

JOHN D. KELLEHER
BRIAN MAC NAMEE
AOIFE D'ARCY

FUNDAMENTALS OF

MACHINE LEARNING FOR PREDICTIVE DATA ANALYTICS

ALGORITHMS, WORKED EXAMPLES, AND CASE STUDIES

SECOND EDITION

Fundamentals of Machine Learning for Predictive Data Analytics

Algorithms, Worked Examples, and Case Studies

Second Edition

John D. Kelleher, Brian Mac Namee, and Aoife D'Arcy

The MIT Press
Cambridge, Massachusetts
London, England

© 2020 Massachusetts Institute of Technology

All rights reserved. No part of this book may be reproduced in any form by any electronic or mechanical means (including photocopying, recording, or information storage and retrieval) without permission in writing from the publisher.

Library of Congress Cataloging-in-Publication Data

Names: Kelleher, John D., 1974- author. |

Mac Namee, Brian, author. |

D'Arcy, Aoife, 1978- author.

Title: Fundamentals of machine learning for predictive data analytics: algorithms, worked examples, and case studies / John D. Kelleher, Brian Mac Namee and Aoife D'Arcy.

Description: Second edition. | Cambridge, Massachusetts: The MIT Press, 2020. | Includes bibliographical references and index.

Identifiers: LCCN 2020002998 | ISBN 9780262044691 (hardcover)

Subjects: LCSH: Machine learning. | Data mining. | Prediction theory.

Classification: LCC Q325.5.K455 2020 | DDC 519.2/870285631–dc23

LC record available at <https://lccn.loc.gov/2020002998>

d_r0

To my wife and family,
thank you for your love, support, and patience.
John

To my family.
Brian

To Grandad D'Arcy, for the inspiration.
Aoife

Contents

Preface

Notation

List of Figures

List of Tables

I INTRODUCTION TO MACHINE LEARNING AND DATA ANALYTICS

1 Machine Learning for Predictive Data Analytics

- 1.1 What Is Predictive Data Analytics?
- 1.2 What Is Machine Learning?
- 1.3 How Does Machine Learning Work?
- 1.4 Inductive Bias Versus Sample Bias
- 1.5 What Can Go Wrong with Machine Learning?
- 1.6 The Predictive Data Analytics Project Lifecycle: CRISP-DM
- 1.7 Predictive Data Analytics Tools
- 1.8 The Road Ahead
- 1.9 Exercises

2 Data to Insights to Decisions

- 2.1 Converting Business Problems into Analytics Solutions
 - 2.1.1 Case Study: Motor Insurance Fraud
- 2.2 Assessing Feasibility
 - 2.2.1 Case Study: Motor Insurance Fraud
- 2.3 Designing the Analytics Base Table
 - 2.3.1 Case Study: Motor Insurance Fraud
- 2.4 Designing and Implementing Features
 - 2.4.1 Different Types of Data
 - 2.4.2 Different Types of Features

- 2.4.3 Handling Time
 - 2.4.4 Legal Issues
 - 2.4.5 Implementing Features
 - 2.4.6 Case Study: Motor Insurance Fraud
- 2.5 Summary
 - 2.6 Further Reading
 - 2.7 Exercises

3 Data Exploration

- 3.1 The Data Quality Report
 - 3.1.1 Case Study: Motor Insurance Fraud
- 3.2 Getting to Know the Data
 - 3.2.1 The Normal Distribution
 - 3.2.2 Case Study: Motor Insurance Fraud
- 3.3 Identifying Data Quality Issues
 - 3.3.1 Missing Values
 - 3.3.2 Irregular Cardinality
 - 3.3.3 Outliers
 - 3.3.4 Case Study: Motor Insurance Fraud
- 3.4 Handling Data Quality Issues
 - 3.4.1 Handling Missing Values
 - 3.4.2 Handling Outliers
 - 3.4.3 Case Study: Motor Insurance Fraud
- 3.5 Advanced Data Exploration
 - 3.5.1 Visualizing Relationships between Features
 - 3.5.2 Measuring Covariance and Correlation
- 3.6 Data Preparation
 - 3.6.1 Normalization
 - 3.6.2 Binning
 - 3.6.3 Sampling
- 3.7 Summary
- 3.8 Further Reading
- 3.9 Exercises

II PREDICTIVE DATA ANALYTICS

4 Information-Based Learning

- 4.1 Big Idea
- 4.2 Fundamentals
 - 4.2.1 Decision Trees
 - 4.2.2 Shannon's Entropy Model
 - 4.2.3 Information Gain
- 4.3 Standard Approach: The ID3 Algorithm
 - 4.3.1 A Worked Example: Predicting Vegetation Distributions
- 4.4 Extensions and Variations
 - 4.4.1 Alternative Feature Selection and Impurity Metrics
 - 4.4.2 Handling Continuous Descriptive Features
 - 4.4.3 Predicting Continuous Targets
 - 4.4.4 Tree Pruning
 - 4.4.5 Model Ensembles
- 4.5 Summary
- 4.6 Further Reading
- 4.7 Exercises

5 Similarity-Based Learning

- 5.1 Big Idea
- 5.2 Fundamentals
 - 5.2.1 Feature Space
 - 5.2.2 Measuring Similarity Using Distance Metrics
- 5.3 Standard Approach: The Nearest Neighbor Algorithm
 - 5.3.1 A Worked Example
- 5.4 Extensions and Variations
 - 5.4.1 Handling Noisy Data
 - 5.4.2 Efficient Memory Search
 - 5.4.3 Data Normalization
 - 5.4.4 Predicting Continuous Targets
 - 5.4.5 Other Measures of Similarity
 - 5.4.6 Feature Selection
- 5.5 Summary
- 5.6 Further Reading
- 5.7 Epilogue
- 5.8 Exercises

6 Probability-Based Learning

- 6.1 Big Idea
 - 6.2 Fundamentals
 - 6.2.1 Bayes' Theorem
 - 6.2.2 Bayesian Prediction
 - 6.2.3 Conditional Independence and Factorization
 - 6.3 Standard Approach: The Naive Bayes Model
 - 6.3.1 A Worked Example
 - 6.4 Extensions and Variations
 - 6.4.1 Smoothing
 - 6.4.2 Continuous Features: Probability Density Functions
 - 6.4.3 Continuous Features: Binning
 - 6.4.4 Bayesian Networks
 - 6.5 Summary
 - 6.6 Further Reading
 - 6.7 Exercises
- 7 Error-Based Learning**
- 7.1 Big Idea
 - 7.2 Fundamentals
 - 7.2.1 Simple Linear Regression
 - 7.2.2 Measuring Error
 - 7.2.3 Error Surfaces
 - 7.3 Standard Approach: Multivariable Linear Regression with Gradient Descent
 - 7.3.1 Multivariable Linear Regression
 - 7.3.2 Gradient Descent
 - 7.3.3 Choosing Learning Rates and Initial Weights
 - 7.3.4 A Worked Example
 - 7.4 Extensions and Variations
 - 7.4.1 Interpreting Multivariable Linear Regression Models
 - 7.4.2 Setting the Learning Rate Using Weight Decay
 - 7.4.3 Handling Categorical Descriptive Features
 - 7.4.4 Handling Categorical Target Features: Logistic Regression
 - 7.4.5 Modeling Non-Linear Relationships
 - 7.4.6 Multinomial Logistic Regression
 - 7.4.7 Support Vector Machines

- 7.5 Summary
- 7.6 Further Reading
- 7.7 Exercises

8 Deep Learning

- 8.1 Big Idea
- 8.2 Fundamentals
 - 8.2.1 Artificial Neurons
 - 8.2.2 Artificial Neural Networks
 - 8.2.3 Neural Networks as Matrix Operations
 - 8.2.4 Why Are Non-Linear Activation Functions Necessary?
 - 8.2.5 Why Is Network Depth Important?
- 8.3 Standard Approach: Backpropagation and Gradient Descent
 - 8.3.1 Backpropagation: The General Structure of the Algorithm
 - 8.3.2 Backpropagation: Backpropagating the Error Gradients
 - 8.3.3 Backpropagation: Updating the Weights in a Network
 - 8.3.4 Backpropagation: The Algorithm
 - 8.3.5 A Worked Example: Using Backpropagation to Train a Feedforward Network for a Regression Task
- 8.4 Extensions and Variations
 - 8.4.1 Vanishing Gradients and ReLUs
 - 8.4.2 Weight Initialization and Unstable Gradients
 - 8.4.3 Handling Categorical Target Features: Softmax Output Layers and Cross-Entropy Loss Functions
 - 8.4.4 Early Stopping and Dropout: Preventing Overfitting
 - 8.4.5 Convolutional Neural Networks
 - 8.4.6 Sequential Models: Recurrent Neural Networks and Long Short-Term Memory Networks
- 8.5 Summary
- 8.6 Further Reading
- 8.7 Exercises

9 Evaluation

- 9.1 Big Idea
- 9.2 Fundamentals
- 9.3 Standard Approach: Misclassification Rate on a Hold-Out Test Set
- 9.4 Extensions and Variations

- 9.4.1 Designing Evaluation Experiments
 - 9.4.2 Performance Measures: Categorical Targets
 - 9.4.3 Performance Measures: Prediction Scores
 - 9.4.4 Performance Measures: Multinomial Targets
 - 9.4.5 Performance Measures: Continuous Targets
 - 9.4.6 Evaluating Models after Deployment
- 9.5 Summary
 - 9.6 Further Reading
 - 9.7 Exercises

III BEYOND PREDICTION

10 Beyond Prediction: Unsupervised Learning

- 10.1 Big Idea
- 10.2 Fundamentals
- 10.3 Standard Approach: The k -Means Clustering Algorithm
 - 10.3.1 A Worked Example
- 10.4 Extensions and Variations
 - 10.4.1 Choosing Initial Cluster Centroids
 - 10.4.2 Evaluating Clustering
 - 10.4.3 Choosing the Number of Clusters
 - 10.4.4 Understanding Clustering Results
 - 10.4.5 Agglomerative Hierarchical Clustering
 - 10.4.6 Representation Learning with Auto-Encoders
- 10.5 Summary
- 10.6 Further Reading
- 10.7 Exercises

11 Beyond Prediction: Reinforcement Learning

- 11.1 Big Idea
- 11.2 Fundamentals
 - 11.2.1 Intelligent Agents
 - 11.2.2 Fundamentals of Reinforcement Learning
 - 11.2.3 Markov Decision Processes
 - 11.2.4 The Bellman Equations
 - 11.2.5 Temporal-Difference Learning

- 11.3 Standard Approach: Q-Learning, Off-Policy Temporal-Difference Learning
 - 11.3.1 A Worked Example
- 11.4 Extensions and Variations
 - 11.4.1 SARSA, On-Policy Temporal-Difference Learning
 - 11.4.2 Deep Q Networks
- 11.5 Summary
- 11.6 Further Reading
- 11.7 Exercises

IV CASE STUDIES AND CONCLUSIONS

12 Case Study: Customer Churn

- 12.1 Business Understanding
- 12.2 Data Understanding
- 12.3 Data Preparation
- 12.4 Modeling
- 12.5 Evaluation
- 12.6 Deployment

13 Case Study: Galaxy Classification

- 13.1 Business Understanding
 - 13.1.1 Situational Fluency
- 13.2 Data Understanding
- 13.3 Data Preparation
- 13.4 Modeling
 - 13.4.1 Baseline Models
 - 13.4.2 Feature Selection
 - 13.4.3 The 5-Level Model
- 13.5 Evaluation
- 13.6 Deployment

14 The Art of Machine Learning for Predictive Data Analytics

- 14.1 Different Perspectives on Prediction Models
- 14.2 Choosing a Machine Learning Approach
 - 14.2.1 Matching Machine Learning Approaches to Projects
 - 14.2.2 Matching Machine Learning Approaches to Data
- 14.3 Beyond Prediction

14.4 Your Next Steps

V APPENDICES

A Descriptive Statistics and Data Visualization for Machine Learning

- A.1 Descriptive Statistics for Continuous Features
 - A.1.1 Central Tendency
 - A.1.2 Variation
- A.2 Descriptive Statistics for Categorical Features
- A.3 Populations and Samples
- A.4 Data Visualization
 - A.4.1 Bar Plots
 - A.4.2 Histograms
 - A.4.3 Box Plots

B Introduction to Probability for Machine Learning

- B.1 Probability Basics
- B.2 Probability Distributions and Summing Out
- B.3 Some Useful Probability Rules
- B.4 Summary

C Differentiation Techniques for Machine Learning

- C.1 Derivatives of Continuous Functions
- C.2 The Chain Rule
- C.3 Partial Derivatives

D Introduction to Linear Algebra

- D.1 Basic Types
- D.2 Transpose
- D.3 Multiplication
- D.4 Summary

Bibliography

Index

Preface

Preface to the 1st Edition

In writing this book our target was to deliver an accessible, introductory text on the fundamentals of machine learning and the ways that machine learning is used in practice to solve predictive data analytics problems in business, science, and other organizational contexts. As such, the book goes beyond the standard topics covered in machine learning books and also covers the lifecycle of a predictive analytics project, data preparation, feature design, and model deployment.

The book is intended for use in machine learning, data mining, data analytics, or artificial intelligence modules of undergraduate and postgraduate computer science, natural and social science, engineering, and business courses. The book provides case studies illustrating the application of machine learning within the industry context of data analytics, which also makes it a suitable text for practitioners looking for an introduction to the field and a textbook for industry training courses in these areas.

The design of the book is informed by our many years of experience in teaching machine learning, and the approach and material in the book has been developed and “road-tested” in the classroom. In writing this book, we have adopted the following guiding principles to make the material accessible:

1. Explain the most important and popular algorithms clearly, rather than overview the full breadth of machine learning. As teachers we believe that giving students a deep knowledge of the core concepts underpinning a field provides them with a solid basis from which they can explore the field themselves. This sharper focus allows us to spend more time introducing, explaining, illustrating, and

contextualizing the algorithms that are fundamental to the field and their uses.

2. Informally explain what an algorithm has been designed to do before presenting the technical formal description of how it does it. Providing this informal introduction to each topic gives students a solid basis from which to attack the more technical material. Our experience with teaching this material to mixed audiences of undergraduates, postgraduates, and professionals has shown that these informal introductions enable students to easily access the topic.
3. Provide *complete* worked examples. In this book we have presented complete workings for all examples, because this enables readers to check their understanding in detail.

Preface to the 2nd Edition

Since the first edition of this book was released in 2015, things have been moving very fast in the world of machine learning. Machine learning models are being used for a more diverse range of applications than ever before, and new developments in machine learning methods are opening up even more opportunities. This has led to the field receiving significant attention from the media (both positive and negative) and a greater interest than ever before from people who want to become machine learning practitioners. For these reasons we felt the time was right for a second edition of the book. In this edition we have sought to expand the topics covered in the first edition to bring them up to date with modern developments, while at the same time staying true to the approach used in the first edition of covering the core concepts in the field in depth with fully worked examples. The main additions in the second edition are the following:

- Due to its expanded size, this edition of the book has been organized into five parts: Part I: Introduction to Machine Learning and Data Analytics; Part II: Predictive Data Analytics; Part III: Beyond Prediction; Part IV: Case Studies and Conclusions; and Part V: Appendices.
- Chapter 8 is a new chapter on **deep learning** that covers the fundamentals of artificial neural networks as well as the most important network architectures used in modern machine learning applications for

images, language, and more. This brings the book right up to date with the most recent developments in machine learning.

- Chapter 10 is a new chapter covering the most important ideas and techniques in **unsupervised learning**. This chapter is one-half of a new part of the book, **Beyond Prediction**, that expands beyond the focus of the first edition on supervised learning to allow broader coverage of machine learning.
- Chapter 11, in the second half of the new **Beyond Prediction** part of the book, describes **reinforcement learning** from the fundamental ideas that underpin it to the use of deep neural networks in modern reinforcement learning systems.
- Section 4.4.5 has been revised to cover **ensemble models** in more detail than in the first edition and includes a new description of **gradient boosting** methods.
- Appendix D is a new section covering the fundamentals of **linear algebra** that underpin the new chapter on deep learning.
- The question sets at the end of each chapter have been revised and expanded—this includes over **50 new questions**.

We hope that these additions and revisions will make the second edition of the book more useful and relevant than the first. We are indebted to all those people—readers, students, instructors, reviewers, colleagues, friends, and family—who gave us feedback on the first edition, which has helped us massively in designing this new edition.

Structure of the Book

In teaching a technical topic, it is important to show the application of the concepts discussed to real-life problems. For this reason, we present machine learning within the context of predictive data analytics, an important industry application of machine learning. The link between machine learning and data analytics runs through every chapter in the book but is especially strong in Part I, which includes Chapters 1 to 3. In Chapter 1 we introduce machine learning and explain its role within a standard data analytics project lifecycle. In Chapter 2 we provide a framework for designing and constructing a predictive analytics solution based on machine learning that meets a business need. All machine learning algorithms

assume that a dataset is available for training; and in Chapter 3 we explain how to design, construct, and quality check a dataset before using it to build a prediction model.

Part II^[117] of the book includes Chapters 4 to 9 and covers the main supervised machine learning material. Each of this part's first five chapters presents a different approach to machine learning: Chapter 4, learning through information gathering; Chapter 5, learning through analogy; Chapter 6, learning by predicting probable outcomes; Chapter 7, learning by searching for solutions that minimize error; and Chapter 8, learning new representations using deep neural networks. All these chapters follow the same two-part structure:

- The first part of each chapter presents an informal introduction to the material presented in the chapter, followed by a detailed explanation of the fundamental technical concepts required to understand the material. Then it presents a standard machine learning algorithm used in that learning approach, along with a detailed worked example.
- The second part of each chapter explains different ways that the standard algorithm can be extended and well-known variations on the algorithm.

The motivation for structuring these technical chapters in two parts is that it provides a natural break in the chapter material. As a result, a topic can be included in a course by covering just the first part of a chapter (Big Idea, fundamentals, standard algorithm, and worked example); and then—time permitting—the coverage of the topic can be extended to some or all of the material in the second part. Chapter 9 explains how to evaluate the performance of prediction models and presents a range of different evaluation metrics. This chapter also adopts the two-part structure of standard approach followed by extensions and variations. Throughout these technical chapters, the link to the broader predictive analytics context is maintained through detailed and complete real-world examples, along with references to the datasets and/or papers on which the examples are based.

Part III covers fundamental techniques in machine learning beyond the supervised machine learning approaches described in Part II. Chapter 10 describes unsupervised machine learning, and Chapter 11 describes reinforcement learning. These chapters follow the same two-part structure as the chapters in Part II.

In Part IV the link between the broader business context and machine learning is shown very clearly in the case studies presented in Chapters 12 (predicting customer churn) and 13 (galaxy classification). In particular, these case studies highlight how a range of issues and tasks beyond model building—such as business understanding, problem definition, data gathering and preparation, and communication of insight—are crucial to the success of a predictive analytics project. Finally, Chapter 14 discusses a range of fundamental topics in machine learning and highlights that the selection of an appropriate machine learning approach for a given task involves factors beyond model accuracy—we must also match the characteristics of the model to the needs of the business.

Part V of the book contains appendices covering background material required to support the content of the other chapters of the book. This includes descriptive statistics and data visualization (Appendix A), probability (Appendix B), differentiation (Appendix C), and linear algebra (Appendix D).

How to Use This Book

Through our years of teaching this material, we have developed an understanding of what is a reasonable amount of material to cover in a one-semester introductory module and in a two-semester more advanced module. To facilitate its use in these different contexts, the book has been designed to be modular—with very few dependencies between chapters. As a result, instructors using this book can plan their courses by simply selecting the sections of the book they wish to cover without worrying about dependencies between the sections. When presented in class, the material in Chapters 1, 2, 12, 13, and 14 typically takes two to three lecture hours per chapter to cover; and the material in Chapters 3, 4, 5, 6, 7, 8, 9, 10, and 11 normally takes four to six lecture hours per chapter to cover.

In [Table 0.1](#) we have listed a number of suggested course plans targeting different contexts. All these courses include Chapter 1 (Machine Learning for Predictive Data Analytics) and Chapter 14 (The Art of Machine Learning for Predictive Data Analytics). The first course listed (column “M.L. (short) (deep)”) is designed to be a one-semester machine learning course with a focus on giving students a deep understanding of two approaches to machine learning, along with an understanding of the correct

methodology to use when evaluating a machine learning model. In our suggested course we have chosen to cover all of Chapters 4 (Information-Based Learning) and 7 (Error-Based Learning). However, Chapter 5 (Similarity-Based Learning) and/or 6 (Probability-Based Learning) could be used instead. The “M.L. (short) (deep)” plan is also an ideal course plan for a short (one-week) professional training course. The second course (“M.L. (short) (broad)” is another one-semester machine learning course. Here, however, the focus is on covering a range of machine learning approaches, and again, evaluation is covered in detail. For a longer two-semester machine learning course (“M.L. (long)”) we suggest covering data preparation (Section 3.6), all the machine learning chapters, and the evaluation chapter.

Table 0.1

Suggested course syllabi.

Chapter	Section	M.L. (short) (deep)	M.L. (short) (broad)	M.L. (long)	P.D.A. (short)	P.D.A. (long)
1		●	●	●	●	●
2					●	●
3	3.1, 3.2, 3.3, 3.4, 3.5 3.6				●	●
4	4.1, 4.2, 4.3 4.4.1, 4.4.2, 4.4.3 4.4.4 4.4.5	● ● ● ●	● ● ● ●	● ● ● ●	●	●
5	5.1, 5.2, 5.3, 5.4.1, 5.4.3, 5.4.6 5.4.2, 5.4.4, 5.4.5		●	●		●
6	6.1, 6.2, 6.3, 6.4.1 6.4.2, 6.4.3, 6.4.4		●	●		●
7	7.1, 7.2, 7.3 7.4.1, 7.4.2, 7.4.3 7.4.4, 7.4.5, 7.4.6, 7.4.7	● ● ●	● ● ●	● ● ●	●	●
8	8.1, 8.2, 8.3 8.4.1, 8.4.2, 8.4.3, 8.4.4, 8.4.5, 8.4.6,		●	●		●
9	9.1, 9.2, 9.3 9.4.1, 9.4.2, 9.4.3, 9.4.4, 9.4.5 9.4.6	● ●	● ● ●	● ● ●	●	●
10	10.1, 10.2, 10.3 10.4.1, 10.4.2, 10.4.4, 10.4.5, 10.4.6		●	●	●	●
11	11.1, 11.2, 11.3 11.4.1, 11.4.2		●	●		
12		●	●	●	●	●
13						●
14		●	●	●	●	●

There are contexts, however, in which the focus of a course is not primarily on machine learning. We also present two course paths that focus on the context of predictive data analytics. The course “P.D.A. (short)” defines a one-semester course. This course gives students an introduction to predictive data analytics, a solid understanding of how machine learning solutions should be designed to meet a business need, insight into how prediction models work and should be evaluated, and one of the case

studies. The “P.D.A. (short)” plan is also an ideal course plan for a short (one-week) professional training course. If there is more time available, then “P.D.A. (long)” expands on the “P.D.A. (short)” course so that students gain a deeper and broader understanding of machine learning, and it includes the second case study.

Online Resources

The following website:

www.machinelearningbook.com

provides access to a wide range of material that supports the book. Worked solutions for all end-of-chapter exercises are available. For questions that are not marked with an *, a solutions manual is available from the book website. Solutions for those questions that are marked with an * are contained in an instructors’ manual available on request from MIT Press.

Acknowledgments

We knew when we began writing this book that it would take a huge amount of work to complete. We underestimated, however, the amount of support we would need and receive from other people. We are delighted to take this opportunity to acknowledge these contributions to the book. We would like to thank our colleagues and students for the help and patience they extended to us over the last few years. We would also like to thank the staff at MIT Press, particularly Marie Lufkin Lee and our editors Melanie Mallon (1st Edition), as well as Theresa Carcaldi of Westchester Publishing Services (2nd Edition). We are also very grateful to the anonymous reviewers who provided insightful and helpful comments on early drafts of the manuscript. Each of us has also been fortunate to have the support of close friends and family, which was invaluable in completing the book.

John would like to thank Lorraine Byrne, Simon Dobnik, Dietmar Frey, Ionella Longo, Alan Mc Donnell, Josef van Genabith, Mary van Genabith, his colleagues and students at Technological University Dublin and in the ADAPT Centre, and all his friends from basketball for their help and encouragement. He would also like to thank his parents (John and Betty) and his sisters (Elizabeth and Marianne), without whose support he would

not have gotten past long division and basic spelling. Finally, he would like to acknowledge and thank Aphra; this book would not have been started without her inspiration and would not have been completed without her support and patience.

Brian would like to thank his parents (Liam and Roisín) and family for all of their support on this book (and everything else). He would also like to thank all his colleagues and students at University College Dublin (and previously at the Dublin Institute of Technology)—especially Pádraig Cunningham and Sarah Jane Delany, who opened his eyes to machine learning.

Aoife would like to thank her parents (Michael and Mairead) and family, and all the people who have supported her throughout her career—especially the much-valued customers of Krisolis who give her data to play with!

Notation

In this section we provide a short overview of the technical notation used throughout this book.

Notational Conventions

Throughout this book we discuss the use of machine learning algorithms to train prediction models based on datasets. The following list explains the notation used to refer to different elements in a dataset. [Figure 0.1](#)^[xxiii] illustrates the key notation using a simple sample dataset.

ID	Name	Age	Country	Rating
1	Brian	24	Ireland	B
2	Mary	57	France	AA
3	Sinead	45	Ireland	AA
4	Paul	38	USA	A
5	Donald	62	Canada	B
6	Agnes	35	Sweden	C
7	Tim	32	USA	B

Annotations:

- $d[1]$: Points to the first row (Brian).
- \mathcal{D} : Points to the entire dataset table.
- $\mathcal{D}_{Rating=AA}$: Points to the subset of rows where Rating is AA (Mary and Sinead).
- t_4 : Points to the row for Donald.
- $d_5[3]$: Points to the row for Agnes.
- d_7 : Points to the row for Tim.

Figure 0.1

How the notation used in the book relates to the elements of a dataset.

Datasets

- \mathcal{D} denotes a dataset.
- A dataset is composed of n instances, (\mathbf{d}_1, t_1) to (\mathbf{d}_n, t_n) , where \mathbf{d} is a set of m descriptive features, and t is a target feature.
- A subset of a dataset is denoted by \mathcal{D} with a subscript to indicate the definition of the subset. For example, $\mathcal{D}_{f=l}$ represents the subset of instances from the dataset \mathcal{D} where the feature f has the value l .

Vectors of Features

- Lowercase boldface letters refer to a vector of features. For example, \mathbf{d} denotes a vector of descriptive features for an instance in a dataset, and \mathbf{q} denotes a vector of descriptive features in a query.

Instances

- Subscripts are used to index into a list of instances.
- \mathbf{x}_i refers to the i^{th} instance in a dataset.
- \mathbf{d}_i refers to the descriptive features of the i^{th} instance in a dataset.

Individual Features

- Lowercase letters represent a single feature (e.g., $f, a, b, c \dots$).
- Square brackets [] are used to index into a vector of features (e.g., $\mathbf{d}[j]$ denotes the value of the j^{th} feature in the vector \mathbf{d}).
- t represents the target feature.

Individual Features in a Particular Instance

- $\mathbf{d}_i[j]$ denotes the value of the j^{th} descriptive feature of the i^{th} instance in a dataset.
- a_i refers to the value for feature a of the i^{th} instance in a dataset.
- t_i refers to the value of the target feature of the i^{th} instance in a dataset

Indexes

- Typically, i is used to index instances in a dataset, and j is used to index features in a vector.

Models

- We use \mathbb{M} to refer to a model.
- \mathbb{M}_w refers to a model \mathbb{M} parameterized by a parameter vector w .

- $\mathbb{M}_w(\mathbf{d})$ refers to the output of a model \mathbb{M} parameterized by parameters w for descriptive features \mathbf{d} .

Set Size

- Vertical bars $| |$ refer to counts of occurrences (e.g., $|a = l|$ represents the number of times that $a = l$ occurs in a dataset).

Feature Names and Feature Values

- We use a specific typography when referring to a feature by name in the text (e.g., POSITION, CREDITRATING, and CLAIM AMOUNT).
- For categorical features, we use a specific typography to indicate the levels in the domain of the feature when referring to a feature by name in the text (e.g., *center*, *aa*, and *soft tissue*).

Notational Conventions for Probabilities

For clarity there are some extra notational conventions used in Chapter 6^[243] on probability.

Generic Events

- Uppercase letters denote generic events where an unspecified feature (or set of features) is assigned a value (or set of values). Typically, we use letters from the end of the alphabet—e.g., X , Y , Z —for this purpose.
- We use subscripts on uppercase letters to iterate over events. So, $\sum_i P(X_i)$ should be interpreted as summing over the set of events that are a complete assignment to the features in X (i.e., all the possible combinations of value assignments to the features in X).

Named Features

- Features explicitly named in the text are denoted by the uppercase initial letters of their names. For example, a feature named MENINGITIS is denoted by M .

Events Involving Binary Features

- Where a named feature is binary, we use the lowercase initial letter of the name of the feature to denote the event where the feature is true and the lowercase initial letter preceded by the \neg symbol to denote the event

where it is false. So, m will represent the event MENINGITIS = *true*, and $\neg m$ will denote MENINGITIS = *false*.

Events Involving Non-Binary Features

- We use lowercase letters with subscripts to iterate across values in the domain of a feature.
- So $\sum_i P(m_i) = P(m) + P(\neg m)$.
- In situations where a letter, for example, X , denotes a joint event, then $\sum_i P(X_i)$ should be interpreted as summing over all the possible combinations of value assignments to the features in X .

Probability of an Event

- The probability that the feature f is equal to the value v is written $P(f = v)$.

Probability Distributions

- We use bold notation $\mathbf{P}()$ to distinguish a probability distribution from a probability mass function $P()$.
- We use the convention that the first element in a probability distribution vector is the probability for a true value. For example, the probability distribution for a binary feature, A , with a probability of 0.4 of being true would be written $\mathbf{P}(A) = < 0.4, 0.6 >$.

Notational Conventions for Deep Learning

For clarity, some additional notational conventions are used in Chapter 8^[381] on deep learning.

Activations

- The activation (or output) of single neuron i is denoted by a_i
- The vector of activations for a layer of neurons is denoted by $\mathbf{a}^{(k)}$ where k identifies the layer.
- A matrix of activations for a layer of neurons processing a batch of examples is denoted by $\mathbf{A}^{(k)}$ where k identifies the layer.

Activation Functions

- We use the symbol φ to generically represent activation functions. In some cases we use a subscript to indicate the use of a particular

activation function. For example, φ_{SM} indicates the use of a softmax function activation function, whereas φ_{ReLU} indicates the use of a rectified linear activation function.

Categorical Targets In the context of handling categorical target features (see Section 8.4.3^[463]) using a softmax function, we use the following symbols:

- We use the \star symbol to indicate the index of the true category in the distribution.
- We use \mathbf{P} to write the true probability distribution over the categories of the target; $\hat{\mathbf{p}}$ to write the distribution over the target categories that the model has predicted; and \mathbf{p} to indicate the predicted probability for the true category.
- We write \mathbf{t} to indicate the one-hot encoding vector of a categorical target.
- In some of the literature on neural networks, the term **logit** is used to refer to the result of a weighted sum calculation in a neuron (i.e., the value we normally denote z). In particular, this terminology is often used in the explanation of softmax functions; therefore, in the section on handling categorical features, we switch from our normal z notation, and instead follow this logit nomenclature, using the notation \mathbf{l} to denote a vector of logits for a layer of neurons, and \mathbf{l}_i to indicate the logit for the i^{th} neuron in the layer.

Elementwise Product

- We use \odot to denote an elementwise product. This operation is sometimes called the **Hadamard product**.

Error Gradients (Deltas) δ

- We use the symbol δ to indicate the rate of change of the error of the network with respect to changes in the weighted sum calculated in a neuron. These δ values are the error gradients that are backpropagated during the backward pass of the backpropagation algorithm. We use a subscript to identify the particular neuron that the δ is associated with; for example, δ_i is the δ for neuron i and is equivalent to the term $\frac{\partial \mathcal{E}}{\partial z_i}$. In some cases we wish to refer to the vector of δ s for the neurons in a layer l ; in these cases we write $\delta^{(l)}$

Network Error

- We use the symbol \mathcal{E} to denote the error of the network at the output layer.

Weights

- We use a lowercase w to indicate a single weight on a connection between two neurons. We use a double subscript to indicate the neurons that are connected, with the convention that the first subscript is the neuron the connection goes to, and the second subscript is the neuron the connection is from. For example, $w_{i,k}$ is the weight on the connection from neuron k to neuron i .
- We use $\Delta w_{i,k}$ to write the sum of error gradients calculated for the weight $w_{i,k}$. We sum errors in this way during batch gradient descent with which we sum over the examples in the batch; see Equation (8.30)^[416] and also in cases in which the weight is shared by a number of neurons, whether in a convolutional neural network or during backpropagation through time.
- We use a bold capital \mathbf{W} to indicate a weight matrix, and we use a superscript in brackets to indicate the layer of the network the matrix is associated with. For example, $\mathbf{W}^{(k)}$ is the weight matrix for the neurons in layer k . In an LSTM network we treat the neurons in the sigmoid and tanh layers within each gate as a separate layer of neurons, and so we write $\mathbf{W}^{(\ell)}$ for the weight matrix for the neurons in the forget gate, and so on for the weight matrices of the other neuron layers in the other gates. However, in a simple recurrent network we distinguish the weight matrices on the basis of whether the matrix is on the connections between the input and the hidden layer, the hidden layer and the output, or the activation memory buffer and the hidden layer. Consequently, for these matrices it is important to highlight the end of the connections the weights are applied to; we use a double subscript (similar to the subscript for a single weight), writing \mathbf{W}_{hx} for the weight matrix on the connections between the input (\mathbf{x}) and the hidden layer (\mathbf{h}).

Weighted Sums and Logits

- We use a lowercase z to represent the result of the weighted sum of the inputs in a neuron. We indicate the identity of the neuron in which the calculation occurred using a subscript. For example, z_i is the result of the weighted sum calculation carried out in neuron i . Note, however, that in the section on Handling Categorical Target features, we switch to the

term *logit* to refer to the output of the weight sum in a neuron and update the notation to reflect this switch; see the previous notation section on Categorical Targets for more details.

- The vector of weighted sums for a layer of neurons is denoted by $\mathbf{z}^{(k)}$ where k identifies the layer.
- A matrix of weighted sums calculations for a layer of neurons processing a batch of examples is denoted by $\mathbf{Z}^{(k)}$ where k identifies the layer.

Notational Conventions for Reinforcement Learning

For clarity there are some extra notational conventions used in Chapter 11^[637] on reinforcement learning (this chapter also heavily uses the notation from the probability chapter).

Agents, States, and Actions

- In reinforcement learning we often describe an agent at time t taking an action, a_t , to move from its current state, s_t , to the next state, s_{t+1} .
- An agent's current state is often modeled as a random variable, S_t . We therefore often describe the probability that an agent is in a specific state, s , at time t as $P(S_t = s)$.
- Often states and actions are explicitly named, in which case we use the following formatting: STATE and *action*.

Transition Probabilities

- We use the \rightarrow notation to represent an agent transitioning from one state to another. Therefore, the probability of an agent moving from state s_1 to state s_2 can be written

$$P(s_1 \rightarrow s_2) = P(S_{t+1} = s_2 \mid S_t = s_1)$$

- Often we condition the probability of an agent transitioning from one state, s_1 , to another, s_2 , on the agent taking a specific action, a . We write this

$$P(s_1 \xrightarrow{a} s_2) = P(S_{t+1} = s_2 \mid S_t = s_1, A_t = a)$$

- The dynamics of an environment in which an agent transitions between states, a Markov process, can be captured in a transition matrix

$$\mathcal{P} = \begin{bmatrix} P(s_1 \rightarrow s_1) & P(s_1 \rightarrow s_2) & \dots & P(s_1 \rightarrow s_n) \\ P(s_2 \rightarrow s_1) & P(s_2 \rightarrow s_2) & \dots & P(s_2 \rightarrow s_n) \\ \vdots & \vdots & \ddots & \vdots \\ P(s_n \rightarrow s_1) & P(s_n \rightarrow s_2) & \dots & P(s_n \rightarrow s_n) \end{bmatrix}$$

- When agent decisions are allowed, leading to a Markov decision process (MDP), then the dynamics of an environment can be captured in a set of transition matrices, one for each action. For example

$$\mathcal{P}^a = \begin{bmatrix} P(s_1 \xrightarrow{a} s_1) & P(s_1 \xrightarrow{a} s_2) & \dots & P(s_1 \xrightarrow{a} s_n) \\ P(s_2 \xrightarrow{a} s_1) & P(s_2 \xrightarrow{a} s_2) & \dots & P(s_2 \xrightarrow{a} s_n) \\ \vdots & \vdots & \ddots & \vdots \\ P(s_n \xrightarrow{a} s_1) & P(s_n \xrightarrow{a} s_2) & \dots & P(s_n \xrightarrow{a} s_n) \end{bmatrix}$$

List of Figures

- 0.1** How the notation used in the book relates to the elements of a dataset.
- 1.1** Predictive data analytics moving from **data** to **insight** to **decision**.
- 1.2** The two steps in supervised machine learning: (a) learning and (b) predicting.
- 1.3** (a)–(d) Striking a balance between overfitting and underfitting in trying to predict income from age.
- 1.4** A diagram of the CRISP-DM process that shows the six key phases and indicates the important relationships between them.
- 2.1** The different data sources typically combined to create an analytics base table.
- 2.2** The hierarchical relationship between an analytics solution, domain concepts, and descriptive features.
- 2.3** Example domain concepts for a motor insurance fraud prediction analytics solution.
- 2.4** Sample descriptive feature data illustrating numeric, binary, ordinal, interval, categorical, and textual types.
- 2.5** Modeling points in time using an observation period and an outcome period.
- 2.6** Observation and outcome periods defined by an event rather than by a fixed point in time (each line represents a prediction subject, and stars signify events). (a) shows the actual data, and (b) shows the event-aligned data.

- 2.7** Modeling points in time for a scenario with no real outcome period (each line represents a customer, and stars signify events). (a) shows the actual data, and (b) shows the event-aligned data.
- 2.8** Modeling points in time for a scenario with no real observation period (each line represents a customer, and stars signify events). (a) shows the actual data, and (b) shows the event-aligned data.
- 2.9** A subset of the domain concepts and related features for a motor insurance fraud prediction analytics solution.
- 2.10** A subset of the domain concepts and related features for a motor insurance fraud prediction analytics solution.
- 2.11** A subset of the domain concepts and related features for a motor insurance fraud prediction analytics solution.
- 2.12** A summary of the tasks in the Business Understanding, Data Understanding, and Data Preparation phases of the CRISP-DM process.
- 3.1** Visualizations of the continuous and categorical features in the motor insurance claims fraud detection ABT in [Table 3.2^{\[56\]}](#).
- 3.2** Histograms for six different sets of data, each of which exhibit well-known, common characteristics.
- 3.3** (a) Three normal distributions with different means but identical standard deviations; and (b) three normal distributions with identical means but different standard deviations.
- 3.4** An illustration of the 68–95–99.7 rule. The gray region defines the area where 95% of values in a sample are expected.
- 3.5** Example scatter plots for pairs of features from the dataset in [Table 3.7^{\[73\]}](#), showing (a) the strong positive covariance between HEIGHT and WEIGHT; (b) the strong negative covariance between SPONSORSHIP EARNINGS and AGE; and (c) the lack of strong covariance between HEIGHT and AGE.
- 3.6** A scatter plot matrix showing scatter plots of the continuous features from the professional basketball team dataset in [Table](#)

[3.7](#)^[73]

- 3.7** Examples of using small multiple bar plot visualizations to illustrate the relationship between two categorical features: (a) the CAREER STAGE and SHOE SPONSOR features; and (b) the POSITION and SHOE SPONSOR features. All data comes from [Table 3.7](#)^[73].
- 3.8** Examples of using stacked bar plot visualizations to illustrate the relationship between two categorical features: (a) CAREER STAGE and SHOE SPONSOR features; and (b) POSITION and SHOE SPONSOR features, all from [Table 3.7](#)^[73].
- 3.9** Example of using small multiple histograms to visualize the relationship between a categorical feature and a continuous feature. All examples use data from the professional basketball team dataset in [Table 3.7](#)^[73]: (a) a histogram of the AGE feature; (b) a histogram of the HEIGHT feature; (c) histograms of the AGE feature for instances displaying each level of the POSITION feature; and (d) histograms of the HEIGHT feature for instances displaying each level of the POSITION feature.
- 3.10** Using box plots to visualize the relationships between categorical and continuous features from [Table 3.7](#)^[73]: (a) and (b) show the relationship between the POSITION feature and the AGE feature; and (c) and (d) show the relationship between the POSITION feature and the HEIGHT feature.
- 3.11** A scatter plot matrix showing scatter plots of the continuous features from the professional basketball team dataset in [Table 3.7](#)^[73] with correlation coefficients included.
- 3.12** Anscombe's quartet. For all four samples, the correlation measure returns the same value (0.816) even though the relationship between the features is very different in each case.
- 3.13** The effect of using different numbers of bins when using binning to convert a continuous feature into a categorical feature.
- 3.14** (a)–(c) Equal-frequency binning of normally distributed data with different numbers of bins; and (d)–(f) the same data binned into the

same number of bins using equal-width binning. The dashed lines illustrate the distribution of the original continuous feature values, and the gray boxes represent the bins.

- 4.1 Cards showing character faces and names for the *Guess Who* game.
- 4.2 The different question sequences that can follow in a game of *Guess Who* beginning with the question *Does the person wear glasses?*
- 4.3 The different question sequences that can follow in a game of *Guess Who* beginning with the question *Is it a man?*
- 4.4 Two decision trees, (a) and (b), that are consistent with the instances in the spam dataset; and (c) the path taken through the tree shown in (a) to make a prediction for the query instance SUSPICIOUS WORDS = *true*, UNKNOWN SENDER = *true*, and CONTAINS IMAGES = *true*.
- 4.5 The entropy of different sets of playing cards measured in bits.
- 4.6 (a) A graph illustrating how the value of a binary log (the log to the base 2) of a probability changes across the range of probability values; and (b) the impact of multiplying these values by – 1.
- 4.7 How the instances in the spam dataset split when we partition using each of the different descriptive features from the spam dataset in [Table 4.2](#)^[121].
- 4.8 The decision tree after the data has been split using ELEVATION.
- 4.9 The state of the decision tree after the \mathcal{D}_1 partition has been split using STREAM.
- 4.10 The state of the decision tree after the \mathcal{D}_2 partition has been split using SLOPE.
- 4.11 The final vegetation classification decision tree.
- 4.12 The vegetation classification decision tree generated using information gain ratio.
- 4.13 The vegetation classification decision tree after the dataset has been split using ELEVATION > 4,175.

- 4.14** The decision tree that would be generated for the vegetation classification dataset listed in [Table 4.9](#)^[147] using information gain.
- 4.15** (a) A set of instances on a continuous number line; (b), (c), and (d) depict some of the potential groupings that could be applied to these instances.
- 4.16** The decision tree resulting from splitting the data in [Table 4.11](#)^[152] using the feature SEASON.
- 4.17** The final decision tree induced from the dataset in [Table 4.11](#)^[152]. To illustrate how the tree generates predictions, this tree lists the instances that ended up at each leaf node and the prediction (PRED.) made by each leaf node.
- 4.18** The decision tree for the post-operative patient routing task.
- 4.19** The iterations of reduced error pruning for the decision tree in [Figure 4.18](#)^[156] using the validation set in [Table 4.13](#)^[157]. The subtree that is being considered for pruning in each iteration is highlighted in black. The prediction returned by each non-leaf node is listed in square brackets. The error rate for each node is given in parentheses.
- 4.20** The process of creating a model ensemble using bagging and subspace sampling.
- 4.21** (a) A plot of the bike rental dataset from [Table 4.14](#)^[162]. (b) An illustration of the final ensemble model trained using the boosting algorithm. (c)–(e) A representation of the changing weights used to generate sample datasets for the first iterations of the boosting process.
- 4.22** (a) A plot of the bike rental dataset from [Table 4.15](#)^[166]. (b)–(e) Visualizations of the prediction models trained in the early iterations of the gradient boosting process. (f) The final ensemble model trained after 20 iterations of gradient boosting.
- 5.1** A feature space plot of the college athlete data in [Table 5.2](#)^[183].
- 5.2** (a) A generalized illustration of the Manhattan and Euclidean distances between two points; and (b) a plot of the Manhattan and

Euclidean distances between instances \mathbf{d}_{12} and \mathbf{d}_5 , and between \mathbf{d}_{12} and \mathbf{d}_{17} from [Table 5.2](#)^[183].

- 5.3 A feature space plot of the data in [Table 5.2](#)^[183], with the position in the feature space of the query represented by the ? marker.
- 5.4 (a) The Voronoi tessellation of the feature space for the dataset in [Table 5.2](#)^[183], with the position of the query represented by the? marker; and (b) the decision boundary created by aggregating the neighboring Voronoi regions that belong to the same target level.
- 5.5 (a) The Voronoi tessellation of the feature space when the dataset has been updated to include the query instance; and (b) the updated decision boundary reflecting the addition of the query instance in the training set.
- 5.6 The decision boundary using majority vote of the nearest 3 and 5 instances.
- 5.7 (a) The decision boundary using majority vote of the nearest 15 neighbors; and (b) the weighted k nearest neighbor model decision boundary (with $k = 21$).
- 5.8 (a) The k - d tree generated for the dataset in [Table 5.4](#)^[191] after the initial split; (b) the partitioning of the feature space by the k - d tree in (a); (c) the k - d tree after the dataset at the left child of the root has been split; and (d) the partitioning of the feature space by the k - d tree in (c).
- 5.9 (a) The final k - d tree generated for the dataset in [Table 5.4](#)^[191]; and (b) the partitioning of the feature space defined by this k - d tree.
- 5.10 (a) The path taken from the root node to a leaf node when we search the tree with a query; and (b) the ? marks the location of the query, and the dashed circle plots the extent of the target.
- 5.11 (a) The target hypersphere after instance \mathbf{d}_{21} has been stored as *best*, and *best-distance* has been updated; and (b) the extent of the search process.

- 5.12** (a) The feature space defined by the SALARY and AGE features in [Table 5.5](#)^[204]; and (b) the normalized SALARY and AGE feature space based on the normalized data in [Table 5.7](#)^[208].
- 5.13** The AGE and RATING feature space for the whiskey dataset. The location of the query instance is indicated by the ? symbol. The circle plotted with a dashed line demarcates the border of the neighborhood around the query when $k = 3$. The three nearest neighbors to the query are labeled with their ID values.
- 5.14** (a) The θ represents the inner angle between the vector emanating from the origin to instance \mathbf{d}_1 and the vector emanating from the origin to instance \mathbf{d}_2 ; and (b) shows \mathbf{d}_1 and \mathbf{d}_2 normalized to the unit circle.
- 5.15** Scatter plots of three bivariate datasets with the same center point A and two queries B and C both equidistant from A ; (a) a dataset uniformly spread around the center point; (b) a dataset with negative covariance; and (c) a dataset with positive covariance.
- 5.16** The coordinate systems defined by the Mahalanobis distance using the covariance matrix for the dataset in [Figure 5.15\(c\)](#)^[219] using three different origins: (a) (50, 50); (b) (63,71); and (c) (42, 35). The ellipses in each figure plot the 1, 3, and 5 unit distance contours.
- 5.17** The effect of using a Mahalanobis versus Euclidean distance. A marks the central tendency of the dataset in [Figure 5.15\(c\)](#)^[219]. The ellipses plot the Mahalanobis distance contours from A that B and C lie on. In Euclidean terms, B and C are equidistant from A ; however, using the Mahalanobis distance, C is much closer to A than B .
- 5.18** A set of scatter plots illustrating the curse of dimensionality.
- 5.19** Feature subset space for a dataset with three features X, Y, and Z.
- 5.20** The process of model induction with feature selection.
- 5.21** A duck-billed platypus.
- 6.1** A game of *find the lady*: (a) the cards used; (b) the cards dealt facedown on a table; (c) the initial likelihoods of the queen ending

up in each position; and (d) a revised set of likelihoods for the position of the queen based on evidence collected.

- 6.2** (a) The set of cards after the wind blows over the one on the right; (b) the revised likelihoods for the position of the queen based on this new evidence; and (c) the final positions of the cards in the game.
- 6.3** Plots of some well-known probability distributions.
- 6.4** Histograms of two unimodal datasets: (a) the distribution has light tails; and (b) the distribution has fat tails.
- 6.5** Illustration of the robustness of the student- t distribution to outliers: (a) a density histogram of a unimodal dataset overlaid with the density curves of a normal and a student- t distribution that have been fitted to the data; and (b) a density histogram of the same dataset with outliers added, overlaid with the density curves of a normal and a student- t distribution that have been fitted to the data.
- 6.6** Illustration of how a mixture of Gaussians model is composed of a number of normal distributions. The curve plotted using a solid line is the mixture of Gaussians density curve, created using an appropriately weighted summation of the three normal curves, plotted using dashed and dotted lines.
- 6.7** (a) The area under a density curve between the limits $x - \frac{\epsilon}{2}$ and $x + \frac{\epsilon}{2}$ (b) the approximation of this area computed by $PDF(x) \times \epsilon$; and (c) the error in the approximation is equal to the difference between area A, the area under the curve omitted from the approximation, and area B, the area above the curve erroneously included in the approximation. Both of these areas will get smaller as the width of the interval gets smaller, resulting in a smaller error in the approximation.
- 6.8** Histograms, using a bin size of 250 units, and density curves for the ACCOUNT BALANCE feature: (a) the fraudulent instances overlaid with a fitted exponential distribution; and (b) the non-fraudulent instances overlaid with a fitted normal distribution.

- 6.9** (a) A Bayesian network for a domain consisting of two binary features. The structure of the network states that the value of feature A directly influences the value of feature B. (b) A Bayesian network consisting of four binary features with a path containing three generations of nodes: D, C, and B.
- 6.10** A depiction of the Markov blanket of a node. The gray nodes define the Markov blanket of the black node. The black node is conditionally independent of the white nodes given the state of the gray nodes.
- 6.11** (a) A Bayesian network representation of the conditional independence asserted by a naive Bayes model between the descriptive features given knowledge of the target feature; and (b) a Bayesian network representation of the conditional independence assumption for the naive Bayes model in the fraud example.
- 6.12** Two different Bayesian networks, each defining the same full joint probability distribution.
- 6.13** A Bayesian network that encodes the causal relationships between the features in the corruption domain. The CPT entries have been calculated using the binned data from [Table 6.18](#)^[295].
- 7.1** (a) A scatter plot of the SIZE and RENTAL PRICE features from the office rentals dataset; and (b) the scatter plot from (a) with a linear model relating RENTAL PRICE to SIZE overlaid.
- 7.2** (a) A scatter plot of the SIZE and RENTAL PRICE features from the office rentals dataset. A collection of possible simple linear regression models capturing the relationship between these two features are also shown. (b) A scatter plot of the SIZE and RENTAL PRICE features from the office rentals dataset showing a candidate prediction model and the resulting errors.
- 7.3** (a) A 3D surface plot and (b) a bird's-eye view contour plot of the error surface generated by plotting the sum of squared errors for the office rentals training set for each possible combination of values for \mathbf{w} [0] (from the range $[-10, 20]$) and \mathbf{w} [1] (from the range $[-2, 3]$).

- 7.4** (a) A 3D plot of an error surface and (b) a bird's-eye view contour plot of the same error surface. The lines indicate the path that the gradient descent algorithm would take across this error surface from four different starting positions to the global minimum—marked as the white dot in the center.
- 7.5** (a) A 3D surface plot and (b) a bird's-eye view contour plot of the error surface for the office rentals dataset showing the path that the gradient descent algorithm takes toward the best-fit model.
- 7.6** A selection of the simple linear regression models developed during the gradient descent process for the office rentals dataset. The bottom-right panel shows the sums of squared errors generated during the gradient descent process.
- 7.7** Plots of the journeys made across the error surface for the simple office rentals prediction problem for different learning rates: (a) a very small learning rate (0.002); (b) a medium learning rate (0.08); and (c) a very large learning rate (0.18). The changing sum of squared errors are also shown.
- 7.8** (a) The journey across the error surface for the office rentals prediction problem when learning rate decay is used ($\alpha_0 = 0.18$, $c = 10$); and (b) a plot of the changing sum of squared errors during this journey.
- 7.9** (a) The journey across the error surface for the office rentals prediction problem when learning rate decay is used ($\alpha_0 = 0.25$, $c = 100$); (b) a plot of the changing sum of squared errors during this journey.
- 7.10** (a) A scatter plot of the RPM and VIBRATION descriptive features from the generators dataset shown in [Table 7.6](#)^[339], where *good* generators are shown as crosses, and *faulty* generators are shown as triangles; and (b) as decision boundary separating *good* generators (crosses) from *faulty* generators (triangles).
- 7.11** (a) A surface showing the value of Equation (7.23)^[339] for all values of RPM and VIBRATION, with the decision boundary given in

Equation (7.23)^[339] highlighted; and (b) the same surface linearly thresholded at zero to operate as a predictor.

- 7.12** (a) A plot of the logistic function (Equation (7.25)^[342]) for the range of values $[-10,10]$; and (b) the logistic decision surface that results from training a model to represent the generators dataset given in [Table 7.6](#)^[339] (note that the data has been normalized to the range $[-1,1]$).
- 7.13** A selection of the logistic regression models developed during the gradient descent process for the machinery dataset from [Table 7.6](#)^[339]. The bottom-right panel shows the sums of squared errors generated during the gradient descent process.
- 7.14** A scatter plot of the extended generators dataset given in [Table 7.7](#)^[347], which results in instances with the different target levels overlapping each other. Instances representing *good* generators are shown as crosses, and those representing *faulty* generators as triangles.
- 7.15** A selection of the logistic regression models developed during the gradient descent process for the extended generators dataset in [Table 7.7](#)^[347]. The bottom-right panel shows the sums of squared errors generated during the gradient descent process.
- 7.16** (a) A scatter plot of the RAIN and GROWTH feature from the grass growth dataset; and (b) the same plot with a simple linear regression model trained to capture the relationship between the grass growth and rainfall.
- 7.17** A selection of the models developed during the gradient descent process for the grass growth dataset from [Table 7.9](#)^[351].
- 7.18** A scatter plot of the P20 and P45 features from the EEG dataset. Instances representing *positive* images are shown as crosses, and those representing *negative* images as triangles.
- 7.19** A selection of the models developed during the gradient descent process for the EEG dataset from [Table 7.10](#)^[355]. The final panel shows the decision surface generated.

- 7.20** An illustration of three different one-versus-all prediction models for the customer type dataset in [Table 7.11](#)^[359], with three target levels: (a) *single* (squares), (b) *business* (triangles), and (c) *family* (crosses).
- 7.21** A selection of the models developed during the gradient descent process for the customer group dataset from [Table 7.11](#)^[359]. Squares represent instances with the *single* target level, triangles the *business* level, and crosses the *family* level. The bottom-right panel illustrates the overall decision boundaries between the three target levels.
- 7.22** A small sample of the generators dataset with two features, RPM and VIBRATION, and two target levels, *good* (shown as crosses) and *faulty* (shown as triangles): (a) a decision boundary with a very small margin; and (b) a decision boundary with a much larger margin. In both cases, the instances along the margins are highlighted.
- 7.23** Different margins that satisfy the constraint in [Equation \(7.44\)](#)^[364], the instances that define the margin are highlighted in each case; (b) shows the maximum margin and also shows two query instances represented as black dots.
- 7.24** (a) The journey across an error surface; and (b) the changing sums of squared errors during this journey.
- 8.1** A high-level schematic of the structure of a neuron.
- 8.2** Plots for activation functions that have been popular in the history of neural networks.
- 8.3** A schematic of an artificial neuron.
- 8.4** A schematic of a feedforward artificial neural network.
- 8.5** An illustration of the correspondence between graphical and matrix representations of a neural network.
- 8.6** An illustration of how a batch of examples can be processed in parallel using matrix operations.
- 8.7** A single-layer network.

- 8.8** The logical AND and OR functions are linearly separable, but the XOR is not.
- 8.9** (left) The XOR function implemented as a two-layer neural network. (right) The network processing the four possible input combinations.
- 8.10** An illustration of how the representational capacity of a network increases as more layers are added to the network.
- 8.11** The calculation of the z values and activations of each neuron during the forward pass of the backpropagation algorithm.
- 8.12** The backpropagation of the δ values during the backward pass of the backpropagation algorithm.
- 8.13** Plots of the logistic function and its derivative.
- 8.14** The forward pass of the examples listed in [Table 8.3](#)^[423] through the network in [Figure 8.4](#)^[390].
- 8.15** An illustration of the forward propagation of \mathbf{d}_2 through the network showing the weights on each connection, and the weighted sum z and activation a value for each neuron in the network.
- 8.16** The δ s for each of the neurons in the network for Example 2.
- 8.17** A plot showing how the sum of squared errors of the network changed during training.
- 8.18** The forward pass of the examples listed in [Table 8.3](#)^[423] through the network in [Figure 8.4](#)^[390] when all the neurons are ReLUs.
- 8.19** An illustration of the forward propagation of \mathbf{d}_2 through the ReLU network showing the weights on each connection, and the weighted sum z and activation a value for each neuron in the network.
- 8.20** A plot showing how the sum of squared errors of the ReLU network changed during training when $\alpha = 0.2$.
- 8.21** A plot showing how the sum of squared errors of the ReLU network changed during training when $\alpha = 0.1$.

- 8.22** The architecture of the neural network used in the weight initialization experiments. Note that the neurons in this network use a linear activation function: $a_i = z_i$.
- 8.23** The internal dynamics of the network in [Figure 8.22^{\[450\]}](#) during the first training iteration when the weights were initialized using a normal distribution with $\mu=0.0$, $\sigma=0.01$.
- 8.24** The internal dynamics of the network in [Figure 8.22^{\[450\]}](#) during the first training iteration when the weights were initialized using a normal distribution with $\mu = 0.0$ and $\sigma = 0.2$.
- 8.25** The internal dynamics of the network in [Figure 8.22^{\[450\]}](#) during the first training iteration when the weights were initialized using Xavier initialization.
- 8.26** The internal dynamics of the network in [Figure 8.22^{\[450\]}](#), using ReLUs, during the first training iteration when the weights were initialized using He initialization.
- 8.27** A schematic of a feedforward artificial neural network with a three-neuron softmax output layer.
- 8.28** The forward pass of the mini-batch of examples listed in [Table 8.13^{\[464\]}](#) through the network in [Figure 8.27^{\[465\]}](#).
- 8.29** An illustration of how different small networks are generated for different training examples by applying dropout to the original large network.
- 8.30** Samples of the handwritten digit images from the MNIST dataset.
- 8.31** A 6-by-6 matrix representation of a grayscale image of a 4, and a neuron with a receptive field that covers the top-left corner of the image.
- 8.32** A 6-by-6 matrix representation of a grayscale image of a 4, and a neuron with a different receptive field from the neuron in [Figure 8.31^{\[480\]}](#).
- 8.33** Illustration of the organization of a set of neurons that share weights (use the same filter) and their local receptive fields such that

together the receptive fields cover the entirety of the input image.

- 8.34** A grayscale image of a 4 after padding has been applied to the original 6-by-6 matrix representation, and the local receptive field of a neuron that includes both valid and padded pixels.
- 8.35** Schematic of the typical sequences of layers found in a convolutional neural network.
- 8.36** Worked example illustrating the dataflow through a multilayer, multifilter CNN.
- 8.37** Schematic of the simple recurrent neural architecture.
- 8.38** A simple RNN model unrolled through time (in this instance, three time-steps).
- 8.39** An illustration of the different iterations of backpropagation during backpropagation through time.
- 8.40** A schematic of the internal structure of a long short-term memory unit.
- 8.41** The flow of activations through a long short-term memory unit during forward propagation when $\mathbf{c}_{t-1} = [0.3, 0.6]$, $\mathbf{h}_t = [0.1, 0.8]$, and $\mathbf{x}_t = [0.9]$.
- 8.42** The flow of error gradients through a long short-term memory unit during backpropagation.
- 9.1** The process of building and evaluating a model using a hold-out test set.
- 9.2** Hold-out sampling can divide the full data into training, validation, and test sets.
- 9.3** Using a validation set to avoid overfitting in iterative machine learning algorithms.
- 9.4** The division of data during the k -fold cross validation process. Black rectangles indicate test data, and white spaces indicate training data.

- 9.5** The division of data during the leave-one-out cross validation process. Black rectangles indicate instances in the test set, and white spaces indicate training data.
- 9.6** The division of data during the ε_0 bootstrap process. Black rectangles indicate test data, and white spaces indicate training data.
- 9.7** The out-of-time sampling process.
- 9.8** Surfaces generated by calculating (a) the arithmetic mean and (b) the harmonic mean of all combinations of features A and B that range from 0 to 100.
- 9.9** Prediction score distributions for two different prediction models. The distributions in (a) are much better separated than those in (b).
- 9.10** Prediction score distributions for the (a) *spam* and (b) *ham* target levels based on the data in [Table 9.11](#)^[557].
- 9.11** (a) The changing values of TPR and TNR for the test data shown in [Table 9.13](#)^[560] as the threshold is altered; and (b) points in ROC space for thresholds of 0.25, 0.5, and 0.75.
- 9.12** (a) A complete ROC curve for the email classification example; and (b) a selection of ROC curves for different models trained on the same prediction task.
- 9.13** The K-S chart for the email classification predictions shown in [Table 9.11](#)^[557].
- 9.14** A series of charts for different model performance on the same large email classification test set used to generate the ROC curves in [Figure 9.12\(b\)](#)^[562]. Each column from top to bottom: a histogram of the *ham* scores predicted by the model, a histogram of the *spam* scores predicted by the model, and the K-S chart.
- 9.15** The (a) gain and (b) cumulative gain at each decile for the email predictions given in [Table 9.11](#)^[557].
- 9.16** The (a) lift and (b) cumulative lift at each decile for the email predictions given in [Table 9.11](#)^[557].

- 9.17** Cumulative gain, lift, and cumulative lift charts for four different models for the extended email classification test set.
- 9.18** The distributions of predictions made by a model trained for the bacterial species identification problem for (a) the original evaluation test set, and for (b) and (c) two periods of time after model deployment; (d) shows how the stability index can be tracked over time to monitor for concept drift.
- 10.1** The three different arrangements of the magnetic letters made by the Murphy children on the Murphy family refrigerator.
- 10.2** Unsupervised machine learning as a single-step process.
- 10.3** (a) A plot of the mobile phone customer dataset given in [Table 10.1](#)^[604]. (b)–(f) The progress of the k -means clustering algorithm, working on the simple customer segmentation dataset. The large symbols represent cluster centroids, and the smaller symbols represent cluster assignments.
- 10.4** (a)–(h) Different clusterings (all with $k = 3$) that can be found for the mobile phone customer dataset given in [Table 10.1](#)^[604] when different initial cluster centroids are used.
- 10.5** (a)–(d) Initial centroids chosen using the k-means++ approach (all with $k = 3$) for the mobile phone customer dataset given in [Table 10.1](#)^[604].
- 10.6** (a) Intra-cluster distance; (b) inter-cluster distance; (c) a *good* clustering; and (d) a *bad* clustering.
- 10.7** The silhouette plot for the final clustering of the mobile phone customer dataset ([Table 10.1](#)^[604]) found using the k -means algorithm (with $k = 3$).
- 10.8** (a)–(f) Different clusterings found for the mobile phone customer dataset in [Table 10.1](#)^[604] for values of k in (2, 9). (g) shows the silhouette for each clustering.
- 10.9** (a)–(b) Visualizations of the distributions of the descriptive features in the mobile phone customer dataset in [Table 10.1](#)^[604] across the

complete dataset, and divided by the clustering found using k -means clustering ($k = 3$).

- 10.10** (a)–(i) A plot of the *blobs*, *circles*, and *half-moons* datasets and the clusterings achieved by the k -means clustering and agglomerative hierarchical clustering algorithms (where k is set to 3, 2, and 2, respectively).
- 10.11** (a)–(d) Different linkage methods that can be used to compare the distances between clusters in agglomerative hierarchical clustering. (Arrows for only some indicative distances are shown in the average linkage diagram (d).)
- 10.12** (a) A plot of a reduced version of the mobile phone customer dataset given in [Table 10.1](#)^[604]. (b)–(d) show details of several iterations of the AHC algorithm.
- 10.13** (a) A plot of the hierarchical grouping of the instances in the mobile phone customer dataset from [Table 10.1](#)^[604] found by the AHC algorithm (using Euclidean distance and single linkage). (b) The clustering returned when the tree is cut at $k = 3$. (c) The clustering returned when the tree is cut at $k = 6$.
- 10.14** The architecture of an auto-encoder network made up of an encoder and a decoder connected by a bottleneck layer.
- 10.15** (a) A selection of images from the handwritten digits dataset; (b)–(d) image reconstructions generated by the auto-encoder network after 0, 10, and 1,000 training epochs.
- 10.16** An image of the digit 2 and reconstructions of this image by the auto-encoder after various amounts of network training. The pixel values of the reconstructed images are shown alongside the images, as is the reconstruction error calculated by comparing these to the pixel values of the original image.
- 10.17** The process of using an unsupervised auto-encoder network to generate a feature representation used to train a supervised model.
- 11.1** An agent behaving in an environment and the observation, reward, action cycle. The transition from observations of the environment to

a state is shown by the state generation function, φ .

- 11.2** A simple Markov process to model the evolution of an infectious disease in individuals during an epidemic using the SUSCEPTIBLE-INFECTED-RECOVERED (S-I-R) model.
- 11.3** A Markov decision process representation for TwentyTwos, a simplified version of the card game Blackjack.
- 11.4** A simple grid world. The start position is annotated with an S and the goal with a G . The squares marked f denote fire, which is very damaging to an agent.
- 11.5** (a)–(c) The evolution of the entries in the action-value table over episodes of Q-learning off-policy temporal-difference learning across the grid world. (d) The cumulative reward earned from each episode. (e) An illustration of the target policy learned by the agent after 350 episodes. (f) The path the agent will take from the start state to the goal state when greedily following the target policy.
- 11.6** (a) A visualization of the final action-value table for an agent trained using SARSA on-policy temporal-difference learning across the grid world after 350 episodes. (b) The cumulative reward earned from each episode. (c) An illustration of the target policy learned by the agent after 350 episodes. (d) The path the agent will take from the start state to the goal state when greedily following the target policy.
- 11.7** The Lunar Lander environment. The aim of the game is to control the spaceship starting from the top of the world and attempting to land on the landing pad.
- 11.8** Framing the action-value function as a prediction problem.
- 11.9** An illustration of the DQN algorithm including experience replay and target network freezing.
- 11.10** (a) Frames from an episode early in the training process in which the agent performs poorly. (b) Frames from an episode near the end of the learning process where the agent is starting to be very effective. (c) Changing episode returns during DQN training. The

gray line shows a 50-episode moving average to better highlight the trend.

- 12.1** The set of domain concepts for the Acme Telephonica customer churn prediction problem.
 - 12.2** (a)–(c) Histograms for the features from the AT ABT with irregular cardinality; (d)–(g) histograms for the features from the AT ABT that are potentially suffering from outliers.
 - 12.3** (a) A stacked bar plot for the REGIONTYPE feature; and (b) histograms for the AVGOVERBUNDLEMINS feature by target feature value.
 - 12.4** An unpruned decision tree built for the AT churn prediction problem (shown only to indicate its size and complexity). The excessive complexity and depth of the tree are evidence that overfitting has probably occurred.
 - 12.5** A pruned decision tree built for the AT churn prediction problem. Gray leaf nodes indicate a churn prediction, and clear leaf nodes indicate a non-churn prediction. For space reasons, we show only the features tested at the top-level nodes.
 - 12.6** (a) Cumulative gain, (b) lift, and (c) cumulative lift charts for the predictions made on the large test data sample.
 - 12.7** A pruned and stunted decision tree built for the Acme Telephonica churn prediction problem.
- 13.1** Examples of the different galaxy morphology categories into which SDSS scientists categorize galaxy objects.
 - 13.2** The first draft of the domain concepts diagram developed by Jocelyn for the galaxy classification task.
 - 13.3** Bar plots of the different galaxy types present in the full SDSS dataset for the 3-level and 5-level target features.
 - 13.4** The revised domain concepts diagram for the galaxy classification task.

- 13.5** SPLOM diagrams of (a) the EXPRAD; and (b) DEVRAD measurements from the raw SDSS dataset. Each SPLOM shows the measure across the five different photometric bands captured by the SDSS telescope (u , g , r , i , and z).
- 13.6** Histograms of a selection of features from the SDSS dataset.
- 13.7** Histograms of the EXPRAD_R feature split by target feature level.
- 13.8** (a)–(c) Small multiple box plots (split by the target feature) of some of the features from the SDSS ABT.
- 14.1** (a) The class conditional densities for two classes (l_1, l_2) with a single descriptive feature \mathbf{d} . (b) The class posterior probabilities plotted for each class for different values of \mathbf{d} .
- 14.2** An illustration of the decision boundaries learned by different machine learning algorithms for three artificial datasets.
- A.1** The members of a school basketball team. The height of each player is listed below the player. The dashed gray line shows the arithmetic mean of the players' heights.
- A.2** The members of the school basketball team from [Figure A.1](#)^[746] with one very tall *ringer* added: (a) the dashed gray line shows the mean of the players' heights; and (b) the dashed gray line shows the median of the players' heights, with the players ordered by height.
- A.3** The members of a rival school basketball team. Player heights are listed below each player. The dashed gray line shows the arithmetic mean of the players' heights.
- A.4** The members of the rival school basketball team from [Figure A.3](#)^[747] ordered by height.
- A.5** Example bar plots for the POSITION feature in [Table A.1](#)^[750]: (a) frequency bar plot, (b) density bar plot, and (c) order density bar plot.
- A.6** Bar plot of the continuous TRAINING EXPENSES feature from [Table A.1](#)^[750].

- A.7** (a) and (b) frequency histograms and (c) and (d) density histograms for the continuous TRAINING EXPENSES feature from [Table A.1](#)^[750], illustrating how using intervals overcomes the problem seen in [Figure A.6](#)^[753] and the effect of varying interval sizes.
- A.8** (a) The structure of a box plot; and (b) a box plot for the TRAINING EXPENSES feature from the basketball team dataset in [Table A.1](#)^[750].
- B.1** The **sample space** for the domain of two dice.
- C.1** (a) The speed of a car during a journey along a minor road before joining a highway and finally coming to a sudden halt; and (b) the acceleration, the derivative of speed with respect to time, for this journey.
- C.2** Examples of continuous functions (shown as solid lines) and their derivatives (shown as dashed lines).
- C.3** (a) A continuous function in two variables, x and y ; (b) the partial derivative of this function with respect to x ; and (c) the partial derivative of this function with respect to y .

List of Tables

- 0.1** Suggested course syllabi.
- 1.1** A credit scoring dataset.
- 1.2** A more complex credit scoring dataset.
- 1.3** A simple retail dataset.
- 1.4** Potential prediction models (a) before and (b) after training data becomes available.
- 1.5** The age-income dataset.
- 2.1** The basic structure of an analytics base table—descriptive features and a target feature.
- 2.2** The ABT for the motor insurance claims fraud detection solution.
- 3.1** The structures of the tables included in a data quality report to describe (a) continuous features and (b) categorical features.
- 3.2** Portions of the ABT for the motor insurance claims fraud detection problem discussed in Section 2.4.6^[42].
- 3.3** A data quality report for the motor insurance claims fraud detection ABT displayed in [Table 3.2](#)^[56].
- 3.4** The structure of a data quality plan.
- 3.5** The data quality plan for the motor insurance fraud prediction ABT.
- 3.6** The data quality plan with potential handling strategies for the motor insurance fraud prediction ABT.
- 3.7** The details of a professional basketball team.

- 3.8** Calculating covariance.
- 3.9** A small sample of the HEIGHT and SPONSORSHIP EARNINGS features from the professional basketball team dataset in [Table 3.7](#)^[73], showing the result of range normalization and standardization.
- 4.1** A dataset that represents the characters in the *Guess Who* game.
- 4.2** An email spam prediction dataset.
- 4.3** The vegetation classification dataset.
- 4.4** Partition sets (Part.), entropy, remainder (Rem.), and information gain (Info. Gain) by feature for the dataset in [Table 4.3](#)^[136].
- 4.5** Partition sets (Part.), entropy, remainder (Rem.), and information gain (Info. Gain) by feature for the dataset \mathcal{D}_7 in [Figure 4.8](#)^[138].
- 4.6** Partition sets (Part.), entropy, remainder (Rem.), and information gain (Info. Gain) by feature for the dataset \mathcal{D}_8 in [Figure 4.9](#)^[139].
- 4.7** Partition sets (Part.), entropy, Gini index, remainder (Rem.), and information gain (Info. Gain) by feature for the dataset in [Table 4.3](#)^[136].
- 4.8** Dataset for predicting the vegetation in an area with a continuous ELEVATION feature (measured in feet).
- 4.9** Dataset for predicting the vegetation in an area sorted by the continuous ELEVATION feature.
- 4.10** Partition sets (Part.), entropy, remainder (Rem.), and information gain (Info. Gain) for the candidate ELEVATION thresholds: ≥ 750 , $\geq 1,350$, $\geq 2,250$ and $\geq 4,175$.
- 4.11** A dataset listing the number of bike rentals per day.
- 4.12** The partitioning of the dataset in [Table 4.11](#)^[152] based on SEASON and WORK DAY features and the computation of the weighted variance for each partitioning.
- 4.13** An example validation set for the post-operative patient routing task.

- 4.14** A simple bicycle demand predictions dataset and the workings of the first three iterations of training an ensemble model using boosting to predict RENTALS given TEMP.
- 4.15** A simple bicycle demand predictions dataset and the workings of the first iterations of training a gradient boosting model.
- 5.1** Matching animals you remember to the features of the unknown animal described by the sailor.
- 5.2** The SPEED and AGILITY ratings for 20 college athletes and whether they were drafted by a professional team.
- 5.3** The distances (Dist.) between the query instance with SPEED = 6.75 and AGILITY = 3.00 and each instance in [Table 5.2](#)^[183].
- 5.4** The extended version of the college athletes dataset.
- 5.5** A dataset listing salary and age information for customers and whether they purchased a product.
- 5.6** The dataset from [Table 5.5](#)^[204] with the Euclidean distance between each instance and the query SALARY = 56,000, AGE = 35 when we use both the SALARY and AGE features, just the SALARY feature, and just the AGE feature.
- 5.7** The updated version of [Table 5.6](#)^[206] once we have applied range normalization to the SALARY and AGE features in the dataset and to the query instance.
- 5.8** A dataset of whiskeys listing the age (in years), the rating (between 1 and 5, with 5 being the best), and the bottle price of each whiskey.
- 5.9** The whiskey dataset after the descriptive features have been normalized.
- 5.10** The calculations for the weighted k nearest neighbor prediction.
- 5.11** A binary dataset listing the behavior of two individuals on a website during a trial period and whether they subsequently signed up for the website.

- 5.12** The similarity between the current trial user, \mathbf{q} , and the two users in the dataset, \mathbf{d}_1 and \mathbf{d}_2 , in terms of co-presence (CP), co-absence (CA), presence-absence (PA), and absence-presence (AP).
- 6.1** A simple dataset for a MENINGITIS diagnosis with descriptive features that describe the presence or absence of three common symptoms of the disease: HEADACHE, FEVER, and VOMITING.
- 6.2** A dataset from a loan application fraud detection domain.
- 6.3** The probabilities needed by a naive Bayes prediction model, calculated from the data in [Table 6.2](#)^[263].
- 6.4** The relevant probabilities, from [Table 6.3](#)^[264], needed by the naive Bayes prediction model to make a prediction for a query with CH = *paid*, GC = *none*, and ACC = *rent*, and the calculation of the scores for each target level.
- 6.5** The relevant probabilities, from [Table 6.3](#)^[264], needed by the naive Bayes prediction model to make a prediction for the query with CH = *paid*, GC = *guarantor*, and ACC = *free*, and the calculation of the scores for each possible target level.
- 6.6** The posterior probability distribution for the GUARANTOR/COAPPLICANT feature under the condition that FRAUD = *false*.
- 6.7** Smoothing the posterior probabilities for the GUARANTOR/COAPPLICANT feature conditioned on FRAUD = *false*.
- 6.8** The Laplace smoothed (with $k = 3$) probabilities needed by a naive Bayes prediction model, calculated from the dataset in [Table 6.2](#)^[263].
- 6.9** The relevant smoothed probabilities, from [Table 6.8](#)^[269], needed by the naïve Bayes prediction model to make a prediction for the query with CH = *paid*, GC = *guarantor*, and ACC = *free*, and the calculation of the scores for each target levels.
- 6.10** Definitions of some standard probability distributions.
- 6.11** The dataset from the loan application fraud detection domain (from [Table 6.2](#)^[263]) with two continuous descriptive features added:

ACCOUNT BALANCE and LOAN AMOUNT.

- 6.12** Partitioning the dataset based on the value of the target feature and fitting the parameters of a statistical distribution to model the ACCOUNT BALANCE feature in each partition.
 - 6.13** The Laplace smoothed (with $k = 3$) probabilities needed by a naive Bayes prediction model, calculated from the dataset in [Table 6.11](#)^[278], extended to include the conditional probabilities for the new ACCOUNT BALANCE feature, which are defined in terms of PDFs.
 - 6.14** The probabilities, from [Table 6.13](#)^[281], needed by the naive Bayes prediction model to make a prediction for the query with CH = *paid*, GC = *guarantor*, ACC = *free*, and AB = 759.07, and the calculation of the scores for each candidate prediction.
 - 6.15** The LOAN AMOUNT continuous feature discretized into four equal-frequency bins.
 - 6.16** The Laplace smoothed (with $k = 3$) probabilities needed by a naive Bayes prediction model, calculated from the data in [Tables 6.11](#)^[278] and [6.15](#)^[283].
 - 6.17** The relevant smoothed probabilities, from [Table 6.16](#)^[284], needed by the naive Bayes model to make a prediction for the query with CH = *paid*, GC = *guarantor*, ACC = *free*, AB = 759.07, and LA = 8,000, and the calculation of the scores for each candidate prediction.
 - 6.18** Some socioeconomic data for a set of countries, and a version of the data after equal-frequency binning has been applied.
 - 6.19** Examples of the samples generated using Gibbs sampling.
- 7.1** A dataset that includes office rental prices and a number of descriptive features for 10 Dublin city-center offices.
 - 7.2** Calculating the sum of squared errors for the candidate model (with $w[0] = 6.47$ and $w[1] = 0.62$) to make predictions for the office rentals dataset.

- 7.3** Details of the first two iterations when the gradient descent algorithm is used to train a multivariable linear regression model for the office rentals dataset (using only the continuous descriptive features).
- 7.4** Weights and standard errors for each feature in the office rentals model.
- 7.5** The office rentals dataset from [Table 7.1](#)^[313] adjusted to handle the categorical ENERGY RATING descriptive feature in linear regression models.
- 7.6** A dataset listing features for a number of generators.
- 7.7** An extended version of the generators dataset from [Table 7.6](#)^[339].
- 7.8** Details of the first two iterations when the gradient descent algorithm is used to train a logistic regression model for the extended generators dataset given in [Table 7.7](#)^[347].
- 7.9** A dataset describing grass growth on Irish farms in July 2012.
- 7.10** A dataset showing participants' responses to viewing *positive* and *negative* images measured on the EEG P20 and P45 potentials.
- 7.11** A dataset of customers of a large national retail chain.
- 8.1** Hourly samples of ambient factors and full load electrical power output of a combined cycle power plant.
- 8.2** The minimum and maximum values for the AMBIENT TEMPERATURE, RELATIVE HUMIDITY, and ELECTRICAL OUTPUT features in the power plant dataset.
- 8.3** The *range-normalized* hourly samples of ambient factors and full load electrical power output of a combined cycle power plant, rounded to two decimal places.
- 8.4** The per example error after the forward pass illustrated in [Figure 8.14](#)^[425], the per example $\partial\mathcal{E}/\partial a_8$, and the **sum of squared errors** for the model over the dataset of four examples.

- 8.5** The $\partial a / \partial z$ for each neuron for Example 2 rounded to four decimal places.
 - 8.6** The $\partial \mathcal{E} / \partial w_{i,k}$ calculations for \mathbf{d}_2 for every weight in the network. We use the neuron index 0 to denote the bias input for each neuron.
 - 8.7** The calculation of $\Delta w_{7,5}$ across our four examples.
 - 8.8** The per example error after each weight has been updated once, the per example $\partial \mathcal{E} / \partial a_8$, and the **sum of squared errors** for the model.
 - 8.9** The per example prediction, error, and the sum of squared errors after training has converged to an $SSE < 0.0001$.
 - 8.10** The per example error of the ReLU network after the forward pass illustrated in [Figure 8.18](#)^[440], the per example $\partial \mathcal{E} / \partial a_8$, and the **sum of squared errors** for the ReLU model.
 - 8.11** The $\partial a / \partial z$ for each neuron for \mathbf{d}_2 rounded to four decimal places.
 - 8.12** The ReLU network's per example prediction, error, and the sum of squared errors after training has converged to an $SSE < 0.0001$.
 - 8.13** The *range-normalized* hourly samples of ambient factors and full load electrical power output of a combined cycle power plant, rounded to two decimal places, and with the (binned) target feature represented using one-hot encoding.
 - 8.14** The calculation of the softmax activation function ϕ_{sm} over a vector of three logits \mathbf{l} .
 - 8.15** The calculation of the softmax activations for each of the neurons in the output layer for each example in the mini-batch, and the calculation of the δ for each neuron in the output layer for each example in the mini-batch.
- 9.1** A sample test set with model predictions.
 - 9.2** The structure of a confusion matrix.
 - 9.3** A confusion matrix for the set of predictions shown in [Table 9.1](#)^[537].

- 9.4** The performance measures from the five individual evaluation experiments and an overall aggregate from the 5-fold cross validation performed on the chest X-ray classification dataset.
- 9.5** A confusion matrix for a k -NN model trained on a churn prediction problem.
- 9.6** A confusion matrix for a naive Bayes model trained on a churn prediction problem.
- 9.7** The structure of a profit matrix.
- 9.8** The profit matrix for the payday loan credit scoring problem.
- 9.9** (a) The confusion matrix for a k -NN model trained on the payday loan credit scoring problem (*average class accuracy_{HM}* = 83.824%); and (b) the confusion matrix for a decision tree model trained on the payday loan credit scoring problem (*average class accuracy_{HM}* = 80.761%).
- 9.10** (a) Overall profit for the k -NN model using the profit matrix in [Table 9.8](#)^[554] and the confusion matrix in [Table 9.9\(a\)](#)^[555]; and (b) overall profit for the decision tree model using the profit matrix in [Table 9.8](#)^[554] and the confusion matrix in [Table 9.9\(b\)](#)^[555].
- 9.11** A sample test set with model predictions and scores.
- 9.12** Confusion matrices for the set of predictions shown in [Table 9.11](#)^[557] using (a) a prediction score threshold of 0.75 and (b) a prediction score threshold of 0.25.
- 9.13** A sample test set with prediction scores and resulting predictions based on different threshold values.
- 9.14** Tabulating the workings required to generate a K-S statistic.
- 9.15** The test set with model predictions and scores from [Table 9.11](#)^[557] extended to include deciles.
- 9.16** Tabulating the workings required to calculate gain, cumulative gain, lift, and cumulative lift for the data given in [Table 9.11](#)^[557].

- 9.17** The structure of a confusion matrix for a multinomial prediction problem with l target levels.
- 9.18** A sample test set with model predictions for a bacterial species identification problem.
- 9.19** A confusion matrix for a model trained on the bacterial species identification problem.
- 9.20** The expected target values for a test set, the predictions made by a model, and the resulting errors based on these predictions for a blood-thinning drug dosage prediction problem.
- 9.21** Calculating the stability index for the bacterial species identification problem given new test data for two periods after model deployment.
- 9.22** The number of customers who left the mobile phone network operator each week during the comparative experiment from both the control group (random selection) and the treatment group (model selection).
- 10.1** A dataset of mobile phone customers described by their average monthly data (DATA USAGE) and call (CALL VOLUME) usage. Details of the first two iterations of the k -means clustering algorithm are also shown. The clustering in the second iteration is actually the final clustering in this simple example.
- 10.2** Calculating the silhouette for the final clustering of the mobile phone customer dataset ([Table 10.1^{\[604\]}](#)) found using the k -means algorithm (with $k = 3$). The overall silhouette index value is 0.66.
- 10.3** Summary statistics for the three clusters found in the mobile phone customer dataset in [Table 10.1^{\[604\]}](#) using k -means clustering ($k = 3$). Note, that the % missing and cardinality columns usually used are omitted here for legibility as these data quality issues will not arise in this simple example. They could be included when this approach is used on *real* datasets.
- 10.4** Information gain for each descriptive feature as a predictor of membership of each cluster based on the clustering of the mobile

phone customer dataset in [Table 10.1](#)^[604] found using k-means clustering ($k = 3$).

- 10.5** **Distance matrices** that detail the first three iterations of the AHC algorithm applied to the reduced version of the mobile phone customer dataset in [Table 10.1](#)^[604].
- 11.1** Some episodes of games played by the TwentyTwos agent showing the cards dealt, as well as the states, actions, and rewards. Note that rewards are shown on the row indicating the action that led to them, not the state that followed that action.
- 11.2** An action-value table for an agent trained to play the card game TwentyTwos (the simplified version of Blackjack described in [Section 11.2.3](#)^[643]).
- 11.3** A portion of the action-value table for the grid world example at its first initialization.
- 11.4** A portion of the action-value table for the grid world example after 350 episodes of Q-learning have elapsed.
- 12.1** The descriptive features in the ABT developed for the Acme Telephonica churn prediction task.
- 12.2** A data quality report for the Acme Telephonica ABT.
- 12.3** The confusion matrix from the test of the AT churn prediction stratified hold-out test set using the pruned decision tree in [Figure 12.5](#)^[699].
- 12.4** The confusion matrix from the test of the AT churn prediction non-stratified hold-out test set.
- 13.1** The structure of the SDSS and Galaxy Zoo combined dataset.
- 13.2** Analysis of a subset of the features in the SDSS dataset.
- 13.3** Features from the ABT for the SDSS galaxy classification problem.
- 13.4** A data quality report for a subset of the features in the SDSS ABT.
- 13.5** The confusion matrices for the baseline models.

- 13.6** The confusion matrices showing the performance of models on the under-sampled training set.
 - 13.7** The confusion matrices for the models after feature selection.
 - 13.8** The confusion matrix for the 5-level logistic regression model (classification accuracy: 77.528%, average class accuracy: 43.018%).
 - 13.9** The confusion matrix for the logistic regression model that distinguished between only the spiral galaxy types (classification accuracy: 68.225%, average class accuracy: 56.621%).
 - 13.10** The confusion matrix for the 5-level two-stage model (classification accuracy: 79.410%, average class accuracy: 53.118%).
 - 13.11** The confusion matrix for the final logistic regression model on the large hold-out test set (classification accuracy: 87.979%, average class accuracy: 67.305%).
- 14.1** The alignment between the phases of CRISP-DM, key questions for analytics projects, and the chapters and sections of this book.
 - 14.2** A taxonomy of models based on the parametric versus non-parametric and generative versus discriminative distinctions.
- A.1** A dataset showing the positions and monthly training expenses of a school basketball team.
 - A.2** A frequency table for the POSITION feature from the school basketball team dataset in [Table A.1^{\[750\]}](#).
 - A.3** Poll results from the run-up to the 2012 U.S. presidential election.
 - A.4** The density calculation for the TRAINING EXPENSES feature from [Table A.1^{\[750\]}](#) using (a) ten 200-unit intervals and (b) four 500-unit intervals.
- B.1** A dataset of instances from the sample space in [Figure B.1^{\[757\]}](#).
 - B.2** A simple dataset for MENINGITIS with three common symptoms of the disease listed as descriptive features: HEADACHE, FEVER, and VOMITING.

I

INTRODUCTION TO MACHINE LEARNING AND DATA ANALYTICS

1

Machine Learning for Predictive Data Analytics

“Study the past if you would define the future.”

—Confucius

Modern organizations collect massive amounts of data. To be of value to an organization, this data must be analyzed to extract **insights** that can be used to make better decisions. The progression from **data** to **insights** to **decisions** is illustrated in [Figure 1.1^{\[4\]}](#). Extracting insights from data is the job of **data analytics**. This book focuses on **predictive data analytics**, which is an important subfield of data analytics.

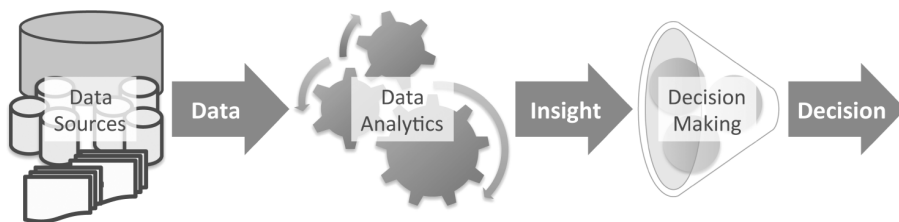


Figure 1.1

Predictive data analytics moving from **data** to **insight** to **decision**.

1.1 What Is Predictive Data Analytics?

Predictive data analytics is the art of building and using **models** that make predictions based on patterns extracted from historical data. Applications of predictive data analytics include

- **Price Prediction:** Businesses such as hotel chains, airlines, and online retailers need to constantly adjust their prices in order to maximize returns based on factors such as seasonal changes, shifting customer demand, and the occurrence of special events. Predictive analytics

models can be trained to predict optimal prices on the basis of historical sales records. Businesses can then use these predictions as an input into their pricing strategy decisions.

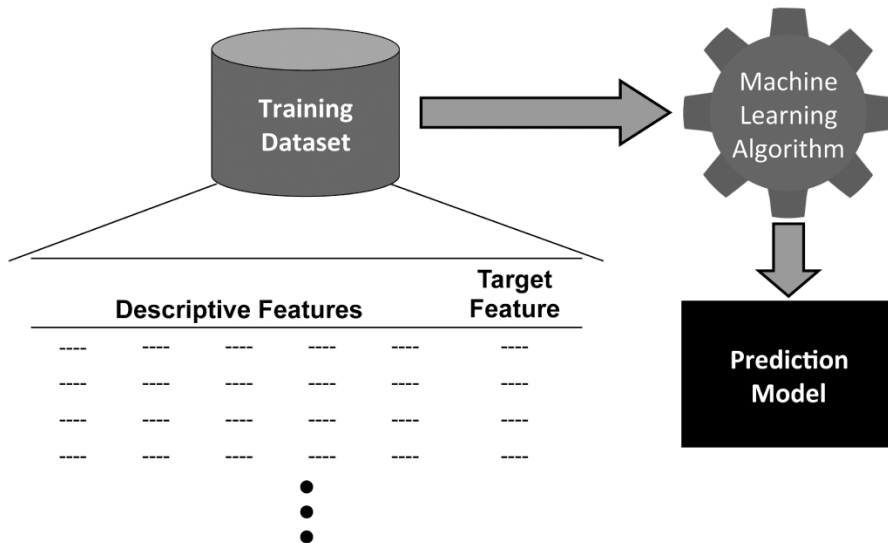
- **Dosage Prediction:** Doctors and scientists frequently decide how much of a medicine or other chemical to include in a treatment. Predictive analytics models can be used to assist this decision making by predicting optimal dosages based on data about past dosages and associated outcomes.
- **Risk Assessment:** Risk is one of the key influencers in almost every decision an organization makes. Predictive analytics models can be used to predict the risk associated with decisions such as issuing a loan or underwriting an insurance policy. These models are trained using historical data from which they extract the key indicators of risk. The output from risk prediction models can be used by organizations to make better risk judgments.
- **Propensity Modeling:** Most business decision making would be much easier if we could predict the likelihood, or **propensity**, of individual customers to take particular actions. Predictive data analytics can be used to build models that predict future customer actions on the basis of historical behavior. Successful applications of **propensity modeling** include predicting the likelihood of customers to leave one mobile phone operator for another, to respond to particular marketing efforts, or to buy different products.
- **Diagnosis:** Doctors, engineers, and scientists regularly make diagnoses as part of their work. Typically, these diagnoses are based on their extensive training, expertise, and experience. Predictive analytics models can help professionals make better diagnoses by leveraging large collections of historical examples at a scale beyond anything one individual would see over his or her career. The diagnoses made by predictive analytics models usually become an input into the professional's existing diagnosis process.
- **Document Classification:** Predictive data analytics can be used to automatically classify documents into different categories. Examples include email spam filtering, news sentiment analysis, customer complaint redirection, and medical decision making. In fact, the definition of a document can be expanded to include images, sounds, and

videos, all of which can be classified using predictive data analytics models.

All these examples have two things in common. First, in each case a model is used to make a prediction to help a person or organization make a decision. In predictive data analytics we use a broad definition of the word **prediction**. In everyday usage, the word prediction has a temporal aspect—we predict what will happen in the future. However, in data analytics a prediction is the assignment of a value to any unknown variable. This could be predicting the price that something will be sold for in the future; alternatively, it could mean predicting the type of document. So, in some cases prediction has a temporal aspect but not in all. The second thing that the examples listed have in common is that a model is trained to make predictions based on a set of historical examples. We use **machine learning** to train these models.

1.2 What Is Machine Learning?

Machine learning is defined as an automated process that extracts patterns from data. To build the models used in predictive data analytics applications, we use **supervised machine learning**. Supervised machine learning¹ techniques automatically learn a model of the relationship between a set of **descriptive features** and a **target feature** based on a set of historical examples, or **instances**. We can then use this model to make predictions for new instances. These two separate steps are shown in [Figure 1.2^{\[5\]}](#).



(a) Learning a model from a set of historical instances



(b) Using a model to make predictions

Figure 1.2

The two steps in supervised machine learning: (a) learning and (b) predicting.

Table 1.1^[6] lists a set of historical instances, or **dataset**, of mortgages that a bank has granted in the past.² This dataset includes descriptive features that describe the mortgage, and a target feature that indicates whether the mortgage applicant ultimately defaulted on the loan or paid it back in full. The descriptive features tell us three pieces of information about the mortgage: the *OCCUPATION* (which can be *professional* or *industrial*) and *AGE* of the applicant and the ratio between the applicant's salary and the amount borrowed (*LOAN-SALARY RATIO*). The target feature, *OUTCOME*, is set to either *default* or *repay*. In machine learning terms, each row in the dataset is referred to as a **training instance**, and the overall dataset is referred to as a **training dataset**.

Table 1.1

A credit scoring dataset.

ID	OCCUPATION	AGE	LOAN-SALARY	OUTCOME
			RATIO	
1	industrial	34	2.96	repay
2	professional	41	4.64	default
3	professional	36	3.22	default
4	professional	41	3.11	default
5	industrial	48	3.80	default
6	industrial	61	2.52	repay
7	professional	37	1.50	repay
8	professional	40	1.93	repay
9	industrial	33	5.25	default
10	industrial	32	4.15	default

An example of a very simple prediction model for this domain is

```

if LOAN-SALARY RATIO > 3 then
    OUTCOME = default
else
    OUTCOME = repay
end if

```

We can say that this model is **consistent** with the dataset because there are no instances in the dataset for which the model does not make a correct prediction. When new mortgage applications are made, we can use this model to predict whether the applicant will repay the mortgage or default on it and make lending decisions on the basis of this prediction.

Machine learning algorithms automate the process of learning a model that captures the relationship between the descriptive features and the target feature in a dataset. For simple datasets like the one presented in [Table 1.1](#)^[6], we may be able to manually create a prediction model; in an example of this scale, machine learning has little to offer us.

Consider, however, the dataset presented in [Table 1.2](#)^[8], which shows a more complete representation of the same problem. This dataset lists more instances, and there are extra descriptive features describing the AMOUNT that a mortgage holder borrows, the mortgage holder's SALARY, the type of

PROPERTY that the mortgage relates to (which can be *farm*, *house*, or *apartment*), and the TYPE of mortgage (which can be *ftb* for first-time buyers or *stb* for second-time buyers).

Table 1.2

A more complex credit scoring dataset.

ID	AMOUNT	SALARY	LOAN-SALARY		OCCUPATION	PROPERTY	TYPE	OUTCOME
			RATIO	AGE				
1	245,100	66,400	3.69	44	industrial	farm	stb	repay
2	90,600	75,300	1.20	41	industrial	farm	stb	repay
3	195,600	52,100	3.75	37	industrial	farm	ftb	default
4	157,800	67,600	2.33	44	industrial	apartment	ftb	repay
5	150,800	35,800	4.21	39	professional	apartment	stb	default
6	133,000	45,300	2.94	29	industrial	farm	ftb	default
7	193,100	73,200	2.64	38	professional	house	ftb	repay
8	215,000	77,600	2.77	17	professional	farm	ftb	repay
9	83,000	62,500	1.33	30	professional	house	ftb	repay
10	186,100	49,200	3.78	30	industrial	house	ftb	default
11	161,500	53,300	3.03	28	professional	apartment	stb	repay
12	157,400	63,900	2.46	30	professional	farm	stb	repay
13	210,000	54,200	3.87	43	professional	apartment	ftb	repay
14	209,700	53,000	3.96	39	industrial	farm	ftb	default
15	143,200	65,300	2.19	32	industrial	apartment	ftb	default
16	203,000	64,400	3.15	44	industrial	farm	ftb	repay
17	247,800	63,800	3.88	46	industrial	house	stb	repay
18	162,700	77,400	2.10	37	professional	house	ftb	repay
19	213,300	61,100	3.49	21	industrial	apartment	ftb	default
20	284,100	32,300	8.80	51	industrial	farm	ftb	default
21	154,000	48,900	3.15	49	professional	house	stb	repay
22	112,800	79,700	1.42	41	professional	house	ftb	repay
23	252,000	59,700	4.22	27	professional	house	stb	default
24	175,200	39,900	4.39	37	professional	apartment	stb	default
25	149,700	58,600	2.55	35	industrial	farm	stb	default

The simple prediction model using only the loan-salary ratio feature is no longer consistent with the dataset. It turns out, however, that there is at least one prediction model that is consistent with the dataset; it is just a little harder to find than the previous one:

```

if LOAN-SALARY RATIO < 1.5 then
    OUTCOME = repay
else if LOAN-SALARY RATIO > 4 then
    OUTCOME = default
else if AGE < 40 and OCCUPATION = industrial then
    OUTCOME = default
else
    OUTCOME = repay
end if

```

To manually learn this model by examining the data is almost impossible. For a machine learning algorithm, however, this is simple. When we want to build prediction models from large datasets with multiple features, machine learning is the solution.

1.3 How Does Machine Learning Work?

Machine learning algorithms work by searching through a set of possible prediction models for the model that best captures the relationship between the descriptive features and target feature in a dataset. An obvious criteria for driving this search is to look for models that are consistent with the data. There are, however, at least two reasons why simply searching for consistent models is not sufficient for learning useful prediction models. First, when we are dealing with large datasets, it is likely that there is **noise**³ in the data, and prediction models that are consistent with noisy data make incorrect predictions. Second, in the vast majority of machine learning projects, the training set represents only a small sample of the possible set of instances in the domain. As a result, machine learning is an **ill-posed problem**, that is, a problem for which a unique solution cannot be determined using only the information that is available.

We can illustrate how machine learning is an ill-posed problem using an example in which the analytics team at a supermarket chain wants to be able to classify customer households into the demographic groups *single*, *couple*, or *family*, solely on the basis of their shopping habits.⁴ The dataset given in [Table 1.3](#)^[9] contains descriptive features describing the shopping habits of five customers. The descriptive features measure whether a customer buys baby food, BBY; alcohol, ALC; or organic vegetable products, ORG. Each feature takes one of two values, *yes* or *no*. Alongside

these descriptive features is a target feature, GRP, that describes the demographic group for each customer (*single*, *couple*, or *family*). The dataset presented in [Table 1.3^{\[9\]}](#) is referred to as a **labeled dataset** because it includes values for the target feature.

Table 1.3

A simple retail dataset.

ID	B BY	ALC	ORG	GRP
1	no	no	no	couple
2	yes	no	yes	family
3	yes	yes	no	family
4	no	no	yes	couple
5	no	yes	yes	single

Imagine that we attempt to learn a prediction model for this retail scenario by searching for a model that is consistent with the dataset. The first thing we need to do is figure out how many different possible models actually exist for the scenario. This step defines the set of prediction models the machine learning algorithm will search. From the perspective of searching for a consistent model, the most important property of a prediction model is that it defines a mapping from every possible combination of descriptive feature values to a prediction for the target feature. For the retail scenario, there are only three binary descriptive features, so there are $2^3 = 8$ possible combinations of descriptive feature values. However, for each of these 8 possible combinations of descriptive feature values, there are 3 possible target feature values, so this means that there are $3^8 = 6,561$ possible prediction models that could be used. [Table 1.4^{\[10\]}](#) illustrates the relationship between combinations of descriptive feature values and prediction models for the retail scenario. The descriptive feature combinations are listed on the left-hand side of the table, and the set of potential models for this domain are shown as M_1 to $M_{6,561}$ on the right-hand side of the table. Using the training dataset from [Table 1.3^{\[9\]}](#), a machine learning algorithm will reduce the full set of 6,561 possible prediction models for this scenario to only those that are consistent with the training instances. [Table 1.4^{\[10\]}](#) illustrates this; the blanked-out columns in the table indicate the models that are not consistent with the training data.

Table 1.4

Potential prediction models (a) before and (b) after training data becomes available.

(a) Before training data becomes available.

(a) Before training data becomes available.

BBY	ALC	ORG	GRP	M ₁	M ₂	M ₃	M ₄	M ₅	...	M ₆₅₆₁
no	no	no	?	couple	couple	single	couple	couple	...	couple
no	no	yes	?	single	couple	single	couple	couple	...	single
no	yes	no	?	family	family	single	single	single	...	family
no	yes	yes	?	single	single	single	single	single	...	couple
yes	no	no	?	couple	couple	family	family	family	...	family
yes	no	yes	?	couple	family	family	family	family	...	couple
yes	yes	no	?	single	family	family	family	family	...	single
yes	yes	yes	?	single	single	family	family	couple	...	family

(b) After training data becomes available.

BBY	ALC	ORG	GRP	M ₂	M ₄	M ₅	...
no	no	no	couple	couple	couple	couple	...
no	no	yes	couple	couple	couple	couple	...
no	yes	no	?	family	single	single	...
no	yes	yes	single	single	single	single	...
yes	no	no	?	couple	family	family	...
yes	no	yes	family	family	family	family	...
yes	yes	no	family	family	family	family	...
yes	yes	yes	?	single	family	couple	...

Table 1.4^[10] also illustrates that the training dataset does not contain an instance for every possible combination of descriptive feature values and that there are still a large number of potential prediction models that remain consistent with the training dataset after the inconsistent models have been excluded.⁵ Specifically, there are three remaining descriptive feature value combinations for which the correct target feature value is not known, and therefore there are $3^3 = 27$ potential models that remain consistent with the training data. Three of these—M₂, M₄, and M₅—are shown in **Table 1.4^[10]**. Because a single consistent model cannot be found on the basis of the sample training dataset alone, we say that machine learning is fundamentally an **ill-posed problem**.

We might be tempted to think that having multiple models that are consistent with the data is a good thing. The problem is, however, that although these models agree on which predictions should be made for the

instances in the training dataset, they disagree with regard to which predictions should be returned for instances that are not in the training dataset. For example, if a new customer starts shopping at the supermarket and buys baby food, alcohol, and organic vegetables, our set of consistent models will contradict each other with respect to the prediction that should be returned for this customer; for example, M_2 will return $GRP = single$, M_4 will return $GRP = family$, and M_5 will return $GRP = couple$.

The criterion of consistency with the training data doesn't provide any guidance with regard to which of the consistent models to prefer in dealing with queries that are outside the training dataset. As a result, we cannot use the set of consistent models to make predictions for these queries. In fact, searching for predictive models that are consistent with the dataset is equivalent to just memorizing the dataset. As a result, no learning is taking place because the set of consistent models tells us nothing about the underlying relationship between the descriptive and target features beyond what a simple look-up of the training dataset would provide.

If a predictive model is to be useful, it must be able to make predictions for queries that are not present in the data. A prediction model that makes the correct predictions for these queries captures the underlying relationship between the descriptive and target features and is said to **generalize** well. Indeed, the goal of machine learning is to find the predictive model that generalizes best. In order to find this single best model, a machine learning algorithm must use some criteria for choosing among the candidate models it considers during its search.

Given that consistency with the dataset is not an adequate criterion to select the best prediction model, which criteria should we use? There are a lot of potential answers to this question, and that is why there are a lot of different machine learning algorithms. Each machine learning algorithm uses different model selection criteria to drive its search for the best predictive model. So, when we choose to use one machine learning algorithm instead of another, we are, in effect, choosing to use one model selection criterion instead of another.

All the different model selection criteria consist of a set of assumptions about the characteristics of the model that we would like the algorithm to induce. The set of assumptions that defines the model selection criteria of a

machine learning algorithm is known as the **inductive bias**⁶ of the machine learning algorithm. There are two types of inductive bias that a machine learning algorithm can use, a restriction bias and a preference bias. A **restriction bias** constrains the set of models that the algorithm will consider during the learning process. A **preference bias** guides the learning algorithm to prefer certain models over others. For example, in Chapter 7^[311] we introduce a machine learning algorithm called **multivariable linear regression with gradient descent**, which implements the restriction bias of considering only prediction models that produce predictions on the basis of a linear combination of the descriptive feature values and applies a preference bias over the order of the linear models it considers in terms of a gradient descent approach through a weight space. As a second example, in Chapter 4^[117] we introduce the **Iterative Dichotomizer 3 (ID3)** machine learning algorithm, which uses a restriction bias of considering only tree prediction models in which each branch encodes a sequence of checks on individual descriptive features but also uses a preference bias by considering shallower (less complex) trees over larger trees. It is important to recognize that using an inductive bias is a necessary prerequisite for learning to occur; without inductive bias, a machine learning algorithm cannot learn anything beyond what is in the data.

In summary, machine learning works by searching through a set of potential models to find the prediction model that best generalizes beyond the dataset. Machine learning algorithms use two sources of information to guide this search, the training dataset and the inductive bias assumed by the algorithm.

1.4 Inductive Bias Versus Sample Bias

Inductive bias is not the only type of bias that affects machine learning. An in-depth review of the range of biases that affect machine learning and the social harms that they can cause are beyond the scope of this book.⁷ However, we highlight **sampling bias**⁸ as a particular form of bias that a data analyst should be aware of and should proactively guard against in any data analytics project.

Sampling bias arises when the sample of data used within a data-driven process is collected in such a way that the sample is not representative of the population the sample is used to represent. One of the most famous

examples of sampling bias was in the 1936 U.S. presidential election, which pitted Franklin D. Roosevelt, the incumbent president, against Alfred Landon, the Republican governor of Kansas. At the time *Literary Digest* was a well-known magazine that had accurately predicted the outcomes of previous presidential elections. For the 1936 election *Literary Digest* ran one of the largest pre-election polls in the U.S. To run the poll *Literary Digest* created a list of 10 million names by integrating every telephone directory in the U.S., and a number of other sources, and then mailing everyone on the list a mock ballot and asking them to return the ballot to the magazine. Nearly 2.4 million people responded to the survey, and on the basis of this sample, *Literary Digest* very publicly and confidently predicted that Alfred Landon would win by a landslide. However, the actual result was a massive win for Roosevelt, with 62% of the votes. *Literary Digest* never recovered from the reputational damage this error in prediction caused and went out of business soon afterward.

There were two fundamental problems with how *Literary Digest* collected its sample, and the result of both was that the sample used for prediction (the survey responses) was not representative of the overall population. First, only about a quarter of the people who were surveyed responded to the survey (2.4 million out of 10 million). It is likely that people who respond to a survey are systematically different from people who don't, and so when the response rate within a population is very low, it is likely that the resulting sample underrepresents particular groups in the population. Second, the selection process used to generate the original list of 10 million people was based on telephone directories. At the time not every household in U.S. had telephones, and of those that did, a disproportionate number (relative to the total voting population of the U.S.) were Republican voters. Consequently, the sample of the population surveyed was skewed toward Republican voters, and so the predictions based on these surveys were also skewed. Importantly, the resulting data was skewed even though the surveys were large.

The key point to remember here is that if a sample of data is not representative of a population, then inferences based on that sample will not generalize to the larger population. This is true no matter how large the sample is. That said, sampling bias is a difficult problem to tackle. One challenge is that bias in a sample can arise in indirect and non-obvious

ways. For example, in 1936 it was not necessarily obvious that using telephone directories to create an initial list of names would skew the resulting sample toward a particular group in the population (in this instance, Republicans). Consequently, data analysts need to think about the sources of the data they are using and understand how the data was collected and whether the collection processes introduced a bias relative to the population. They also need to reflect on the processes they use to preprocess and manage the data, and whether any of these processes introduce bias into the sample.⁹ So, in summary, although inductive bias is necessary for machine learning, and in a sense, a key goal of a data analyst is to find the correct inductive bias, sample bias is something that a data analyst should proactively work hard to remove from the data used in any data analytics project.

1.5 What Can Go Wrong with Machine Learning?

Different machine learning algorithms encode different inductive biases. Because a machine learning algorithm encodes an inductive bias, it can induce models that generalize beyond the instances in a training dataset. An inappropriate inductive bias, however, can lead to mistakes. It has been shown that there is no particular inductive bias that on average is the best one to use.¹⁰ Also, in general, there is no way of knowing for a given predictive task which inductive bias will work best. Indeed, the ability to select the appropriate machine learning algorithm (and hence inductive bias) to use for a given predictive task is one of the core skills that a data analyst must develop.

There are two kinds of mistakes that an inappropriate inductive bias can lead to: **underfitting** and **overfitting**. Underfitting occurs when the prediction model selected by the algorithm is too simplistic to represent the underlying relationship in the dataset between the descriptive features and the target feature. Overfitting, by contrast, occurs when the prediction model selected by the algorithm is so complex that the model fits the dataset too closely and becomes sensitive to noise in the data.

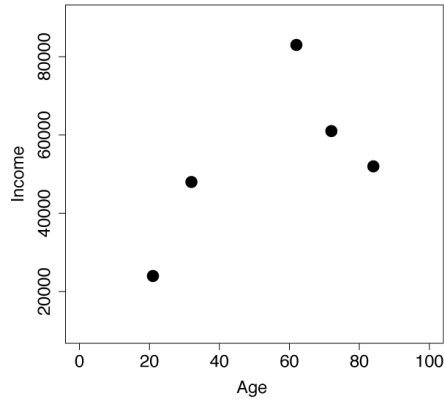
To understand underfitting and overfitting, consider the task of inducing a model to predict a person's INCOME (the target feature) based on AGE (a single descriptive feature). [Table 1.5^{\[14\]}](#) lists a simple dataset that gives ages

and salaries for five people. A visualization¹¹ of this dataset is shown in Figure 1.3(a)^[15].

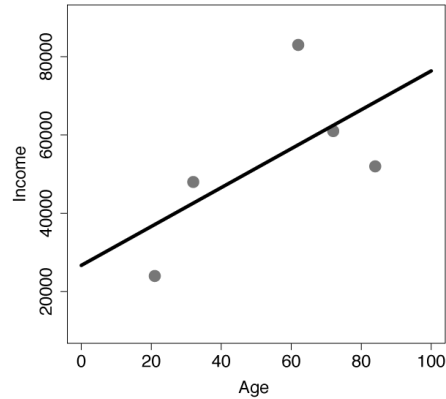
Table 1.5

The age-income dataset.

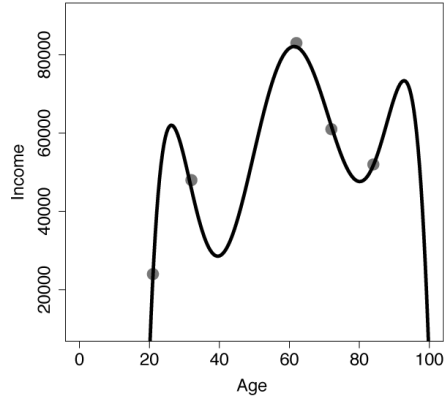
ID	AGE	INCOME
1	21	24,000
2	32	48,000
3	62	83,000
4	72	61,000
5	84	52,000



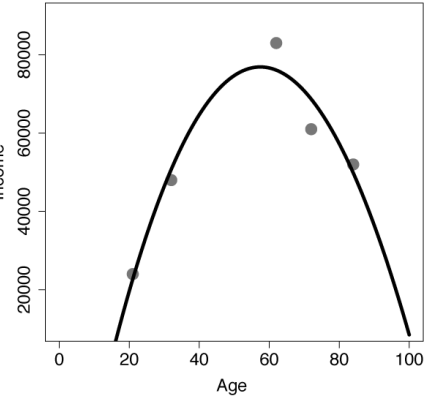
(a) Dataset



(b) Underfitting



(c) Overfitting



(d) Just right

Figure 1.3

(a)–(d) Striking a balance between overfitting and underfitting in trying to predict income from age.

The line in [Figure 1.3\(b\)](#)^[15] represents one model of the relationship between the AGE and INCOME features. This line illustrates a very simple linear function that maps AGE to INCOME. Although this simple model goes some way toward capturing the general trend of the relationship between AGE and INCOME, it does not manage to capture any of the subtlety of the relationship. This model is said to underfit the data as it is not complex enough to fully capture the relationship between the descriptive feature and the target feature. By contrast, the model shown in [Figure 1.3\(c\)](#)^[15], although consistent with the training instances, seems much more complicated than necessary. This model is said to overfit the training data.

Models that either underfit or overfit do not **generalize** well and so will not be able to make good predictions for query instances beyond the content of the training dataset. The prediction model shown in [Figure 1.3\(d\)](#)^[15], however, is a **Goldilocks model**: it is *just right*, striking a good balance between underfitting and overfitting. We find these Goldilocks models by using machine learning algorithms with appropriate inductive biases. This is one of the great arts of machine learning and something that we return to throughout this book.

1.6 The Predictive Data Analytics Project Lifecycle: CRISP-DM

Building predictive data analytics solutions for the kinds of applications described in Section 1.1[3] involves a lot more than just choosing the right machine learning algorithm. As with any other significant project, the chances of success for a predictive data analytics project are greatly increased if a standard process is used to manage the project through the project lifecycle. One of the most commonly used processes for predictive data analytics projects is the **Cross Industry Standard Process for Data Mining (CRISP-DM)**.¹² Key features of the CRISP-DM process that make it attractive to data analytics practitioners are that it is non-proprietary; it is application, industry, and tool neutral; and it explicitly views the data analytics process from both an application-focused and a technical perspective.

[Figure 1.4](#)^[16] shows six key phases of the predictive data analytics project lifecycle that are defined by the CRISP-DM:

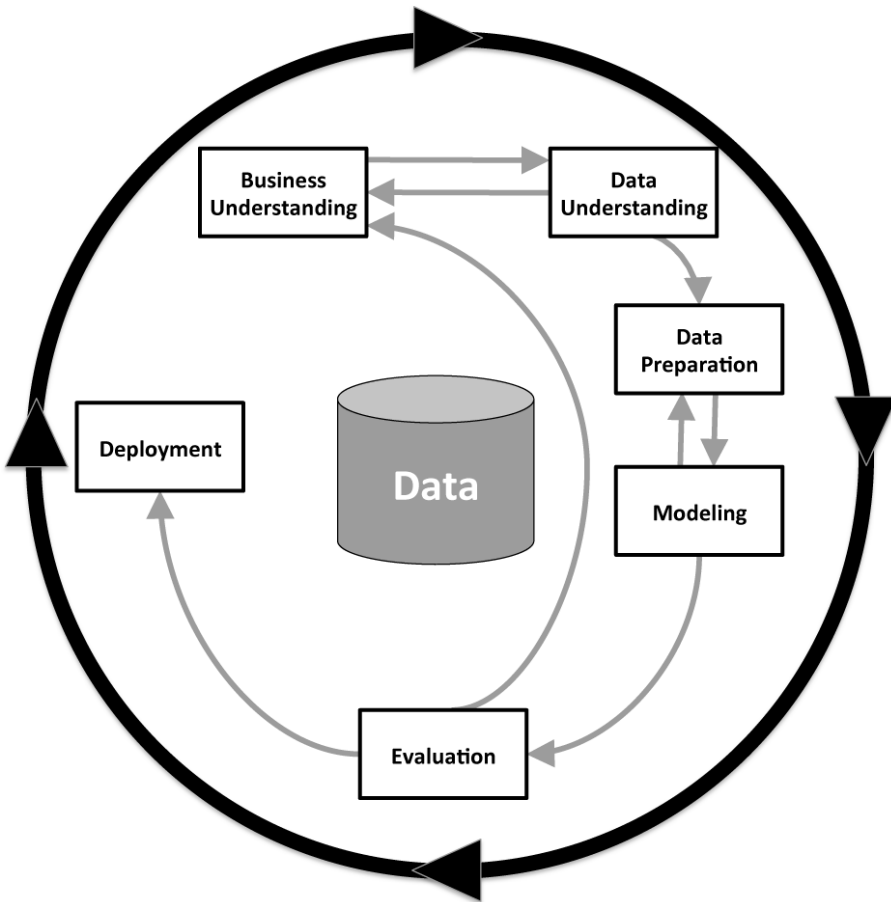


Figure 1.4

A diagram of the CRISP-DM process that shows the six key phases and indicates the important relationships between them. This figure is based on Figure 2 of Wirth and Hipp (2000).

- **Business Understanding:** Predictive data analytics projects never start out with the goal of building a prediction model. Instead, they focus on things like gaining new customers, selling more products, and adding efficiencies to a process. So, during the first phase in any analytics project, the primary goal of the data analyst is to fully understand the business (or organizational) problem that is being addressed and then to design a data analytics solution for it.
- **Data Understanding:** Once the manner in which predictive data analytics will be used to address a business problem has been decided, it is important that the data analyst fully understand the different data sources available within an organization and the different kinds of data that are contained in these sources.

- **Data Preparation:** Building predictive data analytics models requires specific kinds of data, organized in a specific kind of structure known as an **analytics base table (ABT)**.¹³ This phase of CRISP-DM includes all the activities required to convert the disparate data sources that are available in an organization to a well-formed ABT from which machine learning models can be induced.
- **Modeling:** In the Modeling phase of the CRISP-DM process, the machine learning work occurs. Different machine learning algorithms are used to build a range of prediction models from which the best model will be selected for deployment.
- **Evaluation:** Before models can be deployed for use within an organization, it is important that they are fully evaluated and proved to be fit for the purpose. This phase of CRISP-DM covers all the evaluation tasks required to show that a prediction model will be able to make accurate predictions after being deployed and that it does not suffer from overfitting or underfitting.
- **Deployment:** Machine learning models are built to serve a purpose within an organization, and the last phase of CRISP-DM covers all the work that must be done to successfully integrate a machine learning model into the processes within an organization.

[Figure 1.4^{\[16\]}](#) also illustrates the flow between each of these phases and emphasizes that data is at the heart of the process. Certain phases in CRISP-DM are more closely linked together than others. For example, Business Understanding and Data Understanding are tightly coupled, and projects typically spend some time moving back and forth between these phases. Similarly, the Data Preparation and Modeling phases are closely linked, and analytics projects often spend some time alternating between these two phases. Using the CRISP-DM process improves the likelihood that predictive data analytics projects will be successful, and we recommend its use.

1.7 Predictive Data Analytics Tools

Throughout this book we discuss the many different ways we can use machine learning techniques to build predictive data analytics models. In these discussions we do not refer to specific tools or implementations of

these techniques. There are, however, many different, easy-to-use options for implementing machine learning models that interested readers can use to follow along with the examples in this book.

The first decision that must be made in choosing a machine learning platform is whether to use an application-based solution or to use a programming language. We will look at application-based solutions first. Well-designed application-based, or *point-and-click*, tools make it very quick and easy to develop and evaluate models and to perform associated data manipulation tasks. Using one of these tools, it is possible to train, evaluate, and deploy a predictive data analytics model in less than an hour! Important application-based solutions for building predictive data analytics models include IBM SPSS, Knime Analytics Platform, RapidMiner Studio, SAS Enterprise Miner, and Weka.¹⁴ The tools by IBM and SAS are enterprise-wide solutions that integrate with the other offerings by these companies. Knime, RapidMiner, and Weka are interesting because they are all open-source, freely available solutions that readers can begin to use without any financial investment.

An interesting alternative to using an application-based solution for building predictive data analytics models is to use a programming language. Two of the most commonly used programming languages for predictive data analytics are R and Python.¹⁵ Building predictive data analytics models using a language like R or Python is not especially difficult. For example, the following simple lines of code use the R language to build a predictive model for a simple task:

```
creditscoring.train <- read.csv("creditScoringTrain.csv")
glm.mod <- glm(Outcome~Amount+Salary+Age+LoanSalaryRatio,
               family=binomial(link="logit"), data=creditscoring.train)
creditscoring.test <- read.csv("creditScoringTest.csv")
predicted.values <- predict(glm.mod, creditscoring.test)
```

The advantage of using a programming language for predictive data analytics projects is that it gives the data analyst huge flexibility. Anything that the analyst can imagine can be implemented. This is in contrast to application-based solutions, in which the analyst can really achieve only what the tool developers had in mind when they designed the tool. The other main advantage of using a programming language is that, in most cases, the newest advanced analytics techniques become available in

programming languages long before they are implemented in application-based solutions.

Obviously, however, using programming languages also has its disadvantages. The main disadvantage is that programming is a skill that takes time and effort to learn. Using a programming language for advanced analytics has a significantly steeper learning curve than using an application-based solution. The second disadvantage is that in using a programming language, we have very little of the infrastructural support, such as data management, offered with the application-based solutions available to us. This puts an extra burden on developers to implement these supports themselves.

1.8 The Road Ahead

Predictive data analytics projects use machine learning algorithms to induce prediction models from historical data. The insights that these prediction models produce are used to help organizations make data-driven decisions. Machine learning algorithms learn prediction models by inducing a generalized model of the relationship between a set of descriptive features and a target feature from a set of specific training instances. Machine learning, however, is made difficult because there is usually more than one model that is consistent with the training dataset—because of this, machine learning is often described as an ill-posed problem. Machine learning algorithms address this issue by encoding an inductive bias—or set of assumptions—that guide the algorithm to prefer certain models over others. We will see as we proceed through this book that the selection of a machine learning algorithm is not the only way that we can bias the predictive data analytics process. All the other choices that we make, such as the data to use, the descriptive features to use, and the way in which we deploy a model, bias the outcome of the overall process, and this is something that we need to be keenly aware of.

The purpose of this book is to give readers a solid grounding in the theoretical underpinnings of the most commonly used machine learning techniques and a clear view of the ways machine learning techniques are used in practice in predictive data analytics projects. With this in mind, readers can view the book as four parts that are mapped to the phases of the CRISP-DM process.

The first part—Chapters 2^[23] and 3^[53]—covers the Business Understanding, Data Understanding, and Data Preparation phases of the process. In this part we discuss how a business problem is converted into a data analytics solution, how data can be prepared for this task, and the data exploration tasks that should be performed during these phases.

The second part of the book covers the Modeling and Evaluation phase of CRISP-DM. We consider five main families of machine learning algorithm:

- Information-based learning (Chapter 4^[117])
- Similarity-based learning (Chapter 5^[181])
- Probability-based learning (Chapter 6^[243])
- Error-based learning (Chapter 7^[311])
- Deep learning (Chapter 8^[381])

By looking at these five key families, we cover the most commonly used approaches to inductive machine learning that can be used to build most predictive data analytics solutions. The second part of the book concludes with Chapter 9^[533], which describes a range of approaches to evaluating prediction models.

The third part of the book also deals with Modeling, but in this case it looks at modeling approaches beyond prediction. As described previously in this chapter, supervised machine learning is one of three main machine learning paradigms. The other two are **unsupervised learning** and **reinforcement learning**. Chapters 10^[597] and 11^[637] describe these two other approaches as a counterpoint to the descriptions of supervised learning in the rest of the book.

The fourth part of the book covers the Deployment phases of CRISP-DM. Chapters 12^[685] and 13^[703] present case studies describing specific predictive analytics projects from Business Understanding up to Deployment. These case studies demonstrate how everything described in the preceding chapters comes together in a successful predictive data analytics project.

Finally, Chapter 14^[729] provides some overarching perspectives on machine learning for predictive data analytics and summarizes some of the key differences between the different approaches covered in this book.

1.9 Exercises

1. What is **predictive data analytics**?
2. What is **supervised machine learning**?
3. Machine learning is often referred to as an **ill-posed problem**. What does this mean?
4. The following table lists a dataset from the credit scoring domain that we discussed in the chapter. Underneath the table we list two prediction models consistent with this dataset, **Model 1** and **Model 2**.

ID	OCCUPATION	AGE	LOAN-SALARY RATIO	OUTCOME
1	industrial	39	3.40	default
2	industrial	22	4.02	default
3	professional	30	2.70	repay
4	professional	27	3.32	default
5	professional	40	2.04	repay
6	professional	50	6.95	default
7	industrial	27	3.00	repay
8	industrial	33	2.60	repay
9	industrial	30	4.50	default
10	professional	45	2.78	repay

Model 1

```
if LOAN-SALARY RATIO > 3.00 then
    OUTCOME = default
else
    OUTCOME = repay
end if
```

Model 2

```
if AGE= 50 then
    OUTCOME = default
else if AGE= 39 then
    OUTCOME = default
else if AGE= 30 and OCCUPATION = industrial then
    OUTCOME = default
else if AGE= 27 and OCCUPATION = professional then
    OUTCOME = default
else
    OUTCOME = repay
end if
```

- (a) Which of these two models do you think will generalize better to instances not contained in the dataset?

(b) Propose an inductive bias that would enable a machine learning algorithm to make the same preference choice that you made in Part (a).

(c) Do you think that the model that you rejected in Part (a) of this question is overfitting or underfitting the data?

* 5. What is meant by the term **inductive bias**?

* 6. How do machine learning algorithms deal with the fact that machine learning is an **ill-posed problem**?

* 7. What can go wrong when an inappropriate **inductive bias** is used?

* 8. It is often said that 80% of the work done on predictive data analytics projects is done in the Business Understanding, Data Understanding, and Data Preparation phases of **CRISP-DM**, and just 20% is spent on the Modeling, Evaluation, and Deployment phases. Why do you think this would be the case?

* 9. The following table lists a dataset of five individuals described via a set of stroke risk factors and their probability of suffering a stroke in the next five years. This dataset has been prepared by an analytics team who are developing a model as a decision support tool for doctors.¹⁶ The goal of the model is to classify individuals into groups on the basis of their risk of suffering a stroke STROKE RISK. In this dataset there are three categories of risk: *low*, *medium*, and *high*. All the descriptive features are Boolean, taking two levels: *true* or *false*.

ID	HIGH BLOOD PRESSURE	SMOKER	DIABETES	HEART DISEASE	STROKE RISK
1	true	false	true	true	high
2	true	true	true	true	high
3	true	false	false	true	medium
4	false	false	false	false	low
5	true	true	true	false	high

(a) How many possible models exist for the scenario described by the features in this dataset?

(b) How many of these potential models would be consistent with this sample of data?

- * 10. You are using U.S. census data to build a prediction model. On inspecting the data you notice that the RACE feature has a higher proportion of the category *White* than you expected. Why do you think this might be?
- * 11. Why might a prediction model that has very high accuracy on a dataset not generalize well after it is deployed?

1. Other types of machine learning include **unsupervised learning**, **semi-supervised learning**, and **reinforcement learning**. In this book, however, we focus mainly on supervised machine learning and in most of the book use the terms supervised machine learning and machine learning interchangeably. Chapters 10^[597] and 11^[637] provide overviews of unsupervised learning and reinforcement learning, respectively.

2. This dataset has been artificially generated for this example. Siddiqi (2005) gives an excellent overview of building predictive data analytics models for financial credit scoring.

3. For example, some of the feature values will be mislabeled.

4. This kind of classification is not unusual because supermarket chains can collect huge amounts of data about customers' shopping habits through a loyalty card scheme but find it expensive and time consuming to collect more personal data, such as demographic classifications. Demographic classifications, however, are extremely useful to marketing departments in designing special offers and other customer incentives.

5. In this simple example it is easy to imagine collecting a training instance to match every possible combination of descriptive features; because there are only three binary descriptive features, there are only $2^3 = 8$ combinations. In more realistic scenarios, however, there are usually many more descriptive features, which means many more possible combinations. In the credit scoring dataset given in [Table 1.2](#)^[8], for example, a conservative estimate of the number of possible combinations of descriptive features is over 3.6 billion!

6. Learning a general rule from a finite set of examples is called **inductive learning**. This is why machine learning is sometimes described as inductive learning, and the set of assumptions used by the machine algorithm that biases it toward selecting a single model is called the **inductive bias** of the algorithm.

7. For an excellent overview of the different types of biases that affect machine learning and the potential harms these can cause, we recommend Kate Crawford's *The Trouble with Bias* keynote from the NeurIPS 2017 conference (Crawford, 2017). Videos of this talk are freely available online.

8. Sampling bias is closely related to the problem of **selection bias**, and the terms are often treated as synonyms. Sometimes, however, a distinction is made that sampling bias affects the ability of a trained model to generalize appropriately beyond the sample training data to the rest of a population, whereas selection bias is more focused on the validity of similarities and differences found within the sample. For this reason we use the term sampling bias here; however, for the purposes of this book, the distinction is not particularly important and in general we use the terms as synonyms.

9. In this section we have primarily considered the population we are sampling from to be a population of people, but sampling bias can also arise for any population of predictive subjects, be they insurance policies, holidays, cars, or anything else.

10. This is known as the **No Free Lunch Theorem** (Wolpert, 1996).

11. We discuss exactly this type of visualization, a scatter plot, in detail in Chapter 3^[53]. For this example it is sufficient to say that a point is shown for each person in the dataset, placed to represent the person's age (horizontally) and salary (vertically).
12. While the name CRISP-DM refers to **data mining** (a field that overlaps significantly with predictive data analytics), it is equally applicable to predictive analytics projects.
13. All datasets presented in this chapter have been structured as ABTs.
14. For further details, see www.ibm.com/software/ie/analytics/spss, www.knime.org, www.rapidminer.com, www.sas.com, and www.cs.waikato.ac.nz/ml/weka.
15. The website kdnuggets.com runs a regular poll on the most popular programming languages for predictive data analytics, which R and Python regularly top, www.kdnuggets.com/polls/2013/languages-analytics-data-mining-data-science.html. For further details about R and Python, see www.r-project.org and www.python.org.
16. Due to space limitations, this dataset covers only a sample of the risk factors for stroke. There are, for example, a number of non-modifiable risk factors such as age and gender. There is also an array of modifiable risk factors, including alcohol and drug use, unhealthy diet, stress and depression, and lack of physical exercise. Furthermore, this dataset is not based on precise measurements of stroke risk. For more information on stroke and risk factors related to stroke, please see the National Heart, Lung, and Blood Institute on Stroke: <https://www.nhlbi.nih.gov/health-topics/stroke>.

2

Data to Insights to Decisions

“We cannot solve our problems with the same thinking we used when we created them.”

—Albert Einstein

Predictive data analytics projects are not handed to data analytics practitioners fully formed. Rather, analytics projects are initiated in response to a business problem, and it is our job—as analytics practitioners—to decide how to address this business problem using analytics techniques. In the first part of this chapter we present an approach to developing **analytics solutions** that address specific **business problems**. This involves an analysis of the needs of the business, the data we have available for use, and the capacity of the business to use analytics. Taking these factors into account helps to ensure that we develop analytics solutions that are effective and fit for purpose. In the second part of this chapter we move our attention to the data structures that are required to build predictive analytics models, and in particular the **analytics base table (ABT)**. Designing ABTs that properly represent the characteristics of a **prediction subject** is a key skill for analytics practitioners. We present an approach in which we first develop a set of **domain concepts** that describe the prediction subject, and then expand these into concrete **descriptive features**. Throughout the chapter we return to a case study that demonstrates how these approaches are used in practice.

2.1 Converting Business Problems into Analytics Solutions

Organizations don’t exist to do predictive data analytics. Organizations exist to do things like make more money, gain new customers, sell more products, or reduce losses from fraud. Unfortunately, the predictive

analytics models that we can build do not do any of these things. The models that analytics practitioners build simply make predictions based on patterns extracted from historical datasets. These predictions do not solve business problems; rather, they provide insights that help the organization make better decisions to solve their business problems.

A key step, then, in any data analytics project is to understand the **business problem** that the organization wants to solve and, based on this, to determine the kind of insight that a predictive analytics model can provide to help the organization address this problem. This defines the **analytics solution** that the analytics practitioner will set out to build using machine learning. Defining the analytics solution is the most important task in the **Business Understanding** phase of the CRISP-DM process.

In general, converting a business problem into an analytics solution involves answering the following key questions:

1. **What is the business problem? What are the goals that the business wants to achieve?** These first two questions are not always easy to answer. In many cases organizations begin analytics projects because they have a clear issue that they want to address. Sometimes, however, organizations begin analytics projects simply because somebody in the organization feels that this is an important new technique that they should be using. Unless a project is focused on clearly stated goals, it is unlikely to be successful. The business problem and goals should always be expressed in business terms and not yet be concerned with the actual analytics work at this stage.
2. **How does the business currently work?** It is not feasible for an analytics practitioner to learn everything about the businesses with which they work as they will probably move quickly between different areas of an organization, or even different industries. Analytics practitioners must, however, possess what is referred to as **situational fluency**. This means that they understand enough about a business so that they can converse with partners in the business in a way that these business partners understand. For example, in the insurance industry, insurance policyholders are usually referred to as *members* rather than *customers*. Although from an analytics perspective, there is really little difference, using the correct

terminology makes it much easier for business partners to engage with the analytics project. Beyond knowing the correct terminology to use, an analytics practitioner who is situationally fluent will have sufficient knowledge of the quirks of a particular domain to be able to competently build analytics solutions for that domain.

3. **In what ways could a predictive analytics model help to address the business problem?** For any business problem, there are a number of different analytics solutions that we could build to address it. It is important to explore these possibilities and, in conjunction with the business, to agree on the most suitable solution for the business. For each proposed solution, the following points should be described: (1) the predictive model that will be built; (2) how the predictive model will be used by the business; and (3) how using the predictive model will help address the original business problem. The next section provides a case study of the process for converting a business problem into a set of candidate analytics solutions.

2.1.1 Case Study: Motor Insurance Fraud

Consider the following business problem: in spite of having a fraud investigation team that investigates up to 30% of all claims made, a motor insurance company is still losing too much money due to fraudulent claims. The following predictive analytics solutions could be proposed to help address this business problem:

- **[Claim prediction]** A model could be built to predict the likelihood that an insurance claim is fraudulent. This model could be used to assign every newly arising claim a fraud likelihood, and those that are most likely to be fraudulent could be flagged for investigation by the insurance company's claims investigators. In this way the limited claims investigation time could be targeted at the claims that are most likely to be fraudulent, thereby increasing the number of fraudulent claims detected and reducing the amount of money lost to fraud.
- **[Member prediction]** A model could be built to predict the propensity of a member¹ to commit fraud in the near future. This model could be run every quarter to identify those members most likely to commit fraud, and the insurance company could take a risk-mitigation action ranging from contacting the member with some kind of warning to canceling the

member's policies. By identifying members likely to make fraudulent claims before they make them, the company could save significant amounts of money.

- **[Application prediction]** A model could be built to predict, at the point of application, the likelihood that a policy someone has applied for will ultimately result in a fraudulent claim. The company could run this model every time a new application is made and reject those applications that are predicted likely to result in a fraudulent claim. The company would therefore reduce the number of fraudulent claims and reduce the amount of money they would lose to these claims.
- **[Payment prediction]** Many fraudulent insurance claims simply over-exaggerate the amount that should actually be paid out. In these cases the insurance company goes through an expensive investigation process but still must make a reduced payment in relation to a claim. A model could be built to predict the amount most likely to be paid out by an insurance company after having investigated a claim. This model could be run whenever new claims arise, and the policyholder could be offered the amount predicted by the model as settlement as an alternative to going through a claims investigation process. Using this model, the company could save on claims investigations and reduce the amount of money paid out on fraudulent claims.

2.2 Assessing Feasibility

Once a set of candidate analytics solutions that address a business problem have been defined, the next task is to evaluate the feasibility of each solution. This involves considering the following questions:

- Is the data required by the solution available, or could it be made available?
- What is the capacity of the business to utilize the insights that the analytics solution will provide?

The first question addresses data availability. Every analytics solution will have its own set of data requirements, and it is useful, as early as possible, to determine if the business has sufficient data available to meet these requirements. In some cases a lack of appropriate data will simply rule out proposed analytics solutions to a business problem. More likely, the

easy availability of data for some solutions might favor them over others. In general, evaluating the feasibility of an analytics solution in terms of its data requirements involves aligning the following issues with the requirements of the analytics solution:

- **The key objects in the company's data model and the data available regarding them.** For example, in a bricks-and-mortar retail scenario, the key objects are likely to be customers, products, sales, suppliers, stores, and staff. In an insurance scenario, the key objects are likely to be policyholders, policies, claims, policy applications, investigations, brokers, members, investigators, and payments.
- **The connections that exist between key objects in the data model.** For example, in a banking scenario is it possible to connect the multiple accounts that a single customer might own? Similarly, in an insurance scenario is it possible to connect the information from a policy application with the details (e.g., claims, payments, etc.) of the resulting policy itself?
- **The granularity of the data that the business has available.** In a bricks-and-mortar retail scenario, data on sales might only be stored as a total number of sales per product type per day, rather than as individual items sold to individual customers.
- **The volume of data involved.** The amount of data that is available to an analytics project is important because (a) some modern datasets are so large that they can stretch even state-of-the-art machine learning tools; and (b) conversely, very small datasets can limit our ability to evaluate the expected performance of a model after deployment.
- **The time horizon for which data is available.** It is important that the data available covers the period required for the analytics solution. For example, in an online gaming scenario, it might be possible to find out every customer's account balance today but utterly impossible to find out what their balance was last month, or even yesterday.

The second issue affecting the feasibility of an analytics solution is the ability of the business to utilize the insight that the solution provides. If a business is required to drastically revise all their processes to take advantage of the insights that can be garnered from a predictive model, the business may not be ready to do this no matter how good the model is. In

many cases the best predictive analytics solutions are those that fit easily into an existing business process.

Based on analysis of the associated data and capacity requirements, the analytics practitioner can assess the feasibility of each predictive analytics solution proposed to address a business problem. This analysis will eliminate some solutions altogether and for those solutions that appear feasible will generate a list of the data and capacity required for successful implementation. Those solutions that are deemed feasible should then be presented to the business, and one or more should be selected for implementation.

As part of the process of agreeing on the solution to pursue, the analytics practitioner must agree with the business, as far as possible, on the goals that will define a successful model implementation. These goals could be specified in terms of the required accuracy of the model and/or the impact of the model on the business.

2.2.1 Case Study: Motor Insurance Fraud

Returning to the motor insurance fraud detection case study, below we evaluate the feasibility of each proposed analytics solution in terms of data and business capacity requirements.

- **[Claim prediction]** *Data Requirements:* This solution would require that a large collection of historical claims marked as *fraudulent* and *non-fraudulent* exist. Similarly, the details of each claim, the related policy, and the related claimant would need to be available. *Capacity Requirements:* Given that the insurance company already has a claims investigation team, the main requirements would be that a mechanism could be put in place to inform claims investigators that some claims were prioritized above others. This would also require that information about claims become available in a suitably timely manner so that the claims investigation process would not be delayed by the model.
- **[Member prediction]** *Data Requirements:* This solution would not only require that a large collection of claims labeled as either *fraudulent* or *non-fraudulent* exist with all relevant details, but also that all claims and policies can be connected to an identifiable member. It would also require that any changes to a policy are recorded and available historically. *Capacity Requirements:* This solution first assumes that it is

possible to run a process every quarter that performs an analysis of the behavior of each customer. More challenging, there is the assumption that the company has the capacity to contact members based on this analysis and can design a way to discuss this issue with customers highlighted as likely to commit fraud without damaging the customer relationship so badly as to lose the customer. Finally, there are possibly legal restrictions associated with making this kind of contact.

- **[Application prediction]** *Data Requirements:* Again, a historical collection of claims marked as *fraudulent* or *non-fraudulent* along with all relevant details would be required. It would also be necessary to be able to connect these claims back to the policies to which they belong and to the application details provided when the member first applied. It is likely that the data required for this solution would stretch back over many years, as the time between making a policy application and making a claim could cover decades. *Capacity Requirements:* The challenge in this case would be to integrate the automated application assessment process into whatever application approval process currently exists within the company.
- **[Payment prediction]** *Data Requirements:* This solution would require the full details of policies and claims as well as data on the original amount specified in a claim and the amount ultimately paid out. *Capacity Requirements:* Again, this solution assumes that the company has the potential to run this model in a timely fashion whenever new claims rise and also has the capacity to make offers to claimants. This assumes the existence of a customer contact center or something similar.

For the purposes of the case study, we assume that after the feasibility review, it was decided to proceed with the **claim prediction** solution, in which a model will be built that can predict the likelihood that an insurance claim is fraudulent.

2.3 Designing the Analytics Base Table

Once we have decided which analytics solution we are going to develop in response to a business problem, we need to begin to design the data structures that will be used to build, evaluate, and ultimately deploy the model. This work sits primarily in the **Data Understanding** phase of the

CRISP-DM process (see [Figure 1.4^{\[16\]}](#)) but also overlaps with the **Business Understanding** and **Data Preparation** phases (remember that the CRISP-DM process is not strictly linear).

The basic data requirements for predictive models are surprisingly simple. To build a predictive model, we need a large dataset of historical examples of the scenario for which we will make predictions. Each of these historical examples must contain sufficient data to describe the scenario and the outcome that we are interested in predicting. So, for example, if we are trying to predict whether or not insurance claims are fraudulent, we require a large dataset of historical insurance claims, and for each one we must know whether or not that claim was found to be fraudulent.

The basic structure in which we capture these historical datasets is the **analytics base table (ABT)**, a schematic of which is shown in [Table 2.1^{\[29\]}](#). An analytics base table is a simple, flat, tabular data structure made up of rows and columns. The columns are divided into a set of **descriptive features** and a single **target feature**. Each row contains a value for each descriptive feature and the target feature and represents an **instance** about which a prediction can be made.

Table 2.1

The basic structure of an analytics base table—descriptive features and a target feature.

Descriptive Features	Target Feature
—	—
—	—
—	—
—	—

Although the ABT is the key structure that we use in developing machine learning models, data in organizations is rarely kept in neat tables ready to be used to build predictive models. Instead, we need to construct the ABT from the raw data sources that are available in an organization. These may be very diverse in nature. [Figure 2.1^{\[29\]}](#) illustrates some of the different data sources that are typically combined to create an ABT.

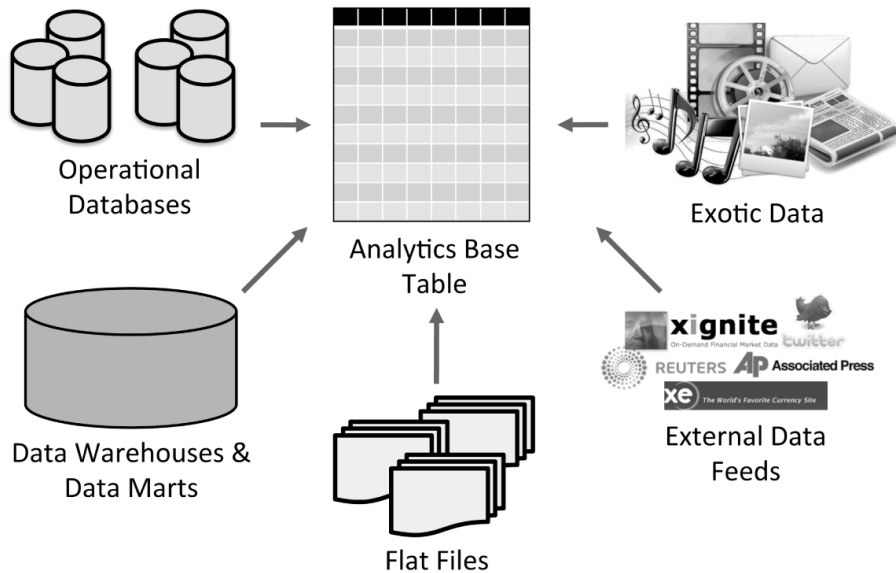


Figure 2.1

The different data sources typically combined to create an analytics base table.

Before we can start to aggregate the data from these different sources, however, a significant amount of work is required to determine the appropriate design for the ABT. In designing an ABT, the first decision an analytics practitioner needs to make is on the **prediction subject** for the model they are trying to build. The prediction subject defines the basic level at which predictions are made, and each row in the ABT will represent one instance of the prediction subject—the phrase **one-row-per-subject** is often used to describe this structure. For example, for the analytics solutions proposed for the motor insurance fraud scenario, the prediction subject of the claim prediction and payment prediction models would be an insurance claim; for the member prediction model, the prediction subject would be a member; and for the application prediction model, it would be an application.

Each row in an ABT is composed of a set of descriptive features and a target feature. The actual features themselves can be based on any of the data sources within an organization, and defining them can appear to be a mammoth task at first. This task can be made easier by making a hierarchical distinction between the actual features contained in an ABT and a set of **domain concepts** upon which features are based—see [Figure 2.2^{\[30\]}](#).

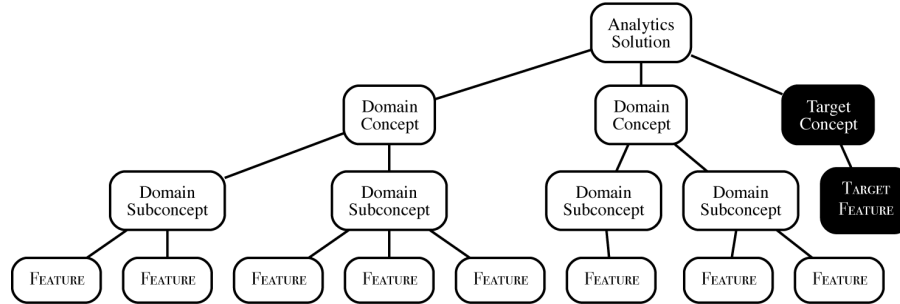


Figure 2.2

The hierarchical relationship between an analytics solution, domain concepts, and descriptive features.

A domain concept is a high-level abstraction that describes some characteristic of the prediction subject from which we derive a set of concrete features that will be included in an ABT. If we keep in mind that the ultimate goal of an analytics solution is to build a predictive model that predicts a target feature from a set of descriptive features, domain concepts are the characteristics of the prediction subject that domain experts and analytics experts believe are likely to be useful in making this prediction. Often, in a collaboration between analytics experts and domain experts, we develop a hierarchy of domain concepts that starts from the analytics solution, proceeds through a small number of levels of abstraction to result in concrete descriptive features. Examples of domain concepts include *customer value*, *behavioral change*, *product usage mix*, and *customer lifecycle stage*. These are abstract concepts that are understood to be likely important factors in making predictions. At this stage we do not worry too much about exactly how a domain concept will be converted into a concrete feature, but rather try to enumerate the different areas from which features will arise.

Obviously, the set of domain concepts that are important change from one analytics solution to another. However, there are a number of general domain concepts that are often useful:

- **Prediction Subject Details:** Descriptive details of any aspect of the prediction subject.
- **Demographics:** Demographic features of users or customers such as age, gender, occupation, and address.

- **Usage:** The *frequency* and *recency* with which customers or users have interacted with an organization. The *monetary value* of a customer's interactions with a service. The *mix* of products or services offered by the organization that a customer or user has used.
- **Changes in Usage:** Any changes in the frequency, recency, or monetary value of a customer's or user's interactions with an organization (for example, has a cable TV subscriber changed packages in recent months?).
- **Special Usage:** How often a user or customer used services that an organization considers special in some way in the recent past (for example, has a customer called a customer complaints department in the last month?).
- **Lifecycle Phase:** The position of a customer or user in their lifecycle (for example, is a customer a new customer, a loyal customer, or a lapsing customer?).
- **Network Links:** Links between an item and other related items (for example, links between different customers or different products, or social network links between customers).

The actual process for determining domain concepts is essentially one of **knowledge elicitation**—attempting to extract from domain experts the knowledge about the scenario we are trying to model. Often, this process will take place across multiple meetings, involving the analytics and domain experts, where the set of relevant domain concepts for the analytics solution are developed and refined.

2.3.1 Case Study: Motor Insurance Fraud

At this point in the motor insurance fraud detection project, we have decided to proceed with the proposed **claim prediction** solution, in which a model will be built that can predict the likelihood that an insurance claim is fraudulent. This system will examine new claims as they arise and flag for further investigation those that look like they might be fraud risks. In this instance the prediction subject is an insurance claim, and so the ABT for this problem will contain details of historical claims described by a set of descriptive features that capture likely indicators of fraud, and a target feature indicating whether a claim was ultimately considered fraudulent. The domain concepts in this instance will be concepts from within the

insurance domain that are likely to be important in determining whether a claim is fraudulent. [Figure 2.3](#)^[32] shows some domain concepts that are likely to be useful in this case. This set of domain concepts would have been determined through consultations between the analytics practitioner and domain experts within the business.

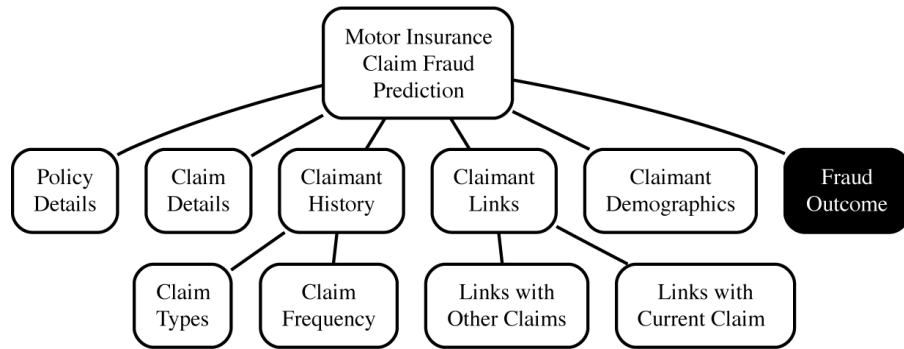


Figure 2.3

Example domain concepts for a motor insurance fraud prediction analytics solution.

The domain concepts shown here are *Policy Details*, which covers information relating to the policy held by the claimant (such as the age of the policy and the type of the policy); *Claim Details*, which covers the details of the claim itself (such as the incident type and claim amount); *Claimant History*, which includes information on previous claims made by the claimant (such as the different types of claims they have made in the past and the frequency of past claims); *Claimant Links*, which captures links between the claimant and any other people involved in the claim (for example, the same people being involved in multiple insurance claims together is often an indicator of fraud); and *Claimant Demographics*, which covers the demographic details of the claimant (such as age, gender, and occupation). Finally, a domain concept, *Fraud Outcome*, is included to cover the target feature. It is important that this is included at this stage because target features often need to be derived from multiple raw data sources, and the effort that will be involved in this should not be forgotten.

In [Figure 2.3](#)^[32] the domain concepts *Claimant History* and *Claimant Links* have both been broken down into a number of **domain subconcepts**. In the case of *Claimant History*, the domain subconcept of *Claim Types* explicitly recognizes the importance of designing descriptive features to capture the different types of claims the claimant has been involved in in

the past, and the *Claim Frequency* domain subconcept identifies the need to have descriptive features relating to the frequency with which the claimant has been involved in claims. Similarly, under *Claimant Links*, the *Links with Other Claims* and *Links with Current Claim* domain subconcepts highlight the fact that the links to or from this claimant can be broken down into links related to the current claim and links relating to other claims. The expectation is that each domain concept, or domain subconcept, will lead to one or more actual descriptive features derived directly from organizational data sources. Together these descriptive features will make up the ABT.

2.4 Designing and Implementing Features

Once domain concepts have been agreed on, the next task is to design and implement concrete features based on these concepts. A feature is any measure derived from a domain concept that can be directly included in an ABT for use by a machine learning algorithm. Implementing features is often a process of approximation through which we attempt to express as much of each domain concept as possible from the data sources that are available to us. Often it will take multiple features to express a domain concept. Also, we may have to use some **proxy features** to capture something that is closely related to a domain concept when direct measurement is not possible. In some extreme cases we may have to abandon a domain concept completely if the data required to express it isn't available. Consequently, understanding and exploring the data sources related to each domain concept that are available within an organization is a fundamental component of feature design. Although all the factors relating to data that were considered during the feasibility assessment of the analytics solution² are still relevant, three key data considerations are particularly important when we are designing features.

The first consideration is **data availability**, because we must have data available to implement any feature we would like to use. For example, in an online payments service scenario, we might define a feature that calculates the average of a customer's account balance over the past six months. Unless the company maintains a historical record of account balances covering the full six-month period, however, it will not be possible to implement this feature.

The second consideration is the **timing** with which data becomes available for inclusion in a feature. With the exception of the definition of the target feature, data that will be used to define a feature must be available before the event around which we are trying to make predictions occurs. For example, if we were building a model to predict the outcomes of soccer matches, we might consider including the attendance at the match as a descriptive feature. The final attendance at a match is not available until midway through the game, so if we were trying to make predictions before kickoff, this feature would not be feasible.

The third consideration is the **longevity** of any feature we design. There is the potential for features to go stale if something about the environment from which they are generated changes. For example, to make predictions on the outcome of loans granted by a bank, we might use the borrower's salary as a descriptive feature. Salaries, however, change all the time based on inflation and other socioeconomic factors. If we were to use a model that includes salary values over an extended period (for example, 10 years) the salary values used to initially train the model may have no relationship to the values that would be presented to the model later on. One way to extend the longevity of a feature is to use a derived ratio instead of a raw feature. For example, in the loan scenario a ratio between salary and requested loan amount might have a much longer useful life span than the salary and loan amount values alone. As a result of these considerations, feature design and implementation is an iterative process in which data exploration informs the design and implementation of features, which in turn inform further data exploration, and so on.

2.4.1 Different Types of Data

The data that the features in an ABT contain can be of a number of different types:

- **Numeric:** True numeric values that allow arithmetic operations (e.g., price, age)
- **Interval:** Values that allow ordering and subtraction, but do not allow other arithmetic operations (e.g., date, time)
- **Ordinal:** Values that allow ordering but do not permit arithmetic (e.g., size measured as small, medium, or large)

- **Categorical:** A finite set of values that cannot be ordered and allow no arithmetic (e.g., country, product type)
- **Binary:** A set of just two values (e.g., gender)
- **Textual:** Free-form, usually short, text data (e.g., name, address)

Figure 2.4^[35] shows examples of these different data types. We often reduce this categorization to just two data types: **continuous** (encompassing the numeric and interval types), and **categorical** (encompassing the categorical, ordinal, binary, and textual types). When we talk about categorical features, we refer to the set of possible values that a categorical feature can take as the **levels** of the feature or the **domain** of the feature. For example, in Figure 2.4^[35] the levels of the CREDIT RATING feature are $\{aa, a, b, c\}$ and the levels of the GENDER feature are $\{male, female\}$. As we will see when we look at the machine learning algorithms covered in Chapters 4^[117] to 7^[311], the presence of different types of descriptive and target features can have a big impact on how an algorithm works.

ID	NAME	DATE OF BIRTH	GENDER	CREDIT RATING	COUNTRY	SALARY
0034	Brian	22/05/78	male	aa	Ireland	67,000
0175	Mary	04/06/45	female	c	France	65,000
0456	Sinead	29/02/82	female	b	Ireland	112,000
0687	Paul	11/11/67	male	a	USA	34,000
0982	Donald	01/12/75	male	b	Australia	88,000
1103	Agnes	17/09/76	female	aa	Sweden	154,000

The diagram illustrates the data types for each column in the table. Arrows point from the column headers to their respective data types: ID and NAME are labeled 'Ordinal'; DATE OF BIRTH is labeled 'Interval'; GENDER and CREDIT RATING are labeled 'Binary'; COUNTRY is labeled 'Categorical'; and SALARY is labeled 'Numeric'.

Figure 2.4

Sample descriptive feature data illustrating numeric, binary, ordinal, interval, categorical, and textual types.

2.4.2 Different Types of Features

The features in an ABT can be of two types: **raw features** or **derived features**. Raw features are features that come directly from raw data

sources. For example, customer age, customer gender, loan amount, or insurance claim type are all descriptive features that we would most likely be able to transfer directly from a raw data source to an ABT.

Derived descriptive features do not exist in any raw data source, so they must be constructed from data in one or more raw data sources. For example, average customer purchases per month, loan-to-value ratios, or changes in usage frequencies for different periods are all descriptive features that could be useful in an ABT but that most likely need to be derived from multiple raw data sources. The variety of derived features that we might wish to use is limitless. For example, consider the number of features we can derive from the monthly payment a customer makes on an electricity bill. From this single raw data point, we can easily derive features that store the average payment over six months; the maximum payment over six months; the minimum payment over six months; the average payment over three months; the maximum payment over three months; the minimum payment over three months; a flag to indicate that a missed payment has occurred over the last six months; a mapping of the last payment made to a *low*, *medium*, or *high* level; the ratio between the current and previous bill payments, and many more.

Despite this limitless variety, however, there are a number of common derived feature types:

- **Aggregates:** These are aggregate measures defined over a group or period and are usually defined as the count, sum, average, minimum, or maximum of the values within a group. For example, the total number of insurance claims that a member of an insurance company has made over his or her lifetime might be a useful derived feature. Similarly, the average amount of money spent by a customer at an online retailer over periods of one, three, and six months might make an interesting set of derived features.
- **Flags:** Flags are binary features that indicate the presence or absence of some characteristic within a dataset. For example, a flag indicating whether or not a bank account has ever been overdrawn might be a useful descriptive feature.
- **Ratios:** Ratios are continuous features that capture the relationship between two or more raw data values. Including a ratio between two

values can often be much more powerful in a predictive model than including the two values themselves. For example, in a banking scenario, we might include a ratio between a loan applicant's salary and the amount for which they are requesting a loan rather than including these two values themselves. In a mobile phone scenario, we might include three ratio features to indicate the mix between voice, data, and SMS services that a customer uses.

- **Mappings:** Mappings are used to convert continuous features into categorical features and are often used to reduce the number of unique values that a model will have to deal with. For example, rather than using a continuous feature measuring salary, we might instead map the salary values to *low*, *medium*, and *high* levels to create a categorical feature.
- **Other:** There are no restrictions to the ways in which we can combine data to make derived features. One especially creative example of feature design was when a large retailer wanted to use the level of activity at a competitor's stores as a descriptive feature in one of their analytics solutions. Obviously, the competitor would not give the retailer this information, and so the analytics team at the retailer sought to find some proxy feature that would give them much the same information. Being a large retailer, they had considerable resources at their disposal, one of which was the ability to regularly take high-resolution satellite photos. Using satellite photos of their competitor's premises, the retailer was able to count the number of cars in the competitor's parking lots and use this as a proxy measure of activity within the competitor's stores!

Although in some applications the target feature is a raw value copied directly from an existing data source, in many others it must be derived. Implementing the target feature for an ABT can demand significant effort. For example, consider a problem in which we are trying to predict whether a customer will default on a loan obligation. Should we count one missed payment as a default or, to avoid predicting that good customers will default, should we consider a customer to have defaulted only after they miss three consecutive payments? Or three payments in a six-month period? Or two payments in a five-month period? Just like descriptive features, target features are based on a domain concept, and we must determine what

actual implementation is useful, feasible, and correct according to the specifics of the domain in question. In defining target features, it is especially important to seek input from domain experts.

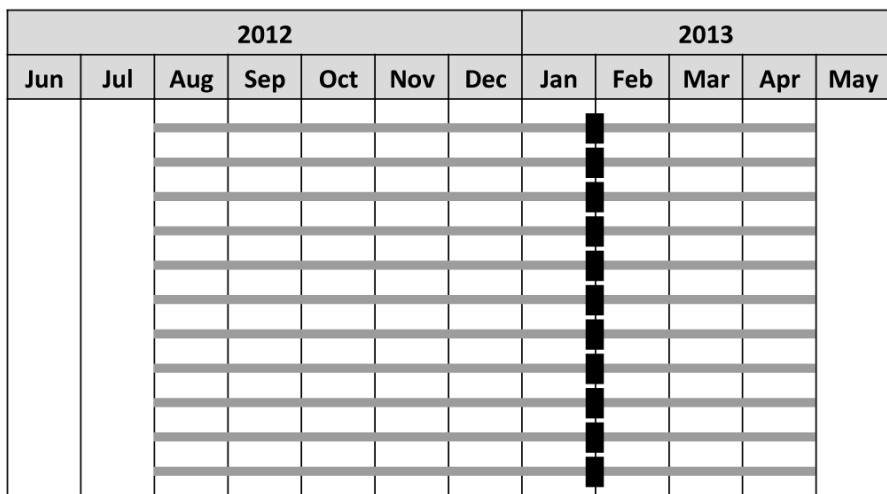
2.4.3 Handling Time

Many of the predictive models that we build are **propensity models**, which predict the likelihood (or propensity) of a future outcome based on a set of descriptive features describing the past. For example, the goal in the insurance claim fraud scenario we have been considering is to make predictions about whether an insurance claim will turn out to be fraudulent after investigation based on the details of the claim itself and the details of the claimant's behavior in *the time preceding the claim*. Propensity models inherently have a temporal element, and when this is the case, we must take time into account when designing the ABT. For **propensity modeling**, there are two key periods: the **observation period**, over which descriptive features are calculated, and the **outcome period**, over which the target feature is calculated.³

In some cases the observation period and outcome period are measured over the same time for all prediction subjects. Consider the task of predicting the likelihood that a customer will buy a new product based on past shopping behavior: features describing the *past shopping behavior* are calculated over the observation period, while the outcome period is the time during which we observe whether the customer bought the product. In this situation, the observation period for all the prediction subjects, in this case, customers, might be defined as the six months prior to the launch of the new product, and the outcome period might cover the three months after the launch. [Figure 2.5\(a\)](#)^[38] shows these two different periods, assuming that the customer's shopping behavior was measured from August 2012 through January 2013, and that whether they bought the product of interest was observed from February 2013 through April 2013. [Figure 2.5\(b\)](#)^[38] illustrates how the observation and outcome period for multiple customers are measured over the same period.

2012							2013				
Jun	Jul	Aug	Sep	Oct	Nov	Dec	Jan	Feb	Mar	Apr	May
Observation Period							Outcome Period				

(a) Observation period and outcome period



(b) Observation and outcome periods for multiple customers (each line represents a customer)

Figure 2.5

Modeling points in time using an observation period and an outcome period.

Often, however, the observation period and outcome period will be measured over different dates for each prediction subject. [Figure 2.6\(a\)](#)^[39] shows an example in which, rather than being defined by a fixed date, the observation period and outcome period are defined relative to an event that occurs at different dates for each prediction subject. The insurance claims fraud scenario we have been discussing throughout this section is a good example of this. In this example the observation period and outcome period are both defined relative to the date of the claim event, which will happen on different dates for different claims. The observation period is the time before the claim event, across which the descriptive features capturing the claimant's behavior are calculated, while the outcome period is the time immediately after the claim event, during which it will emerge whether the claim is fraudulent or genuine. [Figure 2.6\(a\)](#)^[39] shows an illustration of this

kind of data, while [Figure 2.6\(b\)](#)^[39] shows how this is aligned so that descriptive and target features can be extracted to build an ABT. Note that in [Figure 2.6\(b\)](#)^[39] the month names have been abstracted and are now defined relative to the transition between the observation and outcome periods.

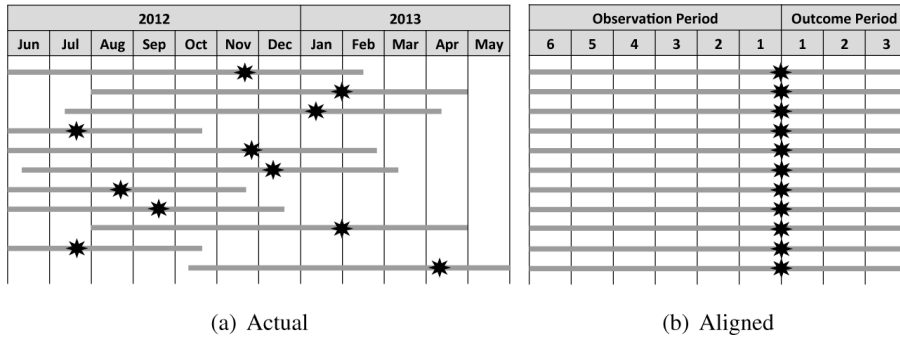


Figure 2.6

Observation and outcome periods defined by an event rather than by a fixed point in time (each line represents a prediction subject, and stars signify events). (a) shows the actual data, and (b) shows the event-aligned data.

When time is a factor in a scenario, the descriptive features and the target feature will not necessarily both be time dependent. In some cases only the descriptive features have a time component to them, and the target feature is time independent. Conversely, the target feature may have a time component and the descriptive features may not.

Next-best-offer models provide an example scenario where the descriptive features are time dependent but the target feature is not. A next-best-offer model is used to determine the least expensive incentive that needs to be offered to a customer who is considering canceling a service, for example, a mobile phone contract, in order to make them reconsider and stay. In this case the customer contacting the company to cancel their service is the key event in time. The observation period that the descriptive features will be based on is the customer's entire behavior up to the point at which they make this contact. There is no outcome period, as the target feature is determined by whether the company is able to entice the customer to reconsider and, if so, the incentive that was required to do this. [Figure 2.7](#)^[39] illustrates this scenario.

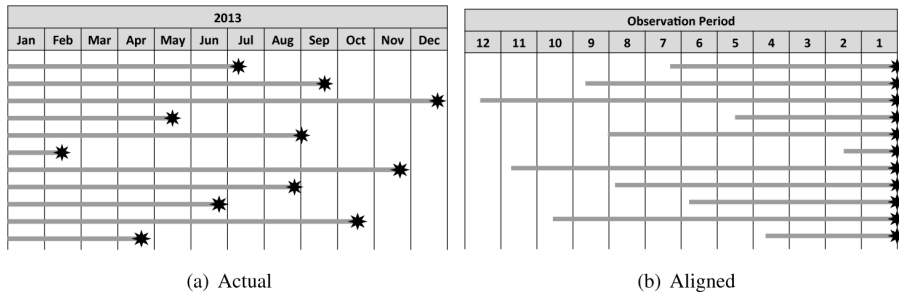


Figure 2.7

Modeling points in time for a scenario with no real outcome period (each line represents a customer, and stars signify events). (a) shows the actual data, and (b) shows the event-aligned data.

Loan default prediction is an example where the definition of the target feature has a time element but the descriptive features are time independent. In loan default prediction, the likelihood that an applicant will default on a loan is predicted based on the information the applicant provides on the application form. There really isn't an observation period in this case, as all descriptive features will be based on information provided by the applicant on the application form, rather than on observing the applicant's behavior over time.⁴ The outcome period in this case is considered the period of the lifetime of the loan during which the applicant will have either fully repaid or defaulted on the loan. In order to build an ABT for such a problem, a historical dataset of application details and subsequent repayment behavior is required (this might stretch back over multiple years depending on the terms of the loans in question). This scenario is illustrated in Figure 2.8^[40].

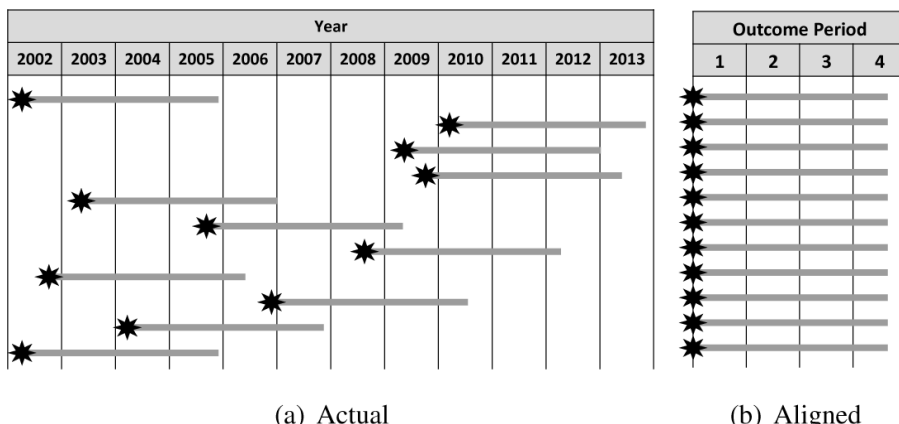


Figure 2.8

Modeling points in time for a scenario with no real observation period (each line represents a customer, and stars signify events). (a) shows the actual data, and (b) shows the event-aligned data.

2.4.4 Legal Issues

Data analytics practitioners can often be frustrated by legislation that stops them from including features that appear to be particularly well suited to an analytics solution in an ABT. Organizations must operate within the relevant legislation that is in place in the jurisdictions in which they operate, and it is important that models are not in breach of this. There are significant differences in legislation in different jurisdictions, but a couple of key relevant principles almost always apply.

The first is related to **anti-discrimination legislation**. Anti-discrimination legislation in most jurisdictions prohibits discrimination on the basis of some set of the following grounds: sex, age, race, ethnicity, nationality, sexual orientation, religion, disability, and political opinions. For example, the United States Civil Rights Act of 1964⁵ made it illegal to discriminate against a person on the basis of race, color, religion, national origin, or sex. Subsequent legislation has added to this list (for example, disability was later added as a further basis for non-discrimination). In the European Union the 1999 Treaty of Amsterdam⁶ prohibits discrimination on the basis of sex, racial or ethnic origin, religion or belief, disability, age, or sexual orientation. The exact implementation details of anti-discrimination law change, however, across the countries in the European Union.

The impact this has on designing features for inclusion in an ABT is that the use of some features in analytics solutions that leads to some people being given preferential treatment is in breach of anti-discrimination law. For example, credit scoring models such as the one discussed in Section 1.2^[5] cannot use race as a descriptive feature because this would discriminate against people on this basis.

The second important principle relates to **data protection legislation**, and in particular the rules surrounding the use of **personal data**. Personal data is defined as data that relates to an identified or identifiable individual, who is known as a **data subject**. Although, data protection legislation changes significantly across different jurisdictions, there are some common tenets on which there is broad agreement. The Organisation for Economic Co-operation and Development (OECD, 2013) defines a set of eight general principles of data protection legislation.⁷ For the design of analytics base tables, three are especially relevant: the **collection limitation principle**, the **purpose specification principle**, and the **use limitation principle**.

The collection limitation principle states that personal data should only be obtained by lawful means with the knowledge and consent of a data subject. This can limit the amount of data that an organization collects and, sometimes, restricts implementing features to capture certain domain concepts because consent has not been granted to collect the required data. For example, the developers of a smartphone app might decide that by turning on location tracking, they could gather data that would be extremely useful in predicting future usage of the app. Doing this without the permission of the users of the app, however, would be in breach of this principle.

The purpose specification principle states that data subjects should be informed of the purpose for which data will be used at the time of its collection. The use limitation principle adds that collected data should not subsequently be used for purposes other than those stated at the time of collection. Sometimes this means that data collected by an organization cannot be included in an ABT because this would be incompatible with the original use for which the data was collected. For example, an insurance company might collect data on customers' travel behaviors through their travel insurance policy and then use this data in a model that predicts personalized prices for life insurance. Unless, however, this second use was stated at the time of collection, this use would be in breach of this principle.

The legal considerations surrounding predictive analytics are of growing importance and need to be seriously considered during the design of any analytics project. Although larger organizations have legal departments to whom proposed features can be handed over for assessment, in smaller organizations analysts are often required to make these assessments themselves, and consequently they need to be aware of the legal implications relating to their decisions.

2.4.5 Implementing Features

Once the initial design for the features in an ABT has been completed, we can begin to implement the technical processes that are needed to extract, create, and aggregate the features into an ABT. It is at this point that the distinction between raw and derived features becomes apparent. Implementing a raw feature is simply a matter of copying the relevant raw

value into the ABT. Implementing a derived feature, however, requires data from multiple sources to be combined into a set of single feature values.

A few key **data manipulation** operations are frequently used to calculate derived feature values: joining data sources, filtering rows in a data source, filtering fields in a data source, deriving new features by combining or transforming existing features, and aggregating data sources. Data manipulation operations are implemented in and performed by **database management systems**, **data management tools**, or **data manipulation tools**, and are often referred to as an **extract-transform-load (ETL)** process.

2.4.6 Case Study: Motor Insurance Fraud

Let's return to the motor insurance fraud detection solution to consider the design and implementation of the features that will populate the ABT. As we noted in our discussion regarding handling time, the motor insurance claim prediction scenario is a good example of a situation in which the observation period and outcome period are measured over different dates for each insurance claim (the prediction subject for this case study). For each claim the observation and output periods are defined relative to the specific date of that claim. The observation period is the time prior to the claim event, over which the descriptive features capturing the claimant's behavior are calculated, and the outcome period is the time immediately after the claim event, during which it will emerge whether the claim is fraudulent or genuine.

The *Claimant History* domain concept that we developed for this scenario indicates the importance of information regarding the previous claims made by the claimant to the task of identifying fraudulent claims. This domain concept is inherently related to the notion of an observation period, and as we will see, the descriptive features derived from the domain subconcepts under *Claimant History* are time dependent. For example, the *Claim Frequency* domain subconcept under the *Claimant History* concept should capture the fact that the number of claims a claimant has made in the past has an impact on the likelihood of a new claim being fraudulent. This could be expressed in a single descriptive feature counting the number of claims that the claimant has made in the past. This single value, however, may not capture all the relevant information. Adding extra descriptive

features that give a more complete picture of a domain concept can lead to better predictive models. In this example we might also include the number of claims made by the claimant in the last three months, the average number of claims made by the claimant per year, and the ratio of the average number of claims made by the claimant per year to the claims made by the claimant in the last twelve months. [Figure 2.9](#)^[43] shows these descriptive features in a portion of the domain concept diagram.

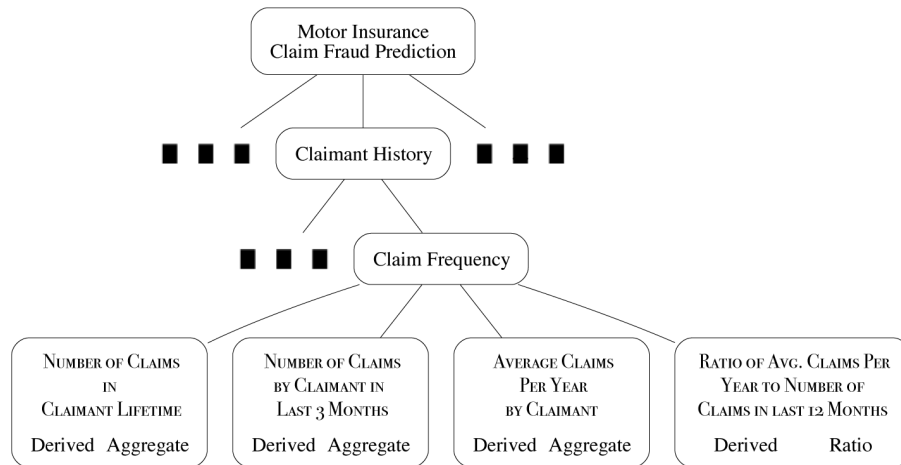


[Figure 2.9](#)

A subset of the domain concepts and related features for a motor insurance fraud prediction analytics solution.

The *Claim Types* subconcept of the *Claim History* is also time dependent. This domain subconcept captures the variety of claim types made by the claimant in the past, as these might provide evidence of possible fraud. The features included under this subconcept, all of which are derived features, are shown in [Figure 2.10](#)^[44]. The features place a particular emphasis on claims relating to soft tissue injuries (for example, whiplash) because it is understood within the insurance industry that these are frequently associated with fraudulent claims. The number of soft tissue injury claims the claimant has made in the past and the ratio between the number of soft tissue injury claims and other claims made by the claimant are both included as descriptive features in the ABT. A flag is also included to indicate that the claimant has had at least one claim refused in the past, because this might be indicative of a pattern of making speculative claims. Finally, a feature is included that expresses the variety of different claim

types made by the claimant in the past. This uses the **entropy** measure that is discussed in Section 4.2^[120] as it does a good job of capturing in a single number the variety in a set of objects.

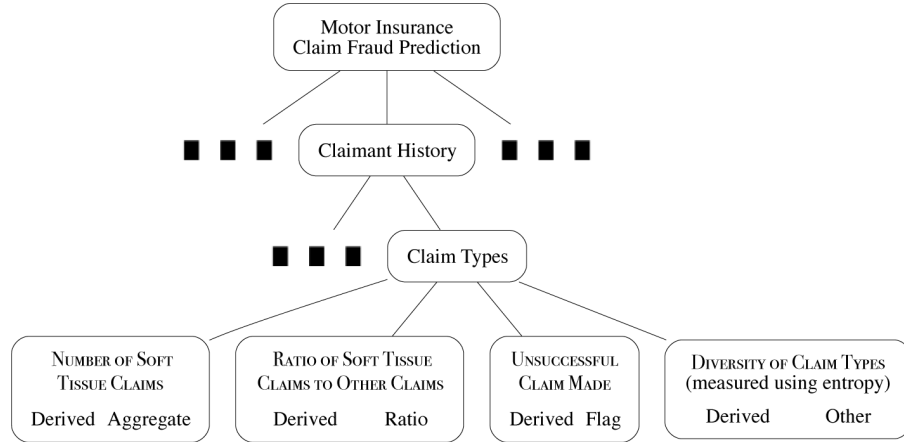


Figure 2.10

A subset of the domain concepts and related features for a motor insurance fraud prediction analytics solution.

However, not all the domain concepts in this scenario are time dependent. The *Claim Details* domain concept, for example, highlights the importance of the details of the claim itself in distinguishing between fraudulent and genuine claims. The type of the claim and amount of the claim are raw features calculated directly from a claims table contained in one of the insurance company's operational databases. A derived feature containing the ratio between the claim amount and the total value of the premiums paid to date on the policy is included. This is based on an expectation that fraudulent claims may be made early in the lifetime of a policy before too much has been spent on premiums. Finally, the insurance company divides their operations into a number of geographic areas defined internally based on the location of their branches, and a feature is included that maps raw address data to these regions.

Table 2.2^[46] illustrates the structure of the final ABT that was designed for the motor insurance claims fraud detection solution.⁸ The table contains more descriptive features than the ones we have discussed in this section.⁹ The table also shows the first four instances. If we examine the table closely, we see a number of strange values (for example, - 99,999) and a number of missing values. In the next chapter, we describe the process we

should follow to evaluate the quality of the data in the ABT and the actions we can take if the quality isn't good enough.

Table 2.2

The ABT for the motor insurance claims fraud detection solution.

ID	TYPE	INC.	MARITAL STATUS	NUM. CLMNTS.	INJURY TYPE	HOSPITAL STAY	CLAIM AMT.
1	ci	0		2	soft tissue	no	1,625
2	ci	0		2	back	yes	15,028
3	ci	54,613	married	1	broken limb	no	-99,999
4	ci	0		3	serious	yes	270,200
		⋮			⋮		

ID	TOTAL CLAIMED	NUM. CLAIMS	NUM. CLAIMS 3 MONTHS	Avg. CLAIMS PER YEAR	Avg. CLAIMS RATIO	NUM. SOFT TISSUE	% SOFT TISSUE
1	3,250	2	0	1	1	2	1
2	60,112	1	0	1	1	0	0
3	0	0	0	0	0	0	0
4	0	0	0	0	0	0	0
	⋮			⋮	⋮		

ID	UNSUCC. CLAIMS	CLAIM AMT. REC.	CLAIM DIV.	CLAIM TO PREM.	REGION	FRAUD FLAG
1	2	0	0	32.500	mn	1
2	0	15,028	0	57.140	dl	0
3	0	572	0	-89.270	wat	0
4	0	270,200	0	30.186	dl	0
	⋮			⋮	⋮	

2.5 Summary

It is important to remember that predictive data analytics models built using machine learning techniques are tools that we can use to help make better decisions within an organization and are not an end in themselves. It is paramount that, when tasked with creating a predictive model, we fully

understand the business problem that this model is being constructed to address and ensure that it does address it. This is the goal behind the process of *converting business problems into analytics solutions* as part of the Business Understanding phase of the CRISP-DM process. When undertaking this process, it is important to take into account the availability of data and the capacity of a business to take advantage of insights arising from analytics models, as otherwise it is possible to construct an apparently accurate prediction model that is in fact useless.

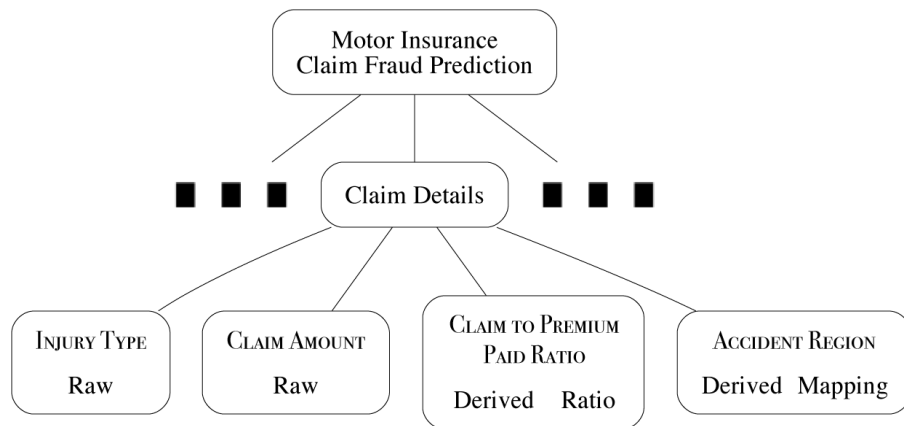


Figure 2.11

A subset of the domain concepts and related features for a motor insurance fraud prediction analytics solution.

Predictive data analytics models are reliant on the data that is used to build them—the **analytics base table (ABT)** is the key data resource in this regard. An ABT, however, rarely comes directly from a single source already existing within an organization. Instead, the ABT has to be created by combining a range of operational data sources together. The manner in which these data resources should be combined must be designed and implemented by the analytics practitioner in collaboration with domain experts. An effective way in which to do this is to start by defining a set of **domain concepts** in collaboration with the business, and then designing **features** that express these concepts in order to form the actual ABT. Domain concepts cover the different aspects of a scenario that are likely to be important in the modeling task at hand.

Features (both descriptive and target) are concrete numeric or symbolic representations of domain concepts. Features can be of many different

types, but it is useful to think of a distinction between **raw features** that come directly from existing data sources and **derived features** that are constructed by manipulating values from existing data sources. Common manipulations used in this process include aggregates, flags, ratios, and mappings, although any manipulation is valid. Often multiple features are required to fully express a single domain concept.

The techniques described in this chapter cover the **Business Understanding**, **Data Understanding**, and (partially) **Data Preparation** phases of the **CRISP-DM** process. Figure 2.12^[47] shows how the major tasks described in this chapter align with these phases. The next chapter will describe the data understanding and data preparation techniques mentioned briefly in this chapter in much more detail. It is important to remember that in reality, the **Business Understanding**, **Data Understanding**, and **Data Preparation** phases of the CRISP-DM process are performed iteratively rather than linearly. The curved arrows in Figure 2.12^[47] show the most common iterations in the process.

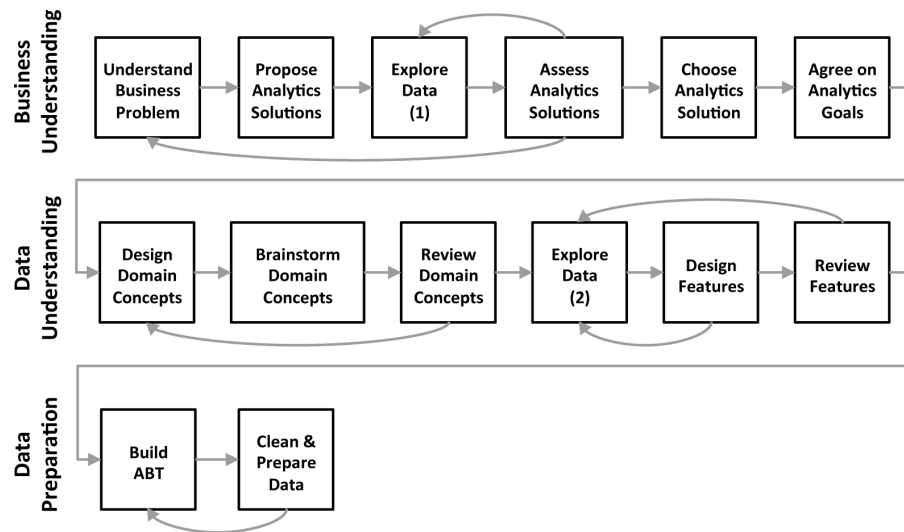


Figure 2.12

A summary of the tasks in the Business Understanding, Data Understanding, and Data Preparation phases of the CRISP-DM process.

2.6 Further Reading

On the topic of converting business problems into analytics solutions, Davenport (2006) and Davenport and Kim (2013) are good business-focused sources. Levitt and Dubner (2005), Ayres (2008), Silver (2012),

and Siegel (2013) all provide nice dicussions of different applications of predictive data analytics.

The CRISP-DM process documentation (Chapman et al., 2000) is surprisingly readable, and adds a lot of extra detail to the tasks described in this chapter. For details on developing business concepts and designing features, Svolba (2007) is excellent (the approaches described can be applied to any tool, not just SAS, which is the focus of Svolba's book).

For further discussion of the legal issues surrounding data analytics, Tene and Polonetsky (2013) and Schwartz (2010) are useful. Chapter 2 of Siegel (2013) discusses the ethical issues surrounding predictive analytics.

2.7 Exercises

1. An online movie streaming company has a business problem of growing **customer churn**—subscription customers canceling their subscriptions to join a competitor. Create a list of ways in which predictive data analytics could be used to help address this business problem. For each proposed approach, describe the predictive model that will be built, how the model will be used by the business, and how using the model will help address the original business problem.
2. A national revenue commission performs audits on public companies to find and fine tax defaulters. To perform an audit, a tax inspector visits a company and spends a number of days scrutinizing the company's accounts. Because it takes so long and relies on experienced, expert tax inspectors, performing an audit is an expensive exercise. The revenue commission currently selects companies for audit at random. When an audit reveals that a company is complying with all tax requirements, there is a sense that the time spent performing the audit was wasted, and more important, that another business who is not tax compliant has been spared an investigation. The revenue commissioner would like to solve this problem by targeting audits at companies who are likely to be in breach of tax regulations, rather than selecting companies for audit at random. In this way the revenue commission hopes to maximize the yield from the audits that it performs.

To help with **situational fluency** for this scenario, here is a brief outline of how companies interact with the revenue commission.

When a company is formed, it registers with the company registrations office. Information provided at registration includes the type of industry the company is involved in, details of the directors of the company, and where the company is located. Once a company has been registered, it must provide a tax return at the end of every financial year. This includes all financial details of the company's operations during the year and is the basis of calculating the tax liability of a company. Public companies also must file public documents every year that outline how they have been performing, details of any changes in directorship, and so on.

- (a) Propose two ways in which predictive data analytics could be used to help address this business problem.¹⁰ For each proposed approach, describe the predictive model that will be built, how the model will be used by the business, and how using the model will help address the original business problem.
 - (b) For each analytics solution you have proposed for the revenue commission, outline the type of data that would be required.
 - (c) For each analytics solution you have proposed, outline the capacity that the revenue commission would need in order to utilize the analytics-based insight that your solution would provide.
3. The table below shows a sample of a larger dataset containing details of policyholders at an insurance company. The descriptive features included in the table describe each policy holders' ID, occupation, gender, age, the value of their car, the type of insurance policy they hold, and their preferred contact channel.

ID	OCCUPATION	GENDER	AGE	MOTOR VALUE	POLICY TYPE	PREF CHANNEL
1	lab tech	female	43	42,632	planC	sms
2	farmhand	female	57	22,096	planA	phone
3	biophysicist	male	21	27,221	planA	phone
4	sheriff	female	47	21,460	planB	phone
5	painter	male	55	13,976	planC	phone
6	manager	male	19	4,866	planA	email
7	geologist	male	51	12,759	planC	phone
8	messenger	male	49	15,672	planB	phone
9	nurse	female	18	16,399	planC	sms
10	fire inspector	male	47	14,767	planC	email

- (a) State whether each descriptive feature contains numeric, interval, ordinal, categorical, binary, or textual data.
- (b) How many levels does each categorical, binary, or ordinal feature have?
4. Select one of the predictive analytics models that you proposed in your answer to Question 2 about the revenue commission for exploration of the design of its **analytics base table (ABT)**.
- (a) What is the prediction subject for the model that will be trained using this ABT?
- (b) Describe the domain concepts for this ABT.
- (c) Draw a domain concept diagram for the ABT.
- (d) Are there likely to be any legal issues associated with the domain concepts you have included?
- * 5. Although their sales are reasonable, an online fashion retailer is struggling to generate the volume of sales that they had originally hoped for when launching their site. List a number of ways in which predictive data analytics could be used to help address this business problem. For each proposed approach, describe the predictive model that will be built, how the model will be used by the business, and how using the model will help address the original business problem.
- * 6. An oil exploration company is struggling to cope with the number of exploratory sites that they need to drill in order to find locations for viable oil wells. There are many potential sites that geologists at the

company have identified, but undertaking exploratory drilling at these sites is very expensive. If the company could increase the percentage of sites at which they perform exploratory drilling that actually lead to finding locations for viable wells, they could save a huge amount of money.

Currently geologists at the company identify potential drilling sites by manually examining information from a variety of different sources. These include ordinance survey maps, aerial photographs, characteristics of rock and soil samples taken from potential sites, and measurements from sensitive gravitational and seismic instruments.

- (a) Propose two ways in which predictive data analytics could be used to help address the problem that the oil exploration company is facing. For each proposed approach, describe the predictive model that will be built, how the model will be used by the company, and how using the model will help address the original problem.
 - (b) For each analytics solution you have proposed, outline the type of data that would be required.
 - (c) For each analytics solution you have proposed, outline the capacity that would be needed in order to utilize the analytics-based insight that your solution would provide.
- * 7. Select one of the predictive analytics models that you proposed in your answer to the previous question about the oil exploration company for exploration of the design of its **analytics base table**.
- (a) What is the prediction subject for the model that will be trained using this ABT?
 - (b) Describe the domain concepts for this ABT.
 - (c) Draw a domain concept diagram for the ABT.
 - (d) Are there likely to be any legal issues associated with the domain concepts you have included?
- * 8. The following table shows a sample of a larger dataset that has been collected to build a model to predict whether newly released movies will be a hit or not.¹¹ The dataset contains details of movies that have already been released, including their title, running time, rating, genre, year of release, and whether or not the actor Kevin Costner had a

starring role. An indicator of whether they were a success—a *hit*—or not—a *miss*—based on box office returns compared to budget is also included.

ID	TITLE	LENGTH	RATING	GENRE	COSTNER	YEAR	HIT
1	Jaws	124	PG	action	false	1975	hit
2	Waterworld	135	PG-13	sci-fi	true	1995	miss
3	Hudson Hawk	100	R	adventure	false	1991	miss
4	Downfall	156	R	drama	false	2004	hit
5	The Postman	177	R	action	true	1997	miss
6	Toy Story	81	G	children's	false	1995	hit
7	Field of Dreams	107	G	drama	true	1989	hit
8	Amelie	122	R	comedy	false	2001	hit

- (a) State whether each descriptive feature contains numeric, interval, ordinal, categorical, binary, or textual data.
- (b) How many levels does each categorical, binary, or ordinal feature have?
- * 9. The management of a large hospital group are concerned about the readmission rate for patients who are hospitalized with problems relating to **diabetes**. An analysis of historical data suggests that the rate of readmission within 30 days of being discharged for patients who were hospitalized for complications relating to diabetes is approximately 20%, compared to an overall average for all patients of approximately 11%. Sometimes patients are readmitted for a recurrence of the same problem for which they were originally hospitalized, but at other times readmission is for different problems. Hospital management are concerned that the cause of the high readmittance rate for diabetes patients might be that they are discharged too early or that their care plans while in the hospital are not addressing all their needs.
Hospital management would like to explore the use of predictive analytics to address this issue.¹² They would like to reduce the readmittance rate of diabetes patients, while at the same time not keeping patients in the hospital longer than they need to be.
 - (a) Propose two ways in which predictive data analytics could be used to help address this problem for the hospital group. For each proposed approach, describe the predictive model that will be built,

how the model will be used by the business, and how using the model will help address the original problem.

- (b) For each analytics solution you have proposed for the hospital group, outline the type of data that would be required.
 - (c) For each analytics solution you have proposed, outline the capacity that the hospital would need in order to use the analytics-based insight that your solution would provide.
- * 10. Select one of the predictive analytics models that you proposed in your answer to the previous question about the readmission of diabetes patients for exploration of the design of its **analytics base table**.
- (a) What is the prediction subject for the model that will be trained using this ABT?
 - (b) Describe the domain concepts for this ABT.
 - (c) Draw a domain concept diagram for the ABT.
 - (d) Are there likely to be any legal issues associated with the domain concepts you have included?

1. Remember that in insurance we don't refer to customers!

2. See the discussion in Section 2.1^[23] relating to data availability, data connections, data granularity, data volume, and data time horizons.

3. It is important to remember for this discussion that all the data from which we construct an ABT for training and evaluating a model will be historical data.

4. Some might argue that the information on the application form summarizes an applicant's entire life, so this constitutes the observation period in this case!

5. The full text of the Civil Rights Act of 1964 is available at www.gpo.gov/fdsys/granule/STATUTE-78/STATUTE-78-Pg241/content-detail.html.

6. The full text of the EU Treaty of Amsterdam is available at www.europa.eu/eu-law/decision-making/pdf/treaty_of_amsterdam/treaty_of_amsterdam_en.pdf.

7. The full discussion of these principles is available at www.oecd.org/sti/ieconomy/privacy.htm.

8. The table is too wide to fit on a page, so it has been split into three sections.

9. The mapping between the features we have discussed here and the column names in [Table 2.2](#)^[46] is as follows: NUMBER OF CLAIMANTS: NUM. CLMNTS.; NUMBER OF CLAIMS IN CLAIMANT LIFETIME: NUM. CLAIMS; NUMBER OF CLAIMS BY CLAIMANT IN LAST 3 MONTHS: NUM. CLAIMS 3 MONTHS; AVERAGE CLAIMS PER YEAR BY CLAIMANT: AVG. CLAIMS PER YEAR; RATIO OF AVERAGE CLAIMS PER YEAR TO NUMBER OF CLAIMS IN LAST 12 MONTHS: AVG. CLAIMS RATIO; NUMBER OF SOFT TISSUE CLAIMS: NUM. SOFT TISSUE; RATIO OF SOFT TISSUE CLAIMS TO OTHER CLAIMS: % SOFT TISSUE; UNSUCCESSFUL CLAIM MADE: UNSUCC. CLAIMS; DIVERSITY OF CLAIM TYPES: CLAIM DIV.;

CLAIM AMOUNT: CLAIM AMT.; CLAIM TO PREMIUM PAID RATIO: CLAIM TO PREM.; ACCIDENT REGION: REGION.

10. Revenue commissioners around the world use predictive data analytics techniques to keep their processes as efficient as possible. Cleary and Tax (2011) is a good example.

11. This dataset has been artificially created for this book, but machine learning has been used for this task, for example, by Mishne and Glance (2006).

12. There are many applications of predictive analytics in healthcare, and predicting readmittance rates for diabetes patients, as well as patients suffering from other issues, is well studied, for example, by Rubin (2015) and Kansagara et al. (2011).

3

Data Exploration

“Fail to prepare, prepare to fail.”

—Roy Keane

In Chapter 2^[23] we described the process of moving from a business problem to an analytics solution and, from there, to the design and construction of an **analytics base table (ABT)**. An ABT for a predictive analytics solution contains a set of instances that are represented by a set of descriptive features and a target feature. Before attempting to build predictive models based on an ABT, it is important that we undertake some exploratory analysis, or **data exploration**, of the data contained in the ABT. **Data exploration** is a key part of both the **Data Understanding** and **Data Preparation** phases of CRISP-DM.

There are two goals in data exploration. The first goal is to fully understand the characteristics of the data in the ABT. It is important that for each feature in the ABT, we understand characteristics such as the types of values a feature can take, the ranges into which the values in a feature fall, and how the values in a dataset for a feature are distributed across the range that they can take. We refer to this as *getting to know* the data. The second goal of data exploration is to determine whether or not the data in an ABT suffer from any **data quality issues** that could adversely affect the models that we build. Examples of typical data quality issues include an instance that is missing values for one or more descriptive features, an instance that has an extremely high value for a feature, or an instance that has an inappropriate level for a feature. Some data quality issues arise due to invalid data and will be corrected as soon as we discover them. Others, however, arise because of perfectly valid data that may cause difficulty to

some machine learning techniques. We note these types of data quality issues during exploration for potential handling when we reach the Modeling phase of a project.

The most important tool used during data exploration is the **data quality report**. This chapter begins by describing the structure of a data quality report and explaining how it is used to *get to know* the data in an ABT and to identify data quality issues. We then describe a number of strategies for handling data quality issues and when it is appropriate to use them. Throughout the discussion of the data quality report and how we use it, we return to the motor insurance fraud case study from Chapter 2^[23]. Toward the end of the chapter, we introduce some more advanced data exploration techniques that, although not part of the standard data quality report, can be useful at this stage of an analytics project and present some data preparation techniques that can be applied to the data in an ABT prior to modeling.

3.1 The Data Quality Report

The **data quality report** is the most important tool of the data exploration process. A data quality report includes tabular reports (one for continuous features and one for categorical features) that describe the characteristics of each feature in an ABT using standard statistical measures of **central tendency** and **variation**. The tabular reports are accompanied by data visualizations that illustrate the distribution of the values in each feature in an ABT. Readers who are not already familiar with standard measures of central tendency (**mean**, **mode**, and **median**), standard measures of variation (**standard deviation** and **percentiles**), and standard data visualization plots (**bar plots**, **histograms**, and **box plots**) should read Appendix A^[745] for the necessary introduction.

The table in a data quality report that describes continuous features should include a row containing the minimum, 1st quartile, mean, median, 3rd quartile, maximum, and standard deviation statistics for that feature as well as the total number of instances in the ABT, the percentage of instances in the ABT that are missing a value for each feature and the **cardinality** of each feature, (cardinality measures the number of distinct values present in the ABT for a feature). [Table 3.1\(a\)](#)^[55] shows the structure of the table in a data quality report that describes continuous features.

Table 3.1

The structures of the tables included in a data quality report to describe (a) continuous features and (b) categorical features.

(a) Continuous Features

Feature	Count	% Miss. Card.			1 st Qrt. Mean			3 rd Qrt. Max.			Std. Dev.
		Min.	Qrt.	Median	Max.						
—	—	—	—	—	—	—	—	—	—	—	—
—	—	—	—	—	—	—	—	—	—	—	—
—	—	—	—	—	—	—	—	—	—	—	—

(b) Categorical Features

Feature	Count	% Miss. Card.			Mode Freq.		Mode %	2 nd Mode Freq.		2 nd Mode %
		Mode	Freq.	%	Mode	Freq.	%	Mode	Freq.	%
—	—	—	—	—	—	—	—	—	—	—
—	—	—	—	—	—	—	—	—	—	—
—	—	—	—	—	—	—	—	—	—	—

The table in the data quality report that describes categorical features should include a row for each feature in the ABT that contains the two most frequent levels for the feature (the mode and 2nd mode) and the frequency with which these appear (both as raw frequencies and as a proportion of the total number of instances in the dataset). Each row should also include the percentage of instances in the ABT that are missing a value for the feature and the cardinality of the feature. [Table 3.1\(b\)](#)^[55] shows the structure of the table in a data quality report that describes categorical features.

The data quality report should also include a histogram for each continuous feature in an ABT. For continuous features with cardinality less than 10, we use bar plots instead of histograms as this usually produces more informative data visualization. For each categorical feature in an ABT, a bar plot should be included in the data quality report.

3.1.1 Case Study: Motor Insurance Fraud

[Table 3.2](#)^[56] shows a portion of the ABT that has been developed for the motor insurance claims fraud detection solution based on the design described in Section 2.4.6^[42].¹ The data quality report for this ABT is shown across [Table 3.3](#)^[57] (tabular reports for continuous and categorical features) and [Figure 3.1](#)^[58] (data visualizations for each feature in the dataset).

Table 3.2

Portions of the ABT for the motor insurance claims fraud detection problem discussed in Section 2.4.6^[42].

ID	TYPE	INC.	MARITAL STATUS	NUM. CLMNTS.	INJURY TYPE	HOSPITAL STAY	CLAIM AMT.	TOTAL CLAIMED	NUM CLAIMS	NUM. SOFT TISS.	% SOFT TISS.	CLAIM AMT. RCVD.	FRAUD FLAG
1	ci	0		2	soft tissue	no	1,625	3,250	2	2	1.0	0	1
2	ci	0		2	back	yes	15,028	60,112	1	0	0	15,028	0
3	ci	54,613	married	1	broken limb	no	-99,999	0	0	0	0	572	0
4	ci	0		4	broken limb	yes	5,097	11,661	1	1	1.0	7,864	0
5	ci	0		4	soft tissue	no	8,869	0	0	0	0	0	1
⋮													
300	ci	0		2	broken limb	no	2,244	0	0	0	0	2,244	0
301	ci	0		1	broken limb	no	1,627	92,283	3	0	0	1,627	0
302	ci	0		3	serious	yes	270,200	0	0	0	0	270,200	0
303	ci	0		1	soft tissue	no	7,668	92,806	3	0	0	7,668	0
304	ci	46,365	married	1	back	no	3,217	0	0	0	0	1,653	0
⋮													
458	ci	48,176	married	3	soft tissue	yes	4,653	8,203	1	0	0	4,653	0
459	ci	0		1	soft tissue	yes	881	51,245	3	0	0	0	1
460	ci	0		3	back	no	8,688	729,792	56	5	0.08	8,688	0
461	ci	47,371	divorced	1	broken limb	yes	3,194	11,668	1	0	0	3,194	0
462	ci	0		1	soft tissue	no	6,821	0	0	0	0	0	1
⋮													
496	ci	0		1	soft tissue	no	2,118	0	0	0	0	0	1
497	ci	29,280	married	4	broken limb	yes	3,199	0	0	0	0	0	1
498	ci	0		1	broken limb	yes	32,469	0	0	0	0	16,763	0
499	ci	46,683	married	1	broken limb	no	179,448	0	0	0	0	179,448	0
500	ci	0		1	broken limb	no	8,259	0	0	0	0	0	1

Table 3.3

A data quality report for the motor insurance claims fraud detection ABT displayed in Table 3.2^[56].

(a) Continuous Features

Feature	Count	% Card.			1 st Quart.			3 rd Quart.			Std. Dev.	
		Miss.	Card.	Min	Qrt.	Mean	Median	Qrt.	Max	Mode	2 nd Quart.	2 nd Quart.
INCOME	500	0.0	171	0.0	0.0	13,740.0	0.0	33,918.5	71,284.0	20,081.5		
NUM. CLAIMANTS	500	0.0	4	1.0	1.0	1.9	2	3.0	4.0	1.0		
CLAIM AMOUNT	500	0.0	493	-99,999	3,322.3	16,373.2	5,663.0	12,245.5	270,200.0	29,426.3		
TOTAL CLAIMED	500	0.0	235	0.0	0.0	9,597.2	0.0	11,282.8	729,792.0	35,655.7		
NUM. CLAIMS	500	0.0	7	0.0	0.0	0.8	0.0	1.0	56.0	2.7		
NUM. SOFT TISSUE	500	2.0	6	0.0	0.0	0.2	0.0	0.0	5.0	0.6		
% SOFT TISSUE	500	0.0	9	0.0	0.0	0.2	0.0	0.0	2.0	0.4		
AMOUNT RECEIVED	500	0.0	329	0.0	0.0	13,051.9	3,253.5	8,191.8	270,200.0	30,547.2		
FRAUD FLAG	500	0.0	2	0.0	0.0	0.3	0.0	1.0	1.0	0.5		

(b) Categorical Features

Feature	Count	% Card.			Mode Freq.			Mode %			2 nd Mode Freq.		2 nd Mode %	
		Miss.	Card.	Mode	Mode	Freq.	Mode	%	Mode	Mode	Freq.	Mode	%	
INSURANCE TYPE	500	0.0	1	ci	500	100.0	—	—	—	—	—	—	—	
MARITAL STATUS	500	61.2	4	married	99	51.0	single	48	42.7					
INJURY TYPE	500	0.0	4	broken limb	177	35.4	soft tissue	172	34.4					
HOSPITAL STAY	500	0.0	2	no	354	70.8	yes	146	29.2					

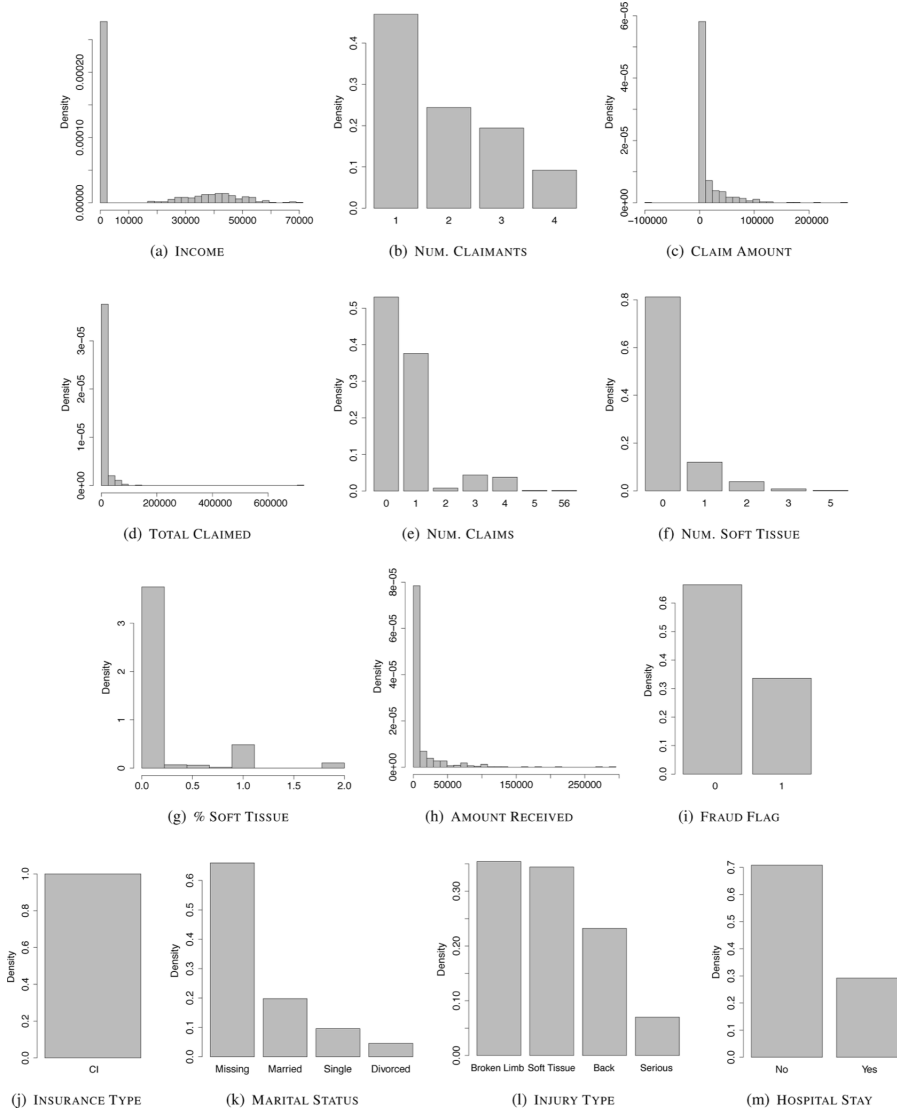


Figure 3.1

Visualizations of the continuous and categorical features in the motor insurance claims fraud detection ABT in Table 3.2^[56].

3.2 Getting to Know the Data

The data quality report gives an in-depth picture of the data in an ABT, and we should study it in detail in order to *get to know* the data that we will work with. For each feature, we should examine the central tendency and variation to understand the types of values that each feature can take. For categorical features, we should first examine the mode, 2nd mode, mode %, and 2nd mode % in the categorical features table in the data quality report. These tell us the most common levels within these features and will identify if any levels dominate the dataset (these levels will have a very high mode

%). The bar plots shown in the data quality report are also very useful here. They give us a quick overview of all the levels in the domain of each categorical feature and the frequencies of these levels.

For continuous features we should first examine the mean and standard deviation of each feature to get a sense of the central tendency and variation of the values within the dataset for the feature. We should also examine the minimum and maximum values to understand the range that is possible for each feature. The histograms for each continuous feature included in a data quality report are a very easy way for us to understand how the values for a feature are distributed across the range they can take.² When we generate histograms of features, there are a number of common, well-understood shapes that we should look out for. These shapes relate to well-known standard **probability distributions**,³ and recognizing that the distribution of the values in an ABT for a feature closely matches one of these standard distributions can help us when building machine learning models. During data exploration we don't need to go any further than simply recognizing that features seem to follow particular distributions, and this can be done from examining the histogram for each feature. [Figure 3.2](#)^[60] shows a selection of histogram shapes that exhibit characteristics commonly seen when analyzing features and that are indicative of standard, well-known probability distributions.

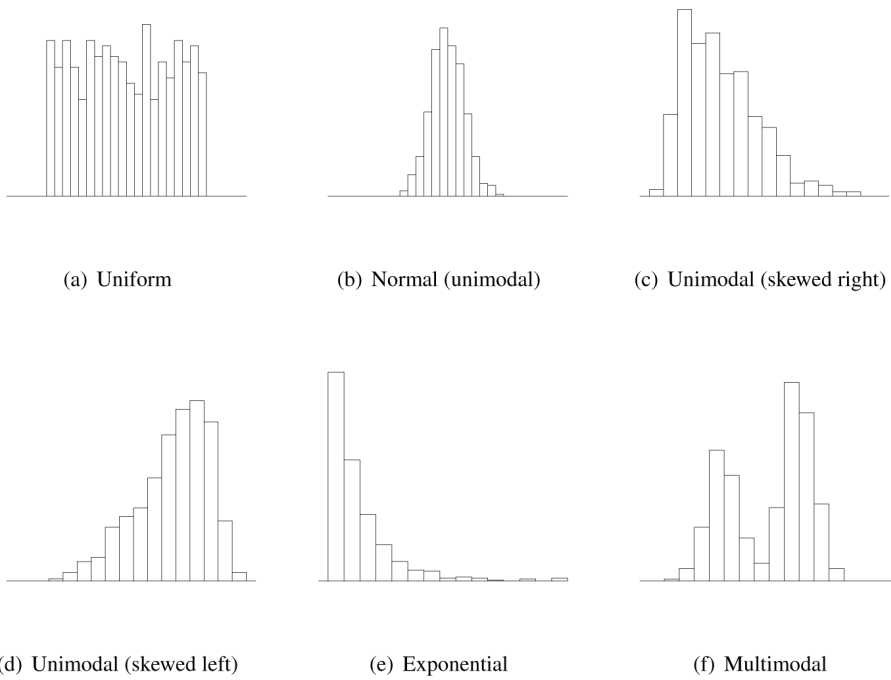


Figure 3.2

Histograms for six different sets of data, each of which exhibit well-known, common characteristics.

[Figure 3.2\(a\)](#)^[60] shows a histogram exhibiting a **uniform distribution**. A uniform distribution indicates that a feature is equally likely to take a value in any of the ranges present. Sometimes a uniform distribution is indicative of a descriptive feature that contains an ID rather than a measure of something more interesting.

[Figure 3.2\(b\)](#)^[60] shows a shape indicative of a **normal distribution**. Features following a normal distribution are characterized by a strong tendency toward a central value and symmetrical variation to either side of this central tendency. Naturally occurring phenomena—for example, the heights or weights of a randomly selected group of men or women—tend to follow a normal distribution. Histograms that follow a normal distribution can also be described as **unimodal** because they have a single peak around the central tendency. Finding features that exhibit a normal distribution is a good thing, as many of the modeling techniques we discuss in later chapters work particularly well with normally distributed data.

[Figures 3.2\(c\)](#)^[60] and [3.2\(d\)](#)^[60] show unimodal histograms that exhibit **skew**. Skew is simply a tendency toward very high (**right skew** as seen in [Figure 3.2\(c\)](#)^[60]) or very low (**left skew** as seen in [Figure 3.2\(d\)](#)^[60]) values. Features recording salaries often follow a right skewed distribution, as most

people are paid salaries near a well-defined central tendency, but there are usually a small number of people who are paid very large salaries. Skewed distributions are often said to have **long tails** toward these very high or very low values.

In a feature following an **exponential distribution**, as shown in [Figure 3.2\(e\)](#)^[60], the likelihood of low values occurring is very high but diminishes rapidly for higher values. Features such as the number of times a person has made an insurance claim or the number of times a person has been married tend to follow an exponential distribution. Recognizing that a feature follows an exponential distribution is another clear warning sign that outliers are likely. As shown in [Figure 3.2\(e\)](#)^[60], exponential distributions have a long tail, and so very high values are not uncommon.

Finally, a feature characterized by a **multimodal distribution** has two or more very commonly occurring ranges of values that are clearly separated. [Figure 3.2\(f\)](#)^[60] shows a **bimodal distribution** with two clear peaks—we can think of this as two normal distributions pushed together. Multimodal distributions tend to occur when a feature contains a measurement made across a number of distinct groups. For example, if we were to measure the heights of a randomly selected group of Irish men and women, we would expect a bimodal distribution with a peak at around 1.635m for women and 1.775m for men.

Observing a multimodal distribution is cause for both caution and optimism. The caution comes from the fact that measures of central tendency and variation tend to break down for multimodal data. For example, consider that the mean value of the distribution shown in [Figure 3.2\(f\)](#)^[60] is likely to sit right in the valley between the two peaks, even though very few instances actually have this value. The optimism associated with finding multimodally distributed data stems from the fact that, if we are lucky, the separate peaks in the distribution will be associated with the different target levels we are trying to predict. For example, if we were trying to predict gender from a set of physiological measurements, height would most likely be a very predictive value, as it would separate people into male and female groups.

This stage of data exploration is mostly an information-gathering exercise, the output of which is just a better understanding of the contents of an ABT. It does, however, also present a good opportunity to discuss

anything unusual that we notice about the central tendency and variation of features within the ABT. For example, a salary feature with a mean of 40 would seem unlikely (40,000 would seem more reasonable) and should be investigated.

3.2.1 The Normal Distribution

The **normal distribution** (also known as a **Gaussian distribution**) is so important that it is worth spending a little extra time discussing its characteristics. Standard probability distributions have associated **probability density functions**, which define the characteristics of the distribution. The probability density function for the normal distribution is

$$N(x, \mu, \sigma) = \frac{1}{\sigma \sqrt{2\pi}} e^{-\frac{(x - \mu)^2}{2\sigma^2}} \quad (3.1)$$

where x is any value, and μ and σ are parameters that define the shape of the distribution. Given a probability density function, we can plot the **density curve** associated with a distribution, which gives us a different way to visualize standard distributions like the normal. Figure 3.3^[62] shows the density curves for a number of different normal distributions. The higher the curve for a particular value on the horizontal axis, the more likely that value is.

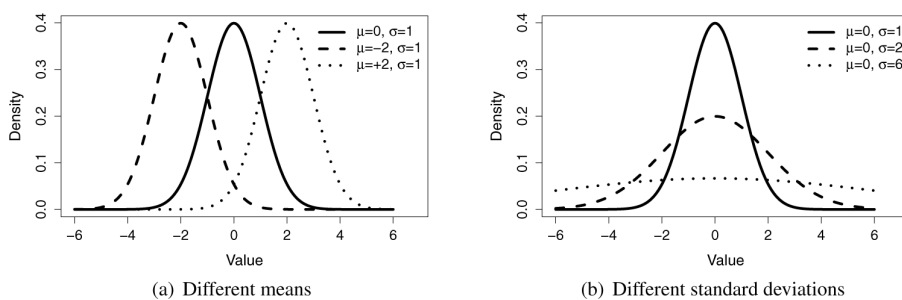


Figure 3.3

(a) Three normal distributions with different means but identical standard deviations; and (b) three normal distributions with identical means but different standard deviations.

The curve defined by a normal probability distribution is symmetric around a single peak value. The location of the peak value is defined by the parameter μ (pronounced *mu*), which denotes the **population mean** (in

other words, the mean value of the feature if we had access to every value that could possibly occur). The height and slope of the curve is dependent on the parameter σ (pronounced *sigma*), which denotes the **population standard deviation**. The larger the value of σ , the lower the maximum height of the curve and the shallower the slope. [Figure 3.3\(a\)](#)^[62] illustrates how the location of the peak moves as the value for μ changes, and [Figure 3.3\(b\)](#)^[62] illustrates how the shape of the curve changes as we vary the value for σ . Notice that in both figures, the normal distribution plotted with the continuous black line has mean $\mu = 0$ and standard deviation $\sigma = 1$. This normal distribution is known as the **standard normal distribution**. The statement $X \sim N(\mu, \sigma)$ is often used as a shorthand for X is a *normally distributed feature with mean μ and standard deviation σ* .⁴ One important characteristic of the normal distribution is often described as the **68–95–99.7 rule**. The rule states that approximately 68% of the values in a sample that follows a normal distribution will be within one σ of μ , 95% of the values will be within two σ of μ , and 99.7% of values will be within three σ of μ . [Figure 3.4](#)^[63] illustrates this rule. This rule highlights that in data that follows a normal distribution, there is a very low probability of observations occurring that differ from the mean by more than two standard deviations.

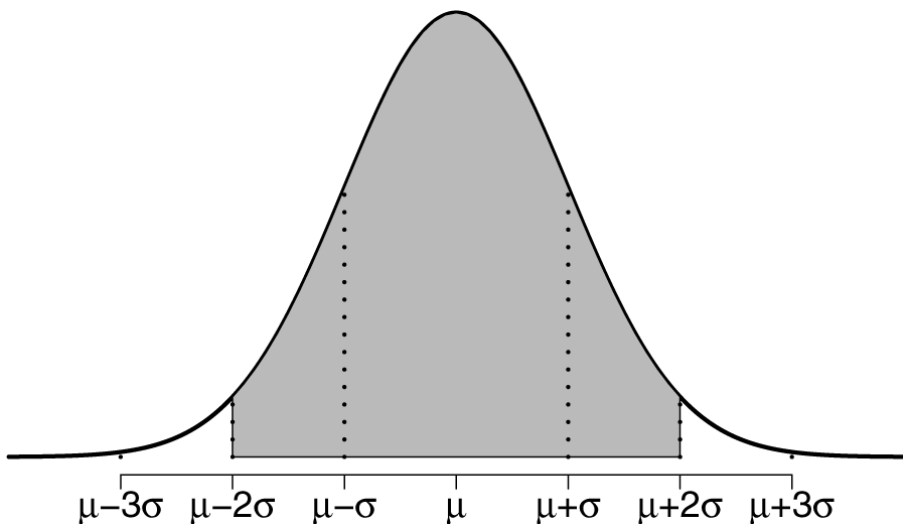


Figure 3.4

An illustration of the 68–95–99.7 rule. The gray region defines the area where 95% of values in a sample are expected.

3.2.2 Case Study: Motor Insurance Fraud

The data quality report in [Table 3.3^{\[57\]}](#) and in [Figure 3.1^{\[58\]}](#) allows us to very quickly become familiar with the central tendency and variation of each feature in the ABT. These were all as the business expected. In the bar plots in [Figure 3.1^{\[58\]}](#), the different levels in the domain of each categorical feature, and how these levels are distributed, are obvious. For example, INJURY TYPE has four levels. Three of these, *broken limb*, *soft tissue*, and *back*, are quite frequent in the ABT, while *serious* is quite rare. The distribution of INSURANCE TYPE is a little strange, as it displays only one level.

From the histograms in [Figure 3.1^{\[58\]}](#), we see that all the continuous features except for INCOME and FRAUD FLAG seem to follow an exponential distribution pretty closely. INCOME is interesting as it seems to follow what looks like a normal distribution except that there is one large bar at about 0. The distribution of the FRAUD FLAG feature that can be seen in its histogram is not typical of a continuous feature.

By analyzing the data quality report, we are able to understand the characteristics of the data in the ABT. We will return to the features that seemed to have slightly peculiar distributions.

3.3 Identifying Data Quality Issues

After getting to know the data, the second goal of data exploration is to identify any data quality issues in an ABT. A **data quality issue** is loosely defined as anything *unusual* about the data in an ABT. The most common data quality issues, however, are **missing values**, **irregular cardinality** problems, and **outliers**. In this section we describe each of these data quality issues and outline how the data quality report can be used to identify them.

The data quality issues we identify from a data quality report will be of two types: data quality issues due to **invalid data** and data quality issues due to **valid data**. Data quality issues due to invalid data typically arise because of errors in the process used to generate an ABT, usually in relation to calculating derived features. When we identify data quality issues due to invalid data, we should take immediate action to correct them, regenerate the ABT, and re-create the data quality report. Data quality issues due to valid data can arise for a range of domain-specific reasons (we discuss

some of these later in this section), and we do not necessarily need to take any corrective action to address these issues. We do not correct data quality issues due to valid data unless the predictive models we will use the data in the ABT to train require that particular data quality issues be corrected. For example, we cannot train error-based models with data that contains missing values, and data that contains outliers significantly damages the performance of similarity-based models. At this stage we simply record any data quality issues due to valid data in a **data quality plan** so that we remain aware of them and can handle them later if required. [Table 3.4](#)^[64] shows the structure of a data quality plan. For each of the data quality issues found, we include the feature it was found in and the details of the data quality issue. Later we add information on potential handling strategies for each data quality issue.

Table 3.4

The structure of a data quality plan.

Feature	Data Quality Issue	Potential Handling Strategies

3.3.1 Missing Values

Often when an ABT is generated, some instances will be missing values for one or more features. The **% Miss.** columns in the data quality report highlight the percentage of missing values for each feature (both continuous and categorical) in an ABT, and so it is very easy to identify which features suffer from this issue. If features have missing values, we must first determine why the values are missing. Often missing values arise from errors in data integration or in the process of generating values for derived fields. If this is the case, these missing values are due to invalid data, so the data integration errors can be corrected, and the ABT can be regenerated to populate the missing values. Missing values can also arise for legitimate reasons, however. Sometimes in an organization, certain values will only have been collected after a certain date, and the data used to generate an ABT might cover time both before and after this date. In other cases,

particularly where data arises from manual entry, certain personally sensitive values (for example, salary, age, or weight) may be entered only for a small number of instances. These missing values are due to valid data, so they do not need to be handled but should instead be recorded in the data quality plan.

There is one case in which we might deal directly with missing values that arise from valid data during data exploration. If the proportion of missing values for a feature is very high, a good rule of thumb is anything in excess of 60%, then the amount of information stored in the feature is so low that it is probably a good idea to simply remove that feature from the ABT.

3.3.2 Irregular Cardinality

The **Card.** column in the data quality report shows the number of distinct values present for a feature within an ABT. A data quality issue arises when the cardinality for a feature does not match what we expect, a mismatch called an **irregular cardinality**. The first things to check the cardinality column for are features with a cardinality of 1. This indicates a feature that has the same value for every instance and contains no information useful for building predictive models. Features with a cardinality of 1 should first be investigated to ensure that the issue is not due to an ABT generation error. If this is the case, then the error should be corrected, and the ABT should be regenerated. If the generation process proves to be error-free, then features with a cardinality of 1, although valid, should be removed from an ABT because they will not be of any value in building predictive models.

The second things to check for in the cardinality column are categorical features incorrectly labeled as continuous. Continuous features will usually have a cardinality value close to the number of instances in the dataset. If the cardinality of a continuous feature is significantly less than the number of instances in the dataset, then it should be investigated. Sometimes a feature is actually continuous but in practice can assume only a small range of values—for example, the number of children a person has. In this case there is nothing wrong, and the feature should be left alone. In other cases, however, a categorical feature will have been developed to use numbers to indicate categories and might be mistakenly identified as a continuous

feature in a data quality report. Checking for features with a low cardinality will highlight these features. For example, a feature might record gender using 1 for female and 0 for male. If treated as a continuous feature in a data quality report, this would have a cardinality of 2. Once identified, these features should be recoded as categorical features.

The third way in which a data quality issue can arise due to an irregular cardinality is if a categorical feature has a much higher cardinality than we would expect given the definition of the feature. For example, a categorical feature storing gender with a cardinality of 6 is worthy of further investigation. This issue often arises because multiple levels are used to represent the same thing—for example, in a feature storing gender, we might find levels of *male*, *female*, *m*, *f*, *M*, and *F*, which all represent male and female in slightly different ways. This is another example of a data quality issue due to invalid data. It should be corrected through a mapping to a standard set of levels, and the ABT should be regenerated.

The final example of a data quality issue due to an irregular cardinality is when a categorical feature simply has a very high number of levels—anything over 50 is worth investigation. There are many genuine examples of features that will have such high cardinality, but some of the machine learning algorithms that we will look at will struggle to effectively use features with such high cardinality. This is an example of a data issue due to valid data, so if this occurs for features in an ABT, it should be noted in the data quality plan.

3.3.3 Outliers

Outliers are values that lie far away from the central tendency of a feature. There are two kinds of outliers that might occur in an ABT: **invalid outliers** and **valid outliers**. Invalid outliers are values that have been included in a sample through error and are often referred to as noise in the data. Invalid outliers can arise for all sorts of different reasons. For example, during a manual data entry process, a *fat fingered*⁵ analyst may have entered 100,000 instead of 1,000. Valid outliers are correct values that are simply very different from the rest of the values for a feature, for example, a billionaire who has a massive salary compared to everyone else in a sample.

There are two main ways that the data quality report can be used to identify outliers within a dataset. The first is to examine the minimum and

maximum values for each feature and use domain knowledge to determine whether these are plausible values. For example, a minimum age value of -12 would jump out as an error. Outliers identified in this way are likely to be invalid outliers and should immediately be either corrected, if data sources allow this, or removed and marked as missing values if correction is not possible. In some cases we might even remove a complete instance from a dataset based on the presence of an outlier.

The second approach to identifying outliers is to compare the gaps between the median, minimum, maximum, 1st quartile, and 3rd quartile values. If the gap between the 3rd quartile and the maximum value is noticeably larger than the gap between the median and the 3rd quartile, this suggests that the maximum value is unusual and is likely to be an outlier. Similarly, if the gap between the 1st quartile and the minimum value is noticeably larger than the gap between the median and the 1st quartile, this suggests that the minimum value is unusual and is likely to be an outlier. The outliers shown in box plots also help to make this comparison. Exponential or skewed distributions in histograms are also good indicators of the presence of outliers.

It is likely that outliers found using the second approach are valid outliers, so they are a data quality issue due to valid data. Some machine learning techniques do not perform well in the presence of outliers, so we should note these in the data quality plan for possible handling later in the project.

3.3.4 Case Study: Motor Insurance Fraud

Using the data quality report in [Table 3.3](#)^[57] and [Figure 3.1](#)^[58] together with the ABT extract in [Table 3.2](#)^[56], we can perform an analysis of this ABT for data quality issues. We do this by describing separately missing values, irregular cardinality, and outliers.

3.3.4.1 Missing values The % Miss. column of the data quality report in [Table 3.3](#)^[57] shows that MARITAL STATUS and NUM. SOFT TISSUE are the only features with an obvious problem with missing values. Indeed, over 60% of the values for MARITAL STATUS are missing, so this feature should almost certainly be removed from the ABT (we return to this feature shortly). Only 2% of the values for the NUM. SOFT TISSUE feature are

missing, so removal would be extreme in this case. This issue should be noted in the data quality plan.

An examination of the histogram for the INCOME feature (shown in [Figure 3.1\(a\)](#)^[58]) and the actual data for this feature in [Table 3.2](#)^[56] reveals an interesting pattern. In the histogram we can see an unusual number of zero values for INCOME that seems set apart from the central tendency of the data, which appears to be at about 40,000. Examining the INCOME row in the data quality report also shows a large difference between the mean and median values, which is unusual. Examining the actual raw data in [Table 3.2](#)^[56] shows that these zeros always co-occur with missing values in the MARITAL STATUS feature. This pattern was investigated with the business to understand whether this was an issue due to valid or invalid data. It was confirmed by the business that the zeros in the INCOME feature actually represent missing values and that MARITAL STATUS and INCOME were collected together, leading to their both being missing for the same instances in the ABT. No other data source existed from which these features could be populated, so it was decided to remove both of them from the ABT.

3.3.4.2 Irregular cardinality Reading down the **Card.** column of the data quality report, we can see that the cardinality of the INSURANCE TYPE feature is 1, an obvious data problem that needs investigation. The cardinality value indicates that every instance has the same value for this feature, ci . Investigation of this issue with the business revealed that nothing had gone wrong during the ABT generation process, and that ci refers to *car insurance*. Every instance in this ABT should have that value, and this feature was removed from the ABT.

Many of the continuous features in the dataset also have very low cardinality values. NUM. CLAIMANTS, NUM. CLAIMS, NUM. SOFT TISSUE, % SOFT TISSUE, and FRAUD FLAG all have cardinality less than 10, which is unusual in a dataset of 500 instances. These low cardinalities were investigated with the business. The low cardinality for the NUM. CLAIMANTS, NUM. CLAIMS, and NUM. SOFT TISSUE features was found to be valid, because these are categorical features and can only take values in a small range, as people tend not to make very many claims. The % SOFT

TISSUE feature is a ratio of the NUM. CLAIMS and NUM. SOFT TISSUE features, and its low cardinality arises from their low cardinality.

The cardinality of 2 for the FRAUD FLAG feature highlights the fact that this is not really a continuous feature. Rather, FRAUD FLAG is a categorical feature that just happens to use 0 and 1 as its category labels, which has led to its being treated as continuous in the ABT. FRAUD FLAG was changed to be a categorical feature. This is particularly important in this case because FRAUD FLAG is the target feature, and as we will see in upcoming chapters, the type of the target feature has a big impact on how we apply machine learning techniques.

3.3.4.3 Outliers From an examination of the minimum and maximum values for each continuous feature in [Table 3.3\(a\)](#)^[57], CLAIM AMOUNT jumps out as having an unusual minimum value of – 99,999. A little investigation revealed that this minimum value arises from \mathbf{d}_3 in [Table 3.2](#)^[56]. The absence of a large bar at – 99,999 in [Figure 3.1\(c\)](#)^[58] confirms that there are not multiple occurrences of this value. The pattern 99,999 also suggests that this is most likely a data entry error or a system default remaining in the ABT. This was confirmed with the business in this case, and this value was treated as an invalid outlier and replaced with a missing value.

CLAIM AMOUNT, TOTAL CLAIMED, NUM. CLAIMS and AMOUNT RECEIVED all seem to have unusually high maximum values, especially when compared to their median and 3rd quartile values. To investigate outliers, we should always start by locating the instance in the dataset that contains the strange maximum or minimum values. In this case the maximum values for TOTAL CLAIMED and NUM. CLAIMS both come from \mathbf{d}_{460} in [Table 3.2](#)^[56]. This policyholder seems to have made many more claims than anyone else, and the total amount claimed reflects this. This deviation from the norm was investigated with the business, and it turned out that although these figures were correct, this policy was actually a company policy rather than an individual policy, which was included in the ABT by mistake. For this reason, instance \mathbf{d}_{460} was removed from the ABT.

The offending large maximums for CLAIM AMOUNT and AMOUNT RECEIVED both come from \mathbf{d}_{302} in [Table 3.2](#)^[56]. Investigation of this claim with the business revealed that this is in fact a valid outlier and represents an unusually large claim for a very serious injury. Examination of the

histograms in Figures 3.1(c)^[58] and 3.1(h)^[58] show that the CLAIM AMOUNT and AMOUNT RECEIVED features have a number of large values (evidenced by the small bars to the right-hand side of these histograms) and that d_{302} is not unique. These outliers should be noted in the data quality plan for possible handling later in the project.

3.3.4.4 The data quality plan Based on the analysis described in the preceding sections, the data quality plan shown in Table 3.5^[68] was created. This records each of the data quality issues due to valid data that have been identified in the motor insurance fraud ABT. During the Modeling phase of the project, we will use this table as a reminder of data quality issues that could affect model training. At the end of the next section, we complete this table by adding potential handling strategies.

Table 3.5

The data quality plan for the motor insurance fraud prediction ABT.

Feature	Data Quality Issue	Potential Handling Strategies
NUM. SOFT TISSUE	Missing values (2%)	
CLAIM AMOUNT	Outliers (high)	
AMOUNT RECEIVED	Outliers (high)	

3.4 Handling Data Quality Issues

When we find data quality issues due to valid data during data exploration, we should note these issues in a data quality plan for potential handling later in the project. The most common issues in this regard are missing values and outliers, which are both examples of **noise** in the data. Although we usually delay handling noise issues until the modeling phase of a project (different predictive model types require different levels of noise handling, and we should in general do as little noise handling as we can), in this section we describe the most common techniques used to handle missing values and outliers. It is a good idea to add suggestions for the best technique to handle each data quality issue in the data quality plan during data exploration as it will save time during modeling.

3.4.1 Handling Missing Values

The simplest approach to handling missing values is to simply drop from an ABT any features that have them. This, however, can result in massive, and frequently needless, loss of data. For example, if in an ABT containing 1,000 instances, one value is missing for a particular feature, it would be pretty extreme to remove that whole feature. As a general rule of thumb, only features that are missing in excess of 60% of their values should be considered for complete removal, and more subtle handling techniques should be used for features missing less data.

An alternative to entirely deleting features that suffer from large numbers of missing values is to derive a missing indicator feature from them. This is a binary feature that flags whether the value was present or missing in the original feature. This can be useful if the reason that specific values for a feature are missing might have some relationship to the target feature—for example, if a feature that has missing values represented sensitive personal data, people’s readiness to provide this data (or not) might tell us something about them. When missing indicator features are used, the original feature is usually discarded.

Another simple approach to handling missing values is **complete case analysis**, which deletes from an ABT any instances that are missing one or more feature values. This approach, however, can result in significant amounts of data loss and can introduce a bias into the dataset if the distribution of missing values in the dataset is not completely random. In general, we recommend the use of complete case analysis only to remove instances that are missing the value of the target feature. Indeed, any instances with a missing value for the target feature should always be removed from an ABT.

Imputation replaces missing feature values with a plausible estimated value based on the feature values that are present. The most common approach to imputation is to replace missing values for a feature with a measure of the central tendency of that feature. For continuous features, the mean or median is most commonly used, and for categorical features, the mode is most commonly used.

Imputation, however, should not be used for features that have very large numbers of missing values because imputing a very large number of missing values will change the central tendency of a feature too much. We would be reluctant to use imputation on features missing in excess of 30%

of their values and would strongly recommend against the use of imputation on features missing in excess of 50% of their values.

There are other, more complex approaches to imputation. For example, we can actually build a predictive model that estimates a replacement for a missing value based on the feature values that are present in a dataset for a given instance. We recommend, however, using simple approaches first and turning to more complex ones only if required.

Imputation techniques tend to give good results and avoid the data loss associated with deleting features or complete case analysis. It is important to note, however, that all imputation techniques suffer from the fact that they change the underlying data in an ABT and can cause the variation within a feature to be underestimated, which can negatively bias the relationships between a descriptive feature and a target feature.

3.4.2 Handling Outliers

The easiest way to handle outliers is to use a **clamp transformation**. This clamps all values above an upper threshold and below a lower threshold to these threshold values, thus removing the offending outliers:

$$a_i = \begin{cases} lower & \text{if } a_i < lower \\ upper & \text{if } a_i > upper \\ a_i & \text{otherwise} \end{cases} \quad (3.2)$$

where a_i is a specific value of feature a , and $lower$ and $upper$ are the lower and upper thresholds.

The upper and lower thresholds can be set manually based on domain knowledge or can be calculated from data. One common way to calculate clamp thresholds is to set the lower threshold to the 1st quartile value minus 1.5 times the **inter-quartile range** and the upper threshold to the 3rd quartile plus 1.5 times the inter-quartile range. This works effectively and takes into account the fact that the variation in a dataset can be different on either side of a central tendency.

If this approach were to be used for the CLAIM AMOUNT feature from the motor claims insurance fraud detection scenario, then the upper and lower thresholds would be defined as follows:

$$lower = 3,322.3 - 1.5 \times 8,923.2 = -10,062.5$$

$$upper = 12,245.5 + 1.5 \times 8,923.2 = 25,630.3$$

where the values used are extracted from [Table 3.3](#)^[57]. Any values outside these thresholds would be converted to the threshold values. Examining the histogram in [Figure 3.1\(c\)](#)^[58] is useful in considering the impact of applying the clamp transformation using these thresholds. Locating 25,630.3 on the horizontal axis shows that this upper threshold would cause a relatively large number of values to be changed. The impact of the clamp transformation can be reduced by changing the multiplier used to calculate the thresholds from 1.5 to a larger value.

Another commonly used approach to setting the upper and lower thresholds is to use the mean value of a feature plus or minus 2 times the standard deviation.⁶ Again this works well, but it does assume that the underlying data follows a normal distribution.

If this approach were to be used for the AMOUNT RECEIVED feature from the motor claims insurance fraud detection scenario, then the upper and lower thresholds would be defined as follows:

$$lower = 13,051.9 - 2 \times 30,547.2 = -48,042.5$$

$$upper = 13,051.9 + 2 \times 30,547.2 = 74,146.3$$

where the values used are again extracted from [Table 3.3](#)^[57]. Examining the histogram in [Figure 3.1\(h\)](#)^[58] is again a good indication of the impact of using this transformation. This impact can be reduced by changing the multiplier used to calculate the thresholds from 2 to a larger value.

Opinions vary widely on when transformations like the clamp transformation should be used to handle outliers in data. Many argue that performing this type of transformation may remove the most interesting and, from a predictive modeling point of view, informative instances from a dataset. On the other hand, some of the machine learning techniques that we discuss in upcoming chapters perform poorly in the presence of outliers. We recommend only applying the clamp transformation in cases where it is suspected that a model is performing poorly due to the presence of outliers. The impact of the clamp transformation should then be evaluated by comparing the performance of different models trained on datasets where the transformation has been applied and where it has not.

3.4.3 Case Study: Motor Insurance Fraud

If we needed to do it, the most sensible approach to handling the missing values in the NUM. SOFT TISSUE feature would be to use imputation. There are very few missing values for this feature (2%), so replacing them with an imputed value should not excessively affect the variance of the feature. In this case the median value of 0.0 (shown in [Table 3.3\(a\)](#)^[57]) is the most appropriate value to use to replace the missing values; because this feature only actually takes discrete values, the mean value of 0.2 never naturally occurs in the dataset.

The outliers present in the CLAIM AMOUNT and AMOUNT RECEIVED features could be easily handled using a clamp transformation. Both features follow a broadly exponential distribution, however, which means that the methods described for setting the thresholds of the clamp will not work especially well (both methods work best for normally distributed data). Therefore, manually setting upper and lower thresholds based on domain knowledge is most appropriate in this case. The business advised that for both features, a lower threshold of 0 and an upper threshold of 80,000 would make sense.

We completed the data quality plan by including these potential handling strategies. The final data quality plan is shown in [Table 3.6](#)^[72]. Together with the data quality report, these are the outputs of the data exploration work for the motor insurance fraud detection project.

Table 3.6

The data quality plan with potential handling strategies for the motor insurance fraud prediction ABT.

Feature	Data Quality Issue	Potential Handling Strategies
NUM. SOFT TISSUE	Missing values (2%)	Imputation (median: 0.0)
CLAIM AMOUNT	Outliers (high)	Clamp transformation (manual: 0, 80,000)
AMOUNT RECEIVED	Outliers (high)	Clamp transformation (manual: 0, 80,000)

3.5 Advanced Data Exploration

All the descriptive statistics and data visualization techniques that we have used in the previous sections of this chapter have focused on the characteristics of individual features. This section will introduce techniques that enable us to examine relationships between pairs of features.

3.5.1 Visualizing Relationships between Features

In preparing to create predictive models, it is always a good idea to investigate the relationships between pairs of features. This can help indicate which descriptive features might be useful for predicting a target feature and help find pairs of descriptive features that are closely related. Identifying pairs of closely related descriptive features is one way to reduce the size of an ABT because if the relationship between two descriptive features is strong enough, we may not need to include both. In this section we describe approaches to visualizing the relationships between pairs of continuous features, pairs of categorical features, and pairs including one categorical and one continuous feature.

For the examples in this section, we introduce a new dataset. [Table 3.7](#)^[73] shows the details of 30 players on a professional basketball team. The dataset includes the HEIGHT, WEIGHT, and AGE of each player; the POSITION that the player normally plays (*guard*, *center*, or *forward*); the CAREER STAGE of the player (*rookie*, *mid-career*, or *veteran*); the average weekly SPONSORSHIP EARNINGS of each player; and whether the player has a SHOE SPONSOR (*yes* or *no*).

Table 3.7

The details of a professional basketball team.

ID	POSITION	HEIGHT	WEIGHT	CAREER		AGE	SPONSORSHIP	SHOE SPONSOR
				STAGE	EARNINGS			
1	forward	192	218	veteran	29		561	yes
2	center	218	251	mid-career	35		60	no
3	forward	197	221	rookie	22		1,312	no
4	forward	192	219	rookie	22		1,359	no
5	forward	198	223	veteran	29		362	yes
6	guard	166	188	rookie	21		1,536	yes
7	forward	195	221	veteran	25		694	no
8	guard	182	199	rookie	21		1,678	yes
9	guard	189	199	mid-career	27		385	yes
10	forward	205	232	rookie	24		1,416	no
11	center	206	246	mid-career	29		314	no
12	guard	185	207	rookie	23		1,497	yes
13	guard	172	183	rookie	24		1,383	yes
14	guard	169	183	rookie	24		1,034	yes
15	guard	185	197	mid-career	29		178	yes
16	forward	215	232	mid-career	30		434	no
17	guard	158	184	veteran	29		162	yes
18	guard	190	207	mid-career	27		648	yes
19	center	195	235	mid-career	28		481	no
20	guard	192	200	mid-career	32		427	yes
21	forward	202	220	mid-career	31		542	no
22	forward	184	213	mid-career	32		12	no
23	forward	190	215	rookie	22		1,179	no
24	guard	178	193	rookie	21		1,078	no
25	guard	185	200	mid-career	31		213	yes
26	forward	191	218	rookie	19		1,855	no
27	center	196	235	veteran	32		47	no
28	forward	198	221	rookie	22		1,409	no
29	center	207	247	veteran	27		1,065	no
30	center	201	244	mid-career	25		1,111	yes

3.5.1.1 Visualizing pairs of continuous features The scatter plot is one of the most important tools in data visualization. A scatter plot is based on two axes: the horizontal axis represents one feature, and the vertical axis represents a second. Each instance in a dataset is represented by a point on the plot determined by the values for that instance of the two features being plotted. [Figure 3.5\(a\)](#)^[74] shows an example scatter plot for the HEIGHT and WEIGHT features from the dataset in [Table 3.7](#)^[73]. The points in this scatter plot are arranged in a broadly linear pattern diagonally across the scatter plot. This suggests that there is a strong, positive, linear relationship between the HEIGHT and WEIGHT features—as height increases, so does weight. We say that features with this kind of relationship are positively covariant. [Figure 3.5\(b\)](#)^[74] shows a scatter plot for the SPONSORSHIP EARNINGS and AGE features from [Table 3.7](#)^[73]. These features are strongly negatively covariant. [Figure 3.5\(c\)](#)^[74] shows a scatter plot of the HEIGHT and AGE features. These features are not strongly covariant either positively or negatively.

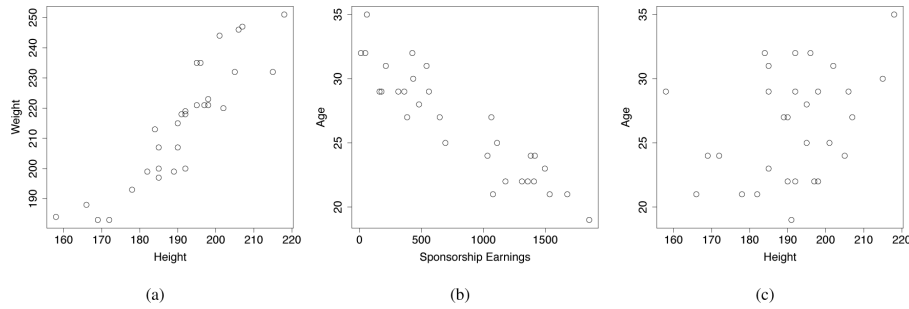


Figure 3.5

Example scatter plots for pairs of features from the dataset in [Table 3.7](#)^[73], showing (a) the strong positive covariance between HEIGHT and WEIGHT; (b) the strong negative covariance between SPONSORSHIP EARNINGS and AGE; and (c) the lack of strong covariance between HEIGHT and AGE.

A **scatter plot matrix (SPLOM)** shows scatter plots for a whole collection of features arranged into a matrix. This is useful for exploring the relationships between groups of features—for example, all the continuous features in an ABT. [Figure 3.6](#)^[75] shows an example scatter plot matrix for the continuous features from the professional basketball team dataset in [Table 3.7](#)^[73]: HEIGHT, WEIGHT, AGE, and SPONSORSHIP EARNINGS. Each row and column represent the feature named in the cells along the diagonal. The

cells above and below the diagonal show scatter plots of the features in the row and column that meet at that cell.

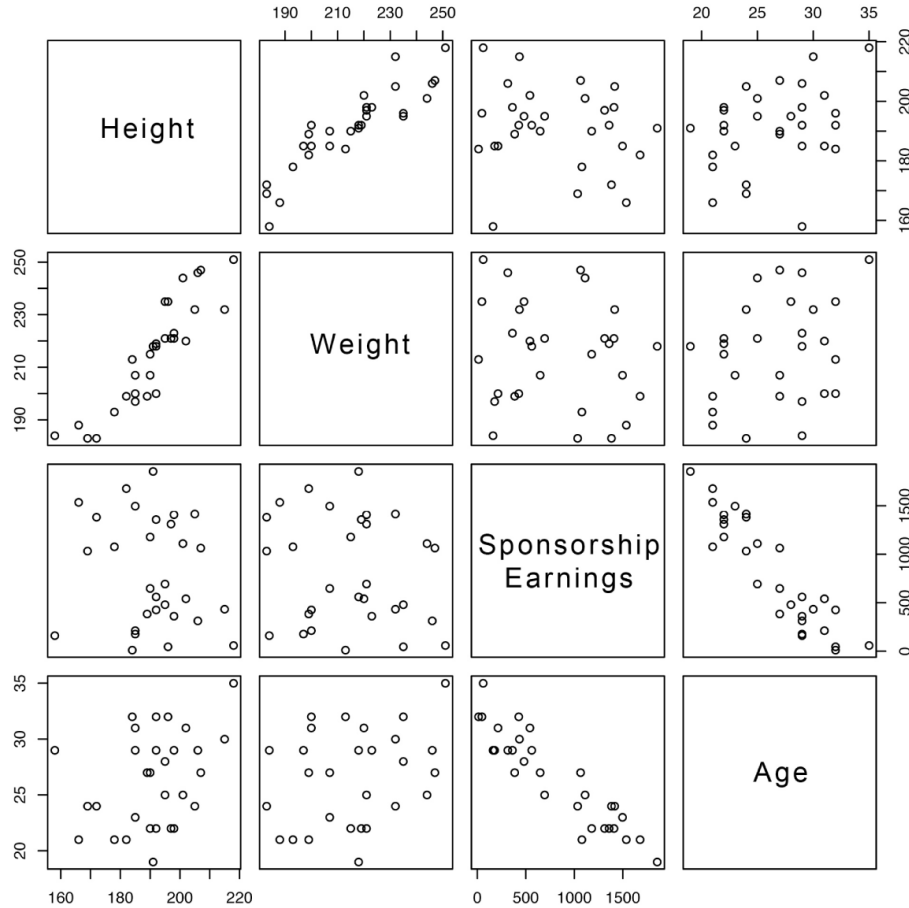


Figure 3.6

A scatter plot matrix showing scatter plots of the continuous features from the professional basketball team dataset in [Table 3.7](#)^[73].

A scatter plot matrix is a very quick way to explore the relationships within a whole set of continuous features. The effectiveness of scatter plot matrices, however, diminishes once the number of features in the set goes beyond 8 because the graphs become too small. Using interactive tools that aid data exploration can help overcome this limitation.

3.5.1.2 Visualizing pairs of categorical features The simplest way to visualize the relationship between two categorical features is to use a collection of bar plots. This is often referred to as a **small multiples** visualization. First, we draw a simple bar plot showing the densities of the different levels of the first feature. Then, for each level of the second

feature, we draw a bar plot of the first feature using only the instances in the dataset for which the second feature has that level. If the two features being visualized have a strong relationship, then the bar plots for each level of the second feature will look noticeably different from one another and from the overall bar plot for the first feature. If there is no relationship, then we should expect that the levels of the first feature will be evenly distributed among the instances having the different levels of the second feature, so all bar plots will look much the same.

[Figure 3.7\(a\)](#)^[76] shows an example for the CAREER STAGE and SHOE SPONSOR features from the professional basketball team dataset in [Table 3.7](#)^[73]. The bar plot on the left shows the distribution of the different levels of the CAREER STAGE feature across the entire dataset. The two plots on the right show the distributions for those players with and without a shoe sponsor. Since all three plots show very similar distributions, we can conclude that no real relationship exists between these two features and that players of any career stage are equally likely to have a shoe sponsor or not.

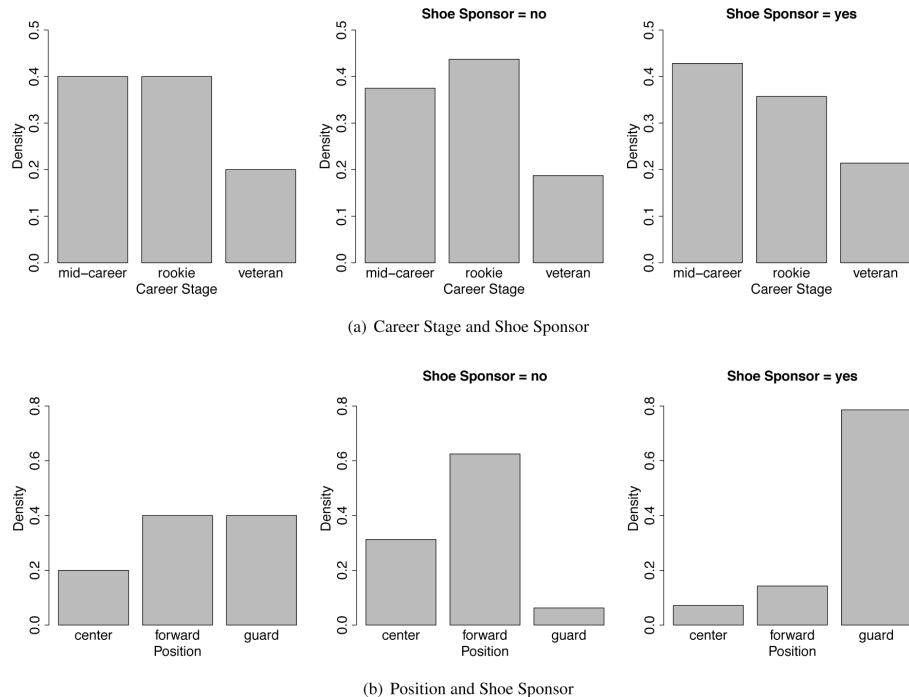


Figure 3.7

Examples of using small multiple bar plot visualizations to illustrate the relationship between two categorical features: (a) the CAREER STAGE and SHOE SPONSOR features; and (b) the POSITION and SHOE SPONSOR features. All data comes from [Table 3.7](#)^[73].

[Figure 3.7\(b\)](#)^[76] shows another example, for the POSITION and SHOE SPONSOR features from the same dataset. In this case, the three plots are very different, so we can conclude that there is a relationship between these two features. It seems that players who play in the guard position are much more likely to have a shoe sponsor than forwards or centers.

When using small multiples, it is important that all the small charts are kept consistent because this ensures that only genuine differences within the data are highlighted, rather than differences that arise from formatting. For example, the scales of the axes must always be kept consistent, as should the order of the bars in the individual bar plots. It is also important that densities are shown rather than frequencies, as the overall bar plots on the left of each visualization cover much more of the dataset than the other two plots, so frequency-based plots would look very uneven.

If the number of levels of one of the features being compared is small (we recommend no more than three), we can use **stacked bar plots** as an alternative to the small multiples bar plots approach. When this approach is used, we show a bar plot of the first feature above a bar plot that shows the relative distribution of the levels of the second feature within each level of the first. Because relative distributions are used, the bars in the second bar plot cover the full range of the space available—these are often referred to as 100% stacked bar plots. If two features are unrelated, then we would expect to see the same proportion of each level of the second feature within the bars for each level of the first.

[Figure 3.8](#)^[79] shows two examples of using stacked bar plots. In the first example, [Figure 3.8\(a\)](#)^[73], a bar plot of the CAREER STAGE feature is shown above a 100% stacked bar plot showing how the levels of the SHOE SPONSOR feature are distributed in instances having each level of CAREER STAGE. The distributions of the levels of SHOE SPONSOR are almost the same for each level of CAREER STAGE, and therefore we can conclude that there is no relationship between these two features. The second example, [Figure 3.8\(b\)](#)^[79], shows the POSITION and SHOE SPONSOR features. In this case we can see that distributions of the levels of the SHOE SPONSOR feature are not the same for each position. From this we can again conclude that guards are more likely to have a shoe sponsor than players in the other positions.

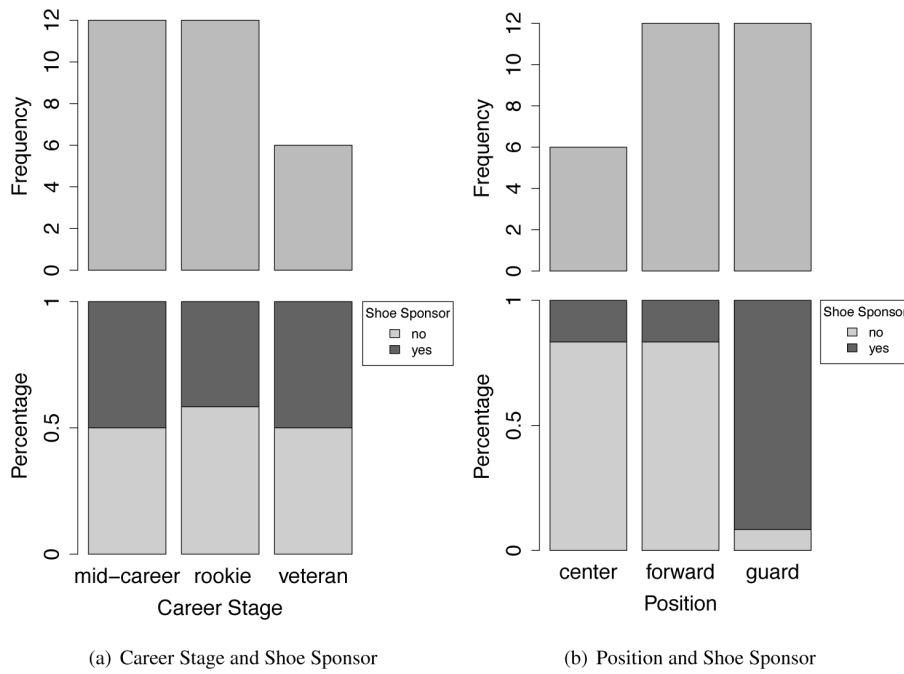


Figure 3.8

Examples of using stacked bar plot visualizations to illustrate the relationship between two categorical features: (a) CAREER STAGE and SHOE SPONSOR features; and (b) POSITION and SHOE SPONSOR features, all from [Table 3.7](#)^[73].

3.5.1.3 Visualizing a categorical feature and a continuous feature

The best way to visualize the relationship between a continuous feature and a categorical feature is to use a small multiples approach, drawing a density histogram of the values of the continuous feature for each level of the categorical feature. Each histogram includes only those instances in the dataset that have the associated level of the categorical feature. Similar to using small multiples for categorical features, if the features are unrelated (or independent), then the histograms for each level should be very similar. If the features are related, however, then the shapes and/or the central tendencies of the histograms will be different.

[Figure 3.9\(a\)](#)^[79] shows a histogram of the AGE feature from the dataset in [Table 3.7](#)^[73]. We can see from this histogram that AGE follows a uniform distribution across a range from about 19 to about 35. [Figure 3.9\(c\)](#)^[79] shows small multiple histograms for values of AGE broken down by the different levels of the POSITION feature. These histograms show a slight tendency for centers to be a little older than guards and forwards, but the relationship does not appear very strong, as each of the smaller histograms

are similar to the overall uniform distribution of the AGE feature. [Figures 3.9\(b\)](#)^[79] and [3.9\(d\)](#)^[79] show a second example, this time for the HEIGHT and POSITION features. From [Figure 3.9\(b\)](#)^[79] we can see that HEIGHT follows a normal distribution centered around a mean of approximately 194. The three smaller histograms depart from this distribution and suggest that centers tend to be taller than forwards, who in turn tend to be taller than guards.

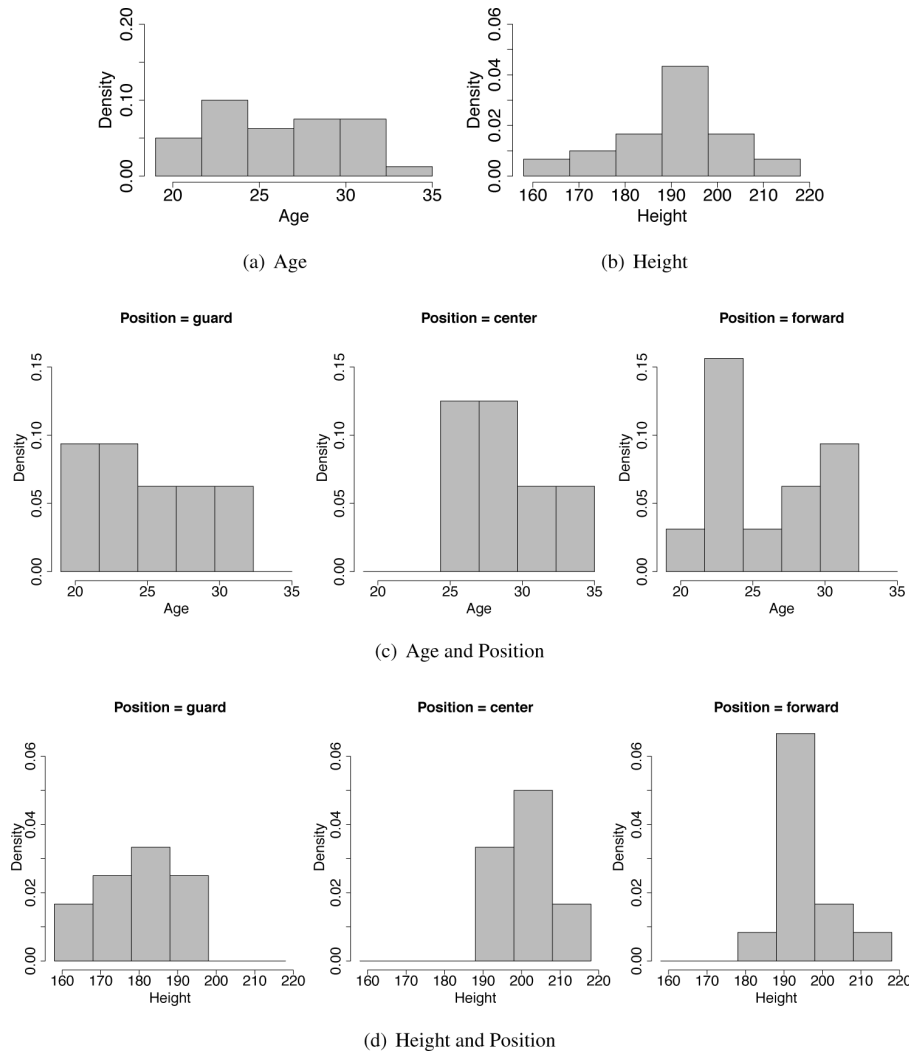


Figure 3.9

Example of using small multiple histograms to visualize the relationship between a categorical feature and a continuous feature. All examples use data from the professional basketball team dataset in [Table 3.7](#)^[73]: (a) a histogram of the AGE feature; (b) a histogram of the HEIGHT feature; (c) histograms of the AGE feature for instances displaying each level of the POSITION feature; and (d) histograms of the HEIGHT feature for instances displaying each level of the POSITION feature.

An alternative approach to using small multiples to visualize the relationship between a categorical feature and a continuous feature is to use a collection of box plots. For each level of the categorical feature, a box plot of the corresponding values of the continuous feature is drawn. This gives multiple box plots that offer an easy comparison of how the central tendency and variation of the continuous feature change for the different levels of the categorical feature. When a relationship exists between the two features, the box plots should show differing central tendencies and variations. When no relationship exists, the box plots should all appear similar.

In [Figures 3.10\(a\)^{\[80\]}](#) and [3.10\(b\)^{\[80\]}](#) we illustrate the multiple box plot approach using the AGE and POSITION features from the dataset in [Table 3.7^{\[73\]}](#). [Figure 3.10\(a\)^{\[80\]}](#) shows a box plot for AGE across the full dataset, while [Figure 3.10\(b\)^{\[80\]}](#) shows individual box plots for AGE for each level of the POSITION feature. Similar to the histograms in [Figure 3.9^{\[79\]}](#), this visualization shows a slight indication that centers tend to be older than forwards and guards, but the three box plots overlap significantly, suggesting that this relationship is not very strong.

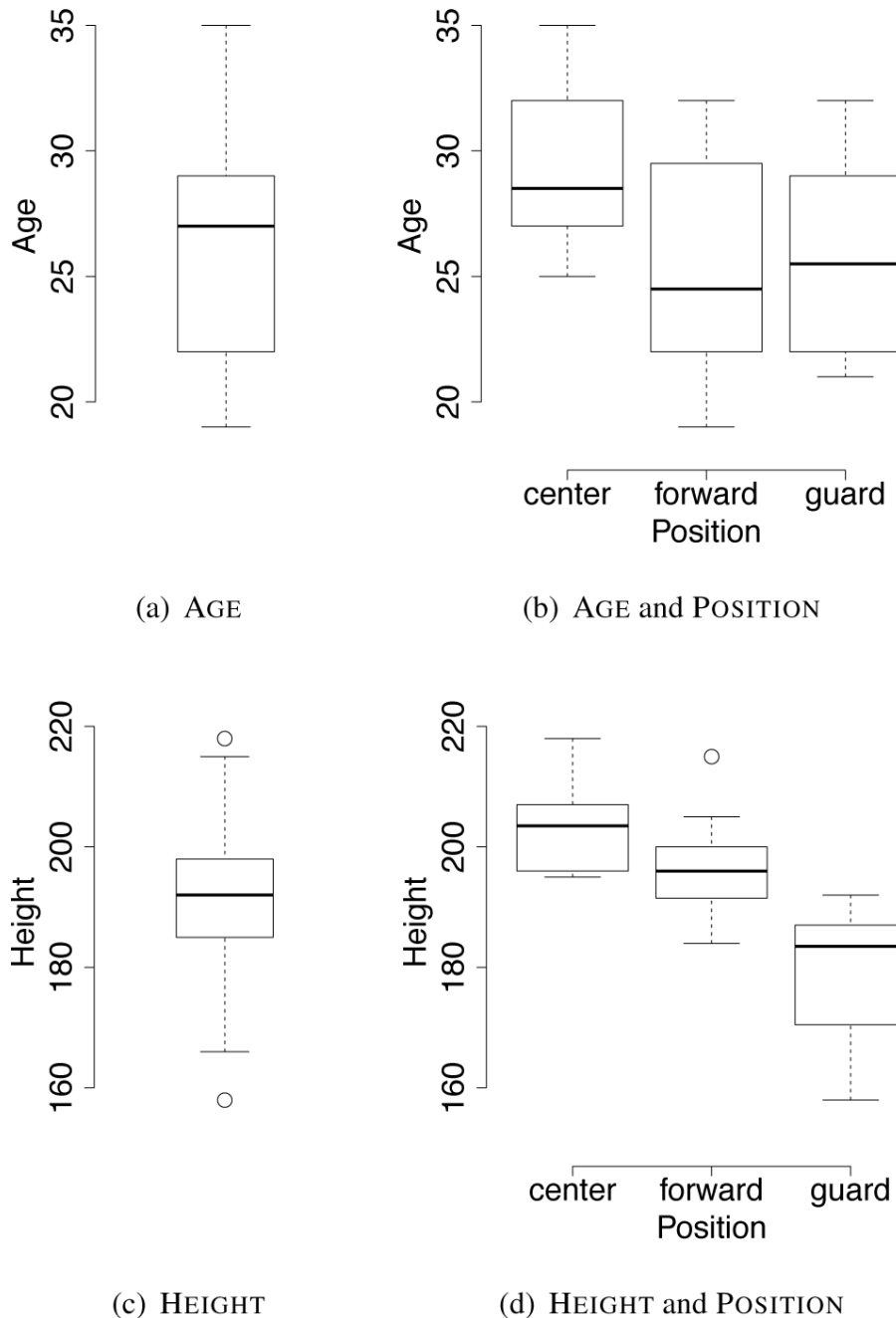


Figure 3.10

Using box plots to visualize the relationships between categorical and continuous features from Table 3.7^[73]: (a) and (b) show the relationship between the POSITION feature and the AGE feature; and (c) and (d) show the relationship between the POSITION feature and the HEIGHT feature.

Figures 3.10(c)^[80] and 3.10(d)^[80] show a similar pair of visualizations for the HEIGHT and POSITION features. Figure 3.10(d)^[80] is typical of a series of box plots showing a strong relationship between a continuous and a categorical feature. We can see that the average height of centers is above

that of forwards, which in turn is above that of guards. Although the whiskers show that there is some overlap between the three groups, they do appear to be well separated.

Histograms show more detail than box plots, so small multiple histograms offer a more detailed view of the relationship between two features. The differences in central tendency and variation between levels can, however, be easier to see in box plots. Box plots are also better suited when the categorical feature has many levels—beyond four levels, small multiple histograms tend to be difficult to interpret. A good approach is to use box plots to initially determine which pairs of features might have a strong relationship and then further investigate these pairs using small multiple histograms.

3.5.2 Measuring Covariance and Correlation

As well as visually inspecting scatter plots, we can calculate formal measures of the relationship between two continuous features using **covariance** and **correlation**. For two features, a and b , in a dataset of n instances, the **sample covariance** between a and b is

$$\text{cov}(a, b) = \frac{1}{n-1} \sum_{i=1}^n ((a_i - \bar{a}) \times (b_i - \bar{b})) \quad (3.3)$$

where a_i and b_i are values of features a and b for the i^{th} instance in a dataset, and \bar{a} and \bar{b} are the sample means of features a and b . Covariance values fall into the range $[-\infty, \infty]$ where negative values indicate a negative relationship, positive values indicate a positive relationship, and values near zero indicate that there is little or no relationship between the features.

Table 3.8

Calculating covariance.

ID	HEIGHT		WEIGHT		$(h - \bar{h}) \times$		AGE	$(h - \bar{h}) \times$	
	(<i>h</i>)	$h - \bar{h}$	(<i>w</i>)	$w - \bar{w}$	(<i>w</i> − \bar{w})	(<i>a</i>)	$a - \bar{a}$	(<i>a</i> − \bar{a})	
1	192	0.9	218	3.0	2.7	29	2.6		2.3
2	218	26.9	251	36.0	967.5	35	8.6		231.3
3	197	5.9	221	6.0	35.2	22	-4.4		-26.0
4	192	0.9	219	4.0	3.6	22	-4.4		-4.0
5	198	6.9	223	8.0	55.0	29	2.6		17.9
					...				
26	191	-0.1	218	3.0	-0.3	19	-7.4		0.7
27	196	4.9	235	20.0	97.8	32	5.6		27.4
28	198	6.9	221	6.0	41.2	22	-4.4		-30.4
29	207	15.9	247	32.0	508.3	27	0.6		9.5
30	201	9.9	244	29.0	286.8	25	-1.4		-13.9
Mean	191.1		215.0				26.4		
Std. Dev.	13.6		19.8				4.2		
Sum					7,009.9				570.8

The table shows how the $((a_i - \bar{a}) \times (b_i - \bar{b}))$ portion of Equation (3.3)^[81] is calculated for each instance in a dataset to arrive at the sum required in the calculation. The relevant means and standard deviations are also shown (standard deviation is not required to calculate covariance but is included as it will be useful later for calculating correlation).

Table 3.8^[82] shows the workings for the calculation of the covariance between the HEIGHT feature and the WEIGHT and AGE features from the dataset in **Table 3.7**^[73]. The table shows how the $((a_i - \bar{a}) \times (b_i - \bar{b}))$ portion of Equation (3.3)^[81] is calculated for each instance in the dataset for the two covariance calculations. Given this table we can calculate the covariances as follows:

$$\begin{aligned} cov(\text{HEIGHT}, \text{WEIGHT}) &= \frac{7,009.9}{29} = 241.72 \\ cov(\text{HEIGHT}, \text{AGE}) &= \frac{570.8}{29} = 19.7 \end{aligned}$$

These figures indicate that there is a strong positive relationship between the height and weight of a player, and a much smaller positive relationship

between height and age. This supports the relationships suggested by the scatter plots of these pairs of features shown in Figures 3.5(a)^[74] and 3.5(c)^[74].

This example also illustrates a problem with using covariance. Covariance is measured in the same units as the features that it measures. As a result, comparing the covariance between pairs of features only makes sense if each pair of features is composed of the same mixture of units. Correlation⁷ is a normalized form of covariance that ranges between – 1 and + 1. We calculate the correlation between two features by dividing the covariance between the two features by the product of their standard deviations. The correlation between two features, a and b , can be calculated as

$$\text{corr}(a, b) = \frac{\text{cov}(a, b)}{\text{sd}(a) \times \text{sd}(b)} \quad (3.4)$$

where $\text{cov}(a,b)$ is the covariance between features a and b and $\text{sd}(a)$ and $\text{sd}(b)$ are the standard deviations of a and b respectively. Because correlation is normalized, it is dimensionless and, consequently, does not suffer from the interpretability difficulties associated with covariance. Correlation values fall into the range [–1, 1], where values close to – 1 indicate a very strong negative correlation (or covariance), values close to 1 indicate a very strong positive correlation, and values around 0 indicate no correlation. Features that have no correlation are said to be **independent**.

The correlations between the HEIGHT and WEIGHT and AGE features can be calculated, using the covariances and standard deviations from Table 3.8^[82], as follows:

$$\begin{aligned} \text{corr}(\text{Height}, \text{Weight}) &= \frac{241.72}{13.6 \times 19.8} = 0.898 \\ \text{corr}(\text{Height}, \text{Age}) &= \frac{19.7}{13.6 \times 4.2} = 0.345 \end{aligned}$$

These correlation values are much more useful than the covariances calculated previously because they are on a normalized scale, which allows us to compare the strength of the relationships to each other. There is a strong positive correlation between HEIGHT and WEIGHT features, but very little correlation between HEIGHT and AGE.

In the majority of ABTs there are multiple continuous features between which we would like to explore relationships. Two tools that can be useful for this are the covariance matrix and the correlation matrix. A covariance matrix contains a row and column for each feature, and each element of the matrix lists the covariance between the corresponding pairs of features. As a result, the elements along the main diagonal list the covariance between a feature and itself, in other words, the variance of the feature. The covariance matrix, usually denoted as Σ , between a set of continuous features, $\{a, b, \dots, z\}$, is given as

$$\sum_{\{a,b,\dots,z\}} = \begin{bmatrix} \text{var}(a) & \text{cov}(a, b) & \cdots & \text{cov}(a, z) \\ \text{cov}(b, a) & \text{var}(b) & \cdots & \text{cov}(b, z) \\ \vdots & \vdots & \ddots & \vdots \\ \text{cov}(z, a) & \text{cov}(z, b) & \cdots & \text{var}(z) \end{bmatrix} \quad (3.5)$$

Similarly, the correlation matrix is just a normalized version of the covariance matrix and shows the correlation between each pair of features:

$$\text{correlation matrix}_{\{a,b,\dots,z\}} = \begin{bmatrix} \text{corr}(a, a) & \text{corr}(a, b) & \cdots & \text{corr}(a, z) \\ \text{corr}(b, a) & \text{corr}(b, b) & \cdots & \text{corr}(b, z) \\ \vdots & \vdots & \ddots & \vdots \\ \text{corr}(z, a) & \text{corr}(z, b) & \cdots & \text{corr}(z, z) \end{bmatrix} \quad (3.6)$$

The covariance and correlation matrices for the HEIGHT, WEIGHT and AGE features are

$$\sum_{\{\text{Height}, \text{Weight}, \text{Age}\}} = \begin{bmatrix} 185.128 & 241.72 & 19.7 \\ 241.72 & 392.102 & 24.469 \\ 19.7 & 24.469 & 17.697 \end{bmatrix}$$

and

$$\text{correlation matrix}_{\{\text{Height}, \text{Weight}, \text{Age}\}} = \begin{bmatrix} 1.0 & 0.898 & 0.345 \\ 0.898 & 1.0 & 0.294 \\ 0.345 & 0.294 & 1.0 \end{bmatrix}$$

The scatter plot matrices (SPLOMs) described in Section 3.5.1^[72] are really a visualization of the correlation matrix. This can be made more obvious by including the correlation coefficients in SPLOMs in the cells above the diagonal. In Figure 3.11^[85] the cells above the diagonal show the correlation coefficients for each pair of features. The font sizes of the correlation coefficients are scaled according to the absolute value of the strength of the correlation to draw attention to those pairs of features with the strongest relationships.

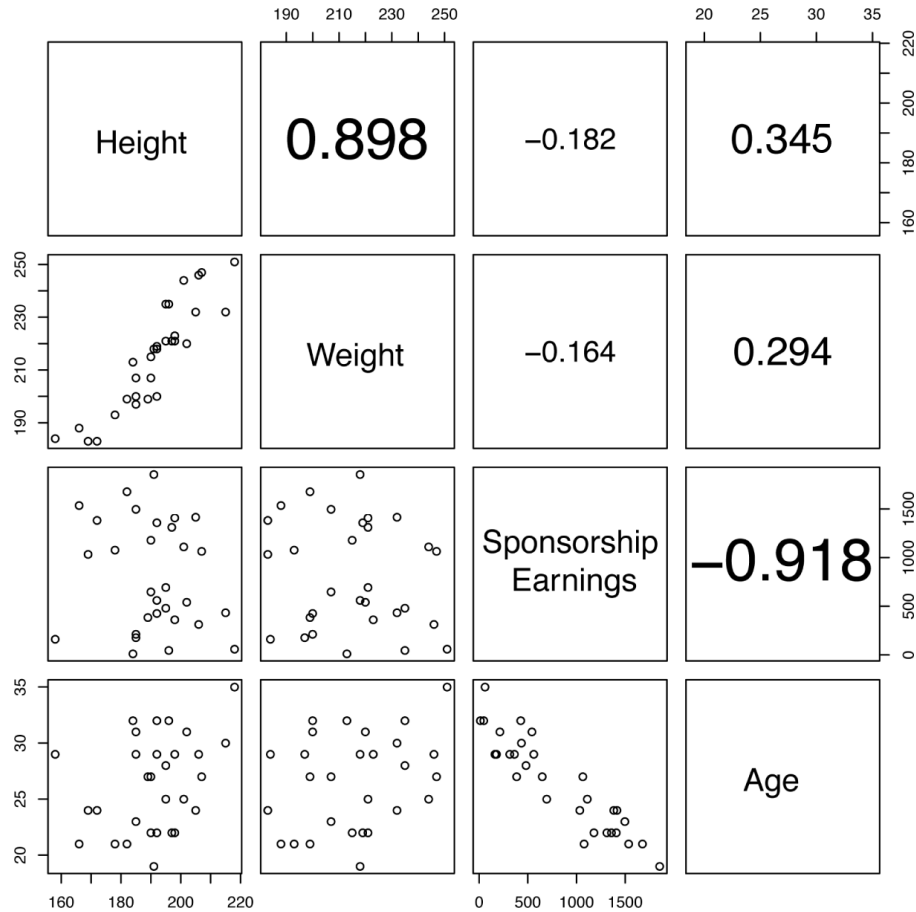


Figure 3.11

A scatter plot matrix showing scatter plots of the continuous features from the professional basketball team dataset in Table 3.7^[73] with correlation coefficients included.

Correlation is a good measure of the relationship between two continuous features, but it is not by any means perfect. First, the correlation measure given in Equation (3.4)^[82] responds only to linear relationships between features. In a linear relationship between two features, as one

feature increases or decreases, the other feature increases or decreases by a corresponding amount. Frequently, features will have very strong non-linear relationships that correlation does not respond to. Also, peculiarities in a dataset can affect the calculation of the correlation between two features.

This problem is illustrated very clearly in the famous example of Anscombe's quartet,⁸ shown in [Figure 3.12](#)^[86]. This is a series of four pairs of features that all have the same correlation value of 0.816, even though they exhibit very different relationships.

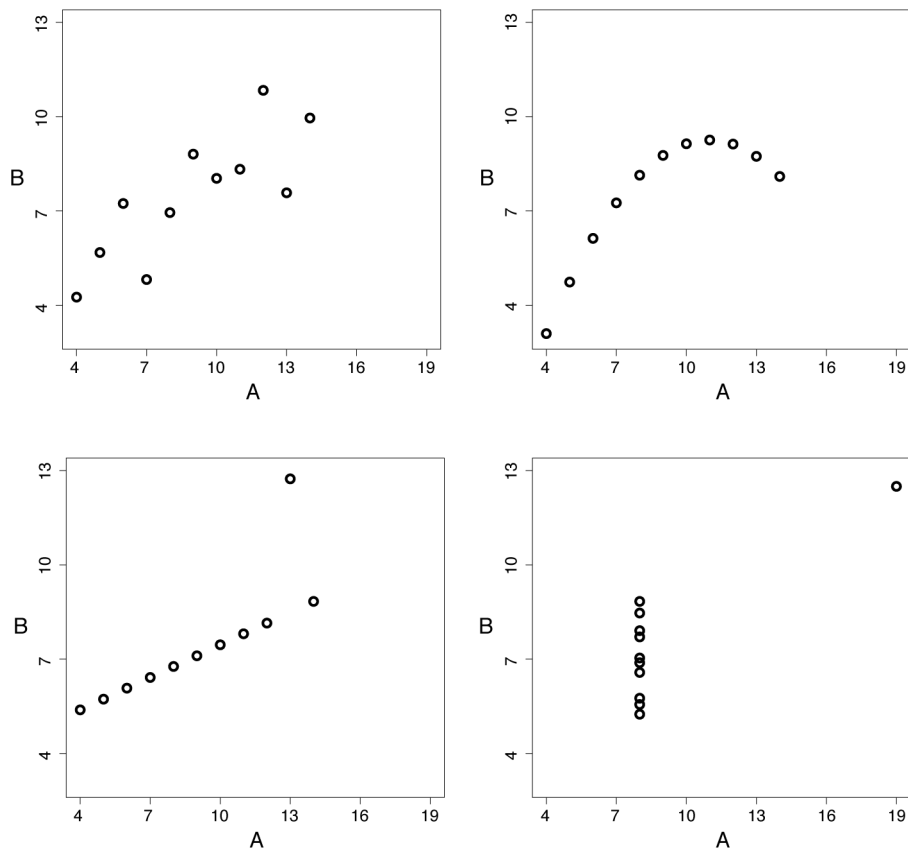


Figure 3.12

Anscombe's quartet. For all four samples, the correlation measure returns the same value (0.816) even though the relationship between the features is very different in each case.

Perhaps the most important thing to remember in relation to correlation is that *correlation does not necessarily imply causation*. Just because the values of two features are correlated does not mean that an actual causal relationship exists between the two. There are two main ways in which causation can be mistakenly assumed. The first is by mistaking the order of a causal relationship. For example, based on correlations tests alone, we

might conclude that the presence of swallows cause hot weather, that spinning windmills cause wind, and that playing basketball causes people to be tall. In fact, swallows migrate to warmer countries, windmills are made to spin by wind, and tall people often choose to play basketball because of the advantage their height gives them in that game.

The second kind of mistake that makes people incorrectly infer causation between two features is ignoring a third important, but hidden, feature. In a famous example of this, an article was published in the prestigious journal *Nature* outlining a causal relationship between young children sleeping with a night-light turned on and these children developing near-sightedness in later life (Quinn et al., 1999). Later studies (Zadnik et al., 2000; Gwiazda et al., 2000), however, could not replicate this link, and eventually a more plausible explanation for the correlation between night-light use and near-sightedness was uncovered. Near-sighted parents, because of their poor night vision, tend to favor the use of night-lights to help them find their way around their children's bedrooms at night. Near-sighted parents are more likely to have near-sighted children, and it is this that accounts for the correlation between night-light use and near-sightedness in children, rather than any causal link. This is an example of a confounding feature, a feature that influences two others and so leads to the appearance of a causal relationship. Confounding features are a common explanation of mistaken conclusions about causal relationships. The lesson to be learned here is that before causation is concluded based on a strong correlation between two features, in-depth studies involving domain experts are required—correlation alone is just not enough. In spite of these difficulties, for machine learning purposes, correlation is a very good measure of the relationship between two continuous features.⁹

3.6 Data Preparation

Instead of explicitly handling problems like noise within the data in an ABT, some data preparation techniques change the way data is represented just to make it more compatible with certain machine learning algorithms. This section describes two of the most common such techniques: binning and normalization. Both techniques focus on transforming an individual feature in some way. There are also situations, however, where we wish to change the size and/or the distributions of target values within the ABT. We

describe a range of different **sampling** techniques that can be used to do this. As with the techniques described in the previous section, sometimes these techniques are performed as part of the Data Preparation phase of CRISP-DM, but sometimes they are performed as part of the Modeling phase.

3.6.1 Normalization

Having continuous features in an ABT that cover very different ranges can cause difficulty for some machine learning algorithms. For example, a feature representing customer ages might cover the range [16,96], whereas a feature representing customer salaries might cover the range [10,000, 100,000]. **Normalization** techniques can be used to change a continuous feature to fall within a specified range while maintaining the relative differences between the values for the feature. The simplest approach to normalization is **range normalization**, which performs a linear scaling of the original values of the continuous feature into a given range. We use range normalization to convert a feature value into the range $[low, high]$ as follows:

$$a'_i = \frac{a_i - min(a)}{max(a) - min(a)} \times (high - low) + low \quad (3.7)$$

where a'_i is the normalized feature value, a_i is the original value, $min(a)$ is the minimum value of feature a , $max(a)$ is the maximum value of feature a , and low and $high$ are the minimum and maximum values of the desired range. Typical ranges used for normalizing feature values are $[0,1]$ and $[-1,1]$. [Table 3.9](#)^[88] shows the effect of applying range normalization to a small sample of the HEIGHT and SPONSORSHIP EARNINGS features from the dataset in [Table 3.7](#)^[73].

Table 3.9

A small sample of the HEIGHT and SPONSORSHIP EARNINGS features from the professional basketball team dataset in [Table 3.7](#)^[73], showing the result of range normalization and standardization.

Values	HEIGHT		SPONSORSHIP EARNINGS		
	Range	Standard	Values	Range	Standard
192	0.500	-0.073	561	0.315	-0.649
197	0.679	0.533	1,312	0.776	0.762
192	0.500	-0.073	1,359	0.804	0.850
182	0.143	-1.283	1,678	1.000	1.449
206	1.000	1.622	314	0.164	-1.114
192	0.500	-0.073	427	0.233	-0.901
190	0.429	-0.315	1,179	0.694	0.512
178	0.000	-1.767	1,078	0.632	0.322
196	0.643	0.412	47	0.000	-1.615
201	0.821	1.017	1,111	0.652	0.384
Max	206		1,678		
Min	178		47		
Mean	193		907		
Std. Dev.	8.26		532.18		

Range normalization has the drawback that it is quite sensitive to the presence of outliers in a dataset. Another way to normalize data is to **standardize** it into **standard scores**.¹⁰ A standard score measures how many standard deviations a feature value is from the mean for that feature. To calculate a standard score, we compute the mean and standard deviation for the feature and normalize the feature values using the following equation:

$$a'_i = \frac{a_i - \bar{a}}{sd(a)} \quad (3.8)$$

where a'_i is the normalized feature value, a_i is the original value, \bar{a} is the mean for feature a , and $sd(a)$ is the standard deviation for a . Standardizing feature values in this way squashes the values of the feature so that the feature values have a mean of 0 and a standard deviation of 1. This results in the majority of feature values being in a range of $[-1,1]$. We should take

care when using standardization as it assumes that data is normally distributed. If this assumption does not hold, then standardization may introduce some distortions. Table 3.9^[88] also shows the effect of applying standardization to the HEIGHT and SPONSORSHIP EARNINGS features.

In upcoming chapters we use normalization to prepare data for use with machine learning algorithms that require descriptive features to be in particular ranges. As is so often the case in data analytics, there is no hard and fast rule that says which is the best normalization technique, and this decision is generally made based on experimentation.

3.6.2 Binning

Binning involves converting a continuous feature into a categorical feature. To perform binning, we define a series of ranges (called **bins**) for the continuous feature that correspond to the levels of the new categorical feature we are creating. The values for the new categorical feature are then created by assigning to instances in the dataset the level of the new feature that corresponds to the range that their value of the continuous feature falls into. There are many different approaches to binning. We will introduce two of the more popular: **equal-width binning** and **equal-frequency binning**.

Both equal-width and equal-frequency binning require that we manually specify how many bins we would like to use. Deciding on the number of bins can be difficult. The general trade-off is this:

- If we set the number of bins to a very low number—for example, two or three bins—(in other words, we abstract to a very low level of resolution), we may lose a lot of information with respect to the distribution of values in the original continuous feature. Using a small number of bins, however, has the advantage of having a large number of instances in each bin.
- If we set the number of bins to a high number—for example, 10 or more —then, just because there are more bin boundaries, it is more likely that at least some of our bins will align with interesting features of the distribution of the original continuous feature. This means that our binning categories will provide a better representation of this distribution. However, the more bins we have, the fewer instances we will have in each bin. Indeed, as the number of bins grows, we can end up with empty bins.

[Figure 3.13](#)^[90] illustrates the effect of using different numbers of bins.¹¹ In this example, the dashed line represents a multimodal distribution from which a set of continuous feature values has been generated. The histogram represents the bins. Ideally the histogram heights should follow the dashed line. In [Figure 3.13\(a\)](#)^[90] there are three bins that are each quite wide, and the histogram heights don't really follow the dashed line. This indicates that this binning does not accurately represent the real distribution of values in the underlying continuous feature. In [Figure 3.13\(b\)](#)^[90] there are 14 bins. In general, the histogram heights follow the dashed line, so the resulting bins can be considered a reasonable representation of the continuous feature. Also, there are no gaps between the histogram bars, which indicates that there are no empty bins. Finally, [Figure 3.13\(c\)](#)^[90] illustrates what happens when we used 60 bins. The histogram heights fit the contour line to an extent, but there is a greater variance in the heights across the bins in this image. Some of the bins are very tall and other bins are empty, as indicated by the gaps between the bars. When we compare, the three images, 14 bins seems to best model the data. Unfortunately, there is no guaranteed way of finding the optimal number of bins for a set of values for a continuous feature. Often, choosing the number of bins comes down to intuition and a process of trial and error experimentation.

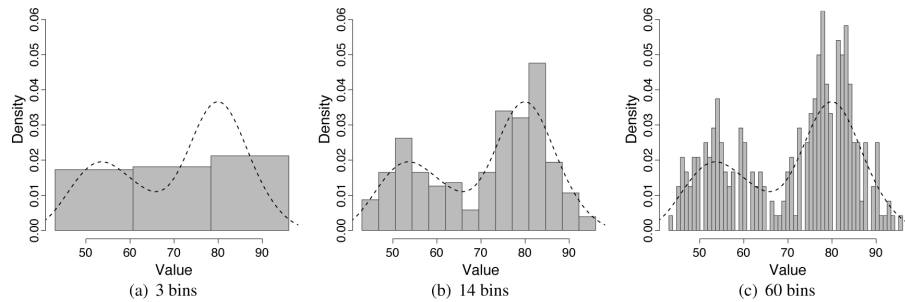


Figure 3.13

The effect of using different numbers of bins when using binning to convert a continuous feature into a categorical feature.

Once the number of bins, b , has been chosen, the equal-width binning algorithm splits the range of the feature values into b bins each of size $\frac{\text{range}}{b}$. For example, if the values for a feature fell between zero and 100 and we wished to have 10 bins, then bin 1 would cover the interval¹² $[0,10)$, bin 2 would cover the interval $[10,20)$, and so on, up to bin 10, which would

cover the interval [90,100]. Consequently, an instance with a feature value of 18 would be placed into bin 2.

Equal-width binning is simple and intuitive, and can work well in practice. However, as the distribution of values in the continuous feature moves away from a uniform distribution, then some bins will end up with very few instances in them, and other bins will have a lot of instances in them. For example, imagine our data followed a normal distribution: then the bins covering the intervals of the feature range at the tails of the normal distribution will have very few instances, and the bins covering the intervals of the feature range near the mean will contain a lot of instances. This scenario is illustrated in [Figures 3.14\(a\)](#)^[92] to [3.14\(c\)](#)^[92], which shows a continuous feature following a normal distribution converted into different numbers of bins using equal-width binning. The problem with this is that we are essentially wasting bins because some of the bins end up representing a very small number of instances (the height of the bars in the diagram shows the number of instances in each bin). If we were able to merge the bins in the regions where there are very few instances, then the resulting spare bins could be used to represent the differences between instances in the regions where lots of instances are clustered together. Equal-frequency binning does this.

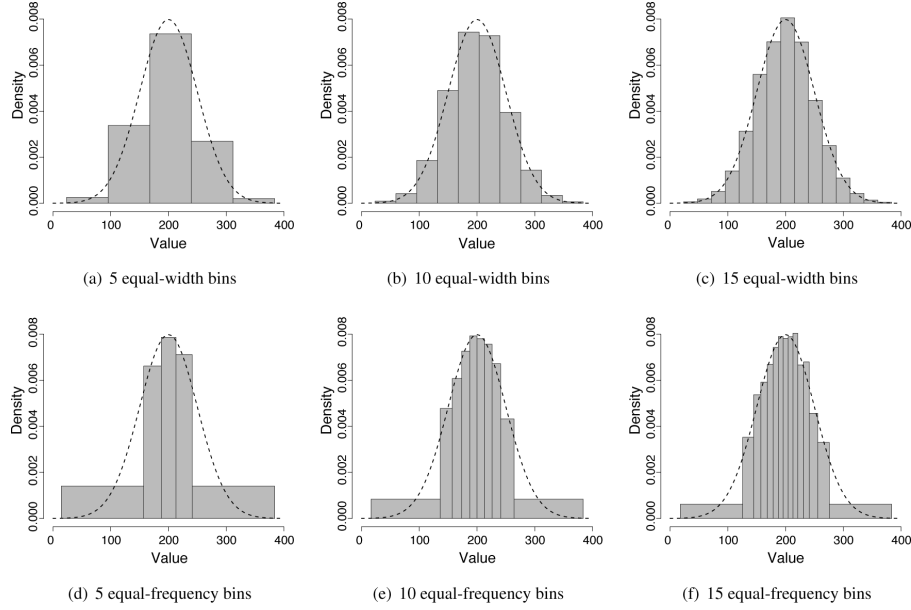


Figure 3.14

(a)–(c) Equal-frequency binning of normally distributed data with different numbers of bins; and (d)–(f) the same data binned into the same number of bins using equal-width binning. The dashed lines illustrate the distribution of the original continuous feature values, and the gray boxes represent the bins.

Equal-frequency binning first sorts the continuous feature values into ascending order and then places an equal number of instances into each bin, starting with bin 1. The number of instances placed in each bin is simply the total number of instances divided by the number of bins, b . For example, if we had 10,000 instances in our dataset and we wish to have 10 bins, then bin 1 would contain the 1,000 instances with the lowest values for the feature, and so on, up to bin 10, which would contain the 1,000 instances with the highest feature values. Figures 3.14(d)^[92] to 3.14(f)^[92] show the same normally distributed continuous feature mentioned previously binned into different numbers of bins using equal-frequency binning.¹³

Using Figure 3.14^[92] to compare these two approaches to binning, we can see that by varying the width of the bins, equal-frequency binning uses bins to more accurately model the heavily populated areas of the range of values the continuous feature can take. The downside to this is that the resulting bins can appear slightly less intuitive because they are of varying sizes.

Regardless of the binning approach used, once the values for a continuous feature have been binned, the continuous feature is discarded

and replaced by a categorical feature, which has a level for each bin—the bin numbers can be used, or a more meaningful label can be manually generated. We will see in forthcoming chapters that using binning to transform a continuous feature into a categorical feature is often the easiest way for some of the machine learning approaches to handle a continuous feature. Another advantage of binning, especially equal-frequency binning, is that it goes some way toward handling outliers. Very large or very small values simply end up in the highest or lowest bin. It is important to remember, though, that no matter how well it is done, binning always discards information from the dataset because it abstracts from a continuous representation to a coarser categorical resolution.

3.6.3 Sampling

In some predictive analytics scenarios, the dataset we have is so large that we do not use all the data available to us in an ABT and instead **sample** a smaller percentage from the larger dataset. We need to be careful when sampling, however, to ensure that the resulting datasets are still representative of the original data and that no unintended bias is introduced during this process. Biases are introduced when, due to the sampling process, the distributions of features in the sampled dataset are very different from the distributions of features in the original dataset. The danger of this is that any analysis or modeling we perform on this sample will not be relevant to the overall dataset.

The simplest form of sampling is **top sampling**, which simply selects the top $s\%$ of instances from a dataset to create a sample. Top sampling runs a serious risk of introducing bias, however, as the sample will be affected by any ordering of the original dataset. For this reason, we recommend that top sampling be avoided.

A better choice, and our recommended default, is **random sampling**, which randomly selects a proportion of $s\%$ of the instances from a large dataset to create a smaller set. Random sampling is a good choice in most cases, as the random nature of the selection of instances should avoid introducing bias.

Sometimes there are very specific relationships in a dataset that we want to maintain in a sample. For example, if we have a categorical target feature, we may want to ensure that the sample has exactly the same

distribution of the different levels of the target feature as the original dataset. In most cases random sampling will maintain distributions; however, if there are one or more levels of a categorical feature that only a very small proportion of instances in a dataset have, there is a chance that these will be omitted or underrepresented by random sampling. **Stratified sampling** is a sampling method that ensures that the relative frequencies of the levels of a specific stratification feature are maintained in the sampled dataset.

To perform stratified sampling, the instances in a dataset are first divided into groups (or strata), where each group contains only instances that have a particular level for the stratification feature. The $s\%$ of the instances in each stratum are then randomly selected, and these selections are combined to give an overall sample of $s\%$ of the original dataset. Remember that each stratum will contain a different number of instances, so by sampling on a percentage basis from each stratum, the number of instances taken from each stratum will be proportional to the number of instances in each stratum. As a result, this sampling strategy is guaranteed to maintain the relative frequencies of the different levels of the stratification feature.

In contrast to stratified sampling, sometimes we would like a sample to contain different relative frequencies of the levels of a particular feature than the distribution in the original dataset. For example, we may wish to create a sample in which the levels of a particular categorical feature are represented equally, rather than with whatever distribution they had in the original dataset. To do this, we can use **under-sampling** or **over-sampling**.

Like stratified sampling, under-sampling begins by dividing a dataset into groups, where each group contains only instances that have a particular level for the feature to be under-sampled. The number of instances in the *smallest* group is the under-sampling target size. Each group containing more instances than the smallest one is then randomly sampled by the appropriate percentage to create a subset that is the under-sampling target size. These under-sampled groups are then combined to create the overall under-sampled dataset.

Over-sampling addresses the same issue as under-sampling but in the opposite way around. After dividing the dataset into groups, the number of instances in the *largest* group becomes the over-sampling target size. From each smaller group, we then create a sample containing that number of

instances. To create a sample that is larger than the size of the group that we are sampling from, we use random sampling with replacement. This means that when an instance is randomly selected from the original dataset, it is replaced into the dataset so that it might be selected again. The consequence of this is that each instance from the original dataset can appear more than once in the sampled dataset.¹⁴ After having created the larger samples from each group, we combine these to form the overall over-sampled dataset.

Sampling techniques can be used to reduce the size of a large ABT to make exploratory analysis easier, to change the distributions of target features in an ABT, and to generate different portions of an ABT to use for training and evaluating a model.

3.7 Summary

For a data analytics practitioner, the key outcomes of the **data exploration** process (which straddles the **Data Understanding** and **Data Preparation** phases of **CRISP-DM**) are that the practitioner should

1. Have *gotten to know* the features within the ABT, especially their central tendencies, variations, and **distributions**.
2. Have identified any **data quality issues** within the ABT, in particular, **missing values**, **irregular cardinality**, and **outliers**.
3. Have corrected any data quality issues due to **invalid data**.
4. Have recorded any data quality issues due to **valid data** in a **data quality plan** along with potential handling strategies.
5. Be confident that enough good-quality data exists to continue with a project.

Although the **data quality report** is just a collection of simple descriptive statistics and visualizations of the features in an **analytics base table**, it is a very powerful tool and the key to achieving the outcomes listed above. By examining the data quality report, analytics practitioners can get a complete picture of the data that they will work with for the rest of an analytics project. In this chapter we have focused on using the data quality report to explore the data in an ABT. A data quality report, however, can also be used to explore any dataset and is commonly used to understand the data in the raw data sources that are used to populate an ABT.

We also took our first steps toward building predictive models in this chapter when we looked at **correlation**. A descriptive feature that correlates strongly with a target feature would be a good place to start building a predictive model, and we return to correlations in later chapters. Examining correlation between features as part of data exploration allows us to add extra outcomes to the list at the beginning of this section:

1. Be aware of the relationships between features in an ABT.
2. Have begun the **feature selection** exercise by removing some features from the ABT.

The previous section of the chapter (Section 3.6^[87]) focused on **data preparation** techniques that we can use on the data in an ABT. It is important to remember that when we perform data preparations (such as those in Section 3.6^[87] or those described in Section 3.4^[69]), we are changing the data that we will use to subsequently train predictive models. If we change the data too much, then the models that we build will not relate well to the original data sources when we deploy them. There is, therefore, a delicate balance that we need to strike between preparing the data so that it is appropriate for use with machine learning algorithms and keeping the data true to the underlying processes that generate it. Well-designed evaluation experiments are the best way to find this balance (we discuss evaluation in detail in Chapter 9^[533]).

The last point worth mentioning is that this chapter relates to deployment. The data in an ABT is historical data from the disparate data sources within an organization. We use this data to train and evaluate a machine learning model that will then be deployed for use on newly arising data. For example, in the motor insurance fraud detection example that we used in this chapter, the claims in the ABT were all historical. The prediction model that we would build using this data would be deployed to predict whether newly arising claims are likely to be fraudulent. It is important that the details of any data preparation techniques we perform on the data in the ABT be saved (usually in the data quality plan) so that we can also apply the same techniques to newly arising data. This is an important detail of model deployment that is sometimes overlooked, which can lead to strange model performance.

3.8 Further Reading

The basis of data exploration is statistics. Montgomery and Runger (2010) is an excellent applied introductory text in statistics and covers, in more detail, all the basic measures used in this chapter. It also covers advanced topics, such as the χ^2 test and **ANOVA test** mentioned in the notes for Section 3.5.2^[81]. Rice (2006) provides a good—if more theoretical—treatment of statistics.

For the practical details of building a data quality report, Svolba (2012, 2007) are very good, even if the SAS language is not being used. Similarly, Dalgaard (2008) is very good even if the R language is not being used. As an example of a detailed investigation into the impact of applying data preparation techniques, Batista and Monard (2003) is interesting.

Data visualization is a mix of statistics, graphic design, art, and psychology. Chang (2012) and Fry (2007) both provide great detail on visualization in general and the R language in particular (the visualizations in this book are almost all generated in R). For more conceptual discussions of data visualization, Tufte (2001) and Bertin (2010) are important works in the field.

3.9 Exercises

1. The table below shows the age of each employee at a cardboard box factory.

ID	1	2	3	4	5	6	7	8	9	10
AGE	51	39	34	27	23	43	41	55	24	25
ID	11	12	13	14	15	16	17	18	19	20
AGE	38	17	21	37	35	38	31	24	35	33

Based on this data, calculate the following **summary statistics** for the AGE feature:

- (a) Minimum, maximum, and range
- (b) Mean and median
- (c) Variance and standard deviation
- (d) 1st quartile (25th percentile) and 3rd quartile (75th percentile)
- (e) Inter-quartile range
- (f) 12th percentile

2. The table below shows the policy type held by customers at a life insurance company.

ID	POLICY	ID	POLICY	ID	POLICY
1	Silver	8	Silver	15	Platinum
2	Platinum	9	Platinum	16	Silver
3	Gold	10	Platinum	17	Platinum
4	Gold	11	Silver	18	Platinum
5	Silver	12	Gold	19	Gold
6	Silver	13	Platinum	20	Silver
7	Bronze	14	Silver		

- (a) Based on this data, calculate the following **summary statistics** for the POLICY feature:
- i. Mode and 2nd mode
 - ii. Mode % and 2nd mode %
- (b) Draw a **bar plot** for the POLICY feature.
3. An analytics consultant at an insurance company has built an **ABT** that will be used to train a model to predict the best communications channel to use to contact a potential customer with an offer of a new insurance product.¹⁵ The following table contains an extract from this ABT—the full ABT contains 5,200 instances.

ID	OCC	GENDER	AGE	LOC	MOTOR INS	MOTOR VALUE	HEALTH INS	HEALTH TYPE	HEALTH		PREF
									ADULTS	KIDS	
1	Student	female	43	urban	yes	42,632	yes	PlanC	1	2	sms
2		female	57	rural	yes	22,096	yes	PlanA	1	2	phone
3	Doctor	male	21	rural	yes	27,221	no				phone
4	Sheriff	female	47	rural	yes	21,460	yes	PlanB	1	3	phone
5	Painter	male	55	rural	yes	13,976	no				phone
14		male	19	rural	yes	48,66	no				email
15	Manager	male	51	rural	yes	12,759	no				phone
16	Farmer	male	49	rural	no		no				phone
17		female	18	urban	yes	16,399	no				sms
18	Analyst	male	47	rural	yes	14,767	no				email
2747		female	48	rural	yes	35,974	yes	PlanB	1	2	phone
2748	Editor	male	50	urban	yes	40,087	no				phone
2749		female	64	rural	yes	156,126	yes	PlanC	0	0	phone
2750	Reporter	female	48	urban	yes	27,912	yes	PlanB	1	2	email
4780	Nurse	male	49	rural	no		yes	PlanB	2	2	email
4781		female	46	rural	yes	18,562	no				phone
4782	Courier	male	63	urban	no		yes	PlanA	2	0	email
4783	Sales	male	21	urban	no		no				sms
4784	Surveyor	female	45	rural	yes	17,840	no				sms
5199	Clerk	male	48	rural	yes	19,448	yes	PlanB	1	3	email
5200	Cook	47	female	rural	yes	16,393	yes	PlanB	1	2	sms

The descriptive features in this dataset are defined as follows:

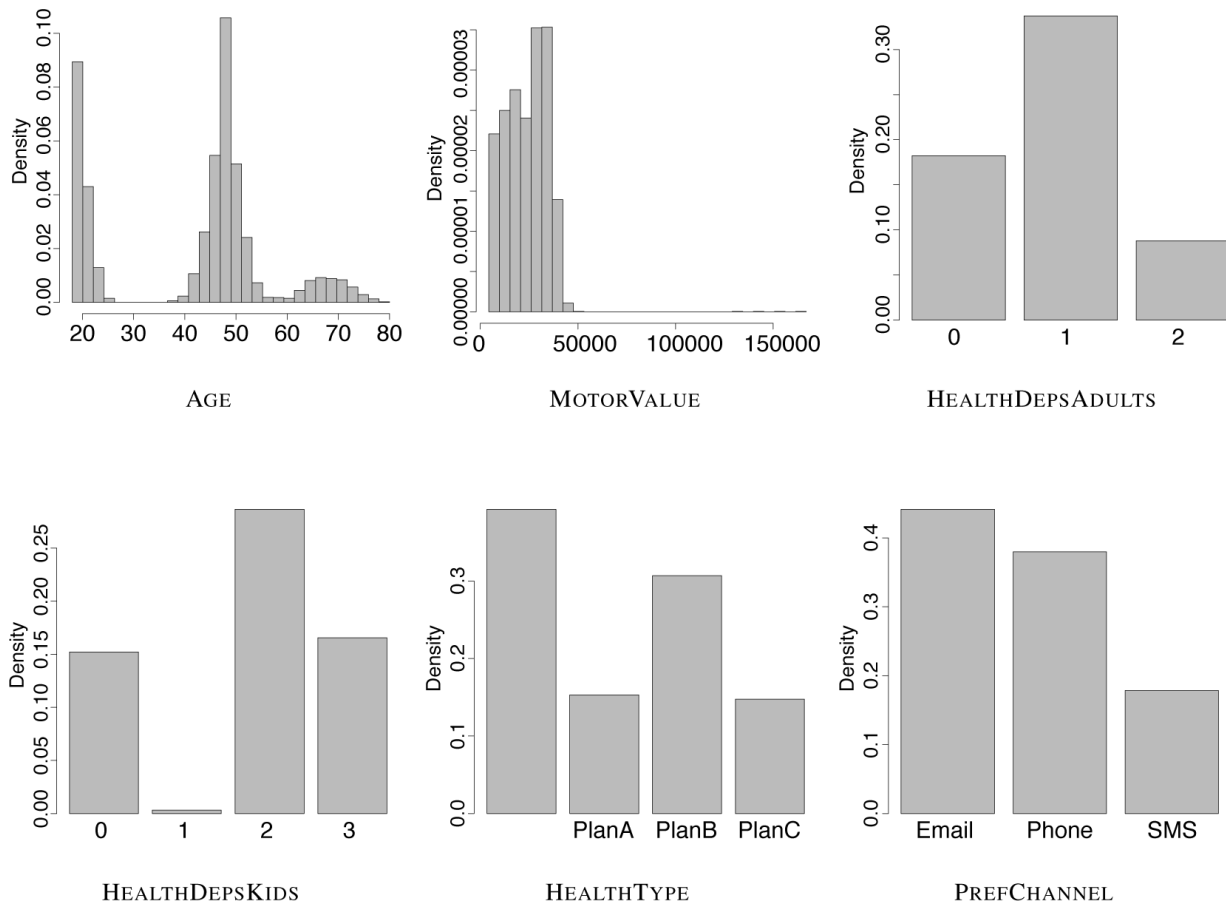
- AGE: The customer's age
- GENDER: The customer's gender (*male* or *female*)
- LOC: The customer's location (*rural* or *urban*)
- OCC: The customer's occupation
- MOTORINS: Whether the customer holds a motor insurance policy with the company (yes or no)
- MOTORVALUE: The value of the car on the motor policy
- HEALTHINS: Whether the customer holds a health insurance policy with the company (yes or no)
- HEALTHTYPE: The type of the health insurance policy (*PlanA*, *PlanB*, or *PlanC*)
- HEALTHDEPSADULTS: How many dependent adults are included on the health insurance policy

- **HEALTHDEPSKIDS**: How many dependent children are included on the health insurance policy
- **PREFCHANNEL**: The customer's preferred contact channel (*email*, *phone*, or *sms*)

The consultant generated the following **data quality report** from the ABT (visualizations of binary features have been omitted for space saving).

Feature	% Count Miss. Card. Min.				1 st Qrt. Mean Median			3 rd Qrt. Max.		Std. Dev.
AGE	5,200	0	51	18	22	41.59	47	50	80	15.66
MOTORVALUE	5,200	17.25	3,934	4,352	15,089.5	23,479	24,853	32,078	166,993	11,121
HEALTHDEPSADULTS	5,200	39.25	4	0	0	0.84	1	1	2	0.65
HEALTHDEPSKIDS	5,200	39.25	5	0	0	1.77	2	3	3	1.11

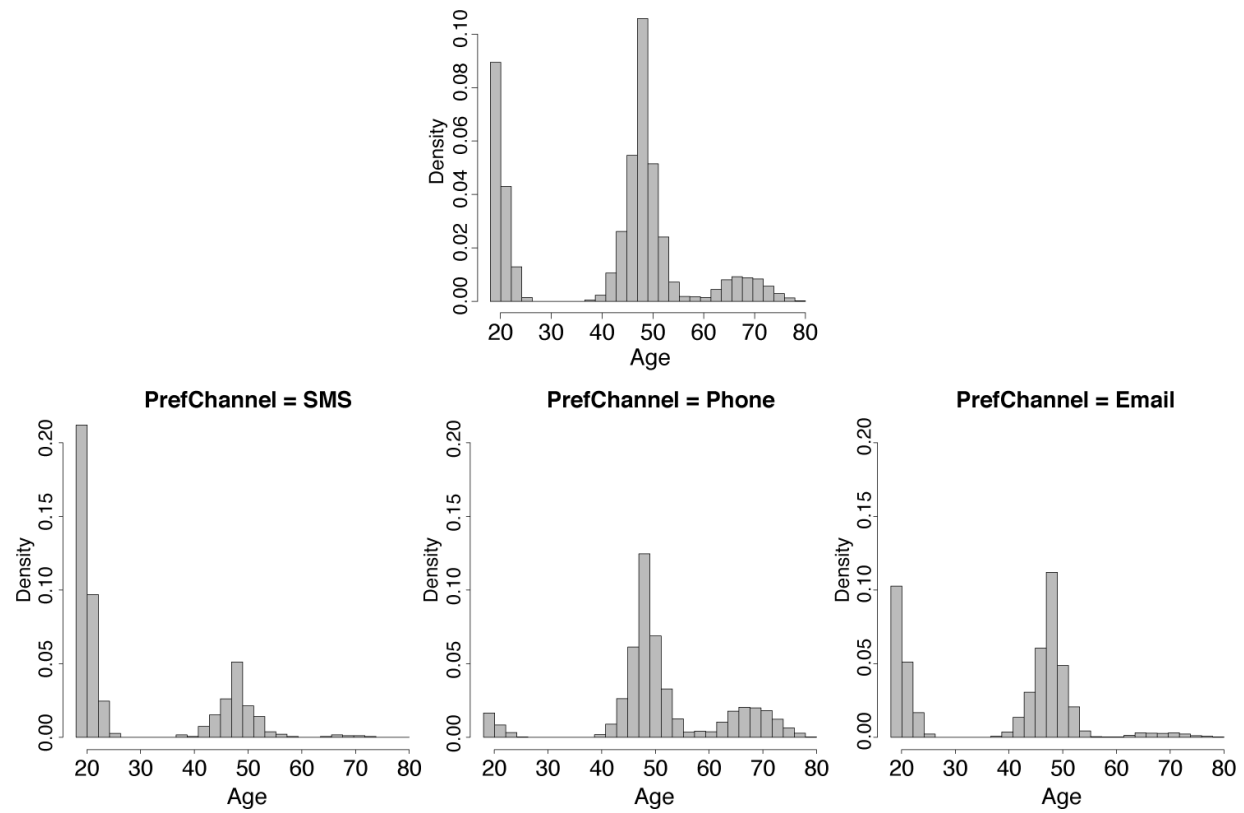
Feature	% Count Miss. Card. Mode				Mode Freq.		2 nd Mode Freq.		2 nd Mode %	
GENDER	5,200	0	2	female	2,626	50.5	male	2,574	49.5	
LOC	5,200	0	2	urban	2,948	56.69	rural	2,252	43.30	
OCC	5,200	37.71	1,828	Nurse	11	0.34	Sales	9	0.28	
MOTORINS	5,200	0	2	yes	4,303	82.75	no	897	17.25	
HEALTHINS	5,200	0	2	yes	3,159	60.75	no	2,041	39.25	
HEALTHTYPE	5,200	39.25	4	PlanB	1,596	50.52	PlanA	796	25.20	
PREFCHANNEL	5,200	0	3	email	2,296	44.15	phone	1,975	37.98	



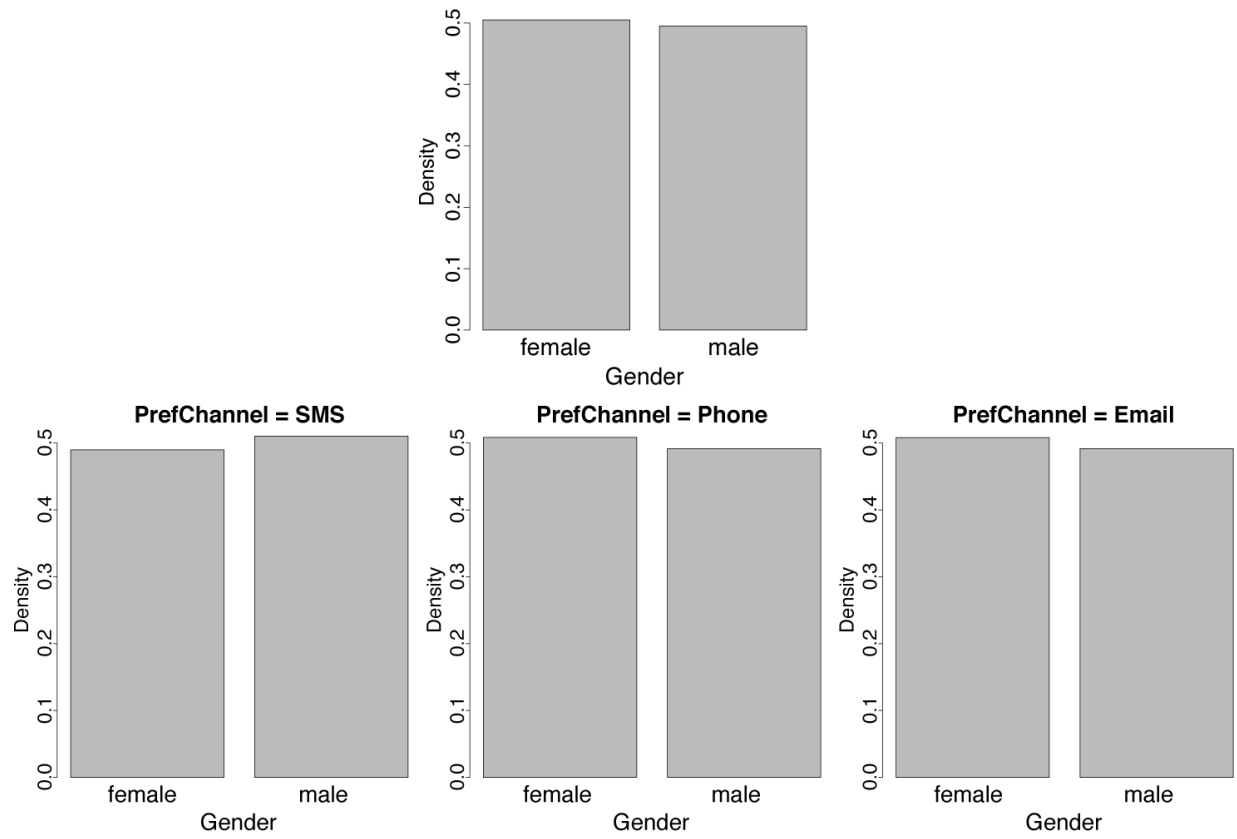
Discuss this data quality report in terms of the following:

- Missing values
 - Irregular cardinality
 - Outliers
 - Feature distributions
4. The following **data visualizations** are based on the channel prediction dataset given in Question 3. Each visualization illustrates the relationship between a descriptive feature and the target feature, **PREFCHANNEL**. Each visualization is composed of four plots: one plot of the distribution of the descriptive feature values in the entire dataset, and three plots illustrating the distribution of the descriptive feature values for each level of the target. Discuss the strength of the relationships shown in each visualization.

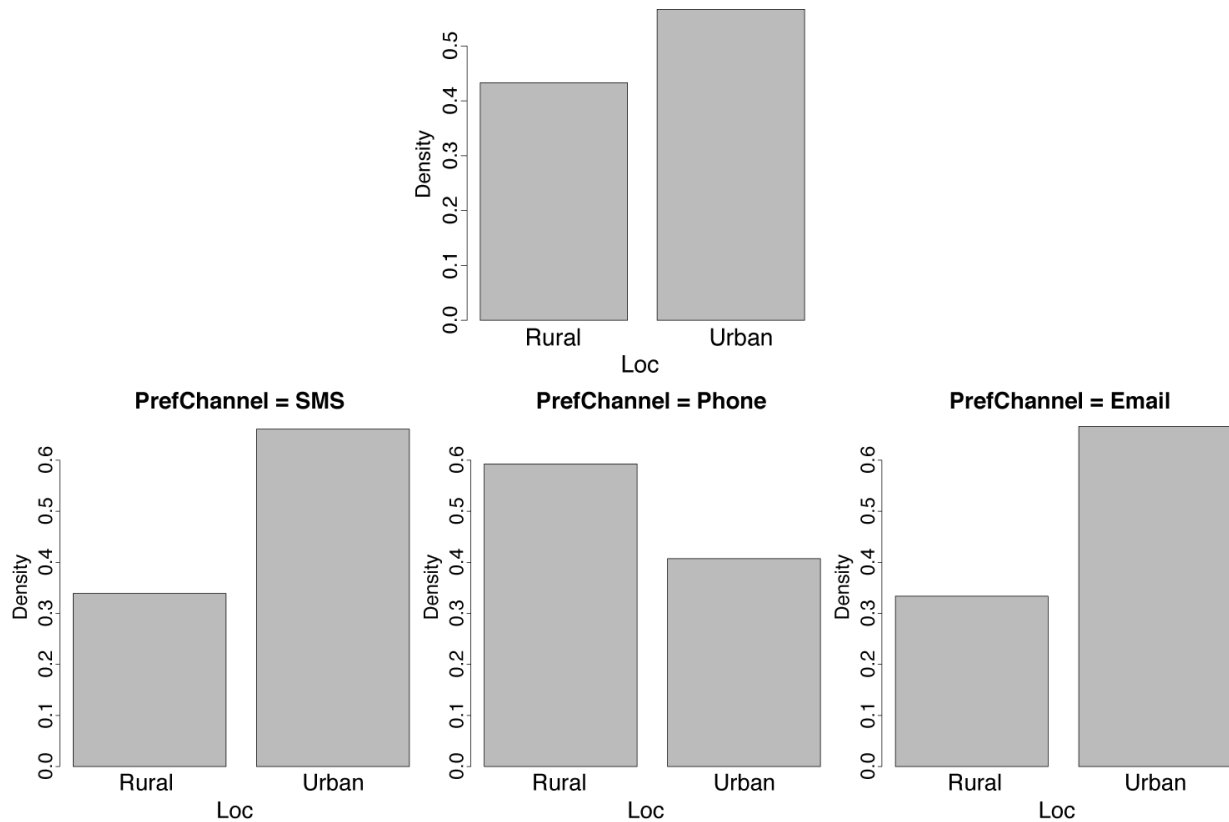
- The visualization below illustrates the relationship between the continuous feature **AGE** and the target feature, **PREFCHANNEL**.



(b) The visualization below illustrates the relationship between the categorical feature GENDER and the target feature PREFCHANNEL.



- (c) The visualization below illustrates the relationship between the categorical feature LOC and the target feature, PREFCHANNEL.



5. The table below shows the scores achieved by a group of students on an exam.

ID	1	2	3	4	5	6	7	8	9	10
SCORE	42	47	59	27	84	49	72	43	73	59
ID	11	12	13	14	15	16	17	18	19	20
SCORE	58	82	50	79	89	75	70	59	67	35

Using this data, perform the following tasks on the SCORE feature:

- (a) A **range normalization** that generates data in the range (0,1)
- (b) A **range normalization** that generates data in the range (-1,1)
- (c) A **standardization** of the data

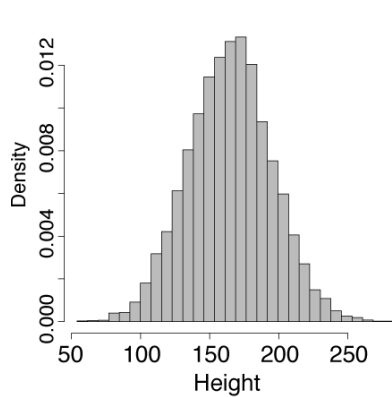
6. The following table shows the IQs for a group of people who applied to take part in a television general-knowledge quiz.

ID	1	2	3	4	5	6	7	8	9	10
IQ	92	107	83	101	107	92	99	119	93	106
ID	11	12	13	14	15	16	17	18	19	20
IQ	105	88	106	90	97	118	120	72	100	104

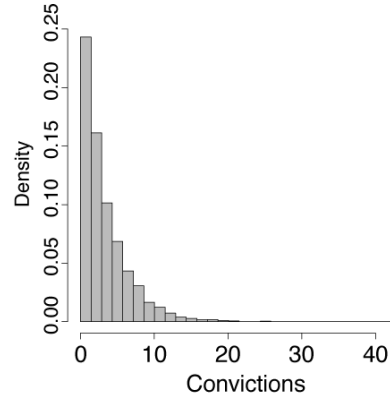
Using this dataset, generate the following **binned** versions of the IQ feature:

- (a) An **equal-width binning** using 5 bins.
- (b) An **equal-frequency binning** using 5 bins

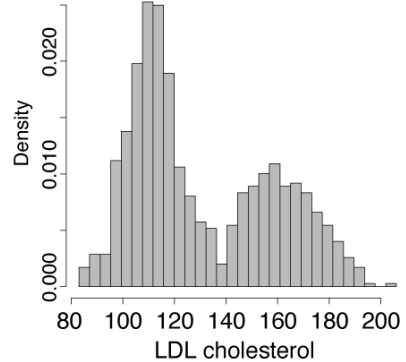
* 7. Comment on the **distributions** of the features shown in each of the following histograms.



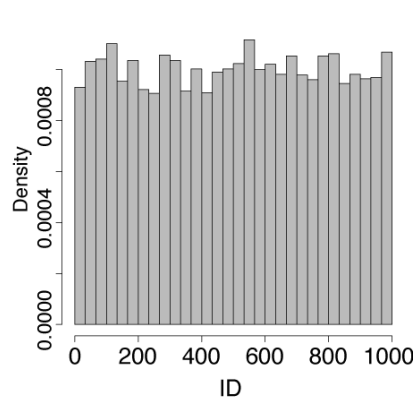
(a)



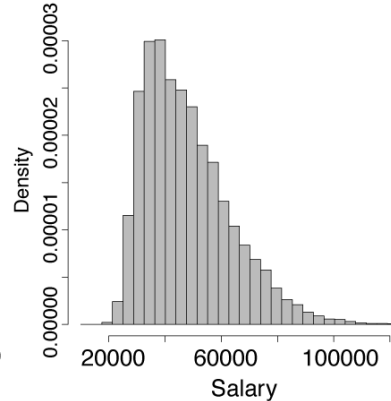
(b)



(c)



(d)



(e)

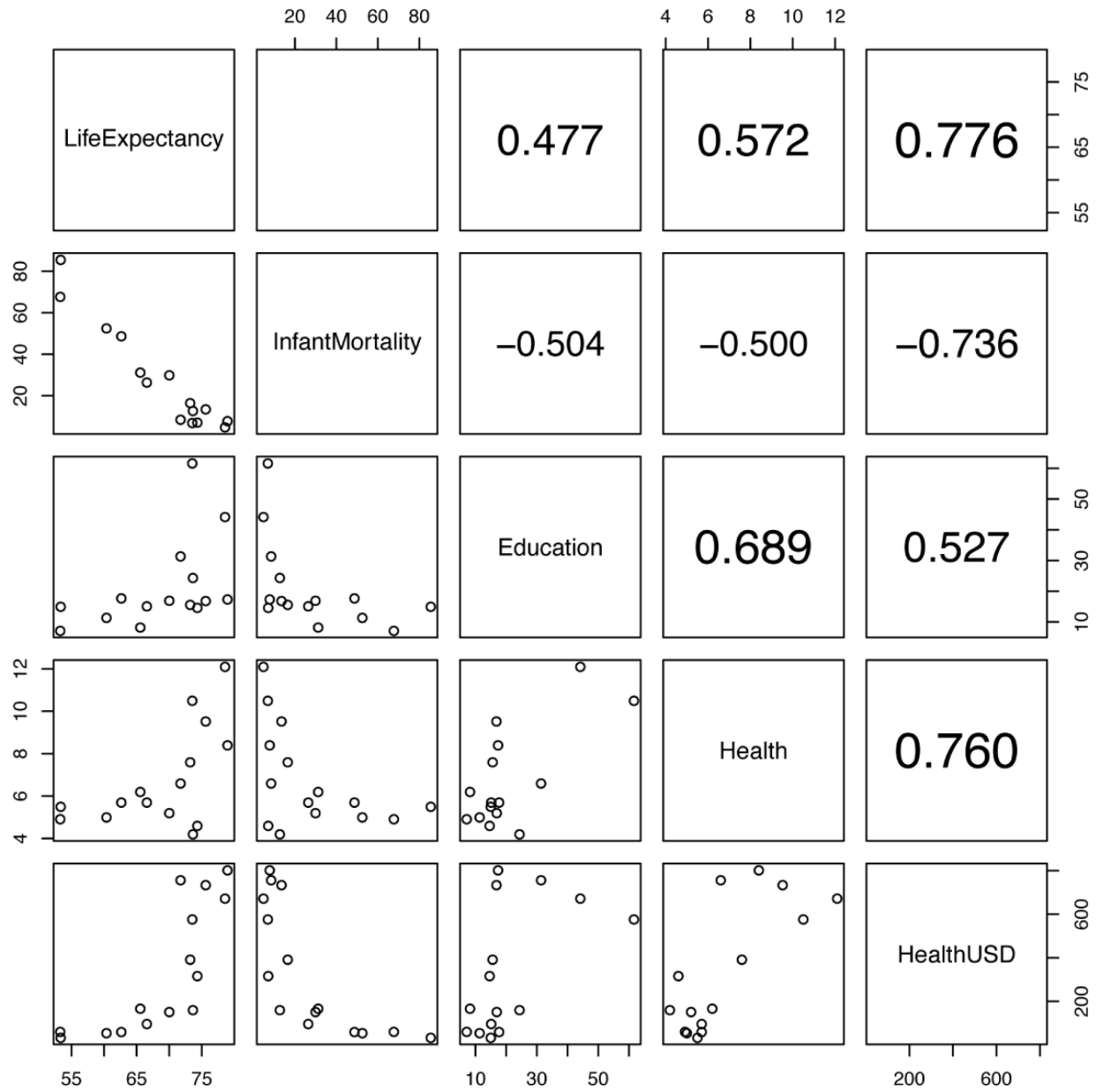
- (a) The height of employees in a trucking company.
- (b) The number of prior criminal convictions held by people given prison sentences in a city district over the course of a full year.
- (c) The LDL cholesterol values for a large group of patients, including smokers and non-smokers.
- (d) The employee ID numbers of the academic staff at a university.
- (e) The salaries of car insurance policyholders.

* 8. The table below shows socioeconomic data for a selection of countries for the year 2009,¹⁶ using the following features:

- COUNTRY: The name of the country
- LIFEEXPECTANCY: The average life expectancy (in years)
- INFANTMORTALITY: The infant mortality rate (per 1,000 live births)
- EDUCATION: Spending per primary student as a percentage of GDP
- HEALTH: Health spending as a percentage of GDP
- HEALTHUSD: Health spending per person converted into US dollars

COUNTRY	LIFE EXPECTANCY	INFANT MORTALITY	EDUCATION	HEALTH	HEALTH USD
Argentina	75.592	13.500	16.841	9.525	734.093
Cameroon	53.288	67.700	7.137	4.915	60.412
Chile	78.936	7.800	17.356	8.400	801.915
Colombia	73.213	16.500	15.589	7.600	391.859
Cuba	78.552	4.800	44.173	12.100	672.204
Ghana	60.375	52.500	11.365	5.000	54.471
Guyana	65.560	31.200	8.220	6.200	166.718
Latvia	71.736	8.500	31.364	6.600	756.401
Malaysia	74.306	7.100	14.621	4.600	316.478
Mali	53.358	85.500	14.979	5.500	33.089
Mongolia	66.564	26.400	15.121	5.700	96.537
Morocco	70.012	29.900	16.930	5.200	151.513
Senegal	62.653	48.700	17.703	5.700	59.658
Serbia	73.532	6.900	61.638	10.500	576.494
Thailand	73.627	12.700	24.351	4.200	160.136

- (a) Calculate the **correlation** between the LIFEEXPECTANCY and INFANTMORTALITY features.
- (b) The image below shows a **scatter plot matrix** of the continuous features from this dataset (the correlation between LIFEEXPECTANCY and INFANTMORTALITY has been omitted). Discuss the relationships between the features in the dataset that this scatter plot highlights.



- * 9. Tachycardia is a condition that causes the heart to beat faster than normal at rest. The occurrence of tachycardia can have serious implications including increased risk of stroke or sudden cardiac arrest. An analytics consultant has been hired by a major hospital to build a predictive model that predicts the likelihood that a patient at a heart disease clinic will suffer from tachycardia in the month following a visit to the clinic. The hospital will use this model to make predictions for each patient when they visit the clinic and offer increased monitoring for those deemed to be at risk. The analytics

consultant has generated an ABT to be used to train this model.¹⁷ The descriptive features in this dataset are defined as follows:

- AGE: The patient's age
- GENDER: The patient's gender (*male* or *female*)
- WEIGHT: The patient's weight
- HEIGHT: The patient's height
- BMI: The patient's body mass index (BMI) which is calculated as $\frac{\text{weight}}{\text{height}^2}$ where weight is measured in kilograms and height in meters.
- SYS. B.P.: The patient's systolic blood pressure
- DIA. B.P.: The patient's diastolic blood pressure
- HEART RATE: The patient's heart rate
- H.R. DIFF.: The difference between the patient's heart rate at this visit and at their last visit to the clinic
- PREV. TACHY.: Has the patient suffered from tachycardia before?
- TACHYCARDIA: Is the patient at high risk of suffering from tachycardia in the next month?

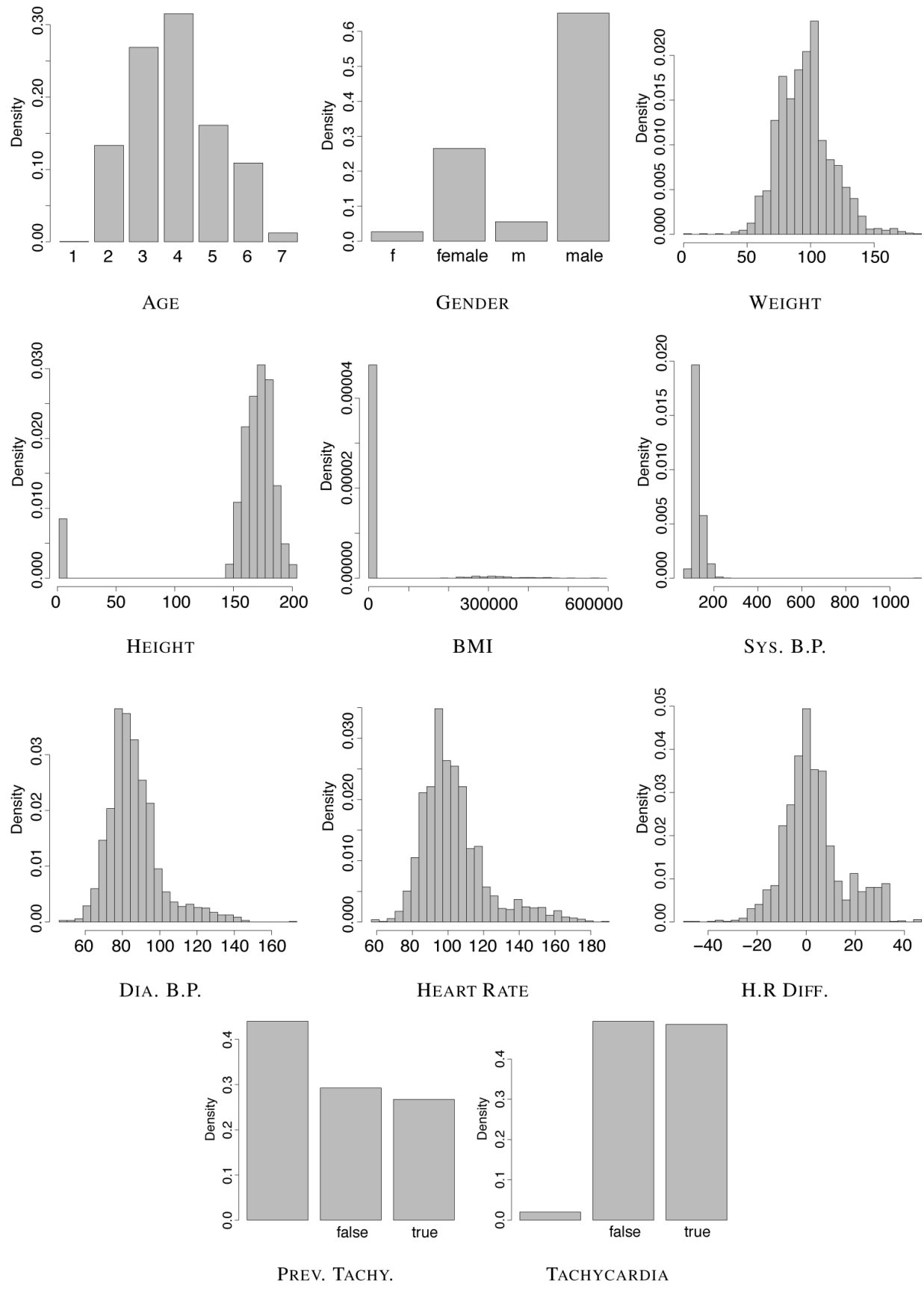
The following table contains an extract from this ABT—the full ABT contains 2,440 instances.

ID	AGE	GENDER	WEIGHT	HEIGHT	BMI	SYS.	DIA.	HEART	H.R.	PREV.	TACHYCARDIA
						B.P.	B.P.	RATE	DIFF.	TACHY.	
1	6	male	78	165	28.65	161	97	143			true
2	5	m	117	171	40.01	216	143	162	17	true	true
			⋮		⋮				⋮		
143	5	male	108	1.88	305,568.13	139	99	84	21	false	true
144	4	male	107	183	31.95	1,144	90	94	-8	false	true
			⋮		⋮				⋮		
1,158	6	female	92	1.71	314,626.72	111	75	75	-5		false
1,159	3	female	151	1.59	596,495.39	124	91	115	23	true	true
			⋮		⋮				⋮		
1,702	3	male	86	193	23.09	138	81	83		false	false
1,703	6	f	73	166	26.49	134	86	84	-4		false
			⋮		⋮				⋮		

The consultant generated the following **data quality report** from the ABT.

Feature	Count	Miss.	Card.	1 st				3 rd		Std.
				Min.	Qrt.	Mean	Median	Qrt.	Max.	
AGE	2,440	0.00	7	1.00	3.00	3.88	4.00	5.00	7.00	1.22
WEIGHT	2,440	0.00	174	0.00	81.00	95.70	95.00	107.00	187.20	20.89
HEIGHT	2,440	0.00	109	1.47	162.00	162.21	171.50	179.00	204.00	41.06
BMI	2,440	0.00	1,385	0.00	27.64	18,523.40	32.02	38.57	596,495.39	77,068.75
SYS .B.P.	2,440	0.00	149	62.00	115.00	127.84	124.00	135.00	1,144.00	29.11
DIA. B.P.	2,440	0.00	109	46.00	77.00	86.34	84.00	92.00	173.60	14.25
HEART RATE	2,440	0.00	119	57.00	91.75	103.28	100.00	110.00	190.40	18.21
H.R. DIFF.	2,440	13.03	78	-50.00	-4.00	3.00	1.00	8.00	47.00	12.38

Feature	Count	Miss.	Card.	Mode	1 st		3 rd		2 nd	
					Mode	Freq.	Mode	%	Mode	Freq.
GENDER	2,440	0.00	4	male	1,591.00	65.20	female	647.00	26.52	
PREV. TACHY.	2,440	44.02	3	false	714.00	52.27	true	652.00	47.73	
TACHYCARDIA	2,440	2.01	3	false	1,205.00	50.40	true	1,186.00	49.60	

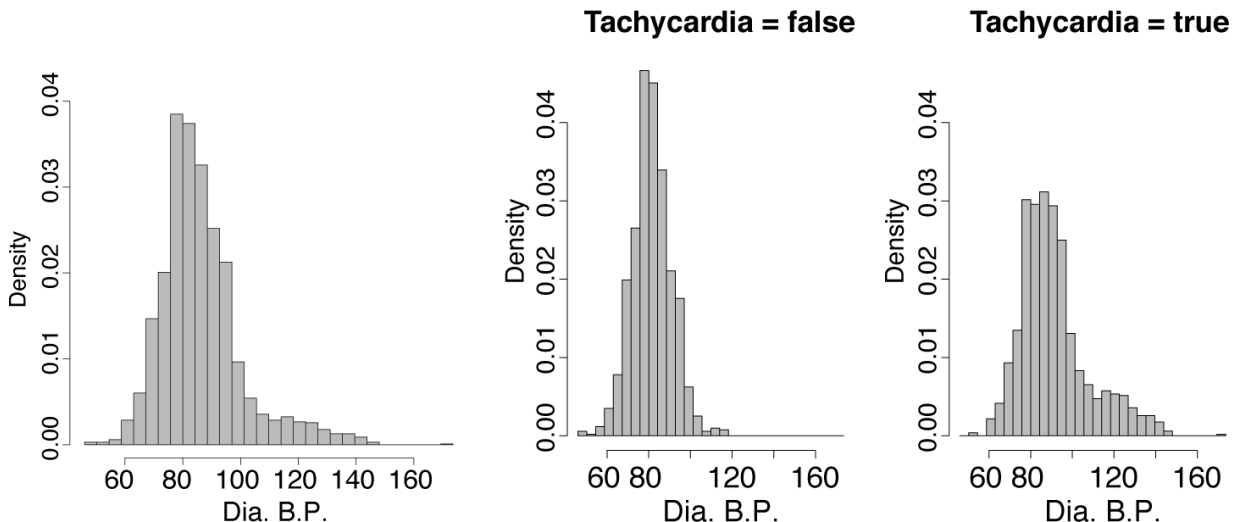


Discuss this data quality report in terms of the following:

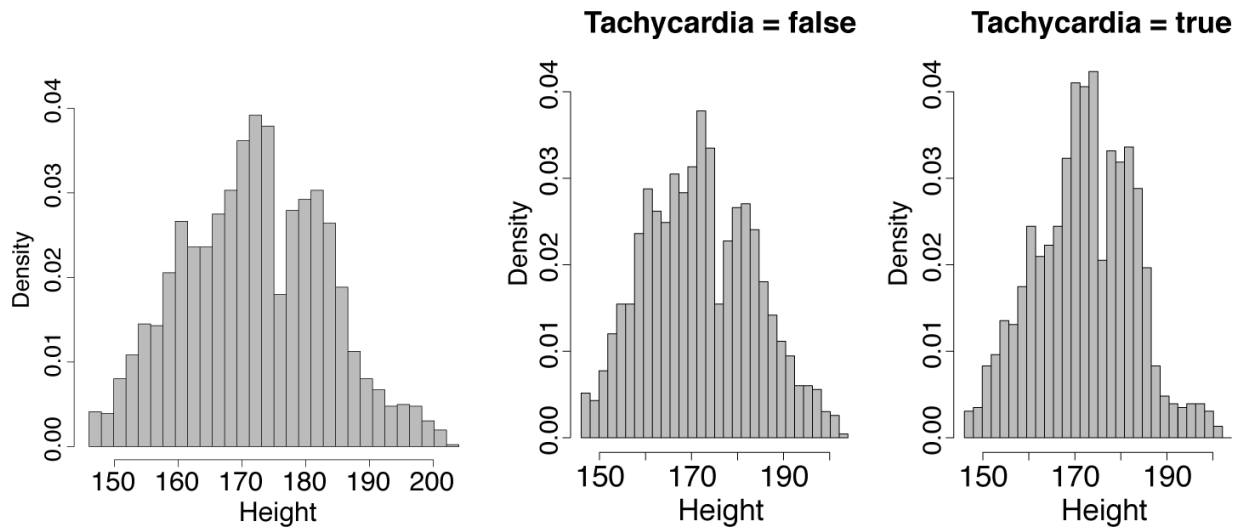
- (a) Missing values
- (b) Irregular cardinality
- (c) Outliers
- (d) Feature distributions

* 10. The following data visualizations are based on the tachycardia prediction dataset from Question 9 (after the instances with missing TACHYCARDIA values have been removed and all outliers have been handled). Each visualization illustrates the relationship between a descriptive feature and the target feature, TACHYCARDIA and is composed of three plots: a plot of the distribution of the descriptive feature values in the full dataset, and plots showing the distribution of the descriptive feature values for each level of the target. Discuss the relationships shown in each visualizations.

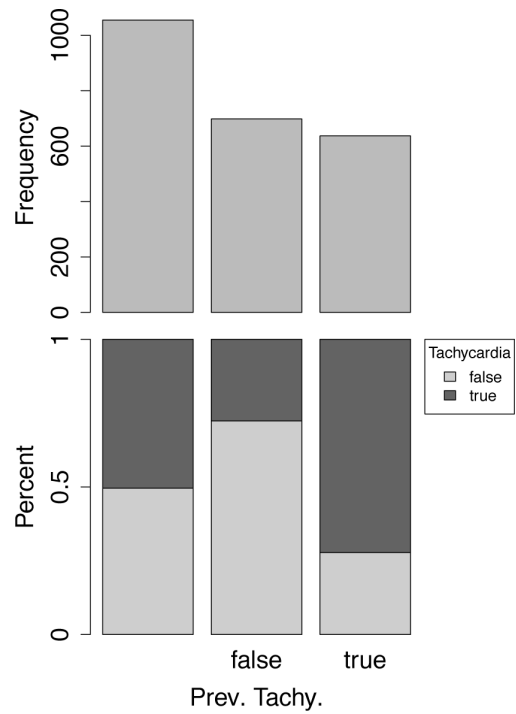
- (a) The visualization below illustrates the relationship between the continuous feature Dia. B.P. and the target feature, TACHYCARDIA.



- (b) The visualization below illustrates the relationship between the continuous HEIGHT feature and the target feature TACHYCARDIA.



(c) The visualization below illustrates the relationship between the categorical feature PREV. TACHY. and the target feature, TACHYCARDIA.



- * 11. Worldwide **breast cancer** is the most common form of cancer for women, and the second most common form of cancer overall.¹⁸ Reliable, population-wide screening is one tool that can be used to reduce the impact of breast cancer, and there is an opportunity for machine learning to be used for this. A large hospital group has

collected a cancer screening dataset for possible use with machine learning that contains features extracted from tissue samples extracted by biopsy from adults presenting for screening. Features have been extracted from these biopsies by lab technicians who rate samples across a number of categories on a scale of 1 to 10. The samples have then been manually categorized by clinicians as either *benign* or *malignant*.¹⁹ The descriptive features in this dataset are defined as follows:

- AGE: The age of the person screened.
- SEX: The sex of the person screened, either *male* or *female*.
- SIZEUNIFORMITY: A measure of the variation in size of cells in the tissue samples, higher values indicate more uniform sizes (1 to 10).
- SHAPEUNIFORMITY: A measure of the variation in shape of cells in the tissue samples, higher values indicate more uniform shapes (1 to 10).
- MARGINALADHESION: A measure of how much cells in the biopsy stick together (1 to 10).
- MITOSES: A measure of how fast cells are growing (1 to 10).
- CLUMPTHICKNESS: A measure of the amount of layering in cells (1 to 10).
- BLANDCHROMATIN: A measure of the texture of cell nuclei (1 to 10).
- CLASS: The clinician's assessment of the biopsy sample as either *benign* or *malignant*.

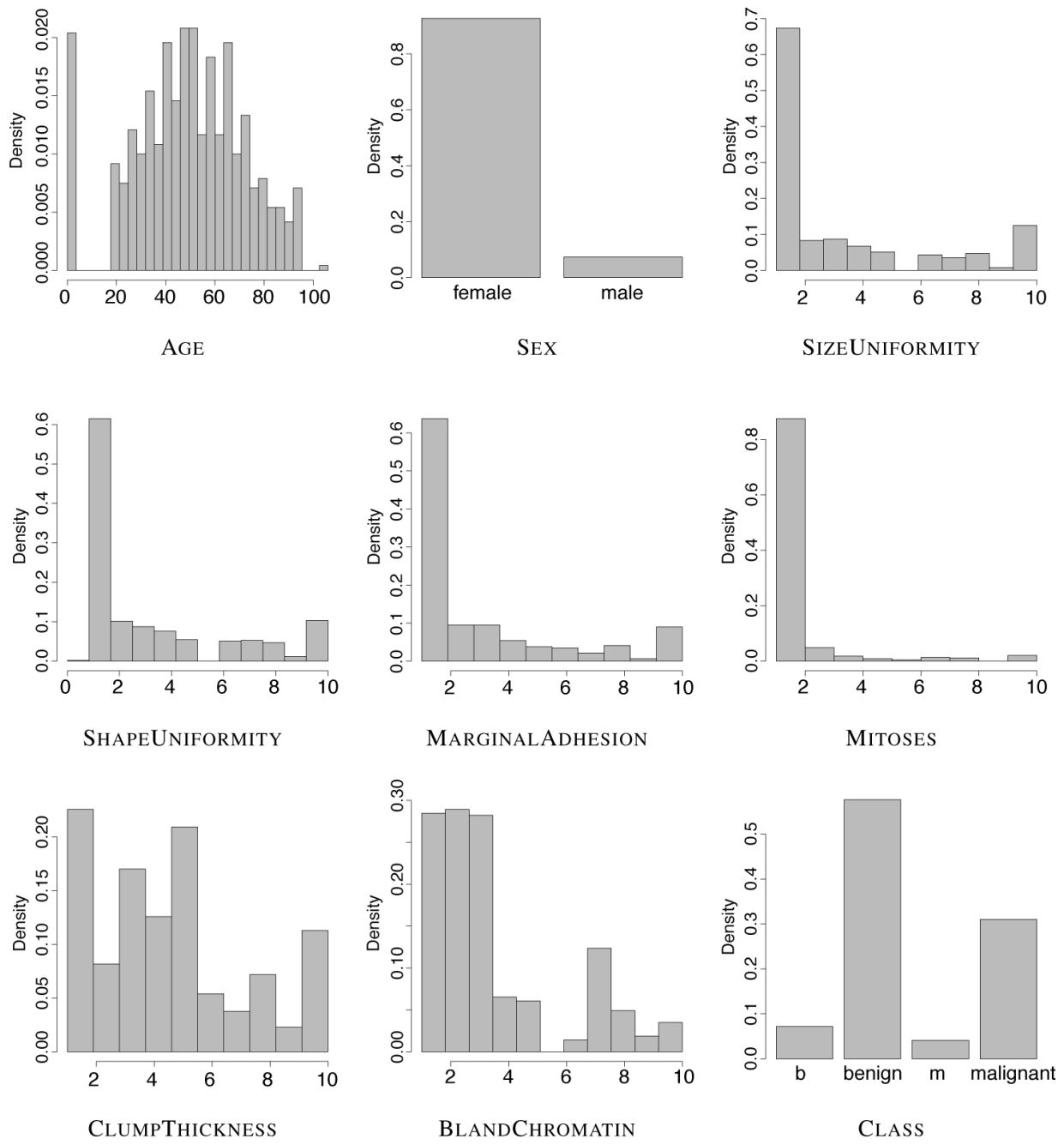
The following table contains an extract from this ABT—the full ABT contains 680 instances.

ID	AGE	SEX	CLUMP		SIZE		SHAPE		MARGINAL		BLAND	
			THICKNESS	UNIFORMITY	UNIFORMITY	ADHESION	CHROMATIN	MITOSES	CLASS			
1	56	<i>female</i>	3	4	5	3	4	1	<i>benign</i>			
2	77	<i>female</i>	2	1	0	1	1	1	<i>benign</i>			
48	34	<i>female</i>	5	2	4	1				1	<i>benign</i>	
49	46	<i>female</i>	5	3	1	2	2	1	<i>b</i>			
50	106	<i>female</i>	2	1	1	1	1	1	<i>benign</i>			
303	95	<i>female</i>	1				1	1		1	<i>benign</i>	
304	28	<i>male</i>	5	1	1	1				1	<i>benign</i>	
305	0	<i>female</i>	3				1	3		1	<i>benign</i>	
679	48	<i>female</i>	10	8	7	4	7	1	<i>m</i>			
680	43	<i>female</i>	5	4	6	7			<i>malignant</i>			

The following **data quality report** has been generated from the ABT.

Feature	Count	% Miss. Card.			Mode Freq.	Mode %	2 nd Mode Freq.		2 nd Mode %	
		Count	Miss.	Card.			Mode	Freq.	%	
SEX	680	0	2	2	<i>female</i>	630	92.65	<i>male</i>	50	7.35
CLASS	680	0	4	4	<i>benign</i>	392	57.65	<i>malignant</i>	211	31.03

Feature	Count	% Miss. Card.			1 st Min. Qrt.			3 rd Median Qrt.			Std. Dev.
		Count	Miss.	Card.	Min.	Qrt.	Mean	Median	Qrt.	Max.	
AGE	680	0.00	80	0	34	49.13	50	65	106	22.95	
CLUMPTHICKNESS	680	0.00	10	1	2	4.45	4	6	10	2.82	
SIZEUNIFORMITY	680	9.26	10	1	1	3.14	1	5	10	3.08	
SHAPEUNIFORMITY	680	9.26	11	0	1	3.20	1	5	10	3.00	
MARGINALADHESION	680	0.00	10	1	1	2.84	1	4	10	2.87	
BLANDCHROMATIN	680	22.94	10	1	2	3.38	3	4	10	2.44	
MITOSES	680	0.00	9	1	1	1.61	1	1	10	1.74	

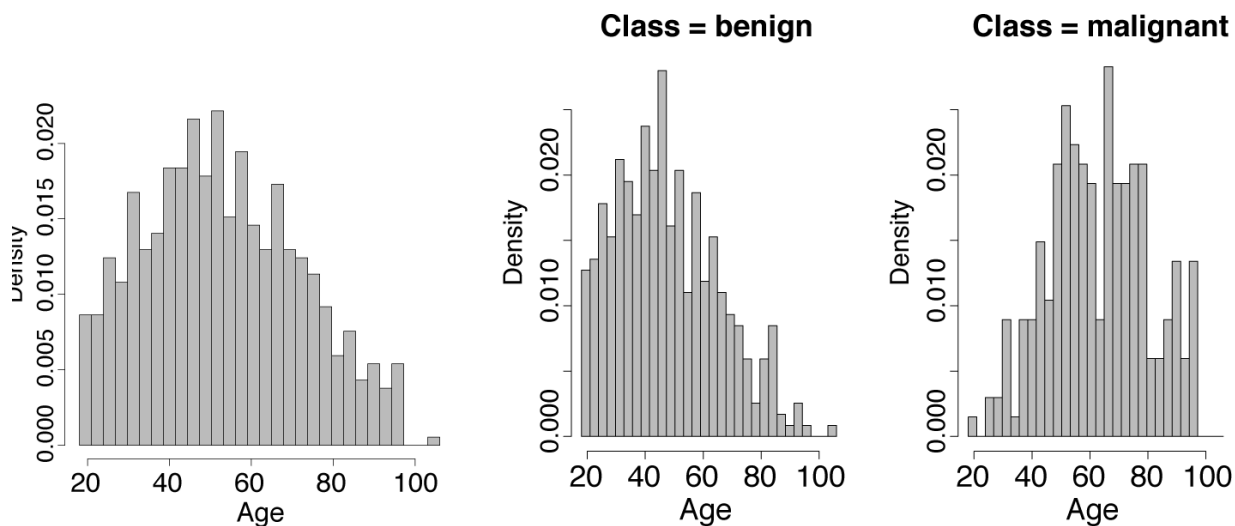


Discuss this data quality report in terms of the following:

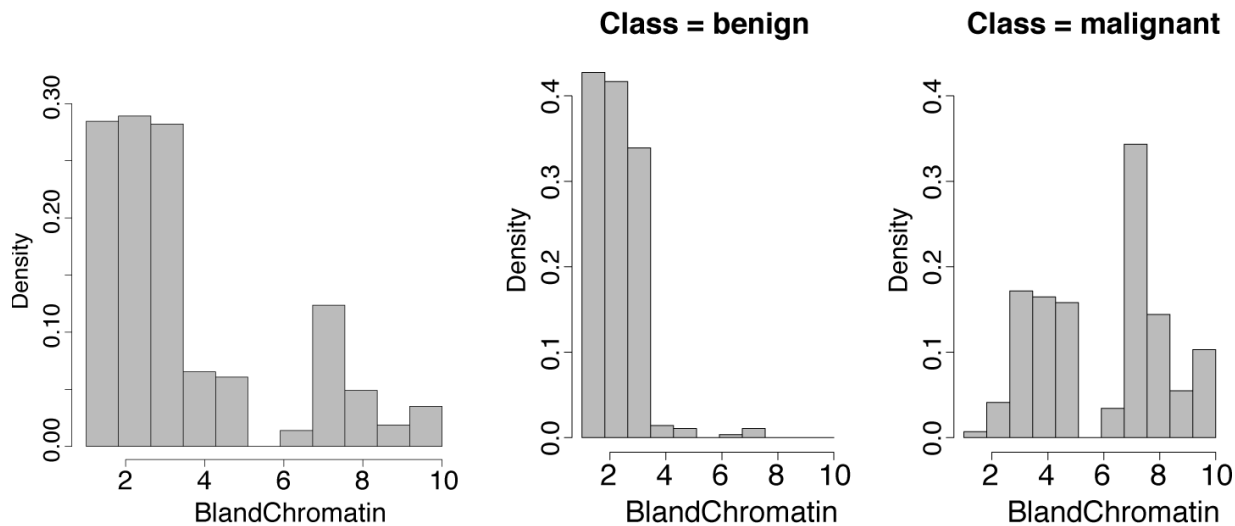
- Missing values
- Irregular cardinality
- Outliers
- Feature distributions

* 12. The following data visualizations are based on the breast cancer prediction dataset from Question 11 (after some data quality issues present in the dataset have been corrected). Each visualization illustrates the relationship between a descriptive feature and the target feature, CLASS and is composed of three plots: a plot of the distribution of the descriptive feature values in the full dataset, and plots showing the distribution of the descriptive feature values for each level of the target. Discuss the relationships shown in each visualizations.

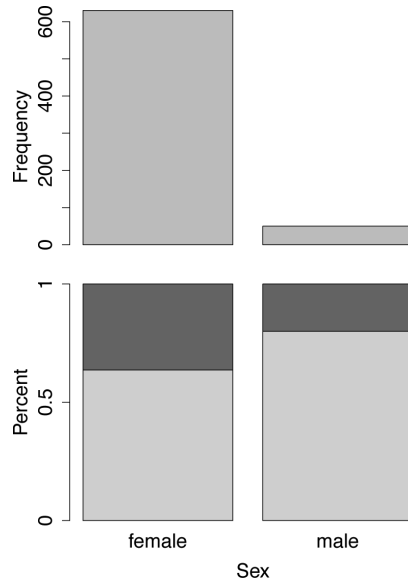
- (a) The visualization below illustrates the relationship between the continuous feature AGE and the target feature, CLASS.



- (b) The visualization below illustrates the relationship between the continuous BLANDCHROMATIN feature and the target feature CLASS.



- (c) The visualization below illustrates the relationship between the categorical feature SEX and the target feature, CLASS.



1. In order to allow this dataset fit on one page, only a subset of the features described in the domain concept diagrams in Figures 2.9^[43], 2.10^[44], and 2.11^[45] are included.
2. Note that in a density histogram, the height of each bar represents the likelihood that a value in the range defining that bar will occur in a data sample (see Section A.4.2^[752]).
3. We discuss probability distributions in more depth in Chapter 6^[243].
4. Sometimes, the variance of a feature, σ^2 , rather than its standard deviation, σ , is listed as the parameter for the normal distribution. In this text we always use the standard deviation σ .
5. *Fat finger* is a phrase often used in financial trading to refer to mistakes that arise when a trader enters extra zeros by mistake and buys or sells much more of a stock than intended.
6. Recall that in Section 3.2^[55] we discussed the 68–95–99.7 rule associated with the normal distribution. This approach to handling outliers is based directly on this rule.
7. The correlation coefficient presented here is more fully known as the Pearson product-moment correlation coefficient or Pearson's r and is named after Karl Pearson, one of the giants of statistics.
8. Francis Anscombe was a famous statistician who published his quartet in 1973 (Anscombe, 1973).
9. There are approaches to formally measuring the relationship between a pair of categorical features (for example, the χ^2 test) and for measuring the relationship between a categorical feature and a continuous feature (for example, the **ANOVA test**). We do not cover these in this book, however, and readers are directed to the further reading section at the end of this chapter for information on these approaches.
10. A standard score is equivalent to a **z-score**, and standardizing in the way described here is also known as applying a **z-transform** to the data.
11. These images were generated using equal-width binning. However, the points discussed in the text are also relevant to equal-frequency binning.

- 12.** In interval notation, a square bracket, [or], indicates that the boundary value is included in the interval, and a parenthesis, (or), indicates that it is excluded from the interval.
- 13.** The bins created when equal-frequency binning is used are equivalent to percentiles (discussed in Section A.1^[745]).
- 14.** Although we didn't mention it explicitly in other cases where we mentioned random sampling, we meant random sampling without replacement.
- 15.** The data used in this question have been artificially generated for this book. Channel propensity modeling is used widely in industry; for example, see Hirschowitz (2001).
- 16.** The data listed in this table is real and was amalgamated from a number of reports that were retrieved from Gapminder (www.gapminder.org). The EDUCATION data is based on a report from the World Bank (data.worldbank.org/indicator/SE.XPD.PRIM.PC.ZS); the HEALTH and HEALTHUSD data are based on reports from the World Health Organization (www.who.int); all the other features are based on reports created by Gapminder.
- 17.** The data used in this question have been artificially generated for this book. This type of application of machine learning techniques, however, is common; for example, see Osowski et al. (2004).
- 18.** Based on data from Bray et al. (2018).
- 19.** The data in this question have been artificially created but were inspired by the famous **Wisconsin breast cancer dataset** first described by Mangasarian and Wolberg (1990), and available from the UCI Machine Learning Repository (Bache and Lichman, 2013).

II

PREDICTIVE DATA ANALYTICS

4

Information-Based Learning

“Information is the resolution of uncertainty.”

—Claude Elwood Shannon

In this chapter we discuss the ways in which concepts from **information theory** can be used to build prediction models. We start by discussing **decision trees**, the fundamental structure used in information-based machine learning, before presenting the fundamental measures of information content that are used: **entropy** and **information gain**. We then present the **ID3** algorithm, the standard algorithm used to induce a decision tree from a dataset. The extensions and variations to this standard approach that we present describe how different data types can be handled, how overfitting can be avoided using decision tree **pruning**, and how multiple prediction models can be combined in **ensembles** to improve prediction accuracy.

4.1 Big Idea

We start off by playing a game. *Guess Who* is a two-player game in which one player chooses a card with a picture of a character on it from a deck, and the other player tries to guess which character is on the card by asking a series of questions to which the answer can be only yes or no. The player asking the questions wins by guessing who is on the card within a small number of questions and loses otherwise. [Figure 4.1](#)^[118] shows the set of cards that we will use for our game. We can represent these cards using the dataset given in [Table 4.1](#)^[118].

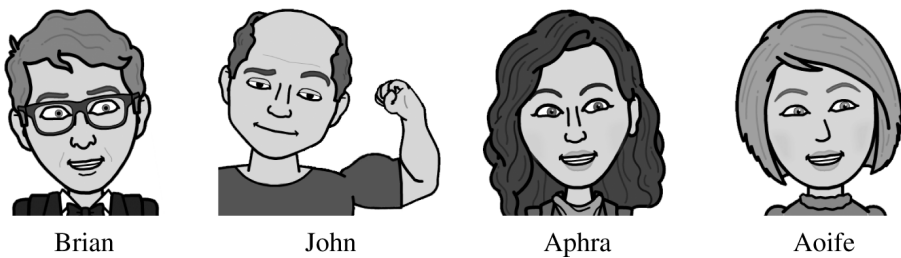


Figure 4.1

Cards showing character faces and names for the *Guess Who* game.

Table 4.1

A dataset that represents the characters in the *Guess Who* game.

Man	Long Hair	Glasses	Name
Yes	No	Yes	Brian
Yes	No	No	John
No	Yes	No	Aphra
No	No	No	Aoife

Now, imagine that we have picked one of these cards and you have to guess which one by asking questions. Which of the following questions would you ask first?

1. Is it a man?
2. Does the person wear glasses?

Most people would ask Question 1 first. Why is this? At first, this choice of question might seem ineffective. For example, if you ask Question 2, and we answer *yes*, you can be sure that we have picked *Brian* without asking any more questions. The problem with this reasoning, however, is that, on average, the answer to Question 2 will be *yes* only one out of every four times you play. That means that three out of every four times you ask Question 2, the answer will be *no*, and you will still have to distinguish between the three remaining characters.

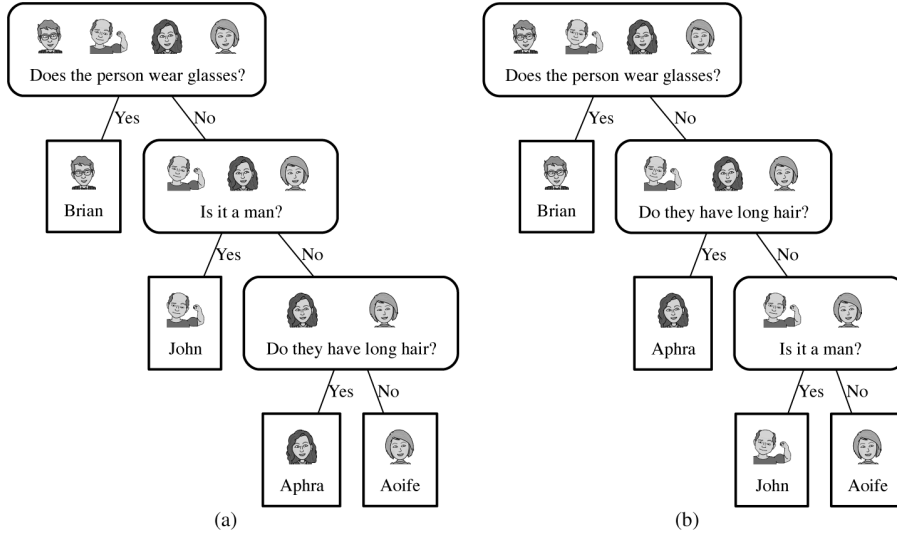


Figure 4.2

The different question sequences that can follow in a game of *Guess Who* beginning with the question *Does the person wear glasses?*

Figure 4.2^[119] illustrates the possible question sequences that can follow in a game beginning with Question 2. In **Figure 4.2(a)**^[119] we next ask, *Is it a man?* and then, if required, *Do they have long hair?* In **Figure 4.2(b)**^[119] we reverse this order. In both of these diagrams, one path to an answer about the character on a card is 1 question long, one path is 2 questions long, and two paths are 3 questions long. Consequently, if you ask Question 2 first, the average number of questions you have to ask per game is

$$\frac{1 + 2 + 3 + 3}{4} = 2.25$$

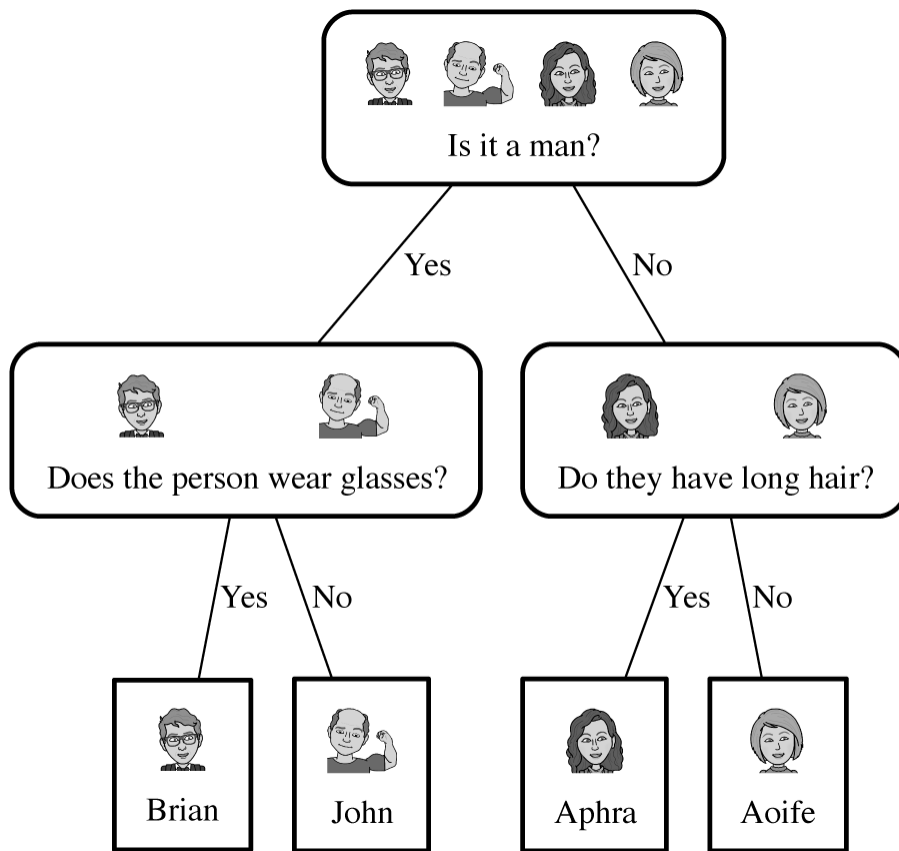


Figure 4.3

The different question sequences that can follow in a game of *Guess Who* beginning with the question *Is it a man?*

On the other hand, if you ask Question 1 first, there is only one sequence of questions with which to follow it. This sequence is shown in [Figure 4.3](#)^[120]. Irrespective of the answers to the questions, you always have to follow a path through this sequence that is 2 questions long to reach an answer about the character on a card. This means that if you always ask Question 1 first, the average number of questions you have to ask per game is

$$\frac{2 + 2 + 2 + 2}{4} = 2$$

What is interesting here is that no matter what question you ask, the answer is always either *yes* or *no*, but, on average, an answer to Question 1 seems to carry more information than an answer to Question 2. This is not because of the literal message in the answer (either *yes* or *no*). Rather, it is because of the way that the answer to each question splits the character

cards into different sets based on the value of the descriptive feature the question is asked about (MAN, LONG HAIR or GLASSES) and the likelihood of each possible answer to the question.

An answer to Question 1, *Is it a man?*, splits the game domain into two sets of equal size: one containing *Brian* and *John* and one containing *Aphra* and *Aoife*. One of these sets contains the solution, which leaves you with just one more question to ask to finish the game. By contrast, an answer to Question 2 splits the game domain into one set containing one element, *Brian*, and another set containing three elements: *John*, *Aphra*, and *Aoife*. This works out really well when the set containing the single element contains the solution. In the more likely case that the set containing three elements contains the solution, however, you may have to ask two more questions to uniquely identify the answer. So, when you consider both the likelihood of an answer and how an answer splits up the domain of solutions, it becomes clear that an answer to Question 2 leaves you with more work to do to solve the game than an answer to Question 1.

So, the big idea here is to figure out which features are the most informative ones to ask questions about by considering the effects of the different answers to the questions, in terms of how the domain is split up after the answer is received and the likelihood of each of the answers. Somewhat surprisingly, people seem to be able to easily do this on the basis of intuition. Information-based machine learning algorithms use the same idea. These algorithms determine which descriptive features provide the most information about a target feature and make predictions by sequentially testing the features in order of their informativeness.

4.2 Fundamentals

In this section we introduce Claude Shannon's approach to measuring information,¹ in particular his model of **entropy** and how it is used in the **information gain** measure to capture the informativeness of a descriptive feature. Before this we introduce **decision trees**, the actual prediction models that we are trying to build.

4.2.1 Decision Trees

Just as we did when we played *Guess Who*, an effective way to generate a prediction is to carry out a series of tests on the values of the descriptive

features describing a query instance and use the answers to these tests to determine the prediction. **Decision trees** take this approach. To illustrate how a decision tree works, we use the dataset listed in [Table 4.2](#)^[121]. This dataset contains a set of training instances that can be used to build a model to predict whether emails are *spam* or *ham* (genuine). The dataset has three binary descriptive features: SUSPICIOUS WORDS is *true* if an email contains one or more words that are typically found in spam email (e.g., *casino*, *viagra*, *bank*, or *account*); UNKNOWN SENDER is *true* if the email is from an address that is not listed in the contacts of the person who received the email; and CONTAINS IMAGES is *true* if the email contains one or more images.

Table 4.2

An email spam prediction dataset.

ID	SUSPICIOUS WORDS	UNKNOWN SENDER	CONTAINS IMAGES	CLASS
376	true	false	true	spam
489	true	true	false	spam
541	true	true	false	spam
693	false	true	true	ham
782	false	false	false	ham
976	false	false	false	ham

[Figure 4.4](#)^[122] shows two decision trees that are **consistent** with the spam dataset. Decision trees look very like the game trees that we developed for the *Guess Who* game. As with all tree representations, a decision tree consists of a **root node** (or starting node), **interior nodes**, and **leaf nodes** (or terminating nodes) that are connected by **branches**. Each non-leaf node (root and interior) in the tree specifies a test to be carried out on a descriptive feature. The number of possible levels that a descriptive feature can take determines the number of downward branches from a non-leaf node. Each of the leaf nodes specifies a predicted level of the target feature.

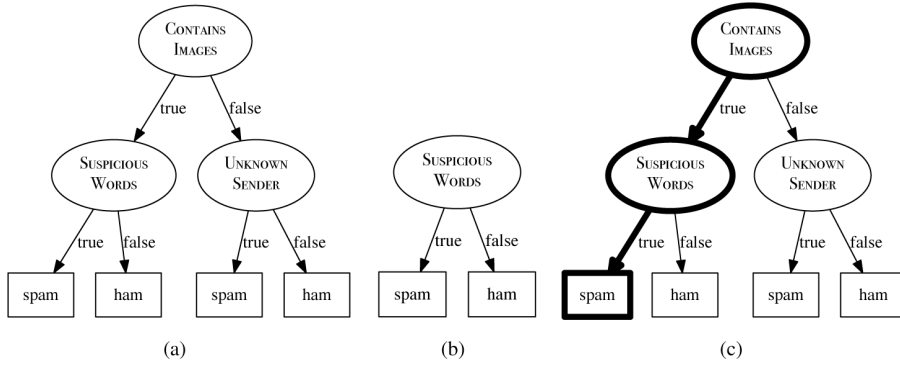


Figure 4.4

Two decision trees, (a) and (b), that are consistent with the instances in the spam dataset; and (c) the path taken through the tree shown in (a) to make a prediction for the query instance SUSPICIOUS WORDS = *true*, UNKNOWN SENDER = *true*, and CONTAINS IMAGES = *true*.

In the diagrams in [Figure 4.4](#)^[122], ellipses represent root or interior nodes, and rectangles represent leaf nodes. The labels of the ellipses indicate which descriptive feature is tested at that node. The labels on each branch indicate one of the possible feature levels that the descriptive feature at the node above can take. The labels on the rectangular leaf nodes indicate the target level that should be predicted when the tests on the interior nodes create a path that terminates at that leaf node.

The process of using a decision tree to make a prediction for a query instance starts with testing the value of the descriptive feature at the root node of the tree. The result of this test determines which of the root node's children the process should then descend to. These two steps of testing the value of a descriptive feature and descending a level in the tree are then repeated until the process comes to a leaf node at which a prediction can be made.

To demonstrate how this process works, imagine that we were given the query email SUSPICIOUS WORDS = *true*, UNKNOWN SENDER = *true*, CONTAINS IMAGES = *true*, and asked to predict whether it is *spam* or *ham*. Applying the decision tree from [Figure 4.4\(a\)](#)^[122] to this query, we see that the root node of this tree tests the CONTAINS IMAGES feature. The query instance value for CONTAINS IMAGES is *true* so the process descends the left branch from the root node, labeled *true*, to an interior node that tests the SUSPICIOUS WORDS feature. The query instance value for this feature is *true*, and so on the basis of the result of the test at this node, the process descends the left branch, labeled *true*, to a leaf node labeled *spam*. As the process has arrived at a

leaf node, it terminates, and the target level indicated by the leaf node, *spam*, is predicted for the query instance. The path through the decision tree for this query instance is shown in [Figure 4.4\(c\)](#)^[122].

The decision tree in [Figure 4.4\(b\)](#)^[122] would have returned the same prediction for the query instance. Indeed, both of the decision trees in [Figures 4.4\(a\)](#)^[122] and [4.4\(b\)](#)^[122] are consistent with the dataset in [Table 4.2](#)^[121] and can generalize sufficiently to make predictions for query instances like the one considered in our example. The fact that there are, at least, two decision trees that can do this raises the question: How do we decide which is the best decision tree to use?

We can apply almost the same approach that we used in the *Guess Who* game to make this decision. Looking at the decision trees in [Figures 4.4\(a\)](#)^[122] and [4.4\(b\)](#)^[122], we notice that the tree in [Figure 4.4\(a\)](#)^[122] performs tests on two features in order to make a prediction, whereas the decision tree in [Figure 4.4\(b\)](#)^[122] needs to test only the value of one feature. The reason for this is that **SUSPICIOUS WORDS**, the descriptive feature tested at the root node of the tree in [Figure 4.4\(b\)](#)^[122], perfectly splits the data into a pure group of *spam* emails and a pure group of *ham* emails. We can say that because of the purity of the splits that it makes, the **SUSPICIOUS WORDS** feature provides more information about the value of the target feature for an instance than the **CONTAINS IMAGES** feature, and so a tree that tests this descriptive feature at the root node is preferable.

This gives us a way to choose between a set of different decision trees that are all consistent with a set of training instances. We can introduce a preference for decision trees that use fewer tests—in other words, trees that are on average shallower.² This is the primary inductive bias that a machine learning algorithm taking an information-based approach encodes. To build shallow trees, we need to put the descriptive features that best discriminate between instances that have different target feature values toward the top of the tree. To do this we need a formal measure of how well a descriptive feature discriminates between the levels of the target feature. Similar to the way that we analyzed the questions in the *Guess Who* game, we measure the discriminatory power of a descriptive feature by analyzing the size and probability of each set of instances created when we test the value of the feature and how pure each set of instances is with respect to the target

feature values of the instances it contains. The formal measure we use to do this is Shannon's entropy model.

4.2.2 Shannon's Entropy Model

Claude Shannon's entropy model defines a computational measure of the impurity of the elements in a set. Before we examine the mathematical definition of entropy, we first provide an intuitive explanation of what it means. Figure 4.5^[124] shows a collection of sets of playing cards of contrasting entropy. An easy way to understand the entropy of a set is to think in terms of the uncertainty associated with guessing the result if you were to make a random selection from the set. For example, if you were to randomly select a card from the set shown in Figure 4.5(a)^[124], you would have zero uncertainty, as you would know for sure that you would select an ace of spades. So, this set has zero entropy. If, however, you were to randomly select an element from the set in Figure 4.5(f)^[124], you would be very uncertain about any prediction as there are 12 possible outcomes, each of which is equally likely. This is why this set has very high entropy. The other sets in Figure 4.5^[124] have entropy values between these two extremes.

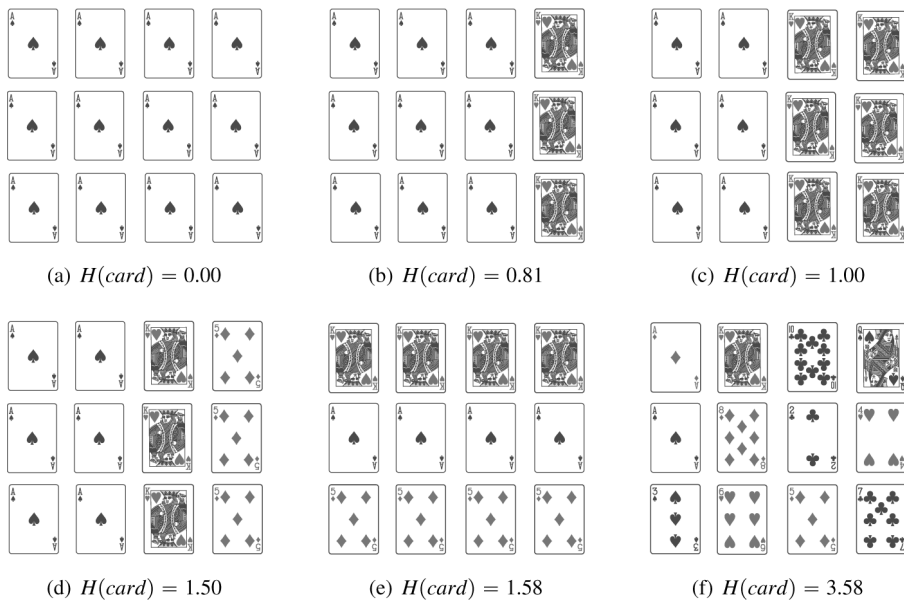


Figure 4.5

The entropy of different sets of playing cards measured in bits.

This gives us a clue as to how we should define a computational model of entropy. We can transform the probabilities³ of the different possible

outcomes when we randomly select an element from a set to entropy values. An outcome with a large probability should map to a low entropy value, and an outcome with a small probability should map to a large entropy value. The mathematical **logarithm**, or **log**, function⁴ does almost exactly the transformation that we need.

If we examine the graph of the **binary logarithm** (a logarithm to the base 2) of probabilities ranging from 0 to 1, shown in [Figure 4.6\(a\)](#)^[125], we see that the logarithm function returns large negative numbers for low probabilities and small negative numbers for high probabilities. Aside from the fact that the logarithm function returns negative numbers, the magnitude of the numbers it returns is ideal as a measure of entropy: large numbers for low probabilities and small numbers (near zero) for high probabilities. It should also be noted that the range of values for the binary logarithm of a probability, $[-\infty, 0]$, is much larger than those taken by the probability itself $[0,1]$. This is also an attractive characteristic of this function. It is more convenient for us to convert the output of the log function to positive numbers by multiplying them by -1 . [Figure 4.6\(b\)](#)^[125] shows the impact of this.

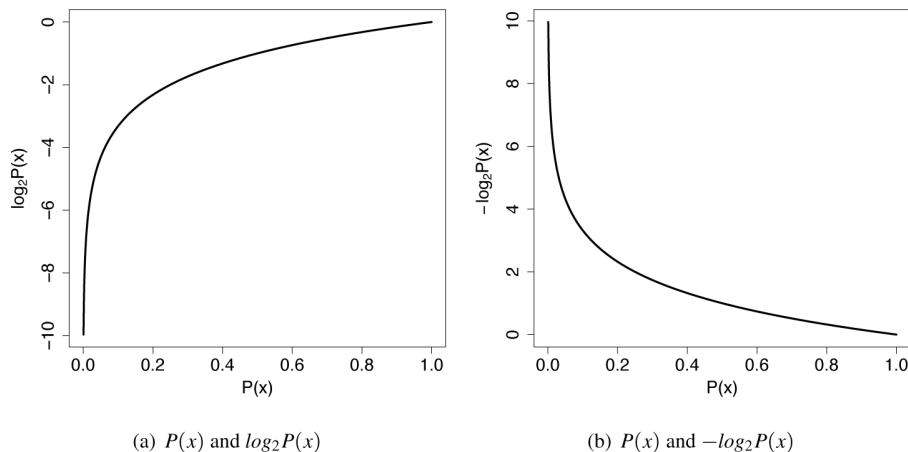


Figure 4.6

(a) A graph illustrating how the value of a binary log (the log to the base 2) of a probability changes across the range of probability values; and (b) the impact of multiplying these values by -1 .

Shannon's model of entropy is a weighted sum of the logs of the probabilities of each possible outcome when we make a random selection from a set. The weights used in the sum are the probabilities of the outcomes themselves, so that outcomes with high probabilities contribute

more to the overall entropy of a set than outcomes with low probabilities. Shannon's model of entropy is defined as

$$H(t) = - \sum_{i=1}^l (P(t = i) \times \log_s(P(t = i))) \quad (4.1)$$

where $P(t = i)$ is the probability that the outcome of randomly selecting an element t is the type i ; l is the number of different types of things in the set; and s is an arbitrary logarithmic base. The minus sign at the beginning of the equation is simply added to convert the negative numbers returned by the log function to positive ones (as described above). We will always use 2 as the base, s , when we calculate entropy, which means that we measure entropy in **bits**.⁵ Equation (4.1)^[125] is the cornerstone of modern **information theory** and is an excellent measure of the impurity—**heterogeneity**—of a set.

To understand how Shannon's entropy model works, consider the example of a set of 52 different playing cards. The probability of randomly selecting any specific card i from this set, $P(card = i)$, is quite low, just $\frac{1}{52}$. The entropy of the set of 52 playing cards is calculated

$$\begin{aligned} H(card) &= - \sum_{i=1}^{52} P(card = i) \times \log_2(P(card = i)) \\ &= - \sum_{i=1}^{52} 0.019 \times \log_2(0.019) \\ &= - \sum_{i=1}^{52} -0.1096 \\ &= 5.700 \text{ bits} \end{aligned}$$

In this calculation, for each possible card Shannon's model multiplies a small probability, $P(card = i)$, by a large negative number, $\log_2(P(card = i))$, resulting in a relatively large negative number. The individual relatively large negative numbers calculated for all the cards are then summed to return one large negative number. The sign of this is inverted to give a large positive value for the entropy of this very impure set.

By contrast, consider the example of calculating the entropy of a set of 52 playing cards if we distinguish between cards on the sole basis of their

suit (hearts ♠, clubs ♣, diamonds ♦ or, spades ♠). This time, there are only four possible outcomes when a random card is selected from this set, each with a reasonably large probability of $\frac{13}{52}$. The entropy associated with this set can be calculated

$$\begin{aligned}
 H(\text{suit}) &= - \sum_{l \in \{\heartsuit, \clubsuit, \diamondsuit, \spadesuit\}} P(\text{suit} = l) \times \log_2(P(\text{suit} = l)) \\
 &= - \left((P(\heartsuit) \times \log_2(P(\heartsuit))) + (P(\clubsuit) \times \log_2(P(\clubsuit))) \right. \\
 &\quad \left. + (P(\diamondsuit) \times \log_2(P(\diamondsuit))) + (P(\spadesuit) \times \log_2(P(\spadesuit))) \right) \\
 &= - \left(\left(\frac{13}{52} \times \log_2\left(\frac{13}{52}\right)\right) + \left(\frac{13}{52} \times \log_2\left(\frac{13}{52}\right)\right) \right. \\
 &\quad \left. + \left(\frac{13}{52} \times \log_2\left(\frac{13}{52}\right)\right) + \left(\frac{13}{52} \times \log_2\left(\frac{13}{52}\right)\right) \right) \\
 &= - ((0.25 \times -2) + (0.25 \times -2) + (0.25 \times -2) + (0.25 \times -2)) \\
 &= 2 \text{ bits}
 \end{aligned}$$

In this calculation Shannon's model multiples the large probability of selecting a specific suit, $P(\text{suit} = l)$, by a small negative number, $\log_2(P(\text{suit} = l))$, to return a relatively small negative number. The relatively small negative numbers associated with each suit are summed to result in a small negative number overall. Again, the sign of this number is inverted to result in a small positive value for the entropy of this much purer set.

To further explore the entropy, we can return to look at the entropy values of each set of cards shown in [Figure 4.5](#)^[124]. In the set shown in [Figure 4.5\(a\)](#)^[124], all the cards are identical. This means that there is no uncertainty about the result when a selection is made from this set. Shannon's model of information is designed to reflect this intuition, and the entropy value for this set is 0.00 bits. In the sets shown in [Figures 4.5\(b\)](#)^[124] and [4.5\(c\)](#)^[124], there is a mixture of two different types of cards, so that these have higher entropy values—in these instances, 0.81 bits and 1.00 bit. The maximum entropy for a set with two types of elements is 1.00 bit, which occurs when there are equal numbers of each type in the set.

The sets shown in [Figures 4.5\(d\)](#)^[124] and [4.5\(e\)](#)^[124] both have three types of cards. The maximum entropy for sets with three elements is 1.58 and occurs when there are equal numbers of each type in the set, as is the case shown in [Figure 4.5\(e\)](#)^[124]. [Figure 4.5\(d\)](#)^[124] shows one card type to be more present than the others, so the overall entropy is slightly lower, 1.50 bits.

Finally, the set shown in [Figure 4.5\(f\)](#)^[124] has a large number of card types, each represented only once, which leads to the high entropy value of 3.58 bits.

This discussion highlights that entropy is essentially a measure of the heterogeneity of a set. As the composition of the sets changed from the set with only one type of element ([Figure 4.5\(a\)](#)^[124]) to a set with many different types of elements, each with an equal likelihood of being selected ([Figure 4.5\(f\)](#)^[124]), the entropy score for the sets increased.

4.2.3 Information Gain

What is the relationship between a measure of heterogeneity of a set and predictive analytics? If we can construct a sequence of tests that splits the training data into pure sets with respect to the target feature values, then we can label queries by applying the same sequence of tests to a query and labeling it with the target feature value of instances in the set in which it ends up.

To illustrate this we return to the spam dataset given in [Table 4.2](#)^[121]. [Figure 4.7](#)^[128] shows how the instances in the spam dataset are split when we partition it using each of the three descriptive features. In [Figure 4.7\(a\)](#)^[128], we can see that splitting the dataset based on the SUSPICIOUS WORDS feature provides a lot of information about whether an email is spam or ham. In fact, partitioning the data by this feature creates two pure sets: one containing only instances with the target level *spam* and the other set containing only instances with the target level *ham*. This indicates that the SUSPICIOUS WORDS feature is a good feature to test if we are trying to decide whether a new email—not listed in the training dataset—is spam or not.

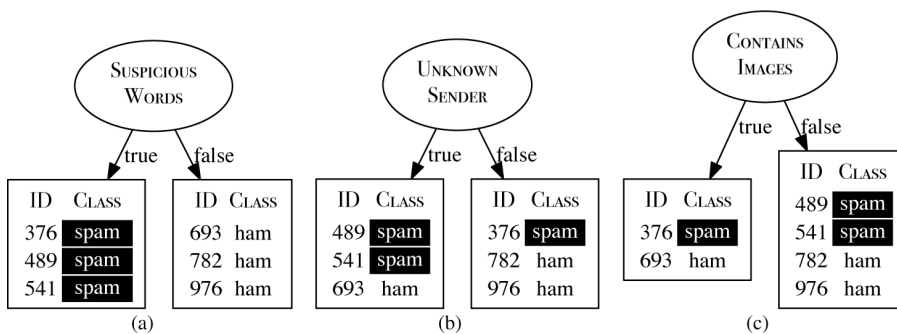


Figure 4.7

How the instances in the spam dataset split when we partition using each of the different descriptive features from the spam dataset in [Table 4.2](#)^[121].

What about the other features? [Figure 4.7\(b\)](#)^[128] shows how the UNKNOWN SENDER feature partitions the dataset. The resulting sets both contain a mixture of *spam* and *ham* instances. This indicates that the UNKNOWN SENDER feature is not as good at discriminating between spam and ham emails as the SUSPICIOUS WORDS feature. Although there is a mixture in each of these sets, however, it seems to be the case that when UNKNOWN SENDER = *true*, the majority of emails are *spam*, and when UNKNOWN SENDER = *false*, the majority of emails are *ham*. Therefore, although this feature doesn't perfectly discriminate between spam and ham, it does give us some information that we might be able to use in conjunction with other features to help decide whether a new email is spam or ham. Finally, if we examine the partitioning of the dataset based on the CONTAINS IMAGES feature, shown in [Figure 4.7\(c\)](#)^[128], it looks like this feature is not very discriminatory for *spam* and *ham* at all. Both the resulting sets contain a balanced mixture of spam and ham instances.

What we need to do at this point is to develop a formal model that captures the intuitions about the informativeness of these features. Unsurprisingly, we do this using Shannon's entropy model. The measure of informativeness that we use is known as **information gain**, which is a measure of the reduction in the overall entropy of a set of instances that is achieved by testing on a descriptive feature. Computing information gain is a three-step process:

1. Compute the entropy of the original dataset with respect to the target feature. This gives us a measure of how much information is required to organize the dataset into pure sets.
2. For each descriptive feature, create the sets that result by partitioning the instances in the dataset using their feature values, and then sum the entropy scores of each of these sets. This gives a measure of the information that remains required to organize the instances into pure sets after we have split them using the descriptive feature.
3. Subtract the remaining entropy value (computed in step 2) from the original entropy value (computed in step 1) to give the information gain.

We need to define three equations to formally specify information gain (one for each step). The first equation calculates the entropy for a dataset with

respect to a target feature⁶

$$H(t, \mathcal{D}) = - \sum_{l \in levels(t)} (P(t = l) \times \log_2(P(t = l))) \quad (4.2)$$

where $levels(t)$ is the set of levels in the domain of the target feature t ; and $P(t = l)$ is the probability of a randomly selected instance having the target feature level l .

The second equation defines how we compute the entropy remaining after we partition the dataset using a particular descriptive feature d . When we partition the dataset \mathcal{D} using the descriptive feature d , we create a number of partitions (or sets) $\mathcal{D}_{d=l_1} \dots \mathcal{D}_{d=l_k}$, where $l_1 \dots l_k$ are the k levels that feature d can take. Each partition, $\mathcal{D}_{d=l_i}$, contains the instances in \mathcal{D} that have a value of level l_i for the d feature. The entropy remaining after we have tested d is a weighted sum of the entropy, still with respect to the target feature, of each partition. The weighting is determined by the size of each partition—so a large partition should contribute more to the overall remaining entropy than a smaller partition. We use the term $rem(d, \mathcal{D})$ to denote this quantity and define it formally

$$rem(d, \mathcal{D}) = \sum_{l \in levels(d)} \underbrace{\frac{|\mathcal{D}_{d=l}|}{|\mathcal{D}|}}_{\text{weighting}} \times \underbrace{H(t, \mathcal{D}_{d=l})}_{\substack{\text{entropy of} \\ \text{partition } \mathcal{D}_{d=l}}} \quad (4.3)$$

Using Equation (4.2)^[129] and Equation (4.3)^[129], we can now formally define information gain made from splitting the dataset \mathcal{D} using the feature d

$$IG(d, \mathcal{D}) = H(t, \mathcal{D}) - rem(d, \mathcal{D}) \quad (4.4)$$

To illustrate how information gain is calculated and to check how well it models our intuitions described at the beginning of this section, we compute the information gain for each descriptive feature in the spam dataset. The first step is to compute the entropy for the whole dataset using Equation (4.2)^[129]

$$\begin{aligned}
H(t, \mathcal{D}) &= - \sum_{l \in \{\text{spam}, \text{ham}\}} (P(t = l) \times \log_2(P(t = l))) \\
&= - ((P(t = \text{spam}) \times \log_2(P(t = \text{spam}))) \\
&\quad + (P(t = \text{ham}) \times \log_2(P(t = \text{ham})))) \\
&= - ((^3/6 \times \log_2(^3/6)) + (^3/6 \times \log_2(^3/6))) \\
&= 1 \text{ bit}
\end{aligned}$$

The next step is to compute the entropy remaining after we split the dataset using each of the descriptive features. The computation for the SUSPICIOUS WORDS feature is⁷

$$\begin{aligned}
rem(\text{WORDS}, \mathcal{D}) &= \left(\frac{|\mathcal{D}_{\text{WORDS}=\text{true}}|}{|\mathcal{D}|} \times H(t, \mathcal{D}_{\text{WORDS}=\text{true}}) \right) \\
&\quad + \left(\frac{|\mathcal{D}_{\text{WORDS}=\text{false}}|}{|\mathcal{D}|} \times H(t, \mathcal{D}_{\text{WORDS}=\text{false}}) \right) \\
&= \left(^3/6 \times \left(- \sum_{l \in \{\text{spam}, \text{ham}\}} P(t = l) \times \log_2(P(t = l)) \right) \right) \\
&\quad + \left(^3/6 \times \left(- \sum_{l \in \{\text{spam}, \text{ham}\}} P(t = l) \times \log_2(P(t = l)) \right) \right) \\
&= (^3/6 \times (-((^3/3 \times \log_2(^3/3)) + (^0/3 \times \log_2(^0/3))))) \\
&\quad + (^3/6 \times (-((^0/3 \times \log_2(^0/3)) + (^3/3 \times \log_2(^3/3))))) \\
&= 0 \text{ bits}
\end{aligned}$$

The remaining entropy for the UNKNOWN SENDER feature is

$$\begin{aligned}
& rem(\text{SENDER}, \mathcal{D}) \\
&= \left(\frac{|\mathcal{D}_{\text{SENDER}=\text{true}}|}{|\mathcal{D}|} \times H(t, \mathcal{D}_{\text{SENDER}=\text{true}}) \right) \\
&\quad + \left(\frac{|\mathcal{D}_{\text{SENDER}=\text{false}}|}{|\mathcal{D}|} \times H(t, \mathcal{D}_{\text{SENDER}=\text{false}}) \right) \\
&= \left(\frac{3}{6} \times \left(- \sum_{l \in \{\text{spam}, \text{ham}\}} P(t = l) \times \log_2(P(t = l)) \right) \right) \\
&\quad + \left(\frac{3}{6} \times \left(- \sum_{l \in \{\text{spam}, \text{ham}\}} P(t = l) \times \log_2(P(t = l)) \right) \right) \\
&= \left(\frac{3}{6} \times \left(- \left(\left(\frac{2}{3} \times \log_2\left(\frac{2}{3}\right) \right) + \left(\frac{1}{3} \times \log_2\left(\frac{1}{3}\right) \right) \right) \right) \right. \\
&\quad \left. + \left(\frac{3}{6} \times \left(- \left(\left(\frac{1}{3} \times \log_2\left(\frac{1}{3}\right) \right) + \left(\frac{2}{3} \times \log_2\left(\frac{2}{3}\right) \right) \right) \right) \right) \right) \\
&= 0.9183 \text{ bits}
\end{aligned}$$

The remaining entropy for the CONTAINS IMAGES feature is

$$\begin{aligned}
& rem(\text{IMAGES}, \mathcal{D}) \\
&= \left(\frac{|\mathcal{D}_{\text{IMAGES}=\text{true}}|}{|\mathcal{D}|} \times H(t, \mathcal{D}_{\text{IMAGES}=\text{true}}) \right) \\
&\quad + \left(\frac{|\mathcal{D}_{\text{IMAGES}=\text{false}}|}{|\mathcal{D}|} \times H(t, \mathcal{D}_{\text{IMAGES}=\text{false}}) \right) \\
&= \left(\frac{2}{6} \times \left(- \sum_{l \in \{\text{spam}, \text{ham}\}} P(t = l) \times \log_2(P(t = l)) \right) \right) \\
&\quad + \left(\frac{4}{6} \times \left(- \sum_{l \in \{\text{spam}, \text{ham}\}} P(t = l) \times \log_2(P(t = l)) \right) \right) \\
&= \left(\frac{2}{6} \times \left(- \left(\left(\frac{1}{2} \times \log_2\left(\frac{1}{2}\right) \right) + \left(\frac{1}{2} \times \log_2\left(\frac{1}{2}\right) \right) \right) \right) \right. \\
&\quad \left. + \left(\frac{4}{6} \times \left(- \left(\left(\frac{2}{4} \times \log_2\left(\frac{2}{4}\right) \right) + \left(\frac{2}{4} \times \log_2\left(\frac{2}{4}\right) \right) \right) \right) \right) \right) \\
&= 1 \text{ bit}
\end{aligned}$$

We can now complete the information gain calculation for each descriptive feature

$$\begin{aligned}
IG(\text{WORDS}, \mathcal{D}) &= H(\text{CLASS}, \mathcal{D}) - rem(\text{WORDS}, \mathcal{D}) \\
&= 1 - 0 \\
&= 1 \text{ bit} \\
IG(\text{SENDER}, \mathcal{D}) &= H(\text{CLASS}, \mathcal{D}) - rem(\text{SENDER}, \mathcal{D}) \\
&= 1 - 0.9183 \\
&= 0.0817 \text{ bits} \\
IG(\text{IMAGES}, \mathcal{D}) &= H(\text{CLASS}, \mathcal{D}) - rem(\text{IMAGES}, \mathcal{D}) \\
&= 1 - 1 \\
&= 0 \text{ bits}
\end{aligned}$$

The information gain of the SUSPICIOUS WORDS feature is 1 bit. This is equivalent to the total entropy for the entire dataset. An information gain score for a feature that matches the entropy for the entire dataset indicates that the feature is perfectly discriminatory with respect to the target feature values. Unfortunately, in more realistic datasets, finding a feature as powerful as the SUSPICIOUS WORDS feature is very rare. The feature UNKNOWN SENDER has an information gain of 0.0817 bits. An information gain score this low suggests that although splitting on this feature provides some information, it is not particularly useful. Finally, the CONTAINS IMAGES feature has an information gain score of 0 bits. This ranking of the features by information gain mirrors the intuitions that we developed about the usefulness of these features during our previous discussion.

We started this section with the idea that if we could construct a sequence of tests that splits the training data into pure sets with respect to the target feature values, then we could do prediction by applying the same sequence of tests to the prediction queries and labeling them with the target feature of the set in which they end up. A key part of doing this is being able to decide which tests should be included in the sequence and in what order. The information gain model we have developed allows us to decide which test we should add to the sequence next because it enables us to select the best feature to use on a given dataset. In the next section, we introduce the standard algorithm for growing decision trees in this way.

4.3 Standard Approach: The ID3 Algorithm

Assuming that we want to use shallow decision trees, is there a way in which we can automatically create them from data? One of the best known decision tree induction algorithms is the **Iterative Dichotomizer 3 (ID3)** algorithm.⁸ This algorithm attempts to create the shallowest decision tree that is consistent with the data given.

The ID3 algorithm builds the tree in a recursive, depth-first manner, beginning at the root node and working down to the leaf nodes. The algorithm begins by choosing the best descriptive feature to test (i.e., the best question to ask first). This choice is made by computing the **information gain** of the descriptive features in the training dataset. A root node is then added to the tree and labeled with the selected test feature. The training dataset is then partitioned using the test. There is one partition created for each possible test result, which contains the training instances that returned that result. For each partition a branch is grown from the node. The process is then repeated for each branch using the relevant partition of the training set in place of the full training set and with the selected test feature excluded from further testing. This process is repeated until all the instances in a partition have the same target level, at which point a leaf node is created and labeled with that level.

The design of the ID3 algorithm is based on the assumption that a correct decision tree for a domain will classify instances from that domain in the same proportion as the target level occurs in the domain. So, given a dataset \mathcal{D} representing a domain with two target levels C_1 and C_2 , an arbitrary instance from the domain should be classified as being associated with target level C_1 with the probability $\frac{|C_1|}{|C_1|+|C_2|}$ and to target level C_2 with the probability $\frac{|C_2|}{|C_1|+|C_2|}$, where $|C_1|$ and $|C_2|$ refer to the number of instances in \mathcal{D} associated with C_1 and C_2 , respectively. To ensure that the resulting decision tree classifies in the correct proportions, the decision tree is constructed by repeatedly partitioning⁹ the training dataset until every instance in a partition maps to the same target level.

Algorithm 1^[134] lists a pseudocode description of the ID3 algorithm. Although the algorithm looks quite complex, it essentially does one of two things each time it is invoked: either it stops growing the current path in the tree by adding a leaf node to the tree, Lines 1–6, or it extends the current

path by adding an interior node to the tree and growing the branches of this node by repeatedly rerunning the algorithm, Lines 7–13.

Algorithm 1 Pseudocode description of the ID3 algorithm.

Require: set of descriptive features \mathbf{d}

Require: set of training instances \mathcal{D}

- 1: **if** all the instances in \mathcal{D} have the same target level C **then return** a decision tree consisting of a leaf node with label C
- 2: **else if** \mathbf{d} is empty **then return** a decision tree consisting of a leaf node with the label of the majority target level in \mathcal{D}
- 3: **else if** \mathcal{D} is empty **then return** a decision tree consisting of a leaf node with the label of the majority target level of the dataset of the immediate parent node
- 4: **else**
- 5: $\mathbf{d}[\text{best}] \leftarrow \arg \max_{d \in \mathbf{d}} IG(d, \mathcal{D})$
- 6: make a new node, $Node_{\mathbf{d}[\text{best}]}$, and label it with $\mathbf{d}[\text{best}]$
- 7: partition \mathcal{D} using $\mathbf{d}[\text{best}]$
- 8: remove $\mathbf{d}[\text{best}]$ from \mathbf{d}
- 9: **for** each partition \mathcal{D}_i of \mathcal{D} **do**
- 10: grow a branch from $Node_{\mathbf{d}[\text{best}]}$ to the decision tree created by rerunning *ID3* with $\mathcal{D} = \mathcal{D}_i$
- 11: **end for**
- 12: **end if**

Lines 1–6 of Algorithm 1^[134] control when a new leaf node is created in the tree. We previously mentioned that the ID3 algorithm constructs the decision tree by recursively partitioning the dataset. An important decision to be made in designing any recursive process is what the base cases that stop the recursion will be. In the ID3 algorithm the base cases are the situations in which we stop splitting the dataset and construct a leaf node with an associated target level. There are two important things to remember in designing these base cases. First, the dataset of training instances considered at each of the interior nodes in the tree is not the complete dataset; rather, it is the subset of instances considered at its parent node that had the relevant feature value for the branch from the parent to the current node. Second, once a feature has been tested, it is not considered for selection again along that path in the tree. A feature will be tested only once

on any path in the tree, but it may occur several times in the tree on different paths. On the basis of these constraints, the algorithm defines three situations where the recursion stops and a leaf node is constructed:

1. All the instances in the dataset have the same target feature level. In this situation, the algorithm returns a single leaf node tree with that target level as its label (Algorithm 1^[134] Lines 1–2).
2. The set of features left to test is empty. This means that we have already tested every feature on the path between the root node and the current node. We have no more features we can use to distinguish between the instances, so we return a single leaf node tree with the majority target level of the dataset as its target level (Algorithm 1^[134] Lines 3–4).
3. The dataset is empty. This can occur when, for a particular partition of the dataset, there are no instances that have a particular feature value. In this case we return a single leaf node tree with the majority target level of the dataset at the parent node that made the recursive call (Algorithm 1^[134] Lines 5–6).

If none of these cases holds, the algorithm continues to recursively create interior nodes, Lines 7–13 of Algorithm 1^[134]. The first step in creating an interior node is to decide which descriptive feature should be tested at this node (Line 8 of Algorithm 1^[134]). When we first mentioned the ID3 algorithm, we stated that it tries to create the shallowest decision tree that is consistent with the data given. The feature of the ID3 algorithm that biases it toward shallow trees is the mechanism that it uses to determine which descriptive feature is the *most informative* one to test at a new node. The ID3 algorithm uses the **information gain** metric to choose the best feature to test at each node in the tree. Consequently, the selection of the best feature on which to split a dataset is based on the purity, or homogeneity, of the resulting partitions in the datasets. Again, remember that each node is constructed in a context consisting of a dataset of instances containing a subset of the instances used to construct its parent node and the set of descriptive features that have not been tested on the path between the root node and parent node. As a result, the information gain for a particular descriptive feature may be different at different nodes in the tree because it will be computed on different subsets of the full training dataset. One

consequence of this is that a feature with a low information gain at the root node (when the full dataset is considered) may have a high information gain score at one of the interior nodes because it is predictive on the subset of instances that are considered at that interior node.

Once the most informative feature, $\mathbf{d}[best]$, has been chosen, the algorithm adds a new node, labeled with the feature $\mathbf{d}[best]$, to the tree (Line 9). It then splits the dataset that was considered at this node, \mathcal{D} , into partitions, $\mathcal{D}_1, \dots, \mathcal{D}_k$, according to the levels that $\mathbf{d}[best]$ can take, $\{l_1, \dots, l_k\}$ (Line 10). Next, it removes the feature $\mathbf{d}[best]$ from the set of features considered for testing later on this path in the tree; this enforces the constraint that a feature can be tested only once on any particular path in the tree (Line 11). Finally, in Lines 12 and 13, the algorithm grows a branch in the tree for each of the values in the domain of $\mathbf{d}[best]$ by recursively calling itself for each of the partitions created at Line 10. Each of these recursive calls uses the partition it is called on as the dataset it considers and is restricted to selecting from the set of features that have not been tested so far on the path from the root node. The node returned by the recursive call to the algorithm may be the root of a subtree or a leaf node. Either way, it is joined to the current node with a branch labeled with the appropriate level of the selected feature.

4.3.1 A Worked Example: Predicting Vegetation Distributions

In this section we work through an example to illustrate how the ID3 is used to induce a decision tree. This example is based on **ecological modeling**, an area of scientific research that applies statistical and analytical techniques to model ecological processes. One of the problems faced by ecological management practitioners is that it is often too expensive to do large-scale, high-resolution land surveys. Using predictive analytics, however, the results of small-scale surveys can be used to create predictive models that can be applied across large regions. These models are used to inform resource management and conservation activities,¹⁰ such as managing the distribution of animal species and vegetation across geographic regions. The descriptive features used by these models often can be automatically extracted from digitized maps, aerial photographs, or satellite imagery—for example, the elevation, steepness, color, and spectral

reflection of the terrain and the presence or absence of features such as rivers, roads, or lakes.

Table 4.3 lists an example dataset from the ecological modeling domain.¹¹ In this example, the prediction task is to classify the type of vegetation that is likely to be growing in areas of land on the sole basis of descriptive features extracted from maps of the areas. Ecological modelers can use information about the type of vegetation that grows in a region as a direct input into their animal species management and conservation programs because areas covered in different types of vegetation support different animal species. By using a predictive model that requires only features from maps, the ecological modelers can avoid expensive ground-based or aerial surveys. There are three types of vegetation that should be recognized by this model. First, *chapparal* is a type of evergreen shrubland that can be fire-prone. The animal species typically found in this vegetation include gray foxes, bobcats, skunks, and rabbits. Second, *riparian* vegetation occurs near streams and is characterized by trees and shrubs. It is usually home to small animals, including raccoons, frogs, and toads. Finally, *conifer* refers to forested areas that contain a variety of tree species (including pine, cedar, and fir trees), with a mixture of shrubs on the forest floor. The animals that may be found in these forests include bears, deer, and cougars. The type of vegetation in an area is stored in the target feature, VEGETATION.

Table 4.3
The vegetation classification dataset.

ID	STREAM	SLOPE	ELEVATION	VEGETATION
1	false	steep	high	chapparal
2	true	moderate	low	riparian
3	true	steep	medium	riparian
4	false	steep	medium	chapparal
5	false	flat	high	conifer
6	true	steep	highest	conifer
7	true	steep	high	chapparal

There are three descriptive features in the dataset. STREAM is a binary feature that describes whether or not there is a stream in the area. SLOPE describes the steepness of the terrain in an area and has the levels *flat*, *moderate*, and *steep*. ELEVATION describes the elevation of an area and has the levels *low*, *medium*, *high*, and *highest*.

The first step in building the decision tree is to determine which of the three descriptive features is the best one to split the dataset on at the root node. The algorithm does this by computing the information gain for each feature. The total entropy for this dataset, which is required to calculate information gain, is computed

$$\begin{aligned}
H(\text{VEGETATION}, \mathcal{D}) &= - \sum_{l \in \{\text{chapparal, riparian, conifer}\}} P(\text{VEGETATION} = l) \times \log_2 (P(\text{VEGETATION} = l)) \\
&= - ((^3/7 \times \log_2 (^3/7)) + (^2/7 \times \log_2 (^2/7)) + (^2/7 \times \log_2 (^2/7))) \\
&= 1.5567 \text{ bits}
\end{aligned} \tag{4.5}$$

[Table 4.4](#)^[137] shows the calculation of the information gain for each feature using this result.

Table 4.4

Partition sets (Part.), entropy, remainder (Rem.), and information gain (Info. Gain) by feature for the dataset in [Table 4.3](#)^[136].

Split by				Partition		Info.
Feature	Level	Part.	Instances	Entropy	Rem.	Gain
STREAM	<i>true</i>	\mathcal{D}_1	$\mathbf{d}_2, \mathbf{d}_3, \mathbf{d}_6, \mathbf{d}_7$	1.5000	1.2507	0.3060
	<i>false</i>	\mathcal{D}_2	$\mathbf{d}_1, \mathbf{d}_4, \mathbf{d}_5$	0.9183		
SLOPE	<i>flat</i>	\mathcal{D}_3	\mathbf{d}_5	0.0	0.9793	0.5774
	<i>moderate</i>	\mathcal{D}_4	\mathbf{d}_2	0.0		
	<i>steep</i>	\mathcal{D}_5	$\mathbf{d}_1, \mathbf{d}_3, \mathbf{d}_4, \mathbf{d}_6, \mathbf{d}_7$	1.3710		
ELEVATION	<i>low</i>	\mathcal{D}_6	\mathbf{d}_2	0.0	0.6793	0.8774
	<i>medium</i>	\mathcal{D}_7	$\mathbf{d}_3, \mathbf{d}_4$	1.0		
	<i>high</i>	\mathcal{D}_8	$\mathbf{d}_1, \mathbf{d}_5, \mathbf{d}_7$	0.9183		
	<i>highest</i>	\mathcal{D}_9	\mathbf{d}_6	0.0		

We can see from the information in [Table 4.4](#)^[137] that ELEVATION has the largest information gain of the three features and therefore is selected by the algorithm at the root node of the tree. [Figure 4.8](#)^[138] shows the state of the tree after the dataset is split using ELEVATION. Notice that the full dataset has been split into four partitions (labeled \mathcal{D}_6 , \mathcal{D}_7 , \mathcal{D}_8 , and \mathcal{D}_9 in [Table 4.4](#)^[137]) and that the feature ELEVATION is no longer listed in these partitions because it has already been used to split the data. The \mathcal{D}_6 and \mathcal{D}_9 partitions each contain just one instance. Consequently they are pure sets, and these partitions can be converted into leaf nodes. The \mathcal{D}_7 and \mathcal{D}_8 partitions, however, contain instances with a mixture of target feature levels, so the algorithm needs to continue splitting these partitions. To do this, the algorithm needs to decide which of the remaining descriptive features has the highest information gain for each partition.

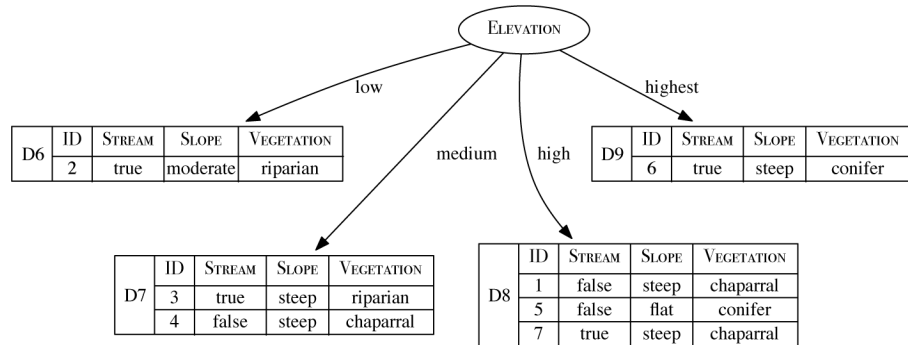


Figure 4.8

The decision tree after the data has been split using ELEVATION.

To address partition \mathcal{D}_7 , first the algorithm computes the entropy of \mathcal{D}_7

$$\begin{aligned}
 H(\text{VEGETATION}, \mathcal{D}_7) &= - \sum_{l \in \{\text{chaparral, riparian, conifer}\}} P(\text{VEGETATION} = l) \times \log_2(P(\text{VEGETATION} = l)) \\
 &= - ((1/2 \times \log_2(1/2)) + (1/2 \times \log_2(1/2)) + (0/2 \times \log_2(0/2))) \\
 &= 1.0 \text{ bits}
 \end{aligned} \tag{4.6}$$

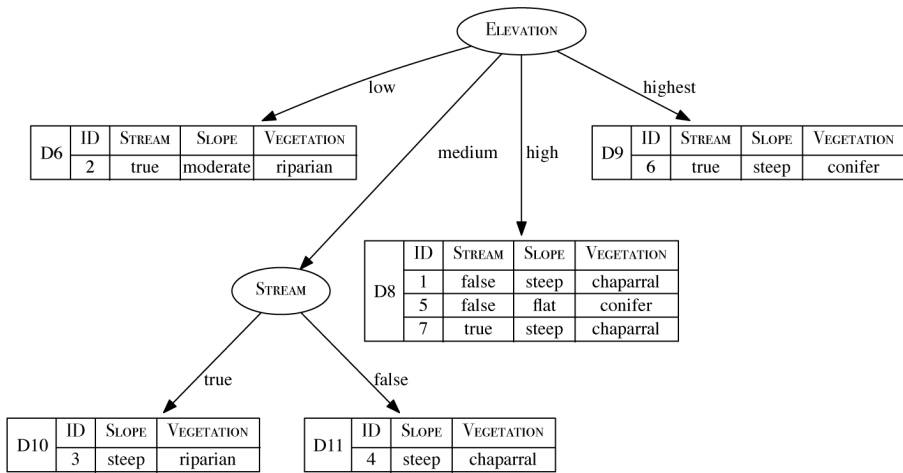
The information gained by splitting \mathcal{D}_7 for using STREAM and SLOPE is then computed as presented in [Table 4.5](#)^[138].

Table 4.5

Partition sets (Part.), entropy, remainder (Rem.), and information gain (Info. Gain) by feature for the dataset \mathcal{D}_7 in Figure 4.8^[138].

Split by Feature	Level	Part.	Instances	Partition Entropy	Rem.	Info. Gain
STREAM	<i>true</i>	\mathcal{D}_{10}	\mathbf{d}_3	0.0	0.0	1.0
	<i>false</i>	\mathcal{D}_{11}	\mathbf{d}_4	0.0		
SLOPE	<i>flat</i>	\mathcal{D}_{12}		0.0	1.0	0.0
	<i>moderate</i>	\mathcal{D}_{13}		0.0		
	<i>steep</i>	\mathcal{D}_{14}	$\mathbf{d}_3, \mathbf{d}_4$	1.0		

The calculations in Table 4.5^[138] show that STREAM has a higher information gain than SLOPE and so is the best feature with which to split \mathcal{D}_7 . Figure 4.9^[139] depicts the state of the decision tree after the \mathcal{D}_7 partition has been split. Splitting \mathcal{D}_7 creates two new partitions (\mathcal{D}_{10} and \mathcal{D}_{11}). Notice that SLOPE is the only descriptive feature that is listed in \mathcal{D}_{10} and \mathcal{D}_{11} . This reflects that ELEVATION and STREAM have already been used on the path from the root node to each of these partitions and so cannot be used again. Both these new partitions are pure sets with respect to the target feature (indeed, they contain only one instance each), and consequently these sets do not need to be split any further and can be converted into leaf nodes.

**Figure 4.9**

The state of the decision tree after the \mathcal{D}_7 partition has been split using STREAM.

At this point \mathcal{D}_8 is the only partition that is not a pure set. There are two descriptive features that can be used to split \mathcal{D}_8 : STREAM and SLOPE. The decision regarding which of these features to use for the split is made by calculating which feature has the higher information gain for \mathcal{D}_8 . The overall entropy for \mathcal{D}_8 is calculated

$$\begin{aligned}
 H(\text{VEGETATION}, \mathcal{D}_8) &= - \sum_{l \in \{\text{chaparral, riparian, conifer}\}} P(\text{VEGETATION} = l) \times \log_2(P(\text{VEGETATION} = l)) \\
 &= - ((^2/3 \times \log_2(^2/3)) + (^0/3 \times \log_2(^0/3)) + (^1/3 \times \log_2(^1/3))) \\
 &= 0.9183 \text{ bits}
 \end{aligned} \tag{4.7}$$

[Table 4.6](#)^[140] details the calculation of the information gain for each descriptive feature in \mathcal{D}_8 using this result. It is clear from the information in [Table 4.6](#)^[140] that in the context of \mathcal{D}_8 , SLOPE has a higher information gain than STREAM.

Table 4.6

Partition sets (Part.), entropy, remainder (Rem.), and information gain (Info. Gain) by feature for the dataset \mathcal{D}_8 in [Figure 4.9](#)^[139].

Split by Feature	Level	Part.	Instances	Partition Entropy	Rem.	Info. Gain
STREAM	<i>true</i>	\mathcal{D}_{15}	\mathbf{d}_7	0.0	0.6666	0.2517
	<i>false</i>	\mathcal{D}_{16}	$\mathbf{d}_1, \mathbf{d}_5$	1.0		
SLOPE	<i>flat</i>	\mathcal{D}_{17}	\mathbf{d}_5	0.0	0.0	0.9183
	<i>moderate</i>	\mathcal{D}_{18}		0.0		
	<i>steep</i>	\mathcal{D}_{19}	$\mathbf{d}_1, \mathbf{d}_7$	0.0		

[Figure 4.10](#)^[140] illustrates the state of the decision tree after \mathcal{D}_8 has been split. Notice that one of the partitions created by splitting \mathcal{D}_8 on the basis of SLOPE is empty: \mathcal{D}_{18} . This is the case because there were no instances in \mathcal{D}_8 that had a value of *moderate* for the SLOPE feature. This empty partition will result in a leaf node that returns a prediction of the majority target level in \mathcal{D}_8 , *chaparral*. The other two partitions created by splitting \mathcal{D}_8 are pure with respect to the target feature: \mathcal{D}_{17} contains one instance with a *conifer* target

level, and \mathcal{D}_{19} contains two instances that both have a *chaparral* target level.

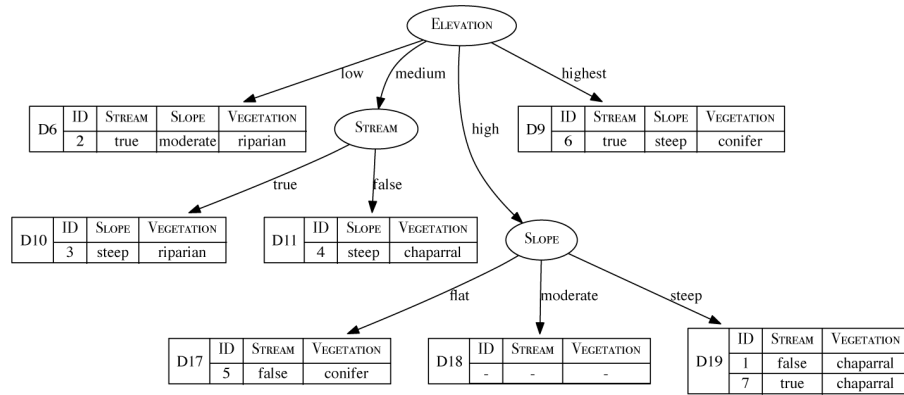


Figure 4.10

The state of the decision tree after the \mathcal{D}_8 partition has been split using SLOPE.

At this point all the remaining partitions are pure with respect to the target feature. Consequently, the algorithm converts each partition into a leaf node and returns the final decision tree. Figure 4.11^[141] shows this decision tree. If the prediction strategy encoded in this tree is applied to the original dataset in Table 4.3^[136], it will correctly classify all the instances in the dataset. In machine learning terms, the induced model is **consistent** with the training data.

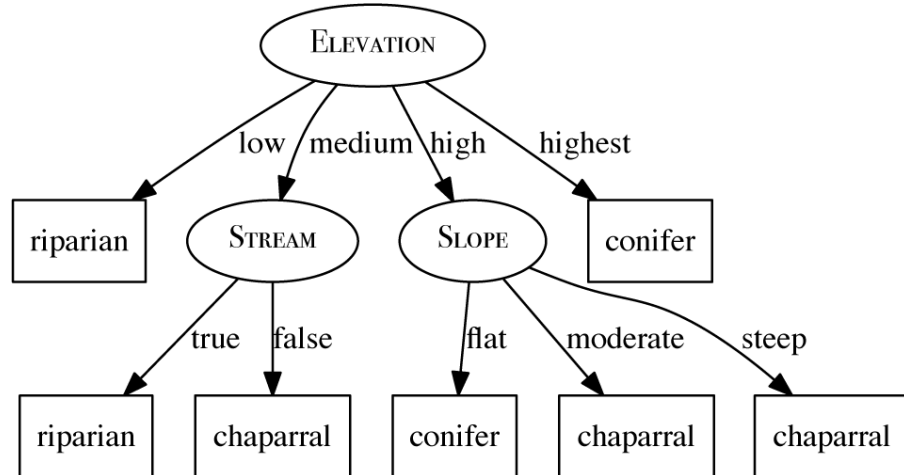


Figure 4.11

The final vegetation classification decision tree.

One final point: remember that the empty partition in [Figure 4.10](#)^[140] (\mathcal{D}_{18}) has been converted into a leaf node that returns the *chapparal* target level. The reason is that *chapparal* is the majority target level in the partition at the parent node (\mathcal{D}_8) of this leaf node. Consequently, this tree will return a prediction of VEGETATION = *chapparal* for the following query:

STREAM = *true*, SLOPE = *moderate*, ELEVATION = *high*

This is interesting because there are no instances listed in [Table 4.3](#)^[136] where SLOPE = *moderate* and VEGETATION = *chapparal*. This example illustrates one way in which the predictions made by the model generalize beyond the dataset. Whether the generalizations made by the model are correct will depend on whether the assumptions used in generating the model (i.e., the **inductive bias**) are appropriate.

The ID3 algorithm works in exactly the same way for larger, more complicated datasets; there is simply more computation involved. Since it was first proposed, there have been many modifications to the original ID3 algorithm to handle variations that are common in real-world datasets. We explore the most important of these modifications in the following sections.

4.4 Extensions and Variations

The ID3 decision tree induction algorithm described in the previous section provides the basic approach to decision tree induction: a top-down, recursive, depth-first partitioning of the dataset beginning at the root node and finishing at the leaf nodes. Although this algorithm works quite well as presented, it assumes categorical features and clean data. It is relatively easy, however, to extend the ID3 algorithm to handle continuous descriptive features and continuous target features. A range of techniques can also be used to make a decision tree more robust to noise in the data. In this section we describe the techniques used to address these issues as well as the use of ensemble methods that allow us to combine the predictions made by multiple models. We begin, however, by introducing some of the metrics, other than entropy-based information gain, that can be used to select the next feature to split on as we build the tree.

4.4.1 Alternative Feature Selection and Impurity Metrics

The information gain measure described in Section 4.2.3^[127] uses entropy to judge the impurity of the partitions that result from splitting a dataset using a particular feature. Entropy-based information gain, however, does have some drawbacks. In particular, it prefers features with many levels because these features split the data into many small subsets, which tend to be pure irrespective of any correlation between the descriptive feature and the target feature. One way of addressing this issue is to use **information gain ratio** instead of entropy. The information gain ratio is computed by dividing the information gain of a feature by the amount of information used to determine the value of the feature

$$GR(d, \mathcal{D}) = \frac{IG(d, \mathcal{D})}{-\sum_{l \in levels(d)} (P(d = l) \times \log_2(P(d = l)))} \quad (4.8)$$

where $IG(d, \mathcal{D})$ is the information gain of the feature d for the dataset \mathcal{D} (computed using Equation (4.4)^[130] from Section 4.2.3^[127]), and the divisor is the entropy of the dataset \mathcal{D} with respect to the feature d (note that $levels(d)$ is the set of levels that the feature d can take). This divisor biases information gain ratio away from features that take on a large number of values and as such counteracts the bias in information gain toward these features.

To illustrate how information gain ratio is computed, we compute the information gain ratio for the descriptive features STREAM, SLOPE, and ELEVATION in the vegetation classification dataset in Table 4.3^[136]. We already know the information gain for these features (see Table 4.4^[137])

$$\begin{aligned} IG(\text{STREAM}, \mathcal{D}) &= 0.3060 \\ IG(\text{SLOPE}, \mathcal{D}) &= 0.5774 \\ IG(\text{ELEVATION}, \mathcal{D}) &= 0.8774 \end{aligned}$$

To convert these information gain scores into information gain ratios, we need to compute the entropy of each feature and then divide the information gain scores by the respective entropy values. The entropy calculations for these descriptive features are

$$\begin{aligned}
H(\text{STREAM}, \mathcal{D}) &= - \sum_{l \in \{\text{true, } \text{false}\}} P(\text{STREAM} = l) \times \log_2(P(\text{STREAM} = l)) \\
&= - ((^4/7 \times \log_2(^4/7)) + (^3/7 \times \log_2(^3/7))) \\
&= 0.9852 \text{ bits}
\end{aligned}$$

$$\begin{aligned}
H(\text{SLOPE}, \mathcal{D}) &= - \sum_{l \in \{\text{flat, } \text{moderate, } \text{steep}\}} P(\text{SLOPE} = l) \times \log_2(P(\text{SLOPE} = l)) \\
&= - ((^1/7 \times \log_2(^1/7)) + (^1/7 \times \log_2(^1/7)) \\
&\quad + (^5/7 \times \log_2(^5/7))) \\
&= 1.1488 \text{ bits}
\end{aligned}$$

$$\begin{aligned}
H(\text{ELEVATION}, \mathcal{D}) &= - \sum_{l \in \{\text{low, } \text{medium, } \text{high, } \text{highest}\}} P(\text{ELEVATION} = l) \times \log_2(P(\text{ELEVATION} = l)) \\
&= - ((^1/7 \times \log_2(^1/7)) + (^2/7 \times \log_2(^2/7)) \\
&\quad + (^3/7 \times \log_2(^3/7)) + (^1/7 \times \log_2(^1/7))) \\
&= 1.8424 \text{ bits}
\end{aligned}$$

Using these results, we can compute the information gain ratio for each descriptive feature by dividing the feature's information gain by the entropy for that feature

$$\begin{aligned}
GR(\text{STREAM}, \mathcal{D}) &= \frac{0.3060}{0.9852} = 0.3106 \\
GR(\text{SLOPE}, \mathcal{D}) &= \frac{0.5774}{1.1488} = 0.5026 \\
GR(\text{ELEVATION}, \mathcal{D}) &= \frac{0.8774}{1.8424} = 0.4762
\end{aligned}$$

From these calculations we can see that SLOPE has the highest information gain ratio score, even though ELEVATION has the highest information gain. The implication is that if we built a decision tree for the

dataset in [Table 4.3](#)^[136] using information gain ratio, then SLOPE (rather than ELEVATION) would be the feature chosen for the root of the tree. [Figure 4.12](#)^[144] illustrates the tree that would be generated for this dataset using information gain ratio.

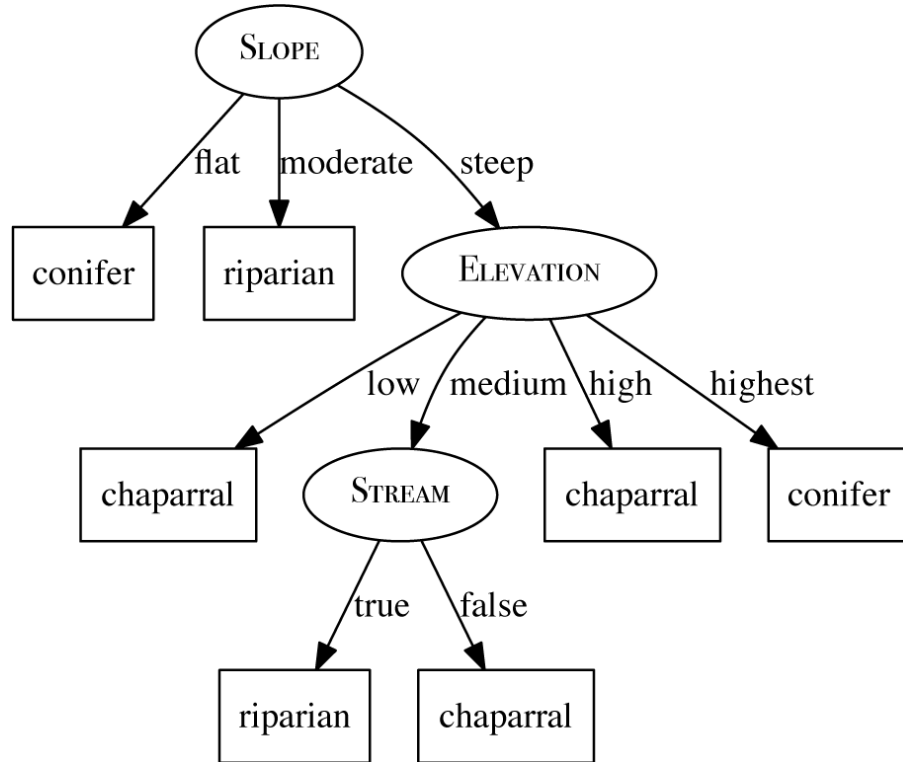


[Figure 4.12](#)

The vegetation classification decision tree generated using information gain ratio.

Notice that there is a *chaparral* leaf node at the end of the branch $\text{ELEVATION} = \text{low}$ even though there are no instances in the dataset where $\text{ELEVATION} = \text{low}$ and $\text{VEGETATION} = \text{chaparral}$. This leaf node is the result of an empty partition being generated when the partition at the ELEVATION node was split. This leaf node was assigned the target level *chaparral* because this was the majority target level in the partition at the ELEVATION node.

If we compare this decision tree to the decision tree generated using information gain (see [Figure 4.11](#)^[141]), it is obvious that the structure of the two trees is very different. This difference illustrates the effect of the metric used to select which feature to split on during tree construction. Another interesting point of comparison between these two trees is that even though

they are both consistent with the dataset given in Table 4.3^[136], they do not always return the same prediction. For example, given the following query:

STREAM = *false*, SLOPE = *moderate*, ELEVATION = *highest*

the tree generated using information gain ratio (Figure 4.12^[144]) will return VEGETATION = *riparian*, whereas the tree generated using information gain (Figure 4.11^[141]) will return VEGETATION = *conifer*. The combination of features listed in this query does not occur in the dataset. Consequently, both the trees are attempting to generalize beyond the dataset. This illustrates how two different models that are both consistent with a dataset can make different generalizations.¹² So, which feature selection metric should be used, information gain or information gain ratio? Information gain has the advantage that it is computationally less expensive than information gain ratio. If there is variation across the number of values in the domain of the descriptive features in a dataset, however, information gain ratio may be a better option. These factors aside, the effectiveness of descriptive feature selection metrics can vary from domain to domain. Therefore, we should experiment with different metrics to find which one results in the best models for each dataset.

Another commonly used measure of impurity is the **Gini index**

$$Gini(t, \mathcal{D}) = 1 - \sum_{l \in levels(t)} P(t = l)^2 \quad (4.9)$$

where \mathcal{D} is a dataset with a target feature t ; $levels(t)$ is the set of levels in the domain of the target feature; and $P(t = l)$ is the probability of an instance of \mathcal{D} having the target level l . The Gini index can be understood as calculating how often the target levels of instances in a dataset would be misclassified if predictions were made on the sole basis of the distribution of the target levels in the dataset. For example, if there were two target levels with equal likelihood in a dataset, then the expected rate of misclassification would be 0.5, and if there were four target levels with equal likelihood, then the expected rate of misclassification would be 0.75. The Gini index is 0 when all the instances in the dataset have the same target level, and it is $1 - \frac{1}{k}$ when there are k possible target levels with equal likelihood. Indeed, a nice feature of the Gini index is that Gini index scores are always between 0 and

1, and in some contexts this may make it easier to compare Gini indexes across features. We can calculate the Gini index for the dataset in [Table 4.3](#)^[136]

$$\begin{aligned}
 Gini(\text{VEGETATION}, \mathcal{D}) &= 1 - \sum_{l \in \{ \text{chaparral, } \\ \text{riparian, } \\ \text{conifer} \}} P(\text{VEGETATION} = l)^2 \\
 &= 1 - \left(\left(\frac{3}{7} \right)^2 + \left(\frac{2}{7} \right)^2 + \left(\frac{2}{7} \right)^2 \right) \\
 &= 0.6531
 \end{aligned}$$

The information gain for a feature based on the Gini index can be calculated in the same way that it is using entropy: calculate the Gini index for the full dataset and then subtract the sum of the weighted Gini index scores for the partitions created by splitting with the feature. [Table 4.7](#)^[146] shows the calculation of the information gain using the Gini index for the descriptive features in the vegetation classification dataset. Comparing these results to the information gain calculated using entropy (see [Table 4.4](#)^[137]), we can see that although the resulting numbers are different, the relative ranking of the features is the same—in both cases ELEVATION has the highest information gain. Indeed, for the vegetation dataset, the decision tree that will be generated using information gain based on the Gini index will be identical to the one generated using information gain based on entropy (see [Figure 4.11](#)^[141]).

Table 4.7

Partition sets (Part.), entropy, Gini index, remainder (Rem.), and information gain (Info. Gain) by feature for the dataset in [Table 4.3](#)^[136].

Split by Feature	Level	Part.	Instances	Partition Gini Index	Rem.	Info. Gain
STREAM	<i>true</i>	\mathcal{D}_1	$\mathbf{d}_2, \mathbf{d}_3, \mathbf{d}_6, \mathbf{d}_7$	0.6250	0.5476	0.1054
	<i>false</i>	\mathcal{D}_2	$\mathbf{d}_1, \mathbf{d}_4, \mathbf{d}_5$	0.4444		
SLOPE	<i>flat</i>	\mathcal{D}_3	\mathbf{d}_5	0.0	0.4000	0.2531
	<i>moderate</i>	\mathcal{D}_4	\mathbf{d}_2	0.0		
	<i>steep</i>	\mathcal{D}_5	$\mathbf{d}_1, \mathbf{d}_3, \mathbf{d}_4, \mathbf{d}_6, \mathbf{d}_7$	0.5600		
ELEVATION	<i>low</i>	\mathcal{D}_6	\mathbf{d}_2	0.0	0.3333	0.3198
	<i>medium</i>	\mathcal{D}_7	$\mathbf{d}_3, \mathbf{d}_4$	0.5000		
	<i>high</i>	\mathcal{D}_8	$\mathbf{d}_1, \mathbf{d}_5, \mathbf{d}_7$	0.4444		
	<i>highest</i>	\mathcal{D}_9	\mathbf{d}_6	0.0		

So, which impurity measure should be used, Gini or entropy? The best advice that we can give is that it is good practice in building decision tree models to try out different impurity metrics and compare the results to see which suits a dataset best.

4.4.2 Handling Continuous Descriptive Features

The easiest way to handle a continuous descriptive feature in a decision tree is to define a threshold within the range of values that the continuous feature can take and to use this threshold to partition the instances on the basis of whether their values for the feature are above or below the threshold.¹³ The only challenge is to determine the best threshold to use. Ideally, we should use the threshold that results in the highest information gain when the feature is used to split the dataset. The problem, however, is that with a continuous feature, there is an infinite number of thresholds to choose from.

There is, however, a simple way to find the optimal threshold, which avoids testing an infinite number of possible thresholds. First, the instances in the dataset are sorted according to the values of the continuous feature. The adjacent instances in the ordering that have different target feature levels are then selected as possible threshold points. It can be shown that the optimal threshold value must lie at one of the boundaries between adjacent instances with different target levels. The optimal threshold is

found by computing the information gain for each of the target level transition boundaries and selecting the boundary with the highest information gain as the threshold. Once a threshold has been set, the continuous feature can compete with the other categorical features for selection as the splitting feature at any node. To illustrate how this is done, we use a modified version of the vegetation classification dataset given in [Table 4.3](#)^[136] in which the ELEVATION feature now contains actual elevations in feet. This dataset is listed in [Table 4.8](#)^[147].

Table 4.8

Dataset for predicting the vegetation in an area with a continuous ELEVATION feature (measured in feet).

ID	STREAM	SLOPE	ELEVATION	VEGETATION
1	false	steep	3,900	chapparal
2	true	moderate	300	riparian
3	true	steep	1,500	riparian
4	false	steep	1,200	chapparal
5	false	flat	4,450	conifer
6	true	steep	5,000	conifer
7	true	steep	3,000	chapparal

To select the best feature to use at the root of the tree, we need to calculate the information gain for each feature. We know from our earlier calculations that the entropy for this dataset is 1.5567 bits (see [Equation 4.5](#)^[137]) and that the information gain for the categorical features are $IG(\text{STREAM}, \mathcal{D}) = 0.3060$ and $IG(\text{SLOPE}, \mathcal{D}) = 0.5774$ (see [Table 4.4](#)^[137]). This leaves us with the tasks of calculating the best threshold on which to split the ELEVATION feature, and calculating the information gain when we partition the dataset with ELEVATION using this optimal threshold. Our first task is to sort the dataset based on the ELEVATION feature. The result is shown in [Table 4.9](#)^[147].

Table 4.9

Dataset for predicting the vegetation in an area sorted by the continuous ELEVATION feature.

ID	STREAM	SLOPE	ELEVATION	VEGETATION
2	true	moderate	300	riparian
4	false	steep	1,200	chapparal
3	true	steep	1,500	riparian
7	true	steep	3,000	chapparal
1	false	steep	3,900	chapparal
5	false	flat	4,450	conifer
6	true	steep	5,000	conifer

Once the instances have been sorted, we look for adjacent pairs that have different target levels. In [Table 4.9](#)^[147] we can see that four pairs of adjacent instances have a transition between the target levels: instances \mathbf{d}_2 and \mathbf{d}_4 , \mathbf{d}_4 and \mathbf{d}_3 , \mathbf{d}_3 and \mathbf{d}_7 , and \mathbf{d}_1 and \mathbf{d}_5 . The boundary value between each of these pairs is simply the average of their ELEVATION values:

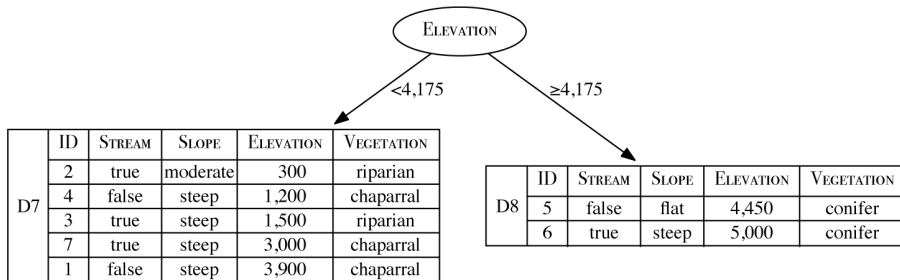
- The boundary between \mathbf{d}_2 and \mathbf{d}_4 is $\frac{300 + 1,200}{2} = 750$
- The boundary between \mathbf{d}_4 and \mathbf{d}_3 is $\frac{1,200 + 1,500}{2} = 1,350$
- The boundary between \mathbf{d}_3 and \mathbf{d}_7 is $\frac{1,500 + 3,000}{2} = 2,250$
- The boundary between \mathbf{d}_1 and \mathbf{d}_5 is $\frac{3,900 + 4,450}{2} = 4,175$

This results in four candidate thresholds: ≥ 750 , $\geq 1,350$, $\geq 2,250$, and $\geq 4,175$. [Table 4.10](#)^[148] shows the computation of information gain for a split using each of these thresholds. The threshold $\geq 4,175$ has the highest information gain of any of the candidate thresholds (0.8631 bits), and this information gain is also higher than the information gain for either of the other two descriptive features. Therefore, we should use $\text{ELEVATION} \geq 4,175$ as the test at the root node of the tree, as shown in [Figure 4.13](#)^[149].

Table 4.10

Partition sets (Part.), entropy, remainder (Rem.), and information gain (Info. Gain) for the candidate ELEVATION thresholds: ≥ 750 , $\geq 1,350$, $\geq 2,250$ and $\geq 4,175$.

Split by Threshold	Part.	Instances	Partition Entropy	Rem.	Info. Gain
≥ 750	\mathcal{D}_1	d_2	0.0	1.2507	0.3060
	\mathcal{D}_2	$d_4, d_3, d_7, d_1, d_5, d_6$	1.4591		
$\geq 1,350$	\mathcal{D}_3	d_2, d_4	1.0	1.3728	0.1839
	\mathcal{D}_4	d_3, d_7, d_1, d_5, d_6	1.5219		
$\geq 2,250$	\mathcal{D}_5	d_2, d_4, d_3	0.9183	0.9650	0.5917
	\mathcal{D}_6	d_7, d_1, d_5, d_6	1.0		
$\geq 4,175$	\mathcal{D}_7	d_2, d_4, d_3, d_7, d_1	0.9710	0.6935	0.8631
	\mathcal{D}_8	d_5, d_6	0.0		

**Figure 4.13**

The vegetation classification decision tree after the dataset has been split using $\text{ELEVATION} \geq 4,175$.

Unlike categorical features, continuous features can be used at multiple points along a path in a decision tree, although the threshold applied to the feature at each of these tests will be different. This is important because it allows multiple splits within a range of a continuous feature to be considered on a path. Consequently, as we build the rest of the tree, we may reuse the ELEVATION feature. This is why that ELEVATION feature is listed in both the partitions (\mathcal{D}_7 and \mathcal{D}_8) shown in Figure 4.13^[149]. We can continue to build the tree by recursively extending each branch as we did in the previous decision tree examples. Figure 4.14^[150] shows the decision tree that is ultimately generated from this process. Notice that the tree uses a mixture of continuous and categorical features and that the ELEVATION feature is used twice with different thresholds in each case.

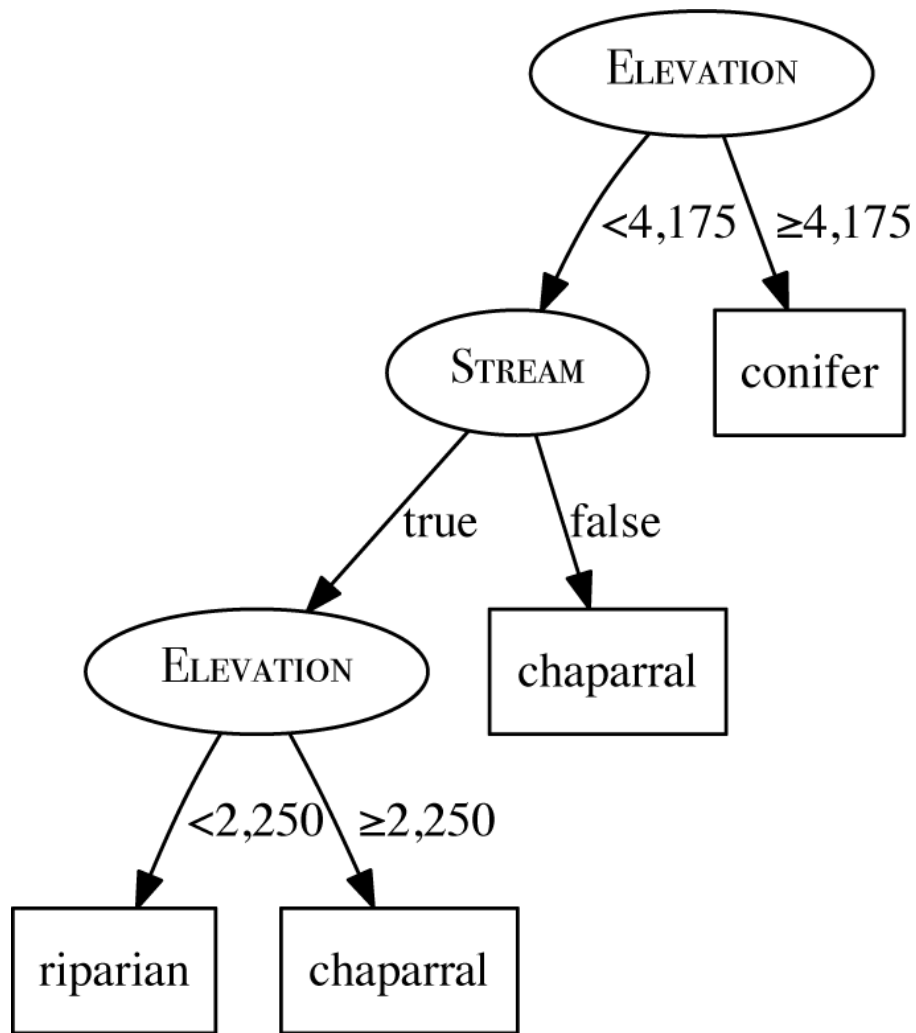


Figure 4.14

The decision tree that would be generated for the vegetation classification dataset listed in Table 4.9^[147] using information gain.

4.4.3 Predicting Continuous Targets

When we use a decision tree to make predictions for a continuous target, we refer to the tree as a **regression tree**.¹⁴ Typically, the value output by the leaf node of a regression tree is the mean of the target feature values of the instances from the training set that reached that node. This means that the error of a regression tree in making a prediction for a query instance is the difference between the mean of the training instances that reached the leaf node that returns the prediction and the correct value that should have been returned for that query. Assuming that the set of training instances reaching a leaf node are indicative of the queries that will be labeled by the node, it

makes sense to construct regression trees in a manner that reduces the **variance** in the target feature values of the set of training instances at each leaf node in the tree. We can do this by adapting the ID3 algorithm to use a measure of variance¹⁵ rather than a measure of entropy in selecting the best feature. Using variance as our measure of impurity, the impurity at a node can be calculated

$$var(t, \mathcal{D}) = \frac{\sum_{i=1}^n (t_i - \bar{t})^2}{n - 1} \quad (4.10)$$

where \mathcal{D} is the dataset that has reached the node; n is the number of instances in \mathcal{D} ; \bar{t} is the mean of the target feature for the dataset \mathcal{D} ; and t_i iterates across the target value of each instance in \mathcal{D} . Using variance as our measure of impurity, we can select which feature to split on at a node by selecting the feature that minimizes the weighted variance across the resulting partitions. The **weighted variance** is computed by summing the variance of the target feature within each partition created by splitting a dataset on a descriptive feature multiplied by the fraction of the dataset in each partition. So, at each node the algorithm will choose the feature to split on by selecting the feature with the lowest weighted variance for the target feature

$$\mathbf{d}[best] = \arg \min_{d \in \mathbf{d}} \sum_{l \in levels(d)} \frac{|\mathcal{D}_{d=l}|}{|\mathcal{D}|} \times var(t, \mathcal{D}_{d=l}) \quad (4.11)$$

where $var(t, \mathcal{D}_{d=l})$ is the variance of the target feature in the partition of the dataset \mathcal{D} containing the instances where $d = l$, $|\mathcal{D}_{d=l}|$ is the size of this partition and $|\mathcal{D}|$ is the size of the dataset. This means that at each decision node, the algorithm will select the feature that partitions the dataset to most reduce the weighted variance of the partitions. This causes the algorithm to cluster instances with similar target feature values. As a result, leaf nodes with small variance in the target feature values across the set of instances at the node are preferred over leaf nodes where the variance in the target feature values across the set of instances at the node is large. To change the

ID3 algorithm in Algorithm 1^[134] to select features to split on based on variance, we replace Line 1 with [Equation 4.11](#)^[150].

The other change we need to make to Algorithm 1^[134] to handle continuous targets relates to the base cases that cause the algorithm to stop processing data partitions and to create a leaf node. In the ID3 algorithm we created a leaf node when there were no instances left in the partition being processed (Line 1), when there were no features left on which to split the data (Line 1), or when we had created a pure partition of the dataset with respect to the target feature levels (Line 1). An algorithm to learn decision trees for a continuous target can use the first two base cases. When these cases occur, the algorithm will create a leaf node that returns the mean value of the target feature in a data partition, rather than the majority level. For continuous targets there is no such thing as a pure split, so we will need to change the final base case.

[Figure 4.15](#)^[151] illustrates the type of partitioning we are trying to achieve when we use a variance measure to select the features to split on in a decision tree. [Figure 4.15\(a\)](#)^[151] depicts a set of instances on the continuous number line. [Figure 4.15\(b\)](#)^[151] depicts one of the extremes for grouping these instances, in which we treat them all as belonging to one partition. The large gap between the two apparent clusters in this dataset results in a large variance, which indicates that we are probably underfitting with this grouping. [Figure 4.15\(c\)](#)^[151] shows that the instances have been gathered into two groups that have a relatively low variance compared with the single group in [Figure 4.15\(b\)](#)^[151]. Intuitively we can see that this grouping is, as Goldilocks put it, *just right* and is the type of grouping we are trying to generate when we use a variance measure to select the splitting point.

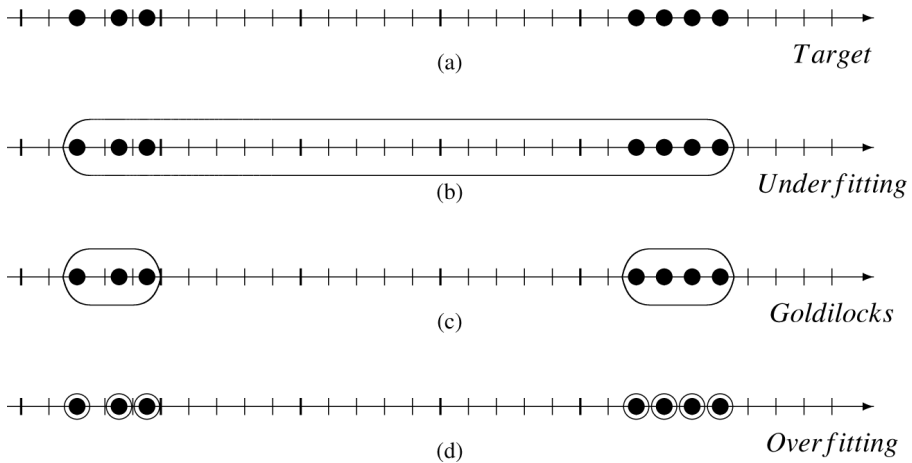


Figure 4.15

(a) A set of instances on a continuous number line; (b), (c), and (d) depict some of the potential groupings that could be applied to these instances.

Figure 4.15(d)^[151] depicts one of the problems that can arise when a variance measure is used to split a continuous target feature. In this example each instance has been put into an individual partition, and although these partitions each have a variance of zero, this is indicative of overfitting the data. This extreme partitioning of the dataset into sets of single instances can happen if there are a lot of descriptive features in the dataset or if there are one or more continuous descriptive features that the algorithm is allowed to split on repeatedly. The reason that partitioning the dataset into single instances is indicative of overfitting is that if there is any noise in the training data (something that is likely in real applications), then the leaf nodes generated due to noisy instances will result in unreliable predictions for queries. To avoid this kind of extreme partitioning, we introduce an **early stopping criterion** into the algorithm for building regression trees. The simplest early stopping criterion is to stop partitioning the dataset if the number of training instances in the partition at the node we are processing is less than some threshold, usually around 5% of the overall dataset size.¹⁶ This early stopping criterion replaces the base case on Line 1 of the ID3 algorithm.

The change to the mechanism for selecting the best feature to split on (made on Line 1) and the introduction of an early stopping criterion (which replaces Line 1) are the only modifications we need to make to the ID3 algorithm (Algorithm 1^[134]) to allow it to handle continuous target features.

To see how this revised algorithm can induce a decision tree, we use the example of predicting the number of bike rentals per day for a city bike sharing program based on the SEASON and whether it is a WORK DAY. Predicting the number of bike rentals on a given day is useful because it can give the administrators of the bike sharing program an insight into the number of resources they need to have ready each day. [Table 4.11](#)^[152] lists a small dataset from this domain.¹⁷

Table 4.11

A dataset listing the number of bike rentals per day.

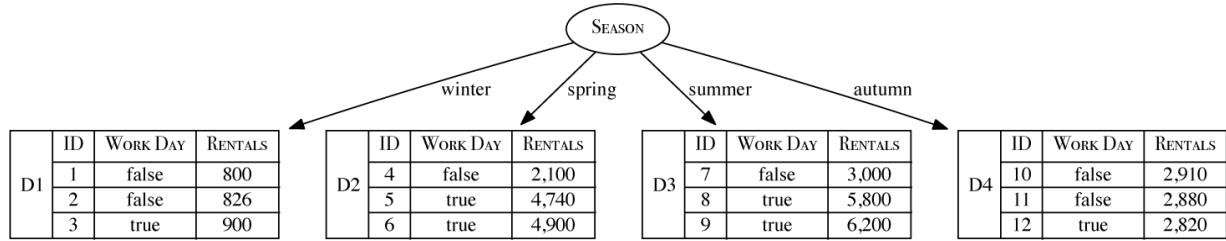
WORK				WORK			
ID	SEASON	DAY	RENTALS	ID	SEASON	DAY	RENTALS
1	winter	false	800	7	summer	false	3,000
2	winter	false	826	8	summer	true	5,800
3	winter	true	900	9	summer	true	6,200
4	spring	false	2,100	10	autumn	false	2,910
5	spring	true	4,740	11	autumn	false	2,880
6	spring	true	4,900	12	autumn	true	2,820

[Table 4.12](#)^[153] illustrates the computation of the weighted variance that results from partitioning the data by SEASON and WORK DAY. It is evident from [Table 4.12](#)^[153] that partitioning the data using SEASON results in a lower weighted variance than partitioning by WORK DAY. This tells us that splitting by SEASON results in a better clustering of the target data than splitting by WORK DAY. [Figure 4.16](#)^[153] illustrates the state of the decision tree after the root node has been created using SEASON.

Table 4.12

The partitioning of the dataset in [Table 4.11](#)^[152] based on SEASON and WORK DAY features and the computation of the weighted variance for each partitioning.

Split by Feature	Level	Part.	Instances	$ \mathcal{D}_{d=l} $	$var(t, \mathcal{D})$	Weighted Variance
				$ \mathcal{D} $		
SEASON	winter	\mathcal{D}_1	$\mathbf{d}_1, \mathbf{d}_2, \mathbf{d}_3$	0.25	2,692	1,379,331
	spring	\mathcal{D}_2	$\mathbf{d}_4, \mathbf{d}_5, \mathbf{d}_6$	0.25	2,472,533	
	summer	\mathcal{D}_3	$\mathbf{d}_7, \mathbf{d}_8, \mathbf{d}_9$	0.25	3,040,000	
	autumn	\mathcal{D}_4	$\mathbf{d}_{10}, \mathbf{d}_{11}, \mathbf{d}_{12}$	0.25	2,100	
WORK DAY	true	\mathcal{D}_5	$\mathbf{d}_3, \mathbf{d}_5, \mathbf{d}_6, \mathbf{d}_8, \mathbf{d}_9, \mathbf{d}_{12}$	0.50	4,026,346	2,551,813
	false	\mathcal{D}_6	$\mathbf{d}_1, \mathbf{d}_2, \mathbf{d}_4, \mathbf{d}_7, \mathbf{d}_{10}, \mathbf{d}_{11}$	0.50	1,077,280	

**Figure 4.16**

The decision tree resulting from splitting the data in [Table 4.11](#)^[152] using the feature SEASON.

[Figure 4.17](#)^[154] illustrates the final decision tree that will be generated for this dataset. This tree will predict the mean target feature value of the leaf node indicated by the descriptive features of a query instance. For example, given a query instance with $SEASON = summer$ and $WORK DAY = true$, this decision tree will predict that there will be 6,000 bike rentals on that day.

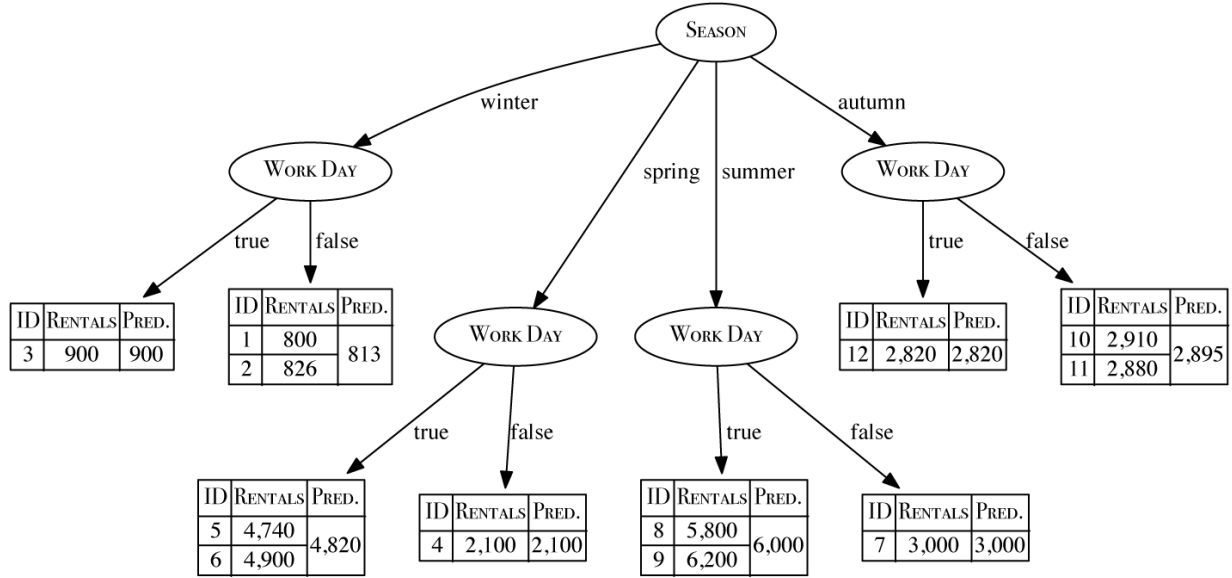


Figure 4.17

The final decision tree induced from the dataset in [Table 4.11](#)^[152]. To illustrate how the tree generates predictions, this tree lists the instances that ended up at each leaf node and the prediction (PRED.) made by each leaf node.

4.4.4 Tree Pruning

A predictive model **overfits** the training set when at least some of the predictions it returns are based on spurious patterns present in the training data used to induce the model. Overfitting happens for a number of reasons, including **sampling variance**¹⁸ and noise in the training set.¹⁹ The problem of overfitting can affect any machine learning algorithm; however, the fact that decision tree induction algorithms work by recursively splitting the training data means that they have a natural tendency to segregate noisy instances and to create leaf nodes around these instances. Consequently, decision trees overfit by splitting the data on irrelevant features that appear relevant only because of noise or sampling variance in the training data. The likelihood of overfitting increases as a tree gets deeper because the resulting predictions are based on smaller and smaller subsets as the dataset is partitioned after each feature test in the path.

Tree pruning identifies and removes subtrees within a decision tree that are likely to be due to noise and sample variance in the training set used to induce it. In cases in which a subtree is deemed to be overfitting, pruning the subtree means replacing the subtree with a leaf node that makes a prediction on the basis of the majority target feature level (or average target

feature value) of the dataset created by merging the instances from all the leaf nodes in the subtree. Obviously, pruning will result in the creation of decision trees that are not consistent with the training set used to build them. In general, however, we are more interested in creating prediction models that generalize well to new data rather than that are strictly consistent with training data, so it is common to sacrifice consistency for generalization capacity.

The simplest way to prune a decision tree is to introduce **early stopping criteria** (similar to the early stopping criterion discussed in the preceding section) into the tree induction algorithm. This is often known as **pre-pruning**. There is a range of simple pre-pruning strategies. For example, we can stop creating subtrees when the number of instances in a partition falls below a threshold, when the information gain (or whatever other feature selection metric is being used) measured at a node is not deemed to be sufficient to make partitioning the data worthwhile,²⁰ or when the depth of the tree goes beyond a predefined limit. More advanced approaches to pre-pruning use statistical significance tests to determine the importance of subtrees, for example, χ^2 **pruning** (pronounced *chi-squared*).²¹

Pre-pruning approaches are computationally efficient and can work well for small datasets. By stopping the partitioning of the data early, however, induction algorithms that use pre-pruning can fail to create the most effective trees because they miss interactions between features that emerge within subtrees that are not obvious when the parent nodes are being considered. Pre-pruning can mean that these useful subtrees are never created.

Post-pruning is an alternative approach to tree pruning in which the tree induction algorithm is allowed to grow a tree to completion, and then each branch on the tree is examined in turn. Branches that are deemed likely to be due to overfitting are pruned. Post-pruning relies on a criterion that can distinguish between subtrees that model relevant aspects of the data and subtrees that model irrelevant random patterns in the data. There is a range of different criteria that can be used, from a very simple threshold on the number of instances at a node in the tree, to statistical significance texts like χ^2 . We recommend the use of criteria that compare the **error rate** in the predictions made by a decision tree when a given subtree is included and when it is pruned. To measure error rate, we set aside some of the training

data as a **validation dataset**²² that is not used during tree induction. We can measure the performance of a decision tree by presenting the instances in the validation to the decision tree and comparing the predictions made for these instances with the actual target feature values in the dataset. The error rate measures the number of predictions made by the tree that are incorrect. A subtree is pruned if the error rate on the validation set of the decision tree with the subtree removed is no greater than the error rate of the decision tree when the subtree is included. Because the instances in the validation set are not used during training, the error rate on the validation set provides a good estimate of the generalization capability of a decision tree.

Reduced error pruning (Quinlan, 1987) is a popular version of post-pruning based on error rates. In reduced error pruning, a decision tree is built to completion and then the tree is searched in an iterative, bottom-up, left-to-right manner for subtrees that can be pruned. The error rate resulting from predictions for the instances in the validation dataset made at the root node of each subtree is compared to the error rate resulting from predictions made at the leaves of the subtree. If the error rate at the subtree root node is less than or equal to the combined error rate at the leaves, the subtree is pruned.

To show how reduced error pruning works, we consider the task of predicting whether a post-operative patient should be sent to an intensive care unit (ICU) or to a general ward for recovery.²³ Hypothermia is a major concern for post-operative patients, so many of the descriptive features relevant to this domain relate to a patient's body temperature. In our example, CORE-TEMP describes the core temperature of the patient (which can be *low* or *high*), and STABLE-TEMP describes whether the patient's current temperature is stable (*true* or *false*). We also include the GENDER of the patient (*male* or *female*). The target feature in this domain, DECISION, records the decision of whether the patient is sent to the *icu* or to a general ward (*gen*) for recovery. Figure 4.18^[156] illustrates a decision tree that has been trained for this post-operative patient routing task. The target level in square brackets at each interior node in the tree shows the majority target level for the data partition at that node.

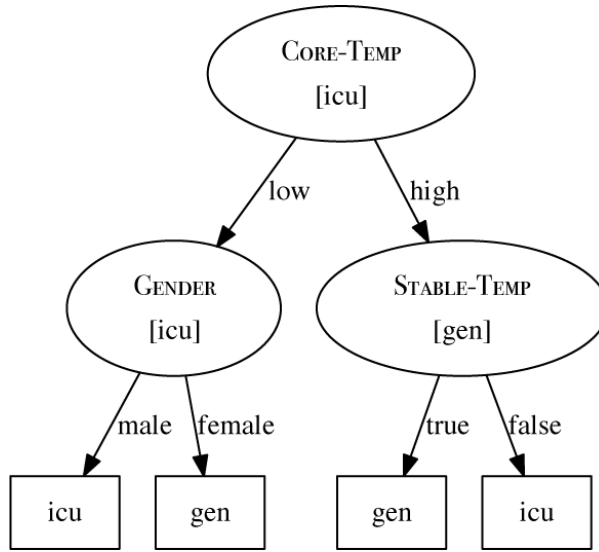


Figure 4.18

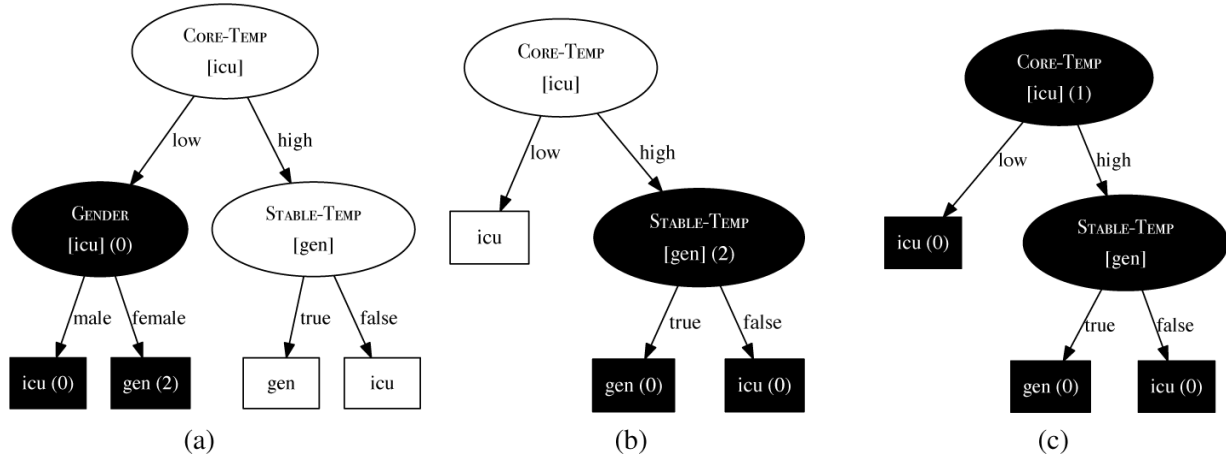
The decision tree for the post-operative patient routing task.

Table 4.13^[157] lists a validation dataset for this domain, and Figure 4.19^[158] illustrates how this validation dataset is used to perform reduced error pruning. In Figure 4.19(a)^[158] the pruning algorithm considers the subtree under the GENDER node for pruning. The path through the tree to make predictions for instances d_2 , d_5 , and d_6 from the validation dataset leads to this subtree. The majority target level predicted at the root node of this subtree (the GENDER node) gives a correct prediction of *icu* for each of the three instances, so the error rate on the validation set for the root node of the subtree is 0. In contrast, the predictions made at the leaf nodes of this subtree are incorrect for d_2 and d_5 (because these patients are *female*, the prediction made is *gen* which does not match the validation dataset), so the error rate for the leaf nodes of this subtree is $0 + 2 = 2$. Because the error rate for the leaf nodes is higher than the error rate for the root node of the subtree, this subtree is pruned and replaced by a leaf node. The result of this pruning is visible on the left branch of the tree shown in Figure 4.19(b)^[158].

Table 4.13

An example validation set for the post-operative patient routing task.

ID	CORE-TEMP	STABLE-TEMP	GENDER	DECISION
1	high	true	male	gen
2	low	true	female	icu
3	high	false	female	icu
4	high	false	male	icu
5	low	false	female	icu
6	low	true	male	icu

**Figure 4.19**

The iterations of reduced error pruning for the decision tree in Figure 4.18^[156] using the validation set in Table 4.13^[157]. The subtree that is being considered for pruning in each iteration is highlighted in black. The prediction returned by each non-leaf node is listed in square brackets. The error rate for each node is given in parentheses.

In the second iteration of the algorithm, the subtree under the **STABLE-TEMP** node is considered for pruning (highlighted in Figure 4.19(b)^[158]). In this instance, the error rate for the root node of this subtree (the **STABLE-TEMP** node) is 2, whereas the error rate of the leaf nodes of the tree is $0 + 0 = 0$. As the error rate of the root node of the subtree is higher than the error rate of the leaf nodes, the tree is not pruned. Figure 4.19(c)^[158] illustrates the final iteration of the algorithm. In this iteration the subtree underneath the root node of the decision tree (the **CORE-TEMP** node) is considered for pruning (i.e., the full decision tree). In this iteration, the error rate of the root node (1) is greater than the error rate of the three leaf nodes, $(0 + 0 + 0 = 0)$, so the tree is left unchanged.

Post-pruning using an error rate criterion is probably the most popular way to prune decision trees.²⁴ One of the advantages of pruning decision trees is that it keeps trees smaller, which in turn makes them easier to interpret. Another advantage is that pruning often increases the accuracy of the trees when there is noise in the training dataset. The reason is that pruning typically affects the lower parts of the decision tree, where noisy training data is most likely to cause overfitting. As such, pruning can be viewed as a **noise dampening mechanism** that removes nodes that have been created because of a small set of noisy instances.

4.4.5 Model Ensembles

Much of the focus of machine learning is on developing the single most accurate prediction model possible for a given task. The techniques we introduce in this section take a slightly different approach. Rather than creating a single model, they generate a set of models and then make predictions by aggregating the outputs of these models. A prediction model that is composed of a set of models is called a **model ensemble**.

The motivation behind using ensemble methods is that a committee of experts working together on a problem are more likely to solve it successfully than a single expert working alone. As is always the case when a committee is working together, however, steps should be taken to guard against **group think**. In the context of model ensembles, this means that each model should make predictions independently of the other models in the ensemble. Given a large population of independent models, an ensemble can be very accurate, even if the individual models in the ensemble perform only marginally better than random guessing.

There are two defining characteristics of ensemble models:

1. They build multiple different models from the same dataset by inducing each model using a modified version of the dataset.
2. They make a prediction by aggregating the predictions of the different models in the ensemble. For categorical target features, this can be done using different types of voting mechanisms; and for continuous target features, this can be done using a measure of the central tendency of the different model predictions, such as the mean or the median.

There are two standard approaches to creating ensembles: **bagging** and **boosting**. The remainder of this section explains each of these basic approaches. Commonly used, high-performing extensions to both of the basic approaches are also described: **random forests** in the case of bagging and **gradient boosting** in the case of boosting.

4.4.5.1 Bagging When we use **bagging** (or **bootstrap aggregating**), each model in the ensemble is trained on a random sample²⁵ of the dataset where, importantly, each random sample is the same size as the dataset, and **sampling with replacement** is used. These random samples are known as **bootstrap samples**, and one model is induced from each bootstrap sample. The reason that we sample with replacement is that this will result in duplicates within each of the bootstrap samples, and consequently every bootstrap sample will be missing some of the instances from the dataset. As a result, each bootstrap sample will be different, and this means that models trained on different bootstrap samples will also be different.²⁶

Decision tree induction algorithms are particularly well suited to use with bagging. The reason is that decision trees are very sensitive to changes in the dataset: a small change in the dataset can result in a different feature being selected to split the dataset at the root or high in the tree, and this can have a ripple effect throughout the subtrees under this node. Frequently, when bagging is used with decision trees, the sampling process is extended so that each bootstrap sample uses only a randomly selected subset of the descriptive features in the dataset. This sampling of the feature set is known as **subspace sampling**. Subspace sampling further encourages the diversity of the trees within the ensemble and has the advantage of reducing the training time for each tree.

Figure 4.20^[160] illustrates the process of creating a model ensemble using bagging and subspace sampling. Model ensembles combining bagging, subspace sampling, and decision trees are known as **random forest** models. Once the individual models in an ensemble have been induced, the ensemble makes predictions by returning the majority vote or the median, depending on the type of prediction required. For continuous target features, the median is preferred to the mean because the mean is more heavily affected by outliers.²⁷

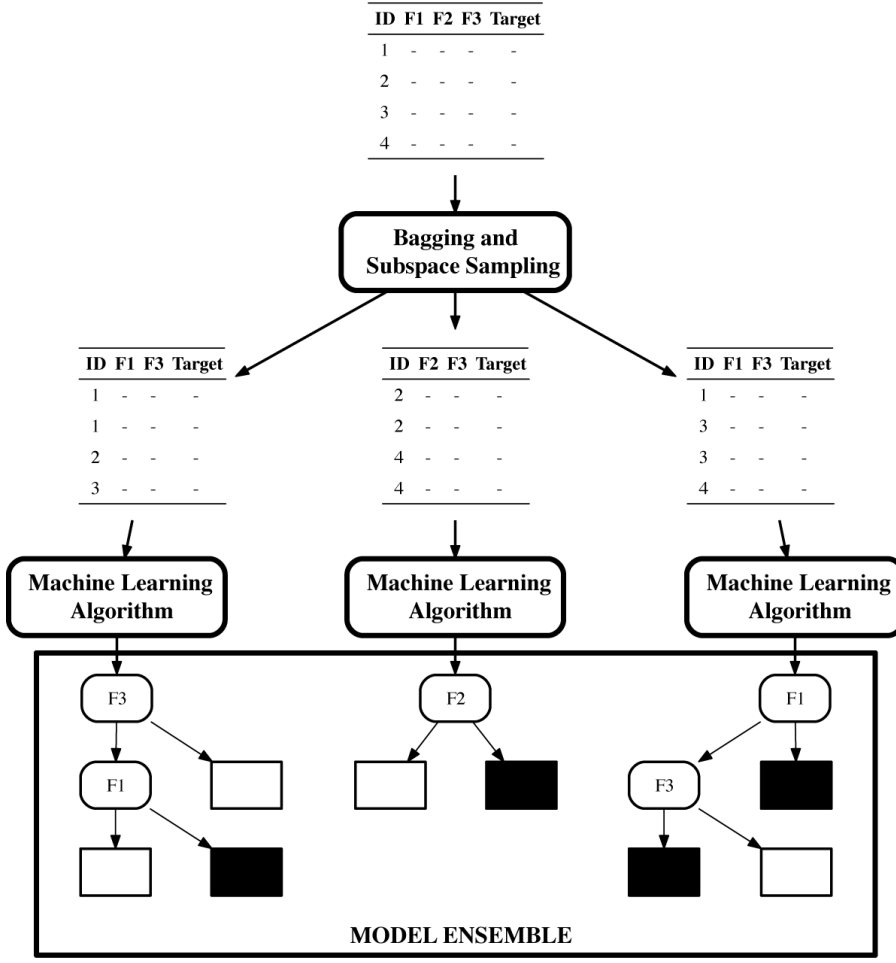


Figure 4.20

The process of creating a model ensemble using bagging and subspace sampling.

4.4.5.2 Boosting When we use **boosting**,²⁸ each new model added to an ensemble is biased to pay more attention to instances that previous models misclassified. This is done by incrementally adapting the dataset used to train the models. To do this we use a **weighted dataset** in which each instance has an associated weight $w_i \geq 0$, initially set to $\frac{1}{n}$ where n is the number of instances in the dataset. These weights are used as a distribution over which the dataset is sampled to create a **replicated training set**, in which the number of times an instance is replicated is proportional to its weight.

Boosting works by iteratively creating models and adding them to the ensemble. The iteration stops when a predefined number of models have been added. During each iteration the algorithm does the following:

1. Induces a model using the weighted dataset and calculates the total error, ϵ , in the set of predictions made by the model for the instances in the training dataset.²⁹ The ϵ value is calculated by summing the weights of the training instances for which the predictions made by the model are incorrect.
2. Increases the weights for the instances misclassified by the model using

$$\mathbf{w}[i] \leftarrow \mathbf{w}[i] \times \left(\frac{1}{2 \times \epsilon} \right) \quad (4.12)$$

and decreases the weights for the instances correctly classified by the model using³⁰

$$\mathbf{w}[i] \leftarrow \mathbf{w}[i] \times \left(\frac{1}{2 \times (1 - \epsilon)} \right) \quad (4.13)$$

3. Calculates a **confidence factor**, α , for the model such that α increases as ϵ decreases. A common way to calculate the confidence factor is

$$\alpha = \frac{1}{2} \times \log_e \left(\frac{1 - \epsilon}{\epsilon} \right) \quad (4.14)$$

Once the set of models has been created, the ensemble makes predictions using a weighted aggregate of the predictions made by the individual models. The weights used in this aggregation are the confidence factors associated with each model. For categorical target features, the ensemble returns the majority target level using a weighted vote. The boosting algorithm presented here can be easily adapted to work with continuous targets by changing the weight update rules to be based on error rather than misclassification, and in this case the aggregation calculates a weighted mean prediction from the base models in the ensemble.³¹

To show how boosting works in practice, we use a modified version of the bike rentals dataset used in Section 4.4.3^[149]. This time we will predict the expected rental demand on the basis of a single descriptive feature, the forecasted temperature for a day. The first columns of Table 4.14^[162] detail a small sample dataset giving temperatures, TEMP, and rental demand,

RENTALS (which can be either *Low* or *High*), for 10 days. The dataset is visualized in [Figure 4.21\(a\)](#)^[163]. At the beginning of the boosting process the sampling distribution is initialized so that each instance has an equal weight of $\frac{1}{10}$ (represented by the equal segments for each instance in the visualization in [Figure 4.21\(b\)](#)^[163]). In the first iteration of the algorithm a dataset is sampled using this distribution, and the number of times each training instance is included in this sample is given in the Freq. column in [Table 4.14](#)^[162]. Instances \mathbf{d}_1 and \mathbf{d}_9 are duplicated in this sample, and instances \mathbf{d}_3 and \mathbf{d}_{10} are not included at all. A decision tree is then trained using the sample, and it is used to make predictions for each instance in the complete training set. In this simple example the decision tree is limited to a single root node with one split based on a value of TEMP (in this case the tree predicts *Low* rental demand for temperatures less than or equal to 8.5 degrees and *High* rental demand for all other temperatures). In [Table 4.14](#)^[162] the column labeled $M_0(\mathbf{d})$ shows the predictions made by this model.

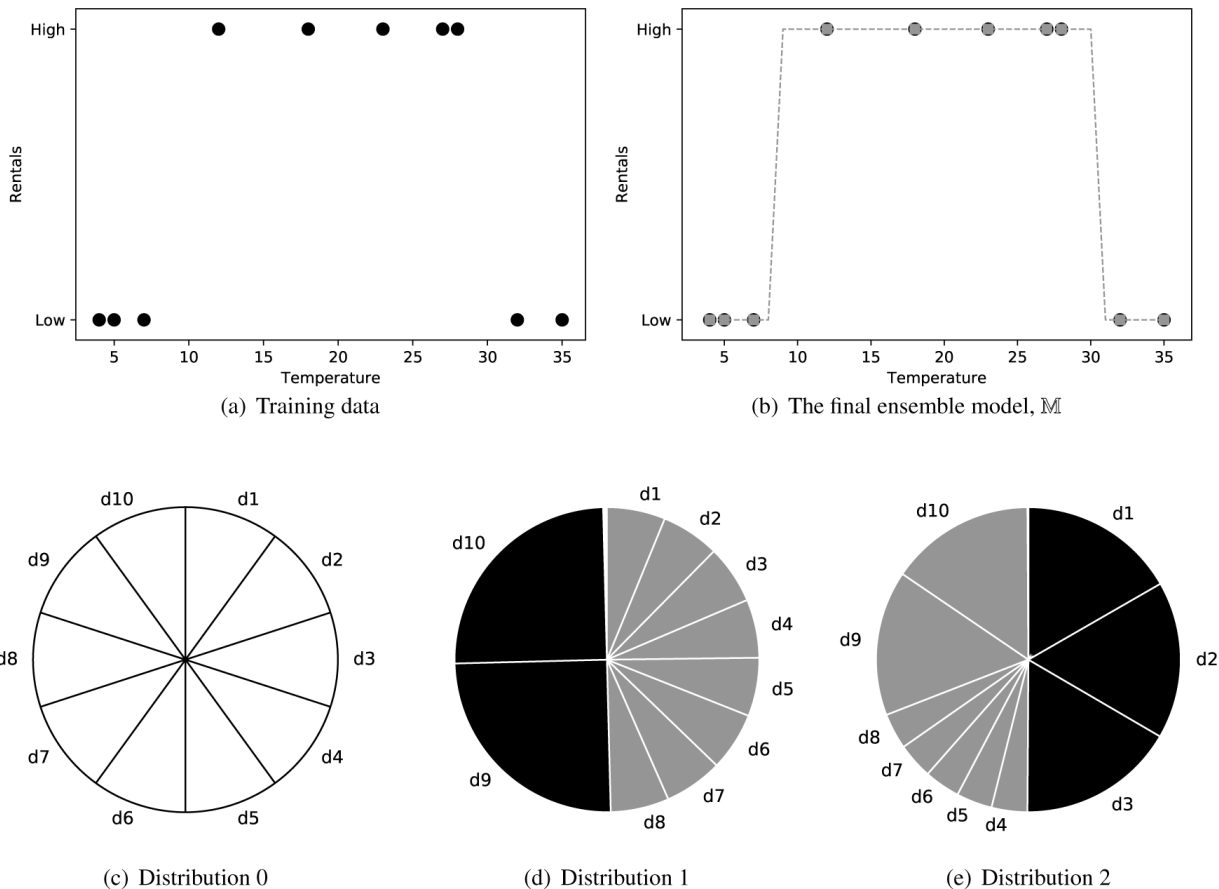


Figure 4.21

(a) A plot of the bike rental dataset from [Table 4.14](#)^[162]. (b) An illustration of the final ensemble model trained using the boosting algorithm. The black circles show the training dataset, the gray squares show the predictions made for the instances in the training dataset by the ensemble model, and the dotted line shows the predictions that would be made by the ensemble model for the full range of input temperatures. (c)–(e) A representation of the changing weights used to generate sample datasets for the first iterations of the boosting process. Black segments represent weights that have increased, and gray segments represent weights that have decreased (all segments for the distribution at the first iteration are white because they have done neither).

Table 4.14

A simple bicycle demand predictions dataset and the workings of the first three iterations of training an ensemble model using boosting to predict RENTALS given TEMP. For each iteration of the boosting process the columns labeled Dist. give the weight in the sampling distribution for each training instance, and the columns labeled Freq. give the number of times a training instance was included in the training set sampled using the sampling distribution. The columns labeled $M_i(\mathbf{d})$ give the predictions made by the model trained at iteration i for each instance in the training dataset.

ID	TEMP	RENTALS	Iteration 0			Iteration 1			Iteration 2		
			Dist.	Freq.	$M_0(\mathbf{d})$	Dist.	Freq.	$M_1(\mathbf{d})$	Dist.	Freq.	$M_2(\mathbf{d})$
1	4	Low	0.100	2	Low	0.062	0	High	0.167	2	Low
2	5	Low	0.100	1	Low	0.062	1	High	0.167	1	Low
3	7	Low	0.100	0	Low	0.062	1	High	0.167	3	Low
4	12	High	0.100	1	High	0.062	2	High	0.038	0	Low
5	18	High	0.100	1	High	0.062	0	High	0.038	0	Low
6	23	High	0.100	1	High	0.062	0	High	0.038	0	Low
7	27	High	0.100	1	High	0.062	1	High	0.038	0	Low
8	28	High	0.100	1	High	0.062	1	High	0.038	1	Low
9	32	Low	0.100	2	High	0.250	3	Low	0.154	1	Low
10	35	Low	0.100	0	High	0.250	1	Low	0.154	2	Low

On the basis of these predictions, ε is calculated as 0.200, the sum of the weights of the two instances misclassified by the model (\mathbf{d}_9 and \mathbf{d}_{10}). The weights of all correctly classified instances are then updated using Equation (4.13)^[161]. For example, the weight for \mathbf{d}_1 is updated

$$\mathbf{w}[1] \leftarrow 0.100 \times \left(\frac{1}{2 \times (1 - 0.200)} \right) \leftarrow 0.0625$$

Similarly, the weights of all incorrectly classified instances are updated using Equation (4.12)^[161]. For example, the weight for \mathbf{d}_9 is updated

$$\mathbf{w}[9] \leftarrow 0.100 \times \left(\frac{1}{2 \times 0.200} \right) \leftarrow 0.250$$

Figure 4.21(d)^[163] illustrates the new distribution that arises from these changes, in which the weight of the segments highlighted in black have increased, and those in gray have decreased. The details of the next iteration of the boosting process are also detailed in Table 4.14^[162] and Figure 4.21(e)^[163].

Figure 4.21(b)^[163] shows an illustration of the final ensemble model trained using five iterations of the boosting algorithm. Even this simple

example can nicely illustrate the power of boosting as, although all the individual decision trees in the ensemble are limited to a single split at the root node of the tree, the ensemble is able to learn a more sophisticated prediction model that none of the individual models within it are capable of representing.

4.4.5.3 Gradient boosting **Gradient boosting** is a more recently developed, and very effective, algorithm for training ensemble models using boosting. Like simpler boosting algorithms, gradient boosting iteratively trains prediction models trying to make later models specialize in areas that earlier models struggled with. Gradient boosting can be said to do this in a more aggressive way than the boosting algorithm described previously. In gradient boosting later models are trained to directly correct errors made by earlier models, rather than the more subtle approach of simply changing weights in a sampling distribution to encourage this.

The gradient boosting algorithm is actually quite straightforward, and it is easiest to explain in the context of a prediction problem with a continuous target. Given a training dataset, \mathcal{D} , made up of descriptive feature and target feature pairs, (\mathbf{d}, t) , the algorithm begins by training a very simple base model, \mathbb{M}_0 . For problems with a continuous target, this model typically simply predicts the overall average target value from the training dataset

$$\mathbb{M}_0(\mathbf{d}) = \frac{1}{n} \sum_i t_i \quad (4.15)$$

Gradient boosting then iteratively adds new models to the ensemble. However, rather than training these models to perform the original prediction task—to predict the target feature t based on the descriptive features \mathbf{d} —these models are trained to predict the errors that the previous model is likely to have made.³² In this way the newly trained models are directly trying to correct, and therefore improve, the predictions made by the models previously added to the ensemble. We write the model trained at the first iteration of gradient boosting

$$\mathbb{M}_1(\mathbf{d}) = \mathbb{M}_0(\mathbf{d}) + \mathbb{M}_{\Delta 1}(\mathbf{d}) \quad (4.16)$$

where $\mathbb{M}_{\Delta 1}$ is the model trained to predict the errors made by the base model, \mathbb{M}_0 .

The gradient boosting algorithm proceeds by adding more and more models where each model is trained to improve the predictions of the previous ones. Equation (4.16)^[164] can be generalized to capture this

$$\mathbb{M}_i(\mathbf{d}) = \mathbb{M}_{i-1}(\mathbf{d}) + \mathbb{M}_{\Delta i}(\mathbf{d}) \quad (4.17)$$

The final model is then a model that makes a basic prediction and adds a number of improvements to this prediction. We can see this if we consider the model trained after four iterations of gradient boosting³³

$$\begin{aligned} \mathbb{M}_4(\mathbf{d}) &= \mathbb{M}_3(\mathbf{d}) + \mathbb{M}_{\Delta 4}(\mathbf{d}) \\ &= (\mathbb{M}_2(\mathbf{d}) + \mathbb{M}_{\Delta 3}(\mathbf{d})) + \mathbb{M}_{\Delta 4}(\mathbf{d}) \\ &= ((\mathbb{M}_1 + \mathbb{M}_{\Delta 2}(\mathbf{d})) + \mathbb{M}_{\Delta 3}(\mathbf{d})) + \mathbb{M}_{\Delta 4}(\mathbf{d}) \\ &= (((\mathbb{M}_0(\mathbf{d}) + \mathbb{M}_{\Delta 1}(\mathbf{d})) + \mathbb{M}_{\Delta 2}(\mathbf{d})) + \mathbb{M}_{\Delta 3}(\mathbf{d})) + \mathbb{M}_{\Delta 4}(\mathbf{d}) \\ &= \mathbb{M}_0(\mathbf{d}) + \mathbb{M}_{\Delta 1}(\mathbf{d}) + \mathbb{M}_{\Delta 2}(\mathbf{d}) + \mathbb{M}_{\Delta 3}(\mathbf{d}) + \mathbb{M}_{\Delta 4}(\mathbf{d}) \end{aligned} \quad (4.18)$$

Although any model can be used at the model training steps in gradient boosting, it is most common to use very shallow decision trees, or **decision stumps**—often just one level deep. This is using the same approach taken in random forests, which aims to combine a large number of **weak learners** into an overall strong learner.

To illustrate gradient boosting, we use another modified version of the bike rentals dataset used in Section 4.4.3^[149]. This will again predict the expected rental demand on the basis of a single descriptive feature, the forecasted temperature for a day. The first columns of Table 4.15^[166] detail a small sample dataset giving temperatures, TEMP, and rental demand, RENTALS (this time as actual numeric values), for 10 days. A visualization of the dataset is provided in Figure 4.22(a)^[167].

Table 4.15

A simple bicycle demand predictions dataset and the workings of the first iterations of training a gradient boosting model.

ID	TEMP	RENTALS	$M_0(\mathbf{d})$	$t - M_0(\mathbf{d})$	$M_{\Delta 1}(\mathbf{d})$	$M_1(\mathbf{d})$	$t - M_1(\mathbf{d})$	$M_{\Delta 2}(\mathbf{d})$	$M_2(\mathbf{d})$	$t - M_2(\mathbf{d})$	$M_{\Delta 3}(\mathbf{d})$	$M_3(\mathbf{d})$
1	4	602	1 287.1	-685.1	-460.9	826.2	-224.2	-167.2	659.0	-57.0	-34.1	624.9
2	5	750	1 287.1	-537.1	-460.9	826.2	-76.2	-167.2	659.0	91.0	-34.1	624.9
3	7	913	1 287.1	-374.1	-460.9	826.2	86.8	71.6	897.8	15.2	-34.1	863.7
4	12	1229	1 287.1	-58.1	-460.9	826.2	402.8	71.6	897.8	331.2	-34.1	863.7
5	18	1827	1 287.1	539.9	691.4	1 978.5	-151.5	71.6	2 050.1	-223.1	-34.1	2 016.1
6	23	2246	1 287.1	958.9	691.4	1 978.5	267.5	71.6	2 050.1	195.9	136.4	2 186.5
7	27	2127	1 287.1	839.9	691.4	1 978.5	148.5	71.6	2 050.1	76.9	136.4	2 186.5
8	28	1714	1 287.1	426.9	691.4	1 978.5	-264.5	71.6	2 050.1	-336.1	-34.1	2 016.1
9	32	838	1 287.1	-449.1	-460.9	826.2	11.8	71.6	897.8	-59.8	-34.1	863.7
10	35	625	1 287.1	-662.1	-460.9	826.2	-201.2	-167.2	659.0	-34.0	-34.1	624.9

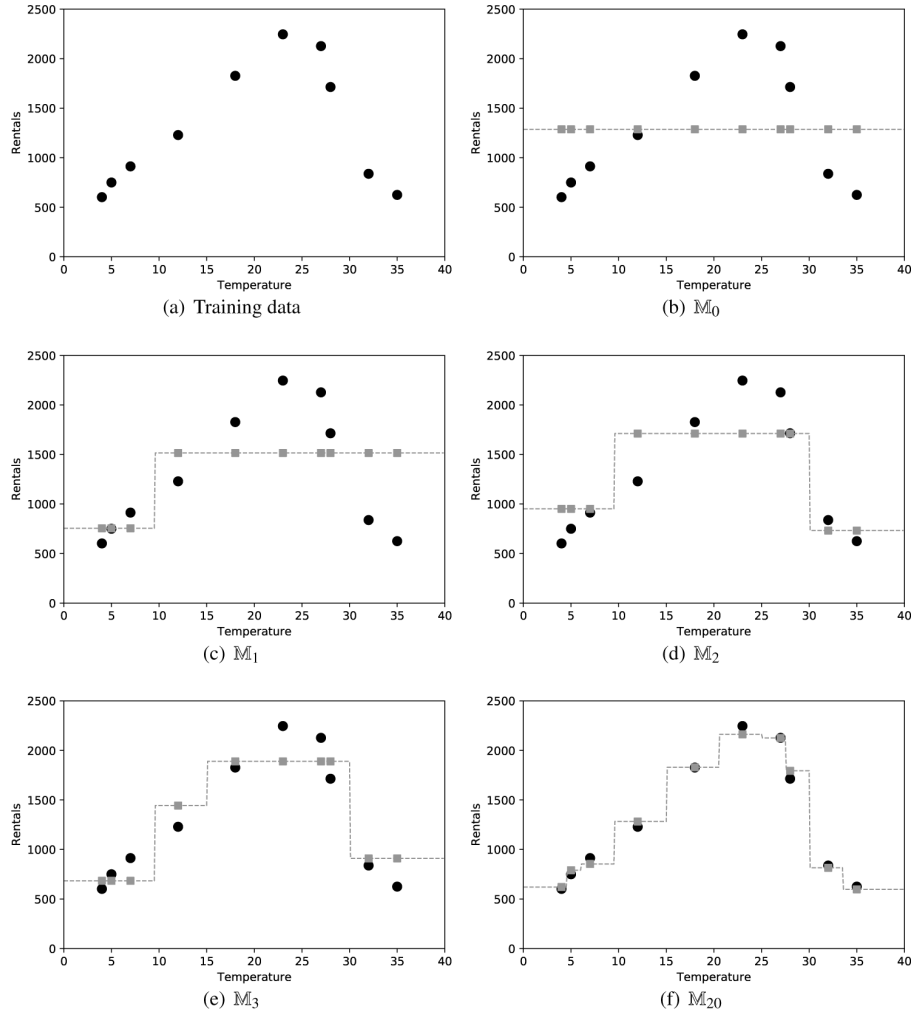


Figure 4.22

(a) A plot of the bike rental dataset from Table 4.15^[166]. (b)–(e) Visualizations of the prediction models trained in the early iterations of the gradient boosting process. (f) The final ensemble model trained after 20 iterations of gradient boosting. In the model visualizations black circles show the training dataset, gray squares show the predictions made for the instances in the training dataset by the current model, and the dotted line shows the predictions that would be made by the current model for the full range of input temperatures.

The first step in building a gradient boosting model for this problem is to train the initial model, M_0 . This always simply predicts the average value of the target feature from the dataset—in this case a rental demand of 1,287.1 bicycles. On the basis of the predictions made by this model, the first set of errors can be calculated. These are shown in the column labeled $t - M_0$ in Table 4.15^[166]; they are simply the difference between the values predicted by the initial model and the target feature value for each instance in the dataset. The first real model trained for this ensemble, $M_{\Delta 1}$, is then trained

to predict these errors on the basis of the descriptive features in the training set. This is a simple one-level decision tree composed of a root note that performs one split on the basis of TEMPERATURE (because TEMPERATURE is a continuous target, the process for training **regression trees** described in Section 4.4.3^[149] is used).

The simple nature of this first trained model is evident from the predictions made by $M_{\Delta 1}$ shown in [Table 4.15](#)^[166]. The model predicts a correction value of -460.9 for input temperatures less than or equal to 9.5 degrees, and a correction value of 691.4 for temperatures above this threshold. These corrections are combined with the M_0 predictions to give the ensemble predictions after the first iteration, M_1 . The predictions for this very simple ensemble model are given in [Table 4.15](#)^[166] and visualized in [Figure 4.22\(c\)](#)^[167], from which the characteristic step pattern of a decision tree is very obvious.

A new set of errors are then calculated by comparing the M_1 predictions to the target feature values. A new model, $M_{\Delta 2}$, is trained to predict these errors on the basis of the original descriptive feature values. The outputs of this model are combined with the M_1 predictions to give the full model for this step in the ensemble building process, M_2 . The outputs of this model for the training dataset instances are shown in [Table 4.15](#)^[166] and [Figure 4.22\(d\)](#)^[167]. To complete the process of building the ensemble model, the algorithm continues to iteratively calculate errors and train new models to predict these errors, which are added as correction terms to the previous model output. [Figure 4.22\(f\)](#)^[167] shows the model output after 20 iterations of model training have been completed.

The gradient boosting algorithm described here does not have an explicit aggregation step, as do the bagging and boosting algorithms described previously (in which individual model predictions were combined through averaging or voting). Instead, the final model trained provides the overall output of the ensemble as it implicitly combines the outputs of all models trained—recall [Equation \(4.18\)](#)^[165]. The simple version of gradient boosting described here can be extended in many ways. For example, a **learning rate**³⁴ parameter, α , can be added to [Equation \(4.17\)](#)^[164] to cause predictions of later errors to have less impact on the overall model than earlier ones, which makes models more robust to outliers.³⁵

$$\mathbb{M}_i(\mathbf{d}) = \mathbb{M}_{i-1}(\mathbf{d}) + \alpha \times \mathbb{M}_{\Delta i}(\mathbf{d}) \quad (4.19)$$

Another way to make models robust to outliers is to train the models to predict only the sign of the errors of the previous predictions rather than the magnitudes of the errors; this is a frequently used adjustment. Although the gradient boosting approach is most easily explained in the context of predicting continuous targets, it can also be easily adapted to work with categorical targets. In this case the initial model predicts a likelihood that an instance belongs to each of the possible target levels, and subsequent models predict corrections to these likelihoods.

The version of the gradient boosting algorithm described here searches for an ensemble model that minimizes the mean squared error between the target feature values from the training dataset and the model predictions. We often describe this as minimizing mean squared error (or L_2) **loss**.³⁶ Gradient boosting can be extended to learn to minimize other loss functions, which makes it an extremely effective and flexible approach to predictive modeling.

4.5 Summary

We have introduced information theory as a method of determining the shortest sequence of descriptive feature tests required to make a prediction. We have also introduced **decision tree** models, which make predictions based on sequences of tests on the descriptive feature values of a query. Consequently, decision trees naturally lend themselves to being trained using information-based metrics. We also introduced the **ID3** algorithm as a standard algorithm for inducing decision trees from a dataset. The ID3 algorithm uses a top-down, recursive, depth-first partitioning of the dataset to build a tree model beginning at the root node and finishing at the leaf nodes. Although this algorithm works quite well as presented, it assumes categorical features with no missing values and clean data. The algorithm can, however, be extended to handle continuous descriptive features and continuous target features. We also discussed how **tree pruning** can be used to help with the problem of overfitting.

The **C4.5** algorithm is a well-known variant of the ID3 algorithm that uses these extensions to handle continuous and categorical descriptive features and missing features. It also uses post-pruning to help with

overfitting. **J48** is an open-source implementation of the C4.5 algorithm that is used in many data analytics toolkits. Another well-known variant of the ID3 algorithm is the **CART** algorithm. The CART algorithm uses the **Gini index** (introduced in Section 4.4.1^[142]) instead of information gain to select features to add to the tree. This algorithm can also handle continuous target features. The variant of the decision tree algorithm that should be used for a particular problem depends on the nature of the problem and the dataset being used. Performing evaluation experiments using different model types is really the only way to determine which variant will work best for a specific problem.

The main advantage of decision tree models is that they are interpretable. It is relatively easy to understand the sequences of tests a decision tree carried out in order to make a prediction. This interpretability is very important in some domains. For example, if a prediction model is being used as a diagnostic tool in a medical scenario, it is not sufficient for the system to simply return a diagnosis. In these contexts both the doctor and the patient would want the system to provide some explanation of how it arrives at the predictions it makes. Decision tree models are ideal for these scenarios.

Decision tree models can be used for datasets that contain both categorical and continuous descriptive features. A real advantage of the decision tree approach is that it has the ability to model the interactions between descriptive features. This arises from the fact that the tests carried out at each node in the tree are performed in the context of the results of the tests on the other descriptive features that were tested at the preceding nodes on the path from the root. Consequently, if there is an **interaction effect** between two or more descriptive features, a decision tree can model this. It is worth noting that this ability is diminished if **pre-pruning** is employed, as pre-pruning may stop subtrees that capture descriptive feature interactions from forming. Finally, as noted earlier, decision tree induction is, relatively, robust to noise in the dataset if **pruning** is used.

There are, however, some situations where decision tree models are not the best option. Although decision trees can handle both categorical and continuous features, they tend to become quite large when dealing with continuous descriptive features. This can result in trees becoming difficult to interpret. Consequently, in dealing with purely continuous data, other

prediction models may be more appropriate, for example, the error-based models discussed in Chapter 7^[311].

Decision trees also have difficulty with domains that have a large number of descriptive features, particularly if the number of instances in the training dataset is small. In these situations overfitting becomes very likely. The probability-based models discussed in Chapter 6^[243] do a better job of handling high-dimensional data.

Another potential issue with decision trees is that they are eager learners. As such, they are not suitable for modeling concepts that change over time, because they will need to be retrained. In these scenarios, the similarity-based prediction models that are the topic of Chapter 5^[181] perform better, as these models can be incrementally retrained.

We concluded by explaining **model ensembles**. We can build a model ensemble using any type of prediction model—or indeed, a mixture of model types. We don’t have to use decision trees. However, decision trees are often used in model ensembles due to the sensitivity of tree induction to changes in the dataset, and this is why we introduced model ensembles in this chapter. Model ensembles are among the most powerful machine learning algorithms; Caruana and Niculescu-Mizil (2006) report a large-scale comparison between seven different types of prediction model in which bagged and boosted tree ensembles are reported as among the best-performing. Which approach should we use? Bagging is simpler to implement and parallelize than boosting, so it may be better with respect to ease of use and training time. With respect to the general ability of bagging and boosting ensembles to make accurate predictions, the results reported in Caruana et al. (2008) indicate that boosted decision tree ensembles were the best-performing model of those tested for datasets containing up to 4,000 descriptive features. For datasets containing more than 4,000 features, random forest ensembles (based on bagging) performed better. Caruana et al. (2008) suggest that a potential explanation for this pattern of results is that boosted ensembles are prone to overfitting, and in domains with large numbers of features, overfitting becomes a serious problem. With all model ensembles, however, the cost of their high performance is increased learning and model complexity.

4.6 Further Reading

Gleick (2011) provides an excellent and accessible introduction to information theory and its history. Shannon and Weaver (1949) is taken as the foundational book in information theory, and Cover and Thomas (1991) is a well-regarded textbook on the topic. MacKay (2003) is an excellent textbook on information theory and machine learning.

Quinlan (1986) originally described the ID3 algorithm, and Quinlan (1993) and Breiman (1993) are two of the best-known books on decision trees. Loh (2011) provides a good overview of more recent developments in tree induction algorithms.

Schapire (1990) described some of the early work on weak learners and computational learning theory. Freund and Schapire (1995) introduced the **AdaBoost** algorithm, which is one of the seminal boosting algorithms. Friedman et al. (2000) generalized the AdaBoost algorithm and developed another popular boosting algorithm, the **LogitBoost** algorithm. Breiman (1996) developed the use of bagging for prediction, and Breiman (2001) introduced **random forests**. The original gradient boosting paper by Friedman (2001) gives a detailed explanation on the fundamentals of gradient boosting. The **XGBoost** (Chen and Guestrin, 2016) gradient boosting implementation played a significant role in popularizing the approach and is a good example of how the basic algorithm can be optimized for performance. Dietterich (2000) give an excellent explanation of the motivations behind using ensembles, and Kuncheva (2004) and Zhou (2012) both provide good overviews of ensemble learning methods.

4.7 Exercises

1. The image below shows a set of eight Scrabble pieces.



- (a) What is the **entropy** in bits of the letters in this set?
- (b) What would be the reduction in entropy (i.e., the **information gain**) in bits if we split these letters into two sets, one containing the vowels and the other containing the consonants?
- (c) What is the maximum possible entropy in bits for a set of eight Scrabble pieces?

- (d) In general, which is preferable when you are playing Scrabble: a set of letters with high entropy or a set of letters with low entropy?
2. A convicted criminal who reoffends after release is known as a *recidivist*. The following table lists a dataset that describes prisoners released on parole and whether they reoffended within two years of release.³⁷

ID	GOOD		DRUG		RECIDIVIST
	BEHAVIOR	AGE < 30	DEPENDENT		
1	false	true	false		true
2	false	false	false		false
3	false	true	false		true
4	true	false	false		false
5	true	false	true		true
6	true	false	false		false

This dataset lists six instances in which prisoners were granted parole. Each of these instances is described in terms of three binary descriptive features (GOOD BEHAVIOR, AGE < 30, DRUG DEPENDENT) and a binary target feature (RECIDIVIST). The GOOD BEHAVIOR feature has a value of *true* if the prisoner had not committed any infringements during incarceration, the AGE < 30 has a value of *true* if the prisoner was under 30 years of age when granted parole, and the DRUG DEPENDENT feature is *true* if the prisoner had a drug addiction at the time of parole. The target feature, RECIDIVIST, has a *true* value if the prisoner was arrested within two years of being released; otherwise it has a value of *false*.

- (a) Using this dataset, construct the decision tree that would be generated by the **ID3** algorithm, using entropy-based information gain.
- (b) What prediction will the decision tree generated in Part (a) of this question return for the following query?

$$\begin{aligned} \text{GOOD BEHAVIOR} &= \textit{false}, \text{AGE} < 30 = \textit{false}, \\ \text{DRUG DEPENDENT} &= \textit{true} \end{aligned}$$

- (c) What prediction will the decision tree generated in Part (a) of this question return for the following query?

GOOD BEHAVIOR = *true*, AGE < 30 = *true*,
DRUG DEPENDENT = *false*

3. The following table lists a sample of data from a census.³⁸

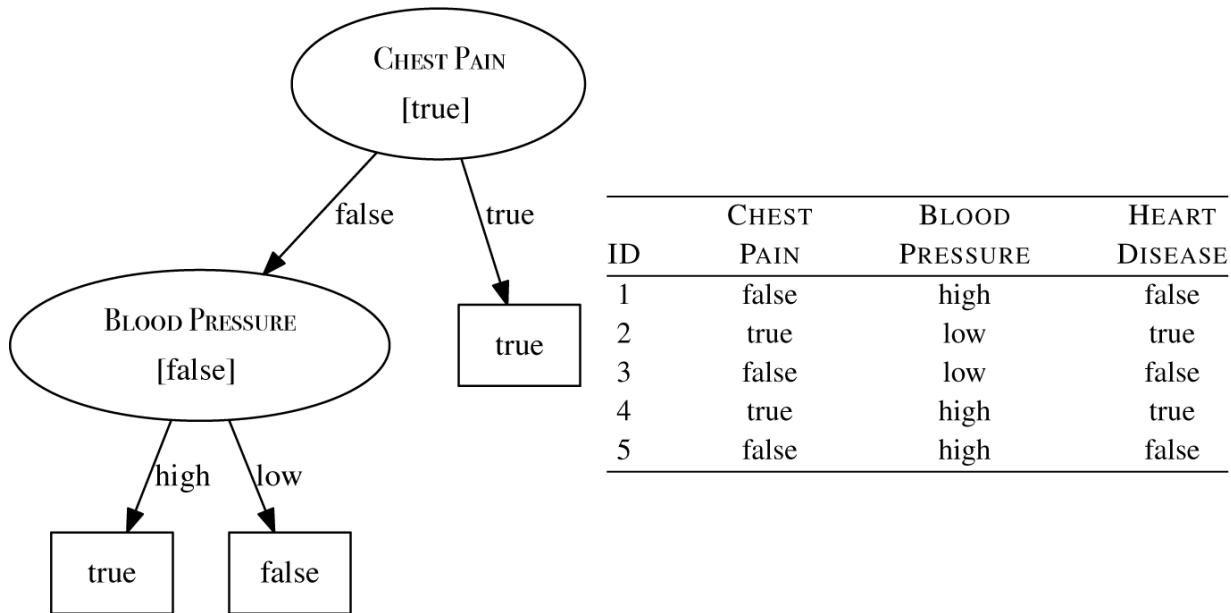
ID	AGE	EDUCATION	MARITAL STATUS	OCCUPATION	ANNUAL INCOME
1	39	bachelors	never married	transport	25K–50K
2	50	bachelors	married	professional	25K–50K
3	18	high school	never married	agriculture	<25K
4	28	bachelors	married	professional	25K–50K
5	37	high school	married	agriculture	25K–50K
6	24	high school	never married	armed forces	<25K
7	52	high school	divorced	transport	25K–50K
8	40	doctorate	married	professional	>50K

There are four descriptive features and one target feature in this dataset, as follows:

- AGE, a continuous feature listing the age of the individual;
- EDUCATION, a categorical feature listing the highest education award achieved by the individual (*high school*, *bachelors*, *doctorate*);
- MARITAL STATUS (*never married*, *married*, *divorced*);
- OCCUPATION (*transport* = works in the transportation industry; *professional* = doctor, lawyer, or similar; *agriculture* = works in the agricultural industry; *armed forces* = is a member of the armed forces); and
- ANNUAL INCOME, the target feature with 3 levels (*<25K*, *25K–50K*, *>50K*).

- (a) Calculate the **entropy** for this dataset.
- (b) Calculate the **Gini index** for this dataset.
- (c) In building a decision tree, the easiest way to handle a continuous feature is to define a threshold around which splits will be made. What would be the optimal threshold to split the continuous AGE feature (use information gain based on entropy as the feature selection measure)?

- (d) Calculate **information gain** (based on entropy) for the EDUCATION, MARITAL STATUS, and OCCUPATION features.
- (e) Calculate the **information gain ratio** (based on entropy) for EDUCATION, MARITAL STATUS, and OCCUPATION features.
- (f) Calculate **information gain** using the **Gini index** for the EDUCATION, MARITAL STATUS, and OCCUPATION features.
4. The following diagram shows a decision tree for the task of predicting heart disease.³⁹ The descriptive features in this domain describe whether the patient suffers from chest pain (CHEST PAIN) and the blood pressure of the patient (BLOOD PRESSURE). The binary target feature is HEART DISEASE. The table beside the diagram lists a pruning set from this domain.



Using the pruning set, apply **reduced error pruning** to the decision tree. Assume that the algorithm is applied in a bottom-up, left-to-right fashion. For each iteration of the algorithm, indicate the subtrees considered as pruning candidates, explain why the algorithm chooses to prune or leave these subtrees in the tree, and illustrate the tree that results from each iteration.

5. The following table⁴⁰ lists a dataset containing the details of five participants in a heart disease study, and a target feature RISK, which

describes their risk of heart disease. Each patient is described in terms of four binary descriptive features

- EXERCISE, how regularly do they exercise
 - SMOKER, do they smoke
 - OBESE, are they overweight
 - FAMILY, did any of their parents or siblings suffer from heart disease

ID	EXERCISE	SMOKER	OBESE	FAMILY	RISK
1	daily	false	false	yes	low
2	weekly	true	false	yes	high
3	daily	false	false	no	low
4	rarely	true	true	yes	high
5	rarely	true	true	no	high

- (a) As part of the study, researchers have decided to create a predictive model to screen participants based on their risk of heart disease. You have been asked to implement this screening model using a **random forest**. The three tables below list three bootstrap samples that have been generated from the above dataset. Using these bootstrap samples, create the decision trees that will be in the random forest model (use entropy-based information gain as the feature selection criterion).

ID	EXERCISE	FAMILY	RISK	ID	SMOKER	OBESE	RISK	ID	OBESE	FAMILY	RISK
1	daily	yes	low	1	false	false	low	1	false	yes	low
2	weekly	yes	high	2	true	false	high	1	false	yes	low
2	weekly	yes	high	2	true	false	high	2	false	yes	high
5	rarely	no	high	4	true	true	high	4	true	yes	high
5	rarely	no	high	5	true	true	high	5	true	no	high

- (b) Assuming the random forest model you have created uses majority voting, what prediction will it return for the following query:

EXERCISE=*rarely*, SMOKER=*false*, OBESE=*true*, FAMILY=*yes*

- * 6. The following table lists a dataset containing the details of six patients. Each patient is described in terms of three binary descriptive

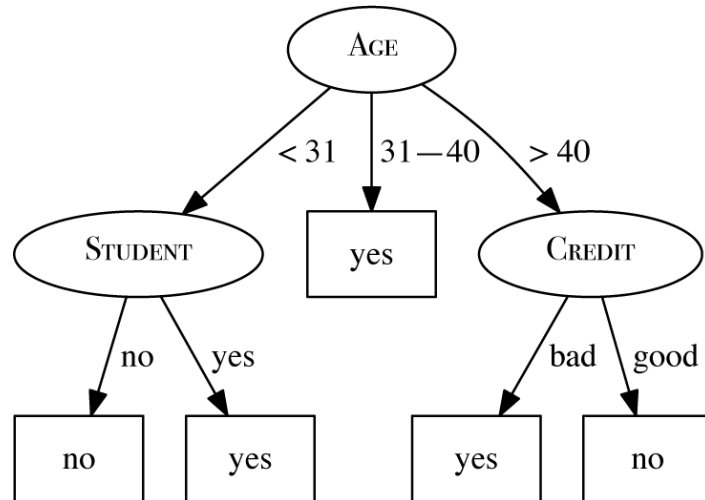
features (OBESE, SMOKER, and DRINKS ALCOHOL) and a target feature (CANCER RISK).⁴¹

ID	OBESE	SMOKER	DRINKS ALCOHOL	CANCER RISK
1	true	false	true	low
2	true	true	true	high
3	true	false	true	low
4	false	true	true	high
5	false	true	false	low
6	false	true	true	high

- (a) Which of the descriptive features will the **ID3** decision tree induction algorithm choose as the feature for the root node of the decision tree?
- (b) In designing a dataset, it is generally a bad idea if all the descriptive features are indicators of the target feature taking a particular value. For example, a potential criticism of the design of the dataset in this question is that all the descriptive features are indicators of the CANCER RISK target feature taking the same level, *high*. Can you think of any descriptive features that could be added to this dataset that are indicators of the *low* target level?
- * 7. The following table lists a dataset collected in an electronics shop showing details of customers and whether they responded to a special offer to buy a new laptop.

ID	AGE	INCOME	STUDENT	CREDIT	BUYS
1	< 31	high	no	bad	no
2	< 31	high	no	good	no
3	31 – 40	high	no	bad	yes
4	> 40	med	no	bad	yes
5	> 40	low	yes	bad	yes
6	> 40	low	yes	good	no
7	31 – 40	low	yes	good	yes
8	< 31	med	no	bad	no
9	< 31	low	yes	good	yes
10	> 40	med	yes	bad	yes
11	< 31	med	yes	good	yes
12	31 – 40	med	no	good	yes
13	31 – 40	high	yes	bad	yes
14	> 40	med	no	good	no

This dataset has been used to build a decision tree to predict which customers will respond to future special offers. The decision tree, created using the **ID3** algorithm, is the following:



- (a) The **information gain** (calculated using entropy) of the feature AGE at the root node of the tree is 0.247. A colleague has suggested that the STUDENT feature would be better at the root node of the tree. Show that this is not the case.

(b) Yet another colleague has suggested that the ID feature would be a very effective at the root node of the tree. Would you agree with this suggestion?

* 8. This table lists a dataset of the scores students achieved on an exam described in terms of whether the student studied for the exam (STUDIED) and the energy level of the lecturer when grading the student's exam (ENERGY).

ID	STUDIED	ENERGY	SCORE
1	yes	tired	65
2	no	alert	20
3	yes	alert	90
4	yes	tired	70
5	no	tired	40
6	yes	alert	85
7	no	tired	35

Which of the two descriptive features should we use as the testing criterion at the root node of a decision tree to predict students' scores?

* 9. Calculate the probability of a **model ensemble** that uses simple majority voting making an incorrect prediction in the following scenarios. (Hint: Understanding how to use the **binomial distribution** will be useful in answering this question.)

(a) The ensemble contains 11 independent models, all of which have an error rate of 0.2.

(b) The ensemble contains 11 independent models, all of which have an error rate of 0.49.

(c) The ensemble contains 21 independent models, all of which have an error rate of 0.49.

* 10. The following table shows the target feature, OUTCOME, for a set of instances in a small dataset. An ensemble model is being trained using this dataset using **boosting**. The table also shows the instance distribution weights, w_4 , for this dataset used at the fifth iteration of the boosting process. The last column of the table shows the

predictions made by the model trained at the fifth iteration of boosting, \mathbb{M}_4 .

ID	OUTCOME	w_4	\mathbb{M}_4
1	<i>Bad</i>	0.167	<i>Bad</i>
2	<i>Good</i>	0.047	<i>Good</i>
3	<i>Bad</i>	0.167	<i>Bad</i>
4	<i>Good</i>	0.071	<i>Bad</i>
5	<i>Good</i>	0.047	<i>Good</i>
6	<i>Bad</i>	0.047	<i>Bad</i>
7	<i>Bad</i>	0.047	<i>Bad</i>
8	<i>Good</i>	0.047	<i>Good</i>
9	<i>Bad</i>	0.167	<i>Bad</i>
10	<i>Good</i>	0.071	<i>Bad</i>
11	<i>Bad</i>	0.047	<i>Bad</i>
12	<i>Good</i>	0.071	<i>Bad</i>

- (a) Calculate the error, ε , associated with the set of predictions made by the model \mathbb{M}_4 given in the table above.
- (b) Calculate the **confidence factor**, α , associated with \mathbb{M}_4 .
- (c) Calculate the updated instance distribution, $\mathbf{w}^{[5]}$, based on the predictions made by \mathbb{M}_4 .

- * 11. The following table shows a set of predictions made by six models in an ensemble and the ground truth of the target feature in a small test dataset, PROGNOSIS.

ID	PROGNOSIS	\mathbb{M}_0	\mathbb{M}_1	\mathbb{M}_2	\mathbb{M}_3	\mathbb{M}_4	\mathbb{M}_5
1	<i>Bad</i>	<i>Bad</i>	<i>Bad</i>	<i>Good</i>	<i>Bad</i>	<i>Bad</i>	<i>Good</i>
2	<i>Good</i>	<i>Good</i>	<i>Good</i>	<i>Good</i>	<i>Bad</i>	<i>Good</i>	<i>Bad</i>
3	<i>Good</i>	<i>Bad</i>	<i>Good</i>	<i>Bad</i>	<i>Good</i>	<i>Good</i>	<i>Good</i>
4	<i>Bad</i>	<i>Bad</i>	<i>Bad</i>	<i>Bad</i>	<i>Bad</i>	<i>Bad</i>	<i>Good</i>
5	<i>Bad</i>	<i>Good</i>	<i>Bad</i>	<i>Good</i>	<i>Bad</i>	<i>Good</i>	<i>Good</i>

- (a) Assuming that these models are part of an ensemble training using **bagging**, calculate the overall output of the ensemble for each instance in the test dataset.
- (b) Measure the performance of this bagged ensemble using **misclassification rate** (**misclassification rate** is discussed in detail

in Section 9.3^[535]; it is simply the percentage of instances in the test dataset that a model has incorrectly classified).

- (c) Assuming that these models are part of an ensemble trained using **boosting** and that the confidence factors, α , for the models are as follows:

M_0	M_1	M_2	M_3	M_4	M_5
0.114	0.982	0.653	0.912	0.883	0.233

calculate the overall output of the ensemble for each instance in the test dataset.

- (d) Measure the performance of this boosted ensemble using **misclassification rate**.

1. Claude Shannon is considered to be the father of information theory. Shannon worked for AT&T Bell Labs, where he worked on the efficient encoding of messages for telephone communication. It was this focus on encoding that motivated his approach to measuring information. In information theory, the meaning of the word **information** deliberately excludes the psychological aspects of the communication and should be understood as measuring the optimal encoding length of a message given the set of possible messages that could be sent within the communication.
2. In fact, it can be argued that a preference toward shallower decision trees is a good idea in general and can be viewed as following **Occam's razor**. Occam's razor is the principle of keeping theories as simple as possible. It is named after a 14th-century Franciscan monk, William of Occam (sometimes spelled *Ockham*), who was one of the first to formulate this principle. The *razor* in the title comes from the idea of shaving off any unnecessary assumptions from a theory.
3. We use some simple elements of probability theory in this chapter. Readers unfamiliar with the way probabilities are calculated based on the relative frequencies of events should read the first section of Appendix B^[757] before continuing with this chapter.
4. The *log* of a to the base b , written as $\log_b(a)$, is the number to which we must raise b to get a . For example, $\log_2(8) = 3$ because $2^3 = 8$ and $\log_5(625) = 4$ because $5^4 = 625$.
5. Using binary logs, the maximum entropy for a set with two types of elements is 1.00 bit, but the entropy for a set with more than two types of elements may be greater than 1.00 bit. The choice of base used in Shannon's model, in the context in which it is used in this chapter, is arbitrary. The choice of base 2 is due partly to a conventional computer science background and partly to its allowing us to use the *bits* unit of information.
6. This is almost identical to the definition of Shannon's entropy model given in Equation (4.1)^[125]. We have extended the definition to include an explicit parameter for the dataset \mathcal{D} for which we are computing the entropy, and we have specified the base as 2.
7. Note that we have shortened feature names in these calculations to save space.
8. This algorithm was first published in Quinlan (1986).
9. Hence the name **Iterative Dichotomizer**.

10. See Guisan and Zimmermann (2000) and Franklin (2009) for an introduction to uses of predictive analytics in ecological modeling.

11. This artificially generated example dataset is inspired by the research reported in Franklin et al. (2000).

12. This is an example of how machine learning is an **ill-posed problem**, as discussed in Section 1.3[7].

13. This approach is related to **binning**, as described in Section 3.6.2^[89]. Simply binning continuous features to convert them into categorical features is another valid approach to handling continuous features in decision trees.

14. Sometimes the task of predicting a continuous target is referred to as a **regression task**.

15. We introduce **variance** in Section A.1.2^[746], and although we extend the formal definition of variance here to include a dataset parameter \mathcal{D} —we do this to explicitly highlight the fact that we are calculating the variance of a feature within a particular dataset, usually the dataset at a node in the tree—the measure of variance we are using is identical to the variance defined in Equation (A.3)^[747].

16. It is also common to use a minimum partition variance as an early stopping criterion. If the variance in the partition being processed is below a set threshold, then the algorithm will not partition the data and will instead create a leaf node.

17. This example is inspired by the research reported in Fanaee-T and Gama (2014). The dataset presented here is synthesized for this example; however, a real bike sharing dataset for this task is available through the UCI Machine Learning Repository (Bache and Lichman, 2013) at archive.ics.uci.edu/ml/datasets/Bike+Sharing+Dataset.

18. This means that the distribution over the target feature will be different between a training set sample and the full population.

19. For example, there might be errors in the target feature or descriptive feature values of one or more of the training instances.

20. **Critical value pruning** (Mingers, 1987) is a well-known version of this pruning technique.

21. See Frank (2000) for a detailed discussion and analysis on the use of statistical tests in decision tree pruning.

22. In the context of decision tree pruning, the validation set is often referred to as the **pruning dataset**.

23. The example of predicting where post-operative patients should be sent is inspired by the research reported in Woolery et al. (1991). A real dataset related to this research is available through the UCI Machine Learning Repository (Bache and Lichman, 2013) at archive.ics.uci.edu/ml/datasets/Post-Operative+Patient/.

24. See Esposito et al. (1997) and Mingers (1989) for overviews and empirical comparisons of a range of decision tree pruning methods based on error rate.

25. See Section 3.6.3^[91].

26. If we have a very large dataset, we may—for computational reasons—want to create bootstrap samples that are smaller than the original dataset. If this is the case, then **sampling without replacement** is preferred. This is known as **subagging**.

27. Question 5 in the Exercises section at the end of this chapter explores bagging and random forest ensemble models in more detail, and worked examples are provided in the solution.

28. Schapire (1999) gives a readable introduction to boosting by one of the originators of the technique.

29. Normally in machine learning, we do not test a model using the same dataset that we use to train it. Boosting, however, is an exception to this rule.
30. Updating the weights using Equations (4.12)^[161] and (4.13)^[161] ensures that the weights always sum to 1.
31. **Adaboost.R2** (Drucker, 1997) is a nice early example of a boosting algorithm designed to work with continuous targets.
32. These errors are often known as the **model residuals**.
33. Because of the way that they make a number of additions to a basic model, gradient boosting models can be considered an instance of a generic family of mathematical models known as **additive models**.
34. **Learning rates** are discussed in much more detail in Chapter 7^[311].
35. Learning rate values are typically in (0, 1], and gradient boosting implementations that use a learning rate often refer to it as **incremental shrinkage**.
36. **Loss functions** are discussed in much more detail in Chapters 7^[311] and 8^[381]. We can view the gradient boosting process as equivalent to the **gradient descent** process described in those chapters.
37. This example of predicting recidivism is based on a real application of machine learning: parole boards do rely on machine learning prediction models to help them when they are making their decisions. See Berk and Bleich (2013) for a recent comparison of different machine learning models used for this task. Datasets dealing with prisoner recidivism are available online, for example, catalog.data.gov/dataset/prisoner-recidivism/. The dataset presented here is not based on real data.
38. This census dataset is based on the Census Income Dataset (Kohavi, 1996), which is available from the UCI Machine Learning Repository (Bache and Lichman, 2013) at archive.ics.uci.edu/ml/datasets/Census+Income/.
39. This example is inspired by the research reported in Palaniappan and Awang (2008).
40. The data in this table has been artificially generated for this question, but is inspired by the results from the Framingham Heart Study: www.framinghamheartstudy.org.
41. The data in this table has been artificially generated for this question. The American Cancer Society does, however, provide information on the causes of cancer: www.cancer.org/cancer/cancercauses/.

5

Similarity-Based Learning

“When I see a bird that walks like a duck and swims like a duck and quacks like a duck, I call that bird a duck.”

—James Whitcomb Riley

Similarity-based approaches to machine learning come from the idea that the best way to make predictions is to simply look at what has worked well in the past and predict the same thing again. The fundamental concepts required to build a system on the basis of this idea are **feature spaces** and **measures of similarity**, and these are covered in the fundamentals section of this chapter. These concepts allow us to understand the standard approach to building similarity-based models: the **nearest neighbor algorithm**. After covering the standard algorithm, we then look at extensions and variations that allow us to handle noisy data (the **k nearest neighbor**, or **k -NN**, algorithm), to make predictions more efficiently (**k -d trees**), to predict continuous targets, and to handle different kinds of descriptive features with varying **measures of similarity**. We also take the opportunity to introduce the use of **data normalization** and **feature selection** in the context of similarity-based learning. These techniques are generally applicable to all machine learning algorithms but are especially important when similarity-based approaches are used.

5.1 Big Idea

The year is 1798, and you are Lieutenant-Colonel David Collins of HMS *Calcutta* exploring the region around Hawkesbury River, in New South Wales. One day, after an expedition up the river has returned to the ship, one of the men from the expedition tells you that he saw a strange animal

near the river. You ask him to describe the animal to you, and he explains that he didn't see it very well because, as he approached it, the animal growled at him, so he didn't approach too closely. However, he did notice that the animal had webbed feet and a duck-billed snout.

In order to plan the expedition for the next day, you decide that you need to classify the animal so that you can determine whether it is dangerous to approach it or not. You decide to do this by thinking about the animals you can remember coming across before and comparing the features of these animals with the features the sailor described to you. **Table 5.1**^[182] illustrates this process by listing some of the animals you have encountered before and how they compare with the growling, web-footed, duck-billed animal that the sailor described. For each known animal, you count how many features it has in common with the unknown animal. At the end of this process, you decide that the unknown animal is most similar to a duck, so that is what it must be. A duck, no matter how strange, is not a dangerous animal, so you tell the men to get ready for another expedition up the river the next day.

Table 5.1

Matching animals you remember to the features of the unknown animal described by the sailor.

<i>Grrr!</i>			Score
	✓	✗	✗
	✗	✓	✗
	✗	✓	✓

Images created by Jan Gillbank, English for the Australian Curriculum website (www.e4ac.edu.au). Used under Creative Commons Attribution 3.0 license.

The process of classifying an unknown animal by matching the features of the animal against the features of animals you have encountered before neatly encapsulates the big idea underpinning similarity-based learning: if you are trying to make a prediction for a current situation, then you should search your memory to find situations that are similar to the current one and make a prediction based on what was true for the most similar situation in your memory. In this chapter we are going to see how this type of reasoning can be implemented as a machine learning algorithm.

5.2 Fundamentals

As the term similarity-based learning suggests, a key component of this approach to prediction is defining a computational measure of similarity between instances. Often this measure of similarity is actually some form of distance measure. A consequence of this, and a somewhat less obvious requirement of similarity-based learning, is that if we are going to compute distances between instances, we need to have a concept of space in the representation of the domain used by our model. In this section we introduce the concept of a feature space as a representation for a training dataset and then illustrate how we can compute measures of similarity between instances in a feature space.

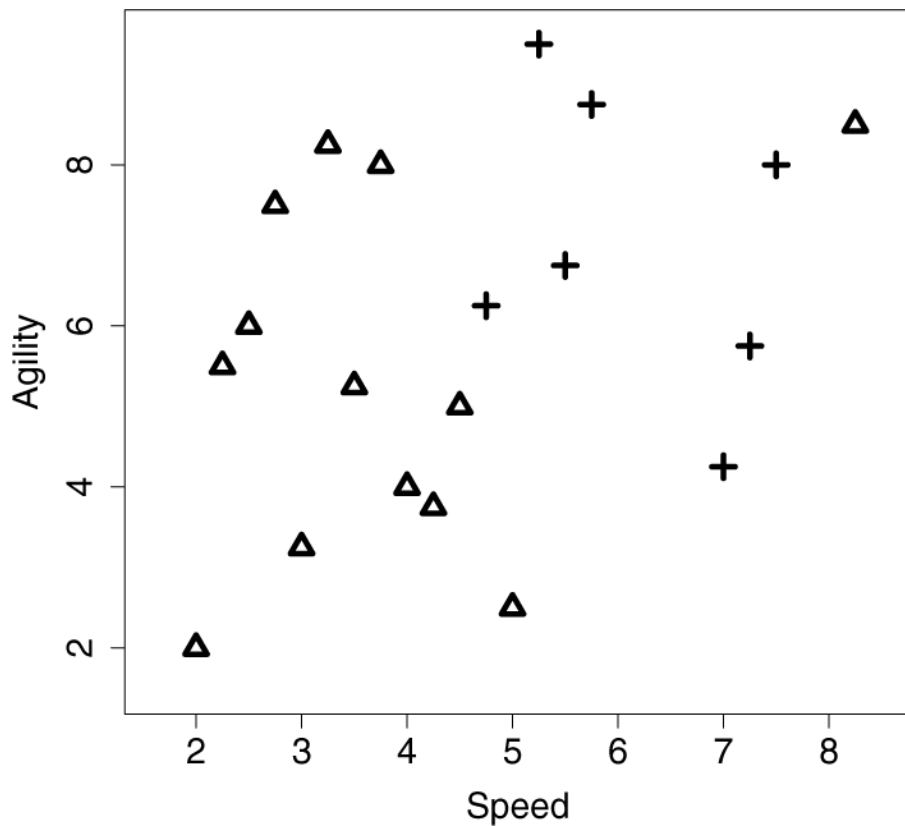
5.2.1 Feature Space

[Table 5.2^{\[183\]}](#) lists an example dataset containing two descriptive features, the SPEED and AGILITY ratings for college athletes (both measures out of 10), and one target feature that lists whether the athletes were drafted to a professional team.¹ We can represent this dataset in a **feature space** by taking each of the descriptive features to be the axes of a **coordinate system**. We can then place each instance within the feature space based on the values of its descriptive features. [Figure 5.1^{\[184\]}](#) is a scatter plot to illustrate the resulting feature space when we do this using the data in [Table 5.2^{\[183\]}](#). In this figure, SPEED has been plotted on the horizontal axis, and AGILITY has been plotted on the vertical axis. The value of the DRAFT feature is indicated by the shape representing each instance as a point in the feature space: triangles for *no* and crosses for *yes*.

Table 5.2

The SPEED and AGILITY ratings for 20 college athletes and whether they were drafted by a professional team.

ID	SPEED	AGILITY	DRAFT	ID	SPEED	AGILITY	DRAFT
1	2.50	6.00	no	11	2.00	2.00	no
2	3.75	8.00	no	12	5.00	2.50	no
3	2.25	5.50	no	13	8.25	8.50	no
4	3.25	8.25	no	14	5.75	8.75	yes
5	2.75	7.50	no	15	4.75	6.25	yes
6	4.50	5.00	no	16	5.50	6.75	yes
7	3.50	5.25	no	17	5.25	9.50	yes
8	3.00	3.25	no	18	7.00	4.25	yes
9	4.00	4.00	no	19	7.50	8.00	yes
10	4.25	3.75	no	20	7.25	5.75	yes

**Figure 5.1**

A feature space plot of the college athlete data in [Table 5.2](#)^[183].

There is always one dimension for every descriptive feature in a dataset. In this example, there are only two descriptive features, so the feature space

is two-dimensional. Feature spaces can, however, have many more dimensions—in document classification tasks, for example, it is not uncommon to have thousands of descriptive features and therefore thousands of dimensions in the associated feature space. Although we can't easily draw feature spaces beyond three dimensions, the ideas underpinning them remain the same.

We can formally define a feature space as an abstract m -dimensional space that is created by making each descriptive feature in a dataset an axis of an m -dimensional coordinate system and mapping each instance in the dataset to a point in this coordinate system based on the values of its descriptive features.

For similarity-based learning, the nice thing about the way feature spaces work is that if the values of the descriptive features of two or more instances in the dataset are the same, then these instances will be mapped to the same point in the feature space. Also, as the differences between the values of the descriptive features of two instances grows, so too does the distance between the points in the feature space that represent these instances. So the distance between two points in the feature space is a useful measure of the similarity of the descriptive features of the two instances.

5.2.2 Measuring Similarity Using Distance Metrics

The simplest way to measure the similarity between two instances, \mathbf{a} and \mathbf{b} , in a dataset is to measure the distance between the instances in a feature space. We can use a **distance metric** to do this: $\text{metric}(\mathbf{a}, \mathbf{b})$ is a function that returns the distance between two instances \mathbf{a} and \mathbf{b} . Mathematically, a **metric** must conform to the following four criteria:

1. **Non-negativity**: $\text{metric}(\mathbf{a}, \mathbf{b}) \geq 0$
2. **Identity**: $\text{metric}(\mathbf{a}, \mathbf{b}) = 0 \iff \mathbf{a} = \mathbf{b}$
3. **Symmetry**: $\text{metric}(\mathbf{a}, \mathbf{b}) = \text{metric}(\mathbf{b}, \mathbf{a})$
4. **Triangular Inequality**: $\text{metric}(\mathbf{a}, \mathbf{b}) \leq \text{metric}(\mathbf{a}, \mathbf{c}) + \text{metric}(\mathbf{b}, \mathbf{c})$

One of the best-known distance metrics is **Euclidean distance**, which computes the length of the straight line between two points. Euclidean distance between two instances \mathbf{a} and \mathbf{b} in an m -dimensional feature space is defined as

$$Euclidean(\mathbf{a}, \mathbf{b}) = \sqrt{\sum_{i=1}^m (\mathbf{a}[i] - \mathbf{b}[i])^2} \quad (5.1)$$

The descriptive features in the college athlete dataset are both continuous, which means that the feature space representing this data is technically known as a **Euclidean coordinate space**, and we can compute the distance between instances in it using Euclidean distance. For example, the Euclidean distance between instances \mathbf{d}_{12} (SPEED = 5.00, AGILITY = 2.50) and \mathbf{d}_5 (SPEED = 2.75, AGILITY = 7.50) from [Table 5.2](#)^[183] is

$$\begin{aligned} Euclidean(\mathbf{d}_{12}, \mathbf{d}_5) &= \sqrt{(5.00 - 2.75)^2 + (2.50 - 7.50)^2} \\ &= \sqrt{30.0625} = 5.4829 \end{aligned}$$

Another, less well-known, distance metric is the **Manhattan distance**.² The Manhattan distance between two instances \mathbf{a} and \mathbf{b} in a feature space with m dimensions is defined as

$$Manhattan(\mathbf{a}, \mathbf{b}) = \sum_{i=1}^m abs(\mathbf{a}[i] - \mathbf{b}[i]) \quad (5.2)$$

where the *abs()* function returns the absolute value. For example, the Manhattan distance between instances \mathbf{d}_{12} (SPEED = 5.00, AGILITY = 2.50) and \mathbf{d}_5 (SPEED = 2.75, AGILITY = 7.50) in [Table 5.2](#)^[183] is

$$\begin{aligned} Manhattan(\mathbf{d}_{12}, \mathbf{d}_5) &= abs(5.00 - 2.75) + abs(2.50 - 7.50) \\ &= 2.25 + 5 = 7.25 \end{aligned}$$

[Figure 5.2\(a\)](#)^[186] illustrates the difference between the Manhattan and Euclidean distances between two points in a two-dimensional feature space. If we compare Equation (5.1)^[185] and Equation (5.2)^[185], we can see that both distance metrics are essentially functions of the differences between the values of the features. Indeed, the Euclidean and Manhattan distances are special cases of the **Minkowski distance**, which defines a family of distance metrics based on differences between features.

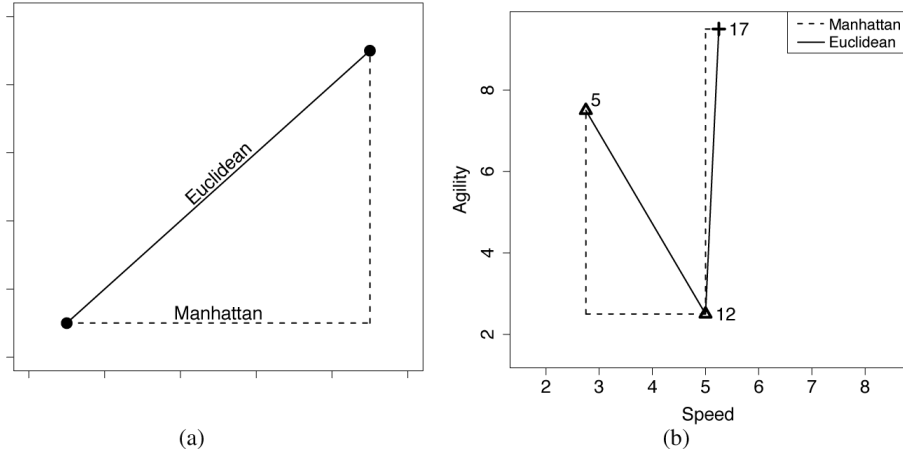


Figure 5.2

(a) A generalized illustration of the Manhattan and Euclidean distances between two points; and (b) a plot of the Manhattan and Euclidean distances between instances \mathbf{d}_{12} and \mathbf{d}_5 , and between \mathbf{d}_{12} and \mathbf{d}_{17} from Table 5.2^[183].

The **Minkowski distance** between two instances \mathbf{a} and \mathbf{b} in a feature space with m descriptive features is defined as

$$Minkowski(\mathbf{a}, \mathbf{b}) = \left(\sum_{i=1}^m \text{abs}(\mathbf{a}[i] - \mathbf{b}[i])^p \right)^{\frac{1}{p}} \quad (5.3)$$

where the parameter p is typically set to a positive value and defines the behavior of the distance metric. Different distance metrics result from adjusting the value of p . For example, the Minkowski distance with $p = 1$ is the Manhattan distance, and with $p = 2$ is the Euclidean distance. Continuing in this manner, we can define an infinite number of distance metrics.

The fact that we can define an infinite number of distance metrics is not merely an academic curiosity. In fact, the predictions produced by a similarity-based model will change depending on the exact Minkowski distance used (i.e., $p = 1, 2, \dots, \infty$). Larger values of p place more emphasis on large differences between feature values than smaller values of p because all differences are raised to the power of p . Consequently, the Euclidean distance (with $p = 2$) is more strongly influenced by a single large difference in one feature than the Manhattan distance (with $p = 1$).³

We can see this if we compare the Euclidean and Manhattan distances between instances \mathbf{d}_{12} and \mathbf{d}_5 with the Euclidean and Manhattan distances between instances \mathbf{d}_{12} and \mathbf{d}_{17} (SPEED = 5.25, AGILITY = 9.50). [Figure 5.2\(b\)](#)^[186] plots the Manhattan and Euclidean distances between these pairs of instances.

The Manhattan distances between both pairs of instances are the same: 7.25. It is striking, however, that the Euclidean distance between \mathbf{d}_{12} and \mathbf{d}_{17} is 8.25, which is greater than the Euclidean distance between \mathbf{d}_{12} and \mathbf{d}_5 , which is just 5.48. This is because the maximum difference between \mathbf{d}_{12} and \mathbf{d}_{17} for any single feature is 7 units (for AGILITY), whereas the maximum difference between \mathbf{d}_{12} and \mathbf{d}_5 on any single feature is just 5 units (for AGILITY). Because these differences are squared in the Euclidean distance calculation, the larger maximum single difference between \mathbf{d}_{12} and \mathbf{d}_{17} results in a larger overall distance being calculated for this pair of instances. Overall the Euclidean distance weights features with larger differences in values more than features with smaller differences in values. This means that the Euclidean difference is more influenced by a single large difference in one feature rather than a lot of small differences across a set of features, whereas the opposite is true of Manhattan distance.

Although we have an infinite number of Minkowski-based distance metrics to choose from, Euclidean distance and Manhattan distance are the most commonly used of these. The question of which is the best one to use, however, still remains. From a computational perspective, the Manhattan distance has a slight advantage over the Euclidean distance—the computation of the squaring and the square root is saved—and computational considerations can become important when dealing with very large datasets. Computational considerations aside, Euclidean distance is often used as the default.

5.3 Standard Approach: The Nearest Neighbor Algorithm

We now understand the two fundamental components of similarity-based learning: a feature space representation of the instances in a dataset and a measure of similarity between instances. We can put these components together to define the standard approach to similarity-based learning: the **nearest neighbor algorithm**. The training phase needed to build a nearest

neighbor model is very simple and just involves storing all the training instances in memory. In the standard version of the algorithm, the data structure used to store training data is a simple list. In the prediction stage, when the model is used to make predictions for new query instances, the distance in the feature space between the query instance and each instance in memory is computed, and the prediction returned by the model is the target feature level of the instance that is nearest to the query in the feature space. The default distance metric used in nearest neighbor models is Euclidean distance. Algorithm 2^[188] provides a pseudocode definition of the algorithm for the prediction stage. The algorithm really is very simple, so we can move straight to looking at a worked example of it in action.

Algorithm 2 Pseudocode description of the nearest neighbor algorithm.

Require: a set of training instances

Require: a query instance

- 1: Iterate across the instances in memory to find the nearest neighbor—this is the instance with the shortest distance across the feature space to the query instance.
 - 2: Make a prediction for the query instance that is equal to the value of the target feature of the nearest neighbor.
-

5.3.1 A Worked Example

Assume that we are using the dataset in [Table 5.2](#)^[183] as our labeled training dataset, and we want to make a prediction to tell us whether a query instance with SPEED = 6.75 and AGILITY = 3.00 is likely to be drafted or not.

[Figure 5.3](#)^[188] illustrates the feature space of the training dataset with the query, represented by the ? marker.

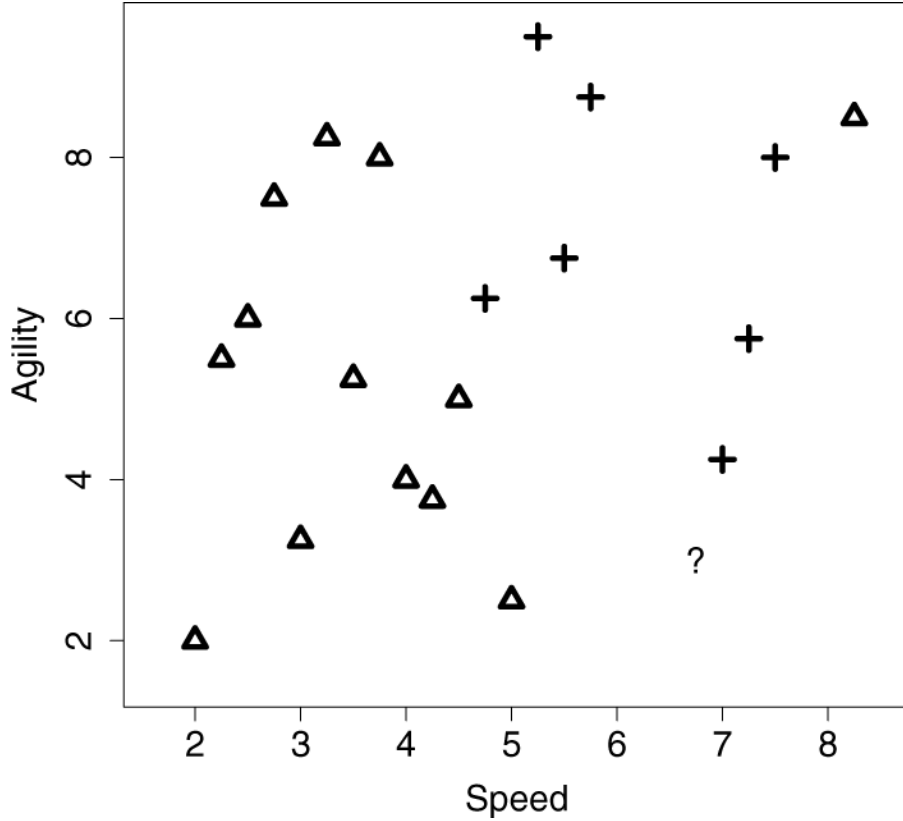


Figure 5.3

A feature space plot of the data in [Table 5.2](#)^[183], with the position in the feature space of the query represented by the ? marker.

Just by visually inspecting [Figure 5.3](#)^[188], we can see that the nearest neighbor to the query instance has a target level of yes, so this is the prediction that the model should return. However, let's step through how the algorithm makes this prediction. Remember that during the prediction stage, the nearest neighbor algorithm iterates across all the instances in the training dataset and computes the distance between each instance and the query. These distances are then ranked from lowest to highest to find the nearest neighbor. [Table 5.3](#)^[189] shows the distances between our query instance and each instance from [Table 5.2](#)^[183] ranked from lowest to highest. Just as we saw in [Figure 5.3](#)^[188], this shows that the nearest neighbor to the query is instance \mathbf{d}_{18} , with a distance of 1.2749 and a target level of yes.

Table 5.3

The distances (Dist.) between the query instance with SPEED = 6.75 and AGILITY = 3.00 and each instance in [Table 5.2](#)^[183].

ID	SPEED	AGILITY	DRAFT	Dist.	ID	SPEED	AGILITY	DRAFT	Dist.
18	7.00	4.25	yes	1.27	11	2.00	2.00	no	4.85
12	5.00	2.50	no	1.82	19	7.50	8.00	yes	5.06
10	4.25	3.75	no	2.61	3	2.25	5.50	no	5.15
20	7.25	5.75	yes	2.80	1	2.50	6.00	no	5.20
9	4.00	4.00	no	2.93	13	8.25	8.50	no	5.70
6	4.50	5.00	no	3.01	2	3.75	8.00	no	5.83
8	3.00	3.25	no	3.76	14	5.75	8.75	yes	5.84
15	4.75	6.25	yes	3.82	5	2.75	7.50	no	6.02
7	3.50	5.25	no	3.95	4	3.25	8.25	no	6.31
16	5.50	6.75	yes	3.95	17	5.25	9.50	yes	6.67

When the algorithm is searching for the nearest neighbor using Euclidean distance, it is partitioning the feature space into what is known as a **Voronoi tessellation**,⁴ and it is trying to decide which **Voronoi region** the query belongs to. From a prediction perspective, the Voronoi region belonging to a training instance defines the set of queries for which the prediction will be determined by that training instance. [Figure 5.4\(a\)](#)^[190] illustrates the Voronoi tessellation of the feature space using the training instances from [Table 5.2](#)^[183] and shows the position of our sample query instance within this decomposition. We can see in this figure that the query is inside a Voronoi region defined by an instance with a target level of yes. As such, the prediction for the query instance should be yes.

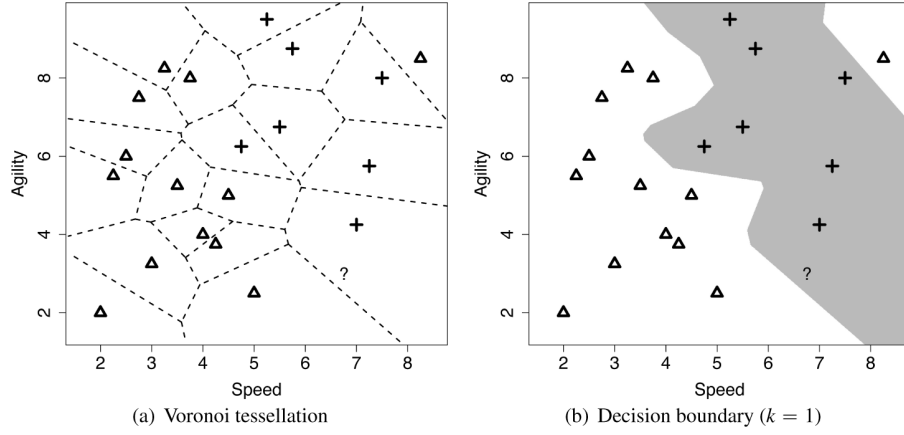


Figure 5.4

(a) The Voronoi tessellation of the feature space for the dataset in [Table 5.2](#)^[183], with the position of the query represented by the ? marker; and (b) the decision boundary created by aggregating the neighboring Voronoi regions that belong to the same target level.

The nearest neighbor prediction algorithm creates a set of **local models**, or neighborhoods, across the feature space where each model is defined by a subset of the training dataset (in this case, one instance). Implicitly, however, the algorithm is also creating a global prediction model based on the full dataset. We can see this if we highlight the decision boundary within the feature space. The **decision boundary** is the boundary between regions of the feature space in which different target levels will be predicted. We can generate the decision boundary by aggregating the neighboring local models (in this case, Voronoi regions) that make the same prediction. [Figure 5.4\(b\)](#)^[190] illustrates the decision boundary within the feature space for the two target levels in the college athlete dataset. Given that the decision boundary is generated by aggregating the Voronoi regions, it is not surprising that the query is on the side of the decision boundary representing the yes target level. This illustrates that a decision boundary is a global representation of the predictions made by the local models associated with each instance in the training set. It also highlights the fact that the nearest neighbor algorithm uses multiple local models to create an implicit global model to map from the descriptive feature values to the target feature.

One of the advantages of the nearest neighbor approach to prediction is that it is relatively straightforward to update the model when new labeled instances become available—we simply add them to the training dataset.

Table 5.4^[191] lists the updated dataset when the example query instance with its prediction of yes is included.⁵ **Figure 5.5(a)**^[192] illustrates the Voronoi tessellation of the feature space that results from this update, and **Figure 5.5(b)**^[192] presents the updated decision boundary. Comparing **Figure 5.5(b)**^[192] with **Figure 5.4(b)**^[190], we can see that the main difference is that the decision boundary in the bottom-right region of the feature space has moved to the left. This reflects the extension of the yes region due to the inclusion of the new instance.

Table 5.4

The extended version of the college athletes dataset.

ID	SPEED	AGILITY	DRAFT	ID	SPEED	AGILITY	DRAFT
1	2.50	6.00	no	12	5.00	2.50	no
2	3.75	8.00	no	13	8.25	8.50	no
3	2.25	5.50	no	14	5.75	8.75	yes
4	3.25	8.25	no	15	4.75	6.25	yes
5	2.75	7.50	no	16	5.50	6.75	yes
6	4.50	5.00	no	17	5.25	9.50	yes
7	3.50	5.25	no	18	7.00	4.25	yes
8	3.00	3.25	no	19	7.50	8.00	yes
9	4.00	4.00	no	20	7.25	5.75	yes
10	4.25	3.75	no	21	6.75	3.00	yes
11	2.00	2.00	no				

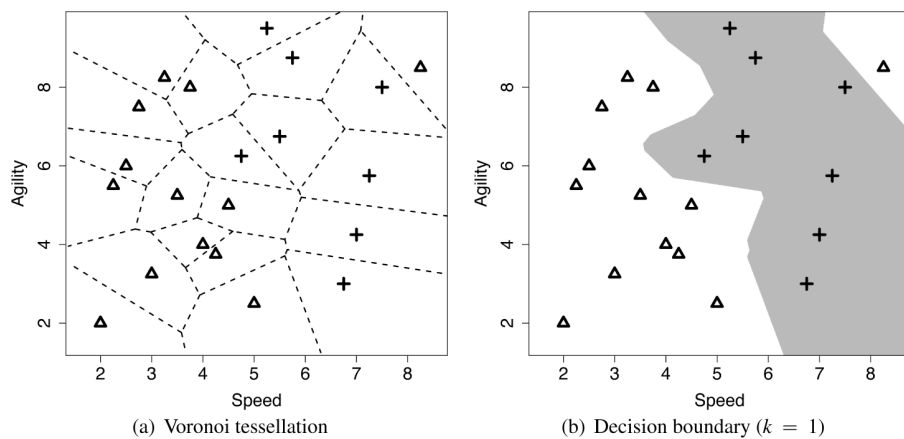


Figure 5.5

(a) The Voronoi tessellation of the feature space when the dataset has been updated to include the query instance; and (b) the updated decision boundary reflecting the addition of the query instance in the training set.

In summary, the inductive bias underpinning similarity-based machine learning algorithms is that things that are similar (i.e., instances that have similar descriptive features) also have the same target feature values. The nearest neighbor algorithm creates an implicit global predictive model by aggregating local models, or neighborhoods. The definition of these neighborhoods is based on similarity within the feature space to the labeled training instances. Predictions are made for a query instance using the target level of the training instance defining the neighborhood in the feature space that contains the query.

5.4 Extensions and Variations

We now understand the standard nearest neighbor algorithm. The algorithm, as presented, can work well with clean, reasonably sized datasets containing continuous descriptive features. Often, however, datasets are noisy, very large, and may contain a mixture of different data types. As a result, a lot of extensions and variations of the algorithm have been developed to address these issues. In this section we describe the most important of these.

5.4.1 Handling Noisy Data

Throughout our worked example using the college athlete dataset, the top-right corner of the feature space contained a *no* region (see [Figure 5.4](#)^[190]). This region exists because one of the *no* instances occurs far away from the rest of the instances with this target level. Considering that all the immediate neighbors of this instance are associated with the *yes* target level, it is likely that either this instance has been incorrectly labeled and should have a target feature value of *yes*, or one of the descriptive features for this instance has an incorrect value and hence it is in the wrong location in the feature space. Either way, this instance is likely to be an example of **noise** in the dataset.

Fundamentally, the nearest neighbor algorithm is a set of local models, each defined using a single instance. Consequently, the algorithm is sensitive to noise because any errors in the description or labeling of training data results in erroneous local models and hence incorrect predictions. The most direct way of mitigating against the impact of noise in the dataset on a nearest neighbor algorithm is to dilute the dependency of the algorithm on individual (possibly noisy) instances. To do this we simply

modify the algorithm to return the majority target level within the set of **k nearest neighbors** to the query \mathbf{q} :

$$\mathbb{M}_k(\mathbf{q}) = \arg \max_{l \in \text{levels}(t)} \sum_{i=1}^k \delta(t_i, l) \quad (5.4)$$

where $\mathbb{M}_k(\mathbf{q})$ is the prediction of the model \mathbb{M} for the query \mathbf{q} given the parameter of the model k ; $\text{levels}(t)$ is the set of levels in the domain of the target feature, and l is an element of this set; i iterates over the instances \mathbf{d}_i in increasing distance from the query \mathbf{q} ; t_i is the value of the target feature for instance \mathbf{d}_i ; and $\delta(t_i, l)$ is the **Kronecker delta** function, which takes two parameters and returns 1 if they are equal and 0 otherwise. [Figure 5.6\(a\)](#)^[193] demonstrates how this approach can regularize the decision boundary for the dataset in [Table 5.4](#)^[191]. In this figure we have set $k = 3$, and this modification has resulted in the *no* region in the top right corner of the feature space disappearing.

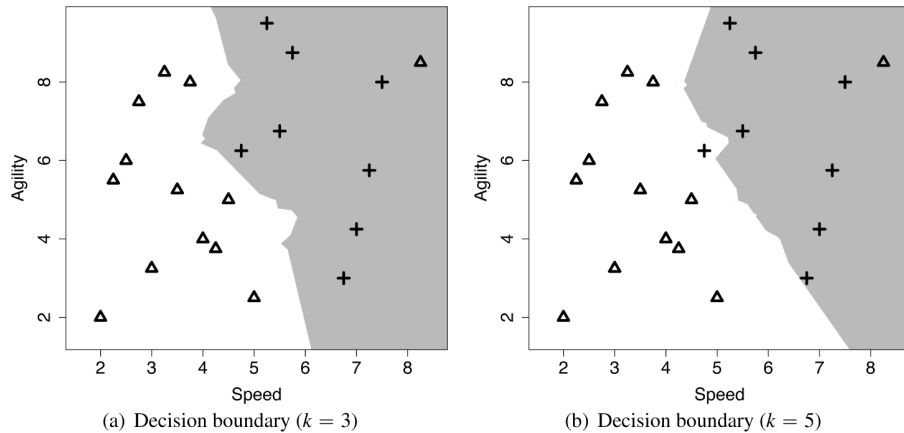


Figure 5.6

The decision boundary using majority vote of the nearest 3 and 5 instances.

Although, in our example, increasing the set of neighbors from 1 to 3 removed the noise issue, $k = 3$ does not work for every dataset. There is always a trade-off in setting the value of k . If we set k too low, we run the risk of the algorithm being sensitive to noise in the data and overfitting. Conversely, if we set k too high, we run the risk of losing the true pattern of the data and underfitting. For example, [Figure 5.6\(b\)](#)^[193] illustrates what happens to the decision boundary in our example feature space when $k = 5$.

Here we can see that the decision boundary may have been pushed too far back into the yes region (one of the crosses is now on the wrong side of the decision boundary). So, even a small increase in k can have a significant impact on the decision boundary.

The risks associated with setting k to a high value are particularly acute when we are dealing with an **imbalanced dataset**. An imbalanced dataset is a dataset that contains significantly more instances of one target level than another. In these situations, as k increases, the majority target level begins to dominate the feature space. The dataset in the college athlete example is imbalanced—there are 13 *no* instances and only 7 *yes* instances. Although this differential between the target levels in the dataset may not seem substantial, it does have an impact as k increases. [Figure 5.7\(a\)](#)^[194] illustrates the decision boundary when $k = 15$. Clearly, large portions of the *yes* region are now on the wrong side of the decision boundary. Moreover, if k is set to a value larger than 15, the majority target level dominates the entire feature space. Given the sensitivity of the algorithm to the value of k , how should we set this parameter? The most common way to tackle this issue is to perform evaluation experiments to investigate the performance of models with different values for k and to select the one that performs best. We return to these kinds of evaluation experiments in Chapter 9^[533].

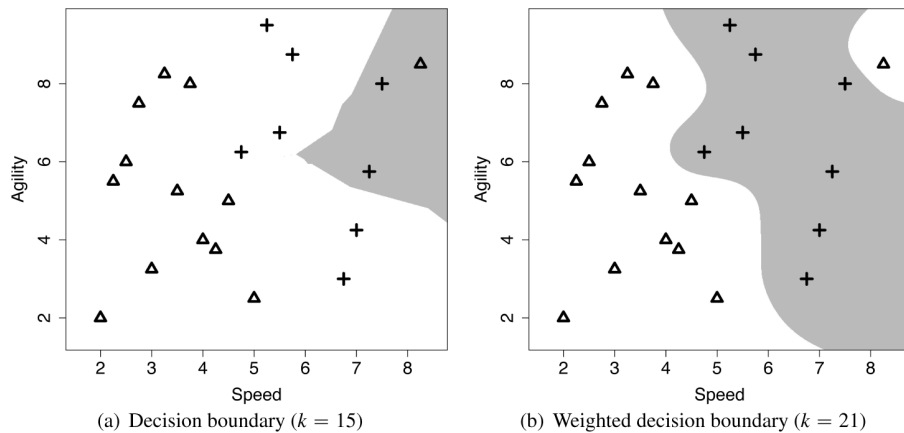


Figure 5.7

(a) The decision boundary using majority vote of the nearest 15 neighbors; and (b) the weighted k nearest neighbor model decision boundary (with $k = 21$).

Another way to address the problem of how to set k is to use a **weighted k nearest neighbor** approach. The problem with setting k to a high value

arises because the algorithm starts taking into account neighbors that are far away from the query instance in the feature space. As a result, the algorithm tends toward the majority target level in the dataset. One way of counterbalancing this tendency is to use a **distance weighted k nearest neighbor** approach. When a distance weighted k nearest neighbor approach is used, the contribution of each neighbor to the prediction is a function of the inverse distance between the neighbor and the query. So when calculating the overall majority vote across the k nearest neighbors, the votes of the neighbors that are close to the query get a lot of weight, and the votes of the neighbors that are farther away from the query get less weight. The easiest way to implement this weighting scheme is to weight each neighbor by the reciprocal⁶ of the squared distance between the neighbor \mathbf{d} and the query \mathbf{q} :

$$\frac{1}{dist(\mathbf{q}, \mathbf{d})^2} \quad (5.5)$$

Using the distance weighted k nearest neighbor approach, the prediction returned for a given query is the target level with the highest score when we sum the weights of the votes of the instances in the neighborhood of k nearest neighbors for each target level. The weighted k nearest neighbor model is defined as

$$\mathbb{M}_k(\mathbf{q}) = \arg \max_{l \in levels(t)} \sum_{i=1}^k \frac{1}{dist(\mathbf{q}, \mathbf{d}_i)^2} \times \delta(t_i, l) \quad (5.6)$$

where $\mathbb{M}_k(\mathbf{q})$ is the prediction of the model \mathbb{M} for the query \mathbf{q} given the parameter of the model k ; $levels(t)$ is the set of levels in the domain of the target feature, and l is an element of this set; i iterates over the instances \mathbf{d}_i in increasing distance from the query \mathbf{q} ; t_i is the value of the target feature for instance \mathbf{d}_i ; and $\delta(t_i, l)$ is the **Kronecker delta** function, which takes two parameters and returns 1 if they are equal and 0 otherwise. The reason we multiply by the Kronecker delta function is to ensure that in calculating the score for each of the candidate target levels, we include only the weights for the instances whose target feature value matches that level.

When we weight the contribution to a prediction of each of the neighbors by the reciprocal of the distance to the query, we can actually set k to be equal to the size of the training set and therefore include all the training instances in the prediction process. The issue of losing the true pattern of the data is less acute now because the training instances that are very far away from the query naturally won't have much of an effect on the prediction.

[Figure 5.7\(b\)](#)^[194] shows the decision boundary for a weighted k nearest neighbor model for the dataset in [Table 5.4](#)^[191] with $k = 21$ (the size of the dataset) and weights computed using the reciprocal of the squared distance. One of the most striking things about this plot is that the top-right region of the feature space again belongs to the *no* region. This may not be a good thing if this instance is due to noise in the data, and this demonstrates that there is no *silver bullet* solution to handling noise in datasets. This is one of the reasons why creating a data quality report⁷ and spending time on cleaning the dataset is such an important part of any machine learning project. That said, there are some other features of this plot that are encouraging. For example, the size of a *no* region in the top right of the feature space is smaller than the corresponding region for the nearest neighbor model with $k = 1$ (see [Figure 5.4\(b\)](#)^[190]). So by giving all the instances in the dataset a weighted vote, we have at least reduced the impact of the noisy instance. Also, the decision boundary is much smoother than the decision boundaries of the other models we have looked at in this section. This may indicate that the model is doing a better job of modeling the transition between the different target levels.

Using a weighted k nearest neighbor model does not require that we set k equal to the size of the dataset, as we did in this example. It may be possible to find a value for k —using evaluation experiments—that eliminates, or further reduces, the effect of the noise on the model. As is so often the case in machine learning, fitting the parameters of a model is as important as selecting which model to use.

Finally, it is worth mentioning two situations where this weighted k nearest neighbor approach can be problematic. The first is if the dataset is very imbalanced, then even with a weighting applied to the contribution of the training instances, the majority target level may dominate. The second is when the dataset is very large, which means that computing the reciprocal

of squared distance between the query and all the training instances can become too computationally expensive to be feasible.

5.4.2 Efficient Memory Search

The fact that the nearest neighbor algorithm stores the entire training dataset in memory has a negative effect on the time complexity of the algorithm. In particular, if we are working with a large dataset, the time cost in computing the distances between a query and all the training instances and retrieving the k nearest neighbors may be prohibitive. Assuming that the training set will remain relatively stable, this time issue can be offset by investing in some one-off computation to create an index of the instances that enables efficient retrieval of the nearest neighbors without doing an exhaustive search of the entire dataset.

The **k -d tree**⁸ which is short for *k -dimensional* tree, is one of the best known of these indices. A k -d tree is a balanced **binary tree**⁹ in which each of the nodes in the tree (both interior and leaf nodes) index one of the instances in a training dataset. The tree is constructed so that nodes that are nearby in the tree index training instances that are nearby in the feature space.

To construct a k -d tree, we first pick a feature and split the data into two partitions using the median value of this feature.¹⁰ We then recursively split each of the two new partitions, stopping the recursion when there are fewer than two instances in a partition. The main decision to be made in this process is how to select the feature to split on. The most common way to do this is to define an arbitrary order over the descriptive features before we begin building the tree. Then, using the feature at the start of the list for the first split, we select the next feature in the list for each subsequent split. If we get to a point where we have already split on all the features, we go back to the start of the feature list.

Every time we partition the data, we add a node with two branches to the k -d tree. The node indexes the instance that had the median value of the feature, the left branch holds all the instances that had values less than the median, and the right branch holds all the instances that had values greater than the median. The recursive partitioning then grows each of these branches in a depth-first manner.

Each node in a k - d tree defines a boundary that partitions the feature space along the median value of the feature the data was split on at that node. Technically these boundaries are **hyperplanes**¹¹ and, as we shall see, play an important role when we are using the k - d tree to find the nearest neighbor for a query. In particular, the hyperplane at a node defines the boundary between the instances stored on each of the subtrees below the node. We will find this useful when we are trying to decide whether to search both branches of a node when we are looking for the nearest neighbor or whether we can prune one of them.

[Figure 5.8](#)^[198] illustrates the creation of the first two nodes of a k - d tree for the college athlete dataset in [Table 5.4](#)^[191]. In generating this figure we have assumed that the algorithm selected the features to split on using the following ordering over the features: SPEED, AGILITY. The non-leaf nodes in the trees list the ID of the instance the node indexes and the feature and value pair that define the hyperplane partition on the feature space defined by the node. [Figure 5.9\(a\)](#)^[199] shows the complete k - d tree generated for the dataset, and [Figure 5.9\(b\)](#)^[199] shows the partitioning of the feature space as defined by the k - d tree. The lines in this figure indicate the hyperplanes partitioning the feature space that were created by the splits encoded in the non-leaf nodes in the tree. The heavier the weight of the line used to plot the hyperplane, the earlier in the tree the split occurred.

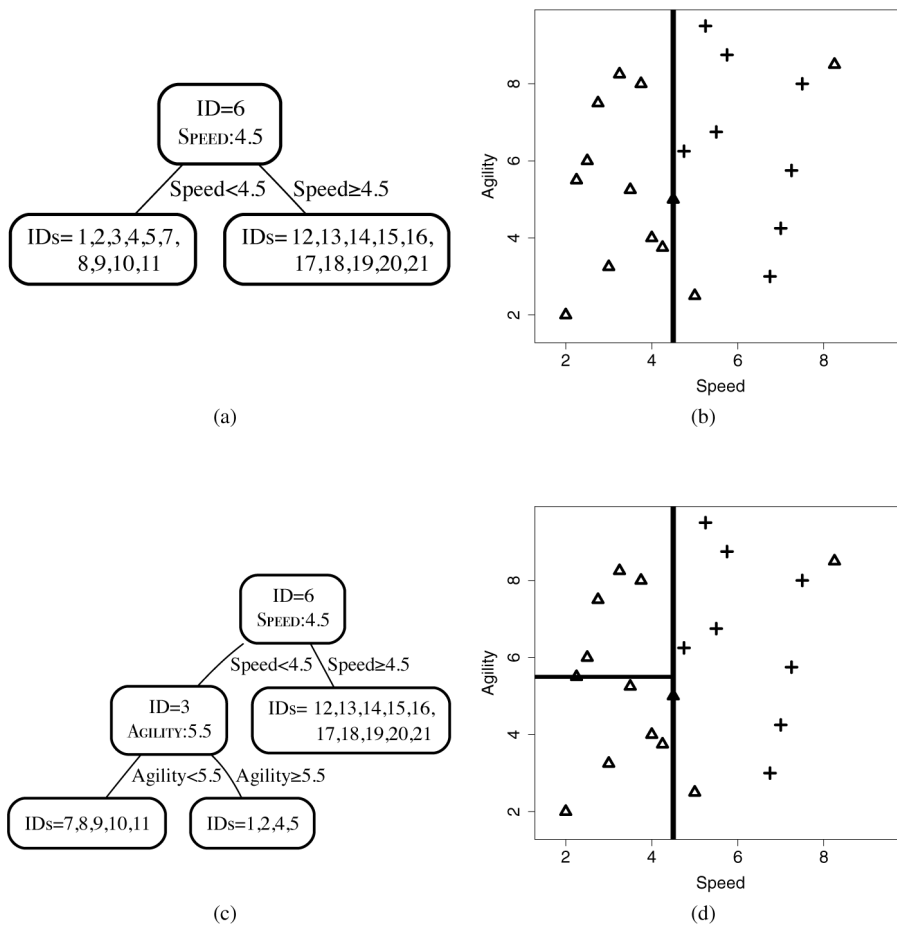
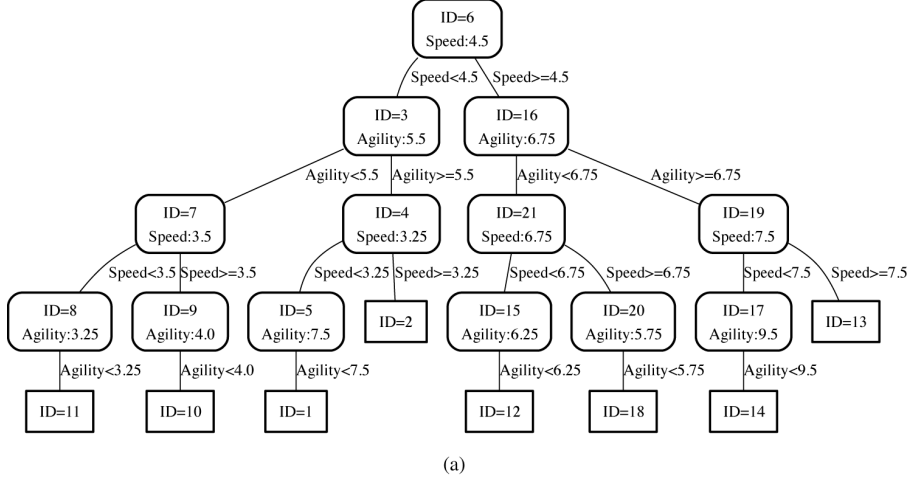
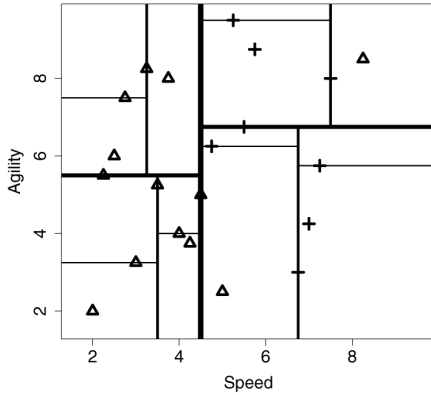


Figure 5.8

(a) The k - d tree generated for the dataset in Table 5.4^[191] after the initial split using the SPEED feature with a threshold of 4.5; (b) the partitioning of the feature space by the k - d tree in (a); (c) the k - d tree after the dataset at the left child of the root has been split using the AGILITY feature with a threshold of 5.5; and (d) the partitioning of the feature space by the k - d tree in (c).



(a)



(b)

Figure 5.9

(a) The final k - d tree generated for the dataset in Table 5.4^[191]; and (b) the partitioning of the feature space defined by this k - d tree.

Once we have stored the instances in a dataset in a k - d tree, we can use the tree to quickly retrieve the nearest neighbor for a query instance. Algorithm 3^[200] lists the algorithm we use to retrieve the nearest neighbor for a query. The algorithm starts by descending through the tree from the root node, taking the branch at each interior node that matches the value of the query for the feature tested at that node, until it comes to a leaf node (Line 3 of the algorithm). The algorithm stores the instance indexed by the leaf node in the *best* variable and sets the *best-distance* variable to the distance between the instance indexed by the leaf node and the query instance (Lines 5, 6, and 7). Unfortunately, there is no guarantee that this instance will be the nearest neighbor, although it should be a good

approximate neighbor for the query. So the algorithm then searches the tree looking for instances that are closer to the query than the instance stored in *best* (Lines 4-11 of the algorithm control this search).

At each node encountered in the search, the algorithm does three things. First, it checks that the node is not `NULL`. If this is the case, then the algorithm has reached the parent node of the root of the tree and should terminate (Line 4) by returning the instance stored in *best* (Line 12). Second, the algorithm checks if the instance indexed by the node is closer to the query than the instance at the current best node. If it is, *best* and *best-distance* are updated to reflect this (Lines 5, 6, and 7). Third, the algorithm chooses which node it should move to next: the parent of the node or a node in the subtree under the other branch of the node (Lines 8, 9, 10, and 11).

The decision of which node to move to next is made by checking if any instances indexed by nodes in the subtree on the other branch of the current node could be the nearest neighbor. The only way that this can happen is if there is at least one instance on the other side of the hyperplane boundary that bisects the node that is closer to the query than the current *best-distance*. Fortunately, because the hyperplanes created by the *k-d* tree are all axis-aligned, the algorithm can test for this condition quite easily. The hyperplane boundary bisecting a node is defined by the value used to split the descriptive feature at the node. This means that we only need to test whether the difference between the value for this feature for the query instance and the value for this feature that defines the hyperplane is less than the *best-distance* (Line 8). If this test succeeds, the algorithm descends to a leaf node of this subtree, using the same process it used to find the original leaf node (Line 9). If this test fails, the algorithm ascends the tree to the parent of the current node and prunes the subtree containing the region on the other side of the hyperplane without testing the instances in that region (Line 11). In either case, the search continues from the new node as before. The search finishes when it reaches the root node and both its branches have been either searched or pruned. The algorithm returns the instance stored in the *best* variable as the nearest neighbor.

Algorithm 3 Pseudocode description of the k - d tree nearest neighbor retrieval algorithm.

Require: query instance \mathbf{q} and a k - d tree \mathbf{kdtree}

```
1: best = null
2: best-distance =  $\infty$ 
3: node = descendTree(kdtree,q)
4: while node! = NULL do
5:   if distance(q,node) < best-distance then
6:     best = node
7:     best-distance = distance(q,node)
8:   end if
9:   if boundaryDist(q, node) < best-distance then
10:    node = descendtree(node,q)
11:   else
12:    node = parent(node)
13:   end if
14: end while
15: return best
```

We can demonstrate how this retrieval algorithm works by showing how the algorithm finds the nearest neighbor for a query instance with SPEED = 6.00 and AGILITY = 3.50. [Figure 5.10\(a\)](#)^[201] illustrates the first stage of the retrieval of the nearest neighbor. The bold lines show the path taken to descend the tree from the root to a leaf node based on the values of the query instance (use [Figure 5.9\(a\)](#)^[199] to trace this path in detail). This leaf node indexes instance \mathbf{d}_{12} (SPEED = 5.00, AGILITY = 2.50). Because this is the initial descent down the tree, *best* is automatically set to \mathbf{d}_{12} , and *best-distance* is set to the distance between instance \mathbf{d}_{12} and the query, which is 1.4142 (we use Euclidean distance throughout this example). At this point the retrieval process will have executed Lines 1–7 of the algorithm.

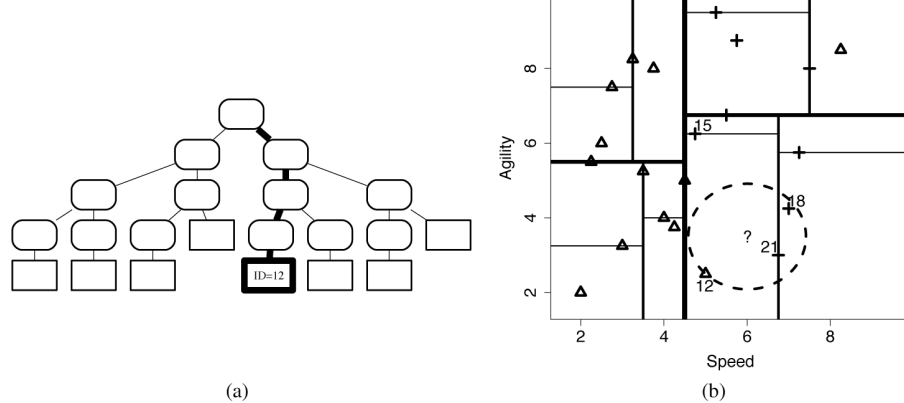


Figure 5.10

(a) The path taken from the root node to a leaf node when we search the tree with a query SPEED = 6.00, AGILITY = 3.50; and (b) the ? marks the location of the query, and the dashed circle plots the extent of the target, and for convenience in the discussion, we have labeled some of the nodes with the IDs of the instances they index (12, 15, 18, and 21).

Figure 5.10(b)^[201] illustrates the location of the query in the feature space (the ?). The dashed circle centered on the query location has a radius equal to the *best-distance*. We can see in Figure 5.10(b)^[201] that this circle intersects with the triangle marking the location of \mathbf{d}_{12} , which is currently stored in *best* (i.e., it is our current best guess for the nearest neighbor). This circle covers the area in the feature space that we know must contain all the instances that are closer to the query than *best*. Although this example is just two dimensional, the k - d tree algorithm can work in a many dimensional feature space, so we will use the term **target hypersphere**¹² to denote the region around the query that is inside the *best-distance*. We can see in Figure 5.10(b)^[201] that instance \mathbf{d}_{12} is not the true nearest neighbor to the query—several other instances are inside the target hypersphere.

The search process must now move to a new node (Lines 8, 9, 10, and 11). This move is determined by Line 8, which checks if the distance between the query and the hyperplane¹³ defined by the current node is less than the value of *best-distance*. In this case, however, the current node is a leaf node, so it does not define a hyperplane on the feature space. As a result, the condition checked in Line 8, fails and the search moves to the parent node of the current node (Line 11).

This new node indexes \mathbf{d}_{15} . The node is not NULL, so the **while** loop on Line 4 succeeds. The distance between instance \mathbf{d}_{15} and the query instance is 3.0208, which is not less than the current value of *best-distance*, so the **if**

statement on Line 5 will fail. We can see this easily in [Figure 5.10\(b\)](#)^[201], as \mathbf{d}_{15} is well outside the target hypersphere. The search will then move to a new node (Lines 8, 9, 10, and 11). To calculate the distance between the query instance and the hyperplane defined by the node indexing \mathbf{d}_{15} (the boundaryDist function on Line 8), we use only the AGILITY feature, as it is the splitting feature at this node. This distance is 2.75, which is greater than *best-distance* (we can see this in [Figure 5.10\(b\)](#)^[201], as the hyperplane defined at the node indexing \mathbf{d}_{15} does not intersect with the target hypersphere). This means that the **if** statement on Line 8 fails, and the search moves to the parent of the current node (Line 11).

This new node indexes \mathbf{d}_{21} , which is not `NULL`, so the **while** loop on Line 4 succeeds. The distance between the query instance and \mathbf{d}_{21} is 0.9014, which is less than the value stored in *best-distance* (we can see this in [Figure 5.10\(b\)](#)^[201], as \mathbf{d}_{21} is inside the target hypersphere). Consequently, the **if** statement on Line 5 succeeds, and *best* is set to \mathbf{d}_{21} , and *best-distance* is set to 0.9014 (Lines 6 and 7). [Figure 5.11\(a\)](#)^[203] illustrates the extent of the revised target hypersphere once these updates have been made.

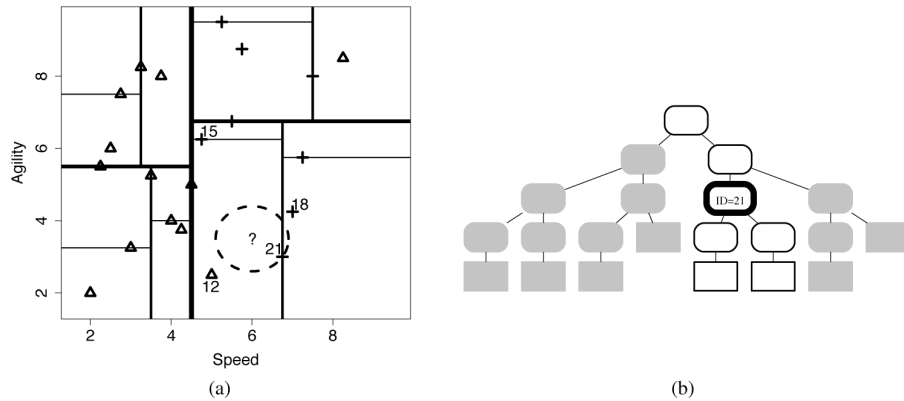


Figure 5.11

(a) The target hypersphere after instance \mathbf{d}_{21} has been stored as *best*, and *best-distance* has been updated; and (b) the extent of the search process: white nodes were checked by the search process, and the node with the bold outline indexed instance \mathbf{d}_{21} , which was returned as the nearest neighbor to the query. Grayed-out branches indicate the portions of the k - d tree pruned from the search.

The **if** statement on Line 8, which tests the distance between the query and the hyperplane defined by the current *best* node, is executed next. The distance between the query instance and the hyperplane defined by the node that indexes instance \mathbf{d}_{21} is 0.75 (recall that because the hyperplane at this

node is defined by the SPEED value of 6.75, we only compare this to the SPEED value of the query instance, 6.00). This distance is less than the current *best-distance* (in [Figure 5.11\(a\)](#)^[203], the hyperplane defined by the node that indexes instance \mathbf{d}_{21} intersects with the target hypersphere). The **if** statement on line 8 will succeed, and the search process will descend down the other branch of the current node (Line 9), because there is possibly an instance closer than the current best instance stored down this branch.

It is obvious from [Figure 5.11\(a\)](#)^[203] that the search process will not find any instances closer to the query than \mathbf{d}_{21} , nor are there any other hyperplanes that intersect with the target hypersphere. So the rest of the search process will involve a descent down to the node, indexing \mathbf{d}_{18} and a direct ascent to the root node where the search process will then terminate and return \mathbf{d}_{21} as the nearest neighbor (we will skip the details of these steps). [Figure 5.11\(b\)](#)^[203] illustrates the parts of the *k-d* tree that were checked or pruned during the search process.

In this example, using a *k-d* tree saved us calculating the distance between the query node and 14 of the instances in the dataset. This is the benefit of using a *k-d* tree and becomes especially apparent when datasets are very large. However, using a *k-d* tree is not always appropriate; *k-d* trees are reasonably efficient when there are a lot more instances than there are features. As a rough rule of thumb, we should have around 2^m instances for m descriptive features. Once this ratio drops, the efficiency of the *k-d* tree diminishes. Other approaches to efficient memory access have been developed, for example, locality sensitivity hashing, R-Trees, B-Trees, M-Trees, and VoRTrees, among others. All these approaches are similar to *k-d* trees in that they are trying to set up indexes that enable efficient retrieval from a dataset. Obviously, the differences between them make them more or less appropriate for a given dataset, and it often requires some experiments to figure out which is the best one for a given problem.

We can extend this algorithm to retrieve the k nearest neighbors by modifying the search to use distance of the k^{th} closest instance found as *best-distance*. We can also add instances to the tree after it has been created. This is important because one of the key advantages of a nearest neighbor approach is that it can be updated with new instances as more labeled data

arrive. To add a new instance to the tree, we start at the root node and descend to a leaf node, taking the left or right branch of each node depending on whether the value of the instance's feature is less than or greater than the splitting value used at the node. Once we get to a leaf node, we simply add the new instance as either the left or the right child of the leaf node. Unfortunately, adding nodes in this way results in the tree becoming unbalanced, which can have a detrimental effect on the efficiency of the tree. So if we add a lot of new instances, we may find that the tree has become too unbalanced and that we will need to construct a new tree from scratch using the extended dataset to restore the efficiency of the retrieval process.

5.4.3 Data Normalization

A financial institution is planning a direct marketing campaign to sell a pension product to its customer base. In preparation for this campaign, the financial institution has decided to create a nearest neighbor model using a Euclidean distance metric to predict which customers are most likely to respond to direct marketing. This model will be used to target the marketing campaign only to those customers who are most likely to purchase the pension product. To train the model, the institution has created a dataset from the results of previous marketing campaigns that list customer information—specifically the annual salary (SALARY) and age (AGE) of the customer—and whether the customer bought a product after they had been contacted via a direct marketing message (PURCH). [Table 5.5](#)^[204] lists a sample from this dataset.

Table 5.5

A dataset listing salary and age information for customers and whether they purchased a product.

ID	SALARY	AGE	PURCH	ID	SALARY	AGE	PURCH
1	53,700	41	no	6	55,900	57	yes
2	65,300	37	no	7	48,600	26	no
3	48,900	45	yes	8	72,800	60	yes
4	64,800	49	yes	9	45,300	34	no
5	44,200	30	no	10	73,200	52	yes

Using this nearest neighbor model, the marketing department wants to decide whether they should contact a customer with the following profile:

$\text{SALARY} = 56,000$ and $\text{AGE} = 35$. Figure 5.12(a)^[205] presents a plot of the feature space defined by the SALARY and AGE features, containing the dataset in Table 5.5^[204]. The location of the query customer in the feature space is indicated by the ?. From inspecting Figure 5.12(a)^[205], it would appear as if instance \mathbf{d}_1 —which has a target level *no*—is the closest neighbor to the query. So we would expect that the model would predict *no* and that the customer would not be contacted.

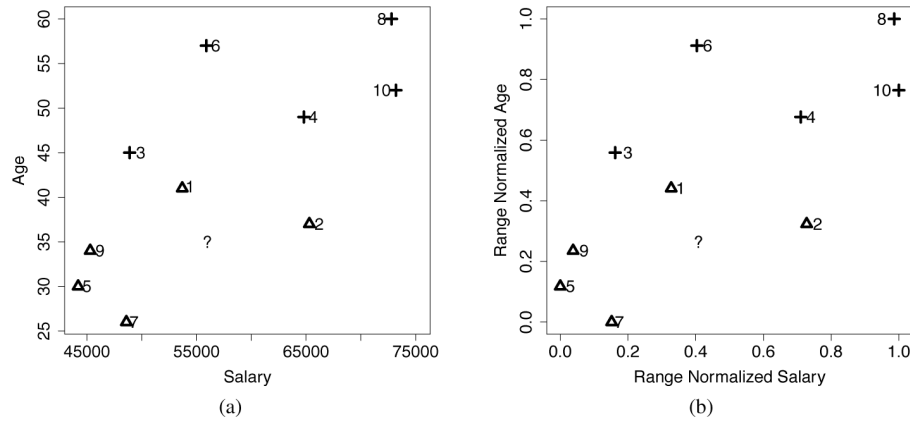


Figure 5.12

(a) The feature space defined by the SALARY and AGE features in Table 5.5^[204]; and (b) the normalized SALARY and AGE feature space based on the normalized data in Table 5.7^[208]. The instances are labeled with their IDs; triangles represent instances with the *no* target level; and crosses represent instances with the *yes* target level. The location of the query $\text{SALARY} = 56,000$, $\text{AGE} = 35$ is indicated by the ?.

The model, however, will actually return a prediction of *yes*, indicating that the customer should be contacted. We can analyze why this happens if we examine the Euclidean distance computations between the query and the instances in the dataset. Table 5.6^[206] lists these distances when we include both the SALARY and AGE features, only the SALARY features, and only the AGE feature in the distance calculation. The nearest neighbor model uses both the SALARY and AGE features when it calculates distances to find the nearest neighbor to the query. The SALARY and AGE section of Table 5.6^[206] lists these distances and the ranking that the model applies to the instances in the dataset using them. From the rankings we can see that the nearest neighbor to the query is instance \mathbf{d}_6 (indicated by its rank of 1). Instance \mathbf{d}_6 has a target value of *yes*, and this is why the model will return a positive prediction for the query.

Table 5.6

The dataset from [Table 5.5](#)^[204] with the Euclidean distance between each instance and the query SALARY = 56,000, AGE = 35 when we use both the SALARY and AGE features, just the SALARY feature, and just the AGE feature.

ID	Dataset			SALARY and AGE		SALARY Only		AGE Only	
	SALARY	AGE	PURCH	Dist.	Rank	Dist.	Rank	Dist.	Rank
1	53,700	41	no	2,300.0078	2	2,300	2	6	4
2	65,300	37	no	9,300.0002	6	9,300	6	2	2
3	48,900	45	yes	7,100.0070	3	7,100	3	10	6
4	64,800	49	yes	8,800.0111	5	8,800	5	14	7
5	44,200	30	no	11,800.0011	8	11,800	8	5	5
6	55,900	57	yes	102.3914	1	100	1	22	9
7	48,600	26	no	7,400.0055	4	7,400	4	9	3
8	72,800	60	yes	16,800.0186	9	16,800	9	25	10
9	45,300	34	no	10,700.0000	7	10,700	7	1	1
10	73,200	52	yes	17,200.0084	10	17,200	10	17	8

The Rank columns rank the distances of each instance to the query (1 is closest, 10 is farthest away).

Considering the distribution of the instances in the feature space as depicted in [Figure 5.12\(a\)](#)^[205], the result that instance \mathbf{d}_6 is the nearest neighbor to the query is surprising. Several other instances appear to be much closer to the query, and importantly, several of these instances have a target level of *no*, for example, instance \mathbf{d}_1 . Why do we get this strange result?

We can get a hint about what is happening by comparing the distances computed using both the SALARY and AGE features with the distances computed using the SALARY feature only, that listed in the SALARY Only section of [Table 5.6](#)^[206]. The distances calculated using only the SALARY feature are almost exactly the same as the distances calculated using both the SALARY and AGE features. This is happening because the salary values are much larger than the age values. Consequently, the SALARY feature dominates the computation of the Euclidean distance whether we include the AGE feature or not. As a result, AGE is being virtually ignored by the metric. This dominance is reflected in the ranking of the instances as neighbors. In [Table 5.6](#)^[206], if we compare the rankings based on SALARY and AGE with the rankings based solely on SALARY, we see that the values in these two columns are identical. The model is using only the SALARY feature and is ignoring the AGE feature when it makes predictions.

This dominance of the distance computation by a feature based solely on the fact that it has a larger range of values than other features is not a good thing. We do not want our model to bias toward a particular feature simply because the values of that feature happen to be large relative to the other features in the dataset. If we allowed this to happen, then our model will be affected by accidental data collection factors, such as the units used to measure something. For example, in a model that is sensitive to the relative size of the feature values, a feature that was measured in millimeters would have a larger effect on the resulting model predictions than a feature that was measured in meters.¹⁴ Clearly we need to address this issue.

Fortunately, we have already discussed the solution to this problem. The problem is caused by features having different **variance**. In Section 3.6.1^[87] we discussed variance and introduced a number of **normalization** techniques that normalize the variances in a set of features. The basic normalization technique we introduced was **range normalization**,¹⁵ and we can apply it to the pension plan prediction dataset to normalize the variance in the SALARY and AGE features. For example, range normalization using the range [0,1] is applied to instance \mathbf{d}_1 from [Table 5.5](#)^[204] as follows:

$$\begin{aligned}\text{SALARY: } & \left(\frac{53,700 - 44,200}{73,200 - 44,200} \right) \times (1.0 - 0.0) + 0 = 0.3276 \\ \text{AGE: } & \left(\frac{41 - 26}{60 - 26} \right) \times (1.0 - 0.0) + 0 = 0.4412\end{aligned}$$

Table 5.7

The updated version of [Table 5.6](#)^[206] once we have applied range normalization to the SALARY and AGE features in the dataset and to the query instance.

ID	Normalized Dataset			SALARY and AGE		SALARY Only		AGE Only	
	SALARY	AGE	PURCH	Dist.	Rank	Dist.	Rank	Dist.	Rank
1	0.3276	0.4412	no	0.1935	1	0.0793	2	0.17647	4
2	0.7276	0.3235	no	0.3260	2	0.3207	6	0.05882	2
3	0.1621	0.5588	yes	0.3827	5	0.2448	3	0.29412	6
4	0.7103	0.6765	yes	0.5115	7	0.3034	5	0.41176	7
5	0.0000	0.1176	no	0.4327	6	0.4069	8	0.14706	3
6	0.4034	0.9118	yes	0.6471	8	0.0034	1	0.64706	9
7	0.1517	0.0000	no	0.3677	3	0.2552	4	0.26471	5
8	0.9862	1.0000	yes	0.9361	10	0.5793	9	0.73529	10
9	0.0379	0.2353	no	0.3701	4	0.3690	7	0.02941	1
10	1.0000	0.7647	yes	0.7757	9	0.5931	10	0.50000	8

The Rank columns rank the distances of each instance to the query (1 is closest, 10 is farthest away).

[Table 5.7](#)^[208] lists the dataset from [Table 5.5](#)^[204] after we have applied range normalization using a range of [0,1] to the SALARY and AGE features. When we normalize the features in a dataset, we also need to normalize the features in any query instances using the same normalization process and parameters. We normalize the query instance with SALARY =56,000 and AGE = 35 as follows:

$$\text{SALARY: } \left(\frac{56,000 - 44,200}{73,200 - 44,200} \right) \times (1.0 - 0.0) + 0 = 0.4069$$

$$\text{AGE: } \left(\frac{35 - 26}{60 - 26} \right) \times (1.0 - 0.0) + 0 = 0.2647$$

[Figure 5.12\(b\)](#)^[205] shows a plot of the feature space after the features have been normalized. The major difference between [Figure 5.12\(a\)](#)^[205] and [Figure 5.12\(b\)](#)^[205] is that the axes are scaled differently. In [Figure 5.12\(a\)](#)^[205] the SALARY axis ranged from 45,000 to 75,000, and the AGE axis ranged from 25 to 60. In [Figure 5.12\(b\)](#)^[205], however, both axes range from 0 to 1. Although this may seem like an insignificant difference, the fact that both features now cover the same range has a huge impact on the performance of a similarity-based prediction model that uses this data.

[Table 5.7](#)^[208] also repeats the calculations from [Table 5.6](#)^[206] using the normalized dataset and the normalized query instance. In contrast with [Table 5.6](#)^[206], where there was a close match between the SALARY and AGE distances and the SALARY only distances and related rankings, in [Table](#)

[5.7](#)^[208] there is much more variation between the SALARY and AGE distances and the SALARY only distances. This increased variation is mirrored in the fact that the rankings based on the distances calculated using the SALARY and AGE features are quite different from the rankings based on the distances calculated using SALARY only. These changes in the rankings of the instances is a direct result of normalizing the features and reflects the fact that the distance calculations are no longer dominated by the SALARY feature. The nearest neighbor model is now factoring both SALARY and AGE into the ranking of the instances. The net effect of this is that instance \mathbf{d}_1 is now ranked as the nearest neighbor to the query—this is in line with the feature space representation in [Figure 5.12\(b\)](#)^[205]. Instance \mathbf{d}_1 has a target level of *no*, so the nearest neighbor model now predicts a target level of *no* for the query, meaning that the marketing department won't include the customer in their list of direct marketing prospects. This is the opposite of the prediction made using the original dataset.

In summary, distance computations are sensitive to the value ranges of the features in the dataset. This is something we need to control for when we are creating a model, as otherwise we are allowing an unwanted bias to affect the learning process. When we normalize the features in a dataset, we control for the variation across the variances of features and ensure that each feature can contribute equally to the distance metric. Normalizing the data is an important thing to do for almost all machine learning algorithms, not just nearest neighbor.

5.4.4 Predicting Continuous Targets

It is relatively easy to adapt the k nearest neighbor approach to handle continuous target features. To do this we simply change the approach to return a prediction of the average target value of the nearest neighbors, rather than the majority target level. The prediction for a continuous target feature by a k nearest neighbor model is therefore

$$\mathbb{M}_k(\mathbf{q}) = \frac{1}{k} \sum_{i=1}^k t_i \quad (5.7)$$

where $\mathbb{M}_k(\mathbf{q})$ is the prediction returned by the model using parameter value k for the query \mathbf{q} , i iterates over the k nearest neighbors to \mathbf{q} in the dataset,

and t_i is the value of the target feature for instance i .

Let's look at an example. Imagine that we are dealers in rare whiskey, and we would like some assistance in setting the reserve price for bottles of whiskey that we are selling at auction. We can use a k nearest neighbor model to predict the likely sale price of a bottle of whiskey based on the prices achieved by similar bottles at previous auctions.¹⁶ [Table 5.8](#)^[209] lists a dataset of whiskeys described by the RATING they were given in a popular whiskey enthusiasts magazine and their AGE (in years). The PRICE achieved at auction by the each bottle is also included.

Table 5.8

A dataset of whiskeys listing the age (in years), the rating (between 1 and 5, with 5 being the best), and the bottle price of each whiskey.

ID	AGE	RATING	PRICE	ID	AGE	RATING	PRICE
1	0	2	30.00	11	19	5	500.00
2	12	3.5	40.00	12	6	4.5	200.00
3	10	4	55.00	13	8	3.5	65.00
4	21	4.5	550.00	14	22	4	120.00
5	12	3	35.00	15	6	2	12.00
6	15	3.5	45.00	16	8	4.5	250.00
7	16	4	70.00	17	10	2	18.00
8	18	3	85.00	18	30	4.5	450.00
9	18	3.5	78.00	19	1	1	10.00
10	16	3	75.00	20	4	3	30.00

One thing that is immediately apparent in [Table 5.8](#)^[209] is that the AGE and RATING features have different ranges. We should normalize these features before we build a model. [Table 5.9](#)^[210] lists the whiskey dataset after the descriptive features have been normalized, using range normalization to the range [0,1].

Table 5.9

The whiskey dataset after the descriptive features have been normalized.

ID	AGE	RATING	PRICE	ID	AGE	RATING	PRICE
1	0.0000	0.25	30.00	11	0.6333	1.00	500.00
2	0.4000	0.63	40.00	12	0.2000	0.88	200.00
3	0.3333	0.75	55.00	13	0.2667	0.63	65.00
4	0.7000	0.88	550.00	14	0.7333	0.75	120.00
5	0.4000	0.50	35.00	15	0.2000	0.25	12.00
6	0.5000	0.63	45.00	16	0.2667	0.88	250.00
7	0.5333	0.75	70.00	17	0.3333	0.25	18.00
8	0.6000	0.50	85.00	18	1.0000	0.88	450.00
9	0.6000	0.63	78.00	19	0.0333	0.00	10.00
10	0.5333	0.50	75.00	20	0.1333	0.50	30.00

Let's now make a prediction using this model for a two-year-old bottle of whiskey that received a magazine rating of 5. Having normalized the dataset, we first need to normalize the descriptive feature values of this query instance using the same normalization process. This results in a query with $\text{AGE} = 0.0667$ and $\text{RATING} = 1.00$. For this example we set $k = 3$. [Figure 5.13](#)^[211] shows the neighborhood that this defines around the query instance. The three closest neighbors to the query are instances \mathbf{d}_{12} , \mathbf{d}_{16} and \mathbf{d}_3 . Consequently, the model will return a price prediction that is the average price of these three neighbors:

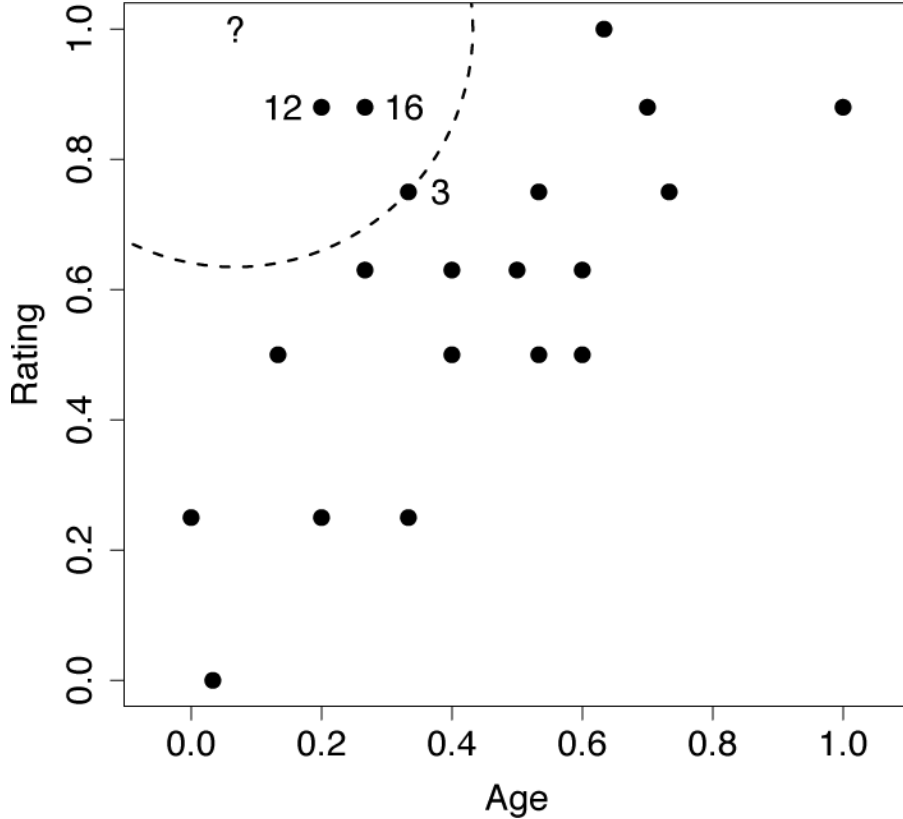


Figure 5.13

The AGE and RATING feature space for the whiskey dataset. The location of the query instance is indicated by the ? symbol. The circle plotted with a dashed line demarcates the border of the neighborhood around the query when $k = 3$. The three nearest neighbors to the query are labeled with their ID values.

$$\mathbb{M}_3(\langle 0.0667, 1.00 \rangle) = \frac{200.00 + 250.00 + 55.00}{3} = 168.33$$

We can also use a **weighted k nearest neighbor** model to make predictions for continuous targets that take into account the distance from the query instance to the neighbors (just like we did for categorical target features in Section 5.4.1^[191]). To do this, the model prediction equation in Equation (5.7)^[208] is changed to

$$\mathbb{M}_k(\mathbf{q}) = \frac{\sum_{i=1}^k \frac{1}{dist(\mathbf{q}, \mathbf{d}_i)^2} \times t_i}{\sum_{i=1}^k \frac{1}{dist(\mathbf{q}, \mathbf{d}_i)^2}} \quad (5.8)$$

where $dist(\mathbf{q}, \mathbf{d}_i)$ is the distance between the query instance and its i^{th} nearest neighbor. This is a weighted average of the target values of the k nearest neighbors, as opposed to the simple average in Equation (5.7)^[208].

Table 5.10

The calculations for the weighted k nearest neighbor prediction.

ID	PRICE	Distance	Weight	PRICE × Weight
1	30.00	0.7530	1.7638	52.92
2	40.00	0.5017	3.9724	158.90
3	55.00	0.3655	7.4844	411.64
4	550.00	0.6456	2.3996	1319.78
5	35.00	0.6009	2.7692	96.92
6	45.00	0.5731	3.0450	137.03
7	70.00	0.5294	3.5679	249.75
8	85.00	0.7311	1.8711	159.04
9	78.00	0.6520	2.3526	183.50
10	75.00	0.6839	2.1378	160.33
11	500.00	0.5667	3.1142	1557.09
12	200.00	0.1828	29.9376	5987.53
13	65.00	0.4250	5.5363	359.86
14	120.00	0.7120	1.9726	236.71
15	12.00	0.7618	1.7233	20.68
16	250.00	0.2358	17.9775	4494.38
17	18.00	0.7960	1.5783	28.41
18	450.00	0.9417	1.1277	507.48
19	10.00	1.0006	0.9989	9.99
20	30.00	0.5044	3.9301	117.90
Totals:			99.2604	16,249.85

Table 5.10^[212] shows the calculation of the numerator and denominator of Equation (5.8)^[210] for our whiskey bottle example, using the normalized dataset with k set to 20 (the full size of the dataset). The final prediction for the price of the bottle of whiskey we plan to sell is

$$\frac{16,249.85}{99.2604} = 163.71$$

The predictions using the $k = 3$ nearest neighbor model and the weighted k nearest neighbor model with k set to the size of the dataset are quite similar: 168.33 and 163.71. So, which model is making the better prediction? In this instance, to find out which model is best, we would really need to put the bottle of whiskey up for auction and see which model predicted the closest price. In situations where we have a larger dataset, however, we could perform evaluation experiments¹⁷ to see which value of k leads to the best-performing model. In general, standard k nearest neighbor models and weighted k nearest neighbor models will produce very similar results when a feature space is well populated. For datasets that only sparsely populate the feature space, however, weighted k nearest neighbor models usually make more accurate predictions, as they take into account the fact that some of the *nearest* neighbors can actually be quite far away.

5.4.5 Other Measures of Similarity

So far we have discussed and used the Minkowski-based Euclidean and Manhattan distance metrics to compute the similarity between instances in a dataset. There are, however, many other ways in which the similarity between instances can be measured. In this section we introduce some alternative measures of similarity and discuss when it is appropriate to use them. Any of these measures of similarity can simply replace the Euclidean measure we used in our demonstrations of the nearest neighbor algorithm.

Throughout this section we use the terms similarity and distance almost interchangeably, because we often judge the similarity between two instances in terms of the distance between them in a feature space. The only difference to keep in mind is that when we use distances, smaller values mean that instances are closer together in a feature space, whereas when we use similarities, larger values indicate this. We will, however, be specific in distinguishing between **metrics** and **indexes**. Recall that in Section 5.2.2^[184] we defined four criteria that a metric must satisfy: **non-negativity**, **identity**, **symmetry**, and **triangular inequality**. It is possible, however, to successfully use measures of similarity in similarity-based models that do not satisfy all four of these criteria. We refer to measures of similarity of this type as **indexes**. Most of the time the technical distinction between a metric and an index is not that important; we simply focus on choosing the right measure of similarity for the type of instances we are comparing. It is

important, however, to know if a measure is a metric or an index, as there are some similarity-based techniques that strictly require measures of similarity to be metrics. For example, the ***k-d trees*** described in Section 5.4.2^[196] require that the measure of similarity used be a metric (in particular that the measure conform to the triangular inequality constraint).

5.4.5.1 Similarity indexes for binary descriptive features There are lots of datasets that contain binary descriptive features—categorical features that have only two levels. For example, a dataset may record whether or not someone liked a movie, a customer bought a product, or someone visited a particular webpage. If the descriptive features in a dataset are binary, it is often a good idea to use a **similarity index** that defines similarity between instances specifically in terms of **co-presence** or **co-absence** of features, rather than an index based on distance.

To illustrate a series of similarity indexes for binary descriptive features, we will use an example of predicting **upsell** in an online service. A common business model for online services is to allow users a free trial period after which time they have to *sign up* to a paid account to continue using the service. These businesses often try to predict the likelihood that users coming to the end of the trial period will accept the upsell offer to move to the paid service. This insight into the likely future behavior of a customer can help a marketing department decide which customers coming close to the end of their trial period the department should contact to promote the benefits of signup to the paid service.

[Table 5.11](#)^[213] lists a small binary dataset that a nearest neighbor model could use to make predictions for this scenario. The descriptive features in this dataset are all binary and record the following information about the behavior of past customers:

- PROFILE: Did the user complete the profile form when registering for the free trial?
- FAQ: Did the user read the frequently asked questions page?
- HELPFORUM: Did the user post a question on the help forum?
- NEWSLETTER: Did the user sign up for the weekly newsletter?
- LIKED: Did the user *Like* the website on Facebook?

Table 5.11

A binary dataset listing the behavior of two individuals on a website during a trial period and whether they subsequently signed up for the website.

ID	PROFILE	FAQ	HELPFORUM	NEWSLETTER	LIKED	SIGNUP
1	true	true	true	false	true	yes
2	true	false	false	false	false	no

The target feature, SIGNUP, indicates whether the customers ultimately signed up to the paid service or not (*yes* or *no*).

The business has decided to use a nearest neighbor model to predict whether a current trial user whose free trial period is about to end is likely to sign up for the paid service. The query instance, \mathbf{q} , describing this user is:

$$\begin{aligned} \text{PROFILE} &= \text{true}, \text{FAQ} = \text{false}, \text{HELPFORUM} = \text{true}, \\ \text{NEWSLETTER} &= \text{false}, \text{LIKED} = \text{false} \end{aligned}$$

Table 5.12

The similarity between the current trial user, \mathbf{q} , and the two users in the dataset, \mathbf{d}_1 and \mathbf{d}_2 , in terms of co-presence (CP), co-absence (CA), presence-absence (PA), and absence-presence (AP).

		\mathbf{q}				\mathbf{q}	
		Pres.	Abs.			Pres.	Abs.
\mathbf{d}_1	Pres.	CP = 2 PA = 0	\mathbf{d}_2	Pres.	CP = 1 PA = 1		
	Abs.	AP = 2 CA = 1		Abs.	AP = 0 CA = 3		

Table 5.12^[214] presents a pairwise analysis of similarity between the current trial user, \mathbf{q} , and the two customers in the dataset in **Table 5.11**^[213] in terms of

- **co-presence (CP)**, how often a true value occurred for the same feature in both the query data \mathbf{q} and the data for the comparison user (\mathbf{d}_1 or \mathbf{d}_2)
- **co-absence (CA)**, how often a false value occurred for the same feature in both the query data \mathbf{q} and the data for the comparison user (\mathbf{d}_1 or \mathbf{d}_2)
- **presence-absence (PA)**, how often a true value occurred in the query data \mathbf{q} when a false value occurred in the data for the comparison user (\mathbf{d}_1 or \mathbf{d}_2) for the same feature
- **absence-presence (AP)**, how often a false value occurred in the query data \mathbf{q} when a true value occurred in the data for the comparison user (\mathbf{d}_1 or \mathbf{d}_2) for the same feature

or \mathbf{d}_2) for the same feature

One way of judging similarity is to focus solely on co-presence. For example, in an online retail setting, co-presence could capture what two users jointly viewed, liked, or bought. The **Russel-Rao** similarity index focuses on this and is measured in terms of the ratio between the number of co-presences and the total number of binary features considered:

$$sim_{RR}(\mathbf{q}, \mathbf{d}) = \frac{CP(\mathbf{q}, \mathbf{d})}{|\mathbf{q}|} \quad (5.9)$$

where \mathbf{q} and \mathbf{d} are two instances, $|\mathbf{q}|$ is the total number of features in the dataset, and $CP(\mathbf{q}, \mathbf{d})$ measures the total number of co-presences between \mathbf{q} and \mathbf{d} . Using Russel-Rao, \mathbf{q} has a higher similarity to \mathbf{d}_1 than to \mathbf{d}_2 :

$$\begin{aligned} sim_{RR}(\mathbf{q}, \mathbf{d}_1) &= \frac{2}{5} = 0.4 \\ sim_{RR}(\mathbf{q}, \mathbf{d}_2) &= \frac{1}{5} = 0.2 \end{aligned}$$

This means that the current trial user is judged to be more similar to the customer represented by instance \mathbf{d}_1 than the customer represented by instance \mathbf{d}_2 .

In some domains co-absence is important. For example, in a medical domain when judging the similarity between two patients, it may be as important to capture the fact that neither patient had a particular symptom as it is to capture the symptoms that the patients have in common. The **Sokal-Michener** similarity index takes this into account and is defined as the ratio between the total number of co-presences and co-absences and the total number of binary features considered:

$$sim_{SM}(\mathbf{q}, \mathbf{d}) = \frac{CP(\mathbf{q}, \mathbf{d}) + CA(\mathbf{q}, \mathbf{d})}{|\mathbf{q}|} \quad (5.10)$$

Using Sokal-Michener for our online services example \mathbf{q} , is judged to be more similar to instance \mathbf{d}_2 than instance \mathbf{d}_1 :

$$sim_{SM}(\mathbf{q}, \mathbf{d}_1) = \frac{3}{5} = 0.6$$

$$sim_{SM}(\mathbf{q}, \mathbf{d}_2) = \frac{4}{5} = 0.8$$

Sometimes, however, co-absences aren't that meaningful. For example, we may be in a retail domain in which there are so many items that most people haven't seen, listened to, bought, or visited the vast majority of them, and as a result, the majority of features will be co-absences. The technical term to describe a dataset in which most of the features have zero values is **sparse data**. In these situations we should use a metric that ignores co-absences. The **Jaccard** similarity index is often used in these contexts. This index ignores co-absences and is defined as the ratio between the number of co-presences and the total number of features, excluding those that record a co-absence between a pair of instances:¹⁸

$$sim_J(\mathbf{q}, \mathbf{d}) = \frac{CP(\mathbf{q}, \mathbf{d})}{CP(\mathbf{q}, \mathbf{d}) + PA(\mathbf{q}, \mathbf{d}) + AP(\mathbf{q}, \mathbf{d})} \quad (5.11)$$

Using Jaccard similarity, the current trial user in the online retail example is judged to be equally similar to instance \mathbf{d}_1 and \mathbf{d}_2 :

$$sim_J(\mathbf{q}, \mathbf{d}_1) = \frac{2}{4} = 0.5$$

$$sim_J(\mathbf{q}, \mathbf{d}_2) = \frac{1}{2} = 0.5$$

The fact that the judgment of similarity between current trial user and the other users in the dataset changed dramatically depending on which similarity index was employed illustrates the importance of choosing the correct index for the task. Unfortunately, beyond highlighting that the Jaccard index is useful for sparse binary data, we cannot give a hard and fast rule for how to choose between these indexes. As is so often the case in predictive analytics, making the right choice requires an understanding of the requirements of the task that we are trying to accomplish and matching these requirements with the features we want to emphasize in our model.

5.4.5.2 Cosine similarity

Cosine similarity is an index that can be used as a measure of the similarity between instances with continuous

descriptive features. The cosine similarity between two instances is the **cosine** of the inner angle between the two **vectors** that extend from the origin of a feature space to each instance. Figure 5.14(a)^[218] illustrates the inner angle, θ , between the vector from the origin to two instances in a feature space defined by two descriptive features, SMS and VOICE.

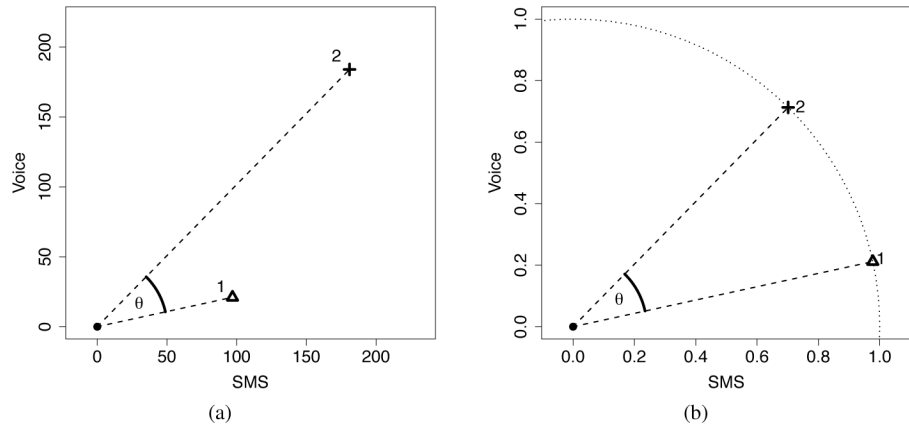


Figure 5.14

(a) The θ represents the inner angle between the vector emanating from the origin to instance d_1 and the vector emanating from the origin to instance d_2 ; and (b) shows d_1 and d_2 normalized to the unit circle.

Cosine similarity is an especially useful measure of similarity when the descriptive features describing instances in a dataset are related to each other. For example, in a mobile telecoms scenario, we could represent customers with just two descriptive features: the average number of SMS messages a customer sends per month, and the average number of VOICE calls a customer makes per month. In this scenario it is interesting to take a perspective on the similarity between customers that focuses on the mix of these two types of services they use, rather than the volumes of the services they use. Cosine similarity allows us to do this. The instances shown in Figure 5.14(a)^[218] are based on this mobile telecoms scenario. The descriptive feature values for d_1 are SMS = 97 and VOICE = 21, and for d_2 are SMS = 181 and VOICE = 184.

We compute the cosine similarity between two instances as the normalized **dot product** of the descriptive feature values of the instances. The dot product is normalized by the product of the lengths of the

descriptive feature value vectors.¹⁹ The dot product of two instances, **a** and **b**, defined by m descriptive features is

$$\mathbf{a} \cdot \mathbf{b} = \sum_{i=1}^m (\mathbf{a}[i] \times \mathbf{b}[i]) = (\mathbf{a}[1] \times \mathbf{b}[1]) + \cdots + (\mathbf{a}[m] \times \mathbf{b}[m]) \quad (5.12)$$

Geometrically, the dot product can be interpreted as equivalent to the cosine of the angle between the two vectors multiplied by the length of the two vectors:

$$\mathbf{a} \cdot \mathbf{b} = \sqrt{\sum_{i=1}^m \mathbf{a}[i]^2} \times \sqrt{\sum_{i=1}^m \mathbf{b}[i]^2} \times \cos(\theta) \quad (5.13)$$

We can rearrange Equation (5.13)^[216] to calculate the cosine of the inner angle between two vectors as the normalized dot product

$$\frac{\mathbf{a} \cdot \mathbf{b}}{\sqrt{\sum_{i=1}^m \mathbf{a}[i]^2} \times \sqrt{\sum_{i=1}^m \mathbf{b}[i]^2}} = \cos(\theta) \quad (5.14)$$

So, in an m -dimensional feature space, the cosine similarity between two instances **a** and **b** is defined as

$$\begin{aligned} sim_{COSINE}(\mathbf{a}, \mathbf{b}) &= \frac{\mathbf{a} \cdot \mathbf{b}}{\sqrt{\sum_{i=1}^m \mathbf{a}[i]^2} \times \sqrt{\sum_{i=1}^m \mathbf{b}[i]^2}} \\ &= \frac{\sum_{i=1}^m (\mathbf{a}[i] \times \mathbf{b}[i])}{\sqrt{\sum_{i=1}^m \mathbf{a}[i]^2} \times \sqrt{\sum_{i=1}^m \mathbf{b}[i]^2}} \end{aligned} \quad (5.15)$$

The cosine similarity between instances will be in the range [0,1], where 1 indicates maximum similarity and 0 indicates maximum dissimilarity.²⁰ We can calculate the cosine similarity between \mathbf{d}_1 and \mathbf{d}_2 from Figure 5.14(a)^[218] as

$$\begin{aligned} sim_{COSINE}(\mathbf{d}_1, \mathbf{d}_1) &= \frac{(97 \times 181) + (21 \times 184)}{\sqrt{97^2 + 21^2} \times \sqrt{181^2 + 184^2}} \\ &= 0.8362 \end{aligned}$$

[Figure 5.14\(b\)](#)^[218] highlights the normalization of descriptive feature values that takes place as part of calculating cosine similarity. This is different from the normalization we have looked at elsewhere in this chapter as it takes place within an instance rather than across all the values of a feature. All instances are normalized so as to lie on a **hypersphere** of radius 1.0 with its center at the origin of the feature space. This normalization is what makes cosine similarity so useful in scenarios in which we are interested in the relative spread of values across a set of descriptive features rather than the magnitudes of the values themselves. For example, if we have a third instance with SMS = 194 and VOICE = 42, the cosine similarity between this instance and \mathbf{d}_1 will be 1.0, because even though the magnitudes of their feature values are different, the relationship between the feature values for both instances is the same: both customers use about four times as many SMS messages as VOICE calls. Cosine similarity is also an appropriate similarity index for sparse data with non-binary features (i.e., datasets with lots of zero values) because the dot product will essentially ignore co-absences in its computation ($0 \times 0 = 0$).

5.4.5.3 Mahalanobis distance The final measure of similarity that we will introduce is the **Mahalanobis distance**, which is a metric that can be used to measure the similarity between instances with continuous descriptive features. The Mahalanobis distance is different from the other distance metrics we have looked at because it allows us to take into account how spread out the instances in a dataset are when judging similarities. [Figure 5.15](#)^[219] illustrates why this is important. This figure shows scatter plots for three bivariate datasets that have the same central tendency, marked A and located in the feature space at (50,50), but whose instances are spread out differently across the feature space. In all three cases the question we would like to answer is, are instance B, located at (30,70), and instance C, located at (70,70), likely to be from the same population from which the dataset has been sampled? In all three figures, B and C are equidistant from A based on Euclidean distance.

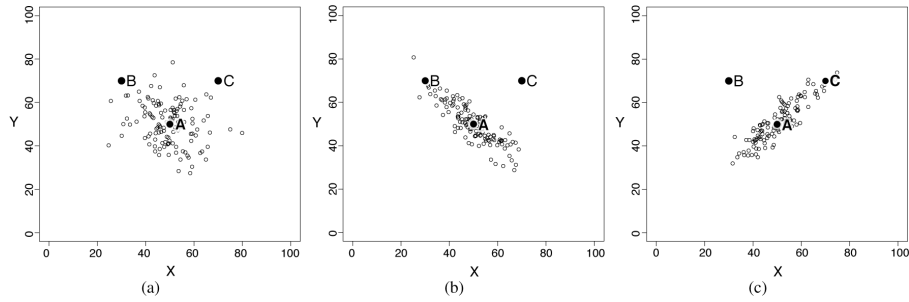


Figure 5.15

Scatter plots of three bivariate datasets with the same center point A and two queries B and C both equidistant from A ; (a) a dataset uniformly spread around the center point; (b) a dataset with negative covariance; and (c) a dataset with positive covariance.

The dataset in Figure 5.15(a)^[219] is equally distributed in all directions around A , and as a result, we can say that B and C are equally likely to be from the same population as the dataset. The dataset in Figure 5.15(b)^[219], however, demonstrates a strong negative **covariance**²¹ between the features. In this context, instance B is much more likely to be a member of the dataset than instance C . Figure 5.15(c)^[219] shows a dataset with a strong positive covariance, and for this dataset, instance C is much more likely to be a member than instance B . What these examples demonstrate is that when we are trying to decide whether a query belongs to a group, we need to consider not only the central tendency of the group, but also how spread out the members in a group are. These examples also highlight that covariance is one way of measuring the spread of a dataset.

The Mahalanobis distance uses covariance to scale distances so that distances along a direction where the dataset is very spread out are scaled down, and distances along directions where the dataset is tightly packed are scaled up. For example, in Figure 5.15(b)^[219] the Mahalanobis distance between B and A will be less than the Mahalanobis distance between C and A , whereas in Figure 5.15(c)^[219] the opposite will be true. The Mahalanobis distance is defined as

$$Mahalanobis(\mathbf{a}, \mathbf{b}) = \sqrt{\left[\mathbf{a}[1] - \mathbf{b}[1], \dots, \mathbf{a}[m] - \mathbf{b}[m] \right] \times \sum^{-1} \times \begin{bmatrix} \mathbf{a}[1] - \mathbf{b}[1] \\ \vdots \\ \mathbf{a}[m] - \mathbf{b}[m] \end{bmatrix}} \quad (5.16)$$

Let's step through Equation (5.16)^[219] bit by bit. First, this equation computes a distance between two instances \mathbf{a} and \mathbf{b} , each with m descriptive features. The first big term we come to in the equation is $[\mathbf{a}[1] - \mathbf{b}[1], \dots, \mathbf{a}[m] - \mathbf{b}[m]]$. This is a row vector that is created by subtracting each descriptive feature value of instance \mathbf{b} from the corresponding feature values of \mathbf{a} . The next term in the equation, Σ^{-1} , represents the **inverse covariance matrix**²² computed across all instances in the dataset. Multiplying the difference in feature values by the inverse covariance matrix has two effects. First, the larger the **variance** of a feature, the less weight the difference between the values for that feature will contribute to the distance calculation. Second, the larger the correlation between two features, the less weight they contribute to the distance. The final element of the equation is a column vector that is created in the same way as the row vector at the beginning of the equation—by subtracting each feature value from \mathbf{b} from the corresponding feature value from \mathbf{a} . The motivation for using a row vector to hold one copy of the feature differences and a column vector to hold the second copy of the features differences is to facilitate matrix multiplication. Now that we know that the row and column vector both contain the difference between the feature values of the two instances, it should be clear that, similar to Euclidean distance, the Mahalanobis distance squares the differences of the features. The Mahalanobis distance, however, also rescales the differences between feature values (using the inverse covariance matrix) so that all the features have unit variance, and the effects of covariance are removed.

The Mahalanobis distance can be understood as defining an orthonormal coordinate system with (1) an origin at the instance we are calculating the distance from (\mathbf{a} in Equation (5.16)^[219]); (2) a primary axis aligned with the direction of the greatest spread in the dataset; and (3) the units of all the axes scaled so that the dataset has unit variance along each axis. The rotation and scaling of the axes are the result of the multiplication by the inverse covariance matrix of the dataset (Σ^{-1}). So, if the inverse covariance matrix is the identity matrix \mathbb{I} , then no scaling or rotation occurs. This is why for datasets such as the one depicted in [Figure 5.15\(a\)](#)^[219], where there is no covariance between the features, the Mahalanobis distance is simply the Euclidean distance.²³

[Figure 5.16](#)^[221] illustrates how the Mahalanobis distance defines this coordinate system, which is translated, rotated, and scaled with respect to the standard coordinates of a feature space. The three scatter plots in this image are of the dataset in [Figure 5.15\(c\)](#)^[219]. In each case we have overlaid the coordinate system defined by the Mahalanobis distance from a different origin. The origins used for the figures were (a) (50,50), (b) (63,71), and (c) (42,35). The dashed lines plot the axes of the coordinate system, and the ellipses plot the 1, 3, and 5 unit distance contours. Notice how the orientation of the axes and the scaling of the distance contours are consistent across the figures. This is because the same inverse covariance matrix based on the entire dataset was used in each case.

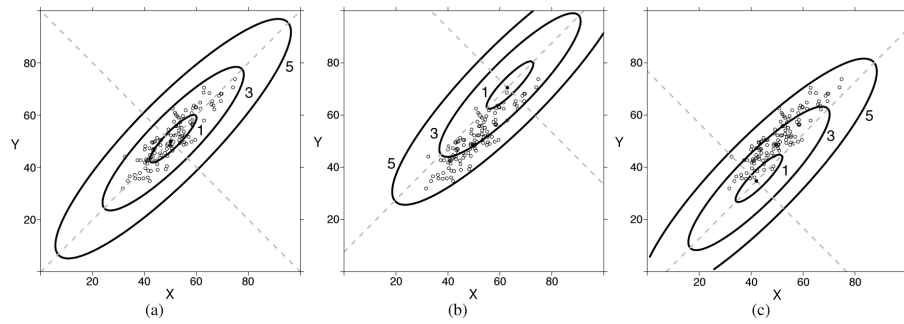


Figure 5.16

The coordinate systems defined by the Mahalanobis distance using the covariance matrix for the dataset in [Figure 5.15\(c\)](#)^[219] using three different origins: (a) (50,50); (b) (63,71); and (c) (42,35). The ellipses in each figure plot the 1, 3, and 5 unit distance contours.

Let's return to the original question depicted in [Figure 5.15](#)^[219]: Are B and C likely to be from the same population from which the dataset has been sampled? Focusing on [Figure 5.15\(c\)](#)^[219], for this dataset it appears reasonable to conclude that instance C is a member of the dataset but that B is probably not. To confirm this intuition we can calculate the Mahalanobis distance between A and B and A and C using Equation (5.16)^[219] as

$$Mahalanobis(A, B)$$

$$= \sqrt{[50 - 30, 50 - 70] \times \begin{bmatrix} 0.059 & -0.521 \\ -0.521 & 0.0578 \end{bmatrix} \times \begin{bmatrix} 50 - 30 \\ 50 - 70 \end{bmatrix}}$$

$$= 9.4049$$

$$Mahalanobis(A, C)$$

$$= \sqrt{[50 - 70, 50 - 70] \times \begin{bmatrix} 0.059 & -0.521 \\ -0.521 & 0.0578 \end{bmatrix} \times \begin{bmatrix} 50 - 70 \\ 50 - 70 \end{bmatrix}}$$

$$= 2.2540$$

where the inverse covariance matrix used in the calculations is based on the covariance matrix²⁴ calculated directly from the dataset:

$$\begin{bmatrix} 82.39 & 74.26 \\ 74.26 & 84.22 \end{bmatrix}$$

[Figure 5.17](#)^[222] shows a contour plot of these Mahalanobis distances. In this figure, A indicates the central tendency of the dataset in [Figure 5.15\(c\)](#)^[219], and the ellipses plot the Mahalanobis distance contours that the distances from A to the instances B and C lie on. These distance contours were calculated using the inverse covariance matrix for the dataset and point A as the origin. The result is that instance C is much closer to A than B and so should be considered a member of the same population as this dataset.

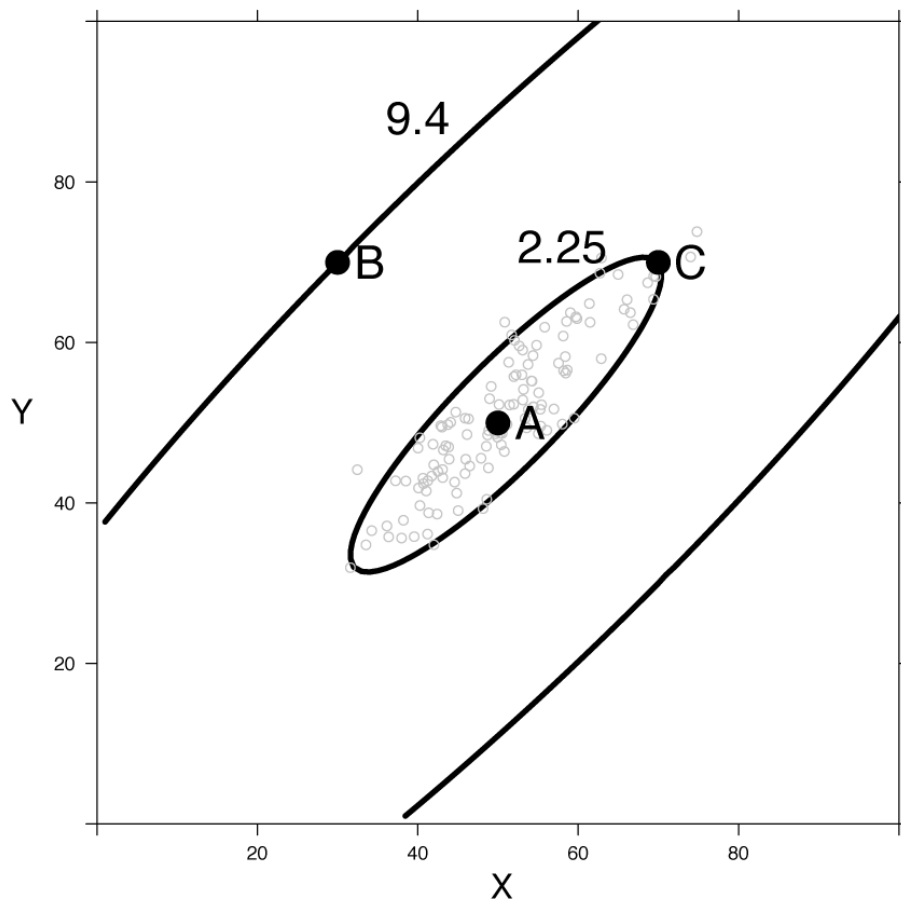


Figure 5.17

The effect of using a Mahalanobis versus Euclidean distance. A marks the central tendency of the dataset in [Figure 5.15\(c\)](#)^[219]. The ellipses plot the Mahalanobis distance contours from A that B and C lie on. In Euclidean terms, B and C are equidistant from A ; however, using the Mahalanobis distance, C is much closer to A than B .

To use Mahalanobis distance in a nearest neighbor model, we simply use the model in exactly the same way as described previously but substitute Mahalanobis distance for Euclidean distance.

5.4.5.4 Summary In this section we have introduced a number of commonly used metrics and indexes for judging similarity between instances in a feature space. These are typically used in situations where a Minkowski distance is not appropriate. For example, if we are dealing with binary features, it may be more appropriate to use the Russel-Rao, Sokal-Michener, or Jaccard similarity metric. Or it may be that the features in the dataset are continuous—typically indicating that a Minkowski distance metric is appropriate—but that the majority of the descriptive features for

each instance have zero values²⁵ in which case we may want to use a similarity index that ignores descriptive features with zero values in both features, for example, **cosine similarity**. Alternatively, we may be dealing with a dataset where there is covariance between the descriptive features, in which case we should consider using the **Mahalanobis distance** as our measure of similarity. There are many other indexes and metrics we could have presented, for example, **Tanimoto similarity** (which is a generalization of the Jaccard similarity to non-binary data), and **correlation-based** approaches such as the **Pearson correlation**. The key things to remember, however, are that it is important to choose a similarity metric or index that is appropriate for the properties of the dataset we are using (be it binary, non-binary, sparse, covariant, etc.) and second, experimentation is always required to determine which measure of similarity will be most effective for a specific prediction model.

5.4.6 Feature Selection

Intuitively, adding more descriptive features to a dataset provides more information about each instance and should result in more accurate predictive models. Surprisingly, however, as the number of descriptive features in a dataset increases, there often comes a point at which continuing to add new features to the dataset results in a decrease in the predictive power of the induced models. The reason for this phenomenon is that, fundamentally, the predictive power of an induced model is based on one of the following:

1. Partitioning the feature space into regions based on clusters of training instances with the same target value, and assigning a query located in a region the target value of the cluster that defines that region.
2. Assigning a query a target value interpolated (for instance, by majority vote or average) from the target values of individual training instances that are near the query in the feature space.

Both of these strategies depend on a reasonable **sampling density** of the training instances across the feature space. The sampling density is the average density of training instances across the feature space. If the sampling density is too low, then large regions of the feature space do not contain any training instances, and it doesn't make sense to associate such a

region with any cluster of training instances or to look for training instances that are nearby. In such instances a model is essentially reduced to guessing predictions. We can measure the **sampling density** across a feature space in terms of the average density of a **unit hypercube**²⁶ in the feature space. The density of a unit hypercube is equal to

$$\text{density} = k^{\left(\frac{1}{m}\right)} \quad (5.17)$$

where k is the number of instances inside the hypercube, and m is the number of dimensions of the feature space.

[Figure 5.18](#)^[226] provides a graphical insight into the relationship between the number of descriptive features in a dataset and the sampling density of the feature space. [Figure 5.18\(a\)](#)^[226] plots a one-dimensional dataset consisting of 29 instances spread evenly between 0.0 and 3.0. We have marked the unit hypercube covering the interval 0 to 1 in this figure. The density of this unit hypercube is $10^{\frac{1}{1}} = 10$ (there are 10 instances inside the hypercube). If we increase the number of descriptive features, the dimensionality of the feature space increases. [Figures 5.18\(b\)](#)^[226] and [5.18\(c\)](#)^[226] illustrate what happens if we increase the number of descriptive features in a dataset but do not increase the number of instances. In [Figure 5.18\(b\)](#)^[226] we have added a second descriptive feature, Y, and assigned each of the instances in the dataset a random Y value in the range [0.0,3.0]. The instances have moved away from each other, and the sampling density has decreased. The density of the marked unit hypercube is now $4^{\frac{1}{2}} = 2$ (there are only 4 instances inside the hypercube). [Figure 5.18\(c\)](#)^[226] illustrates the distribution of the original 29 instances when we move to a three-dimensional feature space (each instance has been given a random value in the range [0.0,3.0] for the Z feature). It is evident that the instances are getting farther and farther away from each other, and the feature space is becoming very sparsely populated, with relatively large areas where there are no or very few instances. This is reflected in a further decrease in the sampling density. The density of the marked hypercube is $2^{\frac{1}{3}} = 1.2599$.

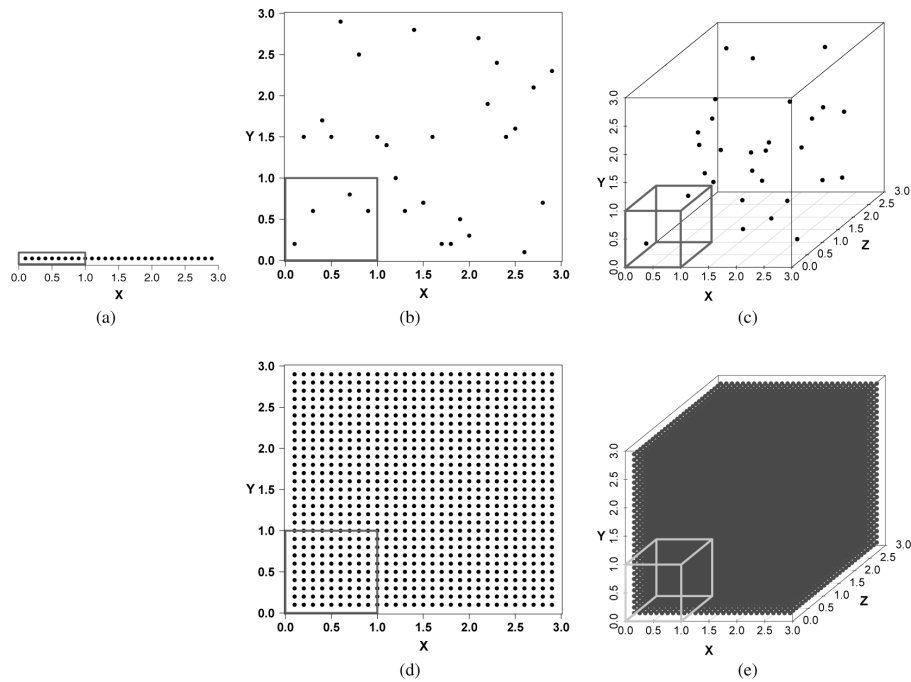


Figure 5.18

A set of scatter plots illustrating the curse of dimensionality. Across (a), (b), and (c), the number of instances remains the same, so the density of the marked unit hypercubes decreases as the number of dimensions increases; (d) and (e) illustrate the cost we must incur, in terms of the number of extra instances required, if we wish to maintain the density of the instances in the feature space as its dimensionality increases.

Figures 5.18(d)^[226] and 5.18(e)^[226] illustrate the cost we would have to incur in extra instances if we wished to maintain the sampling density in the dataset in line with each increase in the dimensionality of the feature space. In the two-dimensional feature space in Figure 5.18(d)^[226], we have maintained the sampling density (the density of the marked unit hypercube is $100^{\frac{1}{2}} = 10$) at the expense of a very large increase in the number of instances—there are $29 \times 29 = 841$ instances plotted in this figure. This is quite a dramatic increase; however, it gets even more dramatic when we increase from two to three descriptive features. In Figure 5.18(e)^[226] we have, again, maintained the sampling density (the density of the marked unit hypercube is $1000^{\frac{1}{3}} = 10$) at the expense of a very large increase in the number of instances—there are $29 \times 29 \times 29 = 24,389$ instances in this figure!

So, in order to maintain the sampling density of the feature space as the number of descriptive features increases, we need to dramatically, indeed, exponentially, increase the number of instances. If we do not do this, then

as we continue to increase the dimensionality of the feature space, the instances will continue to spread out until we reach a point in a high-dimensional feature space where most of the feature space is empty. When this happens, most of the queries will be in locations where none of the training instances are nearby, and as a result, the predictive power of the models based on these training instances will begin to decrease. This trade-off between the number of descriptive features and the density of the instances in the feature space is known as the **curse of dimensionality**.

Typically, we are not able to increase the number of instances in our dataset, and we face the scenario of a sparsely populated feature space,²⁷ as illustrated in Figures 5.18(b)^[226] and 5.18(c)^[226]. Fortunately, several features of real data can help us to induce reasonable models in high-dimensional feature spaces.²⁸ First, although real data does spread out, it doesn't spread out quite as randomly and quickly as we have illustrated here. Real instances tend to cluster. The net effect of this is that the distribution of real data tends to have a lower effective dimensionality than the dimensionality of the feature space. Second, within any small region or neighborhood of the feature space, real data tends to manifest a smooth correlation between changes in descriptive feature values and the values of the target feature. In other words, small changes in descriptive features result in small changes in the target feature. This means that we can generate good predictions for queries by interpolating from nearby instances with known target values.

Another factor that can help us deal with the curse of dimensionality is that some learning algorithms have a natural resistance to the problem. For example, the decision tree learning algorithms we looked at in the last chapter worked by selecting subsets of features from which to build predictive trees and so naturally reduce dimensionality. Even these algorithms, however, do eventually succumb to the curse as the dimensionality grows. Other algorithms, such as the nearest neighbor algorithm, which use all the descriptive features when making a prediction, are particularly sensitive to the curse. The moral here is that the curse of dimensionality is a problem for all inductive learning approaches, and given that acquiring new labeled instances is typically not an option, the best way to avoid it is to restrict the number of descriptive features in a dataset to the smallest set possible, while still providing the learning algorithm with

enough information about the instances to be able to build a useful model. This is difficult, however, because when we design descriptive features, we tend not to know exactly which ones will be predictive and which ones will not.

Fortunately, we can use **feature selection**²⁹ to help reduce the number of descriptive features in a dataset to just the subset that is most useful. Before we begin our discussion of approaches to feature selection, it is useful to distinguish between different types of descriptive features.

- **Predictive:** a predictive descriptive feature provides information that is useful in estimating the correct value of a target feature.
- **Interacting:** by itself, an interacting descriptive feature is not informative about the value of the target feature. In conjunction with one or more other features, however, it becomes informative.
- **Redundant:** a descriptive feature is redundant if it has a strong correlation with another descriptive feature.
- **Irrelevant:** an irrelevant descriptive feature does not provide information that is useful in estimating the value of the target feature.

The goal of any feature selection approach is to identify the smallest subset of descriptive features that maintains overall model performance. Ideally, a feature selection approach will return the subset of features that includes the predictive and interacting features while excluding the irrelevant and redundant features.

The most popular and straightforward approach to feature selection is to **rank and prune**. In this approach the features are ranked using a measure of their predictiveness, and any feature outside the top $X\%$ of the features in the list is pruned. The measures of predictiveness are called **filters** because they are used to filter apparently irrelevant features before learning occurs. Technically, a filter can be defined as a heuristic rule that assesses the predictiveness of a feature using only the intrinsic properties of the data, independently of the learning algorithm that will use the features to induce the model. For example, we can use **information gain**³⁰ as a filter in a rank and prune approach.

Although rank and prune approaches using filters are computationally efficient, they suffer from the fact that the predictiveness of each feature is evaluated in isolation from the other features in the dataset. This leads to

the undesirable result that ranking and pruning can exclude interacting features and include redundant features.

To find the ideal subset of descriptive features to use to train a model, we could attempt to build a model using every possible subset, evaluate the performance of all these models, and select the feature subset that leads to the best model. This is unfeasible, however, as for d features, there are 2^d different possible feature subsets, which is far too many to evaluate unless d is very small. For example, with just 20 descriptive features, there are $2^{20} = 1,048,576$ possible feature subsets. Instead, feature selection algorithms often frame feature selection as a **greedy local search problem**, where each state in the search space specifies a subset of possible features. For example, [Figure 5.19^{\[228\]}](#) illustrates a **feature subset space** for a dataset with three descriptive features: X, Y, and Z. In this figure each rectangle represents a state in the search space that is a particular feature subset. For instance, the rectangle on the very left represents the feature subset that includes no features at all, and the rectangle at the top of the second column from the left represents the feature subset including just the feature X. Each state is connected to all the other states that can be generated by adding or removing a single feature from that state. A greedy local search process moves across a feature subset space like this search in order to find the best feature subset.

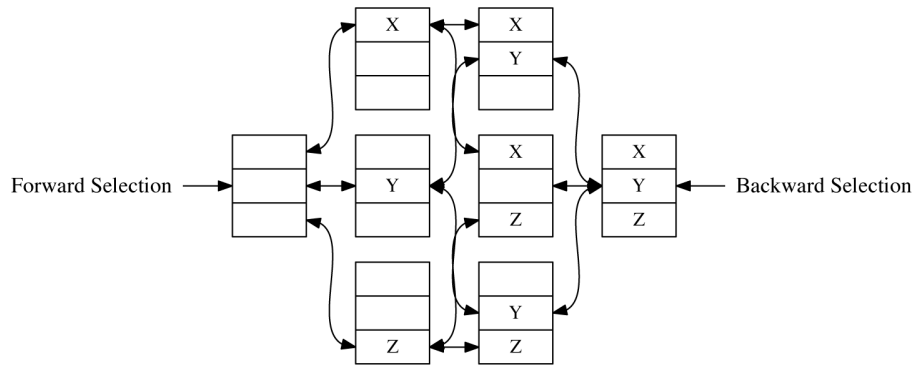


Figure 5.19

Feature subset space for a dataset with three features X, Y, and Z.

When framed as a greedy local search problem, feature selection is defined in terms of an iterative process consisting of the following components:

1. **Subset Generation:** This component generates a set of candidate feature subsets that are successors of the current best feature subset.
2. **Subset Selection:** This component selects the feature subset from the set of candidate feature subsets generated by the subset generation component that is the most desirable for the search process to move to. One way to do this (similar to the ranking and pruning approach described previously) is to use a filter to evaluate the predictiveness of each candidate set of features and select the most predictive one. A more common approach is to use a **wrapper**. A wrapper evaluates a feature subset in terms of the potential performance of the models that can be induced using that subset. This involves performing an evaluation experiment³¹ for each candidate feature subset, in which a model is induced using only the features in the subset, and its performance is evaluated. The candidate feature subset that leads to the best-performing model is then selected. Wrapper approaches are more computationally expensive than filters, as they involve training multiple models during each iteration. The argument for using a wrapper approach is that to get the best predictive accuracy, the inductive bias of the particular machine learning algorithm that will be used should be taken into consideration during feature selection. That said, filter approaches are faster and often result in models with good accuracy.
3. **Termination Condition:** This component determines when the search process should stop. Typically we stop when the subset selection component indicates that none of the feature subsets (search states) that can be generated from the current feature subset is more desirable than the current subset. Once the search process is terminated, the features in the dataset that are not members of the selected feature subset are pruned from the dataset before the prediction model is induced.

Forward sequential selection is a commonly used implementation of the greedy local search approach to feature selection. In forward sequential selection, the search starts in a state with no features (shown on the left of [Figure 5.19](#)^[228]). In the subset generation component of forward sequential selection, the successors of the current best feature subset are the set of

feature subsets that can be generated from the current best subset by adding just a single extra feature. For example, after beginning with the feature subset including no features, the forward sequential search process generates three feature subsets, each containing just one of X, Y, or Z (shown in the second column of [Figure 5.19](#)^[228]). The subset selection component in forward sequential selection can use any of the approaches described above and moves the search process to a new feature subset. For example, after starting with the feature subset including no features, the process will move to the most desirable of the feature subsets containing just one feature. Forward sequential selection terminates when no accessible feature subset is better than the current subset.

Backward sequential selection is a popular alternative to forward sequential selection. In backward sequential selection, we start with a feature subset including all the possible features in a dataset (shown on the right of [Figure 5.19](#)^[228]). The successors of the current best feature subset generated in backward sequential selection are the set of feature subsets that can be generated from the current best subset by removing just a single extra feature. Backward sequential selection terminates when no accessible feature subset is better than or as good as the current subset.

Neither forward nor backward sequential selection consider the effect of adding or removing combinations of features, and as a result, they aren't guaranteed to find the absolute optimal subset of features. So which approach should we use? Forward sequential selection is a good approach if we expect lots of irrelevant features in the dataset, because typically it results in a lower overall computational cost for feature selection due to the fact that on average it generates smaller feature subsets. This efficiency gain, however, is at the cost of the likely exclusion of interacting features. Backward sequential selection has the advantage that it allows for the inclusion of sets of interacting features that individually may not be predictive (because all features are included at the beginning), with the extra computational cost of evaluating larger feature subsets. So if model performance is more important than computational considerations, backward sequential selection may be the better option; otherwise use forward sequential selection.

[Figure 5.20](#)^[230] illustrates how filter selection fits into the model induction process. It is important to remember that feature selection can be

used in conjunction with almost any machine learning algorithm, not just similarity-based approaches. Feature selection is appropriate when there are large numbers of features, so we do not present a worked example here. We do, however, discuss the application of feature selection in the case study in Chapter 13^[703].

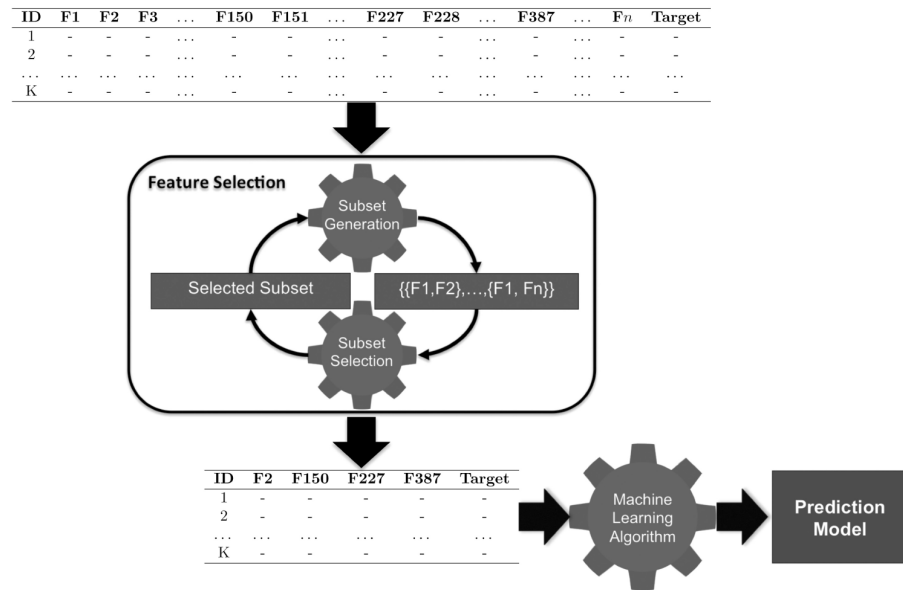


Figure 5.20

The process of model induction with feature selection.

5.5 Summary

Similarity-based prediction models attempt to mimic a very human way of reasoning by basing predictions for a target feature value on the most similar instances in memory. The fact that similarity-based models attempt to mimic a way of reasoning that is natural to humans makes them easy to interpret and understand. This advantage should not be underestimated. In a business context where people are using models to inform decision making, being able to understand how the model works gives people more confidence in the model and, hence, in the insight that it provides.

The standard approach to implementing a similarity-based prediction model is the **nearest neighbor algorithm**. This algorithm is built on two fundamental concepts: (1) a **feature space**, and (2) measures of similarity between instances within the feature space. In this chapter we presented a range of measures of similarity, including **distance metrics** (such as the

Euclidean, **Manhattan**, and **Mahalanobis**) and **similarity indexes** (such as the **Russel-Rao**, **Sokal-Michener**, **Jaccard**, and **Cosine**). Each of these measures is suitable for different types of data, and matching the appropriate measure to the data is an important step in inducing an accurate similarity-based prediction model.

A point that we didn't discuss in this chapter is that it is possible to create custom measures for datasets with both continuous and categorical descriptive features by combining measures. For example, we might use a Euclidean distance metric to handle the continuous features in a dataset and the Jaccard similarity index to handle the categorical features. The overall measure of similarity could then be based on a weighted combination of the two. By combining measures in this way, we can apply nearest neighbor models to any dataset.

Custom metrics aside, the standard distance metrics and similarity indexes weight all features equally. Consequently, the predictions made by a nearest neighbor model are based on the full set of descriptive features in a dataset. This is not true of all prediction models. For example, the predictions made by decision tree models are based on the subset of descriptive features tested on the path from the root of the tree to the leaf node that specifies the prediction. The fact that nearest neighbor models use the full set of descriptive features when making a prediction makes them particularly sensitive to the occurrence of missing descriptive feature values. In Section 3.4^[69] we introduced a number of techniques for handling **missing values**, and particular care should be taken to handle missing values if a nearest neighbor model is being used. The same is true for large range variations across the descriptive features in a dataset and **normalization** techniques (like those described in Section 3.6.1^[87]) should almost always be applied when nearest neighbor models are used.

Nearest neighbor models are essentially a composition of a set of local models (recall our discussion on **Voronoi tessellation**) with the predictions made being a function of the target feature value of the instance in the dataset closest to the query. As a result, these models are very sensitive to noise in the target feature. The easiest way to solve this problem is to employ a **k nearest neighbor** model, which uses a function of the target feature values of the k closest instances to a query. Care must be taken,

however, when selecting the parameter k , particularly when working with imbalanced datasets.

Nearest neighbor models are also sensitive to the presence of redundant and irrelevant descriptive features in training data. Consequently, **feature selection** is a particularly important process for nearest neighbor algorithms. Feature selection excludes redundant and irrelevant features from the induction process and by doing so alleviates the **curse of dimensionality**. The fact that we have emphasized feature selection in this chapter does not mean that it is not important to predictive analytics in general. The issue with redundant and irrelevant features is inherent in any large dataset, and the feature selection techniques described in this chapter are generally applicable when any type of machine learning algorithm is being used.

Finally, the nearest neighbor algorithm is what is known as a **lazy learner**. This contrasts with **eager learners**, such as the information-based (Chapter 4^[117]), probability-based (Chapter 6^[243]), and error-based (Chapter 7^[311]) approaches to machine learning described in other chapters in this book. The distinction between easy learners and lazy learners is based on when the algorithm abstracts from the data. The nearest neighbor algorithm delays abstracting from the data until it is asked to make a prediction. At this point the information in the query is used to define a neighborhood in the feature space, and a prediction is made based on the instances in this neighborhood. Eager learners abstract away from the data during training and use this abstraction to make predictions, rather than directly comparing queries with instances in the dataset. The decision trees described in Chapter 4^[117] are an example of this type of abstraction. One consequence of abstracting away from the training data is that models induced using an eager learning algorithm are typically faster at making predictions than models based on a lazy learner. In the case of a nearest neighbor algorithm, as the number of instances becomes large, the model will become slower because it has more instances to check when defining the neighborhood. Techniques such as the **k -d tree** can help with this issue by creating a fast index at the cost of some preprocessing. This means that a nearest neighbor model may not be appropriate in domains where speed of prediction is of the essence.

An advantage of the lazy learning strategy, however, is that similarity-based machine learning approaches are robust to concept drift. **Concept drift** is a phenomenon that occurs when the relationship between the target feature and the descriptive features changes over time. For example, the characteristics of spam emails change both cyclically through the year (typical spam emails at Christmastime are different from typical spam at other times of the year) and also longitudinally (spam in 2014 is very different from spam in 1994). If a prediction task is affected by concept drift, an eager learner may not be appropriate because the abstraction induced during training will go out of date, and the model will need to be retrained at regular intervals, a costly exercise. A nearest neighbor algorithm can be updated without retraining. Each time a prediction is made, the query instance can be added into the dataset and used in subsequent predictions.³² In this way, a nearest neighbor model can be easily updated, which makes it relatively robust to concept drift (we will return to concept drift in Section 9.4.6^[578]).

To conclude, the weaknesses of similarity-based learning approaches are that they are sensitive to the curse of dimensionality, they are slower than other models at making predictions (particularly with very large datasets), and they may not be able to achieve the same levels of accuracy as other learning approaches. The strengths of these models, however, are that they are easy to interpret, they can handle different types of descriptive features, they are relatively robust to noise (when k is set appropriately), and they may be more robust to concept drift than models induced by eager learning algorithms.

5.6 Further Reading

Nearest neighbor models are based on the concepts of a feature space and measures of similarity within this feature space. We have claimed that this is a very natural way for humans to think, and indeed, there is evidence from cognitive science to support a geometric basis to human thought (Gädenfors, 2004). Gädénfors (2004) also provides an excellent introduction and overview of distance metrics.

Chapter 13 of Hastie et al. (2009) gives an introduction to the statistical theory underpinning nearest neighbor models. The measure used to judge similarity is a key element in a nearest neighbor model. In this chapter, we

have described a number of different distance metrics and similarity indexes. Cunningham (2009) provides a broader introduction to the range of metrics and indexes that are available.

Efficiently indexing and accessing memory is an important consideration in scaling nearest neighbor models to large datasets. In this chapter we have shown how *k-d* trees (Bentley, 1975; Friedman et al., 1977) can be used to speed up the retrieval of nearest neighbors. There are, however, alternatives to *k-d* trees. Samet (1990) gives an introduction to **r-trees** and other related approaches. More recently, hash-based indexes, such as **locality sensitive hashing**, have been developed. Andoni and Indyk (2006) provide a survey of these hash-based approaches. Another approach to scaling nearest neighbor models is to remove redundant or noisy instances from the dataset in which we search for neighbors. For example, the **condensed nearest neighbor** approach (Hart, 1968) was one of the earliest attempts at this and removes the instances not near target level boundaries in a feature space, as they are not required to make predictions. More recent attempts to do this include Segata et al. (2009) and Smyth and Keane (1995).

Nearest neighbor models are often used in text analytics applications. Daelemans and van den Bosch (2005) discuss why nearest neighbor models are so suitable for text analytics. Widdows (2004) provides a very readable and interesting introduction to geometry and linguistic meaning; see, in particular, Chapter 4 for an excellent introduction to similarity and distance. For a more general textbook on **natural language processing**, we recommend Jurafsky and Martin (2008). Finally, nearest neighbor models are the basis of **case-based reasoning (CBR)**, which is an umbrella term for applications based on similarity-based machine learning. Richter and Weber (2013) is a good introduction, and overview, to CBR.

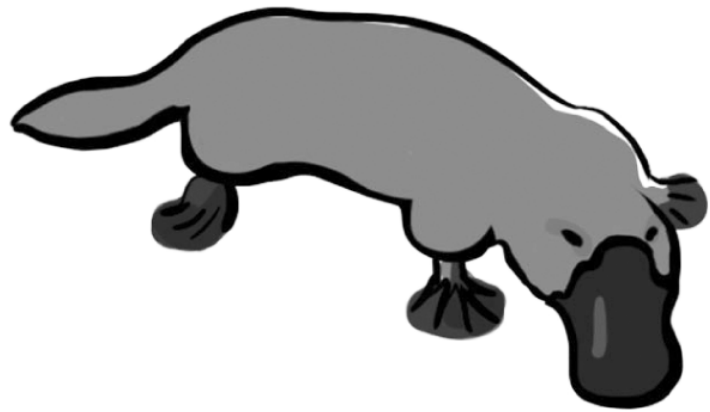


Figure 5.21

A duck-billed platypus. This platypus image was created by Jan Gillbank, English for the Australian Curriculum website (www.e4ac.edu.au). Used under Creative Commons Attribution 3.0 license.

5.7 Epilogue

Returning to 1798 and HMS *Calcutta*, the next day you accompany your men on the expedition up the river, and you encounter the strange animal the sailor had described to you. This time when you see the animal yourself, you realize that it definitely isn't a duck! It turns out that you and your men are the first Europeans to encounter a platypus.³³

This epilogue illustrates two important, and related, aspects of supervised machine learning. First, supervised machine learning is based on the **stationarity assumption**, which states that the data doesn't change—it remains stationary—over time. One implication of this assumption is that supervised machine learning assumes that new target levels—such as previously unknown animals—don't suddenly appear in the data from which queries that are input to the model are sampled. Second, in the context of predicting categorical targets, supervised machine learning creates models that distinguish between the target levels that are present in the dataset from which they are induced. So if a prediction model is trained to distinguish between lions, frogs, and ducks, the model will classify every query instance as being either a lion, a frog, or a duck—even if the query is actually a platypus.

Creating models that can identify queries as being sufficiently different from what was in a training dataset so as to be considered a new type of entity is a difficult research problem. Some of the areas of research relevant to this problem include **outlier detection** and **one-class classification**.

5.8 Exercises

1. The table below lists a dataset that was used to create a nearest neighbor model that predicts whether it will be a good day to go surfing.

ID	WAVE SIZE (FT)	WAVE PERIOD (SECS)	WIND SPEED (MPH)	GOOD SURF
1	6	15	5	yes
2	1	6	9	no
3	7	10	4	yes
4	7	12	3	yes
5	2	2	10	no
6	10	2	20	no

Assuming that the model uses Euclidean distance to find the nearest neighbor, what prediction will the model return for each of the following query instances?

ID	WAVE SIZE (FT)	WAVE PERIOD (SECS)	WIND SPEED (MPH)	GOOD SURF
Q1	8	15	2	?
Q2	8	2	18	?
Q3	6	11	4	?

2. Email spam filtering models often use a **bag-of-words** representation for emails. In a bag-of-words representation, the descriptive features that describe a document (in our case, an email) each represent how many times a particular word occurs in the document. One descriptive feature is included for each word in a predefined dictionary. The dictionary is typically defined as the complete set of words that occur in the training dataset. The table below lists the bag-of-words representation for the following five emails and a target feature, SPAM, whether they are spam emails or genuine emails:

- “*money, money, money*”
- “*free money for free gambling fun*”
- “*gambling for fun*”
- “*machine learning for fun, fun, fun*”
- “*free machine learning*”

ID	Bag-of-Words							SPAM
	MONEY	FREE	FOR	GAMBLING	FUN	MACHINE	LEARNING	
1	3	0	0	0	0	0	0	true
2	1	2	1	1	1	0	0	true
3	0	0	1	1	1	0	0	true
4	0	0	1	0	3	1	1	false
5	0	1	0	0	0	1	1	false

- (a) What target level would a nearest neighbor model using **Euclidean distance** return for the following email: “*machine learning for free*”?
- (b) What target level would a k -NN model with $k = 3$ and using **Euclidean distance** return for the same query?
- (c) What target level would a **weighted k -NN** model with $k = 5$ and using a weighting scheme of the reciprocal of the squared

Euclidean distance between the neighbor and the query, return for the query?

- (d) What target level would a k -NN model with $k = 3$ and using **Manhattan distance** return for the same query?
- (e) There are a lot of zero entries in the spam bag-of-words dataset. This is indicative of **sparse data** and is typical for text analytics. **Cosine similarity** is often a good choice when dealing with sparse non-binary data. What target level would a 3-NN model using cosine similarity return for the query?
3. The predictive task in this question is to predict the level of corruption in a country based on a range of macroeconomic and social features. The table below lists some countries described by the following descriptive features:
- LIFE EXP., the mean life expectancy at birth
 - TOP-10 INCOME, the percentage of the annual income of the country that goes to the top 10% of earners
 - INFANT MORT., the number of infant deaths per 1,000 births
 - MIL. SPEND, the percentage of GDP spent on the military
 - SCHOOL YEARS, the mean number years spent in school by adult females

The target feature is the **Corruption Perception Index** (CPI). The CPI measures the perceived levels of corruption in the public sector of countries and ranges from 0 (highly corrupt) to 100 (very clean).³⁴

COUNTRY ID	LIFE EXP.	TOP-10 INCOME	INFANT MORT.	MIL. SPEND	SCHOOL YEARS	CPI
Afghanistan	59.61	23.21	74.30	4.44	0.40	1.5171
Haiti	45.00	47.67	73.10	0.09	3.40	1.7999
Nigeria	51.30	38.23	82.60	1.07	4.10	2.4493
Egypt	70.48	26.58	19.60	1.86	5.30	2.8622
Argentina	75.77	32.30	13.30	0.76	10.10	2.9961
China	74.87	29.98	13.70	1.95	6.40	3.6356
Brazil	73.12	42.93	14.50	1.43	7.20	3.7741
Israel	81.30	28.80	3.60	6.77	12.50	5.8069
USA	78.51	29.85	6.30	4.72	13.70	7.1357
Ireland	80.15	27.23	3.50	0.60	11.50	7.5360
UK	80.09	28.49	4.40	2.59	13.00	7.7751
Germany	80.24	22.07	3.50	1.31	12.00	8.0461
Canada	80.99	24.79	4.90	1.42	14.20	8.6725
Australia	82.09	25.40	4.20	1.86	11.50	8.8442
Sweden	81.43	22.18	2.40	1.27	12.80	9.2985
New Zealand	80.67	27.81	4.90	1.13	12.30	9.4627

We will use Russia as our query country for this question. The table below lists the descriptive features for Russia.

COUNTRY ID	LIFE EXP.	TOP-10 INCOME	INFANT MORT.	MIL. SPEND	SCHOOL YEARS	CPI
Russia	67.62	31.68	10.00	3.87	12.90	?

- (a) What value would a 3-nearest neighbor prediction model using Euclidean distance return for the CPI of Russia?
- (b) What value would a **weighted k-NN** prediction model return for the CPI of Russia? Use $k = 16$ (i.e., the full dataset) and a weighting scheme of the reciprocal of the squared Euclidean distance between the neighbor and the query.
- (c) The descriptive features in this dataset are of different types. For example, some are percentages, others are measured in years, and others are measured in counts per 1,000. We should always consider normalizing our data, but it is particularly important to do this when the descriptive features are measured in different units. What value would a 3-nearest neighbor prediction model using Euclidean distance return for the CPI of Russia when the descriptive features have been normalized using range normalization?

- (d) What value would a **weighted k -NN** prediction model—with $k = 16$ (i.e., the full dataset) and using a weighting scheme of the reciprocal of the squared Euclidean distance between the neighbor and the query—return for the CPI of Russia when it is applied to the range-normalized data?
- (e) The actual 2011 CPI for Russia was 2.4488. Which of the predictions made was the most accurate? Why do you think this was?
- * 4. You have been given the job of building a recommender system for a large online shop that has a stock of over 100,000 items. In this domain the behavior of customers is captured in terms of what items they have bought or not bought. For example, the following table lists the behavior of two customers in this domain for a subset of the items that at least one of the customers has bought.

	ITEM ID	ITEM 107	ITEM 498	ITEM 7256	ITEM 28063	ITEM 75328
1	true	true	true	false	false	
2	true	false	false	true	true	

- (a) The company has decided to use a similarity-based model to implement the recommender system. Which of the following three similarity indexes do you think the system should be based on?

$$\text{Russell-Rao}(X, Y) = \frac{CP(X, Y)}{P}$$

$$\text{Sokal-Michener}(X, Y) = \frac{CP(X, Y) + CA(X, Y)}{P}$$

$$\text{Jaccard}(X, Y) = \frac{CP(X, Y)}{CP(X, Y) + PA(X, Y) + AP(X, Y)}$$

- (b) What items will the system recommend to the following customer? Assume that the recommender system uses the similarity index you chose in the first part of this question and is trained on the sample dataset listed above. Also assume that the system generates recommendations for query customers by finding the customer most similar to them in the dataset and then recommending the

items that this similar customer has bought but that the query customer has not bought.

	ITEM ID	ITEM 107	ITEM 498	ITEM 7256	ITEM 28063	ITEM 75328
Query	true	false	true	false	false	false

- * 5. You are working as an assistant biologist to Charles Darwin on the *Beagle* voyage. You are at the Galápagos Islands, and you have just discovered a new animal that has not yet been classified. Mr. Darwin has asked you to classify the animal using a nearest neighbor approach, and he has supplied you the following dataset of already classified animals.

ID	BIRTHS LIVE YOUNG	LAYS EGGS	FEEDS OFFSPRING OWN MILK	WARM-BLOODED	COLD-BLOODED	LAND AND WATER BASED	HAS HAIR	HAS FEATHERS	CLASS
1	true	false	true	true	false	false	true	false	mammal
2	false	true	false	false	true	true	false	false	amphibian
3	true	false	true	true	false	false	true	false	mammal
4	false	true	false	true	false	true	false	true	bird

The descriptive features of the mysterious newly discovered animal are as follows:

ID	BIRTHS LIVE YOUNG	LAYS EGGS	FEEDS OFFSPRING OWN MILK	WARM-BLOODED	COLD-BLOODED	LAND AND WATER BASED	HAS HAIR	HAS FEATHERS	CLASS
Query	false	true	false	false	false	true	false	false	?

- (a) A good measure of distance between two instances with categorical features is the **overlap metric** (also known as the **hamming distance**), which simply counts the number of descriptive features that have *different* values. Using this measure of distance, compute

the distances between the mystery animal and each of the animals in the animal dataset.

- (b) If you used a 1-NN model, what class would be assigned to the mystery animal?
 - (c) If you used a 4-NN model, what class would be assigned to the mystery animal? Would this be a good value for k for this dataset?
- * 6. You have been asked by a San Francisco property investment company to create a predictive model that will generate house price estimates for properties they are considering purchasing as rental properties. The table below lists a sample of properties that have recently been sold for rental in the city. The descriptive features in this dataset are SIZE (the property size in square feet) and RENT (the estimated monthly rental value of the property in dollars). The target feature, PRICE, lists the prices that these properties were sold for in dollars.

ID	SIZE	RENT	PRICE
1	2,700	9,235	2,000,000
2	1,315	1,800	820,000
3	1,050	1,250	800,000
4	2,200	7,000	1,750,000
5	1,800	3,800	1,450,500
6	1,900	4,000	1,500,500
7	960	800	720,000

- (a) Create a **k -d tree** for this dataset. Assume the following order over the features: RENT then SIZE.
 - (b) Using the k -d tree that you created in the first part of this question, find the nearest neighbor to the following query: SIZE = 1,000, RENT = 2,200.
- * 7. A data analyst building a k -nearest neighbor model for a continuous prediction problem is considering appropriate values to use for k .
- (a) Initially the analyst uses a simple average of the target variables for the k nearest neighbors in order to make a new prediction. After experimenting with values for k in the range 0–10, it occurs to the

analyst that they might get very good results if they set k to the total number of instances in the training set. Do you think that the analyst is likely to get good results using this value for k ?

- (b) If the analyst was using a distance weighted averaging function rather than a simple average for his or her predictions, would this have made the analyst's idea any more useful?
- * 8. The following table describes a set of individuals in terms of their WEIGHT in kilograms, HEIGHT in meters, and whether or not they have DIABETES:

ID	WEIGHT	HEIGHT	DIABETES
1	68	1.7	true
2	55	1.6	false
3	65	1.6	true
4	100	1.9	true
5	65	1.5	false

- (a) A doctor has carried out a regular checkup on a patient and measured the patient's WEIGHT to be 65 kilograms and their HEIGHT to be 1.7 meters. The doctor inputs these details into a k -NN classifier to check whether the patient is at risk of DIABETES. Assuming that $k = 1$, and that the model uses Euclidean distance as its similarity metric, will the model return *true* or *false* for this patient?
- (b) Clinicians often use BMI as a combined measure of an individual's WEIGHT and HEIGHT. BMI is defined as an individual's weight in kilograms divided by their height in meters-squared. Assuming that the profiles of the five individuals in the system were updated so that the features WEIGHT and HEIGHT were replaced by a single feature BMI and also that the doctor entered the patient's BMI into the system, what prediction would the system return for this patient?
- * 9. A lecturer is about to leave for the airport to go on vacation when they find a script for a student they forgot to mark. They don't have time to manually grade the script before the flight, so they decide to use a k -

nearest neighbor model to grade it instead. The model is designed to award a grade to a student on the basis of how similar they are to other students in the module in terms of their grades on other modules. The following table describes a set of students in terms of their grades out of 100 on two other modules (MODULE 1 and MODULE 2) and the GRADE they got in the lecturer's module: *first-class honors*, *second-class honors*, *pass*, or *fail*.

ID	MODULE		GRADE
	1	2	
1	55	85	first
2	45	30	fail
3	40	20	fail
4	35	35	fail
5	55	75	pass
6	50	95	second

- (a) Looking up the results on the other modules of the student whose script hasn't been corrected, the lecturer finds that the student got the following marks: MODULE 1=60, and MODULE 2=85. Assuming that the k -nearest neighbor model uses $k=1$ and Euclidean distance as its similarity metric, what GRADE would the model assign the student?
- (b) Reviewing the spread of marks for the other two modules, the lecturer notices that there is a larger variance across students in the marks for *Module 2* than there is for *Module 1*. So, the lecturer decides to update the k -nearest neighbor model to use the **Mahalanobis** distance instead of Euclidean distance as its similarity measure. Assuming that the **inverse covariance matrix** for the *Module 1* and *Module 2* results is

$$\sum^{-1} = \begin{bmatrix} 0.046 & -0.009 \\ -0.009 & 0.003 \end{bmatrix}$$

what GRADE would the k -nearest neighbor model assign the student?

1. This example dataset is inspired by the use of analytics in professional and college sports, often referred to as **sabremetrics**. Two accessible introductions to this field are Lewis (2004) and Keri (2007).
2. The Manhattan distance, or **taxi-cab distance**, is so called because it is the distance that a taxi driver would have to cover if going from one point to another on a road system that is laid out in blocks, like the Manhattan road system.
3. In the extreme case with $p = \infty$, the Minkowski metric simply returns the maximum difference between any of the features. This is known as the **Chebyshev distance** but is also sometimes called the **chessboard distance** because it is the number of moves a king must make in chess to go from one square on the board to any other.
4. A Voronoi tessellation is a way of decomposing a space into regions in which each region belongs to an instance and contains all the points in the space whose distance to that instance is less than the distance to any other instance.
5. Instances should be added to the training dataset only if we have determined after making the prediction that the prediction was, in fact, correct. In this example, we assume that at the draft, the query player was drafted.
6. When using the reciprocal of the squared distance as a weighting function, we need to be careful to avoid division by zero in the case in which the query is exactly the same as its nearest neighbor. Typically this problem case is handled by assigning the query the target level of the training instance \mathbf{d} that it exactly matches.
7. See Section 3.1^[54].
8. The primary papers introducing k - d trees are Bentley (1975) and Friedman et al. (1977). Also note that the k here has no relationship with the k used in k nearest neighbor. It simply specifies the number of levels in the depth of the tree, which is arbitrary and typically determined by the algorithm that constructs the tree.
9. A binary tree is simply a tree in which every node in the tree has at most two branches.
10. We use the median value as the splitting threshold because it is less susceptible to the influence of outliers than the mean, and this helps keep the tree as balanced as possible—having a balanced tree helps with the efficiency in retrieval. If more than one instance in a dataset has the median value for a feature we are splitting on, then we select one of these instances to represent the median and place the other instances with the median value in the set containing the instances whose values are greater than the median.
11. A **hyperplane** is a geometric concept that generalizes the idea of a plane into different dimensions. For example, a hyperplane in 2D space is a line and in a 3D space is a plane.
12. Similar to a hyperplane, a hypersphere is a generalization of the geometric concept of a sphere across multiple dimensions. Hence, in a 2D space the term **hypersphere** denotes a circle, in 3D it denotes a sphere, and so on.
13. Recall that each non-leaf node in the tree indexes an instance in the dataset and also defines a hyperplane that partitions the feature space. For example, the horizontal and vertical lines in Figure 5.9(b)^[199] plot the hyperplanes defined by the non-leaf nodes of the k - d tree shown in Figure 5.9(a)^[199].
14. Figure 5.12(a)^[205] further misleads us because when we draw scatter plots, we scale the values to make the plot fit into a square-shaped image. If we were to plot the axis for the SALARY feature to the same scale as the AGE feature in Figure 5.12(a)^[205], it would stretch over almost 400 pages.
15. For convenience, we repeat Equation (3.7)^[87] for range normalization

$$a'_i = \frac{a_i - \min(a)}{\max(a) - \min(a)} \times (\text{high} - \text{low}) + \text{low}$$

16. The example given here is based on artificial data generated for the purposes of this book. Predicting the prices of assets such as whiskey or wine using machine learning is, however, done in reality. For example, Ashenfelter (2008) deals with predicting wine prices and was covered in Ayres (2008).

17. These are covered in Section 9.4.1^[540].

18. One note of caution: the Jaccard similarity index is undefined for pairs of instances in which all the features manifest co-absence, because this leads to a division by zero.

19. The length of a vector, $\|\mathbf{a}\|$, is computed as the square root of the sum of the elements of the vector squared: $\|\mathbf{a}\| = \sum_{i=1}^m \mathbf{a}[i]^2$.

20. If either vector used to calculate a cosine similarity contains negative feature values, then the cosine similarity will actually be in the range $[-1, 1]$. As previously, 1 indicates high similarity, and 0 indicates dissimilarity, but it can be difficult to interpret negative similarity scores. Negative similarity values can be avoided, however, if we use range normalization (see Section 3.6.1^[87]) to ensure that descriptive feature values always remain positive.

21. Covariance between features means that knowing the value of one feature tells us something about the value of the other feature. See Section 3.5.2^[219] for more information.

22. We explain **covariance matrices** in Section 3.5.2^[81]. The **inverse covariance matrix** is the matrix such that when the covariance matrix is multiplied by its inverse, the result is the **identity matrix**: $\Sigma \times \Sigma^{-1} = \mathbb{I}$. The identity matrix is a square matrix in which all the elements of the main diagonal are 1, and all other elements are 0. Multiplying any matrix by the identity matrix leaves the original matrix unchanged—this is the equivalent of multiplying by 1 for real numbers. So the effect of multiplying feature values by an inverse covariance matrix is to rescale the variances of all features to 1 and to set the covariance between all feature pairs to 0. Calculating the inverse of a matrix involves solving systems of linear equations and requires the use of techniques from linear algebra such as **Gauss-Jordan elimination** or **LU decomposition**. We do not cover these techniques here, but they are covered in most standard linear algebra textbooks such as Anton and Rorres (2010).

23. The inverse of the identity matrix \mathbb{I} is \mathbb{I} . Therefore, if there is no covariance between the features, both the covariance and the inverse covariance matrix will be equal to \mathbb{I} .

24. Section 3.5.2^[81] describes the calculation of covariance matrices. The inverse covariance matrix was calculated using the `solve` function from the **R** programming language.

25. Recall that a dataset in which the majority of descriptive features have zero as the value is known as **sparse data**. This often occurs in **document classification** problems, when a **bag-of-words** representation is used to represent documents as the frequency of occurrence of each word in a dictionary (the eponymous bag-of-words). The bag-of-words representation is covered more in Question 2^[236] at the end of this chapter. One problem with sparse data is that with so few non-zero values, the variation between two instances may be dominated by noise.

26. A **hypercube** is a generalization of the geometric concept of a cube across multiple dimensions. Hence in a two-dimensional space, the term hypercube denotes a square; in three-dimensional space, it denotes a cube; and so on. A unit hypercube is a hypercube in which the length of every side is 1 unit.

27. This should not be confused with the concept of **sparse data** that was introduced earlier.

28. The discussion relating to the features of real data that help with the induction of models in high-dimensional spaces is based on Bishop (2006), pp. 33–38.
29. Feature selection is sometimes also known as **variable selection**.
30. See Section 4.2.3^[127].
31. We discuss the design of evaluation experiments in detail in Chapter 9^[533].
32. Obviously we must verify that the prediction made was correct before adding a new instance to the dataset.
33. The story recounted here of the discovery of the platypus is loosely based on real events. See Eco (1999) for a more faithful account of what happened and for a discussion of the implications of this discovery for classification systems in general. The platypus is not the only animal from Australia whose discovery by Europeans has relevance to predictive machine learning. See Taleb (2008) regarding the discovery of black swans and its relevance to predictive models.
34. The data listed in this table is real and is for 2010/11 (or the most recent year prior to 2010/11 when the data was available). The data for the descriptive features in this table was amalgamated from a number of surveys retrieved from **Gapminder** (www.gapminder.org). The Corruption Perception Index is generated annually by **Transparency International** (www.transparency.org).

6

Probability-Based Learning

“When my information changes, I alter my conclusions. What do you do, sir? When my information changes, I alter my conclusions. What do you do, sir?”

—John Maynard Keynes

In this chapter we introduce probability-based approaches to machine learning. Probability-based prediction approaches are heavily based on **Bayes’ Theorem**, and the fundamentals section of this chapter introduces this important cornerstone of computer science after covering some other fundamentals of **probability theory**. We then present the **naive Bayes model**, the standard approach to using probability-based approaches to machine learning. The extensions and variations to this standard approach that we describe are the use of **smoothing** to combat overfitting, the modifications required to the standard naive Bayes model to allow it to handle continuous features, and **Bayesian network** models that give us more control than a naive Bayes model over the assumptions that are encoded in a model.

6.1 Big Idea

Imagine that you are at a county fair and a stall owner is offering all comers a game of *find the lady*. *Find the lady* is a card game that hucksters have been using to earn money from unsuspecting marks for centuries.¹ In a game, the dealer holds three cards—one queen and two aces (as shown in [Figure 6.1\(a\)](#)^[244])—and, typically with a little bit of flair, quickly drops these cards facedown onto a table. Faced with the backs of three cards (as shown in [Figure 6.1\(b\)](#)^[244]), the player then has to guess where the queen has landed. Usually the player bets money on their ability to do this, and the

dealer uses a little manual trickery to misdirect the player toward the wrong card.

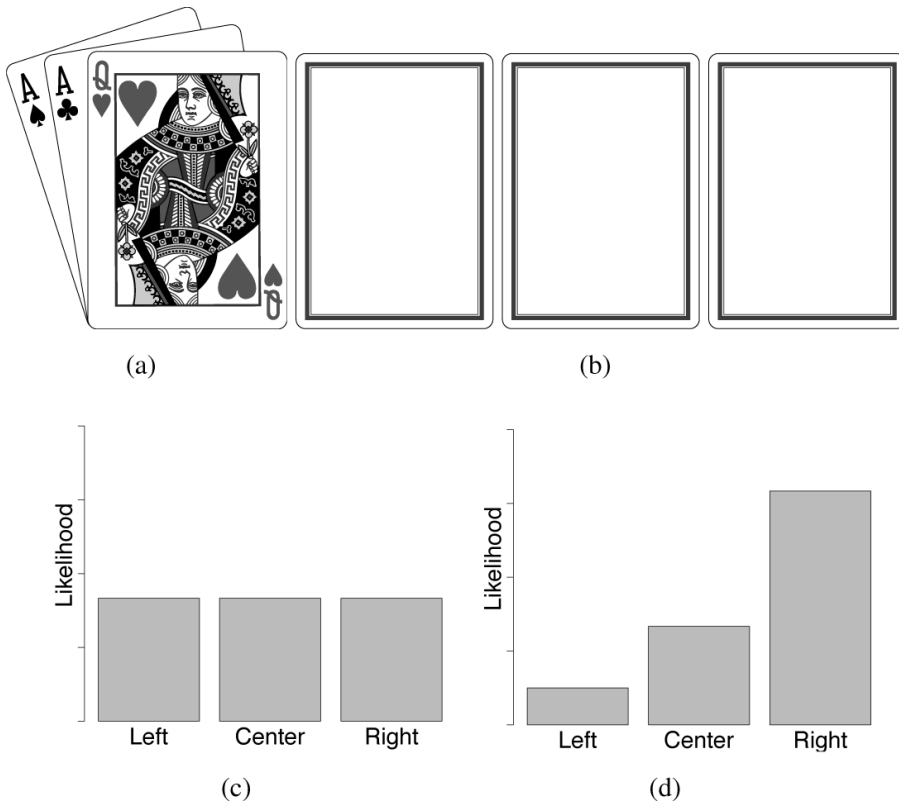


Figure 6.1

A game of *find the lady*: (a) the cards used; (b) the cards dealt facedown on a table; (c) the initial likelihoods of the queen ending up in each position; and (d) a revised set of likelihoods for the position of the queen based on evidence collected.

When you first see the game played, because the dealer lays out the three cards so quickly, you think that there is no way to tell where the queen lands. In this case you can only assume that the queen is equally likely to be in any of the three possible positions: *left*, *center*, or *right*. This is shown in the bar plot in Figure 6.1(c)^[244], which shows an equal likelihood for each position. Not feeling quite brave enough to play a game, you decide to instead study the dealer playing games with other people.

After watching the dealer play 30 games with other players, you notice that he has a tendency to drop the queen in the position on the right (19 times) more than the left (3 times) or center (8 times). Based on this, you update your beliefs about where the queen is likely to land based on the

evidence that you have collected. This is shown in [Figure 6.1\(d\)](#)^[244], where the bars have been redistributed to illustrate the revised likelihoods.

Confident that your study will help you, you lay a dollar down to play a game, ready to guess that the queen is in the position on the right. This time, however, as the dealer drops the cards onto the table, a sudden gust of wind turns over the card on the right to reveal that it is the ace of spades (shown in [Figure 6.2\(a\)](#)^[245]). The extra piece of evidence means that you need to revise your belief about the likelihoods of where the queen will be once again. These revised likelihoods are shown in [Figure 6.2\(b\)](#)^[245]. As you know that the card is not in the position on the right, the likelihood that you had associated with this position is redistributed among the other two possibilities. Based on the new likelihoods, you guess that the queen is in the center position, and happily, this turns out to be correct (see [Figure 6.2\(c\)](#)^[245]). The dealer encourages you to play again, but you know that you've got to know when to walk away, so you head off with an extra dollar in your pocket.

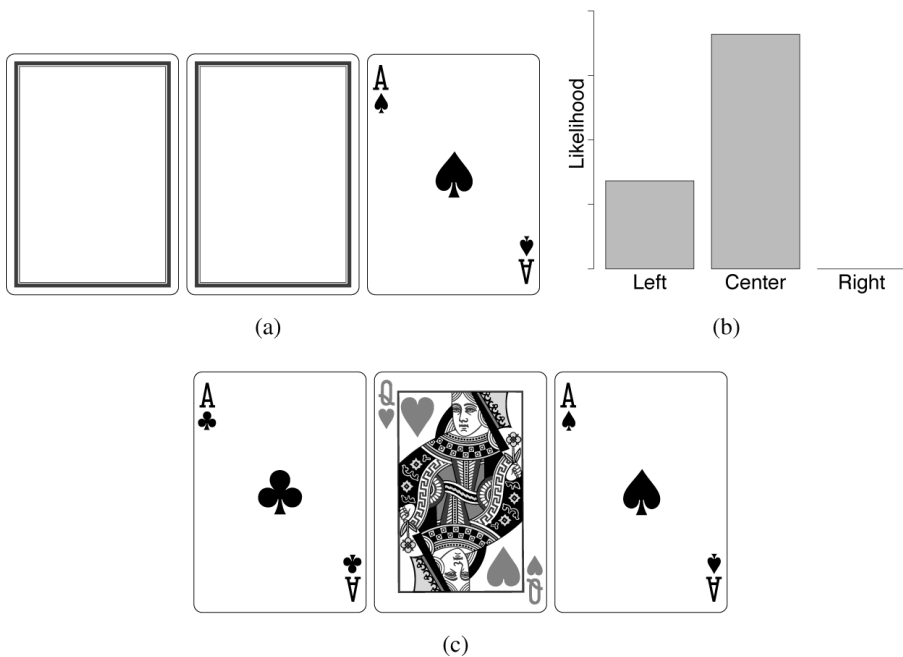


Figure 6.2

(a) The set of cards after the wind blows over the one on the right; (b) the revised likelihoods for the position of the queen based on this new evidence; and (c) the final positions of the cards in the game.

This illustrates the big idea underlying probability-based machine learning. We can use estimates of likelihoods to determine the most likely

predictions that should be made. Most important, though, we revise these predictions based on data we collect and whenever extra evidence becomes available.

6.2 Fundamentals

In this section we describe **Bayes' Theorem** and the important fundamentals of probability theory that are required to use it. This section assumes a basic understanding of probability theory, including the basics of calculating probabilities based on **relative frequencies**, calculating **conditional probabilities**, the probability **product rule**, the probability **chain rule**, and the **Theorem of Total Probability**. Appendix B^[757] provides a comprehensive introduction to these aspects of probability theory, so we recommend that readers unfamiliar with them review this appendix before continuing with this chapter.

We will use the dataset² in Table 6.1^[246] to illustrate how the terminology of probability is mapped into the language of machine learning for predictive data analytics. The target being predicted in this dataset is whether a patient is suffering from MENINGITIS, and the descriptive features are common symptoms associated with this disease (HEADACHE, FEVER, and VOMITING).

Table 6.1

A simple dataset for a MENINGITIS diagnosis with descriptive features that describe the presence or absence of three common symptoms of the disease: HEADACHE, FEVER, and VOMITING.

ID	HEADACHE	FEVER	VOMITING	MENINGITIS
1	true	true	false	false
2	false	true	false	false
3	true	false	true	false
4	true	false	true	false
5	false	true	false	true
6	true	false	true	false
7	true	false	true	false
8	true	false	true	true
9	false	true	false	false
10	true	false	true	true

From a probability point of view, each feature in a dataset is a **random variable**, and the **sample space** for the domain associated with a prediction problem is the set of all possible combinations of assignments of values to features. Each row in a dataset represents an **experiment**, which associates a target feature value with a set of descriptive feature values, and the assignment of a set of descriptive features with values is an **event**. So, for example, each row in [Table 6.1](#)^[246] represents an experiment, and the assignment of the descriptive features to the values shown in each row can be referred to as a distinct event.

A **probability function**, $P()$, returns the probability of an event. For example, $P(\text{FEVER} = \text{true})$ returns the probability of the FEVER feature taking the value *true*. This probability, which is 0.4, can be counted directly from the dataset. Probability functions for categorical features are referred to as **probability mass functions**, while probability functions for continuous features are known as **probability density functions**. In the early part of this chapter, we focus on categorical features, but we return to continuous features in [Section 6.4](#)^[265]. A **joint probability** refers to the probability of an assignment of specific values to multiple different features, for example, $P(\text{MENINGITIS} = \text{true}, \text{HEADACHE} = \text{true}) = 0.2$. Last, a **conditional probability** refers to the probability of one feature taking a specific value given that we already know the value of a different feature, for example, $P(\text{MENINGITIS} = \text{true} | \text{HEADACHE} = \text{true}) = 0.2857$.

It is often useful to talk about the probabilities for all the possible assignments to a feature. To do this we use the concept of a **probability distribution**. A probability distribution is a data structure that describes the probability of each possible value a feature can take. For example, the probability distribution for the binary feature MENINGITIS from [Table 6.1](#)^[246] is $\mathbf{P}(\text{MENINGITIS}) = \langle 0.3, 0.7 \rangle$ (by convention we give the *true* probability first). We use bold notation to distinguish between a probability distribution, $\mathbf{P}()$, and a probability function, $P()$. The sum of a probability distribution must equal 1.0.

A **joint probability distribution** is a probability distribution over more than one feature assignment and is written as a multidimensional matrix in which each cell lists the probability of a particular combination of feature values being assigned. The dimensions of the matrix are dependent on the

number of features and the number of values in the domains of the features. The sum of all the cells in a joint probability distribution must be 1.0. For example, the joint probability distribution for the four binary features from [Table 6.1](#)^[246] (HEADACHE, FEVER, VOMITING, and MENINGITIS) is written³

$$\mathbf{P}(H, F, V, M) = \begin{bmatrix} P(h, f, v, m), & P(\neg h, f, v, m) \\ P(h, f, v, \neg m), & P(\neg h, f, v, \neg m) \\ P(h, f, \neg v, m), & P(\neg h, f, \neg v, m) \\ P(h, f, \neg v, \neg m), & P(\neg h, f, \neg v, \neg m) \\ P(h, \neg f, v, m), & P(\neg h, \neg f, v, m) \\ P(h, \neg f, v, \neg m), & P(\neg h, \neg f, v, \neg m) \\ P(h, \neg f, \neg v, m), & P(\neg h, \neg f, \neg v, m) \\ P(h, \neg f, \neg v, \neg m), & P(\neg h, \neg f, \neg v, \neg m) \end{bmatrix} \quad (6.1)$$

Given a joint probability distribution, we can compute the probability of any event in the domain that it covers by summing over the cells in the distribution where that event is true. For example, to compute the probability of $P(h)$ in the domain specified by the joint probability distribution $\mathbf{P}(H,F,V,M)$, we simply sum the values in the cells containing h (the cells in the first column). Calculating probabilities in this way is known as **summing out**. We can also use summing out to compute conditional probabilities from a joint probability distribution. To calculate the probability $P(h | f)$ from $\mathbf{P}(H,F,V,M)$, we sum the values in all the cells where h and f are the case (the top four cells in the first column).

We are now ready to take on Bayes' Theorem!

6.2.1 Bayes' Theorem

Bayes' Theorem⁴ is so elegant and intuitive that it can be stated in one sentence of plain English:

the probability that an event has happened given a set of evidence for it is equal to the probability of the evidence being caused by the event multiplied by the probability of the event itself

or slightly more succinctly:

$$P(\text{an event given evidence}) = P(\text{the evidence given the event}) \\ \times P(\text{the event})$$

Reading from left to right, the theorem shows us how to calculate the probability of an event given the evidence we have of that event in terms of the likelihood of the event causing this evidence. This is useful because reasoning from the evidence to events (**inverse reasoning**) is often much more difficult than reasoning from an event to the evidence it causes (**forward reasoning**). Bayes' Theorem allows us to easily swap back and forth between these two types of reasoning.

The formal definition of **Bayes' Theorem** is

$$P(X | Y) = \frac{P(Y | X)P(X)}{P(Y)} \quad (6.2)$$

Bayes' Theorem defines the conditional probability of an event, X , given some evidence, Y , in terms of the product of the inverse conditional probability, $P(Y | X)$, and the prior probability of the event $P(X)$.

For an illustrative example of Bayes' Theorem in action, imagine that after a yearly checkup, a doctor informs a patient that there is both bad news and good news. The bad news is that the patient has tested positive for a serious disease and that the test the doctor used is 99% accurate (i.e., the probability of testing positive when a patient has the disease is 0.99, as is the probability of testing negative when a patient does not have the disease). The good news, however, is that the disease is extremely rare, striking only 1 in 10,000 people. So what is the actual probability that the patient has the disease? And why is the rarity of the disease good news given that the patient has tested positive for it?

We can use Bayes' Theorem to answer both of these questions. To calculate the probability that the patient actually has the disease based on the evidence of the test result, $P(d | t)$, we apply Bayes' Theorem:

$$P(d | t) = \frac{P(t | d)P(d)}{P(t)}$$

The information about the scenario gives us the probability of having the disease as $P(d) = 0.0001$ and the probability of not having the disease as $P(\neg d) = 0.9999$. The accuracy of the test is captured as $P(t | d) = 0.99$ and $P(t | \neg d) = 0.01$. The overall probability of the test returning a positive

value, $P(t)$, is not given in the description above, but it can be easily calculated using the **Theorem of Total Probability**⁵ as

$$\begin{aligned} P(t) &= P(t | d)P(d) + P(t | \neg d)P(\neg d) \\ &= (0.99 \times 0.0001) + (0.01 \times 0.9999) \\ &= 0.0101 \end{aligned}$$

We can insert these probabilities into the application of Bayes' Theorem to give

$$\begin{aligned} P(d | t) &= \frac{0.99 \times 0.0001}{0.0101} \\ &= 0.0098 \end{aligned}$$

So, the probability of actually having the disease, in spite of the positive test result, is less than 1%. This is why the doctor said the rarity of the disease was such good news. One of the important characteristics of Bayes' Theorem is its explicit inclusion of the prior probability of an event when calculating the likelihood of that event based on evidence.⁶

Let's look at Bayes' Theorem in a little more detail. Bayes' Theorem is easily derived from the **product rule**.⁷ We know from the product rule and the logical symmetry of the *and* operation⁸ that

$$P(Y | X)P(X) = P(X | Y)P(Y)$$

If we divide both sides of this equation by the prior probability on the left-hand side, $P(Y)$, we get

$$\frac{P(X | Y)P(Y)}{P(Y)} = \frac{P(Y | X)P(X)}{P(Y)}$$

The $P(Y)$ terms on the left-hand side of this equation, however, cancel each other out to give us Bayes' Theorem

$$\begin{aligned} \frac{P(X | Y)\cancel{P(Y)}}{\cancel{P(Y)}} &= \frac{P(Y | X)P(X)}{P(Y)} \\ \Rightarrow P(X | Y) &= \frac{P(Y | X)P(X)}{P(Y)} \end{aligned}$$

There are two important observations regarding the division in Bayes' Theorem by the denominator $P(Y)$. The first is that this division functions as a normalization mechanism ensuring that

$$0 \leq P(X | Y) \leq 1$$

and

$$\sum_i P(X_i | Y) = 1.0$$

where $\sum_i P(X_i)$ should be interpreted as summing over the set of events that are a complete assignment to the features in X . The reason that the division functions as a normalization mechanism is that the prior probability of the evidence, $P(Y)$, is not conditional on X_i , and as a result, it is constant for all X_i .

The second interesting observation about the division of the right-hand side of Bayes' Theorem by $P(Y)$ is that we can calculate $P(Y)$ in two different ways. First, we can calculate $P(Y)$ directly from a dataset as

$$P(Y) = \frac{|\{\text{rows where } Y \text{ is the case}\}|}{|\{\text{rows in the dataset}\}|} \quad (6.3)$$

Alternatively, we can use the **Theorem of Total Probability** to calculate $P(Y)$:

$$P(Y) = \sum_i P(Y | X_i)P(X_i) \quad (6.4)$$

Notice that ignoring the subscripts, the expression we are summing in Equation (6.4)^[250] is identical to the numerator in Bayes' Theorem. This gives us a way to calculate the **posterior probability distribution** over the possible assignment of values to the features in event X conditioned on the event Y , that is, $\mathbf{P}(X | Y)$, which avoids explicitly calculating $P(Y)$. If we let

$$\eta = \frac{1}{\sum_i P(Y | X_i)P(X_i)} \quad (6.5)$$

then

$$P(X_i | Y) = \eta \times P(Y | X_i)P(X_i) \quad (6.6)$$

where the term η explicitly represents a normalization constant. Because Bayes' Theorem can be calculated in this way, it is sometimes written as

$$P(X \mid Y) = \eta \times P(Y \mid X)P(X) \quad (6.7)$$

where η is as defined in Equation (6.5)^[250].

So we have two different definitions of Bayes' Theorem (Equation (6.2)^[248] and Equation (6.7)^[250]), but which one should we use? The choice is really a matter of convenience. If we are calculating the probability of a single event given some evidence, then calculating $P(Y)$ directly from the data using Equation (6.2)^[248] is the easier option. If, however, we need to calculate the posterior probability distribution over X given Y , that is $\mathbf{P}(X \mid Y)$, then we will be actually calculating each of the $P(Y \mid X_i)P(X_i)$ values in Equation (6.5)^[250] as part of this calculation, and it is more efficient to use Equation (6.7)^[250].

We are now ready to use Bayes' Theorem to generate predictions based on a dataset. The next section will examine how this is done.

6.2.2 Bayesian Prediction

To make Bayesian predictions, we generate the probability of the event that a target feature, t , takes a specific level, l , given the assignment of values to a set of descriptive features, \mathbf{q} , from a query instance. We can restate Bayes' Theorem using this terminology and generalize the definition of Bayes' Theorem so that it can take into account more than one piece of evidence (each descriptive feature value is a separate piece of evidence). The **Generalized Bayes' Theorem** is defined as

$$P(t = l \mid \mathbf{q}[1], \dots, \mathbf{q}[m]) = \frac{P(\mathbf{q}[1], \dots, \mathbf{q}[m] \mid t = l)P(t = l)}{P(\mathbf{q}[1], \dots, \mathbf{q}[m])} \quad (6.8)$$

To calculate a probability using the **Generalized Bayes' Theorem**, we need to calculate three probabilities:

1. $P(t = l)$, the **prior probability** of the target feature t taking the level l
2. $P(\mathbf{q}[1], \dots, \mathbf{q}[m])$, the **joint probability** of the descriptive features of a query instance taking a specific set of values

3. $P(\mathbf{q}[1], \dots, \mathbf{q}[m] \mid t = l)$, the **conditional probability** of the descriptive features of a query instance taking a specific set of values given that the target feature takes the level l

The first two of these probabilities are easy to calculate. $P(t = l)$ is simply the relative frequency with which the target feature takes the level l in a dataset. $P(\mathbf{q}[1], \dots, \mathbf{q}[m])$ can be calculated as the relative frequency in a dataset of the joint event that the descriptive features of an instance take on the values $\mathbf{q}[1], \dots, \mathbf{q}[m]$. As discussed in the previous section, it can also be calculated using the **Theorem of Total Probability** (in this instance, summing over all the target levels $\sum_{k \in \text{levels}(t)} P(\mathbf{q}[1], \dots, \mathbf{q}[m] \mid t = k)P(t = k)$), or replaced entirely with a **normalization constant**, η .

The final probability that we need to calculate, $P(\mathbf{q}[1], \dots, \mathbf{q}[m] \mid t = l)$, can be calculated either directly from a dataset (by calculating the relative frequency of the joint event $\mathbf{q}[1], \dots, \mathbf{q}[m]$ within the set of instances where $t = l$), or alternatively, it can be calculated using the probability **chain rule**.⁹ The chain rule states that the probability of a joint event can be rewritten as a product of conditional probabilities. So, we can rewrite $P(\mathbf{q}[1], \dots, \mathbf{q}[m])$ as

$P(\mathbf{q}[1], \dots, \mathbf{q}[m])$ as

$$\begin{aligned} P(\mathbf{q}[1], \dots, \mathbf{q}[m]) &= \\ P(\mathbf{q}[1]) \times P(\mathbf{q}[2] \mid \mathbf{q}[1]) \times \dots \times P(\mathbf{q}[m] \mid \mathbf{q}[m-1], \dots, \mathbf{q}[2], \mathbf{q}[1]) \end{aligned}$$

We can use the chain rule for conditional probabilities by just adding the conditioning term to each term in the expression, so

$$\begin{aligned} P(\mathbf{q}[1], \dots, \mathbf{q}[m] \mid t = l) &= \\ P(\mathbf{q}[1] \mid t = l) \times P(\mathbf{q}[2] \mid \mathbf{q}[1], t = l) \times \dots &\quad (6.9) \\ \dots \times P(\mathbf{q}[m] \mid \mathbf{q}[m-1], \dots, \mathbf{q}[3], \mathbf{q}[2], \mathbf{q}[1], t = l) \end{aligned}$$

This transformation from a joint probability conditioned on a single event into a product of conditional probabilities with just one event being conditioned in each term may not appear to achieve much. We will see shortly, however, that this transformation is incredibly useful.

Let's look at an example of how we can now use Bayes' Theorem to make predictions based on the meningitis diagnosis dataset in [Table 6.1](#)^[246]

for a query instance with HEADACHE = *true*, FEVER = *false*, and VOMITING = *true*. Returning to the shortened notation that we used previously, a predicted diagnosis for this query instance can be given using Bayes' Theorem as

$$P(M \mid h, \neg f, v) = \frac{P(h, \neg f, v \mid M) \times P(M)}{P(h, \neg f, v)}$$

There are two values in the domain of the MENINGITIS feature, *true* and *false*, so we have to do this calculation once for each. Considering first the calculation for *m*, we need the following probabilities, which can be computed directly from [Table 6.1](#)^[246]

$$P(m) = \frac{|\{\mathbf{d}_5, \mathbf{d}_8, \mathbf{d}_{10}\}|}{|\{\mathbf{d}_1, \mathbf{d}_2, \mathbf{d}_3, \mathbf{d}_4, \mathbf{d}_5, \mathbf{d}_6, \mathbf{d}_7, \mathbf{d}_8, \mathbf{d}_9, \mathbf{d}_{10}\}|} = \frac{3}{10} = 0.3$$

$$P(h, \neg f, v) = \frac{|\{\mathbf{d}_3, \mathbf{d}_4, \mathbf{d}_6, \mathbf{d}_7, \mathbf{d}_8, \mathbf{d}_{10}\}|}{|\{\mathbf{d}_1, \mathbf{d}_2, \mathbf{d}_3, \mathbf{d}_4, \mathbf{d}_5, \mathbf{d}_6, \mathbf{d}_7, \mathbf{d}_8, \mathbf{d}_9, \mathbf{d}_{10}\}|} = \frac{6}{10} = 0.6$$

We also need to calculate the likelihood of the descriptive feature values of the query given that the target is *true*. We could calculate this directly from the dataset, but in this example, we will illustrate the chain rule approach just described. Using the chain rule approach, we compute the overall likelihood of the descriptive feature values given a target value of *true* as the product of a set of conditional probabilities that are themselves calculated from the dataset

$$\begin{aligned} P(h, \neg f, v \mid m) &= P(h \mid m) \times P(\neg f \mid h, m) \times P(v \mid \neg f, h, m) \\ &= \frac{|\{\mathbf{d}_8, \mathbf{d}_{10}\}|}{|\{\mathbf{d}_5, \mathbf{d}_8, \mathbf{d}_{10}\}|} \times \frac{|\{\mathbf{d}_8, \mathbf{d}_{10}\}|}{|\{\mathbf{d}_8, \mathbf{d}_{10}\}|} \times \frac{|\{\mathbf{d}_8, \mathbf{d}_{10}\}|}{|\{\mathbf{d}_8, \mathbf{d}_{10}\}|} \\ &= \frac{2}{3} \times \frac{2}{2} \times \frac{2}{2} = 0.6666 \end{aligned}$$

We can now combine the three probabilities just calculated to calculate the overall probability of the target feature taking the level *true* given the query instance

$$\begin{aligned} P(m \mid h, \neg f, v) &= \frac{P(h, \neg f, v \mid m) \times P(m)}{P(h, \neg f, v)} \\ &= \frac{0.6666 \times 0.3}{0.6} = 0.3333 \end{aligned}$$

The corresponding calculation for $P(\neg m | h, \neg f, v)$ is:

$$\begin{aligned}
P(\neg m | h, \neg f, v) &= \frac{P(h, \neg f, v | \neg m) \times P(\neg m)}{P(h, \neg f, v)} \\
&= \frac{\left(P(h | \neg m) \times P(\neg f | h, \neg m) \right.}{P(h, \neg f, v)} \\
&\quad \left. \times P(v | \neg f, h, \neg m) \times P(\neg m) \right) \\
&= \frac{0.7143 \times 0.8 \times 1.0 \times 0.7}{0.6} = 0.6667
\end{aligned}$$

These calculations tell us that it is twice as probable that the patient does not have meningitis as it is that the patient does. This might seem a little surprising given that the patient is suffering from a headache and is vomiting, two key symptoms of meningitis. Indeed, we have a situation where the posterior for a given prediction given the evidence is quite low (here $P(m | h, \neg f, v) = 0.3333$), even though the likelihood of the evidence if we assume the prediction to be correct is quite high, $P(h, \neg f, v | m) = 0.6666$.

What is happening here is that, as Bayes' Theorem states, when calculating a posterior prediction, we weight the likelihood of the evidence given the prediction by the prior of the prediction. In this case, although the likelihood of suffering from a headache and vomiting is quite high when someone has meningitis, the prior probability of having meningitis is quite low. So, even when we take the evidence into account, the posterior probability of having meningitis remains low. This can seem counterintuitive at first. The mistake is to confuse the probability of a prediction given the evidence with the probability of the evidence given the prediction and is another example of the **paradox of the false positive**.¹⁰

Calculating exact probabilities for each of the possible target levels is often very useful to a human decision maker, for example, a doctor. However, if we are trying to build a predictive model that automatically assigns a target level to a query instance, then we need to decide how the model will make a prediction based on the computed probabilities. The obvious way to do this is to have the model return the target level that has the highest posterior probability given the state of the descriptive features in the query. A prediction model that works in this way is making a **maximum a posteriori (MAP)** prediction.¹¹ We can formally define a Bayesian MAP prediction model as

$$\begin{aligned}
M(\mathbf{q}) &= \arg \max_{l \in levels(t)} P(t = l \mid \mathbf{q}[1], \dots, \mathbf{q}[m]) \\
&= \arg \max_{l \in levels(t)} \frac{P(\mathbf{q}[1], \dots, \mathbf{q}[m] \mid t = l) \times P(t = l)}{P(\mathbf{q}[1], \dots, \mathbf{q}[m])}
\end{aligned} \tag{6.10}$$

where $M(\mathbf{q})$ is the prediction returned by the model M using a MAP prediction mechanism for a query, \mathbf{q} , composed of $\mathbf{q}[1], \dots, \mathbf{q}[m]$ descriptive features; $levels(t)$ is the set of levels the target feature can take; and $\arg \max_{l \in levels(t)}$ specifies that we return the level, l , that has the maximum value computed using the function on the right of the arg max term.

Notice that the denominator in Equation (6.10)^[254] is not dependent on the target feature, so it is functioning as a normalization constant. Furthermore, if we want to make a MAP prediction, we don't necessarily have to calculate the actual probabilities for each level in the target domain; we simply need to know which of the levels in the target domain has the largest probability. Consequently, we don't necessarily have to normalize the scores for each target level—something we would have to do if we wanted the actual probabilities. Instead, we can simply return the target level that has the highest score from the numerator term. Using this simplification, the **Bayesian MAP prediction model** can be restated as

$$M(\mathbf{q}) = \arg \max_{l \in levels(t)} P(\mathbf{q}[1], \dots, \mathbf{q}[m] \mid t = l) \times P(t = l) \tag{6.11}$$

Although it might seem that we now have a good solution for building probability-based prediction models, we are not quite done yet. There is one fundamental flaw with the approach that we have developed. To illustrate this, we will consider a second query instance for the meningitis diagnosis problem, this time with descriptive feature values HEADACHE = *true*, FEVER = *true*, and VOMITING = *false*. The probability of MENINGITIS = *true* given this query is

$$\begin{aligned}
P(m \mid h, f, \neg v) &= \frac{\left(P(h \mid m) \times P(f \mid h, m) \right.}{P(h, f, \neg v)} \\
&\quad \left. \times P(\neg v \mid f, h, m) \times P(m) \right) \\
&= \frac{0.6666 \times 0 \times 0 \times 0.3}{0.1} = 0
\end{aligned}$$

and for **MENINGITIS** = *false*

$$P(\neg m \mid h, f, \neg v) = \frac{\left(P(h \mid \neg m) \times P(f \mid h, \neg m) \right.}{\left. \times P(\neg v \mid f, h, \neg m) \times P(\neg m) \right)}{P(h, f, \neg v)}$$

$$= \frac{0.7143 \times 0.2 \times 1.0 \times 0.7}{0.1} = 1.0$$

The calculated posterior probabilities indicate that it is a certainty that the patient does not have meningitis! This is because as we progress along the sequence of conditional probabilities specified by the chain rule, the size of the set of conditioning events for each term increases. As a result, the set of events that fulfill the conditions for each conditional probability in the sequence, and hence that are considered when we compute the probability, get smaller and smaller as more and more conditions are added. The technical term for this splitting of the data into smaller and smaller sets based on larger and larger sets of conditions is **data fragmentation**. Data fragmentation is essentially an instance of the **curse of dimensionality**. As the number of descriptive features grows, the number of potential conditioning events grows. Consequently, an exponential increase is required in the size of the dataset as each new descriptive feature is added to ensure that for any conditional probability, there are enough instances in the training dataset matching the conditions so that the resulting probability is reasonable.

Returning to our example query, in order to calculate $P(h, f, \neg v \mid m)$, the chain rule requires us to define three conditional probabilities, $P(h \mid m)$, $P(f \mid h, m)$, and $P(\neg v \mid f, h, m)$. For the first of these terms, $P(h \mid m)$, only three instances in the dataset fulfill the condition of *m* (**d**₅, **d**₈ and **d**₁₀). In two out of these three rows (**d**₈ and **d**₁₀), *h* is the case, so the conditional probability $P(h \mid m) = 0.6666$. These are also the only two rows that fulfill the conditions of the second term in the chain sequence, $P(f \mid h, m)$. In neither of these rows is *f* the case, so the conditional probability for $P(f \mid h, m)$ is 0. Because the chain rule specifies the product of a sequence of probabilities, if any of the probabilities in the sequence is zero, then the overall probability will be zero. Even worse, because there are no rows in the dataset where *f*, *h*, and *m* are true, there are no rows in the dataset where the conditions for the third term $P(\neg v \mid f, h, m)$ hold, so this probability is

actually undefined, as calculating it involves a division by zero. Trying to compute the probability of $P(h,f,\neg v \mid m)$ directly from the data rather than using the chain rule also suffers from the same problem.

In summary, whether we compute the likelihood term for this example using the chain rule or directly from the dataset, we will end up with a probability of zero, or worse, an undefined probability. This is because there are no instances in the dataset where a patient who had meningitis was suffering from a headache and had a fever but wasn't vomiting. Consequently, the probability for the MENINGITIS feature being *true* given the evidence in the query using this dataset was zero.

Clearly, the probability of a patient who has a headache and a fever having meningitis should be greater than zero. The problem here is that our dataset is not large enough to be truly representative of the meningitis diagnosis scenario, and our model is **overfitting** to the training data. The problem is even more serious than this, however, as in practice, it is almost never possible to collect a dataset that is big enough to sufficiently cover all the possible combinations of descriptive feature values that can occur in a dataset so as to avoid this. All is not lost, however, as the concepts of **conditional independence** and **factorization** can help us overcome this flaw of our current approach.

6.2.3 Conditional Independence and Factorization

So far our treatment of probability has assumed that the evidence we have collected affects the probability of the event we are trying to predict. This is not always the case. For example, it would seem reasonable to argue that the behavior of an octopus in a swimming tank should not affect the outcome of a soccer match.¹² If knowledge of one event has no effect on the probability of another event, and vice versa, then the two events are said to be **independent** of each other. If two events X and Y are independent, then

$$\begin{aligned} P(X \mid Y) &= P(X) \\ P(X, Y) &= P(X) \times P(Y) \end{aligned}$$

Full independence between events is quite rare. A more common phenomenon is that two or more events may be independent if we know that a third event has happened. This is known as **conditional independence**. The typical situation where conditional independence holds

between events is when the events share the same cause. For example, consider the symptoms of meningitis. If we don't know whether the patient has meningitis, then knowing that the patient has a headache may increase the probability we assign to the patient of suffering from a fever. This is because having a headache increases the probability of the patient having meningitis, which in turn increases the probability of the patient having a fever. However, if we already know that the patient has meningitis, then also knowing that the patient has a headache will not affect the probability of the patient having a fever. This is because the information we get from knowing that the patient has a headache is already contained within the information that the patient has meningitis. In this situation, knowing that someone has meningitis makes the events of them having a headache and having a fever independent of each other. For two events, X and Y , that are conditionally independent given knowledge of a third event, here Z , we can say that

$$\begin{aligned} P(X | Y, Z) &= P(X | Z) \\ P(X, Y | Z) &= P(X | Z) \times P(Y | Z) \end{aligned}$$

This allows us an important reformulation of the **chain rule** for situations in which conditional independence applies. Recall that the chain rule for calculating the probability that a set of descriptive features, $\mathbf{q}[1], \dots, \mathbf{q}[m]$, takes a specific set of values when a target feature, t , takes a specific level, l , is

$$\begin{aligned} P(\mathbf{q}[1], \dots, \mathbf{q}[m] | t = l) &= \\ P(\mathbf{q}[1] | t = l) \times P(\mathbf{q}[2] | \mathbf{q}[1], t = l) \times \dots & \quad (6.12) \\ \dots \times P(\mathbf{q}[m] | \mathbf{q}[m-1], \dots, \mathbf{q}[3], \mathbf{q}[2], \mathbf{q}[1], t = l) \end{aligned}$$

If the event of the target feature t taking the level l causes the assignment of values to the descriptive features, $\mathbf{q}[1], \dots, \mathbf{q}[m]$, then the events of each descriptive feature taking a value are conditionally independent of each other given the value of the target feature. This means that the chain rule definition can be simplified as follows:

$$\begin{aligned}
P(\mathbf{q}[1], \dots, \mathbf{q}[m] \mid t = l) &= P(\mathbf{q}[1] \mid t = l) \times P(\mathbf{q}[2] \mid t = l) \times \dots \times P(\mathbf{q}[m] \mid t = l) \\
&= \prod_{i=1}^m P(\mathbf{q}[i] \mid t = l)
\end{aligned} \tag{6.13}$$

The reason that this simplification is so important is that it allows us to simplify the calculations in Bayes' Theorem, under the assumption of conditional independence between the descriptive features, given the level l of the target feature, from

$$P(t = l \mid \mathbf{q}[1], \dots, \mathbf{q}[m]) = \frac{\left(\begin{array}{c} P(\mathbf{q}[1] \mid t = l) \times P(\mathbf{q}[2] \mid \mathbf{q}[1], t = l) \times \\ \dots \times P(\mathbf{q}[m] \mid \mathbf{q}[m-1], \dots, \mathbf{q}[1], t = l) \\ \times P(t = l) \end{array} \right)}{P(\mathbf{q}[1], \dots, \mathbf{q}[m])}$$

to the much simpler

$$P(t = l \mid \mathbf{q}[1], \dots, \mathbf{q}[m]) = \frac{\left(\prod_{i=1}^m P(\mathbf{q}[i] \mid t = l) \right) \times P(t = l)}{P(\mathbf{q}[1], \dots, \mathbf{q}[m])} \tag{6.14}$$

Where appropriate, conditional independence not only simplifies the calculations but also enables us to compactly represent the full joint probability distribution for a domain. Rather than calculating and storing the probabilities of all the joint events in a domain, we can break up the distribution into data structures called **factors**, which define distributions over subsets of features. We can then compute any of the probabilities in the joint probability distribution using the product of these factors.

For example, Equation (6.1)^[247] listed the joint probability distribution for the four binary features in the meningitis diagnosis dataset in [Table 6.1](#)^[246]. This distribution contained 16 entries. If, however, it is in fact the case that HEADACHE, FEVER, and VOMITING are conditionally independent of each other given MENINGITIS, then we would need to store only four factors: $P(M)$, $P(H \mid M)$, $P(F \mid M)$, and $P(V \mid M)$. We can recalculate all the elements of the joint probability distribution using the product of these four factors:

$$P(H, F, V, M) = P(M) \times P(H \mid M) \times P(F \mid M) \times P(V \mid M)$$

Because all the features in this example are binary, we need to store only the probabilities for the events where the features are true under the different combinations of values for the conditioning cases, as the probabilities for the complementary events can be computed by subtracting the stored probabilities from 1.0. Consequently, under this factorization, we need to calculate only seven probabilities directly from the data: $P(m)$, $P(h | m)$, $P(h | \neg m)$, $P(f | m)$, $P(f | \neg m)$, $P(v | m)$, and $P(v | \neg m)$. The four factors required to represent the full joint distribution over the features HEADACHE, FEVER, VOMITING, and MENINGITIS (when the first three are assumed to be conditionally independent given MENINGITIS) can be stated as

$$\begin{aligned} Factor_1 &= \langle P(M) \rangle \\ Factor_2 &= \langle P(h | m), P(h | \neg m) \rangle \\ Factor_3 &= \langle P(f | m), P(f | \neg m) \rangle \\ Factor_4 &= \langle P(v | m), P(v | \neg m) \rangle \end{aligned}$$

and the product required to calculate the probability of any joint event in the domain using these four factors is

$$P(H, F, V, M) = P(M) \times P(H | M) \times P(F | M) \times P(V | M)$$

So, the assumed conditional independence between the features permits us to factorize the distribution and in doing so reduces the number of probabilities we need to calculate and store from the data. The reduction from 16 to 7 probabilities to represent this domain may not seem to achieve much, but there are two things to bear in mind. First, individually, the 7 probabilities have fewer constraints on them than the 16 in the full joint probability distribution. As a result, it is typically easier to collect the data required to calculate these probabilities. Second, as the number of features in the domain grows, the difference between the number of probabilities required for a factorized representation and the number of probabilities in the full joint probability distribution gets larger. For example, in a domain with one target feature and nine descriptive features, all of which are binary, the full joint probability distribution will contain $2^{10} = 1,024$ probabilities. However, if all the descriptive features are conditionally independent given the target feature, we can factorize the joint distribution and represent it

using just 19 probabilities (one for the prior of the target and two conditional probabilities for each descriptive feature).

Apart from making a model more compact, conditional independence and factorization also increase the coverage of a probability-based prediction model by allowing the model to calculate reasonable probabilities for queries with combinations of evidence that do not occur in the training dataset. To illustrate this, let's return to the example query instance for the meningitis diagnosis problem, where HEADACHE = *true*, FEVER = *true*, and VOMITING = *false*. When we originally tried to calculate probabilities for this query, a problem arose from the requirement that we have instances in the training dataset where **all** the evidence events hold. If we treat the evidence events as conditionally independent given the target feature, however, then we can factorize the evidence into its component events and calculate probabilities for each of these events separately. By doing this, we relax the requirement that, to avoid probabilities of zero, all the evidence events must hold in at least one instance for each value in the domain of the target. Instead, to avoid zero probabilities, we require only that for each value in the domain of the target feature, there be at least one instance in the dataset where each event in the evidence holds. For example, this allows us to use the probability of a patient having a fever given that the patient has meningitis, rather than the more constrained conditional probability of the patient having a fever given that the patient has meningitis **and** is suffering from a headache.

We reiterate the factors required to represent the full joint distribution for the meningitis diagnosis scenario when we assume that the descriptive features are conditionally independent given the target, this time including the actual probabilities calculated from the dataset:

$$\begin{aligned}
 Factor_1 &= \langle P(m) = 0.3 \rangle \\
 Factor_2 &= \langle P(h \mid m) = 0.6666, P(h \mid \neg m) = 0.7413 \rangle \\
 Factor_3 &= \langle P(f \mid m) = 0.3333, P(f \mid \neg m) = 0.4286 \rangle \\
 Factor_4 &= \langle P(v \mid m) = 0.6666, P(v \mid \neg m) = 0.5714 \rangle
 \end{aligned} \tag{6.15}$$

Using the factors in Equation (6.15)^[259], we calculate the posterior distribution for meningitis given the query instance using Equation (6.14)

[258] as

$$\begin{aligned}
 P(m \mid h, f, \neg v) &= \frac{P(h \mid m) \times P(f \mid m) \times P(\neg v \mid m) \times P(m)}{\sum_i P(h \mid M_i) \times P(f \mid M_i) \times P(\neg v \mid M_i) \times P(M_i)} \\
 &= \frac{0.6666 \times 0.3333 \times 0.3333 \times 0.3}{(0.6666 \times 0.3333 \times 0.3333 \times 0.3) + (0.7143 \times 0.4286 \times 0.4286 \times 0.7)} \\
 &= 0.1948
 \end{aligned}$$

$$\begin{aligned}
 P(\neg m \mid h, f, \neg v) &= \frac{P(h \mid \neg m) \times P(f \mid \neg m) \times P(\neg v \mid \neg m) \times P(\neg m)}{\sum_i P(h \mid M_i) \times P(f \mid M_i) \times P(\neg v \mid M_i) \times P(M_i)} \\
 &= \frac{0.7143 \times 0.4286 \times 0.4286 \times 0.7}{(0.6666 \times 0.3333 \times 0.3333 \times 0.3) + (0.7143 \times 0.4286 \times 0.4286 \times 0.7)} \\
 &= 0.8052
 \end{aligned}$$

As with our previous calculations, the posterior probabilities for meningitis, calculated under the assumption of conditional independence of the evidence, indicates that the patient probably does not have meningitis, and consequently, a MAP Bayesian model would return MENINGITIS = *false* as the prediction for this query instance. However, the posterior probabilities are not as extreme as those calculated when we did not assume conditional independence. What has happened is that asserting conditional independence has allowed the evidence of the individual symptoms to be taken into account, rather than requiring an exact match across all the symptoms taken together. By doing this, the Bayesian prediction model is able to calculate reasonable probabilities for queries with combinations of evidence that do not occur in the dataset. This results in the model having a higher coverage with respect to the possible queries it can handle. Furthermore, the conditional independence assumption enables us to factorize the distribution of the domain, and consequently we need fewer probabilities with fewer constraints to represent the domain. As we will see, a fundamental component of creating probabilistic prediction models is deciding on the conditional independence assumptions we wish to make and the resulting factorization of the domain.

In the next section we introduce the naive Bayes model, a probability-based machine learning algorithm that asserts a global conditional independence between the descriptive features given the target. As a result

of this conditional independence assumption, naive Bayes models are very compact and relatively robust to overfitting the data, making them one of the most popular predictive modeling approaches.

6.3 Standard Approach: The Naive Bayes Model

A naive Bayes model returns a **MAP** prediction where the posterior probabilities for the levels of the target feature are computed under the assumption of **conditional independence** between the descriptive features in an instance given a target feature level. More formally, the **naive Bayes model** is defined as

$$\mathbb{M}(\mathbf{q}) = \arg \max_{l \in \text{levels}(t)} \left(\left(\prod_{i=1}^m P(\mathbf{q}[i] | t = l) \right) \times P(t = l) \right) \quad (6.16)$$

where t is a target feature with a set of levels, $\text{levels}(t)$, and \mathbf{q} is a query instance with a set of descriptive features, $\mathbf{q}[1], \dots, \mathbf{q}[m]$.

In Section 6.2^[245] we described how a full joint probability distribution could be used to compute the probability for any event in a domain. The problem with this, however, is that generating full joint probability distributions suffers from the curse of dimensionality, and as a result, this approach is not tractable for domains involving more than a few features. In Section 6.2.3^[256], however, we showed how conditional independence between features allows us to factorize the joint distribution, and this helps with the curse of dimensionality problem by reducing the number of probabilities we are required to calculate from the data as well as the number of conditioning constraints on these probabilities. The naive Bayes model leverages conditional independence to the extreme by assuming conditional independence between the assignment of all the descriptive feature values given the target level. This assumption allows a naive Bayes model to radically reduce the number of probabilities it requires, resulting in a very compact, highly factored representation of a domain.

We say that the naive Bayes model is *naive* because the assumption of conditional independence between the features in the evidence given the target level is a simplifying assumption that is made whether or not it is incorrect. Despite this simplifying assumption, however, the naive Bayes approach has been found to be surprisingly accurate across a large range of

domains. This is partly because errors in the calculation of the posterior probabilities for the different target levels do not necessarily result in prediction errors. As we noted when we dropped the denominator of Bayes' Theorem from the MAP prediction model (Equation (6.11)^[254]), for a categorical prediction task, we are primarily interested in the relative size of the posterior probabilities for the different target levels rather than the exact probabilities. Consequently, the relative ranking of the likelihood of the target levels are, to a certain extent, robust to errors in the calculation of the exact probabilities.¹³

The assumption of conditional independence between the features in the evidence given the level of the target feature also makes the naive Bayes model relatively robust to **data fragmentation** and the **curse of dimensionality**. This is particularly important in scenarios with small datasets or with **sparse data**.¹⁴ One application domain where sparse data is the norm rather than the exception is in **text analytics** (for example, **spam filtering**), and naive Bayes models are often successful in this domain.

The naive Bayes model can also be easily adapted to handle missing feature values: we simply drop the conditional probabilities for the evidence events that specify features taking values that are not in the data from the product of the evidence events. Obviously, doing this may have a negative effect on the accuracy of posterior probabilities computed by the model, but again this may not translate directly into prediction errors.

A final advantage of the naive Bayes model is how simple it is to train. For a given prediction task, all that is required to train a naive Bayes model is to calculate the priors for each target level and the conditional probability for each feature given each target level. As a result, a naive Bayes model can be trained relatively quickly compared to many other prediction models. A further advantage that results from this simplicity is the compactness of the naive Bayes model with which a very large dataset can be represented.

Overall, although naive Bayes models may not be as powerful as some other prediction models, they often provide reasonable accuracy results, for prediction tasks with categorical targets, while being robust to the curse of dimensionality and also being easy to train. As a result, a naive Bayes model is often a good prediction model to use to define a baseline accuracy score or when working with limited data.

6.3.1 A Worked Example

We will use the dataset presented in [Table 6.2](#)^[263] to illustrate how to create and use a naive Bayes model for a prediction problem. This dataset relates to a **fraud detection** scenario in which we would like to build a model that predicts whether loan applications are fraudulent or genuine. There are three categorical descriptive features in this dataset. CREDIT HISTORY captures the credit history of the applicant, and its levels are *none* (the applicant has no previous loans), *paid* (the applicant had loans previously and has paid them off), *current* (the applicant has existing loans and are current in repayments), and *arrears* (the applicant has existing loans and are in arrears in repayments). The GUARANTOR/COAPPLICANT feature records whether the loan applicant has a guarantor or coapplicant associated with the application. The levels are *none*, *guarantor*, and *coapplicant*. The ACCOMMODATION feature refers to the applicant's current accommodation, and the levels are *own* (the applicant owns their accommodation), *rent* (the applicant rents their accommodation), and *free* (the applicant has free accommodation). The binary target feature, FRAUD, tells us whether the loan application turned out to be fraudulent (*true* or *false*).

Table 6.2

A dataset from a loan application fraud detection domain.

ID	CREDIT HISTORY	GUARANTOR/ COAPPLICANT	ACCOMMODATION	FRAUD
1	current	none	own	true
2	paid	none	own	false
3	paid	none	own	false
4	paid	guarantor	rent	true
5	arrears	none	own	false
6	arrears	none	own	true
7	current	none	own	false
8	arrears	none	own	false
9	current	none	rent	false
10	none	none	own	true
11	current	coapplicant	own	false
12	current	none	own	true
13	current	none	rent	true
14	paid	none	own	false
15	arrears	none	own	false
16	current	none	own	false
17	arrears	coapplicant	rent	false
18	arrears	none	free	false
19	arrears	none	own	false
20	paid	none	own	false

To train a naive Bayes model using this data, we need to compute the prior probabilities of the target feature taking each level in its domain, and the conditional probability of each feature taking each level in its domain conditioned for each level that the target can take. There are two levels in the target feature domain, four levels in the CREDIT HISTORY domain, three in the GUARANTOR/CoAPPLICANT domain, and three in the ACCOMMODATION domain. This means that we need to calculate $2 + (2 \times 4) + (2 \times 3) + (2 \times 3) = 22$ probabilities. Although this sounds like a lot of probabilities considering the size of the example dataset, it is worth noting that these 22 probabilities would suffice no matter how many new instances are added to the dataset, be it hundreds of thousands, or even millions. This is an

example of the compactness of a naive Bayes representation. Be aware, however, that if new descriptive features were added to the dataset, then the number of probabilities required would grow by $|\text{domain of target}| \times |\text{domain of new feature}|$, and, furthermore, if an extra value were added to the domain of the target, then the number of probabilities would grow exponentially. Once the required probabilities are calculated, our naive Bayes model is ready to make predictions for queries. It is that simple! [Table 6.3](#)^[264] lists the probabilities we need for our naive Bayes fraud detection model.

Table 6.3

The probabilities needed by a naive Bayes prediction model, calculated from the data in [Table 6.2](#)^[263].

$P(fr)$	=	0.3	$P(\neg fr)$	=	0.7
$P(CH = \text{none} fr)$	=	0.1666	$P(CH = \text{none} \neg fr)$	=	0
$P(CH = \text{paid} fr)$	=	0.1666	$P(CH = \text{paid} \neg fr)$	=	0.2857
$P(CH = \text{current} fr)$	=	0.5	$P(CH = \text{current} \neg fr)$	=	0.2857
$P(CH = \text{arrears} fr)$	=	0.1666	$P(CH = \text{arrears} \neg fr)$	=	0.4286
$P(GC = \text{none} fr)$	=	0.8334	$P(GC = \text{none} \neg fr)$	=	0.8571
$P(GC = \text{guarantor} fr)$	=	0.1666	$P(GC = \text{guarantor} \neg fr)$	=	0
$P(GC = \text{coapplicant} fr)$	=	0	$P(GC = \text{coapplicant} \neg fr)$	=	0.1429
$P(ACC = \text{own} fr)$	=	0.6666	$P(ACC = \text{own} \neg fr)$	=	0.7857
$P(ACC = \text{rent} fr)$	=	0.3333	$P(ACC = \text{rent} \neg fr)$	=	0.1429
$P(ACC = \text{free} fr)$	=	0	$P(ACC = \text{free} \neg fr)$	=	0.0714

Notation key: FR = FRAUD, CH = CREDIT HISTORY, GC = GUARANTOR/COAPPLICANT, ACC = ACCOMMODATION.

The following is a query instance for the fraud detection domain:

CREDIT HISTORY = *paid*, GUARANTOR/COAPPLICANT = *none*,
ACCOMMODATION = *rent*

[Table 6.4](#)^[265] shows the relevant probabilities needed to make a prediction for this query and the calculation of the scores for each possible prediction.

Each calculation applies Equation (6.16)^[261] and can be understood as a product of the four factors that the naive Bayes model represents: $P(\text{FR})$, $P(\text{CH} | \text{FR})$, $P(\text{GC} | \text{FR})$, and $P(\text{ACC} | \text{FR})$. The scores are 0.0139 for a prediction of *true* and 0.0245 for a prediction of *false*. It is worth emphasizing that the scores calculated are not the actual posterior probabilities for each target level given the query evidence (to get the actual posterior probabilities we would need to normalize these scores), but they do give us enough information to rank the different target levels based on the relative posterior probabilities. A naive Bayes prediction model returns the MAP prediction, so our naive Bayes model would make a prediction of *false* and so classify this loan application query as not fraudulent.

Table 6.4

The relevant probabilities, from Table 6.3^[264], needed by the naive Bayes prediction model to make a prediction for a query with $\text{CH} = \text{paid}$, $\text{GC} = \text{none}$, and $\text{ACC} = \text{rent}$, and the calculation of the scores for each target level.

$P(\text{fr})$	=	0.3	$P(\neg\text{fr})$	=	0.7
$P(\text{CH} = \text{paid} \text{fr})$	=	0.1666	$P(\text{CH} = \text{paid} \neg\text{fr})$	=	0.2857
$P(\text{GC} = \text{none} \text{fr})$	=	0.8334	$P(\text{GC} = \text{none} \neg\text{fr})$	=	0.8571
$P(\text{ACC} = \text{rent} \text{fr})$	=	0.3333	$P(\text{ACC} = \text{rent} \neg\text{fr})$	=	0.1429
$\left(\prod_{k=1}^m P(\mathbf{q}[k] \text{fr}) \right) \times P(\text{fr}) = 0.0139$					
$\left(\prod_{k=1}^m P(\mathbf{q}[k] \neg\text{fr}) \right) \times P(\neg\text{fr}) = 0.0245$					

There is one, non-obvious, aspect of this example that is particularly interesting. If we look for an instance in the dataset in Table 6.2^[263] that matches all the descriptive feature values in the query, we won't find one. Despite the lack of any instances that perfectly match the evidence, the fact that we were still able to calculate a score for each target level and make a prediction for the query highlights how the conditional independence assumption between the evidence given the target level both increases the coverage of the model and allows the model to generalize beyond the data used to induce it.

6.4 Extensions and Variations

In this section we discuss extensions and variations of the naive Bayes model that increase its ability to generalize and avoid overfitting (smoothing) and that allow it to handle continuous descriptive features. We also describe Bayesian networks, which are a probability-based modeling approach that allows us to include more subtle assumptions in a model than the global assumption of conditional independence between all descriptive features that the naive Bayes model makes.

6.4.1 Smoothing

Although the assumption of conditional independence extends the coverage of a naive Bayes model and allows it to generalize beyond the contents of the training data, naive Bayes models still do not have complete coverage of the set of all possible queries. We can see the reason for this in [Table 6.3](#)^[264], where there are still some probabilities equal to zero, for example, $P(CH = \text{none} | \neg fr)$. These arise when there are no instances in the training data that match a specific combination of target feature and descriptive feature levels. Consequently, a model is likely to overfit the data for any query where one or more of the evidence events match the conditioned event of one of these zero probabilities. For example, consider the following query:

CREDIT HISTORY = *paid*, GUARANTOR/COAPPLICANT = *guarantor*,
ACCOMMODATION = *free*

[Table 6.5](#)^[266] lists the relevant probabilities needed to make a prediction for this query, and the calculation of the scores for each of the possible target levels. In this instance, both possible predictions have a score of zero! Both scores are set to zero because one of the conditional probabilities used to calculate them is zero. For *fr* the probability $P(ACC = \text{free} | fr)$ causes the problem, and for $\neg fr$ the probability $P(GC = \text{guarantor} | \neg fr)$ is the offender. As a result, the model is unable to return a prediction for this query.

Table 6.5

The relevant probabilities, from [Table 6.3](#)^[264], needed by the naive Bayes prediction model to make a prediction for the query with CH = *paid*, GC = *guarantor*, and ACC = *free*, and the calculation of the scores for each possible target level.

$P(fr)$	=	0.3	$P(\neg fr)$	=	0.7
$P(\text{CH} = \text{paid} fr)$	=	0.1666	$P(\text{CH} = \text{paid} \neg fr)$	=	0.2857
$P(\text{GC} = \text{guarantor} fr)$	=	0.1666	$P(\text{GC} = \text{guarantor} \neg fr)$	=	0
$P(\text{ACC} = \text{free} fr)$	=	0	$P(\text{ACC} = \text{free} \neg fr)$	=	0.0714
$\left(\prod_{k=1}^m P(\mathbf{q}[k] fr) \right) \times P(fr) = 0.0$					
$\left(\prod_{k=1}^m P(\mathbf{q}[k] \neg fr) \right) \times P(\neg fr) = 0.0$					

The way to solve this problem is by **smoothing** the probabilities used by the model. We know from the definition of probability that the sum of the probabilities of a feature taking each of its possible levels should equal 1.0:

$$\sum_{l \in \text{levels}(f)} P(f = l) = 1.0$$

where f is a feature and $\text{levels}(f)$ is the set of levels in the domain of the feature. This means that we have a total **probability mass** of 1.0 that is shared out between the different assignments of a level to a feature based on their relative frequency. Smoothing involves taking some of the probability mass from the assignments with probability greater than average and spreading it across the probabilities that are below average, or even equal to zero.

For example, if we sum across the posterior probability distribution for the GUARANTOR/CoAPPLICANT feature under the condition that FRAUD = *false*, we will get a value of 1.0 (see [Table 6.6](#)^[267]). Notice that within this set, $P(\text{GC} = \text{none} | \neg fr)$ is quite large, and at the other extreme, $P(\text{GC} = \text{guarantor} | \neg fr)$ = is equal to zero. Smoothing takes some of the probability mass from the events with high probability and shares this with the events with low probabilities. If this is done correctly, then the total probability mass for the set will remain equal to 1.0, but the spread of probabilities across the set will be smoother (hence the name smoothing).

Table 6.6

The posterior probability distribution for the GUARANTOR/COAPPLICANT feature under the condition that $\text{FRAUD} = \text{false}$.

$P(\text{GC} = \text{none} \mid \neg\text{fr})$	=	0.8571
$P(\text{GC} = \text{guarantor} \mid \neg\text{fr})$	=	0
$P(\text{GC} = \text{coapplicant} \mid \neg\text{fr})$	=	0.1429
$\sum_{l \in \text{levels}(\text{GC})} P(\text{GC} = l \mid \neg\text{fr})$	=	1.0

There are several different ways to smooth probabilities. We will use **Laplace smoothing**. Note, that in general, it does not make sense to smooth the unconditional (prior) probabilities for the different target feature levels,¹⁵ so here we will focus on smoothing the conditional probabilities for the features. Laplace smoothing for conditional probabilities is defined as

$$P(f = l \mid t) = \frac{\text{count}(f = l \mid t) + k}{\text{count}(f \mid t) + (k \times |\text{Domain}(f)|)}$$

where $\text{count}(f = l \mid t)$ is how often the event $f = l$ occurs in the subset of rows in the dataset where the target level is t , $\text{count}(f \mid t)$ is how often the feature, f , took any level in the subset of rows in the dataset where the target level is t , $|\text{Domain}(f)|$ is the number of levels in the domain of the feature, and k is a predetermined parameter. Larger values of k mean that more smoothing occurs—that is, more probability mass is taken from the larger probabilities and given to the small probabilities. Typically k takes small values such as 1, 2, or 3.

Table 6.7^[268] illustrates the steps in smoothing the posterior probabilities for the GUARANTOR/COAPPLICANT feature when conditioned on $\text{FRAUD} = \text{false}$. We can see that after smoothing, the probability mass is more evenly distributed across the events in the set. Crucially, the posterior probability for $P(\text{GC} = \text{guarantor} \mid \neg\text{fr})$ is no longer zero, and as a result, the coverage of the model has been extended to include queries with GUARANTOR/COAPPLICANT values of *guarantor*.

Table 6.7

Smoothing the posterior probabilities for the GUARANTOR/CoAPPLICANT feature conditioned on FRAUD = *false*.

Raw	$P(\text{GC} = \text{none} \mid \neg \text{fr})$	=	0.8571
Probabilities	$P(\text{GC} = \text{guarantor} \mid \neg \text{fr})$	=	0
	$P(\text{GC} = \text{coapplicant} \mid \neg \text{fr})$	=	0.1429
Smoothing		k	= 3
Parameters	$\text{count}(\text{GC} \mid \neg \text{fr})$	=	14
	$\text{count}(\text{GC} = \text{none} \mid \neg \text{fr})$	=	12
	$\text{count}(\text{GC} = \text{guarantor} \mid \neg \text{fr})$	=	0
	$\text{count}(\text{GC} = \text{coapplicant} \mid \neg \text{fr})$	=	2
	$ \text{Domain}(\text{GC}) $	=	3
Smoothed	$P(\text{GC} = \text{none} \mid \neg \text{fr}) = \frac{12 + 3}{14 + (3 \times 3)}$	=	0.6522
Probabilities	$P(\text{GC} = \text{guarantor} \mid \neg \text{fr}) = \frac{0 + 3}{14 + (3 \times 3)}$	=	0.1304
	$P(\text{GC} = \text{coapplicant} \mid \neg \text{fr}) = \frac{2 + 3}{14 + (3 \times 3)}$	=	0.2174

Table 6.8

The Laplace smoothed (with $k = 3$) probabilities needed by a naive Bayes prediction model, calculated from the dataset in [Table 6.2](#)^[263].

$P(fr)$	=	0.3	$P(\neg fr)$	=	0.7
$P(CH = \text{none} fr)$	=	0.2222	$P(CH = \text{none} \neg fr)$	=	0.1154
$P(CH = \text{paid} fr)$	=	0.2222	$P(CH = \text{paid} \neg fr)$	=	0.2692
$P(CH = \text{current} fr)$	=	0.3333	$P(CH = \text{current} \neg fr)$	=	0.2692
$P(CH = \text{arrears} fr)$	=	0.2222	$P(CH = \text{arrears} \neg fr)$	=	0.3462
$P(GC = \text{none} fr)$	=	0.5333	$P(GC = \text{none} \neg fr)$	=	0.6522
$P(GC = \text{guarantor} fr)$	=	0.2667	$P(GC = \text{guarantor} \neg fr)$	=	0.1304
$P(GC = \text{coapplicant} fr)$	=	0.2	$P(GC = \text{coapplicant} \neg fr)$	=	0.2174
$P(ACC = \text{own} fr)$	=	0.4667	$P(ACC = \text{own} \neg fr)$	=	0.6087
$P(ACC = \text{rent} fr)$	=	0.3333	$P(ACC = \text{rent} \neg fr)$	=	0.2174
$P(ACC = \text{free} fr)$	=	0.2	$P(ACC = \text{free} \neg fr)$	=	0.1739

Notation key: FR =FRAUD, CH = CREDIT HISTORY, GC = GUARANTOR/COAPPLICANT, ACC =ACCOMMODATION.

[Table 6.8](#)^[269] lists the prior and smoothed conditional probabilities for the fraud domain that are relevant to a naive Bayes model. Notice that there are no zero probabilities, so the model will be able to return a prediction for any query in this domain. We can illustrate the extended coverage of the model by returning to the query from the beginning of this section:

CREDIT HISTORY = *paid*, GUARANTOR/COAPPLICANT = *guarantor*,
ACCOMMODATION = *free*

[Table 6.9](#)^[270] illustrates how a naive Bayes model would calculate the scores for each candidate target level for this query using the smoothed probabilities from [Table 6.8](#)^[269]. Using our smoothed probabilities, we are able to calculate a score for both target levels: 0.0036 for *true* and 0.0043 for *false*. The target level *false* has the highest score (if only marginally) and is the MAP prediction for this query. Therefore, our naive Bayes model will predict that this loan application is not fraudulent.

Table 6.9

The relevant smoothed probabilities, from [Table 6.8](#)^[269], needed by the naive Bayes prediction model to make a prediction for the query with CH = *paid*, GC = *guarantor*, and ACC = *free*, and the calculation of the scores for each target levels.

$P(fr)$	=	0.3	$P(\neg fr)$	=	0.7
$P(\text{CH} = \text{paid} fr)$	=	0.2222	$P(\text{CH} = \text{paid} \neg fr)$	=	0.2692
$P(\text{GC} = \text{guarantor} fr)$	=	0.2667	$P(\text{GC} = \text{guarantor} \neg fr)$	=	0.1304
$P(\text{ACC} = \text{free} fr)$	=	0.2	$P(\text{ACC} = \text{free} \neg fr)$	=	0.1739
$\left(\prod_{k=1}^m P(\mathbf{q}[m] fr) \right) \times P(fr) = 0.0036$					
$\left(\prod_{k=1}^m P(\mathbf{q}[m] \neg fr) \right) \times P(\neg fr) = 0.0043$					

6.4.2 Continuous Features: Probability Density Functions

To calculate the probability of an event, we have simply counted how often the event occurred and divided this number by how often the event could have occurred. A continuous feature can have an infinite number of values in its domain, so any particular value will occur a negligible amount of the time. In fact, the relative frequency of any particular value for a continuous feature will be indistinguishable from zero given a large dataset.

The way to solve the problem of zero probabilities is to think in terms of how the probability of a continuous feature taking a value is distributed across the range of values that a continuous feature can take. A **probability density function (PDF)** represents the probability distribution of a continuous feature using a mathematical function, and there are a large number of standard, well-defined probability distributions—such as the **normal distribution**—that we can use to model the probability of a continuous feature taking different values in its range.

[Table 6.10](#)^[271] shows the definition of some of the standard probability distributions—the **normal**, **exponential**, and **mixture of Gaussians** distributions—that are commonly used in probabilistic prediction models, and [Figure 6.3](#)^[270] illustrates the shapes of the density curves of these distributions. All standard PDFs have parameters that alter the shape of the density curve defining that distribution. The parameters required for the

normal, exponential, and mixture of Gaussians PDFs are shown in [Table 6.10](#)^[271]. In order to use a PDF to represent the probability of a continuous feature taking different values, we need to choose these parameters to fit the characteristics of the data. We have already described the normal distribution, in some detail, in Section 3.2.1^[61], so we won't repeat that introduction here, but we will describe the other distributions in a little detail.

Table 6.10

Definitions of some standard probability distributions.

Normal

$$x \in \mathbb{R}$$

$$\mu \in \mathbb{R}$$

$$\sigma \in \mathbb{R}_{>0}$$

$$N(x, \mu, \sigma) = \frac{1}{\sigma \sqrt{2\pi}} e^{-\frac{(x - \mu)^2}{2\sigma^2}}$$

Student-*t*

$$x \in \mathbb{R}$$

$$\phi \in \mathbb{R}$$

$$\rho \in \mathbb{R}_{>0}$$

$$\kappa \in \mathbb{R}_{>0}$$

$$z = \frac{x - \phi}{\rho}$$

$$\tau(x, \phi, \rho, \kappa) = \frac{\Gamma(\frac{\kappa+1}{2})}{\Gamma(\frac{\kappa}{2}) \times \sqrt{\pi\kappa} \times \rho} \times \left(1 + \left(\frac{1}{\kappa} \times z^2\right)\right)^{-\frac{\kappa+1}{2}}$$

Exponential

$$x \in \mathbb{R}$$

$$\lambda \in \mathbb{R}_{>0}$$

$$E(x, \lambda) = \begin{cases} \lambda e^{-\lambda x} & \text{for } x > 0 \\ 0 & \text{otherwise} \end{cases}$$

Mixture of *n* Gaussians

$$x \in \mathbb{R}$$

$$\{\mu_1, \dots, \mu_n | \mu_i \in \mathbb{R}\}$$

$$\{\sigma_1, \dots, \sigma_n | \sigma_i \in \mathbb{R}_{>0}\}$$

$$\{\omega_1, \dots, \omega_n | \omega_i \in \mathbb{R}_{>0}\}$$

$$\sum_{i=1}^n \omega_i = 0$$

$$N(x, \mu_1, \sigma_1, \omega_1, \dots, \mu_n, \sigma_n, \omega_n) = \sum_{i=1}^n \frac{\omega_i}{\sigma_i \sqrt{2\pi}} e^{-\frac{(x - \mu_i)^2}{2\sigma_i^2}}$$

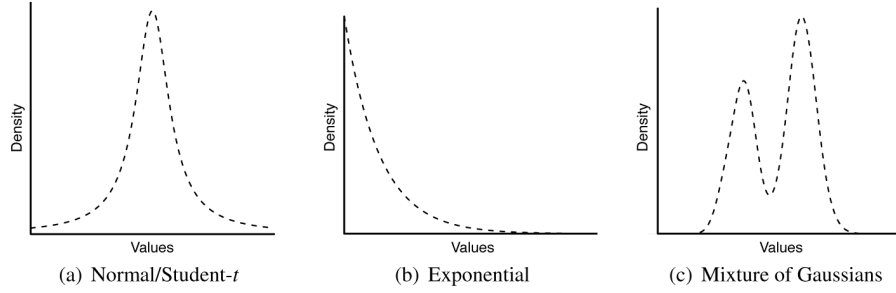


Figure 6.3

Plots of some well-known probability distributions.

The **student- t** distribution is symmetric around a single peak. In fact, it looks very similar to a normal distribution, as shown in Figure 6.3(a)^[270]. The definition of the **student- t** probability density function uses the **gamma function**, $\Gamma()$, which is a standard statistical function.¹⁶ The student- t distribution is a member of the **location-scale** family of distributions.¹⁷ These distributions take two parameters: a **location** parameter ϕ , which specifies the position of the peak density of the distribution, and a non-negative **scale** parameter ρ , which specifies how spread out the distribution is; the higher the scale the more spread out the distribution. The normal distribution is a member of this **location-scale** family, with the mean μ specifying the location, and the standard deviation σ acting as the scale parameter. We use different notation for location and scale parameters, ϕ and ρ , than we do for mean and standard deviation parameters of the normal, μ and σ , because the values of these parameters are estimated using different techniques: generally, the location and scale parameters for distributions are fitted to the data using a guided search process.¹⁸ The student- t distribution, however, takes an extra parameter κ . This parameter is the **degrees of freedom** of the distribution. In statistics the degrees of freedom of a distribution is the number of variables in the calculation of the statistic that are free to vary. For the student- t distribution, the degrees of freedom is always set to the sample size (number of rows in the dataset) minus one.

From a distribution perspective, the main distinction between a normal distribution and a student- t is that a normal distribution has **light tails** whereas the student- t distribution has **fat tails**. Figure 6.4^[273] illustrates the distinction between fat and light tail distributions using histograms of two datasets. The dataset in Figure 6.4(a)^[273] follows a light tail distribution—

the bars at the extreme left and right of the distribution have zero height. The dataset in [Figure 6.4\(b\)](#)^[273] has a fat tail distribution—the bars on the extreme left and right of the distribution are still above zero, if only just. This distinction between fat and light tailed distributions is important because it highlights that when we use a normal distribution, we are implicitly assuming that the likelihood of values that differ from the mean of the distribution drops quite dramatically as we move away from the mean. A common mistake made by many data analysts is to automatically default to modeling unimodally distributed data with a normal distribution.¹⁹ There are statistical tests (such as the **Kolmogorov-Smirnov test**) that can be used to check whether or not a feature is normally distributed, and in cases where the feature is not normally distributed, another **unimodal** distribution, such as the **student-*t* distribution**, may be a better fit.

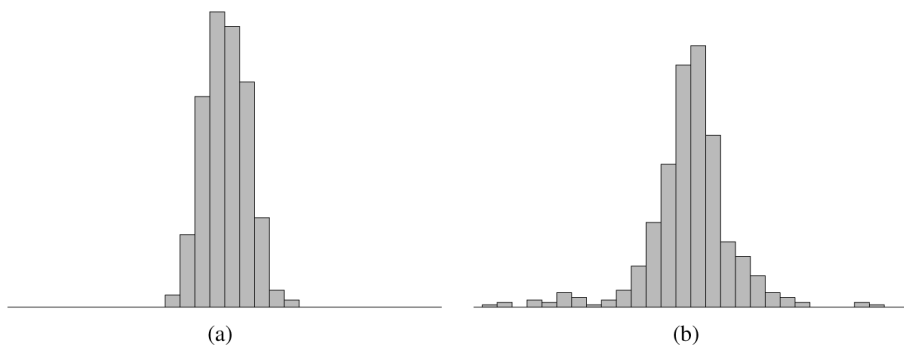


Figure 6.4

Histograms of two unimodal datasets: (a) the distribution has light tails; and (b) the distribution has fat tails.

Another consequence of the normal distribution having light tails is that it is sensitive to outliers in the data. [Figure 6.5](#)^[273] illustrates how outliers affect normal and student-*t* distributions. [Figure 6.5\(a\)](#)^[273] shows a histogram of a dataset that has been overlaid with the curves of a normal and a student-*t* distribution that have been fitted to the data. The normal and the student-*t* distributions are both very similar, and both do a good job of matching the shape of the density histogram. [Figure 6.5\(b\)](#)^[273] shows a histogram of the same dataset after some outliers have been added to the extreme right of the distribution. Again, we have overlaid the histogram with plots of the curves for a normal and a student-*t* distribution that have

been fitted to the updated dataset. Comparing [Figure 6.5\(a\)](#)^[273] and [Figure 6.5\(b\)](#)^[273], we can see clearly that the introduction of outliers has a much larger effect on the normal distribution than it does on the student-*t* distribution. The robustness of the student-*t* to outliers is another reason to consider using this distribution, as opposed to a normal distribution, to model unimodal data in situations with relatively small or possibly noisy datasets.

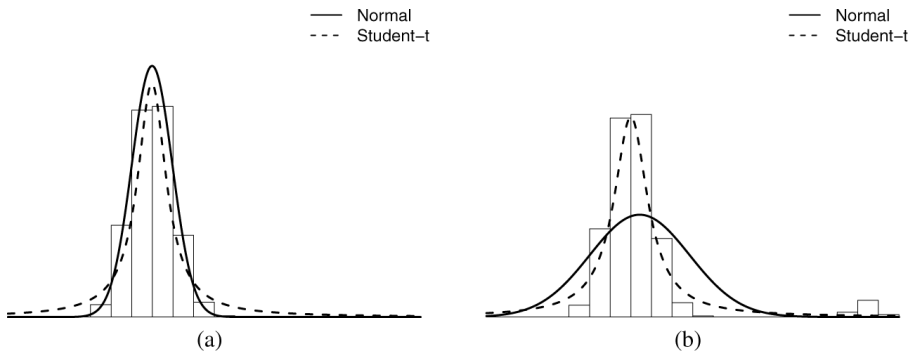


Figure 6.5

Illustration of the robustness of the student-*t* distribution to outliers: (a) a density histogram of a unimodal dataset overlaid with the density curves of a normal and a student-*t* distribution that have been fitted to the data; and (b) a density histogram of the same dataset with outliers added, overlaid with the density curves of a normal and a student-*t* distribution that have been fitted to the data. (This figure is inspired by Figure 2.16 in Bishop (2006).)

The plot of the density curve for the **exponential distribution** ([Figure 6.3\(b\)](#))^[270] shows that it assigns a high probability to values near the left of the distribution and that the probability of a value occurring drops dramatically as we move to the right. The standard range for the exponential distribution is from zero upward (i.e., the density assigned to values less than zero is zero). However, we can adjust this by offsetting the values input into the distribution. The exponential distribution takes one parameter, λ , known as the **rate**. Varying the value λ changes the rate at which the density drops off. As λ gets larger, the peak of the distribution (on the left) gets larger, and the drop-off in density gets steeper. To fit an exponential distribution to a continuous feature, we set λ equal to 1 divided by the mean of the feature. The exponential distribution is often used to model waiting times (for example, how long it will take for a call to be answered at a help desk, how long you will have to wait for a bus, or how

long before a piece of hardware fails), where the parameter λ is equal to 1 divided by the average time it takes for the event.

As the name suggests, the **mixture of Gaussians** distribution is the distribution that results when a number of normal (or Gaussian) distributions are merged. Mixture of Gaussians distributions are used to represent data that is composed of multiple subpopulations. [Figure 6.6\(a\)](#)^[275] illustrates the profile typical of data with multiple subpopulations. The multiple peaks in the density curve arise from the different subpopulations (a distribution with multiple peaks is called **multimodal**). Using a mixture of Gaussians distribution assumes that all the subpopulations in the data are distributed following a normal distribution, but that each of these subpopulation normal distributions has a different mean and may also have a different standard deviation.

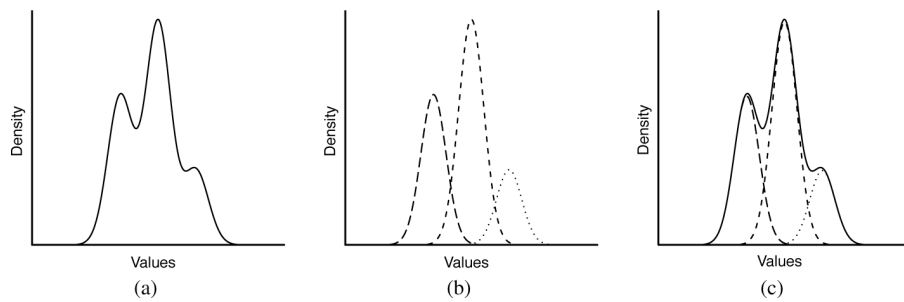


Figure 6.6

Illustration of how a mixture of Gaussians model is composed of a number of normal distributions. The curve plotted using a solid line is the mixture of Gaussians density curve, created using an appropriately weighted summation of the three normal curves, plotted using dashed and dotted lines.

The definition of the mixture of Gaussians distribution in [Table 6.10](#)^[271] shows how the individual normal distributions in a mixture of Gaussians distribution are combined using a weighted sum. Each normal that is merged is known as a **component** of the mixture. The weight of a component in the sum determines the contribution of the component to the overall density of the resulting mixture. A mixture of Gaussians distribution is defined by three parameters for each component: a mean, μ , a standard deviation, σ , and a weight, ω . The set of weight parameters for the mixture must sum to 1.

There is no closed form solution to calculate the parameters to fit a mixture of Gaussians distribution to a set of feature values, as there is for

the exponential and normal distributions. Instead, given the set of values for a continuous feature, we fit a mixture of Gaussians distribution to this data by searching for the number of components and set of parameters for each component that best matches the data. **Guided search** techniques, such as the **gradient descent** algorithm, are used for this task. Analysts will often input a suggested starting point for this search based on their own analysis of the data in order to guide the process.

In [Figure 6.6\(b\)](#)^[275] we can see the three normal distributions used to model the multimodal distribution in [Figure 6.6\(a\)](#)^[275]. Each normal distribution has a different mean but the same standard deviation. The size of the individual normal density curves is proportional to the weight for that normal used in the mixture. [Figure 6.6\(c\)](#)^[275] overlays the multimodal density curve on top of the three weighted normals. It is clear from this figure that the weighted sum of the three normals does an excellent job of modeling the multimodal density distribution.

The fact that we have a range of parameterized distributions to choose from means that in order to define a probability density function (PDF), we must

1. Select which probability distribution we believe will best model the distribution of the values of the feature. The simplest and most direct way to choose a distribution for a feature is to create a density histogram of the feature's values and compare the shape of this histogram to the shapes of the standard distributions. We should choose whichever standard distribution best matches the shape of the histogram to model the feature.
2. Fit the parameters of the selected distribution to the feature values in the dataset. It is relatively straightforward to fit the parameters, μ and σ , of the normal distribution to a dataset by using the sample mean and standard deviation of the feature values in a dataset as estimates of μ and σ respectively. Similar to the normal distribution, the λ parameter for the exponential distribution can be easily calculated by using the value of 1 divided by the mean of the data. However, for many of the other statistical distributions, for example, the mixture of Gaussians distribution, we cannot define an equation over the data that estimates the parameters appropriately. For these distributions, the parameters

are set using guided search techniques such as **gradient descent**. Fortunately, most data analytics packages and programming APIs provide functions that implement methods to fit a specified distribution to a given dataset.²⁰

A PDF is an abstraction over a density histogram and, as such, defines a density curve. The shape of the curve is determined by (a) the statistical distribution that is used to define the PDF, and (b) the values of the statistical distribution parameters. To use a PDF to calculate a probability, we need to think in terms of the area under an interval of the PDF curve. Consequently, to calculate a probability using a PDF, we need to first decide on the interval we wish to calculate the probability for, and then calculate the area under the density curve for that interval to give the probability of a value from that interval occurring. There is no hard and fast rule for deciding on **interval size**. Instead, this decision is made on a case-by-case basis and is dependent on the precision required in answering a question. In some cases, the size of the interval is defined as part of the problem we are trying to solve, or there may be a natural interval to use because of the domain. For example, when we are dealing with a financial feature, we might use intervals that represent cents, while if we were dealing with temperature, we might define the interval to be 1 degree. Once we have selected the interval size, we need to calculate the area under the density curve for that interval.²¹

When we use a PDF to represent the probability distribution of a descriptive feature in a naive Bayes model, however, we don't actually need to calculate exact probabilities. We only need to calculate the relative likelihood of a continuous feature taking a value given different levels of a target feature. The height of the density curve defined by a PDF at a particular feature value gives us this, so we can avoid the effort of calculating the actual probability. We can use a value from a PDF as a relative measure of likelihood because when the interval is very small, the actual area under a PDF curve for that interval can be approximated (with a small error proportional to the width of the interval) by the height of the PDF curve at the center of the interval multiplied by the width of the interval. Figure 6.7^[277] illustrates this approximation.

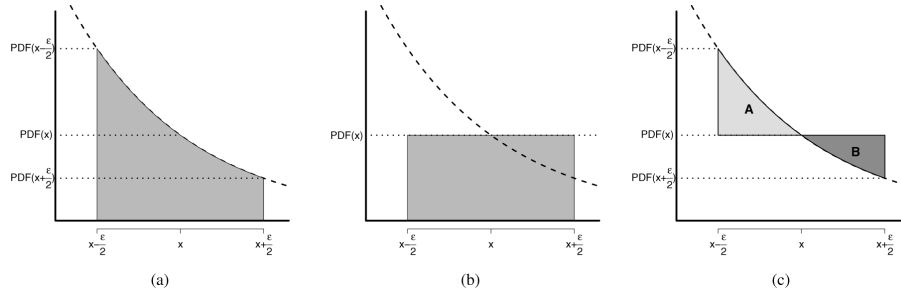


Figure 6.7

(a) The area under a density curve between the limits $x - \frac{\epsilon}{2}$ and $x + \frac{\epsilon}{2}$; (b) the approximation of this area computed by $PDF(x) \times \epsilon$; and (c) the error in the approximation is equal to the difference between area A, the area under the curve omitted from the approximation, and area B, the area above the curve erroneously included in the approximation. Both of these areas will get smaller as the width of the interval gets smaller, resulting in a smaller error in the approximation.

If we were to include the interval width when calculating conditional probabilities for a continuous descriptive feature in a naive Bayes prediction model, using Equation (6.16)^[261], we would multiply the value returned by the PDF by the same interval width each time we calculated the likelihood score for a level of the target feature. Consequently, we can drop this multiplication and just use the value returned by the PDF as a relative measure of the likelihood that the feature takes a specific value.

To ground our discussion of PDFs, and to illustrate how they can be used in making naive Bayes prediction models, we will extend our loan application fraud detection scenario to have two extra continuous features: ACCOUNT BALANCE, which specifies the amount of money in the account of the loan applicant at the time of the application; and LOAN AMOUNT, which specifies the amount of the loan being applied for. Table 6.11^[278] lists this extended dataset. We first use only the extra ACCOUNT BALANCE feature in the dataset (ignoring LOAN AMOUNT, which we return to later in this chapter) to demonstrate how PDFs allow us to include continuous features in a naive Bayes model.

Table 6.11

The dataset from the loan application fraud detection domain (from [Table 6.2](#)^[263]) with two continuous descriptive features added: ACCOUNT BALANCE and LOAN AMOUNT.

ID	CREDIT HISTORY	GUARANTOR/ COAPPLICANT	ACCOMMODATION	ACCOUNT BALANCE	LOAN AMOUNT	FRAUD
1	current	none	own	56.75	900	true
2	current	none	own	1,800.11	150,000	false
3	current	none	own	1,341.03	48,000	false
4	paid	guarantor	rent	749.50	10,000	true
5	arrears	none	own	1,150.00	32,000	false
6	arrears	none	own	928.30	250,000	true
7	current	none	own	250.90	25,000	false
8	arrears	none	own	806.15	18,500	false
9	current	none	rent	1,209.02	20,000	false
10	none	none	own	405.72	9,500	true
11	current	coapplicant	own	550.00	16,750	false
12	current	none	free	223.89	9,850	true
13	current	none	rent	103.23	95,500	true
14	paid	none	own	758.22	65,000	false
15	arrears	none	own	430.79	500	false
16	current	none	own	675.11	16,000	false
17	arrears	coapplicant	rent	1,657.20	15,450	false
18	arrears	none	free	1,405.18	50,000	false
19	arrears	none	own	760.51	500	false
20	current	none	own	985.41	35,000	false

To enable the naive Bayes model to handle the ACCOUNT BALANCE feature, we have to extend the set of probabilities used by the model to represent the domain to include the probabilities for this feature. Recall that the naive Bayes domain representation defines a conditional probability for each possible value in the domain of a descriptive feature for each level in the domain of the target. In our example, the target feature, FRAUD, is binary, so we need to define two conditional probabilities for each value in the domain of the new descriptive feature: $P(\text{AB} = x | \text{fr})$ and $P(\text{AB} = x | \neg\text{fr})$. Because the descriptive feature ACCOUNT BALANCE is continuous, there is an infinite number of values in the feature's domain. However, we

know that using an appropriately defined PDF, we can approximate the probability of the feature taking any value in its domain. As a result, we simply need to define two PDFs for the new feature with each PDF conditioned on a different level of the target feature: $P(AB = x | fr) = PDF_1(AB = x | fr)$ and $P(AB = x | \neg fr) = PDF_2(AB = x | \neg fr)$. These two PDFs do not have to be defined using the same distribution. Once we have selected the distributions we wish to use, to define a PDF for a descriptive feature that is conditioned on a particular target, we fit the parameters of the selected distribution to the subset of the data where the target has that value.

The first step in defining the two PDFs is to decide which distribution we will use to define the PDFs for each target feature level. To make this decision, we partition the training data based on the target feature and generate histograms of the values of the descriptive feature for each of the splits. We then select the statistical distribution that is most similar in shape to each of the resulting histograms. [Figure 6.8](#)^[279] shows the histograms of the values of the ACCOUNT BALANCE feature partitioned on the two levels of the FRAUD target feature. It is clear from these histograms that the distribution of values taken by the ACCOUNT BALANCE feature in the set of instances where FRAUD = *true* follows an exponential distribution; whereas, the distribution of the values taken by the ACCOUNT BALANCE feature in the set of instances where the FRAUD = *false* is similar to a normal distribution.

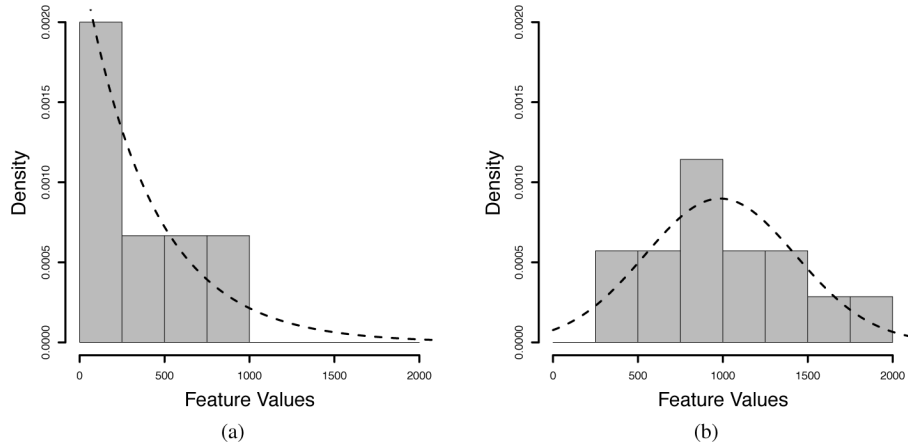


Figure 6.8

Histograms, using a bin size of 250 units, and density curves for the ACCOUNT BALANCE feature: (a) the fraudulent instances overlaid with a fitted exponential distribution; and (b) the non-fraudulent instances overlaid with a fitted normal distribution.

Once we have selected the distributions, the next step is to fit the distributions to the data. To fit the exponential distribution, we compute the sample mean of the ACCOUNT BALANCE feature in the set of instances where FRAUD = *true* and set the λ parameter equal to 1 divided by this value. To fit the normal distribution to the set of instances where FRAUD = *false*, we compute the sample mean and sample standard deviation for the ACCOUNT BALANCE feature for this set of instances and set the parameters of the normal distribution to these values. [Table 6.12](#)^[280] shows how these values are calculated, and the dashed lines in [Figure 6.8](#)^[279] plot the density curves that result from this process. Once distributions have been fitted to the data, we can extend the naive Bayes domain representation to include the PDFs. [Table 6.13](#)^[281] shows the extended domain representation.

Table 6.12

Partitioning the dataset based on the value of the target feature and fitting the parameters of a statistical distribution to model the ACCOUNT BALANCE feature in each partition.

(a) Instances where FRAUD = *true* and the fitted parameters for the exponential distribution

ACCOUNT			
ID	...	BALANCE	FRAUD
1		56.75	true
4		749.50	true
6		928.30	true
10	...	405.72	true
12		223.89	true
13		103.23	true
\overline{AB}		411.22	
$\lambda = {}^1!/\overline{AB}$		0.0024	

(b) Instances where FRAUD = *false* and the fitted parameters for the normal distribution

ACCOUNT			
ID	...	BALANCE	FRAUD
2		1,800.11	false
3		1,341.03	false
5		1,150.00	false
7		250.90	false
8		806.15	false
9		1,209.02	false
11	...	550.00	false
14		758.22	false
15		430.79	false
16		675.11	false
17		1,657.20	false
18		1,405.18	false
19		760.51	false
20		985.41	false
\overline{AB}		984.26	
$sd(AB)$		460.94	

Note: ACCOUNT BALANCE has been shortened to AB in these tables.

Table 6.13

The Laplace smoothed (with $k = 3$) probabilities needed by a naive Bayes prediction model, calculated from the dataset in [Table 6.11](#)^[278], extended to include the conditional probabilities for the new ACCOUNT BALANCE feature, which are defined in terms of PDFs.

$P(fr)$	=	0.3	$P(\neg fr)$	=	0.7
$P(CH = none fr)$	=	0.2222	$P(CH = none \neg fr)$	=	0.1154
$P(CH = paid fr)$	=	0.2222	$P(CH = paid \neg fr)$	=	0.2692
$P(CH = current fr)$	=	0.3333	$P(CH = current \neg fr)$	=	0.2692
$P(CH = arrears fr)$	=	0.2222	$P(CH = arrears \neg fr)$	=	0.3462
$P(GC = none fr)$	=	0.5333	$P(GC = none \neg fr)$	=	0.6522
$P(GC = guarantor fr)$	=	0.2667	$P(GC = guarantor \neg fr)$	=	0.1304
$P(GC = coapplicant fr)$	=	0.2	$P(GC = coapplicant \neg fr)$	=	0.2174
$P(ACC = own fr)$	=	0.4667	$P(ACC = own \neg fr)$	=	0.6087
$P(ACC = rent fr)$	=	0.3333	$P(ACC = rent \neg fr)$	=	0.2174
$P(ACC = free fr)$	=	0.2	$P(ACC = free \neg fr)$	=	0.1739
$P(AB = x fr)$			$P(AB = x \neg fr)$		
		$\approx E \begin{pmatrix} x, \\ \lambda = 0.0024 \end{pmatrix}$			$\approx N \begin{pmatrix} x, \\ \mu = 984.26, \\ \sigma = 460.94 \end{pmatrix}$

Notation key: FR = FRAUD, CH = CREDIT HISTORY, GC = GUARANTOR/COAPPLICANT, ACC = ACCOMMODATION, AB = ACCOUNT BALANCE.

Table 6.14

The probabilities, from [Table 6.13](#)^[281], needed by the naive Bayes prediction model to make a prediction for the query with CH = *paid*, GC = *guarantor*, ACC = *free*, and AB = 759.07, and the calculation of the scores for each candidate prediction.

$P(fr)$	=	0.3	$P(\neg fr)$	=	0.7
$P(CH = paid fr)$	=	0.2222	$P(CH = paid \neg fr)$	=	0.2692
$P(GC = guarantor fr)$	=	0.2667	$P(GC = guarantor \neg fr)$	=	0.1304
$P(ACC = free fr)$	=	0.2	$P(ACC = free \neg fr)$	=	0.1739
$P(AB = 759.07 fr)$			$P(AB = 759.07 \neg fr)$		
$\approx E \begin{pmatrix} 759.07, \\ \lambda = 0.0024 \end{pmatrix}$	=	0.00039	$\approx N \begin{pmatrix} 759.07, \\ \mu = 984.26, \\ \sigma = 460.94 \end{pmatrix}$	=	0.00077
$\left(\prod_{k=1}^m P(\mathbf{q}[k] fr) \right) \times P(fr) = 0.0000014$					
$\left(\prod_{k=1}^m P(\mathbf{q}[k] \neg fr) \right) \times P(\neg fr) = 0.0000033$					

To use the extended domain representation of the model to make a prediction for a query, we calculate the product of the relevant descriptive feature probabilities and the priors for the different target levels as before, but using PDFs to calculate the probabilities for the continuous feature. [Table 6.14](#)^[282] shows how a prediction is made for the following query:

CREDIT HISTORY = *paid*, GUARANTOR/COAPPLICANT = *guarantor*,
ACCOMMODATION = *free*, ACCOUNT BALANCE = 759.07

The calculations for the probabilities for the ACCOUNT BALANCE feature are made using the equations for the normal and exponential distributions in [Table 6.10](#)^[271]. The result is that FRAUD = *false* still has the highest score and will be returned as the prediction for this query.

6.4.3 Continuous Features: Binning

A commonly used alternative to representing a continuous feature using a probability density function is to convert the feature into a categorical feature using **binning**. In Section 3.6.2^[89] we explained two of the best

known binning techniques, **equal-width binning** and **equal-frequency binning**, and discussed some of the general advantages and disadvantages of each technique. One feature of equal-width binning is that it can result in a very uneven distribution of instances across the bins, with some bins containing a large number of instances and other bins being nearly empty. This uneven distribution of instances across bins can have dramatic and unwanted consequences for probability-based models. Bins that contain only a few instances may have extremely small or extremely large conditional probabilities (depending on how the instances are divided when conditioned on the target feature), and these extreme conditional probabilities may bias a model based on the parameters of the binning technique (for example, the number of bins we choose to have) rather than on real distributions in the data. For this reason, we recommend the use of equal-frequency binning to convert continuous features to categorical ones for probability-based models.

Returning to our loan application fraud detection example, we will show how binning can be used to include the LOAN AMOUNT feature (see [Table 6.11](#)^[278]) in a naive Bayes prediction model for this scenario. [Table 6.15](#)^[283] shows the discretization of the LOAN AMOUNT feature into four equal-frequency bins. In this table, the instances in the dataset have been reordered in ascending order based on their LOAN AMOUNT values. Even when using equal-frequency binning, there is still chance that the partitioning of the data will give rise to extreme conditional probabilities. For example, all the *bin3* values have a target feature value of *false*. Consequently, the posterior probability of LOAN AMOUNT = *bin3* conditioned on FRAUD = *true* will be 0.0 and LOAN AMOUNT = *bin3* conditioned FRAUD = *false* will be 1.0. **Smoothing** should be used in conjunction with binning to help with these extreme probabilities.

Table 6.15

The LOAN AMOUNT continuous feature discretized into four equal-frequency bins.

ID	BINNED			BINNED			
	LOAN AMOUNT	LOAN AMOUNT	FRAUD	LOAN ID	LOAN AMOUNT	FRAUD	
15	500	bin1	false	9	20,000	bin3	false
19	500	bin1	false	7	25,000	bin3	false
1	900	bin1	true	5	32,000	bin3	false
10	9,500	bin1	true	20	35,000	bin3	false
12	9,850	bin1	true	3	48,000	bin3	false
4	10,000	bin2	true	18	50,000	bin4	false
17	15,450	bin2	false	14	65,000	bin4	false
16	16,000	bin2	false	13	95,500	bin4	true
11	16,750	bin2	false	2	150,000	bin4	false
8	18,500	bin2	false	6	250,000	bin4	true

$$\begin{aligned}
 bin1 &\leq 9,925 \\
 9,925 < bin2 &\leq 19,250 \\
 19,225 < bin3 &\leq 49,000 \\
 49,000 < bin4
 \end{aligned}$$

Once we have discretized the data using binning, we need to record the raw continuous feature thresholds between the bins. The reason for this is that we need to be able to bin the features of any query instances appropriately before we make predictions for them. To calculate these thresholds, we take the midpoint in the feature range between the instance with the highest feature value in one bin and the feature with the lowest feature value in the next bin. For example, the instances in [Table 6.15](#)^[283] are ordered in ascending order based on the magnitude of their original LOAN AMOUNT value. So, the threshold between *bin1* and *bin2* will be the midpoint between the LOAN AMOUNT values for \mathbf{d}_{12} (9,850) and \mathbf{d}_4 (10,000) which is 9,925. The threshold boundaries for the four bins used to discretize the LOAN AMOUNT feature are

Once we have discretized the continuous features and calculated the thresholds for binning query features, we are ready to create our predictive model. As before, for a naive Bayes model, we calculate the prior probability distribution for the target feature and the posterior distribution for each descriptive feature conditioned on the target feature. Again, we

should smooth the resulting probabilities. [Table 6.16](#)^[284] shows the Laplace smoothed (with $k = 3$) probabilities required by a naive Bayes prediction model calculated from the dataset in [Table 6.11](#)^[278]. Notice that in this domain representation, we blend different approaches to continuous features: we are retaining the PDFs developed in Section 6.4.2^[269] for the ACCOUNT BALANCE feature and extend the representation with the binned version of the LOAN AMOUNT feature, BINNED LOAN AMOUNT.

Table 6.16

The Laplace smoothed (with $k = 3$) probabilities needed by a naive Bayes prediction model, calculated from the data in Tables 6.11^[278] and 6.15^[283].

$P(fr)$	=	0.3	$P(\neg fr)$	=	0.7
$P(CH = \text{none} fr)$	=	0.2222	$P(CH = \text{none} \neg fr)$	=	0.1154
$P(CH = \text{paid} fr)$	=	0.2222	$P(CH = \text{paid} \neg fr)$	=	0.2692
$P(CH = \text{current} fr)$	=	0.3333	$P(CH = \text{current} \neg fr)$	=	0.2692
$P(CH = \text{arrears} fr)$	=	0.2222	$P(CH = \text{arrears} \neg fr)$	=	0.3462
$P(GC = \text{none} fr)$	=	0.5333	$P(GC = \text{none} \neg fr)$	=	0.6522
$P(GC = \text{guarantor} fr)$	=	0.2667	$P(GC = \text{guarantor} \neg fr)$	=	0.1304
$P(GC = \text{coapplicant} fr)$	=	0.2	$P(GC = \text{coapplicant} \neg fr)$	=	0.2174
$P(ACC = \text{own} fr)$	=	0.4667	$P(ACC = \text{own} \neg fr)$	=	0.6087
$P(ACC = \text{rent} fr)$	=	0.3333	$P(ACC = \text{rent} \neg fr)$	=	0.2174
$P(ACC = \text{free} fr)$	=	0.2	$P(ACC = \text{free} \neg fr)$	=	0.1739
$P(AB = x fr)$			$P(AB = x \neg fr)$		
	$\approx E \begin{pmatrix} x, \\ \lambda = 0.0024 \end{pmatrix}$			$\approx N \begin{pmatrix} x, \\ \mu = 984.26, \\ \sigma = 460.94 \end{pmatrix}$	
$P(BLA = \text{bin1} fr)$	=	0.3333	$P(BLA = \text{bin1} \neg fr)$	=	0.1923
$P(BLA = \text{bin2} fr)$	=	0.2222	$P(BLA = \text{bin2} \neg fr)$	=	0.2692
$P(BLA = \text{bin3} fr)$	=	0.1667	$P(BLA = \text{bin3} \neg fr)$	=	0.3077
$P(BLA = \text{bin4} fr)$	=	0.2778	$P(BLA = \text{bin4} \neg fr)$	=	0.2308

Notation key: FR =FRAUD, CH = CREDIT HISTORY, GC = GUARANTOR/COAPPLICANT, ACC =ACCOMMODATION, AB =ACCOUNT BALANCE, BLA =BINNED LOAN AMOUNT.

We are now ready to process a query that has the continuous LOAN AMOUNT feature as part of the evidence:

CREDIT HISTORY = *paid*, GUARANTOR/COAPPLICANT = *guarantor*,
 ACCOMMODATION = *free*, ACCOUNT BALANCE = 759.07,
 LOAN AMOUNT = 8,000

The LOAN AMOUNT value for this query (8,000) is below the threshold for *bin1*. Consequently, the query LOAN AMOUNT feature will be treated as being equal to *bin1* during prediction. [Table 6.17](#)^[285] lists the calculations of the naive Bayes scores for the candidate predictions for this query: 0.000000462 for *true* and 0.000000633 for *false*. The target level *false* has the highest score and will be the prediction made by the model.

Table 6.17

The relevant smoothed probabilities, from [Table 6.16](#)^[284], needed by the naive Bayes model to make a prediction for the query with CH = *paid*, GC = *guarantor*, ACC = *free*, AB = 759.07, and LA = 8,000, and the calculation of the scores for each candidate prediction.

$P(fr)$	=	0.3	$P(\neg fr)$	=	0.7
$P(CH = paid fr)$	=	0.2222	$P(CH = paid \neg fr)$	=	0.2692
$P(GC = guarantor fr)$	=	0.2667	$P(GC = guarantor \neg fr)$	=	0.1304
$P(ACC = free fr)$	=	0.2	$P(ACC = free \neg fr)$	=	0.1739
$P(AB = 759.07 fr)$			$P(AB = 759.07 \neg fr)$		
$\approx E \begin{pmatrix} 759.07, \\ \lambda = 0.0024 \end{pmatrix}$	=	0.00039	$\approx N \begin{pmatrix} 759.07, \\ \mu = 984.26, \\ \sigma = 460.94 \end{pmatrix}$	=	0.00077
$P(BLA = bin1 fr)$	=	0.3333	$P(BLA = bin1 \neg fr)$	=	0.1923
<hr/>					
$\left(\prod_{k=1}^m P(\mathbf{q}[k] fr) \right) \times P(fr) = 0.000000462$					
$\left(\prod_{k=1}^n P(\mathbf{q}[k] \neg fr) \right) \times P(\neg fr) = 0.000000633$					

6.4.4 Bayesian Networks

In this chapter we have introduced two ways to represent the probabilities of events in a domain, a **full joint probability distribution** and a **naive Bayes model**. A full joint probability distribution encodes the probabilities for all joint events in the domain. Using a full joint probability distribution, we can do probabilistic inference by summing out the features we are not interested in. Full joint probability distributions, however, grow at an exponential rate as new features or feature levels are added to the domain.

This exponential growth rate is partially due to the fact that a full joint probability distribution ignores the structural relationships between features, such as direct influence and conditional independence relationships. As a result, full joint distributions are not tractable for any domain of reasonable complexity. By contrast, a naive Bayes model uses a very compact representation of a domain. The reason for this is that the model assumes that all the descriptive features are **conditionally independent** of each other given the value of the target feature. The compactness of the representation is at the cost of making a naive assumption that may adversely affect the predictive accuracy of the model.

Bayesian networks use a graph-based representation to encode the structural relationships (such as direct influence and conditional independence) between subsets of features in a domain. Consequently, a Bayesian network representation is generally more compact than a full joint distribution (because it can encode conditional independence relationships), yet it is not forced to assert a global conditional independence between all descriptive features. As such, Bayesian network models are an intermediary between full joint distributions and naive Bayes models and offer a useful compromise between model compactness and predictive accuracy.

A Bayesian network is a directed acyclical graph (there are no cycles in the graph) that is composed of three basic elements:

- **nodes:** each feature in a domain is represented by a single node in the graph.
- **edges:** nodes are connected by directed links; the connectivity of the links in a graph encodes the influence and conditional independence relationships between nodes.
- **conditional probability tables:** each node has a conditional probability table (**CPT**) associated with it. A CPT lists the probability distribution of the feature represented by the node conditioned on the features represented by the other nodes to which a node is connected by edges.

[Figure 6.9\(a\)](#)^[287] illustrates a simple Bayesian network. This network describes a domain consisting of two features A and B. The directed link from A to B indicates that the value of A directly influences the value of B. In probability terms, the directed edge from A to B in [Figure 6.9\(a\)](#)^[287] states that

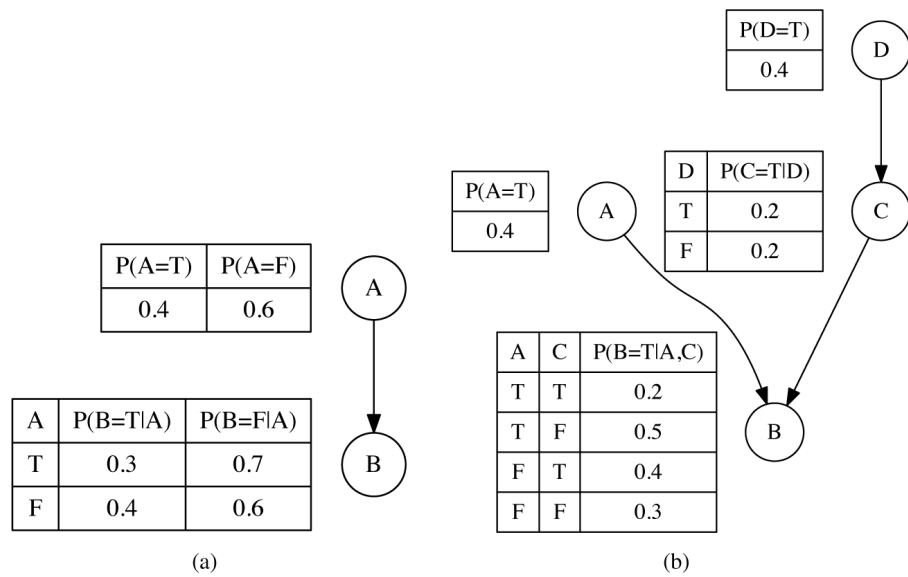


Figure 6.9

(a) A Bayesian network for a domain consisting of two binary features. The structure of the network states that the value of feature A directly influences the value of feature B. (b) A Bayesian network consisting of four binary features with a path containing three generations of nodes: D, C, and B.

$$P(A, B) = P(B \mid A) \times P(A) \quad (6.17)$$

For example, the probability of the event a and $\neg b$ is

$$P(a, \neg b) = P(\neg b | a) \times P(a) = 0.7 \times 0.4 = 0.28$$

where the probabilities used in the calculation are read directly from the CPTs in Figure 6.9(a)^[287]. In the terminology of Bayesian networks, node A is a **parent node** of B, and node B is a **child node** of A, because there is a direct edge from A into B. The CPT associated with each node defines the probabilities of each feature taking a value given the value(s) of its parent node(s). Node A has no parents, so the CPT just lists the unconditional probability distribution for A. Notice that each row in the CPT tables sum to 1. Consequently, for a categorical feature with N levels, we need only $N - 1$ probabilities in each row, with the final probability being understood as equal to 1 minus the sum of the other $N - 1$ probabilities. For example, when dealing with binary features, we need simply state the probability of each feature being *true*, and the *false* value is understood as 1 minus this probability. The network in Figure 6.9(a)^[287] could be simplified in this way, and we will use this simplification for all networks drawn from now on.

The standard approach for handling continuous features in a Bayesian network is to use binning. As a result, the CPT representation is sufficient to handle both categorical and (binned) continuous features.

Equation (6.17)^[286] can be generalized to the statement that for any network with N nodes, the probability of an event x_1, \dots, x_n , can be computed using the following formula:

$$P(x_1, \dots, x_n) = \prod_{i=1}^n P(x_i \mid \text{Parents}(x_i)) \quad (6.18)$$

where $\text{Parents}(x_i)$ describes the set of nodes in the graph that directly link into node x_i . Using this equation, we can compute any joint event in the domain represented by the Bayesian network. For example, using the slightly more complex Bayesian network in Figure 6.9(b)^[287], we can calculate the probability of the joint event $P(a, \neg b, \neg c, d)$ as

$$\begin{aligned} P(a, \neg b, \neg c, d) &= P(\neg b \mid a, \neg c) \times P(\neg c \mid d) \times P(a) \times P(d) \\ &= 0.5 \times 0.8 \times 0.4 \times 0.4 = 0.064 \end{aligned}$$

When we are computing a conditional probability, we need to be aware of the state of both the parents of a node and the children of a node and their parents. This is because knowledge of the state of a child node can tell us something about the state of the parent node. For example, returning to our simple Bayesian network in Figure 6.9(a)^[287], we can compute $P(a \mid \neg b)$ using Bayes' Theorem as follows:

$$\begin{aligned} P(a \mid \neg b) &= \frac{P(\neg b \mid a) \times P(a)}{P(\neg b)} = \frac{P(\neg b \mid a) \times P(a)}{\sum_i P(\neg b \mid A_i)} \\ &= \frac{P(\neg b \mid a) \times P(a)}{(P(\neg b \mid a) \times P(a)) + (P(\neg b \mid \neg a) \times P(\neg a))} \\ &= \frac{0.7 \times 0.4}{(0.7 \times 0.4) + (0.6 \times 0.6)} = 0.4375 \end{aligned}$$

Essentially, here we are using Bayes' Theorem to invert the dependencies between the nodes. So, for a conditional independence, we need to take into account not only the parents of a node but also the state of its children and their parents. If we have knowledge of these parent and children nodes, however, then the node is **conditionally independent** of the rest of the

nodes in the graph. The set of nodes in a graph that make a node independent of the rest of the graph are known as the **Markov blanket** of a node. [Figure 6.10](#)^[288] illustrates the Markov blanket of a node.

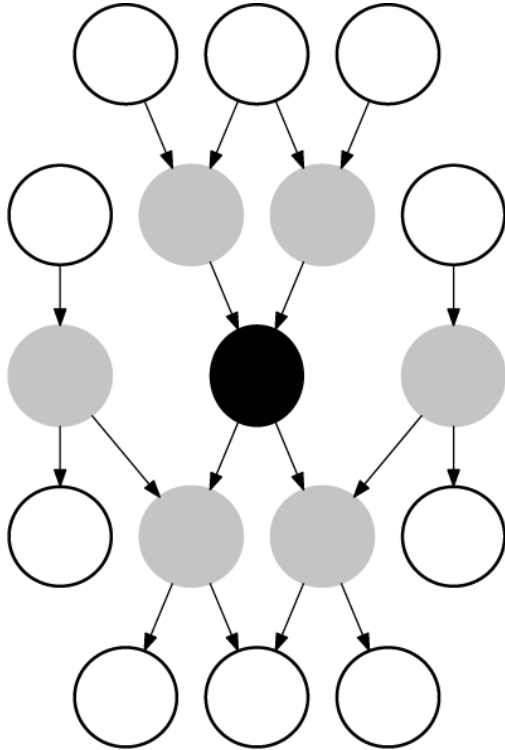


Figure 6.10

A depiction of the Markov blanket of a node. The gray nodes define the Markov blanket of the black node. The black node is conditionally independent of the white nodes given the state of the gray nodes.

So, the conditional probability of a node x_i in a graph with n nodes can be defined as

$$P(x_i \mid x_1, \dots, x_{i-1}, x_{i+1}, \dots, x_n) = \\ P(x_i \mid \text{Parents}(x_i)) \prod_{j \in \text{Children}(x_i)} P(x_j \mid \text{Parents}(x_j)) \quad (6.19)$$

where $\text{Parents}(x_i)$ describes the set of nodes in the graph that directly link into node x_i , and $\text{Children}(x_i)$ describes the set of nodes in the graph that x_i directly links into. Applying this definition to the network in [Figure 6.9\(b\)](#)^[287], we can calculate the probability of $P(c \mid \neg a, b, d)$ as

$$\begin{aligned}
 P(c \mid \neg a, b, d) &= P(c \mid d) \times P(b \mid c, \neg a) \\
 &= 0.2 \times 0.4 = 0.08
 \end{aligned}$$

We already used Equation (6.19)^[288] when we were making predictions for a naive Bayes classifier. A naive Bayes classifier is a Bayesian network with a specific topological structure. Figure 6.11(a)^[290] illustrates the network structure of a naive Bayes classifier and how it encodes the conditional independence between the descriptive features given assumed knowledge of the target. Figure 6.11(b)^[290] illustrates the network structure of the naive Bayes model for predicting a fraudulent loan application that was built in Section 6.3.1^[262]. We can see in this structure that the target feature, FRAUD, has no parents and is the single parent for all the descriptive feature nodes. This structure directly reflects the assumption, made by naive Bayes models, of the conditional independence between descriptive features given knowledge of the target feature and is why the conditional probabilities of the descriptive features in a naive Bayes model are conditioned only on the target feature.

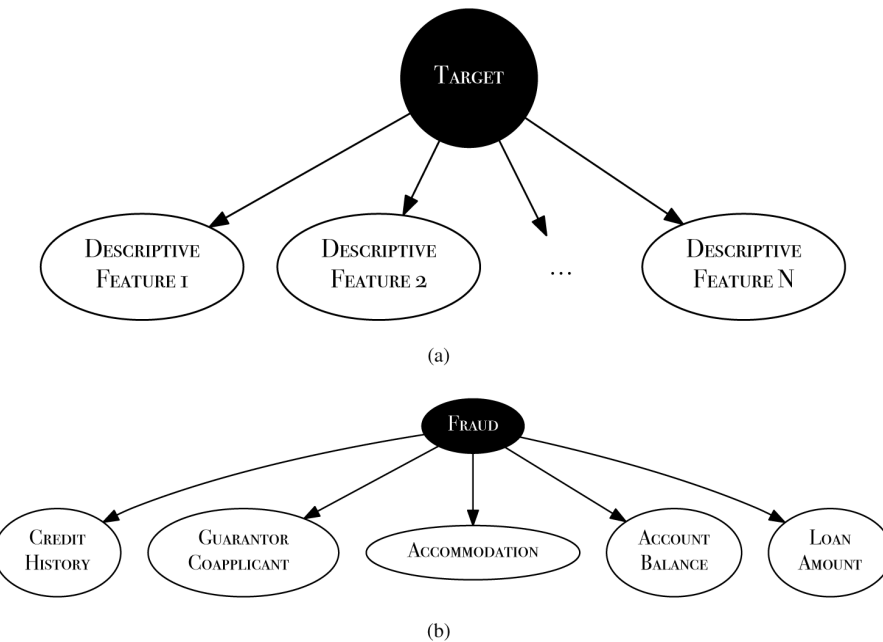


Figure 6.11

(a) A Bayesian network representation of the conditional independence asserted by a naive Bayes model between the descriptive features given knowledge of the target feature; and (b) a Bayesian network representation of the conditional independence assumption for the naive Bayes model in the fraud example.

When we computed a conditional probability for the target feature using a naive Bayes model, we used the following calculation:

$$P(t \mid \mathbf{d}[1], \dots, \mathbf{d}[n]) = P(t) \prod_{j \in \text{Children}(t)} P(\mathbf{d}[j] \mid t)$$

This equation is equivalent to Equation (6.19)^[288]. The fact that the probability $P(t)$ is an unconditional probability simply reflects the structure of the naive Bayes' network where the target feature has no parent nodes (see [Figure 6.11\(a\)](#)^[290]).

Computing a conditional probability for a node becomes more complex if the value of one or more of the parent nodes is unknown. In this situation the node becomes dependent on the ancestors of its unknown parent. This is because if a parent node is unknown, then to compute the distribution for the node, we must sum out this parent. However, to do this summing out, we must know the distribution for the unknown parent, which in turn requires us to sum out the parents of the parent, and so on if necessary. As a result of this recursive summing out, the distribution over a node is dependent on knowledge of the ancestors of any of its parent nodes.²² For example, in [Figure 6.9\(b\)](#)^[287], if the status of node C is not known, then node B becomes dependent on node D. For example, to compute $P(b \mid a, d)$ we would do the following calculations:

1. Compute the distribution for C given D: $P(c \mid d) = 0.2, P(\neg c \mid d) = 0.8$
2. Compute $P(b \mid a, C)$ by summing out C: $P(b \mid a, C) = \sum_i P(b \mid a, C_i)$

$$\begin{aligned} P(b \mid a, C) &= \sum_i P(b \mid a, C_i) = \sum_i \frac{P(b, a, C_i)}{P(a, C_i)} \\ &= \frac{(P(b \mid a, c) \times P(a) \times P(c)) + (P(b \mid a, \neg c) \times P(a) \times P(\neg c))}{(P(a) \times P(c)) + (P(a) \times P(\neg c))} \\ &= \frac{(0.2 \times 0.4 \times 0.2) + (0.5 \times 0.4 \times 0.8)}{(0.4 \times 0.2) + (0.4 \times 0.8)} = 0.44 \end{aligned}$$

This example illustrates the power of Bayesian networks. When complete knowledge of the state of all the nodes in the network is not available, we clamp the values of nodes that we do have knowledge of and sum out the unknown nodes. Furthermore, during these calculations, we only need to condition a node on its Markov blanket, which dramatically reduces the number of probabilities required by the network.

6.4.4.1 Building Bayesian networks Bayesian networks can be constructed by hand or learned from data. Learning both the topology of a Bayesian network and the parameters in the CPTs in the network is a difficult computational task. One of the things that makes learning the structure of a Bayesian network so difficult is that it is possible to define several different Bayesian networks as representations for the same full joint probability distribution. Consider, for example, a probability distribution for three binary features A, B, and C. The probability for a joint event in this domain $P(A,B,C)$ can be decomposed using the **chain rule** in the following way:

$$P(A, B, C) = P(C | A, B) \times P(B | A) \times P(A) \quad (6.20)$$

The chain rule, however, doesn't specify any constraints on which features in the domain we choose to condition on. We could just as easily have decomposed the probability of the joint event as follows:

$$P(A, B, C) = P(A | C, B) \times P(B | C) \times P(C) \quad (6.21)$$

Both of these decompositions are valid, and both define different Bayesian networks for the domain. [Figure 6.12\(a\)](#)^[291] illustrates the Bayesian network representing the decomposition defined in Equation [\(6.20\)](#)^[291], and [Figure 6.12\(b\)](#)^[291] illustrates the Bayesian network representing the decompositions defined in Equation [\(6.21\)](#)^[291].

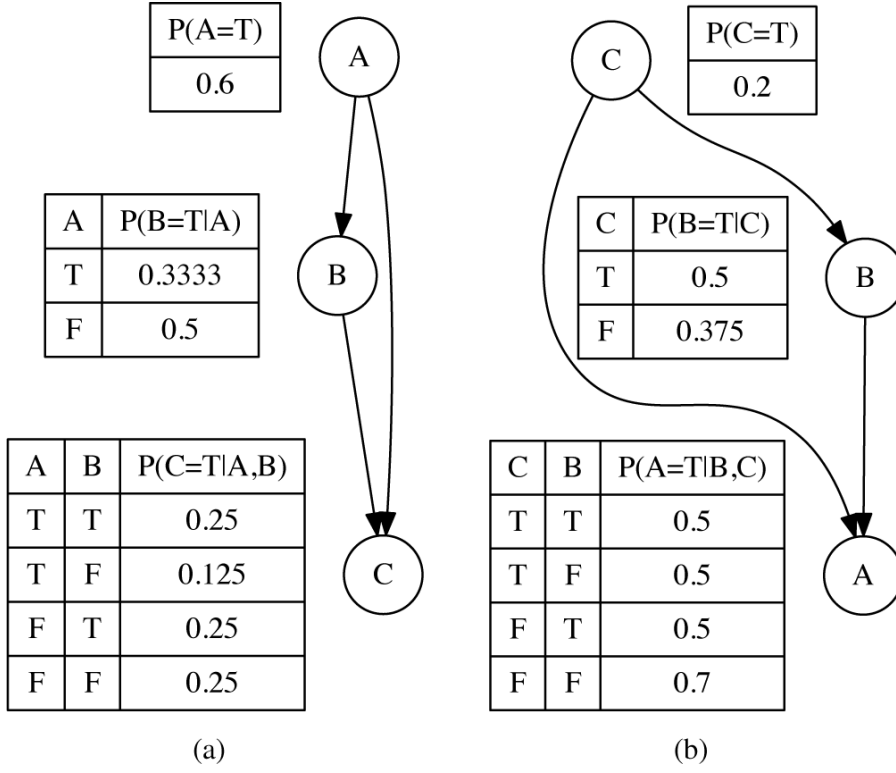


Figure 6.12

Two different Bayesian networks, each defining the same full joint probability distribution.

We can show that both of the networks in Figure 6.12^[291] represent the same joint probability by using each of them to calculate the probability of an arbitrarily chosen joint event from the domain. We should get the same probability for the joint event from both of the networks. For this example, we will calculate the probability of the event $\neg a, b, c$. Using the Bayesian network in Figure 6.12(a)^[291], we would carry out the calculation as follows:

$$\begin{aligned} P(\neg a, b, c) &= P(c | \neg a, b) \times P(b | \neg a) \times P(\neg a) \\ &= 0.25 \times 0.5 \times 0.4 = 0.05 \end{aligned}$$

Using the network in Figure 6.12(b)^[291], the calculation would be

$$\begin{aligned} P(\neg a, b, c) &= P(\neg a | c, b) \times P(b | c) \times P(c) \\ &= 0.5 \times 0.5 \times 0.2 = 0.05 \end{aligned}$$

Both networks return the same probability for the joint event. In fact, these networks will return identical probabilities for all events in this domain.

The basic approach to learning the structure of a Bayesian network is to use a local search algorithm that moves through the space of possible

networks and parameters, and searches for the network topology and CPT parameters that best fit with the data. To start the search, the algorithm is given a seed network and then iteratively adapts this network by adding, removing, or reversing links (and/or adding and removing hidden nodes), accompanied by iterations of parameter learning after each network structure adaptation. One of the difficulties with learning a network structure is that we can always improve the likelihood of the data given a network by simply adding new links into the network. Each time we add a link to a network, we increase the number of CPT entries in the network. The CPT entries are essentially parameters on the network, and the more parameters a network has, the greater its ability to fit (or overfit) the data. So, care must be taken to ensure that the objective function used by the search process avoids overfitting the data by simply creating a very highly connected graph. Consequently, the objective functions used by these algorithms are often based on the **minimum description length principle**, which asserts that the solution with the fewest parameters (shortest description) is the best one. We have already met the minimum description length principle in the more general form of **Occam's razor**. A popular metric used by these algorithms is the **Bayesian information criterion (BIC)**:

$$BIC(\mathcal{G}, D) = \log_e(P(D | \hat{P}, \mathcal{G})) - \left(\frac{d}{2} \times \log_e(n) \right) \quad (6.22)$$

where \mathcal{G} denotes the network graph, D is the training data, \hat{P} is the set of entries in the CPTs of \mathcal{G} , d is the number of parameters of \mathcal{G} (i.e., how many entries in the CPTs of \mathcal{G}), and n is the number of instances in D . This metric contains a term describing how well the model predicts the data $P(D|\hat{P}, \mathcal{G})$ as well as a term that punishes complex models $-(\frac{d}{2} \times \log_e(n))$. As such, it balances the search goals of model accuracy and simplicity. The term $P(D|\hat{P}, \mathcal{G})$ can be computed using metrics such as the **Bayesian score** or the **K2 score**.²³ The search space for these algorithms is exponential in the number of features. Consequently, developing algorithms to learn the structure of Bayesian networks is an ongoing research challenge.²⁴

It is much simpler to construct a Bayesian network using a hybrid approach, where the topology of the network is given to the learning

algorithm, and the learning task involves inducing the CPT entries from the data. This type of learning illustrates one of the real strengths of the Bayesian network framework, namely, that it provides an approach to learning that naturally accommodates human expert information. In this instance, the human expert specifies that topology of the network, and the learning algorithm induces the CPT entries for nodes in the topology in the same way that we computed the conditional probabilities for the naive Bayes model.²⁵

Given that there are multiple Bayesian networks for any domain, an obvious question to ask is, what is the best topological structure to give the algorithm as input? Ideally, we would like to use the network whose structure most accurately reflects the causal relationships in the domain. Specifically, if the value of one feature directly influences, or *causes*, the value taken by another feature, then this should be reflected in the structure of the graph by having a link from the cause feature to the effect feature. Bayesian networks whose topological structure correctly reflects the causal relationships between the features in a dataset are called **causal graphs**. There are two advantages to using a causal graph: (1) people find it relatively easy to think in terms of causal relationships, and as a result, networks that encode these relationships are relatively easy to understand; (2) often networks that reflect the causal structure of a domain are more compact in terms of the number of links between nodes and hence are more compact with respect to the number of CPT entries.

Table 6.18

Some socioeconomic data for a set of countries, and a version of the data after equal-frequency binning has been applied.

COUNTRY ID	Original Feature Values				Binned Feature Values			
	GINI COEF	SCHOOL YEARS	LIFE EXP	CPI	GINI COEF	SCHOOL YEARS	LIFE EXP	CPI
Afghanistan	27.82	0.40	59.61	1.52	low	low	low	low
Argentina	44.49	10.10	75.77	3.00	high	low	low	low
Australia	35.19	11.50	82.09	8.84	low	high	high	high
Brazil	54.69	7.20	73.12	3.77	high	low	low	low
Canada	32.56	14.20	80.99	8.67	low	high	high	high
China	42.06	6.40	74.87	3.64	high	low	low	low
Egypt	30.77	5.30	70.48	2.86	low	low	low	low
Germany	28.31	12.00	80.24	8.05	low	high	high	high
Haiti	59.21	3.40	45.00	1.80	high	low	low	low
Ireland	34.28	11.50	80.15	7.54	low	high	high	high
Israel	39.2	12.50	81.30	5.81	low	high	high	high
New Zealand	36.17	12.30	80.67	9.46	low	high	high	high
Nigeria	48.83	4.10	51.30	2.45	high	low	low	low
Russia	40.11	12.90	67.62	2.45	high	high	low	low
Singapore	42.48	6.10	81.788	9.17	high	low	high	high
South Africa	63.14	8.50	54.547	4.08	high	low	low	low
Sweden	25.00	12.80	81.43	9.30	low	high	high	high
UK	35.97	13.00	80.09	7.78	low	high	high	high
USA	40.81	13.70	78.51	7.14	high	high	high	high
Zimbabwe	50.10	6.7	53.684	2.23	high	low	low	low

We will use an example from **social science** to illustrate how to construct a causal graph using this hybrid approach. In this example, we will build a Bayesian network that enables us to predict the level of corruption in a country based on a number of macroeconomic and social descriptive features. [Table 6.18](#)^[295] lists some countries described using the following features:²⁶

- GINI COEF measures the equality in a society, where a larger Gini coefficient indicates a more unequal society.
- LIFE EXP measures life expectancy at birth.
- SCHOOL YEARS refers to the mean number of years spent in school for adult females.

- CPI is the **Corruption Perception Index (CPI)**, and it is the target feature. The CPI measures the perceived level of corruption in the public sector of a country and ranges from 0 (highly corrupt) to 100 (very clean).

The original feature values shown in [Table 6.18^{\[295\]}](#) are continuous, so we use the standard approach of converting them to categorical features using **equal-frequency binning**, with two bins for each feature: *low* and *high*. The columns labeled Binned Feature Values in [Table 6.18^{\[295\]}](#) show the data after it has been binned.

Once the data has been prepared, there are two stages to building the Bayesian network. First, we define the topology of the network. Second, we create the network CPTs. The topology of the network will be a causal graph that models this domain. In order to build this, we must have a theory of the causal relationships between the features in the domain. A potential causal theory between the features in this dataset is that

the more equal a society, the higher the investment that society will make in health and education, and this in turn results in a lower level of corruption

[Figure 6.13^{\[296\]}](#) illustrates a Bayesian network with a topology that encodes this causal theory. Equality directly affects both health and education, so there are directed arcs from GINI COEF to both LIFE EXP and SCHOOL YEARS. Health and education directly affect corruption, so there is a directed arc from LIFE EXP and from SCHOOL YEARS to CPI. To complete the network, we need to add the CPTs. To do this, we compute the required conditional probabilities from the binned data in [Table 6.18^{\[295\]}](#). The CPTs are shown in [Figure 6.13^{\[296\]}](#).

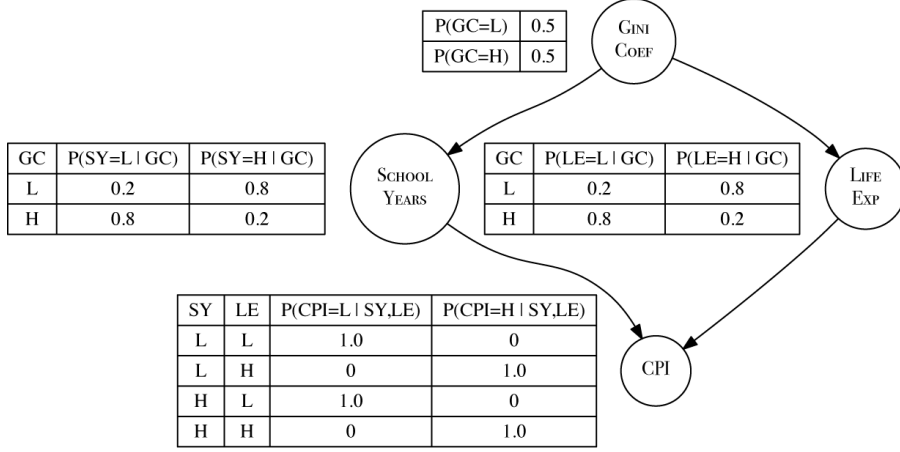


Figure 6.13

A Bayesian network that encodes the causal relationships between the features in the corruption domain. The CPT entries have been calculated using the binned data from Table 6.18^[295].

6.4.4.2 Using a Bayesian network to make predictions Once a network has been created, it is relatively straightforward to use to make a prediction. We simply compute the probability distribution for the target feature conditioned on the state of the descriptive features in the query and return the target feature level with the maximum a posteriori probability:

$$\text{M}(\mathbf{q}) = \arg \max_{l \in \text{levels}(t)} \text{BayesianNetwork}(t = l, \mathbf{q}) \quad (6.23)$$

where $\text{M}(\mathbf{q})$ is the prediction made by the model for the query \mathbf{q} , $\text{levels}(t)$ is the set of levels in the domain of the target feature t , and $\text{BayesianNetwork}(t = l, \mathbf{q})$ returns the probability computed by the network for the event $t = l$ given the evidence specified in the query \mathbf{q} .

For example, imagine we wanted to use the Bayesian network in Figure 6.13^[296] to predict the CPI for a country with the following profile:

GINI COEF = *low*, SCHOOL YEARS = *high*, LIFE EXP = *high*

Because both the parent nodes for CPI are known (SCHOOL YEARS and LIFE EXP), the probability distribution for CPI is independent of the GINI COEF feature. Therefore, we can read the relevant probability distribution for CPI directly from the CPT for the CPI node. From this CPT we can see that when SCHOOL YEARS = *high*, and LIFE EXP = *high*, then the most likely level is CPI = *high*. As a result, CPI = *high* is the MAP CPI value for this query,

and this is the prediction the model will return. In other words, countries that are relatively equal and that have good education and high life expectancy are likely to have a low level of corruption.

6.4.4.3 Making predictions with missing descriptive feature values

One real advantage of Bayesian networks over the other predictive model types that we discuss in this book is they provide an elegant solution to making predictions for a target feature when one or more of the descriptive feature values in a query instance are missing.²⁷ For example, we may wish to predict the CPI for a country with the following profile:

$$\text{GINI COEF} = \text{high}, \text{SCHOOL YEARS} = \text{high}$$

where the value of the LIFE EXP feature is unknown for the country. This means that in the network, one of the parents of the target feature node, CPI, is unknown. Consequently, we need to sum out this feature for each level of the target. We can calculate the probability for $\text{CPI} = \text{high}$ as follows:²⁸

$$\begin{aligned} P(\text{CPI} = \text{high} \mid \text{SY} = \text{high}, \text{GC} = \text{high}) \\ = \frac{P(\text{CPI} = \text{high}, \text{SY} = \text{high}, \text{GC} = \text{high})}{P(\text{SY} = \text{high}, \text{GC} = \text{high})} \\ = \frac{\sum_{i \in \{\text{high, low}\}} P(\text{CPI} = \text{high}, \text{SY} = \text{high}, \text{GC} = \text{high}, \text{LE} = i)}{P(\text{SY} = \text{high}, \text{GC} = \text{high})} \end{aligned}$$

We calculate the numerator in this term as follows:

$$\begin{aligned}
& \sum_{i \in \{\text{high, low}\}} P(\text{CPI} = \text{high}, \text{SY} = \text{high}, \text{GC} = \text{high}, \text{LE} = i) \\
&= \sum_{i \in \{\text{high, low}\}} \left(\begin{array}{l} P(\text{CPI} = \text{high} \mid \text{SY} = \text{high}, \text{LE} = i) \\ \times P(\text{SY} = \text{high} \mid \text{GC} = \text{high}) \\ \times P(\text{LE} = i \mid \text{GC} = \text{high}) \\ \times P(\text{GC} = \text{high}) \end{array} \right) \\
&= \left(P(\text{CPI} = \text{high} \mid \text{SY} = \text{high}, \text{LE} = \text{high}) \right. \\
&\quad \times P(\text{SY} = \text{high} \mid \text{GC} = \text{high}) \times P(\text{LE} = \text{high} \mid \text{GC} = \text{high}) \times P(\text{GC} = \text{high}) \Big) \\
&\quad + \left(P(\text{CPI} = \text{high} \mid \text{SY} = \text{high}, \text{LE} = \text{low}) \right. \\
&\quad \times P(\text{SY} = \text{high} \mid \text{GC} = \text{high}) \times P(\text{LE} = \text{low} \mid \text{GC} = \text{high}) \times P(\text{GC} = \text{high}) \Big) \\
&= (1.0 \times 0.2 \times 0.2 \times 0.5) + (0 \times 0.2 \times 0.8 \times 0.5) = 0.02
\end{aligned}$$

and denominator as:

$$\begin{aligned}
P(\text{SY} = \text{high}, \text{GC} = \text{high}) \\
&= P(\text{SY} = \text{high} \mid \text{GC} = \text{high}) \times P(\text{GC} = \text{high}) \\
&= 0.2 \times 0.5 = 0.1
\end{aligned}$$

We can now calculate the probability for $\text{CPI} = \text{high}$ as

$$P(\text{CPI} = \text{high} \mid \text{SY} = \text{high}, \text{GC} = \text{high}) = \frac{0.02}{0.1} = 0.2$$

We know from this result that the probability for $\text{CPI} = \text{low}$ must be 0.8. So, the network will predict $\text{CPI} = \text{low}$ as the MAP target value for the query. This tells us that an unequal society that has a good education system but for which we have no evidence about the health system is still likely to suffer from corruption.

These calculations make it apparent that even in this small example domain, the calculation of a probability becomes computationally complex very quickly, particularly when we need to sum out one or more features. The complexity of the calculations can be reduced by being careful with the positioning of features with respect to summations and by using dynamic programming techniques to avoid repeated computations. A well-known algorithm that focuses on this approach to reducing the complexity is the **variable elimination** algorithm (Zhang and Poole, 1994). However, even

using the variable elimination algorithm, calculating exact probabilities from a Bayesian network when descriptive feature values are missing is prohibitively complex.

Given the complexity of exact probabilistic inference for Bayesian networks, a popular alternative is to approximate the probability distribution required for a prediction using **Monte Carlo methods**.²⁹ Monte Carlo methods generate a large number of sample events and then use the relative frequency of an event in the set of generated samples as the approximation for the probability of that event in the real distribution. Monte Carlo methods work well in conjunction with Bayesian networks because a Bayesian network models the probability distribution over the features. More specifically, a Bayesian network can be viewed as defining a **Markov chain**. A Markov chain is a system that has a set of finite states and a set of transition probabilities that define the likelihood of the system moving from one state to another. When we view a Bayesian network as a Markov chain, a state is a complete assignment of values to all the nodes in the network (for example, GINI COEF = *high*, SCHOOL YEARS = *low*, LIFE EXP = *high*, CPI = *high* would be a state in the Markov chain defined by the network in [Figure 6.13](#)^[296]), and the CPTs of the network provide a distributed representation of the transition probabilities of the Markov chain. If the distribution used to generate the samples for a Monte Carlo method is a **Markov chain**, then the specific algorithms we use to implement this approach come from a family known as **Markov chain Monte Carlo (MCMC)** algorithms. **Gibbs sampling** is one of the best-known MCMC algorithms and is particularly suitable when we wish to generate probabilities that are conditioned on some evidence, so this is the algorithm we discuss in this section.

The Gibbs sampling algorithm initializes a Bayesian network by clamping the values of the evidence nodes and randomly assigning values to the non-evidence nodes. The algorithm then iteratively generates samples by changing the value of one of the non-evidence nodes. The selection of which non-evidence node to change can be random or follow a predefined list through which the algorithm iterates. The new value for the selected node is drawn from the distribution for the node (the CPT), conditioned on the current state of all the other nodes in the network. Each time a node is updated, a new sample state has been generated. More formally, for a

network with three nodes x_1, x_2, x_3 , using a predefined node selection order of $x_1, x_2, x_3, x_1, \dots$ and assuming that at iteration τ each node has the values $x_1^{(\tau)}, x_2^{(\tau)}, x_3^{(\tau)}$, the next four states generated will be

1. $\langle x_1^{(\tau+1)} \leftarrow P(x_1 | x_2^{(\tau)}, x_3^{(\tau)}), x_2^{(\tau)}, x_3^{(\tau)} \rangle$
2. $\langle x_1^{(\tau+1)}, x_2^{(\tau+2)} \leftarrow P(x_2 | x_1^{(\tau+1)}, x_3^{(\tau)}), x_3^{(\tau)} \rangle$
3. $\langle x_1^{(\tau+1)}, x_2^{(\tau+2)}, x_3^{(\tau+3)} \leftarrow P(x_3 | x_1^{(\tau+1)}, x_2^{(\tau+2)}) \rangle$
4. $\langle x_1^{(\tau+4)} \leftarrow P(x_1 | x_2^{(\tau+2)}, x_3^{(\tau+3)}), x_2^{(\tau+2)}, x_3^{(\tau+3)} \rangle$

There are three technical requirements that must hold for distribution of states generated from Gibbs sampling to converge with the distribution that we are sampling from—in this case, the distribution defined by the Bayesian network. The first is that the distribution we are sampling from must be a **stationary distribution** (also known as an **invariant distribution**). A stationary distribution is a distribution that doesn't change. The distribution defined by a Bayesian network doesn't change during Gibbs sampling, so this requirement always holds in this context. The second requirement is that the Markov chain used to generate the samples must be **ergodic**. A Markov chain is ergodic if every state is reachable from every other state and there are no cycles in the chain. The Markov chain defined by a Bayesian network is ergodic if there are no zero entries in any of the CPTs.³⁰ The third requirement is that the generated states should be independent of each other. As each generated state is a modified version of the preceding state, it is clear that successive states will be correlated with each other. So to obtain independent sample states, we often sub-sample from the sequence (sub-sampling in this way is also known as **thinning**). Once these three conditions hold (stationary distribution, ergodicity, and independent states), the samples generated will eventually converge with the distribution, and it is appropriate to use Gibbs sampling.

Because we start sampling from a random state, however, we do not know whether the initial state is an appropriate state from which to start generating samples. It may, for example, be a state that has a very low probability in the distribution. As a result, it is a good idea to run the network for a number of iterations before the generated states are recorded as samples. This **burn-in time** is to allow the Markov chain to settle into a state that is independent of the initial random state and that is a probable

state for the distribution we are sampling from. The time it takes for the Markov chain to forget the initial random state is called the **mixing time**. Unfortunately, estimating how long the burn-in should be is difficult. For some Markov chains, mixing may require only a few iterations, but for others, it may require hundreds or thousands of iterations. The topology of the network can provide some insight into this problem. Larger graphs will tend to have longer mixing times. Also, an evenly connected network typically has a relatively short mixing time (for the size of the graph). If, however, a graph is composed of a number of clusters connected via bottleneck nodes, this would typically indicate a longer mixing time. Another approach used to determine the appropriate burn-in time is to start several Markov chains with different initial states and wait until all the chains are generating states with similar distribution characteristics (mean state, mode state, etc.). When this happens, it indicates that all the chains are sampling from the same distribution and, hence, that it is likely that they have all forgotten their starting states. Once this happens, the target probability can be computed by calculating the relative frequency of the event within the selected subset of generated states.

Table 6.19

Examples of the samples generated using Gibbs sampling.

Sample Number	Gibbs Iteration	Feature Updated	GINI COEF	SCHOOL YEARS	LIFE EXP	CPI
1	37	CPI	high	high	high	low
2	44	LIFE EXP	high	high	high	low
3	51	CPI	high	high	high	low
4	58	LIFE EXP	high	high	low	high
5	65	CPI	high	high	high	low
6	72	LIFE EXP	high	high	high	low
7	79	CPI	high	high	low	high
8	86	LIFE EXP	high	high	low	low
9	93	CPI	high	high	high	low
10	100	LIFE EXP	high	high	high	low
11	107	CPI	high	high	low	high
12	114	LIFE EXP	high	high	high	low
13	121	CPI	high	high	high	low
14	128	LIFE EXP	high	high	high	low
15	135	CPI	high	high	high	low
16	142	LIFE EXP	high	high	low	low
...						

Table 6.19^[301] lists some of the samples generated using Gibbs sampling for the Bayesian network in [Figure 6.13](#)^[296] for the query

$$\text{GINI COEF} = \text{high}, \text{SCHOOL YEARS} = \text{high}$$

A burn-in of 30 iterations was used, and the samples were thinned by subsampling every 7th iteration. When the algorithm was used to generate 500 samples, the relative frequency of CPI = high was 0.196. When 2,000 samples were generated, the relative frequency rose to 0.1975. This rise in relative frequency illustrates that, as the number of samples generated increases, the resulting distribution approaches the actual distribution. Recall that when we did an exact calculation for this query the probability of CPI = high was 0.2.

We can make predictions using Gibbs sampling in the same way that we made predictions using exact probabilistic inference by predicting the target level with the maximum a posteriori probability:

$$\mathbb{M}(\mathbf{q}) = \arg \max_{l \in levels(t)} Gibbs(t = l, \mathbf{q}) \quad (6.24)$$

where $\mathbb{M}(\mathbf{q})$ is the prediction made by the model for the query \mathbf{q} , $levels(t)$ is the set of levels in the domain of the target feature t , and $Gibbs(t = l, \mathbf{q})$ returns the probability for the event $t = l$ given the evidence specified in the query \mathbf{q} using Gibbs sampling.

6.5 Summary

There are two ways to reason with probabilities forward and inverse. Forward probability reasons from causes to effects: if we know that a particular causal event has happened, then we increase the probability associated with the known effects that it causes. Inverse probability reasons from effects to causes: if we know that a particular event has occurred, then we can increase the probability that one or more of the events that could cause the observed event have also happened. Bayes' Theorem relates these two views of probability by using the notion of a prior probability. Put in subjective terms, Bayes' Theorem tells us that by modifying our initial beliefs about what has happened (our prior beliefs about the world) proportionally with how our observations relate to their potential causes (inverse probability), we can update our beliefs regarding what has happened to cause our observations (forward probability). Put more formally:

$$P(t | \mathbf{d}) = \frac{P(\mathbf{d} | t) \times P(t)}{P(\mathbf{d})} \quad (6.25)$$

The use of prior probabilities in Bayes' Theorem is what distinguishes between Bayesian and **maximum likelihood** approaches to probability.

Bayesian prediction is a very intuitive approach to predicting categorical targets. In order to make a prediction, we have to learn two things:

1. the probability of an instance having a particular set of descriptive feature values given that it has a particular target level $P(\mathbf{d} | t)$
2. the prior probability of that target level $P(t)$

Given these two pieces of information, we can compute the relative likelihood of a particular instance having a particular target level as

$$P(t \mid \mathbf{d}) = P(\mathbf{d} \mid t) \times P(t) \quad (6.26)$$

Once the relative likelihoods for each target level have been calculated, we simply return the maximum a posteriori (MAP) prediction.

The biggest challenge in creating a Bayesian prediction model is overcoming the exponential growth in the number of probabilities (model parameters) that are required as the dimensionality of the feature space increases. The standard approach to addressing this problem is to use the **independence** and **conditional independence** relationships between the features in a domain to **factorize** the **full joint distribution** of the domain. Factorizing the domain representation reduces the number of interactions between the features and reduces the number of model parameters.

A naive Bayes model addresses this problem by naively assuming that each of the descriptive features in a domain is conditionally independent of all the other descriptive features, given the state of the target feature. This assumption, although often wrong, enables the naive Bayes model to maximally factorize the representation that it uses of the domain—in other words, to use the smallest possible number of probabilities to represent the domain.

Surprisingly, given the naivete and strength of the assumption it depends upon, naive Bayes models often perform well. This is partly because naive Bayes models are able to make correct predictions even if the probabilities that they calculate are incorrect, so long as the error in the calculated probabilities does not affect the relative rankings of the different target levels. One consequence of this observation is that naive Bayes models are not really suitable for predicting continuous targets. When predicting a continuous target, every error in the calculation of a probability is reflected in reduced model performance.

The conditional independence assumption means that naive Bayes models use very few parameters to represent a domain. One consequence of this is that naive Bayes models can be trained using a relatively small dataset: with so few parameters and so few conditions on each parameter—only the state of the target feature—it is possible to make reasonable estimates for the parameters using a small dataset. Another benefit of the reduced representation of the model is that the behavior of the model is relatively easy to interpret. It is possible to look at the probabilities for each

descriptive feature and analyze how that value contributed to the final prediction. This information can be useful in informing the development of more powerful models later in a project. Consequently, a naive Bayes model is often a good model to begin with: it is easy to train and has the potential to provide both a baseline accuracy score and some insight into the problem structure. The major drawback of naive Bayes models is the inability of the model to handle the interactions between features.

Bayesian networks provide a more flexible representation for encoding the conditional independence assumptions between the features in a domain. Ideally, the topology of a network should reflect the causal relationships between the entities in a domain. Properly constructed Bayesian networks are relatively powerful models that can capture the interactions between descriptive features in determining a prediction. Although the task of inducing the optimal network structure from data is strictly intractable, algorithms that encode various assumptions exist that allow good models to be learned. Also, in domains where the causal relationships between features are known, Bayesian networks have the advantage of providing a natural framework for integrating expert human knowledge with data-driven induction. Bayesian networks have been successfully applied across a range of fields, including medical diagnosis, object recognition, and natural language understanding.

Several parallels can be drawn between probability-based learning and the other approaches to machine learning that we present in this book. Intuitively, the prior probability of a **nearest neighbor** model predicting a particular target level is simply the relative frequency of that target level in the dataset. For this reason, in general it is wrong to artificially balance the dataset used by a nearest neighbor model,³¹ and doing so biases the target level priors used by the model.

The relationship between probability-based and information-based learning is simply that the amount of information provided by an observation—such as a descriptive feature taking a particular value—is reflected in the difference between the prior and posterior probabilities caused by the observation. If the prior and posterior probabilities are similar, then the information content in the observation was low. If the prior and posterior probabilities are very different, then the information content in the observation was high.

Finally, it can be shown that, under some assumptions, any learning algorithm that minimizes the squared error of the model over the data will output a maximum likelihood prediction.³² The relevance of this finding is that it provides a probabilistic justification for the approach to learning we present in Chapter 7^[311].

6.6 Further Reading

McGrayne (2011) is an accessible book on the development and history of Bayes' Theorem. All data analysts should have at least one good textbook on statistics and probability. We would recommend either Montgomery and Runger (2010) or Tijms (2012) (or both). Jaynes (2003) deals with the use of probability theory in science and is a suitable text for postgraduate students.

Chapter 6 of Mitchell (1997) provides an excellent overview of Bayesian learning. Barber (2012) is a more recent machine learning textbook that adopts a Bayesian approach to learning and inference.

Judea Pearl is recognized as one of the key pioneers in developing the use of Bayesian networks in the field of **artificial intelligence**, and his books (Pearl, 1988, 2000) are accessible and provide good introductions to the theory and methods of Bayesian networks, as well as the more general field of **graphical models**. Neapolitan (2004) is a good textbook on Bayesian networks. Kollar and Friedman (2009) is a comprehensive text on the theory and methods of graphical models and is a good reference text for postgraduate students who are doing research using graphical models.

6.7 Exercises

1. (a) Three people flip a fair coin. What is the probability that exactly two of them will get heads?
(b) Twenty people flip a fair coin. What is the probability that exactly eight of them will get heads?
(c) Twenty people flip a fair coin. What is the probability that at least four of them will get heads?
2. The table below gives details of symptoms that patients presented and whether they were suffering from meningitis.

ID	HEADACHE	FEVER	VOMITING	MENINGITIS
1	true	true	false	false
2	false	true	false	false
3	true	false	true	false
4	true	false	true	false
5	false	true	false	true
6	true	false	true	false
7	true	false	true	false
8	true	false	true	true
9	false	true	false	false
10	true	false	true	true

Using this dataset, calculate the following probabilities:

- (a) $P(\text{VOMITING} = \text{true})$
- (b) $P(\text{HEADACHE} = \text{false})$
- (c) $P(\text{HEADACHE} = \text{true}, \text{VOMITING} = \text{false})$
- (d) $P(\text{VOMITING} = \text{false} | \text{HEADACHE} = \text{true})$
- (e) $P(\text{MENINGITIS} | \text{FEVER} = \text{true}, \text{VOMITING} = \text{false})$

3. Predictive data analytics models are often used as tools for process quality control and fault detection. The task in this question is to create a naive Bayes model to monitor a wastewater treatment plant.³³ The table below lists a dataset containing details of activities at a wastewater treatment plant for 14 days. Each day is described in terms of six descriptive features that are generated from different sensors at the plant. Ss-IN measures the solids coming into the plant per day; SED-IN measures the sediment coming into the plant per day; COND-IN measures the electrical conductivity of the water coming into the plant.³⁴ The features Ss-OUT, SED-OUT, and COND-OUT are the corresponding measurements for the water flowing out of the plant. The target feature, STATUS, reports the current situation at the plant: *ok*, everything is working correctly; *settler*, there is a problem with the plant settler equipment; or *solids*, there is a problem with the amount of solids going through the plant.

ID	Ss -IN	SED -IN	COND -IN	Ss -OUT	SED -OUT	COND -OUT	STATUS
1	168	3	1,814	15	0.001	1,879	ok
2	156	3	1,358	14	0.01	1,425	ok
3	176	3.5	2,200	16	0.005	2,140	ok
4	256	3	2,070	27	0.2	2,700	ok
5	230	5	1,410	131	3.5	1,575	settler
6	116	3	1,238	104	0.06	1,221	settler
7	242	7	1,315	104	0.01	1,434	settler
8	242	4.5	1,183	78	0.02	1,374	settler
9	174	2.5	1,110	73	1.5	1,256	settler
10	1,004	35	1,218	81	1,172	33.3	solids
11	1,228	46	1,889	82.4	1,932	43.1	solids
12	964	17	2,120	20	1,030	1,966	solids
13	2,008	32	1,257	13	1,038	1,289	solids

- (a) Create a naive Bayes model that uses probability density functions to model the descriptive features in this dataset (assume that all the descriptive features are normally distributed).
- (b) What prediction will the naive Bayes model return for the following query?

$$\text{SS-IN} = 222, \text{SED-IN} = 4.5, \text{COND-IN} = 1,518, \text{SS-OUT} = 74, \text{SED-OUT} = 0.25, \text{COND-OUT} = 1,642$$

4. The following is a description of the causal relationship between storms, the behavior of burglars and cats, and house alarms:

Stormy nights are rare. Burglary is also rare, and if it is a stormy night, burglars are likely to stay at home (burglars don't like going out in storms). Cats don't like storms either, and if there is a storm, they like to go inside. The alarm on your house is designed to be triggered if a burglar breaks into your house, but sometimes it can be set off by your cat coming into the house, and sometimes it might not be triggered even if a burglar breaks in (it could be faulty or the burglar might be very good).

- (a) Define the topology of a Bayesian network that encodes these causal relationships.
- (b) The table below lists a set of instances from the house alarm domain. Using the data in this table, create the conditional probability tables (CPTs) for the network you created in Part (a) of this question.

ID	STORM	BURGLAR	CAT	ALARM
1	false	false	false	false
2	false	false	false	false
3	false	false	false	false
4	false	false	false	false
5	false	false	false	true
6	false	false	true	false
7	false	true	false	false
8	false	true	false	true
9	false	true	true	true
10	true	false	true	true
11	true	false	true	false
12	true	false	true	false
13	true	true	false	true

- (c) What value will the Bayesian network predict for ALARM, given that there is both a burglar and a cat in the house but there is no storm?
- (d) What value will the Bayesian network predict for ALARM, given that there is a storm but we don't know if a burglar has broken in or where the cat is?
- * 5. The table below lists a dataset containing details of policyholders at an insurance company. The descriptive features included in the table describe each policy holders' ID, occupation, gender, age, type of insurance policy, and preferred contact channel. The preferred contact channel is the target feature in this domain.

ID	OCCUPATION	GENDER	AGE	POLICY TYPE	PREF CHANNEL
1	lab tech	female	43	planC	email
2	farmhand	female	57	planA	phone
3	biophysicist	male	21	planA	email
4	Sheriff	female	47	planB	phone
5	painter	male	55	planC	phone
6	manager	male	19	planA	email
7	geologist	male	49	planC	phone
8	messenger	male	51	planB	email
9	nurse	female	18	planC	phone

- (a) Using **equal-frequency binning**, transform the AGE feature into a categorical feature with three levels: *young, middle-aged, mature*.

- (b) Examine the descriptive features in the dataset and list the features that you would exclude before you would use the dataset to build a predictive model. For each feature you decide to exclude, explain why you have made this decision.
- (c) Calculate the probabilities required by a **naive Bayes model** to represent this domain.
- (d) What target level will a **naive Bayes model** predict for the following query:

GENDER = *female*, AGE = 30, POLICY = *planA*

- * 6. Imagine that you have been given a dataset of 1,000 documents that have been classified as being about *entertainment* or *education*. There are 700 *entertainment* documents in the dataset and 300 *education* documents in the dataset. The tables below give the number of documents from each topic that a selection of words occurred in.

Word-document counts for the <i>entertainment</i> dataset					
fun	is	machine	christmas	family	learning
415	695	35	0	400	70
Word-document counts for the <i>education</i> dataset					
fun	is	machine	christmas	family	learning
200	295	120	0	10	105

- (a) What target level will a **naive Bayes model** predict for the following query document: “*machine learning is fun*”?
- (b) What target level will a **naive Bayes model** predict for the following query document: “*christmas family fun*”?
- (c) What target level will a **naive Bayes model** predict for the query document in Part (b) of this question, if **Laplace smoothing** with $k = 10$ and a vocabulary size of 6 is used?
- * 7. A **naive Bayes model** is being used to predict whether patients have a high risk of stroke in the next five years (*STROKE=true*) or a low risk of stroke in the next five years (*STROKE=false*). This model uses two continuous descriptive features *AGE* and *WEIGHT* (in kilograms). Both of these descriptive features are represented by probability density

functions, specifically normal distributions. The table below shows the representation of the domain used by this model.

$P(Stroke = true) = 0.25$	$P(Stroke = false) = 0.75$
$P(AGE = x Stroke = true)$ $\approx N \left(\begin{array}{l} x, \\ \mu = 65, \\ \sigma = 15 \end{array} \right)$	$P(AGE = x Stroke = false)$ $\approx N \left(\begin{array}{l} x, \\ \mu = 20, \\ \sigma = 15 \end{array} \right)$
$P(WEIGHT = x Stroke = true)$ $\approx N \left(\begin{array}{l} x, \\ \mu = 88, \\ \sigma = 8 \end{array} \right)$	$P(WEIGHT = x Stroke = false)$ $\approx N \left(\begin{array}{l} x, \\ \mu = 76, \\ \sigma = 6 \end{array} \right)$

- (a) What target level will the **naive Bayes model** predict for the following query:

$$AGE = 45, WEIGHT = 80$$

- * 8. The table below lists a dataset of books and whether or not they were purchased by an individual (i.e., the feature PURCHASED is the target feature in this domain).

ID	SECONDHAND	GENRE	COST	PURCHASED
1	false	romance	expensive	true
2	false	science	cheap	false
3	true	romance	cheap	true
4	false	science	cheap	true
5	false	science	expensive	false
6	true	romance	reasonable	false
7	true	literature	cheap	false
8	false	romance	reasonable	false
9	frue	science	cheap	false
10	true	literature	reasonable	true

- (a) Calculate the probabilities (to four places of decimal) that a **naive Bayes** classifier would use to represent this domain.
- (b) Assuming conditional independence between features given the target feature value, calculate the **probability** (rounded to four places of decimal) of each outcome (PURCHASED=true, and PURCHASED=false) for the following book:

$$\text{SECONDHAND=false, GENRE=literature, COST=expensive}$$

- (c) What prediction would a **naive Bayes** classifier return for the above book?
- * 9. The following is a description of the causal relationship between storms, the behavior of burglars and cats, and house alarms:

Jim and Martha always go shopping separately. If Jim does the shopping he buys wine, but not always. If Martha does the shopping, she buys wine, but not always. If Jim tells Martha that he has done the shopping, then Martha doesn't go shopping, but sometimes Jim forgets to tell Martha, and so sometimes both Jim and Martha go shopping.

- (a) Define the topology of a Bayesian network that encodes these causal relationships between the following Boolean variables: JIM (Jim has done the shopping, *true* or *false*), MARTHA (Martha has done the shopping, *true* or *false*), WINE (wine has been purchased, *true* or *false*).
- (b) The table below lists a set of instances from the house alarm domain. Using the data in this table, create the conditional probability tables (CPTs) for the network you created in the first part of this question, and round the probabilities to two places of decimal.

ID	JIM	MARTHA	WINE
1	false	false	false
2	false	false	false
3	true	false	true
4	true	false	true
5	true	false	false
6	false	true	true
7	false	true	false
8	false	true	false
9	true	true	true
10	true	true	true
11	true	true	true
12	true	true	false

- (c) What value will the Bayesian network predict for WINE if:

$\text{JIM}=\text{true}$ and $\text{MARTHA}=\text{false}$

- (d) What is the probability that JIM went shopping given that $\text{WINE}=\text{true}$?

1. It is appropriate to use a game involving gambling to introduce probability-based machine learning. The origins of probability theory come from attempts to understand gambling and games of chance, in particular, the work of Gerolamo Cardano and the later work of Pierre de Fermat and Blaise Pascal.

2. This data has been artificially generated for this example.

3. To save space, throughout this chapter, named features are denoted by the uppercase initial letters of their names (e.g., the MENINGITIS feature is denoted M). If a named feature is binary, we use either the lowercase initial letter of the feature name to denote that the feature is *true* or the lowercase initial letter preceded by the \neg symbol to denote that it is *false* (e.g., m denotes MENINGITIS = *true*, and $\neg m$ denotes MENINGITIS = *false*).

4. Bayes' Theorem is named after the Reverend Thomas Bayes, who wrote an essay that described how to update beliefs as new information arises. After Thomas Bayes died, this essay was edited and published by the Reverend Richard Price (Bayes and Price, 1763). The modern mathematical form of Bayes' Theorem, however, was developed by Simon Pierre Laplace.

5. The **Theorem of Total Probability** is explained in detail in Section B.3^[762] of Appendix B^[757].

6. Famously, an experiment in which doctors were asked this question about the probability of the patient's having the disease showed that most of them got this question wrong (Casscells et al., 1978).

7. The **product rule** is explained in detail in Section B.3^[762] of Appendix B^[757].

8. That is, a and $b = b$ and a .

9. The probability **chain rule** is explained in detail in Section B.3^[762] of Appendix B^[757].

10. The **paradox of the false positive** states that in order to make predictions about a rare event, the model has to be at least as accurate as the event is rare (i.e., the probability of the model making an error has to be less than the probability of the rare event occurring) or there is a significant chance of **false positive** predictions (i.e., predicting the event when it is not the case). Doctorow (2010) provides an interesting discussion of this phenomenon.

11. The MAP prediction is the prediction mechanism that we assume throughout this book. An alternative mechanism is the **Bayesian optimal classifier**, but we won't discuss it in this text. See Mitchell (1997) for more details.

12. During the European Soccer Championships in 2008 and the 2010 Soccer World Cup, an octopus in Germany, called Paul, was attributed with achieving an 85% success rate at predicting the results of the matches involving Germany. Paul's impressive accuracy should not be taken to suggest that octopus behavior affects soccer matches but rather that independent events may be correlated, at least for an interval of time, without the events actually being dependent. As the oft-quoted maxim states: correlation does not imply causation! (See Section 3.5.2^[81] for further discussion.)

13. One consequence of this, however, is that a naive Bayes model is not a good approach for predicting a continuous target, because errors in calculating posterior probabilities do directly affect the accuracy of the model. This is the only modeling approach covered in this book for which we will not present a way to predict both continuous and categorical target features.

14. Recall that **sparse data**, discussed in Section 5.4.5^[211], refers to datasets where the majority of descriptive features have a value of zero.

15. The primary reason why we apply smoothing is to remove zero probabilities from a model's representation of a domain, and in the vast majority of cases, all the unconditional target level probabilities will be non-zero (because there will be at least one instance with each target level in the training data). Even in cases where one of the target levels is very rare, it may not be appropriate to

smooth the target level priors. See Bishop (2006, pp. 45) for a discussion on how to train a probability-based prediction model in situations where one of the target levels is rare.

16. See Tijms (2012), or any good probability textbook, for an introduction to the gamma function.

17. The student-*t* distribution can be defined in a number of ways. For example, it can be defined so that it takes only one parameter, degrees of freedom. In this text we use the extended location-scale definition.

18. This guided search process is similar to the **gradient descent** search we use to fit our regression models in Chapter 7^[311]. Many data analytics packages and programming APIs provide functions that implement methods to fit a distribution to a dataset.

19. Taleb (2008) discusses the problems that arise when analysts use normal distributions to model social and economic features, where the assumptions regarding light tails don't hold.

20. For example, the R language provides the *fitdistr()* method, as part of the MASS package, that implements a maximum-likelihood fitting of a number of univariate distributions to a given dataset.

21. We can do this either by consulting a probability table or by using **integration** to calculate the area under the curve within the bounds of the interval. There are many excellent statistical textbooks that explain how to do both of these, for example, Montgomery and Runger (2010).

22. The conditional independence relationship between any two nodes in a Bayesian network can be specified using the framework of **d-separation** (the “d” stands for *directed*) (Pearl, 1988). We don't discuss d-separation in this book as it is not required for our discussion.

23. The K2 score is named after the K2 algorithm, one of the earliest and best-known algorithms for learning Bayesian networks (Cooper and Herskovits, 1992).

24. See Kollar and Friedman (2009) for a discussion of algorithms that seek to address this research challenge.

25. In some cases we may not have data for all the features; and in these instances, the standard approach to learning the CPT entries is to use a gradient descent approach (similar to the one we introduce in Chapter 7^[311]), where the objective function of the local search algorithm is simply how well the product of the induced conditional probabilities match the relative frequency of each joint event in the data. In other words, we choose the set of conditional probabilities that maximize the likelihood of the training data.

26. The data listed in this table is real. The Gini coefficient data is for 2013 (or the most recent year prior to 2013 for which the data was available for a country) and was retrieved from the World Bank (data.worldbank.org/indicator/SI.POV.GINI); the life expectancy and mean years in school data was retrieved from Gapminder (www.gapminder.org) and is for 2010/11 (or the most recent year prior to 2010/11 for which the data was available for a country); and the mean years in school were originally sourced from the Institute for Health Metrics and Evaluation (www.healthdata.org). The Corruption Perception Index is for 2011 and was retrieved from Transparency International (www.transparency.org).

27. The most common way to achieve this for the other model types covered in this book is to **impute** the missing values in the query instance using one of the techniques described in Section 3.4.1^[69].

28. In the following calculations we have abbreviated feature names as follows: GC = GINI COEF, LE = LIFE EXP, and SY = SCHOOL YEARS.

29. Monte Carlo methods are named after the Mediterranean principality that is famous for its casino.

30. If there are one or more zero entries in the CPTs, then the Markov chain may still be ergodic, but it is non-trivial to prove ergodicity in these cases.

31. See Davies (2005, pp. 693–696).
32. See Mitchell (1997, pp. 164–167).
33. The dataset in this question is inspired by the Waste Water Treatment Dataset that is available from the UCI Machine Learning repository (Bache and Lichman, 2013) at archive.ics.uci.edu/ml/machine-learning-databases/water-treatment. The creators of this dataset reported their work in Bejar et al. (1991).
34. The conductivity of water is affected by inorganic dissolved solids and organic compounds, such as oil. Consequently, water conductivity is a useful measure of water purity.

7

Error-Based Learning

“Ever tried. Ever failed. No matter. Try again. Fail again. Fail better.”

—Samuel Beckett

In error-based machine learning, we perform a search for a set of parameters for a parameterized model that minimizes the total error across the predictions made by that model with respect to a set of training instances. The Fundamentals section of this chapter introduces the key ideas of a **parameterized model**, measuring **error**, and an **error surface**. We then present the standard approach to building error-based predictive models: **multivariable linear regression with gradient descent**. The extensions and variations to this standard approach that we describe are how to handle categorical descriptive features, the use of **logistic regression** to make predictions for categorical target features, fine-tuning regression models, techniques for building **non-linear** and **multinomial** models, and **support vector machines**, which take a slightly different approach to using error to build prediction models.

7.1 Big Idea

Anyone who has learned a new sport will have had the sometimes painful experience of taking an error-based approach to learning. Take surfing, for example. One of the key skills the novice surfer has to learn is how to successfully *catch a wave*. This involves floating on your surfboard until a wave approaches and then paddling furiously to gain enough momentum for the wave to pick up both you and your board. The position of your body on the board is key to doing this successfully. If you lie too far toward the back of the board, the board will sink and create so much drag that even big

waves will pass by, leaving you behind. If you lie too far forward on your board, you will begin to make great progress before the surfboard tilts nose down into the water and launches you head over heels into the air. Only when you are positioned at the *sweet spot* in the middle of the board—neither too far forward nor too far back—will you be able to use your paddling efforts to successfully catch a wave.

At their first attempt, new surfers will typically position themselves either too far forward or too far backward on their board when they attempt to catch their first wave, resulting in a bad outcome. The outcome of an attempt to catch a wave is a judgment on how well the surfer is doing, so an attempt constitutes an error function: lying too far back on the board leads to a medium error, lying too far forward on the board leads to a more dramatic error, while successfully catching a wave means really no error at all. Armed with the unsuccessful outcome of their first attempt, surfers usually overcompensate on the second attempt, resulting in the opposite problem. On subsequent attempts, surfers will slowly reduce their error by slightly adjusting their position until they home in on the *sweet spot* at which they can keep their board perfectly balanced to allow a seamless transition to *tickling the face of an awesome toob!*

A family of error-based machine learning algorithms takes the same approach. A parameterized prediction model is initialized with a set of random parameters, and an error function is used to judge how well this initial model performs when making predictions for instances in a training dataset. Based on the value of the error function, the parameters are iteratively adjusted to create a more and more accurate model.

7.2 Fundamentals

In this section we introduce a simple model of linear regression, some metrics for measuring the error of a model, and the concept of an error surface. The discussion in this section, and in the rest of this chapter, assumes that you have a basic understanding of differentiation, in particular, what a derivative is, how to calculate a derivative for a continuous function, the chain rule for differentiation, and what a partial derivative is. If you don’t understand any of these concepts, see Appendix C^[765] for the necessary introduction.

7.2.1 Simple Linear Regression

Table 7.1^[313] shows a simple dataset recording the rental price (in Euro per month) of Dublin city-center offices (RENTAL PRICE), along with a number of descriptive features that are likely to be related to rental price: the SIZE of the office (in square feet), the FLOOR in the building in which the office space is located, the BROADBAND rate available at the office (in Mb per second), and the ENERGY RATING of the building in which the office space is located (ratings range from A to C, where A is the most efficient). Over the course of this chapter, we look at the ways in which all these descriptive features can be used to train an error-based model to predict office rental prices. Initially, though, we will focus on a simplified version of this task in which just SIZE is used to predict RENTAL PRICE.

Table 7.1

A dataset that includes office rental prices and a number of descriptive features for 10 Dublin city-center offices.

ID	SIZE	FLOOR	BROADBAND RATE	ENERGY RATING	RENTAL PRICE
1	500	4	8	C	320
2	550	7	50	A	380
3	620	9	7	A	400
4	630	5	24	B	390
5	665	8	100	C	385
6	700	4	8	B	410
7	770	10	7	B	480
8	880	12	50	A	600
9	920	14	8	C	570
10	1,000	9	24	B	620

Figure 7.1(a)^[314] shows a scatter plot of the office rentals dataset with RENTAL PRICE on the vertical (or y) axis and SIZE on the horizontal (or x) axis. From this plot, it is clear that there is a strong linear relationship between these two features: as SIZE increases so does RENTAL PRICE by a similar amount. If we could capture this relationship in a model, we would be able to do two important things. First, we would be able to understand how office size affects office rental price. Second, we would be able to fill

in the gaps in the dataset to predict office rental prices for office sizes that we have never actually seen in the historical data—for example, how much would we expect a 730-square-foot office to rent for? Both of these things would be of great use to real estate agents trying to make decisions about the rental prices they should set for new rental properties.

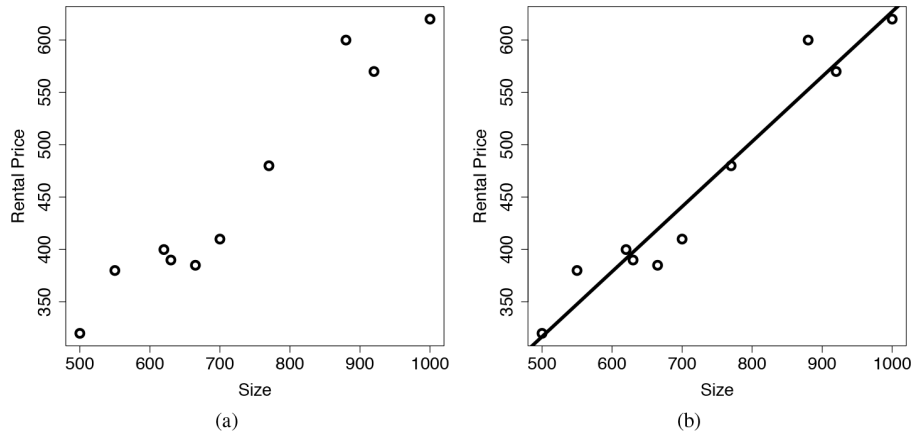


Figure 7.1

(a) A scatter plot of the SIZE and RENTAL PRICE features from the office rentals dataset; and (b) the scatter plot from (a) with a linear model relating RENTAL PRICE to SIZE overlaid.

There is a simple, well-known mathematical model that can capture the relationship between two continuous features like those in our dataset. Many readers will remember from high school geometry that the **equation of a line** can be written

$$y = mx + b \quad (7.1)$$

where m is the slope of the line, and b is known as the y -intercept of the line (i.e., the position at which the line meets the vertical axis when the value of x is set to zero). The equation of a line predicts a y value for every x value given the slope and the y -intercept, and we can use this simple model to capture the relationship between two features such as SIZE and RENTAL PRICE. Figure 7.1(b)^[314] shows the same scatter plot as shown in Figure 7.1(a)^[314] with a simple linear model added to capture the relationship between office sizes and office rental prices. This model is

$$\text{RENTAL PRICE} = 6.47 + 0.62 \times \text{SIZE} \quad (7.2)$$

where the slope of the line is 0.62 and the y -intercept is 6.47.

This model tells us that for every increase of a square foot in SIZE, RENTAL PRICE increases by 0.62 Euro. We can also use this model to determine the expected rental price of the 730-square-foot office mentioned previously by simply plugging this value for SIZE into the model

$$\begin{aligned}\text{RENTAL PRICE} &= 6.47 + 0.62 \times 730 \\ &= 459.07\end{aligned}$$

Hence, we can expect our 730-square-foot office to rent for about 460 Euro per month. This kind of model is known as a **simple linear regression model**. This approach to modeling the relationships between features is extremely common in both machine learning and statistics.

For consistency with the notation that we use in this book, we can rewrite the simple linear regression model

$$M_w(\mathbf{d}) = w[0] + w[1] \times d[1] \quad (7.3)$$

where w is the vector $\langle w[0], w[1] \rangle$; the parameters $w[0]$ and $w[1]$ are referred to as weights;¹ d is an instance defined by a single descriptive feature $d[1]$; and $M_w(d)$ is the prediction output by the model for the instance d . The key to using simple linear regression models is determining the optimal values for the weights in the model. The optimal values for the weights are the ones that allow the model to best capture the relationship between the descriptive features and a target feature. A set of weights that capture this relationship well are said to **fit** the training data. In order to find the optimal set of weights, we need some way to measure how well a model defined using a candidate set of weights fits a training dataset. We do this by defining an **error function** to measure the error between the predictions a model makes on the basis of the descriptive features for each instance in the training data and the actual target values for each instance in the training data.

7.2.2 Measuring Error

The model shown in Equation (7.2)^[313] is defined by the weights $w[0] = 6.47$ and $w[1] = 0.62$. What tells us that these weights suitably capture the relationship within the training dataset? Figure 7.2(a)^[316] shows a scatter

plot of the SIZE and RENTAL PRICE descriptive features from the office rentals dataset and a number of different simple linear regression models that might be used to capture this relationship. In these models the value for $w[0]$ is kept constant at 6.47, and the values for $w[1]$ are set to 0.4, 0.5, 0.62, 0.7, and 0.8 from top to bottom. Out of the candidate models shown, the third model from the top (with $w[1]$ set to 0.62), passes most closely through the actual dataset and is the one that most accurately fits the relationship between office sizes and office rental prices—but how do we measure this formally?

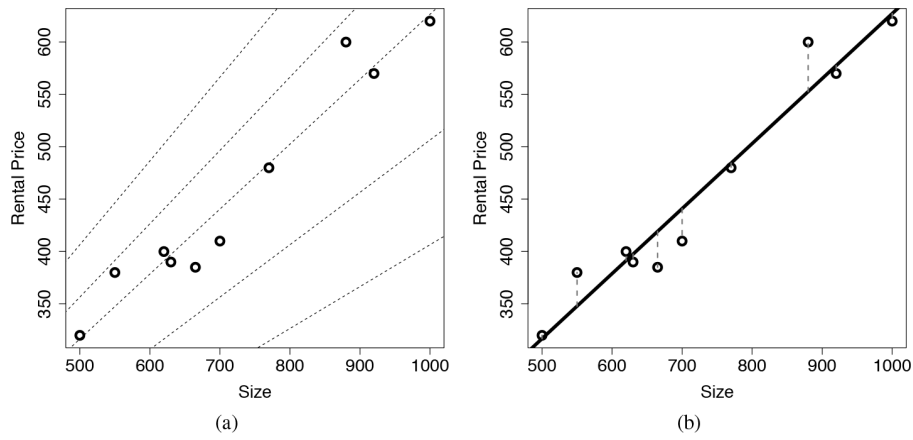


Figure 7.2

(a) A scatter plot of the SIZE and RENTAL PRICE features from the office rentals dataset. A collection of possible simple linear regression models capturing the relationship between these two features are also shown. For all models $w[0]$ is set to 6.47. From top to bottom, the models use 0.4, 0.5, 0.62, 0.7, and 0.8, respectively, for $w[1]$. (b) A scatter plot of the SIZE and RENTAL PRICE features from the office rentals dataset showing a candidate prediction model (with $w[0] = 6.47$ and $w[1] = 0.62$) and the resulting errors.

In order to formally measure the fit of a linear regression model with a set of training data, we require an **error function**. An error function captures the error between the predictions made by a model and the actual values in a training dataset.² There are many different kinds of error functions, but for measuring the fit of simple linear regression models, the most commonly used is the **sum of squared errors** error function, or L_2 . To calculate L_2 we use our candidate model \mathbb{M}_w to make a prediction for each member of the training dataset, \mathcal{D} , and then calculate the error (or **residual**) between these predictions and the actual target feature values in the training set.

[Figure 7.2\(b\)](#)^[316] shows the office rentals dataset and the candidate model with $\mathbf{w}[0] = 6.47$ and $\mathbf{w}[1] = 0.62$ and also includes error bars to highlight the differences between the predictions made by the model and the actual RENTAL PRICE values in the training data. Notice that the model sometimes overestimates the office rental price, and sometimes underestimates the office rental price. This means that some of the errors will be positive and some will be negative. If we were to simply add these together, the positive and negative errors would effectively cancel each other out. This is why, rather than just using the sum of the errors, we use the sum of the *squared* errors because this means all values will be positive.

The sum of squared errors error function, L_2 , is formally defined as

$$L_2(\mathbb{M}_{\mathbf{w}}, \mathcal{D}) = \frac{1}{2} \sum_{i=1}^n (t_i - \mathbb{M}_{\mathbf{w}}(\mathbf{d}_i))^2 \quad (7.4)$$

where the training set is composed of n training instances; each training instance is composed of descriptive features \mathbf{d} and a target feature t ; $\mathbb{M}_{\mathbf{w}}(\mathbf{d}_i)$ is the prediction made by a candidate model $\mathbb{M}_{\mathbf{w}}$ for a training instance with descriptive features \mathbf{d}_i ; and the candidate model $\mathbb{M}_{\mathbf{w}}$ is defined by the weight vector \mathbf{w} . For our simple scenario in which each instance is described with a single descriptive feature, Equation (7.4)^[316] expands to

$$L_2(\mathbb{M}_{\mathbf{w}}, \mathcal{D}) = \frac{1}{2} \sum_{i=1}^n (t_i - (\mathbf{w}[0] + \mathbf{w}[1] \times \mathbf{d}_i[1]))^2 \quad (7.5)$$

[Table 7.2](#)^[317] shows the calculation of the sum of squared errors for the candidate model with $\mathbf{w}[0] = 6.47$ and $\mathbf{w}[1] = 0.62$. In this case, the sum of squared errors is equal to 2,837.08.

Table 7.2

Calculating the sum of squared errors for the candidate model (with $w[0] = 6.47$ and $w[1] = 0.62$) to make predictions for the office rentals dataset.

ID	SIZE	RENTAL PRICE	Model		Squared Error
			Prediction	Error	
1	500	320	316.47	3.53	12.46
2	550	380	347.47	32.53	1,058.20
3	620	400	390.87	9.13	83.36
4	630	390	397.07	-7.07	49.98
5	665	385	418.77	-33.77	1,140.41
6	700	410	440.47	-30.47	928.42
7	770	480	483.87	-3.87	14.98
8	880	600	552.07	47.93	2,297.28
9	920	570	576.87	-6.87	47.20
10	1,000	620	626.47	-6.47	41.86
				Sum	5,674.15
				Sum of squared errors (Sum/2)	2,837.08

If we perform the same calculation for the other candidate models shown in [Figure 7.2\(a\)](#)^[316], we find that with $w[1]$ set to 0.4, 0.5, 0.7, and 0.8, the sums of squared errors are 136,218, 42,712, 20,092, and 90,978 respectively. The fact that the sums of squared errors for these models are larger than for the model with $w[1]$ set to 0.62 demonstrates that our previous visual intuition that this model most accurately fits the training data was correct.

The sum of squared errors function can be used to measure how well any combination of weights fits the instances in a training dataset. The next section explains how the values of an error function for many different potential models can be combined to form an error surface across which we can search for the optimal weights with the minimum sum of squared errors.³

7.2.3 Error Surfaces

For every possible combination of weights, $w[0]$ and $w[1]$, there is a corresponding sum of squared errors value. We can think about all these error values joined to make a surface defined by the weight combinations,

as shown in [Figure 7.3\(a\)](#)^[318]. Here, each pair of weights $\mathbf{w}[0]$ and $\mathbf{w}[1]$ defines a point on the x - y plane, and the sum of squared errors for the model using these weights determines the height of the error surface above the x - y plane for that pair of weights. The x - y plane is known as a **weight space**, and the surface is known as an **error surface**. The model that best fits the training data is the model corresponding to the lowest point on the error surface.

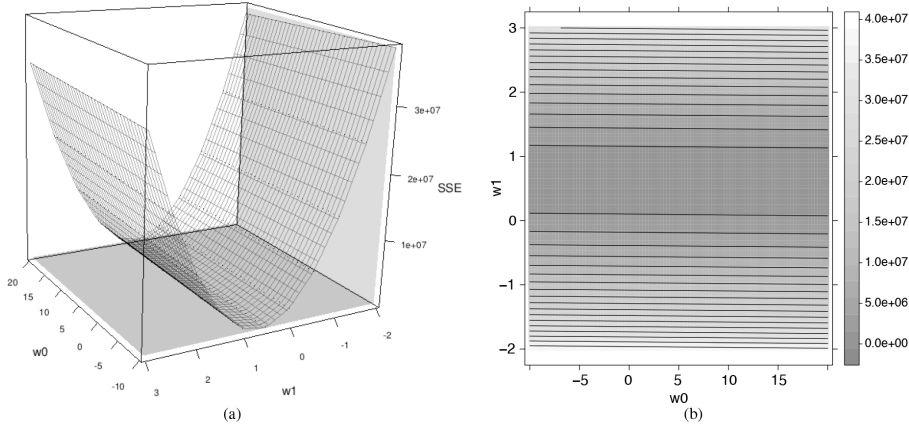


Figure 7.3

(a) A 3D surface plot and (b) a bird's-eye view contour plot of the error surface generated by plotting the sum of squared errors for the office rentals training set for each possible combination of values for $\mathbf{w}[0]$ (from the range $[-10, 20]$) and $\mathbf{w}[1]$ (from the range $[-2, 3]$).

Although for some simple problems, like those presented in our office rentals dataset, it is possible to try out every reasonable combination of weights and through this **brute-force search** find the best combination, for most real-world problems this is not feasible—the computation required would take far too long. Instead, we need a more efficient way to find the best combination of weights. Fortunately, for prediction problems like those posed by the office rentals dataset, the associated error surfaces have two properties that help us find the optimal combination of weights: they are **convex**, and they have a **global minimum**. By convex we mean that the error surfaces are shaped like a bowl. Having a global minimum means that on an error surface, there is a unique set of optimal weights with the lowest sum of squared errors. The reason why the error surface always has these properties is that its overall shape is determined by the linearity of the model, rather than the properties of the data. If we can find the global

minimum of the error surface, we can find the set of weights defining the model that best fits the training dataset. This approach to finding weights is known as **least squares optimization**.

Because we can expect the error surface to be convex and possess a global minimum, we can find the optimal weights at the point where the **partial derivatives** of the error surface with respect to $\mathbf{w}[0]$ and $\mathbf{w}[1]$ are equal to 0. The partial derivatives of the error surface with respect to $\mathbf{w}[0]$ and $\mathbf{w}[1]$ measure the slope of the error surface at the point $\mathbf{w}[0]$ and $\mathbf{w}[1]$. The point on the error surface at which the partial derivatives with respect to $\mathbf{w}[0]$ and $\mathbf{w}[1]$ are equal to 0 is simply the point at the very bottom of the bowl defined by the error surface—there is no slope at the bottom of the bowl. This point is at the **global minimum** of the error surface, and the coordinates of this point define the weights for the prediction model with the lowest sum of squared errors on the dataset. Using Equation (7.5)^[316], we can formally define this point on the error surface as the point at which

$$\frac{\partial}{\partial \mathbf{w}[0]} \frac{1}{2} \sum_{i=1}^n (t_i - (\mathbf{w}[0] + \mathbf{w}[1] \times \mathbf{d}_i[1]))^2 = 0 \quad (7.6)$$

and

$$\frac{\partial}{\partial \mathbf{w}[1]} \frac{1}{2} \sum_{i=1}^n (t_i - (\mathbf{w}[0] + \mathbf{w}[1] \times \mathbf{d}_i[1]))^2 = 0 \quad (7.7)$$

There are a number of different ways to find this point. In this chapter we describe a **guided search** approach known as the **gradient descent** algorithm. This is one of the most important algorithms in machine learning and, as we discuss in other chapters, can be used for many different purposes. The next section describes how gradient descent can be used to find the optimal weights for linear regression models that handle multiple descriptive features: **multivariable linear regression** models.

7.3 Standard Approach: Multivariable Linear Regression with Gradient Descent

The most common approach to error-based machine learning for predictive analytics is to use **multivariable linear regression** with **gradient descent**

to train a best-fit model for a given training dataset. This section explains how this works. First, we describe how we extend the simple linear regression model described in the previous section to handle multiple descriptive features, and then we describe the gradient descent algorithm.

7.3.1 Multivariable Linear Regression

The simple linear regression model we looked at in Section 7.2.1^[312] handled only a single descriptive feature. Interesting problems in predictive analytics, however, are multivariable⁴ in nature. Fortunately, extending the simple linear regression model to a multivariable linear regression model is straightforward. We can define a multivariable linear regression model as

$$\begin{aligned}\mathbb{M}_{\mathbf{w}}(\mathbf{d}) &= \mathbf{w}[0] + \mathbf{w}[1] \times \mathbf{d}[1] + \cdots + \mathbf{w}[m] \times \mathbf{d}[m] \\ &= \mathbf{w}[0] + \sum_{j=1}^m \mathbf{w}[j] \times \mathbf{d}[j]\end{aligned}\tag{7.8}$$

where \mathbf{d} is a vector of m descriptive features, $\mathbf{d}[1] \dots \mathbf{d}[m]$, and $\mathbf{w}[0] \dots \mathbf{w}[m]$ are $(m + 1)$ weights. We can make Equation (7.8)^[320] look a little neater by inventing a dummy descriptive feature, $\mathbf{d}[0]$, that is always equal to 1. This then gives us

$$\begin{aligned}\mathbb{M}_{\mathbf{w}}(\mathbf{d}) &= \mathbf{w}[0] \times \mathbf{d}[0] + \mathbf{w}[1] \times \mathbf{d}[1] + \cdots + \mathbf{w}[m] \times \mathbf{d}[m] \\ &= \sum_{j=0}^m \mathbf{w}[j] \times \mathbf{d}[j] \\ &= \mathbf{w} \cdot \mathbf{d}\end{aligned}\tag{7.9}$$

where $\mathbf{w} \cdot \mathbf{d}$ is the **dot product** of the vectors \mathbf{w} and \mathbf{d} . The dot product of two vectors is the sum of the products of their corresponding elements.

The expansion of the sum of squared errors loss function, L_2 , that we gave in Equation (7.5)^[316] changes slightly to reflect the new regression equation

$$\begin{aligned}L_2(\mathbb{M}_{\mathbf{w}}, \mathcal{D}) &= \frac{1}{2} \sum_{i=1}^n (t_i - \mathbb{M}_{\mathbf{w}}(\mathbf{d}_i))^2 \\ &= \frac{1}{2} \sum_{i=1}^n (t_i - (\mathbf{w} \cdot \mathbf{d}_i))^2\end{aligned}\tag{7.10}$$

where the training dataset is composed of n training instances (\mathbf{d}_i, t_i) ; $\mathbb{M}_w(\mathbf{d}_i)$ is the prediction made by a model \mathbb{M}_w for a training instance with descriptive features \mathbf{d}_i ; and the model \mathbb{M}_w is defined by the weight vector w .

This multivariable model allows us to include all but one of the descriptive features in [Table 7.2](#)^[317] in a regression model to predict office rental prices (we will see how to include the categorical ENERGY RATING in the model in [Section 7.4.3](#)^[336]). The resulting multivariable regression model equation is

$$\begin{aligned} \text{RENTAL PRICE} = & w[0] + w[1] \times \text{SIZE} + w[2] \times \text{FLOOR} \\ & + w[3] \times \text{BROADBAND RATE} \end{aligned}$$

We will see in the next section how the best-fit set of weights for this equation are found, but for now we will set $w[0] = -0.1513$, $w[1] = 0.6270$, $w[2] = -0.1781$, and $w[3] = 0.0714$. This means that the model is rewritten

$$\begin{aligned} \text{RENTAL PRICE} = & -0.1513 + 0.6270 \times \text{SIZE} - 0.1781 \times \text{FLOOR} \\ & + 0.0714 \times \text{BROADBAND RATE} \end{aligned}$$

Using this model, we can, for example, predict the expected rental price of a 690-square-foot office on the 11th floor of a building with a broadband rate of 50 Mb per second

$$\begin{aligned} \text{RENTAL PRICE} &= -0.1513 + 0.6270 \times 690 - 0.1781 \times 11 + 0.0714 \times 50 \\ &= 434.0896 \end{aligned}$$

The next section describes how the weights can be determined using the gradient descent algorithm.

7.3.2 Gradient Descent

In [Section 7.2.3](#)^[317] we said that the best-fit set of weights for a linear regression model can be found at the global minimum of the error surface defined by the weight space associated with the relevant training dataset. We also mentioned that this global minimum can be found at the point at which the partial derivatives of the error surface, with respect to the weights, are equal to zero. Although it is possible to calculate this point directly for some simpler problems, this approach is not computationally feasible for most interesting predictive analytics problems. The number of instances in the training set and the number of weights for which we need to

find values simply make the problem too large. The brute-force search approach that was mentioned in Section 7.2.3^[317] is not feasible either—especially as the number of descriptive features, and subsequently the number of weights, increases.

There is, however, a simple approach to learning weights that we can take based on the facts that, even though they are hard to visualize, the error surfaces that correspond to these high-dimensional weight spaces still have the convex shape seen in Figure 7.3^[318] (albeit in multiple dimensions), and that a single global minimum exists. This approach uses a guided search from a random starting position and is known as **gradient descent**.

To understand how gradient descent works, imagine a hiker unlucky enough to be stranded on the side of a valley on a foggy day. Because of the dense fog, it is not possible for her to see the way to her destination at the bottom of the valley. Instead, it is only possible to see the ground at her feet to within about a three-foot radius. It might, at first, seem like all is lost and that it will be impossible for the hiker to find her way down to the bottom of the valley. There is, however, a reliable approach that the hiker can take that will guide her to the bottom (assuming, somewhat ideally, that the valley is *convex* and has a *global minimum*). If the hiker looks at the slope of the ground at her feet, she will notice that in some directions, the ground slopes up, and in other directions, the ground slopes down. If she takes a small step in the direction in which the ground slopes most steeply downward (the direction of the gradient of the mountain), she will be headed toward the bottom of the mountain. If she repeats this process over and over again, she will make steady progress down the mountain until eventually she arrives at the bottom. Gradient descent works in exactly the same way.

Gradient descent starts by selecting a random point within the weight space (i.e., each weight in the multivariable linear regression equation is assigned a random value within some sensible range) and calculating the sum of squared errors associated with this point based on predictions made for each instance in the training set using the randomly selected weights (as shown in Section 7.2.2^[315]). This defines one point on the error surface. Although the error value at this point in the weight space can be calculated, we know little else about the relative position of this point on the error surface. Just like our imagined mountain climber, the algorithm can use

only very localized information. It is possible, however, to determine the slope of the error surface by determining the derivative of the function used to generate it, and then calculating the value of this derivative at the random point selected in the weight space. This means that, again like our mountain climber, the gradient descent algorithm can use the direction of the slope of the error surface at the current location in the weight space. Taking advantage of this information, the randomly selected weights are adjusted slightly in the direction of the error surface gradient to move to a new position on the error surface. Because the adjustments are made in the direction of the error surface gradient, this new point will be closer to the overall global minimum. This adjustment is repeated over and over until the global minimum on the error surface is reached. [Figure 7.4](#)^[323] shows an error surface (defined over just two weights so that we can visualize the error surface) and some examples of the path down this surface that the gradient descent algorithm would take from different random starting positions.⁵

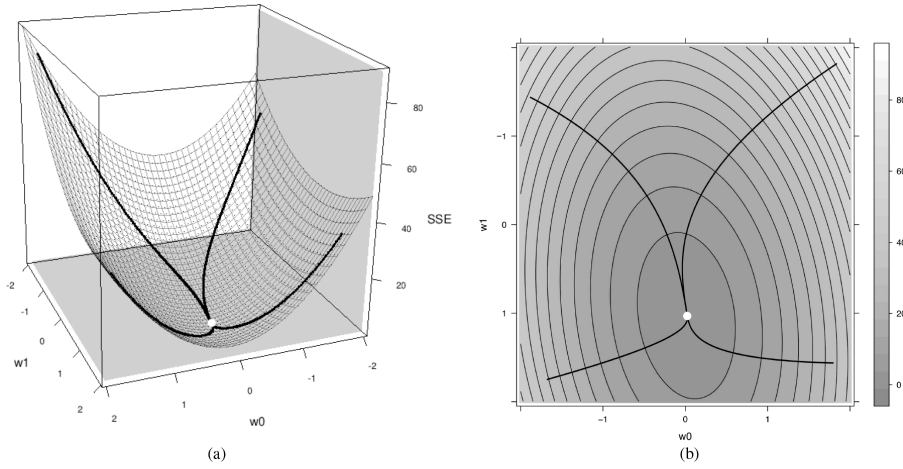


Figure 7.4

(a) A 3D plot of an error surface and (b) a bird's-eye view contour plot of the same error surface. The lines indicate the path that the gradient descent algorithm would take across this error surface from four different starting positions to the global minimum—marked as the white dot in the center.

For the simple version of the office rentals example that uses only the SIZE descriptive feature, described in Section 7.2.1^[312], it is easy to visualize how the gradient descent algorithm would move iteratively toward a model that best fits the training data, making small adjustments each time—with each adjustment reducing the error of the model, just as our surfer from

Section 7.1^[311] did. [Figure 7.5](#)^[324] shows the journey across the error surface that is taken by the gradient descent algorithm when training this model. [Figure 7.6](#)^[325] shows a series of snapshots of the candidate models created at steps along this journey toward the best-fit model for this dataset. Notice how the model gets closer and closer to a model that accurately captures the relationship between SIZE and RENTAL PRICE. This is also apparent in the final panel in [Figure 7.6](#)^[325], which shows how the sum of squared errors decreases as the model becomes more accurate.

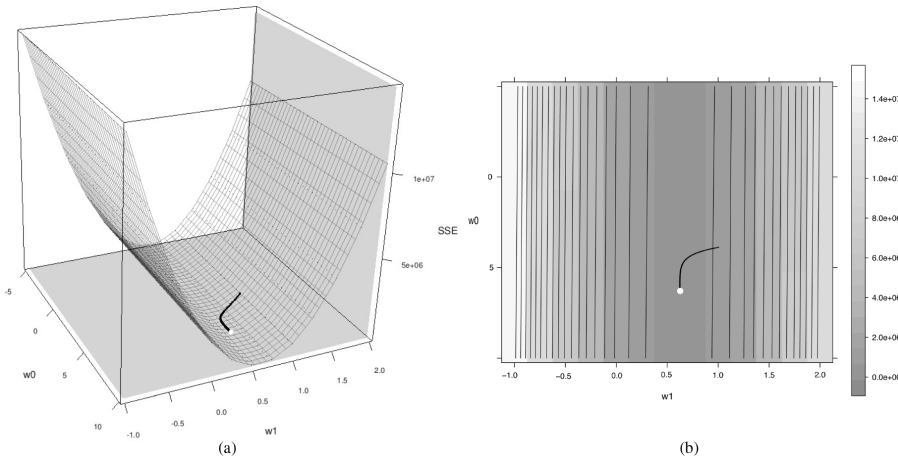


Figure 7.5

(a) A 3D surface plot and (b) a bird's-eye view contour plot of the error surface for the office rentals dataset showing the path that the gradient descent algorithm takes toward the best-fit model.

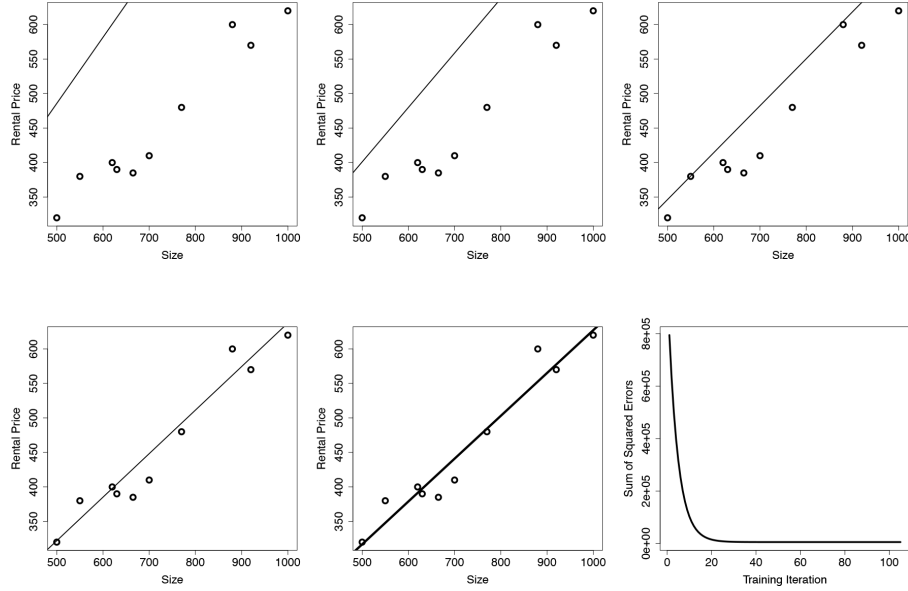


Figure 7.6

A selection of the simple linear regression models developed during the gradient descent process for the office rentals dataset. The bottom-right panel shows the sums of squared errors generated during the gradient descent process.

The gradient descent algorithm for training multivariable regression models is formally presented in Algorithm 4^[326]. Each weight is iteratively adjusted by a small amount based on the error in the predictions made by the current candidate model so as to generate subsequently more and more accurate candidate models. Eventually, the algorithm will converge to a point on the error surface where any subsequent changes to weights do not lead to a noticeably better model (within some tolerance). At this point we can expect the algorithm to have found the global minimum of the error surface and, as a result, the most accurate predictive model possible.

The most important part to the gradient descent algorithm is the line on which the weights are updated, Line 4^[326]. Each weight is considered independently, and for each one a small adjustment is made by adding a small value, called a **delta value**, to the current weight, $w[j]$. This adjustment should ensure that the change in the weight leads to a move *downward* on the error surface. The **learning rate**, α , determines the size of the adjustments made to weights at each iteration of the algorithm and is discussed further in Section 7.3.3^[328].

The remainder of this section focuses on the error delta function, which calculates the delta value that determines the direction (either positive or

negative) and the magnitude of the adjustments made to each weight. The direction and magnitude of the adjustment to be made to a weight is determined by the gradient of the error surface at the current position in the weight space. Recalling that the error surface is defined by the error function, L_2 (given in Equation (7.10)^[320]), the gradient at any point on this error surface is given by the value of the partial derivative of the error function with respect to a particular weight at that point. The error delta function invoked on Line 4^[326] of Algorithm 4^[326] performs this calculation to determine the delta value by which each weight should be adjusted.

To understand how to calculate the value of the partial derivative of the error function with respect to a particular weight, let us imagine for a moment that our training dataset, \mathcal{D} , contains just one training instance: (\mathbf{d}, t) , where \mathbf{d} is a set of descriptive features and t is a target feature. The gradient of the error surface is given as the partial derivative of L_2 with respect to each weight, $\mathbf{w}[j]$

$$\frac{\partial}{\partial \mathbf{w}[j]} L_2(\mathbb{M}_{\mathbf{w}}, \mathcal{D}) = \frac{\partial}{\partial \mathbf{w}[j]} \left(\frac{1}{2} (t - \mathbb{M}_{\mathbf{w}}(\mathbf{d}))^2 \right) \quad (7.11)$$

$$= (t - \mathbb{M}_{\mathbf{w}}(\mathbf{d})) \times \frac{\partial}{\partial \mathbf{w}[j]} (t - \mathbb{M}_{\mathbf{w}}(\mathbf{d})) \quad (7.12)$$

$$= (t - \mathbb{M}_{\mathbf{w}}(\mathbf{d})) \times \frac{\partial}{\partial \mathbf{w}[j]} (t - (\mathbf{w} \cdot \mathbf{d})) \quad (7.13)$$

$$= (t - \mathbb{M}_{\mathbf{w}}(\mathbf{d})) \times -\mathbf{d}[j] \quad (7.14)$$

Equation (7.12)^[324] is calculated from Equation (7.11)^[324] by applying the differentiation **chain rule**.⁶ To understand the move from Equation (7.13)^[324] to Equation (7.14)^[324], imagine a problem with four descriptive features $\mathbf{d}[1] \dots \mathbf{d}[4]$. Remembering that we always include the dummy feature $\mathbf{d}[0]$ with a value of 1, the dot product $\mathbf{w} \cdot \mathbf{d}$ becomes

$$\begin{aligned} \mathbf{w} \cdot \mathbf{d} &= \mathbf{w}[0] \times \mathbf{d}[0] + \mathbf{w}[1] \times \mathbf{d}[1] + \mathbf{w}[2] \times \mathbf{d}[2] \\ &\quad + \mathbf{w}[3] \times \mathbf{d}[3] + \mathbf{w}[4] \times \mathbf{d}[4] \end{aligned}$$

Algorithm 4 The gradient descent algorithm for training multivariable linear regression models.

Require: set of training instances \mathcal{D}

Require: a learning rate α that controls how quickly the algorithm converges

Require: a function, $errorDelta$, that determines the direction in which to adjust a given weight, $\mathbf{w}[j]$, so as to move down the slope of an error surface determined by the dataset, \mathcal{D}

Require: a convergence criterion that indicates that the algorithm has completed

1: $\mathbf{w} \leftarrow$ random starting point in the weight space

2: **repeat**

3: **for** each $\mathbf{w}[j]$ in \mathbf{w} **do**

4: $\mathbf{w}[j] \leftarrow \mathbf{w}[j] + \alpha \times errorDelta(\mathcal{D}, \mathbf{w}[j])$

5: **end for**

6: **until** convergence occurs

If we take the partial derivative of this with respect to $\mathbf{w}[0]$, all the terms that do not contain $\mathbf{w}[0]$ are treated as constants, so

$$\begin{aligned}\frac{\partial}{\partial \mathbf{w}[0]} \mathbf{w} \cdot \mathbf{d} &= \frac{\partial}{\partial \mathbf{w}[0]} (\mathbf{w}[0] \times \mathbf{d}[0] + \mathbf{w}[1] \times \mathbf{d}[1] + \mathbf{w}[2] \times \mathbf{d}[2] \\ &\quad + \mathbf{w}[3] \times \mathbf{d}[3] + \mathbf{w}[4] \times \mathbf{d}[4]) \\ &= \mathbf{d}[0] + 0 + 0 + 0 = \mathbf{d}[0]\end{aligned}$$

Similarly, the partial derivative with respect to $\mathbf{w}[4]$ is

$$\begin{aligned}\frac{\partial}{\partial \mathbf{w}[4]} \mathbf{w} \cdot \mathbf{d} &= \frac{\partial}{\partial \mathbf{w}[4]} (\mathbf{w}[0] \times \mathbf{d}[0] + \mathbf{w}[1] \times \mathbf{d}[1] + \mathbf{w}[2] \times \mathbf{d}[2] \\ &\quad + \mathbf{w}[3] \times \mathbf{d}[3] + \mathbf{w}[4] \times \mathbf{d}[4]) \\ &= 0 + 0 + 0 + 0 + \mathbf{d}[4] = \mathbf{d}[4]\end{aligned}$$

So, in the move between Equations (7.13)^[324] and (7.14)^[324], $\frac{\partial}{\partial \mathbf{w}[j]} (t - (\mathbf{w} \cdot \mathbf{d}))$ becomes $-\mathbf{d}[j]$ (remember that in this equation, t is a constant and so becomes zero when differentiated).

Equation (7.14)^[324] calculates the gradient based only on a single training instance. To take into account multiple training instances, we calculate the sum of the squared errors for each training instance (as we did in all our previous examples). So, Equation (7.14)^[324] becomes

$$\frac{\partial}{\partial \mathbf{w}[j]} L_2(\mathbb{M}_{\mathbf{w}}, \mathcal{D}) = \sum_{i=1}^n ((t_i - \mathbb{M}_{\mathbf{w}}(\mathbf{d}_i)) \times -\mathbf{d}_i[j]) \quad (7.15)$$

where $(\mathbf{d}_1, t_1) \dots (\mathbf{d}_n, t_n)$ are n training instances, and $d_i[j]$ is the j^{th} descriptive feature of training instance (\mathbf{d}_i, t_i) . The direction of the gradient calculated using this equation is toward the highest values on the error surface. The error delta function from Line 4^[326] of Algorithm 4^[326] should return a small step toward a lower value on the error surface. Therefore, we move in the opposite direction of the calculated gradient, and the error delta function can be written

$$\begin{aligned} \text{errorDelta}(\mathcal{D}, \mathbf{w}[j]) &= -\frac{\partial}{\partial \mathbf{w}[j]} L_2(\mathbb{M}_{\mathbf{w}}, \mathcal{D}) \\ &= \sum_{i=1}^n ((t_i - \mathbb{M}_{\mathbf{w}}(\mathbf{d}_i)) \times \mathbf{d}_i[j]) \end{aligned} \quad (7.16)$$

Line 4^[326] of Algorithm 4^[326] can therefore be rewritten as what is known as the weight update rule for multivariable linear regression with gradient descent

$$\mathbf{w}[j] \leftarrow \mathbf{w}[j] + \alpha \times \underbrace{\sum_{i=1}^n ((t_i - \mathbb{M}_{\mathbf{w}}(\mathbf{d}_i)) \times \mathbf{d}_i[j])}_{\text{errorDelta}(\mathcal{D}, \mathbf{w}[j])} \quad (7.17)$$

where $\mathbf{w}[j]$ is any weight, α is a constant learning rate, t_i is the expected target feature value for the i^{th} training instance, $\mathbb{M}_{\mathbf{w}}(\mathbf{d}_i)$ is the prediction made for this training instance by the current candidate model defined by the weight vector \mathbf{w} , and $\mathbf{d}_i[j]$ is the j^{th} descriptive feature of the i^{th} training instance and corresponds with weight $\mathbf{w}[j]$ in the regression model.

To intuitively understand the weight update rule given in Equation (7.17)^[327], it helps to think in terms of what the weight update rule does to weights based on the error in the predictions made by the current candidate model:

- If the errors show that, in general, predictions made by the candidate model are too high, then $\mathbf{w}[j]$ should be decreased if $\mathbf{d}_i[j]$ is positive and increased if $\mathbf{d}_i[j]$ is negative.

- If the errors show that, in general, predictions made by the candidate model are too low, then $w[j]$ should be increased if $d_i[j]$ is positive and decreased if $d_i[j]$ is negative.

The approach to training multivariable linear regression models described so far is more specifically known as **batch gradient descent**. The word **batch** is used because only one adjustment is made to each weight at each iteration of the algorithm based on summing the squared error made by the candidate model for each instance in the training dataset.⁷ Batch gradient descent is a straightforward, accurate, and reasonably efficient approach to training multivariable linear regression models and is used widely in practice. The inductive bias encoded in this algorithm includes a preference bias to prefer models that minimize the sum of squared errors function and a restriction bias introduced by the facts that we consider only linear combinations of descriptive features and that we take a single path through the error gradient from a random starting point.

7.3.3 Choosing Learning Rates and Initial Weights

The values chosen for the learning rate and initial weights can have a significant impact on how the gradient descent algorithm proceeds. Unfortunately, there are no theoretical results that help in choosing the optimal values for these parameters. Instead, these algorithm parameters must be chosen using rules of thumb gathered through experience.

The learning rate, α , in the gradient descent algorithm determines the size of the adjustment made to each weight at each step in the process. We can illustrate this using the simplified version of the RENTAL PRICE prediction problem based only on office size (SIZE). A linear regression model for the problem uses only two weights, $w[0]$ and $w[1]$. Figure 7.7^[329] shows how different learning rates—0.002, 0.08, and 0.18—result in very different journeys across the error surface.⁸ The changing sum of squared errors that result from these journeys are also shown.

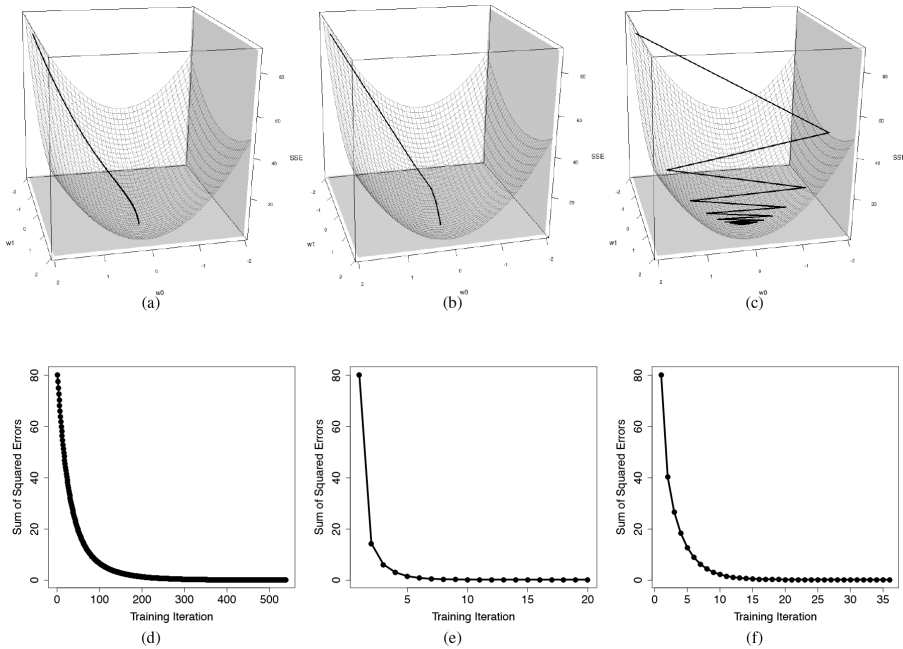


Figure 7.7

Plots of the journeys made across the error surface for the simple office rentals prediction problem for different learning rates: (a) a very small learning rate (0.002); (b) a medium learning rate (0.08); and (c) a very large learning rate (0.18). The changing sum of squared errors are also shown.

Figure 7.7(a)^[329] shows the impact of a very small learning rate. Although the gradient descent algorithm will converge to the global minimum eventually, it takes a very long time as tiny changes are made to the weights at each iteration of the algorithm. Figure 7.7(c)^[329] shows the impact of a large learning rate. The large adjustments made to the weights during gradient descent cause it to jump completely from one side of the error surface to the other. Although the algorithm can still converge toward an area of the error surface close to the global minimum, there is a strong chance that the global minimum itself will be missed, and the algorithm will simply jump back and forth across it. In fact, if inappropriately large learning rates are used, the jumps from one side of the error surface to the other can cause the sum of squared errors to repeatedly increase rather than decrease, leading to a process that will never converge. Figure 7.7(b)^[329] shows that a well-chosen learning rate strikes a good balance, converging quickly but also ensuring that the global minimum is reached. Note that even though the shape of the curve in Figure 7.7(e)^[329] is similar to the shape in Figure 7.7(d)^[329], it takes far fewer iterations to reach the global minimum.

Unfortunately, choosing learning rates is not a well-defined science. Although there are some algorithmic approaches, most practitioners use rules of thumb and trial and error. A typical range for learning rates is [0.000001, 10], and practitioners will usually try out higher values and observe the resulting learning graph. If the graph looks too much like [Figure 7.7\(f\)](#)^[329], a smaller value will be tested until something approaching [Figure 7.7\(e\)](#)^[329] is found.

When the gradient descent algorithm is used to find optimal weights for linear regression models, the initial weights are chosen randomly from a predefined range that must be specified as an input to the algorithm. The choice of the range from which these initial weights are selected affects how quickly the gradient descent algorithm will converge to a solution. Unfortunately, as is the case with the learning rate, there are no well-established, proven methods for choosing initial weights. Normalization also has a part to play here. It is much easier to select initial weights for normalized feature values than for raw feature values, as the range in which weights for normalized feature values might reasonably fall (particularly for the intercept weight, $w[0]$) is much better defined than the corresponding range when raw feature values are used. The best advice we can give is that, based on empirical evidence, choosing random initial weights uniformly from the range $[-0.2, 0.2]$ tends to work well.

7.3.4 A Worked Example

We are now in a position to build a linear regression model that uses all the continuous descriptive features in the office rentals dataset in [Table 7.1](#)^[313] (i.e., all features except for ENERGY RATING). The general structure of the model is

$$\begin{aligned} \text{RENTAL PRICE} = & w[0] + w[1] \times \text{SIZE} + w[2] \times \text{FLOOR} \\ & + w[3] \times \text{BROADBAND RATE} \end{aligned}$$

so there are four weights— $w[0]$, $w[1]$, $w[2]$, and $w[3]$ —for which optimal values must be found. For this example, let's assume that the learning rate, α , is 0.00000002 and the initial weights are chosen from a uniform random distribution in the range $[-0.2, 0.2]$ to be $w[0] = -0.146$, $w[1] = 0.185$, $w[2] = -0.044$, and $w[3] = 0.119$. [Table 7.3](#)^[331] details the important values from

the first two iterations of the gradient descent algorithm when applied to this data.⁹

Table 7.3

Details of the first two iterations when the gradient descent algorithm is used to train a multivariable linear regression model for the office rentals dataset (using only the continuous descriptive features).

Initial Weights								
Iteration 1								
ID	PRICE	RENTAL		Squared Error	errorDelta($\mathcal{D}, \mathbf{w}[j]$)			
		Pred.	Error		$\mathbf{w}[0]$	$\mathbf{w}[1]$	$\mathbf{w}[2]$	$\mathbf{w}[3]$
1	320	93.26	226.74	51,411.08	226.74	113,370.05	906.96	1,813.92
2	380	107.41	272.59	74,307.70	272.59	149,926.92	1,908.16	13,629.72
3	400	115.15	284.85	81,138.96	284.85	176,606.39	2,563.64	1,993.94
4	390	119.21	270.79	73,327.67	270.79	170,598.22	1,353.95	6,498.98
5	385	134.64	250.36	62,682.22	250.36	166,492.17	2,002.91	25,036.42
6	410	130.31	279.69	78,226.32	279.69	195,782.78	1,118.76	2,237.52
7	480	142.89	337.11	113,639.88	337.11	259,570.96	3,371.05	2,359.74
8	600	168.32	431.68	186,348.45	431.68	379,879.24	5,180.17	21,584.05
9	570	170.63	399.37	159,499.37	399.37	367,423.83	5,591.23	3,194.99
10	620	187.58	432.42	186,989.95	432.42	432,423.35	3,891.81	10,378.16
Sum				1,067,571.59	3,185.61	2,412,073.90	27,888.65	88,727.43
Sum of squared errors (Sum/2)				533,785.80				

New Weights (after Iteration 1)								
Iteration 2								
ID	PRICE	RENTAL		Squared Error	errorDelta($\mathcal{D}, \mathbf{w}[j]$)			
		Pred.	Error		$\mathbf{w}[0]$	$\mathbf{w}[1]$	$\mathbf{w}[2]$	$\mathbf{w}[3]$
1	320	117.40	202.60	41,047.92	202.60	101,301.44	810.41	1,620.82
2	380	134.03	245.97	60,500.69	245.97	135,282.89	1,721.78	12,298.44
3	400	145.08	254.92	64,985.12	254.92	158,051.51	2,294.30	1,784.45
4	390	149.65	240.35	57,769.68	240.35	151,422.55	1,201.77	5,768.48
5	385	166.90	218.10	47,568.31	218.10	145,037.57	1,744.81	21,810.16
6	410	164.10	245.90	60,468.86	245.90	172,132.91	983.62	1,967.23
7	480	180.06	299.94	89,964.69	299.94	230,954.68	2,999.41	2,099.59
8	600	210.87	389.13	151,424.47	389.13	342,437.01	4,669.60	19,456.65
9	570	215.03	354.97	126,003.34	354.97	326,571.94	4,969.57	2,839.76
10	620	187.58	432.42	186,989.95	432.42	432,423.35	3,891.81	10,378.16
Sum				886,723.04	2,884.32	2,195,615.84	25,287.08	80,023.74
Sum of squared errors (Sum/2)				443,361.52				

New Weights (after Iteration 2)								
Iteration 3								
ID	PRICE	RENTAL		Squared Error	errorDelta($\mathcal{D}, \mathbf{w}[j]$)			
		Pred.	Error		$\mathbf{w}[0]$	$\mathbf{w}[1]$	$\mathbf{w}[2]$	$\mathbf{w}[3]$
1	320	117.40	202.60	41,047.92	202.60	101,301.44	810.41	1,620.82
2	380	134.03	245.97	60,500.69	245.97	135,282.89	1,721.78	12,298.44
3	400	145.08	254.92	64,985.12	254.92	158,051.51	2,294.30	1,784.45
4	390	149.65	240.35	57,769.68	240.35	151,422.55	1,201.77	5,768.48
5	385	166.90	218.10	47,568.31	218.10	145,037.57	1,744.81	21,810.16
6	410	164.10	245.90	60,468.86	245.90	172,132.91	983.62	1,967.23
7	480	180.06	299.94	89,964.69	299.94	230,954.68	2,999.41	2,099.59
8	600	210.87	389.13	151,424.47	389.13	342,437.01	4,669.60	19,456.65
9	570	215.03	354.97	126,003.34	354.97	326,571.94	4,969.57	2,839.76
10	620	187.58	432.42	186,989.95	432.42	432,423.35	3,891.81	10,378.16
Sum				886,723.04	2,884.32	2,195,615.84	25,287.08	80,023.74
Sum of squared errors (Sum/2)				443,361.52				

Using the initial weights predictions are made for all the instances in the training dataset, as shown in the Predictions column (column 3) of [Table 7.3](#)^[331]. By comparing these predicted values with the actual RENTAL PRICE (column 2), we can compute an error and a squared error term for each training instance, columns 4 and 5 of the table.

To update the weights, we must first calculate the delta value for each weight. This is calculated by summing over all the instances in the training set the prediction error multiplied by the value of the relevant feature for that instance (see [Equation \(7.16\)](#)^[327]). The last four columns on the right of the table list for each instance the product of the prediction error and the feature value. Remember that $\mathbf{d}[0]$ is a dummy descriptive feature, added to match $\mathbf{w}[0]$, with a value of 1 for all training instances. As a result, the values in column 6 are identical to the values in the error column. Focusing on the top cell of column 7, we see the value 113,370.05. This value was calculated by multiplying the prediction error for \mathbf{d}_1 (226.74) by the SIZE value for this instance (500). The other cells in these columns are populated with similar calculations. The $errorDelta(\mathcal{D}, \mathbf{w}[j])$ for each weight is then the summation of the relevant column, for example, $errorDelta(\mathcal{D}, \mathbf{w}[0]) = 3,185.61$ and $errorDelta(\mathcal{D}, \mathbf{w}[1]) = 2,412,073.90$.

Once the $errorDelta(\mathcal{D}, \mathbf{w}[j])$ for a weight has been calculated, we can then update the weight using [Equation \(7.17\)](#)^[327]. This weight update occurs on Line 4^[326] of Algorithm 4^[326]. The update involves multiplying the $errorDelta(\mathcal{D}, \mathbf{w}[j])$ for a given weight by the learning rate and then adding this to the current weight to give a new, updated, weight. The new set of weights is labeled **New Weights (after Iteration 1)** in [Table 7.3](#)^[331].

We can see from Iteration 2 in the bottom half of [Table 7.3](#)^[331] that the new set of predictions made using the updated set of weights calculated in iteration 1 result in a lower sum of squared errors, 443,361.52. Based on this error another new set of weights is calculated using the error deltas shown. The algorithm then keeps iteratively applying the weight update rule until it converges on a stable set of weights beyond which little improvement in model accuracy is possible. In our example, convergence occurred after 100 iterations, and the final values for the weights were $\mathbf{w}[0] = -0.1513$, $\mathbf{w}[1] = 0.6270$, $\mathbf{w}[2] = -0.1781$, and $\mathbf{w}[3] = 0.0714$. The sum of squared errors for the final model was 2,913.5.¹⁰

A last point to make about this example is that careful examination of [Table 7.3](#)^[331] shows why such a low learning rate is used in this example. The large values of the RENTAL PRICE feature, [320,620], cause the squared errors and, in turn, the error delta values to become very large. This means that a very low **learning rate** is required in order to ensure that the changes made to the weights at each iteration of the learning process are small enough for the algorithm to work effectively. Using normalization (see Section 3.6.1^[87]) on the features can help avoid these large squared errors, and we do this in most examples from now on.

7.4 Extensions and Variations

In this section we discuss common and useful extensions to the basic multivariable linear regression with gradient descent approach described in Section 7.3^[319]. Topics covered include interpreting a linear regression model, using weight decay to set the learning rate, handling categorical descriptive and target features, using feature selection, using multivariable linear regression models to model non-linear relationships, and using support vector machines (SVMs) as an alternative to linear regression models.

7.4.1 Interpreting Multivariable Linear Regression Models

A particularly useful feature of linear regression models is that the weights used by the model indicate the effect of each descriptive feature on the predictions returned by the model. First, the signs of the weights indicate whether different descriptive features have a positive or a negative impact on the prediction. [Table 7.4](#)^[333] repeats the final weights for the office rentals model trained in Section 7.3.4^[330]. We can see that increasing office size leads to increasing rental prices; that lower building floors lead to higher rental prices; and that rental prices increase with broadband rates. Second, the magnitudes of the weights show how much the value of the target feature changes for a unit change in the value of a particular descriptive feature. For example, for every increase of a square foot in office size, we can expect the rental price to go up by 0.6270 Euro per month. Similarly, for every floor we go up in an office building, we can expect the rental price to decrease by 0.1781 Euro per month.

Table 7.4

Weights and standard errors for each feature in the office rentals model.

Descriptive Feature	Weight	Standard Error	t-statistic	p-value
SIZE	0.6270	0.0545	11.504	<0.0001
FLOOR	-0.1781	2.7042	-0.066	0.949
BROADBAND RATE	0.071396	0.2969	0.240	0.816

It is tempting to infer the relative importance of the different descriptive features in the model from the magnitude of the weights—that is, the descriptive features associated with higher weights are more predictive than those with lower weights. This is a mistake, however, when the descriptive features themselves have varying scales. For example, in the office rentals dataset, the values of the SIZE feature range from 500 to 1,000, whereas the values for the FLOOR feature range from only 4 to 14. So, direct comparison of the weights tells us little about their relative importance. A better way to determine the importance of each descriptive feature in the model is to perform a **statistical significance test**.

A statistical significance test works by stating a **null hypothesis** and then determining whether there is enough evidence to accept or reject this hypothesis. This accept/reject decision is carried out in three steps:

1. A **test statistic** is computed.
2. The probability of a test-statistic value as big as or greater than the one computed being the result of chance is calculated. This probability is called a **p-value**.
3. The *p*-value is compared to a predefined significance threshold, and if the *p*-value is less than or equal to the threshold (i.e., the *p*-value is small), the null hypothesis is rejected. These thresholds are typically the standard statistical thresholds of 5% or 1%.

The statistical significance test we use to analyze the importance of a descriptive feature $\mathbf{d}[j]$ in a linear regression model is the **t-test**. The null hypothesis that we adopt for this test is that the feature does not have a significant impact on the model. The test statistic we calculate is called the *t*-statistic. In order to calculate this test statistic, we first have to calculate the **standard error** for the overall model and the standard error for the

descriptive feature we are investigating the importance of. The standard error for the overall model is calculated as follows:

$$se = \sqrt{\frac{\sum_{i=1}^n (t_i - \mathbb{M}_{\mathbf{w}}(\mathbf{d}_i))^2}{n - 2}} \quad (7.18)$$

where n is the number of instances in the training dataset. A standard error calculation is then done for a descriptive feature as follows:

$$se(\mathbf{d}[j]) = \frac{se}{\sqrt{\sum_{i=1}^n (\mathbf{d}_i[j] - \bar{\mathbf{d}}[j])^2}} \quad (7.19)$$

where $\mathbf{d}[j]$ is some descriptive feature and $\bar{\mathbf{d}}[j]$ is the mean value of that descriptive feature in the training set.

The t -statistic for this test is calculated as follows:

$$t = \frac{\mathbf{w}[j]}{se(\mathbf{d}[j])} \quad (7.20)$$

where $\mathbf{w}[j]$ is the weight associated with descriptive feature $\mathbf{d}[j]$. Using a standard t -statistic look-up table, we can then determine the p -value associated with this test (this is a two tailed t -test with degrees of freedom set to the number of instances in the training set minus 2). If the p -value is less than the required significance level, typically 0.05, we reject the null hypothesis and say that the descriptive feature has a significant impact on the model; otherwise we say that it does not. We can see from [Table 7.4](#)^[333] that only the SIZE descriptive feature has a significant impact on the model. If a descriptive feature is found to have a significant impact on the model, this indicates that there is a significant linear relationship between it and the target feature.

7.4.2 Setting the Learning Rate Using Weight Decay

In Section 7.3.3^[328] we illustrated the impact of a learning rate parameter on the gradient descent algorithm. In that section we also explained that most

practitioners use rules of thumb and trial and error to set the learning rate. A more systematic approach is to use **learning rate decay**, which allows the learning rate to start at a large value and then decay over time according to a predefined schedule. Although there are different approaches in the literature, a good approach is to use the following decay schedule:

$$\alpha_\tau = \alpha_0 \frac{c}{c + \tau} \quad (7.21)$$

where α_0 is an initial learning rate (this is typically quite large, e.g., 1.0), c is a constant that controls how quickly the learning rate decays (the value of this parameter depends on how quickly the algorithm converges, but it is often set to quite a large value, e.g., 100), and τ is the current iteration of the gradient descent algorithm. [Figure 7.8](#)^[335] shows the journey across the error surface and related plot of the sums of squared errors for the office rentals problem—using just the SIZE descriptive feature—when error decay is used with $\alpha_0 = 0.18$ and $c = 10$ (this is a pretty simple problem, so smaller values for these parameters are suitable). This example shows that the algorithm converges to the global minimum more quickly than any of the approaches shown in [Figure 7.7](#)^[329].

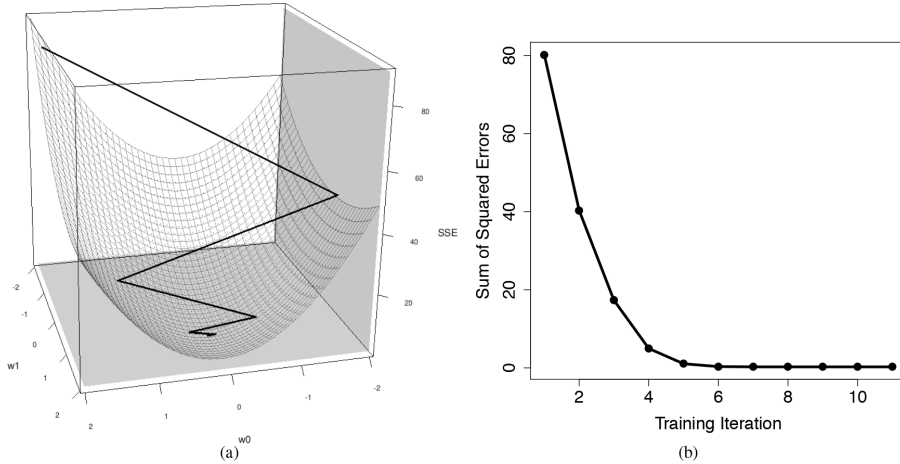


Figure 7.8

(a) The journey across the error surface for the office rentals prediction problem when learning rate decay is used ($\alpha_0 = 0.18$, $c = 10$); and (b) a plot of the changing sum of squared errors during this journey.

The differences between Figures 7.7(f)^[329] and 7.8(b)^[335] most clearly show the impact of learning rate decay as the initial learning rates are the same in these two instances. When learning rate decay is used, there is much less thrashing back and forth across the error surface than when the large static learning rate is used. Using learning rate decay can even address the problem of inappropriately large error rates causing the sum of squared errors to increase rather than decrease. Figure 7.9^[336] shows an example of this in which learning rate decay is used with $\alpha_0 = 0.25$ and $c = 100$. The algorithm starts at the position marked 1 on the error surface, and learning steps actually cause it to move farther and farther up the error surface. This can be seen in the increasing sums of squared errors in Figure 7.9(b)^[336]. As the learning rate decays, however, the direction of the journey across the error surface moves back downward, and eventually the global minimum is reached. Although learning rate decay almost always leads to better performance than a fixed learning rate, it still does require that problem-dependent values are chosen for α_0 and c .

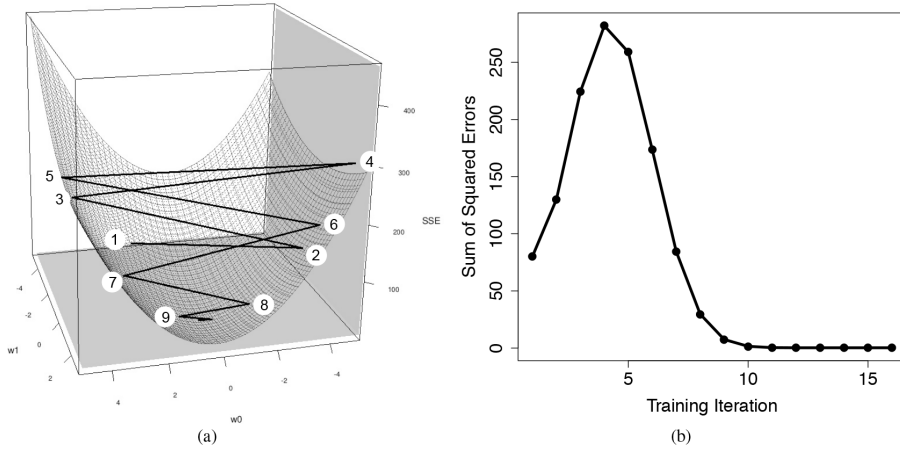


Figure 7.9

(a) The journey across the error surface for the office rentals prediction problem when learning rate decay is used ($\alpha_0 = 0.25$, $c = 100$); (b) a plot of the changing sum of squared errors during this journey.

7.4.3 Handling Categorical Descriptive Features

The regression equation for a multivariable linear regression model for the full dataset shown in Table 7.1^[313] would look like

$$\begin{aligned}\text{RENTAL PRICE} = \mathbf{w}[0] &+ \mathbf{w}[1] \times \text{SIZE} + \mathbf{w}[2] \times \text{FLOOR} \\ &+ \mathbf{w}[3] \times \text{BROADBAND RATE} \\ &+ \mathbf{w}[4] \times \text{ENERGY RATING}\end{aligned}$$

The multiplication of $\mathbf{w}[4] \times \text{ENERGY RATING}$ causes a problem here. Energy rating is a categorical feature, so multiplying the values of this feature by a numeric weight is simply not sensible. The basic structure of the multivariable linear regression model allows for only continuous descriptive features. Obviously, though, in real-world datasets, we often encounter categorical descriptive features, so for the linear regression approach to be really useful, we need a way to handle these.

The most common approach to handling categorical features in linear regression models is to use a transformation that converts a single categorical descriptive feature into a number of continuous descriptive feature values that can encode the levels of the categorical feature. This is done by creating one new binary descriptive feature for every level of the categorical feature. These new features can then be used to encode a level of the original categorical descriptive feature by setting the value of the new feature corresponding to the level of the categorical feature to 1 and the other new continuous features to 0.

For example, if we were to use the ENERGY RATING descriptive feature from [Table 7.1](#)^[313] in a linear regression model, we would convert it into three new continuous descriptive features, as energy rating can have one of three distinct levels: A, B, or C. [Table 7.5](#)^[337] shows this transformed dataset in which the energy rating feature has been replaced with ENERGY RATING A, ENERGY RATING B, and ENERGY RATING C. For training instances in which the original ENERGY RATING feature had a value A, the new ENERGY RATING A feature has a value of 1, and the ENERGY RATING B and ENERGY RATING C are both set to 0. A similar rule is used for instances with the ENERGY RATING feature levels of B and C.

Table 7.5

The office rentals dataset from [Table 7.1](#)^[313] adjusted to handle the categorical ENERGY RATING descriptive feature in linear regression models.

ID	SIZE	FLOOR	BROADBAND RATE	ENERGY RATING A	ENERGY RATING B	ENERGY RATING C	RENTAL PRICE
1	500	4	8	0	0	1	320
2	550	7	50	1	0	0	380
3	620	9	7	1	0	0	400
4	630	5	24	0	1	0	390
5	665	8	100	0	0	1	385
6	700	4	8	0	1	0	410
7	770	10	7	0	1	0	480
8	880	12	50	1	0	0	600
9	920	14	8	0	0	1	570
10	1,000	9	24	0	1	0	620

Returning to our example, the regression equation for this RENTAL PRICE model would change to

$$\begin{aligned} \text{RENTAL PRICE} = & \mathbf{w}[0] + \mathbf{w}[1] \times \text{SIZE} + \mathbf{w}[2] \times \text{FLOOR} \\ & + \mathbf{w}[3] \times \text{BROADBAND RATE} \\ & + \mathbf{w}[4] \times \text{ENERGY RATING A} \\ & + \mathbf{w}[5] \times \text{ENERGY RATING B} \\ & + \mathbf{w}[6] \times \text{ENERGY RATING C} \end{aligned}$$

where the newly added categorical features allow the original ENERGY RATING feature to be included. Everything else about using such a model is exactly the same as before.

The downside to this approach is that it introduces a number of extra weights for which optimal values must be found—in this simple example for only four descriptive features, we need seven weights. This increases the size of the weight space through which we need to search when training the model. One way we can reduce the impact of this is that for each categorical feature we transform, we can reduce the number of newly added features by one by assuming that a zero in all the new features implies that the original feature had the final level. So, for example, for our ENERGY RATING feature, instead of adding three new features (ENERGY RATING A, ENERGY RATING B, and ENERGY RATING C), we could just add ENERGY

RATING A and ENERGY RATING B and assume that whenever they both have a value of 0, ENERGY RATING C is implicitly set.

7.4.4 Handling Categorical Target Features: Logistic Regression

In Section 7.3^[319] we described how a multivariable linear regression model trained using gradient descent can be used to make predictions for continuous target features. Although this is useful for a range of real-world predictive analytics problems, we are also interested in prediction problems with categorical target features. This section covers the reasonably simple adjustments that must be made to the multivariable linear regression with gradient descent algorithm to handle categorical target features, in particular, logistic regression.

7.4.4.1 Predicting categorical targets using linear regression [Table 7.6](#)^[339] shows a sample dataset with a categorical target feature. This dataset contains measurements of the revolutions per minute (RPM) that power station generators are running at, the amount of vibration in the generators (VIBRATION), and an indicator to show whether the generators proved to be working or faulty the day after these measurements were taken. The RPM and VIBRATION measurements come from the day before the generators proved to be operational or faulty. If power station administrators could predict upcoming generator failures before the generators actually fail, they could improve power station safety and save money on maintenance.¹¹ Using this dataset, we would like to train a model to distinguish between properly operating power station generators and faulty generators using the RPM and VIBRATION measurements.

Table 7.6

A dataset listing features for a number of generators.

ID	RPM	VIBRATION	STATUS	ID	RPM	VIBRATION	STATUS
1	568	585	good	29	562	309	faulty
2	586	565	good	30	578	346	faulty
3	609	536	good	31	593	357	faulty
4	616	492	good	32	626	341	faulty
5	632	465	good	33	635	252	faulty
6	652	528	good	34	658	235	faulty
7	655	496	good	35	663	299	faulty
8	660	471	good	36	677	223	faulty
9	688	408	good	37	685	303	faulty
10	696	399	good	38	698	197	faulty
11	708	387	good	39	699	311	faulty
12	701	434	good	40	712	257	faulty
13	715	506	good	41	722	193	faulty
14	732	485	good	42	735	259	faulty
15	731	395	good	43	738	314	faulty
16	749	398	good	44	753	113	faulty
17	759	512	good	45	767	286	faulty
18	773	431	good	46	771	264	faulty
19	782	456	good	47	780	137	faulty
20	797	476	good	48	784	131	faulty
21	794	421	good	49	798	132	faulty
22	824	452	good	50	820	152	faulty
23	835	441	good	51	834	157	faulty
24	862	372	good	52	858	163	faulty
25	879	340	good	53	888	91	faulty
26	892	370	good	54	891	156	faulty
27	913	373	good	55	911	79	faulty
28	933	330	good	56	939	99	faulty

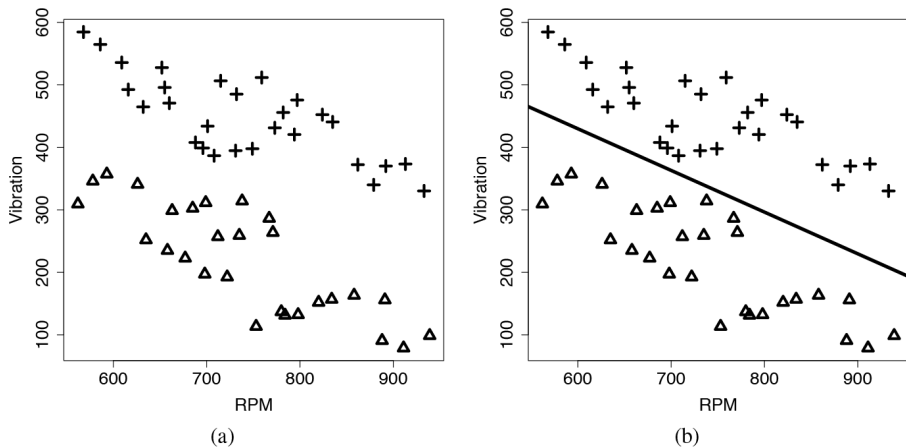


Figure 7.10

(a) A scatter plot of the RPM and VIBRATION descriptive features from the generators dataset shown in Table 7.6^[339], where *good* generators are shown as crosses, and *faulty* generators are shown as triangles; and (b) as decision boundary separating *good* generators (crosses) from *faulty* generators (triangles).

Figure 7.10(a)^[340] shows a scatter plot of this dataset in which we can see that there is a good separation between the two types of generator. In fact, as shown in Figure 7.10(b)^[340], we can draw a straight line across the scatter plot that perfectly separates the *good* generators from the *faulty* ones. This line is known as a decision boundary, and because we can draw this line, this dataset is said to be linearly separable in terms of the two descriptive features used. As the decision boundary is a linear separator, it can be defined using the equation of the line (remember Equation (7.2.1)^[313]). In Figure 7.10(b)^[340] the decision boundary is defined as

$$\text{VIBRATION} = 830 - 0.667 \times \text{RPM} \quad (7.22)$$

or

$$830 - 0.667 \times \text{RPM} - 1 \times \text{VIBRATION} = 0 \quad (7.23)$$

So, for any instance that is actually on the decision boundary, the RPM and VIBRATION values satisfy the equality in Equation (7.23)^[339]. What is more interesting is that instances not actually on the decision boundary behave in a very regular way. The descriptive feature values of all instances above the decision boundary will result in a negative value when plugged into the decision boundary equation, whereas the descriptive features of all

instances below the decision boundary will result in a positive value. For example, applying Equation (7.23)^[339] to the instance RPM = 810, VIBRATION = 495, which is above the decision boundary in Figure 7.10(b)^[340], gives the following result:

$$830 - 0.667 \times 810 - 495 = -205.27$$

By contrast, if we apply Equation (7.23)^[339] to the instance RPM = 650 and VIBRATION = 240, which is below the decision boundary in Figure 7.10(b)^[340], we get

$$830 - 0.667 \times 650 - 240 = 156.45$$

Figure 7.11(a)^[341] illustrates the consistent relationship between Equation (7.23)^[339] and the decision boundary by plotting the value of Equation (7.23)^[339] for all values of RPM and VIBRATION.¹²

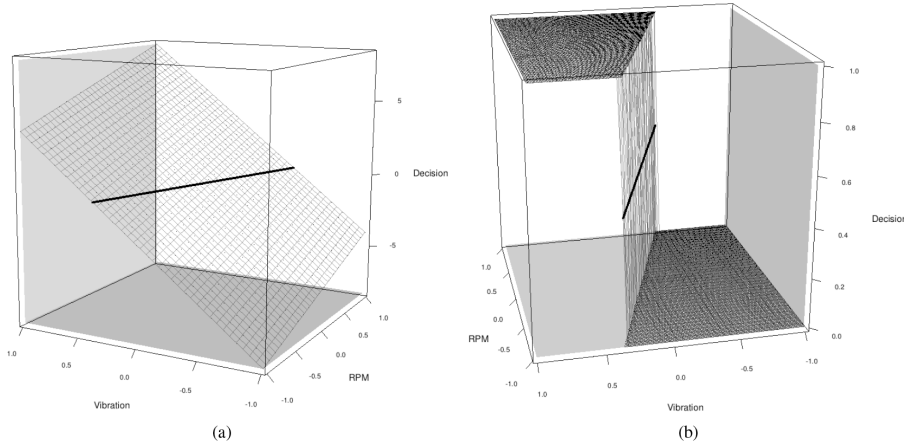


Figure 7.11

(a) A surface showing the value of Equation (7.23)^[339] for all values of RPM and VIBRATION, with the decision boundary given in Equation (7.23)^[339] highlighted; and (b) the same surface linearly thresholded at zero to operate as a predictor.

Because the values of this equation are so well behaved, we can use it to predict a categorical target feature. Reverting to our previous notation, we have

$$\mathbb{M}_{\mathbf{w}}(\mathbf{d}) = \begin{cases} 1 & \text{if } \mathbf{w} \cdot \mathbf{d} \geq 0 \\ 0 & \text{otherwise} \end{cases} \quad (7.24)$$

where \mathbf{d} is a set of descriptive features for an instance; \mathbf{w} is the set of weights in the model; and the *good* and *faulty* generator target feature levels are represented as 0 and 1 respectively. [Figure 7.11\(b\)](#)^[341] shows the value of Equation (7.24)^[341] for every possible value of RPM and VIBRATION. This surface is known as a **decision surface**.

One problem that we need to solve in order to use the model defined in Equation (7.24)^[341] is how to determine the values for the weights, \mathbf{w} , that will minimize the error function for our hypothesis $M_w(\mathbf{d})$. Unfortunately, in this case we cannot just use the gradient descent algorithm. The hard decision boundary given in Equation (7.24)^[341] is **discontinuous**, so is not differentiable, which means we cannot calculate the gradient of the error surface using the derivative. Another problem with this model is that the model always makes completely confident predictions of 0 or 1. A model able to distinguish between instances that are very close to the boundary and those that are farther away would be preferable. We can solve both these problems by using a more sophisticated threshold function that is continuous, and therefore differentiable, and that allows for the subtlety desired: the **logistic function**.¹³

The logistic function¹⁴ is given by

$$\text{logistic}(x) = \frac{1}{1 + e^{-x}} \quad (7.25)$$

where x is a numeric value and e is Euler's number and is approximately equal to 2.7183. A plot of the logistic function for values of x in the range $[-10, 10]$ is shown in [Figure 7.12\(a\)](#)^[343]. We can see that the logistic function is a threshold function that pushes values above zero to 1 and values below zero to 0. This is very similar to the hard threshold function given in Equation (7.24)^[341], except that it has a soft boundary. The next section explains how use of the logistic function allows us to build logistic regression models that predict categorical target features.

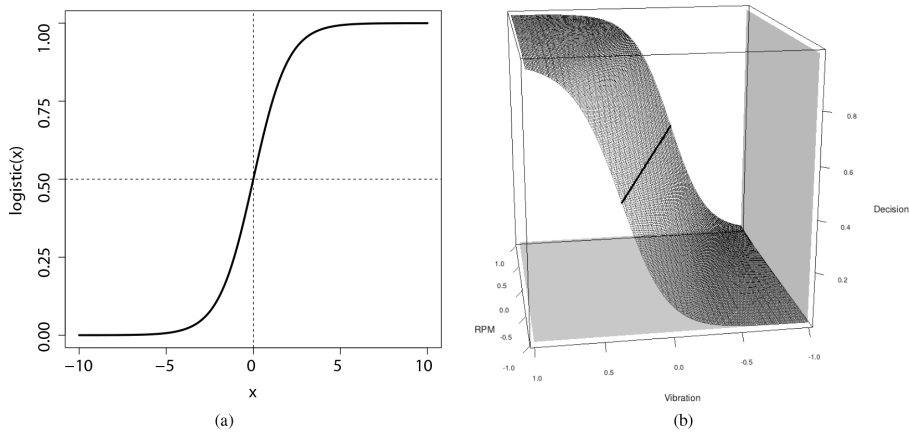


Figure 7.12

(a) A plot of the logistic function (Equation (7.25)^[342]) for the range of values $[-10, 10]$; and (b) the logistic decision surface that results from training a model to represent the generators dataset given in Table 7.6^[339] (note that the data has been normalized to the range $[-1, 1]$).

7.4.4.2 Logistic regression To build a logistic regression model, we threshold the output of the basic linear regression model using the logistic function. So, instead of the regression function simply being the dot product of the weights and the descriptive features (as given in Equation (7.9)^[320]), the dot product of weights and descriptive feature values is passed through the logistic function

$$\begin{aligned} M_w(\mathbf{d}) &= \text{logistic}(\mathbf{w} \cdot \mathbf{d}) \\ &= \frac{1}{1 + e^{-\mathbf{w} \cdot \mathbf{d}}} \end{aligned} \quad (7.26)$$

To see the impact of this, we can build a multivariable logistic regression model for the dataset in Table 7.6^[339]. After the training process (which uses a slightly modified version of the gradient descent algorithm, which we will explain shortly), the resulting logistic regression model is¹⁵

$$M_w(\langle \text{RPM}, \text{VIBRATION} \rangle) = \frac{1}{1 + e^{(-0.4077 + 4.1697 \times \text{RPM} + 6.0460 \times \text{VIBRATION})}} \quad (7.27)$$

The decision surface resulting from Equation (7.27)^[342] is shown in Figure 7.12(b)^[343]. The important thing to notice about this decision surface, in contrast to the decision surface in Figure 7.11(b)^[341], is that there is a gentle transition from predictions of the *faulty* target level to predictions of the

good generator target level. This is one of the key benefits of using logistic regression. Another benefit of using the logistic function is that logistic regression model outputs can be interpreted as probabilities of the occurrence of a target level. So

$$P(t = \text{faulty} | \mathbf{d}) = \mathbb{M}_{\mathbf{w}}(\mathbf{d})$$

and

$$P(t = \text{good} | \mathbf{d}) = 1 - \mathbb{M}_{\mathbf{w}}(\mathbf{d})$$

To find the optimal decision boundary for a logistic regression problem, we use the gradient descent algorithm (Algorithm 4^[326]) to minimize the sum of squared errors based on the training dataset. Figure 7.13^[344] shows a series of the candidate models that were explored on the way to finding this boundary. The final panel in Figure 7.13^[344] shows how the sum of squared errors changed during the training process.

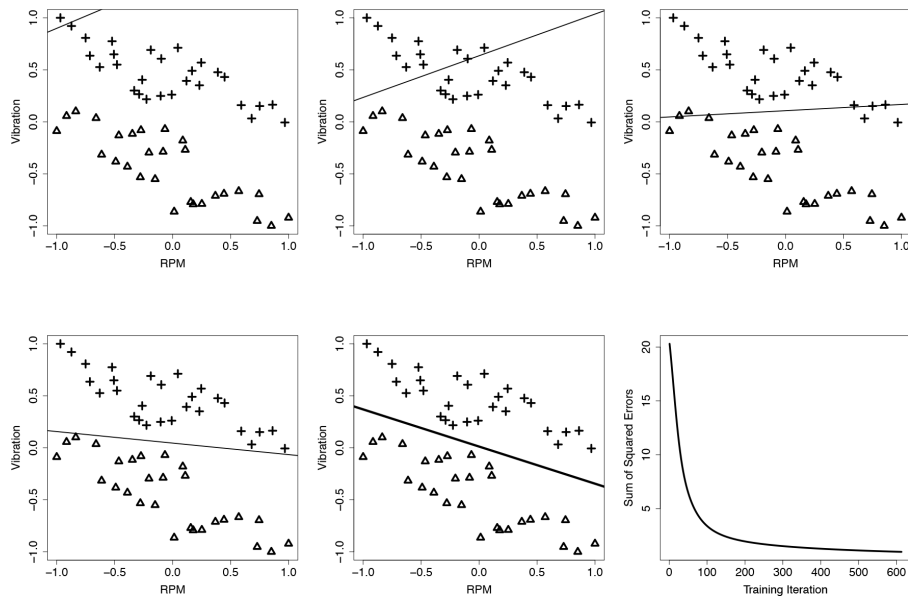


Figure 7.13

A selection of the logistic regression models developed during the gradient descent process for the machinery dataset from Table 7.6^[339]. The bottom-right panel shows the sums of squared errors generated during the gradient descent process.

To repurpose the gradient descent algorithm for training logistic regression models, the only change that needs to be made is in the error delta function, which is used in the weight update rule given on Line 4^[326]

of Algorithm 4^[326]. To derive this new weight update rule, imagine that there is just a single training instance, (\mathbf{d}, t) , in our training dataset. The partial derivative of the error function, L_2 , is then

$$\frac{\partial}{\partial \mathbf{w}[j]} L_2(\mathbb{M}_{\mathbf{w}}, \mathcal{D}) = \frac{\partial}{\partial \mathbf{w}[j]} \frac{1}{2} (t - \mathbb{M}_{\mathbf{w}}(\mathbf{d}))^2$$

where $\mathbf{w}[j]$ is a single weight from the set of weights \mathbf{w} . Applying the chain rule to this, we get

$$\frac{\partial}{\partial \mathbf{w}[j]} L_2(\mathbb{M}_{\mathbf{w}}, \mathcal{D}) = (t - \mathbb{M}_{\mathbf{w}}(\mathbf{d})) \times \frac{\partial}{\partial \mathbf{w}[j]} (t - \mathbb{M}_{\mathbf{w}}(\mathbf{d}))$$

But $\mathbb{M}_{\mathbf{w}}(\mathbf{d}) = \text{logistic}(\mathbf{w} \cdot \mathbf{d})$, so

$$\frac{\partial}{\partial \mathbf{w}[j]} L_2(\mathbb{M}_{\mathbf{w}}, \mathcal{D}) = (t - \text{logistic}(\mathbf{w} \cdot \mathbf{d})) \times \frac{\partial}{\partial \mathbf{w}[j]} (t - \text{logistic}(\mathbf{w} \cdot \mathbf{d}))$$

Applying the chain rule again to the partial derivative part of this equation, and remembering that $\frac{\partial}{\partial \mathbf{w}[j]} \mathbf{w} \cdot \mathbf{d} = \mathbf{d}[j]$, we get

$$\begin{aligned} \frac{\partial}{\partial \mathbf{w}[j]} L_2(\mathbb{M}_{\mathbf{w}}, \mathcal{D}) &= (t - \text{logistic}(\mathbf{w} \cdot \mathbf{d})) \times \frac{\partial}{\partial \mathbf{w}[j]} \text{logistic}(\mathbf{w} \cdot \mathbf{d}) \\ &\quad \times \frac{\partial}{\partial \mathbf{w}[j]} \mathbf{w} \cdot \mathbf{d} \\ &= (t - \mathbb{M}_{\mathbf{w}}(\mathbf{d})) \times \frac{\partial}{\partial \mathbf{w}[j]} \text{logistic}(\mathbf{w} \cdot \mathbf{d}) \times \mathbf{d}[j] \end{aligned}$$

Fortunately, the derivative of the logistic function is well known:

$$\frac{d}{dx} \text{logistic}(x) = \text{logistic}(x)(1 - \text{logistic}(x)) \tag{7.28}$$

So

$$\begin{aligned} \frac{\partial}{\partial \mathbf{w}[j]} L_2(\mathbb{M}_{\mathbf{w}}, \mathcal{D}) &= (t - \text{logistic}(\mathbf{w} \cdot \mathbf{d})) \\ &\quad \times \text{logistic}(\mathbf{w} \cdot \mathbf{d})(1 - \text{logistic}(\mathbf{w} \cdot \mathbf{d})) \times \mathbf{d}[j] \end{aligned} \tag{7.29}$$

Rewriting $\text{logistic}(\mathbf{w} \cdot \mathbf{d})$ as $\mathbb{M}_{\mathbf{w}}(\mathbf{d})$ for readability, we get

$$\frac{\partial}{\partial \mathbf{w}[j]} L_2(\mathbb{M}_{\mathbf{w}}, \mathcal{D}) = (t - \mathbb{M}_{\mathbf{w}}(\mathbf{d})) \quad (7.30)$$

$$\times \mathbb{M}_{\mathbf{w}}(\mathbf{d}) \times (1 - \mathbb{M}_{\mathbf{w}}(\mathbf{d})) \times \mathbf{d}[j] \quad (7.31)$$

This is the partial derivative of the error surface with respect to a particular weight $\mathbf{w}[j]$ and indicates the gradient of the error surface. Using this formulation for the gradient, we can write the weight update rule for logistic regression as

$$\mathbf{w}[j] \leftarrow \mathbf{w}[j] + \alpha \times (t - \mathbb{M}_{\mathbf{w}}(\mathbf{d})) \times \mathbb{M}_{\mathbf{w}}(\mathbf{d}) \times (1 - \mathbb{M}_{\mathbf{w}}(\mathbf{d})) \times \mathbf{d}[j] \quad (7.32)$$

where $\mathbb{M}_{\mathbf{w}}(\mathbf{d}) = \text{logistic}(\mathbf{w} \cdot \mathbf{d}) = \frac{1}{1+e^{-\mathbf{w} \cdot \mathbf{d}}}.$

The rule given in Equation (7.32)^[345] assumes that only a single training instance exists. To modify this to take into account a full training dataset, we simply need to sum across all the training instances as we did before in Equation (7.17)^[327]. This gives us the weight update rule for multivariable logistic regression:

$$\mathbf{w}[j] \leftarrow \mathbf{w}[j] + \alpha \times \sum_{i=1}^n ((t_i - \mathbb{M}_{\mathbf{w}}(\mathbf{d}_i)) \times \mathbb{M}_{\mathbf{w}}(\mathbf{d}_i) \times (1 - \mathbb{M}_{\mathbf{w}}(\mathbf{d}_i)) \times \mathbf{d}_i[j]) \quad (7.33)$$

Other than changing the weight update rule, we don't need to make any other changes to the model training process presented for multivariable linear regression models. To further illustrate this process, the next section presents a worked example of training a multivariable logistic regression model for an extended version of the generators dataset.

7.4.4.3 A worked example of multivariable logistic regression One of the advantages of using a logistic regression model is that it works well for datasets in which the instances with target features set to different levels overlap with each other in the feature space. Table 7.7^[347] shows an extended version of the generators dataset given in Table 7.6^[339], including extra instances that make the separation between *good* generators and *faulty* generators less clear cut. This kind of data is very common in real-world scenarios. A scatter plot of this dataset is shown in Figure 7.14^[349], in which the overlap between the different types of generator in this dataset is clearly visible. Even though the separation between the instances with the different

levels of the target feature in this case is not particularly well defined, a logistic regression model can be trained to distinguish between the two types of generator. In the remainder of this section, we examine this in some detail.

Table 7.7

An extended version of the generators dataset from [Table 7.6](#)^[339].

ID	RPM	VIBRATION	STATUS	ID	RPM	VIBRATION	STATUS
1	498	604	faulty	35	501	463	good
2	517	594	faulty	36	526	443	good
3	541	574	faulty	37	536	412	good
4	555	587	faulty	38	564	394	good
5	572	537	faulty	39	584	398	good
6	600	553	faulty	40	602	398	good
7	621	482	faulty	41	610	428	good
8	632	539	faulty	42	638	389	good
9	656	476	faulty	43	652	394	good
10	653	554	faulty	44	659	336	good
11	679	516	faulty	45	662	364	good
12	688	524	faulty	46	672	308	good
13	684	450	faulty	47	691	248	good
14	699	512	faulty	48	694	401	good
15	703	505	faulty	49	718	313	good
16	717	377	faulty	50	720	410	good
17	740	377	faulty	51	723	389	good
18	749	501	faulty	52	744	227	good
19	756	492	faulty	53	741	397	good
20	752	381	faulty	54	770	200	good
21	762	508	faulty	55	764	370	good
22	781	474	faulty	56	790	248	good
23	781	480	faulty	57	786	344	good
24	804	460	faulty	58	792	290	good
25	828	346	faulty	59	818	268	good
26	830	366	faulty	60	845	232	good
27	864	344	faulty	61	867	195	good
28	882	403	faulty	62	878	168	good
29	891	338	faulty	63	895	218	good
30	921	362	faulty	64	916	221	good
31	941	301	faulty	65	950	156	good
32	965	336	faulty	66	956	174	good
33	976	297	faulty	67	973	134	good
34	994	287	faulty	68	1002	121	good

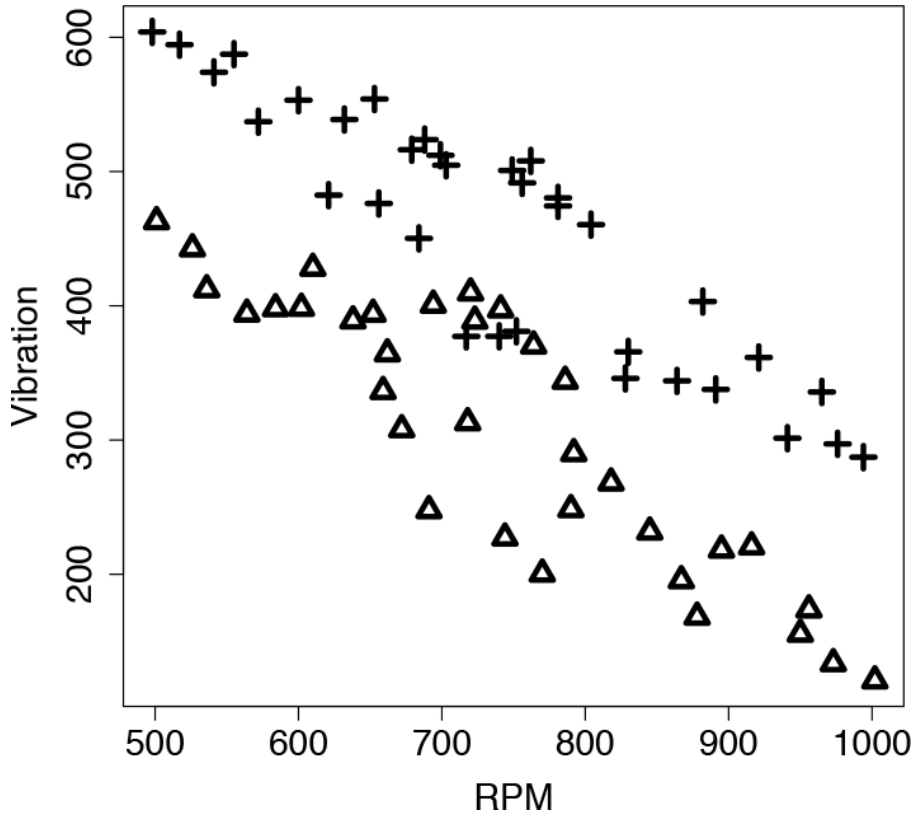


Figure 7.14

A scatter plot of the extended generators dataset given in [Table 7.7](#)^[347], which results in instances with the different target levels overlapping each other. Instances representing *good* generators are shown as crosses, and those representing *faulty* generators as triangles.

There is an ongoing argument regarding whether descriptive features should be **normalized** before being used in linear regression models. The main disadvantage of normalization is that the interpretative analysis discussed in Section 7.4.4^[338] becomes more difficult as the descriptive feature values used in the model do not relate to the actual feature values in the data. For example, if the age of a customer was used as a descriptive feature in a financial credit scoring model, it is more difficult to talk about changes in normalized age on a scale from 0 to 1 than it is to discuss original age values on their natural scale, about 18 to 80. The main advantages of normalizing descriptive feature values are that all weights become directly comparable with each other (as all descriptive features are on the same scale), and the behavior of the gradient descent algorithm used to train the model becomes much less sensitive to the learning rate and the initial weights. Although it is less important for simple linear regression

models, for logistic regression models we recommend that descriptive feature values always be normalized. In this example, before the training process begins, both descriptive features are normalized to the range $[-1, 1]$.

To begin the gradient descent process, random starting values for the weights within the model, $w[0], w[1], w[2]$, are selected. In this example, random values were selected from the range $[-3, 3]$ to give $w[0] = -2.9465$, $w[1] = -1.0147$, and $w[2] = 2.1610$. Using these weights, a prediction is made for every instance in the training dataset, and the resulting sum of squared errors is calculated. The predictions made using these weights and the related error are shown in [Table 7.8](#)^[348] under **Iteration 1**.

Table 7.8

Details of the first two iterations when the gradient descent algorithm is used to train a logistic regression model for the extended generators dataset given in [Table 7.7](#)^[347].

Initial Weights							
Iteration 1							
ID	TARGET	Pred.	Error	Squared Error	<i>errorDelta($\mathcal{D}, \mathbf{w}[j]$)</i>		
					$\mathbf{w}[0]$	$\mathbf{w}[1]$	$\mathbf{w}[2]$
1	1	0.5570	0.4430	0.1963	0.1093	-0.1093	0.1093
2	1	0.5168	0.4832	0.2335	0.1207	-0.1116	0.1159
3	1	0.4469	0.5531	0.3059	0.1367	-0.1134	0.1197
...							
66	0	0.0042	-0.0042	0.0000	0.0000	0.0000	0.0000
67	0	0.0028	-0.0028	0.0000	0.0000	0.0000	0.0000
68	0	0.0022	-0.0022	0.0000	0.0000	0.0000	0.0000
Sum				24.4738	2.7031	-0.7015	1.6493
Sum of squared errors (Sum/2)				12.2369			
New Weights (after Iteration 1)							
Iteration 2							
ID	TARGET	Pred.	Error	Squared Error	<i>errorDelta($\mathcal{D}, \mathbf{w}[j]$)</i>		
					$\mathbf{w}[0]$	$\mathbf{w}[1]$	$\mathbf{w}[2]$
1	1	0.5817	0.4183	0.1749	0.1018	-0.1018	0.1018
2	1	0.5414	0.4586	0.2103	0.1139	-0.1053	0.1094
3	1	0.4704	0.5296	0.2805	0.1319	-0.1094	0.1155
...							
66	0	0.0043	-0.0043	0.0000	0.0000	0.0000	0.0000
67	0	0.0028	-0.0028	0.0000	0.0000	0.0000	0.0000
68	0	0.0022	-0.0022	0.0000	0.0000	0.0000	0.0000
Sum				24.0524	2.7236	-0.6646	1.6484
Sum of squared errors (Sum/2)				12.0262			
New Weights (after Iteration 2)							
Iteration 3							
ID	TARGET	Pred.	Error	Squared Error	<i>errorDelta($\mathcal{D}, \mathbf{w}[j]$)</i>		
					$\mathbf{w}[0]$	$\mathbf{w}[1]$	$\mathbf{w}[2]$
1	1	0.5817	0.4183	0.1749	0.1018	-0.1018	0.1018
2	1	0.5414	0.4586	0.2103	0.1139	-0.1053	0.1094
3	1	0.4704	0.5296	0.2805	0.1319	-0.1094	0.1155
...							
66	0	0.0043	-0.0043	0.0000	0.0000	0.0000	0.0000
67	0	0.0028	-0.0028	0.0000	0.0000	0.0000	0.0000
68	0	0.0022	-0.0022	0.0000	0.0000	0.0000	0.0000
Sum				24.0524	2.7236	-0.6646	1.6484
Sum of squared errors (Sum/2)				12.0262			

This first candidate model is not particularly accurate with an initial sum of squared errors of 12.2369. In fact, instances 1 and 2 are the only instances at this stage that are given predictions of the *faulty* target level, level 1 (note that their prediction values are the only ones greater than 0.5). This can also be seen in the top left-hand image of [Figure 7.15](#)^[350], which shows the candidate model corresponding to this initial set of weights. Based on the errors in these predictions, the delta contributions, labeled as $errorDelta(\mathcal{D}, \mathbf{w}[0])$, $errorDelta(\mathcal{D}, \mathbf{w}[1])$ and $errorDelta(\mathcal{D}, \mathbf{w}[2])$ in [Table 7.8](#)^[348], from each training instance are calculated according to Equation (7.31)^[345]. These individual delta contributions are then summed so that the weight update rule (Equation (7.33)^[346]) can be applied, in this example using a learning rate of 0.02. So, for example, the new value of $\mathbf{w}[0]$ is calculated as the old value plus the learning rate times the sum of the $errorDelta(\mathcal{D}, \mathbf{w}[0])$ contributions to give $-2.9465 + 0.02 \times 2.7031 = -2.8924$. This gives the new set of weights shown as **New Weights (after Iteration 1)**.

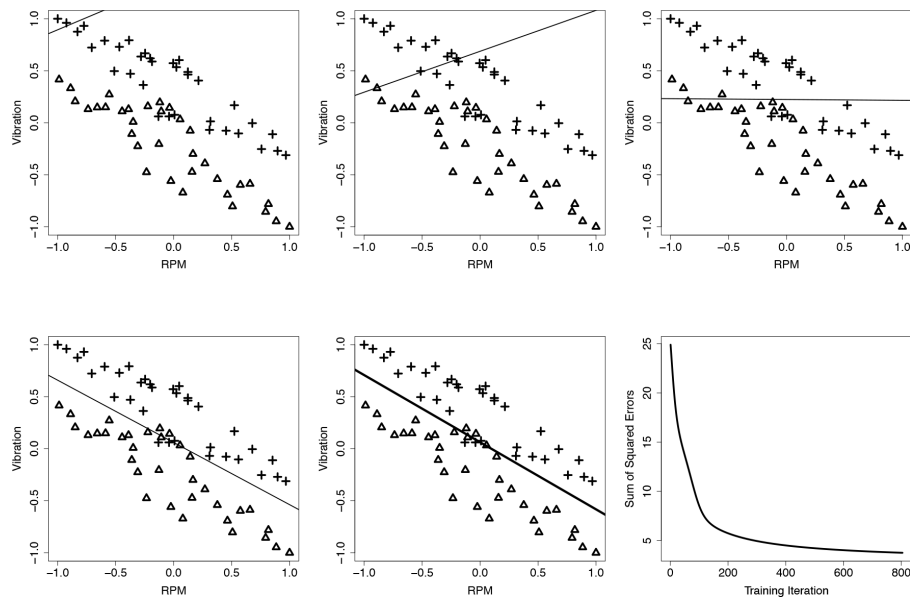


Figure 7.15

A selection of the logistic regression models developed during the gradient descent process for the extended generators dataset in [Table 7.7](#)^[347]. The bottom-right panel shows the sums of squared errors generated during the gradient descent process.

The process then starts again using these new weights as the basis for the predictions and errors marked as **Iteration 2** in [Table 7.8](#)^[348]. The new

weights result in slightly more accurate predictions, evident from the slightly reduced sum of squared errors of 12.0262. Based on the updated errors, a new set of weights is calculated, marked in [Table 7.8](#)^[348] as **New Weights (after Iteration 2)**. [Table 7.8](#)^[348] shows just the first two iterations of the gradient descent process for this model. The continuing process that finds the final model is illustrated in [Figure 7.15](#)^[350], which shows a selection of the candidate models generated on the way to generating the final model, and the bottom-right panel shows how the sum of squared errors changed during the process. The final model trained is

$$M_w(\langle \text{RPM}, \text{VIBRATION} \rangle) = \frac{1}{1 + e^{(-0.4077 + 4.1697 \times \text{RPM} + 6.0460 \times \text{VIBRATION})}}$$

which has a sum of squared errors of 1.8804. Obviously, because there are instances with different levels for the target feature overlapping in the feature space, it is not possible in this case to build a model that perfectly separates the *good* and *faulty* machines. The model trained, however, strikes a good balance between mistaking *good* machines for *faulty* ones and vice versa.

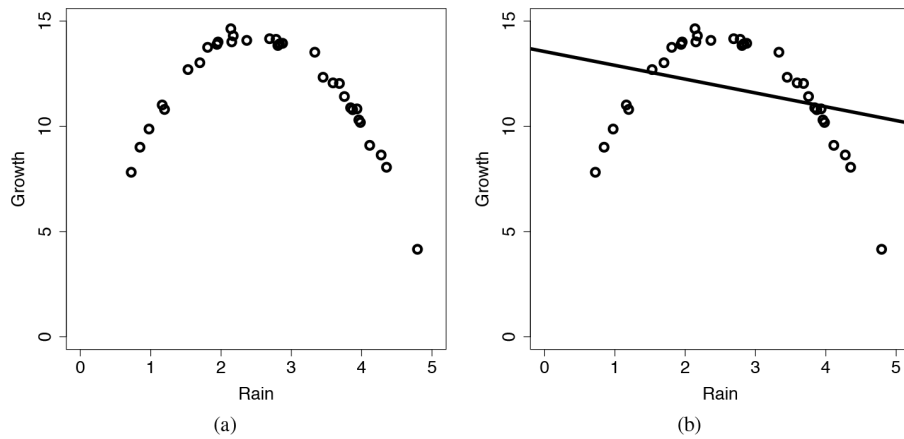
7.4.5 Modeling Non-Linear Relationships

All the simple linear regression and logistic regression models that we have looked at so far model a linear relationship between descriptive features and a target feature. Linear models work very well when the underlying relationships in the data are linear. Sometimes, however, the underlying data will exhibit non-linear relationships that we would like to capture in a model. For example, the dataset in [Table 7.9](#)^[351] is based on an agricultural scenario and shows rainfall (in mm per day), RAIN, and resulting grass growth (in kilograms per acre per day), GROWTH, measured on a number of Irish farms during July 2012. A scatter plot of these two features is shown in [Figure 7.16\(a\)](#)^[352], from which the strong non-linear relationship between rainfall and grass growth is clearly apparent—grass does not grow well when there is very little rain or too much rain, but hits a sweet spot at rainfall of about 2.5mm per day. It would be useful for farmers to be able to predict grass growth for different amounts of forecasted rainfall so that they could plan the optimal times to harvest their grass for making hay.

Table 7.9

A dataset describing grass growth on Irish farms in July 2012.

ID	RAIN	GROWTH	ID	RAIN	GROWTH	ID	RAIN	GROWTH
1	2.153	14.016	12	3.754	11.420	23	3.960	10.307
2	3.933	10.834	13	2.809	13.847	24	3.592	12.069
3	1.699	13.026	14	1.809	13.757	25	3.451	12.335
4	1.164	11.019	15	4.114	9.101	26	1.197	10.806
5	4.793	4.162	16	2.834	13.923	27	0.723	7.822
6	2.690	14.167	17	3.872	10.795	28	1.958	14.010
7	3.982	10.190	18	2.174	14.307	29	2.366	14.088
8	3.333	13.525	19	4.353	8.059	30	1.530	12.701
9	1.942	13.899	20	3.684	12.041	31	0.847	9.012
10	2.876	13.949	21	2.140	14.641	32	3.843	10.885
11	4.277	8.643	22	2.783	14.138	33	0.976	9.876

**Figure 7.16**

(a) A scatter plot of the RAIN and GROWTH feature from the grass growth dataset; and (b) the same plot with a simple linear regression model trained to capture the relationship between the grass growth and rainfall.

A simple linear regression model cannot handle this non-linear relationship. Figure 7.16(b)^[352] shows the best simple linear regression model that can be trained for this prediction problem. This model is

$$\text{GROWTH} = 13.510 + -0.667 \times \text{RAIN}$$

To successfully model the relationship between grass growth and rainfall, we need to introduce non-linear elements. A generalized way in which to do this is to introduce basis functions that transform the raw inputs to the model into non-linear representations but still keep the model itself

linear in terms of the weights. The advantage of this is that, except for introducing the mechanism of basis functions, we do not need to make any other changes to the approach we have presented so far. Furthermore, basis functions work for both simple multivariable linear regression models that predict a continuous target feature and multivariable logistic regression models that predict a categorical target feature.

To use basis functions, we recast the simple linear regression model (see Equation (7.9)^[320]) as follows:

$$\mathbb{M}_{\mathbf{w}}(\mathbf{d}) = \sum_{k=0}^b \mathbf{w}[k] \times \phi_k(\mathbf{d}) \quad (7.34)$$

where \mathbf{d} is a set of m descriptive features, \mathbf{w} is a set of b weights, and ϕ_0 to ϕ_b are a series of b basis functions that each transform the input vector \mathbf{d} in a different way. It is worth noting that there is no reason that b must equal m , and usually b is quite a bit larger than m —that is, there are usually more basis functions than there are descriptive features.

One of the most common uses of basis functions in linear regression is to train models to capture **polynomial** relationships. A linear relationship implies that the target is calculated from the descriptive features using only the addition of the descriptive feature values multiplied by weight values. Polynomial relationships allow multiplication of descriptive feature values by each other and raising of descriptive features to exponents. The most common form of polynomial relationship is the **second order polynomial**, also known as the **quadratic function**, which takes the general form $a = bx + cx^2$. The relationship between rainfall and grass growth in the grass growth dataset can be accurately represented as a second order polynomial through the following model:

$$\text{GROWTH} = \mathbf{w}[0] \times \phi_0(\text{RAIN}) + \mathbf{w}[1] \times \phi_1(\text{RAIN}) + \mathbf{w}[2] \times \phi_2(\text{RAIN})$$

where

$$\begin{aligned}\phi_0(\text{RAIN}) &= 1 \\ \phi_1(\text{RAIN}) &= \text{RAIN} \\ \phi_2(\text{RAIN}) &= \text{RAIN}^2\end{aligned}$$

What makes this approach really attractive is that, although this new model stated in terms of basis functions captures the non-linear relationship between rainfall and grass growth, the model is still linear in terms of the weights and so can be trained using gradient descent without making any changes to the algorithm. [Figure 7.17](#)^[354] shows the final non-linear model that results from this training process, along with a number of the interim steps on the way to this model. The final model is

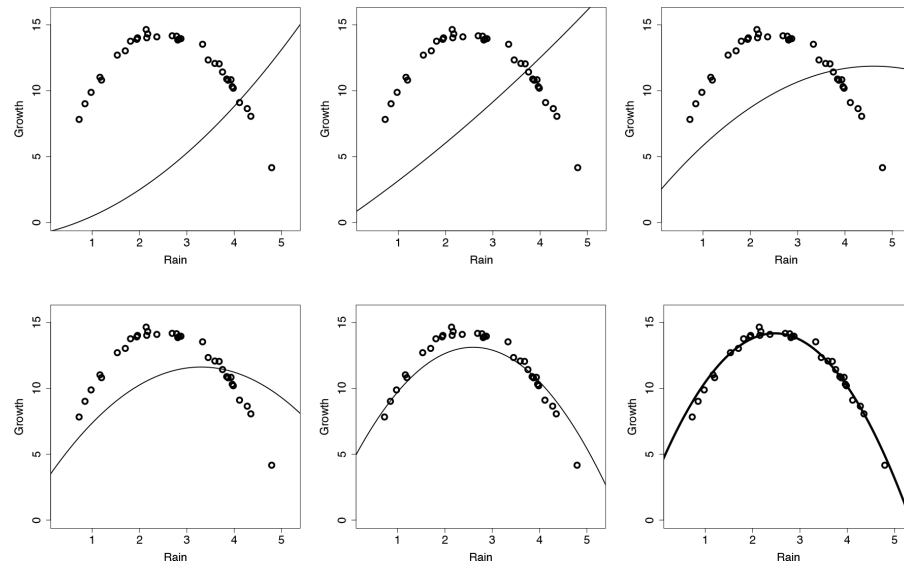


Figure 7.17

A selection of the models developed during the gradient descent process for the grass growth dataset from [Table 7.9](#)^[351].

$$\text{GROWTH} = 3.707 \times \phi_0(\text{RAIN}) + 8.475 \times \phi_1(\text{RAIN}) + -1.717 \times \phi_2(\text{RAIN})$$

where ϕ_0 , ϕ_1 , and ϕ_2 are as described before. This model captures the non-linear relationship in the data very well but was still easy to train using a gradient descent approach. Basis functions can also be used for multivariable simple linear regression models in the same way, the only extra requirement being the definition of more basis functions.

Basis functions can also be used to train logistic regression models for categorical prediction problems that involve non-linear relationships. [Table 7.10](#)^[355] shows a dataset, the EEG dataset, based on a neurological experiment designed to capture how neural responses change when experiment participants view *positive* images (e.g., a picture of a smiling baby) and *negative* images (e.g., a picture of rotting food). In an experiment

performed to capture this data, participants were shown a series of different images, and their neural responses were measured using **electroencephalography (EEG)**. In particular, the values of the commonly used P20 and P45 potentials were measured while a participant viewed each image. These are the descriptive features in this dataset, and the target feature, TYPE, indicates whether the subject was viewing a positive or a negative image. If a model could be trained to classify brain activity as being associated with positive images or negative images, doctors could use this model to help in assessing the brain function of people who have suffered severe brain injuries and are non-communicative.¹⁶ [Figure 7.18](#)^[355] shows a scatter plot of this dataset, from which it is clear that the decision boundary between the two different types of images is not linear—that is, the two types of images are not **linearly separable**.

Table 7.10

A dataset showing participants' responses to viewing *positive* and *negative* images measured on the EEG P20 and P45 potentials.

ID	P20	P45	TYPE	ID	P20	P45	TYPE
1	0.4497	0.4499	negative	26	0.0656	0.2244	positive
2	0.8964	0.9006	negative	27	0.6336	0.2312	positive
3	0.6952	0.3760	negative	28	0.4453	0.4052	positive
4	0.1769	0.7050	negative	29	0.9998	0.8493	positive
5	0.6904	0.4505	negative	30	0.9027	0.6080	positive
6	0.7794	0.9190	negative	31	0.3319	0.1473	positive
⋮				⋮			

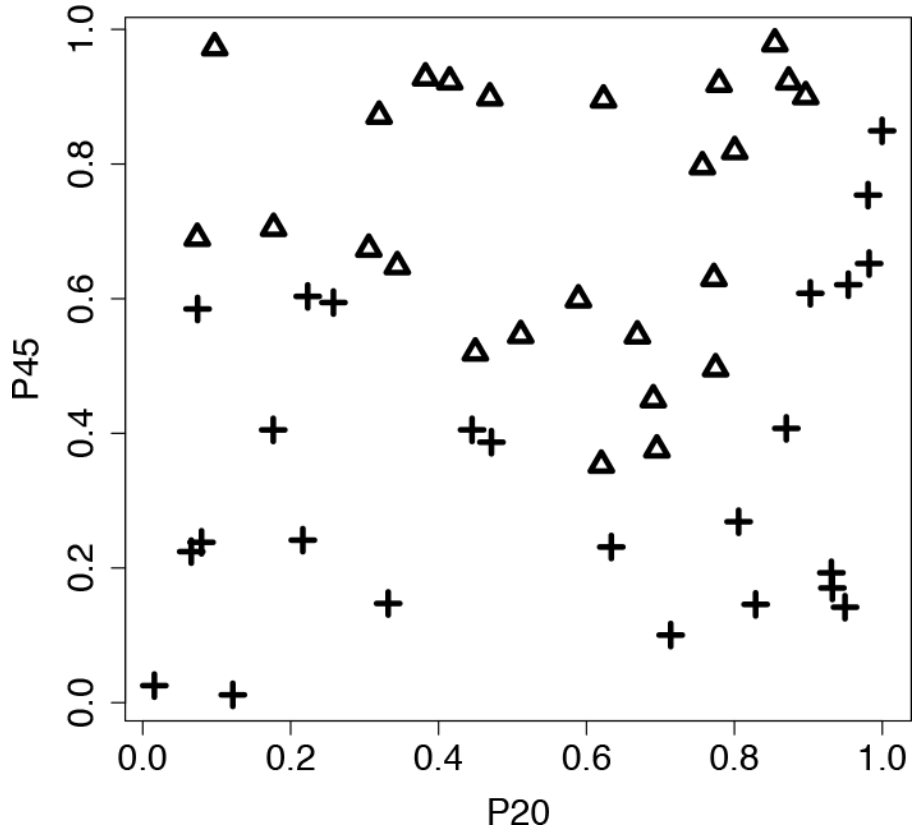


Figure 7.18

A scatter plot of the P20 and P45 features from the EEG dataset. Instances representing *positive* images are shown as crosses, and those representing *negative* images as triangles.

The non-linear decision boundary that is just about perceivable in Figure 7.18^[355] can be represented using a third-order polynomial in the two descriptive features, P20 and P45. The simple regression model we trained previously cannot cope with a non-linear decision boundary like the one seen in Figure 7.18^[355]. We can, however, rewrite the logistic regression equation from Equation (7.26)^[342] to use basis functions as follows:

$$\mathbb{M}_{\mathbf{w}}(\mathbf{d}) = \frac{1}{1 + e^{-\left(\sum_{j=0}^b \mathbf{w}[j] \phi_j(\mathbf{d})\right)}} \quad (7.35)$$

Using this representation with the following set of basis functions will give the learning process the flexibility to find the non-linear decision boundary required to successfully separate the different types of images in the EEG dataset:¹⁷

$$\begin{aligned}
\phi_0(\langle P20, P45 \rangle) &= 1 & \phi_4(\langle P20, P45 \rangle) &= P45^2 \\
\phi_1(\langle P20, P45 \rangle) &= P20 & \phi_5(\langle P20, P45 \rangle) &= P20^3 \\
\phi_2(\langle P20, P45 \rangle) &= P45 & \phi_6(\langle P20, P45 \rangle) &= P45^3 \\
\phi_3(\langle P20, P45 \rangle) &= P20^2 & \phi_7(\langle P20, P45 \rangle) &= P20 \times P45
\end{aligned}$$

This model can be trained using gradient descent to find the optimal decision boundary between the two different types of images. [Figure 7.19](#)^[356] shows a series of the models built during the gradient descent process. The final model can accurately distinguish between the two different types of image based on the measured P20 and P45 activity. [Figure 7.19\(f\)](#)^[356] shows a 3D plot of the final decision surface. Note that although this decision surface is more complex than the ones we have seen before (e.g., [Figure 7.12](#)^[343]), the logistic shape is still maintained.

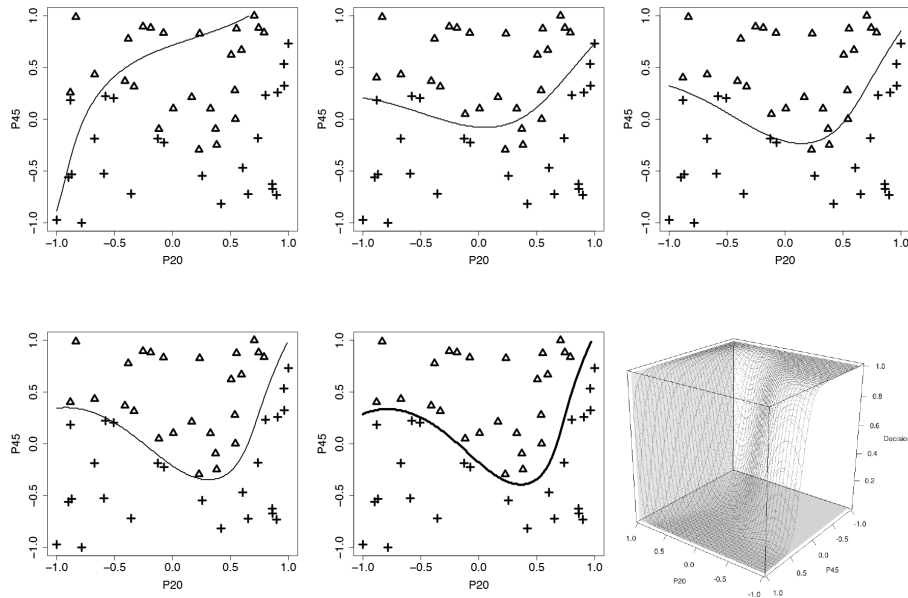


Figure 7.19

A selection of the models developed during the gradient descent process for the EEG dataset from [Table 7.10](#)^[355]. The final panel shows the decision surface generated.

Using basis functions is a simple and effective way in which to capture non-linear relationships within a linear regression model. One way to think about this process is that we change the dataset from two dimensions to a higher-dimensional space. There is no limit to the kinds of functions that can be used as basis functions, and as we have seen in the previous example, the basis functions for different descriptive features in a dataset

can be quite different. One disadvantage of using basis functions, however, is that the analyst has to design the basis function set that will be used. Although there are some well-known sets of functions—for example, different order polynomial functions—this can be a considerable challenge. Second, as the number of basis functions grows beyond the number of descriptive features, the complexity of our models increases, so the gradient descent process must search through a more complex weight space. Using basis functions is an interesting way to change the inductive bias, in particular the restriction bias, encoded in the gradient descent algorithm for learning regression models. By using basis functions such as those given in the examples in this section, we relax the restriction on the algorithm to consider only linear models and instead allow more complex model types such as the higher-order polynomial models seen in these examples.

7.4.6 Multinomial Logistic Regression

The **multinomial logistic regression**¹⁸ model is an extension that handles categorical target features with more than two levels. A good way to build multinomial logistic regression models is to use a set of **one-versus-all** models.¹⁹ If we have r target levels, we create r **one-versus-all** logistic regression models. A **one-versus-all** model distinguishes between one level of the target feature and all the others. Figure 7.20^[358] shows three one-versus-all prediction models for a prediction problem with three target levels (these models are based on the dataset in Table 7.11^[359] that is introduced subsequently in this section).

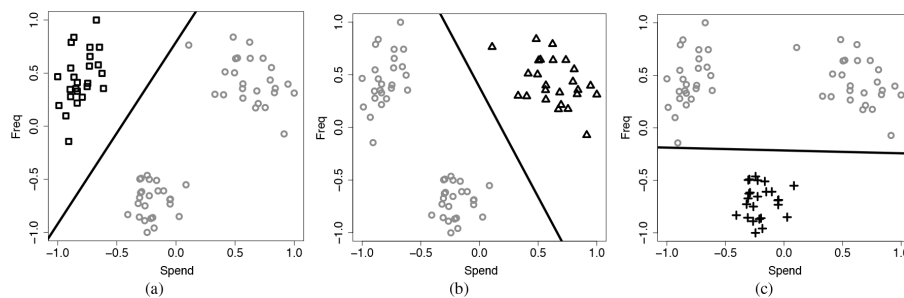


Figure 7.20

An illustration of three different one-versus-all prediction models for the customer type dataset in Table 7.11^[359], with three target levels: (a) *single* (squares), (b) *business* (triangles), and (c) *family* (crosses).

Table 7.11

A dataset of customers of a large national retail chain.

ID	SPEND	FREQ	TYPE	ID	SPEND	FREQ	TYPE
1	21.6	5.4	single	28	122.6	6.0	business
2	25.7	7.1	single	29	107.7	5.7	business
3	18.9	5.6	single				:
4	25.7	6.8	single	47	53.2	2.6	family
	:			48	52.4	2.0	family
26	107.9	5.8	business	49	46.1	1.4	family
27	92.9	5.5	business	50	65.3	2.2	family
	:						:

For r target feature levels, we build r separate logistic regression models $\mathbb{M}_{\mathbf{w}_1}$ to $\mathbb{M}_{\mathbf{w}_r}$:

$$\begin{aligned}\mathbb{M}_{\mathbf{w}_1}(\mathbf{d}) &= \text{logistic}(\mathbf{w}_1 \cdot \mathbf{d}) \\ \mathbb{M}_{\mathbf{w}_2}(\mathbf{d}) &= \text{logistic}(\mathbf{w}_2 \cdot \mathbf{d}) \\ &\vdots \\ \mathbb{M}_{\mathbf{w}_r}(\mathbf{d}) &= \text{logistic}(\mathbf{w}_r \cdot \mathbf{d})\end{aligned}\tag{7.36}$$

where $\mathbb{M}_{\mathbf{w}_1}$ to $\mathbb{M}_{\mathbf{w}_r}$ are r different one-versus-all logistic regression models, and \mathbf{w}_1 to \mathbf{w}_r are r different sets of weights. To combine the outputs of these different models, we normalize their results as follows:

$$\mathbb{M}'_{\mathbf{w}_k}(\mathbf{d}) = \frac{\mathbb{M}_{\mathbf{w}_k}(\mathbf{d})}{\sum_{l \in \text{levels}(t)} \mathbb{M}_{\mathbf{w}_l}(\mathbf{d})}\tag{7.37}$$

where $\mathbb{M}'_{\mathbf{w}_k}(\mathbf{d})$ is a revised, normalized prediction for the one-versus-all model for the target level k . The denominator in this equation sums the predictions of each of the one-versus-all models for the r levels of the target feature and acts as a normalization term. This ensures that the output of all models sums to 1. The r one-versus-all logistic regression models used are trained in parallel, and the revised model outputs, $\mathbb{M}'_{\mathbf{w}_k}(\mathbf{d})$, are used in calculating the sum of squared errors for each model during the training

process. This means that the sum of squared errors function is changed slightly to

$$L_2(\mathbb{M}_{\mathbf{w}_k}, \mathcal{D}) = \frac{1}{2} \sum_{i=1}^n (t_i - \mathbb{M}'_{\mathbf{w}_k}(\mathbf{d}_i[1]))^2 \quad (7.38)$$

The revised predictions are also used in making predictions for query instances. The predicted level for a query, \mathbf{q} , is the level associated with the one-versus-all model that outputs the highest result after normalization. We can write this

$$\mathbb{M}(\mathbf{q}) = \arg \max_{l \in levels(t)} \mathbb{M}'_{\mathbf{w}_l}(\mathbf{q}) \quad (7.39)$$

[Table 7.11](#)^[359] shows a sample from a dataset of mobile customers that includes details of customers' shopping habits with a large national retail chain. Each customer's average weekly spending with the chain, SPEND, and average number of visits per week to the chain, FREQ, are included along with the TYPE of customer: *single*, *business*, or *family*. An extended version of this dataset was used to build a model that can determine the type of a customer based on a few weeks of shopping behavior data. [Figure 7.21](#)^[360] shows the training sequence for a multinomial logistic regression model trained using this data (after the data had been range normalized to $[-1, 1]$). There are three target levels, so three one-versus-all models are built. The evolution of the decision boundary for each model is shown.

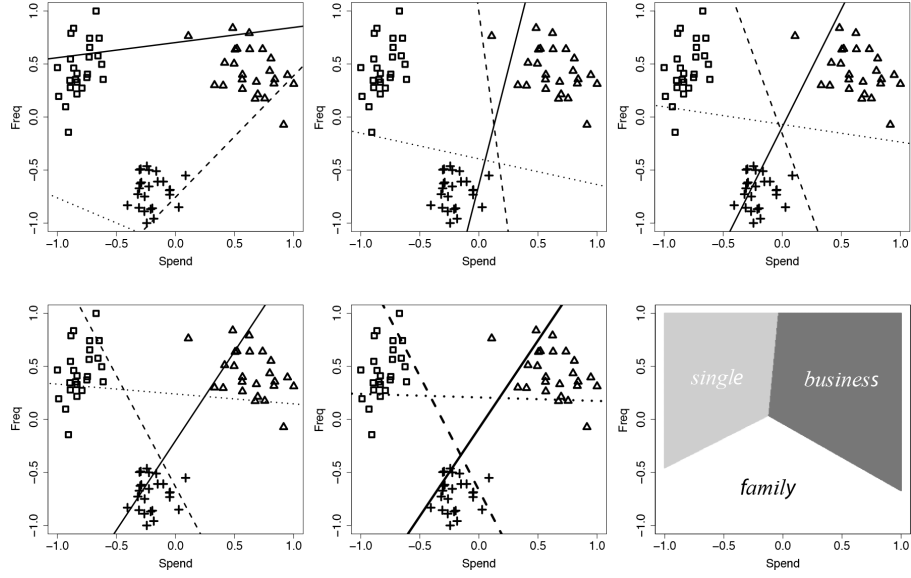


Figure 7.21

A selection of the models developed during the gradient descent process for the customer group dataset from Table 7.11^[359]. Squares represent instances with the *single* target level, triangles the *business* level, and crosses the *family* level. The bottom-right panel illustrates the overall decision boundaries between the three target levels.

The final one-versus-all decision boundaries shown in the bottom-middle panel of Figure 7.21^[360] do not look like the individual one-versus-all decision boundaries shown in Figure 7.20^[358]. The reason for this is that the boundaries shown in Figure 7.20^[358] were trained in isolation, whereas the boundaries shown in Figure 7.21^[360] were trained in parallel and so are interconnected. Although it might look like the decision boundary for the *single* target level shown by the solid line does not discriminate between the instances with the *single* target level and those with the other target levels, when used in conjunction with the other two decision boundaries, it does. We can see this in the **decision boundaries** shown in the bottom-right panel of Figure 7.21^[360]. We use an example to illustrate how a prediction is made using a multinomial regression model.

The parameters of the models learned for the three final decision boundaries in Figure 7.21^[360] are

$$M_{w_{single}}(\mathbf{q}) = \text{logistic}(0.7993 - 15.9030 \times \text{SPEND} + 9.5974 \times \text{FREQ})$$

$$M_{w_{family}}(\mathbf{q}) = \text{logistic}(3.6526 + -0.5809 \times \text{SPEND} - 17.5886 \times \text{FREQ})$$

$$M_{w_{business}}(\mathbf{q}) = \text{logistic}(4.6419 + 14.9401 \times \text{SPEND} - 6.9457 \times \text{FREQ})$$

For a query instance with $\text{SPEND} = 25.67$ and $\text{FREQ} = 6.12$, which are normalized to $\text{SPEND} = -0.7279$ and $\text{FREQ} = 0.4789$, the predictions of the individual models would be

$$\begin{aligned}\mathbb{M}_{\mathbf{w}_{\text{single}}}(\mathbf{q}) &= \text{logistic}(0.7993 - 15.9030 \times (-0.7279) + 9.5974 \times 0.4789) \\ &= 0.9999\end{aligned}$$

$$\begin{aligned}\mathbb{M}_{\mathbf{w}_{\text{family}}}(\mathbf{q}) &= \text{logistic}(3.6526 + -0.5809 \times (-0.7279) - 17.5886 \times 0.4789) \\ &= 0.01278\end{aligned}$$

$$\begin{aligned}\mathbb{M}_{\mathbf{w}_{\text{business}}}(\mathbf{q}) &= \text{logistic}(4.6419 + 14.9401 \times (-0.7279) - 6.9457 \times 0.4789) \\ &= 0.0518\end{aligned}$$

These predictions would be normalized as follows:

$$\begin{aligned}\mathbb{M}'_{\mathbf{w}_{\text{single}}}(\mathbf{q}) &= \frac{0.9999}{0.9999 + 0.01278 + 0.0518} = 0.9393 \\ \mathbb{M}'_{\mathbf{w}_{\text{family}}}(\mathbf{q}) &= \frac{0.01278}{0.9999 + 0.01278 + 0.0518} = 0.0120 \\ \mathbb{M}'_{\mathbf{w}_{\text{business}}}(\mathbf{q}) &= \frac{0.0518}{0.9999 + 0.01278 + 0.0518} = 0.0487\end{aligned}$$

This means the overall prediction for the query instance is *single*, as this gets the highest normalized score.

7.4.7 Support Vector Machines

Support vector machines (SVM) are another approach to predictive modeling that is based on error-based learning. [Figure 7.22\(a\)](#)^[361] shows a scatter plot of a reduced version of the generators dataset (shown in [Table 7.6](#)^[339]) with a decision boundary drawn across it. The instance nearest the decision boundary, based on perpendicular distance, is highlighted. This distance from the decision boundary to the nearest training instance is known as the **margin**. The dashed lines on either side of the decision boundary show the extent of the margin, and we refer to these as the **margin extents**.

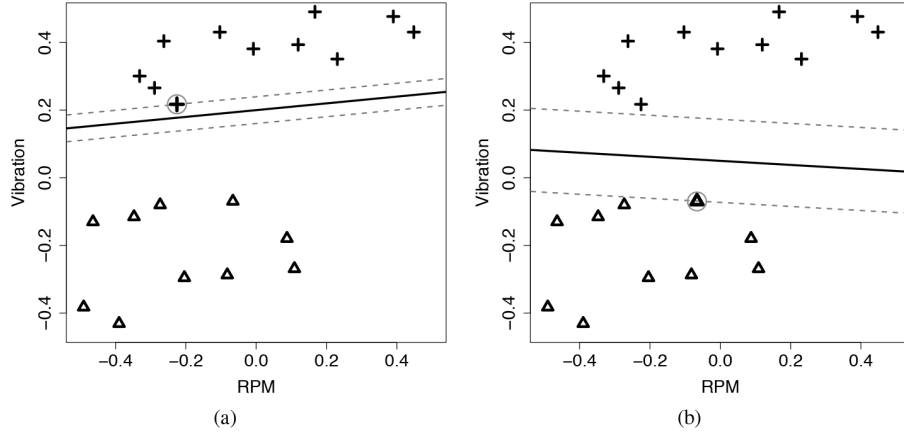


Figure 7.22

A small sample of the generators dataset with two features, RPM and VIBRATION, and two target levels, *good* (shown as crosses) and *faulty* (shown as triangles): (a) a decision boundary with a very small margin; and (b) a decision boundary with a much larger margin. In both cases, the instances along the margins are highlighted.

[Figure 7.22\(b\)](#)^[361] shows a similar diagram but with a different decision boundary, which has a much larger margin. The intuition behind support vector machines is that this second decision boundary should distinguish between the two target levels much more reliably than the first. Training a support vector machine involves searching for the decision boundary, or **separating hyperplane**,²⁰ that leads to the maximum margin because this will best separate the levels of the target feature. Although the goal of finding the best decision boundary is the same for algorithms that build support vector machines as it is for logistic regression models, the inductive bias encoded in the algorithms to select this boundary is different, which leads to different decision boundaries being found.

The instances in a training dataset that fall along the margin extents, and therefore the margins, are known as the **support vectors**. These are the most important instances in the dataset because they define the decision boundary. There will always be at least one support vector for each level of the target feature, but there is no limit to how many support vectors there can be in total.

We define the separating hyperplane in the same way that we did at the beginning of the discussion of logistic regression

$$w_0 + \mathbf{w} \cdot \mathbf{d} = 0 \quad (7.40)$$

Note that this time we have separated w_0 from the other weights, \mathbf{w} , as this will make later equations simpler.²¹ Recall from Section 7.4.4^[338] that for instances above a separating hyperplane

$$w_0 + \mathbf{w} \cdot \mathbf{d} > 0$$

and for instances below a separating hyperplane

$$w_0 + \mathbf{w} \cdot \mathbf{d} < 0$$

For support vector machines, we first set the negative target feature level to -1 and the positive target feature level to $+1$. We then build a support vector machine prediction model so that instances with the negative target level result in the model outputting ≤ -1 and instances with the positive target level result in the model outputting $\geq +1$. The space between the outputs of -1 and $+1$ allows for the margin.

A support vector machine model is defined as

$$\mathbb{M}_{\alpha, w_0}(\mathbf{q}) = \sum_{i=1}^s (t_i \times \alpha[i] \times (\mathbf{d}_i \cdot \mathbf{q}) + w_0) \quad (7.41)$$

where \mathbf{q} is the set of descriptive features for a query instance; $(\mathbf{d}_1, t_1), \dots, (\mathbf{d}_s, t_s)$ are s support vectors (instances composed of descriptive features and a target feature); w_0 is the first weight of the decision boundary; and α is a set of parameters determined during the training process (there is a parameter for each support vector $\alpha[1], \dots, \alpha[s]$).²² When the output of this equation is greater than 1 , we predict the positive target level for the query, and when the output is less than -1 , we predict the negative target level. An important feature of this equation is that the support vectors are a component of the equation. This reflects the fact that a support vector machine uses the support vectors to define the separating hyperplane and hence to make the actual model predictions.

To train a support vector machine, we need to find values for each of the components in Equation (7.41)^[363] (the support vectors, w_0 , and the α parameters) that define the optimal decision boundary between the target levels. This is an instance of a **constrained quadratic optimization problem**, and there are well-known approaches to solving this type of problem. In this book we do not describe this step of the process in detail.²³

Instead, we focus on explaining how the process is set up and how the training process reflects the inductive bias of searching for the separating hyperplane with the maximum margin. As the name **constrained quadratic optimization problem** suggests, this type of problem is defined in terms of (1) a set of constraints and (2) an optimization criterion.

When training a support vector machine, we wish to find a hyperplane that distinguishes between the two target levels, -1 and $+1$. So, the required **constraints** required by the training process are

$$w_0 + \mathbf{w} \cdot \mathbf{d} \leq -1 \text{ for } t_i = -1 \quad (7.42)$$

and

$$w_0 + \mathbf{w} \cdot \mathbf{d} \geq +1 \text{ for } t_i = +1 \quad (7.43)$$

[Figure 7.23](#)^[364] shows two different decision boundaries that satisfy these constraints. Note that the decision boundaries in these examples are equally positioned between positive and negative instances, which is a consequence of the fact that decision boundaries satisfy these constraints. The support vectors are highlighted in [Figure 7.23](#)^[364] for each of the decision boundaries shown. For simplicity in later calculations, we can combine the two constraints in Equations (7.42)^[363] and (7.43)^[363] into a single constraint (remember that t_i is always equal to either -1 or $+1$)

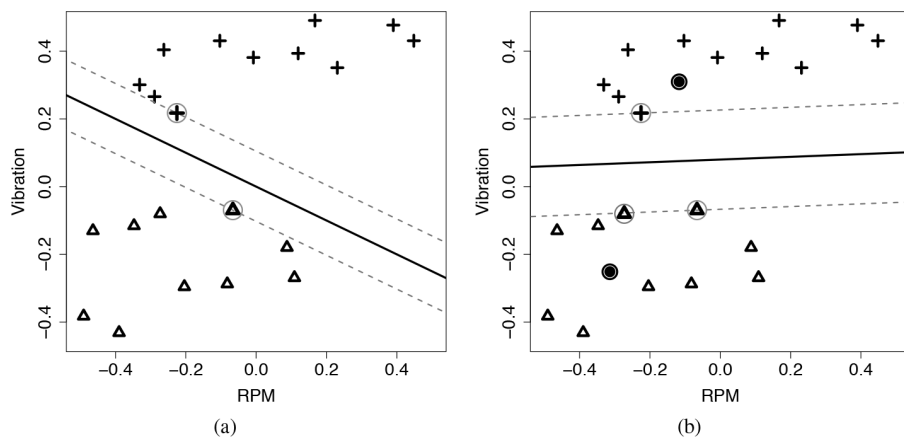


Figure 7.23

Different margins that satisfy the constraint in Equation (7.44)^[364], the instances that define the margin are highlighted in each case; (b) shows the maximum margin and also shows two query instances represented as black dots.

$$t_i \times (w_0 + \mathbf{w} \cdot \mathbf{d}) \geq 1 \quad (7.44)$$

The optimization criterion used when training a support vector machine allows us to choose between multiple different decision boundaries that satisfy the constraint given in Equation (7.44)^[364], such as those shown in Figure 7.23^[364]. The optimization criterion used is defined in terms of the perpendicular distance from any instance to the decision boundary and is given by

$$dist(\mathbf{d}) = \frac{abs(w_0 + \mathbf{w} \cdot \mathbf{d})}{\|\mathbf{w}\|}$$

where $\|\mathbf{w}\|$ is known as the **Euclidean norm** of \mathbf{w} and is calculated

$$\|\mathbf{w}\| = \sqrt{\mathbf{w}[1]^2 + \mathbf{w}[2]^2 + \dots + \mathbf{w}[m]^2}$$

For instances along the margin extents, $abs(w_0 + \mathbf{w} \cdot \mathbf{d}) = 1$ (according to Equation (7.44)^[364]). So, the distance from any instance along the margin extents to the decision boundary is $\frac{1}{\|\mathbf{w}\|}$, and because the margin is symmetrical to either side of the decision boundary, the size of the margin is $\frac{2}{\|\mathbf{w}\|}$. The goal when training a support vector machine is to maximize $\frac{2}{\|\mathbf{w}\|}$ subject to the constraint expressed in Equation (7.44)^[364].

Once the constraints and optimization criterion have been defined, the solution to the constrained quadratic optimization process will identify and define all the components in Equation (7.41)^[363] (the support vectors, w_0 , and the α parameters) for the optimal decision boundary.

The optimal decision boundary and associated support vectors for the example we have been following are shown in Figure 7.23(b)^[364]. In this case *good* is the positive level and set to + 1, and *faulty* is the negative level and set to - 1. The descriptive feature values and target feature values for the support vectors in these cases are ($-0.225, 0.217$, + 1), ($-0.066, -0.069$, -1), and ($-0.273, -0.080$, -1). The value of w_0 is - 0.1838, and the values of the α parameters are (23.056, 6.998, 16.058)). Figure 7.23(b)^[364] shows the position of two new query instances for this problem. The descriptive feature values for these query instances are $\mathbf{q}_1 = \langle -0.314, -0.251 \rangle$ and $\mathbf{q}_2 = \langle -0.117, 0.31 \rangle$. For the first query instance, \mathbf{q}_1 , the output of the support vector machine model is:

$$\begin{aligned}
M_{\alpha, w_0}(\mathbf{q}_1) &= (1 \times 23.056 \times ((-0.225 \times -0.314) + (0.217 \times -0.251))) - 0.1838 \\
&\quad + (-1 \times 6.998 \times ((-0.066 \times -0.314) + (-0.069 \times -0.251))) - 0.1838 \\
&\quad + (-1 \times 16.058 \times ((-0.273 \times -0.314) + (-0.080 \times -0.251))) - 0.1838 \\
&= -2.145
\end{aligned}$$

The model output is less than -1 , so this query is predicted to be a *faulty* generator. For the second query instance, the model output is calculated similarly and is 1.592 . This is greater than $+1$, so this instance is predicted to be a *good* generator.

In the same way we used basis functions with logistic regression models in Section 7.4.5^[351], basis functions can be used with support vector machines to handle training data that is not linearly separable. In order to use basis functions, we must update Equation (7.44)^[364] to

$$t_i \times (w_0 + \mathbf{w} \cdot \phi(\mathbf{d})) \geq 1 \text{ for all } i \quad (7.45)$$

where ϕ is a set of basis functions applied to the descriptive features \mathbf{d} , and \mathbf{w} is a set of weights containing one weight for each member of ϕ . Typically, the number of basis functions in ϕ is larger than the number of descriptive features, so the application of the basis functions moves the data into a higher-dimensional space. The expectation is that a linear separating hyperplane will exist in this higher-dimensional space even though it does not in the original feature space. The prediction model in this case becomes

$$M_{\alpha, \phi, w_0}(\mathbf{q}) = \sum_{i=1}^s (t_i \times \alpha[i] \times (\phi(\mathbf{d}_i) \cdot \phi(\mathbf{q})) + w_0) \quad (7.46)$$

Equation (7.46)^[366] requires a dot product calculation between the result of applying the basis functions to the query instance and to each of the support vectors. During the training process, this is repeated multiple times. A dot product of two high-dimensional vectors is a computationally expensive operation, but a clever trick—the **kernel trick**—is used to avoid it. The same result obtained by calculating the dot product of the descriptive features of a support vector and a query instance after having applied the basis functions can be obtained by applying a much less costly **kernel**

function, *kernel*, to the original descriptive feature values of the support vector and the query.²⁴ The prediction equation becomes

$$\mathbb{M}_{\alpha, \text{kernel}, w_0}(\mathbf{q}) = \sum_{i=1}^s (t_i \times \alpha[i] \times \text{kernel}(\mathbf{d}_i, \mathbf{q}) + w_0) \quad (7.47)$$

A wide range of standard kernel functions can be used with support vector machines. Some popular options are

Linear kernel $\text{kernel}(\mathbf{d}, \mathbf{q}) = \mathbf{d} \cdot \mathbf{q} + c$

where c is an optional constant

Polynomial kernel $\text{kernel}(\mathbf{d}, \mathbf{q}) = (\mathbf{d} \cdot \mathbf{q} + 1)^p$

where p is the degree of a polynomial function

Gaussian radial basis kernel $\text{kernel}(\mathbf{d}, \mathbf{q}) = \exp(-\gamma \|\mathbf{d} - \mathbf{q}\|^2)$

where γ is a manually chosen tuning parameter

The appropriate kernel function for a particular prediction model should be selected by experimenting with different options. It is best to start with a simple linear or low-degree polynomial kernel function and move to more complex kernel functions only if good performance cannot be achieved with this.

The description of the support vector machine approach given in this section assumes that it is possible to separate the instances with the two different target feature levels with a linear hyperplane. Sometimes this is not possible, even after using a kernel function to move the data to a higher-dimensional feature space. In these instances, a margin cannot be defined, as we have done in this example. An extension of the standard support vector machine approach that allows a **soft margin**, however, caters for this and allows overlap between instances with target features of the two different levels. Another extension allows support vector machines to handle multinomial target features using a one-versus-all approach similar to that described in Section 7.4.6^[357]. There are also extensions to handle categorical descriptive features (similar to the approach described in Section 7.4.3^[336]) and continuous target features.

Support vector machines have become a very popular approach to building predictive models in recent times. They can be quickly trained, are not overly susceptible to overfitting, and work well for high-dimensional data. In contrast to logistic regression models, however, they are not very interpretable, and, especially when kernel functions are used, it is very difficult to understand why a particular prediction has been made.

7.5 Summary

The **simple multivariable linear regression** (Section 7.3^[319]) model (for convenience, repeated here as Equation (7.48)^[367]) makes a prediction for a continuous target feature based on a weighted sum of the values of a set of descriptive features. In an error-based model, learning equates to finding the optimal values for these weights. Each of the infinite number of possible combinations of values for the weights will result in a model that **fits**, to some extent, the relationship present in the training data between the descriptive features and the target feature. The optimal values for the weights are the values that define the model with the minimum prediction error.

$$\begin{aligned} M_w(\mathbf{d}) &= \mathbf{w} \cdot \mathbf{d} \\ &= \sum_{j=0}^m \mathbf{w}[j] \times \mathbf{d}[j] \end{aligned} \tag{7.48}$$

We use an **error function** to measure how well a set of weights fits the relationship in the training data. The most common error function used for error-based models is the **sum of squared errors**. The value of the error function for every possible weight combination defines an error surface, similar to the one shown in Figure 7.24(a)^[368]—for each combination of weight values, we get a point on the surface whose coordinates are the weight values, with an elevation defined by the error of the model using the weight values. To find the optimal set of weights, we begin with a set of random weight values that corresponds to some random point on the error surface. We then iteratively make small adjustments to these weights based on the output of the error function, which leads to a journey down the error surface that eventually leads to the optimal set of weights. The zig-zagging line in Figure 7.24(a)^[368] shows an example journey across an error surface,

and [Figure 7.24\(b\)](#)^[368] shows the reduction in the sum of squared errors as the search for the optimal weights progresses down the error surface.

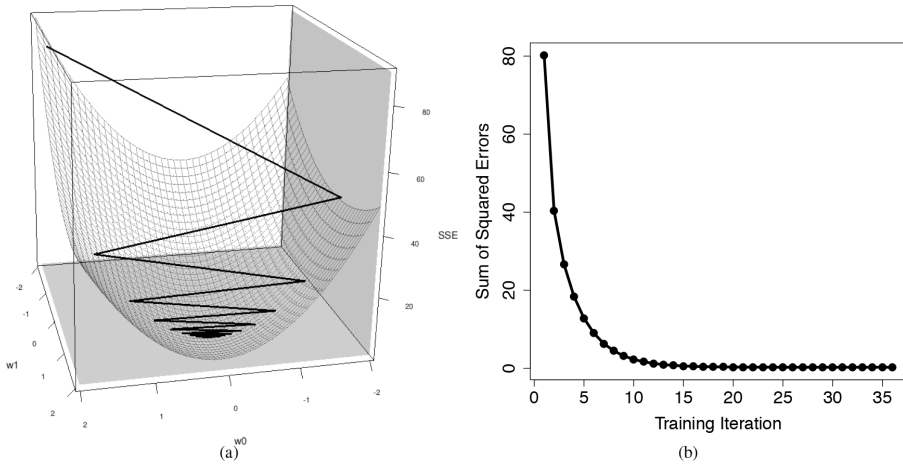


Figure 7.24

(a) The journey across an error surface; and (b) the changing sums of squared errors during this journey.

To ensure that we arrive at the optimal set of weights at the end of this journey across the error surface, we need to ensure that each step we take moves downward on the error surface. We do this by directing our steps according to the **gradient** of the error surface at each step. This is the **gradient descent algorithm**, which is one of the most important algorithms in all of computer science, let alone machine learning.

The simple multivariable linear regression model that we presented at the beginning of this chapter can be extended in many ways, and we presented some of the most important of these. **Logistic regression** models (Section 7.4.4^[338]) allow us to predict categorical targets rather than continuous ones by placing a threshold on the output of the simple multivariable linear regression model using the logistic function.

The simple linear regression and logistic regression models that we first looked at were only capable of representing **linear relationships** between descriptive features and a target feature. In many cases, this limits the creation of an accurate prediction model. By applying a set of **basis functions** (Section 7.4.5^[351]) to descriptive features, models that represent **non-linear relationships** can be created. The advantages of using basis functions is that they allow models that represent non-linear relationships to be built even though these models themselves remain a linear combination

of inputs (e.g., we still use something very similar to Equation (7.48)^[367] to predict continuous targets). Consequently, we can still use the gradient descent process to train them. The main disadvantages of using basis functions are, first, that we must manually decide what set of basis functions to use; and second, that the number of weights in a model using basis functions is usually far greater than the number of descriptive features, so finding the optimal set of weights involves a search across a much larger set of possibilities—that is, a much larger **weight space**.

It is somewhat surprising how often a linear multivariable regression model can accurately represent the relationship between descriptive features and a target feature without the use of basis functions. We recommend that simple linear models be evaluated first and basis functions introduced only when the performance of the simpler models is deemed unsatisfactory.

The logistic regression approach (and the SVM approach) discussed in this chapter is at a disadvantage to those discussed in the previous chapters in that in its basic form, it can only handle categorical target features with two levels. In order to handle categorical target features with more than two levels, that is **multinomial** prediction problems, we need to use a **one-versus-all** approach in which multiple models are trained. This introduces something of an explosion in the number of weights required for a model, as we have an individual set of weights for every target feature level. This is one reason that other approaches are often favored over logistic regression for predicting categorical targets with many levels.

One of the most attractive features of the regression models discussed in this chapter is that they are based on a large body of research and best practice in **statistics**, a much older discipline than machine learning. The maturity of regression-based approaches means that they are easily accepted in other disciplines (e.g., biological, physical, and social sciences) and that there is a range of techniques that allow a degree of analysis of regression models beyond what is possible for other approaches. We saw some of these techniques in Section 7.4.1^[332] when we examined the importance of the different descriptive features in a linear regression model through an analysis of the model weights. A range of other approaches we do not cover in this book can be used to do other in-depth analysis of regression models. Section 7.6^[370] recommends further reading on this topic.

Near the end of this chapter we covered **support vector machines** (SVM). SVM models are trained in a slightly different way than regression models, but the concepts underpinning both approaches are similar. The main advantages of SVM models are that they are robust to overfitting and perform well for very high-dimensional problems. SVM models are just one of a whole range of error-based approaches that are active areas for machine learning research, and new approaches are constantly being developed. In this chapter we have not covered **artificial neural networks**, another popular error-based approach to learning that is a very active research area. One type of artificial neural network can be built by connecting layers of logistic regression models, but there are many other network topologies used in practice. We cover artificial neural networks and deep learning in detail in Chapter 8^[381].

The next section discusses recommended readings for more information on the regression approaches discussed in this chapter and on some of the more recent developments in error-based learning.

7.6 Further Reading

The key component of the gradient descent algorithm presented in this chapter is the use of **differentiation** to compute the slope of the error surface. Differentiation is a part of calculus, which is a large and very important field of mathematics. In Appendix C^[765] we provide an introduction to differentiation that covers all the techniques required to understand how the gradient descent algorithm works. If, however, you wish to get a broader understanding of calculus, we recommend Stewart (2012) as an excellent textbook on all aspects of calculus.

For a more in-depth treatment of regression models and their underpinnings in statistics, Chapter 14 of Rice (2006) offers a nice treatment of the topic, and Kutner et al. (2004) provides massive detail. Ayres (2008) gives a lighter discussion of the many different ways in which regression models are applied in practice.

Burges (1998) is still a good, freely available tutorial on support vector machines. For more details, Cristianini and Shawe-Taylor (2000) is a well-respected textbook on the topic and covers the extensions mentioned in Section 7.4.7^[361], while Vapnik (2000) gives a good overview of the theoretical underpinnings of support vector machines.

7.7 Exercises

1. A multivariate linear regression model has been built to predict the **heating load** in a residential building on the basis of a set of descriptive features describing the characteristics of the building. Heating load is the amount of heat energy required to keep a building at a specified temperature, usually 65° Fahrenheit during the winter regardless of outside temperature. The descriptive features used are the overall surface area of the building, the height of the building, the area of the building's roof, and the percentage of wall area in the building that is glazed. This kind of model would be useful to architects or engineers when designing a new building.²⁵ The trained model is

$$\begin{aligned}\text{HEATING LOAD} = & - 26.030 + 0.0497 \times \text{SURFACE AREA} \\ & + 4.942 \times \text{HEIGHT} - 0.090 \times \text{ROOF AREA} \\ & + 20.523 \times \text{GLAZING AREA}\end{aligned}$$

Use this model to make predictions for each of the query instances shown in the following table.

ID	SURFACE AREA	HEIGHT	ROOF AREA	GLAZING AREA
1	784.0	3.5	220.5	0.25
2	710.5	3.0	210.5	0.10
3	563.5	7.0	122.5	0.40
4	637.0	6.0	147.0	0.60

2. You have been hired by the European Space Agency to build a model that predicts the amount of oxygen that an astronaut consumes when performing five minutes of intense physical work. The descriptive features for the model will be the age of the astronaut and their average heart rate throughout the work. The regression model is

$$\text{OXYCON} = \mathbf{w}[0] + \mathbf{w}[1] \times \text{AGE} + \mathbf{w}[2] \times \text{HEARTRATE}$$

The table that follows shows a historical dataset that has been collected for this task.

HEART				HEART			
ID	OXYCON	AGE	RATE	ID	OXYCON	AGE	RATE
1	37.99	41	138	7	44.72	43	158
2	47.34	42	153	8	36.42	46	143
3	44.38	37	151	9	31.21	37	138
4	28.17	46	133	10	54.85	38	158
5	27.07	48	126	11	39.84	43	143
6	37.85	44	145	12	30.83	43	138

- (a) Assuming that the current weights in a multivariate linear regression model are $w[0] = -59.50$, $w[1] = -0.15$, and $w[2] = 0.60$, make a prediction for each training instance using this model.
- (b) Calculate the sum of squared errors for the set of predictions generated in Part (a).
- (c) Assuming a learning rate of 0.000002, calculate the weights at the next iteration of the gradient descent algorithm.
- (d) Calculate the sum of squared errors for a set of predictions generated using the new set of weights calculated in Part (c).
3. A multivariate logistic regression model has been built to predict the propensity of shoppers to perform a repeat purchase of a free gift that they are given. The descriptive features used by the model are the age of the customer, the socioeconomic band to which the customer belongs (*a*, *b*, or *c*), the average amount of money the customer spends on each visit to the shop, and the average number of visits the customer makes to the shop per week. This model is being used by the marketing department to determine who should be given the free gift. The weights in the trained model are shown in the following table.

Feature	Weight
Intercept ($w[0]$)	-3.82398
AGE	-0.02990
SOCIOECONOMIC BAND B	-0.09089
SOCIOECONOMIC BAND C	-0.19558
SHOP VALUE	0.02999
SHOP FREQUENCY	0.74572

Use this model to make predictions for each of the following query instances.

ID	AGE	SOCIOECONOMIC BAND	SHOP FREQUENCY	SHOP VALUE
1	56	b	1.60	109.32
2	21	c	4.92	11.28
3	48	b	1.21	161.19
4	37	c	0.72	170.65
5	32	a	1.08	165.39

4. The use of the **kernel trick** is key in writing efficient implementations of the **support vector machine** approach to predictive modelling. The kernel trick is based on the fact that the result of a **kernel function** applied to a support vector and a query instance is equivalent to the result of calculating the dot product between the support vector and the query instance after a specific set of basis functions have been applied to both—in other words, $\text{kernel}(d, q) = \phi(d) \cdot \phi(q)$.

(a) Using the support vector $\langle \mathbf{d}[1], \mathbf{d}[2] \rangle$ and the query instance $\langle \mathbf{q}[1], \mathbf{q}[2] \rangle$ as examples, show that applying a polynomial kernel with $p = 2$, $\text{kernel}(\mathbf{d}, \mathbf{q}) = (\mathbf{d} \cdot \mathbf{q} + 1)^2$, is equivalent to calculating the dot product of the support vector and query instance after applying the following set of basis functions:

$$\begin{aligned}\phi_0(\langle \mathbf{d}[1], \mathbf{d}[2] \rangle) &= \mathbf{d}[1]^2 & \phi_1(\langle \mathbf{d}[1], \mathbf{d}[2] \rangle) &= \mathbf{d}[2]^2 \\ \phi_2(\langle \mathbf{d}[1], \mathbf{d}[2] \rangle) &= \sqrt{2} \times \mathbf{d}[1] \times \mathbf{d}[2] & \phi_3(\langle \mathbf{d}[1], \mathbf{d}[2] \rangle) &= \sqrt{2} \times \mathbf{d}[1] \\ \phi_4(\langle \mathbf{d}[1], \mathbf{d}[2] \rangle) &= \sqrt{2} \times \mathbf{d}[2] & \phi_5(\langle \mathbf{d}[1], \mathbf{d}[2] \rangle) &= 1\end{aligned}$$

(b) A support vector machine model has been trained to distinguish between dosages of two drugs that cause a dangerous interaction and those that interact safely. This model uses just two continuous features, DOSE1 and DOSE2, and two target levels, *dangerous* (the positive level, + 1) and *safe* (the negative level, - 1). The support vectors in the trained model are shown in the following table.

DOSE1	DOSE2	CLASS
0.2351	0.4016	+1
-0.1764	-0.1916	+1
0.3057	-0.9394	-1

0.5590	0.6353	-1
-0.6600	-0.1175	-1

In the trained model the value of w_0 is 0.3074, and the values of the α parameters are $\langle 7.1655, 6.9060, 2.0033, 6.1144, 5.9538 \rangle$.

- i. Using the version of the support vector machine prediction model that uses basis functions (see [Equation 7.46](#)) with the basis functions given in Part (a), calculate the output of the model for a query instance with DOSE1 = 0.90 and DOSE2 = -0.90.
- ii. Using the version of the support vector machine prediction model that uses a kernel function (see [Equation 7.47](#)) with the polynomial kernel function, calculate the output of the model for a query instance with DOSE1 = 0.22 and DOSE2 = 0.16.
- iii. Verify that the answers calculated in Parts (i) and (ii) of this question would have been the same if the alternative approach (basis functions or the polynomial kernel function) had been used in each case.
- iv. Compare the amount of computation required to calculate the output of the support vector machine using the polynomial kernel function with the amount required to calculate the output of the support vector machine using the basis functions.
- * 5. In building multivariate logistic regression models, it is recommended that all continuous descriptive features be normalized to the range $[-1, 1]$. The following table shows a data quality report for the dataset used to train the model described in Question 3.

Feature	% Count Miss.			1 st Card. Min. Qrt.			3 rd Mean Median Qrt.			Std. Max. Dev.
	AGE	5,200	6	40	18	22	32.7	32	32	63
SHOP FREQUENCY	5,200	0	316	0.2	1.0	2.2	1.3	4.3	5.4	1.6
SHOP VALUE	5,200	0	3,730	5	11.8	101.9	100.14	174.6	230.7	72.1

Feature	% Count Miss.			Mode Card. Mode		Mode Count	Mode %	2 nd Mode Mode Count	2 nd Mode %
	SOCIOECONOMIC BAND	5,200	8	3	a	2,664	51.2	b	1,315
REPEAT PURCHASE	5,200	0	2	no	2,791	53.7	yes	2,409	46.3

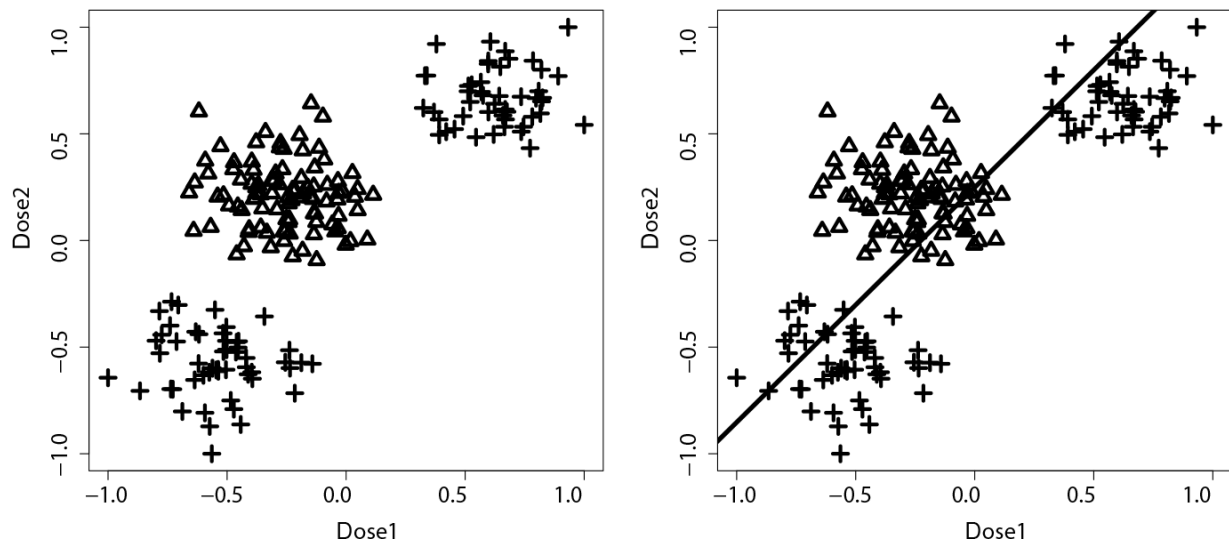
On the basis of the information in this report, all continuous features were normalized using **range normalization**, and any missing values were replaced using **mean imputation** for continuous features and **mode imputation** for categorical features. After applying these data preparation operations, a multivariate logistic regression model was trained to give the weights shown in the following table.

Feature	Weight
Intercept ($w[0]$)	0.6679
AGE	-0.5795
SOCIOECONOMIC BAND B	-0.1981
SOCIOECONOMIC BAND C	-0.2318
SHOP VALUE	3.4091
SHOP FREQUENCY	2.0499

Use this model to make predictions for each of the query instances shown in the following table (question marks refer to missing values).

ID	AGE	SOCIOECONOMIC BAND	SHOP FREQUENCY	SHOP VALUE
1	38	a	1.90	165.39
2	56	b	1.60	109.32
3	18	c	6.00	10.09
4	?	b	1.33	204.62
5	62	?	0.85	110.50

- * 6. The effects that can occur when different drugs are taken together can be difficult for doctors to predict. Machine learning models can be built to help predict optimal dosages of drugs so as to achieve a medical practitioner's goals.²⁶ In the following figure, the image on the left shows a scatter plot of a dataset used to train a model to distinguish between dosages of two drugs that cause a dangerous interaction and those that cause a safe interaction. There are just two continuous features in this dataset, DOSE1 and DOSE2 (both normalized to the range (-1,1) using range normalization), and two target levels, *dangerous* and *safe*. In the scatter plot, DOSE1 is shown on the horizontal axis, DOSE2 is shown on the vertical axis, and the shapes of the points represent the target level—crosses represent *dangerous* interactions and triangles represent *safe* interactions.



In the preceding figure, the image on the right shows a simple linear logistic regression model trained to perform this task. This model is

$$P(\text{TYPE} = \text{dangerous}) =$$

$$\text{Logistic}(0.6168 + 2.7320 \times \text{DOSE1} - 2.4809 \times \text{DOSE2})$$

Plainly, this model is not performing well.

- (a) Would the similarity-based, information-based, or probability-based predictive modeling approaches already covered in this book be likely to do a better job of learning this model than the simple linear regression model?
- (b) A simple approach to adapting a logistic regression model to learn this type of decision boundary is to introduce a set of basis functions that will allow a non-linear decision boundary to be learned. In this case, a set of basis functions that generate a cubic decision boundary will work well. An appropriate set of basis functions is as follows:

$$\begin{aligned}
 \phi_0(\langle \text{DOSE1}, \text{DOSE2} \rangle) &= 1 & \phi_1(\langle \text{DOSE1}, \text{DOSE2} \rangle) &= \text{DOSE1} \\
 \phi_2(\langle \text{DOSE1}, \text{DOSE2} \rangle) &= \text{DOSE2} & \phi_3(\langle \text{DOSE1}, \text{DOSE2} \rangle) &= \text{DOSE1}^2 \\
 \phi_4(\langle \text{DOSE1}, \text{DOSE2} \rangle) &= \text{DOSE2}^2 & \phi_5(\langle \text{DOSE1}, \text{DOSE2} \rangle) &= \text{DOSE1}^3 \\
 \phi_6(\langle \text{DOSE1}, \text{DOSE2} \rangle) &= \text{DOSE2}^3 & \phi_7(\langle \text{DOSE1}, \text{DOSE2} \rangle) &= \text{DOSE1} \times \text{DOSE2}
 \end{aligned}$$

Training a logistic regression model using this set of basis functions leads to the following model:

$$P(\text{TYPE} = \text{dangerous}) =$$

$$\text{Logistic}\left(-0.848 \times \phi_0(\langle \text{DOSE1}, \text{DOSE2} \rangle) + 1.545 \times \phi_1(\langle \text{DOSE1}, \text{DOSE2} \rangle) \right.$$

$$- 1.942 \times \phi_2(\langle \text{DOSE1}, \text{DOSE2} \rangle) + 1.973 \times \phi_3(\langle \text{DOSE1}, \text{DOSE2} \rangle)$$

$$+ 2.495 \times \phi_4(\langle \text{DOSE1}, \text{DOSE2} \rangle) + 0.104 \times \phi_5(\langle \text{DOSE1}, \text{DOSE2} \rangle)$$

$$\left. + 0.095 \times \phi_6(\langle \text{DOSE1}, \text{DOSE2} \rangle) + 3.009 \times \phi_7(\langle \text{DOSE1}, \text{DOSE2} \rangle) \right)$$

Use this model to make predictions for the following query instances:

ID	DOSE1	DOSE2
1	0.50	0.75
2	0.10	0.75
3	-0.47	-0.39
4	-0.47	0.18

- * 7. The following **multinomial logistic regression** model predicts the TYPE of a retail customer (*single*, *family*, or *business*) on the basis of the average amount that they spend per visit, SPEND, and the average frequency of their visits, FREQ:

$$M_{\mathbf{w}_{\text{single}}}(\mathbf{q}) = \text{logistic}(0.7993 - 15.9030 \times \text{SPEND} + 9.5974 \times \text{FREQ})$$

$$M_{\mathbf{w}_{\text{family}}}(\mathbf{q}) = \text{logistic}(3.6526 + -0.5809 \times \text{SPEND} - 17.5886 \times \text{FREQ})$$

$$M_{\mathbf{w}_{\text{business}}}(\mathbf{q}) = \text{logistic}(4.6419 + 14.9401 \times \text{SPEND} - 6.9457 \times \text{FREQ})$$

Use this model to make predictions for the following query instances:

ID	SPEND	FREQ
1	-0.62	0.10
2	-0.43	-0.71
3	0.00	0.00

- * 8. A support vector machine has been built to predict whether a patient is at risk of cardiovascular disease. In the dataset used to train the model, there are two target levels—*high risk* (the positive level, + 1) or *low risk* (the negative level, - 1)—and three descriptive features—AGE, BMI, and BLOOD PRESSURE. The support vectors in the trained model

are shown in the table below (all descriptive feature values have been standardized).

BLOOD			
AGE	BMI	PRESSURE	RISK
-0.4549	0.0095	0.2203	low risk
-0.2843	-0.5253	0.3668	low risk
0.3729	0.0904	-1.0836	high risk
0.558	0.2217	0.2115	high risk

In the model the value of w_0 is -0.0216 , and the values of the α parameters are $\langle 1.6811, 0.2384, 0.2055, 1.7139 \rangle$. What predictions would this model make for the following query instances?

BLOOD			
ID	AGE	BMI	PRESSURE
1	-0.8945	-0.3459	0.5520
2	0.4571	0.4932	-0.4768
3	-0.3825	-0.6653	0.2855
4	0.7458	0.1253	-0.7986

- * 9. A multivariate logistic regression model has been built to diagnose breast cancer in patients on the basis of features extracted from tissue samples extracted by biopsy.²⁷ The model uses three descriptive features—MITOSES, a measure of how fast cells are growing; CLUMPTHICKNESS, a measure of the amount of layering in cells; and BLANDCHROMATIN, a measure of the texture of cell nuclei—and predicts the status of a biopsy as either *benign* or *malignant*. The weights in the trained model are shown in the following table.

Feature	Weight
Intercept ($w[0]$)	-13.92
MITOSES	3.09
CLUMPTHICKNESS	0.63

- (a) Use this model to make predictions for each of the following query instances.

ID	MITOSES	CLUMP THICKNESS	BLAND CHROMATIN
1	7	4	3
2	3	5	1
3	3	3	3
4	5	3	1
5	7	4	4
6	10	4	1
7	5	2	1

- (b) The following are the ground truth labels for the query instances from Part (a).

\mathbf{d}_1	\mathbf{d}_2	\mathbf{d}_3	\mathbf{d}_4	\mathbf{d}_5	\mathbf{d}_6	\mathbf{d}_7
benign	benign	malignant	benign	malignant	malignant	benign

- i. Using the ground truth labels, calculate the **squared error** loss for each query instance (assume that $benign = 0$ and $malignant = 1$).
- ii. **Categorical cross entropy** is another loss function that is commonly used for classification models. Categorical cross entropy is defined as

$$-(t_i \times \ln(\mathbb{M}_{\mathbf{w}}(\mathbf{d}_i)) + (1 - t_i) \times \ln(1 - \mathbb{M}_{\mathbf{w}}(\mathbf{d}_i)))$$

Using the ground truth labels previously given, calculate the categorical cross entropy for the query set. Compare these values to the squared error loss values for each instance.

- * 10. The following images are handwritten instances of the digits 0 and 1.²⁸ The images are small, 8 pixels by 8 pixels, and each pixel contains a gray level from the range [0,7].



Rather than use individual pixel values, which can lead to very high-dimensional feature vectors, a simpler way to represent images for use with regression models is to calculate a histogram for each image and use this as the feature vector instead. In this case the histograms simply count the frequency of occurrence of each possible gray level in each image. The table that follows shows the histograms for a small dataset of 16 images split between examples of digits 0 and 1.

ID	GL-0	GL-1	GL-2	GL-3	GL-4	GL-5	GL-6	GL-7	DIGIT
0	31	3	6	2	7	5	6	4	0
1	37	3	1	4	1	3	2	13	1
2	31	3	4	1	8	7	3	7	0
3	38	2	3	0	1	1	5	14	1
4	31	5	3	2	5	2	5	11	0
5	32	6	3	2	1	1	5	14	1
6	31	3	5	2	3	6	2	12	0
7	31	4	3	4	1	5	5	11	0
8	38	4	2	2	2	4	4	8	1
9	38	3	2	3	4	4	1	9	1

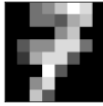
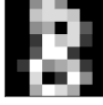
A logistic regression model has been trained to classify digits as either 0 or 1. The weights in this model are as follows:

Intercept	GL-0	GL-1	GL-2	GL-3	GL-4	GL-5	GL-6	GL-7
w[0]	w[1]	w[2]	w[3]	w[4]	w[5]	w[6]	w[7]	w[8]
0.309	0.100	-0.152	-0.163	0.191	-0.631	-0.716	-0.478	-0.171

This model has been used to make predictions for the instances in the training set above. These predictions, and the related calculations required for calculating error and *errorDelta* values are shown in the following table.

ID	$\mathbb{M}_{\mathbf{w}}(\mathbf{d}_i)$	t_i	Error	Squared		$errorDelta(\mathcal{D}, \mathbf{w}[j])$							
				Error	$\mathbf{w}[0]$	$\mathbf{w}[1]$	$\mathbf{w}[2]$	$\mathbf{w}[3]$	$\mathbf{w}[4]$	$\mathbf{w}[5]$	$\mathbf{w}[6]$	$\mathbf{w}[7]$	$\mathbf{w}[8]$
0	0.051	0	-0.051	?	-0.0025	-0.0765	-0.0074	-0.0148	-0.0049	-0.0173	-0.0123	-0.0148	-0.0099
1	?	1	0.003	0.0000	-0.0025	0.0003	0.0000	0.0000	0.0000	0.0000	0.0000	0.0000	0.0001
2	0.019	0	-0.019	0.0004	-0.0025	-0.0110	-0.0011	-0.0014	-0.0004	-0.0028	-0.0025	-0.0011	?
3	0.993	1	0.007	0.0000	?	0.0018	0.0001	0.0001	0.0000	0.0000	0.0000	0.0002	0.0007
4	?	0	-0.489	0.2391	-0.0025	-3.7879	-0.6110	-0.3666	-0.2444	-0.6110	-0.2444	-0.6110	-1.3441
5	0.945	1	?	0.0030	-0.0025	0.0915	0.0172	0.0086	0.0057	0.0029	0.0029	0.0143	0.0400
6	?	0	-0.400	0.1600	-0.0025	-2.9760	-0.2880	-0.4800	-0.1920	-0.2880	-0.5760	-0.1920	-1.1520
7	0.703	0	?	0.4942	-0.0025	-4.5502	?	-0.4403	-0.5871	-0.1468	-0.7339	-0.7339	-1.6146
8	0.980	1	0.020	?	-0.0025	0.0149	0.0016	0.0008	0.0008	0.0008	0.0016	0.0016	0.0031
9	0.986	1	0.014	0.0002	-0.0025	0.0073	0.0006	0.0004	0.0006	0.0008	0.0008	0.0002	0.0017

- (a) Some of the model predictions are missing in the preceding table (marked with a ?). Calculate these.
- (b) Some of the Error and Squared Error values are missing in the preceding table (marked with a ?). Calculate these.
- (c) Some of the $errorDelta$ values are missing in the preceding table (marked with a ?). Calculate these.
- (d) Calculate a new set of weights for this model using a **learning rate** of 0.01.
- (e) The following table shows handwritten examples of the digits 7 and 8 and their corresponding histogram values.

	GL-0	GL-1	GL-2	GL-3	GL-4	GL-5	GL-6	GL-7
	35	1	5	4	5	2	4	8
	30	6	2	0	5	4	4	13

- i. Calculate the output of the model (using the updated weights calculated in the previous part) for these two instances.
- ii. Comment on the appropriateness of these outputs.

- Weights are also known as **model parameters**, and so regression models are often known as **parameterized models**.
- Error functions are commonly referred to as **loss functions** because they represent what we *lose* by reducing the training set to a simple model.

3. One of the best-known and earliest applications of solving a problem by reducing the sum of squared errors occurred in 1801, when **Carl Friedrich Gauss** used it to minimize the measurement error in astronomical data and by doing so was able to extrapolate the position of the dwarf planet Ceres, which had recently been found but then was lost behind the glare of the sun.

4. The words **multivariable** and **multi-feature** are equivalent. The use of multivariable is a sign of the origins of regression in statistics rather than machine learning.

5. In fact, this is the error surface that results from the office rentals dataset when the descriptive features in the dataset are normalized to the range $[-1, 1]$ using range normalization before being used. We discuss normalization subsequently in the chapter.

6. See Appendix C^[765].

7. **Stochastic gradient descent** is a slightly different approach, in which an adjustment to each weight is made on the basis of the error in the prediction made by the candidate model for each training instance individually. This means that many more adjustments are made to the weights. We do not discuss stochastic gradient descent in any detail in this book, although the modifications that need to be made to the gradient descent algorithm for stochastic gradient descent are fairly simple.

8. Note that in this example, we have normalized the RENTAL PRICE and SIZE features to the range $[-1, 1]$, so the error surfaces shown look slightly different from those shown in Figure 7.3^[318] and Figure 7.5^[329].

9. All values in Table 7.3^[331], and similar subsequent tables, are reported at a precision of two places of decimal. Because of this, some error values and squared error values may appear inconsistent. This, however, is only due to rounding differences.

10. Because this is a higher-dimensional problem (three dimensions in the feature space and four dimensions in the weight space), it is not possible to draw the same graphs of the error surfaces that were shown for the previous examples.

11. Gross et al. (2006) describes a real-world example of this kind of application of predictive analytics.

12. Note that in this figure, both the RPM and VIBRATION features have been normalized to the range $[-1, 1]$ (using **range normalization** as described in Section 3.6.1^[87]). It is standard practice to normalize descriptive features whenever we are using regression models to predict a categorical target feature.

13. A hard threshold can be used fairly successfully to train prediction models for categorical targets using the **perceptron learning rule**, although we do not cover that in this book.

14. The logistic function is a real workhorse of mathematical modeling and is used in a huge range of different applications. For example, the logistic function has been used to model how new words enter a language over time, first used very infrequently before moving through a tipping point to become widespread in a language.

15. Note that in this example and in the examples that follow, a normalized version of the generators dataset is used (all descriptive features are normalized to the range $[-1, 1]$ using range normalization), so the weights in Equation (7.27)^[342] are different from those in Equation (7.23)^[339]. If it were not for normalization, these two sets of weights would be the same.

16. This example is very much simplified for illustration purposes, but very interesting work is done on building prediction models from the output of EEG and fMRI scans—for example, Mitchell et al. (2008).

17. The term arising from ϕ_7 is commonly referred to as an **interaction term** because it allows two descriptive features to *interact* in the model.

18. Multinomial logistic regression models are often known as **maximum entropy**, **conditional maximum entropy**, or **MaxEnt** models.
19. This is an example of an ensemble model like those described in Section 4.4.5^[158].
20. Remember that for problems with more than two descriptive features, the decision boundary is a **hyperplane** rather than a **line**.
21. This also means that we no longer use the dummy descriptive feature, **d[0]**, which we previously always set to 1; see Equation (7.9)^[320].
22. These parameters are formally known as **Lagrange multipliers**.
23. We provide references in Section 7.6^[370].
24. Question 4 in the Exercises at the end of this chapter explores the kernel trick in more detail, and worked examples are provided in the solution.
25. This question is inspired by Tsanas and Xifara (2012), and although the data used is artificially generated, it is based on the Energy Efficiency Dataset available from the UCI Machine Learning Repository (Bache and Lichman, 2013) at archive.ics.uci.edu/ml/datasets/Energy+efficiency/.
26. The data used in this question has been artificially generated for this book. Mac Namee et al. (2002) is, however, a good example of prediction models used to help doctors select correct drug dosages.
27. The data in this question has been artificially created but is inspired by the famous **Wisconsin breast cancer dataset** first described in Mangasarian and Wolberg (1990) and is available from the UCI Machine Learning Repository (Bache and Lichman, 2013).
28. These images are based on the dataset from the UCI Machine Learning repository Dua and Graff (2017) and originally described by Alimoglu and Alpaydin (1996).

8

Deep Learning

“A map is not the territory it represents, but, if correct, it has a similar structure to the territory, which accounts for its usefulness.”

—Alfred Korzybski, *Science and Sanity*, p. 58

In this chapter¹ we introduce deep learning, an approach to machine learning that is inspired by how the brain is structured and operates. **Deep learning** is a relatively new term that describes research on modern artificial neural networks. Artificial neural network models are composed of large numbers of simple processing units, called neurons, that typically are arranged into layers and are highly interconnected. Artificial neural networks are some of the most powerful machine learning models, able to learn complex non-linear mappings from inputs to outputs. As such, they generally work well in domains in which there are large numbers of input features (such as image, speech, or language processing), and for which there are very large datasets available for training. Although the history of artificial neural networks can be traced back to the 1940s, the term deep learning came to prominence only in the mid-2000s.² The term deep learning emphasizes that modern networks are deeper (in terms of number of layers) than previous networks. This extra depth enables the networks to learn more complex input-output mappings.

The Fundamentals section of this chapter introduces the standard artificial neural network architecture: a feedforward neural network. We then present the backpropagation algorithm, the standard algorithm used to train neural networks, and illustrate how the algorithm functions with a worked example.

The first two extensions and variations sections explain why the backpropagation algorithm can struggle with unstable gradients when training a deep network and how a number of important hyper-parameter decisions, such as the choice of the network weight initialization process, and activation functions, can help with the challenge of unstable gradients. We then explain how a neural network can be modified and trained to handle categorical target features, using a softmax output layer and the cross-entropy loss function. Then we introduce a well-known extension to backpropagation training known as dropout, which can help stop a network from overfitting. The final two extensions and variations sections introduce well-known neural network architectures, including convolutional neural networks and recurrent neural networks.

8.1 Big Idea

The human brain is an incredibly powerful learning system. Thanks to neuroscience we now know quite a bit about the structure of the brain. For example, we know that the brain works by propagating electrical signals through a massive network of interconnected cells, known as neurons. In fact, it is estimated that the human brain contains around 100 billion interconnected neurons (Herculano-Houzel, 2009).

There are many different types of neurons in the brain; however, in general, neurons have a simple three-part structure consisting of (1) a cell body; (2) a set of relatively short fibers connected to the cell body, called dendrites; and (3) a single long fiber connected to the cell body, called an axon. The dendrites of one neuron connect to the axons of other neurons via connections known as synapses. These synapses allow electrical signals to pass from the axon of one neuron to a dendrite of another. Essentially, the dendrites are the neuron's input channels, and the axon is the output channel. [Figure 8.1](#) presents a schematic of the structure of a neuron that illustrates how the neuron's cell body, dendrites, and axon are interconnected and how one neuron connects to other neurons in the brain. Functionally, an individual neuron can be understood as a simple signal processing system. A neuron functions as an all-or-none switch: if the electrical stimuli gathered by its dendrites are strong enough, the neuron transmits an electrical pulse, known as an action potential, along its axon; otherwise it has no output.

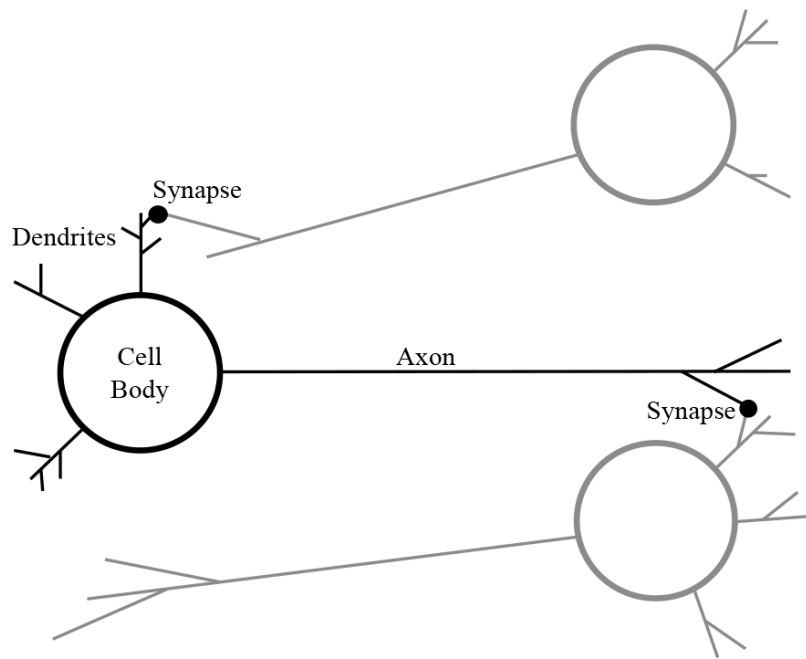


Figure 8.1

A high-level schematic of the structure of a neuron. This figure illustrates three interconnected neurons; the middle neuron is highlighted in black, and the major structural components of this neuron are labeled cell body, dendrites, and axon. Also marked are the synapses connecting the axon of one neuron and the dendrite of another, which allow signals to pass between the neurons.

Although neuroscience has discovered a lot about the neural structure of the brain, neuroscientists are still working on understanding how learning happens in the brain and how high-level human behavior arises from the processing of neurons. In 1949 Donald O. Hebb proposed a theory that attempted to explain how general human behavior emerged from the physiology of the brain. The basis of this theory was that complex behavior emerges from the interactions between massive numbers of highly interconnected neurons rather than from complex processing within neurons. The idea that human mental phenomena emerge through the interconnections between neurons became known as **connectionism**. Hebb also postulated a mechanism for how lasting memories are learned in the brain on the basis of a process of changes to the connections between neurons:

When an axon of a cell A is near enough to excite a cell B and repeatedly or persistently takes part in firing it, some growth process or metabolic change takes place in one or both cells such that A's efficiency, as one of the cells firing B, is increased. (Hebb, 1949, p. 62)

Hebb's theory that learning occurs through changes in the connections between neurons and that behavior emerges through the flow of information across these connections has been very influential both in neuroscience and, as we will discuss, in deep learning.

The big idea in deep learning is to develop computational models that are inspired by the structure and operations of the human brain. The human brain is, of course, much more complex and sophisticated than even the most advanced deep learning models. However, it is because deep learning models are inspired by the human brain that they are known as artificial neural networks: they are designed (at least at a very abstract level) to mirror the structure of the brain, and the adoption of a learning mechanism based on adjusting the connections between neurons can be understood as mimicking Hebb's theory of how the brain learns.

8.2 Fundamentals

We begin this section by introducing the basic building block of all deep learning models, the **artificial neuron** (see Section 8.2.1^[384]); we then describe how the artificial neurons can be connected together to create an **artificial neural network** (see Section 8.2.2^[388]). After we have covered the fundamentals of the models, we explain how these artificial neural networks can be understood as sequences of matrix multiplications (see Section 8.2.3^[390]). Understanding how a neural network can be represented and implemented as a sequence of matrix multiplications has important implications in terms of training time speedups. The matrix representation of a neural network is also useful in terms of understanding why we need to include a non-linear function as part of the information processing within each of the neurons in a network (see Section 8.2.4^[394]) and why the depth of a network (i.e., the number of layers) is important (see Section 8.2.5^[395]). Finally, we use the matrix representation of a network as a compact representation of neural networks in the worked examples. For example, we use the matrix representation to present elements of the worked example in Section 8.3.5^[421], in which we step through the training of a feedforward neural network using backpropagation.

8.2.1 Artificial Neurons

The fundamental building block of a neural network is a computational model known as an artificial neuron. The template structure of these computational models was first defined by McCulloch and Pitts (1943). McCulloch and Pitts were trying to develop a model of the activity in the human brain based on propositional logic. Their inspiration for this work was linking the fact that propositional logic using a Boolean representation (TRUE/FALSE or 1/0) and neurons in the brain are somewhat similar, insofar as they have an all-or-none character (i.e., they act as a switch that responds to a set of inputs by outputting either a high activation or no activation). As a result, they designed a model of the neuron that would take in multiple inputs and then output either a high signal, a 1, or a low signal, a 0. This McCulloch and Pitts model had a two-part structure.

In the first stage of the McCulloch and Pitts model, each input is multiplied by a weight, and the results of these multiplications are then added together. This calculation is known as a weighted sum because it involves summing the weighted inputs. For example, for a weighted sum calculation over two inputs we require two predefined weights. If we assume the two predefined weights are $w_1 = 0.5$ and $w_2 = 3$ and the two inputs are $input_1 = 6$ and $input_2 = 7$, then the weighted sum calculation would proceed as follows:

$$(0.5 \times 6) + (3 \times 7) = 24$$

More generally, we can mathematically define the weighted sum calculation

$$z = \underbrace{w[0] \times d[0] + w[1] \times d[1] + \cdots + w[m] \times d[m]}_{\text{weighted sum}} \quad (8.1)$$

There are, in fact, multiple ways of mathematically defining a weighted sum calculation: we can use the Σ symbol to reduce the length of the equation, or we can represent it as a **dot product** or as a **matrix product**

$$\begin{aligned}
z &= \underbrace{\mathbf{w}[0] \times \mathbf{d}[0] + \mathbf{w}[1] \times \mathbf{d}[1] + \cdots + \mathbf{w}[m] \times \mathbf{d}[m]}_{\text{weighted sum}} \\
&= \sum_{j=0}^m \mathbf{w}[j] \times \mathbf{d}[j] \\
&= \underbrace{\mathbf{w} \cdot \mathbf{d}}_{\text{dot product}} = \underbrace{\mathbf{w}^T \mathbf{d}}_{\text{matrix product}} = [\mathbf{w}_0, \mathbf{w}_1, \dots, \mathbf{w}_m] \begin{bmatrix} d_0 \\ d_2 \\ \vdots \\ d_m \end{bmatrix} \tag{8.2}
\end{aligned}$$

where \mathbf{d} is a vector of $m + 1$ descriptive features, $\mathbf{d}[0]\dots\mathbf{d}[m]$; and $\mathbf{w}[0]\dots\mathbf{w}[m]$ are $(m + 1)$ weights. However, no matter which way we choose to define the weighted sum, the operation remains the same.

The weights can either be excitatory (having a positive value, which increases the probability of the neuron activating) or inhibitory (having a negative value, which decreases the probability of a neuron firing). We have in fact already come across the weighted sum calculation in Chapter 7^[311] when we defined the multivariate linear regression model (see Equation (7.9)^[320]). Recall from Chapter 7^[311] that $\mathbf{w}[0]$ is the equivalent of the y -intercept in the equation of the line from high school geometry (see (7.2.1)^[313]), and $\mathbf{d}[0]$ is a dummy descriptive feature used for notational convenience and is always equal to 1 (see (7.9)^[320]). Including this dummy feature makes the \mathbf{d} and \mathbf{w} vectors have the same length, and this allows us to write the equation as the **dot product** of the two vectors (i.e., $\mathbf{w} \cdot \mathbf{d}$). The inclusion of the weight $\mathbf{w}[0]$ means that there is one more weight term than there are real descriptive features. In other words, there are more weight parameters on the model than there are dimensions in the input space. This extra weight term allows the model to define lines that do not go through the origin of the input space: setting the $\mathbf{w}[0]$ to a value other than 0 translates the line defined by the model away from the origin of the input space, just as changing the value of the y -intercept in the **equation of a line** moves a line up and down the y -axis away from the origin. This $\mathbf{w}[0]$ term is often referred to as the **bias** parameter because in the absence of any other input, the output of the weighted sum is biased to be the value of $\mathbf{w}[0]$. Technically, the inclusion of the bias parameter as an extra weight in this operation changes the function from a linear function on the inputs to

an **affine function**. An affine function is composed of a linear function followed by a translation; this simply means that the mapping defined by an affine function from inputs to outputs is linear but the plot of this mapping does not necessarily pass through the origin. For example, if we dropped the $\mathbf{d}[0]$ dummy feature and then multiplied each of the real descriptive features by a weight and summed the results, we would be applying a linear function to the inputs. A plot of this function would pass through the origin because there is no y -intercept (or bias term) included in the calculation. However, if we then add the bias term (the y -intercept) to the results of the linear function, we are translating the results of the linear function away from the origin. By including the bias term in the set of weights along with a dummy descriptive feature, the function implemented by multiplying the weights by the extended descriptive features is now an affine function. In much of this chapter we discuss matrix representations and calculations, so it is worth noting here that a linear function can always be represented by a single matrix multiplication and that an affine transformation in m dimensions can always be represented as a linear function in $m + 1$ dimensions (as we have done here) and consequently as a single matrix multiplication in $m + 1$ dimensions. In this chapter, affine and linear functions are so closely associated that we often use the term **linear** to refer to affine operations.

In the second stage of the McCulloch and Pitts model, the result of the weighted sum calculation, z , is then converted into a high or a low activation by comparing the value of z with a manually preset threshold; if z is greater than or equal to the threshold, the artificial neuron outputs a 1 (high activation), and otherwise it outputs a 0 (low activation). This threshold is nothing more than a number that is selected by the designer of the artificial neuron. Using the symbol θ to denote the threshold, the second stage of processing in the McCulloch and Pitts model can be defined

$$\mathbb{M}_w(\mathbf{d}) = \begin{cases} 1 & \text{if } z \geq \theta \\ 0 & \text{otherwise} \end{cases} \quad (8.3)$$

In the McCulloch and Pitts model the weights were manually set, but subsequently in this chapter we explain how these weights can be learned

from data using backpropagation. However, the two-part structure of the McCulloch and Pitts model of the neuron is the blueprint for the neurons used in modern neural networks. The main difference between the McCulloch and Pitts model and modern artificial neurons is that the thresholding function is replaced by other functions. Frequently, the term **activation function** is used as a general term to refer to whatever function is employed in the second stage of an artificial neuron, because the function maps the weighted sum value, z , into the output value, or activation, of the neuron. Until recently, one of the most popular functions used in artificial neurons was the **logistic** function introduced in Chapter 7 (see Equation (7.25)^[342] and Figure 7.12^[343]). However, today the most popular choice of function for an activation function is the **rectified linear activation function or rectifier**

$$\text{rectifier}(z) = \max(0, z) \quad (8.4)$$

Note that neurons are often referred to as **units**, and they are distinguished by the type of activation function they use. Hence a neuron that uses a logistic activation function is referred to as a **logistic unit**, and a unit that uses the rectifier function is known as a **rectified linear unit** or **ReLU**. We will explain why the logistic function became so popular as an activation function when we introduce the **backpropagation** algorithm (see Section 8.3^[403]), and why the rectified linear function replaced it when we explain the **vanishing gradient** problem (see Section 8.4.1^[434]). Figure 8.2^[387] shows plots of some of the activation functions that have been popular in neural networks over the last few decades, including the threshold, logistic, **tanh**, and rectifier linear functions.

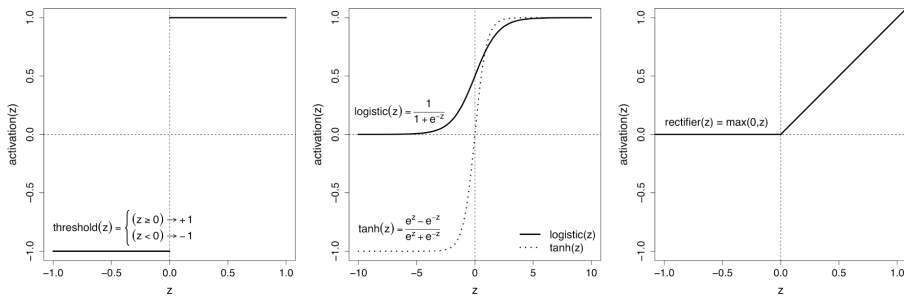


Figure 8.2

Plots for activation functions that have been popular in the history of neural networks.

[Figure 8.2](#)^[387] makes it apparent that a common characteristic of all of these activation functions is that they are not linear functions. This is not a coincidence. In fact, it is the introduction of a non-linearity into the input to output mapping defined by a neuron that enables an artificial neural network to learn complex non-linear mappings; indeed, it is this ability to learn these complex non-linear mappings that makes artificial neural networks such powerful models, in terms of their ability to be accurate on complex tasks. We will explain in more detail why we need non-linear activation functions in neurons in Section 8.2.4^[394].

If we use the symbol φ to represent the activation function of a neuron, we can mathematically define an artificial neuron as follows:

$$\begin{aligned} M_{\mathbf{w}}(\mathbf{d}) &= \varphi(\mathbf{w}[0] \times \mathbf{d}[0] + \mathbf{w}[1] \times \mathbf{d}[1] + \cdots + \mathbf{w}[m] \times \mathbf{d}[m]) \\ &= \varphi \left(\sum_{i=0}^m w_i \times d_i \right) = \varphi \left(\underbrace{\mathbf{w} \cdot \mathbf{d}}_{dot\ product} \right) = \varphi \left(\underbrace{\mathbf{w}^T \mathbf{d}}_{matrix\ product} \right) = \varphi \left([w_0, w_1, \dots, w_m] \begin{bmatrix} d_0 \\ d_1 \\ \vdots \\ d_m \end{bmatrix} \right) \end{aligned} \quad (8.5)$$

where \mathbf{d} is a vector of $m + 1$ descriptive features (including the dummy $\mathbf{d}[0]$ feature), $\mathbf{d}[0], \mathbf{d}[1], \dots, \mathbf{d}[m]$; \mathbf{w} is a vector of $m + 1$ weights (including the bias term) $\mathbf{w}[0], \mathbf{w}[1], \dots, \mathbf{w}[m]$; and φ represents the activation function (threshold, tanh, logistic, or rectifier, etc.) that converts the result of the weighted sum to the output activation. [Figure 8.3](#) presents a graphical representation of this same function. In this figure the arrows carry activations in the direction the arrow is pointing, the weight label on each arrow represents the weight that will be applied to the descriptive feature carried along the arrow, the Σ symbol represents the weighted sum of the inputs, and the φ symbol represents the threshold function being applied to the result of the weighted sum to convert it into an activation.

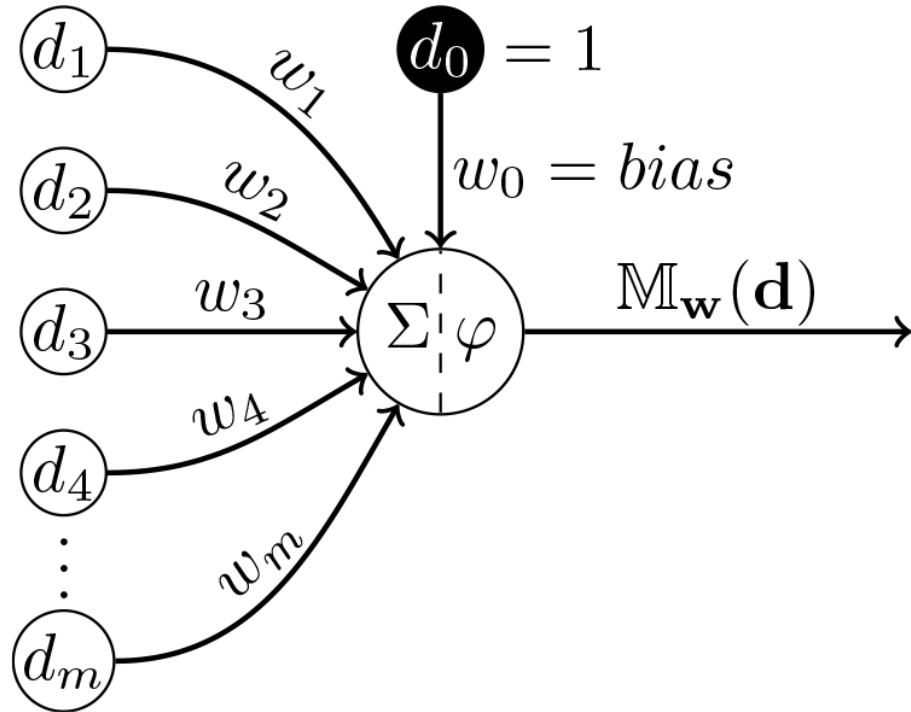


Figure 8.3

A schematic of an artificial neuron.

8.2.2 Artificial Neural Networks

An artificial neural network consists of a network of interconnected artificial neurons. [Figure 8.4](#)^[390] illustrates the structure of a basic artificial neural network. In this network the neurons are organized into a sequence of layers. An artificial neural network can have any structure, but a layer-based organization of neurons is common. There are two types of neurons in this network: sensing neurons and processing neurons. First, the two squares on the left of the figure represent the two memory locations through which inputs are presented to this network. These locations can be thought of as sensing neurons that permit the network to sense the external inputs. Although we consider these memory locations as (sensing) neurons within the network, the inputs presented to the network are not transformed by these sensing neurons. This is why they are represented by squares to visually distinguish them from the other neurons in the network that do transform their inputs. Each of the circles in the network represents a processing neuron that transforms its input using the previously described two-step process of a weighted sum followed by an activation function.

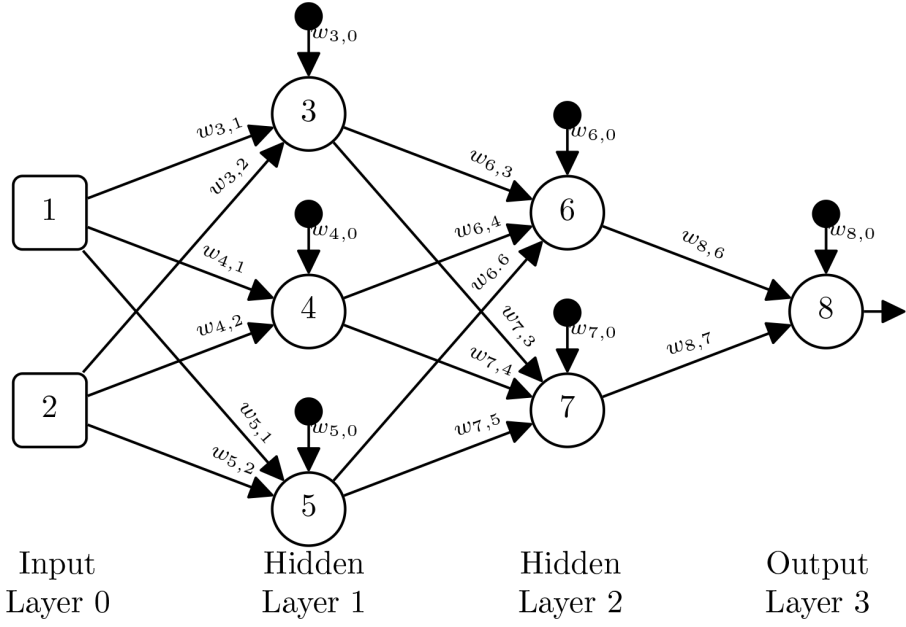


Figure 8.4

A schematic of a feedforward artificial neural network.

The arrows connecting the neurons in the network indicate the flow of information through the network. Examining the arrows in the network shows that the input to the processing neurons can be any of the following: an external input presented to the network via the sensing neurons, the output activation of another processing neuron in the network, or a dummy input that is always set to 1 (the input from a black circle). Also, each arrow is labeled with the weight that the neuron receiving the activation flowing along that connection applies to that activation during the weighted sum calculation. The bias terms are the weights on the dummy inputs. Notice that the indices in the weight subscripts are in reverse order from what might be expected: the first subscript is the index of the neuron to which the activation is flowing, and the second subscript is the index of the neuron that generated the activation. In the case of bias terms, this second index is always equal to zero. The advantage of this index ordering becomes clear when we describe how matrix multiplications can be used to speed up the training and inference in neural networks (see Section 8.2.3^[390]). Training a neural network involves finding a good set of values for these weights.

The network architecture shown in Figure 8.4^[390] is an example of a **feedforward network**. The defining characteristic of a feedforward network is that there are no loops or cycles in the network connections that

would allow the output of a neuron to flow back into the neuron as an input (even indirectly). In other words, in a feedforward network the activations in the network always flow forward through the sequence of layers. This network is also a **fully connected** network because each of the neurons in the network is connected in such a way that it receives inputs from all the neurons in the preceding layer and passes its output activation to all the neurons in the next layer. Subsequently in this chapter we introduce network architectures that are not feedforward and also architectures that are not fully connected.

When this network is processing a set of external inputs, the inputs are presented to the network through sensing neurons in the input layer; this causes the neurons in the next layer to generate activation signals in response to these inputs; and these activations flow forward through the network until the output layer is reached, where the response of the network to the inputs is the activations of the neurons in this final output layer. The internal layers in the network, which are neither input nor output layers, are called **hidden layers**.

The **depth** of a neural network is equal to the number of hidden layers plus the output layer. Therefore, the network in [Figure 8.4](#)^[390] has three layers. The number of layers required for a network to be considered deep is an open question; however, Cybenko (1988) proved that a network with three layers of (processing) neurons (i.e., two hidden layers and an output layer) can approximate any function to arbitrary accuracy. So, here we define the minimum number of hidden layers necessary for a network to be considered deep as two; under this definition the network in shown [Figure 8.4](#)^[390] would be described as a deep network. However, most deep networks have many more than two hidden layers. Today some deep networks have tens or even hundreds of layers. In Section 8.2.5^[395] we discuss how the depth of a neural network affects the ability of the network to represent and learn functions at different levels of complexity.

8.2.3 Neural Networks as Matrix Operations

In Section 8.2.1^[384] we described how adding a dummy feature $\mathbf{d}[0] = 1$ to the input vector of a neuron and also including the y-intercept term (or bias term) from the equation of a line as part of the weight vector of the neuron, as $\mathbf{w}[0]$, permitted us to calculate the weighted sum of the neuron using a

single dot product between the weight vector and the input vector. One advantage of this was notational convenience; we were able to simplify Equation (8.2)^[385]. A much more important advantage, however, is that it can enable significant computational speedups in the training and application of a neural network. There are two ways that this can speed up neural network training and data processing:

1. In a fully connected network, all the neurons in one layer receive activations from all the neurons in the preceding layer; and, because all the neurons in a layer receive the same vector of activations as inputs, we can calculate the weighted sum calculations for all of these neurons using a single vector by matrix multiplication.
2. The fact that we can implement the calculation of the weighted sums for an entire layer of neurons as one matrix multiplication operation can be generalized to implementing an entire network as a sequence of matrix multiplications (one per layer of the network). This means that if we represent a set of input vectors as a matrix of inputs, we can get the network to process all the inputs in parallel. This parallelization of the processing of a number of examples by the network is particularly useful because the standard practice to train a network is to present **batches** of examples to the network, rather than to present examples one at a time.

In order to explain how matrix multiplications are used in a neural network, we need to introduce some notation and then define the order of the matrices in the multiplication. We use the convention of a bold capital letter to denote a matrix and a superscript in parentheses to list the relevant layer. Using this notation and taking the second layer of neurons in a network as an example, if we name the matrix containing the weights on the edges into Layer 2 as $\mathbf{W}^{(2)}$, the column vector of activations coming from the neurons in Layer 1 as $\mathbf{a}^{(1)}$, and the column vector of weighted sums for the neurons in Layer 2 as $\mathbf{z}^{(2)}$, then the order of the matrices in the multiplication operation that we use in this explanation is

$$\mathbf{z}^{(2)} = \mathbf{W}^{(2)}\mathbf{a}^{(1)} \quad (8.6)$$

In the matrix multiplication, each element in a row in the matrix on the left is multiplied by the corresponding element in each column in the matrix on the right, and then the results of these multiplications are summed. This means that each element in $\mathbf{z}^{(2)}$ is the result of multiplying each element in a row in $\mathbf{W}^{(2)}$ by the corresponding element in the column vector $\mathbf{a}^{(1)}$ and summing the results. This is why the indices on weights in [Figure 8.4](#)^[390] were reversed: if we store all the weights for each neuron in a layer in a row in the weight matrix for the layer, then the weights are in the correct position when the weight matrix is multiplied by a column vector of activations from the previous layer.

[Figure 8.5](#)^[392] illustrates how a neural network can be defined as a sequence of matrix multiplication operations, with an elementwise application of an activation function to the results of each multiplication. The left side of [Figure 8.5](#)^[392] presents a graph-based representation of a neural network; this network has a single hidden layer containing three neurons and an output layer with a single neuron in it. The right side of [Figure 8.5](#)^[392] illustrates the sequence of matrix operations that this network would carry out to process a single input vector. [Figure 8.5](#)^[392] highlights how bias terms are introduced into the activation vectors in such a way that they are aligned with the bias term weights during the matrix multiplication. The first column of each weight matrix (filled in black) contains the bias term weights for each neuron in the layer. Each activation vector is augmented with a new first row (filled in black) containing the dummy descriptive feature $\mathbf{d}[0] = 1$. This ensures that the dummy descriptive feature (row 0) will be multiplied by the bias terms weights (column 0) in the multiplication operation.

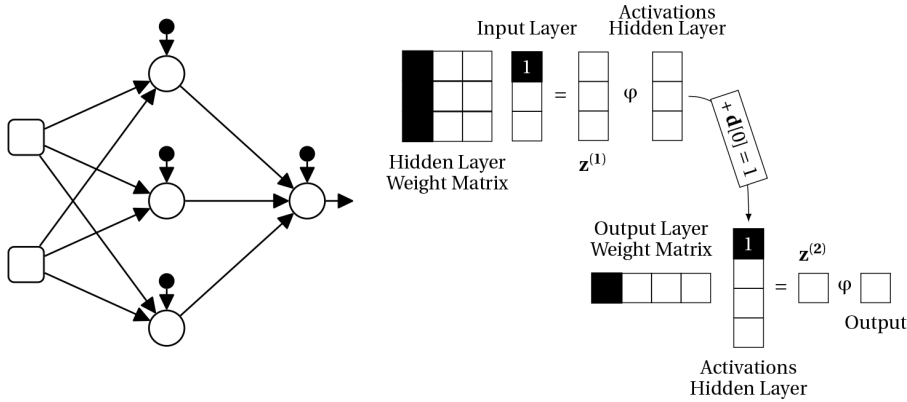


Figure 8.5

An illustration of the correspondence between graphical and matrix representations of a neural network. This figure is inspired by Figure 3.9 of Kelleher (2019).

Stepping through the processing of the network in Figure 8.5^[392], the sequence of calculations necessary to generate the activations for the neurons in the hidden layer is illustrated in the top row of the figure. The first operation in this sequence is the multiplication of the matrix containing the weights on the connections into the neurons in the hidden layer by the outputs of the input layer. The weight matrix is organized so that each row contains the weights for a single neuron. The leftmost element in each row (filled in black) is the bias term weight. The input vector has been augmented with the dummy feature $d[0] = 1$, which is stored in the top row of the vector. Multiplying the weight matrix by the augmented input vector generates the vector of weighted sums for the hidden layer neurons, $\mathbf{z}^{(1)}$. The activation function, φ , is then applied to each of the elements in $\mathbf{z}^{(1)}$ to generate the activations for each of the neurons in the hidden layer. Because this vector of activations from the hidden layer is passed on to another layer for processing, it has to be augmented with the dummy feature $d[0] = 1$; this is represented by the label on the arrow linking the top row of operations with the bottom row.

The bottom row illustrates the operations carried out in the output layer of the network. As with the hidden layer, the first operation is the multiplication of the layer's weight matrix by the (augmented) vector of activations from the previous layer. The weight matrix is again organized with one row of weights per neuron and with the bias term weight as the first element in the row (shown in black). There is only one neuron in the output layer, and so there is only one row in this weight matrix. The

multiplication operation calculates the weighted sum for the output neuron $\mathbf{z}^{(2)}$, and this is passed through the neuron's activation function φ to generate the output of the network.

The fact that we can use a sequence of matrix operations to implement how a neural network processes a single example can be generalized to processing a number of examples in parallel. [Figure 8.6](#)^[393] illustrates how the same sequence of operations shown in [Figure 8.5](#)^[392] to process one example can be used to enable the same network to process four examples in parallel. This is achieved by replacing the input vector containing a single example with an input matrix containing multiple examples. This input matrix is organized so that each column contains the feature vector for a single example. The gray columns in each of the activation and \mathbf{z} matrices trace the processing of the second example through the sequence of operations. Notice that the weight matrices do not change shape, nor does the sequence of operations, and the activation functions φ are still applied elementwise to all the elements in \mathbf{z} matrices. The main difference in processing examples in parallel is that instead of augmenting the input and activation matrices with a single dummy feature value, they are now augmented with a row of dummy features values, one per example.

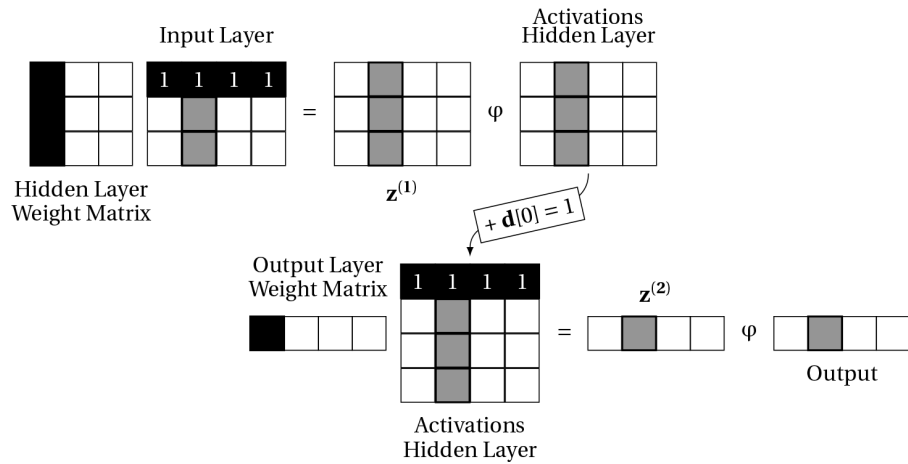


Figure 8.6

An illustration of how a batch of examples can be processed in parallel using matrix operations.

The representation of a network as a sequence of matrix operations provides a transparent view on the depth of the network: a network depth is equal to the number of layers that have a weight matrix associated with

them. This is why the input layer is not counted as part of the depth of the network.

Deep neural networks can contain millions of neurons. Also, as subsequently discussed (and similar to the training regime used for regression models in Chapter 7^[311]), neural networks are trained by iteratively running the network on examples sampled from large datasets. Consequently, unless care is taken, training a network can take an inordinately long time, compared with other machine learning models. The computational speedups achieved by using matrix multiplications address the computational challenge of iterating through both a large number of neurons and a large number of examples. Implementing a network as a sequence of matrix multiplications (1) speeds up the calculation of a weighted sum across each layer in the network, and (2) enables the network to parallelize the processing of examples. Both these speedups enable us to remove expensive *for* loops from the implementation and training of a network: the first removes a *for* loop over the neurons in a layer, and the second removes a *for* loop over the examples in a dataset. A further benefit of implementing a neural network using matrix operations is that it enables the use of specialized hardware known as graphical processing units (**GPUs**). GPUs are designed to carry out matrix operations very quickly. Implementing a neural network as a sequence of matrix operations and then running the network on GPUs is now standard in deep learning.

8.2.4 Why Are Non-Linear Activation Functions Necessary?

A multi-layer feedforward neural network that uses only linear neurons (i.e., neurons that do not include a non-linear activation function) is equivalent to a single-layer network with linear neurons; in other words, it can represent only a linear mapping on the inputs. This equivalence is true no matter how many hidden layers we introduce into the network. We explain subsequently why this is the case, but first we note that for ease of exposition in this discussion, we will ignore the bias terms in the weights of a neuron. This does not affect the generality of the discussion because, as we discussed earlier, a weighted sum that includes a bias term as a weight implements an affine transformation composed of first applying a linear function to the inputs and then translating the result by a bias. Therefore, the inclusion of the translation by the bias term allows the weighted sum to

define a linear function on its inputs that does not pass through the origin. However, in this section, we focus on showing how a sequence of linear layers can be replaced by a single linear function (as distinct from an affine transformation). Furthermore, the combination of the translations that would be applied by including bias terms in each layer can be replaced by applying a single translation (or single bias term) at the end of the processing. Consequently, here we assume that the weight matrices do not include bias terms.

With that caveat regarding bias terms stated, we return to the question of why non-linear activation functions are necessary in a neural network. It turns out that understanding that a neural network can be implemented as a sequence of matrix multiplications with the non-linearity of the activation functions introduced between the matrix multiplications can help answer this question.

Imagine a very simple two layer network (one hidden layer and an output layer) with linear neurons (neurons that don't include an activation function, so that the output activation is just the weighted sum of the inputs).³ The calculation of the activations for the neurons in the first layer can be expressed as follows:

$$\mathbf{A}^{(1)} = \mathbf{W}^{(1)} \mathbf{A}^{(0)} \quad (8.7)$$

Similarly, the calculations of the activations for the second layer can be expressed

$$\mathbf{A}^{(2)} = \mathbf{W}^{(2)} \mathbf{A}^{(1)} \quad (8.8)$$

If we replace $\mathbf{A}^{(1)}$ in Equation (8.8)^[395] with the right-hand side of Equation (8.7)^[395] we get

$$\mathbf{A}^{(2)} = \mathbf{W}^{(2)} \left(\mathbf{W}^{(1)} \mathbf{A}^{(0)} \right) \quad (8.9)$$

However, matrix multiplication is associative (i.e., $\mathbf{X}(\mathbf{Y}\mathbf{Z})$ is equal to $(\mathbf{XY})\mathbf{Z}$); this means that we can rewrite Equation (8.9)^[395]

$$\mathbf{A}^{(2)} = (\mathbf{W}^{(2)} \mathbf{W}^{(1)}) \mathbf{A}^{(0)} \quad (8.10)$$

Also, $\mathbf{W}^{(2)}$ and $\mathbf{W}^{(1)}$ can be replaced by the matrix that is generated by their product; letting $\mathbf{W}' = \mathbf{W}^{(2)}\mathbf{W}^{(1)}$ we get

$$\mathbf{A}^{(2)} = \mathbf{W}' \mathbf{A}^{(0)} \quad (8.11)$$

Furthermore, the transformation implemented by the single weight matrix, generated by the product of weight matrices of the linear layers, will also implement a linear transformation on the input data. Therefore, this rewriting shows that the output of this two-layer network with linear neurons is equivalent to a single-layer network with linear neurons. This reduction of a network to a single weight matrix by using a matrix product can be done no matter how many layers there are in a network, so long as none of the network layers includes non-linear activation functions.

This analysis shows that adding layers to a network without including a non-linear activation function between the layers appears to add complexity to the network, but in reality the network remains equivalent to a single-layer linear network. The conclusion is that in order to create networks that can represent complex non-linear functions, it is not enough to add layers; we must also include non-linearities between these layers. Fortunately, we do not need to add complex non-linearities between the layers; introducing simple non-linearities, such as the logistic or rectifier functions, between each layer is sufficient to enable neural networks to represent arbitrarily complex functions, as long as the network contains enough layers; in other words, as long as the networks are deep enough.

8.2.5 Why Is Network Depth Important?

Given that the preceding analysis in Section 8.2.4^[394] showed that a network with multiple layers of linear neurons is equivalent to a single-layer network of linear functions, a natural question is, *why is adding extra layers to a network (even with non-linearities) a useful thing to do?* This is a particularly pertinent question, considering that the adoption of the term **deep learning** in the mid-2000s to describe modern neural networks was to emphasize that these modern networks are deeper than most of the networks that were developed between the 1940s and the early 2000s.

The fundamental reason to add layers to a network is to increase the **representational capacity** of the network. The representational capacity of a network is the set of functions (or mappings from inputs to outputs) that the network can implement as its weights are varied (Reed and Marks, 1999). A network can represent a function if a set of weights exist for that network for which the network implements the function. Understanding, at least in principle, whether a particular network architecture is capable of representing a function, or not, is very important, because the fundamental task in predictive modeling is to learn functions from data, and if the network cannot represent a function, then it cannot learn it, no matter how much data we provide to the training algorithm.

One way to understand why depth is important to the representational capacity of a neural network is to consider what types of functions a network that has only a single layer of processing neurons, such as the one shown in [Figure 8.7](#)^[397], is capable of representing. Notice that each of the neurons in the output layer (Neurons 3, 4, and 5) are independent of each other; they receive no information from each other. In fact, this figure could be reconfigured as three separate neurons, each receiving the same input vector. For ease of explanation, we will assume that each of these three neurons uses a threshold activation function. This means that each of the neurons in the output layer is equivalent to the McCulloch and Pitts neuron described in [Section 8.2.1](#)^[384]. These thresholded units are also known as **perceptron** networks (Rosenblatt, 1958); we introduce this terminology here because it is useful in the following discussion.

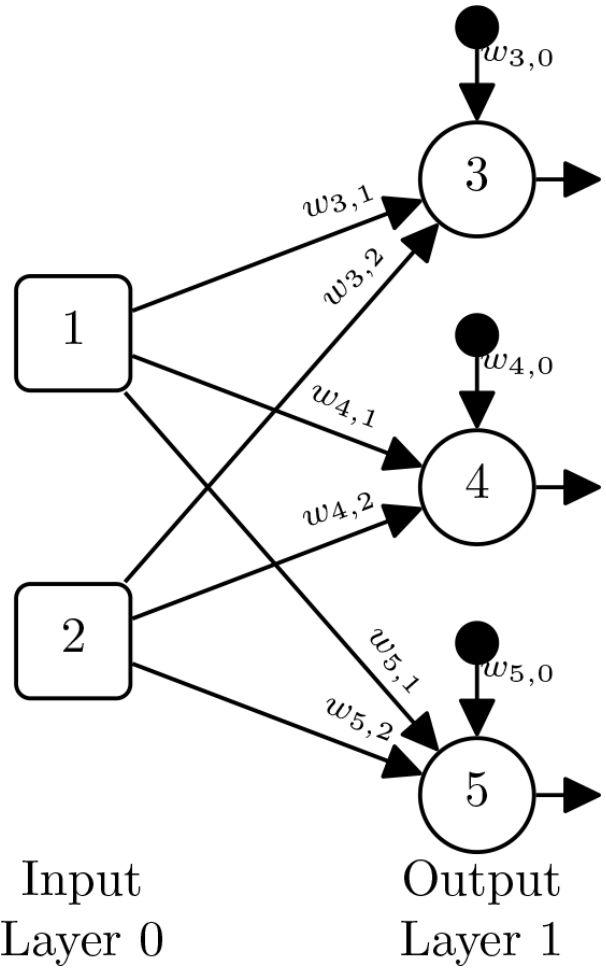


Figure 8.7

A single-layer network.

Equation (8.3)^[386] defines how the McCulloch and Pitts neuron, or perceptron network, maps an input vector to an output activation. If we compare this equation with Equation (7.24)^[341], it is apparent that a perceptron network is identical to a multivariate linear regression model with a threshold applied to it. This means that, similar to the thresholded multivariate linear regression models, a perceptron is able to represent a function that distinguishes between two classes of inputs if these two classes are **linearly separable**. Figure 7.10^[340] illustrates a linearly separable dataset; in that case the two classes of inputs were *good* generators and *faulty* generators. These two classes are linearly separable because as Figure 7.10^{[340](b)} shows, it is possible to draw a single straight line that separates one class from the other. This line is known as a **decision boundary**.

The fact that our single-layer network in [Figure 8.7](#)^[397] contains three independent neurons means that the network has the potential to represent three separate linear decision boundaries. However, none of the neurons in the output layer are capable of representing a non-linear decision boundary on the inputs, and therefore the network as a whole cannot represent a non-linear function.

[Figure 8.8](#)^[398] illustrates the distinction between linearly separable and non-linearly separable functions, using examples from Boolean logic: AND, OR, and XOR functions. These three functions have the same structure; they all take two inputs that can be either *TRUE* or *FALSE*, and they return either *TRUE* or *FALSE*. The AND function returns *TRUE* if both inputs are *TRUE* and *FALSE* otherwise. The plot on the left of [Figure 8.8](#)^[398] shows the input space for the AND with the convention that *FALSE* has been mapped to 0 and *TRUE* has been mapped to 1.⁴ In the plot each of the four possible input combinations is labeled as either triggering a *TRUE* response (shown in the figure by a clear dot) or *FALSE* (shown in the figure by a black dot). As the figure shows, it is possible to draw a straight line between these two classes of inputs. The middle plot shows a similar plot for the OR function, and again it is possible to draw a single straight line to separate the two classes of inputs. The XOR function returns *TRUE* if either but not both of its inputs are *TRUE*. The plot on the right of [Figure 8.8](#)^[398] shows the input space for the XOR and labels the input combinations as resulting in *TRUE* responses or *FALSE* responses. It is apparent from this figure that it is not possible to separate the inputs that generate *TRUE* from those that generate *FALSE* with a single straight line. This is why the XOR function is not linearly separable.

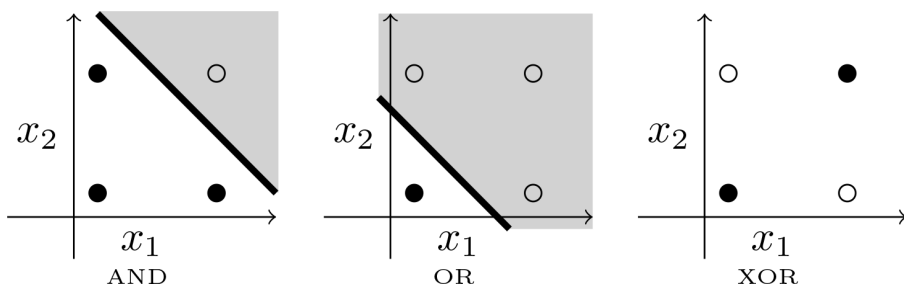


Figure 8.8

The logical AND and OR functions are linearly separable, but the XOR is not. This figure is Figure 4.2 of Kelleher (2019) and is used here with permission.

It may be somewhat surprising, but although the XOR function is very simple, a perceptron cannot represent it because it is not linearly separable. This finding is notorious in the history of neural networks. Through the 1950s and 1960s there was a lot of interest in neural networks. However, in 1969 Marvin Minsky and Seymour Papert published a book entitled *Perceptrons* that was highly critical of neural networks and in particular focused on the fact that single-layer networks (perceptrons) were not able to represent non-linearly separable functions (Minsky and Papert, 1969). This book had a major impact and is attributed with killing interest in neural networks for nearly a decade. In hindsight, the general criticisms of neural networks made by Minsky and Papert have not stood the test of time; however, their criticism of the representational capacity of single-layer networks is valid.

The representational limitation of single-layer networks can be overcome by adding a single hidden layer to the network. Indeed, it is possible to represent the XOR function using a very simple two-layer network. [Figure 8.9](#)^[399] illustrates such a network: the left uses a directed graph representation to show the topology of the network, and the weights on the connections; the right uses the matrix representation of the network to illustrate it processing the four possible input combinations to the XOR function in parallel. All the neurons in this network use the following threshold activation function:

$$\mathbb{M}_w(\mathbf{d}) = \begin{cases} 1 & \text{if } z \geq 1 \\ 0 & \text{otherwise} \end{cases} \quad (8.12)$$

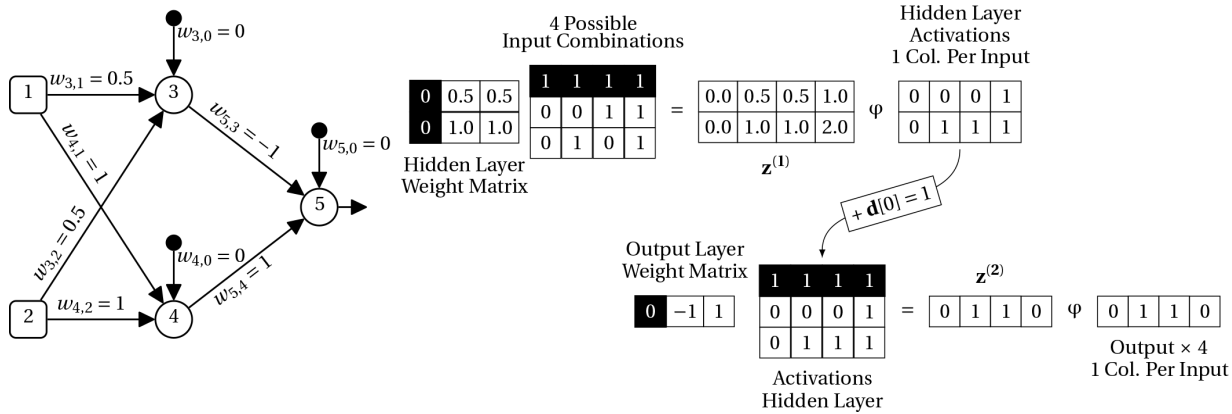


Figure 8.9

(left) The XOR function implemented as a two-layer neural network. (right) The network processing the four possible input combinations, one combination plus bias input per column: [bias, FALSE,FALSE] \rightarrow [1,0,0]; [bias, FALSE,TRUE] \rightarrow [1,0,1]; [bias, TRUE,FALSE] \rightarrow [1,1,0]; [bias, TRUE,TRUE] \rightarrow [1,1,1].

Vertically aligning the columns in the input matrix with the columns in the output matrix shows that the network correctly maps all four inputs combinations to XOR outputs: $< 0,0 > \rightarrow 0$, $< 0,1 > \rightarrow 1$, $< 1,0 > \rightarrow 1$, and $< 1,1 > \rightarrow 0$.

The XOR example shows that a network with a single hidden layer can represent a non-linearly separable function. There are, in fact, mathematical proofs that show that neural networks with a single hidden layer are **universal approximators**; i.e., they can exactly represent any continuous function of multiple inputs. These proofs can be broadly categorized into (1) proofs that bound the number of neurons required in the network but assume that the neurons in the network use complex activation functions (more complex than the smooth functions, such as the logistic function, used in most neural networks) as part of their internal mapping of inputs to an output activation; and (2) proofs that assume that the neurons use smooth functions (such as the logistic, sigmoid, or rectifier) but this simplicity is at the cost of having an exponential number (with respect to the dimensions of the inputs to the network) of neurons in the hidden layer of the network.

The first category of proofs that assume the use of complex functions within the neurons is based on the foundational mathematical theorems from Kolmogorov (1963) and Spercher (1965). Hecht-Nielsen (1987) showed how these proofs could be applied to neural networks. However, as previously noted, these proofs assume that the neurons in the network

include functions that are much more complex (or rougher) than the smooth activation functions used in most networks (such as the logistic functions). In fact, these proofs fail if the neurons are restricted to using smooth functions. This assumption is important because these internal activation functions may be as complex as, or even more complex than, the target function that the network is attempting to represent. Consequently, these theorems are not relevant to the practical task of training a network to learn a function because the inclusion of these complex functions within the neurons of the network shifts the learning burden from approximating the target function to finding these complex internal functions (Reed and Marks, 1999).

The second category of proofs assumes the use of smooth functions within neurons. The **universal approximation theorem** (Hornik et al., 1989; Cybenko, 1989) proved that neural networks with a single hidden layer of neurons using smooth functions (such as sigmoids or logistic functions) can approximate any bounded continuous function, provided there are sufficient neurons in the hidden layer of the network. For many functions the requirement of sufficient neurons turns out to be exponential with respect to the dimensions of the network inputs. More recently, Leshno et al. (1993) extended the universal approximation theorem to include networks with neurons using rectifier activation functions; however, Montúfar (2014) has shown that these networks can also require an exponential number of neurons in the hidden layer. The requirement that networks with a single hidden layer and using smooth activation functions have very wide hidden layers is a serious shortcoming: it may result in the requirement that the network has at least one hidden unit for each input configuration that is being distinguished (Goodfellow et al., 2016). Such a network configuration is likely to result in the network overfitting the training data (i.e., memorizing all the training examples, including the noise, rather than learning the general patterns in the data).

There are two points worth highlighting:

1. Many computational models have the ability of universal approximation of bounded continuous functions; this property is not unique to neural networks (Reed and Marks, 1999). However, these results are still important because they show that neural networks with

at least one hidden layer do have the representational capacity to approximate most functions that we would like them to. If neural networks were not capable of universal approximation, then they would be much less useful for prediction.

2. The fact that a neural network can *represent* a function does not guarantee that we will be able to train it to *learn* the function: the training algorithm may not be able to find the correct set of weights, or it may choose weights that overfit the data (i.e., choose the wrong function) (Goodfellow et al., 2016). For these reasons, the inclusion of more complex functions with the neurons of the network or the inclusion of more neurons within the hidden layer of the network makes the learning task more difficult.

The learning challenges raised by the second point in the preceding list highlight the main motivation for using networks with more than one hidden layer. It is often (but not always) the case that using a deeper network can drastically reduce the number of neurons required to enable the network to represent a target function. For example, some functions can be implemented exactly using a small neural network with two layers but require an infinite number of nodes to approximate with a single hidden layer (Makhoul et al., 1989; Reed and Marks, 1999). Furthermore, Cybenko (1988) proved that a network with at least three layers (two hidden and one output) using sigmoid activation functions can approximate any function (not just bounded continuous functions) with arbitrary accuracy. This does assume that the width of the layers is sufficient to permit the network to represent the function; however, for a given function the number of neurons required in each of the hidden layers is not known, in general.

[Figure 8.10](#) shows how the representational capacity of a neural network increases as more layers are added to the network. The neurons in this network use a simple threshold activation function, but the intuition holds for logistic functions and the rectifier function because these functions also divide the input space of a neuron into two half-spaces: one in which the neuron activates and one in which it doesn't activate. Each subsequent layer in the network is able to use the functions learned by the previous layer to construct a more complex function; this process of using the outputs from one or more functions and inputs to another function to create a new

function is known as function **composition**. The term **representation learning** is sometimes used to describe what the neurons in the hidden layers of a network are doing; in a sense, each subsequent layer in the network projects the inputs it receives into a new representation, and the output layer of the network then learns a mapping from a learned representation to the final output. When this representation learning is successful, the mapping from the representation the output layer receives to the target output is simpler than the mapping from the original input features to the target feature, and this can result in the model's being more accurate. The ability to automatically learn useful representations (features) from data is one of the reasons why deep networks have proven to be so successful on so many tasks. [Figure 8.10](#) illustrates how using just three layers and threshold activation functions, a network is able to represent a function that maps to a convex region. With the addition of more neurons in each layer, the network could represent a function that maps to multiple disconnected convex regions and refines the shapes of these regions. Any function can be approximated by combining disconnected regions.

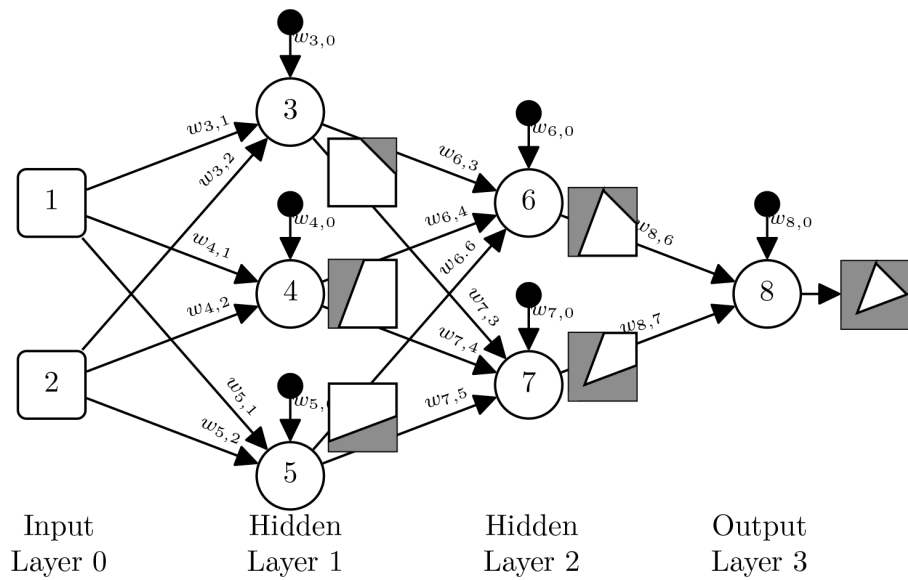


Figure 8.10

An illustration of how the representational capacity of a network increases as more layers are added to the network. The squares overlaying connections coming out of a neuron illustrate the regions of the input space that the neurons activate on: neurons output high activations in response to inputs patterns from the white region in the corresponding square, and low (or no activations) in response to input patterns from the gray regions in the corresponding square. This figure was inspired by Figure 4.2 in (Reed and Marks, 1999) and Figure 3.10 in (Marsland, 2011).

If a three-layer network can represent any function with arbitrary accuracy, is it helpful to go deeper, or is it better to make the layers wider? There is growing empirical evidence that creating deeper networks improves the generalization ability of models across a number of tasks.⁵ However, adding depth to a network comes with a cost. As we see when we discuss the **vanishing gradient** problem, adding depth to a network can slow down the rate at which a network learns. Therefore, when we wish to increase the representational power of a network, there is often a trade-off between making a network deeper and making the layers wider. Finding a good equilibrium for a given prediction task involves experimenting with different architectures to see which performs best.

In summary, neural networks with no hidden layer (i.e., perceptrons) cannot represent non-linearly separable functions. Neural networks with a single hidden layer have been proven to be capable of universal approximation of (bounded) continuous functions as long as either (1) complex functions are integrated into the structure of the neurons, or (2) the hidden layer of the network is *sufficiently* (potentially exponentially) wide. Neural networks with two hidden layers and using smooth activation functions can represent any function and generally can do so using fewer neurons than networks with only a single hidden layer. Also, as [Figure 8.10](#) illustrates, as layers are added to a network, neurons in subsequent layers are able to use the representations learned by the preceding layer as building blocks to construct more complex functions. Overall there is a general trend that deeper networks have better performance than shallower networks, and that deeper networks are often more efficient in terms of the number of neurons they require. However, as networks become deeper they can become more difficult to train. The next section describes how we can train networks with multiple layers of neurons using the **backpropagation** algorithm and explains how the **vanishing gradient** problem can negatively affect the training of deep networks.

8.3 Standard Approach: Backpropagation and Gradient Descent

A neuron is structurally equivalent to a logistic regression model: comparing Equation [\(8.5\)](#)^[387] and Equation [\(7.26\)](#)^[342] makes it apparent that both models calculate a weighted sum over an input vector and then pass the weighted sum value through a non-linear function. Indeed, when a

neuron uses the logistic function as an activation function, then these two models are identical. One consequence of this is that if a neuron uses a logistic activation function, then we can train the neuron in the same way that we train a logistic regression function: using the **gradient descent** algorithm (introduced in Chapter 7^[311]) and with the **weight update rule** defined in Equation (7.33)^[346]. And, if the neuron implements a different activation function, then so long as the function is differentiable, we modify the weight update rule (Equation (7.33)^[346]) by replacing the derivative of the logistic function with the derivative of the new activation function, and apply the gradient descent algorithm as before.⁶ Training a neuron by initializing its weights and then iteratively updating these weights to reduce the error of the neuron on training examples fits with **Hebb's Postulate** (introduced in Section 8.1^[382]) that learning occurs in the brain through a process involving changes in the connections between neurons.

We can, in fact, use the gradient descent algorithm to train a single-layer network (or perceptron), such as the one shown in Figure 8.7^[397]. However, once we introduce one or more hidden layers into a network, it becomes more difficult to use the gradient descent algorithm to train the network. The reason for this is that the gradient descent algorithm uses the error gradient of a model (neuron or regression model) to update the weights on the inputs into the model. Although in a neural network it is relatively straightforward to calculate the gradient of the error for neurons in the output layer by directly comparing the activations of these neurons with the expected outputs, it is not possible to directly compare the activation of a hidden neuron with the expected activation for that neuron, and so we cannot directly calculate an error gradient for hidden neurons.

Consequently, before we can use the gradient descent algorithm to update the weights of a neuron in a hidden layer of the network, we must calculate a measure of how the neuron contributed to the overall error of the network at the output layer. Calculating this measure for each neuron in a network is known as the **blame assignment** problem. The **backpropagation** algorithm solves the blame assignment problem. Once we have used the backpropagation algorithm to solve the blame assignment problem for all the neurons in the network, we can then use the weight update rule from the gradient descent algorithm to update the weights for each of the neurons in the network. The following sections explain (1) the

general structure of the backpropagation algorithm, including the concept of a δ (pronounced *delta*) term that describes the rate of change of the error of a network with respect to changes in the weighted sum of a neuron; (2) the process used to calculate a δ term for each neuron in the network (this process involves backpropagating the error gradients of the network and is the process that gave the algorithm its name); and (3) how the δ terms are used in conjunction with the gradient descent weight update rule to update the weights of the network. Following these explanations we present a worked example to show how the backpropagation and gradient descent algorithm can be used in partnership to train a neural network with hidden layers.

8.3.1 Backpropagation: The General Structure of the Algorithm

The backpropagation algorithm begins by initializing the weights of the network. For the purposes of this explanation we assume that the weights are initialized to random values close to zero (e.g., by sampling from a normal distribution with mean $\mu = 0.0$ and $\sigma = 0.1$). Obviously, a network with random weights is unlikely to implement a useful function. However, it will implement a function, and once the network has been initialized we can now train the network to implement a useful function by iteratively presenting examples to the network and using the error of the network on the examples to update the weights so that the network converges on a set of weights that implement a useful function relative to the patterns in the training data.

The key step in this iterative weight update process is solving the **blame assignment** problem. The general structure of the backpropagation algorithm is a two-step process that results in an assignment of blame (or an error gradient) to each of the neurons in the network:

1. **Forward Pass** An input pattern is presented to the network, and the activations flow forward through the network until an output is generated.
2. **Backward Pass** The error of the network is calculated by comparing the output generated by the forward pass with the target output specified in the dataset. This error is shared back (backpropagated) through the network on a layer-by-layer basis until the input layer is reached. During this backward pass, an error gradient for each neuron

is calculated. These error gradients can then be used by the gradient descent weight update rule to update the weights for each neuron. This backward pass gives the network its name: backpropagation.

[Figure 8.11](#)^[406] illustrates the forward pass in a little more detail. This figure highlights the calculation of the weighted sum at each neuron (e.g., z_3 represents the weighted sum calculation at Neuron 3), and the activations for each neuron (e.g., a_3 represents the activation generated by Neuron 3). The motivation for highlighting the calculation of the weighted sum and activations during the forward pass of the algorithm is that these values are stored in memory after they are calculated and then used as part of the calculations involved in the backpropagation of the error gradients during the backward pass of the algorithm.

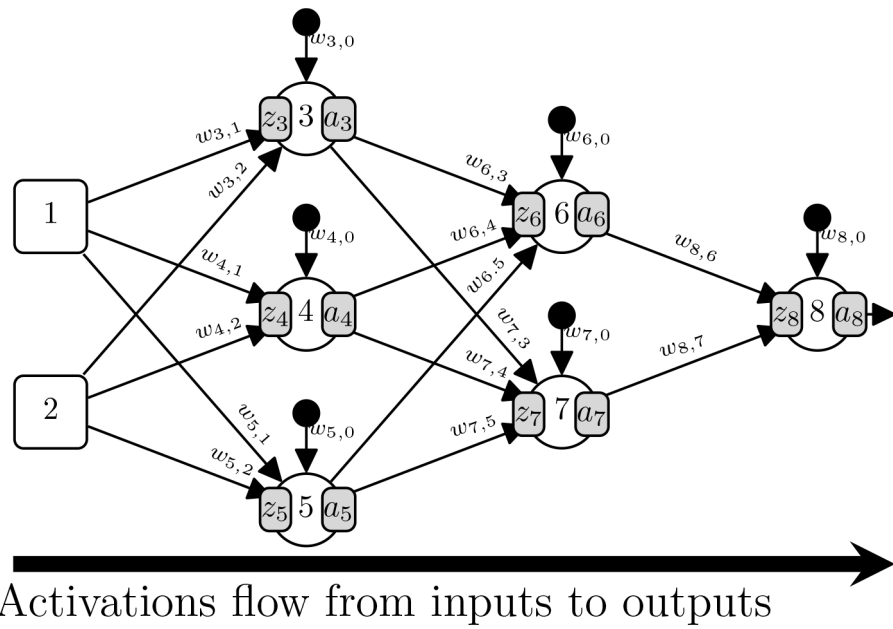


Figure 8.11

The calculation of the z values and activations of each neuron during the forward pass of the backpropagation algorithm. This figure is based on Figure 6.5 of Kelleher (2019).

[Figure 8.12](#)^[407] illustrates the backward pass of the algorithm. Before describing the backward pass of the algorithm, we will distinguish between two types of error gradients that are calculated when we are training a neural network using backpropagation:

1. The first type of error gradient is the *rate of change of the network error with respect to changes in the weighted sum calculation of a neuron*. One of these error gradients is calculated for each neuron in the network. These error gradients are often denoted using the δ symbol with a subscript indicating the relevant neuron. For example, δ_k would denote the error gradient for neuron k . It is these δ error gradients that are calculated and backpropagated during the backward pass of the backpropagation algorithm.
2. The second error gradient is the *rate of change of the network error with respect to changes in the weights of the network*. There is one of these error gradients for each weight in the network. These error gradients are used to update the weights of the network. However, the calculation of these error gradients involves the δ terms. So, we must use the backpropagation algorithm to calculate the δ terms, and once this is done we can calculate the error gradients for each weight. Note that there is only a single δ per neuron, but typically there are many weights associated with each neuron, and so the δ for a neuron will often be used in the calculation of multiple weight error gradients, once for the weight on each connection into the neuron.

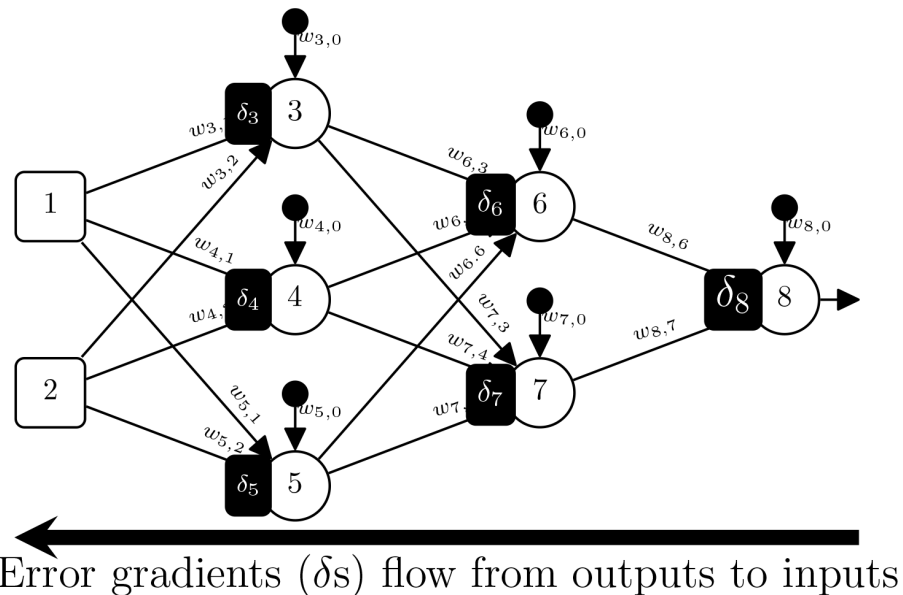


Figure 8.12

The backpropagation of the δ values during the backward pass of the backpropagation algorithm. This figure is based on Figure 6.6 of Kelleher (2019).

Returning to the backward pass of the backpropagation algorithm, [Figure 8.12](#)^[407] shows that the backward pass begins by calculating the δ for each of the neurons in the output layer of the network. In the simplest case, this might be calculated by subtracting the activation of each neuron in the output layer from the target output specified in the dataset. The δ s for the output neurons are then shared back to the neurons in the last hidden layer. This is done by assigning a portion of the δ of each output neuron to each of the hidden neurons connecting to it. This assignment of blame back to the neurons connecting into a neuron is dependent on the weight on the connection between the neurons and also on the activation of the hidden neuron during the forward pass. This is why the activations of all neurons are recorded during the forward pass. The δ for a neuron in the last hidden layer is calculated by summing the portions of the δ s backpropagated to it from all the neurons in the output layer that it connects to. Once the δ s for all the neurons in the last hidden layer is calculated, the process is repeated in order to calculate δ s for the neurons in the preceding hidden layer. This process of apportioning blame for the δ s in one layer back to the neurons in the preceding layer and then summing the blame for each neuron in the preceding layer to calculate its δ is repeated until all the neurons in the first hidden layer of the network have a δ term. At the end of this process, a δ has been calculated for every neuron in the network.

8.3.2 Backpropagation: Backpropagating the Error Gradients

The δ term for a neuron describes the rate of change of the error (i.e., the error gradient) of the network with respect to changes in the weighted sum calculated by the neuron. Using \mathcal{E} to represent the error of the network at the output layer, and z_k to denote the weighted sum calculation in neuron k , the δ for a neuron k can be mathematically defined

$$\delta_k = \frac{\partial \mathcal{E}}{\partial z_k} \quad (8.13)$$

In other words, the δ term for a neuron is the partial derivative of the error of the network with respect to the weighted sum (z) of the neuron. The δ s for all neurons in a network (irrespective of whether they are in the output layer or a hidden layer) are calculated as the product of two terms:

1. the rate of change of the error of the network with respect to changes in the activation of the neuron: $\partial\mathcal{E}/\partial a_k$; and
2. the rate of change of the activation of the neuron with respect to changes in the weighted sum calculated at the neuron: $\partial a_k/\partial z_k$.

$$\delta_k = \frac{\partial a_k}{\partial z_k} \times \frac{\partial \mathcal{E}}{\partial a_k} \quad (8.14)$$

The process used to calculate the term $\partial\mathcal{E}/\partial a_k$ for a neuron k is dependent on whether the neuron is in the output layer or in one of the hidden layers of the network. The difference in how $\partial\mathcal{E}/\partial a_k$ is calculated for output and hidden neurons is how Equation (8.14)^[408] generalizes over all the neurons in the network. However, the same process is used to calculate the term $\partial a_k/\partial z_k$ in the product irrespective of whether the neuron is an output neuron or a hidden neuron. Because the same process is used to calculate $\partial a_k/\partial z_k$ for all neurons we describe this process first, and then we describe how the $\partial\mathcal{E}/\partial a_k$ term is calculated for output neurons and then for hidden neurons.

The term $\partial a_k/\partial z_k$ represents the rate of change of the neuron's activation function with respect to changes in the weighted sum z (i.e., with respect to the input to the activation function). Because this $\partial a_k/\partial z_k$ term is required in order to calculate the δ for a neuron, the backpropagation algorithm assumes that the neurons in the network use differentiable activation functions. The logistic function (see Equation (7.25)^[342]) has a very well-known and relatively simple derivative⁷

$$\frac{d}{dz} \text{logistic}(z) = \text{logistic}(z) \times (1 - \text{logistic}(z)) \quad (8.15)$$

The derivative of a function can be understood as the slope of the graph of the function at each point on the graph. Figure 8.13^[410] illustrates this relationship between the slope of the graph of a function and its derivative. The graph of the logistic function is relatively flat for large (positive or negative) values. We describe these regions as saturated: in economics when a market becomes saturated with a product, the growth in the consumption of the product flattens out; by analogy, regions of curves that are flat are said to be saturated. In these saturated regions the derivative of

the logistic function is approximately 0. The plot of the derivative of the logistic function in [Figure 8.13](#)^[410] illustrates that as the value of z approaches 0 (from either side), the slope of the logistic graph increases until it reaches its maximum value at $z = 0.0$; consequently, we can calculate the maximum value of the derivative of the logistic function using Equation (8.15)^[408] by setting $z = 0.0$ ⁸

$$\begin{aligned}\frac{d}{dz} \text{logistic}(z = 0) &= \text{logistic}(0) \times (1 - \text{logistic}(0)) \\ &= 0.5 \times (1 - 0.5) \\ &= 0.25\end{aligned}\tag{8.16}$$

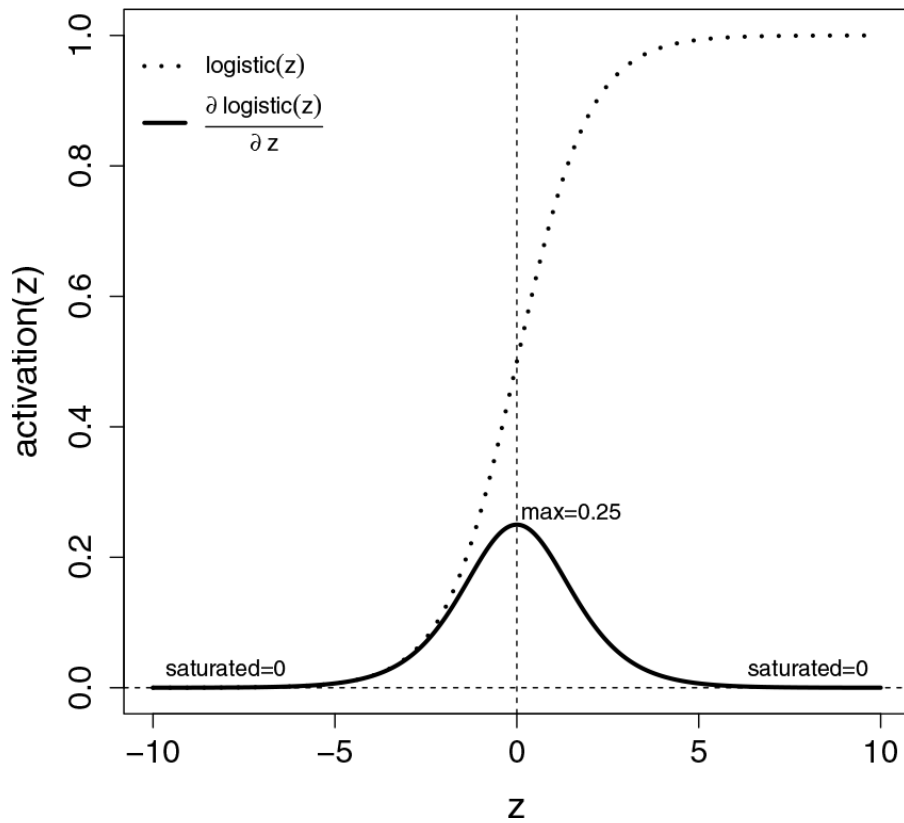


Figure 8.13

Plots of the logistic function and its derivative. This figure is Figure 4.6 of Kelleher (2019) and is used here with permission.

As this example shows, if a neuron k uses the logistic function as its activation function, then we can calculate the term $\partial a_k / \partial z_k$ by simply

inputting the weighted sum for the neuron z_k into Equation (8.15)^[408]. This is why, as Figure 8.11^[406] highlights, the weighted sum for each neuron is stored in the forward pass of the algorithm: it is used to calculate the $\partial a_k / \partial z_k$ term during the backpropagation process. The simplicity of the derivative of the logistic function is one of the reasons why the logistic function was such a popular activation function in neural networks: using logistic activation functions made it relatively easy to implement the backpropagation algorithm.

If, however, a neuron used a different activation function, then we would use the derivative of that function when we are calculating $\partial a_k / \partial z_k$; however, we would do so in the same way, by plugging the z_k value into the derivative.

Once the $\partial a_k / \partial z_k$ term has been calculated for a neuron, the other term needed to calculate the δ for a neuron k using Equation (8.14)^[408] is the rate of change of the error of the network with respect to changes in the activation of the neuron: $\partial \mathcal{E} / \partial a_k$. As noted previously, the calculation of this term is different for output neurons and hidden neurons.

The calculation of $\partial \mathcal{E} / \partial a_k$ for output neurons is dependent on the **error function**⁹ that is used during training. We have already introduced the **sum of squared errors**, or L_2 , error function (see Equation 7.4^[316]), repeated here for convenience

$$L_2(\mathbb{M}_w, \mathcal{D}) = \frac{1}{2} \sum_{i=1}^n (t_i - \mathbb{M}_w(\mathbf{d}_i))^2 \quad (8.17)$$

Equations (7.11)^[324] to (7.14)^[324] step through the derivation of the rate of change of the error of a model (in that case, a linear regression model) for a single input example \mathbf{d} with respect to changes in one of the model's weights $\partial L_2(\mathbb{M}_w, \mathbf{d}) / \partial w[j]$, resulting in

$$\frac{\partial}{\partial w[j]} L_2(\mathbb{M}_w, \mathbf{d}) = (t - \mathbb{M}_w(\mathbf{d})) \times -\mathbf{d}[j] \quad (8.18)$$

This derivation was based on the **chain rule** and is the product of the rate of change of the error of the model with respect to its output—the term ($t -$

$\mathbb{M}_w(\mathbf{d})$)—and the rate of change of the output of the linear regression model with respect to a change in the weight j , the term $-\mathbf{d}[j]$.

The term we want to define is the rate of change of the error of a neuron (a model) with respect to its activation (output): $\partial\mathcal{E}/\partial a_k$. For this we need only the first term from the product in Equation (8.18)^{[410]10}

$$\frac{\partial\mathcal{E}}{\partial a_k} = \frac{\partial L_2(\mathbb{M}_w, \mathbf{d})}{\partial \mathbb{M}_w(\mathbf{d})} = t - \mathbb{M}_w(\mathbf{d}) = t_k - a_k \quad (8.19)$$

The reason why this difference is considered a rate of change is that the larger the difference between a_k and t_k , the faster the error of the network can be changed by changing the activation. However, the direction of the calculated gradient is toward the highest value on the error surface, and therefore to move down the error surface we should multiply it by -1 .¹¹ Hence, using the **sum of squared errors** error function, the error gradient for a single output neuron k on a single example is

$$\frac{\partial\mathcal{E}}{\partial a_k} = -(t_k - a_k) \quad (8.20)$$

The sum of squared errors is a particularly convenient error function to use because the model errors on different examples and also the errors on different outputs (e.g., consider a network that has multiple neurons in the output layer) are independent and therefore the overall error is just the sum of the individual errors. Consequently, if we wish to calculate the error gradient of a network with multiple outputs over multiple examples, we simply sum the error gradients for each output over the examples.

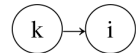
Equation (8.21)^[411] illustrates the calculation of δ_k for neuron k in the output layer. This equation expands Equation (8.14)^[408] using the difference $-(t_k - a_k)$ as the value for $\partial\mathcal{E}/\partial a_k$. Working from the right of the equation, first we calculate $\partial\mathcal{E}/\partial a_k$ by subtracting a_k from t_k and multiplying the result by -1 . Next, $\partial\mathcal{E}/\partial a_k$ is multiplied by $\partial a_k/\partial z_k$ (which is calculated as previously described, by inputting the z_k for the neuron into the derivative of its activation function). For illustrative purposes, in this instance we assume that the output neuron uses a logistic activation function and expand

the definition of $\partial a_k / \partial z_k$ accordingly in the last two lines of the equation. The result of this product is the δ_k for the neuron.

$$\begin{aligned}
\delta_k &= \frac{\partial a_k}{\partial z_k} \times \frac{\partial \mathcal{E}}{\partial a_k} \\
&= \frac{\partial a_k}{\partial z_k} \times -(t_k - a_k) \\
&= \underbrace{\frac{d}{dz} \text{logistic}(z)}_{\text{Assuming a logistic activation function}} \times -(t_k - a_k) \\
&= \underbrace{(\text{logistic}(z) \times (1 - \text{logistic}(z)))}_{\text{Assuming a logistic activation function}} \times -(t_k - a_k) \tag{8.21}
\end{aligned}$$

Switching the focus to the calculation of δ s for hidden neurons, the calculation of $\partial \mathcal{E} / \partial a_k$ for a hidden neuron k requires that the δ s for all downstream neurons be calculated first (i.e., all the neurons that the activation a_k is directly propagated to during the forward pass). The reason for this is that the term $\partial \mathcal{E} / \partial a_k$ connects the activation of the neuron a_k to the output error of the network \mathcal{E} . Specifically, it represents how sensitive the error of the network \mathcal{E} is to changes in a_k . However, for a hidden neuron k , a_k only indirectly affects \mathcal{E} , via the effect it has on the activations of downstream neurons that the a_k is directly propagated to (and the chain reaction that these subsequent activations have on still later neuron activations). Consequently, to connect the activation of a hidden neuron a_k to the network error \mathcal{E} , we have to create a chain of connection via the activations of the downstream neurons. The δ s for the downstream neurons are the links in this chain, and therefore we must calculate these downstream δ s prior to calculating $\partial \mathcal{E} / \partial a_k$.

For example, for each neuron i that neuron k connects forward to



the δ for neuron i connects the z_i value for i to the error of the network \mathcal{E} . Furthermore, the rate of change of z_i with respect to the activation of neuron k (a_k) is the weight on the connection from neuron k to neuron i : $w_{i,k}$. As a result, we can calculate the rate of change of the error of the network \mathcal{E} with

respect to the changes in the activation a_k by taking the product: $w_{i,k} \times \delta_i$. However, the activation a_k may be propagated to many downstream neurons, and therefore to calculate the total sensitivity of the network error \mathcal{E} to changes in a_k , we must sum this product for all n neurons that a_k is directly propagated to

$$\frac{\partial \mathcal{E}}{\partial a_k} = \sum_{i=1}^n w_{i,k} \times \delta_i \quad (8.22)$$

Equation (8.23)^[412] illustrates how the term $\partial \mathcal{E} / \partial a_k$ is calculated for a hidden neuron and how this term is then used to calculate the δ for a hidden neuron by multiplying it by the term $\partial a_k / \partial z_k$ (which, as previously described, is calculated by plugging the z_k into the derivative of the activation function).

$$\begin{aligned} \delta_k &= \frac{\partial a_k}{\partial z_k} \times \frac{\partial \mathcal{E}}{\partial a_k} \\ &= \frac{\partial a_k}{\partial z_k} \times \left(\sum_{i=1}^n w_{i,k} \times \delta_i \right) \\ &= \underbrace{\frac{d}{dz} \text{logistic}(z)}_{\text{Assuming a logistic activation function}} \times \left(\sum_{i=1}^n w_{i,k} \times \delta_i \right) \\ &= \underbrace{(\text{logistic}(z) \times (1 - \text{logistic}(z)))}_{\text{Assuming a logistic activation function}} \times \left(\sum_{i=1}^n w_{i,k} \times \delta_i \right) \end{aligned} \quad (8.23)$$

To summarize, the backward pass of the backpropagation algorithm propagates the δ error gradients back through the network. These δ s are the rate of change of the network error with respect to the weighted sum of a neuron. The backward pass starts by using the calculation illustrated by Equation (8.21)^[411] to calculate a δ for each neuron in the output layer. Then working backward in a layer-by-layer manner, the δ for the hidden neurons are calculated using Equation (8.23)^[412]. This process, working backward from the output to the input layer, constructs for each neuron in the network a chain of connections linking the weighted sum of the neuron to the error of the network. This backward process builds these chains in an efficient

manner because the linking of a new neuron to the chain can be done by extending the chains created for the neurons downstream of it. Once a δ has been calculated for every neuron in the network, the backward pass has completed (and in a sense so has the backpropagation algorithm, at least insofar as the algorithm is a solution to the **blame assignment** problem), and we are now ready to update the weights of the network using the δ s as part of the gradient descent weight update rule.

8.3.3 Backpropagation: Updating the Weights in a Network

The basic principle informing how weights in a neural network should be adjusted is that a weight should be updated in proportion to the sensitivity of the network error to changes in the weight. The rationale is that if the network error is not sensitive to changes in a weight (i.e., the error does not change when the weight changes), then the error is independent of the weight, or to put it another way, the weight did not contribute to the error. However, if the error is sensitive to changes in the weight, then the error is dependent on the weight and accordingly the current weight is to blame for some portion of the error.

The rate of change of the network error with respect to changes in a weight is written mathematically as $\partial\mathcal{E}/\partial w_{i,k}$ for the weight on the connection from neuron k to neuron i . Using the **chain rule**¹² we can rewrite this term as a product of three terms

$$\frac{\partial\mathcal{E}}{\partial w_{i,k}} = \frac{\partial\mathcal{E}}{\partial a_i} \times \frac{\partial a_i}{\partial z_i} \times \frac{\partial z_i}{\partial w_{i,k}} \quad (8.24)$$

Each link in this chain of products is the rate of change of the output of a function (loss function, activation function, or weighted sum function) with respect to one of its inputs. Working from a network weight $w_{i,k}$ forward toward the network error, we have

- the rate of change of the weighted sum function with respect to changes in one of the weights ($\partial z_i/\partial w_{i,k}$);
- the rate of change of the activation function with respect to changes in the weighted sum ($\partial a_i/\partial z_i$); and
- the rate of change of the error of the network with respect to changes in the activation function ($\partial\mathcal{E}/\partial a_i$).

Using the equivalence defined in Equation (8.14)^[408], this product of three terms can be simplified

$$\begin{aligned}\frac{\partial \mathcal{E}}{\partial w_{i,k}} &= \frac{\partial \mathcal{E}}{\partial a_i} \times \frac{\partial a_i}{\partial z_i} \times \frac{\partial z_i}{\partial w_{i,k}} \\ &= \boldsymbol{\delta}_i \times \frac{\partial z_i}{\partial w_{i,k}}\end{aligned}\tag{8.25}$$

This rewriting shows that (1) the backpropagation algorithm is in fact an implementation of the chain rule from calculus and the product used to calculate the $\boldsymbol{\delta}$ terms follows the chain rule; and (2) that we can calculate $\partial \mathcal{E}/\partial w_{i,k}$ (the term we need to update a weight $w_{i,k}$) by multiplying the $\boldsymbol{\delta}$ for a neuron i by the rate of change of the weighted sum calculation for neuron i with respect to changes in the weight $w_{i,k}$. In calculus, when we take the partial derivative of a function with respect to a particular input, all the terms in the function that are not involved in the input disappear, because they are constants when the input changes. This means that the partial derivative of a weighted sum function with respect to a weight simplifies to the derivative of the product of the weight by its input that is equal to the input the weight is applied to

$$\frac{\partial z_i}{\partial w_{i,k}} = a_k\tag{8.26}$$

The implication of this is that once we have calculated the $\boldsymbol{\delta}$ for a neuron, all we need to do to calculate the sensitivity of the network error with respect to a weight on a connection coming into the neuron is to multiply the neuron's $\boldsymbol{\delta}$ by the activation that was propagated forward on that connection. Equation (8.27)^[414] shows how the chain rule product is eventually simplified to the simple product of a $\boldsymbol{\delta}$ by an activation

$$\begin{aligned}\frac{\partial \mathcal{E}}{\partial w_{i,k}} &= \frac{\partial \mathcal{E}}{\partial a_i} \times \frac{\partial a_i}{\partial z_i} \times \frac{\partial z_i}{\partial w_{i,k}} \\ &= \boldsymbol{\delta}_i \times \frac{\partial z_i}{\partial w_{i,k}} \\ &= \boldsymbol{\delta}_i \times a_k\end{aligned}\tag{8.27}$$

This is why, as [Figure 8.11](#)^[406] shows, the activation for each neuron is stored during the forward pass of the algorithm; these activations are used to update the weights on the connections along which they are propagated. We now know how to calculate the sensitivity of the network error with respect to changes in a weight: $\partial\mathcal{E}/\partial w_{i,k}$. How do we use this term to update a weight?

We can get an insight into how we should use this term to update weights by considering the case of a weight $w_{i,k}$ between an output neuron i that uses a logistic activation function and a hidden neuron k . If the output of the neuron i is too high ($a_i > t_i$), then δ_i will be positive because it will be the product of two positive terms:

1. $\partial\mathcal{E}/\partial a_i$ is positive when $a_i > t_i$ (see [Equation \(8.20\)](#)^[411]); and
2. $\partial a_i/\partial z_i$ is always ≥ 0 for a logistic function.

Furthermore, if $a_i > t_i$, we know that we should decrease the output a_i . Therefore,

1. if a_k , the activation from neuron k that the weight $w_{i,k}$ was applied to, is positive, we should decrease the weight $w_{i,k}$. In this case $\partial\mathcal{E}/\partial w_{i,k} = \delta_i \times a_k$ will be positive, because both terms in the product are positive, and so to decrease the weight $w_{i,k}$ we should subtract $\partial\mathcal{E}/\partial w_{i,k}$ from $w_{i,k}$.
2. if a_k is negative, we should increase the weight $w_{i,k}$. However, in this case $\partial\mathcal{E}/\partial w_{i,k} = \delta_i \times a_k$ will be negative, because the product involves a positive and a negative term. And, so to increase $w_{i,k}$, we should again subtract $\partial\mathcal{E}/\partial w_{i,k}$ from $w_{i,k}$.

In both these cases we should subtract $\partial\mathcal{E}/\partial w_{i,k}$ from $w_{i,k}$. The same conclusion can be reached via similar reasoning for the case $a_i < t_i$. Hence we update the weights as follows:

$$w_{i,k} \leftarrow w_{i,k} - \alpha \times \delta_i \times a_k \quad (8.28)$$

where α is the learning rate hyper-parameter and has the same function as the learning rate in gradient descent.¹³ This equation states that the updated weight after processing a training example is equal to the weight used to

process the training example minus α times the sensitivity of the error of the network with respect to changes in the weight.

Equation (8.28)^[415] illustrates how a weight in a network is updated after a single training example has been processed. Updating weights after each training example is known as **on-line**, **sequential**, or **stochastic** gradient descent. One problem with updating the weights of a network after each example is that the error gradient calculated on a single example sampled from the training set is likely to be a noisy approximation of the true gradient over the entire dataset; in other words, the error gradient calculated on a single example may not point in the same direction as the steepest gradient when we average the gradients over the entire dataset. Typically, **stochastic** gradient descent still works because generally descending the error gradient on an individual example will move the weight in a similar direction as descending the gradient over the entire dataset. However, this may not always be the case, because some weight updates may move in an orthogonal direction to the true gradient or even cause the error to increase; this can slow down the training of the network. Ideally, we want to descend the true error gradient for the entire dataset. **Batch gradient descent**¹⁴ involves calculating the error gradients for each weight for all the examples in a dataset and summing the gradients for each weight, and only then updating the weights using the summed error gradients calculated over the entire dataset. Apart from the advantage of descending the true error gradient for the entire dataset, batch gradient descent is also able to take advantage of the fact that a neural network, implemented as a sequence of matrix operations, can process multiple examples in parallel (as illustrated by Figure 8.6^[393] and Figure 8.9^[399]). Furthermore, calculating a direction of descent by taking an average over a set of noisy examples can make the descent of the error surface smoother, which often means that we can use a larger learning rate α with batch gradient descent (i.e., we can take larger steps between weight updates because we are more confident of the direction we are moving). This combination of multiple examples processed in parallel and a larger learning rate can result in much faster training times using batch gradient descent.

However, in order to use batch gradient descent, we must update Equation (8.28)^[415] to accommodate updating a weight using the sum of the

error gradients. To do this, we first introduce the term $\Delta w_{i,k}$ to denote the sum of the error gradients for the weight $w_{i,k}$ over one complete pass through all the examples in the training dataset. Equation (8.29)^[416] defines how $\Delta w_{i,k}$ is calculated for a training dataset containing m examples. In this equation the subscript j indexes over the examples in the dataset and subscripts i and k index over neurons in the network. Hence $\delta_{i,j}$ is the δ value for neuron i for example j . We then rewrite Equation (8.28)^[415] as Equation (8.30)^[416] to use this new term

$$\Delta w_{i,k} = \sum_{j=1}^m \delta_{i,j} \times a_{k,j} \quad (8.29)$$

$$w_{i,k} \leftarrow w_{i,k} - \alpha \times \Delta w_{i,k} \quad (8.30)$$

The distinction between stochastic gradient descent and batch gradient descent can be used to clarify the meanings of two related terms often used in neural network training: **epoch** and **iteration**. An epoch is a single pass through all the examples in the training dataset. Therefore, $\Delta w_{i,k}$ is the error gradient for weight $w_{i,k}$ for one epoch. The term **iteration** is used to refer to a single forward and backward pass plus weight update of the backpropagation algorithm. So if we have a training dataset of m examples in stochastic gradient descent, it would take m iterations to complete a single **epoch**, and this epoch would involve m weight updates. Conversely, in batch gradient descent, assuming we process all the training examples in parallel, we complete a single epoch in each iteration of the algorithm and so there is a single weight update per epoch.

The drawback of batch gradient descent is that the entire dataset must be processed between each weight update. This can be problematic because modern datasets can be very large—it is quite possible to have datasets containing millions or even billions of examples. In these scenarios we need to process millions of examples and to calculate and accumulate millions of error gradients for each weight update. Even with modern computational power and with processing examples in parallel, this can take a long time and ultimately result in network training taking a long time. Consequently, the standard practice in deep learning is to use **mini-batch gradient**

descent. In mini-batch gradient descent, the dataset is split into multiple subsets called **mini-batches** or **batches**.¹⁵

Ideally, each mini-batch should be created by random sampling from the dataset. However, randomly sampling each mini-batch from a very large dataset may be impractical. So, frequently, at the start of training the dataset is shuffled and then split into a sequence of mini-batches. The first iteration of training is done on the first mini-batch in the sequence, the second iteration on the second mini-batch, and so on until the epoch is completed. At the start of the second epoch, the sequence of mini-batches is shuffled and the training iterations are carried out on this new sequence of mini-batches. Equation (8.29)^[416] and Equation (8.30)^[416] work for mini-batch training in much the same way as they do for batch training; the only difference is that the summation in Equation (8.29)^[416] is over the examples in the mini-batch rather than the entire dataset.

Typically mini-batches are all of the same size. There are a number of factors to consider in the choice of the **batch size**, including¹⁶ (1) larger batches provide a more accurate estimate of the true gradient for the entire dataset, but (2) hardware constraints may necessitate the use of smaller batches; for example, if all the examples in a mini-batch are to be processed in parallel, then the larger the batch size, the larger is the memory requirement. Popular batch sizes include 32, 64, 128, and even 256 examples. We noted previously that we can often increase the learning rate α when using batch gradient descent. Generally, finding a good combination of values for the **batch size** and learning rate hyper-parameters involves trial-and-error experimentation.

8.3.4 Backpropagation: The Algorithm

Algorithm 5^[420] brings together the different topics covered in the preceding sections. The algorithm assumes a dataset \mathcal{D} is available; it also requires that values for the learning rate α and the batch size B hyper-parameters have been selected. Finally, the model assumes that a **convergence criterion** has been specified.¹⁷ **Early stopping** is the most popular strategy used to define a convergence criterion; we explain the early stopping algorithm in Section 8.4.4^[472]. However, the general idea of a convergence criterion is that as the training progresses, the error of the network should generally decrease. However, the rate of error reduction after each weight

update will also decrease. Consequently, there is a diminishing return on the improvement of the network relative to the time spent on training. At a certain point in training, further adjustments to the weights will not result in significant changes to the network error, and the convergence criterion specifies a decision process whereby we decide when to stop training.

In Line 1^[420] the data is split into mini-batches where $\mathbf{X}^{(i)}$ is a matrix that contains the descriptive features for each of the examples in mini-batch i , with one column per example, and $\mathbf{Y}^{(i)}$ is a matrix (or vector) containing the corresponding labels for the examples in mini-batch i . The network's weight matrices are initialized in Line 2^[420]. There are L layers in this network and so there are L weight matrices, where $\mathbf{W}^{(i)}$ represents the weight matrix for layer i . The weight matrices are arranged so that there is one row per set of weights per neuron in the layer.

Each loop of the **repeat** loop from Line 3^[420] to Line 33^[420] involves an **epoch** of training (i.e., a full traversal of the training data completed via a single pass through all the mini-batches). Each iteration of the **for** loop (Lines 4^[420] to 31^[420]) involves the processing of a single mini-batch, including both a forward and backward pass of the algorithm and a single set of weight updates. In Line 5^[420] the matrix of descriptive features for the examples in the mini-batch that is about to be processed is presented to the input layer of the network.

The forward pass of the algorithm occurs in the **for** loop Lines 6^[420] to 11^[420]. This forward pass follows the set of operations illustrated in [Figure 8.6](#)^[393]. Each iteration of this **for** loop propagates the activations for the mini-batch forward through the next layer of the network. The vector \mathbf{v} , created on Line 7^[420], is the vector of bias inputs, and it is as wide as the number of neurons in the layer (we use the subscript m here as shorthand for the number of neurons in the layer). On Line 8^[420] the bias inputs vector and the matrix of activations from the previous layer \mathbf{A}^{l-1} are vertically concatenated so that the bias inputs are now stored in the first row of \mathbf{A}^{l-1} ; we use the notation $[\mathbf{v}; \mathbf{A}]$ to represent the vertical concatenation of the vector/matrix \mathbf{v} and \mathbf{A} . This vertical concatenation operation is illustrated in [Figure 8.6](#)^[393] with $\mathbf{d}[0]$ added to the activation matrix as it is propagated forward from one layer to the next. Line 9^[420] is the matrix multiplication of the layer's weights by the activations from the preceding layer. This matrix multiplication generates the weighted sums for all neurons in the layer for

all the examples in the mini-batch and stores the results in the matrix $\mathbf{Z}^{(l)}$. Next, on Line 10^[420], the activation function φ is applied in turn to each element of $\mathbf{Z}^{(l)}$ to generate the activations for each neuron in the layer for each example in the mini-batch. These activations are stored in the matrix $\mathbf{A}^{(l)}$. When the algorithm exits the **for** loop on Line 11^[420], the mini-batch examples will have been propagated through all L layers of the network, and $\mathbf{A}^{(L)}$ will store the activations for all the neurons in the output layer for all the examples in the mini-batch; as per [Figure 8.6](#)^[393] the activations are arranged so that the output layer activations for each example will be stored as a column in $\mathbf{A}^{(L)}$.

This version of the algorithm is for mini-batch training, and so we know that we will need to sum the error gradients for each weight across the examples in the mini-batch. The **for** loop on Lines 12^[420] to 14^[420] is where the variables used to store these totals are initialized. The backpropagation of the δ s and the summation of the error gradients across the examples in the mini-batch are done in the **for** loop from Line 15^[420] to Line 27^[420]. This **for** loop iterates through the examples in the batch, and for each example the δ s for the neurons are calculated and backpropagated. Recall that we use different equations to calculate the δ value for a neuron, depending on whether the neuron is an output neuron or a neuron in a hidden layer. We highlight this distinction by using different **for** loops for each of these conditions. The **for** loop on lines 16^[420] to 18^[420] contains the calculations of the δ s for neurons in the output layer, and the **for** loop on lines 19^[420] to 23^[420] is the calculation of the δ s for neurons in the hidden layers. Once the δ s for all the neurons in the network for an example have been calculated, then for each weight in the network the error gradients are accumulated (Lines 24^[420] to 26^[420]). Consequently, at the end of the processing of the mini-batch (i.e., when the algorithm exits the **for** loop from Line 15^[420] to Line 27^[420]), $\Delta w_{i,k}$ will contain the weight updates for weight $w_{i,k}$ summed across all the examples in the mini-batch. The final **for** loop in each epoch is where the weights of the network are updated (Lines 28^[420] to 30^[420]). On Line 32^[420] the mini-batch sequence is shuffled between epochs.

Algorithm 5 The backpropagation algorithm for a feedforward network with L layers

Require: set of training instances \mathcal{D}

Require: a learning rate α that controls how quickly the algorithm converges

Require: a batch size B specifying the number of examples in each batch

Require: a convergence criterion

```
1: Shuffle  $\mathcal{D}$  and create the mini-batches:  $[(\mathbf{X}^{(1)}, \mathbf{Y}^{(1)}), \dots, (\mathbf{X}^k, \mathbf{Y}^k)]$ 
2: Initialize the weight matrices for each layer:  $\mathbf{W}^{(1)}, \dots, \mathbf{W}^{(L)}$ 
3: repeat                                      $\triangleright$  Each repeat loop is one epoch
4:   for  $t=1$  to number of mini-batches do       $\triangleright$  Each for loop is one iteration
5:      $\mathbf{A}^{(0)} \leftarrow \mathbf{X}^{(t)}$                           $\triangleright$  Forward propagation
6:     for  $l=1$  to  $L$  do
7:        $\mathbf{v} \leftarrow [1_0, \dots 1_m]$                     $\triangleright$  Create  $\mathbf{v}$  the vector of bias terms
8:        $\mathbf{A}^{(l-1)} \leftarrow [\mathbf{v}; \mathbf{A}^{(l-1)}]$          $\triangleright$  Insert  $\mathbf{v}$  into the activation matrix
9:        $\mathbf{Z}^{(l)} \leftarrow \mathbf{W}^l \mathbf{A}^{(l-1)}$ 
10:       $\mathbf{A}^{(l)} \leftarrow \varphi(\mathbf{Z}^{(l)})$             $\triangleright$  Elementwise application of  $\varphi$  to  $\mathbf{Z}^{(l)}$ 
11:    end for
12:    for each weight  $w_{i,k}$  in the network do
13:       $\Delta w_{i,k} = 0$ 
14:    end for
15:    for each example in the mini-batch do           $\triangleright$  Backpropagate the  $\delta$ s
16:      for each neuron  $i$  in the output layer do
17:         $\delta_i = \frac{\partial \mathcal{E}}{\partial a_i} \times \frac{\partial a_i}{\partial z_i}$             $\triangleright$  See Equation (8.21)[411]
18:      end for
19:      for  $l = L-1$  to  $1$  do
20:        for each neuron  $i$  in the layer  $l$  do
21:           $\delta_i = \frac{\partial \mathcal{E}}{\partial a_i} \times \frac{\partial a_i}{\partial z_i}$             $\triangleright$  See Equation (8.23)[412]
22:        end for
23:      end for
24:       $\triangleright$  For each weight  $w_{i,k}$  accumulate  $\Delta w_{i,k}$  across the mini-batch
25:      for each weight  $w_{i,k}$  in the network do
26:         $\Delta w_{i,k} = \Delta w_{i,k} + (\delta_i \times a_k)$             $\triangleright$  Equation (8.29)[416]
27:      end for
28:    end for                                          $\triangleright$  Update the weights
29:    for each weight  $w_{i,k}$  in the network do
30:       $w_{i,k} \leftarrow w_{i,k} - \alpha \times \Delta w_{i,k}$             $\triangleright$  Equation (8.30)[416]
31:    end for
```

```
32:     shuffle([(X(1), Y(1)), ..., (Xk, Yk)])  
33: until convergence occurs
```

8.3.5 A Worked Example: Using Backpropagation to Train a Feedforward Network for a Regression Task

The electrical power output from a combined cycle power plant is influenced by a number of ambient parameters, such as temperature and humidity; being able to accurately predict the output of the power plant working a full load with respect to these parameters can significantly reduce the cost of energy production (Tüfekci, 2014). [Table 8.1](#)^[422] lists the hourly averages for the AMBIENT TEMPERATURE and the RELATIVE HUMIDITY when a power plant is working at full load and the net hourly ELECTRICAL OUTPUT for the plant under these conditions. We use this dataset to illustrate training a deep feedforward network. The ELECTRICAL OUTPUT feature is the target feature for this example. The four examples in [Table 8.1](#)^[422] are only a sample from a larger dataset;¹⁸ however, for this example, for ease of illustration we treat these four examples as if they were our full dataset. Furthermore, we use batch gradient descent for training and treat [Table 8.1](#)^[422] as a batch. Consequently, in each iteration of the training algorithm we will complete a single epoch (a single pass through our four examples and hence through the full dataset), and there will be a single weight update per epoch.

Table 8.1

Hourly samples of ambient factors and full load electrical power output of a combined cycle power plant.

ID	AMBIENT TEMPERATURE °C	RELATIVE HUMIDITY %	ELECTRICAL OUTPUT MW
1	03.21	86.34	491.35
2	31.41	68.50	430.37
3	19.31	30.59	463.00
4	20.64	99.97	447.14

A standard **data preprocessing** practice for neural networks is to **normalize** the descriptive features. Consequently, we begin the worked example by explaining why normalization is important for neural networks

and normalizing the data in [Table 8.1](#)^[422]. During normalization, the values of the descriptive features are mapped to a standard range, for example $[-1, +1]$ or $[0, 1]$, using **range normalization** (see [Equation \(3.7\)](#)^[87]), or **standardized** in order to have a mean of 0 and a standard deviation of 1 (see [Equation \(3.8\)](#)^[88]). The reason is that to ensure that the weight updates for all the weights on the network are on a similar scale. Recall that the update applied to a weight $w_{i,k}$ is always scaled by the a_k term (both in the stochastic setting, [Equation \(8.28\)](#)^[415], and the batch setting, [Equation \(8.29\)](#)^[416]). Now consider what happens to the weights on connections from the input layer to the first hidden layer if there are large differences in the values taken by different descriptive features. For example, consider an input feature recording salaries in dollars; this feature could have a spread of values in the range of millions or more. Contrast this with a feature that measures age in years; this feature is likely to have a spread of values with a maximum of just over 100. In this scenario, everything else being equal, the weight updates for the salary feature will generally be larger than those for the age feature because the weight updates are scaled by the feature values. A similar dynamic emerges between weight updates for the bias inputs, which are always equal to 1 ($a_0 = 1$), and weights on inputs with values much larger than 1. Furthermore, large weight updates can result in instability in model training. Indeed, controlling the size of weight updates in order to stabilize convergence during training is one of the reasons why the **learning rate** hyper-parameter α is included in the weight update rules.¹⁹ In addition, having a large variance on the weight updates applied to input connections can result in the network's having relatively large weights for some features. If a model has a relatively large weight on one input feature, then the output of the model can be very sensitive to small changes in the value of the feature and hence the outputs of the model can be very different for similar input vectors. In summary, non-normalized descriptive features can result in unstable or slow learning and a more unstable model in relation to generalization. If the values of a descriptive feature are normally distributed, then standardizing the feature is appropriate; however, this is relatively rare, and the default is to use **range normalization** into either $[-1, +1]$ or $[0, 1]$ for preprocessing.

In a regression problem, in which the target is continuous, normalization is often applied to both the descriptive features and the target feature. One reason why this makes sense is that many activation functions have a small output range (e.g., the output of the logistic function has the range [0,1]) and it is appropriate that the range of the target feature matches the output range of the activation function. Once the target feature has been normalized, then during training the error of the network on an example can be calculated by directly comparing the output of the network with the normalized target feature value. Doing this does necessitate that in order to retrieve the predicted value of the target in the original range of the target feature, the output from the network must be mapped back to the original scale for the target feature, but generally, this is not a difficult thing to do. For example, if the target feature originally had the range $[min, max]$ and range normalization has been applied to map this to the range of [0,1], then the activation of a logistic unit in the output layer of the network a_i can be mapped to the corresponding value in the original range of the target feature by $max \times a_i$. An alternative strategy for using neural networks for regression is to use linear units in the output layer (i.e., units that do not use an activation function and simply output the weighted sum z as their activation). Using linear units in the output layer means that the output of the network can have the same range as the non-normalized target feature. This has the advantage that the outputs of the network do not have to be transformed back into the original target feature range. However, the downside to not normalizing the target feature in a regression problem is that if the target feature has a large range, then during training the error of the network on an example can be very large, resulting in very large error gradients, which in turn can result in large weight updates and an unstable learning process (similar to the instability that can arise with large inputs, but in this case the instability arises from large errors).

For our example we apply range normalization to both the descriptive features and the target feature. Note that for range normalization of the features we need the minimum and maximum values for each feature. [Table 8.2](#)^[423] lists these values for the original complete dataset²⁰ (as distinct from our sample of four examples). [Table 8.3](#)^[423] lists the examples after the features have been range-normalized into the range [0,1].

Table 8.2

The minimum and maximum values for the AMBIENT TEMPERATURE, RELATIVE HUMIDITY, and ELECTRICAL OUTPUT features in the power plant dataset.

	AMBIENT TEMPERATURE	RELATIVE HUMIDITY	ELECTRICAL OUTPUT
Min	1.81°C	25.56%	420.26MW
Max	37.11°C	100.16%	495.76MW

Table 8.3

The *range-normalized* hourly samples of ambient factors and full load electrical power output of a combined cycle power plant, rounded to two decimal places.

ID	AMBIENT TEMPERATURE °C	RELATIVE HUMIDITY %	ELECTRICAL OUTPUT MW
1	0.04	0.81	0.94
2	0.84	0.58	0.13
3	0.50	0.07	0.57
4	0.53	1.00	0.36

We use the network architecture illustrated in [Figure 8.4^{\[390\]}](#) as the structure for the model we train. We also assume that all the neurons use a logistic activation function. [Figure 8.14^{\[425\]}](#) illustrates the forward pass for the examples in [Table 8.3^{\[423\]}](#) through the network in [Figure 8.4^{\[390\]}](#). This network has a depth of three, and so it has three weight matrices. These weight matrices are organized so that each row contains the weights for the connections coming into one neuron. To help align the elements of the weight matrices shown in [Figure 8.14^{\[425\]}](#) with the connections in the graph representation of the network in [Figure 8.4^{\[390\]}](#), the rows and columns of the weight matrices are labeled using the neuron identifiers from [Figure 8.4^{\[390\]}](#) (the labels are the numbers inside circles). For example, the top row of the matrix shown in [Figure 8.4^{\[390\]}](#) labeled *Hidden layer 1 Weight Matrix* contains the weights on the connections coming into Neuron 3 in [Figure 8.4^{\[390\]}](#); hence this row has the label 3. The middle column in this weight matrix represents the weights on the connections from Neuron 1 to each of the neurons in hidden layer 1: Neurons 3, 4 and 5, respectively. The first column in each weight matrix contains the weights for the bias terms, and so these columns have no label. For this example, the weight matrices were randomly initialized from the range $[-0.5, +0.5]$.

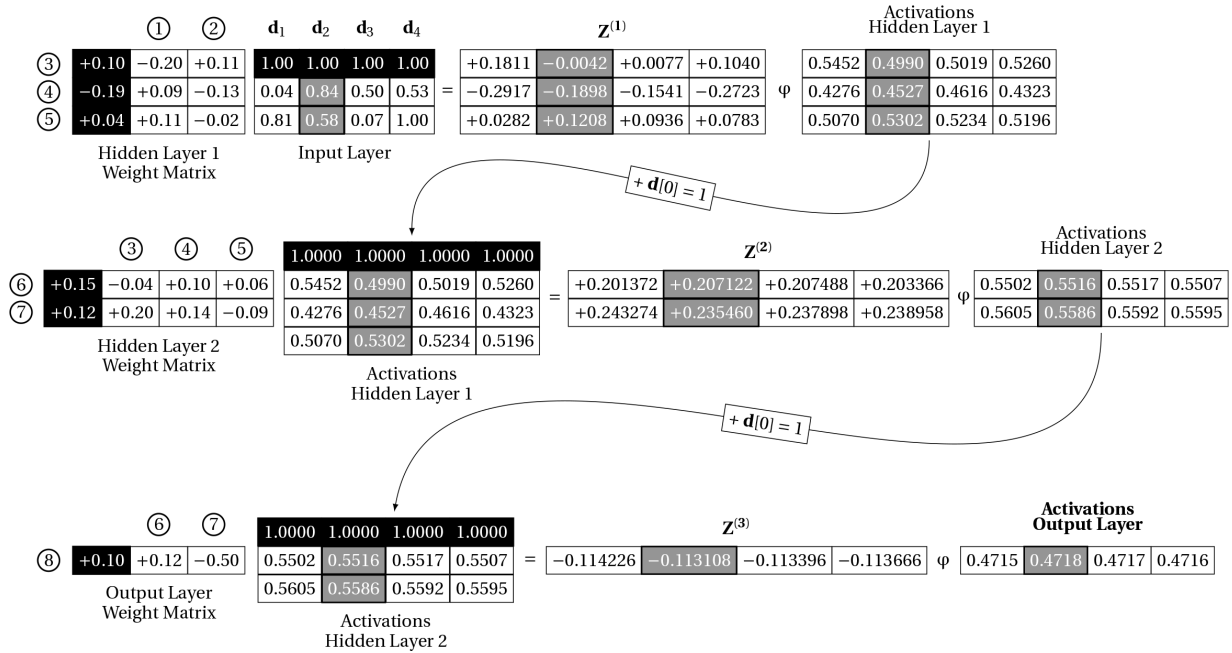


Figure 8.14

The forward pass of the examples listed in [Table 8.3](#)^[423] through the network in [Figure 8.4](#)^[390].

The matrix labeled *Input Layer* contains the inputs for the examples, augmented with the bias inputs for each neuron. Each column in this matrix contains the descriptive features for one of the examples in [Table 8.3](#)^[423]. We have used the convention of a gray background to track the flow of the second example (d_2) through the network: the input vector for d_2 is $\langle \text{bias} = 1, \text{AMBIENT TEMPERATURE} = 0.84, \text{RELATIVE HUMIDITY} = 0.58 \rangle$. The gray column in the matrix $Z^{(1)}$ contains the weighted sums for the neurons 3, 4, and 5 for this input vector; e.g., for Neuron 3 the weighted sum for d_2 is $z_3 = -0.0042$. Tracing d_2 through the logistic activation function, the activation for Neuron 3 for d_2 is $a_3 = 0.4990$. Note that in order to keep the number of decimal points required to represent the calculations through this forward pass manageable for presentation purposes, the outputs of the logistic functions for each layer have been rounded to four decimal places, and these rounded activations were the activations used in the subsequent calculations. Note also that the weight matrix labels on the left of the figure are also the correct neuron labels for the weighted sum Z and activation matrix rows on that line. For example, the first row in $Z^{(1)}$ contains the weighted sum for Neuron 3 (i.e., z_3) for d_1 , d_2 , d_3 , and d_4 , respectively. Similarly, the first row in the *Activations Hidden Layer 1* matrix contains

the activations for Neuron 3 (a_3) for the \mathbf{d}_1 , \mathbf{d}_2 , \mathbf{d}_3 , and \mathbf{d}_4 , respectively. Following the flow of \mathbf{d}_2 through all three layers of the network, the prediction output by the model for this example is 0.4718 (see Cell 2, the gray cell, in the *Activations Output Layer* matrix). [Table 8.4](#)^[426] shows the calculation of the per example error for the four examples and the **sum of squared errors** for the model.

Table 8.4

The per example error after the forward pass illustrated in [Figure 8.14](#)^[425], the per example $\partial\mathcal{E}/\partial a_8$, and the **sum of squared errors** for the model over the dataset of four examples.

	\mathbf{d}_1	\mathbf{d}_2	\mathbf{d}_3	\mathbf{d}_4
Target	0.9400	0.1300	0.5700	0.3600
Prediction	0.4715	0.4718	0.4717	0.4716
Error	0.4685	-0.3418	0.0983	-0.1116
$\partial\mathcal{E}/\partial a_8$: Error $\times -1$	-0.4685	0.3418	-0.0983	0.1116
Error ²	0.21949225	0.11682724	0.00966289	0.01245456
SSE:				0.17921847

The next stage is to backpropagate the δ s for the neurons in the network. When we are processing a batch of examples, we need to do the backpropagation of the δ s for each example. However, for the sake of space, here we illustrate the backpropagation process for a single example. We use \mathbf{d}_2 because the processing of this example has been highlighted in [Figure 8.14](#)^[425], and so it will be easier to identify the relevant z_k and a_k values for each neuron for this example. [Figure 8.15](#)^[427] illustrates the forward pass of \mathbf{d}_2 through the network. This figure shows the weights on each connection and for each neuron shows the weighted sum z calculated by that neuron (the number on the left of the neuron) and the activation z for the neuron (the number on the right of the neuron). Cross-referencing [Figure 8.14](#)^[425], these z and a values are found in the corresponding gray boxes in that figure.

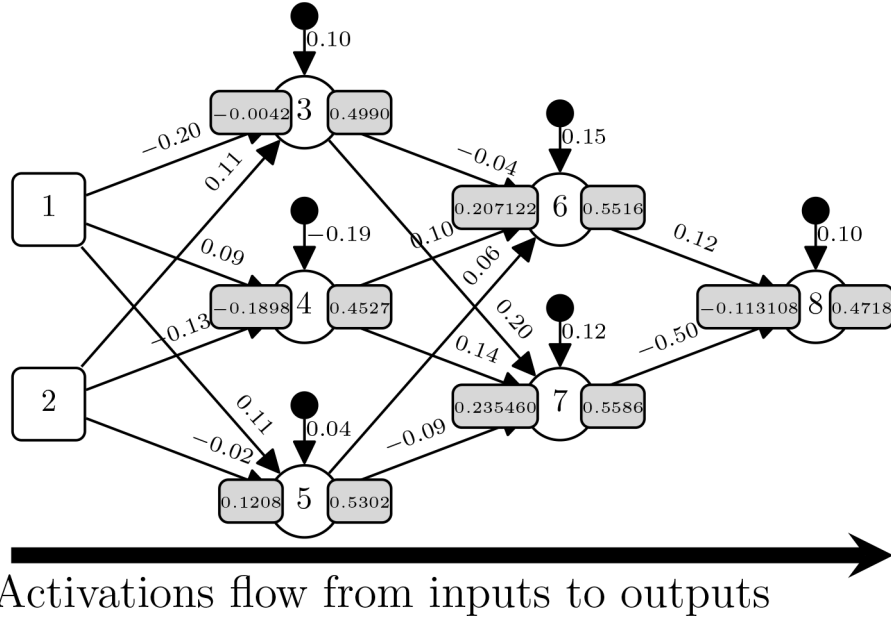


Figure 8.15

An illustration of the forward propagation of \mathbf{d}_2 through the network showing the weights on each connection, and the weighted sum z and activation a value for each neuron in the network.

The first δ we calculate is for Neuron 8: δ_8 . Neuron 8 is an output neuron and so we use the process illustrated in Equation (8.21)^[411]. As shown by Equation (8.21)^[411] and following Equation (8.20)^[411], the term $\partial\mathcal{E}/\partial a$ is the error of the neuron multiplied by -1 , and so from Table 8.4^[426] we see that for \mathbf{d}_2

$$\frac{\partial\mathcal{E}}{\partial a} = 0.3418 \quad (8.31)$$

The second term we need in order to calculate δ_8 is the rate of change of the activation function with respect to the changes in the weighted sum z : $\partial a/\partial z$. This is calculated by plugging the z for the neuron into the derivative of the activation function. The neurons in this network all use the logistic function as their activation function, and so the derivative of this function is given by Equation (8.15)^[408]. As we proceed through the steps of calculating the δ s for each of the neurons, we will need to calculate the $\partial a/\partial z$ term for each neuron, and so for ease of reference, Table 8.5^[428] lists this value for each neuron; for space and convenience considerations we have rounded these values to four decimal places and used the rounded values in our

calculations. From [Table 8.5](#)^[428], for Neuron 8, $\partial a / \partial z = 0.2492$. We now have the two terms we need to calculate δ_8 , and [Equation 8.32](#)^[427] steps through the calculation of δ_8 for \mathbf{d}_2 . Note that for space considerations we have rounded δ_8 to four decimal places, and we will round the δ s for other neurons similarly and use the rounded values in our calculations so that the results of the calculations match the numbers that are presented on the page.

$$\begin{aligned}\delta_8 &= \frac{\partial \mathcal{E}}{\partial a_8} \times \frac{\partial a_8}{\partial z_8} \\ &= 0.3418 \times 0.2492 \\ &= 0.0852\end{aligned}\tag{8.32}$$

Table 8.5

The $\partial a / \partial z$ for each neuron for Example 2 rounded to four decimal places.

NEURON	z	$\partial a / \partial z$
3	-0.004200	0.2500
4	-0.189800	0.2478
5	0.120800	0.2491
6	0.207122	0.2473
7	0.235460	0.2466
8	-0.113108	0.2492

Neuron 8 is the only output neuron in the network, and so once δ_8 has been calculated, we can then proceed to backpropagate the error gradient of the network for \mathbf{d}_2 and calculate the δ s for Neurons 6 and 7. These are hidden neurons, so we use the [Equation \(8.23\)](#)^[412] to calculate δ_6 and δ_7 ; [Equation \(8.33\)](#)^[428] steps through the calculation of δ_6 and [Equation \(8.34\)](#)^[428] steps through the calculation for δ_7 .

$$\begin{aligned}
\delta_6 &= \frac{\partial \mathcal{E}}{\partial a_6} \times \frac{\partial a_6}{\partial z_6} \\
&= (\sum \delta_i \times w_{i,6}) \times \frac{\partial a_6}{\partial z_6} \\
&= (\delta_8 \times w_{8,6}) \times \frac{\partial a_6}{\partial z_6} \\
&= (0.0852 \times 0.12) \times 0.2473 \\
&= 0.0025
\end{aligned} \tag{8.33}$$

$$\begin{aligned}
\delta_7 &= \frac{\partial \mathcal{E}}{\partial a_7} \times \frac{\partial a_7}{\partial z_7} \\
&= (\sum \delta_i \times w_{i,7}) \times \frac{\partial a_7}{\partial z_7} \\
&= (\delta_8 \times w_{8,7}) \times \frac{\partial a_7}{\partial z_7} \\
&= (0.0852 \times -0.50) \times 0.2466 \\
&= -0.0105
\end{aligned} \tag{8.34}$$

Once the δ s for Neurons 6 and 7 have been calculated, we are ready to propagate the error gradients back to the first hidden layer. The process used to calculate the δ s for Neurons 3, 4, and 5 is the same as that used to calculate δ_6 and δ_7 . Equation (8.35)^[429] steps through this calculation for δ_3 , Equation (8.36)^[429] shows the calculation of δ_4 , and Equation (8.37)^[429] lists the calculations of δ_5

$$\begin{aligned}
\delta_3 &= \frac{\partial \mathcal{E}}{\partial a_3} \times \frac{\partial a_3}{\partial z_3} \\
&= \left(\sum \delta_i \times w_{i,3} \right) \times \frac{\partial a_3}{\partial z_3} \\
&= ((\delta_6 \times w_{6,3}) + (\delta_7 \times w_{7,3})) \times \frac{\partial a_3}{\partial z_3} \\
&= ((0.0025 \times -0.04) + (-0.0105 \times 0.20)) \times 0.2500 \\
&= -0.0006
\end{aligned} \tag{8.35}$$

$$\begin{aligned}
\delta_4 &= \frac{\partial \mathcal{E}}{\partial a_4} \times \frac{\partial a_4}{\partial z_4} \\
&= \left(\sum \delta_i \times w_{i,4} \right) \times \frac{\partial a_4}{\partial z_4} \\
&= ((\delta_6 \times w_{6,4}) + (\delta_7 \times w_{7,4})) \times \frac{\partial a_4}{\partial z_4} \\
&= ((0.0025 \times 0.10) + (-0.0105 \times 0.14)) \times 0.2478 \\
&= -0.0003
\end{aligned} \tag{8.36}$$

$$\begin{aligned}
\delta_5 &= \frac{\partial \mathcal{E}}{\partial a_5} \times \frac{\partial a_5}{\partial z_5} \\
&= \left(\sum \delta_i \times w_{i,5} \right) \times \frac{\partial a_5}{\partial z_5} \\
&= ((\delta_6 \times w_{6,5}) + (\delta_7 \times w_{7,5})) \times \frac{\partial a_5}{\partial z_5} \\
&= ((0.0025 \times 0.06) + (-0.0105 \times -0.09)) \times 0.2491 \\
&= 0.0003
\end{aligned} \tag{8.37}$$

We have now calculated the δ s for all the neurons in the network for \mathbf{d}_2 . Figure 8.16^[430] shows the network with each neuron labeled with its corresponding δ . Each δ expresses the rate of change (or sensitivity) of the error of the network with respect to changes in the weighted sum calculation of a specific neuron. In order to update the weights on the connections coming into a neuron, we must connect the rate of change of the error of the network to changes in each weight. Equation (8.27)^[414] defined how the rate of change of the error of a network with respect to a weight in the network $\partial \mathcal{E} / \partial w_{i,k}$ can be calculated using the chain rule. This

calculation reduces to multiplying the δ for the neuron that uses the weight in its weighted sum by the activation that the weight was applied to in the weighted sum. [Table 8.6](#)^[431] lists the calculations of $\partial \mathcal{E} / \partial w_{i,k}$ for each weight in the network for \mathbf{d}_2 . This table is ordered so that the weights for inputs to Neuron 8 are at the top, and then as we move down the table, we move back through the network.

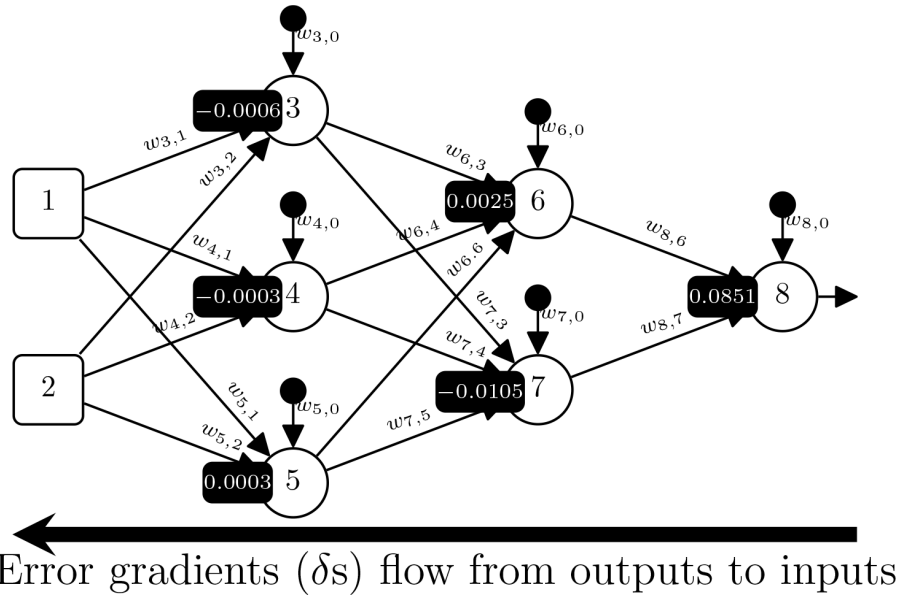


Figure 8.16

The δ s for each of the neurons in the network for Example 2.

Table 8.6

The $\partial\mathcal{E}/\partial w_{i,k}$ calculations for \mathbf{d}_2 for every weight in the network. We use the neuron index 0 to denote the bias input for each neuron.

NEURON _i	NEURON _k	$w_{i,k}$	δ_i	a_k	$\partial\mathcal{E}/\partial w_{i,k}$
8	0	$w_{8,0}$	0.0852	1	$0.0852 \times 1 = 0.0852$
8	6	$w_{8,6}$	0.0852	0.5516	$0.0852 \times 0.5516 = 0.04699632$
8	7	$w_{8,7}$	0.0852	0.5586	$0.0852 \times 0.5586 = 0.04759272$
7	0	$w_{7,0}$	-0.0105	1	$-0.0105 \times 1 = -0.0105$
7	3	$w_{7,3}$	-0.0105	0.4990	$-0.0105 \times 0.4527 = -0.0052395$
7	4	$w_{7,4}$	-0.0105	0.4527	$-0.0105 \times 0.4527 = -0.00475335$
7	5	$w_{7,5}$	-0.0105	0.5302	$-0.0105 \times 0.5302 = -0.0055671$
6	0	$w_{6,0}$	0.0025	1	$0.0025 \times 1 = 0.0025$
6	3	$w_{6,3}$	0.0025	0.4990	$0.0025 \times 0.4527 = 0.0012475$
6	4	$w_{6,4}$	0.0025	0.4527	$0.0025 \times 0.4527 = 0.00113175$
6	5	$w_{6,5}$	0.0025	0.5302	$0.0025 \times 0.5302 = 0.0013255$
5	0	$w_{5,0}$	0.0003	1	$0.0003 \times 1 = 0.0003$
5	1	$w_{5,1}$	0.0003	0.84	$0.0003 \times 0.84 = 0.000252$
5	2	$w_{5,2}$	0.0003	0.58	$0.0003 \times 0.58 = 0.000174$
4	0	$w_{4,0}$	-0.0003	1	$-0.0003 \times 1 = -0.0003$
4	1	$w_{4,1}$	-0.0003	0.84	$-0.0003 \times 0.84 = -0.000252$
4	2	$w_{4,2}$	-0.0003	0.58	$-0.0003 \times 0.58 = -0.000174$
3	0	$w_{3,0}$	-0.0006	1	$-0.0006 \times 1 = -0.0006$
3	1	$w_{3,1}$	-0.0006	0.84	$-0.0006 \times 0.84 = -0.000504$
3	2	$w_{3,2}$	-0.0006	0.58	$-0.0006 \times 0.58 = -0.000348$

If we are using stochastic gradient descent, in which we update the weights after each example has been presented to the network, then to update a weight in the network we first calculate a $\partial\mathcal{E}/\partial w_{i,k}$ term for the weight similarly to the calculations shown in [Table 8.6](#)^[431] for \mathbf{d}_2 and then plug the $\partial\mathcal{E}/\partial w_{i,k}$ value for the weight into [Equation \(8.28\)](#)^[415]. For example, if we assume that \mathbf{d}_2 was the first example processed^[21] and that we have set the learning rate hyper-parameter to $\alpha = 0.2$, then we would update weight $w_{7,5}$ as follows:

$$\begin{aligned}
w_{7,5} &= w_{7,5} - \alpha \times \delta_7 \times a_5 \\
&= w_{7,5} - \alpha \times \frac{\partial \mathcal{E}}{\partial w_{i,k}} \\
&= -0.09 - 0.2 \times -0.0055671 \\
&= -0.08888658
\end{aligned} \tag{8.38}$$

However, in this example we use batch gradient descent training, and so for each weight update we must first calculate a table equivalent to [Table 8.6](#)^[431] for each example. Once these tables have been created, for each weight we sum the $\partial \mathcal{E} / \partial w_{i,k}$ for that weight across the tables. This summation gives us the $\Delta w_{i,k}$ term in [Equation \(8.30\)](#)^[416]. [Table 8.7](#)^[432] illustrates this calculation for weight $w_{7,5}$, and [Equation 8.39](#)^[432] shows how the $\Delta w_{7,5}$ is used as part of [Equation 8.30](#)^[416] to update the weight after the batch of four examples has been processed; again, in this weight update we assume that $\alpha = 0.2$.

Table 8.7

The calculation of $\Delta w_{7,5}$ across our four examples.

MINI-BATCH EXAMPLE	$\frac{\partial \mathcal{E}}{\partial w_{7,5}}$
\mathbf{d}_1	0.00730080
\mathbf{d}_2	-0.00556710
\mathbf{d}_3	0.00157020
\mathbf{d}_4	-0.00176664
$\Delta w_{7,5} =$	0.00153726

$$\begin{aligned}
w_{7,5} &= w_{7,5} - \alpha \times \Delta w_{i,k} \\
&= -0.09 - 0.2 \times 0.00153726 \\
&= -0.0903074520
\end{aligned} \tag{8.39}$$

If we update all the weights in the network using the process illustrated in [Equation 8.39](#)^[432] for weight $w_{7,5}$ and then run the same examples through a forward pass of the network, we reduce the error of the model by a small amount; [Table 8.8](#)^[433] lists the per example error and sum of squared errors for the four examples after all the weights have been updated. Comparing [Table 8.8](#)^[433] with [Table 8.4](#)^[426], we see that the model made a slightly

different prediction for each example; the prediction for \mathbf{d}_2 is now 0.4741 whereas the original prediction was 0.4718. Also, the total error of the model on the dataset, measured here by the sum of squared errors, has dropped slightly from 0.17921847 to 0.17896823, an error reduction of 0.00025024. Admittedly, this drop in error is tiny, but it is a reduction in error, and this reduction was achieved by updating randomly initialized weights once. In a full network training scenario there would be many such weight updates as the training progressed through multiple epochs and, for each epoch, multiple mini-batches; the reduction of the network error would accumulate over these weight updates. For example, assuming that we continue to train the network on just our small sample dataset with $\alpha = 0.2$ and updating the weights after each pass through our data, then the training of the network would converge to an $SSE < 0.0001$ after 7,656 epochs.²² [Table 8.9](#)^[433] lists the model predictions for each of the examples and the calculation of the sum of squared errors once training has converged. [Figure 8.17](#)^[434] illustrates how the sum of squared errors of the network changes during the training. This plot shows that the reduction in the error achieved by each weight update (one per epoch) is initially quite small. However, after approximately 5,000 epochs, the rate of decrease of the error increases dramatically until it flattens out again around 6,000 epochs. From then on, the sum of squared errors of the network continues to slowly reduce until it reaches the convergence criterion of $SSE < 0.0001$. As with the regression examples in Chapter 7^[311], the profile of this error reduction over the course of the training is sensitive to a number of factors, for example, the learning rate α and how it is updated throughout the training (see Section 7.3.3^[328]).

Table 8.8

The per example error after each weight has been updated once, the per example $\partial\mathcal{E}/\partial a_8$, and the **sum of squared errors** for the model.

	d₁	d₂	d₃	d₄
Target	0.9400	0.1300	0.5700	0.3600
Prediction	0.4738	0.4741	0.4740	0.4739
Error	0.4662	-0.3441	0.0960	-0.1139
$\partial\mathcal{E}/\partial a_8$: Error $\times -1$	-0.4662	0.3441	-0.0960	0.1139
Error ²	0.21734244	0.11840481	0.009216	0.01297321
SSE:				0.17896823

Table 8.9

The per example prediction, error, and the sum of squared errors after training has converged to an SSE < 0.0001.

	d₁	d₂	d₂	d₂
Target	0.9400	0.1300	0.5700	0.3600
Prediction	0.9266	0.1342	0.5700	0.3608
Error	0.0134	-0.0042	0.0000	-0.0008
Error ²	0.00017956	0.00001764	0.00000000	0.00000064
SSE:				0.00009892

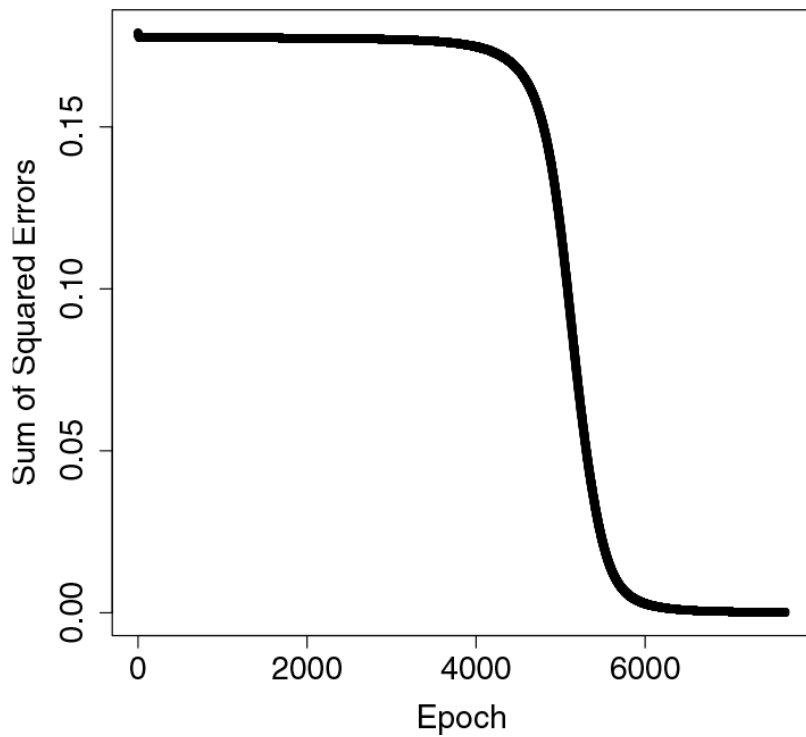


Figure 8.17

A plot showing how the sum of squared errors of the network changed during training.

8.4 Extensions and Variations

One of the biggest challenges in training a deep neural network is to ensure that the flow of error gradients back through the layers of a network is stable during training. Consequently, in Sections 8.4.1^[434] and 8.4.2^[447] we explain and motivate the current standard approaches to deciding on two of the most important hyper-parameter decisions for keeping error gradients stable: the selection of the activation function, and the initialization of the weights. Then in Section 8.4.3^[463] we explain how to adapt the design of a neural network to classification problems by using a **softmax** output layer and the **cross-entropy** loss function. Whether deep learning is applied to regression or classification, the size and complexity of deep learning models make them susceptible to **overfitting**, and so in Section 8.4.4^[472] we cover the two most popular extensions to backpropagation that are used to try to avoid overfitting: **early stopping** and **dropout**. We then conclude the extensions and variations of deep learning by introducing two of the most popular network architectures used in deep learning: **convolutional neural**

networks (Section 8.4.5^[477]) and **recurrent neural networks** (Section 8.4.6^[499]).

8.4.1 Vanishing Gradients and ReLUs

Figure 8.16^[430] shows the network from the worked example in a graph form with each of the neurons labeled with the δ for the neuron. These δ s were calculated by backpropagating the error on Example 2. If we compare the δ for Neuron 8 (the output neuron) with the δ s for the neurons in the first hidden layer (Neurons 3, 4, and 5), it becomes clear that the δ values become smaller as they are propagated back from the output layer to the earlier layers in the network: $\delta_8 = 0.0851$, whereas $\delta_3 = -0.0006$, $\delta_4 = -0.0003$, and $\delta_5 = 0.0003$ are all smaller in magnitude. This phenomenon is known as the **vanishing gradient** problem, because in deep networks the δ terms tend toward zero and vanish as we propagate the δ s back to the early layers.

Vanishing gradients are a serious challenge for training deep networks because the δ s are the learning signal that tells each neuron how it should update its weights in order to improve the network's performance on an example. In other words, the updates applied to a weight are a function of the δ for the neuron that uses the weight in its weighted sum. However, as the δ s vanish, the learning signal attenuates, and this can slow down the rate at which the early layers of the network learn. Concretely, this means that in each weight update, the weights in the earlier layers in the network are updated by smaller amounts than the neurons in the later layers. This differential in the weight updates is apparent in Table 8.6^[431], which is arranged so that $\partial\mathcal{E}/\partial w_{i,k}$ terms for the weights on inputs to output layer (Neuron 8) are at the top of the table, and then as we move down the table, we move back through the network. Inspecting the right-hand column of this table and comparing the magnitude of the $\partial\mathcal{E}/\partial w_{i,k}$ terms, the most significant digit in the $\partial\mathcal{E}/\partial w_{i,k}$ terms for weights on inputs to Neuron 8 are at 10^{-2} ; by comparison the most significant digit for the $\partial\mathcal{E}/\partial w_{i,k}$ terms for the weights on inputs to Neurons 3, 4, and 5 (the first hidden layer) are at 10^{-4} . This differential means that the neurons in the first hidden layer will learn more slowly than the neurons output layer. Furthermore, the deeper the network becomes, the slower the earlier layers learn (because the

learning signal, the error gradient, attenuates as it is backpropagated through the layers).

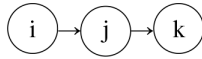
This is a serious problem because the ability of a deep neural network to learn a useful representation of the inputs works by the earlier layers of the network extracting low-level features from the raw data and then the later layers learning to combine these features in useful ways (see [Figure 8.10](#)^[402] for an illustration of this for a three-layer network). However, if the neurons in the early layers of the network take a long time to train, then the neurons in the later layers cannot efficiently build upon the outputs of these early neurons. The net result is that the vanishing gradient problem can cause deep networks to take a very long time to train. The vanishing gradient problem is a direct consequence of the fact that the backpropagation algorithm is based on the **chain rule**. Using backpropagation, the error gradient at any point in the network is a product of the gradients up to that point; for convenience, we repeat [Equation \(8.25\)](#)^[414] here

$$\begin{aligned}\frac{\partial \mathcal{E}}{\partial w_{i,k}} &= \frac{\partial \mathcal{E}}{\partial a_i} \times \frac{\partial a_i}{\partial z_i} \times \frac{\partial z_i}{\partial w_{i,k}} \\ &= \delta_i \times \frac{\partial z_i}{\partial w_{i,k}}\end{aligned}\tag{8.40}$$

Reading from left to right, the first term in this product is the rate of change of the error gradient of the network with respect to changes in the activation (or output) of a neuron i ; the second term is the rate of change of the activation of neuron i with respect to changes in z_i (the weighted sum for neuron i); and the third term is the rate of change of z_i with respect to changes in the weight $w_{i,k}$.

The earlier in the network a weight occurs, the more terms there are in the product. This expansion in the number of terms arises from the fact that for all hidden neurons the δ term is calculated by a product of (1) $\partial \mathcal{E}/\partial a_i$, which itself is a product of the weighted sum of the δ s backpropagated to the neuron; and (2) the derivative of the neuron's activation function, that is, a term of the form $\partial a_k/\partial z_k$ (see [Equation \(8.23\)](#)^[412]). However, if these backpropagated δ s came from hidden neurons, then they were also calculated as a product of the weighted sum of the δ s backpropagated to

those hidden neurons and the $\partial a_k / \partial z_k$ term for those neurons. To illustrate this growth in the number of terms in the chain of products as we move back through a network, imagine a simple feedforward network with just three neurons, i , j , and k , arranged so that i feeds forward into j and j into k



[Equation 8.41](#)^[436] illustrates the expansion of the chain of products as the error gradient is propagated back through the network. By the time the original error gradient term $\partial \mathcal{E} / \partial a_k$ is propagated back to δ_i it is multiplied by two weights, $w_{j,i}$ and $w_{k,j}$, and three times by the derivative of the activation function of a neuron with respect to the weighted sum of the neuron: $\partial a_k / \partial z_k$, $\partial a_j / \partial z_j$, $\partial a_i / \partial z_i$. We return to the discussion of weights in the next section, [Section 8.4.2](#)^[447]; our focus in this section is on the effect of repeatedly multiplying the error gradient by the derivative of an activation function

$$\begin{aligned}
\delta_i &= \frac{\partial \mathcal{E}}{\partial a_i} \times \frac{\partial a_i}{\partial z_i} \\
&= \overbrace{w_{j,i} \times \delta_j}^{} \times \frac{\partial a_i}{\partial z_i} \\
&= w_{j,i} \times w_{k,j} \times \overbrace{\delta_k}^{} \times \frac{\partial a_j}{\partial z_j} \times \frac{\partial a_i}{\partial z_i} \\
&= w_{j,i} \times w_{k,j} \times \overbrace{\frac{\partial \mathcal{E}}{\partial a_k} \times \frac{\partial a_k}{\partial z_k}}^{} \times \frac{\partial a_j}{\partial z_j} \times \frac{\partial a_i}{\partial z_i}
\end{aligned} \tag{8.41}$$

Multiplying a number by a number less than 1 makes the number smaller. With this in mind, it is instructive to refer to [Figure 8.13](#)^[410], which plots the logistic function and the derivative of the logistic function. [Figure 8.13](#)^[410] shows that the maximum value of the derivative of the logistic function is 0.25. The figure also shows that the derivative is 0 (or near 0) for the **saturated** regions of the function: the logistic function saturates for large negative ($\approx z < -2$) or positive values ($z > +2$); this means that the rate of change of the output of the logistic function with respect to small changes in z , when z has a large negative or positive value, is 0 (or near 0).

[Equation 8.41](#)^[436] shows that during backpropagation the error gradient is repeatedly multiplied by a derivative of activation functions, one multiplication for each neuron that the error gradient is backpropagated through. When a neuron uses a logistic function as its activation function, then the maximum value the derivative can take is 0.25. Consequently, backpropagating the error gradient through the neuron that uses a logistic activation function involves multiplying the error term by a value ≤ 0.25 and that is ≈ 0 for z values in the saturated regions of the logistic function. If all the neurons in a network use a logistic activation function or another activation function whose derivative has a small range less than 1, then the error gradient will get smaller and smaller as it is backpropagated through the networks layers, and the scaling down of the gradient is particularly severe for neurons whose z value is in the saturated region of the activation function.

Given that the vanishing gradient problem arises from repeatedly multiplying the error gradients by the derivative of the activation functions, one way to address the vanishing gradient problem is to use a different activation function. At the start of the chapter we introduced the rectified linear function:²³

$$\text{rectifier}(z) = \max(0, z) = \begin{cases} z & \text{if } z > 0 \\ 0 & \text{otherwise} \end{cases} \quad (8.42)$$

The derivative of the rectifier function is:

$$\frac{d}{dz} \text{rectifier}(z) = \begin{cases} 1 & \text{if } z > 0 \\ 0 & \text{otherwise} \end{cases} \quad (8.43)$$

The fact that the derivative of the rectifier function takes either a 0 or a 1 value means that during backpropagation for some neurons in a network, the δ value will be pushed to zero. However, this is not necessarily a problem: if we consider the backpropagation process as error gradients, δ_s , flowing through a layer of neurons then, although for some neurons in the layer the δ_s will go to zero, for others the gradients will pass through unscaled. In particular, in any neuron where the input to the rectifier

function is greater than zero ($z > 0$) then the neuron will activate during the forward pass and the partial derivative of the activation function will be 1 during the backward pass. In these cases the error gradients are able to be backpropagated through the neuron without scaling. Consequently, the error gradients in the backward pass can propagate along the paths of active neurons in the network, and because $\partial a_k / \partial z_k = 1$ along these paths, the gradients can flow back through a deeper network (Glorot et al., 2011). Note that neurons that use a rectified linear activation function are known as ReLUs (short for *rectified linear units*).

Technically, the derivative of the rectifier function is undefined when $z_k = 0$, so strictly, the rectifier function is not an appropriate choice for gradient descent and backpropagation, which assume differentiable functions. However, a common practice in neural networks is to choose a derivative value for $z_k = 0$ of zero, and we have integrated this convention into the definition of Equation (8.43)^[437]. This convention has been found generally to work well.

[Figure 8.18](#)^[440] shows the forward propagation of the examples in [Table 8.3](#)^[423] through the same network that we used in the worked example, with the single difference that all the neurons in the network are now ReLUs.²⁴ [Table 8.10](#)^[441] lists the per example error of this ReLU network resulting from the forward pass in [Figure 8.18](#)^[440]. This table also lists the sum of squared errors for the ReLU model.²⁵

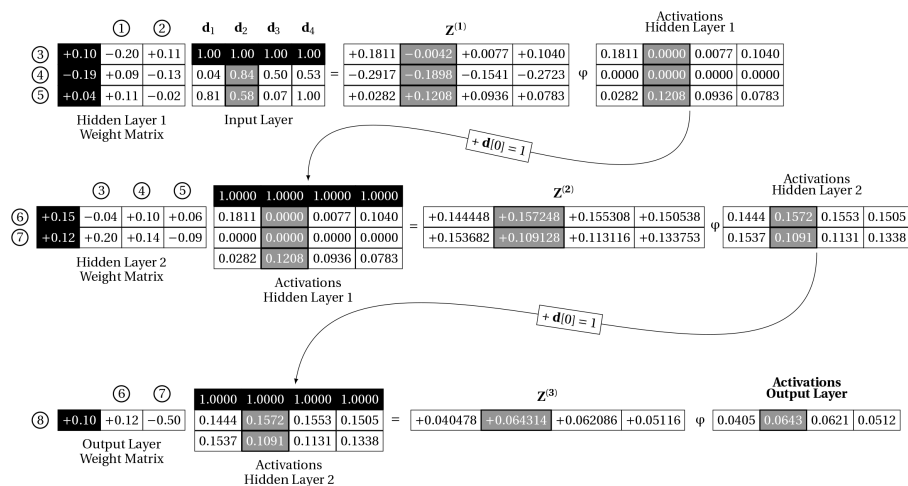


Figure 8.18

The forward pass of the examples listed in [Table 8.3](#)^[423] through the network in [Figure 8.4](#)^[390] when all the neurons are ReLUs.

Table 8.10

The per example error of the ReLU network after the forward pass illustrated in [Figure 8.18^{\[440\]}](#), the per example $\partial\mathcal{E}/\partial a_8$, and the **sum of squared errors** for the ReLU model.

	\mathbf{d}_1	\mathbf{d}_2	\mathbf{d}_3	\mathbf{d}_4
Target	0.9400	0.1300	0.5700	0.3600
Prediction	0.0405	0.0643	0.0621	0.0512
Error	0.8995	0.0657	0.5079	0.3088
$\partial\mathcal{E}/\partial a_8$: Error $\times -1$	-0.8995	-0.0657	-0.5079	-0.3088
Error ²	0.80910025	0.00431649	0.25796241	0.09535744
SSE:				0.58336829

To illustrate the effect that switching to a rectified linear activation function has on a network, we step through the forward and backward pass of the backpropagation algorithm for \mathbf{d}_2 . [Figure 8.19^{\[441\]}](#) illustrates the forward pass for \mathbf{d}_2 through the ReLU network. This figure shows the weights on each connection and for each neuron shows the weighted sum z calculated by that neuron (the number on the left of the neuron) and the activation a for the neuron (the number on the right of the neuron). These z and a values will be found in the corresponding gray boxes in [Figure 8.18^{\[440\]}](#). Notice that both Neurons 3 and 4 have an activation of zero for \mathbf{d}_2 . The reason is that both these neurons happen to have large negative weights on at least one of their inputs. However, the forward propagation through the network still occurs along an active path through Neuron 5.

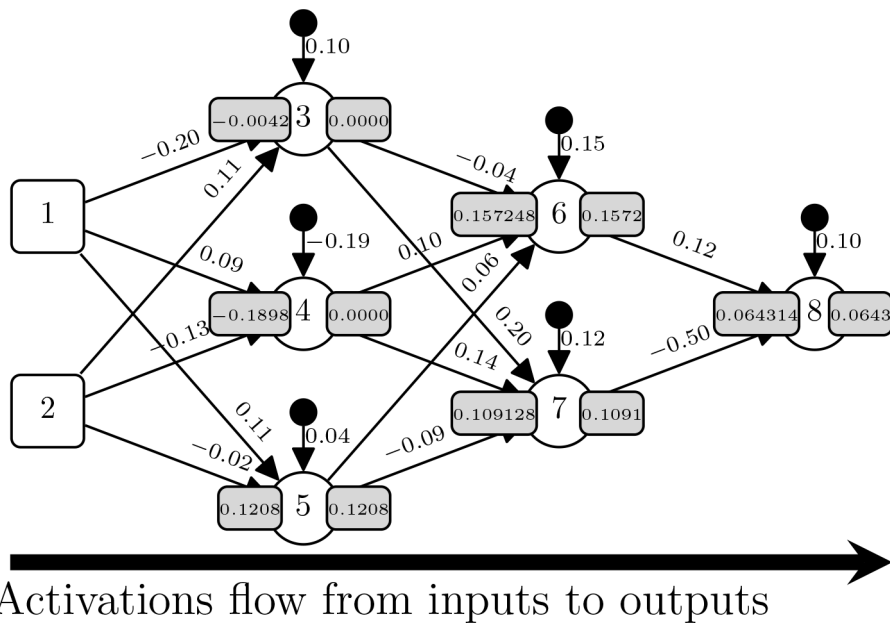


Figure 8.19

An illustration of the forward propagation of \mathbf{d}_2 through the ReLU network showing the weights on each connection, and the weighted sum z and activation a value for each neuron in the network.

In order to calculate and backpropagate the δ s for \mathbf{d}_2 through the network, we need the $\partial a / \partial z$ for each neuron in the network for this example, Table 8.11^[442] lists these values; because all the neurons use a rectified linear activation function, the $\partial a / \partial z$ are either 0 or 1 (as per derivative of the rectified linear function given in Equation 8.43^[437]). From these values we can see that the error gradient will be able to flow backward through Neurons 8, 7, and 6 without being scaled down by the multiplication by $\partial a / \partial z$ in the δ calculations. Equation 8.44^[442] lists the calculations of the δ s for \mathbf{d}_2 for all the neurons in the ReLU network. Comparing the δ s for the ReLU network with those calculated for the logistic network for the same example (see Figure 8.16^[430]) shows that, where the derivative of the ReLU has not pushed the δ to 0, the drop in the magnitude of the δ s as we move back through the network is not as severe; for example, in Figure 8.16^[430] there is a consistent reduction in the magnitude of the δ values from 10^{-2} in the output layer to 10^{-4} in the first hidden layer, and in the ReLU network the drop is from 10^{-2} in the output layer to 10^{-3} in the first hidden layer. The fact that both of these neurons had an activation of 0 in response to \mathbf{d}_2 resulted in both of these neurons having a $\delta = 0$. This means that weights for these neurons will not be updated for this example.

Table 8.11

The $\partial a/\partial z$ for each neuron for \mathbf{d}_2 rounded to four decimal places.

NEURON	z	$\partial a/\partial z$
3	-0.004200	0
4	-0.189800	0
5	0.120800	1
6	0.157248	1
7	0.109128	1
8	0.064314	1

We can illustrate the speed up in training that can be achieved by switching a network from using the logistic activation function to a rectified linear activation function if we compare the number of epochs required for the network from the worked example to converge to an $SSE < 0.0001$ when it uses ReLUs instead of logistic units. If we initialize the network with the same initial set of weights that we used in Section 8.3.5 [421] and use the same data, training regime, and learning rate ($\alpha = 0.2$), then the ReLU version of the network converges to an $SSE < 0.0001$ in just 424 epochs, as compared with the 7,656 epochs required to train the logistic network. **Table 8.12**^[443] lists the predictions of the trained ReLU network for each of the examples and the calculation of the sum of squared errors once training has converged. **Figure 8.20**^[443] illustrates how the sum of squared errors of the ReLU network changes during the training of the network. The plot shows that the initial sum of squared errors of the network is just under 0.6, and this drops to < 0.2 after the first epoch. After approximately 150 epochs the rate of decrease of the sum of squared errors increases, but training also becomes a bit unstable with the sum of squared errors of the network sometimes increasing and decreasing dramatically. This type of instability can be indicative that the learning rate α is too high. In fact, because the rectifier linear function is unbounded,²⁶ it is often the case that smaller learning rates are necessary in training a ReLU network than in training a network with logistic units. **Figure 8.21**^[444] plots the SSE of the ReLU network across the training epochs when we use a smaller learning rate, in this case $\alpha = 0.1$. Not only is the learning more stable (i.e., smoother) but the training of the network actually converges on the stop criterion of $SSE < 0.0001$ in fewer epochs, 412 instead of 424. This illustrates how sensitive

the training of a deep neural network can be to a range of hyper-parameters, such as the learning rate and activation function.

Table 8.12

The ReLU network's per example prediction, error, and the sum of squared errors after training has converged to an $SSE < 0.0001$.

	d_1	d_2	d_3	d_4
Target	0.9400	0.1300	0.5700	0.3600
Prediction	0.9487	0.1328	0.5772	0.3679
Error	-0.0087	-0.0028	-0.0072	-0.0079
Error ²	0.00007569	0.00000784	0.00005184	0.00006241
SSE:				0.00009889

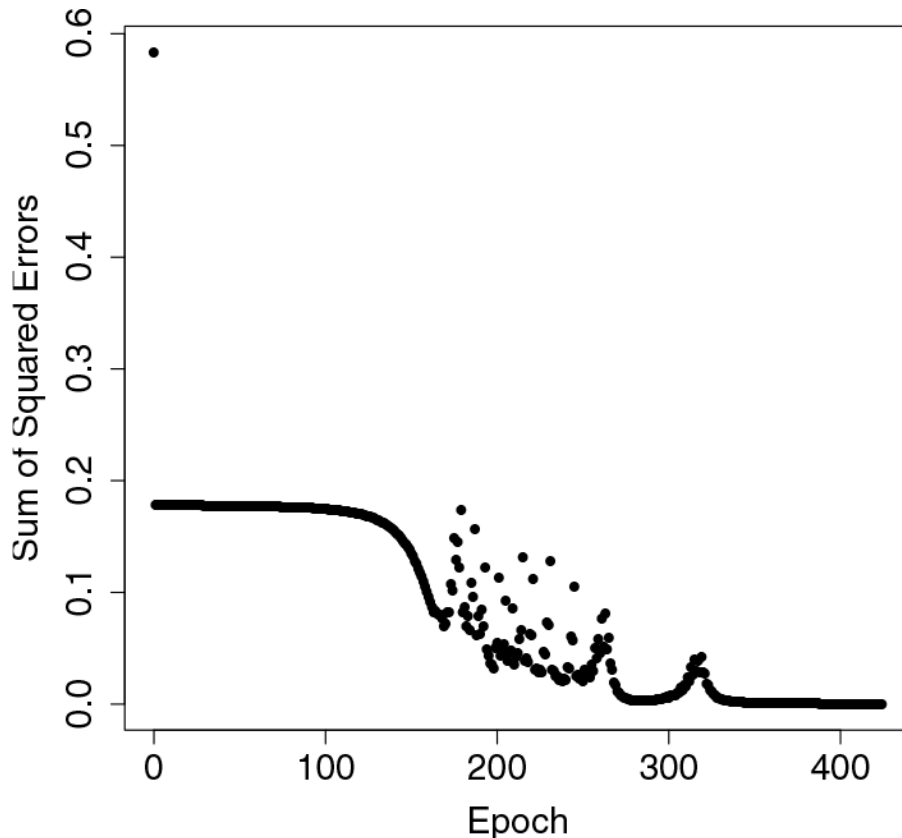


Figure 8.20

A plot showing how the sum of squared errors of the ReLU network changed during training when $\alpha = 0.2$.

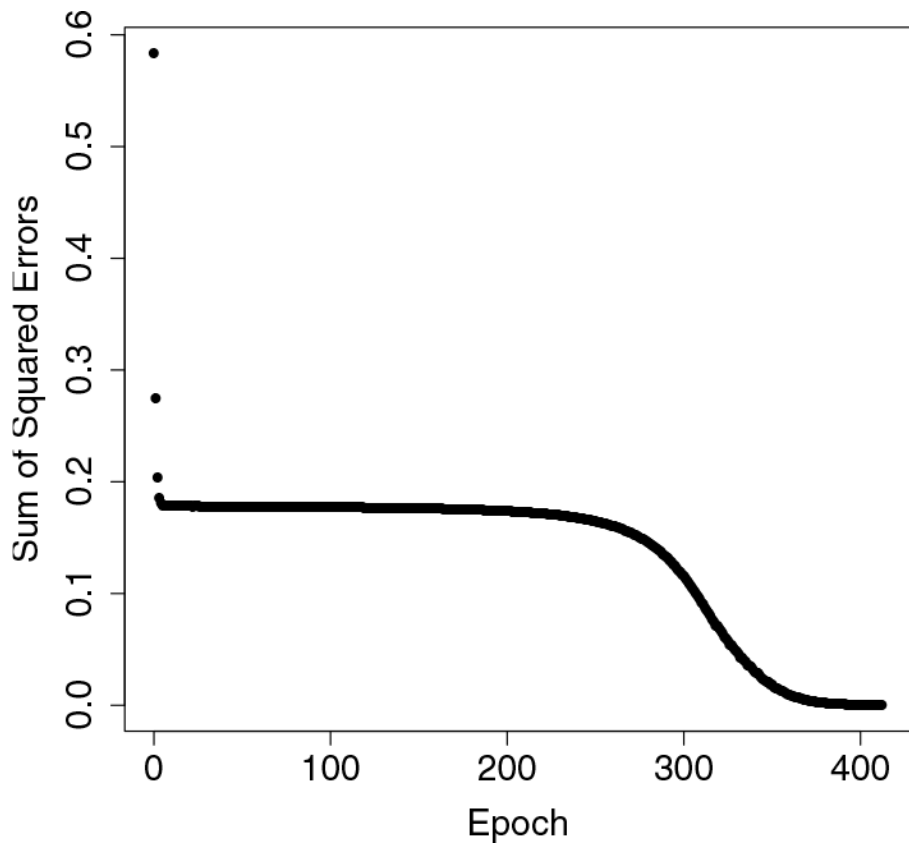


Figure 8.21

A plot showing how the sum of squared errors of the ReLU network changed during training when $\alpha = 0.1$.

$$\begin{aligned}
\delta_k &= \frac{\partial \mathcal{E}}{\partial a_k} \times \frac{\partial a_k}{\partial z_i} \\
\delta_8 &= -0.0657 \times 1.0 \\
&= -0.0657 \\
\delta_7 &= (\delta_8 \times w_{8,7}) \times \frac{\partial a_7}{\partial z_7} \\
&= (-0.0657 \times -0.50) \times 1 \\
&= 0.0329 \\
\delta_6 &= (\delta_8 \times w_{8,6}) \times \frac{\partial a_6}{\partial z_6} \\
&= (-0.0657 \times 0.12) \times 1 \\
&= -0.0079 \\
\delta_5 &= ((\delta_6 \times w_{6,5}) + (\delta_7 \times w_{7,5})) \times \frac{\partial a_5}{\partial z_5} \\
&= ((-0.0079 \times 0.06) + (0.0329 \times -0.09)) \times 1 \\
&= -0.0034 \\
\delta_4 &= ((\delta_6 \times w_{6,4}) + (\delta_7 \times w_{7,4})) \times \frac{\partial a_4}{\partial z_4} \\
&= ((-0.0079 \times 0.10) + (0.0329 \times 0.14)) \times 0 \\
&= 0 \\
\delta_3 &= ((\delta_6 \times w_{6,3}) + (\delta_7 \times w_{7,3})) \times \frac{\partial a_3}{\partial z_3} \\
&= ((-0.0079 \times -0.04) + (0.0329 \times 0.20)) \times 0 \\
&= 0
\end{aligned} \tag{8.44}$$

We have seen that switching a network from a logistic activation function to a rectified linear activation function can speed up training; however, a less obvious effect of this switch is that it also tends to make the representations learned by a network **sparse**. What this means is that for any given input vector, only a subset of the neurons in the network will activate (i.e., $a_i > 0$). This is because the rectified linear function has a zero output value for half its domain (i.e., for all $z \leq 0$). For example, consider a feedforward network that has been initialized with weights randomly sampled with uniform probability from a range such as $[-0.5, +0.5]$. In such

a network, immediately after initialization, approximately half the hidden neurons in the network will have activations equal to zero; in a sense, in a network with a sparse representation, each input vector flows through a subset of active pathways in the network (Glorot et al., 2011). By contrast in a network using logistic activation functions, the vast majority of neurons will be active for all inputs. Using a sparse representation can reduce the energy consumed by a network (Reagen et al., 2017) and is also more biologically plausible (Glorot et al., 2011). However, if the representations become too sparse, then the performance of the network may deteriorate.

For example, consider Neuron 4 in our example network. This neuron has two large negative weights ($w_{4,0} = -0.19$ and $w_{4,2} = -0.13$). The effect of these negative weights is apparent in the $\mathbf{Z}^{(1)}$ matrix in forward pass of the mini-batch through the ReLU network in [Figure 8.18](#)^[440]: for all four examples of the mini-batch $z_4 < 0$, and hence $a_4 = 0$. The fact that the ReLU activation function for Neuron 4 is saturated for all four examples means that Neuron 4 is essentially dead during the forward pass of the algorithm (it does not activate for any example) and this reduces the representational capacity of the network. Furthermore, during the backward pass of the algorithm the derivative of the rectified linear function for Neuron 4 is zero for all four examples, causing the error gradient to be pushed to zero for all four examples, and so the weights on connections into Neuron 4 receive no updates. Consequently, no matter how long we train the network, Neuron 4 will remain in this dead state. This dynamic of a ReLU being in a state where it is inactive for all (or nearly all) inputs and consequently it never updated and so never becomes active is known as the **dying ReLU** problem. If too many neurons in a network are dead, then the network will not converge during training. For example, in our example network, if Neuron 8 is dead, the network will never converge on the training stop criterion, because no error gradients will be backpropagated to the earlier layers and so no training will occur. Similarly, if Neurons 6 and 7 are dead, then no error gradients will be backpropagated past this layer of neurons and the network is essentially reduced to a perceptron network composed of just Neuron 8, as none of the other neurons will have their input weights updated during training.

A simple heuristic that is sometimes used to try to avoid dead ReLUs is to initialize all the bias weights of a network to small positive values, such as 0.1, because this increases the likelihood that most of the neurons will initially be active for most of the training examples and so these neurons can learn from these examples (Goodfellow et al., 2016, p. 187). However, this heuristic is not guaranteed to avoid dead ReLUs: returning to the forward propagation of \mathbf{d}_2 through the ReLU network (see [Figure 8.19^{\[441\]}](#)), in this network Neuron 3 already has a bias of $w_{3,0} = 0.1$, but this positive bias is dominated by the large negative weight $w_{3,1} = -0.20$. Therefore, Neuron 3 illustrates that even with the heuristic of setting the bias weights to 0.1, a ReLU may still not activate to every (or in extreme cases any) input pattern. We return to the topic of weight initialization strategies in [Section 8.4.2^{\[447\]}](#). Another approach to avoiding dead ReLUs is to modify the rectified linear function so that it does not saturate for $z < 0$. Two popular variants of ReLU that adopt this strategy are the **Leaky ReLU** (Maas et al., 2013) and the **Parametric ReLU** (He et al., 2015).

The leaky rectified linear function has a small (predefined) non-zero gradient when $z < 0$. Maas et al. (2013) set the non-zero gradient for $z < 0$ to 0.01, giving the following definition of this function:

$$\text{rectifier}_{\text{leaky}}(z) = \begin{cases} z & \text{if } z > 0 \\ 0.01 \times z & \text{otherwise} \end{cases} \quad (8.45)$$

The derivative we use to backpropagate a δ through the $\text{rectifier}_{\text{leaky}}$ function is

$$\frac{d}{dz} \text{rectifier}_{\text{leaky}}(z) = \begin{cases} 1 & \text{if } z > 0 \\ 0.01 & \text{otherwise} \end{cases} \quad (8.46)$$

Not surprisingly, neurons that use the leaky rectified linear function as their activation function are known as Leaky ReLUs. When we switch a network from ReLUs to Leaky ReLUs, we sacrifice the potential benefits in terms of energy efficiency of sparse representations for a gradient that may potentially be more robust during training. Leaky ReLUs always activate to some extent for every input; however, given that for $z \leq 0$ the derivative of

the $\text{rectifier}_{\text{leaky}}$ function is very small (0.01), a leaky ReLU with large negative weight will still learn very slowly.

He et al. (2015) introduced the **Parametric ReLU** (PReLU) for which the main distinction from the Leaky ReLU was that rather than using a fixed predefined gradient for $z \leq 0$, this gradient can be learned as a parameter for each neuron in the network. In other words, each neuron in the network learns a separate gradient for its activation function for the region $z \leq 0$. As a result, when we define the activation function for a PReLU, we introduce a subscript on the terms to identify the neuron and the corresponding gradient being used. Hence for a PReLU i , the activation function is defined as

$$\text{rectifier}_{\text{parametric}}(z_i) = \begin{cases} z_i & \text{if } z_i > 0 \\ \lambda_i \times z_i & \text{otherwise} \end{cases} \quad (8.47)$$

The derivative used to backpropagate δ s through the $\text{rectifier}_{\text{parametric}}$ function is then defined as

$$\frac{d}{dz} \text{rectifier}_{\text{parametric}}(z_i) = \begin{cases} 1 & \text{if } z_i > 0 \\ \lambda_i & \text{otherwise} \end{cases} \quad (8.48)$$

The parameter λ is learned in tandem with the weights of the network. Similar to the weights of the network, the λ parameter is initialized to a value and is then iteratively updated as training progresses. In their experiments He et al. (2015) initialized the λ parameters in their networks to 0.25. Also similar to the weights in a network, the updating of a λ is proportional to the error gradient of the network with respect to changes in that parameter

$$\frac{\partial \mathcal{E}}{\partial \lambda_i} = \frac{\partial \mathcal{E}}{\partial a_i} \times \frac{\partial a_i}{\partial \lambda_i} \quad (8.49)$$

The first term in this product, $\partial \mathcal{E}/\partial a_i$, is the rate of change of the error of the network with respect to changes in the activation function and is calculated as it would be for the weights in the network; for neurons in the output layer, it is calculated using [Equation 8.20](#)^[411], and for neurons in the

hidden layer, it is calculated as the weighted sum of the δ s backpropagated to the neuron, per [Equation 8.22](#)^[412]. The second term in the product, $\partial a_i / \partial \lambda_i$, is the gradient of the activation function with respect to changes in λ_i . This gradient is given by

$$\frac{\partial a_i}{\partial \lambda_i} = \begin{cases} 0 & \text{if } z_i > 0 \\ z_i & \text{otherwise} \end{cases} \quad (8.50)$$

Once we have calculated the $\partial \mathcal{E} / \partial \lambda_i$ term, we update λ_i using the following update rule:²⁷

$$\lambda_i \leftarrow \lambda_i - \alpha \times \frac{\partial \mathcal{E}}{\partial \lambda_i} \quad (8.51)$$

where α is a learning rate.

To summarize, although the inclusion of a non-linear activation function within neurons in a network enables the network to represent non-linear mappings from inputs to outputs, the selection of which non-linear function we use can have a significant effect on the training speed of a deep network. For many years the logistic function was the default activation function used in neural networks. The primary reason was that it had such a simple derivative. However, although its derivative is simple, that it has a max value of 0.25 contributes to the vanishing gradient problem in neural networks. This is why in recent years most researchers have switched to using the rectifier function (or variants) as the default activation function. Similar to the logistic function, the rectifier function saturates in part of its domain, and this can lead to a dying ReLU dynamic in which a unit does not activate for any of the training instances, and consequently the neuron is stuck in a dead non-active state. The leaky ReLU and parametric ReLU were developed to address this potential problem. However, the particular choice of which variant of ReLU to use is network- and task-dependent, and, similarly to most hyper-parameters, needs to be decided upon through experimentation. We noted in this section that a heuristic that is used to help avoid saturating the rectifier function is to initialize the bias weights in the network to 0.1. This heuristic highlights the interaction between how we choose to initialize the weights in the network and how the error gradients

flow during backpropagation. The next section discusses this interaction in more detail and introduces some popular weight initialization schemes for deep networks.

8.4.2 Weight Initialization and Unstable Gradients

So far in this chapter we have been initializing the bias terms and weights in our worked examples by sampling from a uniform distribution with a range of $[-0.5, +0.5]$. The main advantage of this initialization regime is its simplicity. However, using this regime also allowed us to highlight some of the problems that arise when weights are set naively, such as the problem of vanishing gradients, and dead neurons. If we wish to train a deep network, we want the behavior of the network, in terms of the variance of the layer's z values, activations, and error gradients, to be similar across all the layers of the network. The reason why keeping the behavior of a network across its layers similar is useful in creating deep networks is that it allows us to add more layers to the network. However, naively initializing weights can result in unstable behavior within the dynamics of a network during training, resulting in saturated activation functions (as a consequence of z values becoming too large or small) or unstable error gradients.

The first way that a naive weight initialization can result in instability during training is that the weights on the connections into a neuron are too large. Then the z value for the neuron will be large, which can result in the activation function for the neuron becoming **saturated**. For example, a large negative z value ($\approx z < -2$) or a large positive z value ($\approx z > +2$) will cause the logistic function to saturate, and a large negative $z < 0$ will cause the rectified linear function to saturate. The derivative of a saturated activation function is 0 (or near 0). Consequently, saturated activation functions are problematic for gradient-descent-based algorithms (such as backpropagation) because these algorithms work by iteratively adjusting the weights using small increments that are scaled by the derivative of the activation function. This means that neurons with saturated activation functions can get stuck: their weights never change substantially during training because the incremental updates are either 0 or are tiny. For example, recall Neuron 4 in the ReLU network in Section 8.4.1^[434]; this neuron was inactive for all the input examples and so the weights of the neuron would never be updated, and it was therefore stuck in this dead

state. A general principle that we can derive from this is that neurons with saturated activation functions learn slowly (or not at all), and so we should take care when initializing weights to avoid saturating neurons. For most activation functions, avoiding saturation at initialization is achieved by avoiding large (positive or negative) z values, which in turn are avoided by initializing the weights to be close to 0.

The second way that a naive weight initialization can lead to instability during training is that very small or large weights can result in unstable gradients. [Equation 8.41](#)^[436] showed how the chain of products used to backpropagate an error gradient through a network of three neurons (i , j , and k) expands. [Equation 8.52](#)^[449] shows the last line from [Equation 8.41](#)^[436] and is annotated to explain how extreme weights can make gradients unstable. Notice that the error term $\partial\mathcal{E}/\partial a_k$ is multiplied by two weights: $w_{j,i}$ and $w_{k,j}$. If both these weights are > 1 , then the error gradient term will get larger each time it is multiplied; conversely, if both these weights are < 1 , then the error gradient term will get smaller each time it is multiplied. The problem of gradients becoming too large is known as **exploding gradients**. Extreme cases of exploding gradients can result in numerical overflow generating **NaN** (not-a-number) gradients. However, even when the gradients are defined, very large gradients are a problem. The calculation of an error derivative with respect to a weight is valid only for small changes in that weight. If the error gradient (the derivative) becomes too large, then the weights will be updated by a large amount, and the resulting changes in the output of a neuron, from one iteration to the next, will be so large that the training will become unstable.²⁸ Conversely, if weights are very small (too close to 0), then the error gradient will tend to vanish, and the weight updates will be so small that training the network will take an inordinate amount of time. The complementary problems of exploding and vanishing gradients can be understood as examples of the more general challenge of **unstable gradients**

$$\delta_i = \underbrace{w_{j,i} \times w_{k,j}}_{\substack{\text{extreme weights} \\ \rightarrow \text{unstable gradients}}} \times \underbrace{\frac{\partial\mathcal{E}}{\partial a_k} \times \underbrace{\frac{\partial a_k}{\partial z_k} \times \underbrace{\frac{\partial a_j}{\partial z_j} \times \underbrace{\frac{\partial a_i}{\partial z_i}}_{\substack{\text{extreme weights} \\ \rightarrow \text{saturated activations} \\ \rightarrow \text{vanishing gradients}}}}}_{\substack{\text{vanishing gradients}}}} \quad (8.52)$$

The third way in which naive weights initialization can cause unstable gradients arises from the fact that the variance of the output of a weighted sum is a function of three factors: the number of inputs to the weighted sum, the variance of the inputs, and the variance of the weights. Consequently, if the relationship between the number of inputs to a weighted sum and the variance of the weights is incorrect, then the result of a weighted sum can have either a larger variance than the variance of its inputs or a smaller variance than the variance of its inputs. This property of weighted sum calculations can result in unstable dynamics in both the forward and backward pass of the backpropagation algorithm because weighted sum calculations are used in both these phases; in the forward pass the calculation of the z value for each neuron is done using a weighted sum, and in the backward pass the calculation of a δ for a neuron includes the calculation of the term $\partial\mathcal{E}/\partial a_k$ which is a weighted sum of the δ s backpropagated to that neuron (see [Equation 8.22^{\[412\]}](#)). Later in this section we return to the question of how to counteract this property of weighted sum calculations. First, we will empirically show how different variations of weight initialization can interact with this property of weighted sum calculations in order to introduce different types instability into the internal training dynamics within a network.

To illustrate how adjusting the variance of the sample distribution used to initialize the weights of a network affects the dynamics of the network during training, we will scale up our example network so that the effects become apparent. Our new network is designed to work with our scenario of predicting the electrical output of a combined cycle power plant: the network has two neurons in the input layer for the inputs AMBIENT TEMPERATURE and the RELATIVE HUMIDITY, and one neuron in the output layer for the target ELECTRICAL OUTPUT. However, the network now has five fully connected hidden layers with 100 neurons in each layer. [Figure 8.22^{\[450\]}](#) illustrates this new network architecture. Furthermore, in order to isolate the effect of weight initialization on training dynamics from the problem of saturated activation functions, the neurons in this network use a linear activation function that outputs the same value that it receives as input: $a_i = z_i$. The derivative of this activation function with respect to z is always 1: each unit change in the value of z_i results in a unit change in the

value of a_i . Consequently, the gradients in this network will not be affected by saturated activation functions.²⁹ Apart from adjusting the network architecture, we also increase the size of the training data to a sample of 100 examples, and we **standardize**³⁰ all the features to have a mean of 0 and a standard deviation of 1.³¹

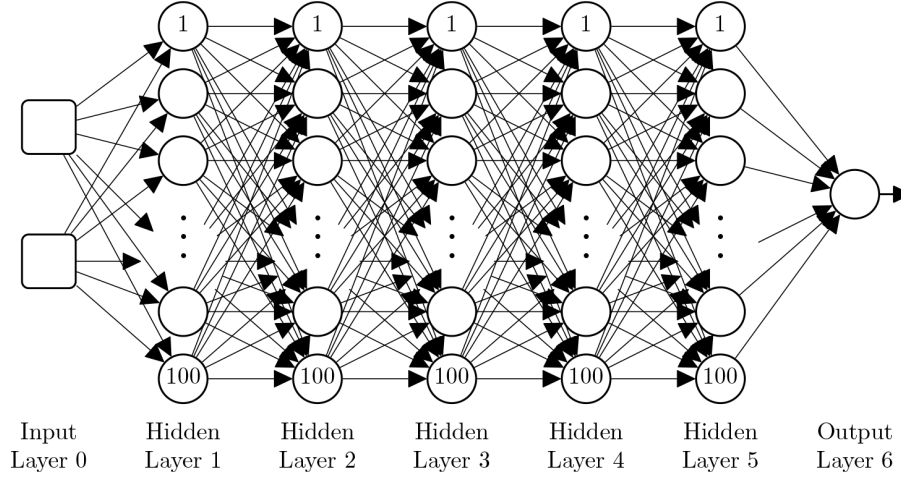


Figure 8.22

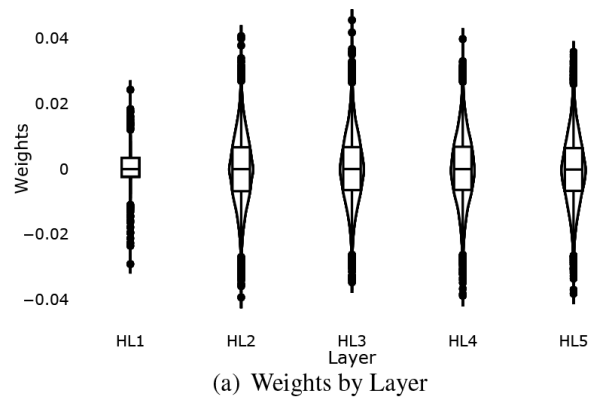
The architecture of the neural network used in the weight initialization experiments. Note that the neurons in this network use a linear activation function: $a_i = z_i$.

With this extended network architecture, the question arises of how we will initialize the weights. Although weight initialization is clearly important, at present relatively little is known in principle about how to select a good set of initial weights. Most weight initialization processes are based on heuristics that try to ensure that the weights are neither too big nor too small. Different heuristics are often used for the bias terms and the weights. Typically, bias terms are initialized to 0. However, in some instances we may wish to set bias terms to non-zero values; for example, ReLUs saturate when $z < 0$, and so to avoid dead ReLUs, the heuristic of initializing the bias terms for ReLU units to a small positive number (such as 0.1) is sometimes used (Goodfellow et al., 2016, pp. 296–297). For the discussion in this section, however, we assume that biases are initialized to 0.

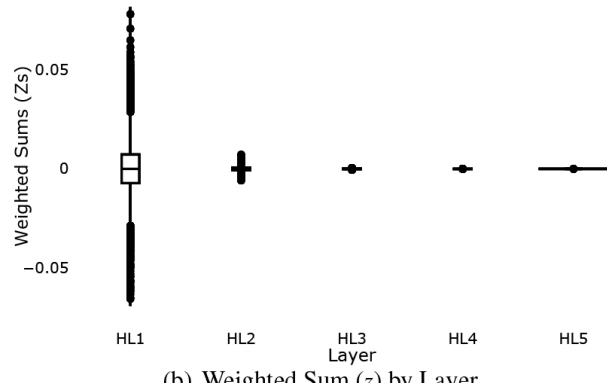
Traditionally, the most frequent heuristic used to initialize the weights of a neural network was randomly sampling values from a normal or uniform distribution with a mean of 0. For example, we might sample the weights

from a normal distribution with mean $\mu = 0.0$ and $\sigma = 0.01$. When weights are initialized in this way, we can control the initial scale of the weights by controlling the variance of the normal distribution. Figure 8.23^[453] illustrates the internal dynamics of the network shown in Figure 8.22^[450] during the first iteration of training if we initialize the weights of the network by sampling from a normal distribution with $\mu = 0.0$ and $\sigma = 0.01$ and pass our 100 examples through the network as a single mini-batch. Each of the four figures in Figure 8.23^[453] uses side-by-side violin plots³² to illustrate the distribution of a network property (weights, weighted sums, activations, or δ s) across the five hidden layers in the architecture during the first training iteration. Figure 8.23(a)^[453] illustrates the distribution of weight values across each of the five hidden layers immediately after initialization. The difference in the distribution between hidden layer 1 (*HL1*) and the other hidden layers is caused by the fact that there are only two inputs into each of the neurons in *HL1* whereas there are 100 inputs into each of the neurons in the other hidden layers. Consequently, the plot of values for *HL1* is generated from a much smaller sample of weight values than the plots for the other hidden layers. Figure 8.23(b)^[453] illustrates how the *z* values vary across the layers of the network during the forward pass of the algorithm. It is clear that the variance of the distribution of *z* values dramatically reduces as we move forward through the network, and this reduction in the variance together with the fact that the median of the *z* values is 0 across all the layers indicates that the *z* values are consistently getting smaller. This vanishing *z* values dynamic is a result of the fact that the *z* values are calculated using a weighted sum, and in this network configuration the relationship between the number of inputs to each weighted sum and the variances of the weights is such that the variance of the *z* values is scaled down at each layer in the network. We return subsequently to this vanishing *z* dynamic to explain in more detail how it arises. The plot of activation values directly mirrors the plot of the *z* values because the neurons are using a linear activation function. Figure 8.23(d)^[453] clearly illustrates **vanishing gradients** across layers in the network; that the δ values are tending toward 0 is indicated by the fact that the median of the δ values across the layers is 0 but the variance of δ values rapidly shrinks as we move backward from the last hidden layer (*HL5*) to the first layer (*HL1*). Remember that the neurons in this network all use a linear activation function that has a

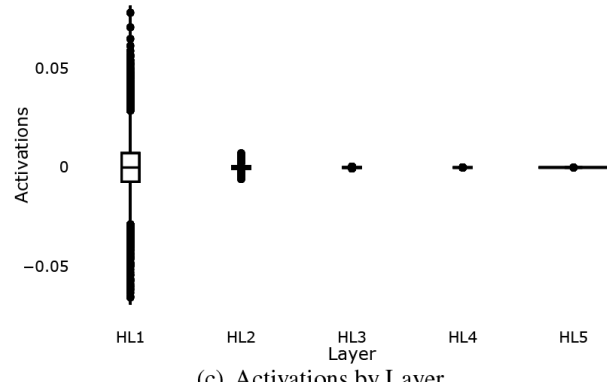
derivative value of 1. This removes the scaling of the δ s by the derivative of the activation function, and so in this instance these vanishing gradients are caused by both the repeated multiplication by small weights during backpropagation and the fact that the calculation of a δ for a neuron involves a weighted sum calculation³³ that in this network configuration results in the variance of the δ s shrinking as they are backpropagated through the layers.



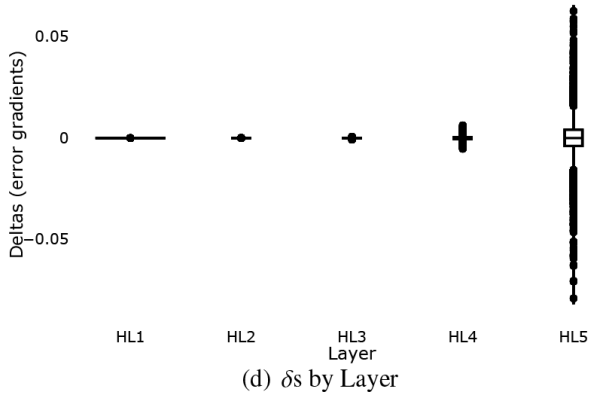
(a) Weights by Layer



(b) Weighted Sum (z) by Layer



(c) Activations by Layer



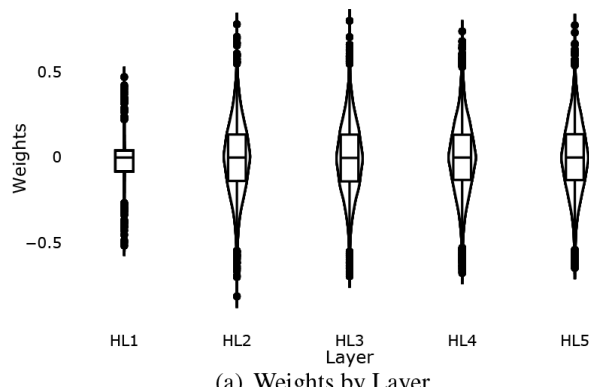
(d) δ s by Layer

Figure 8.23

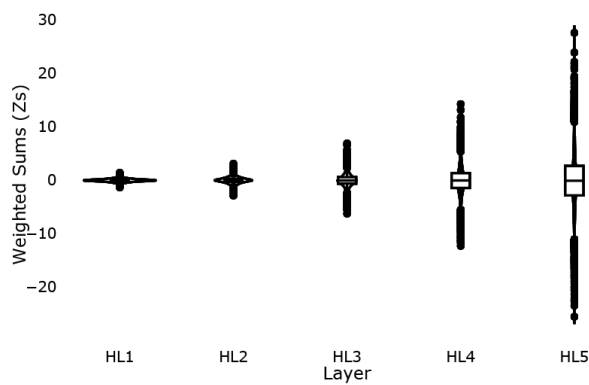
The internal dynamics of the network in [Figure 8.22](#)^[450] during the first training iteration when the weights were initialized using a normal distribution with $\mu=0.0, \sigma=0.01$.

Given that the vanishing gradients exhibited in [Figure 8.23\(d\)](#)^[453] are partly caused by the repeated multiplication by small weights, we can try to avoid this problem by making the network weights larger. [Figure 8.24](#)^[454] illustrates what happens in the internal dynamics of the network if we increase the standard deviation of the distribution from which we sample, in this instance a normal distribution with $\mu = 0.0$ and $\sigma = 0.2$. The impact of this larger standard deviation on the weights in the network is evident if we compare [Figure 8.23\(a\)](#)^[453] with [Figure 8.24\(a\)](#)^[454]: although the distribution of weights within each layer looks similar in the two figures, the scales on the weights axes show that the weights plotted in [Figure 8.24\(a\)](#)^[454] have a larger variance from the median 0, indicating that the weights tend to be larger. It turns out that these slightly larger weight values can dramatically affect the internal dynamics of the network during training. First, [Figure 8.24\(b\)](#)^[454] shows that now the z values consistently become larger as we move forward through the network; this is a complete reversal of the vanishing z value dynamic shown in [Figure 8.23\(b\)](#)^[453]. This exploding z value dynamic is a problem because if we wish to avoid saturated activation functions, we need to stop the z values in neurons taking an extreme value (where the concept of *extreme* is dependent on the activation function). We subsequently explain what is causing both these vanishing and exploding z values. Second, [Figure 8.24\(d\)](#)^[454] shows that the network now has an **exploding gradient** dynamic during backpropagation, with the variance of δ values rapidly increasing as they are backpropagated through the network. As in the previous analysis, in this network the instability in gradient propagation (in this instance exploding gradients) is not due to a scaling of the gradients by the derivative of the activation function; the linear activation function used by the neurons in this network has a derivative of 1, and so the gradients are not changed by this derivative during backpropagation. Instead, the exploding exploding gradients exhibited in [Figure 8.24\(d\)](#)^[454] is caused by a similar process to the vanishing z values plotted in [Figure 8.23\(b\)](#)^[453] and the exploding z values plotted in [Figure](#)

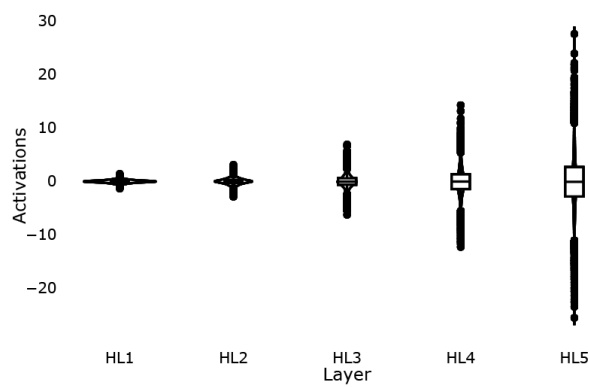
8.24(b)^[454]; the connection between these three processes is that they all involve a weighted sum.



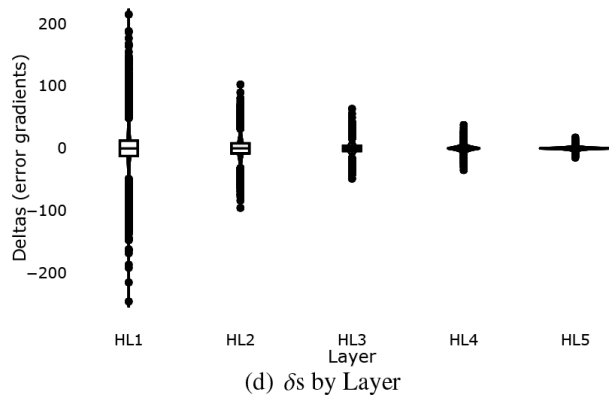
(a) Weights by Layer



(b) Weighted Sum (z) by Layer



(c) Activations by Layer



(d) δ s by Layer

Figure 8.24

The internal dynamics of the network in [Figure 8.22](#)^[450] during the first training iteration when the weights were initialized using a normal distribution with $\mu = 0.0$ and $\sigma = 0.2$.

To explain the relationship between the weighted sum calculation and the phenomena of vanishing and exploding z and δ values, we will analyze the relationship between the variance of z for a single neuron in the first hidden layer of a network and the variance of the weights used in calculating that z . This neuron receives n_{in} inputs $d_1, \dots, d_{n_{in}}$ (note that for this discussion we ignore the bias input and weight, and we drop the layer (k) superscript when we are discussing a single neuron). Consequently, this neuron will use n_{in} weights in its weighted sum $\mathbf{w} = \langle w_1, \dots, w_{n_{in}} \rangle$

$$z = (w_1 \times d_1) + (w_2 \times d_2) + \dots + (w_{n_{in}} \times d_{n_{in}}) \quad (8.53)$$

The starting point for our explanation of the relationship between weighted sum calculations and vanishing and exploding z and δ values is the **Bienaym  formula** from statistics, which states that the variance of the sum of uncorrelated random variables is the sum of their variance

$$\text{var} \left(\sum_{i=1}^n X_i \right) = \sum_{i=1}^n \text{var}(X_i) \quad (8.54)$$

Assuming that all the weights and the inputs are independent and identically distributed,³⁴ then the products in the weighted sum can be considered uncorrelated and we can state the variance of z as follows:

$$\begin{aligned} \text{var}(z) &= \text{var}((w_1 \times d_1) + (w_2 \times d_2) + \dots + (w_{n_{in}} \times d_{n_{in}})) \\ &= \sum_{i=1}^{n_{in}} \text{var}(w_i \times d_i) \end{aligned} \quad (8.55)$$

Also assuming that each weight w_i is independent of the corresponding input d_i , then variance of each of these products is given:³⁵

$$\text{var}(w \times d) = [E(\mathbf{W})]^2 \text{var}(\mathbf{d}) + [E(\mathbf{d})]^2 \text{var}(\mathbf{W}) + \text{var}(\mathbf{W}) \text{var}(\mathbf{d}) \quad (8.56)$$

Note that we have dropped the subscript on w because every w_i is sampled from the same distribution and hence has the same expected value and variance: $E(\mathbf{W})$ is the expected value of a weight (i.e., the probabilistic average, or mean value, of the weights), and $\text{var}(\mathbf{W})$ is the shared scalar variance of all the weights. Similarly, we have dropped the subscript from d because we are assuming that the inputs have been **standardized** to have a mean of 0 and a standard deviation of 1, and so all the inputs have the same mean and variance: $E(\mathbf{d})$ is the mean value of an input, and $\text{var}(\mathbf{d})$ is the shared scalar variance of all the inputs. If we have sampled our weights from a distribution with mean 0, then $E(W) = 0$, and if the inputs have been standardized, then $E(\mathbf{d}) = 0$, and so the Equation (8.56)^[455] simplifies to

$$\text{var}(w \times d) = \text{var}(\mathbf{W})\text{var}(\mathbf{d}) \quad (8.57)$$

This identity permits us to rewrite the variance of z in our case study neuron

$$\text{var}(z) = \sum_{i=1}^{n_{in}} \text{var}(w_i \times d_i) = n_{in} \text{var}(\mathbf{W}) \text{var}(\mathbf{d}) \quad (8.58)$$

Equation 8.58^[456] states that the variance of z is equal to the variance of the inputs ($\text{var}(\mathbf{d})$) scaled by $n_{in} \text{var}(\mathbf{W})$. On one hand, this analysis reveals that the variance of z is dependent on the number of inputs the neuron receives, n_{in} ; in general, the larger the number of inputs, the larger the variance. However, it also tells us that the scaling of the variance of z is dependent on the product $n_{in} \text{var}(\mathbf{W})$. Consequently, we can counteract this scaling by the number of inputs by setting $\text{var}(\mathbf{W}) = 1/n_{in}$; that is, by setting the variance of the distribution that the weights for a neuron are sampled from to $1/n_{in}$. When $\text{var}(\mathbf{W}) = 1/n_{in}$ then $n_{in} \text{var}(\mathbf{W}) = 1$ and the variance of z for the neuron is solely dependent on the variance of the inputs, which if standardized will have a variance of 1. In a fully connected network n_{in} is the same for all the neurons in a layer, and so for these networks we can set the variance of the distribution from which the weights are sampled on a layer-by-layer basis.

This analysis explains the vanishing z values plotted in Figure 8.23(b)^[453]. Recall that this plot was generated using input data that had been

standardized, and so $\text{var}(\mathbf{d}) = 1$. In this network, for the neurons in the first hidden layer $n_{in}^{(HL1)} = 2$ and for neurons in all the other hidden layers $n_{in} = 100$. Furthermore, the weights in the network were sampled from a normal distribution with $\mu = 0.0$ and $\sigma = 0.01$, and therefore the weights in each layer have a variance of $\text{var}(\mathbf{W}) = \sigma^2 = 0.01^2 = 0.0001$. This configuration means that variance of z values across the neurons in layer $HL1$ is

$$\begin{aligned}\text{var}(Z^{(HL1)}) &= n_{in}^{(HL1)} \times \text{var}(\mathbf{W}^{(HL1)}) \times \text{var}(\mathbf{d}^{(HL1)}) \\ &= 2 \times 0.0001 \times 1 \\ &= 0.0002\end{aligned}\tag{8.59}$$

where $\text{var}(Z^{(HL1)})$ denotes the shared scalar variance of all the z values across the neurons in layer $HL1$; $n_{in}^{(HL1)}$ is the number of inputs coming into each neuron in layer $HL1$; $\text{var}(\mathbf{W}^{(HL1)})$ denotes the shared scalar variance of all the weights across the neurons in layer $HL1$; and $\text{var}(\mathbf{d}^{(HL1)})$ denotes the shared scalar variance of all the inputs to layer $HL1$. When checking this against [Figure 8.23\(b\)](#)^[453], note that a variance of $\sigma^2 = 0.0002$ is equivalent to a standard deviation of $\sigma \approx 0.014$. That the neurons in this network use a linear activation function means that $\text{var}(Z^{(HL1)})$ is also the variance of the activations propagated forward to the next hidden layer, and so it is also the variance of the inputs to the next layer: $\text{var}(Z^{(HL1)}) = \text{var}(A^{(HL1)}) = \text{var}(\mathbf{d}^{(HL2)})$. For $HL2$ we know that $n_{in}^{(HL2)} = 100$ and $\text{var}(\mathbf{W}^{(HL2)}) = 0.0001$, and so we can now calculate the variance of z across the neurons in layer $HL2$ as follows:

$$\begin{aligned}\text{var}(Z^{(HL2)}) &= n_{in}^{(HL2)} \times \text{var}(\mathbf{W}^{(HL2)}) \times \text{var}(\mathbf{d}^{(HL2)}) \\ &= 100 \times 0.0001 \times 0.0002 \\ &= 0.000002\end{aligned}\tag{8.60}$$

Essentially, in this network, because of the use of linear activations, the variance of z for layer k in the network is the variance of z in the preceding layer, $\text{var}(z^{(k-1)})$, scaled by $n_{in}^{(k)} \times \text{var}(\mathbf{W}^{(k)})$. For all the remaining hidden layers in this network $n_{in} = 100$, and so this process of scaling the variance of z by $100 \times 0.0001 = 0.01$ will continue through each of the subsequent hidden layers in this network. This is why the variance of z rapidly

decreases for each layer as we move forward through the network as shown in [Figure 8.23\(b\)](#)^[453].

This analysis also explains the exploding z values plotted in [Figure 8.24](#)^[454]. In this instance the weights in the network were sampled from a normal distribution with $\mu = 0.0$ and $\sigma = 0.2$, which means that for all k : $\text{var}(\mathbf{W}^{(k)}) = \sigma^2 = 0.2^2 = 0.04$. As a result, the variance of the z values across the neurons in $HL1$ is $\text{var}(Z^{(HL1)}) = 2 \times 0.04 = 0.08$ (i.e., $\sigma \approx 0.283$), and this is then scaled by $100 \times 0.04 = 4$ at each of the other hidden layers in the network. This is why the variance of the z values rapidly increases as we move forward through the network as shown in [Figure 8.24\(b\)](#)^[454].

A similar analysis also explains the exploding δ values plotted in [Figure 8.24\(d\)](#)^[454]. In this case, however, the number of inputs to the weighted sum calculation within a neuron during the backpropagation process is the number of neurons that the neuron propagated its activation to during the forward pass (see [Equation 8.22](#)^[412]). If we use n_{out} to denote this number, then for the neurons in the last hidden layer $n_{out}^{(HL5)} = 1$ because there is only a single neuron in the output layer, and for the neurons in all the other layers in the network $n_{out} = 100$. As with the analysis of the scaling of the variances for z in the forward pass, the scaling of the variance of the δ values as they are backpropagated through each layer k is a function of number of inputs to each neuron in the layer (here $n_{out}^{(k)}$) multiplied by the variance of the weights for that layer $\text{var}(\mathbf{W}^{(k)})$. The same weights are used during the forward and backward passes of a single iteration of backpropagation. Consequently, the weights used during the backpropagation of the δ s plotted in [Figure 8.24\(d\)](#)^[454] are sampled from a normal distribution with $\mu = 0.0$ and $\sigma = 0.2$, which means that for all the layers $\text{var}(\mathbf{W}^{(k)}) = \sigma^2 = 0.2^2 = 0.04$. If for the purposes of this discussion we naively assume that the variance of the δ values backpropagated to the neurons in $HL5$ is equal to 1, then we can expect the variance of the δ s backpropagated to $HL4$ to be equal to $100 \times 0.04 \times 1 = 4$. Furthermore, for each subsequent layer that the δ s are backpropagated through, the variance will increase by a factor of 4, and it is this scaling that causes the exploding gradients evident in [Figure 8.24\(d\)](#)^[454].

We noted at the start of this section that in order to train a deep network, it is important to keep the internal behavior of the network (i.e., the

variance of the z values, activations, and δ s) similar across all the layers during training, because doing so allows us to add more layers to the network while avoiding saturated units (by avoiding extreme z values) and exploding or vanishing δ s. The preceding analysis highlighted that the variance of output of a weighted sum is dependent on the number of inputs to the weighted sum (be it n_{in} during forward propagation or n_{out} during backward propagation). This observation is the basis for a number of weight initialization regimes that adjust the variance of the distribution used to sample the weights for a neuron based on its connections to other neurons in the network. For example, we noted previously that in a fully connected feedforward network, if we set $var(\mathbf{W}^{(k)}) = 1/n_{in}^{(k)}$, then the variance of the z values in layer k is dependent solely on the variance of the inputs to that layer; and if the inputs are standardized, then the variance of the z values will not be scaled for that layer. If we do this when sampling the weights for each of the layers in the network, then the variance of the z values across all the layers will be stable. The different weight initialization regimes that have been developed vary, depending on whether they take both n_{in} and n_{out} into account and the activation functions with which they work best.

One of the best known of these weight initialization regimes is called **Xavier initialization**.³⁶ There are a number of variants of Xavier initialization used in practice, but the original version of Xavier initialization was designed for fully connected feedforward networks and worked on a layer-by-layer basis. The original version of Xavier initialization considered both the forward activation through the network and the backward propagation of gradients, and so the calculation of the variance of the distribution from which the weights for a layer are sampled takes both the inputs to a layer $n_{in}^{(k)}$ and the number of outputs from a layer $n_{out}^{(k)}$ into account; it is calculated as follows:

$$var(\mathbf{W}^{(k)}) = \frac{2}{n_{in}^{(k)} + n_{out}^{(k)}} \quad (8.61)$$

where $var(\mathbf{W}^{(k)})$ is the variance of all the weights in layer k ; $n_{in}^{(k)}$ is the number of neurons that feed inputs to layer k ; and $n_{out}^{(k)}$ is the number of

neurons that neurons in layer k connect forward to (in a fully connected feedforward network $n_{in}^{(k)}$ is equal to the number of neurons in layer $k - 1$ and $n_{out}^{(k)}$ is the number of neurons in layer $k + 1$). Often in practice, however, a simpler variant of **Xavier initialization** is used that just considers $n_{in}^{(k)}$

$$var(\mathbf{W}^{(k)}) = \frac{1}{n_{in}^{(k)}} \quad (8.62)$$

[Figure 8.25](#)^[460] illustrates the internal dynamics of the network in [Figure 8.22](#)^[450] during the first training iteration when the weights of each layer in the network are sampled from a normal distribution with a mean of 0 and a variance calculated using Equation (8.62)^[459]. Notice that the z values, activations, and δ s have a relatively similar distribution across each of the layers of the network; that is, the training of the network is not suffering from either exploding z values (which would saturate activation functions if they were used) or exploding or vanishing δ s.

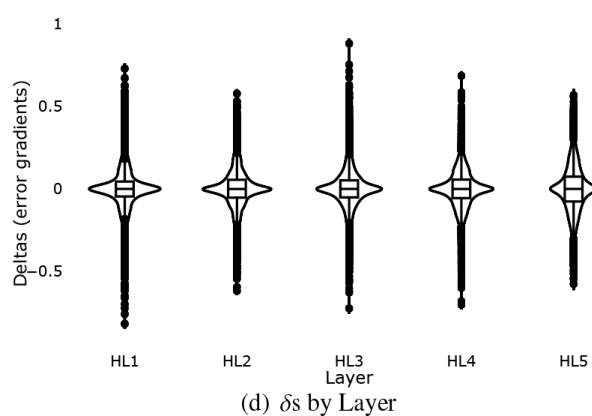
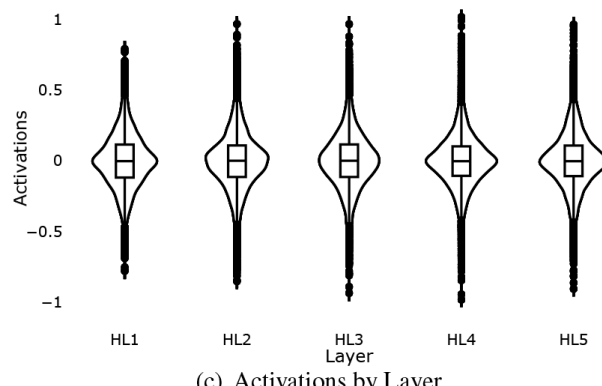
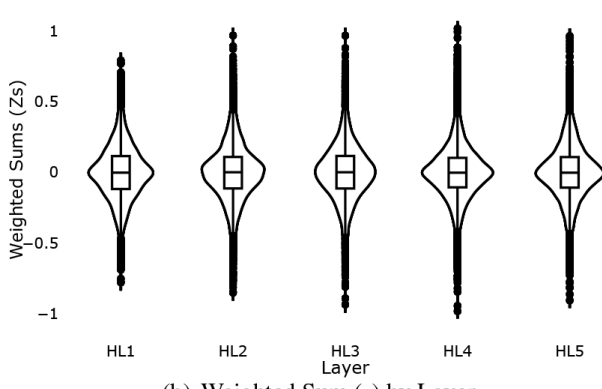
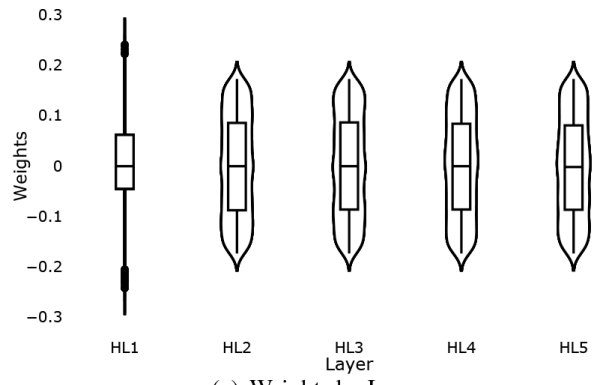


Figure 8.25

The internal dynamics of the network in [Figure 8.22](#)^[450] during the first training iteration when the weights were initialized using Xavier initialization.

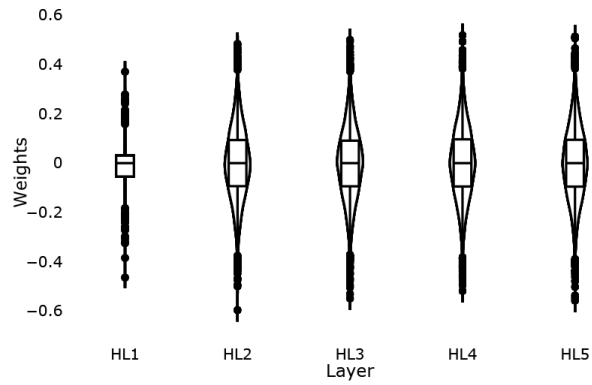
Xavier initialization has empirically been shown to often lead to faster training and is one of the most popular weight initialization approaches in deep learning. It is generally used when networks use **logistic** or **tanh** activation functions. However, a modified version of this weight initialization heuristic is recommended when the network uses rectified linear units (He et al., 2015). This weight initialization heuristic is known as **He initialization** (or sometimes it is called **Kaiming initialization**) and is defined as follows:

$$var(\mathbf{W}^{(k)}) = \frac{2}{n_{in}^{(k)}} \quad (8.63)$$

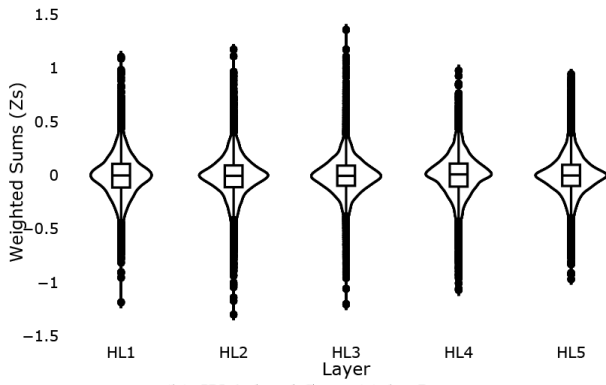
Sometimes a blend of **Xavier** and **He** initialization is used. For example, in a network using ReLUs, Xavier initialization (Equation (8.62)^[459]) could be used to define the variance for the weights in the first layer, because the rectified function has not been applied to the inputs, and then He initialization (Equation (8.63)^[461]) could then be used for the later layers in the network (He et al., 2015). Following this strategy, for a fully connected three-layer ReLU network with 100 inputs, 80 neurons in the first hidden layer, 50 neurons in the second hidden layer, and 5 neurons in the output layer, the weight matrix for each layer would be initialized as shown in Equation (8.64)^[461], where the notation $\mathbf{W}^{(k)} \sim \mathcal{N}(\mu, \sigma)$ indicates that the values in the weight matrix for layer k should be sampled from a normal distribution with mean μ and standard deviation σ .

$$\begin{aligned} \mathbf{W}^{(1)} &\sim \mathcal{N}\left(0, \sqrt{\frac{1}{100}}\right) \\ \mathbf{W}^{(2)} &\sim \mathcal{N}\left(0, \sqrt{\frac{2}{80}}\right) \\ \mathbf{W}^{(3)} &\sim \mathcal{N}\left(0, \sqrt{\frac{2}{50}}\right) \end{aligned} \quad (8.64)$$

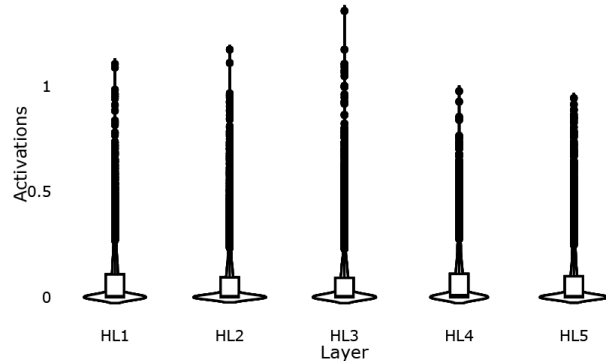
[Figure 8.26](#)^[462] illustrates the internal dynamics of the network in [Figure 8.22](#)^[450] during the first training iteration when ReLUs are used and the weights for neurons in $HL1$ are sampled using Xavier initialization and the weights for the neurons in the later layers are sampled using He initialization. The effect of the rectified linear activation function is evident in [Figure 8.26\(c\)](#)^[462], where the activations are all positive. Notice as well that the distribution of the z and δ values is relatively stable across the layers (see [Figure 8.26\(b\)](#)^[462] and [Figure 8.26\(d\)](#)^[462]). This stability in the internal dynamics of the network, particularly with respect to the gradients, is likely to result in the network learning much faster than networks affected by vanishing or exploding gradients, and it is a result of careful weight initialization.



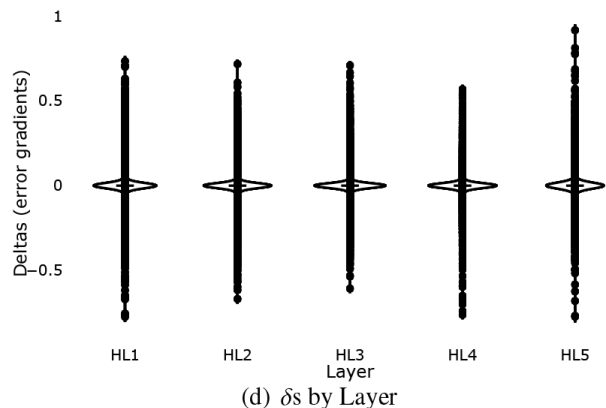
(a) Weights by Layer



(b) Weighted Sum (z) by Layer



(c) Activations by Layer



(d) δ s by Layer

Figure 8.26

The internal dynamics of the network in Figure 8.22^[450], using ReLUs, during the first training iteration when the weights were initialized using He initialization.

8.4.3 Handling Categorical Target Features: Softmax Output Layers and Cross-Entropy Loss Functions

All the examples that we have looked at so far have been regression problems. To create a neural network that can predict a multi-level categorical feature, we make three adjustments:

1. we represent the target feature using **one-hot encoding**;
2. we change the output layer of the network to be a **softmax layer**; and
3. we change the error (or loss) function we use for training to be the **cross-entropy** function.

A **one-hot encoding** is a vector-based representation of a categorial feature value.³⁷ A one-hot vector has one element per level of the categorical feature. For example, if a feature can take three levels (e.g., *low*, *medium*, *high*), then the vector would have three elements. It is known as a one-hot representation because at most one element in the vector will have the value 1 and all the other elements will be 0, with the value of the feature indicated by whichever element is 1. For our three-level categorical feature we might decide that $\langle 1,0,0 \rangle$ indicates *low*, $\langle 0,1,0 \rangle$ indicates *medium*, and $\langle 0,0,1 \rangle$ indicates *high*. When we are representing the target feature in a dataset using a one-hot encoding, then for each instance in the dataset there is a one-hot vector encoding the level of the target for that instance. Table 8.13^[464] lists the power plant dataset after the target feature ELECTRICAL OUTPUT has been converted to a three-level categorical feature, by applying binning to the range-normalized values ($low \leq 0.33$, $medium \leq 0.66$, $high > 0.66$), and then encoded using one-hot encoding.

Table 8.13

The *range-normalized* hourly samples of ambient factors and full load electrical power output of a combined cycle power plant, rounded to two decimal places, and with the (binned) target feature represented using one-hot encoding.

ID	AMBIENT TEMPERATURE °C	RELATIVE HUMIDITY %	Electrical Output		
			low	medium	high
1	0.04	0.81	0	0	1
2	0.84	0.58	1	0	0
3	0.50	0.07	0	1	0
4	0.53	1.00	0	1	0

In a **softmax output layer** there is a single neuron for each level of the target feature. For example, if the prediction task is to predict the level of a categorical feature that can take three levels (e.g., *low*, *medium*, *high*), then the output layer of the network would have three neurons. The activation function used by the neurons in a softmax layer is the **softmax function**; for an output layer with m neurons, the softmax activation function is defined as follows:

$$\varphi_{sm}(z_i) = \frac{e^{z_i}}{\sum_{j=1}^m e^{z_m}} \quad (8.65)$$

The softmax activation function normalizes the z scores for a layer of neurons so that the sum of the activations of the neurons is 1. Hence using the softmax function, the activation of each neuron is dependent on the size of its z value relative to the z values of the other neurons in the output layer. The softmax function will always return a positive value for every neuron because e^z is always positive, even if z is negative. Another useful property of e^z is that e^0 is 1; as a result, even in the unlikely event that all the z s are 0, we avoid the problem of a division by 0, and each neuron will have an activation of $1/m$.

In the context of a softmax layer, the non-normalized z values are often referred to as **logits**. Therefore, to align with this general terminology, for this discussion we switch from discussing z values for a neuron to discussing the logit of the neuron. We use the notation \mathbf{l} to denote a vector of logits for a layer of neurons, and \mathbf{l}_i to indicate the logit for the i^{th} neuron

in the layer. Using the notation φ_{sm} to denote the softmax activation function, $\varphi_{sm}(\mathbf{l})$ denotes applying the softmax function to the vector of logits \mathbf{l} , and $\varphi_{sm}(\mathbf{l}_i)$ refers to the calculation of the softmax value for the i^{th} logit, that is, the output activation of the i neuron in the layer. Note that $\varphi_{sm}(\mathbf{l}_i)$ can be understood as equivalent to $\varphi_{sm}(z_i)$ in Equation (8.65)^[463]; the notational differences arise because we are now specifying the parameter as an index of a logit rather than specifying the z score directly. [Table 8.14](#)^[464] illustrates the calculation of the softmax function for a vector of three logits (i.e., three z values),

Table 8.14

The calculation of the softmax activation function φ_{sm} over a vector of three logits \mathbf{l} .

	\mathbf{l}_0	\mathbf{l}_1	\mathbf{l}_2
\mathbf{l}	1.5	-0.9	0.6
$e^{\mathbf{l}_i}$	4.48168907	0.40656966	1.8221188
$\sum_i e^{\mathbf{l}_i}$			6.71037753
$\varphi_{sm}(\mathbf{l}_i)$	0.667874356	0.060588195	0.27153745

The fact that the softmax function returns a normalized set of positive values across the layer allows us to interpret the activation of each neuron in the layer as a probability. There is one neuron in an output softmax layer per target feature level, and so the softmax function returns one probability per level. The natural consequence of this is that using a softmax layer, each neuron is trained to predict the probability of one of the levels of the categorical target feature. The final prediction is then made by taking the feature level whose neuron predicts the highest probability. [Figure 8.27](#)^[465] illustrates a fully connected feedforward neural network with a softmax output layer with three neurons for our three-level (*low*, *medium* and *high*) target feature; the dotted rectangle around the softmax layer highlights that the activation function φ normalizes the logit values across the neurons in the layer.

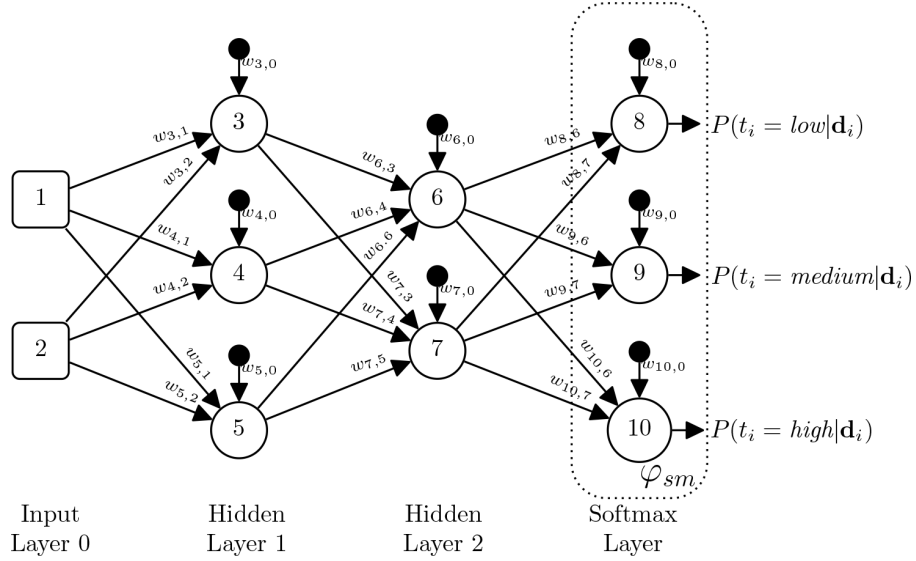


Figure 8.27

A schematic of a feedforward artificial neural network with a three-neuron softmax output layer.

The **cross-entropy** error (or loss) function is generally used in contexts in which the output of a network can be interpreted as a probability distribution over a set of exclusive categories. In the general scenario of a model predicting a distribution over a set of categories, the cross-entropy loss function is defined as

$$L_{CE} (\mathbf{t}, \hat{\mathbf{P}}) = - \sum_j \mathbf{t}_j \ln (\hat{\mathbf{P}}_j) \quad (8.66)$$

where L_{CE} is the cross-entropy loss; \mathbf{t} is the target feature represented using one-hot encoding (the target distribution over the categories); $\hat{\mathbf{P}}$ is the distribution over the categories that the model has predicted; \ln is the natural logarithm function; and j is an index over both the target distribution \mathbf{t} and the predicted distribution $\hat{\mathbf{P}}$. This loss function is called **cross-entropy** because in information theory **cross-entropy** is used to describe a measure of the difference in nats between two probability distributions over the same set of events. The information theory basis for this function can be seen in the similarity between Equation (8.66)^[465] and the equation for Shannon's entropy, Equation (4.1)^[125].

The cross-entropy loss measures the dissimilarity between the true distribution \mathbf{t} and the predicted distribution $\hat{\mathbf{P}}$. In situations where the true

distribution \mathbf{t} is encoded as a one-hot vector, the cross-entropy loss function can be simplified to:

$$L_{CE} (\mathbf{t}, \hat{\mathbf{P}}) = -\ln (\hat{\mathbf{P}}_*) \quad (8.67)$$

$\hat{\mathbf{P}}_*$ indicates the predicted probability for the true category (i.e., the category encoded as a 1 in the one-hot encoded vector \mathbf{t}). To illustrate this simplification with a case study, we assume that our distribution is over three categories, and the target distribution is encoded as a one-hot vector. Now if the target distribution over a particular instance is $\mathbf{t} = [0,1,0]$ (i.e., the second category is the correct category), then the cross-entropy summation in Equation (8.66)^[465] expands as follows:

$$\begin{aligned} L_{CE} (\mathbf{t}, \hat{\mathbf{P}}) &= - \sum_j \mathbf{t}_j \ln (\hat{\mathbf{P}}_j) \\ &= - ((\mathbf{t}_0 \ln (\hat{\mathbf{P}}_0)) + (\mathbf{t}_1 \ln (\hat{\mathbf{P}}_1)) + (\mathbf{t}_2 \ln (\hat{\mathbf{P}}_2))) \\ &= - ((0 \ln (\hat{\mathbf{P}}_0)) + (1 \ln (\hat{\mathbf{P}}_1)) + (0 \ln (\hat{\mathbf{P}}_2))) \\ &= -1 \ln (\hat{\mathbf{P}}_1) \end{aligned} \quad (8.68)$$

Equation (8.68)^[466] shows that all the terms that involve a 0 element from \mathbf{t} disappear, and the loss simplifies to the negative log of the predicted probability for the true class.

To understand why Equation (8.67)^[466] is an appropriate measure to use as the loss function for categorical training, we should first remember that the loss function is the function that we wish to minimize during training, and so we wish the loss function to return a large value when there is a large difference between the true and predicted probability distributions, and a small value when \mathbf{t} and $\hat{\mathbf{P}}$ are similar or identical. For this discussion it may be useful to quickly refer to Figure (4.6)^[125] to see a plot of how the negative log of a probability changes as the probability changes (Figure (4.6)^[125] shows this plot for binary logs, but the general shape of the plot is similar for natural logs). For probabilities near 0, the negative log returns a large number, and for probabilities near 1 the negative log returns a value near 0. Now, imagine a scenario in which the model makes a correct prediction and the maximum probability in $\hat{\mathbf{P}}$ is assigned to the correct category. In this scenario, then $\hat{\mathbf{P}}_*$ will be relatively close to 1 (and the better

the model's prediction the closer to one \hat{p} will be). As \hat{p} approaches 1, then the negative log of this probability approaches 0. In other words, the loss of the model reduces as the model's predictions improve. In the complementary scenario, the model makes an incorrect prediction and the maximum probability in \hat{p} is assigned to the incorrect category. Because a probability distribution must sum to 1, an increase in one probability results in a decrease in one or more of the other probabilities in the distribution. Hence if the model assigns the maximum probability mass to an incorrect category, this will reduce \hat{p} , and, as Figure (4.6)^[125] illustrates, this will result in the negative log of the \hat{p} rapidly increasing. This is exactly the behavior we desire from a loss function: small values for correct predictions and large values for incorrect predictions.

Using Equation (8.67)^[466] we can now calculate a loss for the network's predictions over a set of exclusive categories. However, to train the network we must backpropagate this loss through the network. To do this we must adjust the derivatives used in the calculation of the δ s for the output neurons because we have changed the activation function used by these neurons. However, we do not need to change anything with regard to the calculation of the δ s for the hidden neurons; once we have updated the calculation of the δ s for the output neurons, then the error gradients can flow back through the network as previously.

Equations (8.69)^[467] to (8.72)^[467] step through the definition of the δ_k for a neuron in a softmax output layer when a cross-entropy loss function is used. Equation (8.69)^[467] is a restatement of Equation (8.13)^[408], which provides the general definition of the δ for a neuron k as the partial derivative for the error (or loss) of the network with respect to the weighted sum of neuron k : $\partial\mathcal{E}/\partial z_k$. Equation (8.70)^[467] restates this definition in terms of the error of the network as calculated using the cross-entropy loss function and also taking the partial derivative with respect to a change in the logit for neuron k in the output layer. Equation (8.71)^[467] specifies that the cross-entropy loss for the network is dependent solely on the negative natural log of the probability of the correct prediction, per Equation (8.67)^[466]. The logit for an output neuron k , l_k , can only indirectly affect the loss in terms of how it changes the predicted probability for the true category: \hat{p}_* . Equation (8.72)^[467] uses the chain rule to make this explicit by defining δ_k as

the product of the rate of change of the negative natural log of the predicted probability of the true category with respect to changes in that probability and the rate of change of the predicted probability of the true category with respect to changes in the logit (we encountered this expansion step previously in a different guise; recall that $\partial\mathcal{E}/\partial z_k = \partial\mathcal{E}/\partial a_k \times \partial a_k/\partial z_k$).

$$\delta_k = \frac{\partial\mathcal{E}}{\partial z_k} \quad (8.69)$$

$$= \frac{\partial L_{CE}(\mathbf{t}, \hat{\mathbf{P}})}{\partial \mathbf{l}_k} \quad (8.70)$$

$$= \frac{\partial -\ln(\hat{\mathbf{P}}_*)}{\partial \mathbf{l}_k} \quad (8.71)$$

$$= \frac{\partial -\ln(\hat{\mathbf{P}}_*)}{\partial (\hat{\mathbf{P}}_*)} \times \frac{\partial (\hat{\mathbf{P}}_*)}{\partial \mathbf{l}_k} \quad (8.72)$$

From calculus, the derivative of the natural log is

$$\frac{d \ln x}{dx} = \frac{1}{x} \quad (8.73)$$

Using this identity, we can define the first term in the product in Equation (8.72)^[467]

$$\frac{\partial -\ln(\hat{\mathbf{P}}_*)}{\partial (\hat{\mathbf{P}}_*)} = -\frac{1}{\hat{\mathbf{P}}_*} \quad (8.74)$$

This is simply 1 divided by the model's predicted probability for the correct category.

The second term in the product in Equation (8.72)^[467] is the rate of change of the predicted probability for the true category with respect to the logit for one of the neurons in the softmax layer. In other words, this is the rate of change of the softmax calculation for the activation of the output neuron for the true class with respect to the logits of a neuron in the output layer. There are two cases that we need to handle with this derivative (1) when \mathbf{l}_k is the logit for the neuron whose activation is the probability of the

correct category (i.e., $k = \star$), and (2) when \mathbf{l}_k is the logit for a neuron whose activation is the probability for one of the incorrect categories (i.e., $k \neq \star$).

The reason why we need two different derivatives for the softmax function to handle these two cases is that when we are taking the derivative with respect to changes in the logit for the neuron whose activation is $\hat{\mathbf{P}}_\star$ (i.e. $k = \star$), then adjusting logit k changes both the numerator and the denominator in the softmax for the calculation of $\hat{\mathbf{P}}_\star$, whereas in the case that the logit with respect to which we are taking the derivative is for a neuron corresponding to another category, changing the logit changes only the denominator of the softmax. We do not derive the derivatives of the softmax for each of these cases, as that is relatively convoluted, involving in quotient rule from calculus; instead, we simply state them

$$\frac{\partial (\hat{\mathbf{P}}_\star)}{\partial \mathbf{l}_k} = \begin{cases} \hat{\mathbf{P}}_\star (1 - \hat{\mathbf{P}}_k) & \text{if } k = \star \\ -\hat{\mathbf{P}}_\star \hat{\mathbf{P}}_k & \text{otherwise} \end{cases} \quad (8.75)$$

We can now define the calculation of the δ for a neuron in a softmax output layer using a cross-entropy loss function as follows:

$$\delta_k = \frac{\partial - \ln (\hat{\mathbf{P}}_\star)}{\partial (\hat{\mathbf{P}}_\star)} \times \frac{\partial (\hat{\mathbf{P}}_\star)}{\partial \mathbf{l}_k} \quad (8.76)$$

$$= -\frac{1}{\hat{\mathbf{P}}_\star} \times \frac{\partial (\hat{\mathbf{P}}_\star)}{\partial \mathbf{l}_k} \quad (8.77)$$

$$= -\frac{1}{\hat{\mathbf{P}}_\star} \times \begin{cases} \hat{\mathbf{P}}_\star (1 - \hat{\mathbf{P}}_k) & \text{if } k = \star \\ -\hat{\mathbf{P}}_\star \hat{\mathbf{P}}_k & \text{otherwise} \end{cases} \quad (8.78)$$

$$= \begin{cases} -(1 - \hat{\mathbf{P}}_k) & \text{if } k = \star \\ \hat{\mathbf{P}}_k & \text{otherwise} \end{cases} \quad (8.79)$$

Equation (8.76)^[469] is taken from Equation (8.72)^[467]; the step to Equation (8.77)^[469] uses Equation (8.74)^[468]; the rewrite in Equation (8.78)^[469] uses Equation (8.75)^[468]; and finally Equation (8.79)^[469] is the simplification we get when the terms cancel out after the product. Equation (8.79)^[469] states that δ for the neuron in the softmax output layer whose activation is the

predicted probability for the correct category as specified by a 1 in the one-hot encoded target vector using the cross-entropy loss function is

$$\delta_{k=\star} = - (1 - \hat{\mathbf{P}}_k) \quad (8.80)$$

For each of the other neurons in the softmax output layer, their δ is simply their activation

$$\delta_{k \neq \star} = \hat{\mathbf{P}}_k \quad (8.81)$$

We illustrate the calculation of δ s for neurons in a softmax output layer using the mini-batch of examples listed in [Table 8.13](#)^[464] and the network architecture shown in [Figure 8.27](#)^[465]. [Figure 8.28](#)^[470] illustrates the forward pass for this mini-batch through this network. Note that we are assuming the neurons in the hidden layers are ReLUs and that the final layer is a softmax layer. To highlight this change in activation functions between the layers, we have labeled the φ symbol in the figure with the name of the activation function it represents. The weights in this network have been initialized so that all the bias terms are equal to + 1.0 and the other weights are listed in the weight matrices shown in [Figure 8.28](#)^[470]. Further, to aid in presentation we have rounded the activations for each layer to four decimal places and used these rounded activations as inputs to the later calculations. Focusing on the softmax activations for the output layer for all four examples, all three neurons output similar values; this is not surprising given that this is a randomly initialized network. However, for the purpose of illustration it is worth noting that the model would return the class label with the highest probability for each example; hence the model would return a prediction of *low* for all four examples in the mini-batch.

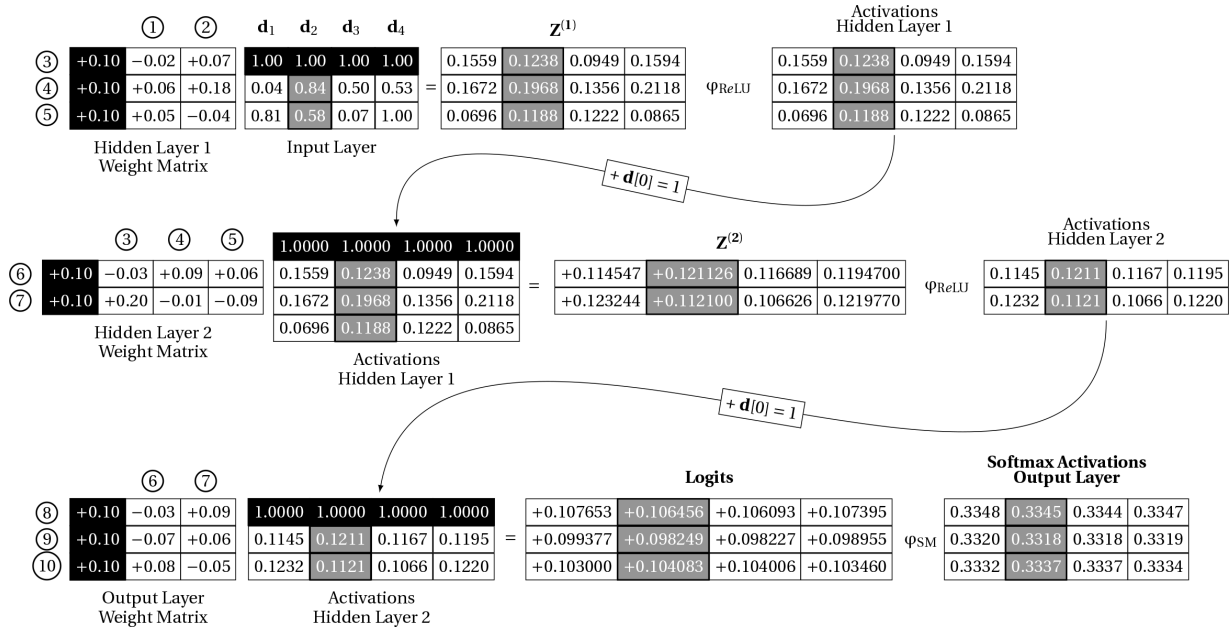


Figure 8.28

The forward pass of the mini-batch of examples listed in [Table 8.13](#)^[464] through the network in [Figure 8.27](#)^[465].

[Table 8.15](#)^[471] steps through the calculations that bring us from the logits for each of the neurons for each example to the corresponding softmax activations and then to the δ s for each neuron for each example. [Table 8.15](#)^[471] is split into five segments with each segment containing information on Neurons 8, 9, and 10, and the calculations flow from the top of the table to the bottom. The top segment of [Table 8.15](#)^[471] lists the logit values for Neurons 8, 9, and 10 for each of the examples in the mini-batch (these logits are taken directly from [Figure 8.28](#)^[470]). The second segment in [Table 8.15](#)^[471] lists e raised to the power of the corresponding logit (e^{l_i}) and also the per example sum of these values ($\sum_i e^{l_i}$). The third segment lists the per neuron and per example softmax activations; these values are calculated by dividing the e^{l_i} value in the corresponding cell in the second segment by the sum for that column $\sum_i e^{l_i}$. For example, the calculation of the softmax activation for Neuron 8 and example d_1 is $1.113661238/3.326635258 \approx 0.3348$. These softmax activations are also shown in [Figure 8.28](#)^[470]. The bottom two segments of the table illustrate the calculation of the δ s for each neuron for each example. The fourth segment of the table lists the per example one-hot encoding of the target for each example in the mini-batch. These 0 and 1 values tell us which equation to use in order to calculate the

corresponding δ (below) based on the corresponding softmax activation (above). Whenever the target one-hot encoding is a 0, we use Equation (8.81)^[469] to calculate the δ ; and whenever it is a 1, we use Equation (8.80)^[469] to calculate the δ . For example, for \mathbf{d}_1 the target one-hot encoding for Neuron 8 is 0, and as a result we use Equation (8.81)^[469] to calculate the δ ; this entails simply copying the softmax activation. However, for the same example, the target one-hot encoding for Neuron 10 is 1, and so we use Equation (8.80)^[469] to calculate the δ for neuron 10 in this example. The result of this calculation is -0.6668 .

Table 8.15

The calculation of the softmax activations for each of the neurons in the output layer for each example in the mini-batch, and the calculation of the δ for each neuron in the output layer for each example in the mini-batch.

	\mathbf{d}_1	\mathbf{d}_2	\mathbf{d}_3	\mathbf{d}_4
Per Neuron Per Example logits				
Neuron 8	0.107653	0.106456	0.106093	0.107395
Neuron 9	0.099377	0.098249	0.098227	0.098955
Neuron 10	0.103000	0.104083	0.1040060	0.103460
Per Neuron Per Example e^{l_i}				
Neuron 8	1.113661238	1.112328983	1.111925281	1.11337395
Neuron 9	1.104482611	1.103237457	1.103213186	1.104016618
Neuron 10	1.108491409	1.109692556	1.109607113	1.109001432
$\sum_i e^{l_i}$	3.326635258	3.325258996	3.324745579	3.326392
Per Neuron Per Example Softmax Activations				
Neuron 8	0.3348	0.3345	0.3344	0.3347
Neuron 9	0.3320	0.3318	0.3318	0.3319
Neuron 10	0.3332	0.3337	0.3337	0.3334
Per Neuron Target One-Hot Encodings				
Neuron 8	0	1	0	0
Neuron 9	0	0	1	1
Neuron 10	1	0	0	0
Per Neuron Per Example δ s				
Neuron 8	0.3348	-0.6655	0.3344	0.3347
Neuron 9	0.3320	0.3318	-0.6682	-0.6681
Neuron 10	-0.6668	0.3337	0.3337	0.3334

Once the δ s for the output neurons have been calculated, the backpropagation of the δ s through the network and the updating of the

weights progresses as in the previous examples. For example, to update weight $w_{9,6}$ we would first calculate $\Delta w_{9,6}$ using Equation (8.29)^[416]. Equation (8.82)^[472] shows this calculation with the per example δ_s for neuron 9 taken from Table 8.15^[471], and the activations for Neuron 6 are from Figure 8.28^[470]

$$\begin{aligned}
 \Delta w_{9,6} &= \sum_{j=1}^4 \delta_{9,j} \times a_{6,j} \\
 &= (0.3320 \times 0.1145) + (0.3318 \times 0.1211) \\
 &\quad + (-0.6682 \times 0.1167) + (-0.6681 \times 0.1195) \\
 &= 0.038014 + 0.04018098 + -0.07797894 + -0.07983795 \\
 &= -0.07962191
 \end{aligned} \tag{8.82}$$

The weight can then be updated using the batch weight update rule (see Equation (8.30)^[416]), where we assume a learning rate of $\alpha = 0.01$, as shown in Equation (8.83)^[472]

$$\begin{aligned}
 w_{9,6} &= w_{9,6} - \alpha \times \Delta w_{9,6} \\
 &= -0.07 - 0.01 \times -0.07962191 \\
 &= -0.07 - (-0.000796219) \\
 &= -0.069203781
 \end{aligned} \tag{8.83}$$

8.4.4 Early Stopping and Dropout: Preventing Overfitting

Deep learning models can have millions of parameters, and this complexity makes them prone to **overfitting**. Two of the most commonly used methods to avoid overfitting in neural networks are **early stopping** and **dropout** (Srivastava et al., 2014).

The fundamental idea underpinning **early stopping** is that we can identify the point during an iterative training algorithm (such as backpropagation) when a model begins to overfit the training data as being the point when the error of the model on a **validation dataset** begins to increase. This idea of using a validation set to identify when overfitting occurs is illustrated in Figure 9.3^[542] in Chapter 9^[533] in which we discuss the use of a validation set in the general setting of designing a model evaluation experiment. Building on this idea, the early stopping algorithm

uses the performance of the model on a validation dataset to determine when to stop training the model. To apply early stopping, we first set aside a portion of the training data as a validation set. Then during training after each iteration (or number of iterations), the current model is run on the validation set and its error is recorded. If the error on the validation starts to increase, then we should stop training. One slight complication of this approach is that during training, the error of a model can fluctuate even without the occurrence of overfitting, for example if the learning rate is too high; therefore, applying a strict rule of stopping training immediately after the first time the validation error increases can be too conservative a criterion for stopping. Consequently, it is standard to use a **patience** parameter to control early stopping. The patience parameter is a predefined threshold (i.e., it is a hyper-parameter) that specifies the number of times in a row we will permit the error on the validation set to be higher than the lowest recorded so far before we stop training. For example, if the patience parameter is set to 10 and we test the model on the validation set after every iteration, then we would allow training to continue until we observe 10 successive validation errors higher than the lowest recorded so far at which point our patience would run out and we stop training. Note that each time we observe a decrease in the best validation error, we reset the patience count to zero. Using a patience parameter allows the validation error to fluctuate a bit during training while still allow training to progress; it is only when we have observed a clear trend over multiple iterations of a relatively high validation error that we stop training. Naturally, when our patience runs out, we roll back training to the version of the model that produced the lowest validation set error. Doing this requires us to store the parameters of the model each time we observe a drop in the validation error. Algorithm 6^[474] lists the early stopping algorithm. We recommend using early stopping as the default strategy to control when to stop training a neural network.

Algorithm 6 The early stopping algorithm

Require: p the patience parameter
Require: \mathcal{D}_v a validation set

```
1: bestValidationModelError =  $\infty$ 
2: tmpValidationModelError = 0
3:  $\theta$  = initial model parameters
4:  $\theta^{best}$  = 0
5: patienceCount = 0
6: while patienceCount <  $p$  do
7:    $\theta$  = new model parameters after most recent weight update
8:   tmpValidationModelError = calculateValidationModelError( $\theta$ ,  $\mathcal{D}_v$ )
9:   if bestValidationModelError  $\geq$  tmpValidationModelError then
10:    bestValidationModelError = tmpValidationModelError
11:     $\theta^{best}$  =  $\theta$ 
12:    patienceCount = 0
13:   else
14:     patienceCount = patienceCount + 1
15:   end if
16: end while
17: return Best Model Parameters  $\theta^{best}$ 
```

Another simple and very effective technique to stop overfitting is called **dropout**. When we use dropout, each time we load a training example we choose a random set of neurons from the input and hidden layers and drop (or delete) them from the network for that training instance. We then do the forward and backward pass of the backpropagation and the weight update as usual for that example; the distinction is just that these processes will be run on the smaller network that remains after the selected neurons were dropped. For example, the weights connected to neurons that are dropped for an example do not receive updates on that example. Then for the next example we randomly choose a new set of nodes to drop and then do backpropagation as usual for this new example, but this time on the new reduced version of the network. In fact, not only is a different randomly selected set of neurons dropped for each training example, but a different set of neurons is randomly selected for each presentation of a training example. Consequently, for a given example, a different set of neurons is dropped each time it is presented to the network (i.e., for each epoch).

Figure 8.29^[475] illustrates how different small networks are generated for each training example by randomly dropping neurons from the original large network.

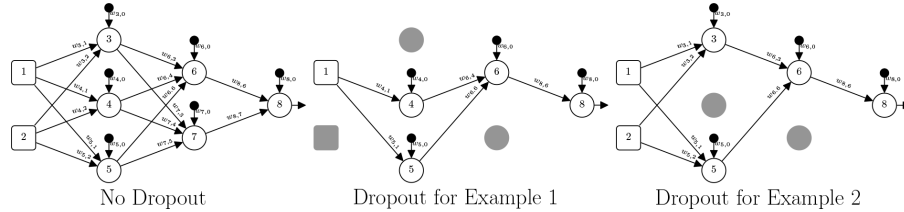


Figure 8.29

An illustration of how different small networks are generated for different training examples by applying dropout to the original large network. The gray nodes mark the neurons that have been dropped from the network for the training example.

The most popular method for implementing dropout is known as **inverted dropout**.³⁸ When we use inverted dropout we *drop* a neuron by multiplying the activation of the neuron during the forward pass by zero. This means that its activation does not flow forward through the network, and hence it has no effect on the output of the model. Also, during backpropagation no error gradients flow back through the dropped neurons; their δ s are set to 0. This makes sense because their activation will not have been used to generate the output of the model and so will not have contributed to the error of the model. As a consequence, the weights on a dropped neuron won't receive any weight updates for that example.

Algorithm 7^[476] provides a pseudocode definition of how the forward and backward passes of the backpropagation algorithm are modified to include inverted dropout. This implementation works on a layer-by-layer basis. During the forward pass for each input and hidden layer in the network a vector **DropMask** of 0 or 1 values is sampled from a Bernoulli distribution with probability ρ that a sampled value will be 1. The length of **DropMask** should be equal to the number of neurons in the layer (see Line 7^[476]). In Line 7^[476] the elementwise multiplication of the vector containing the activations of the neurons in the layer and the **DropMask** vector is performed (we use the notation \odot to denote an elementwise product).³⁹ In the updated activation vector $\mathbf{a}^{(l)'}$ generated by this multiplication, the activations for all the neurons whose position in the activation vector correspond with a 0 value in **DropMask** will be 0. Next, in Line 7^[476] each

element in new activation vector $\mathbf{a}^{(l)''}$ is divided by the parameter ρ . The name **inverted dropout** comes from this division of the non-zeroed activations by the ρ parameter. The reason we perform this division by ρ is to scale up the non-zero activations in the new activation vector so that the weighted sum calculations in the next layer are of a similar magnitude to what they would have been if none of the activations had been set to 0. The benefit of this is that the z values for the neurons in the next layer will be of a similar magnitude during training, when we are using dropout, as they will be during testing/inference (when we do not use dropout). The activation vector created by this division $\mathbf{a}^{(l)''}$ is the activation vector propagated forward to the next layer. During the backward pass, once we have calculated the δ s for the neurons in a layer, we multiply each neuron's δ by the corresponding element the **DropMask** vector that was created for that layer during the forward pass (Line 7^[476]). As a result of this multiplication for any neuron whose activation in the forward pass was set to 0 by the multiplication with **DropMask**, the δ value of the neuron will also be set to 0. This ensures that no error gradients flow back through the neurons that were dropped for this example. We then use the updated δ s to backpropagate the error gradients to the preceding layer and also for the weight update calculations.

Algorithm 7 Extensions to Backpropagation to Use Inverted Dropout

Require: ρ probability that a neuron in a layer will not be dropped

▷ Forward Pass

- 1: **for** each input or hidden layer l **do**
- 2: $\mathbf{DropMask}^{(l)} = (m_1, \dots, m_{\text{size}(l)}) \sim \text{Bernoulli}(\rho)$
- 3: $\mathbf{a}^{(l)'} = \mathbf{a}^{(l)} \odot \mathbf{DropMax}^{(l)}$
- 4: $\mathbf{a}^{(l)''} = \frac{1}{\rho} \mathbf{a}^{(l)'}$
- 5: **end for**

▷ Backward Pass

- 6: **for** each layer l in backward pass **do**
- 7: $\delta^{(l)} = \delta^{(l)} \odot \mathbf{DropMax}^{(l)}$
- 8: **end for**

Once the model has been trained we do not use dropout. Using dropout during inference would introduce random noise to the inference process.

Dropout is both simple and very effective, and applying dropout is standard practice in most deep learning research today. The ρ parameter is a hyper-parameter that is preset before training. Typical values for ρ are 0.8 for the input layer, and 0.5 for hidden layers (Goodfellow et al., 2016, p. 253).

Randomly dropping neurons from a network during training may seem like a surprising way to improve the performance of the model. There are a number of perspectives on understanding how dropout helps with overfitting. One way to understand how dropout helps is to recognize that because we use a different network on each training example, we are in effect training an **ensemble** of a very large number of smaller networks rather than training a single large model, and these smaller networks are less complex and so are less likely to overfit. Another way to understand how dropout helps is to notice that the training data looks different at every epoch because each time an example is presented to a network a different set of input neurons is set to 0. This variation in the data stops the model from memorizing the training data and forces it to learn patterns that generalize over sets of features rather than relying on a particular feature (or small subset of features). The fact that more features contribute to the predictions made by the model has the effect that the weight updates get spread out across more weights because more weights will have been involved in the prediction and hence will have contributed to the error. Spreading out the weight updates means that the weight will in general remain smaller. Keeping all the weights in a network small helps to keep a model's predictions relatively stable with respect to small changes in the input: if a model has some relatively large weights, then the model can be very sensitive to small changes in features to which these weights are applied. Models whose output changes drastically in response to small changes in the input are likely overfitting the data, because a small amount of noise in the input data can have a large effect on the outputs generated by the model. The approach of avoiding overfitting by modifying the learning algorithm in order to generate models that are stable with respect to changes in the input is generally known as **regularization**. Hence dropout can be understood as a regularization technique that improves the stability of the resulting model. Indeed, **early stopping** can also be understood as a regularization technique because it limits the number of updates to the

weights in a model and by so doing keeps individual weights from getting too large.

8.4.5 Convolutional Neural Networks

An artificial neural network is built up by connecting lots of simple processing units, and therefore neural networks have a very flexible structure. This flexibility in the network design space can be exploited to tailor a network to process different types of data. For example, rather than using full connectivity between layers (as we have done so far), we might decide to constrain the connectivity between layers so that each neuron in one layer connects only to a subset of the neurons in the next layer. Done correctly, tailoring the architecture of a network can help the network to learn a particular task by guiding the network to learn useful functions for the target task.

In this section we motivate and explain the key architectural characteristics of **convolutional neural networks** (or CNNs) which are primarily tailored to process grid like data, such as image data. The CNN architecture was originally applied to handwritten digit recognition, and much of the early work on CNNs was based on the **MNIST** (pronounced *em-nist*) dataset⁴⁰ (Le Cun et al., 1998). The dataset contains 60,000 training and 10,000 test images of handwritten digits from approximately 250 writers. Each image contains a single digit that has been size-normalized and centered. [Figure 8.30](#)^[478] shows some examples of the images from the dataset. Each image is labeled with the digit it contains, and the prediction task is to return the correct label for each image. Each image is grayscale and can be represented as a grid of 28 by 28 integers in the range [0,255] where a 0 value indicates a white pixel, a value of 255 indicates a black pixel, and numbers between 0 and 255 indicate shades of gray. We use this handwritten digit recognition task as the basis for our examples in this section. In particular, we use the 6-by-6 matrix grayscale encoding of a 4, shown in [Equation \(8.84\)](#)^[478] as the input pattern for our examples



Figure 8.30

Samples of the handwritten digit images from the MNIST dataset. Image attribution: Josef Steppan, used here under the Creative Commons Attribution-Share Alike 4.0 International license (<https://creativecommons.org/licenses/by-sa/4.0>) and was sourced via Wikimedia Commons (<https://commons.wikimedia.org/wiki/File:MnistExamples.png>).

$$\begin{bmatrix} 000 & 000 & 000 & 000 & 000 & 000 \\ 000 & \mathbf{255} & 000 & 000 & 000 & 000 \\ 000 & \mathbf{255} & 000 & \mathbf{255} & 000 & 000 \\ 000 & \mathbf{255} & \mathbf{255} & \mathbf{255} & \mathbf{255} & 000 \\ 000 & 000 & 000 & \mathbf{255} & 000 & 000 \\ 000 & 000 & 000 & 000 & 000 & 000 \end{bmatrix} \quad (8.84)$$

Convolutional neural networks have three distinctive characteristics:

1. local receptive fields;
2. weight sharing; and
3. sub-sampling (pooling).

8.4.5.1 Local receptive fields and filters The concept of **local receptive field** comes from research on visual perception in cats. In the early 1960s Hubel and Wiesel carried out a series of experiments in which they used probes to track the neural activity in the brains of sedated cats while simple visual features such as horizontal or vertical lines of light were projected onto different locations on a dark screen (Hubel and Wiesel, 1962). They discovered neurons in the brains of cats that activated only

when a visual feature appeared at specific locations in the visual field. For a given neuron to react, a specific visual feature had to occur at a particular location in the visual field; if the feature was moved to a different location in the visual field, then the neuron did not activate, nor did it activate if a different feature occurred at its target location. Furthermore, some groups of neurons reacted to the same visual feature, but each neuron in the group reacted when the feature occurred at different locations; for example, one neuron would react to the feature if it occurred in the bottom-right of the screen whereas a different neuron would react if the feature occurred in the top-left of the screen. Together this set of neurons could determine whether the visual feature occurred anywhere in the screen. By having multiple such groups of neurons, in which each group contained neurons that specialized in identifying a particular visual feature and that as a whole inspected the entire visual field for the target feature, the cat was able to perceive multiple different features occurring at different locations at the same time. However, each of the neurons in each group only inspected a local region of the visual field for a single feature, and these local regions became known as **local receptive fields**. The advantage of a local receptive field is that for a given neuron, the learning task is simplified to learning whether a particular feature occurs in a specific local region rather than learning to activate when one or more features occur anywhere in the visual field.

Inspired by these results, neural network research started to design networks in which neurons in one layer received input only from a localized subset of neurons in the preceding layer, that is, each neuron had a local receptive field in the preceding layer. Using local receptive fields, neurons can learn to extract low-level features in the input (such as a segment or an oriented edge in an image), and these features can be passed on to neurons in later layers that combine these low-level features into more complex features. [Figure 8.31](#)^[480] illustrates the concept of a local receptive field in a neural network. In this figure, the input to the network is a 6-by-6 matrix of grayscale values to represent a 6-by-6 image⁴¹ of a 4; the 4 is shown in the matrix by 255 values. The neuron in the figure takes 9 inputs, arranged in a two-dimensional 3-by-3 grid, mirroring the two-dimensional nature of the image. Apart from the grid nature of the inputs, the rest of the processing within the neuron is the same as previously described in this chapter: the result of a weighted sum of inputs is passed through a non-linear activation

function. It is relatively standard in image processing to use ReLUs for the network, and so we assume throughout this section that the neurons use the rectified linear function as their activation function. Furthermore, for the purpose of simplifying the discussion and examples in this section, we drop the **bias term** in this figure and throughout most of this section. However, it is important to remember that neurons in a convolutional network do have bias terms and that they are learned in the same way, as they are feedforward networks. As previously, the bias term is simply an extra weight that is multiplied by the dummy input value 1, and the result of this product is included in the weighted sum of the neuron. The bias term is also updated in the same way that any other weight would be updated. In [Figure 8.31](#)^[480], the key thing to note about this figure is that the neuron receives inputs only from a small predefined region of the input; in other words, the neuron receives inputs only from the pixels in its local receptive field.

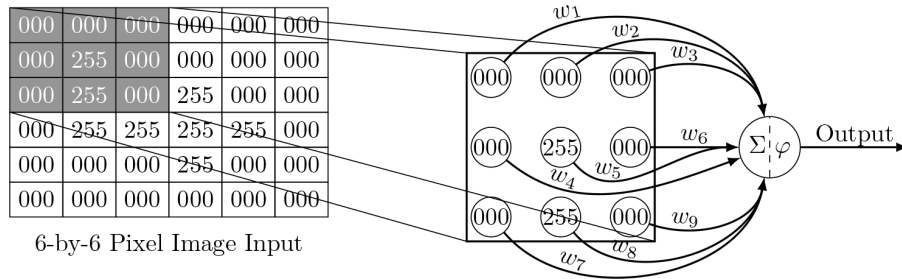


Figure 8.31

A 6-by-6 matrix representation of a grayscale image of a 4, and a neuron with a receptive field that covers the top-left corner of the image. This figure was inspired by Figure 2 of Kelleher and Dobnik (2017).

For the purpose of illustration, let us assume that the neuron shown in [Figure 8.31](#)^[480] uses the set of weights listed in Equation (8.85)^[480]

$$\begin{bmatrix} 0 & 0 & 0 \\ 1 & 1 & 1 \\ 0 & 0 & 0 \end{bmatrix} \quad (8.85)$$

Equation (8.86)^[481] lists the calculation of the activation for this neuron for this set of inputs.

$$\begin{aligned}
a_i &= \text{rectifier}((w_1 \times 000) + (w_2 \times 000) + (w_3 \times 000) \\
&\quad + (w_4 \times 000) + (w_5 \times 255) + (w_6 \times 000) \\
&\quad + (w_7 \times 000) + (w_8 \times 255) + (w_9 \times 000)) \\
&= \text{rectifier}((0 \times 000) + (0 \times 000) + (0 \times 000) \\
&\quad + (1 \times 000) + (1 \times 255) + (1 \times 000) \\
&\quad + (0 \times 000) + (0 \times 255) + (0 \times 000)) \\
&= 255
\end{aligned} \tag{8.86}$$

This calculation shows that if a neuron uses the set of weights in Equation (8.85)^[480], then the activation of the neuron is solely dependent on the values along the middle row of inputs. All the other input values are ignored because they are given a weight of 0. Consequently, neurons using this set of weights can be thought of as rudimentary detectors for horizontal edges because they will have maximum activation if there is a horizontal line across the middle row of their inputs. For example, Figure 8.32^[481] shows a second neuron with a different local receptive field, and Equation (8.87)^[482] shows the calculation of the activation of this neuron if it uses the same set of weights. In this case, there are maximum grayscale values (255) across the middle row of the neurons receptive field, and as a result of the interaction between this input pattern and the weights in Equation (8.85)^[480], this neuron has a very large activation for this input.

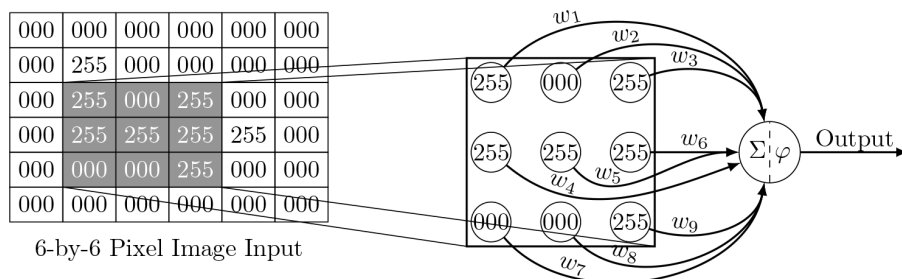


Figure 8.32

A 6-by-6 matrix representation of a grayscale image of a 4, and a neuron with a different receptive field from the neuron in Figure 8.31^[480]. This figure was inspired by Figure 2 of Kelleher and Dobnik (2017).

$$\begin{aligned}
a_i &= \text{rectifier}((w_1 \times 255) + (w_2 \times 000) + (w_3 \times 255) \\
&\quad + (w_4 \times 255) + (w_5 \times 255) + (w_6 \times 255) \\
&\quad + (w_7 \times 000) + (w_8 \times 000) + (w_9 \times 255)) \\
&= \text{rectifier}((0 \times 255) + (0 \times 000) + (0 \times 255) \\
&\quad + (1 \times 255) + (1 \times 255) + (1 \times 255) \\
&\quad + (0 \times 000) + (0 \times 000) + (0 \times 255)) \\
&= 765
\end{aligned} \tag{8.87}$$

Equation (8.88)^[482] shows some other sets of weights that our example neurons could use. It is relatively straightforward to see that neurons using the weight matrix on the left will have a high activation if their local receptive field contains high values down the central column of the field, neurons using the weight matrix in the middle will respond if there are high values down the left-right diagonal of the receptive field, neurons using the third weight matrix will have a high activation if there are more high values down the central column of the receptive field than there are in the other pixels in the input, and similarly the distribution of positive and negative values in the matrix on the right means that neurons using this set of weights will have a high activation if there are more high values across the middle row of the receptive field than in other places in the input. There are, of course, many different weight matrices that could be defined, each of which would cause a neuron to activate in response to a different visual pattern in the neuron's local receptive field. In fact, given that the weights are real numbers, there are infinitely many combinations of weights, and we are using only integer values in the examples for the sake of clarity in presentation.

The set of weights used by a neuron determine the type of visual feature to which the neuron activates in response; consequently, these weight matrices are called **filters** because they filter the input by returning high activations for certain patterns of inputs and low activations for others. In this discussion on local receptive fields, the filters we have presented are hand designed for the purpose of illustration. In reality, these filters are learned by the convolutional network in the same way that weights are learned in a fully connected feedforward network. Allowing the network to learn the filter weights means that the network is able to learn which visual

patterns are useful to extract from the visual input in order to be successful at the prediction task on which it is being trained.

$$\begin{bmatrix} 0 & 1 & 0 \\ 0 & 1 & 0 \\ 0 & 1 & 0 \end{bmatrix} \quad \begin{bmatrix} 1 & 0 & 0 \\ 0 & 1 & 0 \\ 0 & 0 & 1 \end{bmatrix} \quad \begin{bmatrix} -1 & +1 & -1 \\ -1 & +1 & -1 \\ -1 & +1 & -1 \end{bmatrix} \quad \begin{bmatrix} -1 & -1 & -1 \\ +1 & +1 & +1 \\ -1 & -1 & -1 \end{bmatrix} \quad (8.88)$$

8.4.5.2 Weight sharing and translation equivariant feature detection When a neuron applies a filter to its local receptive field, it is a local visual feature detector for which the visual feature is a pattern of input values. If the feature occurs in the neuron's local receptive field, then the neuron will have a high activation. However, an image processing system should be able to detect whether a visual feature occurs in an image irrespective of where in the image it occurs. Technically, this property is described as the model being **equivariant** to the translation of features.

Convolutional neural networks achieve translation equivariant feature detection through **weight sharing**. This is done by organizing neurons into groups in which all the neurons in the group apply the same filter to their inputs. In other words, in a convolutional neural network, when two neurons share weights, they share all their weights, because they use the same filter. When two or more neurons share a filter, then each weight in the filter is used multiple times during the forward pass of the training algorithm to process a given input (once by each neuron that uses the filter). During the backward pass of the algorithm, we calculate a separate weight update for each neuron that uses the weight, and then the final weight update that is applied is the sum of these separate weight updates. By summing the weight updates across the neurons that use it, we retain a single consistent weight for all the neurons. This is similar to the way we summed the weight updates for a weight during batch training (see Equation (8.30)^[416]); the difference here is that for each training example we sum over the weight updates for each neuron that uses the weight (as opposed to weight updates for different training examples). So, if a weight is shared by m different neurons, then the weight update after processing a single example is defined as follows:

$$\begin{aligned}\Delta w_{i,*} &= \sum_{i=1}^m \delta_i \times a_* \\ w_{i,*} &\leftarrow w_{i,*} - \alpha \times \Delta w_{i,*}\end{aligned}\tag{8.89}$$

where i iterates over the neurons that share the weight; and $*$ is a wildcard placeholder for the index of the appropriate input neuron to each neuron that uses the weight. When we are using batch gradient descent, this summation can be extended to include a summation over the examples in the batch.

The way that a convolutional neural network uses weight sharing to achieve translation equivariant feature detection is by organizing the local receptive fields of a set of neurons that share a filter (and hence share their weights) so that (1) each neuron's receptive field covers a slightly different region of the visual field compared with the other neurons in the set; and (2) together the receptive fields of the neurons in the set cover the entire visual field. [Figure 8.33](#)^[484] illustrates how the local receptive fields of a set of neurons can be organized so that together they cover the entirety of the input. This figure contains 16 subfigures, with each subfigure containing a matrix of input data (on the left) representing the input image and a grid of 16 circles (on the right) in which each circle represents a neuron. Each subfigure highlights the local receptive field in the input of the highlighted neuron in the set of neurons.

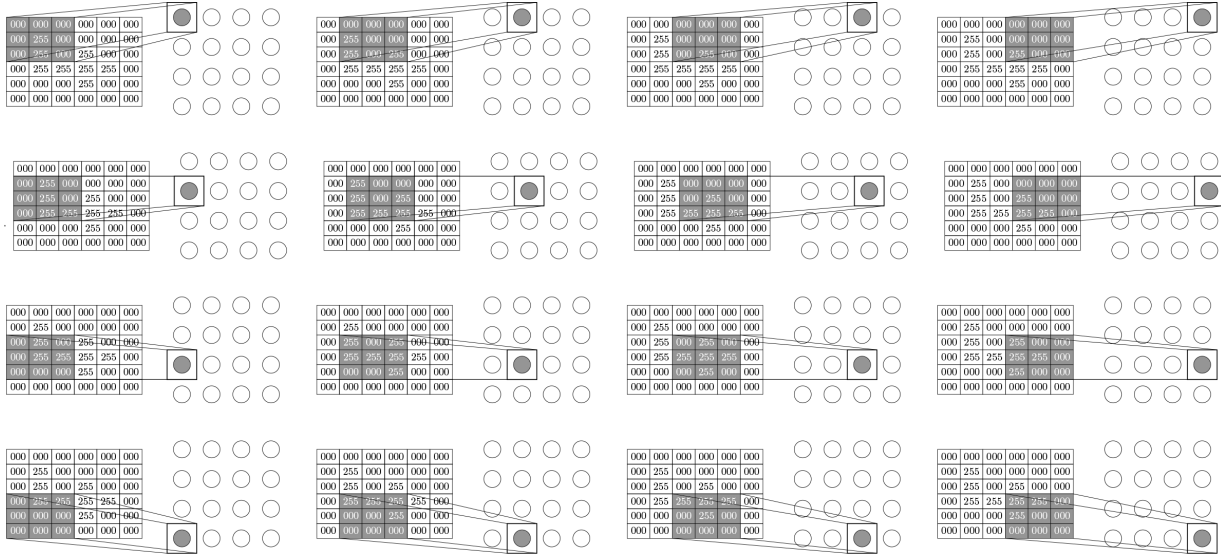


Figure 8.33

Illustration of the organization of a set of neurons that share weights (use the same filter) and their local receptive fields such that together the receptive fields cover the entirety of the input image.

The name **convolutional neural network** comes from the fact that it is possible to implement the processing of an image by a set of neurons that share a filter with a single neuron that applies the filter to each region of the image in sequence and stores the result for each region. In mathematics, the process of passing a function over a sequence of values is known as **convolving a function**, and by analogy a set of neurons that share a filter (and thereby each implements the same function) and that are organized such that together their receptive fields cover the input are convolving a function over the input.⁴²

The fact that the joint receptive fields of the neurons in each set cover the entire input means that if the relevant visual feature (where relevance is defined by the filter used by a set of neurons) occurs anywhere in the input, then at least one of the neurons in the set will have a high activation. Indeed, the activations of the neurons in a set provide a map of where in the input the relevant visual feature occurred, and for this reason the set of activations for a set of neurons that share a filter is called a **feature map**. Equation (8.90)^[486] and Equation (8.91)^[486] illustrate how the feature map generated by the neurons in Figure 8.33^[484] changes if the filter used by the neurons to process the example input is changed. Note that in generating the feature map for each of these equations, we have applied the rectified linear

activation function to the results of the weighted sum of each receptive field and the filter.⁴³

$$\underbrace{\begin{bmatrix} 000 & 000 & 000 & 000 & 000 & 000 \\ 000 & \mathbf{255} & 000 & 000 & 000 & 000 \\ 000 & \mathbf{255} & 000 & \mathbf{255} & 000 & 000 \\ 000 & \mathbf{255} & \mathbf{255} & \mathbf{255} & \mathbf{255} & 000 \\ 000 & 000 & 000 & \mathbf{255} & 000 & 000 \\ 000 & 000 & 000 & 000 & 000 & 000 \end{bmatrix}}_{\text{Input Image}} \rightarrow \underbrace{\begin{bmatrix} -1 & +1 & -1 \\ -1 & +1 & -1 \\ -1 & +1 & -1 \end{bmatrix}}_{\text{Convolved Filter}} \rightarrow \underbrace{\begin{bmatrix} 510 & 0 & 255 & 0 \\ 510 & 0 & 0 & 0 \\ 255 & 0 & 255 & 0 \\ 0 & 0 & 0 & 0 \end{bmatrix}}_{\text{Feature Map}} \quad (8.90)$$

$$\underbrace{\begin{bmatrix} 000 & 000 & 000 & 000 & 000 & 000 \\ 000 & \mathbf{255} & 000 & 000 & 000 & 000 \\ 000 & \mathbf{255} & 000 & \mathbf{255} & 000 & 000 \\ 000 & \mathbf{255} & \mathbf{255} & \mathbf{255} & \mathbf{255} & 000 \\ 000 & 000 & 000 & \mathbf{255} & 000 & 000 \\ 000 & 000 & 000 & 000 & 000 & 000 \end{bmatrix}}_{\text{Input Image}} \rightarrow \underbrace{\begin{bmatrix} -1 & -1 & -1 \\ +1 & +1 & +1 \\ -1 & -1 & -1 \end{bmatrix}}_{\text{Convolved Filter}} \rightarrow \underbrace{\begin{bmatrix} 0 & 0 & 0 & 0 \\ 0 & 0 & 0 & 0 \\ 255 & 0 & 255 & 0 \\ 0 & 0 & 0 & 0 \end{bmatrix}}_{\text{Feature Map}} \quad (8.91)$$

8.4.5.3 Filter hyper-parameters: Dimension, stride, and padding

The dimensionality of a feature map generated by applying a filter to an input is determined by the number of neurons used to process the input (each element in a feature map corresponds to the output of one neuron). We can see this if we compare the dimensionality of the features maps in Equation (8.90)^[486] and Equation (8.91)^[486] with the number of neurons shown in Figure 8.33^[484]. There are three hyper-parameters that affect the number of neurons required to cover the entirety of an input and hence the dimensionality of the resulting feature map; these are filter dimensions, the stride, and the padding.

The **filter dimension** hyper-parameter specifies the size of the filter in each dimension. The illustration in Figure 8.33^[484] assumes that the neurons are using a two-dimensional 3-by-3 (height by width) filter. However, larger and smaller filters are possible, and as filters become larger the number of neurons required to cover the input naturally gets smaller and vice versa. For example, if we decreased the dimension of our filter to a 2-by-2 dimension then we would need to increase the set of neurons to a 5-by-5 layer in order to cover the input, and this would result in a 5-by-5 feature map. Conversely, if we increased the dimension of our filter to a 4-by-4 filter, then we could cover the input with a 3-by-3 layer of neurons

generating a 3-by-3 feature map. Choosing a good filter size for a given dataset often involves a trial-and-error process of experimenting with different options. Also, all our filter examples so far have been two-dimensional filters. The reason is that we have been focusing on processing a grayscale image that is a two-dimensional input. However, it is quite possible to use one-dimensional filters or filters with three or more dimensions. For now we continue with using two-dimensional filters, but we return to this topic in Section 8.4.5.5^[492].

The **stride** parameter specifies the distance between the center of the local receptive field of one neuron and the center of the local receptive fields of its horizontal or vertical neighbor in the set of neurons sharing the filter. The configuration of receptive fields in Figure 8.33^[484] uses a horizontal and vertical stride of 1; this means that as we move from one neuron to the next horizontally, the corresponding receptive fields also move by one column in the input space. Similarly, as we move from one neuron to the next vertically, the receptive fields also move by one row in the input space. Using a horizontal and vertical stride of 1 means that there is a relatively large overlap in the receptive fields between a neuron and its neighbors. Other strides are possible, and it is possible to use different horizontal and vertical strides. For example, if we used a horizontal and vertical stride of 3 in Figure 8.33^[484], then there would be no overlap between the receptive fields of different neurons, and this would also reduce the number of neurons required to cover the input. Similar to the filter dimensions, finding the appropriate stride for a given dataset involves trial-and-error experimentation.

There are two related phenomena in Figure 8.33^[484] that, in some instances, maybe undesirable consequences of how the receptive fields for the neurons have been defined. The first is that if we use a 4-by-4 layer of neurons, to cover a 6-by-6 input matrix, the dimensionality of the resulting feature map is also 4-by-4. In some cases we may wish to avoid this reduction in dimensionality between the input and the feature map. The second phenomenon is that there is a difference in the number of times that each pixel in the image is used as an input to a neuron in the grid. This differential is largest between the pixels at the corners of the image versus the pixels in the middle of the image; only one of the receptive fields covers the top-left pixel in the image, whereas nine receptive fields cover the pixel

at coordinate (3,3). Both of these phenomena are a consequence of the fact that we are applying the filter only to **valid** pixels in the image. We are using the term **valid** here to distinguish the pixels that occur in the image from imaginary (or **padding**) pixels that we might invent around the border of an image. [Figure 8.34](#)^[488] illustrates what happens if we pad the boundary of an image with imaginary pixels. In this figure, the imaginary pixels are shown in gray, and the valid (real) pixels are in the center of the matrix, shown in black. The boundary between imaginary and valid pixels is highlighted by a thickly outlined rectangle enclosing the valid pixels. All the imaginary pixels have been given a value of 000. The figure also illustrates the local receptive field of the first neuron in the grid; note that this receptive field includes imaginary pixels. Adding this padding to the image increases the number of neurons required to cover the image, assuming that the filter size and horizontal and vertical strides are maintained. In fact, there are now as many neurons in the grid as there are valid pixels in the image. Furthermore, although there is still a differential between some of the valid pixels in terms of the number of neurons that take them as input, this differential has been decreased; each of the valid corner pixels is now present in four receptive fields, as opposed to one as previously, whereas the count of receptive fields covering a pixel in the center of the image is not affected by the padding. When padding is applied it is generally added to all edges as equally as is possible. As with filter size and stride length, the selection of whether to use padding or not is task dependent and is often based on trial and error.

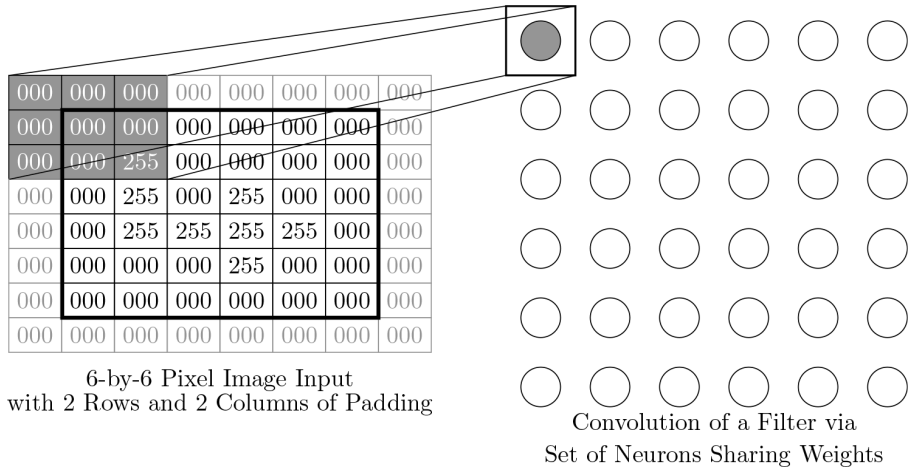


Figure 8.34

A grayscale image of a 4 after padding has been applied to the original 6-by-6 matrix representation, and the local receptive field of a neuron that includes both valid and padded pixels.

The particular choices of filter size, stride length, and padding is task dependent. However, a popular combination is to use a stride length of 1 and to pad the image with imaginary pixels (Charniak, 2019, p. 56). This combination ensures that the output from a layer of neurons applying a filter across an image has the same dimensions as the input image. Maintaining the dimensionality between input and output becomes important in convolutional neural networks when we use multiple layers of neurons, the output for one layer being interpreted as the *image* input to the next layer. In these cases, unless the dimensionality is maintained by using imaginary pixels, then the dimensionality of the input to each layer reduces for each subsequent layer. Equation (8.92)^[489] and Equation (8.93)^[489] each list a filter weight matrix and the feature map generated by using a set of neurons to process our example input in Equation (8.84)^[478] after the input has had padding applied and using a stride length of 1. The generated feature maps have the same 6-by-6 dimensionality as the input image (before padding was applied). As a comparator, the filters used in these two equations are the same as those used in Equation (8.90)^[486] and Equation (8.91)^[486]; the difference now is that the generated feature maps are larger, and indeed some of the new cells have positive values.

$$\begin{array}{ccccccccc}
 0 & 0 & 0 & 0 & 0 & 0 & 0 & 0 & 0 \\
 0 & 0 & 0 & 0 & 0 & 0 & 0 & 0 & 0 \\
 0 & 0 & 0 & 255 & 0 & 0 & 0 & 0 & 0 \\
 0 & 0 & 0 & 255 & 0 & 0 & 255 & 0 & 0 \\
 0 & 0 & 0 & 255 & 255 & 255 & 255 & 0 & 0 \\
 0 & 0 & 0 & 0 & 0 & 0 & 0 & 0 & 0 \\
 0 & 0 & 0 & 0 & 0 & 0 & 0 & 0 & 0 \\
 0 & 0 & 0 & 0 & 0 & 0 & 0 & 0 & 0
 \end{array} \xrightarrow{\text{Convolved Filter}} \begin{bmatrix} -1 & +1 & -1 \\ -1 & +1 & -1 \\ -1 & +1 & -1 \end{bmatrix} \rightarrow
 \begin{array}{cccccc}
 0 & 255 & 0 & 0 & 0 & 0 \\
 0 & 510 & 0 & 255 & 0 & 0 \\
 0 & 510 & 0 & 0 & 0 & 0 \\
 0 & 255 & 0 & 255 & 0 & 0 \\
 0 & 0 & 0 & 0 & 0 & 0 \\
 0 & 0 & 0 & 255 & 0 & 0
 \end{array} \xrightarrow{\text{Feature Map}}$$

Input Image

(8.92)

$$\begin{array}{ccccccccc}
 0 & 0 & 0 & 0 & 0 & 0 & 0 & 0 & 0 \\
 0 & 0 & 0 & 0 & 0 & 0 & 0 & 0 & 0 \\
 0 & 0 & 0 & 255 & 0 & 0 & 0 & 0 & 0 \\
 0 & 0 & 0 & 255 & 0 & 0 & 255 & 0 & 0 \\
 0 & 0 & 0 & 255 & 255 & 255 & 255 & 0 & 0 \\
 0 & 0 & 0 & 0 & 0 & 0 & 0 & 0 & 0 \\
 0 & 0 & 0 & 0 & 0 & 0 & 0 & 0 & 0 \\
 0 & 0 & 0 & 0 & 0 & 0 & 0 & 0 & 0
 \end{array} \xrightarrow{\text{Convolved Filter}} \begin{bmatrix} -1 & -1 & -1 \\ +1 & +1 & +1 \\ -1 & -1 & -1 \end{bmatrix} \rightarrow
 \begin{array}{cccccc}
 0 & 0 & 0 & 0 & 0 & 0 \\
 0 & 0 & 0 & 0 & 0 & 0 \\
 0 & 0 & 0 & 0 & 0 & 0 \\
 0 & 255 & 0 & 255 & 0 & 255 \\
 0 & 0 & 0 & 0 & 0 & 0 \\
 0 & 0 & 0 & 0 & 0 & 0
 \end{array} \xrightarrow{\text{Feature Map}}$$

Input Image

(8.93)

8.4.5.4 Pooling The precise location of a visual feature in an image may not be relevant for an image-processing task. For example, knowing that there is an eye in the top-left region of an image is useful for face recognition, but the extra precision of knowing that it is centered at pixel (998,742) may not be useful. Indeed, in training an image processing model we typically want the model to generalize over the precise locations of features in training images so that it can still use these features when they occur in offset configurations in new images. The most straightforward way to make a model abstract away from the precise location of visual features is to sub-sample the feature maps. In convolutional neural networks, sub-sampling is done using **sub-sampling layers**. Each neuron in a sub-sampling layer has a local receptive field in a feature map generated by the previous layer, which will have convolved a filter over the input to that layer. However, typically the local receptive fields of neurons in a sub-sampling layer do not overlap (in contrast with the overlapping receptive fields used when we arrange neurons to convolve a filter). Consequently, there are fewer output activations from a sub-sampling layer than there are inputs: one output per local receptive field and multiple inputs per field. The amount of sub-sampling applied is dependent on the dimensions of the

receptive fields of the neurons; for example, using non-overlapping 2-by-2 receptive fields, the output from a sub-sampling layer will have half the number of rows and columns as the feature map input to the layer. In early convolution networks, the activation of sub-sampling neurons was often the average of the values in the feature map covered by the local receptive field of the neuron. Many modern convolutional networks use a **max** function that simply returns the maximum value in the region of the feature map covered by the local receptive field. Applying a max function to a local receptive field is often referred to as **max pooling**. Equation (8.94)^[490] illustrates the result of applying max pooling to the feature map from Equation (8.93)^[489] using non-overlapping local receptive fields with a dimensionality of 2-by-2.

$$\begin{array}{c}
 \text{Input Image} \\
 \left[\begin{array}{cccccccc} 000 & 000 & 000 & 000 & 000 & 000 & 000 & 000 \\ 000 & 000 & 000 & 000 & 000 & 000 & 000 & 000 \\ 000 & 000 & \mathbf{255} & 000 & 000 & 000 & 000 & 000 \\ 000 & 000 & \mathbf{255} & 000 & \mathbf{255} & 000 & 000 & 000 \\ 000 & 000 & \mathbf{255} & \mathbf{255} & \mathbf{255} & 000 & 000 & 000 \\ 000 & 000 & 000 & 000 & \mathbf{255} & 000 & 000 & 000 \\ 000 & 000 & 000 & 000 & 000 & 000 & 000 & 000 \\ 000 & 000 & 000 & 000 & 000 & 000 & 000 & 000 \end{array} \right] \rightarrow \left[\begin{array}{ccc} -1 & -1 & -1 \\ +1 & +1 & +1 \\ -1 & -1 & -1 \end{array} \right] \rightarrow \\
 \text{Convolved Filter} \\
 \\
 \text{Feature Map} \\
 \rightarrow \left[\begin{array}{ccccc} 0 & 0 & 0 & 0 & 0 \\ 0 & 0 & 0 & 0 & 0 \\ 0 & 0 & 0 & 0 & 0 \\ 0 & 255 & 0 & 255 & 0 & 255 \\ 0 & 0 & 0 & 0 & 0 & 0 \\ 0 & 0 & 0 & 0 & 0 & 0 \end{array} \right] \rightarrow \text{max pooling} \rightarrow \left[\begin{array}{ccc} 0 & 0 & 0 \\ 255 & 255 & 255 \\ 0 & 0 & 0 \end{array} \right] \\
 \text{Output from Sub-sampling}
 \end{array} \tag{8.94}$$

Using a max function requires that the backward pass in the backpropagation algorithm be updated slightly. The reason is that a max function allows through only the maximum value from its inputs, and so the non-max values did not affect the output (and hence the error) of the network. As a result, there is no error gradient with respect to the non-max

values that the max function received. Furthermore, the gradient for the max function ($\partial a / \partial z$) for the max value is 1, because the output of the activation function will be linear for small changes in the input value that achieved the max (i.e., it will change by the same amount as that input value is changed). Consequently, in backpropagating through a max function, the entire error gradient is backpropagated to the neuron that propagated forward the max value, and the other neurons receive an error gradient of zero.

To illustrate the backpropagation process through a convolutional layer, we need to shift our focus from the flow of data through the layer to the neural architecture of the layer. Equation (8.95)^[491] illustrates an extended version of the convolutional network that would implement the data processing illustrated in Equation (8.94)^[490]. Note that in Equation (8.95)^[491] each symbol in a matrix represents a neuron in a layer, rather than a data point. The matrix on the left of Equation (8.95)^[491] represents the 6-by-6 layer of neurons that share the filter listed in Equation (8.94)^[490]. It is the output of this layer of neurons that generates the feature map in Equation (8.94)^[490]. The matrix in the middle of Equation (8.95)^[491] represents the 3-by-3 sub-sampling layer. Each neuron in this layer has a local receptive field of dimensions 2-by-2, and there is no overlap between the receptive fields of the neurons in this layer. The matrix on the right of Equation (8.95)^[491] represents an extension to the architecture that we have discussed. This matrix contains two neurons that are fully connected to the sub-sampling layer; that is, each neuron in this layer receives inputs from all the neurons in the sub-sampling layer. For ease of reference, we have explicitly labeled a number of neurons in this architecture A, B, C, D, and E

$$\begin{array}{c}
 \left[\begin{array}{cccccc} O & O & O & O & O & O \\ O & O & O & O & O & O \\ A & O & O & O & O & O \\ O & B & O & O & O & O \\ O & O & O & O & O & O \\ O & O & O & O & O & O \end{array} \right] \xrightarrow{\text{Sub-sampling Layer}} \left[\begin{array}{ccc} O & O & O \\ C & O & O \\ O & O & O \end{array} \right] \xrightarrow{\text{Fully Connected Layer}} \underbrace{\left[\begin{array}{c} D \\ E \end{array} \right]}_{\text{Fully Connected Layer}}
 \end{array} \quad (8.95)$$

Neurons that convolve the Filter

To begin the backpropagation process through the convolutional layer, we assume that the δ s for the neurons D and E have already been calculated. We can now calculate the δ for Neuron C

$$\begin{aligned}\delta_C &= \frac{\partial \mathcal{E}}{\partial a_C} \times \frac{\partial a_C}{\partial z_C} \\ &= ((\delta_D \times w_{D,C}) + (\delta_E \times w_{E,C})) \times 1\end{aligned}\tag{8.96}$$

This is the standard calculation we would use to calculate the δ for any hidden neuron, see Equation (8.23)^[412], with the slight simplification that, as mentioned previously, the gradient of the activation function $\partial a_c / \partial z_c = 1$. We calculate the δ s for the other neurons in the sub-sampling layer in a similar fashion.

Once we have calculated a δ for each of the neurons in the sub-sampling layer, we can then backpropagate these δ s to the layer of neurons that convolve the filter. Recall that the receptive fields of the neurons in the sub-sampling layer do not overlap. Consequently, each of the neurons in the first layer connects only to a single neuron in the sub-sampling layer. For example, neurons A and B are both in the receptive field of Neuron C, but neither A nor B feeds forward into any of the other neurons in the sub-sampling layer. From the feature map in Equation (8.94)^[490] we can ascertain that $a_A = 0$ and $a_B = 255$. In fact, Neuron B has the highest activation for any of the neurons in the local receptive field of Neuron C. This means that $\delta_A = 0$ because Neuron A did not have the maximum value in the local receptive field of the sub-sampling neuron to which it is connected. The activation for Neuron B, however, was the maximum value for the local receptive field the neuron is in, and so the δ value for Neuron B is calculated as shown in Equation (8.97)^[492]. Notice that $w_{C,B} = 1$. The reason is that the max function does not apply weights to its inputs or, to put it another way, all the inputs have a weight of 1. Also, Neuron B is a ReLU and so $\partial a_B / \partial z_B = 1$ because $a_B > 0$

$$\begin{aligned}
\delta_B &= \frac{\partial \mathcal{E}}{\partial a_B} \times \frac{\partial a_B}{\partial z_B} \\
&= (\delta_D \times w_{C,B}) \times \frac{\partial a_B}{\partial z_B} \\
&= (\delta_D \times 1) \times 1
\end{aligned} \tag{8.97}$$

The δ s for the other neurons in the first layer will either be 0 (if they, like Neuron A, did not produce the maximum value in the local receptive field of the sub-sampling neuron to which they connect) or can be calculated in a similar way to Neuron B. Once the δ for each of the neurons in this layer has been calculated, the weight updates for each weight in the filter can be calculated by summing weight updates across the neuron in the layer, per Equation (8.89)^[483].

8.4.5.5 Handling color images and multiple filters All the example filters that we previously presented were two-dimensional. The reason is that the MNIST handwriting recognition case study we are using in this section involves grayscale images. Consequently we require only a two-dimensional filter because all pixel information for an image can be represented in a two-dimensional matrix indexing over the height and width of the grayscale image. However, color images typically encode three types of information for each pixel—the red, green and blue information, with other colors generated via the combination of these three primary colors. Encoding the red, green, and blue (RGB) information is normally done using a separate two-dimensional matrix for each color, with the dimensions of each of these two-dimensional matrices equal to the pixel resolution of the image. The term **channel** is used to describe the number of matrices used to encode the information in an image. An RGB image has three channels, and a grayscale image will have one channel. If we were processing RGB images, then we would use three-dimensional filters: height by width by channel.

Typically, the third dimension of a filter is referred to as the **depth** of the filter, with the term **channel** specifically used to describe the depth of the data representation of a color image. The depth of a filter must match the depth of the input. Consequently, if we are designing a filter to process a

color image, with three color channels (red, green, and blue), we can vary the height and width dimensions of the filter, but the depth dimension must be 3. For example, we could experiment with using a 2-by-2-by-3 filter (height by width by depth). Equation (8.98)^[493] illustrates the structure of such a three-dimensional filter. We have included the **bias term** w_0 in this filter in order to highlight that although the filter now has three dimensions, there is still only one bias term.

$$\underbrace{w_0}_{\text{bias}} \begin{bmatrix} w_1 & w_2 \\ w_3 & w_4 \end{bmatrix} \begin{bmatrix} w_5 & w_6 \\ w_7 & w_8 \end{bmatrix} \begin{bmatrix} w_9 & w_{10} \\ w_{11} & w_{12} \end{bmatrix} \quad (8.98)$$

Adding depth to a filter does not involve a major change in the way a neuron applies a filter to its local receptive field. For example, if a neuron is applying a 2-by-2-by-3 filter, then its local receptive field will have the same dimensions (this is why the depth of the filter must match the depth of the input). If the input happens to be a color image, then we can distinguish the different layers of depth by the color channels. In this context, the neuron will apply a different 2-by-2 filter to each color channel: one 2-by-2 filter is applied to the red values of the pixels in the receptive field; another 2-by-2 filter is applied to the green values of the pixels in the receptive field; and the third 2-by-2 filter is applied to the blue values of the pixels in the receptive field. Then the results of these three calculations are summed together along with the bias, to generate a single scalar value that is pushed through the activation function and then stored in the feature map.⁴⁴ Equation (8.99)^[493] lists a 2-by-2-by-3 filter that has been annotated to indicate which parts of the filter are applied to which channel

$$\underbrace{w_0 = 0.5}_{\text{bias}} \underbrace{\begin{bmatrix} w_1 = 1 & w_2 = 1 \\ w_3 = 0 & w_4 = 0 \end{bmatrix}}_{\text{Red Channel}} \underbrace{\begin{bmatrix} w_5 = 0 & w_6 = 1 \\ w_7 = 0 & w_8 = 1 \end{bmatrix}}_{\text{Green Channel}} \underbrace{\begin{bmatrix} w_9 = 1 & w_{10} = 0 \\ w_{11} = 0 & w_{12} = 1 \end{bmatrix}}_{\text{Blue Channel}} \quad (8.99)$$

For the purposes of illustration, imagine that we are using this filter to process the following 3-by-3 RGB image (the pixel values here are not real; they have been selected to ease the calculations in the example):

$$\left[\begin{array}{ccc} \underbrace{\begin{bmatrix} 1 & 1 & 1 \\ 0 & 0 & 0 \\ 0 & 0 & 0 \end{bmatrix}}_{\text{Red Channel}} & \underbrace{\begin{bmatrix} 0 & 0 & 2 \\ 0 & 0 & 2 \\ 0 & 0 & 2 \end{bmatrix}}_{\text{Green Channel}} & \underbrace{\begin{bmatrix} 3 & 0 & 0 \\ 0 & 3 & 0 \\ 0 & 0 & 3 \end{bmatrix}}_{\text{Blue Channel}} \end{array} \right] \quad (8.100)$$

Assuming a stride length of 1 and no padding on the input, we would require a 2-by-2 layer of neurons to convolve the filter over this image. The top-left neuron in this layer would have a local receptive field covering the 2-by-2 square in the top-left of each of the channels. [Equation 8.101](#)^[494] lists the values from the image that are inside this neuron's local receptive field

$$\left[\begin{array}{ccc} \underbrace{\begin{bmatrix} 1 & 1 \\ 0 & 0 \end{bmatrix}}_{\text{Red Channel}} & \underbrace{\begin{bmatrix} 0 & 0 \\ 0 & 0 \end{bmatrix}}_{\text{Green Channel}} & \underbrace{\begin{bmatrix} 3 & 0 \\ 0 & 3 \end{bmatrix}}_{\text{Blue Channel}} \end{array} \right] \quad (8.101)$$

The output activation for this neuron would be calculated as follows:

$$\begin{aligned} z &= ((w_0 \times 1) \\ &\quad + (w_1 \times 1) + (w_2 \times 1) + (w_3 \times 0) + (w_4 \times 0) \\ &\quad + (w_5 \times 0) + (w_6 \times 0) + (w_7 \times 0) + (w_8 \times 0) \\ &\quad + (w_9 \times 3) + (w_{10} \times 0) + (w_{11} \times 0) + (w_{12} \times 3)) \\ &= 0.5 + 1 + 1 + 0 + 0 + 0 + 0 + 0 + 3 + 0 + 0 + 3 \\ &= 8.5 \\ a &= \text{rectifier}(z) \\ &= \text{rectifier}(8.5) \\ &= 8.5 \end{aligned} \quad (8.102)$$

The activations for the other three neurons using this filter would be calculated in a similar way, resulting in the following feature map being generated by this 2-by-2 layer of neurons:

$$\left[\begin{array}{cc} 8.5 & 6.5 \\ 0.5 & 10.5 \end{array} \right] \quad (8.103)$$

Adding depth to a filter not only enables a convolutional neural network to process color images that contain multiple channels; it also enables a convolutional network to have a sequence of multi-filter convolutional layers. The reason is that although a convolutional layer that runs multiple filters in parallel over its input will generate multiple feature maps, the next convolutional layer can treat these multiple feature maps as if they were a single multi-channel input. In this case, the number of channels in the input to this layer would be equal to the number of filters in the preceding convolutional layer. This is done by stacking the feature maps together. In these stacked feature map inputs, each channel then encodes the information from a particular filter spectrum (for example, the information from the horizontal edge detector filter spectrum) instead of encoding the information in a particular color spectrum (Charniak, 2019). Consequently, adding depth to filters not only enables convolutional neural networks to process multi-dimensional input; it also enables the networks to apply multiple filters in parallel to the same input and for later layers in the network to integrate information from across these layers. As a result, convolutional networks can learn to identify, extract, and use multiple different features in the input.

The sequence of convolving a filter over an input, then applying a non-linear activation function, and finally sub-sampling the resulting feature maps is relatively standard in most modern convolutional networks, and often this sequence of operations is taken as defining a convolutional layer. As we discussed previously, a network may have multiple convolutional layers in sequence because the outputs from a sub-sampling layer may be passed as an input to another filter convolution, and so this sequence of operations may be repeated multiple times. Padding may be applied to retain dimensionality, and in some cases the non-linearity activation or sub-sampling may be dropped in some convolutional layers. Generally, the later layers of a convolutional network will include one or more fully connected layers (such as those shown in previous examples) with a softmax output layer if the model is being used for classification. [Figure 8.35](#)^[497] presents a schematic of how two convolutional layers might be sequenced in a simple convolutional neural network. [Figure 8.35](#)^[497] also shows that there may be multiple filters applied in parallel in a convolutional layer. In this network, Convolutional layer 1 includes Filters 1 and 2 and so generates two feature

maps. These two feature maps are then stacked together and fed forward as input to the second convolutional layer. Convolutional layer 2 includes Filters 3 and 4, and it does not include a sub-sampling layer.⁴⁵ Filters 3 and 4 will both have a depth of 2 because the input to the second convolutional layer is the two stacked features maps generated by Convolutional layer 1. The last two layers of the network are typical of the types of layers that are used near the output of a convolutional network when it is used for image classification. The second-to-last layer is a dense fully connected layer (i.e., each neuron in this layer receives the complete feature maps generated by Filters 3 and 4 as input) that feeds forward to the **softmax** output layer.

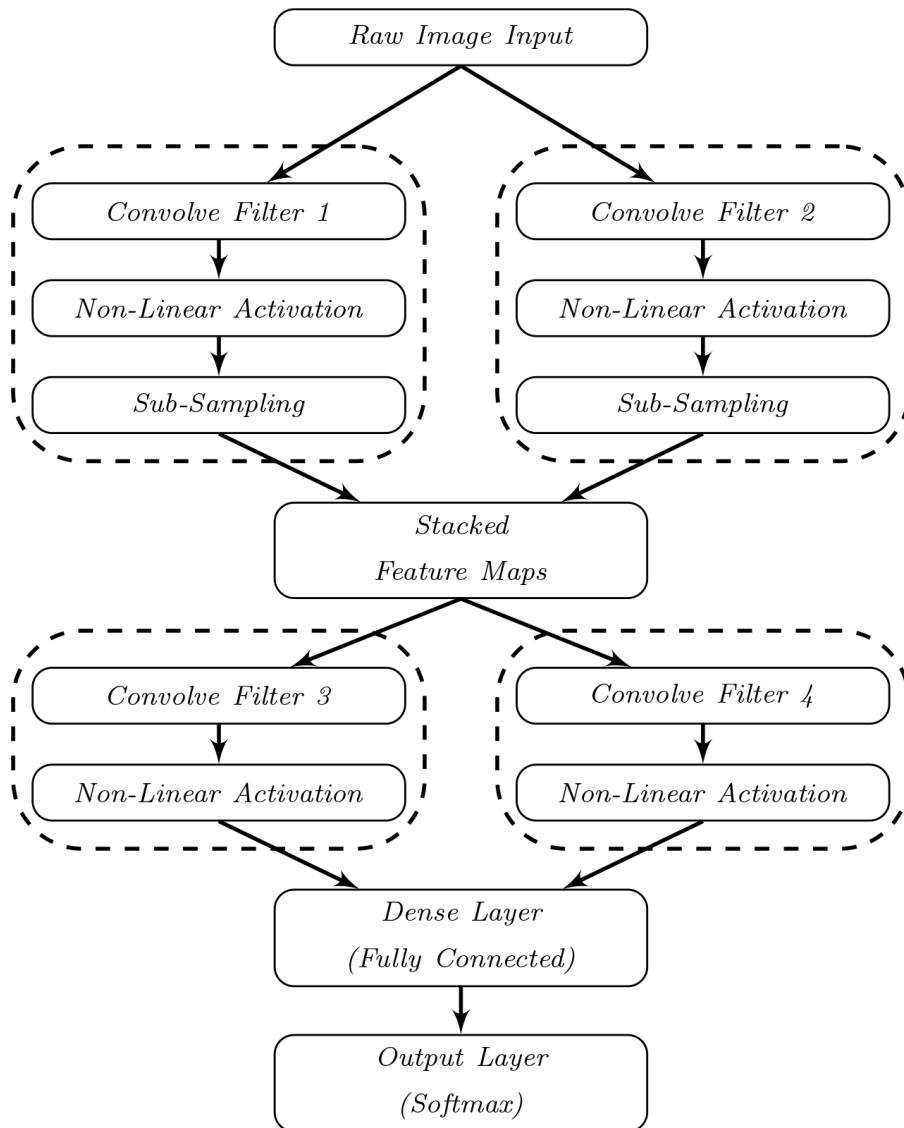


Figure 8.35

Schematic of the typical sequences of layers found in a convolutional neural network.

[Figure 8.36](#)^[498] provides a worked example of data processing and flow through a convolutional network similar in structure to the architecture blueprint shown in [Figure 8.35](#)^[497]. The main structural difference is that the network in [Figure 8.36](#)^[498] does not include a **softmax** output layer. For ease of presentation we have reduced the input image to be a single column of 7 color pixels. We have also simplified the RGB values to be only 1s or 0s, and similarly we have selected values for the filter weight that, hopefully, make it easier to follow the flow of the data processing (rather than filter values that encode meaningful feature detectors). These simplifications

aside, the processing and flow of data through [Figure 8.36](#)^[498] is representative of the flow through a multi-layer, multi-filter convolutional neural network. Starting on the left of the figure, the column of 7 three-channel (RGB) pixels is fed into the first convolutional layer. This first convolutional layer contains two layers of 6 neurons. The 6 neurons in the top layer share the weights in Filter 1, and the 6 neurons in the bottom layer share the weights in Filter 2. Both Filters 1 and 2 have a dimensionality of 2-by-1-by-3. There are 6 neurons in each of these layers because we are assuming a step size of 1, and so it requires six neurons to convolve one of these filters over the 7-by-1-by-3 input. Feature map 1 contains the 6 activations for the 6 neurons that applied Filter 1 to the input, and Feature map 2 contains the 6 activations for the 6 neurons that applied Filter 2 to the input. Note that all the neurons in this network are ReLU, so each of these activations was calculated in each neuron by passing the result of the weighted sum calculation through a rectified linear activation function (similar to the calculation listed in [Equation \(8.102\)](#)^[494]). The first convolutional layer uses a max pooling layer to sub-sample each of the feature maps. The neurons in these max pooling layers have non-overlapping local receptive fields, and each local receptive field covers two cells in a feature map. The results of each of the max pooling layers are then stacked together to create a multi-channel input for the second layer. The dimensions of this input are 3-by-2-by-2, and so all the filters in the second layer have a depth of 2. The second convolutional layer uses two filters (Filters 3 and 4) and so contains two layers of neurons that share weights. The top layer of neurons share the weights in Filter 3, and the bottom layer share the weights in Filter 4. There are two neurons in each of these layers because we are assuming a step size of 1, and so it requires two neurons to convolve a 2-by-1-by-2 filter over the 3-by-2-by-2 input. Feature map 3 and Feature map 4 contain the activations of the neurons in each of these two layers. The final output of the network is generated by a single ReLU that is fully connected to both Feature map 3 and Feature map 4. The weights used by this ReLU are shown on the edges feeding into the unit.

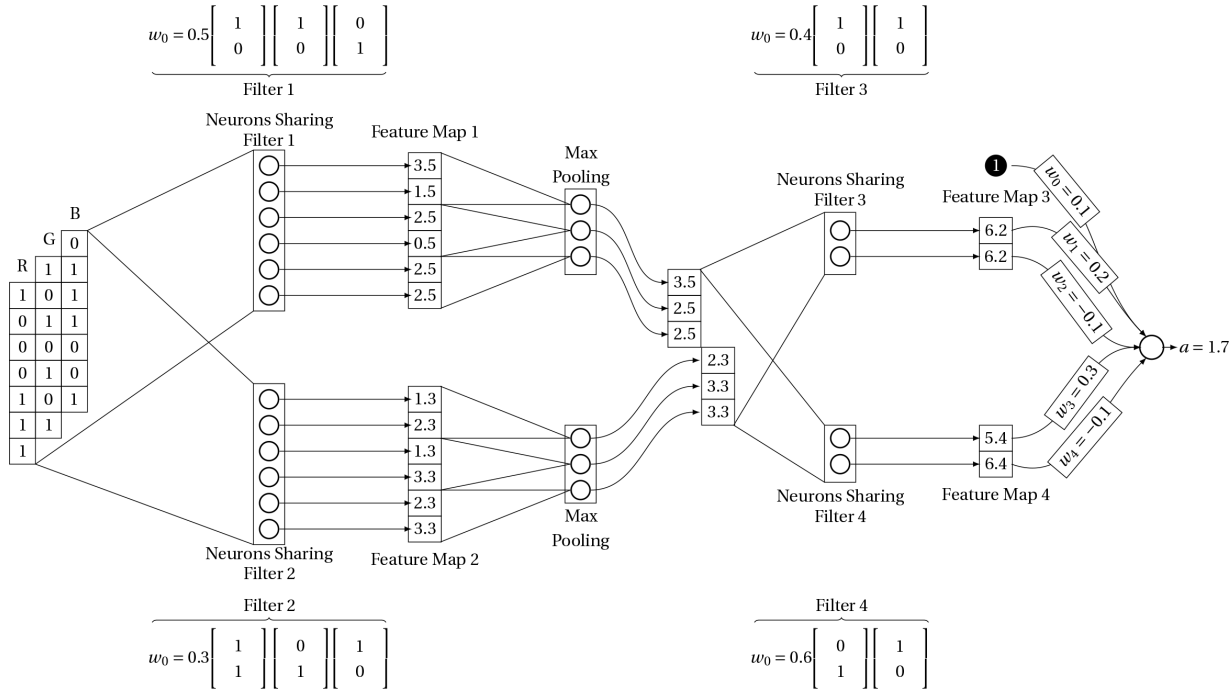


Figure 8.36

Worked example illustrating the dataflow through a multilayer, multifilter CNN.

The data, filter weights, and scale of the network shown in Figure 8.36^[498] have been simplified for the purposes of illustration. Consequently, the overall network output of 1.7 has no particular meaning. A more realistic example of the complexity and scale of a modern convolutional network is the AlexNet network (Krizhevsky et al., 2012). AlexNet is one of the most famous convolutional networks in the history of deep learning. The reason for its fame is that its victory in the ImageNet LargeScale Visual Recognition Challenges (ILSVRC) in 2012 was a watershed moment for deep learning that reinvigorated a lot of interest in the field of neural networks. The AlexNet architecture included five convolutional layers, followed by three fully connected (dense) layers. The first convolutional layer had 96 different filters and used a ReLU non-linearity and max pooling. The second convolutional layer had 256 filters, and also used a ReLU non-linearity and max pooling. The third, fourth, and fifth convolutional layers had 384, 384, and 256 filters, respectively, and none of these layers included a non-linearity or a max pooling operation. The final three dense layers had 4096 neurons each. In total, AlexNet had 60 million weights and 650,000 neurons. Since 2012, however, several larger

convolutional networks have been developed, and new and larger models continue to be announced.

8.4.6 Sequential Models: Recurrent Neural Networks and Long Short-Term Memory Networks

The convolutional neural networks discussed in Section 8.4.5^[477] are ideally suited to processing data that have a fixed-size grid-like structure and where the basic features have a local extent, such as images. There are, however, many domains in which the data has a sequential varying-length structure and in which interactions between data points may span long distances in the sequence. Natural language is an example of this type of data: it is naturally sequential, one word follows the other, each sentence may have a different number of words (varying length), and it contains long-distance dependencies between elements. For example, in English, the subject and verb of a sentence should agree. Compare the sentences “The dog in that house is aggressive” with “The dogs in that house are aggressive.” In the first sentence, the subject of the sentence is singular, *dog*, and so we use the singular form of the verb *is*; in the second sentence, the subject is plural, *dogs*, and so we use the plural form of the verb *are*.⁴⁶ Processing data of this type requires a model that has the capacity to remember relevant information from earlier in the sequence. **Recurrent neural networks** (RNN) are designed to process this type of data.

A recurrent neural network works in discrete time. In processing a sequence, the network takes one input from the sequence at each time point. The defining characteristic of a recurrent neural network is that it contains feedback connections, and so, unlike a feedforward network, which is a directed **acyclic** graph, a recurrent neural network is a directed **cyclic** graph. These cycles, or recurrent links, are the reason these networks are called **recurrent** networks. That a recurrent network contains cycles means that the output from a neuron at one time point may be fed back into the same neuron at another time point. A consequence of this is that the network has a memory over past activations (and hence past inputs that contributed to these activations). This is why these networks are useful for processing sequential data that exhibit long-distance dependencies. There are a variety of different recurrent neural network architectures; in this section we introduce two of the most popular: simple recurrent networks (also known

as Elman networks (Elman, 1990)), and long short-term memory (LSTM) networks (Hochreiter and Schmidhuber, 1997).

8.4.6.1 Simple recurrent neural networks A simple recurrent neural network architecture is a feedforward architecture with one hidden layer that has been extended with a memory buffer that is used to store the activations from the hidden layer for one time-step. On each time-step, the information stored in the memory buffer is concatenated with the next input to each neuron. This process of storing activations in the memory buffer at one time-step and reading from the buffer at the next time-step is how the recurrent connections are implemented.

[Figure 8.37](#)^[502] illustrates the architecture of a simple recurrent network. Note that for ease of presentation the network schematics in this figure have been rotated so that the forward flow of information through each network is from the input layer at the bottom to the output layer at the top. Furthermore, to align with most explanations of recurrent neural networks, in the subsequent discussion we adopt the following conventions: x denotes an input; h denotes a hidden layer; and y denotes the output from the network. The goal of the network schematic on the left of [Figure 8.37](#)^[502] is to provide a high-level overview of the template structure of a simple recurrent neural network. Consequently, in this schematic we have abstracted away from some of the details of a network architecture: for example, the layers of neurons are represented by rectangles with rounded corners; and the (multiple) connections between neurons in different layers are represented by single arrows labeled with the name of the weight matrix for the weights on those connections. The labels on the rectangles indicate whether the rectangle represents the input layer \mathbf{x}_t , the hidden layer \mathbf{h}_t , the output layer \mathbf{y}_t , or the activation buffer that stores the activations of the hidden layer from the previous time-step \mathbf{h}_{t-1} .

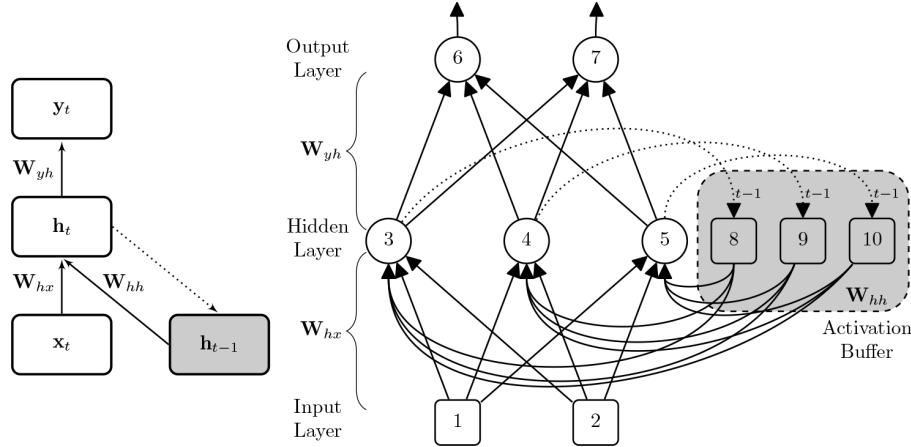


Figure 8.37

Schematic of the simple recurrent neural architecture.

Although there are four sets of connections in this network (input to hidden, hidden to output, hidden to buffer, and buffer to hidden), there are only three weight matrices in the network. There are no weights on the connections between the output of the hidden layer and the memory buffer. The reason is that the transfer of hidden neuron activations to the memory buffer is a simple copy operation. That there are no weights on these connections is indicated in [Figure 8.37^{\[502\]}](#) by a dashed arrow that represents these connections. There are, however, weights on the connections from the memory buffer to each of the neurons. These weights are necessary because the information read from the memory buffer is processed by the hidden neurons in the same way that each of the inputs is. The three weight matrices are

1. \mathbf{W}_{hx} containing the weights for the connections between the input layer (x) and the hidden layer (h);
2. \mathbf{W}_{yh} containing the weights for the connections between the hidden layer (h) and the output layer (y); and
3. \mathbf{W}_{hh} containing the weights for the connections between the memory buffer and the hidden layer. This matrix has the subscript hh because in actuality these weights are applied to recurrent connections from the hidden layer back to the hidden layer.

The network schematic on the right of [Figure 8.37^{\[502\]}](#) illustrates the details of how neurons within the different layers of a specific example

simple recurrent network are connected. This example network has two neurons in the input layer (Neurons 1 and 2), three neurons in the hidden layer (Neurons 3, 4, and 5), and two neurons in the output layer (Neurons 6 and 7). In this example we assume that the hidden neurons and the output layer are ReLUs. At each time-step a new input vector is presented to the network; this flows forward to the hidden layer. Each of the hidden layer neurons receives both the input vector and a vector containing the information stored in the memory buffer at the same time. Processing these inputs, the hidden neurons generate activations that are then propagated forward to the output layer and also written to the activation memory buffer (overwriting whatever information was in the memory buffer). At the next time-step, these new activations are then fed back to the hidden neurons in parallel with the new input.

The forward propagation of the activations through a simple recurrent network is defined as follows (where the subscript t denotes the time-step of the system; and there is one input per time-step—although this input may be a vector of values—and so the subscript t also defines the index in the input sequence of the current input):

$$\mathbf{h}_t = \varphi((\mathbf{W}_{hh} \cdot \mathbf{h}_{t-1}) + (\mathbf{W}_{hx} \cdot \mathbf{x}_t) + \mathbf{w}_0) \quad (8.104)$$

$$\mathbf{y}_t = \varphi(\mathbf{W}_{yh} \cdot \mathbf{h}_t) \quad (8.105)$$

Equation (8.104)^[501] defines how the activations for the hidden layer for input t are generated. This is done in the same way as the previous examples (a weighted summation of inputs followed by the application of a non-linear activation function). The reason why Equation 8.104^[501] has a more complicated form than previously is that the neuron has two sets of inputs (from the input layer and the activation buffer), and so it has two separate weight matrices; also, to be as transparent as possible, we have explicitly represented the bias terms for the weights in a separate vector \mathbf{w}_0 . Stepping through Equation 8.104^[501] we have the following four operations:

1. a dot product between the information stored in the memory buffer (the hidden layer activations from the previous time-step encoded as vector \mathbf{h}_{t-1}) and the weight matrix for the weights on the connections from the memory buffer to the hidden neurons;

2. a dot product between the input vector for this time-step \mathbf{x}_t and the weight matrix for the weights on the connections between the input layer and the hidden layer \mathbf{W}_{hx} ;
3. the summation of the results of these two dot products with the bias terms for the hidden layer neurons; and finally,
4. the weighted sum calculated in Step (3) is passed through a non-linear activation function φ .

As noted, the activation vector \mathbf{h}_t of the hidden layer for input t is propagated forward to the output layer, and also to the memory buffer where it is stored for one time-step. Equation (8.105)^[501] specifies how the output activations \mathbf{y}_t for input t are then generated: a weighted sum is calculated via a dot product operation between the weight matrix \mathbf{W}_{yh} and the activations vector from the hidden layer \mathbf{h}_t , and this is passed through a non-linear activation function φ .

8.4.6.2 Backpropagation through time The fact that a recurrent neural network is fundamentally an augmented feedforward network means that training a network using backpropagation is quite similar to training a normal feedforward network. For example, if the network shown on the right of Figure 8.37^[502] was applied only to a single input, then we would calculate the δ s for the neurons in the output layer.⁴⁷ and then backpropagate these δ s to the hidden layer neurons. The main novelty in this scenario is that the neurons in the hidden layer of a simple recurrent neural network have two weight matrices associated with them: \mathbf{W}_{hx} and \mathbf{W}_{hh} . However, for the purposes of updating the weights on the connections into a hidden layer neuron, this distinction is irrelevant and the same δ is used to update all the weights on the connections into a neuron.

Things become a little more complex when a recurrent network is applied to a sequence of inputs. The variant of backpropagation used to train a recurrent neural network is called **backpropagation through time**. A recurrent neural network is deliberately designed so that when the network processes an input at time t in a sequence, the output generated is dependent not only on input t but also on the previous inputs in the sequence. This means that the error for the output at time t is also dependent on the states of the network for all the previous inputs in the sequence ($t-1$,

$t-2$, and so on) back to the start of the sequence. Backpropagation works by using the chain rule to assign blame to each of the model's parameters (weights) in proportion to the sensitivity of the network's error to changes in those weights. This means that we must backpropagate the error at time t to all the parameters that contributed to the error. In other words we must backpropagate the error back through the previous states of the network. Hence the name *backpropagation through time*: as we backpropagate through the previous states of the network, we are in effect going back through time.

[Figure 8.38](#)^[504] provides a graphical representation of a recurrent neural network unrolled through three time-steps.⁴⁸ The subscripts on the \mathbf{x} , \mathbf{h} , and \mathbf{y} layer labels indicate that these layers have a different state at each time-step. The box labeled \mathbf{h}_0 represents that state of the activation memory buffer when the model is initialized. The activation memory buffer is not shown in this figure because the feedback loop of storing the hidden state activations from one time-step in the buffer and reading from the buffer at the next time-step is represented by the horizontal arrows between each \mathbf{h}_t layer. Notice that unlike the layers, the weight matrices do not have a time subscript on them. The reason is that the network uses the same weights to process Input 1 as it does to process Input 3. This means that even though the network is unrolled through three time-steps, it still has only 3 weight matrices (not 9). In a sense, the unrolled recurrent neural network is similar to a convolutional neural network in that weights are shared between different neurons: the neurons in the hidden layer at time $t = 1$ use exactly the same weights as the neurons in the hidden layer at time $t = 2$ and $t = 3$, and so on. Understanding that we are dealing with shared weights is important because the standard process for updating a shared weight is (a) to calculate the weight update for the weight at each location in the network where it is used; (b) to sum these weight updates together; and (c) finally to update the weight once using this summed weight update. This is exactly what we do to update the weights in our recurrent neural network.

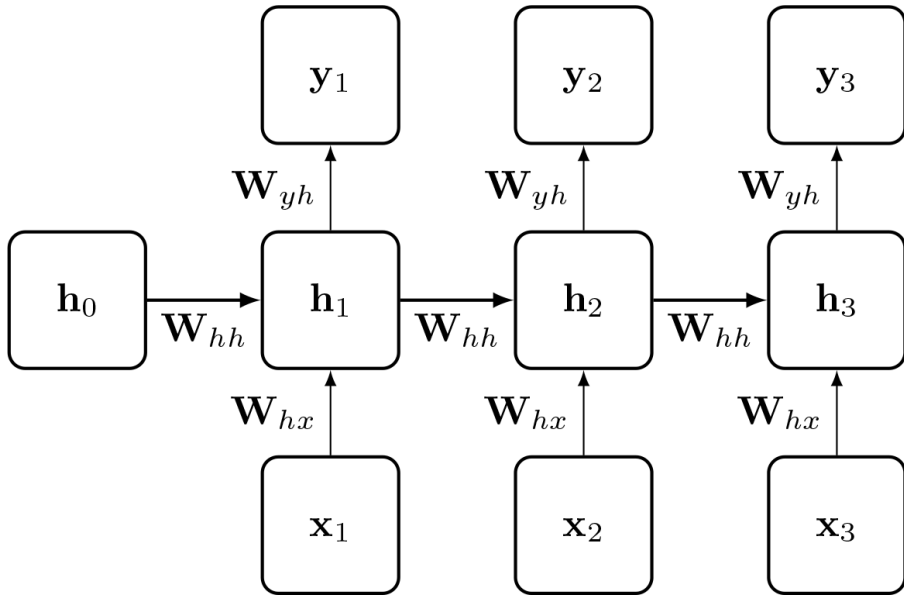


Figure 8.38

A simple RNN model unrolled through time (in this instance, three time-steps).

To train a recurrent neural network using backpropagation through time, we first do a forward pass by presenting each input in the sequence in turn and unrolling the network through time (as shown in [Figure 8.38^{\[504\]}](#)). The unrolling of the network through time during the forward pass means that some neurons⁴⁹ will occur multiple times in the unrolled network, and we store the weighted sum z value and activation value a of each neuron at each time-step. This is the same process that we use for the forward pass of a standard feedforward network (see [Figure 8.11^{\[406\]}](#)); the slightly complicating factor here is that in an unrolled recurrent network a neuron may occur multiple times (for example, neurons in the hidden layer will occur once for each time-step), and so for each neuron we have a timestamped sequence of z and a values.

Once the forward pass is complete, we calculate an error term for each of the outputs of the network. The total error of the network is then the sum of these individual errors. For the network in [Figure 8.38^{\[504\]}](#) we would calculate three errors: one for y_1 , one for y_2 , and one for y_3 . Each of these errors is then backpropagated through the unrolled network. [Figure 8.39^{\[506\]}](#) illustrates the path taken by the error gradients as each error for each time-step is backpropagated through the network. [Figure 8.39^{\[506\]}](#) also shows how often each weight matrix was used in the generation of each output. For

example, \mathbf{W}_{yh} was involved once in the generation of \mathbf{y}_3 whereas \mathbf{W}_{hh} and \mathbf{W}_{hx} were involved three times. The fact that a weight matrix may be involved multiple times in the generation of an output means that backpropagating the error for an output can result in multiple error gradients being calculated for a weight: one error gradient for each time the weight was involved in generating the output. For example, if we examine [Figure 8.39](#)^[506] we see that when $\mathcal{E}_{t=3}$ is backpropagated through the network, a single error gradient is calculated for each weight in \mathbf{W}_{yh} because this matrix occurs only once in the unrolled network, but three separate error gradients are calculated for each weight in \mathbf{W}_{hh} and \mathbf{W}_{hx} . This is why during the forward pass we unrolled the network and stored a separate weighted sum z and activation a for each occurrence of a neuron in the unrolled network. As we backpropagate through each time-step in the unrolled network, we use the corresponding weighted sum z and activation a for a neuron at that time-step to backpropagate the error gradient for that neuron. In backpropagating the error $\mathcal{E}_{t=2}$ we will calculate a single error gradient for each weight in \mathbf{W}_{yh} and two error gradients for each weight in \mathbf{W}_{hh} and \mathbf{W}_{hx} ; when we backpropagated the error for \mathbf{y}_1 we calculated one error gradient for each weight in each of the three weight matrices. Once we have calculated all these error gradients for a sequence, we then update each weight by summing all the error gradients for that weight and then using the summed error gradient to update the weight. This means that for the example in [Figure 8.39](#)^[506] we would sum three error gradients for each weight in \mathbf{W}_{yh} and six error gradients for each weight in \mathbf{W}_{hh} and each weight in \mathbf{W}_{yx} . As we mentioned previously, this is similar to the way the error gradients for shared weights in a convolutional neural network are summed, and then the weight is updated once using this summed gradient.

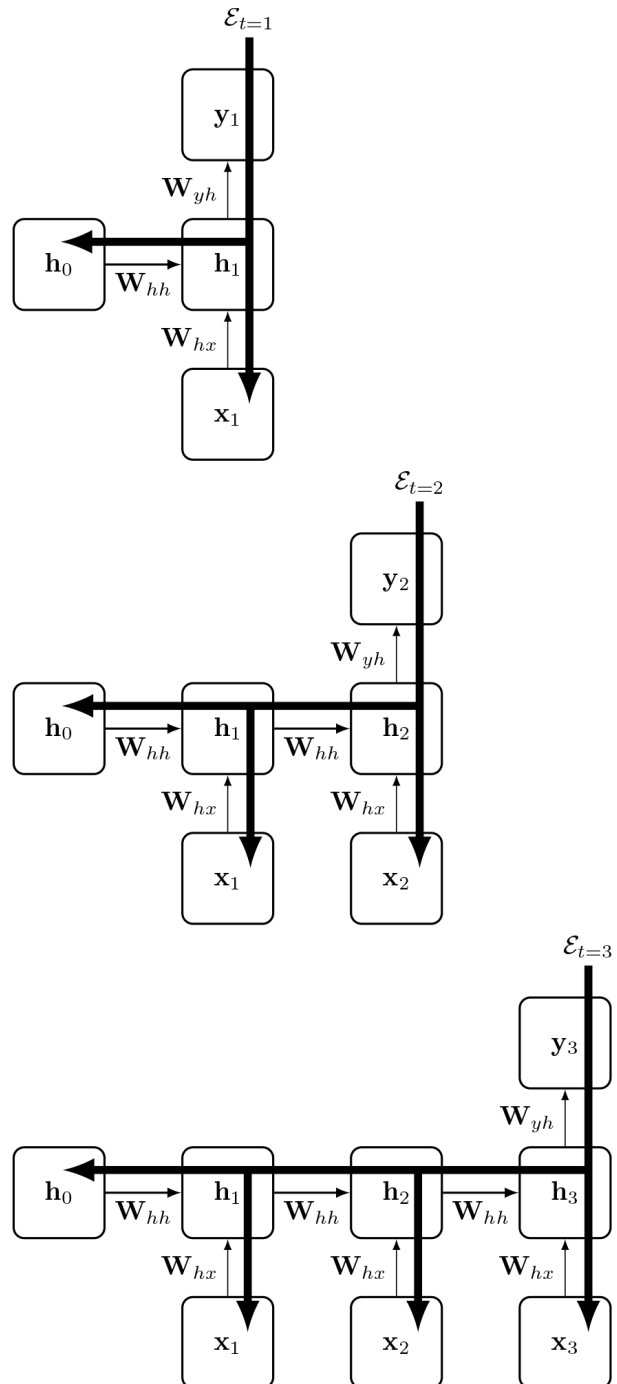


Figure 8.39

An illustration of the different iterations of backpropagation during backpropagation through time.

Note that in [Figure 8.38](#)^[504] we have shown the network generating an output for each input it receives. However, recurrent networks are quite flexible and can be deployed in different scenarios. For example, it may be that the network outputs only a single value once it has processed the whole

sequence; this scenario might hold if we were training a network to process a sentence and then return a label describing the sentiment—*positive* or *negative*—expressed in the sentence. In this case we would calculate an error (or loss) only at the output at the end of the sequence. This error is then backpropagated through the unrolled network, in the same way that $\mathcal{E}_{t=3}$ is backpropagated in Figure 8.39^[506] resulting in a single error gradient for each weight in \mathbf{W}_{yh} and three separate error gradients for each weight in \mathbf{W}_{hh} and \mathbf{W}_{hx} . Again, the error gradients for a weight are summed and then the weight is updated once.

For long sequences of inputs it can become cumbersome and also computationally expensive to keep track of all the error gradients for all the different weights in the unrolled network. Consequently, a common practice when training a recurrent neural network to process a long sequence is to break the sequence up into subsequences. A typical size for a subsequence might be 20 inputs. The forward and backward pass is then carried out on each subsequence in turn: in the forward pass the network is unrolled over a subsequence, and in the backward pass the error gradients are backpropagated only through this truncated unrolled network. Information can flow forward from one subsequence to the next by using the hidden state of the network at the end of processing one subsequence to initialize the activation buffer at the start of the next subsequence. Algorithm 8^[507] provides a pseudocode definition of the backpropagation through time algorithm for a single sequence of input-output pairs of length n .

Algorithm 8 The Backpropagation Through Time Algorithm

Require: h_0 initialized hidden state
Require: \mathbf{x} a sequence of inputs
Require: \mathbf{y} a sequence of target outputs
Require: n length of the input sequence
Require: Initialized weight matrices (with associated biases)
Require: $\Delta\mathbf{w}$ a data structure to accumulate the summed weight updates for each weight across time-steps

- 1: **for** $t = 1$ to n **do**
- 2: $Inputs = [x_0, \dots, x_t]$
- 3: $h_{tmp} = h_0$
- 4: **for** $i = 0$ to t **do** ▷ Unroll the network through t steps
- 5: $h_{tmp} = ForwardPropagate(Inputs[i], h_{tmp})$
- 6: **end for**
- 7: $\hat{y}_t = OutputLayer(h_{tmp})$ ▷ Generate the output for time-step t
- 8: $\mathcal{E}_t = \mathbf{y}[t] - \hat{y}_t$ ▷ Calculate the error at time-step t
- 9: $Backpropagate(\mathcal{E}_t)$ ▷ Backpropagate \mathcal{E}_t through t steps
- 10: For each weight, sum the weight updates across the unrolled network and update $\Delta\mathbf{w}$
- 11: **end for**
- 12: Update the network weights using $\Delta\mathbf{w}$

In Section 8.4.4^[472] we introduced **dropout** as one of the standard methods used to stop a deep learning network from overfitting. Using dropout during the training of a recurrent neural network can be problematic because dropping different neurons from the network at different time-steps across a sequence can stop the network from propagating important information forward through the sequence. The standard technique for applying dropout to a recurrent neural network during training is known as **variational RNN** (Goldberg, 2017). In variational RNN, the dropout mask is selected once per sequence (rather than at each input), and so the same neurons are dropped across all time-steps in the sequence; for more details see Gal and Ghahramani (2016).

8.4.6.3 Long short-term memory networks Recurrent neural networks are particularly susceptible to the **exploding gradients** and **vanishing gradients** problems we discussed in Section 8.4.1^[434] and Section 8.4.2^[447].

The reason is that during the backward pass, error gradients will be multiplied by the \mathbf{W}_{hh} matrix multiple times—once for each time-step through which we backpropagate. This repeated multiplication of the error gradient can rapidly scale up the size of the gradient if a weight in \mathbf{W}_{hh} is > 1 (causing our weight updates to become too large and our training to become unstable) or cause the gradient to vanish if the weight is very small. As a result, although in principle a recurrent neural network has the ability to propagate information across the spans of long-distance dependencies in input sequences, the vanishing and exploding gradient problems limit the ability of these networks to learn these dependencies.

Long short-term memory (LSTM) networks are specifically designed to improve the ability of a recurrent network to model dependencies over long distances in a sequence (Hochreiter and Schmidhuber, 1997). They achieve this goal by removing the repeated multiplication by the \mathbf{W}_{hh} matrix during backpropagation. [Figure 8.40](#)^[509] illustrates the internal structure of an LSTM unit. Note that each line in [Figure 8.40](#)^[509] represents a vector of activations, and the $+$ symbol represents an elementwise vector addition and \odot represents an elementwise vector product. The fundamental element in an LSTM network is the **cell**. In [Figure 8.40](#)^[509] the cell is depicted by the line extending from \mathbf{c}_{t-1} to \mathbf{c}_t across the top of the diagram. The cell provides a path that carries the activations of the network forward through the time-steps as the network processes a sequence. The activations in the cell can take values in the range $[-1, +1]$. The propagation of activations along the cell is controlled by three **gates**: the **forget gate**, the **input gate**, and the **output gate**. The forget gate removes information from the cell, the input gate adds information to the cell, and the output gate decides which information should be output by the network at the current time-step.

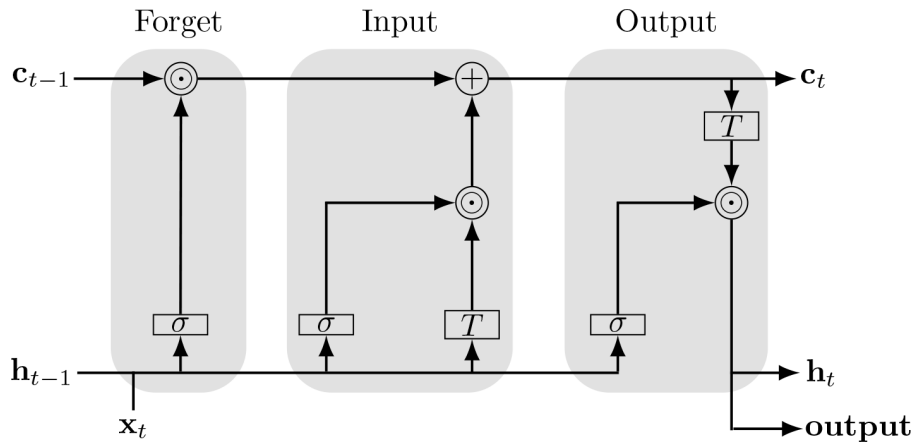


Figure 8.40

A schematic of the internal structure of a long short-term memory unit. In this figure a σ represents a layer of neurons that use a sigmoid activation function, a T represents a layer of neurons that use a tanh activation function, the \odot symbols represent elementwise vector multiplication (i.e., the Hadamard product), and $+$ represents an elementwise vector addition operation. This figure is based on Figure 5.4 of Kelleher (2019), which in turn was inspired by an image by Christopher Olah (available at: <http://colah.github.io/posts/2015-08-Understanding-LSTMs/>).

The input to all three of these gates is the vector of hidden state activations propagated forward from the previous time-step h_{t-1} concatenated with the current input vector x_t . In Figure 8.40^[509] this concatenation is depicted by the intersection of the h_{t-1} and x_t lines in the bottom-left corner of the figure. We use the term hx_t to write the vector that is the result of concatenating h_{t-1} with x_t . For example, if $h_{t-1} = [a,b]$ and $x_t = [c,d]$, then $hx_t = [a,b,c,d]$.

The flow of information in Figure 8.40^[509] is from left to right. The **forget gate** is the leftmost gate in Figure 8.40^[509], and it is the first gate to process the inputs to the time-step. The **forget gate** works by passing hx_t through a layer of neurons that use sigmoid activation functions. This layer of neurons is the same width as the LSTM cell, and so there is one activation in the output of the sigmoid layer for each activation in the cell state. Next, an elementwise product of the vector of activations in the cell state c_{t-1} with the vector of activations from the sigmoid layer is performed. This elementwise product is depicted in Figure 8.40^[509] by the \odot symbol at the intersection of the cell state and the output of the forget gate sigmoid layer in the top-left of the figure. The sigmoid activation function outputs values in the range 0 to 1 so that the multiplication of the cell state by the

sigmoid layer activations has the effect of pushing all the cell state activations that have a corresponding sigmoid activation near 0 to 0 (i.e., these activations are forgotten) and all the cell state activations that have a corresponding sigmoid activation near 1 to be maintained (i.e., they are remembered) and propagated forward. Equation (8.106)^[509] defines the calculation of the forget mask for time-step t , and Equation (8.107)^[509] defines the filtering of the cell state by the forget mask. Note that we use the notation \mathbf{c}^\ddagger to represent the vector of activations in the cell state in the interval between the update by the forget gate and the subsequent update by the input gate

$$\mathbf{f}_t = \varphi_{sigmoid}(\mathbf{W}^{(f)} \cdot \mathbf{hx}_t) \quad (8.106)$$

$$\mathbf{c}^\ddagger = \mathbf{c}_{t-1} \odot \mathbf{f}_t \quad (8.107)$$

where \mathbf{hx}_t is the concatenation of \mathbf{h}_{t-1} and \mathbf{x}_t ; and $\mathbf{W}^{(f)}$ is the forget gate matrix of weights. For example, imagine an LSTM unit with the inputs and $\mathbf{W}^{(f)}$ matrix (the zeros are the bias terms) as listed in Equation (8.108)^[510]

$$\begin{aligned} \mathbf{c}_{t-1} &= \begin{bmatrix} 1 \\ 1 \\ 1 \end{bmatrix} \mathbf{h}_{t-1} = \begin{bmatrix} 1 \\ 1 \end{bmatrix} \mathbf{x}_t = [4] \\ \mathbf{W}^{(f)} &= \begin{bmatrix} 0 & 1 & 1 & 1 \\ 0 & -1 & -1 & -1 \\ 0 & 0 & 0 & 0 \end{bmatrix} \end{aligned} \quad (8.108)$$

Given this context, the processing of the forget gate would be as follows (note that in this calculation \mathbf{hx}_t is augmented with a bias input 1):

$$\begin{aligned}
& \underbrace{\begin{bmatrix} 0 & 1 & 1 & 1 \\ 0 & -1 & -1 & -1 \\ 0 & 0 & 0 & 0 \end{bmatrix}}_{\mathbf{w}^{(f)}} \times \underbrace{\begin{bmatrix} 1 \\ 1 \\ 1 \\ 4 \end{bmatrix}}_{\mathbf{h}\mathbf{x}_t} = \underbrace{\begin{bmatrix} 6 \\ -6 \\ 0 \end{bmatrix}}_{\mathbf{z}_t^{(f)}} \rightarrow \varphi_{sigmoid} \rightarrow \underbrace{\begin{bmatrix} 0.997527377 \\ 0.002472623 \\ 0.500000000 \end{bmatrix}}_{\mathbf{f}_t} \\
& \underbrace{\begin{bmatrix} 0.997527377 \\ 0.002472623 \\ 0.500000000 \end{bmatrix}}_{\mathbf{f}_t} \odot \underbrace{\begin{bmatrix} 1 \\ 1 \\ 1 \end{bmatrix}}_{\mathbf{c}_{t-1}} = \underbrace{\begin{bmatrix} 0.997527377 \\ 0.002472623 \\ 0.500000000 \end{bmatrix}}_{\mathbf{c}^{\ddagger}}
\end{aligned} \tag{8.109}$$

Notice that because of the way that the sigmoid activation function operates, large positive values in the $\mathbf{Z}_t^{(f)}$ vector (i.e., + 6) are mapped to values close to 1 in \mathbf{f}_t : 0.002472623, whereas large negative values in $\mathbf{Z}_t^{(f)}$ (such as - 6) are mapped to values near 0; and $\mathbf{Z}_t^{(f)}$ values near 0 are mapped to values around 0.5. Comparing each term in \mathbf{c}_{t-1} with the corresponding term in \mathbf{c}^{\ddagger} illustrates how the elementwise product of \mathbf{f}_t updates the cell state. For example, the first value in \mathbf{c}_{t-1} is 1, and this is multiplied by an \mathbf{f}_t value near 1 resulting in a \mathbf{c}^{\ddagger} value of 0.997527377. This \mathbf{c}^{\ddagger} value is very close to the original \mathbf{c}_{t-1} , which shows that the forget gate has largely retained the value in the cell state (or in other words, the cell state has largely remembered this value). However, the second value in \mathbf{c}_{t-1} is also 1 but this is multiplied by an \mathbf{f}_t value near zero resulting in a \mathbf{c}^{\ddagger} value of 0.002472623. In this case, the forget gate has largely erased the original cell value from the cell state (i.e., the cell state has now forgotten the original value). Finally, the third term in \mathbf{c}_{t-1} is multiplied by an \mathbf{f}_t of 0.5, which results in the value of 0.5 in \mathbf{c}^{\ddagger} . This last term illustrates an intermediate behavior in the forget gate in which the original cell state is half-forgotten/half-retained.

The fundamental information processing pattern within the forget gate can be characterized as passing the concatenated $\mathbf{h}\mathbf{x}_t$ vector through a layer of sigmoid neurons in order to generate a vector mask, and then using an elementwise product of this mask with the cell state to update (or filter) the cell's activations. This information processing pattern of creating a vector

mask and then using it in an elementwise product to update another activation vector is present in both of the other gates in an LSTM.

The task of the **input gate** is to decide, on the basis of the current input and the propagated hidden state (\mathbf{hx}_t), *which* elements of the cell state, \mathbf{c}^\pm , should be updated and *how* these elements should be updated. The input gate uses separate paths of information processing to make each of these decisions and then merges the results of these decisions using an elementwise product. The first path of information processing in the input gate decides *which* elements of the cell state should be updated. In this first path of processing \mathbf{hx}_t is passed through a layer of sigmoid units that is the same width as the cell state. The output of this layer of neurons is a vector mask, in which each element in the vector is in the range [0,1]. A value near 1 indicates that the corresponding element of the cell state should be updated, and a value near 0 indicates that the corresponding element of the cell state should be preserved as is. This first path of information processing in the input gate is similar to the process used in the forget gate; however, in this case the generate vector mask is not applied directly to the cell state but rather is used to filter the vector of output activations generated by the second path of processing in the input gate. In this second path of processing \mathbf{hx}_t is passed through a layer of tanh units. The layer of tanh units is as wide as the cell state and so there is one tanh activation per activation in the cell state. The tanh activation function outputs values in the range [-1,+1]. The fact that the tanh function has a range of [-1,+1] means that activations in the cell state can be both increased and decreased at each time-step. If the LSTM used only sigmoid units, then the activations in the cell would monotonically increase across time and this would have the unwanted consequence of the cell state tending to saturate with maximum activations as the sequence of time-steps increases, irrespective of the inputs. These two paths of processing are then merged using an elementwise product operation between the tanh activations and the sigmoid activations (i.e., the vector mask). The cell state is then updated by adding the vector generated by the elementwise produce of the tanh and sigmoid activations. The state of the cell after the update gate is the cell state that is propagated forward to the next time-step, and so after this

update the cell state is now \mathbf{c}_t (rather than \mathbf{c}^\ddagger). The calculations in the input gate are defined by the following equations:

$$\mathbf{i}_t^\dagger = \varphi_{\text{sigmoid}}(\mathbf{W}^{(i\dagger)} \cdot \mathbf{h}\mathbf{x}_t) \quad (8.110)$$

$$\mathbf{i}_t^\ddagger = \varphi_{\text{tanh}}(\mathbf{W}^{(i\ddagger)} \cdot \mathbf{h}\mathbf{x}_t) \quad (8.111)$$

$$\mathbf{i}_t = \mathbf{i}_t^\dagger \odot \mathbf{i}_t^\ddagger \quad (8.112)$$

$$\mathbf{c}_t = \mathbf{c}^\ddagger + \mathbf{i}_t \quad (8.113)$$

The fact that the input gate has two paths of processing means that it uses two separate weight matrices to process the input, one on each processing path. In these equations we distinguish between these two paths of data processing and the weight matrices using the \dagger and \ddagger . The \dagger symbol marks the path of processing that generates the vector mask that controls *which* activations in the cell state are updated (see Equation (8.110)^[511]). The \ddagger symbol marks the path of processing that generates the candidate cell update, prior to the filtering by the vector mask (see Equation (8.111)^[511]). This distinction between the processing paths is why the weight matrix in Equation (8.110)^[511] has a \dagger in the superscript (i.e., $\mathbf{W}^{(i\dagger)}$) whereas the weight matrix in Equation (8.111)^[511] has a \ddagger . Equation (8.112)^[511] defines how these the two paths of processing are merged using an elementwise product, denoted by the \odot term. Finally, Equation (8.113)^[511] specifies how the cell state, post the forget gate, is updated by the input gate to generate the cell state for this time-step \mathbf{c}_t .

The task of the **output gate** is to decide which parts of the \mathbf{c}_t should be passed to the output layer of the network and on to the next time-step as the propagated hidden state. Similar to the input gate, the **output gate** has two paths of processing, one involving a sigmoid layer and the other involving a tanh layer. The functioning of the output gate has a similar interpretation as the input gate: the tanh layer decides what information might be relevant to output from the current cell state, and the sigmoid layer uses the $\mathbf{h}\mathbf{x}_t$ vector to decide which activations are most relevant to output at this time-step. The output gate uses a three-step process:

1. the vector of cell activations \mathbf{c}_t is passed through a layer of tanh units to create a vector of candidate output activations;

2. the \mathbf{hx}_t vector is passed through a layer of sigmoid units to generate a vector mask that in this instance will control which of the activations within the candidate output vector will actually be propagated to the output layer; and
3. the two vectors of activations generated by Steps 1 and 2 are merged using an elementwise product, and the result of this operation is the vector of activations that is propagated to the output layer.

These processing steps are described mathematically in the following equations:

$$\mathbf{o}^\dagger_t = \varphi_{sigmoid}(\mathbf{W}^{(o\dagger)} \cdot \mathbf{hx}_t) \quad (8.114)$$

$$\mathbf{o}^\ddagger_t = \varphi_{tanh}(\mathbf{W}^{(o\ddagger)} \cdot \mathbf{c}_t) \quad (8.115)$$

$$\mathbf{o}_t = \mathbf{o}^\dagger_t \odot \mathbf{o}^\ddagger_t \quad (8.116)$$

$$\mathbf{h}_{t+1} = \mathbf{o}_t \quad (8.117)$$

Similar to the equations for the input gate, we use the symbols \dagger and \ddagger to distinguish the different paths of information processing in the output gate. Equation (8.114)^[512] describes how the output gate uses the \mathbf{hx}_t vector to generate the vector mask \mathbf{o}^\dagger_t , that filters what activations are sent to the output layer and also propagated forward as the next hidden state; Equation (8.115)^[512] specifies how the current cell state \mathbf{c}_t is passed through a layer of tanh units to generate a candidate output vector \mathbf{o}^\ddagger_t ; and Equation (8.116)^[512] describes how the actual output vector that is propagated to the output layer \mathbf{o}_t is generated using an elementwise product of the vector mask \mathbf{o}^\dagger_t and the candidate output vector \mathbf{o}^\ddagger_t . Finally, Equation (8.117)^[512] ensures that the vector of activations that is propagated to the output layer is the same vector that is propagated to the next time-step as the LSTM hidden state.

Bringing all the LSTM equations together specifies the sequence of calculations that occur in the forward pass of an LSTM

$$\begin{aligned}
\mathbf{f}_t &= \varphi_{sigmoid}(\mathbf{W}^{(f)} \cdot \mathbf{h}_{t-1}) \\
\mathbf{c}_t^{\pm} &= \mathbf{c}_{t-1} \odot \mathbf{f}_t \\
\mathbf{i}_t^{\dagger} &= \varphi_{sigmoid}(\mathbf{W}^{(i\dagger)} \cdot \mathbf{h}_{t-1}) \\
\mathbf{i}_t^{\ddagger} &= \varphi_{tanh}(\mathbf{W}^{(i\ddagger)} \cdot \mathbf{h}_{t-1}) \\
\mathbf{i}_t &= \mathbf{i}_t^{\dagger} \odot \mathbf{i}_t^{\ddagger} \\
\mathbf{c}_t &= \mathbf{c}_t^{\pm} + \mathbf{i}_t \\
\mathbf{o}_t^{\dagger} &= \varphi_{sigmoid}(\mathbf{W}^{(o\dagger)} \cdot \mathbf{h}_{t-1}) \\
\mathbf{o}_t^{\ddagger} &= \varphi_{tanh}(\mathbf{W}^{(o\ddagger)} \cdot \mathbf{c}_t) \\
\mathbf{o}_t &= \mathbf{o}_t^{\dagger} \odot \mathbf{o}_t^{\ddagger} \\
\mathbf{h}_{t+1} &= \mathbf{o}_t
\end{aligned}$$

LSTMs have a complex internal structure containing multiple layers of neurons, and they can be considered networks in their own right. However, they can also be used as the building block of a recurrent neural network. This is achieved by replacing the hidden layer in a recurrent neural network with an LSTM unit. LSTMs have proven very successful at processing language; for example, they are currently the standard network used for speech recognition on mobile phones.

[Figure 8.41](#)^[514] presents a worked example of the forward propagation of activations through an LSTM unit. In this example, the cell state propagated forward from the previous time-step is $\mathbf{c}_{t-1} = [0.3, 0.6]$; the hidden state propagated forward from the previous time-step is $\mathbf{h}_t = [0.1, 0.8]$; and the input at the $\mathbf{x}_t = [0.9]$. In this instance, the weights for the different matrices in the LSTM unit are randomly sampled from a normal distribution $\mu = 0, \sigma = 0.1$, and the bias terms have been initialized to 0. In this figure, the activation flow through the gates is ordered vertically: the top row of the figure illustrates the flow through the forget gate; the next two rows illustrate the flow through the two paths of the input gate; and the bottom two rows illustrate the flow through the two paths of the output gate. The vector of activations that the unit would propagate forward as the cell state for the next time (\mathbf{c}_t) step is shown on the top right of the figure, and the vector of activations \mathbf{o}_t that the unit would propagate both to the output layer for this time-step and on to the next time-step as the hidden state is shown in the bottom-right of the figure.

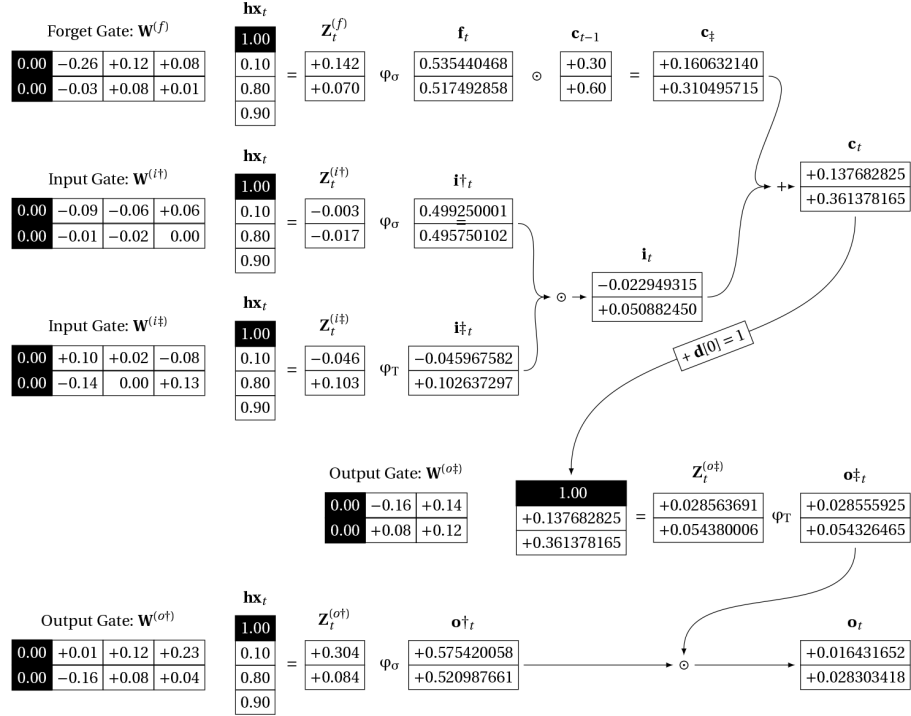


Figure 8.41

The flow of activations through a long short-term memory unit during forward propagation when $\mathbf{c}_{t-1} = [0.3, 0.6]$, $\mathbf{h}_t = [0.1, 0.8]$, and $\mathbf{x}_t = [0.9]$.

It is standard that hidden state \mathbf{h} and the cell state \mathbf{c} have the same size. The larger the size of the hidden state, the larger the representational capacity of the LSTM. In this example, the hidden state has a size of 2; however, typically the size of the hidden state is much larger. For example, it is not uncommon to see sizes of 128, 256, 512, and 1,024. The dimensions of the weight matrices are determined by the size of the hidden state. If \mathbf{H} is the size of the hidden state, and the input \mathbf{x} has a dimension of n (in this example $n = 1$), then the dimensions of the weight matrices in the forget gate and input gate ($\mathbf{W}^{(f)}$, $\mathbf{W}^{(i†)}$, and $\mathbf{W}^{(i‡)}$) and the sigmoid layer in the output gate ($\mathbf{W}^{(o†)}$), including bias terms is: $\mathbf{H} \times (1 + n + \mathbf{H})$. This ensures that there are \mathbf{H} neurons in the layers in these gates. As a result, irrespective of the width of the input \mathbf{x} , the activation vectors for these layers will be the same size as the cell state \mathbf{c} , and so the dimensions of the vectors in the elementwise operations that update the cell state will match. Figure 8.41^[514] shows the dimensions of the different weight matrices in the unit where $\mathbf{H} = 2$ and $n = 1$. In this unit each of these weight matrices has dimensions 2×4 . The weight matrix for the tanh layer in the output gate ($\mathbf{W}^{(o‡)}$, including bias

terms, has dimensions $\mathbf{H} \times (1 + \mathbf{H})$. This ensures that the output vector from this layer \mathbf{o}_t^\dagger is the same size as \mathbf{H} and so is the correct dimensions for the elementwise product with the \mathbf{o}_t^\dagger vector, and also that the vector resulting from this operation will have a size of \mathbf{H} . This is important because it ensures that \mathbf{h}_{t-1} and \mathbf{h}_t are the same size.

8.4.6.4 Backpropagating through an LSTM cell Figure 8.42^[516] illustrates the flow of error gradients through an LSTM during backpropagation. In this figure the error gradients flow from right to left. The backpropagation process within an LSTM begins with three vectors of error gradients

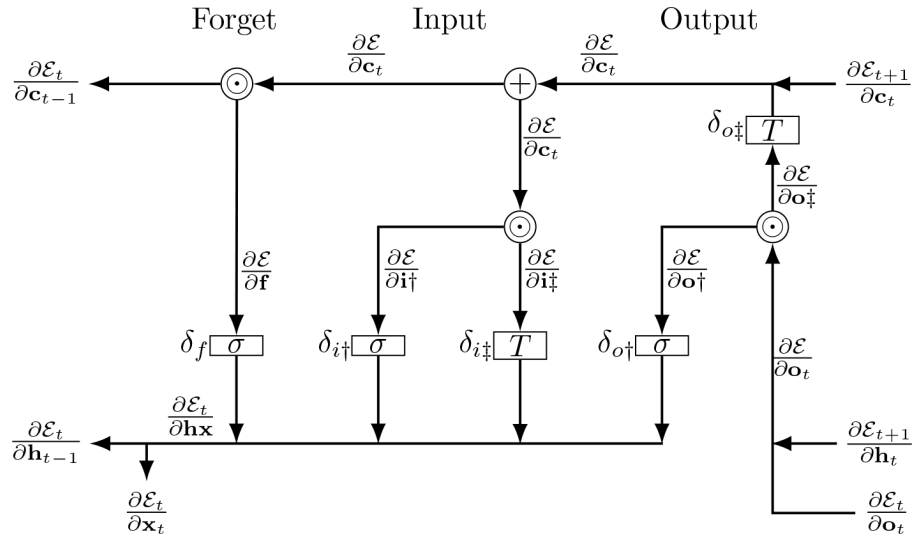


Figure 8.42

The flow of error gradients through a long short-term memory unit during backpropagation.

1. $\partial\mathcal{E}/\partial\mathbf{o}_t$: the rate of change of the error of the network at time-step t with respect to changes in the activation vector \mathbf{o}_t that was propagated to the output layer during the forward pass;
2. $\partial\mathcal{E}_{t+1}/\partial\mathbf{h}_t$: the rate of change of the error of the network at time-step $t+1$ with respect to changes in the activation vector \mathbf{h}_t that was propagated forward to the next time-step during the forward pass; and
3. $\partial\mathcal{E}_{t+1}/\partial\mathbf{c}_t$: the rate of change of the error of the network at time-step $t+1$ with respect to changes in the cell state \mathbf{c}_t that was propagated forward to the next time-step during the forward pass.

During the forward pass of an LSTM unit, there are three operations on activation vectors that are novel with respect to the other network architectures we have examined: forks in computational flow, elementwise products of vectors, and elementwise addition of vectors. To be able to backpropagate error gradients through an LSTM, we need to understand how the novel operations in the forward pass are handled in the backward pass.

A fork in computational flow during forward propagation results in the same activation vector flowing in two directions, with each path generating error gradients that must be merged in the backpropagation stage. This occurs twice in an LSTM: (1) the cell state \mathbf{c}_t vector flows forward into the next time-step and is also passed through a tanh layer as part of the output layer; and (2) the vector of output activations \mathbf{o}_t flows forward to both the output layer and the next time-step (as the propagated hidden state \mathbf{h}_t). Forks in the forward computation flow are handled in backpropagation by summing the derivatives that are flowing back along each of the fork branches. For example, in [Figure 8.42](#)^[516] the vector of error gradients $\partial\mathcal{E}/\partial\mathbf{o}_t$ is calculated using an elementwise addition of $\partial\mathcal{E}_t/\partial\mathbf{o}_t$ and $\partial\mathcal{E}_{t+1}/\partial\mathbf{h}_t$

$$\frac{\partial\mathcal{E}}{\partial\mathbf{o}_t} = \frac{\partial\mathcal{E}_t}{\partial\mathbf{o}_t} + \frac{\partial\mathcal{E}_{t+1}}{\partial\mathbf{h}_t} \quad (8.118)$$

All three gates in an LSTM involve an elementwise product of two activation vectors (see Equations [\(8.107\)](#)^[509], [\(8.112\)](#)^[511], and [\(8.116\)](#)^[512]). For each of these cases, what we wish to calculate during backpropagation is the rate of change of the error with respect to changes in each of the inputs to the product. This means that we will generate two sets of error gradients when we backpropagate through an elementwise vector product, one for each branch of data that flows into the product. In backpropagation, the error gradient with respect to an input to a product of two terms is the error gradient with respect to the result of the product multiplied by the other input to the product. In dealing with an elementwise vector product, this is applied to each of the separate products in turn. So, for example, backpropagating the error gradient $\partial\mathcal{E}/\partial\mathbf{o}_t$ through the elementwise vector product in the output gate (see Equation [\(8.116\)](#)^[512]) produces the following two error gradient vectors:

$$\frac{\partial \mathcal{E}}{\partial \mathbf{o}^\ddagger} = \frac{\partial \mathcal{E}}{\partial \mathbf{o}_t} \odot \mathbf{o}^\dagger \quad (8.119)$$

$$\frac{\partial \mathcal{E}}{\partial \mathbf{o}^\dagger} = \frac{\partial \mathcal{E}}{\partial \mathbf{o}_t} \odot \mathbf{o}^\ddagger \quad (8.120)$$

where \odot is an elementwise vector product, \mathbf{o}^\dagger was calculated in the forward pass using Equation (8.114)^[512]; and \mathbf{o}^\ddagger was calculated in the forward pass using Equation (8.115)^[512]. Figure 8.42^[516] indicates the flow of error gradients back through the elementwise product in the output gate by labeling each path emerging from the operation with its respective error gradient vector: $\partial \mathcal{E} / \partial \mathbf{o}^\ddagger$ and $\partial \mathcal{E} / \partial \mathbf{o}^\dagger$, respectively. We backpropagate through the other elementwise products that occur in the forward pass within the LSTM using a similar strategy: in order to calculate the backpropagated error gradient for one input to a product, we multiply the error gradient for the result of the product by the other input to the product.

The forward computational flow through the LSTM input gates include an elementwise addition of two activation vectors. This operation is used in the input gate to update the cell state (see Equation (8.113)^[511]). The term $\partial \mathcal{E} / \partial \mathbf{c}_t$ describes the vector of error gradients that are backpropagated through this operation. The same error gradient vector flows back along both paths that feed into the elementwise summation in the forward path. This is why in Figure 8.42^[516] both of the paths emerging from the elementwise summation are labeled with the same term as the input arrow: $\partial \mathcal{E} / \partial \mathbf{c}_t$.

Having covered how we backpropagate through branches, elementwise products, and elementwise additions in the forward pass, we are now able to backpropagate the error gradients through the LSTM. Starting on the right, we calculate $\partial \mathcal{E} / \partial \mathbf{o}_t$ per Equation (8.118)^[516] and then backpropagate this through the output gate elementwise product to calculate $\partial \mathcal{E} / \partial \mathbf{o}^\ddagger$ (Equation (8.119)^[516]) and $\partial \mathcal{E} / \partial \mathbf{o}^\dagger$ (Equation (8.120)^[516]). Next we calculate $\partial \mathcal{E} / \partial \mathbf{c}_t$. To calculate these error gradients we must backpropagate $\partial \mathcal{E} / \partial \mathbf{o}^\ddagger$ through a tanh layer and then merge the resulting gradients with the error gradients from the next time-step with respect to the current cell state. This is done as follows:

$$\delta_{o_t^{\dagger}} = \frac{\partial \mathcal{E}}{\partial \mathbf{o}_t^{\dagger}} \odot \frac{\partial \mathbf{o}_{t+1}^{\dagger}}{\partial \mathbf{c}_t^{\dagger}} = \frac{\partial \mathcal{E}}{\partial \mathbf{o}_t^{\dagger}} \odot \underbrace{(\mathbf{1} - \tanh^2(\mathbf{c}_t^{\dagger}))}_{\text{Derivate of tanh, i.e.: } \frac{\partial a}{\partial z}} \quad (8.121)$$

$$\frac{\partial \mathcal{E}}{\partial \mathbf{c}_t} = \delta_{o_t^{\dagger}} + \frac{\partial \mathcal{E}_{t+1}}{\partial \mathbf{c}_t} \quad (8.122)$$

In Equation (8.121)^[517] we calculate a vector containing δ values for the neurons in the output gate tanh layer by backpropagating the error gradients $\partial \mathcal{E} / \partial \mathbf{o}_t^{\dagger}$ back through that tanh activation function. Then in Equation (8.122)^[517] we merge the two sets of gradients that arise from the fork in the forward propagation of \mathbf{c}_t to both the next time-step (as the cell state) and the output layer for this time-step.

Focusing on the input gate, the gradients for each of the inputs to the elementwise product can now be calculated as follows:

$$\frac{\partial \mathcal{E}}{\partial \mathbf{i}_t^{\dagger}} = \frac{\partial \mathcal{E}}{\partial \mathbf{c}_t} \odot \mathbf{i}_t^{\dagger} \quad (8.123)$$

$$\frac{\partial \mathcal{E}}{\partial \mathbf{i}^{\dagger}} = \frac{\partial \mathcal{E}}{\partial \mathbf{c}_t} \odot \mathbf{i}^{\dagger} \quad (8.124)$$

Similarly, the gradients for the inputs to the elementwise product in the forget gate are calculated

$$\frac{\partial \mathcal{E}}{\partial \mathbf{c}_{t-1}} = \frac{\partial \mathcal{E}}{\partial \mathbf{c}_t} \odot \mathbf{f}_t \quad (8.125)$$

$$\frac{\partial \mathcal{E}}{\partial \mathbf{f}} = \frac{\partial \mathcal{E}}{\partial \mathbf{c}_t} \odot \mathbf{c}_{t-1} \quad (8.126)$$

Each of the terms $\partial \mathcal{E} / \partial \mathbf{f}$ (Equation (8.126)^[518]), $\partial \mathcal{E} / \partial \mathbf{i}^{\dagger}$ (Equation (8.124)^[518]), $\partial \mathcal{E} / \partial \mathbf{i}^{\dagger}$ (Equation (8.123)^[518]), and $\partial \mathcal{E} / \partial \mathbf{o}^{\dagger}$ (Equation (8.120)^[516]) describes a vector of error gradients with respect to the output activations of the neurons in one of the sigmoid and tanh layers in the LSTM. In order to calculate the δ s for the neurons in each of these layers, we must multiply these error gradients by the derivative of the activation function for the layer with respect to the inputs to the activation function (i.e., $\partial \mathbf{a} / \partial \mathbf{z}$). Recall that we are dealing with vectors of gradients, and so for each layer we will do an elementwise product with a vector of activation function derivatives;

also, the derivatives of the activation functions are dependent on whether the neurons in the layer are using a sigmoid or tanh function.

$$\delta_f = \frac{\partial \mathcal{E}}{\partial \mathbf{f}} \odot \frac{\partial \mathbf{f}_t}{\partial \mathbf{z}_f} = \frac{\partial \mathcal{E}}{\partial \mathbf{f}} \odot (\mathbf{f}_t \odot (\mathbf{1} - \mathbf{f}_t)) \quad (8.127)$$

$$\delta_{i\dagger} = \frac{\partial \mathcal{E}}{\partial \mathbf{i}\dagger} \odot \frac{\partial \mathbf{i}\dagger_t}{\partial \mathbf{z}_{i\dagger}} = \frac{\partial \mathcal{E}}{\partial \mathbf{i}\dagger} \odot (\mathbf{i}\dagger_t \odot (\mathbf{1} - \mathbf{i}\dagger_t)) \quad (8.128)$$

$$\delta_{i\dagger} = \frac{\partial \mathcal{E}}{\partial \mathbf{i}\dagger} \odot \frac{\partial \mathbf{i}\dagger_t}{\partial \mathbf{z}_{i\dagger}} = \frac{\partial \mathcal{E}}{\partial \mathbf{i}\dagger} \odot (\mathbf{1} - \tanh^2(\mathbf{i}\dagger_t)) \quad (8.129)$$

$$\delta_{o\dagger} = \frac{\partial \mathcal{E}}{\partial \mathbf{o}\dagger} \odot \frac{\partial \mathbf{o}\dagger_t}{\partial \mathbf{z}_{o\dagger}} = \frac{\partial \mathcal{E}}{\partial \mathbf{o}\dagger} \odot (\mathbf{o}\dagger_t \odot (\mathbf{1} - \mathbf{o}\dagger_t)) \quad (8.130)$$

Once we have calculated the δ s for the neurons in these layers, we have two further sets of calculations to perform in order to complete the backpropagation through the LSTM. First, we need to calculate the updates for each weight in each of these layers; and second, we need to calculate the vector of gradients $\partial \mathcal{E} / \partial \mathbf{h}_{t-1}$ that are backpropagated to the previous time-step.

Assuming that we are training the LSTM network using **backpropagation through time**, then for each time-step, we calculate the update for each weight by multiplying the δ for the neuron that uses the weight by the input value that weight was applied to, and then we sum these weight updates across the time-steps. The weight is then updated using the summed weight update. For example, the update for the weights in $\mathbf{W}^{(f)}$ would be calculated as follows:

$$\Delta \mathbf{W}^{(f)} = \delta_f \cdot \mathbf{h} \mathbf{x}^\top \quad (8.131)$$

Note that here we use the notation $\mathbf{h} \mathbf{x}^\top$ to write the transpose of the vector $\mathbf{h} \mathbf{x}$; we use transpose of the vector to ensure that this matrix and vector product is defined. We can illustrate the process of calculating a weight update for the weights in $\mathbf{W}^{(f)}$ by using the context provided by the forward pass example shown in [Figure 8.41](#)^[514]. For the purposes of this example, we assume that the following error gradients are already calculated:

$$\frac{\partial \mathcal{E}_{t+1}}{\partial \mathbf{c}_t} = \begin{bmatrix} 0.35 \\ 0.50 \end{bmatrix} \quad \frac{\partial \mathcal{E}_{t+1}}{\partial \mathbf{h}_t} = \begin{bmatrix} 0.75 \\ 0.25 \end{bmatrix} \quad \frac{\partial \mathcal{E}_t}{\partial \mathbf{o}_t} = \begin{bmatrix} 0.15 \\ 0.60 \end{bmatrix}$$

Given these terms we calculate the update for the weights in $\mathbf{W}^{(f)}$ using the sequence of calculations listed in Equations (8.132)^[519] to (8.138)^[520]

$$\frac{\partial \mathcal{E}}{\partial \mathbf{o}_t} = \underbrace{\begin{bmatrix} 0.75 \\ 0.25 \end{bmatrix}}_{\frac{\partial \mathcal{E}_{t+1}}{\partial \mathbf{h}_t}} + \underbrace{\begin{bmatrix} 0.15 \\ 0.60 \end{bmatrix}}_{\frac{\partial \mathcal{E}_t}{\partial \mathbf{o}_t}} = \begin{bmatrix} 0.9 \\ 0.85 \end{bmatrix} \quad (8.132)$$

$$\frac{\partial \mathcal{E}}{\partial \mathbf{o}^\ddagger} = \underbrace{\begin{bmatrix} 0.9 \\ 0.85 \end{bmatrix}}_{\frac{\partial \mathcal{E}}{\partial \mathbf{o}_t}} \odot \underbrace{\begin{bmatrix} 0.575420058 \\ 0.52098661 \end{bmatrix}}_{\mathbf{o}^\ddagger} = \begin{bmatrix} 0.517878052 \\ 0.442839512 \end{bmatrix} \quad (8.133)$$

$$\delta_{o^\ddagger} = \underbrace{\begin{bmatrix} 0.517878052 \\ 0.442839512 \end{bmatrix}}_{\frac{\partial \mathcal{E}}{\partial \mathbf{o}^\ddagger}} \odot \underbrace{\begin{bmatrix} 0.999184559 \\ 0.997048635 \end{bmatrix}}_{1 - \tanh(\mathbf{c}_t)} = \begin{bmatrix} 0.517455753 \\ 0.441532531 \end{bmatrix} \quad (8.134)$$

$$\frac{\partial \mathcal{E}}{\partial \mathbf{c}_t} = \underbrace{\begin{bmatrix} 0.517455753 \\ 0.441532531 \end{bmatrix}}_{\delta_{o^\ddagger}} + \underbrace{\begin{bmatrix} 0.35 \\ 0.50 \end{bmatrix}}_{\frac{\partial \mathcal{E}_{t+1}}{\partial \mathbf{c}_t}} = \begin{bmatrix} 0.867455753 \\ 0.941532531 \end{bmatrix} \quad (8.135)$$

$$\frac{\partial \mathcal{E}}{\partial \mathbf{f}} = \underbrace{\begin{bmatrix} 0.867455753 \\ 0.941532531 \end{bmatrix}}_{\frac{\partial \mathcal{E}}{\partial \mathbf{c}_t}} \odot \underbrace{\begin{bmatrix} 0.3 \\ 0.6 \end{bmatrix}}_{\mathbf{c}_{t-1}} = \begin{bmatrix} 0.260236726 \\ 0.564919518 \end{bmatrix} \quad (8.136)$$

$$\delta_f = \underbrace{\begin{bmatrix} 0.260236726 \\ 0.564919518 \end{bmatrix}}_{\frac{\partial \mathcal{E}}{\partial \mathbf{f}}} \odot \underbrace{\begin{bmatrix} 0.248743973 \\ 0.249694 \end{bmatrix}}_{\mathbf{f}_t \odot (1 - \mathbf{f}_t)} = \begin{bmatrix} 0.064732317 \\ 0.141057014 \end{bmatrix} \quad (8.137)$$

$$\begin{aligned} \Delta \mathbf{W}^{(f)} &= \underbrace{\begin{bmatrix} 0.064732317 \\ 0.141057014 \end{bmatrix}}_{\delta_f} \cdot \underbrace{\begin{bmatrix} 1.00 & 0.10 & 0.80 & 0.90 \end{bmatrix}}_{\mathbf{h} \mathbf{x}^\top} \\ &= \begin{bmatrix} 0.064732317 & 0.006473232 & 0.051785854 & 0.058259085 \\ 0.141057014 & 0.014105701 & 0.112845611 & 0.126951313 \end{bmatrix} \end{aligned} \quad (8.138)$$

To calculate the vector of gradients $\partial \mathcal{E} / \partial \mathbf{h}_{t-1}$, we first need to calculate the error gradient with respect to changes in $\mathbf{h} \mathbf{x}_t$ for each of the four layers

of neurons that receive \mathbf{hx}_t as input: the forget gate sigmoid layer, the input gate sigmoid layer, the input gate tanh layer, and the output gate sigmoid layer. For each of these layers we calculate the error gradient with respect to the layer's input (\mathbf{hx}_t) by multiplying the δ values for the neurons in the layer by the weights the neuron uses. This is similar to the way we calculate the error gradients with respect to the weights of a neuron, the difference here being that we want the error gradient with respect to the input \mathbf{hx}_t , and so in this case we multiply the δ by the weights rather than the inputs. Once the vector of error gradients with respect to \mathbf{hx}_t has been calculated for each of the layers, $\partial\mathcal{E}/\partial\mathbf{hx}$ is calculated using an elementwise sum of these vectors of gradients

$$\frac{\partial\mathcal{E}}{\partial\mathbf{hx}} = \left(\mathbf{W}^{(f)\top} \cdot \delta_f\right) + \left(\mathbf{W}^{(i^\dagger)\top} \cdot \delta_{i^\dagger}\right) + \left(\mathbf{W}^{(i^\ddagger)\top} \cdot \delta_{i^\ddagger}\right) + \left(\mathbf{W}^{(o^\dagger)\top} \cdot \delta_{o^\dagger}\right) \quad (8.139)$$

The vector of gradients $\partial\mathcal{E}/\partial\mathbf{hx}$ includes error gradients for each element of \mathbf{h}_{t-1} and \mathbf{x}_t . This is because \mathbf{h}_{t-1} and \mathbf{x}_t were concatenated together in the forward pass. Hence the vector of gradients $\partial\mathcal{E}_t/\partial\mathbf{h}_{t-1}$ is extracted from $\partial\mathcal{E}/\partial\mathbf{hx}$ by splitting the vector at the index that joined \mathbf{h}_{t-1} and \mathbf{x}_t when they were concatenated.

LSTMs were specifically designed to be able to model long-distance dependencies in a sequence. The fundamental element in the design of these networks was to remove the repeated multiplication of error gradients by weight matrices during backpropagation through time. Equation (8.139)^[520] may appear to undermine this design goal, because the calculation of the backpropagated error gradients in the vector $\partial\mathcal{E}_t/\partial\mathbf{h}_{t-1}$ involves a multiplication by weight matrices. However, this is not the only vector of error gradients that are backpropagated; recall, the $\partial\mathcal{E}/\partial\mathbf{c}_{t-1}$ is also backpropagated to the previous time-step. Equation (8.140)^[521] expands out the full set of operations and terms that are used in the calculation of $\partial\mathcal{E}_t/\partial\mathbf{c}_{t-1}$. The point to note in this equation is that the calculation does not involve a weight term. Consequently, error gradients with respect to the cell state, \mathbf{c} , are not repeatedly multiplied by a (weight) term that is shared across time-steps, and so these gradients are relatively stable as they flow backward along the cell state path. It is primarily this path of error gradients

flow (rather than the backpropagated hidden state $\partial\mathcal{E}/\partial\mathbf{h}_{t-1}$ gradients) that enable LSTMs to learn long-distance dependencies

$$\begin{aligned}
 \frac{\partial\mathcal{E}}{\partial\mathbf{c}_{t-1}} &= \mathbf{f}_t \odot \frac{\partial\mathcal{E}}{\partial\mathbf{c}_t} \\
 &= \mathbf{f}_t \odot \left(\frac{\partial\mathcal{E}_{t+1}}{\partial\mathbf{c}_t} + \delta_{o^\ddagger} \right) \\
 &= \mathbf{f}_t \odot \left(\frac{\partial\mathcal{E}_{t+1}}{\partial\mathbf{c}_t} + \left((\mathbf{1} - \tanh^2(\mathbf{c}_{t,t}^\ddagger)) \odot \frac{\partial\mathcal{E}}{\partial\mathbf{o}_t^\ddagger} \right) \right) \\
 &= \mathbf{f}_t \odot \left(\frac{\partial\mathcal{E}_{t+1}}{\partial\mathbf{c}_t} + \left((\mathbf{1} - \tanh^2(\mathbf{c}_{t,t}^\ddagger)) \odot \left(\mathbf{o}_t^\dagger \odot \frac{\partial\mathcal{E}}{\partial\mathbf{o}_t} \right) \right) \right) \\
 &= \mathbf{f}_t \odot \left(\frac{\partial\mathcal{E}_{t+1}}{\partial\mathbf{c}_t} + \left((\mathbf{1} - \tanh^2(\mathbf{c}_{t,t}^\ddagger)) \odot \left(\mathbf{o}_t^\dagger \odot \left(\frac{\partial\mathcal{E}_{t+1}}{\partial\mathbf{h}_t} + \frac{\partial\mathcal{E}_t}{\partial\mathbf{o}_t} \right) \right) \right) \right)
 \end{aligned} \tag{8.140}$$

8.5 Summary

The distinctive characteristic of deep learning models is that they are deeper and larger than older neural networks. The depth of a network is measured by the number of layers of neurons within the network. The reason why depth is important is that by introducing multiple layers into a network, the network is able to learn a hierarchy of features with later layers in the network building on the features that previous layers have learned to extract from the raw input. A consequence of this layer-wise transformation of the input data into new representations is that as the network becomes deeper, the ability of the network to represent more complex relationships between descriptive and target features is increased.

The standard algorithm for training a deep neural network combines the backpropagation algorithm (which solves the blame assignment problem) with stochastic gradient descent (which we use to update the weights in the network after blame has been assigned to each neuron). A difficulty with training a deep network with backpropagation and gradient descent is unstable gradients (either vanishing or exploding gradients). Two key innovations that helped with the unstable gradient problem were the adoption of the rectified linear activation function and the development of new techniques for weight initialization.

The ability of deep neural networks to learn and represent complex mappings from inputs to outputs is why these networks have been so successful at so many complex tasks. However, this representational capacity also means that deep networks are likely to suffer from overfitting. Dropout is a very simple and effective method that helps to stop overfitting.

Finally, the fact that deep learning models are combined by connecting artificial neurons together means that we can tailor the structure of a network toward the characteristics of the data on which we are planning to run the network. Convolutional neural networks are a network architecture that have been very successful at image processing tasks. Convolutional neural networks combine local receptive fields, weight sharing, and sub-sampling. They generally work very well on data that has a grid-like structure and in which the low-level features in the data have a local extent. By contrast, recurrent neural networks are designed to process sequential data that may have long distances between dependent features in the input sequence. These recurrent models use a feedback loop to maintain, evolve, and propagate a representation of the pertinent information within the sequence history. Recurrent networks also use weight sharing with the same weight matrices being reused at each time-step in a sequence. The fact that the same weights are applied on the feedback loop within a recurrent network means that these networks are very susceptible to unstable gradients, as the repeated multiplication by the same weight of the gradient as it is propagated back through the unrolled network can cause the gradient to explode or vanish. Long short-term memory (LSTM) networks have addressed instability in the propagation of weights through a sequential model by removing this repeated multiplication by the shared weights.

In terms of using deep learning for a machine learning task, the first question to ask is whether deep learning is really necessary or appropriate. Deep learning works best in complex domains with lots of features and large datasets. Further, deep learning generally requires relatively powerful computer hardware. If the domain is not complex, or if the available data is small, or if the available hardware is not powerful enough for deep learning, then it is likely that you will have more success by exploring whether an alternative machine learning model can be used to develop a viable solution for the task. Once the decision to use deep learning has been made, the next decision is to choose the network architecture to use. We have covered three

architectures in this chapter: feedforward networks are appropriate if the descriptive features are in a fixed-sized vector; if the input data has a grid-like structure, then consider a convolutional neural network; and if the input may be a variable length sequence, then a recurrent neural network or LSTM network will be most appropriate. As mentioned in the chapter, ReLUs (or variants) are now the default activation function to use, although if a network architecture specifies a particular activation function, then follow the specification (e.g., LSTMs specify the use of sigmoid and tanh activations). With regard to the network training, take care with the weight initialization process, and it is generally a good idea to include dropout. Finally, as discussed in the Information Based Learning chapter, in which we discussed tree pruning to avoid overfitting, using the performance of the model on the validation set to decide when to stop the training and weight updates is nearly always the case in training a neural network.

8.6 Further Reading

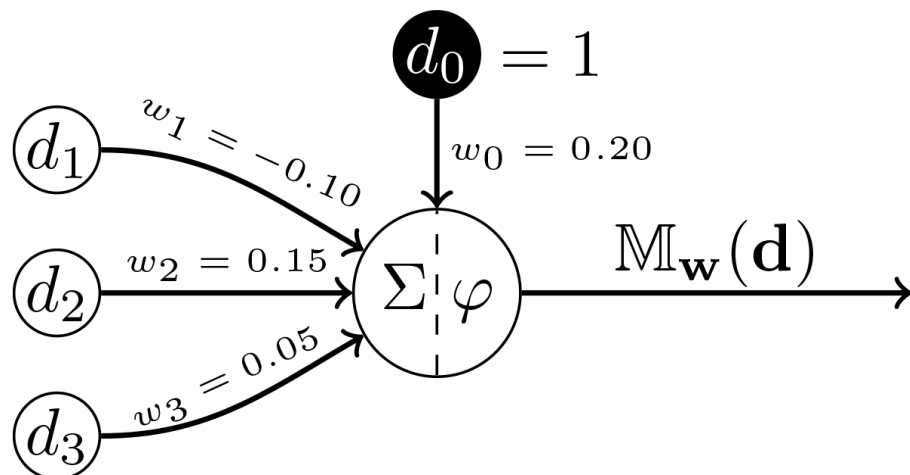
Deep learning has grown out of research on neural networks. Consequently, many books on neural networks cover the fundamentals of deep learning. Neural network texts that we would recommend include Bishop (1996) and Reed and Marks (1999). Kelleher (2019) provides an overview of the history of deep learning that highlights the major developments in the field and the trends that are driving its adoption across a broad range of domains, and it discusses likely future developments in the field. The explanation of the backpropagation algorithm presented in this chapter is based on Chapter 6 of Kelleher (2019). Goodfellow et al. (2016) provides a comprehensive overview of the field. From a programming perspective, we would recommend Charniak (2019) as an introduction to programming deep learning models using TensorFlow, and Trask (2019) provides a great introduction to implementing neural networks using Numpy. Finally, we also recommend Goldberg (2017) for an accessible introduction to the use of deep learning for natural language processing and Reagen et al. (2017) for a computer architecture perspective on deep learning.

Deep learning is currently attracting a huge amount of attention within the machine learning community. Consequently, there is rapid progress within the field, with new techniques and network architectures being published every month. As a result, it is not possible in a single chapter to

cover all possible deep learning topics. Some of the topics that, space permitting, we would have included are **batch normalization** (Ioffe and Szegedy, 2015), which can speed up the training of very deep networks; algorithms that adaptively adjust the learning rate parameter such as **Adam** (Kingma and Ba, 2014); and more recent neural network architectures such as **Generative Adversarial Networks** (Goodfellow et al., 2014), and attention-based architectures, such as the **Transformer** (Vaswani et al., 2017).

8.7 Exercises

1. The following image shows an artificial neuron that takes three inputs

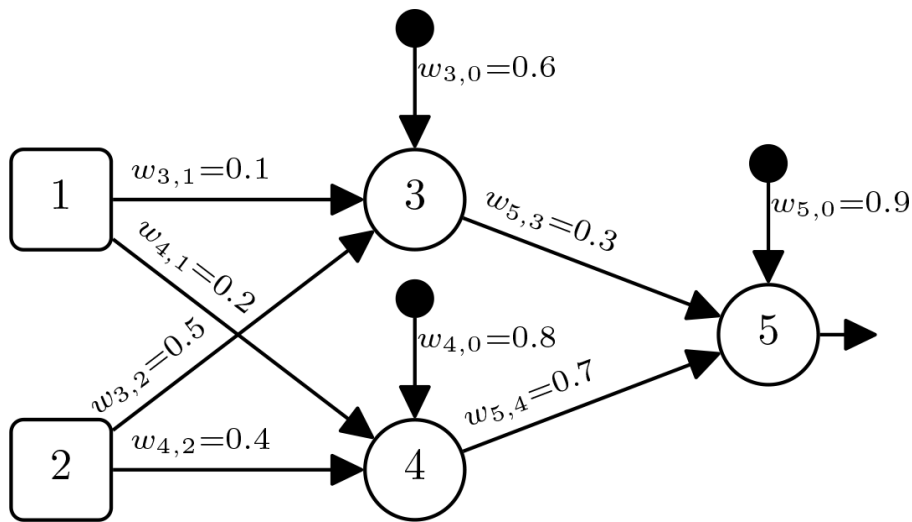


- (a) Calculate the **weighted sum** for this neuron for the input vector

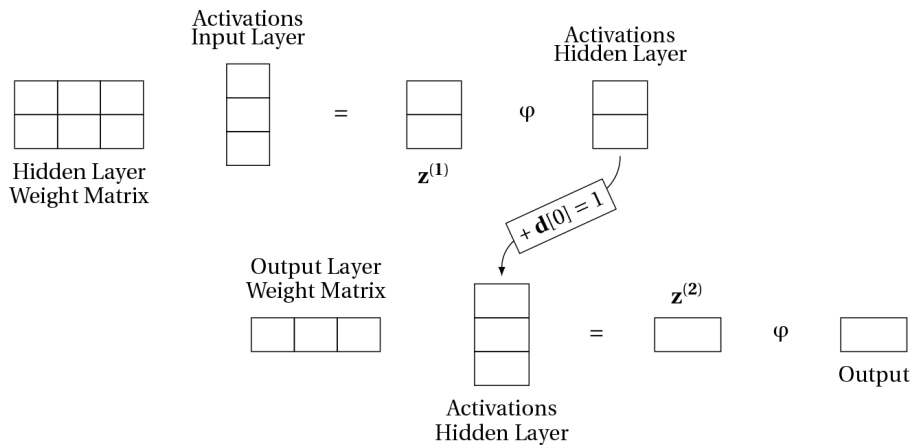
$$\mathbf{d} = [0.2, 0.5, 0.7]$$

- What would be the output from this neuron if the activation function φ is a threshold activation with $\theta = 1$?
- What would be the output from this neuron if the activation function φ is the logistic function?
- What would be the output from this neuron if the activation function φ is the rectified linear function?

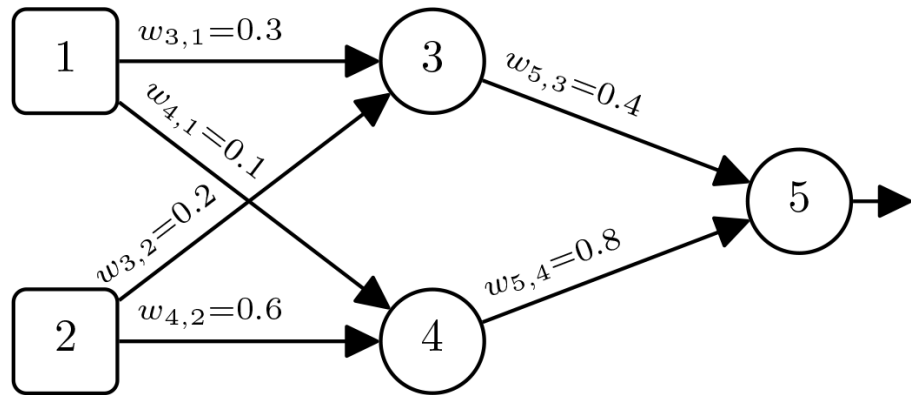
2. The following image shows an artificial neural network with two sensing neurons (Neurons 1 and 2) and 3 processing neurons (Neurons 3, 4, and 5)



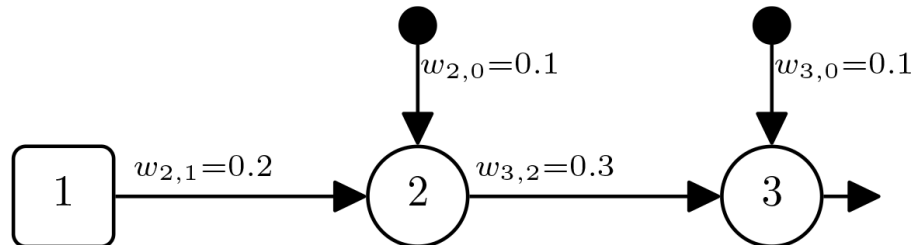
- (a) Assuming that the processing neurons in this network use a **logistic** activation function, what would be the output of Neuron 5 if the network received the input vector: Neuron 1 = 0.7 and Neuron 2 = 0.3?
- (b) Assuming that the processing neurons in this network use a **ReLU** activation function, what would be the output of Neuron 5 if the network received the input vector: Neuron 1 = 0.7 and Neuron 2 = 0.3?
- (c) The following image provides a template diagram for the sequence of matrix operations that our neural network would use to process the input vector Neuron 1 = 0.7 and Neuron 2 = 0.3. Assuming that the processing neurons in the network use a ReLU activation function, fill in the diagram with the appropriate weights, bias terms, weighted sum values, and activations.



3. The following image shows an artificial network with two layers of **linear neurons** (i.e., neurons that have no activation function and whose output is simply the result of the weighted sum of their inputs). Furthermore, these neurons have no bias terms.



- (a) Calculate the output for Neuron 5 for the input vector: Neuron 1 = 0.9, Neuron 2 = 0.5.
 - (b) Calculate the weight matrix for the single layer network that would implement the equivalent mapping that this two-layer network implements.
 - (c) Show that the single-layer network using the weight matrix you calculated in Part 2 generates the same output as the network for the input vector: Neuron 1 = 0.9, Neuron 2 = 0.5.
4. The following image illustrates the topology of a simple feedforward neural network that has a single sensing neuron (Neuron 1), a single hidden processing neuron (Neuron 2), and a single processing output neuron (Neuron 3).

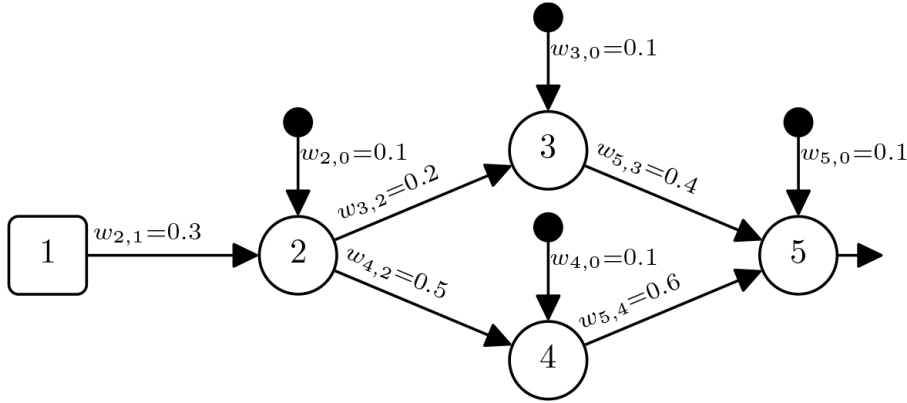


- (a) Assuming that the processing neurons use **logistic** activation functions, that the input to the network is Neuron 1 = 0.2 and that the desired output for this input is 0.7:

- i. Calculate the output generated by the network in response to this input.
- ii. Calculate the δ values for each of the neurons in the network (i.e., δ_3, δ_2).
- iii. Using the δ values you calculated above, calculate the sensitivity of the error of the network to changes in each of the weights of the network (i.e., $\partial E/\partial w_{3,2}, \partial E/\partial w_{3,0}, \partial E/\partial w_{2,1}, \partial E/\partial w_{2,0}$).
- iv. Assuming a learning rate of $\alpha = 0.1$, calculate the updated values for each of the weights in the network ($w_{3,2}, w_{3,0}, w_{2,1}, w_{2,0}$) after the processing of this single training example.
- v. Calculate the reduction in the error of the network for this example using the new weights, compared with using the original weights.

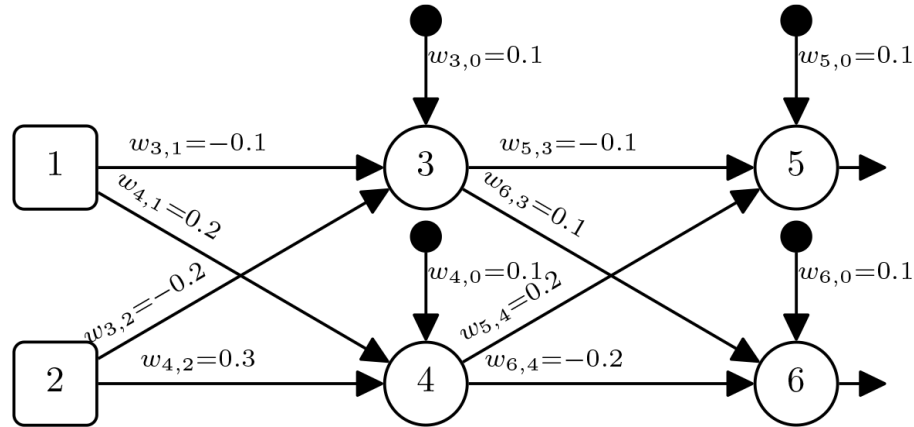
- (b) Assuming that the processing neurons are **ReLUs**, that the input to the network is Neuron 1 = 0.2, and that the desired output for this input is 0.7:
- i. Calculate the output generated by the network in response to this input.
 - ii. Calculate the δ values for each of the neurons in the network (i.e., δ_3, δ_2).
 - iii. Using the δ values you have calculated in the preceding, calculate the sensitivity of the error of the network to changes in each of the weights of the network (i.e., $\partial E/\partial w_{3,2}, \partial E/\partial w_{3,0}, \partial E/\partial w_{2,1}, \partial E/\partial w_{2,0}$).
 - iv. Assuming a learning rate of $\alpha = 0.1$, calculate the updated values for each of the weights in the network ($w_{3,2}, w_{3,0}, w_{2,1}, w_{2,0}$) after the processing of this single training example.
 - v. Calculate the reduction in the error for this example using the new weights for the network, compared with using the original weights.

5. The following image illustrates the topology of a simple feedforward neural network that has a single sensing neuron (Neuron 1), three hidden processing neuron (Neurons 2, 3, and 4), and a single processing output neuron (Neuron 5).



- (a) Assuming that the processing neurons use **logistic** activation functions, that the input to the network is Neuron 1 = 0.5 and that the desired output for this input is 0.9:
- Calculate the output generated by the network in response to this input.
 - Calculate the δ values for each of the processing neurons in the network (i.e., $\delta_5, \delta_4, \delta_3, \delta_2$).
 - Using the δ values you have calculated, calculate the sensitivity of the error of the network to changes in each of the weights of the network (i.e., $\partial E / \partial w_{5,4}, \partial E / \partial w_{5,3}, \partial E / \partial w_{5,0}, \partial E / \partial w_{4,2}, \partial E / \partial w_{4,0}, \partial E / \partial w_{3,2}, \partial E / \partial w_{3,0}, \partial E / \partial w_{2,1}, \partial E / \partial w_{2,0}$).
 - Assuming a learning rate of $\alpha = 0.1$, calculate the updated values for each of the weights in the network ($w_{5,4}, w_{5,3}, w_{5,0}, w_{4,2}, w_{4,0}, w_{3,2}, w_{3,0}, w_{2,1}, w_{2,0}$) after the processing of this single training example.
 - Calculate the reduction in the error of the network for this example using the new weights, compared with using the original weights.
- (b) Assuming that the processing neurons are **ReLUs**, that the input to the network is Neuron 1 = 0.5 and that the desired output for this input is 0.9
- Calculate the output generated by the network in response to this input.
 - Calculate the δ values for each of the processing neurons in the network (i.e., $\delta_5, \delta_4, \delta_3, \delta_2$).

- iii. Using the δ values you have calculated, calculate the sensitivity of the error of the network to changes in each of the weights of the network (i.e., $\partial E / \partial w_{5,4}$, $\partial E / \partial w_{5,3}$, $\partial E / \partial w_{5,0}$, $\partial E / \partial w_{4,2}$, $\partial E / \partial w_{4,0}$, $\partial E / \partial w_{3,2}$, $\partial E / \partial w_{3,0}$, $\partial E / \partial w_{2,1}$, $\partial E / \partial w_{2,0}$).
- iv. Assuming a learning rate of $\alpha = 0.1$, calculate the updated values for each of the weights in the network ($w_{5,4}$, $w_{5,3}$, $w_{5,0}$, $w_{4,2}$, $w_{4,0}$, $w_{3,2}$, $w_{3,0}$, $w_{2,1}$, $w_{2,0}$) after the processing of this single training example.
- v. Calculate the reduction in the error of the network for this example using the new weights, compared with using the original weights.
6. The following image illustrates the topology of a feedforward neural network that has two sensing neurons (Neurons 1 and 2), two hidden processing neuron (Neurons 3, and 4), and two processing output neurons (Neurons 5 and 6).



- (a) Assuming that the processing neurons use **logistic** activation functions, that the input to the network is Neuron 1 = 0.3 and Neuron 2 = 0.6, and that the desired output for this input is Neuron 5 = 0.7 and Neuron 6 = 0.4:
- Calculate the output generated by the network in response to this input.
 - Calculate the sum of squared errors for this network for this example.
 - Calculate the δ values for each of the processing neurons in the network (i.e., δ_6 , δ_5 , δ_4 , δ_3).

- iv. Using the δ values you calculated above, calculate the sensitivity of the error of the network to changes in each of the weights of the network (i.e., $\partial E / \partial w_{6,4}$, $\partial E / \partial w_{6,3}$, $\partial E / \partial w_{6,0}$, $\partial E / \partial w_{5,4}$, $\partial E / \partial w_{5,3}$, $\partial E / \partial w_{5,0}$, $\partial E / \partial w_{4,2}$, $\partial E / \partial w_{4,1}$, $\partial E / \partial w_{4,0}$, $\partial E / \partial w_{3,2}$, $\partial E / \partial w_{3,1}$, $\partial E / \partial w_{3,0}$).
 - v. Assuming a learning rate of $\alpha = 0.1$, calculate the updated values for each of the weights in the network ($w_{6,4}, w_{6,3}, w_{6,0}, w_{5,4}, w_{5,3}, w_{5,0}, w_{4,2}, w_{4,1}, w_{4,0}, w_{3,2}, w_{3,1}, w_{3,0}$) after the processing of this single training example.
 - vi. Calculate the reduction in the sum of squared error of the network for this example using the new weights, compared with using the original weights.
- (b) Assuming that the processing neurons use a **rectifier** activation functions, that the input to the network is Neuron 1 = 0.3 and Neuron 2 = 0.6 and that the desired output for this input is Neuron 5 = 0.7 and Neuron 6 = 0.4:
- i. Calculate the output generated by the network in response to this input.
 - ii. Calculate the sum of squared errors for this network on this example.
 - iii. Calculate the δ values for each of the processing neurons in the network (i.e., $\delta_6, \delta_5, \delta_4, \delta_3$).
 - iv. Using the δ values you calculated above, calculate the sensitivity of the error of the network to changes in each of the weights of the network (i.e., $\partial E / \partial w_{6,4}$, $\partial E / \partial w_{6,3}$, $\partial E / \partial w_{6,0}$, $\partial E / \partial w_{5,4}$, $\partial E / \partial w_{5,3}$, $\partial E / \partial w_{5,0}$, $\partial E / \partial w_{4,2}$, $\partial E / \partial w_{4,1}$, $\partial E / \partial w_{4,0}$, $\partial E / \partial w_{3,2}$, $\partial E / \partial w_{3,1}$, $\partial E / \partial w_{3,0}$).
 - v. Assuming a learning rate of $\alpha = 0.1$, calculate the updated values for each of the weights in the network ($w_{6,4}, w_{6,3}, w_{6,0}, w_{5,4}, w_{5,3}, w_{5,0}, w_{4,2}, w_{4,1}, w_{4,0}, w_{3,2}, w_{3,1}, w_{3,0}$) after the processing of this single training example.
 - vi. Calculate the reduction in the sum of squared error of the network for this example using the new weights, compared with using the original weights.

7. Assuming a fully connected feedforward network where all the neurons uses a linear activation function (i.e., $a_i = z_i$) and with the following topology:

- (a) 100 neurons in the input layer
- (b) 5 hidden layers with 2,000 neurons in each layer
- (c) 10 neurons in the output layer

If all the inputs to the network have been standardized to have a mean value of 0 and a standard deviation of 1, and the initial weights for the network are sampled from a normal distribution with mean 0.0 and standard deviation of $\sigma = 0.01$, then:

- (a) Calculate the variance of the z values across for the neurons in the first hidden layer in the first iteration of training.
- (b) Calculate the variance of the z values across for the neurons in the last hidden layer in the first iteration of training.

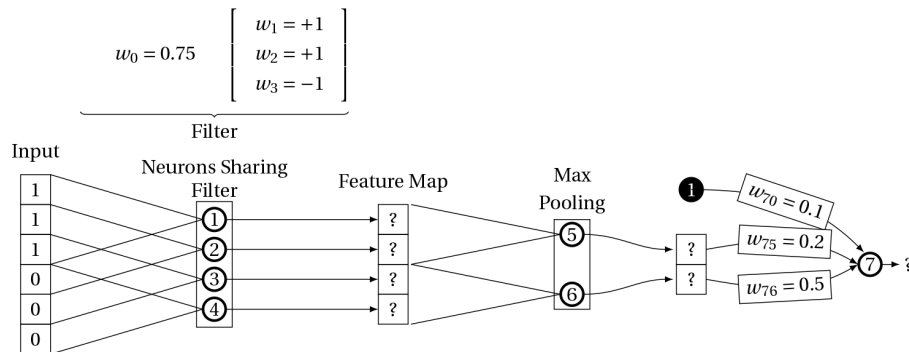
Assuming that the variance of the δs for the output layer is equal to 1:

- (a) Calculate the variance of the δs across for the neurons in the last hidden layer in the first iteration of training.
- (b) Calculate the variance of the δs values across for the neurons in the first hidden layer in the first iteration of training.
- (c) Is the training dynamic of this network stable, or is it suffering from vanishing or exploding gradients?

* 8. Assuming a network architecture that has four neurons in a **softmax** output layer. If the one-hot encoding of the target for the current training example is $t = [0,0,1,0]$ and the logits for the four neurons in the softmax output layer for this example are $[0,0.5,0.25,0.75]$, then what is the δ value for each of the four neurons?

* 9. Assuming a feedforward neural network that has 4 neurons in hidden layer k and that we are training this network using **inverted dropout** with $\rho = 0.5$. If the activations for the neurons in layer k are as follows: $[0.2,0.4,0.3,0.1]$ and the **DropMask** for layer k is $[1,0,1,0]$, calculate the activation vector that is actually propagated to layer $k + 1$ after inverted dropout has been applied.

- * 10. The figure below illustrates a layer of a convolutional neural network that is processing a one-dimensional input. For ease of reference each of the neurons in the network has been labeled: 1,2,3,4,5,6,7. The architecture of the network consists of ReLUs that share a filter (Neurons 1,2,3,4), followed by a sub-sampling layer containing two max pooling units (Neurons 5,6), and then a fully connected layer containing a single ReLU (Neuron 7). The ReLU in the first layer has a 3-by-1 receptive field, and there is a stride of 1 used in this layer. The max pooling units have a receptive field of 2-by-1, and there is no overlap between the receptive fields of the max pooling units.



- (a) What value will this network output?
- (b) Assuming the target output for this input is 1, calculate the δ for each neuron in the network.
- (c) Calculate the weight update for each weight in the filter: w_0, w_1, w_2, w_3 .

- * 11. Assume a simple recurrent neural network architecture matching the one shown in the detailed schematic on the left of [Figure 8.37](#)^[502]. This network has two input neurons, three ReLUs in the hidden layer, and two ReLUs in the output layer. Also, all the bias terms in the network are equal to 0.1, and the weight matrices of the network (excluding bias terms) are listed in Equation (8.141)^[530].

$$\underbrace{\begin{bmatrix} -0.07 & 0.05 \\ -0.04 & 0.1 \\ -0.05 & -0.05 \end{bmatrix}}_{\mathbf{W}_{hx}} \underbrace{\begin{bmatrix} -0.22 & -0.1 & 0.05 \\ -0.04 & -0.09 & -0.06 \\ -0.09 & 0 & -0.08 \end{bmatrix}}_{\mathbf{W}_{hh}} \underbrace{\begin{bmatrix} 0.06 & -0.01 & -0.18 \\ -0.06 & 0.13 & 0.14 \end{bmatrix}}_{\mathbf{W}_{yh}}$$

(8.141)

- (a) If $\mathbf{x}_t = [1, 0.5]$ and $\mathbf{h}_{t-1} = [0.05, 0.2, 0.15]$, calculate the value of \mathbf{y}_t .
- (b) Assuming that the target output for time $t = [0, 1]$, calculate the δ value for each neuron in the network.

- * 12. Assuming that the LSTM cell state propagated forward from the last time-step is

$$\mathbf{c}_{t-1} = \begin{bmatrix} +0.5 \\ -0.5 \end{bmatrix}$$

- (a) What will be the value of \mathbf{c}_t if

$$\mathbf{f}_t = \begin{bmatrix} +1.00 \\ +1.00 \end{bmatrix} \quad \mathbf{i}_t^f = \begin{bmatrix} +1.00 \\ +1.00 \end{bmatrix} \quad \mathbf{i}_t^i = \begin{bmatrix} -0.25 \\ +0.25 \end{bmatrix}$$

- (b) What will be the value of \mathbf{c}_t if

$$\mathbf{f}_t = \begin{bmatrix} +1.00 \\ +1.00 \end{bmatrix} \quad \mathbf{i}_t^f = \begin{bmatrix} 0.00 \\ 0.00 \end{bmatrix} \quad \mathbf{i}_t^i = \begin{bmatrix} -0.25 \\ +0.25 \end{bmatrix}$$

- (c) What will be the value of \mathbf{c}_t if

$$\mathbf{f}_t = \begin{bmatrix} 0.00 \\ 0.00 \end{bmatrix} \quad \mathbf{i}_t^f = \begin{bmatrix} +1.00 \\ +1.00 \end{bmatrix} \quad \mathbf{i}_t^i = \begin{bmatrix} -0.25 \\ +0.25 \end{bmatrix}$$

- (d) What will be the value of \mathbf{c}_t if

$$\mathbf{f}_t = \begin{bmatrix} 0.00 \\ 0.00 \end{bmatrix} \quad \mathbf{i}_t^f = \begin{bmatrix} 0.00 \\ 0.00 \end{bmatrix} \quad \mathbf{i}_t^i = \begin{bmatrix} -0.25 \\ +0.25 \end{bmatrix}$$

- * 13. Equations (8.132)^[519] to (8.138)^[520] step through the calculation of the weight update for $\mathbf{W}^{(f)}$ in the context of the forward pass presented in Figure 8.41^[514] and under the assumption that the following error gradients are already calculated:

$$\frac{\partial \mathcal{E}_{t+1}}{\partial \mathbf{c}_t} = \begin{bmatrix} 0.35 \\ 0.50 \end{bmatrix} \quad \frac{\partial \mathcal{E}_{t+1}}{\partial \mathbf{h}_t} = \begin{bmatrix} 0.75 \\ 0.25 \end{bmatrix} \quad \frac{\partial \mathcal{E}_t}{\partial \mathbf{o}_t} = \begin{bmatrix} 0.15 \\ 0.60 \end{bmatrix}$$

- (a) Given this context, calculate $\frac{\partial \mathcal{E}_t}{\partial \mathbf{c}_{t-1}}$.

- (b) Given this context, calculate the vector of error gradients with respect to the input $\mathbf{h}\mathbf{x}_t$ for the forget gate sigmoid layer.

1. Parts of this chapter assume a familiarity with calculus, in particular the concepts of a partial derivative and the chain rule; see Appendix C^[765] for an introduction to these concepts. This chapter

also draws on a number of concepts introduced in Chapter 7^[311], including the gradient descent algorithm, and logistic regression models.

2. See Kelleher (2019) for a history of the development of neural network models and the emergence of deep learning.

3. This explanation is inspired by the discussion in Reagen et al. (2017, p. 14).

4. The axes in Figure 8.8^[398] are slightly offset for ease of reading.

5. See Goodfellow et al. (2016, p. 195) for relevant references.

6. Subsequently, in this chapter we illustrate how this can be done for ReLU, neurons using rectifier activation functions.

7. We have already discussed the derivative of the logistic function in Chapter 7^[311] (see Equation (7.28)^[345]); we rewrite it here using z in place of x for convenience.

8. As Figure 8.13^[410] illustrates, $\text{logistic}(0) = 0.5$

9. Also known as the **loss function** or **cost function**.

10. We introduce the subscript k on the target t_k into this equation to allow for situations in which the network has multiple neurons in the output layer, and the target output then defines a separate target t_k for each of these neurons.

11. In Chapter 7^[311] we discussed dropping the minus sign from the front of $-\mathbf{d}[j]$; compare Equation (7.15)^[326] with Equation (7.16)^[327].

12. See Appendix C^[765].

13. See Section 7.3.3^[328] for further discussions on the role of the learning rate, and Section 7.4.2^[334] for a discussion on different approaches to setting the learning rate.

14. This is the same as the batch gradient descent discussed in Chapter 7^[311].

15. The reuse of the term **batch** in mini-batch learning can lead to confusion. To clarify the distinctive meanings: the terms **batch learning** or **batch gradient descent** typically indicate that the entire training set is processed between each weight update, whereas the term **batch** can also be used to indicate a set of examples in a mini-batch training regime (as in *a batch of examples*), and the term **batch size** describes the number of examples in each batch (or mini-batch).

16. See Goodfellow et al. (2016, p. 272) and references therein for further discussion on the trade-offs in batch size.

17. The concept of a convergence criterion is also used in the gradient decent algorithm discussed in Chapter 7^[311]; see Algorithm 4^[326].

18. This example and dataset is based on the Combined Cycle Power Plant dataset available from the UCI repository at <https://archive.ics.uci.edu/ml/datasets/combined+cycle+power+plant> and originally collected for the work reported in Tüfekci (2014)

19. See Section 7.4.2^[334].

20. Available from the UCI repository at <https://archive.ics.uci.edu/ml/datasets/combined+cycle+power+plant>.

21. This assumption of treating \mathbf{d}_2 as the first example permits us to use the original $w_{7,5} = -0.09$ in our example calculation rather than the updated value for the weight that would be used if \mathbf{d}_1 had already been processed and the weights updated accordingly.

22. The most popular strategy to define a convergence criterion to stop training a neural network is **early stopping**. Early stopping is designed to avoid a model **overfitting** the training data. We explain the early stopping algorithm in Section 8.4.4^[472]. However, for ease of explanation in this section,

we have simply used a threshold of $SSE < 0.0001$ as our convergence criterion. Using a threshold on the error of the model error on the training set as a convergence criterion—as we are doing here—is very likely to result in the model overfitting the training data. Hence it is worth emphasizing that we are using this convergence criterion only for ease of explanation, and in general we recommend that you use early stopping when you are training a neural network.

23. See Equation (8.4)^[386] and Figure 8.2^[387].

24. Note that as with the worked example, to keep the number of decimal points required to represent the calculations through this forward pass manageable, the outputs of the activation function (in this instance the rectified linear function) for each layer have been rounded to four decimal places, and these rounded activations were the activations used in the subsequent calculations.

25. Note that comparing the sum of squared errors for the logistic network in Table 8.4^[426] with the sum of squared errors for the ReLU model in Table 8.10^[441] is not useful, because both of these are errors for random networks.

26. By *unbounded*, we mean that, unlike the logistic function where the maximum value it will return is 1, the rectifier linear function may return any value up to $+\infty$.

27. The similarity of this update rule to the standard weight update rule is apparent if we compare this equation with Equation 8.28^[415].

28. This is why we use a learning rate α to scale the weight updates. Scaling a weight update using a learning rate works because the error derivative defines only the direction the weight update should take and not the update size; and, scaling by the learning rate changes only the step size and not the direction of the update. However, even when we use a learning rate to scale updates, large weights can still result in exploding gradients, which in turn result in inappropriately large weight updates. We discussed the problem of large weight updates in Chapter 7^[311] Section 7.4.2^[334], in which we compared the effect of different learning rates and introduced the idea of using learning rate decay. A relevant point from that discussion was that large weight updates could result in the error actually increasing (see Figure 7.9^[336]).

29. Note that using linear activation functions in this way means that the network as a whole implements a linear function. However, in this instance, this simplification is appropriate because the purpose of this network architecture design is to illustrate the effect of different weight initialization regimes rather than to be accurate on the task.

30. For more on the standardization of inputs, see the discussion on data preprocessing at the start of the worked example in Section 8.3.5^[421].

31. In this case, we chose to standardize the features in the data rather than range-normalize them, in order to align the data configurations used to generate the plots in this section with the assumptions made in the accompanying mathematical analysis.

32. A **violin plot** is a **box plot** that has been augmented to show the probability density of a data at different values in the range. The use of violin plots to illustrate the variance across layers within a network was inspired by a blog post by Daniel Godoy (see <https://towardsdatascience.com/hyperparameters-in-action-part-ii-weight-initializers-35aee1a28404>).

33. Specifically, the calculation of the term $\partial\mathcal{E}/\partial a_k$ (see Equation 8.22^[412]).

34. This is a *naive* assumption because we are making it to simplify the discussion irrespective of whether or not it is true.

35. The variance of the product of two independent random variables X and Y is given by $\text{var}(X \times Y) = [E(X)]^2\text{var}(Y) + [E(Y)]^2\text{var}(X) + \text{var}(X)\text{var}(Y)$.

36. Xavier initialization is named after the first author (Xavier Glorot) of the paper that introduced this layer-wise approach to weight initialization, Glorot and Bengio (2010). However, in some places the author's second name is used instead of his first name to describe the same initialization algorithm, so that it is sometimes called **Glorot initialization**.

37. We can also use one-hot encodings to represent categorical descriptive features (see Section 7.4.3^[336]).

38. This explanation of inverted dropout is inspired by a description given in Andrew Ng's Coursera course; the video is available at <https://www.youtube.com/watch?v=D8PJAL-MZv8&feature=youtu.be>.

39. This operation is sometimes called the **Hadamard product** (see Appendix D^[771]).

40. *NIST* is the acronym for the institute that collected the data, the National Institute for Standards and Technology, and *M* indicates that the original data has been modified to make it easier to use for machine learning. The MNIST dataset is available at <http://yann.lecun.com/exdb/mnist/>.

41. We are using this smaller 6-by-6 image rather than the full 28-by-28 MNIST digit image dimensions to simplify the illustration.

42. Technically, what a convolution network is actually calculating should be called a **cross-correlation** (Charniak, 2019, p. 52), but we ignore this technicality for the purposes of this discussion.

43. In some texts, such as Goodfellow et al. (2016), the application of the activation function is treated as a separate step after the feature map has been generated by the application of the filter. Here we include the application function as part of the generation of the feature map.

44. As noted previously, in some texts, such as Goodfellow et al. (2016), the application of the activation function is treated as a separate step after the feature map has been generated by the application of the filter. In these scenarios, the raw scalar value would be stored in the feature map.

45. This omission of the sub-sampling layer is done simply to illustrate that it is optional.

46. This example is taken from (Mahalunkar and Kelleher, 2018), which reports on experiments that use formal grammars to understand the representational capacity of recurrent neural networks to model long-distance dependencies.

47. The details of how this is done depend on how the output layer is organized. For networks trained using the sum of squared errors loss function, the δ for output neurons is calculated using Equation (8.21)^[411]; for neurons in a softmax output layer the δ is calculated using Equation 8.72^[467].

48. Figure 8.38^[504] is based on a figure from Kelleher (2016). As with the schematic on the left of Figure 8.37^[502], this figure abstracts over some of the details of the network. For example, the layers of neurons are here represented by rectangles with rounded corners with the labels on the rectangles indicating whether the rectangle represents the input layer \mathbf{x}_t , the hidden layer \mathbf{h}_t , the output layer \mathbf{y}_t , or the hidden layer from the previous time-step \mathbf{h}_{t-1} ; and the (multiple) connections between neurons in different layers are here represented by a single arrow labeled with the name of the weight matrix for the weights on those connections.

49. For this discussion we treat all neurons in an unrolled network that use the same set of weights as instances of the same neuron; for example, for a neuron in the hidden layer, a different instance of that neuron will occur in each time-step.

9

Evaluation

“Essentially, all models are wrong, but some are useful.”
—George E. P. Box

In this chapter we describe how to evaluate machine learning models built for predictive data analytics tasks. We start by outlining the fundamental goals of evaluation before describing the standard approach of measuring the **misclassification rate** for a model on a **hold-out test set**. We then present extensions and variations of this approach that describe different performance measures for models predicting categorical, continuous, and multinomial targets; how to design effective evaluation experiments; and how to continually measure the performance of models after deployment.

9.1 Big Idea

The year is 1904, and you are a research assistant working in the lab of physicist Professor René Blondlot, at the University of Nancy, in France. Until recently, spirits have been very high in the lab due to the discovery earlier the previous year of a new form of electromagnetic radiation called **N rays** (Blondlot, 1903). The existence of N rays was first hinted at in an experiment performed at the lab that was designed to answer questions about the exact nature of the recently discovered X-ray radiation. This experiment showed behavior uncharacteristic of X-rays, which Professor Blondlot interpreted to mean that another, different type of electromagnetic radiation must exist. This new type of radiation was named the N ray (after the University of Nancy), and experiments were designed to demonstrate its existence. These experiments were performed in Nancy and confirmed, to the satisfaction of everyone involved, that N rays did indeed exist. This new

discovery caused ripples of great excitement in the international physics community and greatly enhanced the reputations of the lab at Nancy and Professor Blondlot.

Doubt has begun to surround the phenomenon of N rays, however, as a number of international physicists have not been able to reproduce the results of the experiments that demonstrate their existence. You are currently preparing for a visit by the American physicist Professor Robert W. Wood to whom Professor Blondlot has agreed to demonstrate the experiments that show the effects of N rays. In one of these experiments, the brightening of a small spark that occurs when an object that supposedly emits N rays is brought close to it is measured. In a second experiment, the refractive effect of passing N rays through a prism (something that does not happen to X-rays) is demonstrated. You carefully prepare the apparatus for these experiments, and on the 21st of September 1904, you spend three hours assisting Professor Blondlot in demonstrating them to Professor Wood.

Just over a week later, you are very disappointed to read an article published by Wood in the journal *Nature* (Wood, 1904) that completely refutes the existence of N rays. He dismisses the experimental setup for the experiments you demonstrated as entirely inappropriate. Even more dramatically, he reports that he actually interfered with the second experiment by removing the prism from the apparatus during the demonstration (because the experiment was completed in darkness, Wood was able to do this without anybody noticing), which made no difference to the results that you measured and reported, so it completely undermines them. Within a few years of the publication of this article, the consensus within the physics research community is that N rays do not exist.

The story of Professor Blondlot and N rays is true,¹ and it is one of the most famous examples in all of science of how badly designed experiments can lead to completely inappropriate conclusions. There was no fraud involved in the work at the Nancy lab. The experiments designed to show the existence of N rays simply relied too much on subjective measurements (the changes in the brightness of the spark was measured by simple human observation) and did not account for all the reasons other than the presence of N rays that could have created the phenomena observed.

The *big idea* to take from this example to predictive data analytics projects is that when we evaluate predictive models, we must ensure that the evaluation experiments are designed so that they give an accurate estimate of how the models will perform when deployed. The most important part of the design of an evaluation experiment for a predictive model is ensuring that the data used to evaluate the model is not the same as the data used to train the model.

9.2 Fundamentals

Over the last four chapters, we have discussed a range of approaches to building machine learning models that make various kinds of predictions. The question that we must answer in the **Evaluation** phase of the **CRISP-DM** process (recall Section 1.6^[15]) is *Can the model generated do the job that it has been built for?* The purpose of evaluation is threefold:

- to determine which of the models that we have built for a particular task is most suited to that task
- to estimate how the model will perform when deployed
- to convince the business for whom a model is being developed that the model will meet their needs

The first two items in this list focus on measuring and comparing the performance of a group of models to determine which model *best* performs the prediction task that the models have been built to address. The definition of *best* is important here. No model will ever be perfect, so some fraction of the predictions made by every model will be incorrect. There are, though, a range of ways in which models can be incorrect, and different analytics projects will emphasize some over others. For example, in a medical diagnosis scenario, we would require that a prediction model be very accurate in its diagnoses and, in particular, never incorrectly predict that a sick patient is healthy, as that patient will then leave the health-care system and could subsequently develop serious complications. On the other hand, a model built to predict which customers would be most likely to respond to an online ad only needs to do a slightly better than random job of selecting those customers that will actually respond in order to make a profit for the company. To address these different project requirements, there is a spectrum of different approaches to measuring the performance of

a model, and it is important to align the correct approach with a given modeling task. The bulk of this chapter discusses these different approaches and the kinds of modeling tasks that they best suit.

As indicated by the third item in the list above, there is more to evaluation than measuring model performance. For a model to be successfully deployed, we must consider issues like how quickly the model makes predictions, how easy it is for human analysts to understand the predictions made by a model, and how easy it is to retrain a model should it go stale over time. We return to these issues in the final section of this chapter.

9.3 Standard Approach: Misclassification Rate on a Hold-Out Test Set

The basic process for evaluating the effectiveness of predictive models is simple. We take a dataset for which we know the predictions that we expect the model to make, referred to as a **test set**, present the instances in this dataset to a trained model, and record the predictions that the model makes. These predictions can then be compared to the predictions we expected the model to make. Based on this comparison, a **performance measure** can be used to capture, numerically, how well the predictions made by the model match those that were expected.

There are different ways in which a test set can be constructed from a dataset, but the simplest is to use what is referred to as a **hold-out test set**. A hold-out test set is created by randomly sampling a portion of the data in the ABT we created in the **Data Preparation** phase. This random sample *is never used in the training process* but reserved until after the model has been trained, when we would like to evaluate its performance. [Figure 9.1](#)^[536] illustrates this process.

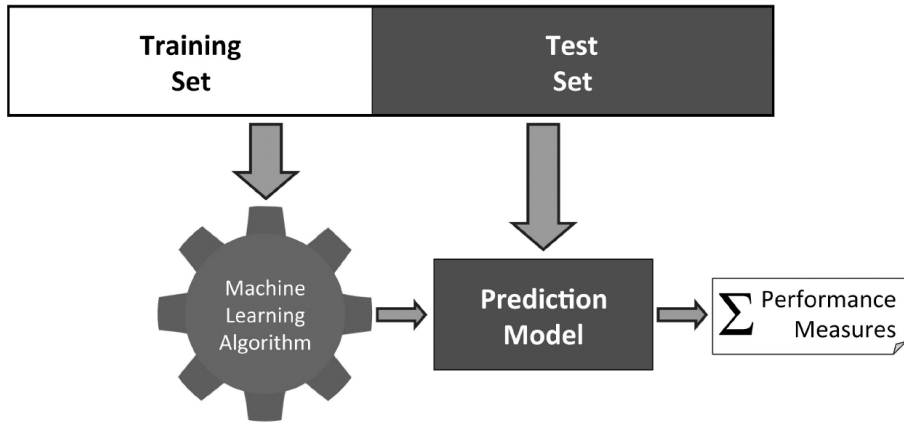


Figure 9.1

The process of building and evaluating a model using a hold-out test set.

Using a hold-out test set avoids the issue of **peeking**, which arises when the performance of a model is evaluated on the same data used to train it; because the data was used in the training process, the model has already *seen* this data, so it is probable that it will perform very well when evaluated on this data. An extreme case of this problem happens when k nearest neighbor models are used. If the model is asked to make a prediction about an instance that was used to train it, the model will find as the nearest neighbor, for this instance, the instance itself. Therefore, if the entire training set is presented to this model, its performance will appear to be perfect. Using a hold-out test set avoids this problem, because none of the instances in the test set will have been used in the training process. Consequently, the performance of the model on the test set is a better measure of how the model is likely to perform when actually deployed and shows how well the model can **generalize** beyond the instances used to train it. The most important rule in evaluating models is not to use the same data sample both to evaluate the performance of a predictive model and to train it.

For a first example of how to evaluate the performance of a predictive model, let us assume that we are dealing with an email classification problem with a binary categorical target feature distinguishing between *spam* and *ham* emails. When making predictions about categorical targets, we need performance measures that capture how often the model makes correct predictions and the severity of the mistakes that the model makes when it is incorrect. [Table 9.1](#)^[537] shows the expected targets for a small

sample test set and a set of predictions made by a model trained for this prediction problem (the FP and FN comments in the Outcome column will be explained shortly).

Table 9.1

A sample test set with model predictions.

ID	Target	Pred.	Outcome	ID	Target	Pred.	Outcome
1	spam	ham	FN	11	ham	ham	TN
2	spam	ham	FN	12	spam	ham	FN
3	ham	ham	TN	13	ham	ham	TN
4	spam	spam	TP	14	ham	ham	TN
5	ham	ham	TN	15	ham	ham	TN
6	spam	spam	TP	16	ham	ham	TN
7	ham	ham	TN	17	ham	spam	FP
8	spam	spam	TP	18	spam	spam	TP
9	spam	spam	TP	19	ham	ham	TN
10	spam	spam	TP	20	ham	spam	FP

The simplest performance measure we can use to assess how well this model has performed for this problem is the **misclassification rate**. The misclassification rate is the number of incorrect predictions made by the model divided by the total number of predictions made:

$$\text{misclassification rate} = \frac{\text{number incorrect predictions}}{\text{total predictions}} \quad (9.1)$$

In the example in [Table 9.1](#)^[537], 20 predictions are made in total, and out of these, 5 are incorrect (instances \mathbf{d}_1 , \mathbf{d}_2 , \mathbf{d}_{12} , \mathbf{d}_{17} , and \mathbf{d}_{20}). Therefore, the misclassification rate is calculated as $\frac{5}{20} = 0.25$, which is usually expressed as a percentage: 25%. This tells us that the model is incorrect about a quarter of the time. Misclassification rate can assume values in the range [0,1], and lower values indicate better performance.

The **confusion matrix** is a very useful analysis tool to capture what has happened in an evaluation test in a little more detail and is the basis for calculating many other performance measures. The confusion matrix calculates the frequencies of each possible outcome of the predictions made by a model for a test dataset in order to show, in detail, how the model is

performing. For a prediction problem with a binary target feature (where, by convention, we refer to the two levels as **positive** and **negative**), there are just four outcomes when the model makes a prediction:

- **True Positive (TP):** an instance in the test set that had a positive target feature value and that was predicted to have a positive target feature value
- **True Negative (TN):** an instance in the test set that had a negative target feature value and that was predicted to have a negative target feature value
- **False Positive (FP):** an instance in the test set that had a negative target feature value but that was predicted to have a positive target feature value
- **False Negative (FN):** an instance in the test set that had a positive target feature value but that was predicted to have a negative target feature value

The Outcome column of [Table 9.1](#)^[537] shows the category to which each prediction made by the model belongs. One thing worth keeping in mind is that there are two ways in which the prediction made by a model can be correct—true positive or true negative—and two ways in which the prediction made by a model can be incorrect—false positive or false negative.² The confusion matrix allows us to capture these different types of correct and incorrect predictions made by the model.

Each cell in a confusion matrix represents one of these outcomes (TP, TN, FP, FN) and counts the number of times this outcome occurred when the test dataset was presented to the model. The structure of a confusion matrix for a simple prediction task with two target levels is shown in [Table 9.2](#)^[538]. The columns in the table are labeled *Prediction-positive* and *Prediction-negative* and represent the predictions generated by a model, which is either positive or negative. The rows in the table are labeled *Target-positive* and *Target-negative* and represent the target feature values that were expected. The top left cell in the confusion matrix, labeled TP, shows the number of instances in a test set that have a positive target feature value that were also predicted by the model to have a positive target feature value. Similarly, the bottom left cell in the matrix, labeled FP, shows the number of instances in a test set that have a negative target feature value

that were in fact predicted by the model to have a positive target feature value. TN and FN are defined similarly.

Table 9.2

The structure of a confusion matrix.

		Prediction	
		positive	negative
Target	positive	TP	FN
	negative	FP	TN

At a glance, the confusion matrix can show us that a model is performing well if the numbers on its diagonal, representing the true positives and true negatives, are high. Looking at the other cells within the confusion matrix can show us what kind of mistakes the model is making. [Table 9.3](#)^[539] shows the confusion matrix for the set of predictions shown in [Table 9.1](#)^[537] (in this case, we refer to the *spam* target level as the positive level and *ham* as the negative level).³

Table 9.3

A confusion matrix for the set of predictions shown in [Table 9.1](#)^[537].

		Prediction	
		<i>spam</i>	<i>ham</i>
Target	<i>spam</i>	6	3
	<i>ham</i>	2	9

It is clear from the values along the diagonal, the true positives and true negatives, that the model is doing a reasonably good job of making accurate predictions. We can actually calculate the **misclassification rate** directly from the confusion matrix as follows:

$$\text{misclassification rate} = \frac{(FP + FN)}{(TP + TN + FP + FN)} \quad (9.2)$$

In the email classification example we have been following, the misclassification rate would be

$$\text{misclassification rate} = \frac{(2 + 3)}{(6 + 9 + 2 + 3)} = 0.25$$

For completeness, it is worth noting that **classification accuracy** is the opposite of misclassification rate. Again, using the confusion matrix, classification accuracy is defined as

$$\text{classification accuracy} = \frac{(TP + TN)}{(TP + TN + FP + FN)} \quad (9.3)$$

Classification accuracy can assume values in the range [0,1], and higher values indicate better performance. For the email classification task, classification accuracy would be

$$\text{classification accuracy} = \frac{(6 + 9)}{(6 + 9 + 2 + 3)} = 0.75$$

We can also use the confusion matrix to begin to investigate the kinds of mistakes that the prediction model is making. For example, the model makes a prediction of *ham* incorrectly 3 times out of the 9 times that the correct prediction should be *spam* (33.333% of the time), while it makes a prediction of *spam* incorrectly just 2 times out the 11 times that the correct prediction should be *ham* (18.182% of the time). This suggests that when the model makes mistakes, it more commonly incorrectly predicts the *spam* level than the *ham* level. This kind of insight that we can get from the confusion matrix can help in trying to improve a model, as it can suggest to us where we should focus our work.

This section has presented a basic approach to evaluating prediction models. The most important things to take away from this example are:

1. It is crucial to use data to evaluate a model that has not been used to train the model.
2. The overall performance of a model can be captured in a single performance measure, for example, misclassification rate.
3. To fully understand how a model is performing, it can often be useful to look beyond a single performance measure.

There are, however, a range of variations to this standard approach to evaluating prediction model performance, and the remainder of this chapter

covers the most important of these.

9.4 Extensions and Variations

When evaluating the performance of prediction models, there is always a tension between the need to fully understand the performance of the model and the need to reduce model performance to a single measure that can be used to rank models by performance. For example, a set of confusion matrices gives a detailed description of how a set of models trained on a categorical prediction problem performed and can be used for a detailed comparison of performances. Confusion matrices, however, cannot be ordered and so cannot be used to rank the performance of the set of models. To perform this ranking, we need to reduce the information contained in the confusion matrix to a single measure, for example, misclassification rate. Any information reduction process will result in some information loss, and a single measure of model performance will be designed to emphasize some aspects of model performance and de-emphasize, or lose, others. For this reason, there are a variety of different performance measures and no single approach that is appropriate for all scenarios.

This section covers a selection of the most important performance measures. We also describe different experimental designs for evaluating prediction models and ways to monitor model performance after a model has been deployed.

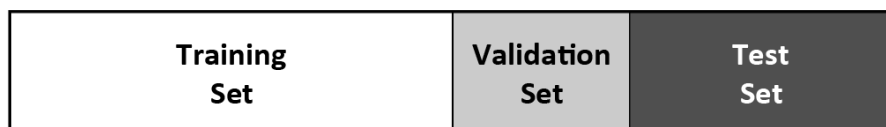
9.4.1 Designing Evaluation Experiments

As well as being required to select appropriate performance measures to use when evaluating trained models, we also need to ensure that we are using the appropriate evaluation experiment design. The goal here is to ensure that we calculate the best estimate of how a prediction model will perform when actually deployed *in the wild*. In this section we will describe the most important evaluation experiment designs and indicate when each is most appropriate.

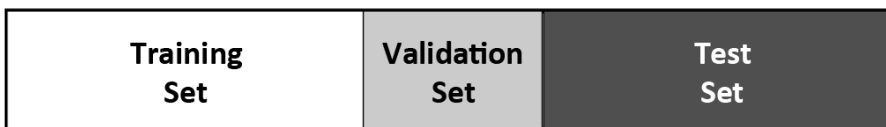
9.4.1.1 Hold-out sampling In Section 9.3^[535] we used a **hold-out test set** to evaluate the performance of a model. The important characteristic of this test set was that it was not used in the process of training the model. Therefore, the performance measured on this test set should be a good indicator of how well the model will perform on future unseen data for

which it will be used to make predictions after deployment. This is an example of using a **sampling method** to evaluate the performance of a model, as we take distinct, random, non-overlapping **samples** from a larger dataset and use these for training and testing a prediction model. When we use a hold-out test set, we take one sample from the overall dataset to use to train a model and another separate sample to test the model.

Hold-out sampling is probably the simplest form of sampling that we can use and is most appropriate when we have very large datasets from which we can take samples. This ensures that the training set and test set are sufficiently large to train an accurate model and fully evaluate the performance of that model. Hold-out sampling is sometimes extended to include a third sample, the **validation set**. The validation set is used when data outside the training set is required in order to tune particular aspects of a model. For example, when **wrapper-based feature selection** techniques are used, a validation set is required in order to evaluate the performance of the different feature subsets on data not used in training. It is important that after the feature selection process is complete, a separate test set still exists that can be used to evaluate the expected performance of the model on future unseen data after deployment. [Figure 9.2](#)^[541] illustrates how a large ABT can be divided into a **training set**, a **validation set**, and a **test set**. There are no fixed recommendations for how large the different datasets should be when hold-out sampling is used, although training:validation:test splits of 50:20:30 or 40:20:40 are common.



(a) A 50:20:30 split



(b) A 40:20:40 split

Figure 9.2

Hold-out sampling can divide the full data into training, validation, and test sets.

One of the most common uses of a validation set is to avoid **overfitting** when using machine learning algorithms that iteratively build more and more complex models. The **ID3** algorithm for building **decision trees** and the **gradient descent** algorithm for building regression models are two examples of this type of approach. As the algorithm proceeds, the model that it is building will become more and more fitted to the nuances of the training data. We can see this in the solid line in [Figure 9.3^{\[542\]}](#). This shows how the misclassification rate made by a model on a set of training instances changes as the training process continues. This will continue almost indefinitely as the model becomes more and more tuned to the instances in the training set. At some point in this process, however, overfitting will begin to occur, and the ability of the model to generalize well to new query instances will diminish.

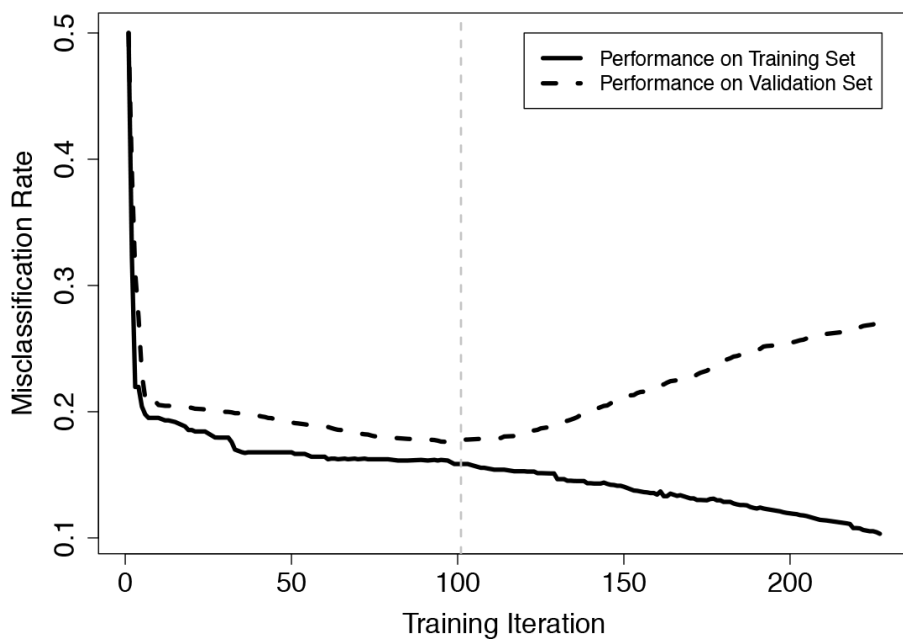


Figure 9.3

Using a validation set to avoid overfitting in iterative machine learning algorithms.

We can find the point at which overfitting begins to happen by comparing the performance of a model at making predictions for instances in the training dataset used to build it versus its ability to make predictions for instances in a validation dataset as the training process continues. The dashed line in [Figure 9.3^{\[542\]}](#) shows the performance of the model being trained on a validation dataset. We can see that, initially, the performance of

the model on the validation set falls almost in line with the performance of the model on the training dataset (we usually expect the model to perform slightly better on the training set). About halfway through the training process, however, the performance of the model on the validation set begins to disimprove. This is the point at which we say overfitting has begun to occur (this is shown by the vertical dashed line, at Training Iteration = 100, in [Figure 9.3](#)^[542]). To combat overfitting, we allow algorithms to train models beyond this point but save the model generated at each iteration. After the training process has completed, we find the point at which performance on the validation set began to disimprove and revert back to the model trained at that point. This process is essentially the same as the decision tree post-pruning process described in [Section 4.4.4](#)^[153].

Two issues arise when using hold-out sampling. First, using hold-out sampling requires that we have enough data available to make suitably large training, test, and if required, validation sets. This is not always the case, and making any of these partitions too small can result in a poor evaluation. Second, performance measured using hold-out sampling can be misleading if we happen to make a **lucky split** of the data that places the *difficult* instances into the training set and the *easy* ones into the test set. This will make the model appear much more accurate than it will actually be when deployed. An example of a commonly used sampling method that attempts to address these two issues is **k-fold cross validation**.

9.4.1.2 k-Fold cross validation When **k-fold cross validation** is used, the available data is divided into k equal-sized **folds** (or partitions), and k separate evaluation experiments are performed. In the first evaluation experiment, the data in the 1st fold is used as the test set, and the data in the remaining $k - 1$ folds is used as the training set. A model is trained using the training set, and the relevant performance measures on the test set are recorded. A second evaluation experiment is then performed using the data in the 2nd fold as the test set and the data in the remaining $k - 1$ folds as the training set. Again the relevant performance measures are calculated on the test set and recorded. This process continues until k evaluation experiments have been conducted and k sets of performance measures have been recorded. Finally, the k sets of performance measures are aggregated to give one overall set of performance measures. Although k can be set to any

value, 10-fold cross validation is probably the most common variant used in practice. [Figure 9.4](#)^[543] illustrates how the available data is split during the k -fold cross validation process. Each row represents a fold in the process, in which the black rectangles indicate the data used for testing while the white spaces indicate the data used for training.

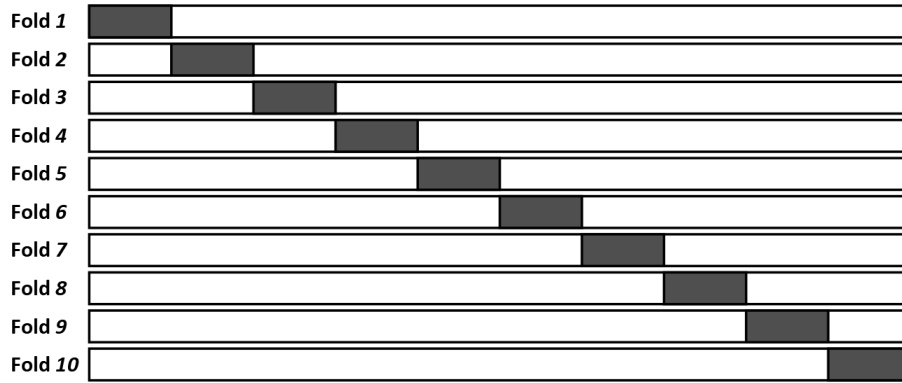


Figure 9.4

The division of data during the k -fold cross validation process. Black rectangles indicate test data, and white spaces indicate training data.

Let's consider an example. As part of a medical decision making system, a prediction system that can automatically determine the orientation of chest X-rays (the orientations can be *lateral* or *frontal*) is built.⁴ Based on a full dataset of 1,000 instances, we decide to evaluate the performance of this system with classification accuracy using 5-fold cross validation. So, the full dataset is divided into 5 folds (each containing 200 instances), and five evaluation experiments are performed using 1 fold as the test set and the remaining folds as the training set. The confusion matrices and class accuracy measures arising from each fold are shown in [Table 9.4](#)^[544].

Table 9.4

The performance measures from the five individual evaluation experiments and an overall aggregate from the 5-fold cross validation performed on the chest X-ray classification dataset.

Fold	Confusion Matrix				Classification
		Prediction		Accuracy	
		<i>lateral frontal</i>			
1	Target	<i>lateral</i>	43	9	81%
		<i>frontal</i>	10	38	
2	Target	<i>lateral</i>	46	9	88%
		<i>frontal</i>	3	42	
3	Target	<i>lateral</i>	51	10	82%
		<i>frontal</i>	8	31	
4	Target	<i>lateral</i>	51	8	85%
		<i>frontal</i>	7	34	
5	Target	<i>lateral</i>	46	9	84%
		<i>frontal</i>	7	38	
Overall	Target	<i>lateral</i>	237	45	84%
		<i>frontal</i>	35	183	

The performance measures for each fold (in this case, a confusion matrix and a class accuracy measure) can be aggregated into summary performance measures that capture the overall performance across the 5 folds. The aggregate confusion matrix, generated by summing together the corresponding cells in the individual confusion matrices for each fold, is shown at the bottom of [Table 9.4](#)^[544]. The aggregate class accuracy measure can then be calculated from this combined confusion matrix and, in this case, turns out to be 84%. When different performance measures are used, the aggregates can be calculated in the same way.

There is a slight shift in emphasis here from evaluating the performance of one model, to evaluating the performance of a set of k models. Our goal, however, is still to estimate the performance of a model after deployment. When we have a small dataset (introducing the possibility of a lucky split), measuring aggregate performance using a set of models gives a better estimate of post-deployment performance than measuring performance using a single model. After estimating the performance of a deployed model using k -fold cross validation, we typically train the model that will be deployed using all of the available data. This contrasts with the hold-out sampling design, in which we simply deploy the model that has been evaluated.

9.4.1.3 Leave-one-out cross validation **Leave-one-out cross validation**, also known as **jackknifing**, is an extreme form of k -fold cross validation in which the number of folds is the same as the number of training instances. This means that each fold of the test set contains only one instance, and the training set contains the remainder of the data. Leave-one-out cross validation is useful when the amount of data available is too small to allow big enough training sets in a k -fold cross validation. [Figure 9.5](#)^[546] illustrates how the available data is split during the leave-one-out cross validation process. Each row represents a fold in the process, in which the black rectangles indicate the instance that is used for testing while the white spaces indicate the data used for training.

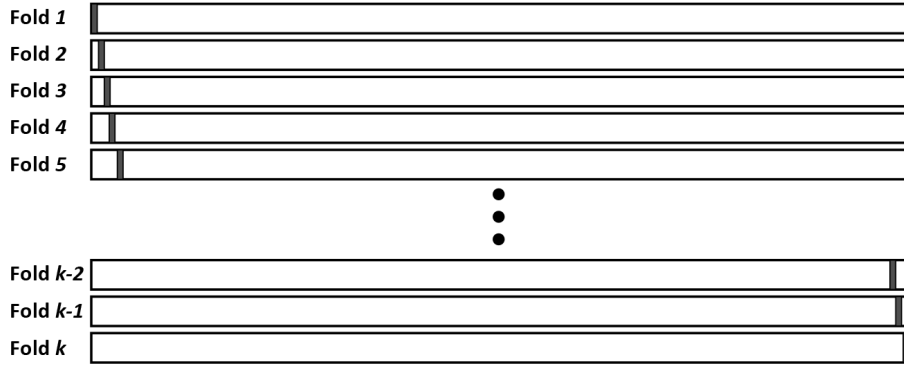


Figure 9.5

The division of data during the leave-one-out cross validation process. Black rectangles indicate instances in the test set, and white spaces indicate training data.

At the conclusion of the leave-one-out cross validation process, a performance measure will have been calculated for every instance in the dataset. In the same way as we saw in [Table 9.4](#)^[544] for k -fold cross validation, these performance measures are aggregated across all the folds to arrive at an overall measure of model performance.

9.4.1.4 Bootstrapping The next sampling method we will look at is **bootstrapping**, and in particular the ε_0 **bootstrap**. Bootstrapping approaches are preferred over cross validation approaches in contexts with very small datasets (approximately fewer than 300 instances). Similar to k -fold cross validation, the ε_0 bootstrap iteratively performs multiple evaluation experiments using slightly different training and test sets each time to evaluate the expected performance of a model. To generate these partitions for an iteration of the ε_0 bootstrap, a random selection of m instances is taken from the full dataset to generate a test set, and the remaining instances are used as the training set. Using the training set to train a model and the test set to evaluate it, a performance measure (or measures) is calculated for this iteration. This process is repeated for k iterations, and the average of the individual performance measures, the titular ε_0 , gives the overall performance of the model. Typically, in the ε_0 bootstrap, k is set to values greater than or equal to 200, much larger values than when k -fold cross validation is used. [Figure 9.6](#)^[547] illustrates how the data is divided during the ε_0 bootstrap process. Each row represents an iteration of the process, in which the black rectangles indicate the data used for testing while the white spaces indicate the data used for training.

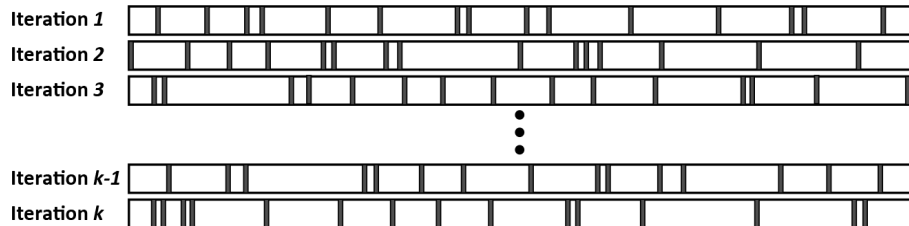


Figure 9.6

The division of data during the ε_0 bootstrap process. Black rectangles indicate test data, and white spaces indicate training data.

9.4.1.5 Out-of-time sampling The sampling methods discussed in the previous section all rely on random sampling from a large dataset in order to create test sets. In some applications there is a natural structure in the data that we can take advantage of to form test sets. In scenarios that include a time dimension, this can be particularly effective and is often referred to as **out-of-time sampling**, because we use data from one period to build a training set and data out of another period to build a test set. For example, in a customer churn scenario, we might use details of customer behavior from one year to build a training set and details of customer behavior from a subsequent year to build a test set. [Figure 9.7^{\[547\]}](#) illustrates the process of out-of-time sampling.

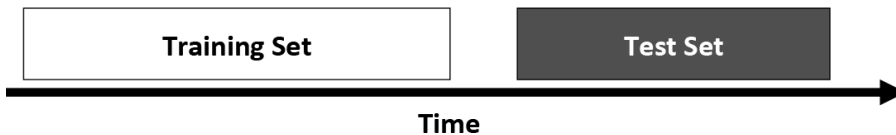


Figure 9.7

The out-of-time sampling process.

Out-of-time sampling is essentially a form of hold-out sampling in which the sampling is done in a targeted rather than a random fashion. When using out-of-time sampling, we should be careful to ensure that the times from which the training and test sets are taken do not introduce a bias into the evaluation process, because the two different time samples are not really representative. For example, imagine we wished to evaluate the performance of a prediction model built to estimate the daily energy demand in a residential building based on features describing the family that lives in the house, the weather on a given day, and the time of the year. If the training sample covered a period in the summer and the testing

sample covered a period in the winter, the results of any evaluation would not provide a reliable measure of how likely the model might actually perform when deployed. It is important when choosing the periods for out-of-time sampling that the time spans are large enough to take into account any cyclical behavioral patterns or that other approaches are used to account for these.

9.4.2 Performance Measures: Categorical Targets

This section describes the most important performance measures for evaluating the performance of models with categorical target features.

9.4.2.1 Confusion matrix-based performance measures Confusion matrices are a convenient way to fully describe the performance of a predictive model when applied to a test set. They are also the basis for a whole range of different performance measures that can highlight different aspects of the performance of a predictive model. The most basic of these measures are **true positive rate (TPR)**, **true negative rate (TNR)**, **false negative rate (FNR)**, and **false positive rate (FPR)**, which convert the raw numbers from the confusion matrix into percentages.⁵ These measures are defined as follows:

$$TPR = \frac{TP}{(TP + FN)} \quad (9.4)$$

$$TNR = \frac{TN}{(TN + FP)} \quad (9.5)$$

$$FPR = \frac{FP}{(TN + FP)} \quad (9.6)$$

$$FNR = \frac{FN}{(TP + FN)} \quad (9.7)$$

There are strong relationships between these measures, for example: $FNR = 1 - TPR$, and $FPR = 1 - TNR$.

All these measures can have values in the range [0,1]. Higher values of TPR and TNR indicate better model performance, while the opposite is the case for FNR and FPR. Confusion matrices are often presented containing these measures rather than the raw counts, although we recommend using

raw counts so that the number of instances with each of the different levels of the target feature remains apparent.

For the email classification data given in [Table 9.1](#)^[537], the confusion matrix-based values can be calculated as follows:

$$\begin{aligned} TPR &= \frac{6}{(6+3)} = 0.667 \\ TNR &= \frac{9}{(9+2)} = 0.818 \\ FPR &= \frac{2}{(9+2)} = 0.182 \\ FNR &= \frac{3}{(6+3)} = 0.333 \end{aligned}$$

These values immediately suggest that the model is better at predicting the *ham* level (TNR) than it is at predicting the *spam* level (TPR).

9.4.2.2 Precision, recall, and F_1 measure Precision, recall, and the F_1 measure are another frequently used set of performance measures that can be calculated directly from the confusion matrix. Precision and recall are defined as follows:

$$precision = \frac{TP}{(TP + FP)} \tag{9.8}$$

$$recall = \frac{TP}{(TP + FN)} \tag{9.9}$$

Recall is equivalent to true positive rate (TPR) (compare Equations (9.4)^[548] and (9.9)^[549]). Recall tells us how confident we can be that all the instances with the positive target level have been found by the model. Precision captures how often, when a model makes a positive prediction, this prediction turns out to be correct. Precision tells us how confident we can be that an instance predicted to have the positive target level actually has the positive target level. Both precision and recall can assume values in the range [0,1], and higher values in both cases indicate better model performance.

Returning to the email classification example, and assuming again that *spam* emails are the positive level, precision measures how often the emails marked as spam actually are spam, whereas recall measures how often the spam messages in the test set were actually marked as *spam*. The precision

and recall measures for the email classification data shown in [Table 9.1](#)^[537] are

$$\begin{aligned} \text{precision} &= \frac{6}{(6+2)} = 0.750 \\ \text{recall} &= \frac{6}{(6+3)} = 0.667 \end{aligned}$$

Email classification is a good application scenario in which the different information provided by precision and recall is useful. The precision value tells us how likely it is that a genuine *ham* email could be marked as *spam* and, presumably, deleted: 25% ($1 - \text{precision}$). Recall, on the other hand, tells us how likely it is that a spam email will be missed by the system and end up in our in-box: 33.333% ($1 - \text{recall}$). Having both of these numbers is useful as it allows us to think about tuning the model toward one kind of error or the other. Is it better for a genuine email to be marked as *spam* and deleted, or for a spam email to end up in our in-box? The performance recorded in [Table 9.1](#)^[537] shows that this system is slightly more likely to make the second kind of mistake than the first.

Precision and recall can be collapsed to a single performance measure known as the **F_1 measure**,⁶ which offers a useful alternative to the simpler misclassification rate. The F_1 measure is the **harmonic mean** of precision and recall and is defined as

$$F_1 \text{ measure} = 2 \times \frac{(\text{precision} \times \text{recall})}{(\text{precision} + \text{recall})} \quad (9.10)$$

In Section A.1^[745] we talk about how measures of **central tendency** attempt to capture the average value of a list of numbers. Although the **arithmetic mean** and **median** are two of the most commonly known such measures, there are more, including the **harmonic mean**. The harmonic mean tends toward the smaller values in a list of numbers and so can be less sensitive to large outliers than the arithmetic mean, which tends toward higher values. This characteristic is useful in the generation of performance measures like the F_1 measure, as we typically prefer measures to highlight shortcomings in our models rather than hide them. The F_1 measure can assume values in the range $(0,1]$, and higher values indicate better performance.

For the email classification dataset shown in [Table 9.1](#)^[537], the F_1 measure (again assuming that the *spam* level is the positive level) is calculated as

$$F_1 \text{ measure} = 2 \times \frac{\left(\frac{6}{(6+2)} \times \frac{6}{(6+3)} \right)}{\left(\frac{6}{(6+2)} + \frac{6}{(6+3)} \right)} \\ = 0.706$$

Precision, recall, and the F_1 measure work best in prediction problems with binary target features and place an emphasis on capturing the performance of a prediction model on the positive, or most important, level. These measures place less emphasis on the performance of the model on the negative target level. This is appropriate in many applications. For example, in medical applications, a prediction that a patient has a disease is much more important than a prediction that a patient does not. In many cases, however, it does not make sense to consider one target level as being more important. The **average class accuracy** performance measure can be effective in these cases.

9.4.2.3 Average class accuracy Classification accuracy can mask poor performance. For example, the confusion matrices shown in [Tables 9.5](#)^[551] and [9.6](#)^[551] show the performance of two different models on a test dataset that relates to a prediction problem in which we would like to predict whether a customer will churn or not. The accuracy for the model associated with the confusion matrix shown in [Table 9.5](#)^[551] is 91%, while for the model associated with the confusion matrix shown in [Table 9.6](#)^[551], the accuracy is just 78%. In this example the test dataset is quite **imbalanced**, containing 90 instances with the *non-churn* level and just 10 instances with the *churn* level. This means that the performance of the model on the *non-churn* level overwhelms the performance on the *churn* level in the accuracy calculation and illustrates how classification accuracy can be a misleading measure of model performance.

Table 9.5

A confusion matrix for a k -NN model trained on a churn prediction problem.

		Prediction	
		<i>non-churn</i>	<i>churn</i>
Target	<i>non-churn</i>	90	0
	<i>churn</i>	9	1

Table 9.6

A confusion matrix for a naive Bayes model trained on a churn prediction problem.

		Prediction	
		<i>non-churn</i>	<i>churn</i>
Target	<i>non-churn</i>	70	20
	<i>churn</i>	2	8

To address this issue, we can use **average class accuracy**⁷ instead of classification accuracy.⁸ The average class accuracy is calculated as

$$\text{average class accuracy} = \frac{1}{|levels(t)|} \sum_{l \in levels(t)} recall_l \quad (9.11)$$

where $levels(t)$ is the set of levels that the target feature, t , can assume; $|levels(t)|$ is the size of this set; and $recall_l$ refers to the recall achieved by a model for level l .⁹ The average class accuracies for the model performances shown in Tables 9.5^[551] and 9.6^[551] are $\frac{1}{2}(1 + 0.1) = 55\%$ and $\frac{1}{2}(0.778 + 0.8) = 78.889\%$ respectively, which would indicate that the second model is actually a better performer than the first. This result is contrary to the conclusion drawn from classification accuracy but is more appropriate in this case due to the target level imbalance present in the data.

The average class accuracy measure shown in Equation (9.11)^[551] uses an **arithmetic mean** and so can be more fully labeled $average class accuracy_{AM}$. While this is an improvement over raw classification accuracy, many people prefer to use a **harmonic mean**¹⁰ instead of an arithmetic mean when calculating average class accuracy. Arithmetic means are susceptible to influence of large outliers, which can inflate the apparent performance of a model. The **harmonic mean**, on the other hand, emphasizes the importance of smaller values and so can give a slightly more realistic measure of how well a model is performing. The harmonic mean is defined as follows:

$$\text{average class accuracy}_{HM} = \frac{1}{\frac{1}{|levels(t)|} \sum_{l \in levels(t)} \frac{1}{recall_l}} \quad (9.12)$$

where the notation meanings are the same as for Equation (9.11)^[551]. The *average class accuracy*_{HM} for the model performances shown in Tables 9.5^[551] and 9.6^[551] are

$$\frac{1}{\frac{1}{2} \left(\frac{1}{1.0} + \frac{1}{0.1} \right)} = \frac{1}{5.5} = 18.2\%$$

and

$$\frac{1}{\frac{1}{2} \left(\frac{1}{0.778} + \frac{1}{0.800} \right)} = \frac{1}{1.268} = 78.873\%$$

The harmonic mean results in a more pessimistic view of model performance than an arithmetic mean. To further illustrate the difference between arithmetic mean and harmonic mean, Figure 9.8^[553] shows the arithmetic mean and the harmonic mean of all combinations of two features A and B that range from 0 to 100. The curved shape of the harmonic mean surface shows that the harmonic mean emphasizes the contribution of smaller values more than the arithmetic mean—note how the sides of the surface are pulled down to the base of the graph by the harmonic mean. We recommend that, in general, when calculating average class accuracy, the harmonic mean should be used rather than the arithmetic mean.

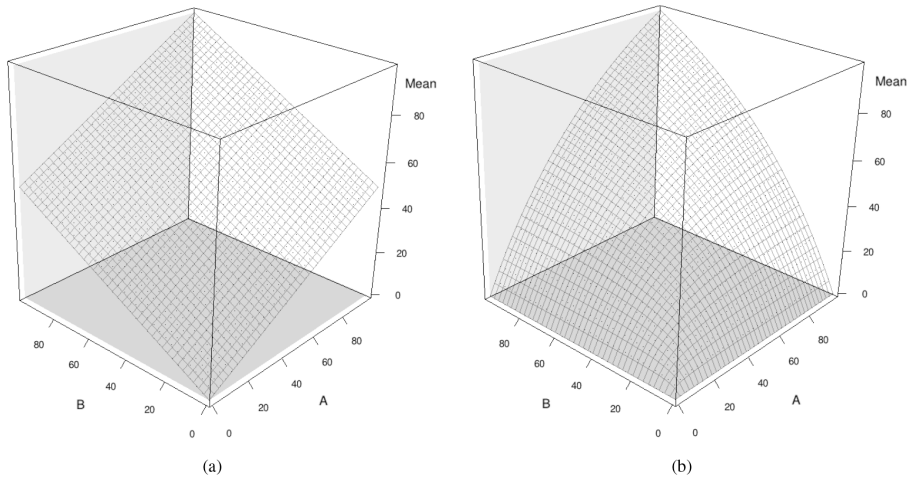


Figure 9.8

Surfaces generated by calculating (a) the arithmetic mean and (b) the harmonic mean of all combinations of features A and B that range from 0 to 100.

9.4.2.4 Measuring profit and loss One of the problems faced by all the performance measures discussed so far is that they place the same value on all the cells within a confusion matrix. For example, in the churn prediction example, correctly classifying a customer as likely to churn is *worth* the same as correctly classifying a customer as not likely to churn. It is not always correct to treat all outcomes equally. For example, if a customer who really was not a churn risk is classified as likely to churn, the cost incurred by the company because of this mistake is the cost of a small bonus offer that would be given to the customer to entice the customer to stay with the company. On the other hand, misclassifying a customer who really was a churn risk probably has a much larger cost associated with it because that customer will be lost when a small bonus may have enticed the customer to stay. When evaluating the performance of models, it would be useful to be able to take into account the costs of different outcomes.

One way in which to do this is to calculate the profit or loss that arises from each prediction we make and to use these to determine the overall performance of a model. To do this we first need to create a **profit matrix** that records these. Table 9.7^[553] shows the structure of a profit matrix, which is the same as the structure of a confusion matrix. TP_{Profit} represents the profit arising from a correct positive prediction, FN_{Profit} is the profit arising from an incorrect negative prediction, and so on (note that profit can refer

to a positive or a negative value). The actual values in a profit matrix are determined through domain expertise.

Table 9.7

The structure of a profit matrix.

		Prediction	
		positive	negative
Target	positive	TP_{Profit}	FN_{Profit}
	negative	FP_{Profit}	TN_{Profit}

To see the use of a profit matrix in action, consider a prediction problem in which a payday loan company has built a credit scoring model to predict the likelihood that a borrower will default on a loan. Based on a set of descriptive features extracted from the loan application (e.g., AGE, OCCUPATION, and ASSETS), the model will classify potential borrowers as belonging to one of two groups: *good* borrowers, who will repay their loans in full; and *bad* borrowers, who will default on some portion of their loans. The company can run this model whenever a new loan application is made and only extend credit to those borrowers predicted to belong to the *good* target level. [Table 9.8](#)^[554] shows the profit matrix for this problem.

Table 9.8

The profit matrix for the payday loan credit scoring problem.

		Prediction	
		<i>good</i>	<i>bad</i>
Target	<i>good</i>	140	-140
	<i>bad</i>	-700	0

The values in this matrix are based on historical data that the company has on loans given out in the past. The typical value of a loan is \$1,000, and the interest rate charged is 14%. So, when a loan is repaid in full, the profit made by the company is usually \$140. Therefore, the profit arising from correctly predicting the *good* level for a potential borrower is \$140. Incorrectly predicting the *bad* level for a potential borrower who would have repaid the loan in full will result in a negative profit (or loss) of - \$140, as the company has forgone potential interest payments. Correctly

predicting the *bad* level for a potential borrower results in no profit as no money is loaned.¹¹ Incorrectly predicting the *good* level for a potential borrower who goes on to default on the loan, however, results in a loan not being repaid. Based on historical examples, the expected loss in this case, referred to as the **loss given default**, is \$700 (most borrowers will repay some of their loan before defaulting). The values in [Table 9.8](#)^[554] are based on these figures. It is clear that the different outcomes have different profit and loss associated with them. In particular, extending a loan to a borrower who turns out to be *bad* is a very costly mistake.

[Tables 9.9\(a\)](#)^[555] and [9.9\(b\)](#)^[555] show confusion matrices for two different prediction models, a *k*-NN model and a decision tree model, trained for the payday loans credit scoring problem. The average class accuracy (using a harmonic mean) for the *k*-NN model is 83.824% and for the decision tree model is 80.761%, which suggests that the *k*-NN model is quite a bit better than the decision tree.

Table 9.9

(a) The confusion matrix for a *k*-NN model trained on the payday loan credit scoring problem (*average class accuracy_{HM}* = 83.824%); and (b) the confusion matrix for a decision tree model trained on the payday loan credit scoring problem (*average class accuracy_{HM}* = 80.761%).

(a) *k*-NN model

		Prediction	
		<i>good</i>	<i>bad</i>
Target	<i>good</i>	57	3
	<i>bad</i>	10	30

(b) decision tree

		Prediction	
		<i>good</i>	<i>bad</i>
Target	<i>good</i>	43	17
	<i>bad</i>	3	37

We can, however, use the values in the profit matrix to calculate the overall profit associated with the predictions made by these two models. This is achieved by multiplying the values in the confusion matrix by the corresponding values in the profit matrix and summing the results. [Tables 9.10\(a\)](#)^[555] and [9.10\(b\)](#)^[555] show this calculation for the *k*-NN and the decision tree models. The overall profit for the *k*-NN model is \$560, while it is \$1,540 for the decision tree model. As well as showing that it is hard to make money in the payday loans business, this reverses the ordering implied using the average class accuracy. The predictions made by the

decision tree model result in a higher profit than those made by the k -NN model. This is because the k -NN makes the mistake of misclassifying a *bad* borrower as *good* more often than the decision tree model, and this is the more costly mistake. Ranking the models by profit, we are able to take this into account, which is impossible using classification accuracy or average class accuracy.

Table 9.10

(a) Overall profit for the k -NN model using the profit matrix in [Table 9.8](#)^[554] and the confusion matrix in [Table 9.9\(a\)](#)^[555]; and (b) overall profit for the decision tree model using the profit matrix in [Table 9.8](#)^[554] and the confusion matrix in [Table 9.9\(b\)](#)^[555].

		Prediction			
		<i>good</i>	<i>bad</i>		
Target	<i>good</i>	7,980	-420	<i>good</i>	6,020
	<i>bad</i>	-7,000	0		-2,100
Profit		560		Profit	1,540

It is worth mentioning that to use profit as a performance measure, we don't need to quantify the profit associated with each outcome as completely as we have done in this example. The minimal amount of information we need is the relative profit associated with each of the different outcomes (TP, TN, FP, or FN) that can arise when a model makes a prediction. For example, in the spam filtering problem described previously, all we need to use are the relative profits of classifying a *ham* email as *spam*, classifying a *spam* email as *ham*, and so on.

While using profit might appear to be the ideal way to evaluate model performance for categorical targets, unfortunately, this is not the case. It is only in very rare scenarios that we can accurately fill in a profit matrix for a prediction problem. In many cases, although it may be possible to say that some outcomes are more desirable than others, it is simply not possible to quantify this. For example, in a medical diagnosis problem, we might confidently say that a false negative (telling a sick patient that they do not have a disease) is worse than a false positive (telling a healthy patient that they do have a disease), but it is unlikely that we will be able to quantify this as twice as bad, or four times as bad, or 10.75 times as bad. When a

profit matrix is available, however, profit is a very effective performance measure to use.

9.4.3 Performance Measures: Prediction Scores

Careful examination of the workings of the different classification models that we have discussed in Chapters 4^[117] to 7^[311] shows that none of them simply produces a target feature level as its output. In all cases, a **prediction score** (or scores) is produced, and a threshold process is used to convert this score into one of the levels of the target feature. For example, the naive Bayes model produces probabilities that are converted into categorical predictions using the maximum a posteriori probability approach, and logistic regression models produce a probability for the positive target level that is converted into a categorical prediction using a threshold. Even in decision trees, the prediction is based on the majority target level at a leaf node, and the proportion of this level gives us a prediction score. In a typical scenario with two target levels, a prediction score in the range [0,1] is generated by a model, and a threshold of 0.5 is used to convert this score into a categorical prediction as follows:

$$\text{threshold}(\text{score}, 0.5) = \begin{cases} \text{positive} & \text{if } \text{score} \geq 0.5 \\ \text{negative} & \text{otherwise} \end{cases} \quad (9.13)$$

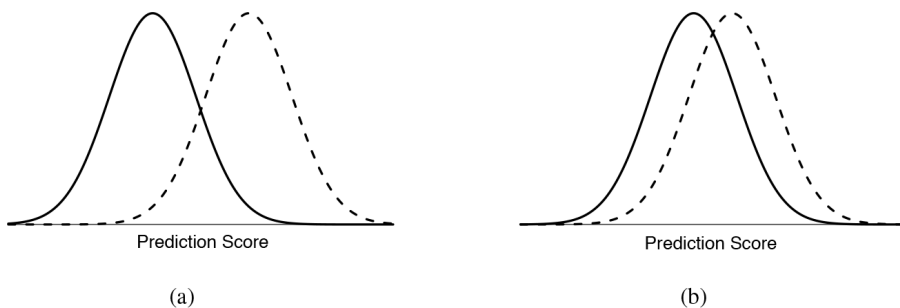
To illustrate this, [Table 9.11](#)^[557] shows the underlying scores that the predictions shown in [Table 9.1](#)^[537] were based on, assuming a threshold of 0.5—that is, instances with a prediction score greater than or equal to 0.5 were given predictions of the *spam* (positive) level, and those with prediction scores less than 0.5 were given predictions of the *ham* (negative) level. The instances in this table have been sorted by these scores in ascending order; as a result, the thresholding on the scores to generate predictions is very much apparent. An indication of the performance of the model is also evident from this ordering—the Target column shows that the instances that actually should get predictions of the *ham* level generally have lower scores, and those that should get predictions of the *spam* level generally have higher scores.

Table 9.11

A sample test set with model predictions and scores.

ID	Target	Prediction	Score	Outcome	ID	Target	Prediction	Score	Outcome
7	ham	ham	0.001	TN	5	ham	ham	0.302	TN
11	ham	ham	0.003	TN	14	ham	ham	0.348	TN
15	ham	ham	0.059	TN	17	ham	spam	0.657	FP
13	ham	ham	0.064	TN	8	spam	spam	0.676	TP
19	ham	ham	0.094	TN	6	spam	spam	0.719	TP
12	spam	ham	0.160	FN	10	spam	spam	0.781	TP
2	spam	ham	0.184	FN	18	spam	spam	0.833	TP
3	ham	ham	0.226	TN	20	ham	spam	0.877	FP
16	ham	ham	0.246	TN	9	spam	spam	0.960	TP
1	spam	ham	0.293	FN	4	spam	spam	0.963	TP

A range of performance measures use this ability of a model, to rank instances that should get predictions of one target level higher than the other, to better assess how well a prediction model is performing. The basis of most of these approaches is measuring how well the distributions of scores produced by the model for different target levels are separated. [Figure 9.9](#)^[557] illustrates this: assuming that prediction scores are normally distributed, the distributions of the scores for the two target levels are shown for two different classification models. The prediction score distributions shown in [Figure 9.9\(a\)](#)^[557] are much better separated than those in [Figure 9.9\(b\)](#)^[557]. We can use the separation of the prediction score distributions to construct performance measures for categorical prediction models.

**Figure 9.9**

Prediction score distributions for two different prediction models. The distributions in (a) are much better separated than those in (b).

If the distributions of prediction scores from predictive models perfectly followed a normal distribution, similar to those in [Figure 9.9](#)^[557], calculating the degree of separation between distributions would be very simple and only involve a simple comparison of means and standard deviations. Unfortunately, this is not the case, as the distribution of prediction scores for a model can follow any distribution. For example, the density histograms in [Figure 9.10](#)^[558] show the distributions of prediction scores for the *spam* and *ham* target levels based on the data in [Table 9.11](#)^[557]. There are a number of performance measures based on the idea of comparing prediction score distributions that attempt to cater to the peculiarities of real data. This section describes some of the most important of these measures.

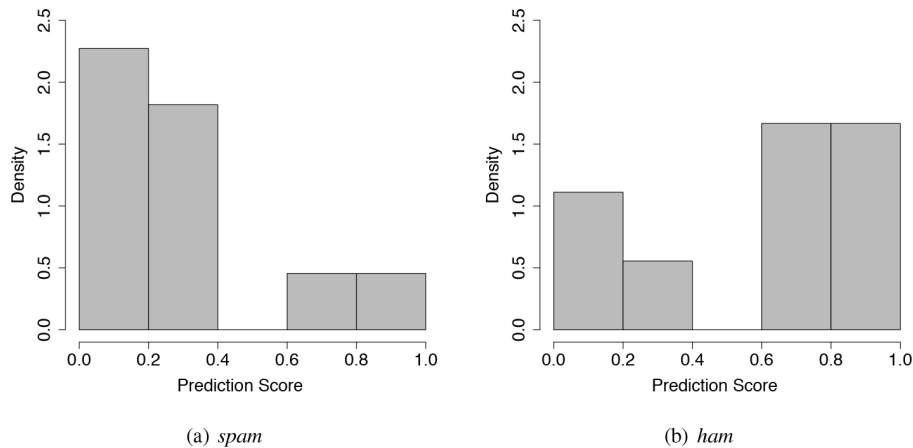


Figure 9.10

Prediction score distributions for the (a) *spam* and (b) *ham* target levels based on the data in [Table 9.11](#)^[557].

9.4.3.1 Receiver operating characteristic curves The **receiver operating characteristic index (ROC index)**, which is based on the **receiver operating characteristic curve (ROC curve)**,¹² is a widely used performance measure that is calculated using prediction scores. We saw in [Section 9.4.2](#)^[547] how the true positive rate (TPR) and true negative rate (TNR) can be calculated from a confusion matrix. These measures, however, are intrinsically tied to the threshold used to convert prediction scores into target levels. The predictions shown in [Table 9.11](#)^[557] and in the confusion matrix in [Table 9.3](#)^[539] are based on a prediction score threshold of 0.5. This threshold can be changed, however, which leads to different predictions and a different confusion matrix. For example, if we changed

the threshold used to generate the predictions shown in [Table 9.11](#)^[557] from 0.5 to 0.75, the predictions for instances \mathbf{d}_{17} , \mathbf{d}_8 , and \mathbf{d}_6 would change from *spam* to *ham*, resulting in their outcomes changing to TN, FN, and FN respectively. This would mean that the confusion matrix would change to that shown in [Table 9.12\(a\)](#)^[559] and, in turn, that the TPR and TNR measures would change to 0.5 and 0.833 respectively.

Table 9.12

Confusion matrices for the set of predictions shown in [Table 9.11](#)^[557] using (a) a prediction score threshold of 0.75 and (b) a prediction score threshold of 0.25.

		Prediction		Prediction	
		<i>spam</i>	<i>ham</i>	<i>spam</i>	<i>ham</i>
Target	<i>spam</i>	4	4	7	2
	<i>ham</i>	2	10	4	7

Similarly, if we changed the threshold from 0.5 to 0.25, the predictions for instances \mathbf{d}_{14} , \mathbf{d}_5 , and \mathbf{d}_1 would change from *ham* to *spam*, resulting in their outcomes changing to FP, FP, and TP respectively. This would mean that the confusion matrix would change to that shown in [Table 9.12\(b\)](#)^[559] and, in turn, that the TPR and TNR measures would change to 0.777 and 0.636 respectively.

For every possible value of the threshold, in the range [0,1], there are corresponding TPR and TNR values. The pattern that is evident in the two examples presented above continues as the threshold value is modified: as the threshold increases, TPR decreases and TNR increases, and as the threshold decreases, the opposite occurs. [Table 9.13](#)^[560] shows how the predictions made for test instances change as the threshold changes. Also shown are the resulting TPR, TNR, FPR, and FNR values, as well as the misclassification rate for each threshold. We can see that the misclassification rate doesn't change that much as the threshold changes. This is due to the trade-offs between false positives and false negatives.

Table 9.13

A sample test set with prediction scores and resulting predictions based on different threshold values.

ID	Target	Score	Pred. (0.10)	Pred. (0.25)	Pred. (0.50)	Pred. (0.75)	Pred. (0.90)
7	ham	0.001	ham	ham	ham	ham	ham
11	ham	0.003	ham	ham	ham	ham	ham
15	ham	0.059	ham	ham	ham	ham	ham
13	ham	0.064	ham	ham	ham	ham	ham
19	ham	0.094	ham	ham	ham	ham	ham
12	spam	0.160	spam	ham	ham	ham	ham
2	spam	0.184	spam	ham	ham	ham	ham
3	ham	0.226	spam	ham	ham	ham	ham
16	ham	0.246	spam	ham	ham	ham	ham
1	spam	0.293	spam	spam	ham	ham	ham
5	ham	0.302	spam	spam	ham	ham	ham
14	ham	0.348	spam	spam	ham	ham	ham
17	ham	0.657	spam	spam	spam	ham	ham
8	spam	0.676	spam	spam	spam	ham	ham
6	spam	0.719	spam	spam	spam	ham	ham
10	spam	0.781	spam	spam	spam	spam	ham
18	spam	0.833	spam	spam	spam	spam	ham
20	ham	0.877	spam	spam	spam	spam	ham
9	spam	0.960	spam	spam	spam	spam	spam
4	spam	0.963	spam	spam	spam	spam	spam
Misclassification Rate			0.300	0.300	0.250	0.300	0.350
True Positive Rate (TPR)			1.000	0.778	0.667	0.444	0.222
True Negative rate (TNR)			0.455	0.636	0.818	0.909	1.000
False Positive Rate (FPR)			0.545	0.364	0.182	0.091	0.000
False Negative Rate (FNR)			0.000	0.222	0.333	0.556	0.778

Figure 9.11(a)^[561] shows the changing values for TPR and TNR for the prediction scores shown in Table 9.13^[560] as the threshold is varied from 0 to 1.¹³ This graph shows that changing the value of the threshold results in a trade-off between accuracy for predictions of positive target levels and accuracy for predictions of negative target levels. Capturing this trade-off is the basis of the ROC curve.

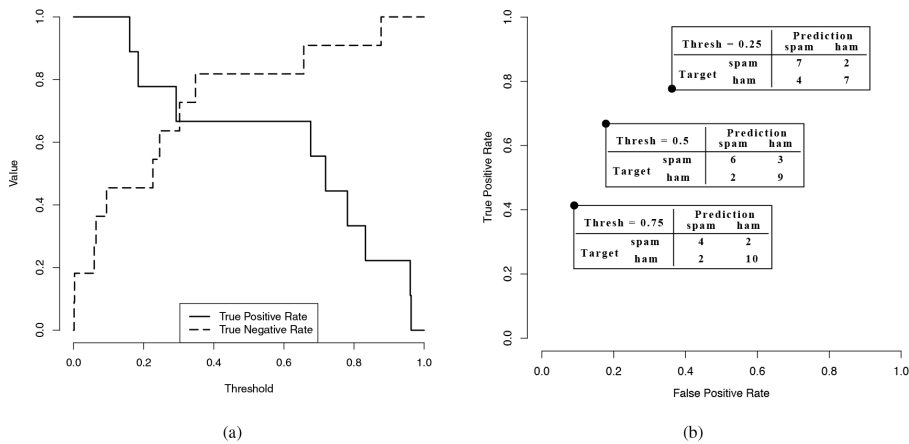


Figure 9.11

(a) The changing values of TPR and TNR for the test data shown in [Table 9.13](#)^[560] as the threshold is altered; and (b) points in ROC space for thresholds of 0.25, 0.5, and 0.75.

To plot an ROC curve, we create a chart with true positive rate on the vertical access and false positive rate (or $1 - \text{true negative rate}$) on the horizontal axis.¹⁴ The values for these measures, when any threshold value is used on a collection of score predictions, gives a point on this plot, or a point in **receiver operating characteristic space (ROC space)**. [Figure 9.11\(b\)](#)^[561] shows three such points in ROC space and associated confusion matrices for the email classification dataset for thresholds of 0.25, 0.5, and 0.75.

The ROC curve is drawn by plotting a point for every feasible threshold value and joining them. [Figure 9.12\(a\)](#)^[562] shows a complete ROC curve for the email predictions in [Table 9.13](#)^[560]. A line along the diagonal of ROC space from $(0,0)$ to $(1,1)$, shown as a dotted line in [Figure 9.12\(a\)](#)^[562], is a reference line representing the expected performance of a model that makes random predictions. We always expect the ROC curve for a trained model to be above this random reference line.¹⁵ In fact, as the strength of a predictive model increases, the ROC curve moves farther away from the random line toward the top left-hand corner of ROC space—toward a TPR of 1.0 and an FPR of 0.0. So, the ROC curve gives us an immediate visual indication of the strength of a model—the closer the curve is to the top left, the more predictive the model.

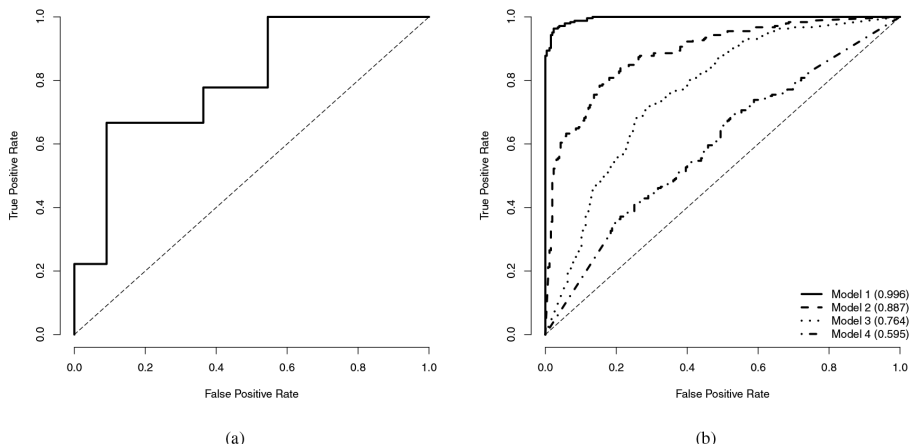


Figure 9.12

(a) A complete ROC curve for the email classification example; and (b) a selection of ROC curves for different models trained on the same prediction task.

Often the ROC curves for multiple predictive models will be plotted on a single ROC plot, allowing easy comparison of their performance. Figure 9.12(b)^[562] shows ROC curves for four models tested on a version of the email classification test set in Table 9.13^[560], containing many more instances than the one we have been discussing so far, which is why the curves are so much smoother than the curve shown in Figure 9.12(a)^[562]. These smoother curves are more representative of the kind of ROC curves we typically encounter in practice. In this example, Model 1 approaches perfect performance, Model 4 is barely better than random guessing, and Models 2 and 3 sit somewhere in between these two extremes.

Although it is useful to visually compare the performance of different models using an ROC curve, it is often preferable to have a single numeric performance measure with which models can be assessed. Fortunately, there is an easy calculation that can be made from the ROC curve that achieves this. The **ROC index** or **area under the curve (AUC)** measures the area underneath an ROC curve. Remembering that the perfect model will appear in the very top left-hand corner of ROC space, it is fairly intuitive that curves with higher areas will be closer to this maximum possible value. The area under an ROC curve is calculated as the integral of the curve. Because ROC curves are discrete and stepped in nature, finding their integrals is actually very easily done using the **trapezoidal method**. The ROC index can be calculated as

$$ROC\ index = \sum_{i=2}^{|T|} \frac{(FPR(T[i]) - FPR(T[i-1])) \times (TPR(T[i]) + TPR(T[i-1]))}{2} \quad (9.14)$$

where \mathbf{T} is a set of thresholds, $|T|$ is the number of thresholds tested, and $TPR(\mathbf{T}[i])$ and $FPR(\mathbf{T}[i])$ are the true positive and false positive rates at threshold i respectively.

The ROC index can take values in the range [0,1] (although values less than 0.5 are unlikely and indicative of a target labeling error), and larger values indicate better model performance. So, for example, the ROC index for the ROC curve shown in [Figure 9.12\(a\)](#)^[562] is 0.798, and the ROC indices for Models 1 to 4 in [Figure 9.12\(b\)](#)^[562] are 0.996, 0.887, 0.764, and 0.595 (as shown in the legend). While there are no hard and fast rules about what constitutes an acceptable value for the ROC index, and this is really an application-specific decision, a good rule of thumb is that a value above 0.7 indicates a *strong* model, while a value below 0.6 indicates a *weak* model. The ROC index is quite robust in the presence of imbalanced data, which makes it a common choice for practitioners, especially when multiple modeling techniques are being compared to one another.

The ROC index can be interpreted probabilistically as the probability that a model will assign a higher rank to a randomly selected positive instance than to a randomly selected negative instance.¹⁶ The **Gini coefficient**¹⁷ is another commonly used performance measure that is just a linear rescaling of the ROC index:

$$Gini\ coefficient = (2 \times ROC\ index) - 1 \quad (9.15)$$

The Gini coefficient can take values in the range [0,1], and higher values indicate better model performance. The Gini coefficient for the model shown in [Figure 9.12\(a\)](#)^[562] is 0.596, and the Gini coefficients for the four models shown in [Figure 9.12\(a\)](#)^[562] are 0.992, 0.774, 0.527, and 0.190. The Gini coefficient is very commonly used in financial modeling scenarios such as credit scoring.

9.4.3.2 Kolmogorov-Smirnov statistic

The **Kolmogorov-Smirnov statistic** (K-S statistic) is another performance measure that captures the

separation between the distribution of prediction scores for the different target levels in a classification problem. To calculate the K-S statistic, we first determine the cumulative probability distributions of the prediction scores for the positive and negative target levels. This is done as follows:

$$CP(\text{positive}, ps) = \frac{\text{num positive test instances with score} \leq ps}{\text{num positive test instances}} \quad (9.16)$$

$$CP(\text{negative}, ps) = \frac{\text{num negative test instances with score} \leq ps}{\text{num negative test instances}} \quad (9.17)$$

where ps is a prediction score value, $CP(\text{positive}, ps)$ is the cumulative probability distribution of positive value scores, and $CP(\text{negative}, ps)$ is the cumulative probability distribution of negative value scores. These cumulative probability distributions can be plotted on a **Kolmogorov-Smirnov chart (K-S chart)**. [Figure 9.13](#)^[564] shows the K-S chart for the test set predictions shown in [Table 9.11](#)^[557]. We can see how the cumulative likelihood of finding a *ham* (or negative) instance increases much more quickly than that of finding a *spam* (or positive) instance. This makes sense because if a model is performing accurately, we would expect negative instances to have low scores (close to 0.0) and positive instances to have high scores (close to 1.0).

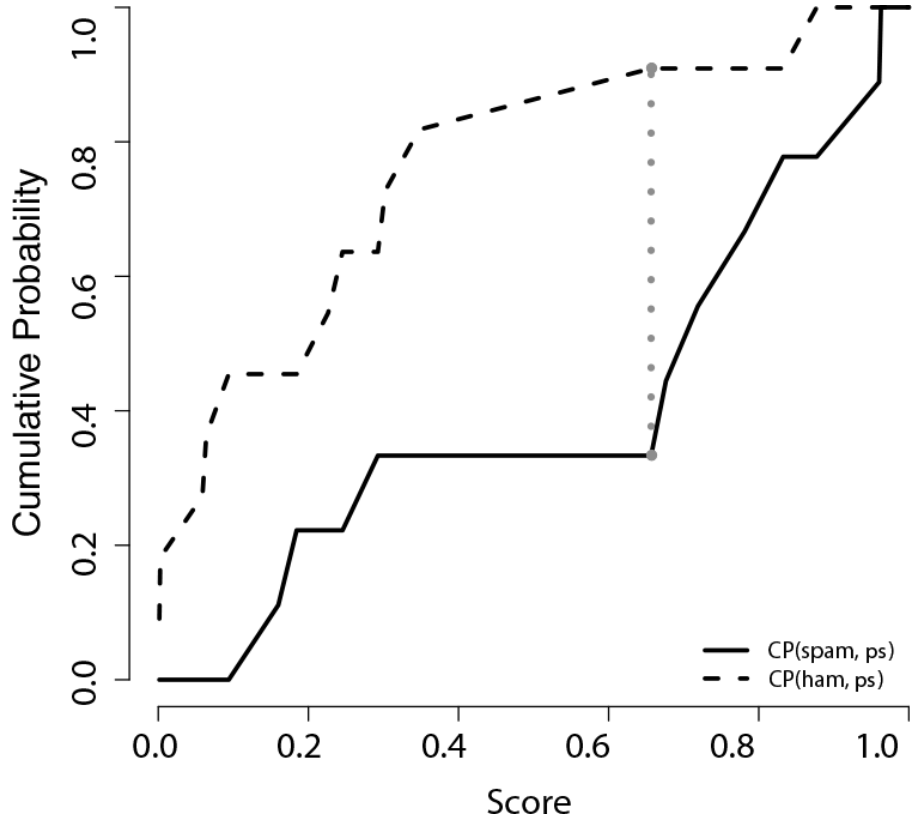


Figure 9.13

The K-S chart for the email classification predictions shown in [Table 9.11](#)^[557].

The K-S statistic is calculated by determining the maximum difference between the cumulative probability distributions for the positive and negative target levels. This can be given formally as

$$K-S = \max_{ps} (CP(positive, ps) - CP(negative, ps)) \quad (9.18)$$

where $CP(positive, ps)$ and $CP(negative, ps)$ are as described above. This distance is indicated by the vertical dotted line in [Figure 9.13](#)^[564], from which it is clear that the K-S statistic is the largest distance between the positive and negative cumulative distributions. The K-S statistic ranges from 0 to 1, and higher values indicate better model performance, reflecting the fact that there is a clear distinction between the distributions of the scores predicted by the model for the negative and the positive instances.

In practice, the simplest way to calculate a K-S statistic for the predictions made by a model for a test dataset is to first tabulate the positive and negative cumulative probabilities for the scores predicted for each

instance in the test dataset, in ascending order by prediction score. For the score predicted by the model for each instance in the test set, the distance between the positive and negative cumulative probabilities at that score can then be calculated. The K-S statistic is the maximum of these distances. [Table 9.14](#)^[565] shows an example for the email classification problem predictions given in [Table 9.11](#)^[557]. We have highlighted in bold and marked with a * the instance that results in the maximum distance between $CP(spam, ps)$ and $CP(ham, ps)$. This distance is 0.576, which is the K-S statistic for this example.

Table 9.14

Tabulating the workings required to generate a K-S statistic.

ID	Prediction	Positive (spam)		Negative (ham)		Positive (spam)	Negative (ham)
		Cumulative Score	Count	Cumulative Count	Cumulative Probability		
7	0.001		0	1	0.000	0.091	0.091
11	0.003		0	2	0.000	0.182	0.182
15	0.059		0	3	0.000	0.273	0.273
13	0.064		0	4	0.000	0.364	0.364
19	0.094		0	5	0.000	0.455	0.455
12	0.160		1	5	0.111	0.455	0.343
2	0.184		2	5	0.222	0.455	0.232
3	0.226		2	6	0.222	0.545	0.323
16	0.246		2	7	0.222	0.636	0.414
1	0.293		3	7	0.333	0.636	0.303
5	0.302		3	8	0.333	0.727	0.394
14	0.348		3	9	0.333	0.818	0.485
17	0.657		3	10	0.333	0.909	*0.576
8	0.676		4	10	0.444	0.909	0.465
6	0.719		5	10	0.556	0.909	0.354
10	0.781		6	10	0.667	0.909	0.242
18	0.833		7	10	0.778	0.909	0.131
20	0.877		7	11	0.778	1.000	0.222
9	0.960		8	11	0.889	1.000	0.111
4	0.963		9	11	1.000	1.000	0.000

* marks the maximum distance, which is the K-S statistic.

To illustrate how a K-S statistic and K-S chart can give insight into model performance, [Figure 9.14](#)^[566] shows a series of charts for the four different prediction models trained on the email classification task and evaluated on a large test set. The charts are a histogram of the *spam* scores predicted by the model, a histogram of the *ham* scores predicted by the model, and the resulting K-S chart with the K-S statistic highlighted.

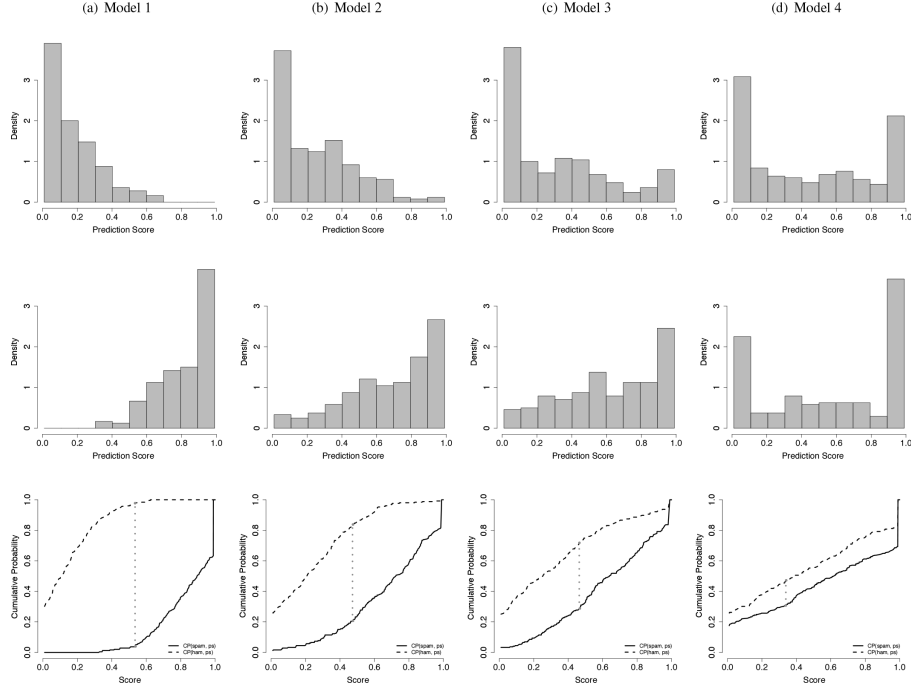


Figure 9.14

A series of charts for different model performance on the same large email classification test set used to generate the ROC curves in Figure 9.12(b)^[562]. Each column from top to bottom: a histogram of the *ham* scores predicted by the model, a histogram of the *spam* scores predicted by the model, and the K-S chart.

The resulting K-S statistics are 0.940, 0.631, 0.432, and 0.164. These results show that Model 1 is doing a much better job of separating the two target levels than the other models. We can see this in the score histograms and the K-S charts, but it is also nicely captured in the K-S statistics.

9.4.3.3 Measuring gain and lift In scenarios in which we have a positive target level that we are especially interested in (for example, spam emails, fraudulent transactions, or customers who will respond to an offer), it can often be useful to focus in on how well a model is making predictions for just those instances, rather than how well the model is distinguishing between two target levels. This is a subtle difference but can lead to a change in the ordering of models compared to other performance measures. Two useful performance measures in this regard are **gain** and **lift** (we will see that the related performance measures of **cumulative gain** and **cumulative lift** are also useful).

The basic assumption behind both gain and lift is that if we were to rank the instances in a test set in descending order of the prediction scores

assigned to them by a well-performing model, we would expect the majority of the positive instances to be toward the top of this ranking. The gain and lift measures attempt to measure to what extent a set of predictions made by a model meet this assumption.

To calculate gain and lift, we first rank the predictions made for a test set in descending order by prediction score and then divide them into **deciles**.¹⁸ A decile is a group containing 10% of a dataset. [Table 9.15](#)^[568] shows the data from [Table 9.11](#)^[557] divided into deciles. There are 20 instances, so each decile contains just 2 instances. The first decile contains instances 9 and 4, the second decile contains instances 18 and 20, and so on.

Table 9.15

The test set with model predictions and scores from [Table 9.11](#)^[557] extended to include deciles.

Decile	ID	Target	Prediction	Score	Outcome
1 st	9	spam	spam	0.960	TP
	4	spam	spam	0.963	TP
2 nd	18	spam	spam	0.833	TP
	20	ham	spam	0.877	FP
3 rd	6	spam	spam	0.719	TP
	10	spam	spam	0.781	TP
4 th	17	ham	spam	0.657	FP
	8	spam	spam	0.676	TP
5 th	5	ham	ham	0.302	TN
	14	ham	ham	0.348	TN
6 th	16	ham	ham	0.246	TN
	1	spam	ham	0.293	FN
7 th	2	spam	ham	0.184	FN
	3	ham	ham	0.226	TN
8 th	19	ham	ham	0.094	TN
	12	spam	ham	0.160	FN
9 th	15	ham	ham	0.059	TN
	13	ham	ham	0.064	TN
10 th	7	ham	ham	0.001	TN
	11	ham	ham	0.003	TN

Gain is a measure of how many of the positive instances in the overall test set are found in a particular decile. To find this, we count the number of positive instances (based on the known target values) found in each decile and divide these by the total number of positive instances in the test set. So, the gain in a given decile is calculated as

$$gain(dec) = \frac{\text{num positive test instances in decile } dec}{\text{num positive test instances}} \quad (9.19)$$

where dec refers to a particular decile. [Table 9.16](#)^[568] shows how gain is calculated for each decile in the email classification test set. The number of positive and negative instances in each decile is shown. Based on these numbers, the gain for each decile is calculated using Equation (9.19)^[567] (the calculation of some other measures are also included in this table, and these will be explained shortly).

Table 9.16

Tabulating the workings required to calculate gain, cumulative gain, lift, and cumulative lift for the data given in [Table 9.11](#)^[557].

Decile	Positive (spam)		Negative (ham)		Cum. Gain	Lift	Cum. Lift
	Count	Count	Gain				
1 st	2	0	0.222	0.222	2.222	2.222	2.222
2 nd	1	1	0.111	0.333	1.111	1.667	
3 rd	2	0	0.222	0.556	2.222	1.852	
4 th	1	1	0.111	0.667	1.111	1.667	
5 th	0	2	0.000	0.667	0.000	1.333	
6 th	1	1	0.111	0.778	1.111	1.296	
7 th	1	1	0.111	0.889	1.111	1.270	
8 th	1	1	0.111	1.000	1.111	1.250	
9 th	0	2	0.000	1.000	0.000	1.111	
10 th	0	2	0.000	1.000	0.000	1.000	

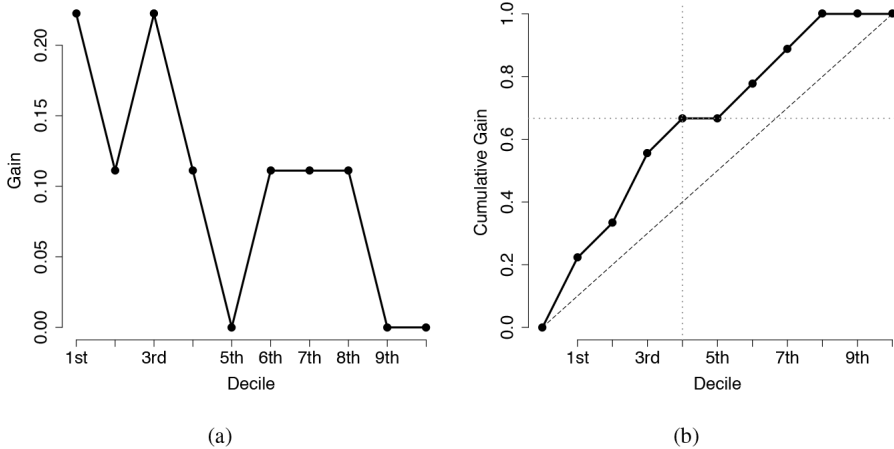


Figure 9.15

The (a) gain and (b) cumulative gain at each decile for the email predictions given in [Table 9.11](#)^[557].

[Figure 9.15\(a\)](#)^[569] graphs the gain for each decile to produce a **gain chart**. We can see from this chart that the gain is higher for the lower deciles, which contain the instances with the highest scores. This is indicative of the fact that the model is performing reasonably well. **Cumulative gain** is calculated as the fraction of the total number of positive instances in a test set identified up to a particular decile (i.e., in that decile and all deciles below it):

$$\text{cumulative gain}(dec) = \frac{\text{num positive test instances in all deciles up to } dec}{\text{num positive test instances}} \quad (9.20)$$

The cumulative gain for each decile of the email classification dataset is shown in [Table 9.16](#)^[568]. [Figure 9.15\(b\)](#)^[569] shows a **cumulative gain chart** of this data. That cumulative gain chart allows us to understand how many of the positive instances in a complete test set we can expect to have identified at each decile of the dataset. So, for example, [Figure 9.15\(b\)](#)^[569] shows that by the 4th decile (40% of the test data), 66.667% of the spam emails in the entire test set will have been identified. This is evidence of just how well the model is performing. The dotted diagonal line on the cumulative gain chart shows the performance we would expect from random guessing, and the closer the cumulative gain line is to the top left-hand corner of the chart, the better the model is performing.

The **gain** in a particular decile can be interpreted as a measure of how much better than random guessing the predictions made by a model are.

Lift captures this more formally. If a model were performing no better than random guessing, we would expect that within each decile, the percentage of positive instances should be the same as the percentage of positive instances overall in the complete dataset. Lift tells us how much higher the actual percentage of positive instances in a decile dec is than the rate expected. So, the lift at decile dec is the ratio between the percentage of positive instances in that decile and the percentage of positive instances overall in the population:

$$lift(dec) = \frac{\% \text{ of positive test instances in decile } dec}{\% \text{ of positive test instances}} \quad (9.21)$$

In the email classification example, the percentage of positive (*spam*) instances in the full test dataset is $\frac{9}{20} = 0.45$. Therefore, the lift at each decile dec is the percentage of *spam* instances in that decile divided by 0.45. [Table 9.16](#)^[568] shows the lift for each decile for the predictions shown in [Table 9.11](#)^[557] for the email classification problem. If we compare the visualization of lift for these predictions shown in [Figure 9.16\(a\)](#)^[570] to the gain chart for the same set of predictions in [Figure 9.15\(a\)](#)^[569], we can see that the shapes are the same. For a well-performing model, the lift curve should start well above 1.0 and cross 1.0 at one of the lower deciles. Lift can take values in the range $[0, \infty]$, and higher values indicate that a model is performing well at a particular decile.

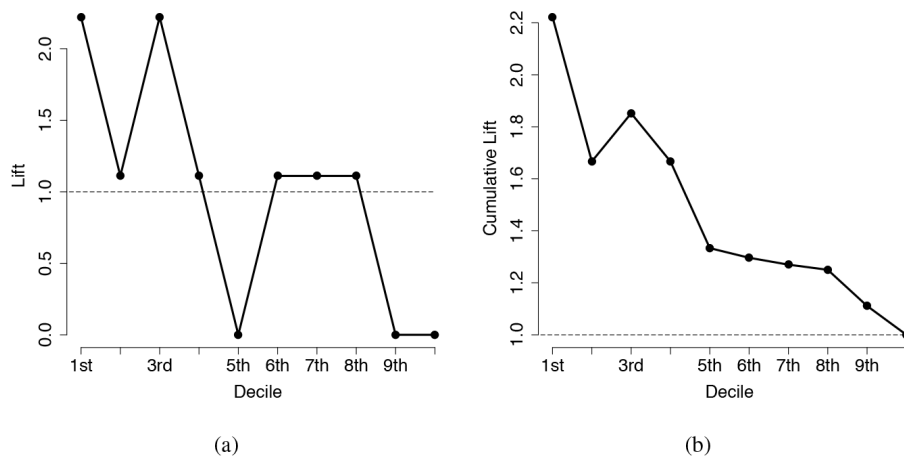


Figure 9.16

The (a) lift and (b) cumulative lift at each decile for the email predictions given in [Table 9.11](#)^[557].

In the same way we calculated cumulative gain, we can calculate lift cumulatively. The **cumulative lift** at decile dec is defined as

$$cumulative\ lift(dec) = \frac{\% \text{ of positive instances in all deciles up to } dec}{\% \text{ of positive test instances}} \quad (9.22)$$

[Table 9.16](#)^[568] shows the cumulative lift for each decile for the predictions shown in [Table 9.11](#)^[557] for the email classification problem, and these values are plotted in a **cumulative lift curve** in [Figure 9.16\(b\)](#)^[570].

[Figure 9.17](#)^[571] shows cumulative gain, lift, and cumulative lift charts (the gain chart is not shown as it is essentially the same as the lift chart) for four different sets of model predictions for the larger version of the email classification test set (these are the same predictions for which ROC charts and K-S charts were plotted in [Figures 9.12\(b\)](#)^[562] and [9.14](#)^[566]). Focusing on the cumulative gain charts, we can see that for Model 1, 80% of the spam messages are identified in the top 40% of the model predictions. For Model 2, we need to look almost as far as the top 50% of predictions to find the same percentage of spam messages. For Models 3 and 4, we need to go as far as 60% and 75% respectively. This indicates that Model 1 distinguishes between the target levels most effectively.

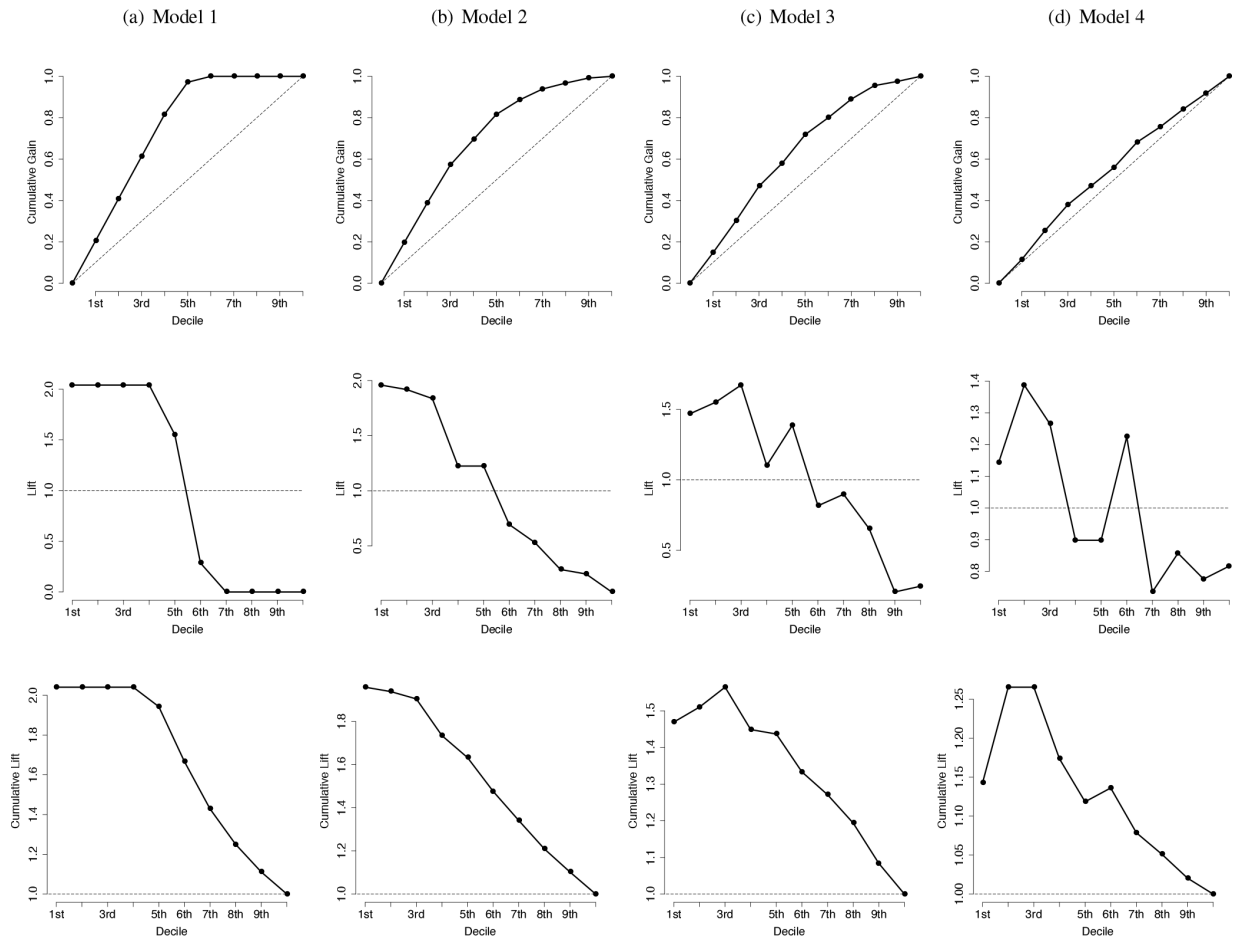


Figure 9.17

Cumulative gain, lift, and cumulative lift charts for four different models for the extended email classification test set.

Cumulative gain is especially useful in **customer relationship management (CRM)** applications such as **cross-sell** and **upsell** models. The cumulative gain tells us how many customers we need to contact in order to reach a particular percentage of those who are likely to respond to an offer, which is an incredibly useful piece of information to know when planning customer contact budgets.

9.4.4 Performance Measures: Multinomial Targets

All the performance measures described in the previous section assumed that the prediction problem being evaluated had only two target levels. Many of the prediction problems for which we build models are **multinomial**, that is, there are multiple target levels. When we deal with multinomial prediction problems, we need a different set of performance

measures. This section describes the most common of these. We begin by discussing how the confusion matrix can be extended to handle multiple target levels.

If we have multiple target levels, the structure of the confusion matrix shown in [Figure 9.2](#)^[538] no longer fits the data. Similarly, the notion of thinking about a positive level and a negative level doesn't apply any more. The confusion matrix can, however, be easily extended to handle multiple target levels by including a row and column for each one. [Table 9.17](#)^[572] shows the structure of a confusion matrix for a multinomial prediction problem in which the target feature has l levels.

Table 9.17

The structure of a confusion matrix for a multinomial prediction problem with l target levels.

		Prediction					Recall
		level 1	level 2	level 3	...	level l	
Target	level 1	-	-	-	-	-	-
	level 2	-	-	-	-	-	-
	level 3	-	-	-	-	-	-
	:				⋮		⋮
	level l	-	-	-	-	-	-
Precision		-	-	-	...	-	

In [Table 9.17](#)^[572] we have included precision and recall measures for each target level. Precision and recall are calculated in almost exactly the same way for multinomial problems as for binary problems. Abandoning the notion of positive and negative target levels, we get

$$precision(l) = \frac{TP(l)}{TP(l) + FP(l)} \quad (9.23)$$

$$recall(l) = \frac{TP(l)}{TP(l) + FN(l)} \quad (9.24)$$

where $TP(l)$ refers to the number of instances correctly given a prediction of the target level l , $FP(l)$ refers to the number of instances that are incorrectly given a prediction of target level l , and $FN(l)$ refers to the number of instances that should have been given a prediction of target level l but were given some other prediction.

[Table 9.18](#)^[573] shows the expected targets and a set of model predictions for a multinomial prediction problem in which the species of a bacteria present in a sample is determined using the results of spectrography performed on the sample.¹⁹ In this example, we are trying to distinguish between four species of the bacterial genus *Fructobacillus*, namely, *durionis*, *ficulneus*, *fructosus*, and *pseudoficulneus* (abbreviated as *pseudo*. in all tables). [Table 9.19](#)^[574] shows the associated confusion matrix for these predictions, including measures of precision and recall.

Table 9.18

A sample test set with model predictions for a bacterial species identification problem.

ID	Target	Prediction	ID	Target	Prediction
1	<i>durionis</i>	<i>fructosus</i>	16	<i>ficulneus</i>	<i>ficulneus</i>
2	<i>ficulneus</i>	<i>fructosus</i>	17	<i>ficulneus</i>	<i>ficulneus</i>
3	<i>fructosus</i>	<i>fructosus</i>	18	<i>fructosus</i>	<i>fructosus</i>
4	<i>ficulneus</i>	<i>ficulneus</i>	19	<i>durionis</i>	<i>durionis</i>
5	<i>durionis</i>	<i>durionis</i>	20	<i>fructosus</i>	<i>fructosus</i>
6	<i>pseudo.</i>	<i>pseudo.</i>	21	<i>fructosus</i>	<i>fructosus</i>
7	<i>durionis</i>	<i>fructosus</i>	22	<i>durionis</i>	<i>durionis</i>
8	<i>ficulneus</i>	<i>ficulneus</i>	23	<i>fructosus</i>	<i>fructosus</i>
9	<i>pseudo.</i>	<i>pseudo.</i>	24	<i>pseudo.</i>	<i>fructosus</i>
10	<i>pseudo.</i>	<i>fructosus</i>	25	<i>durionis</i>	<i>durionis</i>
11	<i>fructosus</i>	<i>fructosus</i>	26	<i>pseudo.</i>	<i>pseudo.</i>
12	<i>ficulneus</i>	<i>ficulneus</i>	27	<i>fructosus</i>	<i>fructosus</i>
13	<i>durionis</i>	<i>durionis</i>	28	<i>ficulneus</i>	<i>ficulneus</i>
14	<i>fructosus</i>	<i>fructosus</i>	29	<i>fructosus</i>	<i>fructosus</i>
15	<i>fructosus</i>	<i>ficulneus</i>	30	<i>fructosus</i>	<i>fructosus</i>

Table 9.19

A confusion matrix for a model trained on the bacterial species identification problem.

		Prediction				Recall
		<i>durionis</i>	<i>ficulneus</i>	<i>fructosus</i>	<i>pseudo.</i>	
Target	<i>durionis</i>	5	0	2	0	0.714
	<i>ficulneus</i>	0	6	1	0	0.857
	<i>fructosus</i>	0	1	10	0	0.909
	<i>pseudo.</i>	0	0	2	3	0.600
Precision		1.000	0.857	0.667	1.000	

While the overall classification accuracy for this set of predictions is 80%,²⁰ the individual recall scores for each target level show that the performance of the model is not the same for all four levels: the accuracy on the *ficulneus* and *fructosus* levels is quite high (85.714% and 90.909% respectively), while for the *durionis* and *pseudoficulneus* levels, the accuracy is considerably lower (71.429% and 60.000%). The $\text{averageclassaccuracy}_{HM}$ performance measure can be applied to multinomial prediction problems and is an effective option for measuring performance. Using Equation (9.12)^[552], we can calculate the average class accuracy for this problem:

$$\frac{1}{\frac{1}{4} \left(\frac{1}{0.714} + \frac{1}{0.857} + \frac{1}{0.909} + \frac{1}{0.600} \right)} = \frac{1}{1.333} = 75.000\%$$

It is not easy to apply the measures based on prediction scores to multinomial problems. Although there are some examples of doing it, there is no broad consensus in the community on how it should best be done in all cases, so we do not discuss it further in this book.

9.4.5 Performance Measures: Continuous Targets

All the performance measures that we have discussed so far focus on prediction problems with categorical targets. When evaluating the performance of prediction models built for continuous targets, there are fewer options to choose from. In this section we describe the most popular

performance measures used for continuous targets. The basic process is the same as for categorical targets. We have a test set containing instances for which we know the correct target values, and we have a set of predictions made by a model. We would like to measure how accurately the predicted values match the correct target values.

9.4.5.1 Basic measures of error In Section 7.2.2^[315], when covering error-based learning, we discussed the basis of the most common performance measure for continuous targets: **sum of squared errors**. The sum of squared errors function, L_2 , for a set of predictions made by a model, \mathbb{M} , is defined as

$$\text{sum of squared errors} = \frac{1}{2} \sum_{i=1}^n (t_i - \mathbb{M}(\mathbf{d}_i))^2 \quad (9.25)$$

where $t_1 \dots t_n$ is a set of n expected target values, and $\mathbb{M}(d_1) \dots \mathbb{M}(d_n)$ is a set of n predictions for a set of test instances, $d_1 \dots d_n$. We modify this very slightly to give us the **mean squared error** performance measure, which captures the average difference between the expected target values in the test set and the values predicted by the model. The **mean squared error (MSE)** performance measure is defined as

$$\text{mean squared error} = \frac{\sum_{i=1}^n (t_i - \mathbb{M}(\mathbf{d}_i))^2}{n} \quad (9.26)$$

The mean squared error allows us to rank the performance of multiple models on a prediction problem with a continuous target. Mean squared error values fall in the range $[0, \infty]$, and smaller values indicate better model performance.

[Table 9.20](#)^[576] shows the expected target values for a test set, the predictions made by two different models (a multivariable linear regression model and a k -NN model), and the resulting errors based on these predictions (the additional error measures will be explained shortly). The prediction problem in this case is to determine the dosage of a blood-thinning drug (in milligrams) that should be given to a patient in order to

achieve a particular level of blood-thinning. The descriptive features in this case would be the level of blood-thinning desired, demographic details for the patient, and the results of various medical tests performed on the patient. Doctors could use the outputs of such a system to help them make better dosing decisions.²¹ The mean squared error for the multivariable linear regression model is 1.905 and for the k -NN model is 4.394. This indicates that the regression model is more accurately predicting the correct drug dosages than the nearest neighbor model.

Table 9.20

The expected target values for a test set, the predictions made by a model, and the resulting errors based on these predictions for a blood-thinning drug dosage prediction problem.

ID	Target	Linear Regression		k -NN	
		Prediction	Error	Prediction	Error
1	10.502	10.730	0.228	12.240	1.738
2	18.990	17.578	-1.412	21.000	2.010
3	20.000	21.760	1.760	16.973	-3.027
4	6.883	7.001	0.118	7.543	0.660
5	5.351	5.244	-0.107	8.383	3.032
6	11.120	10.842	-0.278	10.228	-0.892
7	11.420	10.913	-0.507	12.921	1.500
8	4.836	7.401	2.565	7.588	2.752
9	8.177	8.227	0.050	9.277	1.100
10	19.009	16.667	-2.341	21.000	1.991
11	13.282	14.424	1.142	15.496	2.214
12	8.689	9.874	1.185	5.724	-2.965
13	18.050	19.503	1.453	16.449	-1.601
14	5.388	7.020	1.632	6.640	1.252
15	10.646	10.358	-0.288	5.840	-4.805
16	19.612	16.219	-3.393	18.965	-0.646
17	10.576	10.680	0.104	8.941	-1.634
18	12.934	14.337	1.403	12.484	-0.451
19	10.492	10.366	-0.126	13.021	2.529
20	13.439	14.035	0.596	10.920	-2.519
21	9.849	9.821	-0.029	9.920	0.071
22	18.045	16.639	-1.406	18.526	0.482
23	6.413	7.225	0.813	7.719	1.307
24	9.522	9.565	0.043	8.934	-0.588
25	12.083	13.048	0.965	11.241	-0.842
26	10.104	10.085	-0.020	10.010	-0.095
27	8.924	9.048	0.124	8.157	-0.767
28	10.636	10.876	0.239	13.409	2.773
29	5.457	4.080	-1.376	9.684	4.228
30	3.538	7.090	3.551	5.553	2.014
		MSE	1.905		4.394
		RMSE	1.380		2.096
		MAE	0.975		1.750
		R^2	0.889		0.776

One complaint that is often leveled against mean squared error is that, although it can be used to effectively rank models, the actual mean squared error values themselves are not especially meaningful in relation to the scenario that a model is being used for. For example, in the drug dosage prediction problem, we cannot say by how many milligrams we expect the model to be incorrect based on the mean squared error values. This is due to the use of the squared term in the mean squared error calculation but can easily be addressed by using **root mean squared error** instead. The **root mean squared error (RMSE)** for a set of predictions made by a model on a test set is calculated as

$$\text{root mean squared error} = \sqrt{\frac{\sum_{i=1}^n (t_i - \mathbb{M}(\mathbf{d}_i))^2}{n}} \quad (9.27)$$

where the terms have the same meaning as before. Root mean squared error values are in the same units as the target value and so allow us to say something more meaningful about what the error for predictions made by the model will be. For example, for the drug dosage prediction problem, the root mean squared error value is 1.380 for the regression model and 2.096 for the nearest neighbor model. This means that we can expect the predictions made by the regression model to be 1.38mg out on average, whereas those made by the nearest neighbor model will be, on average, 2.096mg out.

Due to the inclusion of the squared term, the root mean squared error tends to overestimate error slightly as it overemphasizes individual large errors. An alternative measure that addresses this problem is the **mean absolute error (MAE)**, which does not include a squared term.²² Mean absolute error is calculated as

$$\text{mean absolute error} = \frac{\sum_{i=1}^n \text{abs}(t_i - \mathbb{M}(\mathbf{d}_i))}{n} \quad (9.28)$$

where the terms in the equation have the same meaning as before, and abs refers to the absolute value. Mean absolute error values fall in the range $[0, \infty]$, and smaller values indicate better model performance.

For the drug dosage predictions given in [Table 9.20](#)^[576], the mean absolute error is 0.975 for the regression model and 1.750 for the nearest neighbor model. Mean absolute errors are in the same units as the predictions themselves, so we can say that, based on mean absolute error, we can expect the regression model to make errors of approximately 0.9575mg in each of its predictions and the nearest neighbor model to be out by approximately 4.020mg. These are not massively different from the values calculated using root mean squared error. As we recommended the use of harmonic mean over arithmetic mean when calculating average class accuracy, we recommend the use of root mean squared error over mean absolute error because it is better to be pessimistic when estimating the performance of models.

9.4.5.2 Domain independent measures of error The fact that root mean squared error and mean absolute error are in the same units as the target feature itself can be attractive, as it gives a very intuitive measure of how well a model is performing—for example, a model is typically 1.38mg out in its dosage predictions. The disadvantage of this, however, is that these types of measures by themselves are not sufficient to judge whether a model is making accurate predictions without deep knowledge of a domain. For example, how can we judge whether a drug dosage prediction model that has a root mean squared error of 1.38mg is actually making accurate predictions without also understanding the domain of drug dosage prediction. To make these judgments it is necessary to have a normalized, domain independent measure of model performance.

The R^2 coefficient is a domain independent measure of model performance that is frequently used for prediction problems with a continuous target. The R^2 coefficient compares the performance of a model on a test set with the performance of an imaginary model that always predicts the average values from the test set. The R^2 coefficient is calculated as

$$R^2 = 1 - \frac{\text{sum of squared errors}}{\text{total sum of squares}} \quad (9.29)$$

where the **sum of squared errors** is computed using Equation (9.25)^[575], and the **total sum of squares** is given by

$$\text{total sum of squares} = \frac{1}{2} \sum_{i=1}^n (t_i - \bar{t})^2 \quad (9.30)$$

R^2 coefficient values fall in the range [0,1) and larger values indicate better model performance. A useful interpretation of the R^2 coefficient is as the amount of variation in the target feature that is explained by the descriptive features in the model.

The average target value for the drug dosage prediction test set given in Table 9.20^[576] is 11.132. Using this, the R^2 coefficient for the regression model can be calculated as 0.889 and for the nearest neighbor model as 0.776. This leads to the same conclusion with regard to model ranking as the root mean squared error measures: namely, that the regression model has better performance on this task than the nearest neighbor model. The R^2 coefficient, however, has the advantage that it allows assessment of model performance in a domain-independent way.

9.4.6 Evaluating Models after Deployment

Predictive models are based on the assumption that the patterns learned in the training data will be relevant to unseen instances that are presented to the model in the future. Data, however, like everything else in the world, is not constant. People grow older, inflation drives up salaries, the content of the spam emails changes, and the way people use technologies changes. This phenomenon is often referred to as **concept drift**. Concept drift means that almost all the predictive models that we build will at some point go **stale**, and the relationships that they have learned between descriptive features and target features will no longer apply. It is important that once a model is deployed, we put in place an **ongoing model validation** scheme to monitor the model to catch the point at which it begins to go stale. If we can catch this point, we can take appropriate action.

To monitor the ongoing performance of a model, we need a signal that indicates that something has changed. There are three sources from which we can extract such a signal:

- The performance of the model measured using appropriate performance measures
- The distributions of the outputs of a model
- The distributions of the descriptive features in query instances presented to the model

Once a signal has identified that concept drift has occurred and that a model has indeed gone stale, corrective action is required. The nature of this corrective action depends on the application and the type of model being used. In most cases, however, corrective action involves gathering a new labeled dataset and restarting the model building process using this new dataset.

9.4.6.1 Monitoring changes in performance measures The simplest way to get a signal that concept drift has occurred is to repeatedly evaluate models with the same performance measures used to evaluate them before deployment. We can calculate performance measures for a deployed model and compare these to the performance achieved in evaluations before the model was deployed. If the performance changes significantly, this is a strong indication that concept drift has occurred and that the model has gone stale. For example, if we had used root mean squared error on a hold-out test set to evaluate the performance of a model before deployment, we could collect all the query instances presented to the model for a period after deployment and, once their true target feature values became available, calculate the root mean squared error on this new set of query instances. A *large* change in the root mean squared error value would flag that the model had gone stale. One of the drawbacks of using this method to detect that a model has gone stale is that estimating how *large* this change needs to be in order to signal that the model has gone stale is entirely domain dependent.²³

Although monitoring changes in the performance of a model is the easiest way to tell whether it has gone stale, this method makes the rather large assumption that the correct target feature value for a query instance will be made available shortly after the query has been presented to a

deployed model. There are many scenarios in which this is the case. For example, for churn models, customers will either churn or not churn; for credit scoring models, customers will either repay their loans or not; and for models predicting athlete performance, athletes will either match expectations or not. There are many more scenarios, however, in which the correct target feature values either never become available or do not become available early enough to be useful for ongoing model validation. In these scenarios, this approach to ongoing model validation simply doesn't work.

9.4.6.2 Monitoring model output distribution changes An alternative to using changing model performance is to use changes in the distribution of model outputs as a signal for concept drift. If the distribution of model outputs changes dramatically, for example, if a model that previously made positive predictions 80% of the time is suddenly making positive predictions only 20% of the time, then we can assume that there is a strong possibility that concept drift has occurred and that the model has gone stale. In order to compare distributions, we measure the distribution of model outputs on the test set that was used to originally evaluate a model and then repeat this measurement on new sets of query instances collected during periods after the model has been deployed. We then use an appropriate measure to calculate the difference between the distributions collected after deployment and the original distribution. One of the most commonly used measures for this is the **stability index**. The stability index is calculated as

$$stability\ index = \sum_{l \in levels(t)} \left(\left(\frac{|\mathcal{A}_{t=l}|}{|\mathcal{A}|} - \frac{|\mathcal{B}_{t=l}|}{|\mathcal{B}|} \right) \times \log_e \left(\frac{|\mathcal{A}_{t=l}|}{|\mathcal{A}|} / \frac{|\mathcal{B}_{t=l}|}{|\mathcal{B}|} \right) \right) \quad (9.31)$$

where $|\mathcal{A}|$ refers to the size of the test set on which performance measures were originally calculated, $|\mathcal{A}_{t=l}|$ refers to the number of instances in the original test set for which the model made a prediction of level l for target t , $|\mathcal{B}|$ and $|\mathcal{B}_{t=l}|$ refer to the same measurements on the newly collected dataset, and \log_e is the **natural logarithm**.²⁴ In general,

- If the value of the stability index is less than 0.1, then the distribution of the newly collected test set is broadly similar to the distribution in the

original test set.

- If the value of the stability index is between 0.1 and 0.25, then some change has occurred and further investigation may be useful.
- A stability index value greater than 0.25 suggests that a significant change has occurred and corrective action is required.

[Table 9.21](#)^[581] shows an example of how the stability index could be calculated for two different sets of query instances collected at two different times after model deployment based on the bacterial species identification problem given in [Table 9.18](#)^[573]. For the original test set and the two new test sets, referred to as New Sample 1 and New Sample 2, the count and percentage for each target value is given (note that the tests sets do not have to be the same size because relative distributions are used). The original baseline target frequencies are based on the predictions in [Table 9.18](#)^[573] and are visualized in [Figure 9.18\(a\)](#)^[582].

Table 9.21

Calculating the stability index for the bacterial species identification problem given new test data for two periods after model deployment.

Target	Original		New Sample 1			New Sample 2		
	Count	%	Count	%	SI _t	Count	%	SI _t
<i>durionis</i>	7	0.233	12	0.267	0.004	12	0.200	0.005
<i>ficulneus</i>	7	0.233	8	0.178	0.015	9	0.150	0.037
<i>fructosus</i>	11	0.367	16	0.356	0.000	14	0.233	0.060
<i>pseudo.</i>	5	0.167	9	0.200	0.006	25	0.417	0.229
Sum	30		45		0.026	60		0.331

The frequency and percentage of each target level are shown for the original test set and for two samples collected after deployment. The column marked SI_t shows the different parts of the stability index sum based on Equation (9.31)^[580].

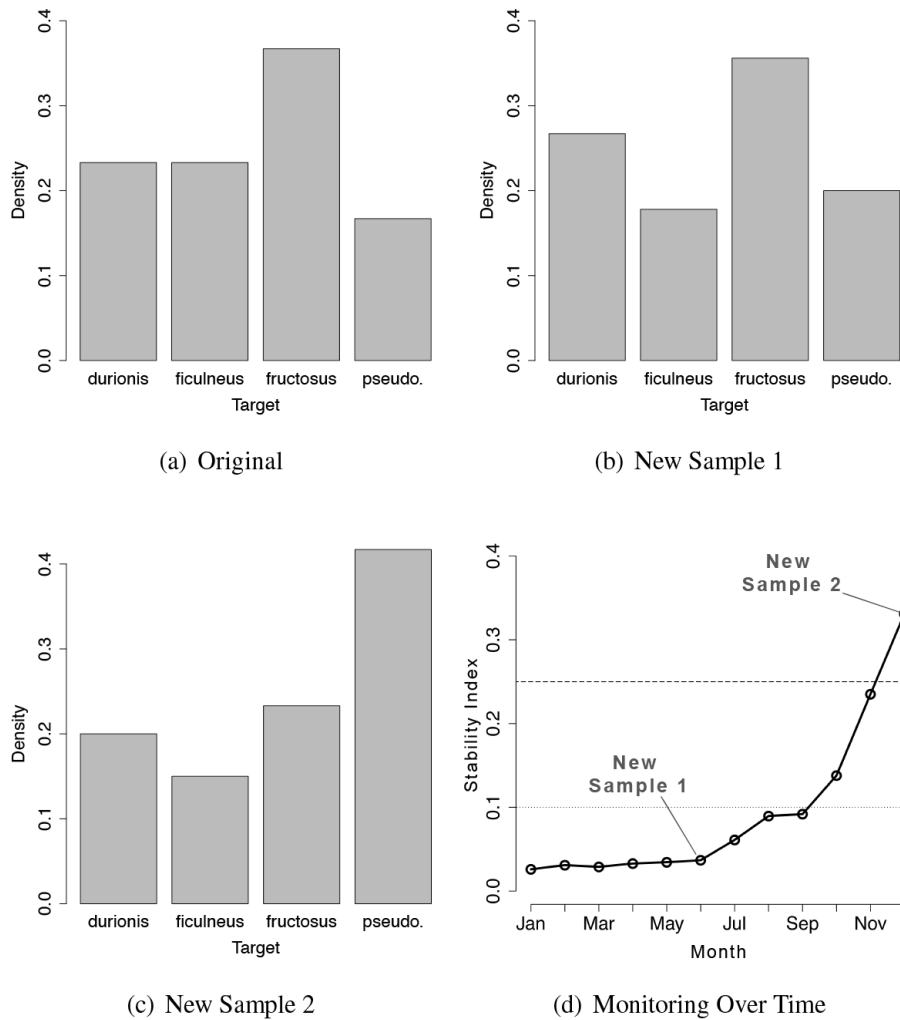


Figure 9.18

The distributions of predictions made by a model trained for the bacterial species identification problem for (a) the original evaluation test set, and for (b) and (c) two periods of time after model deployment; (d) shows how the stability index can be tracked over time to monitor for concept drift.

Figures 9.18(b)^[582] and 9.18(c)^[582] show the target distributions for the two points in time after deployment for which the stability index is to be calculated. These bar plots show that the distribution of target levels for New Sample 1 is similar to the original test set, but that the distribution of target levels for New Sample 2 is quite different. This is reflected in the stability index calculations in Table 9.21^[581], which are determined using Equation (9.31)^[580]. For example, for New Sample 1, the stability index is

$$\begin{aligned}
\text{stability index} &= \left(\frac{7}{30} - \frac{12}{45} \right) \times \log_e \left(\frac{7}{30} / \frac{12}{45} \right) \\
&\quad + \left(\frac{7}{30} - \frac{8}{45} \right) \times \log_e \left(\frac{7}{30} / \frac{8}{45} \right) \\
&\quad + \left(\frac{11}{30} - \frac{16}{45} \right) \times \log_e \left(\frac{11}{30} / \frac{16}{45} \right) \\
&\quad + \left(\frac{5}{30} - \frac{9}{45} \right) \times \log_e \left(\frac{5}{30} / \frac{9}{45} \right) \\
&= 0.026
\end{aligned}$$

where the counts come from [Table 9.21](#)^[581]. The stability index for New Sample 2, calculated in the same way, is 0.331. This suggests that at the point in time at which New Sample 1 was collected, the outputs produced by the model followed much the same distribution as when the model was originally evaluated, but that when New Sample 2 was collected, the distribution of the outputs produced by the model had changed significantly.

To monitor models for the occurrence of concept drift, it is important that the stability index be continuously tracked over time. [Figure 9.18\(d\)](#)^[582] shows how the stability index could be tracked for the bacterial species identification problem every month for a period of 12 months after model deployment. The dotted line indicates a stability index value of 0.1, above which a model should be closely monitored, and the dashed line indicates a stability index of 0.25, above which corrective action is recommended.

The stability index can be used for both categorical and continuous targets. When a model predicts a continuous target, the target range is divided into bins, and the distribution of values into these bins is used in the calculation. It is particularly common to use deciles for this task. The same can actually be done for models that predict binary categorical targets by dividing the prediction scores into deciles. The stability index is just one measure of the difference between two different distributions, and there are many other options that can be used. For example, for categorical targets, the χ^2 statistic is often used, and for continuous targets, the **K-S statistic** can also be used.

The advantage of using evaluation approaches based on comparing the distribution of a model's output, such as the stability index, is that they do not require that the true targets for query instances become available shortly after predictions have been made. The downside, however, is that such

measures do not directly measure the performance of the model, and consequently, a high stability index may reflect a change in the underlying population rather than a change in model performance. So, relying solely on a stability index can lead to models being rebuilt when it is not required.

9.4.6.3 Monitoring descriptive feature distribution changes In the same way we can compare the distributions of model outputs between the time that the model was built and after deployment, we can also make the same type of comparison for the distributions of the descriptive features used by the model. We can use any appropriate measure that captures the difference between two different distributions for this, including the stability index, the χ^2 statistic, and the K-S statistic.

There is, however, a challenge here, as usually, there are a large number of descriptive features for which measures need to be calculated and tracked. Furthermore, it is unlikely that a change in the distribution of just one descriptive feature in a multi-feature model will have a large impact on model performance. For this reason, unless a model uses a very small number of descriptive features (generally fewer than 10), we do not recommend this approach. Measuring the difference in descriptive feature distributions can be useful, however, in understanding what has changed to make a model go stale. So, we recommend that if a model has been flagged as having gone stale using either performance measure monitoring or output distribution monitoring, then the distributions of the descriptive features at the time that the model was built and the distributions of the features at the time that the model went stale should be compared in an effort to understand what has changed. This information should help if the model is to be rebuilt to address the fact that it has gone stale.

9.4.6.4 Comparative experiments using a control group At the beginning of this chapter, we emphasized that it is important that the evaluation of prediction models not just focus on predictive power but also take into account the suitability of the model for the task to which it will be deployed. As part of this type of broader evaluation, the use of **comparative experiments** that include a **control group** can be quite effective. The idea of a control group might be familiar to readers from reading about medical trials. To test a new medicine, doctors typically

assemble a group of patients who suffer from the problem that the medicine is designed to address. During a trial period, half of the patients, the **treatment group**, are given the new drug, and the other half, the control group, are given a **placebo** (essentially a fake drug that has no actual medical effect). Patients are not aware which group they have been assigned to during the trial (hence the need for the placebo). As long as both the treatment group and the control group are representative of the overall population, at the end of the trial period, the doctors running the trial can be confident that any improvement they see in the patients in the treatment group that they do not see in the control group is due to the new medicine.

We can use exactly the same idea to evaluate the impact of predictive models. It is important to note here that we use control groups not to evaluate the predictive power of the models themselves, but rather to evaluate how good they are at helping with the business problem when they are deployed. If we have developed a predictive model that is used in a particular business process, we can run that business process in parallel both with the predictive model, the treatment group, and without the predictive model, the control group, in order to evaluate how much the use of the predictive model has improved the business process.

For example, consider a mobile phone network operator that has built a churn prediction model to help address a problem with customers leaving to join other networks. The company would like to evaluate how well the model is helping to address the churn problem. Before the churn model was put in place, every week the company would randomly select 1,000 customers from their customer base and have their customer contact center call these customers to discuss how satisfied they were with the network's performance and offer assistance with any issues. This was based on the assumption that such a call made to customers considering switching to a different network would encourage them to stay with their current network. The churn model replaced the random selection of customers by assigning every customer in the company's customer base a churn risk score and selecting the 1,000 customers with the highest churn risk scores to receive a call from the customer contact center. Everything else about the process was the same as before.

In order to evaluate the effect this model was having on the company's churn problem, they performed a comparative experiment. The company's

entire customer base was divided randomly into two groups, the treatment group and the control group—and each group contained approximately 400,000 customers. For the customers in the treatment group, the company applied the process using the predictive model to determine which customers to contact regarding customer satisfaction. For the customers in the control group, the random selection process was used. These two approaches ran in parallel for 12 weeks, and at the end of this period, the company measured the number of customers within each group who had left the company to join another network. [Table 9.22](#)^[584] shows the number of customers who churned from each of these two groups during the 12 weeks of the trial, and the associated means and standard deviations. These figures show that, on average, fewer customers churn when the churn prediction model is used to select which customers to call. This tells us not only something about how accurate the churn prediction model is but, more important, that using the model actually made a difference in the business problem that the company was trying to address.²⁵

Table 9.22

The number of customers who left the mobile phone network operator each week during the comparative experiment from both the control group (random selection) and the treatment group (model selection).

Week	Control Group (Random Selection)	Treatment Group (Model Selection)
1	21	23
2	18	15
3	28	18
4	19	20
5	18	15
6	17	17
7	23	18
8	24	20
9	19	18
10	20	19
11	18	13
12	21	16
Mean		
Std.	20.500	17.667
Dev.	3.177	2.708

In order to use control groups in evaluation, we need to be able to divide a population into two groups, run two versions of a business process in parallel, and accurately measure the performance of the business process. Therefore, using control groups is not suitable in all scenarios, but when it is applicable, it adds an extra dimension to our evaluations that takes into account not just how well a model can make predictions, but also how much the predictive model helps to address the original business problem.

9.5 Summary

This chapter covers a range of approaches for evaluating the performance of prediction models. The choice of the correct performance measure for a particular problem depends on a combination of the nature of the prediction problem (e.g., continuous versus categorical), the characteristics of the dataset (e.g., balanced versus imbalanced), and the needs of the application (e.g., medical diagnosis versus marketing response prediction). This last issue is interesting because sometimes particular performance measures become especially popular in certain industries, and in many cases, this dictates the choice of performance measure. For example, in financial credit scoring, the **Gini coefficient** is almost always used to evaluate model performance.

For those struggling to choose an appropriate performance measure, in the absence of other information, we recommend:

- For categorical prediction problems, use **average class accuracy** based on a **harmonic mean**.
- For continuous prediction problems, use the **R²** coefficient.

There are also a number of different ways in which evaluation experiments can be performed, as described in Section 9.4.1^[540]. The choice of which one to use mostly depends on how much data is available. The following rules of thumb may be useful (although the usual caveats that all scenarios are slightly different apply). In cases with very small datasets (approximately fewer than 300 instances), bootstrapping approaches are preferred over cross validation approaches. Cross validation approaches are generally preferred unless datasets are very large, in which case the likelihood of the **lucky split** becomes very low, and hold-out approaches can be used. As with everything else, there is an application-specific

component to the selection of an experimental design—for example, **out-of-time sampling** is a good choice in scenarios where a time dimension is important.

9.6 Further Reading

The evaluation of machine learning models is a live research issue, and a large body of material addresses all the questions that have been discussed in this chapter. For a detailed discussion of the issues associated with evaluating models for categorical prediction problems (and model evaluation in general), Japkowicz and Shah (2011) is excellent. David Hand has also written extensively on the appropriateness of different evaluation measures and is always worth reading. For example, Hand and Anagnostopoulos (2013) discusses issues with the use of the ROC index.

Japkowicz and Shah (2011) also discusses the issue of performing statistical significance tests to compare the performance of multiple models. Demsar (2006) gives another excellent overview of comparing multiple modeling types and has been the basis for much discussion in the machine learning community. This is slightly more of a concern to machine learning researchers who are interested in comparing the overall power of different machine learning algorithms. By contrast, in most predictive analytics projects, our focus is on determining the best model for a specific problem.

The design of model evaluation experiments is an example of the application of techniques from the larger discipline of experimental design, which is used extensively in the manufacturing industry amongst others. Montgomery (2012) is an excellent reference for this topic and well worth reading.

Finally, for those interested in experimenting with different evaluation measures, the ROCR package (Sing et al., 2005) for the R programming language includes a wide range of measures.

9.7 Exercises

1. The table below shows the predictions made for a categorical target feature by a model for a test dataset. Based on this test set, calculate the evaluation measures listed below.

ID	Target	Prediction	ID	Target	Prediction	ID	Target	Prediction
1	false	false	8	true	true	15	false	false
2	false	false	9	false	false	16	false	false
3	false	false	10	false	false	17	true	false
4	false	false	11	false	false	18	true	true
5	true	true	12	true	true	19	true	true
6	false	false	13	false	false	20	true	true
7	true	true	14	true	true			

- (a) A confusion matrix and the misclassification rate
(b) The average class accuracy (harmonic mean)
(c) The precision, recall, and F_1 measure
2. The table below shows the predictions made for a continuous target feature by two different prediction models for a test dataset.

ID	Model 1		Model 2		ID	Model 1		Model 2	
	Target	Prediction	Target	Prediction		Target	Prediction	Prediction	
1	2,623	2,664	2,691		16	2,570	2,577	2,612	
2	2,423	2,436	2,367		17	2,528	2,510	2,557	
3	2,423	2,399	2,412		18	2,342	2,381	2,421	
4	2,448	2,447	2,440		19	2,456	2,452	2,393	
5	2,762	2,847	2,693		20	2,451	2,437	2,479	
6	2,435	2,411	2,493		21	2,296	2,307	2,290	
7	2,519	2,516	2,598		22	2,405	2,355	2,490	
8	2,772	2,870	2,814		23	2,389	2,418	2,346	
9	2,601	2,586	2,583		24	2,629	2,582	2,647	
10	2,422	2,414	2,485		25	2,584	2,564	2,546	
11	2,349	2,407	2,472		26	2,658	2,662	2,759	
12	2,515	2,505	2,584		27	2,482	2,492	2,463	
13	2,548	2,581	2,604		28	2,471	2,478	2,403	
14	2,281	2,277	2,309		29	2,605	2,620	2,645	
15	2,295	2,280	2,296		30	2,442	2,445	2,478	

- (a) Based on these predictions, calculate the evaluation measures listed below for each model.
- The sum of squared errors
 - The R^2 measure
- (b) Based on the evaluation measures calculated, which model do you think is performing better for this dataset?

3. A credit card issuer has built two different credit scoring models that predict the propensity of customers to default on their loans. The outputs of the first model for a test dataset are shown in the table below.

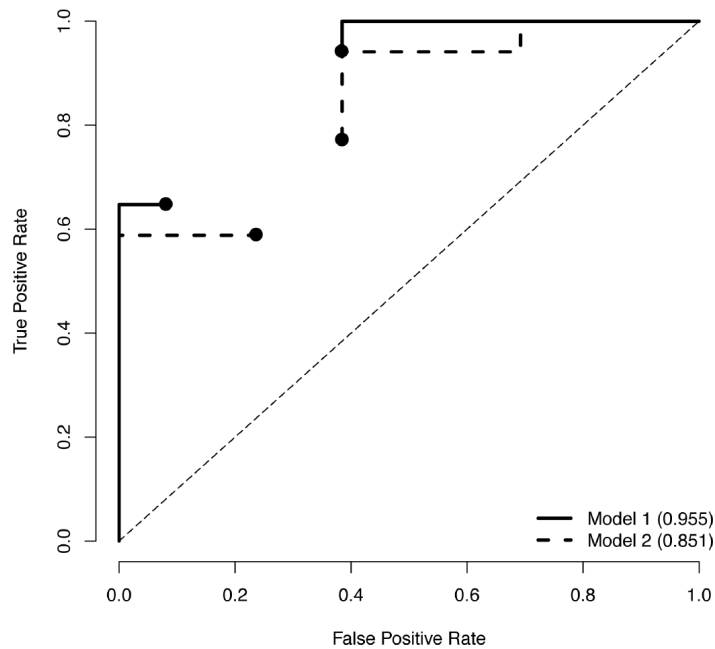
ID	Target	Score	Prediction	ID	Target	Score	Prediction
1	bad	0.634	bad	16	good	0.072	good
2	bad	0.782	bad	17	bad	0.567	bad
3	good	0.464	good	18	bad	0.738	bad
4	bad	0.593	bad	19	bad	0.325	good
5	bad	0.827	bad	20	bad	0.863	bad
6	bad	0.815	bad	21	bad	0.625	bad
7	bad	0.855	bad	22	good	0.119	good
8	good	0.500	good	23	bad	0.995	bad
9	bad	0.600	bad	24	bad	0.958	bad
10	bad	0.803	bad	25	bad	0.726	bad
11	bad	0.976	bad	26	good	0.117	good
12	good	0.504	bad	27	good	0.295	good
13	good	0.303	good	28	good	0.064	good
14	good	0.391	good	29	good	0.141	good
15	good	0.238	good	30	good	0.670	bad

The outputs of the second model for the same test dataset are shown in the table below.

ID	Target	Score	Prediction	ID	Target	Score	Prediction
1	bad	0.230	bad	16	good	0.421	bad
2	bad	0.859	good	17	bad	0.842	good
3	good	0.154	bad	18	bad	0.891	good
4	bad	0.325	bad	19	bad	0.480	bad
5	bad	0.952	good	20	bad	0.340	bad
6	bad	0.900	good	21	bad	0.962	good
7	bad	0.501	good	22	good	0.238	bad
8	good	0.650	good	23	bad	0.362	bad
9	bad	0.940	good	24	bad	0.848	good
10	bad	0.806	good	25	bad	0.915	good
11	bad	0.507	good	26	good	0.096	bad
12	good	0.251	bad	27	good	0.319	bad
13	good	0.597	good	28	good	0.740	good
14	good	0.376	bad	29	good	0.211	bad
15	good	0.285	bad	30	good	0.152	bad

Based on the predictions of these models, perform the following tasks to compare their performance.

- (a) The image below shows an **ROC curve** for each model. Each curve has a point missing.



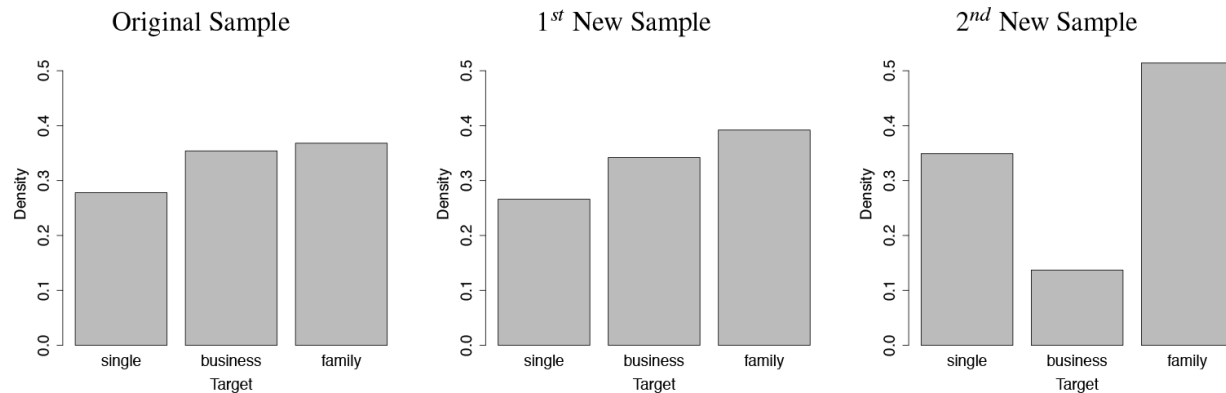
Calculate the missing point in the ROC curves for Model 1 and Model 2. To generate the point for Model 1, use a threshold value of 0.51. To generate the point for Model 2, use a threshold value of 0.43.

- (b) The **area under the ROC curve** (AUC) for Model 1 is 0.955 and for Model 2 is 0.851. Which model is performing best?
- (c) Based on the AUC values for Model 1 and Model 2, calculate the **Gini coefficient** for each model.
4. A retail supermarket chain has built a prediction model that recognizes the household that a customer comes from as being one of *single*, *business*, or *family*. After deployment, the analytics team at the supermarket chain uses the **stability index** to monitor the performance of this model. The table below shows the frequencies of predictions of the three different levels made by the model for the original validation dataset at the time the model was built, for the month after deployment, and for a monthlong period six months after deployment.

Target	Original Sample	1 st New Sample	2 nd New Sample
--------	-----------------	----------------------------	----------------------------

<i>single</i>	123	252	561
<i>business</i>	157	324	221
<i>family</i>	163	372	827

Bar plots of these three sets of prediction frequencies are shown in the following images.



Calculate the **stability index** for the two new periods and determine whether the model should be retrained at either of these points.

- * 5. Explain the problem associated with measuring the performance of a predictive model using a single accuracy figure.
- * 6. A marketing company working for a charity has developed two different models that predict the likelihood that donors will respond to a mailshot asking them to make a special extra donation. The prediction scores generated for a test set for these two models are shown in the table below.

ID	Target	Model 1	Model 2	ID	Target	Model 1	Model 2
		Score	Score			Score	Score
1	false	0.1026	0.2089	16	true	0.7165	0.4569
2	false	0.2937	0.0080	17	true	0.7677	0.8086
3	true	0.5120	0.8378	18	false	0.4468	0.1458
4	true	0.8645	0.7160	19	false	0.2176	0.5809
5	false	0.1987	0.1891	20	false	0.9800	0.5783
6	true	0.7600	0.9398	21	true	0.6562	0.7843
7	true	0.7519	0.9800	22	true	0.9693	0.9521
8	true	0.2994	0.8578	23	false	0.0275	0.0377
9	false	0.0552	0.1560	24	true	0.7047	0.4708
10	false	0.9231	0.5600	25	false	0.3711	0.2846
11	true	0.7563	0.9062	26	false	0.4440	0.1100
12	true	0.5664	0.7301	27	true	0.5440	0.3562
13	true	0.2872	0.8764	28	true	0.5713	0.9200
14	true	0.9326	0.9274	29	false	0.3757	0.0895
15	false	0.0651	0.2992	30	true	0.8224	0.8614

- (a) Using a classification threshold of 0.5, and assuming that *true* is the positive target level, construct a **confusion matrix** for each of the models.
 - (b) Calculate the simple accuracy and **average class accuracy** (using an **arithmetic mean**) for each model.
 - (c) Based on the average class accuracy measures, which model appears to perform best at this task?
 - (d) Generate a **cumulative gain chart** for each model.
 - (e) The charity for which the model is being built typically has only enough money to send a mailshot to the top 20% of its contact list. Based on the cumulative gain chart generated in the previous part, would you recommend that Model 1 or Model 2 would perform best for the charity?
- * 7. A prediction model is going to be built for in-line quality assurance in a factory that manufactures electronic components for the automotive industry. The system will be integrated into the factory's production line and determine whether components are of an acceptable quality standard based on a set of test results. The prediction subject is a component, and the descriptive features are a set of characteristics of

the component that can be gathered on the production line. The target feature is binary and labels components as *good* or *bad*.

It is extremely important that the system not in any way slow the production line and that the possibility of defective components being passed by the system be minimized as much as possible. Furthermore, when the system makes a mistake, it is desirable that the system can be retrained immediately using the instance that generated the mistake. When mistakes are made, it would be useful for the production line operators to be able to query the model to understand why it made the prediction that led to a mistake. A large set of historical labeled data is available for training the system.

- (a) Discuss the different issues that should be taken into account when evaluating the suitability of different machine learning approaches for use in this system.
- (b) For this task, discuss the suitability of the decision tree, k nearest neighbor, naive Bayes, and logistic regression models. Which one do you think would be most appropriate?
- * 8. The following matrices list the confusions matrices for two models and the **profit matrix** for this prediction task. Calculate the overall profit for each model.

$$\mathbb{M}_1 = \begin{bmatrix} 50 & 10 \\ 20 & 80 \end{bmatrix} \quad \mathbb{M}_2 = \begin{bmatrix} 35 & 25 \\ 40 & 60 \end{bmatrix} \quad Profit = \begin{bmatrix} +100 & -20 \\ -110 & +10 \end{bmatrix}$$

- * 9. The following table lists the scores returned by a prediction model for a test set of 12 examples. The prediction task is a binary classification task, and the instances in the test set are labeled as belonging to the *positive* or *negative* class. For ease of reading, the instances have been ordered in descending order of the score the model assigned to each instance.

ID	Target	Score
1	positive	0.75
2	positive	0.72
3	positive	0.64
4	negative	0.62
5	negative	0.55

6	positive	0.48
7	negative	0.45
8	negative	0.44
9	negative	0.38
10	negative	0.35
11	negative	0.32
12	negative	0.31

- (a) Calculate the **ROC index** for this model using the **trapezoidal method** and the following set of thresholds: 1.0, 0.5, and 0.0.
- (b) The following table lists the scores returned by the same prediction model for a new test set of 12 examples. Again, the prediction task is a binary classification task, and the instances in the test set are labeled as belonging to the *positive* or *negative* class. For ease of reading, the instances have been ordered in descending order of the score the model assigned to each instance. Calculate the ROC index for this model using the **trapezoidal method** and the following set of thresholds: 1.0, 0.5, and 0.0.

ID	Target	Score
1	positive	0.71
2	positive	0.70
3	positive	0.66
4	positive	0.65
5	positive	0.62
6	positive	0.60
7	negative	0.58
8	positive	0.48
9	positive	0.34
10	negative	0.30
11	negative	0.28
12	negative	0.25

- (c) The ROC index is insensitive to changes in class distribution within the test set. This means that if the proportion of positive to negative instances changes in a test set, the ROC index will remain the same if the performance of the models on each class is constant. Consequently, the ROC index is robust to class imbalance or skew in the test set. Why do you think this is the case?²⁶

- * 10. As part of a natural language processing project, a company is creating a dictionary of idiomatic phrases.²⁷ The company has used an automatic process to extract a set of 50,000 candidate idioms from a large corpus and now are planning to use a machine learning model to filter this set of candidates before presenting them to a human annotator who decides whether a candidate phrase should be added to the dictionary or not. In order to evaluate which machine learning model to use as the pre-annotator filter, the company created a test set of 10 phrases extracted at random from the set of 50,000 candidates.
- (a) The following table presents the scoring by two models of the test set of candidate idioms. Which model would be chosen to filter candidate idioms if the decision were taken on the basis of the F_1 score for each model, assuming both models use a threshold of > 0.5 for classifying a candidate as an idiom.

Model Scoring			
ID	Idiom	M_1	M_2
1	true	0.70	0.80
2	true	0.56	0.80
3	true	0.55	0.70
4	true	0.54	0.45
5	true	0.45	0.44
6	false	0.73	0.55
7	false	0.72	0.54
8	false	0.35	0.40
9	false	0.34	0.38
10	false	0.33	0.30

- (b) There is a cost associated with each item presented to the human annotator, and the company wants to maximize the number of items that end up in the dictionary. The company estimates that it has an annotation budget that will cover the human annotation of 20,000 phrases (i.e., 40% of the set of candidate phrases). Calculate the **cumulative gain** of each of the models for the 4th decile. Again, assume both models use a threshold of > 0.5 for the idiom class. Finally, on the basis of cumulative gain scores, which

model would you recommend the company use for the pre-annotation filtering task?

1. Detailed descriptions of the story of Professor Blondlot and N rays are available in Klotz (1980) and Ashmore (1993).
2. Statisticians will often refer to false positives as **type I errors** and false negatives as **type II errors**. Similarly, false positives are often also referred to as **false alarms**, true positives as **hits**, and false negatives as **misses**.
3. Typically, the level that is of most interest is referred to as the **positive level**. In email classification, identifying spam emails is the most important issue, so the *spam* level is referred to as the positive level. Similarly, in fraud detection, the fraud events would most likely be the positive level; in credit scoring, the default events would most likely be the positive level; and in disease diagnosis, a confirmation that a patient has the disease would most likely be the positive level. The choice, however, is arbitrary.
4. Lehmann et al. (2003) discusses building prediction models to perform this task.
5. The terms **sensitivity** and **specificity** are often used for true positive rate and true negative rate.
6. The F_1 measure is often also referred to as the **F measure**, **F score**, or **F_1 score**.
7. Sometimes target levels in categorical prediction problems are referred to as **classes**, which is where this name comes from.
8. Target level imbalance affects misclassification rate in the same way, and average misclassification rate can also be calculated to combat this problem.
9. Whereas previously we referred to recall as something calculated only for the positive level, we can calculate recall for any level as the accuracy of the predictions made for that level.
10. Remember that a harmonic mean is used in the F_1 measure given in Equation (9.10)^[550].
11. This is always an interesting category to determine a value for. Some people might argue that some profit arises as no loss was made.
12. The slightly strange name *receiver operating characteristic* comes from the fact that this approach was first used for tuning radar signals in World War II.
13. The staircase nature of this graph arises from the fact that there are ranges for the threshold in which no instances occur (for example, from 0.348 to 0.657), during which the TPR and TNR values do not change. Larger test sets cause these curves to smoothen significantly.
14. ROC curves are often plotted with sensitivity on the vertical axis and $1 - \text{specificity}$ on the horizontal axis. Recall that sensitivity is equal to TPR, and specificity is equal to TNR, so these are equivalent.
15. If an ROC curve appears below the diagonal random reference line, this means that the model is consistently making predictions of the positive level for instances that should receive predictions of the negative level and vice versa, and that it could actually be quite a powerful model. This usually arises when a transcription error of some kind has been made and should be investigated.
16. The ROC index is in fact equivalent to the **Wilcoxon-Mann-Whitney statistic** used in significance testing.
17. The Gini coefficient should not be confused with the **Gini index** described in Section 4.4.1^[142]. Their only connection is that they are both named after the Italian statistician Corrado Gini.
18. Any **percentiles** (see Section A.1^[745]) can be used, but deciles are particularly common.

19. See De Bruyne et al. (2011) for an example of machine learning models being used for this task.
20. It is important to remember that for a prediction problem with four target levels, uniform random guessing will give an accuracy of just 25%.
21. A nice example of building machine learning models for drug dosage prediction can be found in Mac Namee et al. (2002).
22. This is very similar to the difference between **Euclidean distance** and **Manhattan distance** discussed in Section 5.2.2^[184].
23. Systems like the **Western Electric rules** (Montgomery, 2004), used widely in process engineering to detect *out-of-control* processes, can be useful in this regard.
24. The natural logarithm of a value a , $\log_e(a)$, is the logarithm of a to the base e , where e is **Euler's number**, equal to approximately 2.718.
25. A formal test for **statistical significance** could easily be used to reinforce this conclusion.
26. We recommend Fawcett (2006) as an excellent introduction and overview to ROC analysis that covers the topic of imbalance in the test set. Note also that in very highly imbalanced data where there is a very large number of negative examples, the false positive rate is not very sensitive to changes in the number of false positives (because the denominator is so large) and in these contexts, if the focus of the model is on detecting the positive class, it is probably advisable to use precision as the evaluation metric, as it focuses more on the ability to detect the positive class, rather than on the ability to distinguish between classes (which the ROC index captures).
27. This question is inspired by the work reported in Klubička et al. (2018).

III

BEYOND PREDICTION

10

Beyond Prediction: Unsupervised Learning

“Dick: I guess it looks as if you’re reorganizing your records. What is this though? Chronological?

Rob: No...

Dick: Not alphabetical...

Rob: Nope...

Dick: What?

Rob: Autobiographical.”

—Nick Hornby, High Fidelity

The examples throughout this book so far have focused on supervised machine learning methods for building predictive models. In this chapter we shift the focus to **unsupervised machine learning** methods. We begin by illustrating the key differences between supervised and unsupervised machine learning before describing clustering, one of the main applications of unsupervised learning; and the standard approach for clustering, the **k -means clustering** algorithm. We then explain some variations on the standard algorithm as well as how clustering can be evaluated and interpreted. Finally, we cover a second use case of unsupervised learning, to generate representations that will be used in other machine learning approaches rather than as an end result in their own right. Unsupervised learning is a huge topic in its own right, and so the goal of this chapter is to give a flavor of the most important approaches involved. Suggestions for further reading are given at the end of the chapter.

10.1 Big Idea

Like lots of other families, the Murphys have a set of magnetic letters on the refrigerator in their kitchen. Struggling to entertain his daughter one afternoon, Mr. Murphy asked little Abigail to tidy them up. A shorter time

later than Mr. Murphy would have liked, Abigail skipped back in to her father to say that she was finished. After going along to admire her work, Mr. Murphy congratulated his daughter on organizing the letters so well. Not long afterward, however, Mr. Murphy's son, Andrew, ran in to say that he had fixed the letters in the kitchen because they had been so badly organized. Mr. Murphy walked to the kitchen to have a look and agreed with his son that he too had done a great job of organizing the letters. Having encouraged his two younger children to play outside, Mr. Murphy had just sat down to read the newspaper when his third child Amalia ran in to say that she had fixed the letters on the fridge because they were all out of order. Once again he went to the kitchen to inspect and agreed that Amalia had also done a great job of organizing the letters. Not long afterward the three Murphy children came to their father together to ask how it was that he had told each of them that they had done a great job of arranging the letters when they had all done something different.

Figure 10.1^[598] shows how the three Murphy children organized the letters on the fridge. From the disorganized letters at the beginning, Abigail divided the letters into six different-colored groups, Andrew organized them into a lowercase group and an uppercase group, and Sarah made a group for each letter of the alphabet. All are correct, although they focus on different characteristics of the letter magnets—color, case, and character. This illustrates the *big idea* behind unsupervised learning. In contrast with supervised learning, there is no target feature that we build a model to predict; rather, we perform modeling to find structure within a set of instances defined by descriptive features alone.

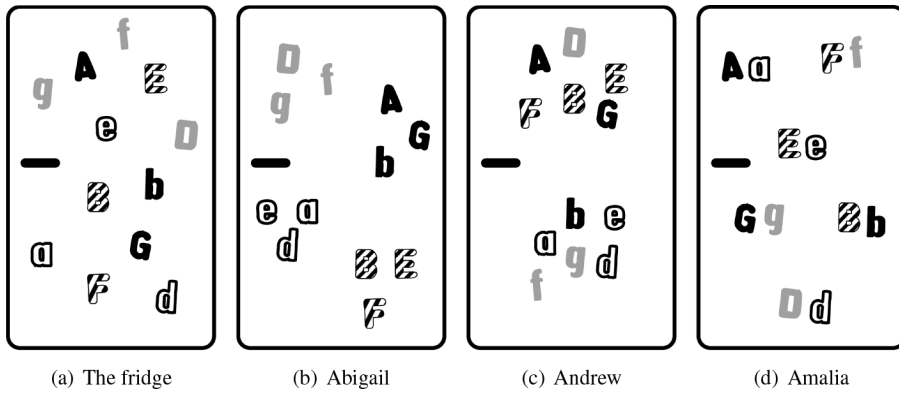


Figure 10.1

The three different arrangements of the magnetic letters made by the Murphy children on the Murphy family refrigerator.

10.2 Fundamentals

In Chapter 1[3] of this book we described supervised machine learning techniques as automatically learning a model of the relationship between a set of **descriptive features** and a **target feature** on the basis of a set of historical instances. In contrast with this, **unsupervised machine learning** techniques are used in the absence of a target feature and model the underlying structure within the descriptive features in a dataset. This structure is typically captured in new generated features that can be appended to the original dataset and so **augment** or **enrich** it. [Figure 10.2](#)^[599] illustrates this.

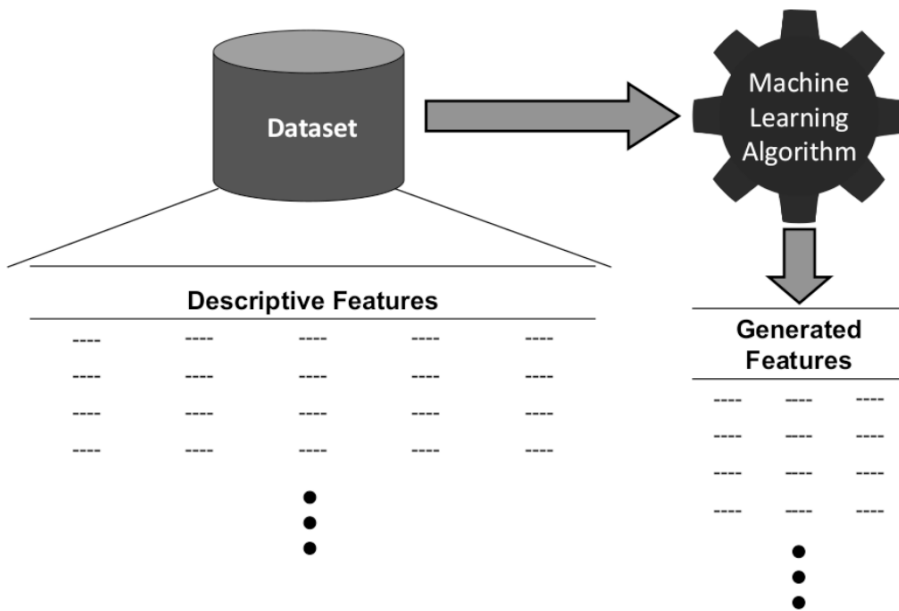


Figure 10.2

Unsupervised machine learning as a single-step process.

There are two key use cases for unsupervised learning: clustering and representation learning. **Clustering** is a technique that partitions the instances in a dataset into groups, or **clusters**, that are similar to each other. The end result of clustering is a single new generated feature that indicates the cluster that an instance belongs to, and the generation of this new feature is typically the end goal of the clustering task. One of the most common applications of clustering is **customer segmentation** with which organizations attempt to discover meaningful groupings into which they can group their customers so that targeted offers or treatments can be designed.

In **representation learning** the goal of unsupervised machine learning is to create a new way to represent the instances in a dataset, usually with the expectation that this new representation will be more useful for a later, usually supervised, machine learning process. The origins of deep learning discussed in Chapter 8^[381] lie in this application of unsupervised machine learning.

The fundamentals of unsupervised learning have already largely been covered in previous chapters. The clustering methods discussed in this chapter use the ideas of a **feature space** and a **distance measure** discussed in Chapter 5^[181], and the feature generation techniques largely build upon

the ideas of **error-based learning** and **neural networks** discussed in Chapters 7^[311] and 8^[381].

Converting business problems into solutions based on unsupervised machine learning also relies mainly on the techniques discussed in the context of supervised learning in Chapter 2^[23]. CRISP-DM remains an appropriate process to follow, the approach to designing data representations based on domain concepts is still very useful, and the project flow presented in Section 2.5^[44] is still appropriate. In all these tasks, the absence of a target feature makes determining what descriptive features are likely to be useful in an **ABT** and evaluating the performance of a proposed solution a little more challenging. For these reasons, analysts often must rely more heavily on domain experts in projects using unsupervised learning than in performing supervised machine learning tasks.

In the next section we discuss the standard approach to clustering, the k -means clustering algorithm.

10.3 Standard Approach: The k -Means Clustering Algorithm

The **k -means clustering** algorithm is the most well-known approach to clustering. As well as being simple to understand and computationally efficient, it is also quite effective and often a good solution to clustering problems. The goal of k -means clustering is to take a dataset, \mathcal{D} , consisting of n instances, \mathbf{d}_1 to \mathbf{d}_n , where \mathbf{d}_i is a set of m descriptive features, and divide this dataset into k disjoint clusters, \mathcal{C}_1 to \mathcal{C}_k . The number of clusters to be found, k , is an input to the algorithm and each instance can belong to only one cluster. The algorithm finds the division of instances into clusters by minimizing

$$\sum_{i=1}^n \min_{\mathbf{c}_1, \dots, \mathbf{c}_k} \text{Dist}(\mathbf{d}_i, \mathbf{c}_j) \quad (10.1)$$

where \mathbf{c}_1 to \mathbf{c}_k are the centers of the k clusters, referred to as **cluster centroids**; and Dist is a distance measure used to compare instances to centroids. Algorithm 9^[601] provides a pseudocode definition of the k -means clustering algorithm.¹

The algorithm begins by randomly selecting k cluster centroids, \mathbf{c}_1 to \mathbf{c}_k , where a cluster centroid is composed of a value for each descriptive feature present in a dataset (these initial cluster centroids are often referred to as **seeds**). The values for these cluster centroids can be selected randomly following uniform distributions bounded by the minimum and maximum values of each feature. The distance of each instance in the dataset to each of these cluster centroids is then calculated using the distance measure $Dist$. It is usual in k -means clustering for $Dist$ to calculate Euclidean distance.² As discussed in Section 5.4.3^[204] in relation to similarity models for predictive modeling, it is important that all descriptive features are normalized before using k -means clustering so that distance contributions across features are comparable. Each instance in the dataset is then assigned to be a *member* of the cluster, C_i , to whose cluster centroid, \mathbf{c}_i , it is closest. The cluster centroids are then updated to the average value of the descriptive features of the members of a cluster. In this way the cluster centroids are moved to be representative of the members of that cluster.

Algorithm 9 Pseudocode description of the **k -means clustering** algorithm.

Require: a dataset \mathcal{D} containing n training instances, $\mathbf{d}_1, \dots, \mathbf{d}_n$

Require: the number of clusters to find k

Require: a distance measure, $Dist$, to compare instances to cluster centroids

- 1: Select k random cluster centroids, \mathbf{c}_1 to \mathbf{c}_k , each defined by values for each descriptive feature, $\mathbf{c}_i = <\mathbf{c}_i[1], \dots, \mathbf{c}_i[m]>$
- 2: **repeat**
- 3: calculate the distance of each instance, \mathbf{d}_i , to each cluster centroid, \mathbf{c}_1 to \mathbf{c}_k , using $Dist$
- 4: assign each instance, \mathbf{d}_i , to belong to the cluster, C_i , to whose cluster centroid, \mathbf{c}_i , it is closest
- 5: update each cluster centroid, \mathbf{c}_i , to the average of the descriptive feature values of the instances that belong to cluster C_i
- 6: **until** no cluster reassessments are performed during an iteration

This process repeats until convergence occurs—where *convergence* is defined as having occurred when no cluster memberships change on an iteration of the algorithm and therefore the cluster centroids are stable. Once the algorithm has completed, its two outputs are a vector of

assignments of each instance in the dataset to one of the clusters, \mathcal{C}_1 to \mathcal{C}_k , and the k cluster centroids, \mathbf{c}_1 to \mathbf{c}_k . This first output can be used to enrich the original dataset with a new generated feature, the cluster memberships.

10.3.1 A Worked Example

[Table 10.1](#)^[604] shows a simple dataset with just two descriptive features that describe the average number of minutes of calls, CALL VOLUME, and average megabytes of data, DATA USAGE, used per month by customers of a mobile phone company.³ From [Figure 10.3\(a\)](#)^[602], which illustrates this dataset, it is clear to a human viewer that three clusters exist in this dataset, however, we require an algorithm such as k -means clustering to find them automatically (especially in real-world datasets with many more dimensions when we can't create this type of data visualization).

Table 10.1

A dataset of mobile phone customers described by their average monthly data (DATA USAGE) and call (CALL VOLUME) usage. Details of the first two iterations of the k -means clustering algorithm are also shown. The clustering in the second iteration is actually the final clustering in this simple example.

ID	DATA USAGE	CALL VOLUME	Cluster Distances Iter. 1			Iter. 1 Cluster	Cluster Distances Iter. 2			Iter. 2 Cluster
			$Dist(\mathbf{d}_i, \mathbf{c}_1)$	$Dist(\mathbf{d}_i, \mathbf{c}_2)$	$Dist(\mathbf{d}_i, \mathbf{c}_3)$		$Dist(\mathbf{d}_i, \mathbf{c}_1)$	$Dist(\mathbf{d}_i, \mathbf{c}_2)$	$Dist(\mathbf{d}_i, \mathbf{c}_3)$	
1	-0.9531	-0.3107	0.2341	0.9198	0.6193	C_1	0.4498	1.9014	1.1099	C_1
2	-1.1670	-0.7060	0.5770	0.6108	0.9309	C_1	0.87	2.0554	1.558	C_1
3	-1.2329	-0.4188	0.3137	0.8945	0.6388	C_1	0.7464	2.152	1.3661	C_1
4	1.0684	-0.4560	2.1972	2.06	2.438	C_2	1.6857	0.3813	1.7651	C_2
5	-1.1104	0.1090	0.2415	1.3594	0.1973	C_3	0.5669	2.1905	0.923	C_1
6	-0.8431	0.1811	0.4084	1.405	0.4329	C_1	0.3694	1.9842	0.6651	C_1
7	-0.3666	0.6905	1.1055	1.9728	1.0231	C_3	0.7885	1.9406	0.0837	C_3
8	0.9285	-0.2168	2.0351	2.0378	2.2455	C_1	1.5083	0.5759	1.5127	C_2
9	1.1175	-0.6028	2.2715	2.0566	2.529	C_2	1.772	0.298	1.895	C_2
10	0.8404	-1.0450	2.1486	1.693	2.4636	C_2	1.7165	0.258	2.0328	C_2
11	-1.005	-0.0337	0.1404	1.2012	0.3692	C_1	0.4339	2.0376	0.9295	C_1
12	0.2410	0.7360	1.6017	2.2398	1.6013	C_3	1.1457	1.6581	0.5908	C_3
13	0.2021	0.4364	1.4253	1.9619	1.4925	C_1	0.9259	1.4055	0.5668	C_3
14	0.2153	0.8360	1.6372	2.3159	1.6125	C_3	1.2012	1.7602	0.5956	C_3
15	0.8770	-0.2459	1.985	1.9787	2.201	C_2	1.4603	0.5454	1.4865	C_2
16	-0.0345	1.0502	1.595	2.4136	1.4929	C_3	1.2433	2.0589	0.5321	C_3
17	0.8785	-1.3601	2.3325	1.727	2.6698	C_2	1.9413	0.569	2.3167	C_2
18	0.9164	-0.8517	2.1454	1.7984	2.4383	C_2	1.6815	0.0674	1.9271	C_2
19	-1.0423	0.1193	0.2593	1.3579	0.2525	C_3	0.5065	2.133	0.8608	C_1
20	-0.7426	0.0119	0.3899	1.2399	0.5706	C_1	0.1889	1.8164	0.7247	C_1
21	0.6259	-1.1834	2.0248	1.4696	2.3616	C_2	1.6355	0.4709	2.0374	C_2
22	0.7684	-0.5844	1.927	1.7338	2.195	C_2	1.4362	0.2382	1.6289	C_2
23	-0.2596	0.7450	1.2183	2.0535	1.1432	C_3	0.8736	1.9167	0.1535	C_3
24	-0.3414	0.4215	0.9432	1.7202	0.9548	C_1	0.5437	1.7259	0.1909	C_3

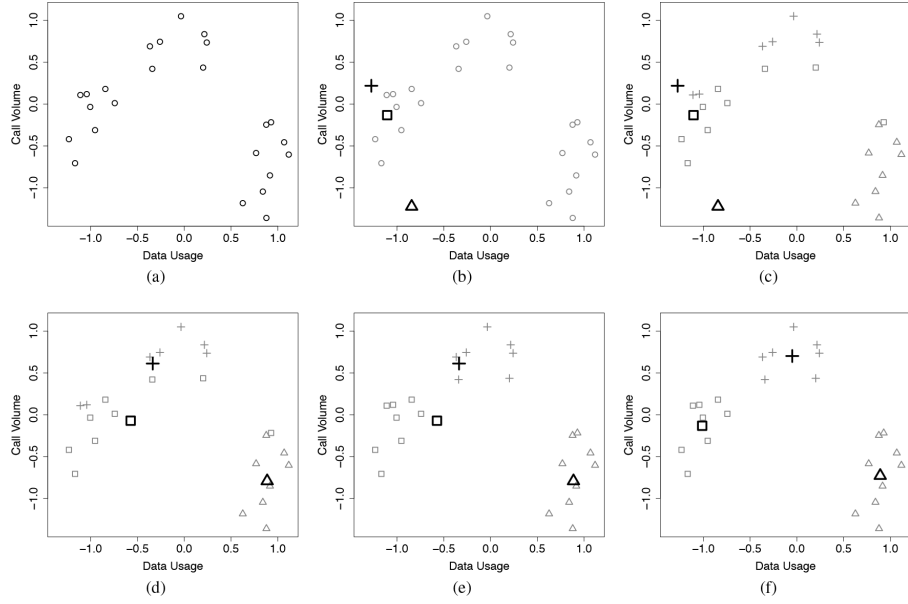


Figure 10.3

(a) A plot of the mobile phone customer dataset given in [Table 10.1](#)^[604]. (b)–(f) The progress of the k -means clustering algorithm, working on the simple customer segmentation dataset. The large symbols represent cluster centroids, and the smaller symbols represent cluster assignments.

[Figure 10.3\(b\)](#)^[602] shows the initial randomly selected cluster centroids overlaid onto the dataset, where $\mathbf{c}_1 = \langle -1.1048, -0.1324 \rangle$, $\mathbf{c}_2 = \langle -0.8431, -1.2239 \rangle$, and $\mathbf{c}_3 = \langle -1.2744, 0.2187 \rangle$. After selection of the initial cluster centroids, the next step in the algorithm is to calculate the Euclidean distance from each instance in the dataset to each cluster centroid. In this example we use Euclidean distance as the distance measure. In [Table 10.1](#)^[604] the columns labeled *Cluster Distances Iter. 1* show the distances between each instance and these initial cluster centroids. On the basis of these distances, each instance in \mathcal{D} is assigned to one of these clusters, as shown in the column labeled *Cluster*. These memberships are illustrated in [Figure 10.3\(c\)](#)^[602].

Each cluster centroid is then updated by calculating the mean value of each descriptive feature for all instances that are a member of the cluster. For example, there are nine members of \mathcal{C}_1 : $\{\mathbf{d}_1, \mathbf{d}_2, \mathbf{d}_3, \mathbf{d}_6, \mathbf{d}_8, \mathbf{d}_{11}, \mathbf{d}_{13}, \mathbf{d}_{20}, \mathbf{d}_{24}\}$. So, \mathbf{c}_1 is updated to

$$\begin{aligned}
\mathbf{c}_1[\text{DATA USAGE}] &= (-0.9531 + -1.167 + -1.2329 + -0.8431 + 0.9285 \\
&\quad + -1.005 + 0.2021 + -0.7426 + -0.3414)/9 \\
&= -0.5727 \\
\mathbf{c}_1[\text{CALL VOLUME}] &= (-0.3107 + -0.706 + -0.4188 + 0.1811 + -0.2168 \\
&\quad + -0.0337 + 0.4364 + 0.0119 + 0.4215)/9 \\
&= -0.0706
\end{aligned}$$

The other cluster centroids are updated similarly, so that $\mathbf{c}_1 = \langle -0.5727, -0.0706 \rangle$, $\mathbf{c}_2 = \langle 0.8866, -0.7912 \rangle$, and $\mathbf{c}_3 = \langle -0.3367, 0.6123 \rangle$. These are illustrated in [Figure 10.3\(d\)](#)^[602].

The previous process is then repeated, and the distances of each instance in \mathcal{D} to these updated cluster centroids are given in [Table 10.1](#)^[604] in the columns labeled *Cluster Distances Iter. 2*. The updated cluster memberships based on these distances are shown in the rightmost column of [Table 10.1](#)^[604]. [Figures 10.3\(e\)](#)^[602] and [10.3\(f\)](#)^[602] show the remaining steps of the k -means clustering process. In this simple example no cluster reassessments are made at the third iteration, and so the process is considered to have converged.

The final results of the clustering are the cluster centroid values of $\mathbf{c}_1 = \langle -1.012, -0.131 \rangle$, $\mathbf{c}_2 = \langle 0.8912, -0.7273 \rangle$, and $\mathbf{c}_3 = \langle -0.0491, 0.7022 \rangle$; and the cluster assignments of

$$\begin{aligned}
C_1 &= \{\mathbf{d}_1, \mathbf{d}_2, \mathbf{d}_3, \mathbf{d}_5, \mathbf{d}_6, \mathbf{d}_{11}, \mathbf{d}_{19}, \mathbf{d}_{20}\} \\
C_2 &= \{\mathbf{d}_4, \mathbf{d}_8, \mathbf{d}_9, \mathbf{d}_{10}, \mathbf{d}_{15}, \mathbf{d}_{17}, \mathbf{d}_{18}, \mathbf{d}_{21}, \mathbf{d}_{22}\} \\
C_3 &= \{\mathbf{d}_7, \mathbf{d}_{12}, \mathbf{d}_{13}, \mathbf{d}_{14}, \mathbf{d}_{16}, \mathbf{d}_{23}, \mathbf{d}_{24}\}
\end{aligned}$$

These cluster assignments are also shown in the rightmost column of [Table 10.1](#)^[604] (as cluster assignments did not change after the second iteration of the algorithm) in context with the original dataset. A set of cluster assignments is usually referred to as a **clustering**.

The sample dataset used in this section has been purposefully selected to include just two descriptive features so that the visualizations in [Figure 10.3](#)^[602] could be easily shown. The algorithm, however, proceeds in exactly the same way for larger datasets and usually converges after tens of iterations. Long after it was first proposed, k -means remains a commonly used clustering algorithm; however, there have been many modifications

and alternatives proposed over the years. We explore the most important of these modifications in the following sections.

10.4 Extensions and Variations

The k -means clustering algorithm is simple and reasonably effective, but this simple version leaves a number of questions unanswered—can we make the process more efficient, how are clusterings evaluated, how is k chosen, and how are clusters interpreted?—and it works only for clusterings of a certain underlying structure. In this section we look at extensions and modifications of the k -means clustering algorithm that answer these questions and address these shortcomings. At the end of the chapter, unsupervised machine learning for feature generation will be discussed.

10.4.1 Choosing Initial Cluster Centroids

In the basic form of k -means clustering, the initial cluster centroids, or seeds, are chosen at random uniformly within the feature space. This choice of these initial seeds, unfortunately, can have a big impact on the performance of the algorithm. Different randomly selected starting points can lead to different, often sub-optimal, clusterings. [Figure 10.4](#)^[606] illustrates this, showing other clusterings that are possible given different random initial cluster centroids for the mobile phone customer dataset presented in [Table 10.1](#)^[604]. In [Figures 10.4\(a\)](#)^[606] and [10.4\(b\)](#)^[606], a very different seed from that shown in [Figure 10.3\(b\)](#)^[602] is shown to lead to the same clustering found previously ([Figure 10.3\(f\)](#)^[602]), whereas in [Figures 10.4\(a\)](#)^[606] to [10.4\(h\)](#)^[606], seeds that lead to very different clusterings are shown. It is clear that the clusterings shown in [Figures 10.4\(d\)](#)^[606], [10.4\(f\)](#)^[606], and [10.4\(h\)](#)^[606] are quite different from the clustering found previously (shown in [Figure 10.3\(f\)](#)^[602]) and are sub-optimal compared with the result we would intuitively expect from looking at the visualization of this dataset. The clustering in [Figure 10.4\(h\)](#)^[606] is particularly *unlucky*, as one of the clusters has remained empty!⁴

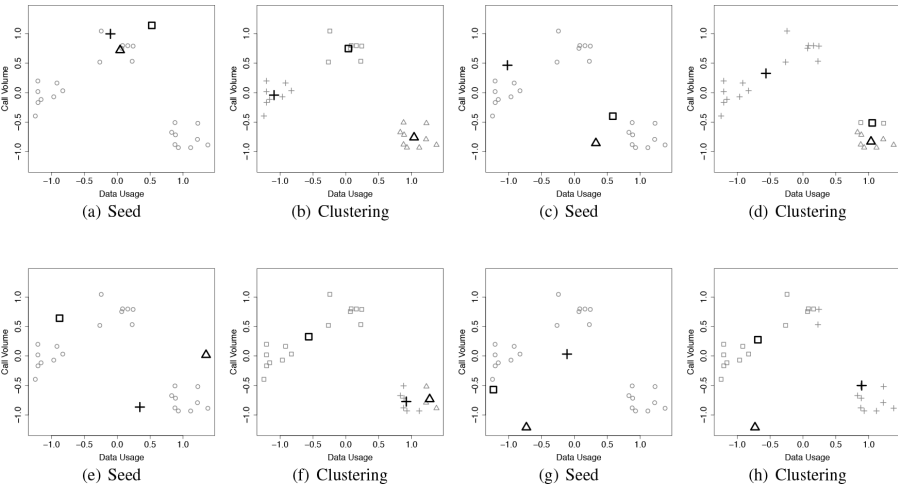


Figure 10.4

(a)–(h) Different clusterings (all with $k = 3$) that can be found for the mobile phone customer dataset given in Table 10.1^[604] when different initial cluster centroids are used.

These sub-optimal clusterings are rare—for this dataset the vast majority of initial centroid choices will lead to the clustering in Figure 10.3(f)^[602]—but they can occur. In large multivariate datasets they are more common, and the algorithm can very easily arrive in one—we don’t have the luxury of simply visualizing high-dimensional datasets to check against an *intuitive* clustering.

An easy way to address this issue is to perform multiple runs of the k -means clustering algorithm starting from different initial centroids and then aggregate the results. In this way the most common clustering is chosen as the final result. There are, however, a number of methods designed to more carefully select the initial centroids. These methods offer two advantages over basic k -means: they can find initial centroids less likely to lead to sub-optimal clusterings, and they can select initial centroids that allow the algorithm to converge much more quickly than when seeds are randomly chosen. The **k-means++** algorithm is a well-known example of this kind of algorithm and is used as the default clustering implementation in many machine learning packages and tools.

Algorithm 10^[607] shows a pseudocode description of the k-means++ algorithm. In this approach, an instance is chosen randomly (following a uniform distribution) from the dataset as the first centroid. Subsequent centroids are then chosen randomly but following a distribution defined by the square of the distances between an instance and the nearest cluster

centroid out of those found so far. This means that instances far away from the current set of centroids are much more likely to be selected than those close to already selected centroids.

[Figure 10.5](#)^[607] shows a selection of sets of initial centroids selected by the k-means++ process. From these it is clear that instances from the dataset are being used as cluster centroids and that typically there is good diversity across the feature space in the centroids shown. The k-means++ algorithm is still stochastic in the manner in which initial cluster centroids are selected, and it does not completely remove the possibility of a poor starting point that leads to a sub-optimal clustering. Hence, an aggregate across multiple runs should still be used.

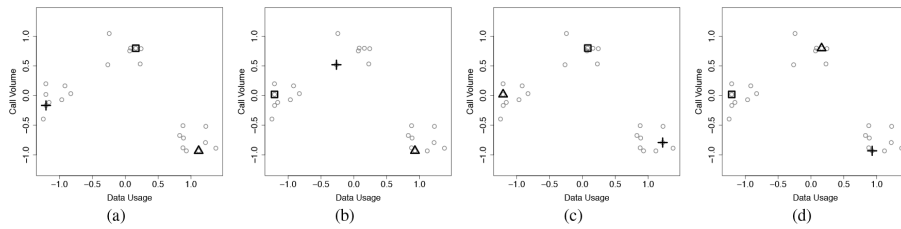


Figure 10.5

(a)–(d) Initial centroids chosen using the k-means++ approach (all with $k = 3$) for the mobile phone customer dataset given in [Table 10.1](#)^[604].

Algorithm 10 Pseudocode description of the **k-means++** algorithm.

Require: a dataset \mathcal{D} containing n training instances, $\mathbf{d}_1, \dots, \mathbf{d}_n$

Require: k , the number of cluster centroids to find

Require: a distance measure $Dist$ to compare instances to cluster centroids

- 1: choose \mathbf{d}_i randomly (following a uniform distribution) from \mathcal{D} to be the position of the initial centroid, \mathbf{c}_1 , of the first cluster, C_1
 - 2: **for** cluster C_j in C_2 to C_k **do**
 - 3: for each instance, \mathbf{d}_i , in \mathcal{D} let $Dist(\mathbf{d}_i)$ be the distance between \mathbf{d}_i and its nearest cluster centroid
 - 4: calculate a selection weight for each instance, \mathbf{d}_i , in \mathcal{D} as $\frac{Dist(\mathbf{d}_i)^2}{\sum_{p=1}^n Dist(\mathbf{d}_p)^2}$
 - 5: choose \mathbf{d}_i as the position of cluster centroid, \mathbf{c}_j , for cluster C_j randomly following a distribution based on the selection weights
 - 6: **end for**
 - 7: proceed with k -means as normal using $\{\mathbf{c}_1, \dots, \mathbf{c}_k\}$ as the initial centroids.
-

10.4.2 Evaluating Clustering

Unsupervised learning presents us with a more complicated evaluation challenge than supervised learning. All the performance measures described in Chapter 9^[533] for supervised learning relied on the existence of **ground truth** labels to which the predictions made by a model can be compared to measure its performance. The essence of the unsupervised scenario is that no ground truth exists—we don’t know what it is that we are looking for! This means that we typically need to move beyond the performance measures described in Chapter 9^[533].

One common approach to evaluating clustering is to use an **internal criterion** to evaluate how well the clustering found by an algorithm matches some idealized notion of what a *good* clustering would look like. Many of these methods make an assumption that a good clustering is a clustering in which the instances that belong to a given cluster are very close together, whereas the instances that belong to different clusters are far apart. That is, a good clustering minimizes **intra-cluster distances** and maximizes **inter-cluster distances**. [Figure 10.6](#)^[608] illustrates these two types of distances along with examples of a *good* and a *bad* clustering—according to this definition.

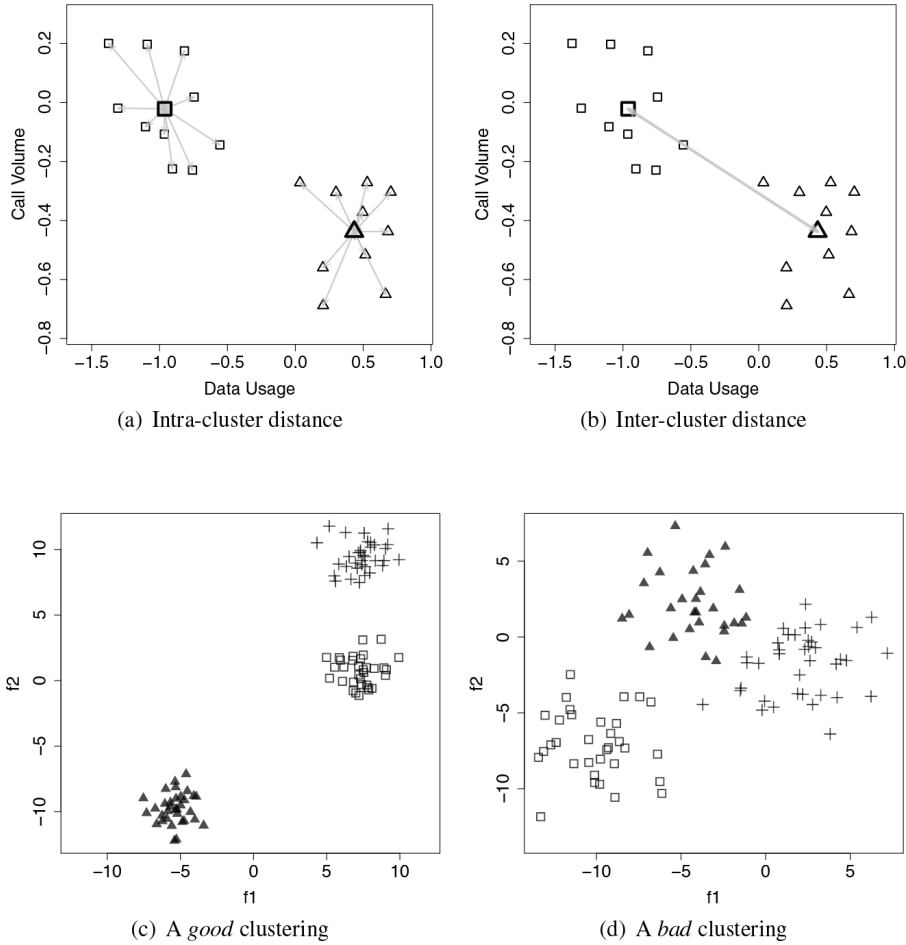


Figure 10.6

(a) Intra-cluster distance; (b) inter-cluster distance; (c) a *good* clustering; and (d) a *bad* clustering.

The **silhouette** is a well-known and widely used performance measure that assesses how well a clustering meets these criteria.⁵ Calculating the silhouette for a clustering involves a reasonable amount of computation. Algorithm 11^[610] outlines the steps involved. To calculate the silhouette for a clustering, \mathcal{C} , over a dataset, \mathcal{D} , we calculate a **silhouette width** for each instance, \mathbf{d}_i , in \mathcal{D} and average these over all instances in the dataset.

The silhouette width for an individual instance is essentially a localized ratio of inter-cluster and intra-cluster distances capturing how well the instance \mathbf{d}_i has been clustered. If for \mathbf{d}_i the average intra-cluster distance, $a(i)$, is much smaller than the average inter-cluster distance to members of the nearest next cluster, $b(i)$, then the silhouette width, $s(i)$, will be close to 1 and we can be confident that \mathbf{d}_i really belongs to the cluster in which it has been placed. On the other hand, if $a(i)$ is much larger than $b(i)$, then \mathbf{d}_i

is closer on average to members of another cluster than it is on average to the members of its own cluster, and $s(i)$ will be close to -1 . This means that \mathbf{d}_i doesn't really *belong* to the cluster in which it has been placed.

Averaging across these localized values gives an overall measure of the overall quality of the clustering. The silhouette for a clustering will always be in the range from -1 to 1 . A value near 1 suggests a good clustering, while a value near -1 suggests a poor clustering (with the caveat that these scores are based on the assumption about desired characteristics of a clustering described previously).

[Table 10.2^{\[611\]}](#) shows an example of calculating the silhouette for the final clustering of the mobile phone customer dataset found using the k -means algorithm (with $k = 3$) ([Table 10.1^{\[604\]}](#)). The cluster to which each instance has been assigned, the nearest other cluster to each instance, the values of $a(i)$ and $b(i)$, and the final silhouette value, $s(i)$, are all shown. We discuss in detail the calculation of the silhouette width for the first instance in the dataset, \mathbf{d}_1 .

Table 10.2

Calculating the silhouette for the final clustering of the mobile phone customer dataset ([Table 10.1^{\[604\]}](#)) found using the k -means algorithm (with $k = 3$). The overall silhouette index value is 0.66.

Nearest						Nearest					
ID	Cluster	Cluster	$a(i)$	$b(i)$	$s(i)$	ID	Cluster	Cluster	$a(i)$	$b(i)$	$s(i)$
1	C_1	C_3	0.401	1.374	0.708	13	C_3	C_1	0.5136	1.3592	0.6221
2	C_1	C_3	0.695	1.811	0.616	14	C_3	C_1	0.4349	1.5738	0.7236
3	C_1	C_3	0.503	1.644	0.694	15	C_2	C_3	0.5776	1.3480	0.5715
4	C_2	C_3	0.484	1.628	0.703	16	C_3	C_1	0.4955	1.5409	0.6784
5	C_1	C_3	0.387	1.232	0.686	17	C_2	C_1	0.7369	2.2757	0.6762
6	C_1	C_3	0.445	0.970	0.541	18	C_2	C_3	0.4312	1.8473	0.7666
7	C_3	C_1	0.452	1.056	0.572	19	C_1	C_3	0.3711	1.1682	0.6823
8	C_2	C_3	0.599	1.364	0.561	20	C_1	C_3	0.4334	1.0006	0.5669
9	C_2	C_3	0.470	1.768	0.734	21	C_2	C_1	0.6520	1.9710	0.6692
10	C_2	C_3	0.504	1.978	0.745	22	C_2	C_3	0.4504	1.5457	0.7086
11	C_1	C_3	0.327	1.223	0.732	23	C_3	C_1	0.3954	1.1654	0.6607
12	C_3	C_1	0.433	1.537	0.719	24	C_3	C_1	0.5339	0.8880	0.3988

In this clustering \mathbf{d}_1 is a member of C_1 . The first step is calculating the silhouette value for \mathbf{d}_1 is to calculate $a(i)$, the average distance between \mathbf{d}_1

and the other members of cluster \mathcal{C}_1 . The distance from \mathbf{d}_1 to each other member of \mathcal{C}_1 is

$$\mathbf{d}_1 \quad \begin{matrix} \mathbf{d}_2 & \mathbf{d}_3 & \mathbf{d}_5 & \mathbf{d}_6 & \mathbf{d}_{11} & \mathbf{d}_{19} & \mathbf{d}_{20} \\ [0.45 & 0.30 & 0.45 & 0.50 & 0.28 & 0.44 & 0.39] \end{matrix}$$

The average distance between \mathbf{d}_1 and the other members of \mathcal{C}_1 , the average intra-cluster distance, is the average of these values, which is equal to 0.401, the $a(i)$ value for \mathbf{d}_1 given in [Table 10.2](#)^[611].

The next step in the algorithm is to calculate the average distance from \mathbf{d}_1 to each member of the other two clusters, \mathcal{C}_2 and \mathcal{C}_3 —the inter-cluster distances. The distances from \mathbf{d}_1 to the members of \mathcal{C}_2 are

$$\mathbf{d}_1 \quad \begin{matrix} \mathbf{d}_4 & \mathbf{d}_8 & \mathbf{d}_9 & \mathbf{d}_{10} & \mathbf{d}_{15} & \mathbf{d}_{17} & \mathbf{d}_{18} & \mathbf{d}_{21} & \mathbf{d}_{22} \\ [2.03 & 1.88 & 2.09 & 1.94 & 1.83 & 2.11 & 1.95 & 1.80 & 1.74] \end{matrix}$$

which gives an average of 1.931. For \mathcal{C}_3 the distances are

$$\mathbf{d}_1 \quad \begin{matrix} \mathbf{d}_7 & \mathbf{d}_{12} & \mathbf{d}_{13} & \mathbf{d}_{14} & \mathbf{d}_{16} & \mathbf{d}_{23} & \mathbf{d}_{24} \\ [1.16 & 1.59 & 1.38 & 1.64 & 1.64 & 1.26 & 0.95] \end{matrix}$$

which gives an average of 1.3743. Based on these two average distances, \mathcal{C}_3 is the closest other cluster to \mathbf{d}_1 and so $b(i) = 1.3743$, as shown in [Table 10.2](#)^[611]. The silhouette width for \mathbf{d}_1 is then calculated using Equation (10.2)^[610]

$$\frac{1.3743 - 0.401}{\max(0.401, 1.374)} = 0.7081$$

The $a(i)$, $b(i)$, and $s(i)$ values in [Table 10.2](#)^[611] are calculated similarly for each other instance, and the overall silhouette for the clustering is the average of these values, in this case, 0.656. This suggests a reasonably *good* clustering.

Algorithm 11 Pseudocode description of the algorithm for calculating the **silhouette** for internal cluster evaluation.

Require: a dataset \mathcal{D} containing n training instances, $\mathbf{d}_1, \dots, \mathbf{d}_n$

Require: a clustering C of dataset \mathcal{D} into k clusters, C_1, \dots, C_k

Require: a distance measure, $Dist$, to compare distances between instances

- 1: **for** each instance \mathbf{d}_i in \mathcal{D} **do**
 - 2: let $a(i)$ be the average distance between instance \mathbf{d}_i and all of the other instances within the cluster to which \mathbf{d}_i belongs, C_j (*average intra-cluster distance*)
 - 3: calculate the average distance between instance \mathbf{d}_i and the members of each of the other clusters $C \setminus C_j$
 - 4: let $b(i)$ be the lowest average distance between instance \mathbf{d}_i and any other cluster (*average inter-cluster distance*)
 - 5: calculate the silhouette index for \mathbf{d}_i as
- $$s(i) = \frac{b(i) - a(i)}{\max(a(i), b(i))} \quad (10.2)$$
- 6: **end for**
 - 7: calculate final silhouette for the clustering as $s = \frac{1}{n} \sum_{i=1}^n s(i)$
-

The individual silhouette widths for the instances in a dataset can also be used to produce a useful visual tool for inspecting a clustering. A **silhouette plot** shows the silhouette width for each instance in the dataset grouped by the clusters to which they belong. [Figure 10.7](#)^[612] shows the silhouette plot for the clustering of the mobile phone customer dataset. Silhouette plots show a useful overview of a clustering, including the size of each cluster and an indication of how well each instance belongs to its cluster, which can be an easy way to identify outliers in clusterings.

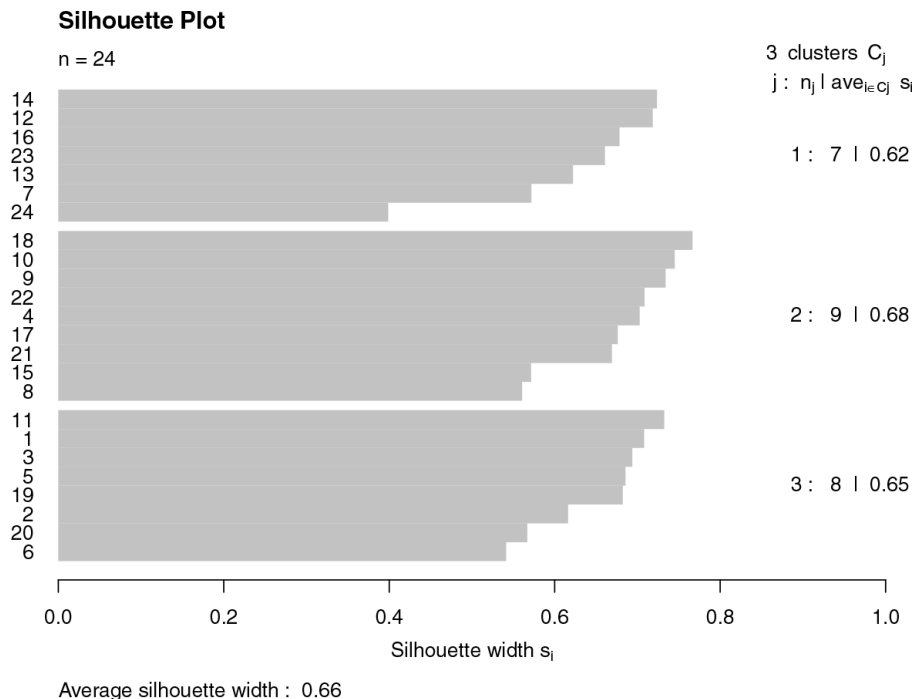


Figure 10.7

The silhouette plot for the final clustering of the mobile phone customer dataset (Table 10.1^[604]) found using the k -means algorithm (with $k = 3$).

Another approach to evaluating clustering is to use external criteria in which some measure from outside the clustering is used as a proxy ground truth. For example, for the sample mobile phone customer data used in this section, the type of tariff that customers had (e.g. *gold*, *silver*, or *bronze*) could be used as a proxy ground truth, and the ability of the clustering to separate the dataset into groups of the same tariff type could be used as a measure of the quality of the clustering. This assumes that we should expect the clustering to find groups with similar tariff types, an assumption that could be based only on detailed knowledge of the domain. The performance measures used for classification problems described in Chapter 9^[533] can be used for this—for example, the **F_1 measure** is commonly used. There are also specific measures that are often used for this, for example **normalized mutual information** (NMI), which is based on information-theoretic ideas including **entropy**, as discussed in Chapter 4^[117]; however, these are outside the scope of this chapter.

One thing about evaluating unsupervised machine learning approaches that is a little easier than the supervised case is that we can do it without the

need to divide a dataset into training, testing, and validation partitions. Although techniques such as ***k*-fold cross validation** can be useful in using external criteria for evaluation, in using internal criteria for evaluation we typically just use all the data both for generating the clustering and evaluating the clustering.

10.4.3 Choosing the Number of Clusters

The *k*-means clustering algorithm, like many other clustering algorithms, requires that the analyst choose the value for *k* as an input to the algorithm. The absence of ground truth, as discussed in the previous section, makes this choice notoriously difficult. Analysts need to balance the needs of their application—for example, in the mobile phone customer scenario, how many customer groups could the organization usefully make decisions about?—with the ability of an algorithm to find meaningful groupings within a given dataset. The former criterion is very domain specific, and so it is not discussed further here. The silhouette described in the previous section, however, can be used effectively to achieve the latter, and this approach to choosing *k* is described in this section.

Regardless of the dataset used, the *k*-means clustering algorithm will always find the number of clusters requested from it regardless of whether these define meaningful structure within the dataset. To determine the best value for *k* we can repeatedly cluster the data for all values of *k* within a given range, calculate a clustering performance measure for each clustering found, and then select the value of *k* that gives the clustering with the highest performance measure. When the silhouette is used in this approach, it is often referred to as the **silhouette method**. [Figure 10.8^{\[613\]}](#) shows each of the clusterings found in the mobile phone customer dataset for values of *k* in [2,9] using *k*-means clustering, and their corresponding silhouettes ([Figure 10.8\(g\)^{\[613\]}](#)). This shows that the clustering with three clusters has the highest silhouette score and could be chosen as the *most appropriate* clustering given the assumptions that underlie the silhouette.

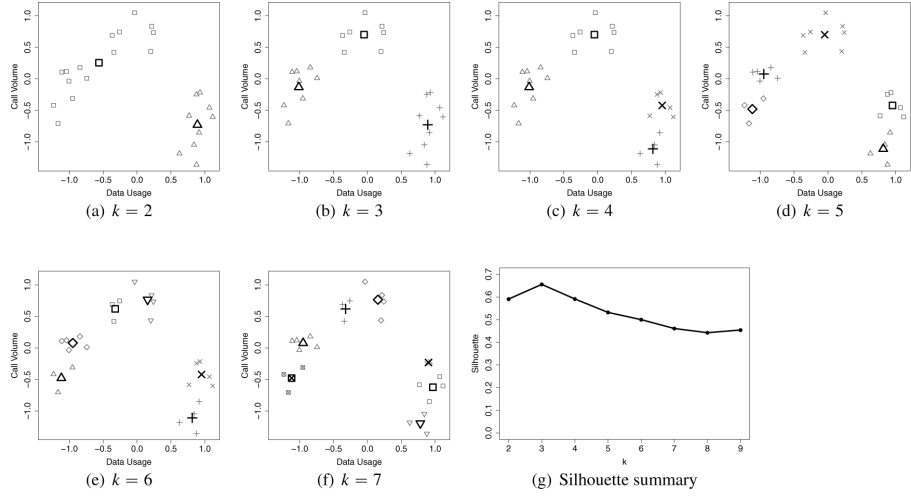


Figure 10.8

(a)–(f) Different clusterings found for the mobile phone customer dataset in Table 10.1^[604] for values of k in {2,9}. (g) shows the silhouette for each clustering.

10.4.4 Understanding Clustering Results

Although internal measures such as the silhouette and external measures calculated against a proxy ground truth are useful in measuring how well a clustering matches an ideal expectation, they do not tell analysts anything about what has been found in the clustering, or whether or not the clustering will be *useful* for a particular task. Unfortunately, automated approaches to answering this question don't really exist, and it falls on analysts to understand what a clustering result tells them about a dataset. The fundamental question that analysts must answer is how do the members of a particular cluster differ from the overall population—*what makes the members of this cluster special?*

Although fully automated approaches to answering this question do not exist, analysts can use an approach based on the data exploration tools presented in Chapter 3^[53] to understand the results of a clustering. The first thing that should always be done is a careful examination of a set of summary statistics describing the members of each cluster. This can be done by preparing a **data quality report**⁶ for each cluster that describes the instances that belong to that cluster. The second useful thing that can be done is to prepare a series of data visualizations that examine the distribution of each feature for the members of each cluster found. This is equivalent to the approach described in Section 3.5.1^[72] for visually examining associations between descriptive features and a target feature, in

which the cluster that instances belong to are used instead of an actual target feature.

A final useful tool is to rank the importance of each descriptive feature in defining membership of each cluster. Some features are particularly important in defining membership of certain clusters but not important for defining membership of others. This can help analysts know where to focus when investigating the data quality reports and visualizations created describing each cluster. This can easily be done by calculating the **information gain**⁷ for each descriptive feature as a predictor of binary flags indicating membership of each cluster and ranking features according to these information gain values.⁸

To illustrate this approach using a simple example, [Table 10.3](#)^[614] shows a data quality report for each cluster found using k -means clustering (with $k = 3$) on the mobile phone customer dataset (see [Table 10.1](#)^[604]). [Figure 10.9](#)^[615] shows the distributions of each feature for the full population and for each cluster so that the differences can be compared. Finally, [Table 10.4](#)^[616] lists the features in the mobile phone customer dataset in order of importance in defining membership of each of the three clusters found.

Table 10.3

Summary statistics for the three clusters found in the mobile phone customer dataset in [Table 10.1](#)^[604] using k -means clustering ($k = 3$). Note, that the % missing and cardinality columns usually used are omitted here for legibility as these data quality issues will not arise in this simple example. They could be included when this approach is used on *real* datasets.

Feature	Cluster	Count	1 st		3 rd		Max	Std. Dev.
			Min.	Qrt.	Mean	Median		
DATA USAGE	C_1	8	-1.2329	-1.1246	-1.0121	-1.0237	-0.9256	-0.7426 0.1639
	C_2	9	0.6259	0.8404	0.8912	0.8785	0.9285	1.1175 0.1471
	C_3	7	-0.3666	-0.3005	-0.0491	-0.0345	0.2087	0.241 0.2732
CALL VOLUME	C_1	8	-0.7060	-0.3377	-0.1310	-0.0109	0.1116	0.1811 0.3147
	C_2	9	-1.3601	-1.0450	-0.7273	-0.6028	-0.4560	-0.2168 0.4072
	C_3	7	0.4215	0.5635	0.7022	0.7360	0.7905	1.0502 0.2204

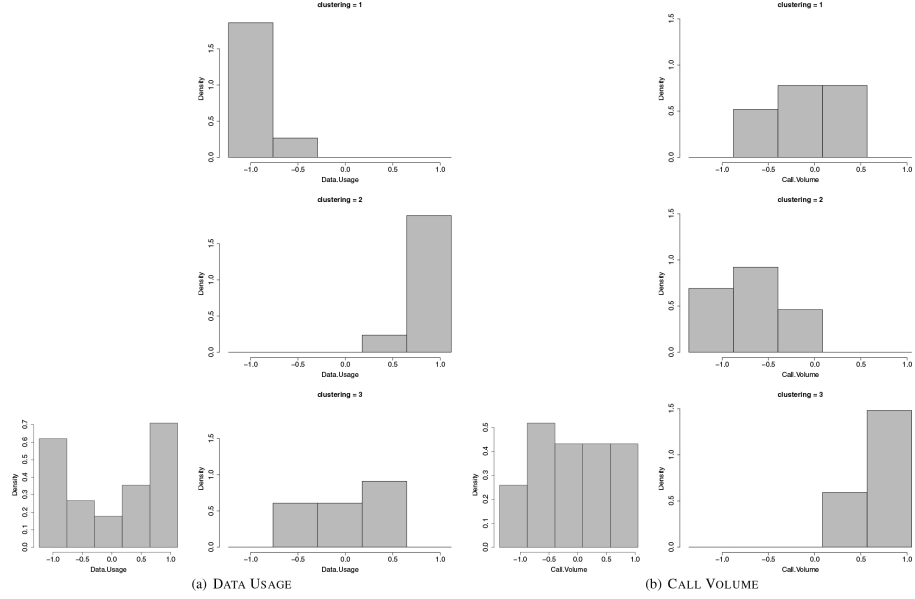


Figure 10.9

(a)–(b) Visualizations of the distributions of the descriptive features in the mobile phone customer dataset in [Table 10.1](#)^[604] across the complete dataset, and divided by the clustering found using k -means clustering ($k = 3$).

Table 10.4

Information gain for each descriptive feature as a predictor of membership of each cluster based on the clustering of the mobile phone customer dataset in [Table 10.1](#)^[604] found using k -means clustering ($k = 3$).

Feature	C_1		C_2		C_3	
	Info.	Gain	Info.	Gain	Info.	Gain
DATA.USAGE	0.9183		DATA.USAGE	0.9544	CALL.VOLUME	0.8709
CALL.VOLUME	0.2117		CALL.VOLUME	0.5488	DATA.USAGE	0.2479

[Table 10.4](#)^[616] shows that membership of clusters \mathcal{C}_1 and \mathcal{C}_2 is most associated with DATA USAGE, whereas membership of \mathcal{C}_3 is most associated with CALL VOLUME. In looking at the summary statistics and visualizations with these priorities in mind, it is clear that the customers in \mathcal{C}_1 are characterized most strongly by their low *Data Usage*, customers in \mathcal{C}_2 by their high *Data Usage*, and customers in \mathcal{C}_3 by their high *Call Volume*. Although this example is small, the same approach can be used effectively for large multivariate datasets, with the only difference being a need to examine summary statistics and visualizations for many more features. The

prioritization given by the information gain values is extremely helpful for dealing with this.

10.4.5 Agglomerative Hierarchical Clustering

The k -means clustering algorithm and other algorithms like it impose an expected global structure onto the clustering process—essentially, the k -means algorithm searches for tightly packed spherical clusters. Sometimes this expected global structure does not match actual patterns within a dataset that we might want to take advantage of. [Figure 10.10](#)^[617] illustrates this using three well-known simple two-dimensional artificial datasets: *blobs*, *circles*, and *half-moons*. In each case there is an *intuitive* clustering that we can observe in the visualizations—for the *blobs* dataset there are three clusters, one for each blob; for the *circles* dataset there are two clusters, one for each ring; and for the *half-moons* dataset there are two clusters, one for each half-moon shape. The clustering returned by the k -means clustering algorithm, however, can accurately find these intuitive clusterings only for the *blobs* dataset. The reason is that the *intuitive* clusters in the other two datasets do not conform to the assumption of spherical clusters that underlies the k -means clustering algorithm. To find these other types of clusterings, it can be more useful to use a clustering algorithm that is driven more by local relationships in a dataset than an expected global structure.

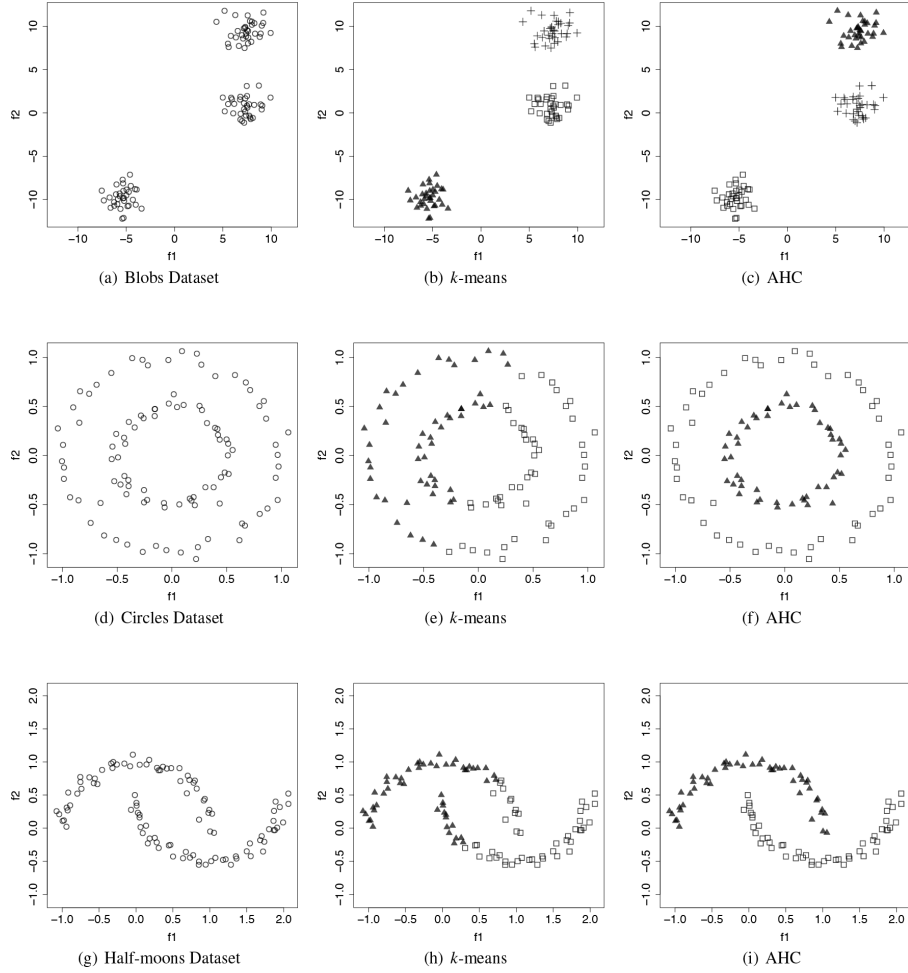


Figure 10.10

(a)–(i) A plot of the *blobs*, *circles*, and *half-moons* datasets and the clusterings achieved by the k -means clustering and agglomerative hierarchical clustering algorithms (where k is set to 3, 2, and 2, respectively).

The **agglomerative hierarchical clustering** (AHC) algorithm is a simple, effective, bottom-up clustering approach that is driven by local structure within a dataset rather than a global expectation of what a cluster structure should be. A pseudocode description of the AHC algorithm is given in Algorithm 9^[601].

Algorithm 12 Pseudocode description of the **agglomerative hierarchical clustering** algorithm.

Require: a dataset \mathcal{D} containing n training instances, $\mathbf{d}_1, \dots, \mathbf{d}_n$

Require: a distance measure, $Dist$, to compare distances between instances

Require: a linkage method, \mathcal{L} , to compare distances between clusters

- 1: initialize the hierarchy level, $h = 1$
- 2: divide \mathcal{D} into a set of n disjoint clusters, $C = \{C_1, \dots, C_n\}$, with one instance in each cluster
- 3: **repeat**
- 4: using distance measure $Dist$ and linkage method \mathcal{L} , find the nearest pair of clusters, C_i and C_j , in the current clustering
- 5: merge C_i and C_j to form a new cluster C_{n+h}
- 6: remove the old clusters from the clustering: $C \leftarrow C \setminus \{C_i, C_j\}$
- 7: add the new cluster to the clustering: $C \leftarrow C \cup C_{n+h}$
- 8: $h \leftarrow h + 1$
- 9: **until** all the instances join into a single cluster

The AHC algorithm begins by considering each instance in a dataset to be the only member of a cluster, which gives n initial clusters, \mathcal{C}_1 to \mathcal{C}_n . The two clusters that are nearest are then merged (or *agglomerated*) to form a new cluster. This process repeats over and over until a single cluster containing all instances in the dataset is formed. [Figure 10.10](#)^[617] shows how AHC can be used for find the intuitive clusterings in the half-moons and circles datasets as well as the blobs dataset.

This AHC algorithm requires two decisions to be made in order for it to be complete. The first is the distance measure, $Dist$, to be used to compare instances and clusters. Any of the distance measures discussed in this book (as well as many others not discussed in this book) can be used for this. The second is the **linkage method**, \mathcal{L} , that will be used to allow distances between whole clusters rather than just single instances to be compared. The challenge is if two clusters, each containing multiple instances, have been found, how should the distance between them be calculated? Should it be based on the distance between the centroids of two clusters, or the distance between the two closest instances in two clusters, or the average distance between all instances in two clusters, or some other method?

Several different linkage methods for AHC exist in the literature; some of the most common are

- **single linkage:** the distance between the most similar instances in two clusters is used as the overall distance between the clusters;
- **complete linkage:** the distance between the most dissimilar instances in two clusters is used as the overall distance between the clusters;
- **average linkage:** the average of the distances between all pairs of instances in two clusters is used as the overall distance between the clusters; and
- **centroid linkage:** the distance between the centroids of two clusters is used as the overall distance between the clusters.

[Figure 10.11^{\[619\]}](#) illustrates these options. In the AHC examples shown in [Figure 10.10^{\[617\]}](#), Euclidean distance and single linkage are used. The choice of linkage method can lead to quite different results when AHC is used. For example, using centroid linkage leads to results very similar to a k -means clustering approach, whereas using single linkage leads to results much more heavily reliant on local distances within a dataset.

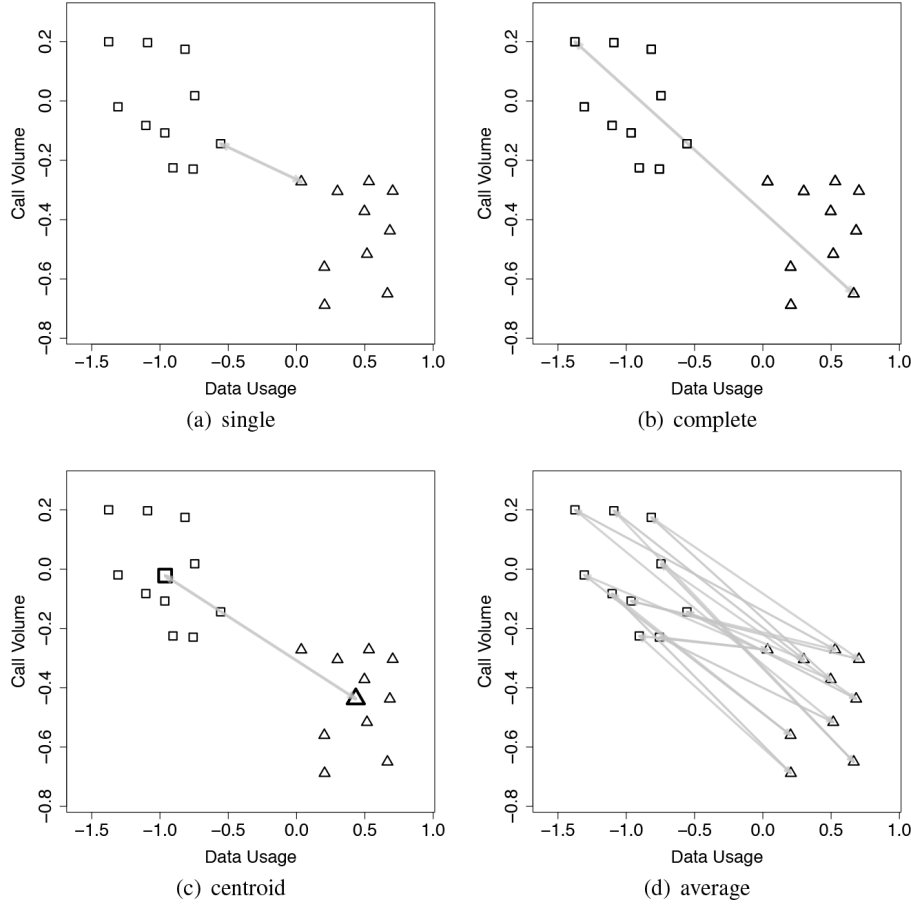


Figure 10.11

(a)–(d) Different linkage methods that can be used to compare the distances between clusters in agglomerative hierarchical clustering. (Arrows for only some indicative distances are shown in the average linkage diagram (d).)

We can illustrate how the AHC algorithm works using a reduced version of the mobile phone customer dataset from [Table 10.1](#)^[604]. This dataset contains just nine instances (the instance labels have been kept consistent so that this example can be compared with previous ones) and is shown in [Figure 10.12\(a\)](#)^[621]. AHC begins by considering each instance in the dataset as a simple cluster containing just one instance. The distance between each of these single-instance clusters is then calculated (in this example Euclidean distance is used). [Table 10.5\(a\)](#)^[620] shows these distances and is referred to as a **distance matrix**.⁹ The pair of instances in the dataset that are closest together are then selected and combined into a cluster. In this example d_{15} and d_8 are separated by a distance of just 0.06 and are

combined together into the cluster \mathcal{C}_{10} . This is illustrated in Figure 10.12(b) [621].

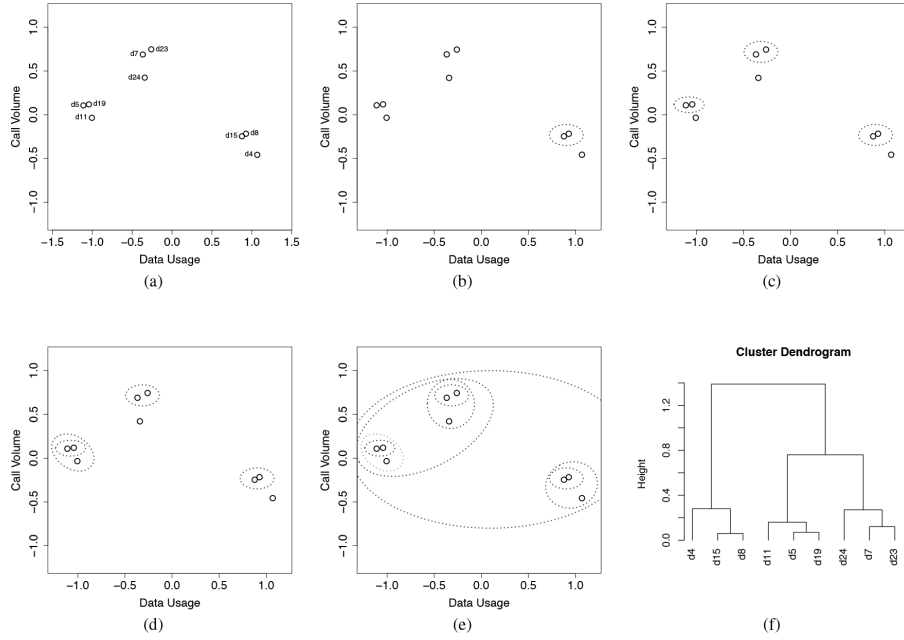


Figure 10.12

(a) A plot of a reduced version of the mobile phone customer dataset given in Table 10.1^[604]. (b) At the first iteration of the AHC algorithm the first pair of instances is combined into a cluster, \mathcal{C}_{10} . (c) After three iterations of the AHC algorithm, three pairs of instances have been combined into clusters, \mathcal{C}_{10} , \mathcal{C}_{11} , and \mathcal{C}_{12} . (d) At the fourth iteration of AHC, the first hierarchical cluster combination is created when a single instance, d_{11} is combined with the cluster \mathcal{C}_{10} to create a new cluster, \mathcal{C}_{13} .

Table 10.5

Distance matrices that detail the first three iterations of the AHC algorithm applied to the reduced version of the mobile phone customer dataset in [Table 10.1](#)^[604].

(a) A distance matrix for the instances in the dataset.

	d_4	d_{15}	d_8	d_{11}	d_5	d_{19}	d_{24}	d_7	d_{23}
d_4	0.00								
d_{15}	0.28	0.00							
d_8	0.28	0.06	0.00						
d_{11}	2.12	1.89	1.94	0.00					
d_5	2.25	2.02	2.06	0.18	0.00				
d_{19}	2.19	1.95	2.00	0.16	0.07	0.00			
d_{24}	1.66	1.39	1.42	0.81	0.83	0.76	0.00		
d_7	1.84	1.56	1.58	0.96	0.94	0.89	0.27	0.00	
d_{23}	1.79	1.51	1.53	1.08	1.06	1.00	0.33	0.12	0.00

(b) The distance matrix after one iteration of AHC.

	d_4	C_{10}	d_{11}	d_5	d_{19}	d_{24}	d_7	d_{23}	
d_4	0.00								
C_{10}	0.28	0.00							
d_{11}	2.12		1.89	0.00					
d_5	2.25		2.02	0.18	0.00				
d_{19}	2.19		1.95	0.16	0.07	0.00			
d_{24}	1.66		1.39	0.81	0.83	0.76	0.00		
d_7	1.84		1.56	0.96	0.94	0.89	0.27	0.00	
d_{23}	1.79		1.51	1.08	1.06	1.00	0.33	0.12	0.00

(c) The distance matrix after two iterations of AHC.

	d_4	C_{10}	d_{11}	C_{11}	d_{24}	C_{12}	
d_4	0.00						
C_{10}	0.28	0.00					
d_{11}	2.12		1.89	0.00			
C_{11}	2.19		1.95	0.16	0.00		
d_{24}	1.66		1.39	0.81	0.76	0.00	
C_{12}	1.79		1.51	0.97	0.89	0.27	0.00

(d) The distance matrix after three iterations of AHC.

	d_4	C_{13}	C_{11}	d_{24}	C_{12}	
d_4	0.00					
C_{13}	0.28	0.00				
C_{11}	2.19		0.16	0.00		
d_{24}	1.66		0.81	0.76	0.00	
C_{12}	1.79		0.97	0.89	0.27	0.00

In the next iteration of the AHC algorithm the distance between this new cluster and all other clusters is calculated. In this example single linkage is used and so the distance between two clusters is calculated as the minimum distance between their member instances. [Table 10.5\(b\)](#)^[620] shows an updated distance matrix including \mathcal{C}_{10} . Over the next two iterations, two more pairs of instances from the original dataset are combined into clusters: d_5 and d_{19} into \mathcal{C}_{11} , and d_7 and d_{23} into \mathcal{C}_{12} . This is illustrated in [Figure 10.12\(c\)](#)^[621], and [Table 10.5\(b\)](#)^[620] shows an updated distance matrix including these new clusters.

The next iteration of the algorithm is interesting because the smallest distance found in the distance matrix is a distance of 0.16 between cluster \mathcal{C}_{10} and instance d_{11} . These are merged into a new cluster, \mathcal{C}_{13} , as shown in [Figure 10.12\(d\)](#)^[621]. This is the clearest indication so far of the hierarchical nature of AHC, as a cluster created at a previous iteration of the algorithm

will be merged into a larger cluster. [Table 10.5\(d\)](#)^[620] shows the distance matrix after this new cluster has been created. The algorithm then continues merging clusters until only a single cluster containing all instances remains. This process is illustrated in [Figure 10.12\(e\)](#)^[621]. It is also possible to directly illustrate the hierarchical nature of AHC using a **dendrogram**. In a dendrogram each instance in a dataset is represented by its ID label at the bottom of the figure,¹⁰ and the horizontal linkages indicate where clusters have been created. The vertical gaps between cluster linkages indicate the distance between the two clusters that have been merged. For example, at the bottom of the hierarchy the vertical gaps between clusterings are very small because the clusters are very close, and as we move farther up the hierarchy, the gaps get larger as clusters that are farther apart are merged.

One advantage of AHC is that the number of clusters to be found, k , is not a required input for the algorithm. Rather, the algorithm finds a hierarchical agglomeration (or grouping) of the instances in a dataset that can then be used to cluster the instances into any number of groups. To illustrate this, [Figure 10.13\(a\)](#)^[623] returns to the full mobile phone customer dataset from [Table 10.1](#)^[604] and shows the dendrogram capturing the result of running the AHC algorithm on this dataset. Once this hierarchical tree structure has been found, it can be **cut** to any level to give a clustering with that many clusters. [Figure 10.13\(b\)](#)^[623] shows the tree cut for three clusters and the resultant clustering, and [Figure 10.13\(c\)](#)^[623] shows the same illustrations for six clusters. The techniques described in Section 10.4.2^[607] for evaluating clusterings can be used here to set the best value for k .

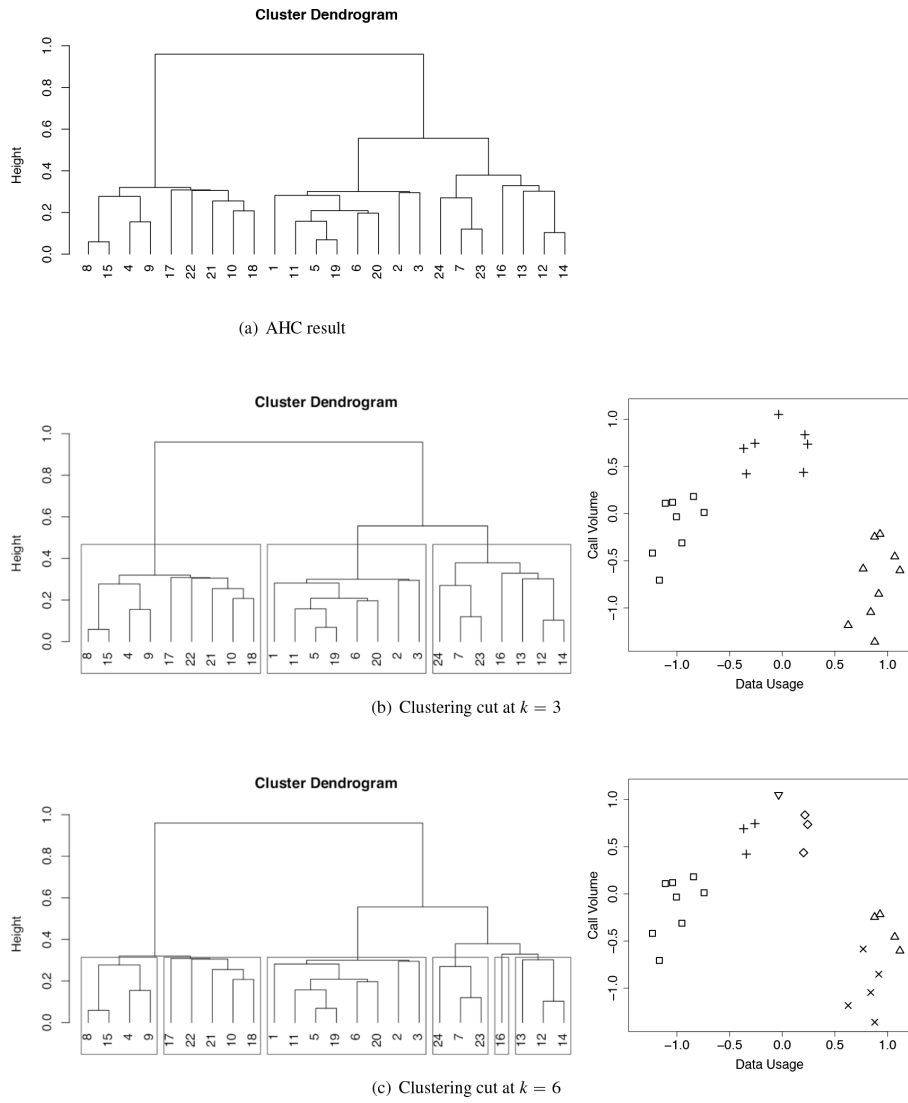


Figure 10.13

(a) A plot of the hierarchical grouping of the instances in the mobile phone customer dataset from Table 10.1^[604] found by the AHC algorithm (using Euclidean distance and single linkage). (b) The clustering returned when the tree is cut at $k = 3$. (c) The clustering returned when the tree is cut at $k = 6$.

Another advantage of AHC is that it is deterministic, and doesn't suffer from the impact of different seeds as k -means or k -means++ does. This means that it will give exactly the same result every time it is run on the same dataset and that the issues around finding seeds discussed in Section 10.4.1^[605] do not arise. These two advantages are present in most hierarchical clustering algorithms.

10.4.6 Representation Learning with Auto-Encoders

The second use case we described for unsupervised learning in Section 10.2^[598] was **representation learning**. Representation learning essentially tries to automatically extract new descriptive features from a dataset. This can be an attractive alternative to the manual work of designing features that we described in Chapter 2^[23]. In this use case, unsupervised machine learning is used as one part of a larger machine learning pipeline. Usually the outputs from the unsupervised work are consumed in a supervised machine learning task, or another unsupervised machine learning task. **Neural network** models are particularly useful for representation learning, and this is a large part of the promise of **deep learning**, as discussed in Chapter 8^[381]. In this section we look at how **auto-encoder** models, a particular type of neural network, can be used to learn a new feature representation that can be a useful step as part of a larger machine learning process.

An **auto-encoder** model is a special type of *feedforward neural network* that is trained to reproduce its inputs at its output layer. This may seem like a trivial task—it is essentially an **identity function**—but it is made more interesting by a network architecture that transforms the data through a series of narrower and narrower layers. This has the impact of first greatly reducing the dimensionality of the input data, before reproducing the inputs from this lower-dimensional representation. [Figure 10.14](#)^[625] shows the architecture of a typical auto-encoder network. The first half of an auto-encoder, up to the output of the narrowest layer in the middle, is known as an **encoder**, and the second half of the network is known as a **decoder**. The narrow middle layer is often referred to as a **bottleneck layer**.

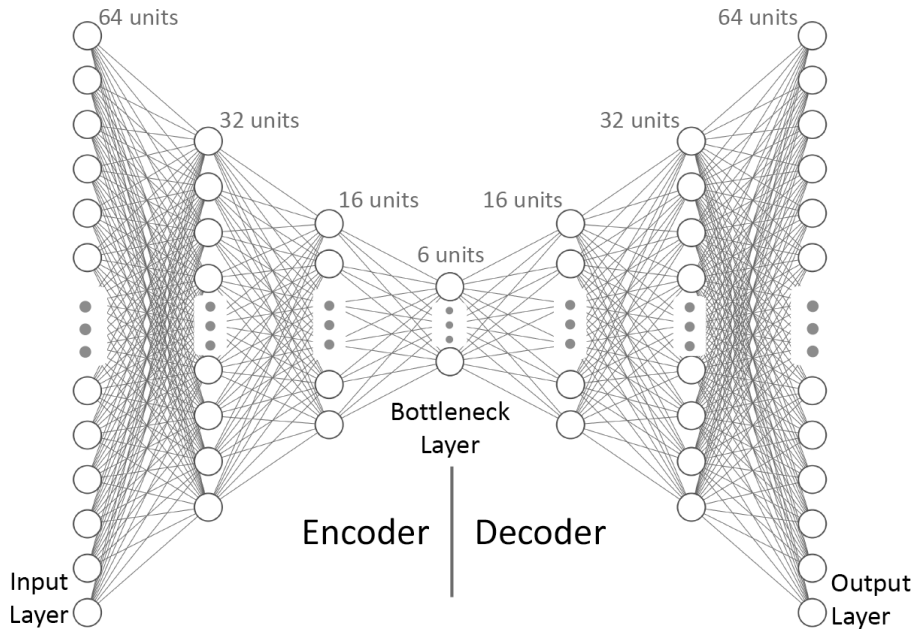


Figure 10.14

The architecture of an auto-encoder network made up of an encoder and a decoder connected by a bottleneck layer.

For an auto-encoder network to be able to reproduce the feature values for a query instance that are presented at its input layer at its output layer, the low-dimensional representation at the middle bottleneck layer needs to capture almost all the useful information contained in the original input features. This is what makes auto-encoders useful for representation learning. The outputs of the bottleneck layer in the network can be used as a new representation of the original input features. This type of representation is often referred to as an **embedding** because the original features have been embedded into a new lower-dimensional space.

An auto-encoder model can be trained like any other feedforward neural network using the **backpropagation of error algorithm**.¹¹ The only difference is that rather than having a separate target feature vector against which **loss** is measured, the loss functions used to train these measure the ability of the network to reproduce the inputs for particular instances at its output layer. For this type of network, it is common to use **rectified linear** activation functions in the units in all layers except for the final output layer, at which either **sigmoid** or **linear** activation functions are usually used.¹² Loss in auto-encoder networks is typically measured using **mean**

squared error loss,¹³ rather than the loss functions more commonly used for classification problems.

To illustrate the use of an auto-encoder network for feature generation, we use a dataset of simple handwritten digits.¹⁴ This dataset contains a library of 1,797 small (8 pixels by 8 pixels) grayscale images of handwritten digits (0–9). Figure 10.15(a)^[626] shows a selection of these digits. Grayscale images are stored as a matrix of pixel values in the range [0,1] where 0 represents a black pixel and 1 represents a white one. The pixels from an 8-by-8 pixel image can be flattened into a single vector of 64 values to give an **ABT** in which each descriptive feature for an instance (an image) represents the grayscale value for a particular pixel in that image. This gives a large set of low-information descriptive features.

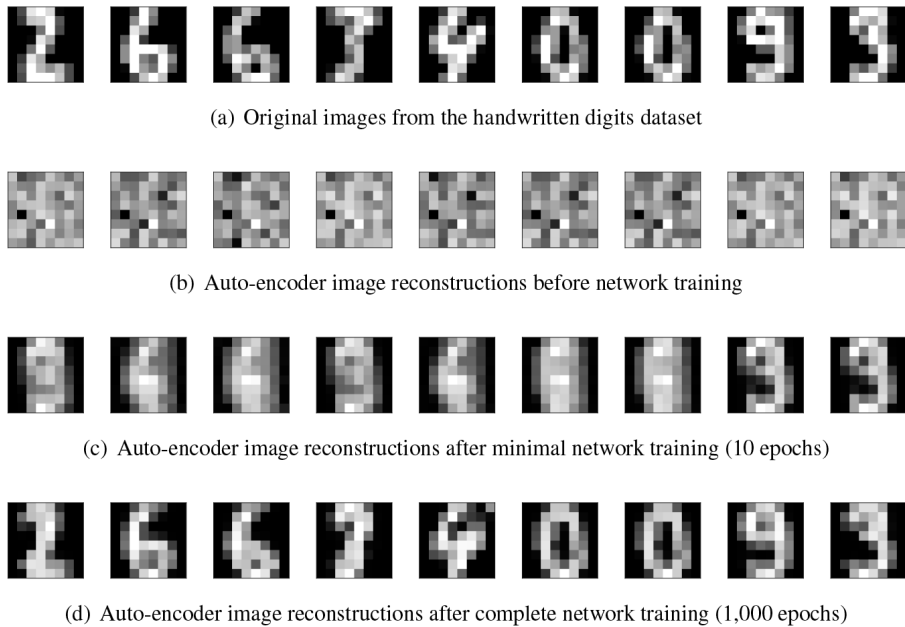


Figure 10.15

(a) A selection of images from the handwritten digits dataset; (b) image reconstructions generated by the auto-encoder network before training; (c) image reconstructions generated by the auto-encoder network after minimal training (10 epochs); and (d) image reconstructions generated by the auto-encoder network after complete training (1,000 epochs).

An auto-encoder can be trained to learn a more compact representation of these images. The architecture of the auto-encoder used in this example is shown in Figure 10.14^[625]. The units in all hidden layers use a **rectified linear** activation function. The units in the output layer use a **sigmoid** activation function. The bottleneck layer contains six units, and this is the

dimensionality of the new representation, or **embedding**, generated. The network is trained for 1,000 epochs using mini-batch gradient descent with a batch size of 32.¹⁵

Figure 10.15(b)^[626] shows examples of the reconstructions generated by the auto-encoder network before it has been trained for the digits shown in Figure 10.15(a)^[626]. The initial weights in the auto-encoder are randomly initialized, and therefore it should not be a surprise that these reconstructions bear no resemblance to the original images and are basically noise. Figure 10.15(c)^[626] shows reconstructions of the same images after just five epochs of network training. At this stage, these reconstructed images are already beginning to resemble the originals on which they are based. Figure 10.15(d)^[626] shows the final reconstructions generated by the network after 1,000 epochs of network training. Although there is some blurring around the edges, these look remarkably similar to the original images.

Figure 10.16^[627] shows a more detailed view of the reconstructions of the first example from Figure 10.15(a)^[626], an image of the digit 2. Reconstructed images and the underlying pixel values from before, during, and after training are shown, as well as the corresponding reconstruction errors. It is clear from both the quality of the image shown and the reconstruction errors that the quality of the reconstruction improves as training progresses.

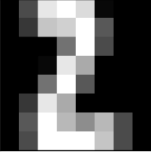
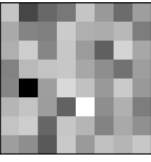
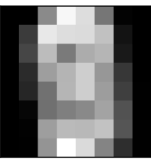
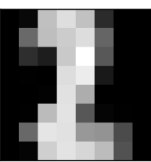
Training	Image	Pixel Values	Error
Original		$\begin{bmatrix} 0.00 & 0.19 & 0.94 & 1.00 & 0.88 & 0.06 & 0.00 & 0.00 \\ 0.00 & 0.12 & 0.75 & 0.81 & 1.00 & 0.25 & 0.00 & 0.00 \\ 0.00 & 0.00 & 0.00 & 0.38 & 1.00 & 0.19 & 0.00 & 0.00 \\ 0.00 & 0.00 & 0.06 & 0.94 & 0.62 & 0.00 & 0.00 & 0.00 \\ 0.00 & 0.00 & 0.38 & 1.00 & 0.25 & 0.00 & 0.00 & 0.00 \\ 0.00 & 0.12 & 0.94 & 0.62 & 0.00 & 0.00 & 0.00 & 0.00 \\ 0.00 & 0.25 & 1.00 & 0.69 & 0.50 & 0.69 & 0.19 & 0.00 \\ 0.00 & 0.19 & 1.00 & 1.00 & 0.75 & 0.19 & 0.00 & 0.00 \end{bmatrix}$	
0 Epochs		$\begin{bmatrix} 0.51 & 0.48 & 0.49 & 0.49 & 0.51 & 0.50 & 0.49 & 0.50 \\ 0.51 & 0.50 & 0.49 & 0.52 & 0.51 & 0.51 & 0.51 & 0.49 \\ 0.51 & 0.52 & 0.50 & 0.51 & 0.50 & 0.49 & 0.52 & 0.50 \\ 0.50 & 0.51 & 0.51 & 0.51 & 0.50 & 0.50 & 0.49 & 0.50 \\ 0.50 & 0.47 & 0.50 & 0.52 & 0.51 & 0.50 & 0.52 & 0.50 \\ 0.51 & 0.51 & 0.50 & 0.49 & 0.53 & 0.50 & 0.51 & 0.49 \\ 0.51 & 0.52 & 0.49 & 0.51 & 0.51 & 0.50 & 0.51 & 0.50 \\ 0.50 & 0.50 & 0.48 & 0.51 & 0.50 & 0.51 & 0.51 & 0.51 \end{bmatrix}$	0.1876
10 Epochs		$\begin{bmatrix} 0.00 & 0.00 & 0.42 & 0.83 & 0.76 & 0.33 & 0.03 & 0.00 \\ 0.01 & 0.12 & 0.80 & 0.76 & 0.74 & 0.62 & 0.06 & 0.00 \\ 0.00 & 0.15 & 0.60 & 0.35 & 0.54 & 0.58 & 0.07 & 0.00 \\ 0.00 & 0.09 & 0.49 & 0.57 & 0.68 & 0.46 & 0.11 & 0.00 \\ 0.00 & 0.08 & 0.31 & 0.57 & 0.68 & 0.48 & 0.13 & 0.01 \\ 0.00 & 0.05 & 0.31 & 0.37 & 0.41 & 0.51 & 0.19 & 0.00 \\ 0.00 & 0.02 & 0.49 & 0.59 & 0.59 & 0.63 & 0.21 & 0.01 \\ 0.00 & 0.01 & 0.45 & 0.85 & 0.74 & 0.39 & 0.09 & 0.01 \end{bmatrix}$	0.0685
1,000 Epochs		$\begin{bmatrix} 0.00 & 0.06 & 0.71 & 0.87 & 0.71 & 0.10 & 0.00 & 0.00 \\ 0.00 & 0.32 & 0.70 & 0.77 & 0.86 & 0.30 & 0.00 & 0.00 \\ 0.00 & 0.11 & 0.09 & 0.75 & 0.97 & 0.24 & 0.00 & 0.00 \\ 0.00 & 0.00 & 0.00 & 0.86 & 0.93 & 0.08 & 0.00 & 0.00 \\ 0.00 & 0.00 & 0.02 & 0.88 & 0.62 & 0.00 & 0.00 & 0.00 \\ 0.00 & 0.01 & 0.68 & 0.89 & 0.24 & 0.04 & 0.01 & 0.00 \\ 0.00 & 0.32 & 0.91 & 0.89 & 0.53 & 0.51 & 0.19 & 0.00 \\ 0.00 & 0.03 & 0.78 & 0.89 & 0.83 & 0.69 & 0.21 & 0.00 \end{bmatrix}$	0.0179

Figure 10.16

An image of the digit 2 and reconstructions of this image by the auto-encoder after various amounts of network training. The pixel values of the reconstructed images are shown alongside the images, as is the reconstruction error calculated by comparing these to the pixel values of the original image.

After it has been trained to accurately encode its inputs into a low-dimensional space and then decode them back into the original feature space, an auto-encoder can be used for feature generation by focusing on the output of the first encoder part of the network. The outputs of the final layer in the encoder, the **bottleneck layer**, can be used as a new transformed representation of the original dataset. A full dataset can be passed through the encoder network, and the outputs of the bottleneck layer can be saved as new generated features. These new generated features can then replace the original descriptive features in an ABT for later tasks in a pipeline, for example, training a supervised machine learning model. This process is illustrated in [Figure 10.17](#)^[628].

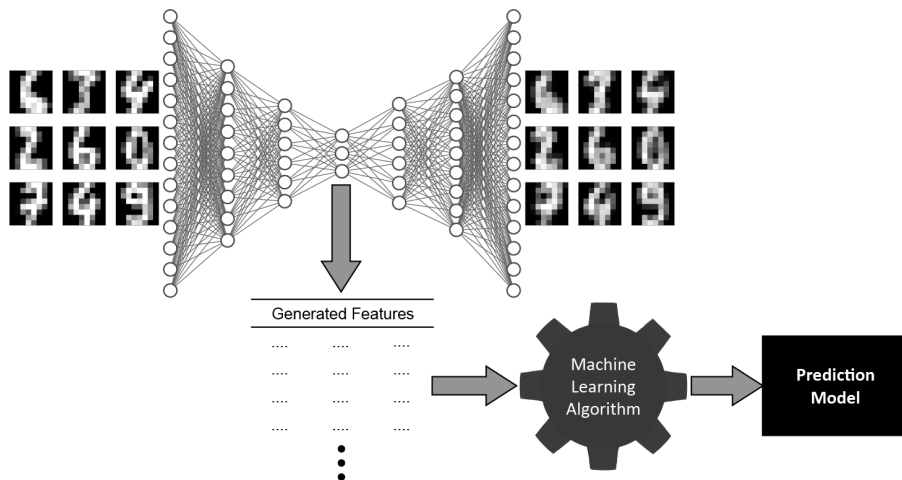


Figure 10.17

The process of using an unsupervised auto-encoder network to generate a feature representation used to train a supervised model.

10.5 Summary

This chapter moved away from the supervised machine learning techniques for training predictive models discussed in the rest of the book to focus on **unsupervised machine learning**. Unsupervised machine learning techniques are used in the absence of a target feature and model the underlying structure within the descriptive features in a dataset. We can think of the output of most unsupervised machine learning models as new generated features that can be appended to the original dataset to **augment** or **enrich** it. There are two key main use cases for unsupervised learning: clustering and representation learning.

In **clustering**, unsupervised algorithms are used to partition the instances in a dataset into coherent groups. The assignment of each instance in a dataset to one of these groups is the output of the clustering process, and a generated feature capturing these assignments can be appended to the original dataset. Two clustering techniques were presented in detail: ***k*-means clustering** and **agglomerative hierarchical clustering** (AHC). These are well-known, reasonably effective approaches to clustering. AHC has an advantage over *k*-means that it does not require *k* to be set before the algorithm starts. AHC is, however, much more computationally expensive than *k*-means, which can be a barrier to using it on very large datasets.

The other unsupervised machine learning use case covered in this chapter was **representation learning**. Here unsupervised machine learning

techniques are used to learn new sets of generated features to represent instance in a dataset. **Neural network** models are especially effective in this use case, and the chapter presented an example of using an **auto-encoder** to learn a feature representation that could be used by a supervised machine learning model. Using unsupervised learning to generate feature representations that could be used in later supervised models (e.g., Hinton et al. (2006) and Hinton (2005)) was the starting point for the wave of renewed interest in neural network models that began in the early 2000s and became known as **deep learning**.

Applications of unsupervised learning are widespread, including customer segmentations (Berry and Linoff, 2004), anomaly detection (Chandola et al., 2009), and analyzing people's movement patterns (Li et al., 2015). Designing solutions based on unsupervised machine learning techniques can be more creative than designing solutions based on supervised learning because the solutions tend not to follow quite so obvious a pattern. Finally, unsupervised learning is a fascinating research area, and it is probably fair to say that it has many more significant open research challenges than supervised learning.

10.6 Further Reading

For more detail on unsupervised machine learning algorithms (Friedman et al., 2001) has a fairly comprehensive unsupervised learning section that gives a broader sweep of approaches than those covered in this chapter. As discussed in the introduction, the goal of this chapter is to give a flavor of the most important unsupervised machine learning techniques, and there are many more clustering algorithms not covered here. For example, *k*-means is a special case of the **Gaussian mixture model** (Murphy, 2012) approach to clustering (assuming spherical distributions), which in turn has been extended into **model-based clustering** (Scrucca et al., 2016) algorithms, all of which can be very effective. The **expectation maximization algorithm** sits behind all of these and more than warrants careful study (Moon, 1996). **Spectral clustering** (Ng et al., 2002) is another approach worth investigating, and for very large spatial datasets, the **DBScan** (Ester et al., 1996) can be a good approach.

Berry and Linoff (2004) provide a good specialized treatment of clustering algorithms for customer segmentation applications. Han et al.

(2011) is also very good on describing unsupervised machine learning techniques with customer applications in mind.

The auto-encoders presented in this chapter are fairly simple, and more sophisticated approaches have emerged, for example, **convolutional auto-encoders**, **de-noising auto-encoders**, and **variational auto-encoders**. Guo et al. (2016) provide a readable, coherent overview of these different types.

10.7 Exercises

1. The following table shows a small dataset in which each instance describes measurements taken using three sensors when a valve in an oil well was opened. The three descriptive features, PRESSURE, TEMPERATURE, and VOLUME measure characteristics of the oil flowing through the valve when it was opened. The **k -means clustering** approach is to be applied to this dataset with $k = 3$ and using **Euclidean distance**. The initial cluster centroids for the three clusters \mathcal{C}_1 , \mathcal{C}_2 , and \mathcal{C}_3 are $\mathbf{c}_1 = \langle -0.929, -1.040, -0.831 \rangle$, $\mathbf{c}_2 = \langle -0.329, -1.099, 0.377 \rangle$, and $\mathbf{c}_3 = \langle -0.672, -0.505, 0.110 \rangle$. The following table also shows the distance to these three cluster centers for each instance in the dataset.

ID	PRESSURE	TEMPERATURE	VOLUME	Cluster Distances Iter. 1		
				$Dist(\mathbf{d}_i, \mathbf{c}_1)$	$Dist(\mathbf{d}_i, \mathbf{c}_2)$	$Dist(\mathbf{d}_i, \mathbf{c}_3)$
1	-0.392	-1.258	-0.666	0.603	1.057	1.117
2	-0.251	-1.781	-1.495	1.204	1.994	2.093
3	-0.823	-0.042	1.254	2.314	1.460	1.243
4	0.917	-0.961	0.055	2.049	1.294	1.654
5	-0.736	-1.694	-0.686	0.697	1.284	1.432
6	1.204	-0.605	0.351	2.477	1.611	1.894
7	0.778	-0.436	-0.220	1.911	1.422	1.489
8	1.075	-1.199	-0.141	2.125	1.500	1.896
9	-0.854	-0.654	0.771	1.650	0.793	0.702
10	-1.027	-0.269	0.893	1.891	1.201	0.892
11	-0.288	-2.116	-1.165	1.296	1.848	2.090
12	-0.597	-1.577	-0.618	0.666	1.136	1.298
13	-1.113	-0.271	0.930	1.930	1.267	0.960
14	-0.849	-0.430	0.612	1.569	0.879	0.538
15	1.280	-1.188	0.053	2.384	1.644	2.069

- (a) Assign each instance to its nearest cluster to generate the clustering at the first iteration of k -means on the basis of the initial cluster

centroids.

- (b) On the basis of the clustering calculated in Part (a), calculate a set of new cluster centroids.

2. The following table shows details of two different clusterings of the dataset from Question 1—one with $k = 2$ and one with $k = 3$ —and partial workings to calculate the silhouette for the clusterings.

$k = 2$ clustering						$k = 3$ clustering					
Nearest						Nearest					
ID	Cluster	Cluster	$a(i)$	$b(i)$	$s(i)$	ID	Cluster	Cluster	$a(i)$	$b(i)$	$s(i)$
d₁	<i>C</i> ₁	<i>C</i> ₂	??	1.898	??	d₁	<i>C</i> ₁	<i>C</i> ₂	0.732	1.681	0.565
d₂	<i>C</i> ₁	<i>C</i> ₂	1.608	2.879	0.442	d₂	<i>C</i> ₁	??	??	??	??
d₃	<i>C</i> ₂	<i>C</i> ₁	0.624	2.594	0.76	d₃	<i>C</i> ₃	<i>C</i> ₂	0.624	2.422	0.742
d₄	<i>C</i> ₁	<i>C</i> ₂	1.261	2.142	0.411	d₄	<i>C</i> ₂	<i>C</i> ₁	0.482	1.884	??
d₅	<i>C</i> ₁	<i>C</i> ₂	1.452	2.098	0.308	d₅	<i>C</i> ₁	<i>C</i> ₃	0.619	2.098	0.705
d₆	<i>C</i> ₁	??	??	??	??	d₆	<i>C</i> ₂	<i>C</i> ₃	0.68	2.24	0.697
d₇	<i>C</i> ₁	<i>C</i> ₂	1.42	2.061	0.311	d₇	<i>C</i> ₂	<i>C</i> ₁	0.777	1.935	0.598
d₈	<i>C</i> ₁	<i>C</i> ₂	1.272	2.432	??	d₈	<i>C</i> ₂	<i>C</i> ₁	0.558	1.842	0.697
d₉	<i>C</i> ₂	<i>C</i> ₁	0.496	2.067	0.76	d₉	<i>C</i> ₃	<i>C</i> ₁	0.496	2.04	0.757
d₁₀	<i>C</i> ₂	<i>C</i> ₁	0.344	2.375	??	d₁₀	<i>C</i> ₃	??	0.344	??	??
d₁₁	<i>C</i> ₁	<i>C</i> ₂	1.565	2.802	0.441	d₁₁	<i>C</i> ₁	<i>C</i> ₂	0.769	2.201	0.651
d₁₂	<i>C</i> ₁	<i>C</i> ₂	1.338	??	??	d₁₂	<i>C</i> ₁	<i>C</i> ₂	0.592	1.935	0.694
d₁₃	<i>C</i> ₂	<i>C</i> ₁	0.379	2.444	0.845	d₁₃	<i>C</i> ₃	<i>C</i> ₁	0.379	2.436	0.844
d₁₄	<i>C</i> ₂	<i>C</i> ₁	??	2.056	??	d₁₄	<i>C</i> ₃	<i>C</i> ₁	0.459	2.038	??
d₁₅	<i>C</i> ₁	<i>C</i> ₂	1.425	2.53	0.437	d₁₅	<i>C</i> ₂	<i>C</i> ₁	0.579	2.101	0.725

- (a) A number of values are missing from these workings (indicated by ??). Calculate the missing values. The distances between each instance in the dataset from Question 1 (using **Euclidean distance**) are shown in the following distance matrix, and will be useful for this exercise.

	d_1	d_2	d_3	d_4	d_5	d_6	d_7	d_8	d_9	d_{10}	d_{11}	d_{12}	d_{13}	d_{14}	d_{15}
d_1	0.00														
d_2	0.99	0.00													
d_3	2.31	3.30	0.00												
d_4	1.52	2.11	2.30	0.00											
d_5	0.56	0.95	2.55	1.95	0.00										
d_6	2.00	2.63	2.29	0.55	2.46	0.00									
d_7	1.50	2.12	2.21	0.61	2.02	0.73	0.00								
d_8	1.56	1.98	2.62	0.35	1.96	0.78	0.82	0.00							
d_9	1.63	2.60	0.78	1.94	1.79	2.10	1.92	2.20	0.00						
d_{10}	1.95	2.93	0.47	2.23	2.15	2.32	2.13	2.52	0.44	0.00					
d_{11}	1.00	0.47	3.23	2.07	0.78	2.61	2.20	1.94	2.49	2.86	0.00				
d_{12}	0.38	0.96	2.43	1.77	0.19	2.26	1.83	1.78	1.69	2.04	0.83	0.00			
d_{13}	2.01	2.98	0.49	2.32	2.19	2.41	2.22	2.61	0.49	0.09	2.91	2.09	0.00		
d_{14}	1.59	2.57	0.75	1.93	1.81	2.08	1.83	2.21	0.28	0.37	2.51	1.70	0.44	0.00	
d_{15}	1.82	2.26	2.68	0.43	2.21	0.66	0.94	0.28	2.31	2.62	2.19	2.03	2.71	2.33	0.00

- (b) On the basis of the completed table, calculate the silhouette for each clustering.
- (c) On the basis of the silhouette, would you choose 2 or 3 for the value of k for this dataset?
3. A city tax service has performed a clustering of individual taxpayers using k -means clustering in order to better understand groups that might exist within their taxpayer base. The clustering has divided the taxpayers into three clusters. Four descriptive features have been used to describe each taxpayer:
- AGE: The age of the taxpayer.
 - YEARSINCURRENTEMPLOYMENT: The number of years that the taxpayer has been in their current job.
 - TOTALINCOME: The taxpayer's total income for the current tax year.
 - EFFECTIVETAXRATE: The effective tax rate paid by the taxpayer (this is simply tax paid divided by total income).

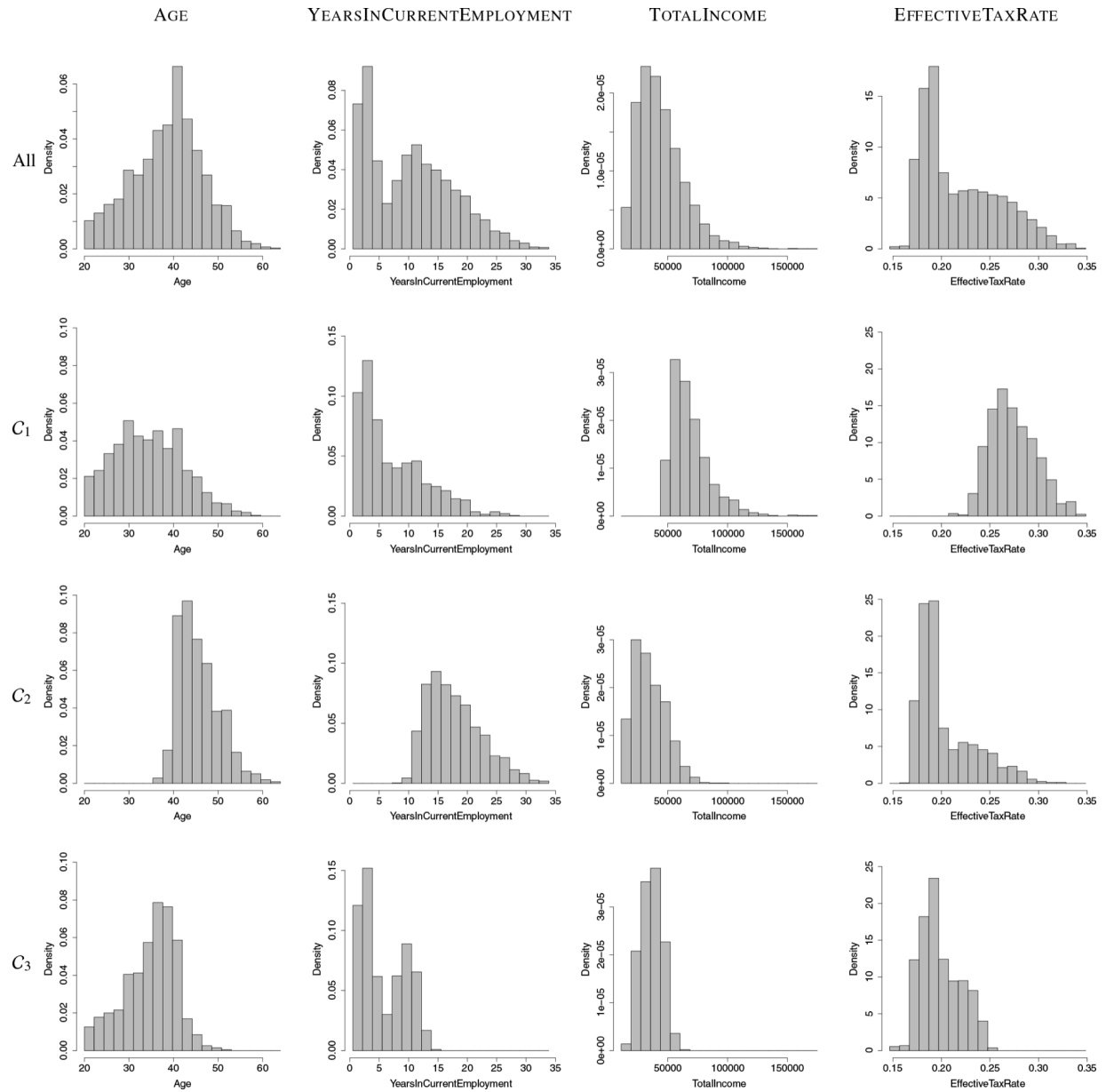
The following table shows summary statistics of the four descriptive features for each of the three clusters found.

Feature	Cluster	1 st			3 rd			Std. Dev.
		Min.	Qrt.	Mean	Median	Qrt.	Max	
AGE	C_1	20	28	34.6	34	40	59	7.8
	C_2	36	43	45.8	45	48	64	4.5
	C_3	20	32	34.9	36	39	52	5.8
YEARSIN CURRENT EMPLOYMENT	C_1	0.50	2.74	7.18	5.11	10.76	27.40	5.56
TOTALINCOME	C_2	8.16	14.25	17.81	17.04	20.71	33.89	4.60
	C_3	0.50	2.44	5.73	4.38	9.32	14.12	3.73
	C_1	46 247.70	57 355.06	68 843.26	64 977.64	75 967.11	175 000	16 387.77
EFFECTIVE TAXRATE	C_2	11 182.46	24 222.04	34 711.67	32 637.42	44 102.08	93 800.98	13 412.08
	C_3	15 505.02	29 636.07	36 370.00	36 421.53	42 912.04	64 075.62	8 744.26
	C_1	0.210	0.256	0.274	0.271	0.291	0.349	0.024
	C_2	0.167	0.183	0.204	0.192	0.220	0.321	0.030
	C_3	0.147	0.183	0.199	0.194	0.214	0.252	0.021

The following table shows the information gain calculated when each descriptive feature is used to predict the membership of a single cluster versus the rest of the population.

Feature	Information Gain		
	\mathcal{C}_1	\mathcal{C}_2	\mathcal{C}_3
AGE	0.0599	0.4106	0.1828
YEARSINCURRENTEMPLOYMENT	0.0481	0.5432	0.3073
TOTALINCOME	0.5015	0.0694	0.1830
EFFECTIVETAXRATE	0.5012	0.0542	0.2166

The following images show histograms of the values of the four descriptive features both for the full dataset and when divided into the three clusters found.



Using the information provided, write a description of what it means for a taxpayer to be a member of each of the clusters.

- * 4. The following table shows a *customer-item matrix* describing items from an online store that customers have bought.

ID	I_1	I_2	I_3	I_4	I_5	I_6	I_7	I_8	I_9	I_{10}	I_{11}	I_{12}	I_{13}	I_{14}
1	1	1	1	1	1	1	0	0	0	0	0	0	0	0
2	1	1	1	1	0	1	1	1	0	0	0	0	0	0
3	1	1	0	1	0	1	1	1	1	0	0	0	1	0
4	1	0	1	0	1	1	1	0	0	0	0	0	0	0
5	0	0	0	0	0	0	0	1	1	1	1	1	1	1
6	0	1	0	0	0	0	0	0	1	1	1	1	1	0
7	0	0	0	1	0	0	1	1	1	1	0	1	0	1
8	0	1	0	0	0	0	0	0	0	1	0	1	1	1

The online store would like to cluster their customers to see if they could define meaningful groups to whom they could target special offers. The table below shows a distance matrix calculated using the **Jaccard similarity measure** (see Section 5.4.5^[211]). A number of items have been left out of this matrix (indicated by ??).

$$\begin{array}{ccccccccc}
 & \mathbf{d}_1 & \mathbf{d}_2 & \mathbf{d}_3 & \mathbf{d}_4 & \mathbf{d}_5 & \mathbf{d}_6 & \mathbf{d}_7 & \mathbf{d}_8 \\
 \mathbf{d}_1 & 0.000 & & & & & & & \\
 \mathbf{d}_2 & ?? & 0.000 & & & & & & \\
 \mathbf{d}_3 & 0.600 & ?? & 0.000 & & & & & \\
 \mathbf{d}_4 & 0.429 & 0.500 & 0.700 & 0.000 & & & & \\
 \mathbf{d}_5 & 1.000 & 0.923 & 0.750 & 1.000 & 0.000 & & & \\
 \mathbf{d}_6 & 0.909 & ?? & 0.727 & 1.000 & 0.375 & 0.000 & & \\
 \mathbf{d}_7 & 0.917 & 0.727 & 0.636 & 0.909 & 0.444 & ?? & 0.000 & \\
 \mathbf{d}_8 & 0.900 & 0.909 & 0.818 & 1.000 & 0.500 & 0.429 & 0.667 & 0.000
 \end{array}$$

- (a) Using the Jaccard similarity index (reproduced here from Section 5.4.5^[211])

$$dist_J(\mathbf{q}, \mathbf{d}) = 1 - \frac{CP(\mathbf{q}, \mathbf{d})}{CP(\mathbf{q}, \mathbf{d}) + PA(\mathbf{q}, \mathbf{d}) + AP(\mathbf{q}, \mathbf{d})}$$

calculate these missing distances in the preceding distance matrix (note that because this is a distance (or dissimilarity) matrix rather than a similarity matrix, the values shown are $1 - sim_J(\mathbf{q}, \mathbf{d})$).

- (b) **Agglomerative hierarchical clustering** (AHC) can easily be applied to this distance matrix. If **single linkage** is used with AHC, which agglomerations will be made in the first three iterations of the algorithm?
- (c) If **average linkage** were used with AHC instead of single linkage, which agglomerations would be made in the first three iterations of the algorithm?

* 5. The following table shows a small dataset used for human activity recognition from a wearable accelerometer sensor.¹⁶ Each instance describes the average acceleration in the X, Y, and Z directions within a short time window. There are no labels, so this data is being clustered in an attempt to recognize different activity from this simple data stream. The **k-means clustering** approach is to be applied to this dataset with $k = 2$ and using **Euclidean distance**. The initial cluster centroids for the two clusters \mathcal{C}_1 and \mathcal{C}_2 are $\mathbf{c}_1 = \langle -0.235, 0.253, 0.438 \rangle$ and $\mathbf{c}_2 = \langle 0.232, 0.325, -0.159 \rangle$. The following table also shows the distance to these three cluster centers for each instance in the dataset.

ID	X	Y	Z	Cluster Distances Iter. 1	
				$Dist(\mathbf{d}_i, \mathbf{c}_1)$	$Dist(\mathbf{d}_i, \mathbf{c}_2)$
1	-0.154	0.376	0.099	0.370	0.467
2	-0.103	0.476	-0.027	0.532	0.390
3	0.228	0.036	-0.251	0.858	0.303
4	0.330	0.013	-0.263	0.932	0.343
5	-0.114	0.482	0.014	0.497	0.417
6	0.295	0.084	-0.297	0.922	0.285
7	0.262	0.042	-0.304	0.918	0.319
8	-0.051	0.416	-0.306	0.784	0.332

- (a) Assign each instance to its nearest cluster to generate the clustering at the first iteration of k -means on the basis of the initial cluster centroids.
- (b) On the basis of the clustering calculated in Part (a), calculate a set of new cluster centroids.
- (c) Calculate the distances of each instance to these new cluster centers and perform another clustering iteration.

1. There are several different ways to explain the k -means clustering algorithm. For example, as k -means is actually a special case of the **expectation maximization algorithm** (Moon, 1996), it is often described in a probabilistic context more similar to typical descriptions of that algorithm. To align with Chapter 5^[181] we present a similarity-based description of the algorithm.

2. Described in Section 5.2.2^[184]. Although it is possible to use other distance measures, such as those described in Chapter 5^[181], in k -means clustering this can break the guarantees that the algorithm makes about convergence. The k -medoids clustering algorithm (Kaufman and Rousseeuw, 1990) was developed to address these problems.

3. The example given here is based on artificial data generated for the purposes of this book. Performing customer segmentation in this way, however, is very common (see, for example, Berry

and Linoff (2004)).

4. A common modification to k -means clustering in which actual instances are chosen as initial centroids, rather than random points in the feature space, easily stops this from happening.
5. The silhouette (Rousseeuw, 1987) is just one example of how clusterings can be evaluated. Others include the **cubic clustering criterion** (Sarle, 1983) and the **Dunn index** (Dunn, 1974); however, these are based on very similar ideas to the silhouette.
6. See Section 3.1^[54].
7. See Section 4.2.3^[127].
8. This is much like the rank and prune approach to feature selection described in Section 5.4.6^[223].
9. Because Euclidean distance between any two points is symmetrical ($dist(a,b) = dist(b,a)$), we show only half of the distance matrix.
10. The instances have been arranged in an order that leads to a nice dendrogram visualization, and this was also the order used in the distance matrices to make it easy to follow the combination of instances into clusters.
11. See Chapter 8^[381].
12. See Chapter 8^[381] for descriptions of these different activation functions.
13. See Section 9.4.5^[574].
14. This dataset is from the UCI Machine Learning repository Dua and Graff (2017) and was originally described by Alimoglu and Alpaydin (1996).
15. See Chapter 8^[381] for a discussion of mini-batch gradient descent.
16. The data in this question has been artificially created but is inspired by the **Human Activity Recognition Using Smartphones Dataset** first described by Anguita et al. (2013) and available from the UCI Machine Learning Repository (Bache and Lichman, 2013).

11

Beyond Prediction: Reinforcement Learning

“Live. Die. Repeat.”

—Edge of Tomorrow

This chapter discusses **reinforcement learning**, an approach to machine learning that is sufficiently different from supervised and unsupervised machine learning to be often considered the third leg of the machine learning stool. Although reinforcement learning can be used for many different tasks, its most common application is in learning to control the behaviors of autonomous systems—for example, training robots to perform tasks, or automated players to play games—and this is the application that this chapter focuses on. The other key differentiating factor between reinforcement learning and the other approaches we have looked at in this book is that reinforcement learning relies less on using a dataset to drive learning and more on the ability to repeatedly attempt tasks in an environment.

This chapter begins by establishing the fundamental setup of the reinforcement learning scenario and then describes **temporal-difference learning**, a common approach to reinforcement learning. The standard reinforcement learning approach, **Q-learning**, a form of temporal-difference learning, is then described. After discussing some extensions and variations of this approach, the chapter focuses on how **deep learning** techniques have been recently integrated into reinforcement learning to impressive effect. The chapter finishes by describing the **deep Q network** algorithm.

11.1 Big Idea

Sarah is a young venture scout in training for her pioneering badge. One of the more unusual challenges involved in earning this badge is to learn to cross a stream using a set of stepping-stones while wearing an electronic blindfold. In this challenge the scout begins at the edge of the bank on one side of the stream and has to make a series of steps to get to the other side. The goal is to get across the river in the fewest steps possible without getting wet. The blindfold makes this quite challenging! The blindfold, however, is electronic and controlled by the scout leader administering the test. Before the scout attempts a step, the blindfold is made transparent for 0.5 seconds to give the scout a quick view of their environment so that they make a decision about which direction they will step in and how far.

Sarah spent days training to get better at this challenge. At first she was terrible at it, and almost every step she took led to the disappointing sensation of wet feet. The first time that Sarah took a step that reached a stepping-stone, however, she felt a huge rush of excitement. As time went by, Sarah found herself feeling this excitement more and more often as she became better and better at quickly assessing her situation when the blindfold was cleared and making better decisions about which direction to step in. She even occasionally made it all the way across the stream without stepping into the water and experienced the elation of landing on the grassy bank of the far side of the river. Still, throughout her training Sarah would occasionally still step into the water and experience the disappointing feeling of soggy feet, which reminded her to be more careful about her decisions next time. On other occasions she would take a series of successful steps but then experience a sinking feeling realizing that she had turned back on herself and arrived back on the starting bank.

Sarah's training for the stepping-stone challenge has many of the characteristics of a reinforcement learning problem. Sarah had a task that she wanted to get better at, and so she practiced it many times. In each practice episode, each one of the decisions Sarah made led to immediate feedback: either splashing into the river (negative feedback), landing successfully on the next stepping-stone (positive feedback), turning back on her tracks (very negative feedback), or landing on the far riverbank (very positive feedback). On the basis of this feedback, Sarah learned what constituted a good decision and became better and better at assessing her situation and choosing which direction to step in next and how far. By

optimizing her decisions to maximize these immediate rewards, Sarah learned how to complete the overall task successfully. This is what we try to achieve in reinforcement learning.

By the time her test came around, Sarah had become an expert at the river-crossing challenge. No matter how awkwardly the scout leaders laid out the stepping-stones, she could quickly assess the situation each time the blindfold was cleared and choose the right direction to step in. She completed the challenge in record time and was awarded the pioneering badge.

11.2 Fundamentals

This section introduces the fundamentals of **reinforcement learning**. We begin by explaining the concept of an **intelligent agent** and then describe the fundamental building blocks of reinforcement learning. **Markov decision processes** (MDPs) are an extremely useful mathematical tool for framing reinforcement learning problems; these are covered next. Finally, the **temporal-difference learning** approach, which is the basis for the standard approach to reinforcement learning that will be discussed in the following chapter, is explained.

11.2.1 Intelligent Agents

The stepping-stone crossing challenge described in Section 11.1^[637] nicely illustrates the intelligent agent approach that underpins reinforcement learning. We can consider the scout to be an **intelligent agent** (or simply **agent**) attempting to complete a task within an environment. The **goal** of the agent is to complete the task as successfully as possible. Each attempt at the task is referred to as an **episode**. At any point in time, t , the agent observes the current state of its environment, o_t ; considers these observations to select an action, a_t ; and takes this action, receiving immediate feedback, r_t , from the environment about whether this was a good or bad action to take. We use r_t to refer to feedback, as in reinforcement learning feedback is more commonly referred to as **reward** (where reward can be either positive or negative). This gives a series of discrete steps that make up an episode

$$(o_1, a_1, r_1), (o_2, a_2, r_2), (o_3, a_3, r_3), \dots, (o_e, a_e, r_e) \quad (11.1)$$

where the episode proceeds through time-steps $t = 1, \dots, e$. At each time-step the agent makes an observation, o_t , of the environment, takes an action, a_t , and receives a reward, r_t , based on that action. This cycle is illustrated in Figure 11.1^[639].

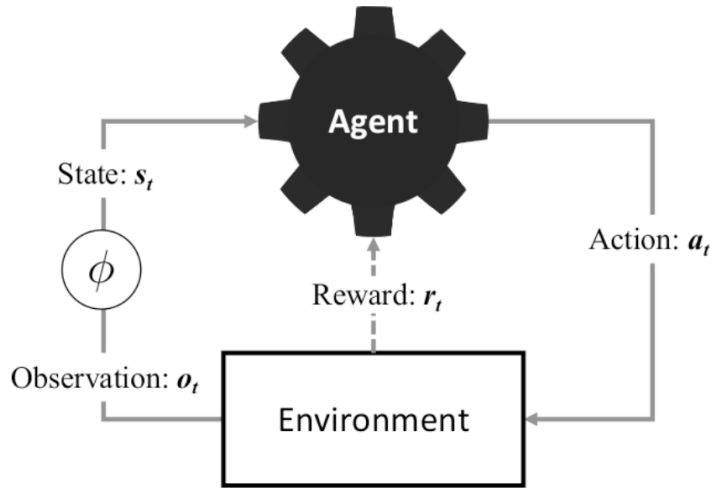


Figure 11.1

An agent behaving in an environment and the observation, reward, action cycle. The transition from observations of the environment to a state is shown by the state generation function, ϕ .

The sequence of observations, actions and rewards that precede any time-step, t , is referred to as a **history**, H_t . The job of the agent in the environment is to make decisions at each time-step, t , about what action to take next on the basis of its current observations of the environment, o_t , and the history, H_t .

Maintaining long histories of actions, rewards, and observations (which are possibly only very slightly different from one iteration to the next) is not a very efficient way to reason about the world, particularly as episodes might cover hundreds or thousands of time-steps. Instead, we collapse this information into a single representation, referred to as a **state**. The state at time-step t , s_t , should contain all the important information about the environment at that time-step, any important information about what has been happening in the environment at preceding time-steps, and any important information about the internal composition of the agent. For example, for a robot deployed within a hospital to deliver equipment to operating theaters, the state might include the robot's position in the environment, the positions of people nearby, whether the robot is on the

way to collect items or to deliver them, and the current levels of the robot’s batteries.

In Figure 11.1^[639] we show how the observations made about the environment at time-step t are converted into a state, s_t , using a **state generation function**, ϕ . In many cases, if the environment is **fully observable** this function is a simple identity function because the observation fully defines the state. It is also possible, however, for this function to be more elaborate when the observations over multiple time-steps are accumulated into a state.¹ Using states instead of observations, Equation (11.1)^[639] can be restated²

$$(s_1, a_1, r_1), (s_2, a_2, r_2), (s_3, a_3, r_3), \dots, (s_e, a_e, r_e) \quad (11.2)$$

We see in subsequent examples that designing good state representations is one of the *arts* of reinforcement learning.

The goal of the intelligent agent is to complete a task as *successfully* as possible. To frame the reinforcement learning problem, this needs to be more formally defined—what does it mean to successfully complete a task? The next section explores this.

11.2.2 Fundamentals of Reinforcement Learning

The fundamental idea underpinning reinforcement learning is that the only goal of an intelligent agent is to maximize **cumulative reward** across an episode.³ The cumulative reward earned across an episode is referred to as the **return** from the episode and can be defined as

$$G = r_t + r_{t+1} + r_{t+2} + r_{t+3} + \dots + r_e \quad (11.3)$$

That *intelligent* behavior can be driven by the singular goal of maximizing return is a bold statement—it is often argued that it is very ambitious to expect sophisticated, long-term behavior to emerge from simple accumulation of instantaneous rewards. Reward is often delayed, and the real value of an action is not reflected immediately but rather by the fact that an action takes us toward a later state that will ultimately allow an agent to earn a reward. For example, early moves in a game of chess do not lead to large positive rewards but set the ground for later high-reward

moves. Rewards can also often be somewhat contradictory, and an action that gives an immediate positive reward may turn out to be a bad one in the longer term. For example, eating cake almost always seems like a good idea in the moment, but in terms of long-term health is probably not always a strong choice. It has been shown repeatedly, however, that it is in fact possible to learn sophisticated, long-term behaviors using the maximization of cumulative reward alone. This introduces the second *art* of reinforcement learning: the design of effective reward functions.

The key decision making component of a reinforcement learning agent is referred to as a **policy**, π . A policy is simply a mapping from states to actions

$$a_t = \pi(s_t) \quad (11.4)$$

that tells the agent which action, a_t , to take when in a given state, s_t . We can also define a policy in probabilistic terms

$$P(A_t = a | S_t = s) = \pi(S_t = s) \quad (11.5)$$

where A_t and S_t are random variables that can be assigned specific states and actions; and the policy, π , returns a probability distribution across the possible actions that an agent can take in a given state.

The policy can be thought of as a simple lookup table that records the action that should be taken in every state, and reinforcement learning problems can be framed as an effort to learn this table directly.⁴ Policies can also be encoded as a rule used to choose an action from those available in a particular state, and this is the approach we focus on in this chapter. For example, we might use a **greedy action selection policy** that says the agent should always take the action that will give it the highest immediate reward. This would, however, ignore the fact that sometimes reward is delayed and that taking an action that gives a low immediate reward can be a good idea if it leads the agent to a state that could give it large positive rewards later on. This suggests the need for a more sophisticated measure of the value of taking an action in a given state and leads to the final fundamental component of a reinforcement learning agent: a **value function**.

In reinforcement learning a **value function** returns the cumulative reward that an agent can expect to earn if it starts from a particular state, s_t , and follows a specific policy, π all the way to the end of an episode. We can write this

$$V_\pi(s_t) = E_\pi[r_t + r_{t+1} + r_{t+2} + r_{t+3} + \dots + r_e \mid s_t] \quad (11.6)$$

where E is the expectation. This value function returns the expected cumulative reward that an agent will earn if it follows policy π starting from state s_t .

We can also calculate the expected value from the starting point of an agent's taking a specific action, a_t , in a given state, s_t . This is known as an **action-value function** and returns the cumulative reward that an agent can expect to earn if it takes an action a_t in state s_t and then continues to select actions using policy, π , all the way to the end of an episode. We can write this⁵

$$Q_\pi(s_t, a_t) = E_\pi[r_t + r_{t+1} + r_{t+2} + r_{t+3} + \dots + r_e \mid s_t, a_t] \quad (11.7)$$

The output of the action-value function is referred to as the **expected return** of pursuing action a_t in state s_t . We will see that the action-value function formulation of expected return is the more useful of these two.

In the formulation given in Equation (11.7)^[642] expected future rewards are considered to be as valuable as the immediate reward that the agent will receive from taking the next immediate action, a_t . Just as we might be more excited about receiving a gift of \$100 today than a promise to receive a gift of \$100 in a year's time, it is reasonable when calculating expected return to pay more attention to the immediate reward we expect to receive from taking the next action than to the rewards that we expect to receive in 10 or even 100 actions' time. This is known as **discounted return**. We can modify Equation (11.3)^[641] to define discounted return

$$G_\gamma = r_t + \gamma r_{t+1} + \gamma^2 r_{t+2} + \gamma^3 r_{t+3} + \dots + \gamma^{e-t} r_e \quad (11.8)$$

where γ is a **discount rate** and is a value in [0,1]. This implements an exponential discounting so that future expected rewards have less and less

impact on the value calculated for an action. Choosing a low value for γ makes the action-value function focus heavily on the most immediate rewards. For example, with $\gamma = 0.1$

$$G_{\gamma=0.1} = r_t + 0.1 \times r_{t+1} + 0.01 \times r_{t+2} + 0.001 \times r_{t+3} + \dots$$

Choosing a high value for γ gives almost equal importance to all rewards. For example, with $\gamma = 0.9$

$$G_{\gamma=0.9} = r_t + 0.9 \times r_{t+1} + 0.81 \times r_{t+2} + 0.729 \times r_{t+3} + \dots$$

To use discounted return in the **action-value function** it is restated

$$Q_\pi(s_t, a_t) = E_\pi[r_t + \gamma r_{t+1} + \gamma^2 r_{t+2} + \gamma^3 r_{t+3} + \dots + \gamma^{3-t} r_e | s_t, a_t] \quad (11.9)$$

Discounting makes intuitive sense, makes some of the mathematics associated with reinforcement learning more straightforward, and avoids any issues with circular paths through states that can arise in some scenarios. Discounted return is widely used in reinforcement learning.

In summary, in a reinforcement learning scenario, an **agent** inhabiting an **environment** attempts to achieve a **goal** by taking a sequence of **actions** to move it between **states**. On completion of each action the agent receives an immediate scalar **reward** indicating whether the outcome of the action was positive or negative, and to what degree. In reinforcement learning the degree to which an agent has achieved a goal is measured only by the **cumulative rewards** it has received from each action taken in pursuit of that goal. To choose which action to take in a given state the agent uses a **policy**. Policies rely on being able to assess the **expected return** of taking an action in a particular state, and an **action-value function** can be used to calculate this.⁶

None of this, however, yet explains how any actual learning takes place! This explanation appears subsequently, but before discussing reinforcement learning algorithms we will explain **Markov decision processes**, a useful mathematical framework into which we can place the key components of reinforcement learning to allow learning to take place.

11.2.3 Markov Decision Processes

Markov decision processes (MDPs) are an attractive mathematical framework within which to reason about decision making scenarios in which outcomes are partly under the control of a decision maker, but also partly random. This has made them an attractive framework for applications ranging from financial modeling, to robot control, to modeling the flow of human conversation. This also makes them ideal for reasoning about reinforcement learning.

A **Markov process**, a more basic framework than an MDP that does not include decision making, can be used to model a discrete random process that transitions through a finite set of states, S . For example, we could use a Markov process to model how infection progresses in an individual when a disease epidemic breaks out. Individuals can belong to one of three states: SUSCEPTIBLE, INFECTED, or RECOVERED (these are often referred to as **S-I-R models**). An individual can belong to only one of these states at a time and moves between them according to a Markov process. [Figure 11.2\(a\)](#)^[644] shows these states and how an individual can move between them.⁷

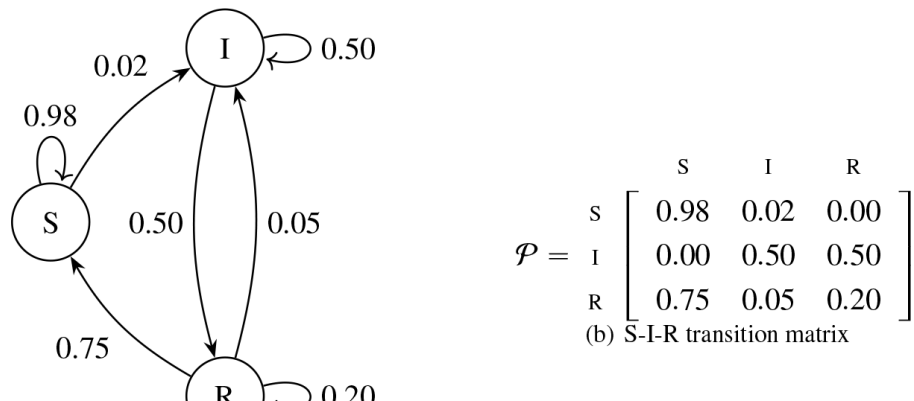


Figure 11.2

A simple Markov process to model the evolution of an infectious disease in individuals during an epidemic using the SUSCEPTIBLE-INFECTED-RECOVERED (S-I-R) model.

Markov processes are built on the **Markov assumption** that the probability of transitioning to a particular state at the next time-step relies only on the current state, and does not require any knowledge of the history of states that came before that, or

$$P(S_{t+1} | S_t, S_{t-1}, S_{t-2}, \dots) = P(S_{t+1} | S_t) \quad (11.10)$$

Given the Markov assumption, we can write the probability of transitioning between two states

$$P(s_1 \rightarrow s_2) = P(S_{t+1} = s_2 | S_t = s_1) \quad (11.11)$$

where S_t and S_{t+1} are random variables to which the states at time t and $t + 1$ are assigned. The full dynamics of a Markov process can be captured in a transition matrix

$$\mathcal{P} = \begin{bmatrix} P(s_1 \rightarrow s_1) & P(s_1 \rightarrow s_2) & \dots & P(s_1 \rightarrow s_n) \\ P(s_2 \rightarrow s_1) & P(s_2 \rightarrow s_2) & \dots & P(s_2 \rightarrow s_n) \\ \vdots & \vdots & \ddots & \vdots \\ P(s_n \rightarrow s_1) & P(s_n \rightarrow s_2) & \dots & P(s_n \rightarrow s_n) \end{bmatrix}$$

where s_1 to s_n are n different states. A Markov process can be fully characterized by the set of states, S , and the transition matrix, \mathcal{P} .

The numbers along the arrows in [Figure 11.2](#)^[644] show the probabilities of moving between the different states in this model. The transition matrix is also shown. Most people will remain in the SUSCEPTIBLE state indefinitely, $P(S \rightarrow S) = 0.98$, but with a small probability, $P(S \rightarrow I) = 0.02$, can transition to the INFECTED state. Individuals will most likely remain in the INFECTED state for some time, $P(I \rightarrow I) = 0.50$, but will transition eventually to the RECOVERED state, $P(I \rightarrow R) = 0.50$. After remaining in the RECOVERED state for some time, $P(R \rightarrow R) = 0.20$, most people will soon transition back to the SUSCEPTIBLE state, $P(R \rightarrow S) = 0.75$, but a small part of the population will instead relapse and return to the INFECTED state, $P(R \rightarrow I) = 0.05$.

A **Markov decision process** (MDP) extends the Markov process by adding decision making and rewards. We extend the formulation of the Markov process to include a finite set of actions that can be taken, A , and add actions from this set to the formulation of transition probabilities

$$P(s_1 \xrightarrow{a} s_2) = P(S_{t+1} = s_2 | S_t = s_1, A_t = a) \quad (11.12)$$

Retaining the Markov assumption that only the current time-step is required to model what will happen next, the probability of transitioning to a particular state depends only on the current state and the action just taken. Each transition to a new state based on a particular action now also carries with it a reward

$$R(s_1 \xrightarrow{a} s_2) = E(r_t | S_t = s_1, S_{t+1} = s_2, A_t = a) \quad (11.13)$$

To illustrate MDPs in a little more detail we develop an MDP representation for an agent designed to play the card game **TwentyTwos**, a simplified version of the popular game **Blackjack**, that has been invented for this example. TwentyTwos is a game played between a single player and a dealer. In TwentyTwos the player tries to collect a hand of cards that have a total value higher than the total value of the cards in the dealer's hand, but not exceeding 22—a player is said to go *bust* when they exceed 22. Cards are worth their number value, with picture cards worth 10, and aces always worth 11 (this is one of the simplifications of this version of the game). The player and dealer are initially each dealt two cards. The player is allowed to see one of the two cards dealt to the dealer, but the dealer's other card remains hidden until the player is finished taking their actions. The player then repeatedly chooses to either be dealt another card, *Twist*, or to stop on their current total, *Stick*.⁸ When the player is finished, the dealer turns over their second card and must continue to deal themselves cards until they reach a total value of 17 or more, or go bust by exceeding a value of 22. The dealer's play strictly follows these rules and so we can say that the dealer does not make any decisions during the game. We also assume cards are dealt from an infinite deck, which simplifies some of the modeling of the game.⁹

The player wins if their total is less than or equal to 22 and is greater than the dealer's total, or if the dealer goes bust. In the rare event that the player is dealt two aces, giving a total of 22, they are awarded a *TwentyTwo* and win regardless of the cards dealt to the dealer. The game is tied if the dealer and the player have the same total, less than or equal to 22. The player loses in all other cases. The player wins \$2 in the event of a *TwentyTwo* (two aces), wins \$1 if they beat the dealer in the normal way, neither wins nor loses anything if the game is tied, and loses \$1 if the dealer

wins.¹⁰ Table 11.1^[647] shows some episodes of the TwentyTwos game being played including the the player’s hand, the dealer’s hand, the actions the player takes, and the rewards earned by the player.

Table 11.1

Some episodes of games played by the TwentyTwos agent showing the cards dealt, as well as the states, actions, and rewards. Note that rewards are shown on the row indicating the action that led to them, not the state that followed that action.

Iter	Player Hand	Dealer Hand	State	Action	Reward
1	2 ♦ 7 ♣	(9)	8 ♥	(8) PL-DH	<i>Twist</i> 0
2	2 ♦ 7 ♣ K ♣	(19)	8 ♥	(8) PH-DH	<i>Stick</i> +1
3	2 ♦ 7 ♣ K ♣	(19)	8 ♥ Q ♦	(18) WIN	
1	4 ♠ A ♥	(15)	Q ♥	(10) PM-DH	<i>Twist</i> -1
2	4 ♠ A ♥ 9 ♣	(24)	Q ♥	(10) BUST	
1	2 ♦ 4 ♦	(6)	3 ♥	(3) PL-DL	<i>Twist</i> 0
2	2 ♦ 4 ♦ 3 ♥	(9)	3 ♥	(3) PL-DL	<i>Twist</i> 0
3	2 ♦ 4 ♦ 3 ♥ 6 ♣	(15)	3 ♥	(3) PM-DL	<i>Twist</i> 0
4	2 ♦ 4 ♦ 3 ♥ 6 ♣ 6 ♦	(21)	3 ♥	(3) PH-DL	<i>Stick</i> 0
5	2 ♦ 4 ♦ 3 ♥ 6 ♣ 6 ♦	(21)	3 ♥ 7 ♥ A ♠	(21) TIE	
1	Q ♦ J ♣	(20)	A ♥	(11) PH-DH	<i>Stick</i> +1
2	Q ♦ J ♣	(20)	A ♠ 5 ♣ Q ♠	(26) WIN	
1	A ♦ A ♥	(22)	2 ♥	(2) PH-DL	<i>Stick</i> +2
2	A ♦ A ♥	(22)	2 ♥	(2) TWENTYTWO	

There are lots of options for the state representation that can be used to model an agent playing the game TwentyTwos. Card suits have no impact on the game (for example, 10 ♦ is equivalent to 10 ♥) and because there is an infinite deck, tracking the actual cards that have been dealt gives no advantage to the player. So, the only thing that needs to be taken into account in the state representation is the total value of the cards in the player’s hand and the value of the visible card dealt to the dealer. The total value of the initial two cards dealt to the player can range from 4 (for example, 2 ♥ and 2 ♣) to 22 (for example, A ♠ and A ♥), giving 19 unique values. There are 10 values that the dealer’s visible card can represent: 2 to 11. This means that there are 190 different combinations of the values of the hands held by the player and the dealer. To fully capture the game dynamics we could represent TwentyTwos using the 190 different hand states plus five more terminal states representing the outcomes of going bust, losing,

tying, winning, and winning with a *TwentyTwo*. This would give a total of 195 different states. Many of these states, however, or not significantly different from each other and so it makes sense to discretize the hand representation so as to have a smaller number of states. In designing state representations the principle of **parsimony** applies: we should strive for the simplest representation that gives sufficient flexibility to model the important aspects of an environment and task.

To make things manageable for this example, we aggressively discretize the representation of the value of the cards in the player's and dealer's hands. For the player's hand, just three levels (*low*, *medium*, and *high*) are modeled

- Player Low (PL): 4 – 14
- Player Medium (PM): 15 – 18
- Player High (PH): 19 – 22

For the value of the visible card dealt to the dealer, just two levels (*low* and *high*) are modeled

- Dealer Low (DL): 2 – 7
- Dealer High (DH): 8 – 11

This gives a state representation with six states to represent all possible combinations of the value of the cards in the player's hand and the value of the dealer's visible card: PL-DL, PM-DL, PH-DL, PL-DH, PM-DH, and PH-DH. Adding the five terminal states—**BUST**, **LOSE**, **TIE**, **WIN**, and **TWENTYTWO**—gives 11 states in total. [Figure 11.3](#)^[648] shows a visualization of an MDP for **TwentyTwos** using this representation where the circles represent the 11 states. Note that in this diagram the **BUST** state has been included twice to make the illustration a little more clear by avoiding too many overlapping arrows.

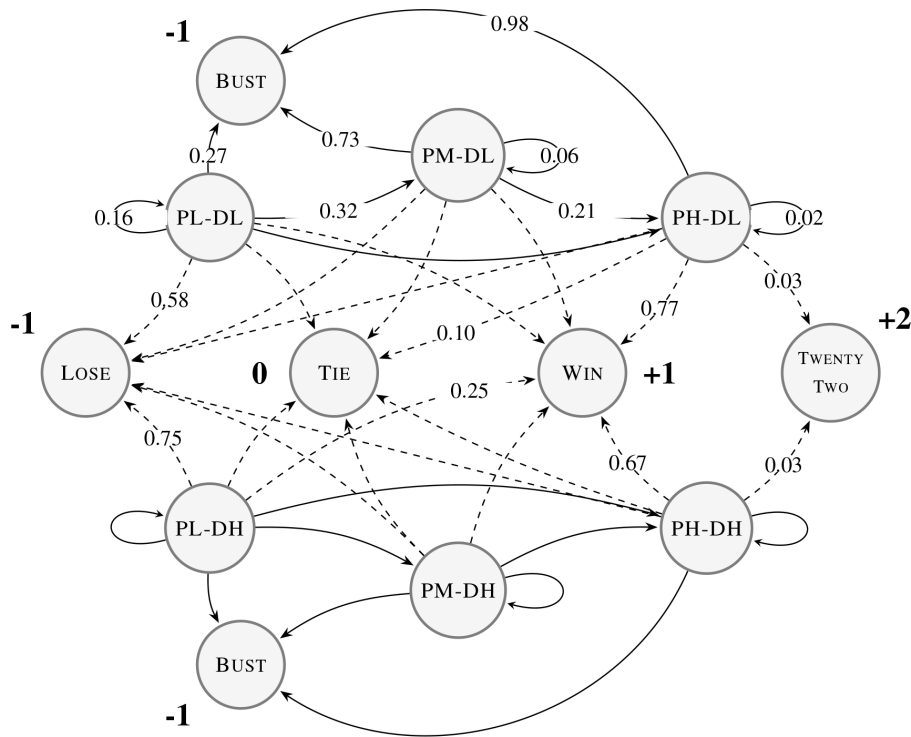


Figure 11.3

A Markov decision process representation for TwentyTwos, a simplified version of the card game Blackjack. The eleven states are shown as the nodes in the graph with transitions based on different actions represented by the edges (transitions for *Twist* actions are shown as solid lines and transitions for *Stick* actions are shown as dashed lines). For clarity in the graph, rewards at non-terminal nodes are left out and rewards are shown just once at each terminal node; the *BUST* state is shown twice to avoid overlapping transition arrows; and only an illustrative selection of transition probabilities are shown (the full set of transitions probabilities is shown in the transition matrices in Equations (11.15)^[650] and (11.14)^[650]).

In TwentyTwos the player has two actions available to them in each non-terminal state: *Stick* or *Twist*. Once the player enters one of the terminal states (*BUST*, *LOSE*, *TIE*, *WIN*, or *TWENTYTWO*) the game is over and there are no more actions to take. Figure 11.3^[648] shows the possible transitions between states in TwentyTwos based on these actions. Transitions related to a *Twist* action are shown as solid lines, and transitions related to a *Stick* action are shown with dashed lines. Choosing to *Twist* in any of the non-terminal states will take the agent to the same non-terminal state, another non-terminal state representing a higher player hand value, or—if they are unlucky—the *BUST* state. After the player chooses to *Stick*, the dealer will reveal their hidden card and keep dealing more cards until they reach a total greater than or equal to 17. Depending on how the value of the dealer's

hand that results from this compares to the value of the player's hand the agent will move into one of the terminal states: LOSE, TIE, WIN, or TWENTYTWO.

[Figure 11.3](#)^[648] shows a selection of the transition probabilities between states in the TwentyTwos MDP (only a selection of probabilities are shown to make the graph less cluttered). The probabilities associated with each *Twist* transition shown in [Figure 11.3](#)^[648] have been calculated based on what can happen in a game of TwentyTwos, under the assumption of an infinite deck from which cards are dealt. Consider, for example, the probability of an agent in the PM-DH state remaining in that state after choosing the *Twist* action: $P(\text{PM-DH} \xrightarrow{\text{Twist}} \text{PM-DH})$. If the agent is in the PM-DH state, they must have a total value in their hand of either 15, 16, 17, or 18. If the agent chooses the *Twist* action they will be dealt one of the 13 types of cards in a deck with a value between 2 and 11 (remember that there are four cards in the deck with a value of 10: 10, J, Q, and K). This means that there are 52 different scenarios that could occur if a player is in the PM-DH state and chooses the *Twist* action (the player is dealt one of 13 possible cards when their hand has one of 4 possible values, so $4 \times 13 = 52$). Only 3 of these scenarios, however, will lead to the agent staying in the PM-DH state. The agent can only stay in the PM-DH state if they have a hand value of 15 and are dealt a 2 or a 3; or if they have a hand value of 16 and are dealt a 2. So, $P(\text{PM-DH} \xrightarrow{\text{Twist}} \text{PM-DH}) = \frac{3}{52} = 0.058$. All state transition probabilities based on the *Twist* action can be calculated in a similar way. For transitions based on the *Stick* action a large number of games of TwentyTwos have been simulated and transition probabilities have been calculated based on this simulation.¹¹

We can capture the full dynamics of the TwentyTwos MDP in a pair of transition matrices, one for each possible action. For the *Twist* action the structure of the state transition matrix, $\mathcal{P}^{\text{Twist}}$, is

$$\mathcal{P}^{\text{Twist}} = \begin{bmatrix} P(\text{PL-DL} \xrightarrow{\text{Twist}} \text{PL-DL}) & P(\text{PL-DL} \xrightarrow{\text{Twist}} \text{PM-DL}) & \dots & P(\text{PL-DL} \xrightarrow{\text{Twist}} \text{TWENTYTWO}) \\ P(\text{PM-DL} \xrightarrow{\text{Twist}} \text{PL-DL}) & P(\text{PM-DL} \xrightarrow{\text{Twist}} \text{PM-DL}) & \dots & P(\text{PM-DL} \xrightarrow{\text{Twist}} \text{TWENTYTWO}) \\ \vdots & \vdots & \ddots & \vdots \\ P(\text{TWENTYTWO} \xrightarrow{\text{Twist}} \text{PL-DL}) & P(\text{TWENTYTWO} \xrightarrow{\text{Twist}} \text{PM-DL}) & \dots & P(\text{TWENTYTWO} \xrightarrow{\text{Twist}} \text{TWENTYTWO}) \end{bmatrix}$$

and for the *Stick* action the structure of the state transition matrix, $\mathcal{P}^{\text{Stick}}$, is

$$\mathcal{P}^{Stick} = \begin{bmatrix} P(PL-DL \xrightarrow{Stick} PL-DL) & P(PL-DL \xrightarrow{Stick} PM-DL) & \dots & P(PL-DL \xrightarrow{Stick} TWENTYTWO) \\ P(PM-DL \xrightarrow{Stick} PL-DL) & P(PM-DL \xrightarrow{Stick} PM-DL) & \dots & P(PM-DL \xrightarrow{Stick} TWENTYTWO) \\ \vdots & \vdots & \ddots & \vdots \\ P(TWENTYTWO \xrightarrow{Stick} PL-DL) & P(TWENTYTWO \xrightarrow{Stick} PM-DL) & \dots & P(TWENTYTWO \xrightarrow{Stick} TWENTYTWO) \end{bmatrix}$$

The completed transition matrix for the *Twist* action, \mathcal{P}^{Twist} , is

$$\mathcal{P}^{Twist} = \begin{bmatrix} & PL-DL & PM-DL & PH-DL & PL-DH & PM-DH & PH-DH & BUST & LOSE & TIE & WIN & TWENTYTWO \\ PL-DL & \begin{bmatrix} 0.16 & 0.32 & 0.34 & 0.00 & 0.00 & 0.00 & 0.17 & 0.00 & 0.00 & 0.00 & 0.00 \\ 0.00 & 0.06 & 0.29 & 0.00 & 0.00 & 0.00 & 0.65 & 0.00 & 0.00 & 0.00 & 0.00 \\ 0.00 & 0.00 & 0.08 & 0.00 & 0.00 & 0.00 & 0.92 & 0.00 & 0.00 & 0.00 & 0.00 \\ 0.00 & 0.00 & 0.00 & 0.16 & 0.32 & 0.34 & 0.17 & 0.00 & 0.00 & 0.00 & 0.00 \\ 0.00 & 0.00 & 0.00 & 0.00 & 0.06 & 0.29 & 0.65 & 0.00 & 0.00 & 0.00 & 0.00 \\ PH-DH & 0.00 & 0.00 & 0.00 & 0.00 & 0.08 & 0.92 & 0.00 & 0.00 & 0.00 & 0.00 & 0.00 \\ BUST & 0.00 & 0.00 & 0.00 & 0.00 & 0.00 & 0.00 & 0.00 & 0.00 & 0.00 & 0.00 & 0.00 \\ LOSE & 0.00 & 0.00 & 0.00 & 0.00 & 0.00 & 0.00 & 0.00 & 0.00 & 0.00 & 0.00 & 0.00 \\ TIE & 0.00 & 0.00 & 0.00 & 0.00 & 0.00 & 0.00 & 0.00 & 0.00 & 0.00 & 0.00 & 0.00 \\ WIN & 0.00 & 0.00 & 0.00 & 0.00 & 0.00 & 0.00 & 0.00 & 0.00 & 0.00 & 0.00 & 0.00 \\ TWENTYTWO & 0.00 & 0.00 & 0.00 & 0.00 & 0.00 & 0.00 & 0.00 & 0.00 & 0.00 & 0.00 & 0.00 \end{bmatrix} \end{bmatrix} \quad (11.14)$$

The completed transition matrix for the *Stick* action, \mathcal{P}^{Stick} , is

$$\mathcal{P}^{Stick} = \begin{bmatrix} & PL-DL & PM-DL & PH-DL & PL-DH & PM-DH & PH-DH & BUST & LOSE & TIE & WIN & TWENTYTWO \\ PL-DL & \begin{bmatrix} 0.00 & 0.00 & 0.00 & 0.00 & 0.00 & 0.00 & 0.00 & 0.68 & 0.00 & 0.32 & 0.00 \\ 0.00 & 0.00 & 0.00 & 0.00 & 0.00 & 0.00 & 0.00 & 0.58 & 0.06 & 0.36 & 0.00 \\ 0.00 & 0.00 & 0.00 & 0.00 & 0.00 & 0.00 & 0.00 & 0.20 & 0.10 & 0.68 & 0.03 \\ 0.00 & 0.00 & 0.00 & 0.00 & 0.00 & 0.00 & 0.00 & 0.81 & 0.00 & 0.19 & 0.00 \\ 0.00 & 0.00 & 0.00 & 0.00 & 0.00 & 0.00 & 0.00 & 0.00 & 0.73 & 0.06 & 0.21 \\ PM-DH & 0.00 & 0.00 & 0.00 & 0.00 & 0.00 & 0.00 & 0.00 & 0.00 & 0.00 & 0.00 & 0.00 \\ PH-DH & 0.00 & 0.00 & 0.00 & 0.00 & 0.00 & 0.00 & 0.00 & 0.00 & 0.22 & 0.15 & 0.60 \\ BUST & 0.00 & 0.00 & 0.00 & 0.00 & 0.00 & 0.00 & 0.00 & 0.00 & 0.00 & 0.00 & 0.00 \\ LOSE & 0.00 & 0.00 & 0.00 & 0.00 & 0.00 & 0.00 & 0.00 & 0.00 & 0.00 & 0.00 & 0.00 \\ TIE & 0.00 & 0.00 & 0.00 & 0.00 & 0.00 & 0.00 & 0.00 & 0.00 & 0.00 & 0.00 & 0.00 \\ WIN & 0.00 & 0.00 & 0.00 & 0.00 & 0.00 & 0.00 & 0.00 & 0.00 & 0.00 & 0.00 & 0.00 \\ TWENTYTWO & 0.00 & 0.00 & 0.00 & 0.00 & 0.00 & 0.00 & 0.00 & 0.00 & 0.00 & 0.00 & 0.00 \end{bmatrix} \end{bmatrix} \quad (11.15)$$

Some of these probabilities are highlighted along the edges in [Figure 11.3](#)^[648].

The final component of the MDP shown in [Figure 11.3](#)^[648] is the reward associated with each transition to a new state based on taking a particular action. The rewards are shown as the large numbers beside some states. In this model, the reward for all transitions to non-terminal states (e.g., PL-DL or PM-DH) is 0; these are not shown in [Figure 11.3](#)^[648]. The remaining rewards are based on the winnings earned within the game. Transitions into the BUST or LOSE states return a reward of -1, transitions into the TIE state earn a reward of 0, transitions into the WIN state return a reward of +1, and transitions into the TWENTYTWO state return a reward of +2. Although it makes sense to do it, the rewards do not have to be so closely tied to the

winnings within the game, and different reward structures could be designed to encourage different playing strategies—for example, more conservative or more aggressive play.

This MDP captures the dynamics of the TwentyTwos game, and it also hints toward some strategies for successful play. For example, choosing to *Stick* when the value of the player’s hand is low and the value of the dealer’s hand is high, state PL-DH, rarely leads to the player winning, $P(\text{PL-DH} \xrightarrow{\text{Stick}} \text{WIN}) = 0.19$. The MDP alone, however, is not sufficient to describe optimal behavior for successfully playing the game. The next section describes how an MDP can be used as the basis for reasoning about optimal behavior.

11.2.4 The Bellman Equations

Although an MDP tells us everything we need to know about how an agent can take actions to move between states in an environment, it does not tell us anything about what actions the agent should take to be most successful. However, the **action-value function** given in Equation (11.9)^[643] can be expressed in terms of the components of an MDP to do just this. Before presenting the formal version of this, it is worth stating the intuition. We can calculate the value of taking a particular action in a given state as the **expected reward** for taking the action plus the value of the state that the agent arrives in after taking that action.

To restate Equation (11.9)^[643] in terms of the components of an MDP, we modify Equation (11.9)^[643] to sum to infinity rather than just the end of an episode,¹² and we state the equation a little more succinctly

$$\begin{aligned} Q_\pi(s_t, a_t) &= E_\pi [r_t + \gamma r_{t+1} + \gamma^2 r_{t+2} + \dots + \gamma^3 r_\infty \mid s_t, a_t] \\ &= E_\pi \left[\sum_{k=0}^{\infty} \gamma^k r_{t+k} \mid s_t, a_t \right] \end{aligned} \tag{11.16}$$

$$= E_\pi \left[r_t + \gamma \sum_{k=0}^{\infty} \gamma^k r_{t+k+1} \mid s_t, a_t \right] \tag{11.17}$$

This states that the expected return of taking action a_t in state s_t is the immediate expected reward from taking that action plus the sum of

discounted expected rewards that will arise if we continue to follow policy π .

To restate Equation (11.17)^[651] using the components of an MDP we must explicitly represent the uncertainty associated with state transitions. This uncertainty is one of the key things that the MDP formulation allows us to model. We don't know exactly what state an agent will arrive in after taking action a_t from state s_t , but from the transition matrix, \mathcal{P}^{a_t} , we do know the probability of each possible transition between states, $P(s_t \xrightarrow{a_t} s_{t+1})$. To calculate the expected return of taking action a_t from state s_t we can calculate a weighted sum across the expected returns that the agent could receive in every state, s_{t+1} , that the agent could reach after taking action a_t in state s_t . The weights in this weighted sum are the probabilities of the state transitions¹³

$$Q_\pi(s_t, a_t) = \sum_{s_{t+1}} P(s_t \xrightarrow{a_t} s_{t+1}) \left[R(s_t \xrightarrow{a_t} s_{t+1}) + \gamma E_\pi \left[\sum_{k=0}^{\infty} \gamma^k r_{t+k+1} \mid s_{t+1} \right] \right] \quad (11.18)$$

Recall that $R(s_t \xrightarrow{a_t} s_{t+1})$ is the reward received when state s_{t+1} is reached from state s_t after taking action a_t .

Equation (11.18)^[652] still includes the expected return that arises from taking all of the actions after a_t essentially as it was stated before in Equation (11.17)^[651]. In fact, the final part of Equation (11.18)^[652] is almost identical to Equation (11.16)^[651] except for the explicit reference to an action in the latter. By adding an explicit reference to action a_{t+1} , we can arrive at a very elegant recursive definition of the action-value function. First the expected return can be written as a sum across the expected returns of all possible actions a_{t+1} that could be taken in state s_{t+1}

$$Q_\pi(s_t, a_t) = \sum_{s_{t+1}} P(s_t \xrightarrow{a_t} s_{t+1}) \left[R(s_t \xrightarrow{a_t} s_{t+1}) + \gamma \sum_{a_{t+1}} E_\pi \left[\sum_{k=0}^{\infty} \gamma^k r_{t+k+1} \mid s_{t+1}, a_{t+1} \right] \right] \quad (11.19)$$

The calculation of expected return for actions a_{t+1} and beyond refers to the policy, π , that is used to select the action that will be taken in each state (as did all other calculations of expected return). We can define the policy as a

function that returns a probability distribution over the set of possible actions that can be taken from a state, as described in Equation (11.5)^[641]. Using this definition we can rewrite Equation (11.19)^[652]

$$Q_\pi(s_t, a_t) = \sum_{s_{t+1}} P(s_t \xrightarrow{a_t} s_{t+1}) \left[R(s_t \xrightarrow{a_t} s_{t+1}) + \gamma \sum_{a_{t+1}} \pi(s_{t+1}, a_{t+1}) Q_\pi(s_{t+1}, a_{t+1}) \right] \quad (11.20)$$

where $\pi(s_{t+1}, a_{t+1})$ returns the likelihood of taking action a_{t+1} from state s_{t+1} under policy π , and $Q_\pi(s_{t+1}, a_{t+1})$ is a recursive call to the action-value function itself. This is one of the **Bellman Equations**,¹⁴ which are the foundation stones of reinforcement learning. This final formulation of the action-value function simply states that the expected *return* from taking action a_t in state s_t is the expected *reward* for taking that action plus the expected *return* from all of the subsequent actions that the agent will take as it moves between states if it continues to follow the policy π .

Given that it is the policy, π , that determines which action an agent will take in a given state, it is reasonable to assume that if an agent follows different policies, then the agent can expect to earn different levels of return —some higher and some lower. It can be shown, however, that for any MDP an optimal policy, π^* , exists, where following π^* will lead to returns as good as or better than the returns that would be earned following any other policy. Using this idea and Equation (11.19)^[652] the **Bellman optimality equation** for action-value functions can be written

$$Q_*(s_t, a_t) = \sum_{s_{t+1}} P(s_t \xrightarrow{a_t} s_{t+1}) \left[R(s_t \xrightarrow{a_t} s_{t+1}) + \gamma \max_{a_{t+1}} Q_*(s_{t+1}, a_{t+1}) \right] \quad (11.21)$$

which states that the maximum cumulative return following an action a_t taken in a state s_t is earned by continuing to take the action that will return the maximum return. The Bellman optimality equation for action-value functions can be used to establish a non-linear series of simultaneous equations (one for each pair of states and actions, (s_t, a_t)) which, if solved, will give the true values of $Q_*(s_t, a_t)$ for all states and actions. After these values have been found, a simple policy that gives a zero probability to any

action that does not give the maximum return available from a state and a non-zero probability to any action (there might be more than one) that does lead to the maximum return available from that state is an optimal policy to use with any MDP. Directly solving the large series of simultaneous equations that arise from the Bellman optimality equation for MDPs of interesting scale, however, is computationally very expensive and requires full knowledge of the dynamics of an MDP for a given scenario that can be unavailable in practice. In the **optimal control domain** in which the Bellman optimality equations were originally conceived, solutions are calculated using **dynamic programming**. In modern reinforcement learning, however, iterative approaches that calculate approximate solutions are typically used. The next section describes one of the most important of these, **temporal-difference learning**.

11.2.5 Temporal-Difference Learning

Temporal-difference learning is a simple, iterative, tabular approach to learning the action-value function, $Q_\pi(s_t, a_t)$, that is quite effective. We say that temporal-difference learning is tabular because an **action-value table** is used to store estimates of the expected return from taking each available action, a_t , in each possible state, s_t —the value of $Q_\pi(s_t, a_t)$. Recall that the expected return is the cumulative reward that the agent expects to receive if it takes action a_t in state s_t and then follows the policy π all the way to the end of the episode. All entries in the action-value table are first initialized to random values (or sometimes zeros). [Table 11.2](#)^[654] shows an example action-value table for the TwentyTwos playing agent discussed in Section 11.2.3^[643]. Note that there is an entry for each action-state combination and that the terminal states always have a value of 0.000 for every action.

Table 11.2

An action-value table for an agent trained to play the card game TwentyTwos (the simplified version of Blackjack described in Section 11.2.3^[643]).

State	Action	Value	State	Action	Value	State	Action	Value
PL-DL	<i>Twist</i>	0.039	PH-DL	<i>Twist</i>	-0.666	PM-DH	<i>Twist</i>	-0.668
PL-DL	<i>Stick</i>	-0.623	PH-DL	<i>Stick</i>	0.940	PM-DH	<i>Stick</i>	-0.852
PM-DL	<i>Twist</i>	-0.597	PL-DH	<i>Twist</i>	-0.159	PH-DH	<i>Twist</i>	-0.883
PM-DL	<i>Stick</i>	-0.574	PL-DH	<i>Stick</i>	-0.379	PH-DH	<i>Stick</i>	0.391
BUST	<i>Twist</i>	0.000	TIE	<i>Twist</i>	0.000	WIN	<i>Twist</i>	0.000
BUST	<i>Stick</i>	0.000	TIE	<i>Stick</i>	0.000	WIN	<i>Stick</i>	0.000
LOSE	<i>Twist</i>	0.000				TWENTYTWO	<i>Twist</i>	0.000
LOSE	<i>Stick</i>	0.000				TWENTYTWO	<i>Stick</i>	0.000

The goal in temporal-difference learning is to find the true values for each entry in this table, and this is achieved by deploying the agent into the environment and updating the values in the table on the basis of the performance of the agent. Over time, we can expect the table to converge toward optimal values. In temporal-difference learning, the relevant value in the table is updated after each action that the agent takes. When an agent in state s_t takes action a_t , the difference between the current estimated return in the action-value table for that action in that state, $Q_\pi(s_t, a_t)$, and the actual return received after taking the action is calculated. On the basis of this difference, the estimate for the action-value entry $Q_\pi(s_t, a_t)$ is updated slightly. If the current estimate is higher than the actual return, then the estimate is lowered slightly, and vice versa. A **learning rate** is used to control the size of the changes that are made to the action-value estimates at each iteration. We can write this action-value table update rule

$$Q_\pi(s_t, a_t) \leftarrow Q_\pi(s_t, a_t) + \alpha \underbrace{(G(s_t, a_t) - Q_\pi(s_t, a_t))}_{\text{difference between actual and expected returns}} \quad (11.22)$$

where $G(s_t, a_t)$ is the actual return received from the point of taking action a_t to the end of the episode. By repeatedly applying this update rule, the values in the action-value table slowly converge to good estimates of their true values.¹⁵

Careful readers might note a contradiction in the paragraph above, however. Equation (11.22)^[655] states that the action-value table is updated

using the actual return received by an agent across a full episode, whereas we also said that this update takes place after every action. It is not possible to know the actual return that will be earned by the agent across the entire episode until the episode is complete, and so it would not be possible to apply this update rule after early actions in the episode. To overcome this contradiction temporal-difference learning uses an approach known as **bootstrapping**. Bootstrapping uses the existing estimates of expected returns in the action-value table to make action-value table updates rather than waiting for an episode to finish to discover what the actual return is.

We can see bootstrapping quite clearly in the definition of the actual temporal-difference learning update rule

$$Q_{\pi}(s_t, a_t) \leftarrow Q_{\pi}(s_t, a_t) + \alpha \underbrace{(r_t + \gamma Q_{\pi}(s_{t+1}, a_{t+1}))}_{\text{actual return}} - \underbrace{Q_{\pi}(s_t, a_t)}_{\text{expected return}} \quad (11.23)$$

Rather than waiting for the episode to complete to find out the actual return of taking action a_t in state s_t , the update rule uses the current estimate of the expected return, $Q_{\pi}(s_{t+1}, a_{t+1})$. This formulation of temporal-difference learning that performs an action-value table update after every action is known as **TD(0)**. As TD(0) updates an entry in the action-value table every time an action has been taken, it has the advantage that an agent can start to learn very quickly; however, this approach can take a long time to converge toward the optimal values in the action-value table.¹⁶

To allow learning to take place in temporal-difference learning, we need to revisit the idea of a policy, and use policies that allow a balance of **exploration** and **exploitation**. To help illustrate this, imagine Conor has gone to a small **Gaeltacht** town in Ireland on a two-week business trip. In Gaeltacht towns people speak the native Irish language rather than English (spoken in the rest of the country). It is important for Conor to have a good meal each evening so that he is ready for work again the next day, and he is worried about getting things he doesn't like in the hotel restaurant. Unfortunately, Conor doesn't speak any Irish and the staff in the hotel restaurant don't speak any English. Conor does, however, recognize the Irish word for chicken, *sicín*, on the hotel restaurant menu, and he does like chicken. The menu is quite simple, displaying only five words: *sicín*,

mairteoil, muiceoil, muisiriún, and bradán. So what would be a reasonable policy for Conor to use to order his dinner each evening?

Conor could take the approach of always pointing to *sicín* on the menu, as he knows what this is and he likes chicken. This is an example of a **greedy action selection policy**. Conor knows the expected reward for ordering chicken is high compared with the expected reward for ordering the other unknown items (which he assumes to be low), and so this policy will return a consistently high reward. A greedy policy **exploits** current knowledge of the rewards that actions are expected to return. Following this policy will lead to the best outcomes on the basis of current knowledge, but does not allow any opportunities for learning. Perhaps one of the other items on the menu is even better than chicken, but following a greedy policy will never allow Conor the opportunity to learn this.

Learning requires an opportunity to **explore** as well as to exploit. To ensure maximum exploration Conor could randomly pick one of the menu items each evening. This would allow him to sample every item and update his knowledge about what he likes and what he doesn't like. Sometimes Conor would be very happy with his choices (his reward would be high), but sometimes he would be disappointed (his reward would be low). While this **random action selection policy** is good for learning, pursuing it into the second week of Conor's stay would seem like a bad idea. He would have no opportunity to exploit the knowledge he established in the first week about the rewards associated with ordering different items.

Instead, the best policy for Conor to take for learning is to balance exploration and exploitation. Some days Conor should order the item he knows he likes best, and some days he should choose something new. This will allow Conor to make good choices based on his current knowledge, but also to explore new items and learn about the rewards associated with them. The ϵ -**greedy action selection policy** is a simple action selection policy that balances exploration and exploitation. When an ϵ -greedy policy is used, an agent chooses the best action most of the time, but occasionally—with a probability of ϵ —selects a random action uniformly from those available. So, if on alternate evenings Conor swapped between choosing his favorite menu item and choosing a menu item at random ($\epsilon = 0.5$), by the end of the two weeks he will have enjoyed a whole selection of meals from the hotel restaurant's dishes of *chicken, beef, pork, mushrooms, and salmon*.¹⁷

In reinforcement learning scenarios where episodes involve long sequences of actions, balancing exploration and exploitation is even more important. Agents need to make sequences of good decisions in order to get the opportunity to explore deeper into action sequences and so need to exploit before exploring in some episodes. For example, if a chess-playing agent never took good early moves, the agent would never have a chance to learn how to behave in potentially game-winning situations. In talking about reinforcement learning policies, it is worthwhile to distinguish between a **behavior policy** that an agent uses during learning and a **target policy** that an agent will use when deployed into the world after learning has taken place. After deployment it can often make sense to restrict an agent to greedy action selection and allow no further exploration. This will ensure that the agent never takes potentially dangerous random actions but limits the ability of an agent to continue to learn after being deployed, which could be useful if aspects of the environment changed over time.¹⁸

One final thing worth noting is that temporal-difference learning is **model-free**. The agent does not need to know anything about the dynamics of the environment in which it is acting. The only knowledge an agent using temporal-difference learning requires is a list of states that exist in the environment, a way to recognize what state it is in, and a list of the actions that it is possible for the agent to take. With this minimal information temporal-difference learning can be used to learn sophisticated, long-term behaviors. Note especially that we do not need to know the full dynamics of an MDP, in particular the state transition probabilities that are captured in a transition matrix. This is useful because often in real-life applications it can be difficult to capture these values.

In the next section we combine the ideas of temporal-difference learning and a specific behavior policy to define the standard approach to reinforcement learning: **Q-learning**.

11.3 Standard Approach: Q-Learning, Off-Policy Temporal-Difference Learning

Algorithm 13^[658] shows the algorithm for the **Q-learning** approach to temporal-difference learning. In this approach an agent is deployed into the world and acts sequentially, observing the state of the world and taking actions that move it to new states and generate reward. This algorithm

assumes an episodic scenario in which the agent will repeat multiple episodes of the task that it is performing (for example, multiple iterations of a game or attempts to navigate an environment). During learning, after completing an episode the agent will return to the initial state and start again. This will repeat for some pre-specified number of episodes after which the expectation is that the agent will have learned to perform the task well. The ϵ -greedy policy is often used together with Q-learning for choosing actions that balance exploration and exploitation and will be used in this section.¹⁹

Algorithm 13 Pseudocode description of the Q-learning algorithm for off-policy temporal-difference learning.

Require: a behavior policy, π , that chooses actions
Require: an action-value function Q that performs a lookup into an action-value table with entries for every possible action, a , and state, s
Require: a learning rate, α , a discount-rate, γ , and a number of episodes to perform

- 1: initialize all entries in the action-value table to random values (except for terminal states which receive a value of 0)
- 2: **for** each episode **do**
- 3: reset s_t to the initial agent state
- 4: **repeat**
- 5: select an action, a_t , based on policy, π , current state, s_t , and action-value function, Q
- 6: take action a_t observing reward, r_t , and new state s_{t+1}
- 7: update the record in the action-value table for the action, a_t , just taken in the last state, s_t , using:
$$Q(s_t, a_t) \leftarrow Q(s_t, a_t) + \alpha \left(r_t + \gamma \max_{a_{t+1}} Q(s_{t+1}, a_{t+1}) - Q(s_t, a_t) \right) \quad (11.24)$$
- 8: let $s_t = s_{t+1}$
- 9: **until** agent reaches a terminal state
- 10: **end for**

The learning in Q-learning takes place when an entry in the action-value table is updated after an action has taken place using Equation (13)^[658] at Line 13.²⁰ The intuition behind this update is that the value of taking a

specific action in a specific state, $Q(s_t, a_t)$, should increase if that action leads to an immediate positive reward and/or it takes the agent to a state from which the agent can expect to receive a positive future return. The value of taking the action in the state should decrease if the reward and/or future return are negative.

Q-learning is referred to as **off-policy** learning, as when the update to the value function is made the **behavior policy** (for example, ϵ -greedy action selection) to select the action used to calculate the expected future return. Rather, the agent uses a greedy policy—it is assumed that the agent will always take the best possible next action (based on the current action-value table). This leads Q-learning to be optimistic about what will happen in the future.

The values in [Table 11.2](#)^[654] actually show the entries in the action-value table learned for TwentyTwos after 100,000 episodes of Q-learning.²¹ Examining the actions with the maximum expected return in each state shows that the target policy learned is overwhelmingly to *Stick*, with *Twist* being the best action only in the PL-DL, PL-DH, and PM-DH states. Even with this cautious strategy, in an evaluation in which an agent plays a bout of 1,000 hands of TwentyTwos 100,000 times, this player will on average earn a profit of $\$198 \pm 24$ in 1,000 hands. This compares favorably to a random player that will expect to lose on average $\$197 \pm 25$ out of 1,000 hands. Given that the agent started with no knowledge of the game and has learned playing strategy through maximization of cumulative reward alone in a simple state space, this is pretty impressive.²²

11.3.1 A Worked Example

Grid worlds have long been used as a good way to illustrate the operation of reinforcement learning algorithms, and we will use this type of example in this section. In a grid world scenario an agent must learn to navigate an environment from a start position to a goal position, often avoiding obstacles along the way. A grid world environment is defined by a rectangular grid in which an agent occupies a single cell and can move horizontally or vertically, one cell at a time, across the world. The agent has no map of the environment and begins with knowledge only of the actions that can be taken—*left*, *right*, *up*, or *down*—and its current state. The state representation is simple, with each cell that an agent can occupy in the grid

world defining a state. Grid worlds are an excellent environment in which to study reinforcement learning because, as we will see, it is easy to examine how the action-value table evolves over time.

[Figure 11.4](#)^[660] shows a grid world in which an agent must traverse an environment fraught with dangers. The starting position is shown marked with an S and the goal position is marked with a G . The cells marked with an f represent fiery ground that will damage the agent if it is crossed. The agent's task is to navigate the environment from the start state to the goal state as quickly as possible while avoiding damage from fiery ground. To achieve this a reward structure has been designed. The reward for moving between any two normal cells is -1 , the reward for arriving at the goal is 50 , and the reward for entering a fiery cell is -20 . The agent always starts in the start cell marked with an S . To demonstrate the workings of the Q-learning algorithm, we examine the process of using it to train an agent to navigate this environment. In this example the ϵ -greedy policy with $\epsilon = 0.1$ is used throughout, and the hyper-parameters α and γ are set to $\alpha = 0.2$ and $\gamma = 0.9$.²³

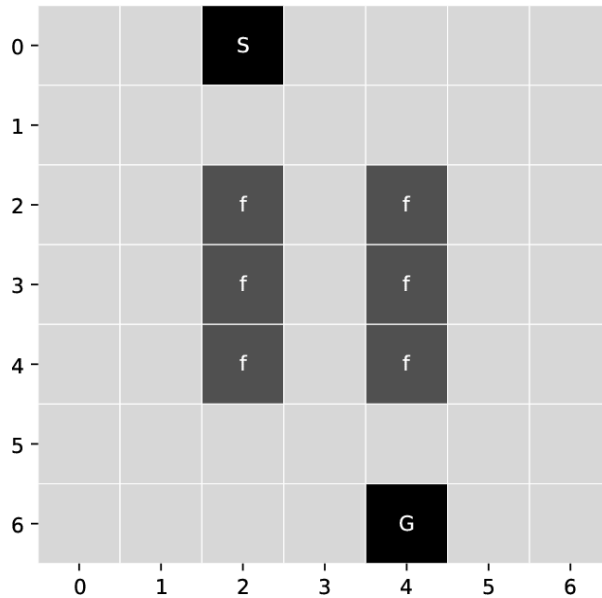


Figure 11.4

A simple grid world. The start position is annotated with an S and the goal with a G . The squares marked f denote fire, which is very damaging to an agent.

The Q-learning algorithm (Algorithm 13^[658]) starts by randomly initializing the action-value table (Line 13^[658]). In this example all entries

have been initialized to random numbers in $[-1,1]$. There are 196 entries in the full action-value table—one for each of the four actions that can be taken in each of the 49 states that make up the grid world. [Table 11.3](#)^[661] shows a portion of the action-value table.

Table 11.3

A portion of the action-value table for the grid world example at its first initialization.

State	Action	Value	State	Action	Value	State	Action	Value
0-0	<i>up</i>	0.933		
0-0	<i>down</i>	-0.119	2-0	<i>left</i>	-0.691	6-2	<i>right</i>	0.201
0-0	<i>left</i>	-0.985	2-0	<i>right</i>	0.668	6-3	<i>up</i>	-0.588
0-0	<i>right</i>	0.822	2-1	<i>up</i>	-0.918	6-3	<i>down</i>	0.038
0-1	<i>up</i>	0.879	2-1	<i>down</i>	-0.228	6-3	<i>left</i>	0.859
0-1	<i>down</i>	0.164	2-1	<i>left</i>	-0.301	6-3	<i>right</i>	-0.085
0-1	<i>left</i>	0.343	2-1	<i>right</i>	-0.317	6-4	<i>up</i>	0.000
0-1	<i>right</i>	-0.832	2-2	<i>up</i>	0.633	6-4	<i>down</i>	0.000
0-2	<i>up</i>	0.223	2-2	<i>down</i>	-0.048	6-4	<i>left</i>	0.000
0-2	<i>down</i>	0.582	2-2	<i>left</i>	0.566	6-4	<i>right</i>	0.000
0-2	<i>left</i>	0.672	2-2	<i>right</i>	-0.058	6-5	<i>up</i>	0.321
0-2	<i>right</i>	0.084	2-3	<i>up</i>	0.635	6-5	<i>down</i>	-0.793
0-3	<i>up</i>	-0.308	2-3	<i>down</i>	0.763	6-5	<i>left</i>	-0.267
0-3	<i>down</i>	0.247	2-3	<i>left</i>	-0.121	6-5	<i>right</i>	0.588
0-3	<i>left</i>	0.963	2-3	<i>right</i>	0.562	6-6	<i>up</i>	-0.870
0-3	<i>right</i>	0.455	2-4	<i>up</i>	0.629	6-6	<i>down</i>	-0.720
0-4	<i>up</i>	-0.634	2-4	<i>down</i>	-0.409	6-6	<i>left</i>	0.811
		6-6	<i>right</i>	0.176

At the beginning of the first episode of the Q-learning process (Line 13^[658]), the agent is placed in the starting cell in the grid world ($s_0 = 0-3$). From [Table 11.3](#)^[661] we can see the Q values of the actions available to the agent from the starting state: $Q(0-3, \text{up}) = -0.308$, $Q(0-3, \text{down}) = 0.247$, $Q(0-3, \text{left}) = 0.963$, and $Q(0-3, \text{right}) = 0.455$. The *left* action is the most attractive in this instance on the basis of its Q value. The agent chooses the next action to take, however, using its policy (Line 13^[658]), in this case ε -greedy with $\varepsilon = 0.1$. Following the ε -greedy policy, the agent generates a random number (uniformly from $[0,1]$) of 0.634, which is greater than ε , and the agent uses greedy action selection and chooses $a_0 = \text{left}$. The agent

performs this action (Line 13^[658]), moving to the left, and records the next state, $s_1 = 0\text{-}2$, and the reward received, $r_0 = -1$.

On the basis of the action it has taken, the agent now makes an update to $Q(0\text{-}3, \text{left})$ (Line 13^[658]) using Equation (13)^[658]. The Q values of the actions available to the agent from state 0-2 are $Q(0\text{-}2, \text{up}) = 0.223$, $Q(0\text{-}2, \text{down}) = 0.582$, $Q(0\text{-}2, \text{left}) = 0.672$, and $Q(0\text{-}2, \text{right}) = 0.084$ (based on [Table 11.3](#)^[661]). The action with the highest Q value from state 0-2 is therefore *left* and this is the one used in the update equation. It is this selection of the best action, rather than one selected using the behavior policy, that makes Q-learning an *off-policy* approach. Equation (13)^[658] is used to perform the update as follows:

$$\begin{aligned} Q(0\text{-}3, \text{left}) &\leftarrow Q(0\text{-}3, \text{left}) + \alpha \times (R(0\text{-}3, \text{left}) + \gamma \times Q(0\text{-}2, \text{left}) - Q(0\text{-}3, \text{left})) \\ &0.963 + 0.2 \times (-1 + 0.9 \times 0.672 - 0.963) \\ &0.691 \end{aligned}$$

As the experience of moving left from state 0-3 to state 0-2 has not led to a large positive reward or opened up the potential for a new action that will give significant positive return, the value of this action in this state has been reduced. The agent then updates its current state (Line 13^[658]), $s_0 = s_1 = 0\text{-}2$, and returns to the beginning of the algorithm to choose the next action according to the policy. Again, following the ϵ -greedy policy a random number is generated, 0.073, which this time is below ϵ , and so a random action from those available from state 0-2 is selected. The random action selected in this case is *down*. Note that this action is different from the action used in the update equation previously (*left*). This is because the action is now selected using the ϵ -greedy policy, whereas the action used during the update was selected *off-policy*.

The agent then continues to move across the environment making sequential updates to the action-value table until eventually it reaches the goal state after making 150 moves and accumulating a total reward of -891 . [Figure 11.5\(a\)](#)^[663] shows a representation of the action-value table after this first episode. A grid for each action (*up*, *down*, *left*, and *right*) is shown where the shading in the grid illustrates the current estimate of the expected return of that action in the state corresponding to the grid cell position (darker shading indicates higher expected return with lighter shading indicating lower expected return).

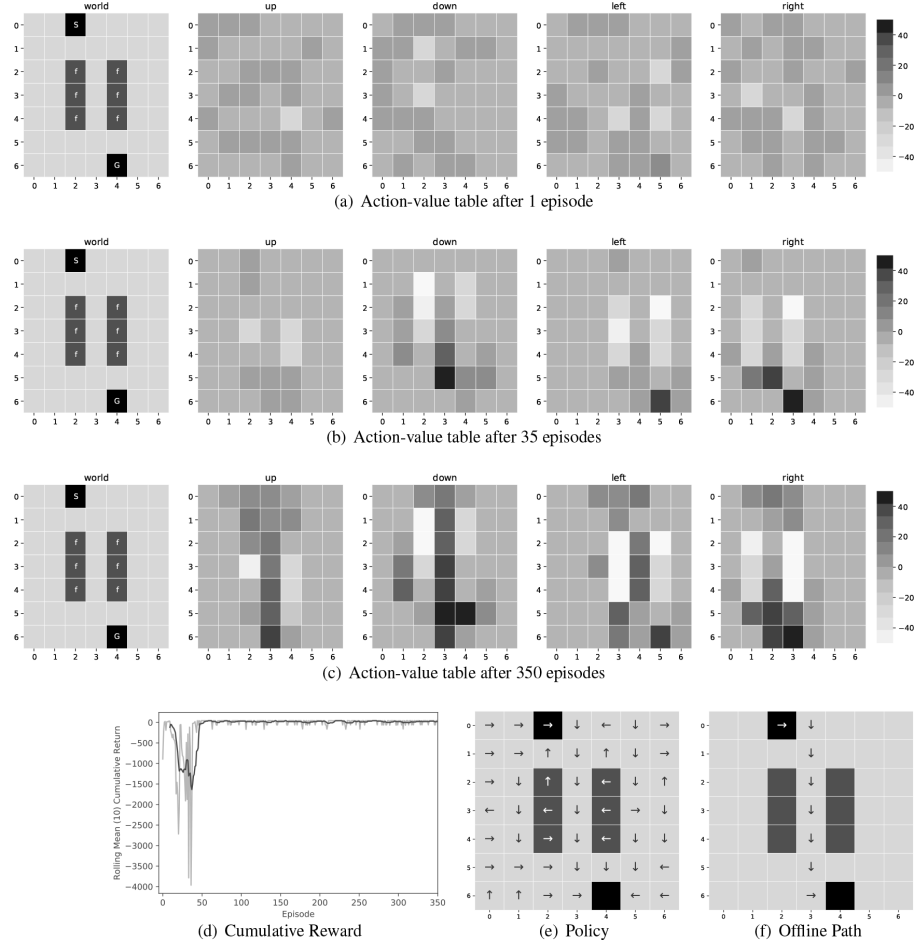


Figure 11.5

(a)–(c) The evolution of the entries in the action-value table over episodes of Q-learning off-policy temporal-difference learning across the grid world. (d) The cumulative reward earned from each episode. (e) An illustration of the target policy learned by the agent after 350 episodes. The arrows show the direction with the highest entry in the action-value table for each state. (f) The path the agent will take from the start state to the goal state when greedily following the target policy.

The action-value table is still fairly sparse after the first iteration with most combinations having changed little from their randomly initialized values. There are a couple of interesting things that are evident, however. At the end of the first episode the agent reached the goal cell, state 6-4, by moving *left* from state 6-5. This led to a large positive reward of 50. Before this action $Q(6\text{-}5, \text{left})$ gave an expected return from the action-value table of -0.267 . Following this action it was updated as follows:

$$\begin{aligned}
 Q(6\text{-}5, \text{left}) &\leftarrow Q(6\text{-}5, \text{left}) + \alpha \times (R(6\text{-}5, \text{left}) + \gamma \times Q(6\text{-}4, \text{up}) - Q(6\text{-}5, \text{left})) \\
 &\quad -0.267 + 0.2 \times (50 + 0.9 \times 0 - -0.267) \\
 &= 9.786
 \end{aligned}$$

This value can be seen in the dark shading of the cell corresponding to state 6-5 in the *right* grid in [Figure 11.5\(a\)](#)^[663]. There are also some very lightly shaded cells in [Figure 11.5\(a\)](#)^[663]—for example, cell 1-2 in the *down* panel —illustrating large negative values resulting from trips into the fiery cells and subsequent negative reward.

The reason that only the states immediately surrounding those that led to large positive or negative rewards reflect these rewards is that Q-learning, and temporal-difference learning in general, uses **bootstrapping** and updates Q values immediately after actions rather than waiting until the end of an episode. So the large positive reward achieved when moving to the terminal state can only impact the Q value of the state that immediately preceded it. As learning continues, however, values start to propagate across the states in the environment on subsequent episodes. This is clear in the visualization of the action-value table after 35 episodes of Q-learning have elapsed that is shown in [Figure 11.5\(b\)](#)^[663]. We can see here that the large positive Q values from actions taken in states near the goal state have started to propagate through the environment, although there are not yet large positive values near the start state. The emergence of knowledge about how to traverse the environment is also reflected in the fact that the cumulative reward earned by the agent at episode 35 is -115 based on a journey taking 50 actions.

[Figure 11.5\(d\)](#)^[663] shows the total cumulative reward (or return) earned by the agent for each of 350 learning episodes that the agent performs in this grid world environment (to make it easier to see the overall trend in this graph a rolling mean across 10 episodes is shown). This graph shows that the agent's performance initially declined, and it started to perform quite badly, until after about 40 episodes its performance began to improve. Performance then became stable with a return of about 40 after the agent learned a useful path through the environment. [Figure 11.5\(c\)](#)^[663] visualizes the action-value table after 350 episodes have elapsed. By this time a clear optimal route through the graph has emerged running straight down from the top to the bottom, and we can say that the agent has learned to perform the navigation task. [Table 11.4](#)^[665] shows the same portion of the action-value table shown in [Table 11.3](#)^[661] after the final episode has completed. Extracting the action with the highest Q value in each state from the action-value table gives the greedy **target policy** that the agent, now trained to

complete the task, would use after deployment. This is shown in [Figure 11.5\(e\)](#)^[663]. The path that the agent would take from the start state to the goal state following this policy is shown in [Figure 11.5\(f\)](#)^[663].

Table 11.4

A portion of the action-value table for the grid world example after 350 episodes of Q-learning have elapsed.

State	Action	Value	State	Action	Value	State	Action	Value
0-0	<i>up</i>	-1.627		
0-0	<i>down</i>	-1.255	2-0	<i>left</i>	-1.583	6-2	<i>right</i>	40.190
0-0	<i>left</i>	-1.655	2-0	<i>right</i>	-1.217	6-3	<i>up</i>	34.375
0-0	<i>right</i>	-1.000	2-1	<i>up</i>	-1.493	6-3	<i>down</i>	40.206
0-1	<i>up</i>	1.302	2-1	<i>down</i>	4.132	6-3	<i>left</i>	24.784
0-1	<i>down</i>	-1.900	2-1	<i>left</i>	-1.643	6-3	<i>right</i>	50.000
0-1	<i>left</i>	-1.900	2-1	<i>right</i>	-36.301	6-4	<i>up</i>	0.000
0-1	<i>right</i>	15.173	2-2	<i>up</i>	13.247	6-4	<i>down</i>	0.000
0-2	<i>up</i>	13.299	2-2	<i>down</i>	-46.862	6-4	<i>left</i>	0.000
0-2	<i>down</i>	12.009	2-2	<i>left</i>	-0.858	6-4	<i>right</i>	0.000
0-2	<i>left</i>	8.858	2-2	<i>right</i>	-1.157	6-5	<i>up</i>	-0.353
0-2	<i>right</i>	18.698	2-3	<i>up</i>	16.973	6-5	<i>down</i>	-0.793
0-3	<i>up</i>	13.921	2-3	<i>down</i>	29.366	6-5	<i>left</i>	36.823
0-3	<i>down</i>	21.886	2-3	<i>left</i>	-88.492	6-5	<i>right</i>	-0.342
0-3	<i>left</i>	15.900	2-3	<i>right</i>	-77.447	6-6	<i>up</i>	-0.870
0-3	<i>right</i>	13.846	2-4	<i>up</i>	-1.016	6-6	<i>down</i>	-0.720
0-4	<i>up</i>	1.637	2-4	<i>down</i>	-20.255	6-6	<i>left</i>	1.008
		6-6	<i>right</i>	-0.802

It is worth reflecting for a moment that the agent has learned to navigate this grid world without any knowledge of the overall structure of the environment or indication about what it should do. Rather, the agent—equipped with only knowledge of the states in the world and the actions that it can take—was able to learn a long-term strategy to complete a somewhat sophisticated task using only the instantaneous rewards that is received for each move that it made.

11.4 Extensions and Variations

In this section we cover two important extensions to the temporal-difference learning approach introduced in the previous section. The first is the

SARSA on-policy modification to temporal-difference learning. The second is an extension that uses a predictive machine learning model to replace the action-value table to accommodate environments in which the state-action space is too large for tabular methods to work. Specifically we present the **deep Q network** (DQN) algorithm.

11.4.1 SARSA, On-Policy Temporal-Difference Learning

The Q -learning algorithm discussed in Section 11.3^[657] is referred to as *off-policy* as the **behavior policy** is not used to select the action to be taken in the next state when Q values are updated (a greedy target policy is used instead). *On-policy* temporal-difference learning is an alternative in which the behavior policy is used to select the next action at the update step. **SARSA**²⁴ is the most well-known on-policy temporal-difference learning algorithm, and is described in Algorithm 14^[666]. This algorithm is very similar to the Q -learning algorithm in Algorithm 13^[658]. The main difference is in the Q value update step, where the next action to be taken, a_{t+1} , from the new state, s_{t+1} , is chosen using the behavior policy (Line 14^[666]) and then used in updating the value of $Q(s_t, a_t)$ (Line 14^[666]). This is in contrast to Q -learning, which always assumes the action with the highest expected return will be chosen when computing the update. If an ε -greedy behavior policy (or any other similar behavior policy that encourages exploration) is used, then occasionally random actions rather than the best action will be used in this step.

Algorithm 14 Pseudocode description of the **SARSA** algorithm for on-policy temporal-difference learning.

Require: a behavior policy, π , that chooses actions
Require: an action-value function Q that performs a lookup into an action-value table with entries for every possible action, a , and state, s
Require: a learning rate, α , a discount-rate, γ , and a number of episodes to perform

- 1: initialize all entries in the action-value table to random values (except for terminal states which receive a value of 0)
- 2: **for** each episode **do**
- 3: reset s_t to the initial agent state
- 4: select an action, a_t , based on policy, π , current state, s_t , and action-value function, Q
- 5: **repeat**
- 6: take action a_t observing reward, r_t , and new state, s_{t+1}
- 7: select the next action, a_{t+1} , based on policy, π , new state, s_{t+1} , and action-value function, Q
- 8: update the record in the action-value table for the action, a_t , just taken in the last state, s_t , using:
$$Q(s_t, a_t) \leftarrow Q(s_t, a_t) + \alpha(r_t + \gamma Q(s_{t+1}, a_{t+1}) - Q(s_t, a_t))$$
- 9: let $s_t = s_{t+1}$ and $a_t = a_{t+1}$
- 10: **until** agent reaches terminal state
- 11: **end for**

The differences between SARSA and Q -learning can be illustrated by examining the behavior of a SARSA agent in the same grid world environment used in Section 11.3.1^[659] (we assume the same sequence of random numbers are generated for easy comparison). The algorithm starts by initializing the Q values for every action in every state to the same values used before, shown in Table 11.3^[661]. At Line 14^[666] the agent selects the first action²⁵ using the ϵ -greedy policy. Assuming that the agent generates the same random number as before (0.634), which is greater than ϵ , greedy action selection will be used and, again, $a_0 = \text{left}$ will be chosen as it has the highest Q value for the start state, 0-3. After taking this action (Line 14^[666]) and recording the reward, $r_0 = -1$, and next state, $s_1 = 0\text{-}2$, the

behavior policy is used to select the next action that the agent will take (Line 14^[666]). Assuming again that the same random number as before (0.0728) that is less than ϵ is generated, random action selection will be used and $a_1 = \text{down}$ will again be selected. Now, when updating the value for $Q(0\text{-}3, \text{left})$, the Q value for this action, *down*, from the next state is used rather than the Q value for the best possible action, *left*, that was used in Q -learning. So, $Q(0\text{-}3, \text{left})$ is updated to:

$$\begin{aligned} Q(0\text{-}3, \text{left}) &\leftarrow Q(0\text{-}3, \text{left}) + \alpha \times (R(0\text{-}3, \text{left}) + \gamma \times Q(0\text{-}2, \text{down}) - Q(0\text{-}3, \text{left})) \\ &0.963 + 0.2 \times (-1 + 0.9 \times 0.582 - 0.963) \\ &0.675 \end{aligned}$$

The value calculated is not terribly different from the value calculated before. Cumulatively, however, these differences will lead to quite different behavior. Agents trained using SARSA tend to learn more conservative strategies than agents trained using Q -learning. Since agents using SARSA use a policy with some exploration in their action-value table update equation, they will often base their estimation of expected return on next actions with quite poor return. This is evident in [Figure 11.6](#)^[667], which shows a visualization of the final action-value table learned by an agent training using SARSA for the grid world. Here we see that the SARSA agent favors staying away from any possibility of falling into one of the dangerous cells rather than taking the more direct route.

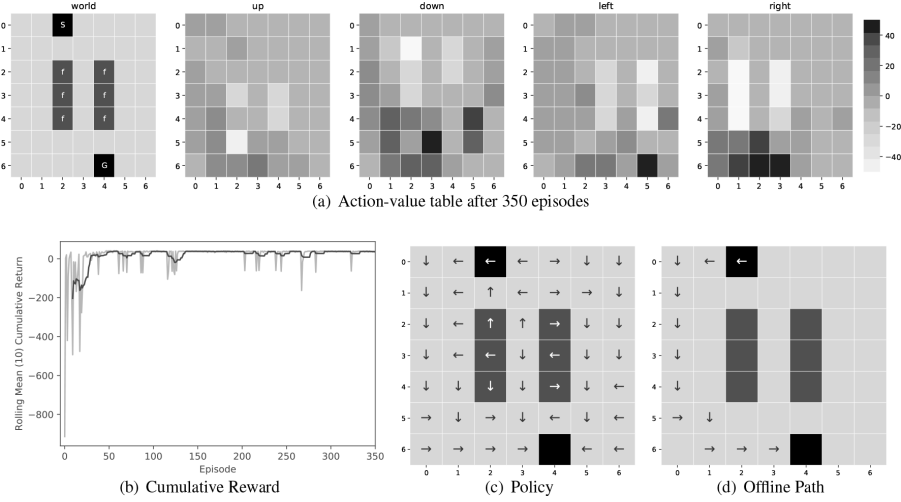


Figure 11.6

(a) A visualization of the final action-value table for an agent trained using SARSA on-policy temporal-difference learning across the grid world after 350 episodes. (b) The cumulative reward earned from each episode. (c) An illustration of the target policy learned by the agent after 350 episodes. The arrows show the direction with the highest entry in the action-value table for each state. (d) The path the agent will take from the start state to the goal state when greedily following the target policy.

This preference for caution is often the reason for choosing between SARSA and Q-Learning (although this can also be managed through careful design of rewards). On top of a preference for caution in a final target policy, if training is being undertaken in the real world with potentially expensive equipment, SARSA might be favored over Q-Learning. There is more likelihood of Q-Learning choosing actions that do damage to equipment as random action selections made by a behavior policy coupled with a target policy favoring risky states could lead to the occasional disaster.

11.4.2 Deep Q Networks

In many environments to which we would like to apply reinforcement learning, it becomes difficult to define a state representation that captures the nuances of the environment and does not lead to so many states as to become impossible to use with the tabular approaches described so far. Consider, for example, the version of the classic **Lunar Lander** video game shown in Figure 11.7^{[669], 26}. In this game the player must land the spacecraft on the Moon's surface without damaging it. The player has just three controls: thrusters that turn the spacecraft left and right, and one that

pushes it up. An episode involves an attempt to land the spaceship from a position at the top of the screen and ends when either the spaceship successfully touches down gently on the landing pad or crashes.

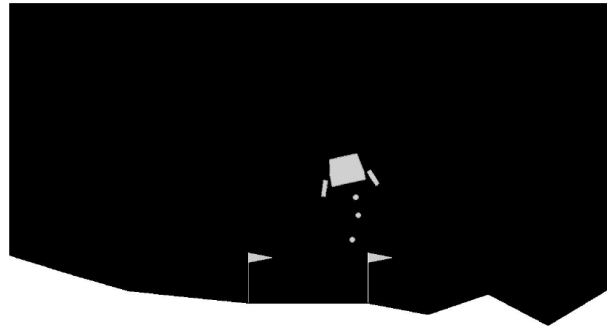


Figure 11.7

The Lunar Lander environment. The aim of the game is to control the spaceship starting from the top of the world and attempting to land on the landing pad.

Just about any state representation we could design that would accurately capture the dynamics of this game would result in an action-value table with thousands or hundreds of thousands of entries. For example, we could represent state using a vector storing the position of the spaceship (in x and y coordinates), the velocity of the spaceship (again in x and y directions), the angular velocity of the spaceship, the spaceship's altitude above the surface, and the slope of the line connecting the spaceship to the landing pad. Even if we discretized each of these 7 characteristics allowing just 5 levels (*very low*, *low*, *medium*, *high*, and *very high*), which would be a gross approximation, this would lead to $7^5 = 16,807$ possible states. Adding 4 possible actions (*left*, *right*, *up*, and *none*) to this would give an action-value table with 67,228 entries. Dealing with an action-value table of this scale is computationally troublesome, but more important, such a large state space would most likely mean that any training process would inevitably leave much of the action-value table unexplored.

For large problems like this, instead of implementing the action-value function, $Q_\pi(s_t, a_t)$, as a table storing the value of every action in every state, it would be better to learn a generalized version of the action-value function from observation of a small number of state and action pairs. Approaches that do this are referred to as **approximate methods**. Learning generalized functions from a small training dataset is exactly what predictive modeling

does, and we can use predictive models, trained using a combination of ideas from supervised machine learning and reinforcement learning, for this task! A predictive model can be trained to learn the action-value function

$$\mathbb{M}(s_t, a_t) \approx Q_\pi(s_t, a_t) \quad (11.25)$$

If a **neural network** (see Chapter 8^[381]) is used for this task (and that is what we will use in the approach described in this section), we can output the value of all actions in a given state at the same time across the output layer of a network. So, the problem is reframed

$$\mathbb{M}(s_t) \approx Q_\pi(s_t, a_t) \quad (11.26)$$

where for a given state the model outputs the value of the action-value function for every action that could be taken in that state. To simplify notation we refer to action-value functions implemented as predictive models as $Q_{\mathbb{M}}$. Figure 11.8^[669] illustrates this framing of the action-value function learning problem.

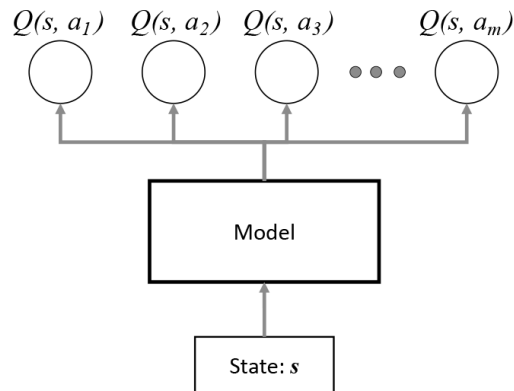


Figure 11.8
Framing the action-value function as a prediction problem.

Neural networks are a useful modeling approach to use for this prediction problem because, as long as a **loss function** can be formulated, we can use iterative approaches like the gradient descent algorithm²⁷ to train them. The link between temporal-difference learning and gradient descent was already made in Section 11.2.5^[654]. Temporal-difference learning is based on calculating the error between a predicted value for the expected

return from taking an action in a given state and the actual return that is earned when the agent takes that action (Equation (11.23)^[655]). We can use exactly this idea to define a loss function that can be used to train a neural network

$$\mathcal{L}(Q_{\mathbb{M}_W}(s_t)) = (t_i - Q_{\mathbb{M}_W}(s_t, a_t))^2 \quad (11.27)$$

$$= \left(r_t + \gamma \max_{a_{t+1}} Q_{\mathbb{M}_W}(s_{t+1}, a_{t+1}) - Q_{\mathbb{M}_W}(s_t, a_t) \right)^2 \quad (11.28)$$

where \mathbf{W} are the network weights; and t_i , the target feature value, is defined as the actual return earned from taking an action. We can calculate a gradient of this function

$$\frac{\partial \mathcal{L}(Q_{\mathbb{M}_W}(s_t, a_t))}{\partial \mathbf{W}} = \left(r_t + \gamma \max_{a_{t+1}} Q_{\mathbb{M}_W}(s_{t+1}, a_{t+1}) - Q_{\mathbb{M}_W}(s_t, a_t) \right) \frac{\partial Q_{\mathbb{M}_W}(s_t, a_t)}{\partial \mathbf{W}} \quad (11.29)$$

The naive approach to training a neural network using this loss function would be to use the backpropagation of error algorithm with stochastic gradient descent. This would mean that every time the agent took an action, a_t , to move from s_t to s_{t+1} , accumulating reward r_t , a loss would be calculated using Equation (11.27)^[670] and the gradient of this loss Equation (11.28)^[670] would be backpropagated through the network to update the weights. Algorithm 15^[671] outlines this naive approach.

In practice, unfortunately, this doesn't work, for a number of reasons. First, recall that when gradient descent was discussed, the instances in the training data were shuffled at the beginning of each epoch. Gradient-descent-like algorithms for training neural networks assume training instances are independent from each other. In this naive approach each instance presented to the network would be highly correlated with the previous instance presented (similar states would follow each other on the basis of actions taken) and independence would no longer be the case. This would make the training process likely to become stuck in something approaching a local minimum. The other problem is that the network being used to generate targets is the actual network being trained. This network is changing frequently during the training process, which can cause the

training to oscillate wildly. The **deep Q network** (DQN) algorithm addresses these issues using two key ideas: **experience replay** and **network freezing**.

Algorithm 15 Pseudocode description of the **naive neural Q-learning** algorithm.

```

1: initialize weights,  $\mathbf{W}$ , in action-value function network,  $Q_{\mathbb{M}}$ , to random values
2: for each episode do
3:   reset  $s_t$  to the initial agent state
4:   repeat
5:     select action,  $a_t$ , based on policy,  $\pi$ , the current state,  $s_t$ , and action-value net-
       work output,  $Q_{\mathbb{M}}(s_t, a_t)$ 
6:     take action  $a_t$  and observing reward,  $r_t$ , and new state,  $s_{t+1}$ 
7:     generate a target feature

$$t = r_t + \gamma \max_{a_{t+1}} Q_{\mathbb{M}}(s_{t+1}, a_{t+1})$$

8:     perform an iteration of stochastic gradient descent using a single training in-
       stance  $< s_t, t >$ 
9:   until agent reaches terminal state
10:  end for

```

When **experience replay** is used, each time an agent uses an action-value network $Q_{\mathbb{M}_w}$ to select and take an action, a_t , in a state, s_t , earning a reward, r_t , and moving the agent to a new state, s_{t+1} , an instance of the form $\langle s = s_t, a = a_t, r = r_t, s' = s_{t+1} \rangle$ is added to a **replay memory**, \mathcal{D} . After taking the action, instead of performing a single step of stochastic gradient descent, the agent randomly selects a random sample of b instances from the replay memory, and performs an iteration of **mini-batch gradient descent**²⁸ using this sample as the mini-batch. The target feature values for the instances in the mini-batch are generated as described in Algorithm 15^[671]. This means that the training process is using its experience of the environment much more efficiently because each step is used in network training multiple times. Furthermore, the correlations between instances are broken because mini-batches are randomly selected from the replay memory. The replay memory is given a maximum size, N (usually greater

than 10,000), and when it reaches this the oldest instances are dropped as new ones are added. [Figure 11.9](#)^[672] illustrates this process.

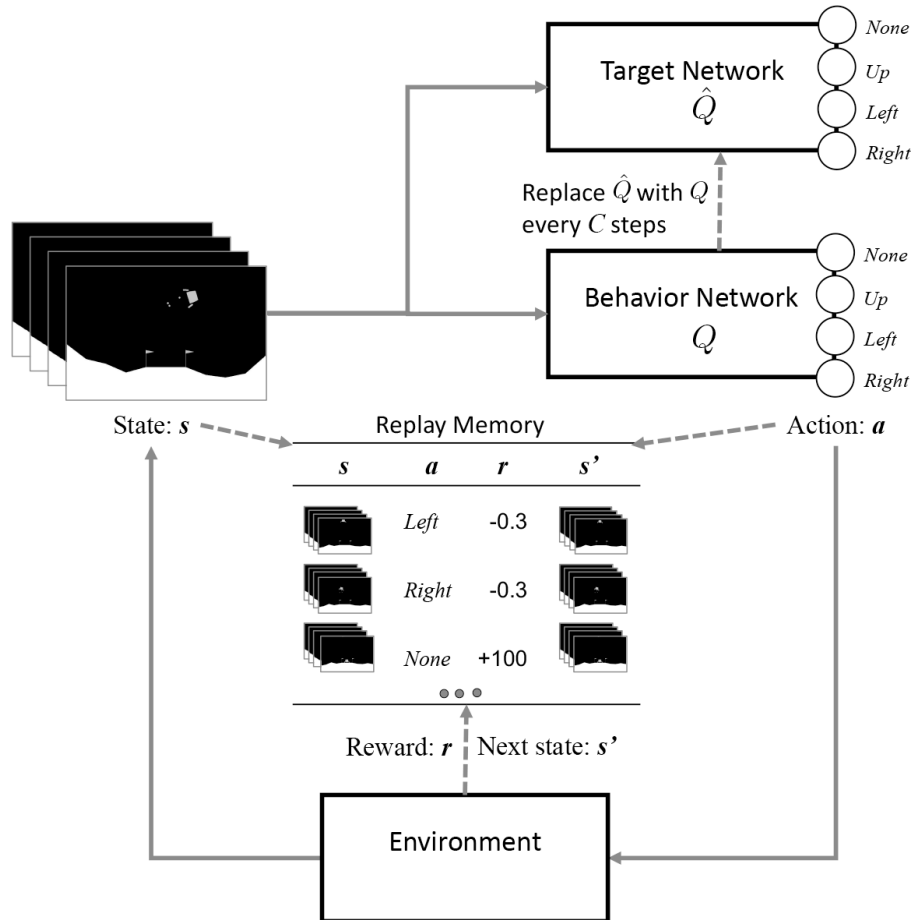


Figure 11.9

An illustration of the DQN algorithm including experience replay and target network freezing.

In the naive approach described in Algorithm 15^[671] the network being trained is also being used to generate target feature values (Line 15). This can cause the network training process to become unstable as small change in the outputs of the action-value network can lead to sudden changes in the policy as a different action is suddenly favored in a type of state. **Target network freezing** is used to address this. Two different networks are used in the training process: an **action-value behavior network** that is used to predict the values of actions for making decisions and an **action-value target network** that is used to predict the value of taking subsequent actions in subsequent states when generating target feature values. The action-value target network is *frozen* and not updated at each iteration of the

algorithm. It does, however, need to be updated occasionally because otherwise the estimated values used in the loss function will be inaccurate. Therefore, after every C steps the current action-value target network is replaced with a copy of the action-value behavior network. This is also illustrated in [Figure 11.9](#)^[672]. Target network freezing makes the training process more stable and leads to faster convergence. A pseudocode description of the deep Q network algorithm is given in [Algorithm 16](#)^[673].

Algorithm 16 Pseudocode description of the **deep Q network** (DQN) algorithm.

- 1: initialize replay memory \mathcal{D} with N steps based on random actions
 - 2: initialize weights, \mathbf{W} in behavior action-value function network, $Q_{\mathbb{M}}$, to random values
 - 3: initialize weights, $\widehat{\mathbf{W}}$ in target action-value function network, $\widehat{Q}_{\mathbb{M}}$ to \mathbf{W}
 - 4: **for** each episode **do**
 - 5: reset s_t to the initial agent state
 - 6: **repeat**
 - 7: select action, a_t , based on agent's policy, π , the current state, s_t , and behavior network output, $Q_{\mathbb{M}}(s_t, a_t)$
 - 8: take action a_t and observe the resulting reward, r_t , and new state, s_{t+1}
 - 9: add tuple $\langle s = s_t, a = a_t, r = r_t, s' = s_{t+1} \rangle$ as a new instance in \mathcal{D}
 - 10: randomly select a mini-batch of b instances from \mathcal{D} to give \mathcal{D}_b
 - 11: generate target feature values for each instance, $\langle s_i, a_i, r_i, s'_i \rangle$ in \mathcal{D}_b as:
- $$t_i = r_i + \gamma \max_{a'} \widehat{Q}_{\mathbb{M}}(s'_i, a')$$
- 12: perform an iteration of mini-batch gradient descent using \mathcal{D}_b
 - 13: every C steps let $\widehat{Q}_{\mathbb{M}} = Q_{\mathbb{M}}$
 - 14: **until** agent reaches terminal state
 - 15: **end for**
-

The deep Q network algorithm can be used with any state representation that can be input into a neural network, and can use different neural network architectures. The simplest version of this would be a numeric state vector input into a **multi-layer perceptron** feedforward network. The algorithm was first proposed, however, as an approach to playing video games in which the only inputs were screenshots of the game. To best handle image inputs a **convolutional neural network**²⁹ was used. A single screenshot of a game does not contain sufficient information about the state of an

environment and an agent for the environment to be considered **fully observable**, and so the Markov assumption does not hold. For example, in the single screenshot of the Lunar Lander environment in [Figure 11.7](#)^[669], it is not possible to tell at what velocity the spaceship is moving. To overcome this, sequences of the last k screenshots stacked together can be used as the state representation. This is an example of using a **state generation function** as discussed in Section 11.2^[638]. Usually small stacks of screenshots (e.g. $k = 4$) provide enough information to capture the state.

It is difficult to provide a detailed worked example of the DQN algorithm because the number of weights to be learned and steps required for anything interesting is too large for clear presentation. Instead, to illustrate the DQN algorithm we will examine at a higher level how an automated player of the Lunar Lander game can be trained. As mentioned before this game has four actions available to the agent: *None*, *Up*, *Left*, and *Right*. State can be represented as a stack of the last 4 frames in the game. This is illustrated in [Figure 11.9](#)^[672]. There are two ways that an episode can end: an agent can either land successfully or crash. The agent earns a reward of + 100 for landing successfully and a reward of - 100 for crashing. During landing the agent receives a reward of + 10 each time one of its legs touches the ground gently. For every step that the agent is firing one of its thrusters it receives a reward of - 0.3.

A **convolutional neural network** was used as the action-value network. Input images were scaled to 84×84 and the network contained hidden convolutional layers with 32, 64 and 64 units.³⁰ Filter sizes were 8×8 (stride 4), 4×4 (stride 3), and 3×3 (stride 1). **Rectified linear activation** functions were used in all hidden layer units. A final hidden layer flattened the outputs of the previous convolutional layer and contained 512 fully connected units with rectified linear activations. The output layer was a fully connected layer with 4 outputs (one per action) using **linear activations**. [Figure 11.9](#)^[672] illustrates this architecture. The behavior policy used was ϵ **greedy**, but **linear annealing** was also used. Linear annealing allows the value for ϵ used in ϵ greedy policy to change over time. At the beginning, a large value 0.9 is used and this slowly moves down toward a small value 0.05. During DQN training the size of the replay memory was

50,000 and the target action-value function network, \widehat{Q}_M , was replaced every 10,000 steps.

[Figure 11.10\(c\)](#)^[675] shows the changing cumulative reward for the DQN agent as it learns to play the Lunar Lander game. The steady increase of return clearly shows that the agent was improving its performance over time. [Figure 11.10\(a\)](#)^[675] shows a series of screens from an episode early in the training process in which the agent performed quite poorly. This can be compared to the screens in [Figure 11.10\(b\)](#)^[675] which are from an episode much later in training at which the agent is performing quite well.

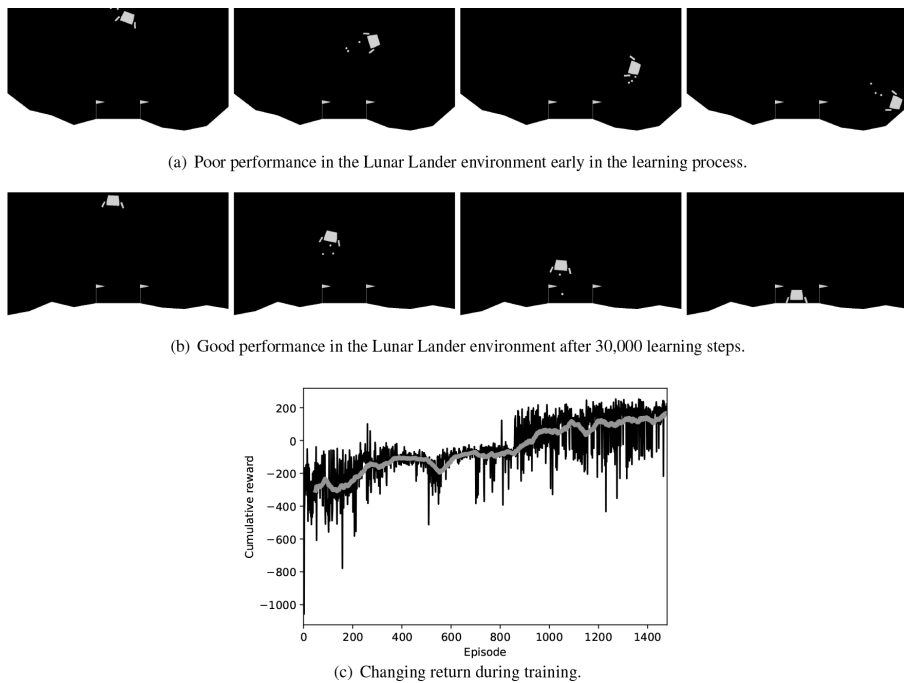


Figure 11.10

(a) Frames from an episode early in the training process in which the agent performs poorly. (b) Frames from an episode near the end of the learning process where the agent is starting to be very effective. (c) Changing episode returns during DQN training. The gray line shows a 50-episode moving average to better highlight the trend.

This example demonstrates that, using the DQN algorithm, it is possible to train agents to perform very sophisticated tasks using modern deep neural networks combined with very basic state representations—in this case just screenshots from the game. This ability led to a resurgence of interest in reinforcement learning in the 2010s after somewhat of a quiet period. New methods that expand on the ideas described in this section are being

proposed all the time and some of the most promising are discussed in section 11.6^[677].

11.5 Summary

This chapter introduced **reinforcement learning**, an alternative approach to **supervised** or **unsupervised** machine learning. Some argue that reinforcement learning is closer to supervised learning because the reward signal is a form of supervision. The key difference, however, is that reinforcement learning does not require a labeled dataset containing examples of correct behavior to learn from. Instead, a reinforcement learning agent can be deployed into an environment and learn from experimenting within that environment. This is particularly attractive for problems in which automated systems are to be trained to perform a control task—for example, robotics or automated game playing. To use supervised learning for these types of tasks would require an expert controller to operate the system in order to generate a dataset containing examples of correct behavior. This is often very time consuming and expensive to generate. Moreover, reinforcement learning agents can often find exceptional solutions to problems that a human operator would not be aware of. This has been the case in the recent deep reinforcement learning successes at games like go, chess, and poker at which reinforcement learning agents are playing at world class level and use play strategies that are a total surprise to human players.

In a reinforcement learning scenario an **agent** inhabiting an **environment** attempts to achieve a **goal** by taking a sequence of **actions** to move it between **states**. On completion of each action the agent receives an immediate scalar **reward** indicating whether the outcome of the action was positive or negative and to what degree. In reinforcement learning, the degree to which an agent has achieved a goal is measured only by the **cumulative rewards** it has received from each action taken in pursuit of that goal. To choose which action to take in a given state the agent uses a **policy**. Policies rely on being able to assess the **expected return** of taking an action in a particular state, and an **action-value function** is used to calculate this. Markov decision processes are particularly useful for formalizing this structure and provide the scaffolding for reasoning about reinforcement learning problems.

The learning approaches described in this chapter are **value-based** and **model-free**. That is, they optimize the action-value function and do not rely on having a model of how the world behaves. This means that they can learn to behave effectively in an environment with only minimal knowledge of that environment—the states that can be occupied and the actions that the agent can take are all that the agent needs to know. **Temporal-difference learning**, and its **Q-learning (off-policy)** and **SARSA (on-policy)** variants, are standard approaches to reinforcement learning and have been used effectively in a variety of environments. They take a **bootstrapping** approach where estimates of action-value are iteratively improved on the basis of other estimates of action-value. The advantage of this is that learning can happen quickly as updates are made after each action the agent takes. The disadvantage is that these approaches can struggle to learn very long-term strategies in which reward does not accrue until long after actions have been taken.

The SARSA and Q-learning approaches are both tabular methods which are limited in terms of the size of state space they can handle. **Approximate methods** are an alternative to tabular approaches to reinforcement learning that learn a generalized version of the **action-value function** (or the value function) and can handle much larger state spaces than tabular methods. These methods have been in existence since at least the early 1990s but have seen a resurgence of interest in the 2010s with the emergence of **deep learning**. **Deep Q networks** are a temporal-difference based approach that use a deep neural network to learn a generalize action-value function. These networks have been shown to be especially effective, particularly when states are stored in very low-level representations, such as the arrangement of pieces on a game board or a screenshot of a game.

One overarching point about reinforcement learning that is worth mentioning is that it comes at the cost of hugely increased computation. Training reinforcement learning agents for sophisticated tasks in complex, dynamic environments can required large computational resources for significant amounts of time. This is especially the case when approximate methods based on deep neural networks are used.

11.6 Further Reading

Reinforcement learning is built upon the framework of an **intelligent agent**. The intelligent agent view of **artificial intelligence** overlaps to a large extent with machine learning but is a vibrant field in its own right. Wooldridge and Jennings (1995) remains a key introduction to the field and the more recent Wooldridge (2009) adds useful information about systems where multiple agents compete or cooperate is very useful. Mac Namee (2009) provides an overview of the dominant approaches in using intelligent agent systems in games and entertainment applications.

The ideas of reinforcement learning and Markov decision processes stem from early work by Howard (1960) and Bellman (1957a,b). One fascinating early example is by Michie (1961, 1963) who built an automated tic-tac-toe player based on ideas of reinforcement learning. Due to a lack of access to computing resources, however, this was built using over two hundred matchboxes filled with colored marbles rather than in software!

Sutton and Barto's textbook has been the definitive work on reinforcement learning since it was first published in (Sutton and Barto, 1998), and their recent 2nd edition (Sutton and Barto, 2018) is an excellent update. This covers a deep theoretical framing of the reinforcement learning problem, as well as a collection of approaches including dynamic programming, Monte Carlo methods, temporal-difference learning, and other extensions. The book is detailed, rigorous, and easy to read. Bertsekas (2017) is also an excellent and detailed textbook that covers the fundamentals of reinforcement learning, with a leaning toward solutions based on **dynamic programming**.

For a more broad discussion, Isaac Asimov's *I, Robot* (Asimov, 1950), in which the **Three Laws of Robotics** first appear, is a fun exploration of the challenges of defining reward and utility functions. Similarly, Bostrom's **paperclip maximizer** thought experiment (Bostrom, 2003) is an interesting exploration of the potential negative consequences of a highly functional intelligent agent pursuing cumulative reward.

Reinforcement learning approaches have been used in automated game playing since **TD-Gammon** (Tesauro, 1994) was developed in the 1990s. This trend has continued and recent, high-profile successes include **Deep Q Learning** for Atari video games (Mnih et al., 2013), **AlphaGo** for Go (Silver et al., 2017), **AlphaZero** for chess (Silver et al., 2018), and the OpenAI Five player for DOTA 2 (McCandlish et al., 2018). For more recent

advances at the junction of reinforcement learning and deep learning, Sejnowski (2018) gives a nice overview of some key application areas and recent developments, and again, Sutton and Barto (2018) provides a good overview.

11.7 Exercises

1. An agent in an environment completes an episode and receives the following rewards:

$$\{r_0 = -33, r_1 = -11, r_2 = -12, r_3 = 27, r_4 = 87, r_5 = 156\}$$

- (a) Calculate the discounted return at time $t = 0$ on the basis of this sequence of rewards using a discounting factor of 0.72.
 (b) Calculate the discounted return at time $t = 0$ on the basis of this sequence of rewards using a discount rate of 0.22.
2. To try to better understand the slightly baffling behavior of her new baby, Maria—a scientifically minded new mother—monitored her baby girl over the course of a day recording her activity at 20 minute intervals. The activity stream looked like this (with time flowing down through the columns):

SLEEPING	SLEEPING	SLEEPING	CRYING	SLEEPING	SLEEPING
CRYING	SLEEPING	HAPPY	HAPPY	CRYING	HAPPY
SLEEPING	SLEEPING	CRYING	HAPPY	SLEEPING	HAPPY
SLEEPING	CRYING	SLEEPING	HAPPY	SLEEPING	HAPPY
SLEEPING	CRYING	SLEEPING	HAPPY	SLEEPING	HAPPY
HAPPY	SLEEPING	HAPPY	HAPPY	SLEEPING	HAPPY
HAPPY	SLEEPING	HAPPY	SLEEPING	HAPPY	HAPPY
HAPPY	HAPPY	HAPPY	SLEEPING	HAPPY	SLEEPING
SLEEPING	SLEEPING	HAPPY	SLEEPING	HAPPY	SLEEPING
SLEEPING	HAPPY	HAPPY	SLEEPING	SLEEPING	SLEEPING
SLEEPING	HAPPY	HAPPY	SLEEPING	HAPPY	SLEEPING
SLEEPING	CRYING	CRYING	SLEEPING	SLEEPING	SLEEPING

Maria noticed that her baby could occupy one of three states—HAPPY, CRYING, or SLEEPING—and moved quite freely between them.

- (a) On the basis of this sequence of states, calculate a transition matrix that gives the probability of moving between each of the three states.

- (b) Draw a **Markov process** diagram to capture the behavior of a small baby as described.
3. The following table shows the action-value table for a reinforcement learning agent learning to play the **TwentyTwos** game after 20 episodes of training have elapsed.

State	Action	Value	State	Action	Value	State	Action	Value
PL-DL	<i>Twist</i>	0.706	PH-DL	<i>Twist</i>	-0.038	PM-DH	<i>Twist</i>	0.533
PL-DL	<i>Stick</i>	0.284	PH-DL	<i>Stick</i>	0.164	PM-DH	<i>Stick</i>	-0.526
PM-DL	<i>Twist</i>	-0.985	PL-DH	<i>Twist</i>	0.386	PH-DH	<i>Twist</i>	0.154
PM-DL	<i>Stick</i>	0.589	PL-DH	<i>Stick</i>	-0.832	PH-DH	<i>Stick</i>	0.103
BUST	<i>Twist</i>	0.000	TIE	<i>Twist</i>	0.000	WIN	<i>Twist</i>	0.000
BUST	<i>Stick</i>	0.000	TIE	<i>Stick</i>	0.000	WIN	<i>Stick</i>	0.000
LOSE	<i>Twist</i>	0.000				TWENTYTWO	<i>Twist</i>	0.000
LOSE	<i>Stick</i>	0.000				TWENTYTWO	<i>Stick</i>	0.000

In the answers to the following questions, assume that after the initial cards have been dealt to the player and the dealer, the following cards are coming up next in the deck: 10 ♠, 2 ♣, 7 ♣, K ♥, 9 ♦.

- (a) At the beginning of the first episode the player is dealt (2 ♥, K ♣), the dealer is dealt (A ♦, 3 ♦), and the dealer's visible card is the A ♦. Given these cards, what state is the TwentyTwos playing agent in?
- (b) Assuming that the next action that the agent will take is selected using a **greedy action selection policy**, what action will the agent choose to take (*Stick* or *Twist*)?
- (c) Simulate taking the action that the agent selected in Part (b) and determine the state that the agent will move to following this action and the reward that they will receive. (**Note:** If cards need to be dealt to the player or dealer, use cards from the list given at the beginning of this question.)
- (d) Assuming that **Q-learning** is being used with $\alpha = 0.2$ and $\gamma = 0.9$, update the entry in the action-value table for the action simulated in Part (c).
- (e) Assuming that a **greedy action selection policy** is used again and that **Q-learning** is still being used with $\alpha = 0.2$ and $\gamma = 0.9$, select the next action that the agent will perform, simulate this action, and update the entry in the action-value table for the action. (**Note:** If

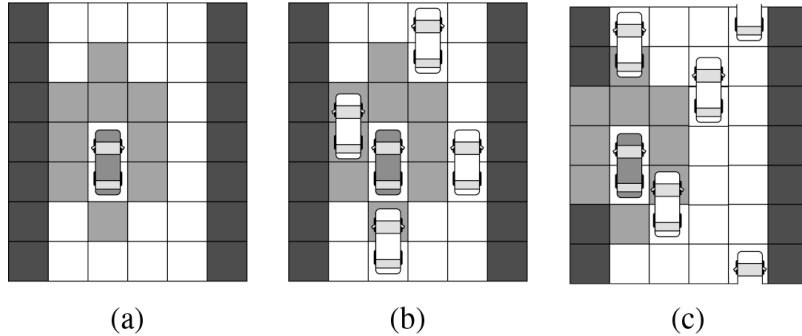
cards need to be dealt to the player or dealer, continue to use cards from the list given at the beginning of this question.)

- (f) On the basis of the changes made to the TwentyTwos playing agent's action-value table following the two actions taken in the previous parts of this question, how has the agent's **target policy** changed?
- * 4. As part of a project to develop a self-driving taxi system, the behavior of a taxi driver has been observed over a work day. During their shift the taxi driver can CRUISE looking for work, wait for a fare at a taxi RANK, take a FARE and deliver a passenger to their destination, or take a BREAK. The behavior of the taxi driver over the shift looked like this (with time flowing down through the columns):

CRUISE	RANK	RANK	FARE	CRUISE	CRUISE
FARE	CRUISE	BREAK	FARE	FARE	BREAK
CRUISE	CRUISE	CRUISE	FARE	FARE	RANK
CRUISE	FARE	CRUISE	FARE	FARE	RANK
CRUISE	FARE	CRUISE	FARE	CRUISE	RANK
FARE	CRUISE	FARE	FARE	CRUISE	FARE
FARE	RANK	FARE	CRUISE	FARE	FARE
FARE	FARE	FARE	CRUISE	FARE	CRUISE
CRUISE	CRUISE	FARE	CRUISE	FARE	CRUISE
CRUISE	FARE	FARE	CRUISE	CRUISE	CRUISE
CRUISE	FARE	FARE	CRUISE	FARE	CRUISE
CRUISE	RANK	FARE	CRUISE	CRUISE	CRUISE

- (a) On the basis of this behavior sequence, calculate a transition matrix that gives the probability of moving between all the four states.
- (b) Draw a **Markov process** diagram to capture the behavior of the taxi driver as described.
- * 5. The following image labeled (a) shows a simple schematic of a system used to train a self-driving car to drive on a four-lane highway. The car has sensors on the front, the rear, and the sides that indicate the presence of other cars or lane barriers in the area immediately surrounding the car. The shaded cells in Image (a) below show the region that these sensors cover. The region around the car is divided into cells that can be empty, occupied by another car, or occupied by a barrier. Cars occupy an area covered by two cells (one above the other

as shown in Image (a)). Images (b) and (c) show the car in other positions where other cars and barriers are sensed by the car, but other cars and barriers are out of range of the sensors.



The car can move at three speeds: *stationary*, *slow*, and *fast*. When moving fast, the car moves forward two cells per time-step; when moving slowly the car moves forward one cell per time-step; and when stationary does not move forward at all. The actions that the car can take are to (1) maintain its current speed, (2) increase its speed (move up one level in the speed categories stationary, slow, and fast), (3) decrease its speed (move down one level in the speed categories), (4) move to the left, and (5) move to the right.

When the car changes speed, the action has an immediate effect on the car's progress in the current time-step. If the car is stationary, taking the action to move left or right has no effect on the car's position. If the car is moving slowly, then moving left or right moves the car one cell in that direction at that time-step, but not any distance forward. If the car is moving fast, then moving left or right moves the car one cell in that direction at that time-step and one cell forward.

The goal that the agent is being trained to achieve is to learn to drive as far as possible in the shortest amount of time possible without crashing. The car moves forward along an infinite highway, and an episode ends if the car crashes into a barrier or another car.

- (a) Design a state representation for the car agent in this scenario. How many states will exist in the representation?
- (b) Given the state representation that you have defined in Part (a) and the actions available to the agent, how many entries would the

action-value function table for a tabular reinforcement learning agent trained for this task have?

(c) Design a reward function for this scenario.

1. Environments in which the state contains all information about the environment and any agents in it are known as **fully observable** environments. Environments in which this is not the case are known as **partially observable environments**. The use of a state generation function allows us to treat some partially observable environments as if they were fully observable and apply the mechanics of reinforcement learning where otherwise it would not be possible.
2. There is some argument in the reinforcement learning literature about whether the reward that follows an action, a_t , taken in a state, s_t , should be referred to as r_t or r_{t+1} . The argument stems from a disagreement about when a discrete moment of time ends—after the action completes or after the reward is received? From a computational point of view it makes no difference, as long as consistency is maintained in notation and computation. Throughout this chapter we use r_t to refer to the reward received after taking an action, a_t , at time-step t .
3. This is captured in Sutton's **reward hypothesis** (Sutton and Barto, 2018): "*That all of what we mean by goals and purposes can be well thought of as maximization of the expected value of the cumulative sum of a received scalar signal (reward).*"
4. Approaches taking this approach include **policy gradient** and **evolutionary reinforcement learning** approaches.
5. We use Q here to be consistent with the framing of Q -learning later in this chapter.
6. We have presented this discussion on the context of episodic, model-free, policy-based reinforcement learning. There are other framings of the reinforcement learning problem under which different framings are used and extra components are added—for example, **policy-based reinforcement learning** and **model-based reinforcement learning**. For clarity of explanation, however, we have ignored these in this discussion of the fundamentals required to understand the approaches to reinforcement learning that are discussed in this chapter. Interested readers are directed to the suggestions for further reading presented in Section 11.6^[677], in which these alternatives are discussed.
7. This is a simple manufactured example for this book, but this type of model is often used in epidemiology Hunter et al. (2018).
8. Advanced features of Blackjack, like *doubling down*, *insurance*, and *splitting pairs*, are not allowed in our TwentyTwos game.
9. This is not as extreme an assumption as it might sound, as cards in Blackjack are usually dealt from a shoe containing 6 to 8 standard playing card decks.
10. In this simplified version of Blackjack, the complication of the player having to choose a wager for each hand is ignored.
11. Understanding the probabilities associated with the dynamics of card games has a history stretching back to the origins of probability theory (Bernstein, 1996), through early applications of computing technology (Scarne, 1986), right to the modern day (Brown and Sandholm, 2017).
12. This is a slight departure from Equation (11.9)^[643] as it sums to infinity rather than to the end of an episode. This, however, makes no difference in the discussion that follows but is the normal formulation of the Bellman Equations.

13. This is simply the definition of **expectation** as defined in probability theory for any **random variable**: $E[X] = \sum_{i=1}^k x_i p_i + x_2 p_2 + x_3 p_3 + \dots + x_k p_k$, where X is a random variable, x_1 to x_k are the possible values of the random variable, and p_1 to p_k are the probabilities of these different values occurring.
14. The Bellman Equations were first introduced by Richard Bellman in the 1950s (Bellman, 1957a,b) as part of very early work on reinforcement learning.
15. It is worth noting that the temporal-difference learning approach to reinforcement learning takes a very similar approach to the **gradient descent** algorithm described in Section 7.3^[319].
16. An alternative TD(λ) uses an approach known as **eligibility traces** to take account of the actual rewards received from multiple actions.
17. If we extended this example so that the restaurant was slightly hip and prepared different dishes based on the main ingredient chosen every night, some that Conor likes more than others (for example, chicken satay one night and chicken pie the next), this would become an example of a **multi-armed bandit problem**. Multi-armed bandit problems are a common framework for solving optimization problems where choices have uncertain outcomes and can be viewed as a very simple form of reinforcement learning.
18. This is related to the idea of **concept drift** discussed in Section 9.4.6^[578].
19. There are many other action-selection policies that can be used together with temporal-difference learning. For example, a simple modification to the ε -greedy policy is to reduce ε over time so that the amount of exploration that the agent performs reduces over time. **Boltzmann action selection** is another commonly used alternative that uses the action-value function values, $Q(s_t, a_t)$, for each possible action to build a **softmax** probability distribution, $\pi(s_t, a_t) = e^{Q(s_t, a_t)} / \sum_{a_t} e^{Q(s_t, a_t)}$. Actions are then selected randomly following this distribution.
20. This is just a slight modification of Equation (11.23)^[655].
21. Because of the random nature of state transitions in TwentyTwos, a lot of episodes are needed for learning to converge.
22. Note that TwentyTwos is a much easier game to win than Blackjack, in which it is well known that *the house always wins!*
23. These values are recommended by Sutton and Barto (2018) but can be tuned through experimentation.
24. The name SARSA comes from the terms s_t , a_t , r_t , s_{t+1} , and a_{t+1} used in the algorithm and the order in which they appear.
25. This action selection is required here to seed the first iteration of the loop beginning on Line 14^[666].
26. The implementation of Lunar Lander used in this example comes from the **Gym** toolkit developed by **OpenAI** (Brockman et al., 2016). This is a fantastic resource for experimenting with reinforcement learning agents.
27. See Section 7.3^[319].
28. See Chapter 8^[319].
29. See Chapter 8^[381].
30. The architecture followed the architecture described by Mnih et al. (2013).

IV

CASE STUDIES AND CONCLUSIONS

12

Case Study: Customer Churn

“There is only one boss. The customer. And he can fire everybody in the company from the chairman on down, simply by spending his money somewhere else.”

—Sam Walton

Acme Telephonica (AT) is a mobile phone operator that has customers across every state of the USA. Like every telecommunications company, AT struggles with customer **churn**—customers leaving AT for other mobile phone operators. AT is always looking for new ways to address the churn issue and in 2008 founded a **customer retention** team. The customer retention team monitors the number of calls made to the AT customer support center by each customer and identifies the customers who make a large number of customer support calls as churn risks. The customer retention team contacts these customers with special offers designed to entice them to stay with AT. This approach, however, has not proved particularly successful, and churn has been steadily increasing over the last five years.

In 2010 AT hired Ross, a predictive data analytics specialist, to take a new approach to reducing customer churn. This case study describes the work carried out by Ross when he took AT through the CRISP-DM process¹ in order to develop a predictive data analytics solution to this business problem. The remainder of this chapter will discuss how each phase of the CRISP-DM process was addressed in this project.

12.1 Business Understanding

As is the case in most predictive data analytics projects, AT did not approach Ross with a well-specified predictive analytics solution. Instead,

the company approached him with a business problem—reducing customer churn. Therefore, Ross's first goal was to convert this business problem into a concrete analytics solution. Before attempting this conversion, Ross had to fully understand the business objectives of AT. This was reasonably straightforward as AT management had stated that their goal was to reduce their customer churn rates. The only factor left unspecified was what the magnitude of that reduction was expected to be. Based on previous projects he had worked on, the current approach to customer retention that AT was taking, and AT's historical data, Ross agreed with AT management that a target reduction from the current high of approximately 10% to approximately 7.5% was realistic and probably achievable. Ross did stress to AT management that until he actually examined the data, he could not know how useful a model he would be able to build.

Ross's next task was to fully assess the current situation within AT. In particular, Ross needed to understand the current analytics capability of the company and its readiness to take action in response to the insights that an analytics solution would provide. AT already had a customer retention team proactively making interventions in an effort to reduce customer churn. Furthermore, this team was already using data from within the organization to choose which customers to target for intervention, which suggested that the team members were in a position to use predictive data analytics models.

Ross spent a significant amount of time meeting with Kate, the leader of the customer retention team, in order to understand how they worked. Kate explained that at the end of every month, a call list was generated, capturing the customers who had made more than three calls to the AT customer support service in the previous two months. These customers were deemed to be at risk of churning in the coming month, so the customer retention team set about contacting them with a special offer. Typically, the offer was a reduced call rate for the next three months, although retention team members had the freedom to make other offers.

Ross also spoke to the chief technology officer (CTO) at AT, Grace, in order to understand the available data resources. Ross learned that AT had reasonably sophisticated transactional systems for recording recent call activity and billing information. Historic call and bill records as well as customer demographic information were stored in a data warehouse. Grace

had played a significant role in developing the process that had made information about customer support contacts available to the customer retention team. Ross hoped that this would make his task a little easier because Grace was the main gatekeeper to all the data resources at AT, and having her support for the project would be important. Other parts of the business that Ross spent significant time interviewing included the billing department, the sales and marketing team, and the network management.

Throughout the early stages of the project, Ross had been consciously working on developing his **situational fluency**. Through his discussions with the AT management team, Kate, and Grace, he had learned a lot about the mobile phone industry. The basic structure of the AT business was that customers had a contract for call services that AT provided. These contracts did not have a fixed time and were essentially renewed every month when a customer paid a fixed **recurring charge** for that month. Paying the recurring charge entitled a customer to a **bundle** of minutes of call time that were offered at a reduction to the standard call rate. For different recurring fees, customers received different-sized bundles of call time. When a customer used up all the call time in his or her bundle, subsequent call time was referred to as **over bundle minutes**. These tended to be more expensive than the minutes included as part of a customer's bundle. At AT, all calls were classified as either **peak time calls** or **off-peak time calls**. Peak time was 08:00 to 18:00 from Monday to Friday, and calls made during peak time were more expensive than calls made during off-peak times.

Based on his assessment of the current situation within AT, Ross developed a list of ways that predictive analytics could help address the customer churn problem at AT. These included finding answers to the following questions:

- **What is the overall lifetime value of a customer?** A model could be built to predict the overall value that AT was likely to receive from a particular customer over the person's entire customer lifecycle. This could be used to identify customers who currently did not look valuable but that were likely to be valuable customers later in their customer lifecycles (college students often fall into this category). By offering these customers incentives now to prevent them from churning, AT

would ensure that it received the full value from these customers in the future.

- **Which customers were most likely to churn in the near future?** A prediction model could be trained to identify the customers from the AT customer base who were most likely to churn in the near future. The retention team could focus their retention efforts on these customers. The process that the AT retention team had in place at the beginning of the project to identify customers likely to churn took a single feature approach to this identification—they looked only at how many calls a customer had made to the AT customer support service. It was likely that a machine learning model that looked at multiple features would do a better job of identifying customers likely to churn.
- **What retention offer would a particular customer best respond to?** A system could be built to predict which offer, from a set of possible retention offers, a particular customer would be most likely respond to when contacted by the AT retention team. This could help the retention team convince more customers to stay with AT.
- **Which pieces of the network infrastructure were likely to fail in the near future?** Using information about network loads, network usage, and equipment diagnostics, a predictive model could be built to flag upcoming equipment failures so that pre-emptive action could be taken. Network outages are a driver of customer dissatisfaction and ultimately customer churn, so reducing these could have a positive impact on churn rates.

After discussion with the AT executive team, it was decided that the analytics solution most appropriate to focus on was predicting *which customers are most likely to churn in the near future*. There were a number of reasons this project was selected:

- Ross's previous discussions with Grace, the AT CTO, had established that the data required to build a churn prediction model were likely to be available and reasonably easily accessible.
- The prediction model could be easily integrated with AT's current business processes. AT already had a retention team in place that was making proactive interventions to help prevent churn, albeit using a very simple system to identify which customers to contact. By creating a

more sophisticated model to identify those customers, this existing process would be improved.

- Building a churn prediction model was also attractive to the AT executive team, as they hoped that as well as being useful in reducing churn rates, it would help to explain the main drivers behind customer churn. A better understanding of the main drivers of customer churn would be useful to many other parts of the AT business.

By contrast, the other analytics solutions developed suffered from a lack of available data (e.g., AT had no data available on the success or otherwise of various retention offers made); from being too significant a change in the business processes used by AT to be considered achievable at the time (e.g., generating a prediction of the overall lifetime value of a customer); or from not being based on sufficiently well-grounded assumptions (e.g., the fact that customer churn is heavily influenced by network failures).

Once the analytics solution had been defined, the next step was to agree on the expected performance of the new analytics model. Based on a recent evaluation of historical performance, AT management believed at the time of this project that their current system for identifying likely churners had an accuracy of approximately 60%, so any newly developed system would have to perform considerably better than this to be deemed worthwhile. In consultation with the members of the AT executive team and the retention team, Ross agreed that his goal would be to create a churn prediction system that would achieve a prediction accuracy in excess of 75%.

12.2 Data Understanding

During the process of determining which analytics solution was most suitable for the current situation at AT, Ross had already begun to understand the data resources available. His next task was to add much more depth to this understanding, following the process described in Section 2.3^[28]. This involved working very closely with Grace to understand what data was available, the formats that the data was kept in, and where the data resided. This understanding would form the basis of Ross's work on designing the **domain concepts** and **descriptive features** that would make up the **analytics base table (ABT)**, which would drive the creation of the predictive model. This was an iterative process in which Ross moved

back and forth between Kate at the AT retention team, Grace, the CTO, and other parts of the business identified as having insight into the data associated with customer churn. It quickly became apparent that the key data resources within AT that would be important for this project were

- The customer demographic records from the AT data warehouse
- The customer billing records stored in the AT billing database, where records stretch back over a time horizon of five years
- The transactional record of calls made by individuals, stretching back over a time horizon of 18 months
- The sales team's transactional database, containing details of phone handsets issued to customers
- The retention team's simple transactional database, containing all the contacts they had made with customers, and the outcomes of these contacts, stretching back to a time horizon of 12 months

Before going any further, Ross had to define the **prediction subject** for the ABT and the target feature. The goal was to develop a model that would predict whether a customer would churn in the coming months. This meant that the prediction subject in this case was a customer, so the ABT would need to be built to contain one row per customer.

Predicting churn is a form of **propensity modeling**,² where the event of interest in this case is a customer making the decision to churn. Consequently, Ross needed to agree with the business (in particular the customer retention team) on a definition of churn. The definition would be used to identify churn events in AT's historical data and, consequently, was fundamental to building the ABT for the project. The business agreed that a customer who had been inactive for one month (i.e., had not made any calls or paid a bill) or who had explicitly canceled or not renewed a contract would be considered to have churned. Ross also needed to define the lengths of the **observation period** and the **outcome period** for the model. He decided that the **observation period**, during which he would collect data on customer behavior, would stretch back for 12 months. This was a decision made based on the data available and Ross's expectation that anything farther back than this was likely to have little impact on predicting churn. With regard to defining the **outcome period**, the company agreed that it would be most useful to make a prediction that a customer was likely

to churn three months before the churn event took place, as this gave them time to take retention actions. Consequently, the outcome period was defined as three months.³

With the target feature suitably defined, Ross's next task was to determine the domain concepts that would underpin the design of the ABT. The domain concepts are those areas that the business believes have an impact on a customer's decision to churn. The domain concepts were developed through a series of workshops with representatives of various parts of the AT business—in particular the retention team, but also sales and marketing and billing. AT believed that the main concepts that affected churn were underlying customer demographics (e.g., perhaps younger customers were more likely to churn); customer billing information, and in particular changes in billing patterns (e.g., perhaps customers whose bill suddenly increased were more likely to churn); the details of a customer's handset (e.g., perhaps customers who have had a handset for a long time are more likely to churn); the interactions a customer has had with AT customer care (e.g., perhaps customers who are making a large number of calls to customer care are having difficulties with the AT network and so are likely to churn); and the actual calls the customer is making, in particular, changing call patterns (e.g., perhaps customers who have started making calls to new groups of people are more likely to churn). This set of domain concepts was felt to be extensive enough to cover all the characteristics that were likely to contribute to a customer's likelihood to churn and is shown in [Figure 12.1](#)^[690].

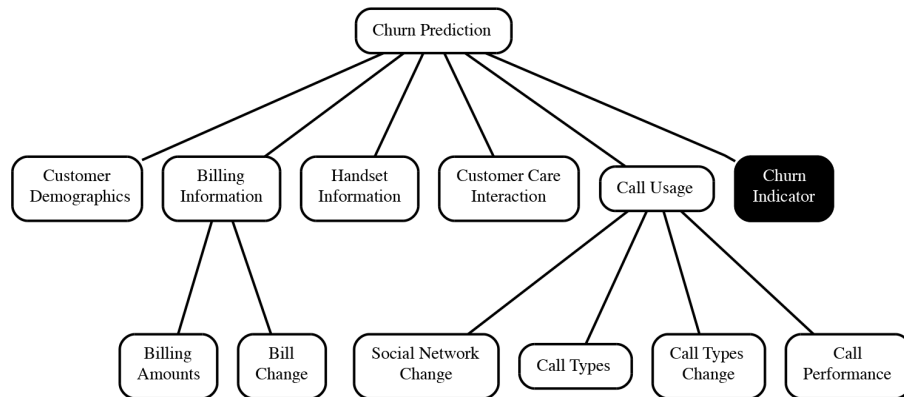


Figure 12.1

The set of domain concepts for the Acme Telephonica customer churn prediction problem.

From these domain concepts, Ross worked on deriving a set of descriptive features. Some of the descriptive features were simply copies of available raw data. For example, the AGE, GENDER, CREDITRATING, and OCCUPATION columns from the customer demographics data warehouse could be directly included as descriptive features in the ABT to capture the CUSTOMER DEMOGRAPHICS domain concept. The more interesting descriptive features were ones that had to be derived from the raw data sources. For example, Ross learned that the retention team believed that one of the main reasons customers churned was the availability of new, high-end handsets at other networks. To try to capture the HANDSET INFORMATION domain concept, Ross designed three descriptive features:

- SMARTPHONE: This feature indicated whether the customer's current handset was a smartphone, which was derived from the customer's most recent handset entry.
- NUMHANDSETS: This was a count of how many different handsets the customer had had in the past three years. This was derived from a count of all the handset entries for a particular customer.
- HANDSETAGE: Based on a customer's latest handset entry, this feature captured the number of days that the customer had had his or her current handset.

In churn analysis, and in any sort of propensity modeling, change is usually a key driver of customer behavior. For this reason, and based on discussions with the AT team, Ross included the BILL CHANGE and SOCIAL NETWORK CHANGE domain concepts. It was understood by the AT retention team that customers often made a decision to churn if their bill increased significantly due to changing call patterns, or when they began to make large numbers of calls to new friends or colleagues on other networks. For these reasons, Ross designed the following descriptive features:

- CALLMINUTESCHANGEPCT: Derived from the raw call data, this feature captured the amount by which the number of minutes a customer used had changed that month compared to the previous month.
- BILLAMOUNTCHANGEPCT: Derived from the raw call data, this feature captured the amount by which a customer's bill had changed that month compared to previous month.

- NEWFREQUENTNUMBERS: Derived from analysis of the actual numbers dialed in the raw call data, this feature attempted to capture how many new numbers a customer has begun calling frequently that month. A frequent number was defined as a number that constituted more than 15% of a customer’s total calls.

Often descriptive features that are likely to be very useful cannot be implemented due to the unavailability of data. For example, the AT team felt that a customer beginning to frequently call other networks would be a good indicator of churn, but a suitable data feature could not be extracted to capture this. In its call records, AT did not include information about which network calls are made to, and with the free movement of numbers among operators, numbers themselves were no longer a reliable indicator of network.

The full set of descriptive features Ross developed, along with a short description of each, is shown in [Table 12.1](#)^[692].

Table 12.1

The descriptive features in the ABT developed for the Acme Telephonica churn prediction task.

Feature	Description
BILLAMOUNTCHANGEPCT	The percentage by which the customer’s bill has changed from last month to this month
CALLMINUTESCHANGEPCT	The percentage by which the call minutes used by the customer has changed from last month to this month
AVGBILL	The average monthly bill amount
AVGRECURRINGCHARGE	The average monthly recurring charge paid by the customer
AVGDROPPEDCALLS	The average number of customer calls dropped each month
PEAKRATIOCHANGEPCT	The percentage by which the customer’s peak calls to off-peak calls ratio has changed from last month to this month
AVG RECEIVED MINS	The average number of calls received each month by the customer
AVGMINS	The average number of call minutes used by the customer each month
AVGOVERBUNDLEMINS	The average number of out-of-bundle minutes used by the customer each month
AVGROAMCALLS	The average number of roaming calls made by the customer each month
PEAKOFFPEAKRATIO	The ratio between peak and off-peak calls made by the customer this month
NEWFREQUENTNUMBERS	How many new numbers the customer is frequently calling this month
CUSTOMERCARECALLS	The number of customer care calls made by the customer last month

Feature	Description
NUMRETENTIONCALLS	The number of times the customer has been called by the retention team
NUMRETENTIONOFFERS	The number of retention offers the customer has accepted
AGE	The customer's age
CREDITRATING	The customer's credit rating
INCOME	The customer's income level
LIFETIME	The number of months the customer has been with AT
OCCUPATION	The customer's occupation
REGIONTYPE	The type of region the customer lives in
HANDSETPRICE	The price of the customer's current handset
HANDSETAGE	The age of the customer's current handset
NUMHANDSETS	The number of handsets the customer has had in the past 3 years
SMARTPHONE	Whether the customer's current handset is a smartphone
CHURN	The target feature

12.3 Data Preparation

With help from Grace to implement the actual data manipulation and data integration scripts using the tools available at AT, Ross populated an ABT containing all the features listed in [Table 12.1](#)^[692]. Ross sampled data from the period 2008 to 2013. Using the definition of churn as a customer who had not made any calls or paid a bill for one month, Ross was able to identify churn events throughout this time period. To collect instances of customers who had not churned, Ross randomly sampled customers who did not match the churn definition but who also could be deemed active customers. Working with Kate, Ross defined an active customer as a current customer who made at least five calls per week and who had been a customer for at least six months.⁴ This definition ensured that the non-churn instances in the dataset would include only customers with a relatively normal behavior profile and for which there was a long enough data history that realistic descriptive features could be calculated for them.

The final ABT contained 10,000 instances equally split between customers who churned and customers who did not churn. In the raw data, customers who did not churn outnumber those who churned at a ratio of over 10 to 1. This is an example of an **imbalanced dataset**, in which the different levels of the target feature—in this case, churners and non-churners—are not equally represented in the data. Some of the machine learning approaches we have discussed in the preceding chapters perform

better when a **balanced sample** is used to train them, and this is why Ross created an ABT with equal numbers of instances with each target level.⁵

Ross then developed a full data quality report for the ABT including a range of data visualizations. The data quality report tables are shown in [Table 12.2](#)^[694]. Ross first assessed the level of **missing values** within the data. Within the continuous features, only AGE stood out with 11.47% of values missing. This could be handled reasonably easily using an imputation approach,⁶ but Ross held off on performing this at this stage. The REGIONTYPE and OCCUPATION categorical features both suffered from a significant number of missing values—74% and 47.8% respectively. Ross strongly considered removing these features entirely.

Table 12.2

A data quality report for the Acme Telephonica ABT.

(a) Data quality report for continuous features

Feature	% Count Miss. Card.			1 st Min. Qrt. Mean Median			3 rd Qrt. Max. Std.			
	Count	Miss.	Card.	Min.	Qrt.	Mean	Median	Qrt.	Max.	Dev.
AGE	10,000	11.47	40	0.00	0.00	30.32	34.00	48.00	98.00	22.16
INCOME	10,000	0.00	10	0.00	0.00	4.30	5.00	7.00	9.00	3.14
NUMHANDSETS	10,000	0.00	19	1.00	1.00	1.81	1.00	2.00	21.00	1.35
HANDSETAGE	10,000	0.00	1,923	52.00	590.00	905.52	887.50	1,198.00	2,679.00	453.75
HANDSETPRICE	10,000	0.00	16	0.00	0.00	35.73	0.00	59.99	499.99	57.07
AVGBILL	10,000	0.00	5,588	0.00	33.33	58.93	49.21	71.76	584.23	43.89
AVGMINS	10,000	0.00	4,461	0.00	150.63	521.17	359.63	709.19	6,336.25	540.44
AVGRECURRINGCHARGE	10,000	0.00	1,380	0.00	30.00	46.24	44.99	59.99	337.98	23.97
AVGOVERBUNDLEMINS	10,000	0.00	2,808	0.00	0.00	40.65	0.00	37.73	513.84	81.12
AVGROAMCALLS	10,000	0.00	850	0.00	0.00	1.19	0.00	0.26	177.99	6.05
CALLMINUTESCHANGEPCT	10,000	0.00	10,000	-16.422	-1.49	0.76	0.50	2.74	19.28	3.86
BILLAMOUNTCHANGEPCT	10,000	0.00	10,000	-31.67	-2.63	2.96	1.96	7.56	42.89	8.51
AVG RECEIVED MINS	10,000	0.00	7,103	0.00	7.69	115.27	52.54	154.38	2,006.29	169.98
AVGOUTCALLS	10,000	0.00	524	0.00	3.00	25.29	13.33	33.33	610.33	35.66
AVGINCALLS	10,000	0.00	310	0.00	0.00	8.37	2.00	9.00	304.00	17.68
PEAKOFFPEAKRATIO	10,000	0.00	8,307	0.00	0.78	2.22	1.40	2.50	160.00	3.88
PEAKRATIOCHANGEPCT	10,000	0.00	10,000	-41.32	-6.79	-0.05	0.01	6.50	37.78	9.97
AVGDROPPEDCALLS	10,000	0.00	1,479	0.00	0.00	0.50	0.00	0.00	9.89	1.41
LIFETIME	10,000	0.00	56	6.00	11.00	18.84	17.00	24.00	61.00	9.61
CUSTOMERCARECALLS	10,000	0.00	109	0.00	0.00	1.74	0.00	1.33	365.67	5.76
NUMRETENTIONCALLS	10,000	0.00	5	0.00	0.00	0.05	0.00	0.00	4.00	0.23
NUMRETENTIONOFFERS	10,000	0.00	5	0.00	0.00	0.02	0.00	0.00	4.00	0.155
NEWFREQUENTNUMBERS	10,000	0.00	4	0.00	0.00	0.20	0.00	0.00	3.00	0.64

(b) Data quality report for categorical features

Feature	% Count Miss. Card.				Mode	Freq.	% Mode	2 nd Mode Freq.	
	Count	Miss.	Card.	Mode				Mode	Freq.
OCCUPATION	10,000	74.00	8	professional	1,705	65.58	crafts	274	10.54
REGIONTYPE	10,000	47.80	8	suburb	3,085	59.05	town	1,483	28.39
MARRIAGESTATUS	10,000	0.00	3	unknown	3,920	39.20	yes	3,594	35.94
CHILDREN	10,000	0.00	2	false	7,559	75.59	true	2,441	24.41
SMARTPHONE	10,000	0.00	2	true	9,015	90.15	false	985	9.85
CREDITRATING	10,000	0.00	7	b	3,785	37.85	c	1,713	17.13
HOMEOWNER	10,000	0.00	2	false	6,577	65.77	true	3,423	34.23
CREDITCARD	10,000	0.00	6	true	6,537	65.37	false	3,146	31.46
CHURN	10,000	0.00	2	false	5,000	50.00	true	5,000	50.00

When he considered **cardinality**, Ross noticed that a number of the continuous features had very low cardinality—for example, INCOME, AGE,

`NUMHANDSETS`, `HANDSETPRICE`, and `NUMRETENTIONCALLS`. In most cases, Ross confirmed with Kate and Grace that these were valid because the range of values that the features could take was naturally low. For example, `HANDSETPRICE` can take only a small number of values—e.g., 59.99, 129.99, 499.99, and so on. The `INCOME` feature stood out as unusual with only 10 distinct values (the histogram for this feature confirmed this; see [Figure 12.2\(a\)](#)^[695]). Grace explained to Ross that incomes were actually recorded in bands rather than as exact values, so this was really a categorical feature. The cardinality of the `CREDITCARD` and `REGIONTYPE` categorical features were higher than expected (the histograms for these features are shown in [Figures 12.2\(b\)](#)^[695] and [12.2\(c\)](#)^[695]). The issue was that some levels had multiple representations—for example, for the `REGIONTYPE` feature, towns were represented as *town* and as *t*. Ross easily corrected this issue by mapping the levels of the feature to one consistent labeling scheme.

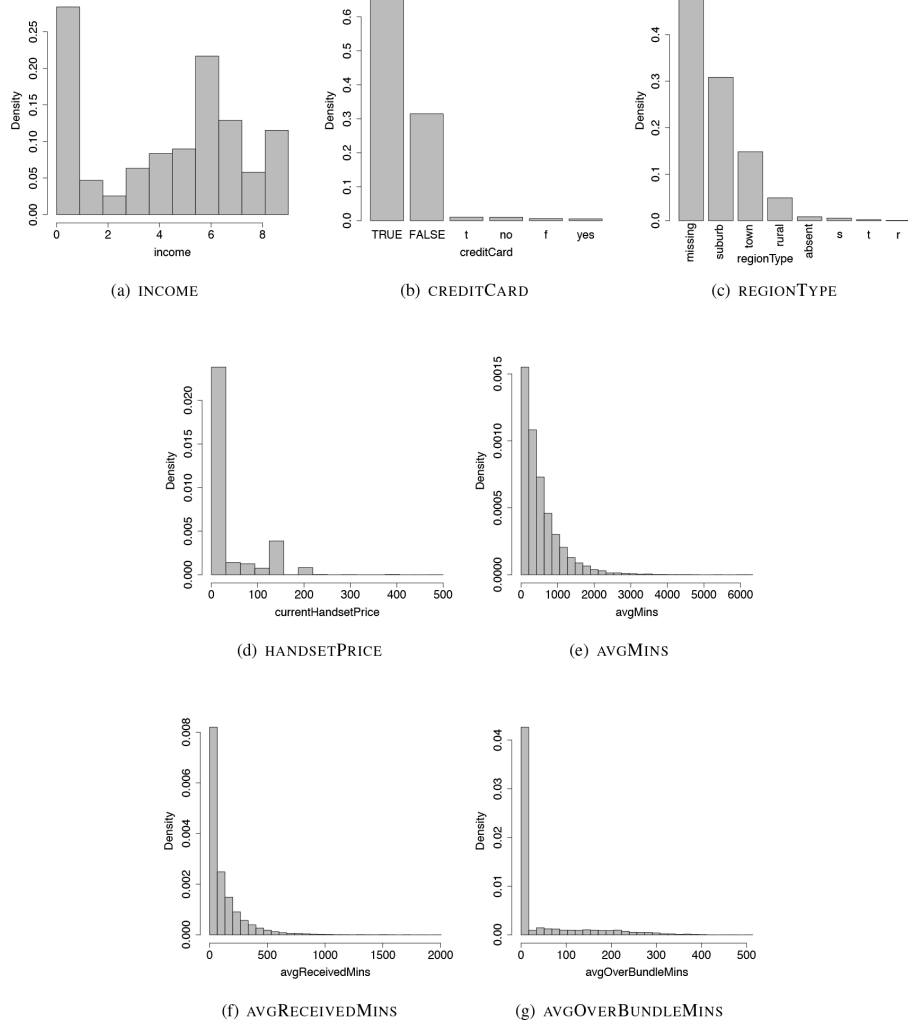


Figure 12.2

(a)–(c) Histograms for the features from the AT ABT with irregular cardinality; (d)–(g) histograms for the features from the AT ABT that are potentially suffering from outliers.

Four continuous features stood out as possibly suffering from the presence of **outliers**: HANDSETPRICE, with a minimum value of 0, which seemed unusual; AVGMINES, with a maximum of 6,336.25, which was very different from the mean and the 3rd quartile values for that feature; AVGRECEIVEDMINS, with a maximum of 2,006.29, which was also very different from the mean and the 3rd quartile values for that feature; and AVGOVERBUNDLEMINS, with minimum, 1st quartile, and median values of 0 compared to a mean of 40. Figure 12.2^[695] presents the histograms for these features. Ross confirmed with Grace and Kate that these were valid outliers—for example, some handsets are given away for free, and some customers just make a lot of calls. They did spend some time, however, discussing the

AVGOVERBUNDLEMINS. The histogram for this feature has an unusual shape that results in the unusual minimum, 1st quartile, and median values (see [Figure 12.2\(g\)](#)^[695]). By examining the data for this feature more closely, they eventually explained this shape by the fact that most customers did not go over the number of minutes in their bundle, which accounts for the large bar for 0 in this histogram. The values above zero seem to follow something close to a wide normal distribution, and the large number of, albeit valid, zero values account for the unusual minimum, 1st quartile, and median values. At this point Ross just made note of these outliers as something he might have to deal with during the modeling phase.

Ross then turned his attention to examining the data visualizations of the relationship between each descriptive feature and the target feature. No individual feature stood out as having a very strong relationship, but the evidence of connections between the descriptive features and the target feature could be seen. For example, [Figure 12.3\(a\)](#)^[697] shows a slightly higher propensity of people in rural areas to churn. Similarly, [Figure 12.3\(b\)](#)^[697] shows that customers who churned tended to make more calls outside their *bundle* than those who did not.

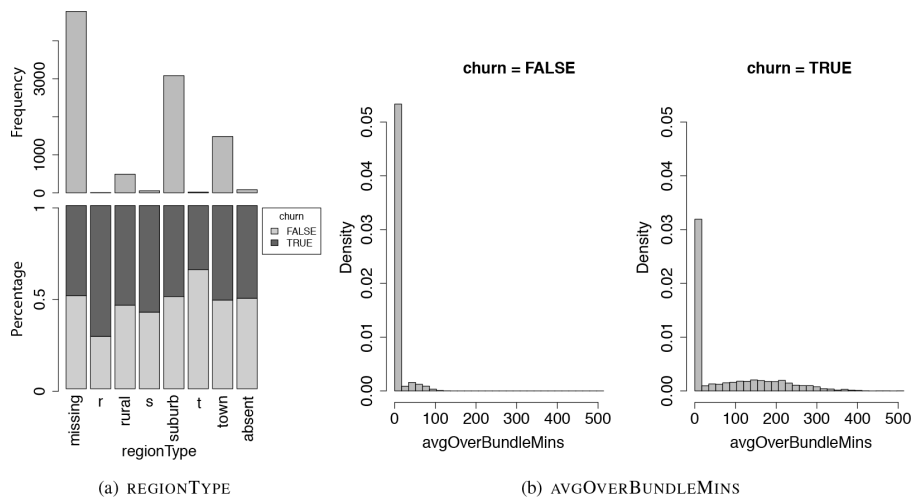


Figure 12.3

(a) A stacked bar plot for the REGIONTYPE feature; and (b) histograms for the AVGOVERBUNDLEMINS feature by target feature value.

Once Ross had reviewed the full data quality report in detail, he made the following decisions regarding the problematic features he had identified. First, he decided to delete the AGE and OCCUPATION features

because of the level of missing values in each of these features. He decided to keep the REGIONTYPE feature, however, because it appeared to have some relationship with the target. He also applied the planned mapping of the REGIONTYPE values to a consistent labeling scheme: $\{s|suburb\} \rightarrow suburb$; $\{t|town\} \rightarrow town$; $\{missing|absent\} \rightarrow missing$.

Ross further divided this dataset into three randomly sampled partitions —a training partition (50%), a validation partition (20%) and a test partition (30%). The training partition was used as the core training data for the prediction models built. The validation partition was used for tuning tasks, and the test partition was used for nothing other than a final test of the model to evaluate its performance.

12.4 Modeling

The requirements for this model were that it be accurate, that it be capable of being integrated into the wider AT processes, and, possibly, that it act as a source of insight into the reasons people might churn. In selecting the appropriate model type to use, all these aspects, along with the structure of the data, should be taken into account. In this case, the ABT was composed of a mixture of continuous and categorical descriptive features and had a categorical target feature. The categorical target feature, in particular, makes decision trees a suitable choice for this modeling task. Furthermore, decision tree algorithms are capable of handling both categorical and continuous descriptive features as well as handling missing values and outliers without any need to transform the data. Finally, decision trees are relatively easy to interpret, which means that the structure of the model can give some insight into customer behavior. All these factors taken together indicated that decision trees were an appropriate modeling choice for this problem.

Ross used the ABT to train, tune, and test a series of decision trees to predict churn given the set of descriptive features. The first tree that Ross built used an entropy-based information gain as the splitting criterion, limited continuous splits to binary choices, and no pruning. Ross had decided, again in consultation with the business, that a simple classification accuracy rate was the most appropriate evaluation measure for this task. The first tree constructed achieved an **average class accuracy**⁷ of 74.873% on the hold-out test set, which was reasonably encouraging.

This tree is shown in [Figure 12.4](#)^[698], and the lack of pruning is obvious in its complexity. This complexity and the excessive depth of the tree suggest overfitting. In the second tree that he built, Ross employed **post-pruning using reduced error pruning**,⁸ which used the validation partition that was created from the initial dataset. The reasonably large dataset that Ross had to begin with, which in turn led to a reasonably large validation partition, meant that reduced error pruning was appropriate in this case.⁹ [Figure 12.5](#)^[699] shows the tree resulting from this training iteration. It should be clear that this is a much simpler tree than the previous one. The features used at the top levels of both trees, and deemed most informative by the algorithm, were the same: AVGOVERBUNDLEMINS, BILLAMOUNTCHANGEPCT, and HANDSETAGE.

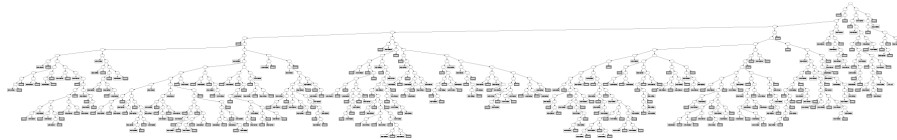


Figure 12.4

An unpruned decision tree built for the AT churn prediction problem (shown only to indicate its size and complexity). The excessive complexity and depth of the tree are evidence that overfitting has probably occurred.

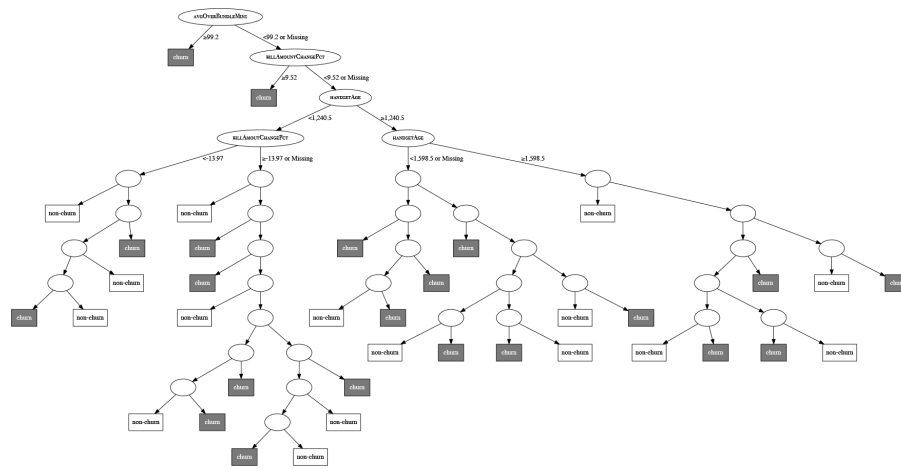


Figure 12.5

A pruned decision tree built for the AT churn prediction problem. Gray leaf nodes indicate a churn prediction, and clear leaf nodes indicate a non-churn prediction. For space reasons, we show only the features tested at the top-level nodes.

Using pruning, Ross was able to increase the average class accuracy on the hold-out test set to 79.03%, a significant improvement over the previous model. [Table 12.3](#)^[699] shows the confusion matrix from this test. The confusion matrix shows that this model was slightly more accurate when classifying instances with the *non-churn* target level than with the *churn* target level. Based on these, results Ross was confident that this tree was a good solution for the AT churn prediction problem.

Table 12.3

The confusion matrix from the test of the AT churn prediction stratified hold-out test set using the pruned decision tree in [Figure 12.5](#)^[699].

		Prediction		Recall
		<i>churn</i>	<i>non-churn</i>	
Target	<i>churn</i>	1,058	442	70.53
	<i>non-churn</i>	152	1,348	89.86

12.5 Evaluation

The model evaluations based on misclassification rate described in the previous section are the first step in evaluating the performance of the prediction model created. The classification accuracy of 79.03% is well above the target agreed on with the business. This is misleading, however. This performance is based on a stratified hold-out test set, which contains the same number of churners and non-churners. The underlying distribution of churners and non-churners within the larger AT customer base, however, is much different. Rather than a 50:50 split of churners to non-churners, the actual underlying ratio is, in fact, closer to 10:90. For this reason, it is very important to perform a second evaluation in which the test data reflect the actual distribution of target feature values in the business scenario.

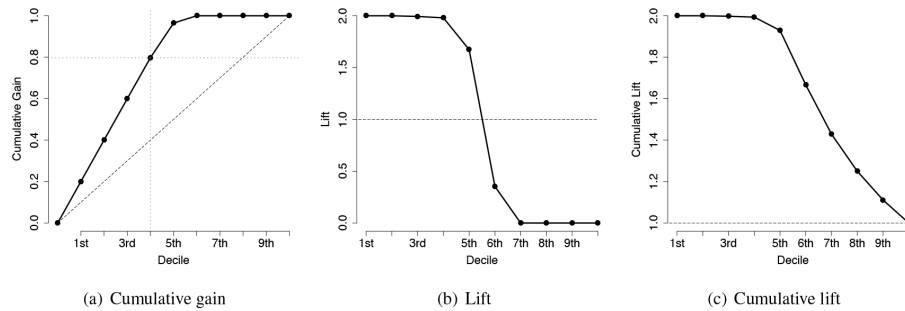
Ross had AT generate a second data sample (which did not overlap with the sample taken previously) that was not stratified according to the target feature values. The confusion matrix illustrating the performance of the prediction model on this test set is shown in [Table 12.4](#)^[700].

Table 12.4

The confusion matrix from the test of the AT churn prediction non-stratified hold-out test set.

		Prediction		Recall
		<i>churn</i>	<i>non-churn</i>	
Target	<i>churn</i>	1,115	458	70.88
	<i>non-churn</i>	1,439	12,878	89.95

The average class accuracy on the non-stratified hold-out test set was 79.284%. Ross also generated **cumulative gain**, **lift**, and **cumulative lift** charts for the dataset.¹⁰ These are shown in [Figure 12.6](#)[⁷⁰⁰]. The cumulative gain chart in particular shows that if AT were to call just 40% of their customer base, they would identify approximately 80% of the customers who are likely to churn, which is strong evidence that the model is doing a good job of distinguishing between different customer types.

**Figure 12.6**

(a) Cumulative gain, (b) lift, and (c) cumulative lift charts for the predictions made on the large test data sample.

Given these good results Ross decided that it was appropriate to present the model to other parts of the business. This was an important step in gaining credibility for the model. The tree shown in [Figure 12.5](#)[⁶⁹⁹] is reasonably straightforward to interpret, but when taken out to other parts of the business, it may be hard for people to deal with this much information, so Ross decided to create a purposefully stunted version of the decision tree, with only a small number of levels shown for the presentation of the model to the business (although he intended to use the larger pruned tree for actual deployment). The idea behind this was that stunting the tree made it more interpretable. The fact that the most informative features occupy berths toward the top of a tree means that stunted trees usually capture the

most important information. Many machine learning tools will allow the maximum depth of a tree to be specified as a parameter, which allows for the creation of such **stunted trees**.

Figure 12.7^[701] shows the stunted tree Ross generated for the churn problem, where the depth of the tree is limited to five layers. This tree results in a slightly lower classification accuracy on the test partition, 78.5%, but is very easy to interpret—the key features in determining churn are clearly AVGOVERBUNDLEMINS, BILLAMOUNTCHANGEPCT, and HANDSETAGE. It seems, from this data, that customers are most likely to churn when their bill changes dramatically, when they begin to exceed the bundled minutes in their call package, or when they have had a handset for a long time and are considering changing to something newer. This is useful information that the business can use to attempt to devise other churn handling strategies in parallel to using this model to create call lists for the retention team. The business was interested in the features that were selected as important to the tree, and there was a good deal of discussion on the omission of the features describing customers' interactions with AT customer care (these had been the basis of the organization's previous model).

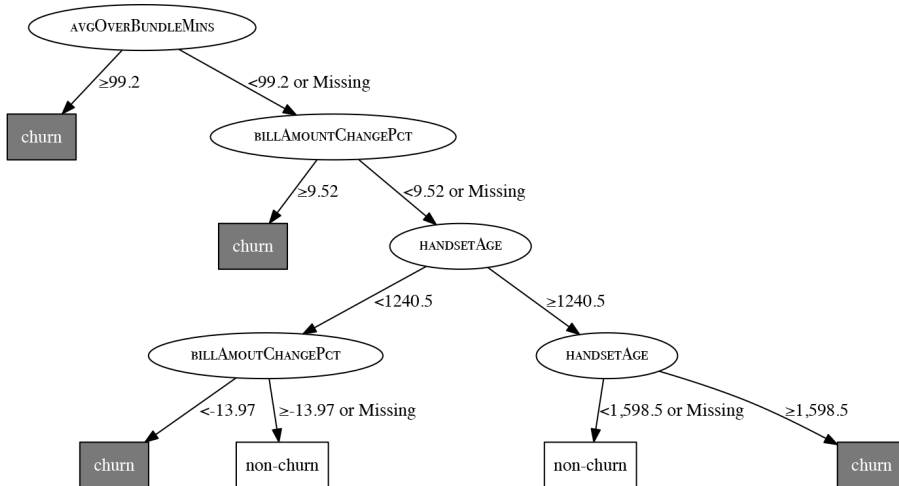


Figure 12.7

A pruned and stunted decision tree built for the Acme Telephonica churn prediction problem.

To further support his model, Ross organized a control group test (see Section 9.4.6^[578]) in which for two months, the AT customer base was randomly divided into two groups, and call lists for the retention team were

selected from the first group using the old approach based on calls to customer care, and for the second group using the new decision tree model. It was shown after two months that the churn rate within the sample for which the retention team used the new model to build their call list was approximately 7.4%, while for the group using the old model, it was over 10%. This experiment showed the AT executive team that the new decision tree model could significantly reduce churn rates within the AT customer base.

12.6 Deployment

Because AT was already using a process in which its retention team generated call lists based on collected data, deployment of the new decision tree model was reasonably straightforward. The main challenge was a return to the Data Preparation phase to make the routines used to extract the data for the ABT robust and reliable enough to be used to generate new query instances every month. This involved working with the AT IT department to develop deployment-ready **extract-transform-load** (ETL) routines. Code was then written to replace the previous simple rule about customer care contacts with the decision tree when retention call lists were generated.

The last step in deployment was to put in place an **ongoing model validation** plan to raise an alarm if evidence arose indicating that the deployed model had gone **stale**. In this scenario, feedback on the performance of the model implicitly arises within a reasonably short amount of time after predictions are made—churn predictions can be easily compared to actual customer behavior (taking into account interventions made by the business). The monitoring system that Ross put in place generated a report at the end of every quarter that evaluated the performance of the model in the previous quarter by comparing how many of the people not contacted by the retention team actually churned. If this number changed significantly from what was seen in the data used to build the model, the model would be deemed stale, and retraining would be required.

1. See Section 1.6^[15].

2. See Section 2.4.3^[36].

3. Obviously, churn events will happen on different dates for different customers; therefore, to build the ABT, the observation and outcome periods for different customers would have to be aligned. This situation is an example of the propensity model scenario illustrated in Figure 2.6^[39] in Section 2.4.3^[36].

4. The fact that active customers were defined as *current customers* means that they were all active on the same date—namely, whatever day the ABT was generated. This could be problematic: a model trained on this data might ignore seasonal effects such as Christmas. The alternative is to define active customers as any customer in the AT data that was active at some point. Such a definition, however, has the complication that the same customer could appear in the ABT as both an active and a churn customer, although admittedly the descriptive features for these two instances would be calculated over different periods of time.

5. We return to this discussion in Section 12.5^[698] and Section 13.4.1^[719].

6. See Section 3.4^[69].

7. All average class accuracies used in this section use a **harmonic mean**.

8. See Section 4.4.4^[153].

9. If data had been more scarce, pruning using a statistical test, such as χ^2 , would have been a more sensible route to take.

10. **Cumulative gain**, **lift**, and **cumulative lift** are introduced in Section 9.4.3.3^[565].

13

Case Study: Galaxy Classification

“The history of astronomy is a history of receding horizons.”

—Edwin Powell Hubble

Astronomy has gone through a revolution in recent years as the reducing costs of digital imaging has made it possible to collect orders of magnitude more data than ever before. Large-scale sky scanning projects are being used to map the whole of the night sky in intricate detail. This offers huge potential for new science based on this massive data collection effort. This progress comes at a cost, however, as all this data must be labeled, tagged, and cataloged. The old approach of doing all this manually has become obsolete because the volume of data involved is just too large.

The **Sloan Digital Sky Survey (SDSS)** is a landmark project that is cataloging the night sky in intricate detail and is facing exactly the problem described above.¹ The SDSS telescopes collect over 175GB of data every night, and for the data collected to be fully exploited for science, each night sky object captured must be identified and cataloged within this data in almost real time. Although the SDSS has been able to put in place algorithmic solutions to identifying certain objects within the images collected, there have been a number of difficulties. In particular, it has not been possible for the SDSS to develop a solution to automatically categorize galaxies into the different **morphological** groups—for example, spiral galaxies or elliptical galaxies.

This case study² describes the work undertaken when, in 2011, the SDSS hired Jocelyn, an analytics professional, to build a galaxy morphology classification model to include in their data processing pipeline. The

remainder of this chapter describes the work undertaken by Jocelyn on this project within each phase of the CRISP-DM process.

13.1 Business Understanding

When Jocelyn first arrived at SDSS, she was pleased to find that the business problem she was being asked to help with was already pretty well defined in predictive analytics terms. The SDSS pipeline takes the data captured by the SDSS instruments and processes it, before storing the results of this processing in a centrally accessible database. At the time Jocelyn arrived, the SDSS pipeline included rule-based systems that could classify night sky objects into broad categories—for example, stars and galaxies. SDSS scientists, however, were struggling to build rule-based systems that could accurately perform more fine-grained classifications. In particular, the SDSS scientists wanted a system that could reliably classify galaxies into the important morphological (i.e., shape) types: **elliptical galaxies** and **spiral galaxies**. Classifying galaxies according to **galaxy morphology** is standard practice in astronomy,³ and morphological categories have been shown to be strongly correlated with other important galaxy features. So, grouping galaxies by morphological type is a fundamentally important step in analyzing the characteristics of galaxies.

This was the challenge that the SDSS had hired Jocelyn to address. The scientists at SDSS wanted Jocelyn to build a machine learning model that could examine sky objects that their current rule-based system had flagged as being galaxies and categorize them as belonging to the appropriate morphological group. Although there remained some details left to agree on, the fact that the SDSS had defined their problem in terms of analytics meant that Jocelyn very easily completed the important step of converting a business problem into an analytics solution. Edwin was assigned to Jocelyn as her key scientific contact from SDSS and was eager to answer any questions Jocelyn had as he saw real value in the model she was developing.

The first detail that Jocelyn needed to agree on with Edwin was the set of categories into which sky objects should be categorized. The scientists at SDSS listed two key galaxy morphologies of interest: *elliptical* and *spiral*. The spiral category further divided into *clockwise spiral* and *anti-clockwise spiral* subcategories. [Figure 13.1](#)^[705] shows illustrations of these different

galaxy types. Jocelyn suggested that she would first work on the coarse classification of galaxies into elliptical and spiral categories, and then, depending on how this model performed, look at classifying spirals into the more fine-grained categories. Jocelyn also suggested that a third *other* category be included to take into account the fact that all the sky objects labeled as galaxies in the previous step in the SDSS may not actually be galaxies. Edwin agreed with both of these suggestions.

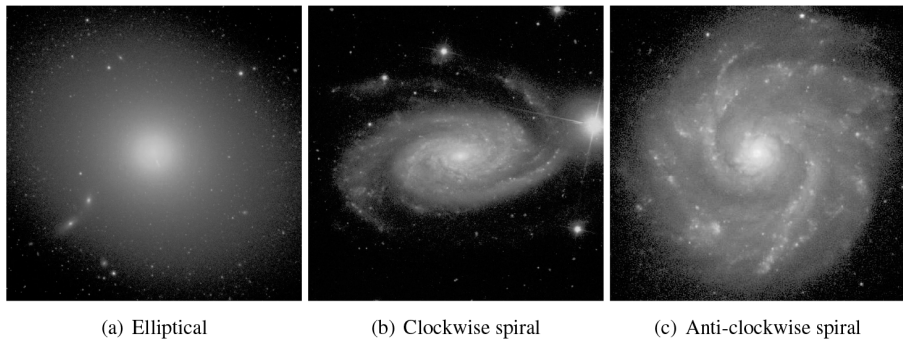


Figure 13.1

Examples of the different galaxy morphology categories into which SDSS scientists categorize galaxy objects. Credits for these images belong to the Sloan Digital Sky Survey, www.sdss3.org.

The second detail that Jocelyn needed to agree on with Edwin was the target accuracy that would be required by the system she would build in order for it to be of use to scientists at SDSS. It is extremely important that analytics professionals manage the expectations of their clients during the business understanding process, and agreeing on expected levels of model performance is one of the easiest ways in which to do this. This avoids disappointment and difficulties at later stages in a project. After lengthy discussion, both Jocelyn and Edwin agreed that in order for the system to be useful, a classification accuracy of approximately 80% would be required. Jocelyn stressed that until she had looked at the data and performed experiments, she could not make any predictions as to what classification accuracy would be possible. She did, however, explain to Edwin that because the categorization of galaxy morphologies is a somewhat subjective task (even human experts don't always fully agree on the category that a night sky object should belong to), it was unlikely that classification accuracies beyond 90% would be achievable.

Finally, Edwin and Jocelyn discussed how fast the model built would need to be to allow its inclusion in the existing SDSS pipeline. Fully processed data from the SDSS pipeline is available to scientists approximately one week after images of night sky objects are captured by the SDSS telescopes.⁴ The system that Jocelyn built would be added to the end of this pipeline because it would require outputs from existing data processing steps. It was important that the model Jocelyn deployed not add a large delay to data becoming available to scientists. Based on the expected volumes of images that would be produced by the SDSS pipeline, Jocelyn and Edwin agreed that the model developed should be capable of performing approximately 1,000 classifications per second on a dedicated server of modest specification.

13.1.1 Situational Fluency

The notion of **situational fluency**⁵ is especially important when dealing with scientific scenarios. It is important that analytics professionals have a basic grasp of the work their scientific partners are undertaking so that they can converse fluently with them. The real skill in developing situational fluency is determining how much knowledge about the application domain the analytics professional requires in order to complete the project successfully. It was not reasonable, nor necessary, to expect that Jocelyn would become fully familiar with the intricacies of the SDSS and the astronomy that it performs. Instead, she needed enough information to understand the key pieces of equipment involved, the important aspects of the night sky objects that she would be classifying, and the key terminology involved.

While complex scientific scenarios can make this process more difficult than is the case for more typical business applications, there is also the advantage that scientific projects typically produce publications clearly explaining their work. These kinds of publications are an invaluable resource for an analytics professional trying to come to grips with a new topic. Jocelyn read a number of publications by the SDSS team⁶ before spending several sessions with Edwin discussing the work that he and his colleagues did. The following short summary of the important things she learned illustrates the level of situational fluency required for this kind of scenario.

The SDSS project captures two distinct kinds of data—images of night-sky objects and **spectrographs** of night sky objects—using two distinct types of instrument, an imaging camera and a spectrograph.

The SSDS imaging camera captures images in *five* distinct **photometric bands**:⁷ ultra-violet (*u*), green (*g*), red (*r*), far-red (*i*), and near infrared (*z*). The raw imaging data captured from the SDSS telescopes is passed through a processing pipeline that identifies individual night sky objects and extracts a number of properties for each object. For galaxy classification, the most important properties extracted from the images are brightness, color, and shape. The measure of brightness used in the SDSS pipeline is referred to as **magnitude**. **Flux** is another measure that attempts to standardize measures of brightness, taking into account how far away different objects are from the telescope. Measures of flux and magnitude are made in each of the five photometric bands used by the SDSS imaging system. To measure the **color** of night sky objects, the flux measured in different photometric bands is compared. The image-based measures of overall galaxy shape are extracted from the images using **morphological** and **moment** image processing operations. These measures capture how well objects match template shapes—although none is accurate enough to actually perform the galaxy morphology prediction itself.

A **spectrograph** is a device that disperses the light emitted by an object into different wavelengths and measures the intensity of the emission of each wavelength—this set of measures is referred to as a **spectrogram**. The SDSS spectrographs perform this task for manually identified night sky objects and produce spectrograms across wavelengths from visible blue light to near-infrared light. Spectrography data may be useful in galaxy classification because different galaxy types are likely to emit different amounts of different light wavelengths, so spectrograms might be a good indicator for galaxy type. Spectrography also allows measurement of **redshift**, which is used to determine the distance of night sky objects from the viewer.

Once Jocelyn felt that she was suitably fluent with the SDSS situation, she proceeded to the Data Understanding phase of the CRISP-DM process so as to better understand the data available.

13.2 Data Understanding

Jocelyn's first step in fully understanding the data available to her was to define the **prediction subject**. In this case the task was to categorize galaxies according to morphology, and therefore galaxy made sense as the prediction subject. The structure of the dataset required for this task would contain one row per galaxy, and each row would include a set of descriptive features describing the characteristics of that galaxy object and a target feature indicating the morphological category of the galaxy object.

Based on her understanding of the SDSS process, Jocelyn sketched out the first draft of the domain concepts diagram for the galaxy classification problem shown in [Figure 13.2](#)^[708]. Jocelyn felt that the important **domain concepts** were likely to be the target (galaxy type), galaxy appearance measures (e.g., color), spectrography information (e.g., red shift), and position information (the position of each object in the night sky was also available from the SDSS pipeline). Data with which to implement features based on these domain concepts would likely come from the raw camera imaging and spectrograph images themselves, or from the results of the SDSS processing pipeline.

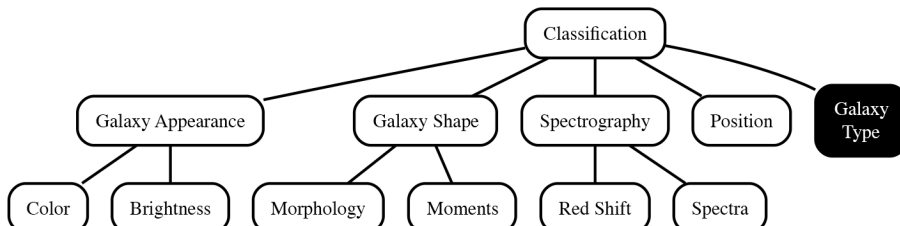


[Figure 13.2](#)

The first draft of the domain concepts diagram developed by Jocelyn for the galaxy classification task.

Jocelyn took this first domain concept draft along to a meeting with Ted, the SDSS chief data architect, to discuss the data resources that would be available for model building. Ted quickly made two observations. First, the spectrograph data collected by the SDSS telescopes was not nearly as extensive as the camera imaging data collected—while there was imaging data for millions of galaxies, there were spectrograms for only hundreds of thousands. Collecting spectrographic information involves a much more complicated process than capturing imaging data, so it is done for a much smaller portion of the sky. This was likely to continue to be the case, so any

solution that relied on spectrographic data as well as imaging data to classify galaxy types would work for only a fraction of the observations made by the SDSS telescopes.

Ted's second observation was that, although there was a huge amount of data available on past observations of night sky objects, only a tiny fraction of these contained manual labels indicating the morphological category to which they belonged. This meant that the data available at the SDSS did not contain a suitable target feature that Jocelyn could use to train prediction models. This is a very common scenario and a real thorn in the side of the predictive model builder—although there is often an almost endless amount of data available for training, little or none of it is labeled with the relevant target feature, making it effectively useless.

Jocelyn's options at this stage were (1) to embark on a large-scale manual data labeling project for which she would hire experts to manually label a suitably large set of historical night sky object observations, or (2) to find some other data source that she could add to the SDSS data to use as a target feature. While the first option is often used, Jocelyn was lucky that another data source became available. Through conversations with Edwin, Jocelyn became aware of a parallel project to the SDSS that offered an intriguing solution to her problem. **Galaxy Zoo**⁸ is a **crowdsourced, citizen science** effort in which people can log on to a website and categorize images of galaxies—taken from the SDSS—into different groups. The Galaxy Zoo project started in 2007 and since then has collected millions of classifications of hundreds of thousands of galaxies.

The galaxy types that Galaxy Zoo citizen scientists could choose from were *elliptical*, *clockwise spiral*, *anti-clockwise spiral*, *edge-on disk*, *merger*, and *don't know*. The first three types are self-explanatory and match directly with the categories of interest to the SDSS project. An *edge-on disk* is a spiral galaxy viewed from the edge, which makes the direction of the spiral arms unclear. A *merger* is a sky object in which multiple galaxies appear grouped together. Examples were labeled as *don't know* when a Galaxy Zoo participant could not place the object in question into one of the other categories.

The data from the Galaxy Zoo project was publicly available and therefore easily accessible to Jocelyn. Galaxy Zoo labels were available for approximately 600,000 SDSS galaxies, which Jocelyn felt would be more

than enough to use to train and test a galaxy morphology classification model. Conveniently, this also determined the subset of the SDSS dataset (those galaxies used in the Galaxy Zoo project) that Jocelyn would use for this project. With the knowledge that the Galaxy Zoo labels would provide her with a target feature, Jocelyn returned to speak with Ted again about getting access to the SDSS data.

Accessing the results of the SDSS processing pipeline turned out to be reasonably straightforward, as it was already collected into a single large table in the SDSS data repository. Ted organized a full download of the SDSS photo imaging data repository for all the objects for which Galaxy Zoo labels existed. This dataset contained 600,000 rows and 547 columns,⁹ with one row for each galaxy observation, containing identifiers, position information, and measures describing the characteristics of the galaxy.

Jocelyn decided to begin her data exploration work by focusing on the target feature. The structure of the data available from the Galaxy Zoo project is shown in [Table 13.1](#)^[709]. The category of each galaxy is voted on by multiple Galaxy Zoo participants, and the data includes the fraction of these votes for each of the categories.

Table 13.1

The structure of the SDSS and Galaxy Zoo combined dataset.

Name	Type	Description
OBJID	Continuous	Unique SDSS object identifier
P_EL	Continuous	Fraction of votes for elliptical galaxy category
P_CW	Continuous	Fraction of votes for clockwise spiral galaxy category
P_ACW	Continuous	Fraction of votes for anti-clockwise spiral galaxy category
P_EDGE	Continuous	Fraction of votes for edge-on disk galaxy category
P_MG	Continuous	Fraction of votes for merger category
P_DK	Continuous	Fraction of votes for don't know category

The raw data did not contain a single column that could be used as a target feature, so Jocelyn had to design one from the data sources that were present. She generated two possible target features from the data provided. In both cases, the target feature level was set to the galaxy category that received the majority of the votes. In the first target feature, just three levels were used: *elliptical* (P_{EL} majority), *spiral* (P_{CW} , P_{ACW} , or P_{EDGE} majority), and *other* (P_{MG} or P_{DK} majority). The second target feature

allowed three levels for spiral galaxies: *spiral_cw* (*p_CW* majority), *spiral_acw* (*p_ACW* majority), and *spiral_edge* (*p_EDGE* majority). Figure 13.3^[710] shows bar plots of the frequencies of the 3-level and the 5-level target features. The main observation that Jocelyn made from these is that galaxies in the dataset were not evenly distributed across the different morphology types. Instead, the *elliptical* level was much more heavily represented than the others in both cases. Using the 3-level target feature as her initial focus, Jocelyn began to look at the different descriptive features in the data downloaded from the SDSS repository that might be useful in building a model to predict galaxy morphology.

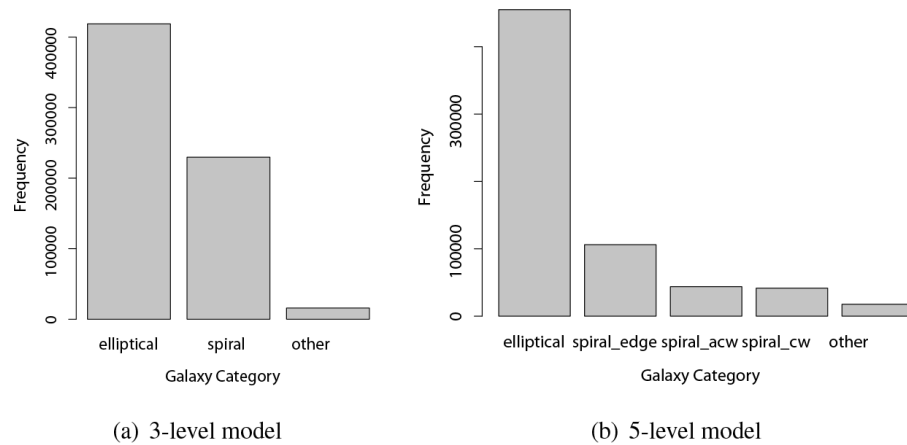


Figure 13.3

Bar plots of the different galaxy types present in the full SDSS dataset for the 3-level and 5-level target features.

The SDSS download that Jocelyn had access to was a big dataset—over 600,000 rows. Although modern predictive analytics and machine learning tools can handle data of this size, a large dataset can be cumbersome when performing data exploration operations—calculating summary statistics, generating visualizations, and performing correlation tests can just take too long. For this reason, Jocelyn extracted a small sample of 10,000 rows from the full dataset for exploratory analysis using **stratified sampling**.

Given that (1) the SDSS data that Jocelyn downloaded was already in a single table; (2) the data was already at the right prediction subject level (one row per galaxy); and (3) many of the columns in this dataset would most likely be used directly as features in the ABT that she was building, Jocelyn decided to produce a **data quality report** on this dataset. Table

[13.2](#)^[711] shows an extract from this data quality report. At this point Jocelyn was primarily interested in understanding the amount of data available, any issues that might arise from missing values, and the types of each column in the dataset.

Table 13.2

Analysis of a subset of the features in the SDSS dataset.

Feature	% Count Miss. Card.			1 st Min. Qrt.			3 rd Mean Median Qrt.			Std. Max. Dev.	
	Count	Miss.	Card.	Min.	Qrt.	Mean	Median	Max.	Dev.		
RUN	10,000	0.00	380	109.00	2,821.00	3,703.45	3,841.00	4,646.00	8,095.00	1,378.82	
RA.1	10,000	0.00	9,964	0.03	151.38	185.26	185.02	220.56	359.99	59.12	
DEC.1	10,000	0.00	9,928	-11.23	9.71	24.87	23.41	39.11	69.83	18.92	
ROWC_U	10,000	0.00	1	0.00	0.00	0.00	0.00	0.00	0.00	0.00	
ROWC_G	10,000	0.00	1	0.00	0.00	0.00	0.00	0.00	0.00	0.00	
ROWC_R	10,000	0.00	1	0.00	0.00	0.00	0.00	0.00	0.00	0.00	
ROWC_I	10,000	0.00	1	0.00	0.00	0.00	0.00	0.00	0.00	0.00	
ROWC_Z	10,000	0.00	1	0.00	0.00	0.00	0.00	0.00	0.00	0.00	
SKYIVAR_U	10,000	0.00	9,986	-9,999.00	459.81	78.89	798.27	1,083.65	2,197.09	450.26	
SKYIVAR_G	10,000	0.00	9,989	-9,999.00	439.55	965.88	2,957.92	6,005.71	9,913.59	2,766.70	
SKYIVAR_R	10,000	0.00	9,988	-9,999.00	123.31	201.91	1,091.78	3,347.77	4,623.07	1,514.50	
SKYIVAR_I	10,000	0.00	9,986	-9,999.00	46.02	174.79	434.48	1,825.93	2,527.57	851.42	
SKYIVAR_Z	10,000	0.00	9,986	-9,999.00	13.60	-234.23	49.57	75.39	205.07	44.51	
PSFMAG_U	10,000	0.00	9,768	7.47	20.60	21.08	21.13	21.598	26.19	0.85	
PSFMAG_G	10,000	0.00	9,743	8.30	19.06	19.48	19.54	19.967	26.17	0.78	
PSFMAG_R	10,000	0.00	9,744	7.45	18.23	18.65	18.68	19.113	26.49	0.76	
PSFMAG_I	10,000	0.00	9,744	7.33	17.83	18.27	18.26	18.722	25.46	0.80	
PSFMAG_Z	10,000	0.00	9,747	7.40	17.47	17.93	17.90	18.381	23.92	0.82	
DEVFLUX_U	10,000	0.00	9,990	-3.68	11.64	43.05	23.07	44.31	28,616.04	194.73	
DEVFLUX_G	10,000	0.00	9,987	-1,278.28	48.79	143.71	77.06	133.46	614,662.80	2,401.59	
DEVFLUX_R	10,000	0.00	9,983	-4.37	111.04	267.74	152.75	250.65	137,413.00	993.65	
DEVFLUX_I	10,000	0.00	9,980	-4.06	160.42	390.98	216.57	351.21	608,862.80	3,041.20	
DEVFLUX_Z	10,000	0.00	9,983	-14.72	204.72	528.69	276.99	447.45	2,264,700.00	9,073.95	

Jocelyn was surprised that none of the columns had any missing values. Although this is not unheard of (particularly in cases like the SDSS project in which data is generated in a fully automated process), it is very unusual. The minimum values of - 9,999 for the SKYIVAR_U/G/R/I/Z columns (and some others not shown in [Table 13.2](#)^[711]), which were so different from the means for those columns, suggested that maybe there were missing values after all.¹⁰ There were also a number of columns, such as ROWC_U/G/R/I/Z, that had cardinality of 1 (and standard deviations of zero) indicating that

every row had the same. These features contained no actual information, so should be removed from the dataset. Having performed this initial analysis, Jocelyn met again with Edwin and Ted to discuss the data quality issues and, more generally, to review the domain concepts outlined in [Figure 13.2](#)^[708] so as to begin designing the actual descriptive features that would populate the ABT. Edwin was broadly in agreement with the set of domain concepts that Jocelyn had developed and was very positive about the use of Galaxy Zoo classifications as a source for generating the target feature. He did explain, however, that Jocelyn's suggestion of using position information was very unlikely to be useful, so that was removed from the set of domain concepts. Edwin also agreed that Ted was correct about the unavailability of spectrograph data for most objects, so this was also removed. The final domain concept diagram is shown in [Figure 13.4](#)^[712]. Edwin helped Jocelyn align the columns in the raw SDSS dataset with the different domain concepts, which generated a good set of descriptive features within each domain concept.

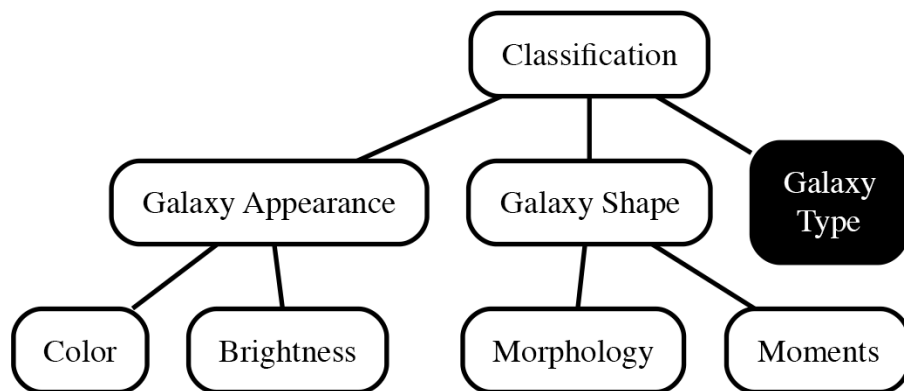


Figure 13.4

The revised domain concepts diagram for the galaxy classification task.

Both Edwin and Ted were surprised to see missing values in the data, as it was produced through a fully automated process. Simply through eyeballing the data, Jocelyn uncovered the fact that, in almost all cases, when one suspect – 9,999 value was present in a row in the dataset, that row contained a number of suspect – 9,999 values (this was the case for 2% of the rows in the dataset). Although neither Edwin nor Ted could understand exactly how this had happened, they agreed that something had obviously gone wrong in the processing pipeline in those cases and that the

– 9,999 values must refer to missing values.¹¹ **Complete case analysis** was used to entirely remove any rows containing two or more – 9,999, or missing, values. Before performing this operation, however, Jocelyn first checked that the percentage of missing values was approximately 2% in each of the 3 levels (and in each of the levels in the 5-level model) to ensure that there was no relationship between missing values and galaxy type. There was no obvious relationship, so Jocelyn was confident that removing rows containing missing values would not affect one target level more than the others.

One of the advantages of working in scientific scenarios is that there is a body of literature that discusses how other scientists have addressed similar problems. Working with Edwin, Jocelyn reviewed the relevant literature and discovered a number of very informative articles discussing descriptive features that were likely to be useful in classifying galaxy morphologies.¹² In particular, a number of interesting features that could be derived from the flux and magnitude measurements already in the SDSS dataset were described in the literature. Jocelyn implemented these derived features for inclusion in the final ABT.

In many instances the SDSS dataset contained the same measurement for a night sky object measured separately for each of the five photometric bands covered by the SDSS telescope. Because of this, Jocelyn suspected that there would be a large amount of redundancy in the data as the measurements in the different bands were likely to be highly correlated. To investigate this idea, she generated SPLOM charts for different photometric band versions of a selection of columns from the dataset (see [Figure 13.5^{\[714\]}](#)), and these showed significant relationships, which confirmed her suspicion. Jocelyn showed these charts to Edwin. Edwin agreed that it was likely that correlations existed between measurements in the different photometric bands but stressed, however, that differences across these bands would exist and might be quite important in predicting galaxy morphology. The existence of a high level of correlation between measurements indicated to Jocelyn that feature selection would be important later during the modeling phase as it had the potential to massively reduce the dimensionality of the dataset.

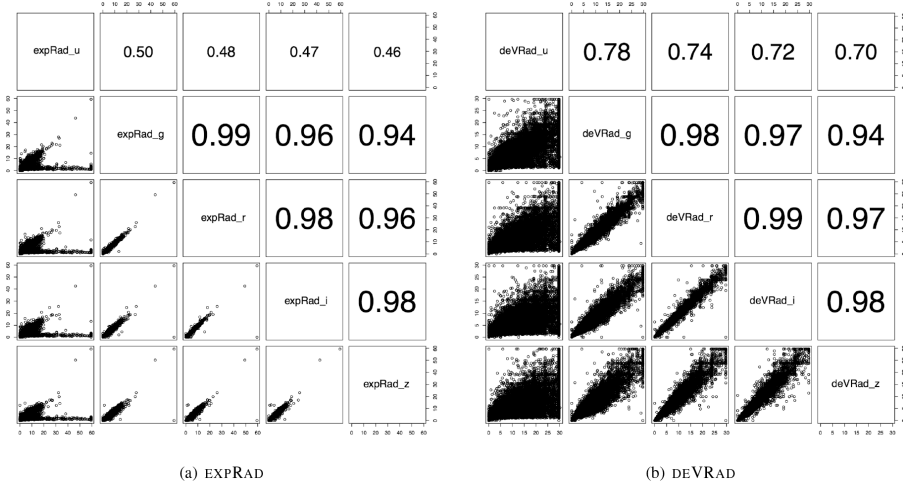


Figure 13.5

SPLOM diagrams of (a) the EXPRAD; and (b) DEVRAD measurements from the raw SDSS dataset. Each SPLOM shows the measure across the five different photometric bands captured by the SDSS telescope (u , g , r , i , and z).

At this point the design of the ABT had fallen into place. For the most part, Jocelyn would use descriptive features directly from the raw SDSS data. These would be augmented with a small number of derived features that the literature review undertaken with Edwin had identified. Jocelyn was now ready to move into the **Data Preparation** phase, during which she would populate the ABT, analyze its contents in detail, and perform any transformations that were required to handle data quality issues.

13.3 Data Preparation

After removing a large number of the columns from the raw SDSS dataset, introducing a number of derived features, and generating two target features, Jocelyn generated an ABT containing 327 descriptive features and two target features. [Table 13.3](#)^[715] lists these features (features that occur over all five photometric bands are listed as NAME_U/G/R/I/Z to save space).^[13]

Table 13.3

Features from the ABT for the SDSS galaxy classification problem.

Feature	Feature	Feature
SKYIVAR_U/G/R/I/Z	UERR_U/G/R/I/Z	EXPFLUX_U/G/R/I/Z
PSFMAG_U/G/R/I/Z	ME1_U/G/R/I/Z	EXPFLUXIVAR_U/G/R/I/Z
PSFMAGERR_U/G/R/I/Z	ME2_U/G/R/I/Z	MODELFLUXIVAR_U/G/R/I/Z
FIBERMAG_U/G/R/I/Z	ME1E1ERR_U/G/R/I/Z	CMODELFLUX_U/G/R/I/Z
FIBERMAGERR_U/G/R/I/Z	ME1E2ERR_U/G/R/I/Z	CMODELFLUXIVAR_U/G/R/I/Z

FIBER2MAG_U/G/R/I/Z	ME2E2ERR_U/G/R/I/Z	APERFLUX7_U/G/R/I/Z
FIBER2MAGERR_U/G/R/I/Z	MRRCC_U/G/R/I/Z	APERFLUX7IVAR_U/G/R/I/Z
PETROMAG_U/G/R/I/Z	MRRCCERR_U/G/R/I/Z	LNLSTAR_U/G/R/I/Z
PETROMAGERR_U/G/R/I/Z	MCR4_U/G/R/I/Z	LNLEXP_U/G/R/I/Z
PSFFLUX_U/G/R/I/Z	DEVRAD_U/G/R/I/Z	LNLDEV_U/G/R/I/Z
PSFFLUXIVAR_U/G/R/I/Z	DEVRADERR_U/G/R/I/Z	FRACDEV_U/G/R/I/Z
FIBERFLUX_U/G/R/I/Z	DEVAB_U/G/R/I/Z	DERED_U/G/R/I/Z
FIBERFLUXIVAR_U/G/R/I/Z	DEVABERR_U/G/R/I/Z	DEREDDIFF_U_G
FIBER2FLUX_U/G/R/I/Z	DEVMAG_U/G/R/I/Z	DEREDDIFF_G_R
FIBER2FLUXIVAR_U/G/R/I/Z	DEVMAGERR_U/G/R/I/Z	DEREDDIFF_R_I
PETROFLUX_U/G/R/I/Z	DEVFLUX_U/G/R/I/Z	DEREDDIFF_I_Z
PETROFLUXIVAR_U/G/R/I/Z	DEVFLUXIVAR_U/G/R/I/Z	PETRORATIO_I
PETRORAD_U/G/R/I/Z	EXPRAD_U/G/R/I/Z	PETRORATIO_R
PETRORADERR_U/G/R/I/Z	EXPRADERR_U/G/R/I/Z	AE_I
PETROR50_U/G/R/I/Z	EXPAB_U/G/R/I/Z	PETROMAGDIFF_U_G
PETROR50ERRQ_U/G/R/I/Z	EXPABERR_U/G/R/I/Z	PETROMAGDIFF_G_R
PETROR90_U/G/R/I/Z	EXP MAG_U/G/R/I/Z	PETROMAGDIFF_R_I
PETROR90ERRQ_U/G/R/I/Z	EXP MAGERR_U/G/R/I/Z	PETROMAGDIFF_I_Z
Q_U/G/R/I/Z	CMODELMAG_U/G/R/I/Z	GALAXY_CLASS_3
QERR_U/G/R/I/Z	CMODELMAGERR_U/G/R/I/Z	GALAXY_CLASS_5
U_U/G/R/I/Z		

Once Jocelyn had populated the ABT, she generated a data quality report (the initial data quality report covered the data in the raw SDSS dataset only, so a second one was required that covered the actual ABT) and performed an in-depth analysis of the characteristics of each descriptive feature. An extract from this data quality report is shown in [Table 13.4](#)^[716].

Table 13.4

A data quality report for a subset of the features in the SDSS ABT.

Feature	Count	% Miss.		Min.	1 st Qrt.		Median	3 rd Qrt.		Max.	Std. Dev.
		Card.	Qrt.		Mean	Median		Qrt.	Max.		
SKYIVAR_U	640,432	0.00	639,983	0.00	465.53	784.78	793.20	1,079.53	2,190.05	447.36	
SKYIVAR_G	640,432	0.00	640,081	0.00	442.55	3,318.72	2,949.62	6,008.31	9,898.47	2,769.84	
SKYIVAR_R	640,432	0.00	640,178	0.00	127.18	1,629.86	1,094.93	3,342.65	4,596.46	1,513.38	
SKYIVAR_I	640,432	0.00	640,042	0.00	48.28	842.18	436.13	1,825.88	2,515.35	852.73	
SKYIVAR_Z	640,432	0.00	640,042	0.00	13.90	52.19	49.76	75.10	205.69	44.19	
ME2_G	640,432	0.00	629,246	-0.96	-0.13	0.01	0.01	0.15	0.97	0.28	
FIBER2FLUXIVAR_U	640,432	0.00	639,827	0.00	20.31	27.24	25.96	32.40	170.70	11.02	
PSFMAG_U	640,432	0.00	632,604	13.76	20.59	21.05	21.12	21.58	25.56	0.81	
PETROFLUXIVAR_U	640,432	0.00	627,391	0.00	0.16	0.40	0.31	0.53	6.29	0.36	
LNLSTAR_R	640,432	0.00	639,690	-218,875.30	-12,623.05	-12,009.95	-6,771.37	-4,308.99	0.00	16,193.73	
PETROMAG_R	640,432	0.00	628,562	11.72	16.76	17.08	17.29	17.61	22.72	0.75	
EXPAB_I	640,432	0.00	623,467	0.05	0.49	0.65	0.67	0.81	1.00	0.20	
DEREDDIFF_U_G	640,432	0.00	630,319	-2.47	1.29	1.61	1.67	1.89	6.67	0.40	
DEREDDIFF_G_R	640,432	0.00	631,627	-1.06	0.64	0.82	0.84	0.99	4.70	0.27	
DEREDDIFF_R_I	640,432	0.00	611,597	-4.46	0.36	0.39	0.40	0.44	2.22	0.10	
DEREDDIFF_LZ	640,432	0.00	615,131	-2.29	0.23	0.28	0.30	0.34	5.33	0.11	
PETRORATIO_I	640,432	0.00	640,432	1.12	2.33	2.67	2.68	3.01	25.52	0.46	
PETRORATIO_R	640,432	0.00	640,432	1.18	2.29	2.63	2.64	2.96	10.05	0.42	
AE_I	640,432	0.00	640,432	0.00	0.13	0.27	0.23	0.38	0.90	0.18	
MODELMAJDIFF_U_G	640,432	0.00	630,476	-2.45	1.33	1.65	1.71	1.94	6.83	0.40	
MODELMAJDIFF_G_R	640,432	0.00	630,437	-1.05	0.68	0.85	0.87	1.03	4.75	0.27	
MODELMAJDIFF_R_I	640,432	0.00	613,667	-4.46	0.38	0.41	0.42	0.47	2.25	0.10	
MODELMAJDIFF_LZ	640,432	0.00	615,346	-2.27	0.25	0.29	0.32	0.35	5.34	0.11	
PETROMAGDIFF_G_R	640,432	0.00	631,901	-1.99	0.64	0.83	0.84	1.00	5.13	0.28	
PETROMAGDIFF_R_I	640,432	0.00	612,827	-3.32	0.35	0.39	0.41	0.45	2.83	0.11	
PETROMAGDIFF_LZ	640,432	0.00	620,422	-4.43	0.19	0.24	0.27	0.33	3.69	0.15	

The magnitude of the maximum values for the FIBER2FLUXIVAR_U feature in comparison to the median and 3rd quartile value was unusual and suggested the presence of outliers. The difference between the mean and median values for the SKYIVAR_R feature also suggested the presence of outliers. Similarly, the difference between the mean and median values for the LNLSTAR_R feature suggested that the distribution of this feature was heavily skewed and also suggested the presence of outliers. Figure 13.6^[717] shows histograms for these features. The problems of outliers and skewed distributions is clearly visible in these distributions. A number of other features exhibited a similar pattern.

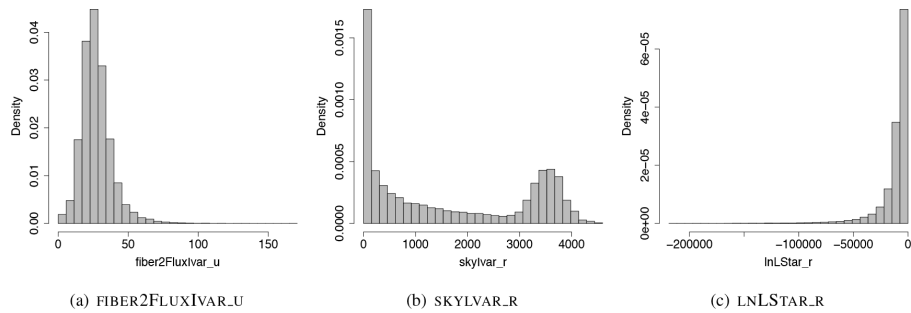


Figure 13.6

Histograms of a selection of features from the SDSS dataset.

With Edwin’s help, Jocelyn investigated the actual data in the ABT to determine whether the extreme values in the features displaying significant skew or the presence of outliers were due to **valid outliers** or **invalid outliers**. In all cases the extreme values were determined to be valid outliers. Jocelyn decided to use the **clamp transformation** to change the values of these outliers to something closer to the central tendency of the features. Any values beyond the 1st quartile value plus 2.5 times the inter-quartile range were reduced to this value. The standard value of 1.5 times the inter-quartile range was changed to 2.5 to slightly reduce the impact of this operation.

Jocelyn also made the decision to normalize all the descriptive features into **standard scores**. The differences in the ranges of values of the set of descriptive features in the ABT was huge. For example, `deVAB_R` had a range as small as [0.05,1.00] while `APERFLUX7IVAR_U` had a range as large as [-265,862,15,274]. Standardizing the descriptive feature in this way was likely to improve the accuracy of the final predictive models. The only drawback to standardization is that the models become less interpretable. Interpretability, however, was not particularly important for the SDSS scenario (the model built would be added to the existing SDSS pipeline and process thousands of galaxy objects per day), so standardization was appropriate.

Jocelyn also performed a simple first-pass feature selection using the 3-level model to see which features might stand out as predictive of galaxy morphology. Jocelyn used the **information gain** measure to rank the predictiveness of the different features in the dataset (for this analysis, missing values were simply omitted). The columns identified as being most

predictive of galaxy morphology were EXPRAD_G (0.3908), EXPRAD_R (0.3649), DEVRADE_G (0.3607), EXPRAD_I (0.3509), DEVRADE_R (0.3467), EXPRAD_Z (0.3457), and MRRCC_G (0.3365). Jocelyn generated histograms for all these features compared to the target feature—for example, [Figure 13.7](#)^[718] shows the histograms for the EXPRAD_R feature. It was encouraging that in many cases distinct distributions for each galaxy type were apparent in the histograms. [Figure 13.8](#)^[718] shows small multiple box plots divided by galaxy type for a selection of features from the ABT. The differences between the three box plots in each plot gives an indication of the likely predictiveness of each feature. The presence of large numbers of outliers can also be seen.

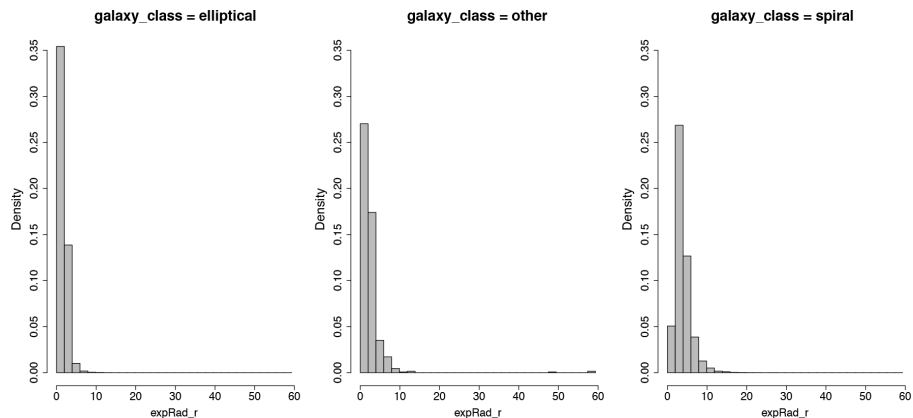


Figure 13.7

Histograms of the EXPRAD_R feature split by target feature level.

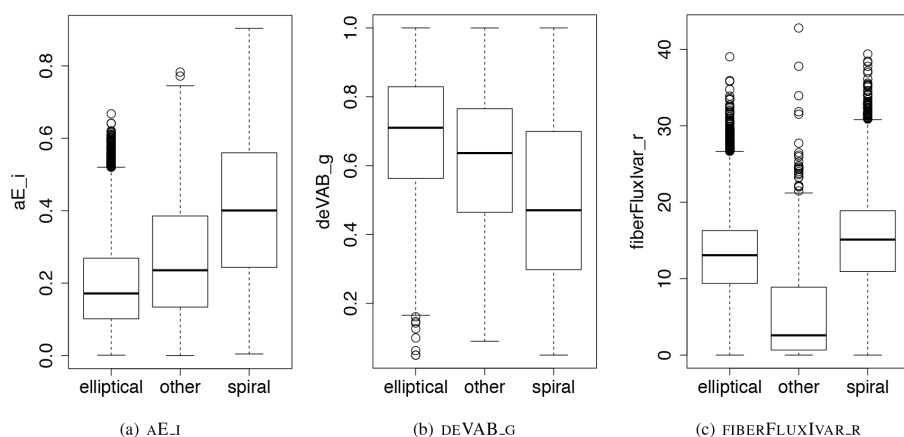


Figure 13.8

(a)–(c) Small multiple box plots (split by the target feature) of some of the features from the SDSS ABT.

13.4 Modeling

The descriptive features in the SDSS dataset are primarily continuous. For this reason, Jocelyn considered trying a similarity-based model, the ***k* nearest neighbor**, and two error-based models, the **logistic regression** model and the **support vector machine**. Jocelyn began by constructing a simple baseline model using the 3-level target feature.

13.4.1 Baseline Models

Because of the size of the ABT, Jocelyn decided to split the dataset into a **training set** and a large **hold-out test set**. Subsets of the training set would be also used for **validation** during the model building process. The training set consisted of 30% of the data in the ABT (approximately 200,000 instances), and the test set consisted of the remaining 70% (approximately 450,000 instances).¹⁴ Using the training set, Jocelyn performed a 10-fold cross validation experiment on models trained to use the full set of descriptive features to predict the 3-level target. These would act as baseline performance scores that she would try to improve upon. The classification accuracies achieved during the cross validation experiment were 82.912%, 86.041%, and 85.942% by the *k* nearest neighbor, logistic regression, and support vector machine models respectively. The confusion matrices from the evaluation of these models are shown in [Table 13.5](#)^[720].

Table 13.5

The confusion matrices for the baseline models.

(a) k nearest neighbor model (classification accuracy: 82.912%, average class accuracy: 54.663%)

		Prediction			Recall
		<i>elliptical</i>	<i>spiral</i>	<i>other</i>	
Target	<i>elliptical</i>	115,438	10,238	54	91.814%
	<i>spiral</i>	19,831	50,368	18	71.731%
	<i>other</i>	2,905	1,130	18	0.442%

(b) logistic regression model (classification accuracy: 86.041%, average class accuracy: 62.137%)

		Prediction			Recall
		<i>elliptical</i>	<i>spiral</i>	<i>other</i>	
Target	<i>elliptical</i>	115,169	10,310	251	91.600%
	<i>spiral</i>	13,645	56,321	251	80.209%
	<i>other</i>	2,098	1,363	592	14.602%

(c) support vector machine model (classification accuracy: 85.942%, average class accuracy: 58.107%)

		Prediction			Recall
		<i>elliptical</i>	<i>spiral</i>	<i>other</i>	
Target	<i>elliptical</i>	114,721	10,992	18	91.244%
	<i>spiral</i>	13,089	57,092	36	81.307%
	<i>other</i>	2,654	1,327	72	1.770%

These initial baseline results were promising; however, one key issue did emerge. It was clear that the performance of the models trained using the SDSS data was severely affected by the **target level imbalance** in the data —there were many more examples of the *elliptical* target level than either the *spiral* or, especially, the *other* target level. Having a dominant target level, like the *elliptical* target level in this example, means that models trained on this data can overcompensate for the majority target level and ignore the minority ones. For example, based on the confusion matrix in [Table 13.5\(c\)](#)^[720], the misclassification rate for the *elliptical* target level is only 8.756%, while for the *spiral* target level, it is higher, at 18.693%, and

for the *other* target level, it is a fairly dire 98.230%. The single classification accuracy performance measure hides this poor performance on the minority target levels. An average class accuracy performance measure, however, brings this issue to the fore. The average class accuracy scores achieved by the models were 54.663%, 62.137%, and 58.107% by the k nearest neighbor, logistic regression, and support vector machine models respectively. Jocelyn decided to build a second set of models in which she would address the target level imbalance issue.

The target level imbalance in the SDSS dataset arises through **relative rarity**.¹⁵ In the large SDSS dataset, there are plenty of galaxies in the *other* and *spiral* categories; there are just many more in the *elliptical* category. In this case, Jocelyn addressed the target level imbalance problem by using **under-sampling** to generate a new training dataset in which all three target levels had an equal distribution. This was referred to as the **under-sampled training set**. Jocelyn performed the same baseline test on the three model types using this new dataset. The resulting confusion matrices are shown in [Table 13.6](#)^[721].

Table 13.6

The confusion matrices showing the performance of models on the under-sampled training set.

(a) k nearest neighbor model (classification accuracy: 73.965%)

		Prediction			Recall
		<i>elliptical</i>	<i>spiral</i>	<i>other</i>	
Target	<i>elliptical</i>	23,598	4,629	5,253	70.483%
	<i>spiral</i>	4,955	24,734	3,422	74.700%
	<i>other</i>	3,209	4,572	25,628	76.711%

(b) logistic regression model (classification accuracy: 78.805%)

		Prediction			Recall
		<i>elliptical</i>	<i>spiral</i>	<i>other</i>	
Target	<i>elliptical</i>	25,571	4,203	3,706	76.378%
	<i>spiral</i>	3,677	26,267	3,166	79.331%
	<i>other</i>	2,684	3,763	26,963	80.705%

(c) support vector machine model (classification accuracy: 78.226%)

		Prediction			Recall
		<i>elliptical</i>	<i>spiral</i>	<i>other</i>	
Target	<i>elliptical</i>	24,634	4,756	4,089	73.579%
	<i>spiral</i>	3,763	26,310	3,038	79.460%
	<i>other</i>	2,584	3,550	27,275	81.640%

The resulting classification accuracies (average class accuracies and classification accuracies are the same in this case because the dataset is balanced) from the 10-fold cross validation experiment were 73.965%, 78.805%, and 78.226% for the k nearest neighbor, logistic regression, and support vector machine models respectively. The overall performance on

this balanced dataset was not as good as the performance on the original dataset; however, balancing the training set did result in the performance on each target level being more equal. Predictions for the *other* target level are actually being performed this time, whereas in the previous example, this target level was essentially being ignored. Choosing between models in this sort of scenario is difficult as it really comes down to balancing the needs of the application—when the system makes errors (as it inevitably will from time to time), what error is least bad? In this example, is it better to classify a galaxy that should be *other* as an *elliptical* galaxy or vice versa? Jocelyn discussed this issue and the results of these two baseline experiments with Edwin, and both decided that it would be best to pursue the optimal performance measured by overall classification accuracy because, in practice, the important thing for the SDSS system was to classify *elliptical* and *spiral* galaxies as accurately as possible.

With these baseline performance measures established, Jocelyn turned her attention to feature selection in an effort to improve on these performance scores.

13.4.2 Feature Selection

In the SDSS dataset, many of the features are represented multiple times for each of the five different photometric bands, and this made Jocelyn suspect that many of these features might be redundant and so ripe for removal from the dataset. **Feature selection** approaches that search through subsets of features (known as **wrapper** approaches) are better at removing redundant features than rank and prune approaches because they consider groups of features together. For this reason, Jocelyn chose to use a **step-wise sequential search** for feature selection for each of the three model types. In all cases overall classification accuracy was used as the fitness function that drove the search. After feature selection, the classification accuracy of the models on the test set were 85.557%, 88.829%, and 87.188% for the k nearest neighbor, logistic regression, and support vector machine models respectively. The resulting confusion matrices are shown in [Table 13.7](#)^[723]. In all cases performance of the models improved with feature selection. The best performing model is the logistic regression model. For this model, just 31 out of the total 327 features were selected.^{[16](#)}

This was not surprising given the large amount of redundancy within the feature set.

Table 13.7

The confusion matrices for the models after feature selection.

(a) k nearest neighbor model (classification accuracy: 85.557%, average class accuracy: 57.617%)

		Prediction			Recall
		<i>elliptical</i>	<i>spiral</i>	<i>other</i>	
Target	<i>elliptical</i>	116,640	9,037	54	92.770%
	<i>spiral</i>	15,833	54,366	18	77.426%
	<i>other</i>	2,815	1,130	108	2.655%

(b) logistic regression model (classification accuracy: 88.829%, average class accuracy: 67.665%)

		Prediction			Recall
		<i>elliptical</i>	<i>spiral</i>	<i>other</i>	
Target	<i>elliptical</i>	117,339	8,302	90	93.326%
	<i>spiral</i>	10,812	59,297	108	84.448%
	<i>other</i>	1,757	1,273	1,022	25.221%

(c) support vector machine model (classification accuracy: 87.188%, average class accuracy: 60.868%)

		Prediction			Recall
		<i>elliptical</i>	<i>spiral</i>	<i>other</i>	
Target	<i>elliptical</i>	115,152	10,561	18	91.586%
	<i>spiral</i>	11,243	58,938	36	83.938%
	<i>other</i>	2,528	1,237	287	7.080%

Based on these results, Jocelyn determined that the logistic regression model trained using the reduced set of features was the best model to use for galaxy classification. This model gave the best prediction accuracy and offered the potential for very fast classification times, which was attractive for integration into the SDSS pipeline. Logistic regression models also produce confidences along with the predictions, which was attractive to

Edwin as it meant that he could build tests into the pipeline that would redirect galaxies with low confidence classifications for manual confirmation of the predictions made by the automated system.

13.4.3 The 5-Level Model

To address the finer grained 5-level (*elliptical*, *spiral_cw*, *spiral_acw*, *spiral_eo*, and *other*) classification task, Jocelyn attempted two approaches. First, she used a 5-target-level model to make predictions. Second, she used a **two-stage model**. In this case the logistic regression model used for the 3-level target feature would first be used, and then a model trained to distinguish only between different spiral galaxy types (*clockwise*, *anti-clockwise*, and *edge-on*) would be used to further classify those galaxy objects classified as *spiral* by the first stage.

Based on the performance of the logistic regression model on the 3-level classification problem, Jocelyn trained a logistic regression classifier on the 5-level dataset and evaluated it using a 10-fold cross validation. Following the same approach as in earlier models, Jocelyn performed feature selection using a **step-wise sequential search** to find the best subset of features for this model. Just 11 features from the full set were selected.¹⁷ The resulting classification accuracy on the best performing model that Jocelyn could build was 77.528% (with an average class accuracy of 43.018%). The confusion matrix from this test is shown in [Table 13.8](#)^[724]. The overall accuracy of this model is somewhat comparable with the overall accuracy of the 3-level model. The classifier accurately predicts the type of galaxies with the *elliptical* target level and, to a lesser extent, with the *spiral_eo* target level. The ability of the model to distinguish between clockwise (*spiral_cw*) and anti-clockwise (*spiral_acw*) spiral galaxies, however, is extremely poor.

Table 13.8

The confusion matrix for the 5-level logistic regression model (classification accuracy: 77.528%, average class accuracy: 43.018%).

		Prediction					Recall
		<i>elliptical</i>	<i>spiral_cw</i>	<i>spiral_acw</i>	<i>spiral_eo</i>	<i>other</i>	
Target	<i>elliptical</i>	120,625	46	1,515	3,450	95	95.939%
	<i>spiral_cw</i>	7,986	373	4,715	2,176	30	2.443%
	<i>spiral_acw</i>	8,395	435	4,928	2,272	35	30.673%
	<i>spiral_eo</i>	8,719	75	1,018	28,981	78	74.556%
	<i>other</i>	3,038	30	218	619	148	3.660%

To test the two-stage classifier, Jocelyn extracted a small ABT containing only spiral galaxies from the original ABT. Using this new ABT, Jocelyn trained a logistic regression model to distinguish between the three spiral galaxy types (*spiral_cw*, *spiral_acw*, and *spiral_eo*). She used step-wise sequential feature selection again, and this time 32 features were chosen.¹⁸ This model was able to achieve a classification accuracy of 68.225% (with an average class accuracy of 56.621%). The resulting confusion matrix is shown in Table 13.9^[724]. Although it is evident from the confusion matrix that the model could distinguish between the edge-on spiral galaxies and the other two types, it could not accurately distinguish between the clockwise and anti-clockwise spiral galaxies.

Table 13.9

The confusion matrix for the logistic regression model that distinguished between only the spiral galaxy types (classification accuracy: 68.225%, average class accuracy: 56.621%).

		Prediction			Recall
		<i>spiral_cw</i>	<i>spiral_acw</i>	<i>spiral_eo</i>	
Target	<i>spiral_cw</i>	5,753	6,214	3,319	37.636%
	<i>spiral_acw</i>	6,011	6,509	3,540	40.528%
	<i>spiral_eo</i>	1,143	2,084	35,643	91.698%

In spite of the model's difficulty distinguishing between the clockwise and anti-clockwise spiral galaxies, Jocelyn did perform an evaluation of the

two-stage model. This model first used a 3-level logistic regression model to distinguish between the *elliptical*, *spiral*, and *other* target levels. Any objects classified as belonging to the *spiral* target level were then presented to a model trained to distinguish between the three different spiral types. The two-stage model achieved a classification accuracy of 79.410%. The resulting confusion matrix is shown in [Table 13.10](#)^[725].

Table 13.10

The confusion matrix for the 5-level two-stage model (classification accuracy: 79.410%, average class accuracy: 53.118%).

		Prediction					Recall
		<i>elliptical</i>	<i>spiral_cw</i>	<i>spiral_acw</i>	<i>spiral_eo</i>	<i>other</i>	
Target	<i>elliptical</i>	117,339	76	2,510	5,716	90	93.326%
	<i>spiral_cw</i>	2,354	4,859	5,242	2,802	23	31.799%
	<i>spiral_acw</i>	2,473	5,079	5,499	2,990	25	34.229%
	<i>spiral_eo</i>	5,985	965	1,760	30,102	60	77.439%
	<i>other</i>	1,757	98	341	834	1,022	25.222%

Although the performance of the two-stage model was better than the performance of the simpler 5-level model, it still did a very poor job of distinguishing between the different spiral galaxy types. Jocelyn discussed this model with Edwin, and they both agreed that the performance was not at the level required by the SDSS scientists for inclusion in the SDSS processing pipeline. It would most likely be possible to create a model that could distinguish between the clockwise and anti-clockwise spiral galaxies, but this would probably require the calculation of new features based on the application of image processing techniques to the raw galaxy images. Based on the time available to the project, Jocelyn did not pursue this avenue and, in consultation with Edwin, decided to continue with just the 3-level model. The best-performing model was the 3-level logistic regression model after feature selection (the performance of this model is shown in [Table 13.7\(b\)](#)^[723]). With this model selected as the best performing approach, Jocelyn was ready to perform the final evaluation experiment.

13.5 Evaluation

The final evaluation that Jocelyn performed was in two parts. In the first part, she performed a performance test of the final model selected—the 3-level logistic regression model using the selected feature subset—on the large test dataset mentioned at the beginning of Section 13.4^[719]. This dataset had not been used in the training process, so the performance of the model on this dataset should give a fair indication of how well the model would perform when deployed on real, unseen data. The confusion matrix resulting from this test is shown in [Table 13.11](#)^[726]. The classification accuracy was 87.979% (with an average class accuracy of 67.305%), which was similar to performance on the training data and well above the target that Jocelyn and Edwin had agreed on at the beginning of the project.

Table 13.11

The confusion matrix for the final logistic regression model on the large hold-out test set (classification accuracy: 87.979%, average class accuracy: 67.305%).

		Prediction			Recall
		<i>elliptical</i>	<i>spiral</i>	<i>other</i>	
Target	<i>elliptical</i>	251,845	19,159	213	92.857%
	<i>spiral</i>	25,748	128,621	262	83.179%
	<i>other</i>	4,286	2,648	2,421	25.879%

The purpose of the second part of the evaluation was to encourage confidence in the models that Jocelyn had built among the SDSS scientists. In this evaluation, Edwin and four of his colleagues independently examined 200 galaxy images randomly selected from the final test set and classified them as belonging to one of the three galaxy types. A single majority classification was calculated from the five manual classifications for each galaxy. Jocelyn extracted two key measurements by comparing these manual classifications to the classifications made by the model she had built. First, Jocelyn calculated an average class accuracy by comparing the predictions made by her model for the same 200 galaxies with the manual classifications made by the SDSS scientists. The average class

accuracy was 78.278%, which was similar to the accuracies measured on the overall test set.

Second, Jocelyn calculated an **inter-annotator agreement** statistic for the manual classifications given by the five SDSS scientists. Using the **Cohen's kappa**¹⁹ measure of **inter-annotator agreement** to measure how closely the manual classifications matched each other, Jocelyn calculated a measure of 0.6. Jocelyn showed that even the SDSS scientists themselves disagreed on the types of certain galaxies. This is not uncommon in this kind of scenario, in which the classifications have a certain amount of fuzziness around their boundaries—e.g., the exact line between an *elliptical* and a *spiral* galaxy can be hard to define—and led to very interesting discussions for the scientists!

Together the strong performance by the model on the large test dataset and the confidence built through the manual annotation exercise meant that Edwin and his colleagues were happy to integrate the 3-level model into the SDSS processing pipeline.

13.6 Deployment

Once Edwin had approved the models that Jocelyn had built, Jocelyn met again with Ted to begin the process of integrating the models into the SDSS processing pipeline. This was a reasonably straightforward process with just a few issues that needed discussion. First, Jocelyn had put the SDSS data through a preprocessing step, standardizing all descriptive features. The standardization parameters (the mean and standard deviation of each feature) needed to be included in the pipeline so that the same preprocessing step could be applied to newly arriving instances before presenting them to the models.

Second, a process was put in place that allowed manual review by SDSS experts to be included in the galaxy classification process. One of the advantages of using a logistic regression model is that along with classifications, it also produces probabilities. Given that there are three target levels, a prediction probability of approximately 0.333 indicates that the prediction made by the model is really quite unsure. A system was put in place in the SDSS processing pipeline to flag for manual review any galaxies given low probability predictions.

Last, a strategy needed to be put in place to monitor the performance of the models over time so that any **concept drift** that might take place could be flagged. Jocelyn agreed with Ted to put in place an alert system using the **stability index**. This would raise an alert whenever the stability index went above 0.25 so that someone could consider retraining the model.

1. Full details of the SDSS project, which is fascinating, are available at www.sdss.org.
2. Although this case study is based on real data downloaded from the SDSS, the case study itself is entirely fictitious and developed only for the purposes of this book. Very similar work to that described in this section has, however, actually been undertaken, and details of representative examples are given in Section 13.6^[727].
3. This practice was first systematically applied by Edwin Hubble in 1936 (Hubble, 1936).
4. In an interesting example of the persistence of good solutions using older technology, the data captured by the telescopes at the SDSS site in New Mexico is recorded onto magnetic tapes that are then couriered to the Feynman Computing Center at Fermilab in Illinois, over 1,000 miles away. This is the most effective way to transport the massive volumes of data involved!
5. See Chapter 2^[23].
6. Stoughton et al. (2002) provides an in-depth discussion of the data collected by the SDSS. A shorter overview is provided at skyserver.sdss3.org/dr9/en/sdss/data/data.asp.
7. Most consumer digital cameras capture full-color images by capturing separate images on red, green, and blue imaging sensors and combining these. The colors red, green, and blue are known as **photometric bands**. The photometric bands captured by the SDSS imaging camera are the same as these bands; they are just defined on different parts of the spectrum.
8. Full details of the Galaxy Zoo project and the data released by it are described in Lintott et al. (2008, 2011). The Galaxy Zoo (www.galaxyzoo.org) project referred to in this example is Galaxy Zoo I.
9. The fact that the SDSS and Galaxy Zoo make all their data available for free online is a massive contribution to global science. The data used in this case study can be accessed by performing a simple SQL query at skyserver.sdss3.org/dr9/en/tools/search/sql.asp. The query to select all the camera imaging data from the SDSS data release for each of the objects covered by the Galaxy Zoo project along with the Galaxy Zoo classifications is `SELECT * FROM PhotoObj AS p JOIN ZooSpec AS zs ON zs.objid = p.objid ORDER BY p.objid`. Full details of all the data tables available from the SDSS are available at skyserver.sdss3.org/dr9/en/help/docs/tabledesc.asp.
10. Many systems use values like – 9,999 to indicate that values are actually missing.
11. The co-occurrence of multiple missing values in a row is something that it is hard to find through summary analysis of the data and one of the reasons analytics practitioners should always eyeball extracts from a dataset during the data exploration process.
12. Interested readers might find Tempel et al. (2011), Ball et al. (2004) and Banerji et al. (2010) good references on this topic.
13. We direct the interested reader to <http://skyserver.sdss3.org/dr9/en/sdss/data/data.asp> for a overview of what these features represent.
14. It is more common to split an ABT in the opposite proportions (70% for the training set and 30% for the test set). In this case, however, because the ABT was so large it was more useful to have a

very large test sample, as 200,000 instances should be more than enough for the training set.

15. Target level imbalance typically arises through either **absolute rarity** or **relative rarity** of the minority target levels. Absolute rarity refers to scenarios in which there simply do not exist many examples of the minority target levels—for example, in automated inspection tasks on production lines, it is often the case that there are simply very few examples of defective products that can be used for training. Relative rarity, on the other hand, refers to scenarios in which the proportion of examples of the majority target levels in a dataset is much higher than the proportion of examples of the minority target level, but there is actually no shortage of examples of the minority target level.

16. The features selected were AE_I, APERFLUX7IVAR_G, APERFLUX7IVAR_I, APERFLUX7_U, DERED_U, DEVAB_R, DEVRADEERR_Z, DEVRAD_U, DEREDDIFF_G_R, EXPRAD_G, EXPRAD_R, FIBER2FLUXIVAR_Z, FIBER2MAGERR_G, FIBERFLUXIVAR_R, FRACDEV_Z, LNLDDEV_G, LNLDDEV_R, LNLDDEV_U, LNLDDEV_Z, MCR4_Z, PETROFLUXIVAR_G, PETROFLUXIVAR_I, PETROR50ERR_R, PETROR50_G, PETROR90_G, PETROR90_R, PETROR90_U, PSFFLUXIVAR_I, PSFMAGERR_R, PSFMAG_R, SKYIVAR_U, and SKYIVAR_Z.

17. The features selected were SKYIVAR_U, PETROFLUXIVAR_I, PETROR50ERR_G, DEVRADEERR_G, DEVRADEERR_R, DEVRADEERR_I, DEVAB_G, EXPFLUX_Z, APERFLUX7_Z, APERFLUX7IVAR_R, and MODELMAGDIFF_I_Z.

18. The features selected were AE_I, APERFLUX7IVAR_R, CMODELFLUXIVAR_U, DEVABERR_G, DEVABERR_Z, DEVAB_G, DEVAB_I, DEVFLUXIVAR_U, DEVFMAGERR_U, DEVRADEERR_G, DEVRADEERR_U, DEREDDIFF_U_G, EXPABERR_U, EXPAB_G, EXPMAG_Z, EXPRADERR_U, FIBER2FLUXIVAR_R, FIBER2MAG_I, FIBERFLUXIVAR_G, FIBERFLUX_G, FIBERFLUX_R, FIBERFLUX_Z, LNLDDEV_R, MCR4_Z, ME1E1ERR_Z, ME1_U, MODELMAGDIFF_R_I, PETROMAGDIFF_R_I, PETROR90_R, PSFMAG_U, SKYIVAR_U, and U_R.

19. The Cohen's kappa statistic was first described in Cohen (1960). Using the Cohen's kappa statistic, a value of 1.0 indicates total agreement, while a value of 0.0 indicates agreement no better than chance. Values around 0.6 are typically understood to indicate an *acceptable* level of agreement, although the exact nature of what is and is not acceptable is very task dependent.

14

The Art of Machine Learning for Predictive Data Analytics

“It is a capital mistake to theorize before one has data. Insensibly one begins to twist facts to suit theories, instead of theories to suit facts.”

—Sherlock Holmes

Predictive data analytics projects use machine learning to build models that capture the relationships in large datasets between descriptive features and a target feature. A specific type of learning, called inductive learning, is used, where learning entails inducing a general rule from a set of specific instances. This observation is important because it highlights that machine learning has the same properties as inductive learning. One of these properties is that a model learned by induction is not guaranteed to be correct. In other words, the general rule that is induced from a sample may not be true for all instances in a population.

Another important property of inductive learning is that learning cannot occur unless the learning process is biased in some way. This means that we need to tell the learning process what types of patterns to look for in the data. This bias is referred to as inductive bias. The inductive bias of a learning algorithm comprises the set of assumptions that define the search space the algorithm explores, and the search process it uses.

On top of the inductive bias encoded in a machine learning algorithm, we also bias the outcome of a predictive data analytics project in lots of other ways. Consider the following questions:

What is the predictive analytics target? What descriptive features will we include/exclude? How will we handle missing values? How will we normalize our features? How will we represent continuous features? What types of models will we create? How will we set the parameters of the learning algorithms? What evaluation process will we follow? What performance measures will we use?

These questions are relevant when building any prediction model, and the answer to each one introduces a specific bias. Often we are forced to answer these questions, and others like them, based on intuition, experience, and experimentation. This is what makes machine learning something of an art, rather than strictly a science. But it is also what makes machine learning such a fascinating and rewarding area in which to work.

En masse all the questions that must be answered to successfully complete a predictive data analytics project can seem overwhelming. This is why we recommend using the **CRISP-DM** process to manage a project through its lifecycle. [Table 14.1](#)^[730] shows the alignment between the phases of CRISP-DM, some of the key questions that must be answered during a predictive data analytics project, and the chapters in this book dealing with these questions.

Table 14.1

The alignment between the phases of CRISP-DM, key questions for analytics projects, and the chapters and sections of this book.

CRISP-DM	Open Questions	Chapter
Business Understanding	<i>What is the organizational problem being addressed? In what ways could a prediction model address the organizational problem? Do we have situational fluency? What is the capacity of the organization to utilize the output of a prediction model? What data is available?</i>	Chapter 2 ^[23]
Data Understanding	<i>What is the prediction subject? What are the domain concepts? What is the target feature? What descriptive features will be used?</i>	Chapter 2 ^[23]
Data Preparation	<i>Are there data quality issues? How will we handle missing values? How will we normalize our features? What features will we include?</i>	Chapter 3 ^[53]
Modeling	<i>What types of models will we use? How will we set the parameters of the machine learning algorithms? Have underfitting or overfitting occurred?</i>	Chapters 4 ^[117] , 5 ^[181] , 6 ^[243] , 7 ^[311] and 8 ^[381]
Evaluation	<i>What evaluation process will we follow? What performance measures will we use? Is the model fit for purpose?</i>	Chapter 9 ^[533]
Deployment	<i>How will we continue to evaluate the model after deployment? How will the model be integrated into the organization?</i>	Section 9.4.6 ^[578]

and
Chapters
12^[685] and
13^[703]

Remember, an analytics project is often iterative, with different stages of the project feeding back into later cycles. It is also important to remember that the purpose of an analytics project is to solve a real-world problem and to keep focus on this rather than being distracted by the, admittedly sometimes fascinating, technical challenges of model building. We strongly believe that the best way to keep an analytics project focused, and to improve the likelihood of a successful conclusion, is to adopt a structured project lifecycle, such as CRISP-DM, and we recommend its use.

14.1 Different Perspectives on Prediction Models

A key step in any predictive analytics project is deciding which type of predictive analytics model to use. In this book we have presented some of the most commonly used prediction models and the machine learning algorithms used to build them. We have structured this presentation around five approaches to learning: information-based, similarity-based, probability-based, error-based, and deep learning. The mathematical foundation of these approaches can be described using five simple (but important) equations: Claude Shannon's model of **entropy** (Equation (14.1)^[731]), **Euclidean distance** (Equation (14.2)^[731]), **Bayes' Theorem** (Equation (14.3)^[731]), the **sum of squared errors** (Equation (14.4)^[731]), and the application of the **chain rule** to backpropagate error gradients in a neural network (Equation (14.5)^[731]).

$$H(t, \mathcal{D}) = - \sum_{l \in levels(t)} (P(t = l) \times \log_2(P(t = l))) \quad (14.1)$$

$$dist(\mathbf{q}, \mathbf{d}) = \sqrt{\sum_{i=1}^m (\mathbf{q}[i] - \mathbf{d}[i])^2} \quad (14.2)$$

$$P(t = l | \mathbf{q}) = \frac{P(\mathbf{q}|t = l)P(t = l)}{P(\mathbf{q})} \quad (14.3)$$

$$L_2(\mathbb{M}_{\mathbf{w}}, \mathcal{D}) = \frac{1}{2} \sum_{i=1}^n (t_i - \mathbb{M}_{\mathbf{w}}(\mathbf{d}_i))^2 \quad (14.4)$$

$$\frac{\partial \mathcal{E}}{\partial w_{i,k}} = \frac{\partial \mathcal{E}}{\partial a_i} \times \frac{\partial a_i}{\partial z_i} \times \frac{\partial z_i}{\partial w_{i,k}} \quad (14.5)$$

An understanding of these five equations is a strong basis for understanding the mathematical fundamentals of many areas of scientific modeling. Adding an understanding of how these five equations are used in the machine learning algorithms we have described (ID3, k nearest neighbor, multivariable linear regression with gradient descent, naive Bayes, and the backpropagation of error algorithm) is a strong foundation on which to build a career in predictive data analytics.

The taxonomy we have used to distinguish between different machine learning algorithms is based on human approaches to learning that the algorithms can be said to emulate. This is not the only set of distinctions that can be made between the algorithms and the resulting models. It is useful to understand some of the other commonly used distinctions, because this understanding can provide insight into which learning algorithm and related model is most appropriate for a given scenario.

The first distinction between models that we will discuss is the distinction between **parametric** and **non-parametric** models. This distinction is not absolute, but it generally describes whether the size of the **domain representation** used to define a model is solely determined by the number of features in the domain or is affected by the number of instances in the dataset. In a parametric model the size of the domain representation (i.e., the number of parameters) is independent of the number of instances in the dataset. Examples of parametric models include the naive Bayes and Bayesian network models in Chapter 6^[243] and the simple linear and logistic

regression models in Chapter 7^[311]. For example, the number of factors required by a naive Bayes model is only dependent on the number of features in the domain and is independent of the number of instances. Likewise, the number of weights used in a linear regression model is defined by the number of descriptive features and is independent of the number of instances in the training data.

In a non-parametric model the number of parameters used by the model increases as the number of instances increases. Nearest neighbor models are an obvious example of a non-parametric model. As new instances are added to the feature space, the size of the model’s representation of the domain increases. Decision trees are also considered non-parametric models. The reason for this is that when we train a decision tree from data, we do not assume a fixed set of parameters prior to training that define the tree. Instead, the tree branching and the depth of the tree are related to the complexity of the dataset it is trained on. If new instances were added to the dataset and we rebuilt the tree, it is likely that we would end up with a (potentially very) different tree. Support vector machines are also non-parametric models. They retain some instances from the dataset—potentially all of them, although in practice, relatively few—as part of the domain representation. Hence, the size of the domain representation used by a support vector machine may change as instances are added to the dataset.

In general, parametric models make stronger assumptions about the underlying distributions of the data in a domain. A linear regression model, for example, assumes that the relationship between the descriptive features and the target is linear (this is a strong assumption about the distribution in the domain). Non-parametric models are more flexible but can struggle with large datasets. For example, a 1-NN model has the flexibility to model a discontinuous decision surface; however, it runs into time and space complexity issues as the number of instances grows.

When datasets are small, a parametric model may perform well because the strong assumptions made by the model—if correct—can help the model to avoid overfitting. However, as the size of the dataset grows, particularly if the decision boundary between the classes is very complex, it may make more sense to allow the data to inform the predictions more directly. Obviously the computational costs associated with non-parametric models

and large datasets cannot be ignored. However, support vector machines are an example of a non-parametric model that, to a large extent, avoids this problem. As such, support vector machines are often a good choice in complex domains with lots of data.

The other important distinction that is often made between classification models is whether they are **generative** or **discriminative**. A model is generative if it can be used to generate data that will have the same characteristics as the dataset from which the model was produced. In order to do this, a generative model must learn, or encode, the distribution of the data belonging to each class. The Bayesian network models described in Chapter 6^[243] are examples of generative models.¹ Indeed, Markov chain Monte Carlo methods for estimating probabilities are based on the fact that we can run these models to generate data that approximate the distributions of the dataset from which the model was induced. Because they explicitly model the distribution of the data for each class k nearest neighbor models are also generative models.

In contrast, discriminative models learn the boundary between classes rather than the characteristics of the distributions of the different classes. Support vector machines and the other classification models described in Chapter 7^[311] are examples of discriminative prediction models. In some cases they learn a hard boundary between the classes; in other cases—such as logistic regression—they learn a soft boundary, which takes into account the distance from the boundary. However, all these models learn a boundary. Decision trees are also discriminative models. Decision trees are induced by recursively partitioning the feature space into regions belonging to the different classes, and consequently they define a decision boundary by aggregating the neighboring regions belonging to the same class. Decision tree **model ensembles** based on **bagging** and **boosting** are also discriminative models. Most of the deep network models described in Chapter 8^[381] are also discriminative models, although the **auto-encoder** network described in Chapter 10^[597] is a nice example of a generative neural network.

This generative versus discriminative distinction is more than just a labeling exercise. Generative and discriminative models learn different concepts. In probabilistic terms, using \mathbf{d} to represent the vector of

descriptive feature values and t_l to represent a target level, a generative model works by

1. learning the class conditional densities (i.e., the distribution of the data for each target level) $P(\mathbf{d}|t_l)$ and the class priors $P(t_l)$;
2. then using Bayes' Theorem to compute the class posterior probabilities $P(t_l|\mathbf{d})$;²
3. and then applying a decision rule over the class posteriors to return a target level.

By contrast, a discriminative model works by

1. learning the class posterior probability $P(t_l|\mathbf{d})$ directly from the data,
2. and then applying a decision rule over the class posteriors to return a target level.

This distinction between what generative and discriminative models try to learn is important because the class conditional densities, $P(\mathbf{d}|t_l)$, can be very complex compared to the class posteriors, $P(t_l|\mathbf{d})$ (see [Figure 14.1](#)^[734]). Consequently, generative models try to learn more complex solutions to the prediction problem than discriminative models.

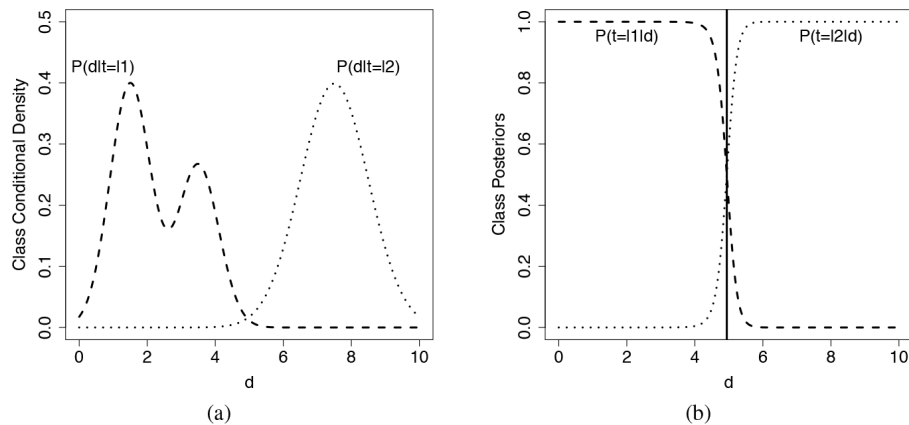


[Figure 14.1](#)

(a) The class conditional densities for two classes (l_1, l_2) with a single descriptive feature \mathbf{d} . The height of each curve reflects the density of the instances from that class for that value of \mathbf{d} . (b) The class posterior probabilities plotted for each class for different values of \mathbf{d} . Notice that the class posterior probability $P(t = l_1|\mathbf{d})$ is not affected by the multimodal structure of the corresponding class conditional density $P(\mathbf{d}|t = l_1)$. This illustrates how the class posterior probabilities can be simpler than the class conditional densities. The solid vertical line in (b) plots the decision boundary for \mathbf{d} that gives the minimum misclassification rate assuming uniform prior for the two target levels (i.e., $P(t = l_1) = P(t = l_2)$). This figure is based on Figure 1.27 from Bishop (2006).

The potential difficulty in learning the class conditional densities, relative to the posterior class probabilities, is exacerbated in situations where we have a lot of descriptive features because, as the dimensionality of \mathbf{d} increases, we will need more and more data to create good estimates for $P(t_l|\mathbf{d})$. So, in complex domains, discriminative models are likely to be more accurate. However, as is so often the case in machine learning, this is not the end of the generative versus discriminative debate. Generative models tend to have a higher bias—they make more assumptions about the form of the distribution they are learning. For example, as we discussed in Chapter 6^[243] on probability, generative models encode independence assumptions about the descriptive features in \mathbf{d} . This may sound like another problem for generative models. However, in domains where we have good prior knowledge of the independence relationships between features, we can encode this prior structural information into a generative model. This structural information can bias the model in such a way as to help it avoid overfitting the data. As a result, a generative model may outperform a discriminative model when trained on a small dataset with good prior knowledge. Conversely, however, as the amount of training data increases, the bias imposed on a generative model can become larger than the error of the trained model. Once this tipping point in dataset size has been surpassed, a discriminative model will outperform a generative model.

The debate regarding the advantages and disadvantages of generative and discriminative models can be extended beyond model accuracy to include their ability to handle missing data, unlabeled data, and feature preprocessing, among other topics. We will not discuss these topics here. Instead, we will simply note that the appropriate choice of generative versus discriminative model is context-dependent, and evaluating a range of different types of models is the safest option. [Table 14.2](#)^[735] summarizes the different perspectives on the model types that we have presented in this book.

Table 14.2

A taxonomy of models based on the parametric versus non-parametric and generative versus discriminative distinctions.

Model	Parametric/ Non-Parametric	Generative/ Discriminative
-------	-------------------------------	-------------------------------

k Nearest Neighbor	Non-Parametric	Generative
Decision Trees	Non-Parametric	Discriminative
Bagging/Boosting	Parametric*	Discriminative
Naive Bayes	Parametric	Generative
Bayesian Network	Parametric	Generative
Linear Regression	Parametric	Discriminative
Logistic Regression	Parametric	Discriminative
SVM	Non-Parametric	Discriminative
Neural networks	Parametric**	Discriminative

*Although the individual models in an ensemble could be non-parametric (for example, when decision trees are used), the ensemble model itself is considered parametric. **We have classified neural networks as parametric models; however, it can be argued that deep networks are non-parametric because they have so many parameters that they have a representational overcapacity.

14.2 Choosing a Machine Learning Approach

Each of the approaches to machine learning that we have presented in this book induces distinct types of prediction models with different strengths and weaknesses. This raises the question of when to use which machine learning approach. The first thing to understand is that there is not one best approach that always outperforms the others. This is known as the **No Free Lunch Theorem** (Wolpert, 1996). Intuitively, this theorem makes sense because each algorithm encodes a distinct set of assumptions (i.e., the **inductive bias** of the learning algorithm), and a set of assumptions that are appropriate in one domain may not be appropriate in another domain.

We can see the assumptions encoded in each algorithm reflected in the distinctive characteristics of the **decision boundaries** that they learn for categorical prediction tasks. To illustrate these characteristics, we have created three artificial datasets and trained four different models on each of these datasets. The top row of images in [Figure 14.2](#)^[737] illustrates how the three artificial datasets were created. Each of the images in the top row shows a feature space defined by two continuous descriptive features, F1 and F2, partitioned into *good* and *bad* regions by three different, artificially created decision boundaries.³ In the subsequent images, we show the decision boundaries that are learned by four different machine learning algorithms based on training datasets generated according to the decision boundaries shown in the top row. In order from top to bottom, we show decision trees (without pruning), nearest neighbor models (with $k = 3$ and using majority voting), naive Bayes models (using normal distributions to

represent the two continuous feature values), and logistic regression models (using a simple linear model). In these images the training data instances are shown as symbols on the feature space (triangles for *good* and crosses for *bad*), the decision boundaries learned by each algorithm are represented by thick black lines, and the underlying *actual* decision boundaries are shown by the background shading.

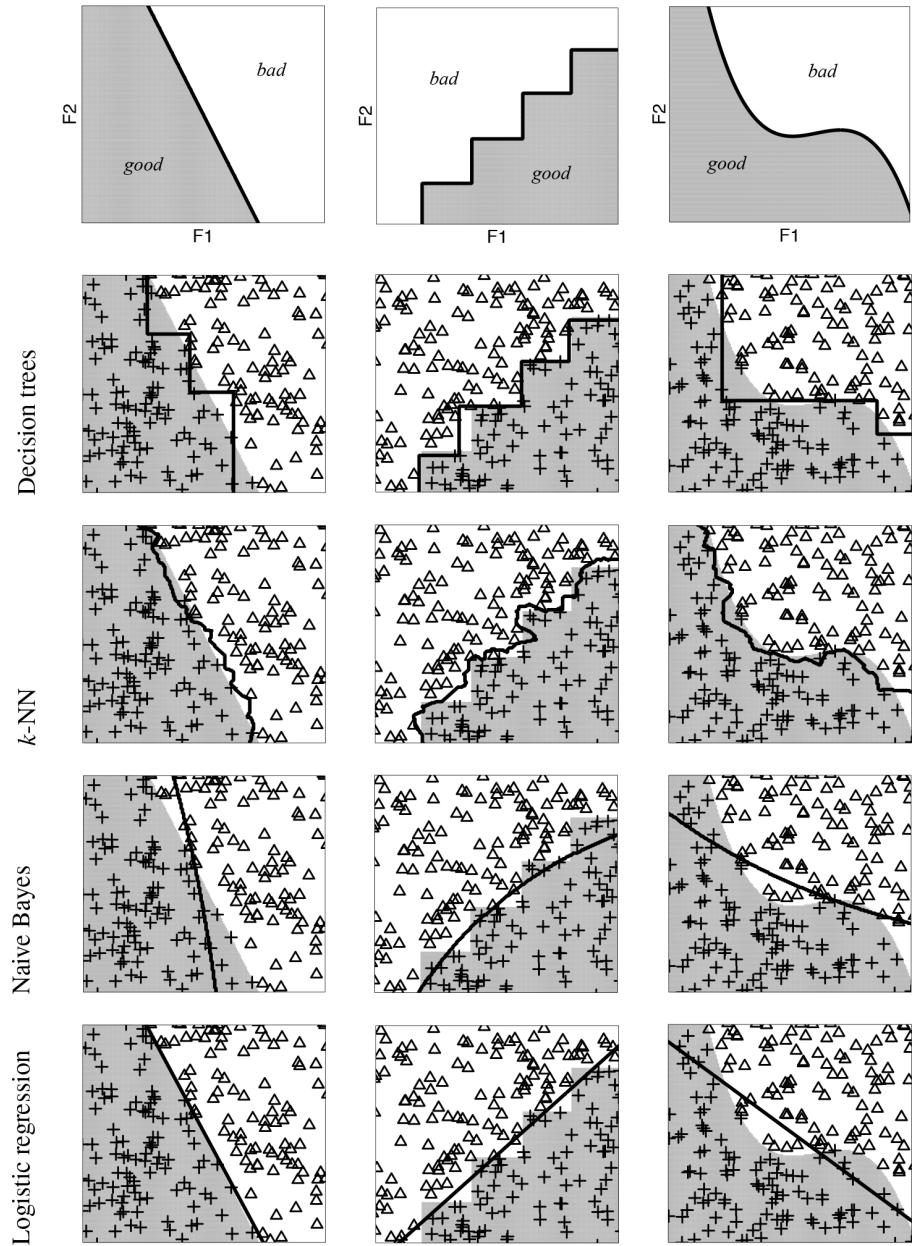


Figure 14.2

An illustration of the decision boundaries learned by different machine learning algorithms for three artificial datasets.

These examples show two things. First, the decision boundaries learned by each algorithm are characteristic of that algorithm. For example, the decision boundaries associated with decision trees have a characteristic stepped appearance because of the way feature values are split in a decision tree, while the decision boundaries associated with k -NN models are noticeably jagged because of their local focus. The characteristic appearance of the decision boundaries is related to the representations used within the models and the inductive biases that the algorithms used to build them encode. The second thing that is apparent from the images in [Figure 14.2](#)^[737] is that some of the models do a better job of representing the underlying decision boundaries than others. The decision boundary learned by the logistic regression model best matches the underlying decision boundary for the dataset in the first column, the decision tree model seems most appropriate for the dataset in the second column, and the k -NN model appears best for the dataset in the third column.

Real predictive data analytics projects use datasets that are much more complex than those shown in [Figure 14.2](#)^[737]. For this reason selecting which type of model to use should be informed by the specific priorities of a project and the types of the descriptive and target features in the data. Also, in general, it is not a good idea to select just one machine learning approach at the beginning of a project and to exclusively use that. Instead, it is better to choose a number of different approaches and to run experiments to evaluate which is best for the particular project. However, this still requires the selection of a set of initial approaches. There are two questions to consider:

1. Does a machine learning approach match the requirements of the project?
2. Is the approach suitable for the type of prediction we want to make and the types of descriptive features we are using?

14.2.1 Matching Machine Learning Approaches to Projects

In many cases the primary requirement of a project is to create an accurate prediction model. Accuracy can often be related to the power of a machine learning algorithm to capture the interaction between descriptive features and the target feature. Caruana and Niculescu-Mizil (2006) and Caruana et al. (2008) report empirical evaluations of the accuracy of a range of model

types across a range of domains. They found that on average, ensemble models and support vector machines were among the most accurate models. A consistent finding in both of these experiments, however, was the fact that for some domains, these more powerful models performed quite poorly, and other models, that in other domains were quite weak, achieved the best results. The main conclusions from this, and other similar studies, is that no machine learning approach is universally best, and experimentation with different approaches is the best way to ensure that an accurate model is built.

When evaluating models against a particular deployment scenario, model accuracy is not the only issue we need to consider. In order to successfully address a business problem, a model must be accurate, but it must also meet the other requirements of the business scenario. Three issues are important to consider:

- **Prediction speed:** How quickly can a model make predictions? Logistic regression models, for example, are very fast at making predictions as all that is involved is calculating the regression equation and performing a thresholding operation. On the other hand, k nearest neighbor models are very slow to make predictions as they must perform a comparison of a query instance to every instance in a, typically large, training set. The time differences arising from these different computational loads can have an influence on model selection. For example, in a real-time credit card fraud prediction system, it may be required that a model perform thousands of predictions per second. Even if significant computational resources were to be deployed for such a problem, it may not be possible for a k nearest neighbor model to perform fast enough to meet this requirement.
- **Capacity for retraining:** In Section 9.4.6^[578] we discussed approaches that can be used to monitor the performance of a model so as to flag the occurrence of concept drift and indicate if a model has gone stale. When this occurs, the model needs to be changed in some way to adapt to the new scenario. For some modeling approaches this is quite easy, while for others it is almost impossible to adapt a model, and the only option is to discard the current model and train a new one using an updated dataset. Naive Bayes and k nearest neighbor models are good examples of the

former type, while decision trees and regression models are good examples of the latter.

- **Interpretability:** In many instances a business will not be happy to simply accept the predictions made by a model and incorporate these into their decision making. Rather, they will require the predictions made by a model to be explained and justified. Different models offer different levels of explanation capacity and therefore different levels of interpretability. For example, decision trees and linear regression models are very easily interpreted, while support vector machines, ensembles, and deep neural networks are almost entirely uninterpretable (because of this, they are often referred to as a **black box**).

In summary, ensembles, support vector machines, neural networks, and Bayesian networks are, in general, more powerful machine learning approaches than the others we have presented. However, these approaches are more complex, take a longer time to train, and are harder to interpret than the simpler approaches that we have presented. Furthermore, the selection of a machine learning approach also depends on the aspects of an application scenario described above (speed, capacity for retraining, interpretability), and often, these factors are a bigger driver for the selection of a machine learning approach than prediction accuracy.

14.2.2 Matching Machine Learning Approaches to Data

When matching machine learning approaches to the characteristics of a dataset, it is important to remember that almost every approach can be made to work for both continuous and categorical descriptive and target features. Certain approaches, however, are a more natural fit for some kinds of data than others, so we can make some recommendations. The first thing to consider in regard to data is whether the target feature is continuous or categorical. Models trained by reducing the sum of squared errors, for example, linear regression, are the most natural fit for making predictions for continuous target features. Out of the different approaches we have considered, the information-based and probability-based approaches are least well suited in this case. If, on the other hand, the target feature is categorical, then information-based and probability-based approaches are likely to work very well. Models trained using error-based approaches can become overly complicated when the number of levels of the target feature

goes above two, although deep neural network models handle these scenarios easily.

If all the descriptive features in a dataset are continuous, then a similarity-based approach is a natural fit, especially when there is also a categorical target feature. Error-based models would be preferred if the target feature is also continuous. When there are many continuous features, probability-based and information-based models can become complicated, but if all the features in a dataset are categorical, then information-based and probability-based models are appropriate. Error-based and deep learning models are less suitable in this case as they require categorical features to be converted into sets of binary features, which causes an increase in dimensionality. In many cases datasets will contain both categorical and continuous descriptive features. The most naturally suited learning approaches in these scenarios are probably those that are best suited for the majority feature type.

The last issue to consider in relation to data when selecting machine learning approaches is the **curse of dimensionality**. If there are a large number of descriptive features, then we will need a large training dataset. **Feature selection** is an important process in any machine learning project and should generally be applied no matter what type of models are being developed. That said, some models are more susceptible to the curse of dimensionality than others. Similarity-based approaches are particularly sensitive to the curse of dimensionality and can struggle to perform well for a dataset with large numbers of descriptive features. Decision tree models have a feature selection mechanism built into the algorithm and so are more robust to this issue. Also, some of the unsupervised learning approaches described in Chapter 10^[597] can be used to address the curse of dimensionality by learning new more compact representations.

14.3 Beyond Prediction

The majority of this book is focused on building predictive models. Machine learning, however, can be used for many other tasks. In Chapters 10^[597] and 11^[637] we described two of the major uses of machine learning that go *beyond prediction*: unsupervised learning and reinforcement learning.

Unsupervised machine learning techniques are used in the absence of a target feature and model the underlying structure within the descriptive features in a dataset. Usually this is done either to divide a dataset into clusters of similar examples, or to generate new features that can be appended to a dataset.

In reinforcement learning an agent inhabiting an environment learns to perform a task by pursuing actions that achieve the highest cumulative reward, where a reward is immediate feedback that follows an action to indicate how successful it was. The main application of reinforcement learning is to learn control strategies, for example, in robotics.

As we did with predictive modeling we can capture the mathematical foundations of these further approaches to machine learning in two key equations: the function minimized by the k -means clustering algorithm (Equation (14.6)^[741]) and the action-value function update rule used in Q-learning (Equation (14.7)^[741]).

$$\sum_{i=1}^n \min_{\mathbf{c}_1, \dots, \mathbf{c}_k} Dist(\mathbf{d}_i, \mathbf{c}_j) \quad (14.6)$$

$$Q(s_t, a_t) \leftarrow Q(s_t, a_t) + \alpha \left(r_t + \gamma \max_{a_{t+1}} Q(s_{t+1}, a_{t+1}) - Q(s_t, a_t) \right) \quad (14.7)$$

Understanding these two equations, and the core algorithms that they underpin (k -means clustering and Q-learning), is an excellent step toward broadening your knowledge out to the many other uses of machine learning beyond prediction. Most of the advice given in the previous sections on choosing machine learning approaches and completing successful projects, also equally applies to these machine learning approaches, and a good grounding in predictive modeling makes adding these approaches to your toolkit relatively straight-forward.

14.4 Your Next Steps

In many ways, the easy part of a predictive data analytics project is building the models. The machine learning algorithms tell us how to do this. What makes predictive data analytics difficult, but also fascinating, is figuring out how to answer all the questions that surround the modeling phase of a project. Throughout the course of a predictive data analytics project, we are

forced to use our intuition and experience, and experimentation, to steer the project toward the best solution. To ensure a successful project outcome, we should inform the decisions that we make by

- becoming situationally fluent so that we can converse with experts in the application domain;
- exploring the data to understand it correctly;
- spending time cleaning the data;
- thinking hard about the best ways to represent features;
- and spending time designing the evaluation process correctly.

A distinctive aspect of this book is that we have chosen to present machine learning in context. In order to do this, we have included topics that are not covered in many machine learning books, including discussions on business understanding, data exploration and preparation, and case studies. We have also provided an in-depth introduction to some of the most popular machine learning approaches with examples that illustrate how these algorithms work. We believe that this book will provide you with an understanding of the broader context and core techniques of machine learning that will enable you to have a successful career in predictive data analytics.

Machine learning is a huge topic, however, and one book can only be so long. As a result, we have had to sacrifice coverage of some aspects of machine learning in order to include other topics and worked examples. We believe that this book will give you the knowledge and skills that you will need to explore these topics yourself. To help with this, we would recommend Hastie et al. (2001), Bishop (2006), and Murphy (2012) for broad coverage of machine learning algorithms, including more in-depth coverage of unsupervised and reinforcement learning approaches than included in this book. These books are suitable as reference texts for experienced practitioners and postgraduate researchers in machine learning. Some of the other machine learning topics that you might like to explore include **semi-supervised learning** (Chapelle et al., 2009), **multi-label classification** (Tsoumakas et al., 2012), and **graphical models** (Kollar and Friedman, 2009). Finally, we hope that you find machine learning as fascinating and rewarding a topic as we do, and we wish you the best in your future learning.

1. In this discussion, when we categorize models as being generative or discriminative, we are speaking in the general case. In fact, all models can be trained in either a generative or a discriminative manner. However, some models lend themselves to generative training and others to discriminative training, and it is this perspective that we use in this discussion.
2. We could also formulate the generative model as learning the joint distribution $P(\mathbf{d}, t_l)$ directly and then computing the required posteriors from this distribution.
3. This example is partly inspired by the “machine learning classifier gallery” by Tom Fawcett at home.comcast.net/~tom.fawcett/public_html/ML-gallery/pages/

V

APPENDICES

A

Descriptive Statistics and Data Visualization for Machine Learning

In this appendix we introduce the fundamental statistical measures of **central tendency** and **variation**. We also introduce three of the most important and useful data visualization techniques that can be used to visualize a single feature: the **bar plot**, the **histogram**, and the **box plot**.

A.1 Descriptive Statistics for Continuous Features

To understand the characteristics of a continuous feature, there are two things that are important to measure: the **central tendency** of the feature and the **variation** within the feature. These are the basic building blocks of everything else that will follow, so it is important to fully understand them.

A.1.1 Central Tendency

The central tendency of a sample refers to the value that is *typical* of the sample and therefore can be used to summarize it. Measures of central tendency are an approximation of this notional value. The **arithmetic mean** (or **sample mean** or just **mean**) is the best-known measure of central tendency. The arithmetic mean of a set of n values for a feature a is denoted by the symbol \bar{a} and is calculated as

$$\bar{a} = \frac{1}{n} \sum_{i=1}^n a_i \tag{A.1}$$

Figure A.1^[746] shows a group of players on a school basketball team and their heights. Using Equation (A.1)^[745] we can calculate the arithmetic mean of these players' heights as

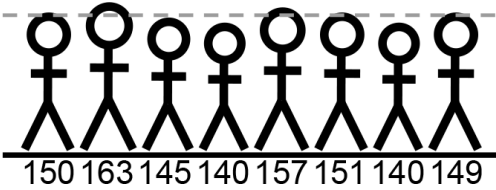


Figure A.1

The members of a school basketball team. The height of each player is listed below the player. The dashed gray line shows the arithmetic mean of the players' heights.

$$\overline{\text{HEIGHT}} = \frac{1}{8} \times (150 + 163 + 145 + 140 + 157 + 151 + 140 + 149) \\ = 149.375$$

This mean height is shown by the dashed gray line in [Figure A.1](#)^[746]. The arithmetic mean is one measure of the central tendency of a **sample** (for our purposes, a sample is just a set of values for a feature in an ABT). Because it is easy to calculate and easy to interpret, the mean is commonly used as part of the data exploration process as a good estimate of the central tendencies of features in an ABT.

Any measure of central tendency is, however, just an approximation, so we must be aware of the limitations of any measure that we use. The arithmetic mean, for example, is very sensitive to very large or very small values in a sample. For example, suppose our basketball team manages to sign a *ringer* measuring in at 229cm, as shown in [Figure A.2\(a\)](#)^[746]. The arithmetic mean for the full group is now 158.222cm and, as shown by the dashed gray line in [Figure A.2\(a\)](#)^[746], no longer really represents the central tendency of the group. An unusually large or small value like this is referred to as an **outlier**, and the arithmetic mean is very sensitive to the presence of outliers.

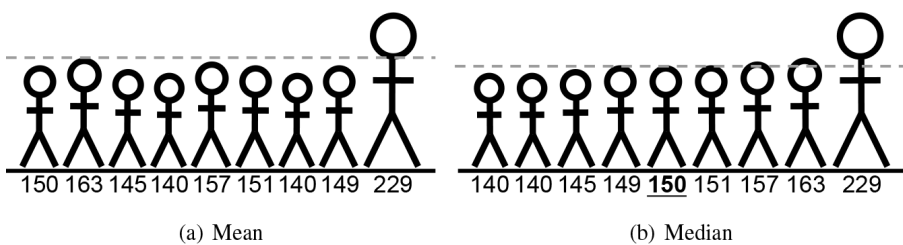


Figure A.2

The members of the school basketball team from [Figure A.1](#)^[746] with one very tall *ringer* added: (a) the dashed gray line shows the mean of the players' heights; and (b) the dashed gray line shows the median of the players' heights, with the players ordered by height.

There are other statistics that we can use to measure central tendency that are not as sensitive to outliers. The **median** is another very useful measure of the central tendency of a sample. The median of a set of values can be calculated by ordering the values from lowest to highest and selecting the middle value. If there is an even number of values in the sample, then the median is obtained by calculating the arithmetic mean of the middle two values. The median is not as sensitive to outliers as the arithmetic mean and therefore can be a more accurate estimate of the central tendency of a set of values if outliers exist. In fact, a large difference between the mean and median of a feature is an indication that there may be outliers among the feature values.

Figure A.2(b)^[746] shows the extended basketball team ordered from smallest to tallest, with the height of each player listed below the player. The median value of this set is 150 and is shown as the dashed gray line in Figure A.2(b)^[746]. In this case the median better captures the central tendency of the set of values.

Another commonly used measure of central tendency is the **mode**. The mode is simply the most commonly occurring value in a sample (determined by counting the frequency with which each value occurs in the sample). If all values in a sample occur with equal frequency, then there is no mode. For the heights of the players in the extended basketball team in Figure A.2^[746], the mode is 140, as it is the only value that appears twice. The mode is not particularly effective in this case at measuring the central tendency of the values. Mode is more frequently useful for categorical features than for continuous ones, but it can be useful for continuous features when the sample is large enough.

A.1.2 Variation

Having used the measures of central tendency to describe where our data is centered, we will now turn our attention to the **variation** in our data. Figure A.3^[747] shows a rival school basketball team of that shown in Figure A.1^[746]. The height of each player is listed below the player, and the dashed gray line shows the arithmetic mean of the players' heights, which is 149.375, the same as for the original team. The heights of the players in this second team vary much more than those of the first team (see Figures A.1^[746] and A.3^[747]). Descriptive statistics provides us with a range of tools that we can

use to formally measure variation and so distinguish between the sets of heights in the two basketball teams. In essence, most of statistics, and in turn, analytics, is about describing and understanding variation.

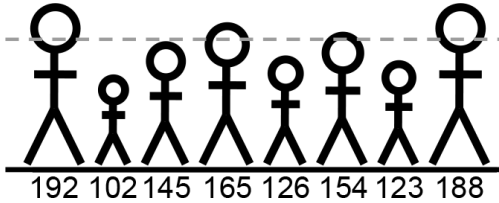


Figure A.3

The members of a rival school basketball team. Player heights are listed below each player. The dashed gray line shows the arithmetic mean of the players' heights.

The most easily calculated measure of variation is **range**. The range of a sample of n values for a feature a is calculated as

$$\text{range} = \max(a) - \min(a) \quad (\text{A.2})$$

The range of the basketball player heights in [Figure A.1](#)^[746] is $163 - 140 = 23$ and for those in [Figure A.3](#)^[747] is $192 - 102 = 90$. These measures match what we intuitively see in these figures—the heights of the second team vary much more than those of the first team. The main advantage of using the range is the ease with which it is calculated. The major disadvantage of the range, however, is that it is highly sensitive to outliers.

The **variance** of a sample is a more useful measure of variation. Variance measures the average difference between each value in a sample and the mean of that sample. The variance of the n values of a feature a is denoted $\text{var}(a)$ and is calculated as

$$\text{var}(a) = \frac{\sum_{i=1}^n (a_i - \bar{a})^2}{n - 1} \quad (\text{A.3})$$

In order to allow for the fact that some of the differences between values and the mean will be positive and some will be negative, we square each difference.¹

For the players' heights given in [Figure A.1](#)^[746], the mean is 149.375, so the variance can be calculated as

$$\begin{aligned} \text{var(HEIGHT)} &= \frac{(150 - 149.375)^2 + (163 - 149.375)^2 + \dots + (149 - 149.375)^2}{8 - 1} \\ &= 63.125 \end{aligned}$$

For the players' heights given in [Figure A.3](#)^[747], the mean is also 149.375, so the variance can be calculated as

$$\begin{aligned} \text{var(HEIGHT)} &= \frac{(192 - 149.375)^2 + (102 - 149.375)^2 + \dots + (188 - 149.375)^2}{8 - 1} \\ &= 1,011.411 \end{aligned}$$

This example illustrates that the variance also captures the intuition that the heights of the players in the second team vary much more than those in the first team. It also, however, illustrates an issue with using variance. Due to the fact that the differences are squared, variances are not in the same units as the original values, so they are not especially informative—telling someone that the variance of the heights on one team is 63.125 and on another is 1,011.411 doesn't give them any particularly useful information other than the fact that the variance of one team is bigger than that of the other.

The **standard deviation**, sd , of a sample is calculated by taking the square root of the variance of the sample:

$$\begin{aligned} sd(a) &= \sqrt{\text{var}(a)} \\ &= \sqrt{\frac{\sum_{i=1}^n (a_i - \bar{a})^2}{n - 1}} \end{aligned} \tag{A.4}$$

This means that the standard deviation is measured in the original units of the sample, which makes it much more interpretable than the variance. It is very common to see the mean and standard deviation provided as a full description of a sample.

The standard deviation of the heights of the players on the first basketball team is 7.945 and for the second team is 31.803. As these measures are in the same units as the heights, they afford us a more intuitive understanding of the data and make comparison easier. We can say that, on average, players on the first team vary by almost 8cm from the average of 149.375cm, while on the second team, they vary by approximately 32cm.

Percentiles are another useful measure of the variation of the values for a feature. A proportion of $\frac{i}{100}$ of the values in a sample take values equal to or lower than the i^{th} percentile of that sample. Conversely, a proportion of $(100 - i)/100$ values in a sample take values larger than the i^{th} percentile. To calculate the i^{th} percentile of the n values of a feature a , we first order the values in ascending order and then multiply n by $\frac{i}{100}$ to determine the *index*. If the *index* is a whole number, we take the value at that position in the ordered list of values as the i^{th} percentile. If *index* is not a whole number, then we interpolate the value for the i^{th} percentile as

$$i^{th} \text{ percentile} = (1 - \text{index_f}) \times a_{\text{index_w}} + \text{index_f} \times a_{\text{index_w}+1} \quad (\text{A.5})$$

where *index_w* is the whole part of *index*, *index_f* is the fractional part of *index*, and $a_{\text{index_w}}$ is the value in the ordered list at position *index_w*.

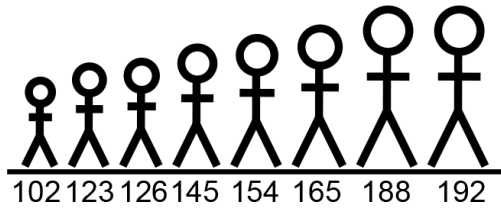


Figure A.4

The members of the rival school basketball team from [Figure A.3](#)^[747] ordered by height.

For example, [Figure A.4](#)^[749] shows the basketball team from [Figure A.3](#)^[747] ordered by height. To calculate the 25^{th} percentile, we first calculate *index* as $\frac{25}{100} \times 8 = 2$. So, the 25^{th} percentile is the second value in the ordered list, which is 123. To calculate the 80^{th} percentile, we first calculate *index* as $\frac{80}{100} \times 8 = 6.4$. Because *index* is not a whole number, we set *index_w* to the whole part of *index*, 6, and *index_f* to the fractional part, 0.4. Then we can calculate the 80^{th} percentile as

$$(1 - 0.4) \times 165 + 0.4 \times 188 = 174.2$$

using the 6^{th} and 7^{th} values in the list, 165 and 188. We have actually already come across a percentile in the measures of central tendency. The median is the 50^{th} percentile.

We can use percentiles to describe another measure of variation known as the **inter-quartile range (IQR)**. The inter-quartile range is calculated as

the difference between the 25th percentile and the 75th percentile. These percentiles are also known as the **lower quartile** (or 1st quartile) and the **upper quartile** (or 3rd quartile), hence the name inter-quartile range. For the heights of the first basketball team, the inter-quartile range is $151 - 140 = 11$, while for the second team, it is $165 - 123 = 42$.

A.2 Descriptive Statistics for Categorical Features

The statistics outlined in the previous section work well to describe continuous features, but they do not work for categorical features. For categorical features we are interested primarily in **frequency counts** and **proportions**. The frequency count of each level² of a categorical feature is calculated by counting the number of times that level appears in the sample. The proportion for each level is calculated by dividing the frequency count for that level by the total sample size. Frequencies and proportions are typically presented in a **frequency table**, which shows the frequency and proportion of each level for a particular feature—usually sorted by descending frequency.

For example, [Table A.1^{\[750\]}](#) lists the position that each player on a school basketball team plays at, and the average training expenses accrued each month by each player on the team. [Table A.2^{\[750\]}](#) shows the frequencies and proportions of the positions that players in the team play at, based on counts of the occurrences of the different levels of the POSITION feature in [Table A.1^{\[750\]}](#). We can see from this example that the *guard* level is the most frequent, followed by *forward* and *center*.

Table A.1

A dataset showing the positions and monthly training expenses of a school basketball team.

TRAINING EXPENSES			TRAINING EXPENSES		
ID	POSITION		ID	POSITION	
1	center	56.75	11	center	550.00
2	guard	1,800.11	12	center	223.89
3	guard	1,341.03	13	center	103.23
4	forward	749.50	14	forward	758.22
5	guard	1,150.00	15	forward	430.79
6	forward	928.30	16	forward	675.11
7	center	250.90	17	guard	1,657.20
8	guard	806.15	18	guard	1,405.18
9	guard	1,209.02	19	guard	760.51
10	forward	405.72	20	forward	985.41

Table A.2

A frequency table for the POSITION feature from the school basketball team dataset in [Table A.1](#)^[750].

Level	Count	Proportion
guard	8	40%
forward	7	35%
center	5	25%

Based on these frequency counts and proportions, the **mode** of a categorical feature can be calculated. The mode is a measure of the central tendency of a categorical feature and is simply the most frequent level. Based on the counts in [Table A.2](#)^[750], the mode of the POSITION feature is *guard*. We often also calculate a **second mode**, which is just the second most common level of a feature. In this example, the second mode is *forward*.

A.3 Populations and Samples

Throughout the discussion in the previous sections about central tendency and variation, we consistently used the word **sample** to refer to the set of values in an ABT for a particular feature. In statistics it is very important to understand the difference between a **population** and a sample. The term population is used in statistics to represent all possible measurements or outcomes that are of interest to us in a particular study or piece of analysis.

The term sample refers to the subset of the population that is selected for analysis.

For example, consider [Table A.3](#)^[751], which shows a set of results for polls run shortly before the 2012 United States presidential election, in which Mitt Romney and Barack Obama were the front-runners.³ In the first poll in the table, from Pew Research, we can see that a sample of just 2,709 likely voters⁴ was used. This poll put Obama ahead of Romney in the race to the White House. In this example the actual population of interest was the voting population of the United States, which was approximately 240,926,957 people. It would be almost impossible to ask the full voting population their voting intentions before an actual election—after all, that is what the actual election is for—so polling companies take a sample.

Table A.3

Poll results from the run-up to the 2012 U.S. presidential election.

Poll	Obama	Romney	Other	Date	Margin of Error	Sample Size
Pew Research	50	47	3	04-Nov	±2.2	2,709
ABC News/Wash Post	50	47	3	04-Nov	±2.5	2,345
CNN/Opinion Research	49	49	2	04-Nov	±3.5	963
Pew Research	50	47	3	03-Nov	±2.2	2,709
ABC News/Wash Post	49	48	3	03-Nov	±2.5	2,069
ABC News/Wash Post	49	49	2	30-Oct	±3.0	1,288

While the sample of 2,709 voters out of a population of 240,926,957 might appear quite small, we can also see from the table that the **margin of error** for the poll is given as $\pm 2.2\%$. The margin of error takes into account the fact that this is just a sample from a much larger population.⁵ All the other polls in the table were conducted with similar-sized samples. You should notice, however, that, in general, the larger the sample, the smaller the margin of error. This reflects the fact that if we use a bigger sample, we can be more confident in our approximations of the characteristics of the full population.

In choosing a sample, it is important that it be representative of the population. In this example the sample should represent the voting

population—for example, there should be a representative proportion of males compared to females and of different age categories within the sample. If a sample is not representative, we say that the sample is **biased**. Using a **simple random sample** is the most straightforward way of avoiding biased samples. In a simple random sample, each item in the population is equally likely to make it into the sample. Other, more sophisticated sampling methods can be used to ensure that a sample maintains relationships that exist in a population. We discuss sampling methods in more detail in Section 3.6.3^[91].

In the context of a predictive analytics scenario, the sample is the set of values that occur in an ABT. The population is the set of all the values that could possibly occur. For example, in an ABT for a motor insurance claims fraud prediction problem, we may include details of 500 claims that have happened in the past. This would be our sample. The population would be all the claims that have ever happened.

Up to this point we have outlined descriptive statistics that we can use to describe the values in a sample. How do we relate these values to the actual underlying population? Statistics that describe the population are referred to as **population parameters**. In general we use the sample statistics, which we have already calculated, as estimates for the population parameters. The population mean of a feature is usually denoted by μ , and in general, given a sufficiently large sample, we use the sample mean \bar{a} as a point estimate of μ . The population variance of a feature is usually denoted by σ^2 . In general, given a sufficiently large sample, we use the sample variance, $\text{var}(a)$, as a point estimate of σ^2 . This process is known as **statistical inference**.

Careful readers will have noticed that in the equation for variance given in Equation (A.3)^[747], we divided the sum of the differences between the values of the feature a and \bar{a} not by n , the number of values for a in the ABT, but by $n - 1$. We divide by $n - 1$ so that the sample variance is an unbiased estimate of the population variance. We say that the estimate is unbiased if its variance, on average, equals that of the population variance. If we divided by n , we would have a biased estimator that on average underestimates the variance. It is in small differences like this that we see the impact of working on samples rather than populations.

A.4 Data Visualization

When performing data exploration, **data visualization** can help enormously. In this section we describe three important data visualization techniques that can be used to visualize the values in a single feature: the **bar plot**, the **histogram**, and the **box plot**. For the examples throughout this section, we will use the dataset in [Table A.1](#)^[750], which lists the position that each player on a school basketball team plays at and the average training expenses they accrue each month.

A.4.1 Bar Plots

The simplest form of data visualization we can use for data exploration is the bar plot. A bar plot includes a vertical bar for each level of a categorical feature. The height of each bar indicates the frequency of the associated level (readers will most likely already be familiar with the bar plot). In a slight variation of the bar plot, we can show **densities** rather than frequencies by dividing each frequency by the total number of values in the dataset. This makes bar plots comparable across datasets or samples of different sizes and is referred to as a **probability distribution**, because the densities actually tell us the probability that we would pick each level if we were to select one instance at random from the dataset.

Another simple variant of the basic bar plot orders the bars in descending order.⁶ Typically we use bar plots to discover the most frequent levels for a feature, and this ordering makes this more apparent. [Figure A.5](#)^[753] shows example bar plots of all three types for the POSITION feature from the dataset in [Table A.1](#)^[750]. We can see that *guard* is the most frequent level.

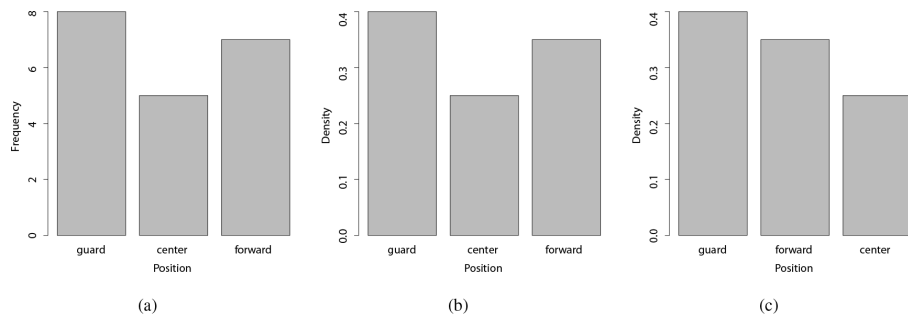


Figure A.5

Example bar plots for the POSITION feature in [Table A.1](#)^[750]: (a) frequency bar plot, (b) density bar plot, and (c) order density bar plot.

A.4.2 Histograms

[Figure A.6](#)^[753] is a bar plot of the TRAINING EXPENSES feature from [Table A.1](#)^[750]. The figure illustrates why a bar plot is not an appropriate graphic to use to visualize a continuous feature: as is generally the case with a continuous feature, there are as many distinct values as there are instances in the dataset, and therefore there are as many bars in the histogram as there are instances, each bar having a height of 1.0.

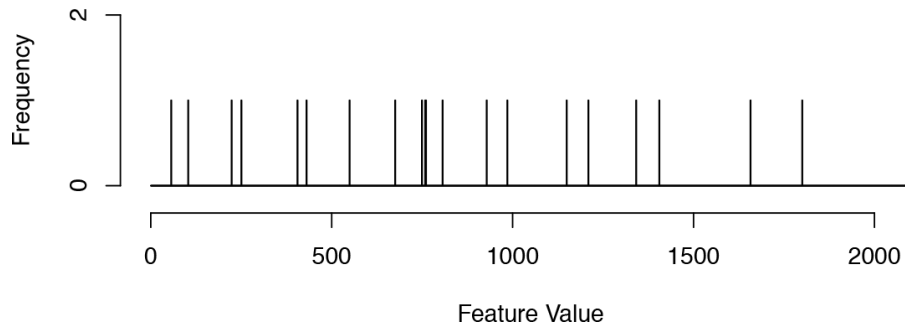


Figure A.6

Bar plot of the continuous TRAINING EXPENSES feature from [Table A.1](#)^[750].

The way to solve this problem is to visualize intervals rather than specific values, and this is what a **histogram** does. [Figure A.7\(a\)](#)^[754] shows the frequency histogram for the TRAINING EXPENSES feature when we define ten 200-unit intervals spanning the range that this feature can take (the frequencies come from [Table A.4\(a\)](#)^[755]). In this histogram the width of each bar indicates the extent of the interval the bar represents, and the height of each bar is based on the number of instances in the dataset that have a value inside the interval. This type of histogram is often referred to as a **frequency histogram**. Generally, there is not an optimal set of intervals for a given feature. For example, we could have used four 500-unit intervals to generate the histogram instead—see [Figure A.7\(b\)](#)^[754], based on frequencies from [Table A.4\(b\)](#)^[755]—or, indeed, any other set of intervals.

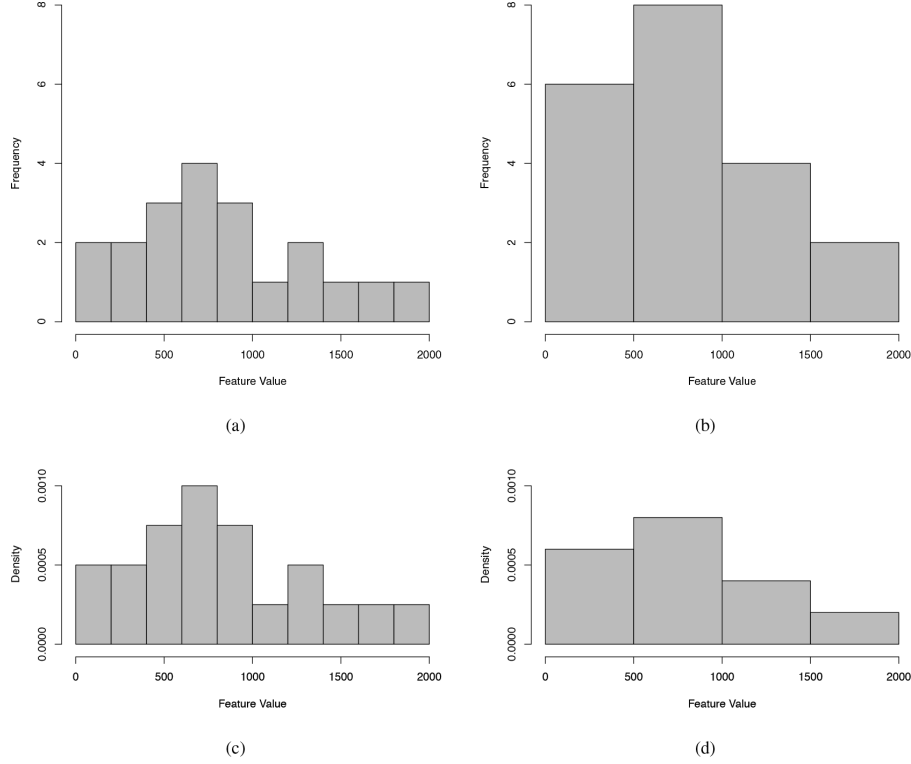


Figure A.7

(a) and (b) frequency histograms and (c) and (d) density histograms for the continuous TRAINING EXPENSES feature from [Table A.1](#)^[750], illustrating how using intervals overcomes the problem seen in [Figure A.6](#)^[753] and the effect of varying interval sizes.

Table A.4

The density calculation for the TRAINING EXPENSES feature from [Table A.1](#)^[750] using (a) ten 200-unit intervals and (b) four 500-unit intervals.

(a) 200-unit intervals

Interval	Count	Density	Prob
[0, 200)	2	0.00050	0.1
[200, 400)	2	0.00050	0.1
[400, 600)	3	0.00075	0.15
[600, 800)	4	0.00100	0.2
[800, 1000)	3	0.00075	0.15
[1000, 1200)	1	0.00025	0.05
[1200, 1400)	2	0.00050	0.1
[1400, 1600)	1	0.00025	0.05
[1600, 1800)	1	0.00025	0.05
[1800, 2000)	1	0.00025	0.02

(b) 500-unit intervals

Interval	Count	Density	Prob
[0, 500)	6	0.0006	0.3
[500, 1000)	8	0.0008	0.4
[1000, 1500)	4	0.0004	0.2
[1500, 2000)	2	0.0002	0.1

We can convert a histogram to a probability distribution by dividing the count for each interval by the total number of observations in the dataset multiplied by the width of the interval. As a result, the area of each bar (the bar height times the bar width) gives the probability for the feature taking a value in the interval represented by that bar. The resulting histogram is called a **density histogram** because the height of each bar represents how densely the instances in the dataset that fall within the interval are packed into the area of the bar.

Figure A.7(c)^[754] illustrates the density histogram of the TRAINING EXPENSES feature using ten 200-unit intervals, and Figure A.7(d)^[754] illustrates the density histogram using four 500-unit intervals. Notice that the vertical axes in these histograms are labeled **density**, rather than frequency. Table A.4(a)^[755] shows the density and probability calculations for the TRAINING EXPENSES feature when we use ten 200-unit intervals, and Table A.4(b)^[755] shows the same calculations when we use four 500-unit intervals.⁷ Recall that we compute the density for each interval by dividing the number of observations in the interval by the width of the interval multiplied by the total number of observations. Notice that the sum of the probabilities (the bar areas in the histograms) in both of these tables is 1.0, which is what we would expect with a probability distribution—all probability distributions sum to 1.0.

A.4.3 Box Plots

The last data visualization technique we will discuss for visualizing the values of a single feature is the **box plot**.⁸ A box plot is a visual representation of the five key descriptive statistics for a continuous feature: minimum, 1st quartile, median, 3rd quartile, and maximum. Figure A.8(a)^[756] shows the structure of a box plot. In a box plot the vertical axis shows the range of values that a feature can take. The extent of the rectangular box in the middle of the plot is determined by the 3rd quartile at the top and the 1st quartile at the bottom. The height of this rectangle, then, also shows the inter-quartile range. The strong black line across the middle of the rectangle shows the median.

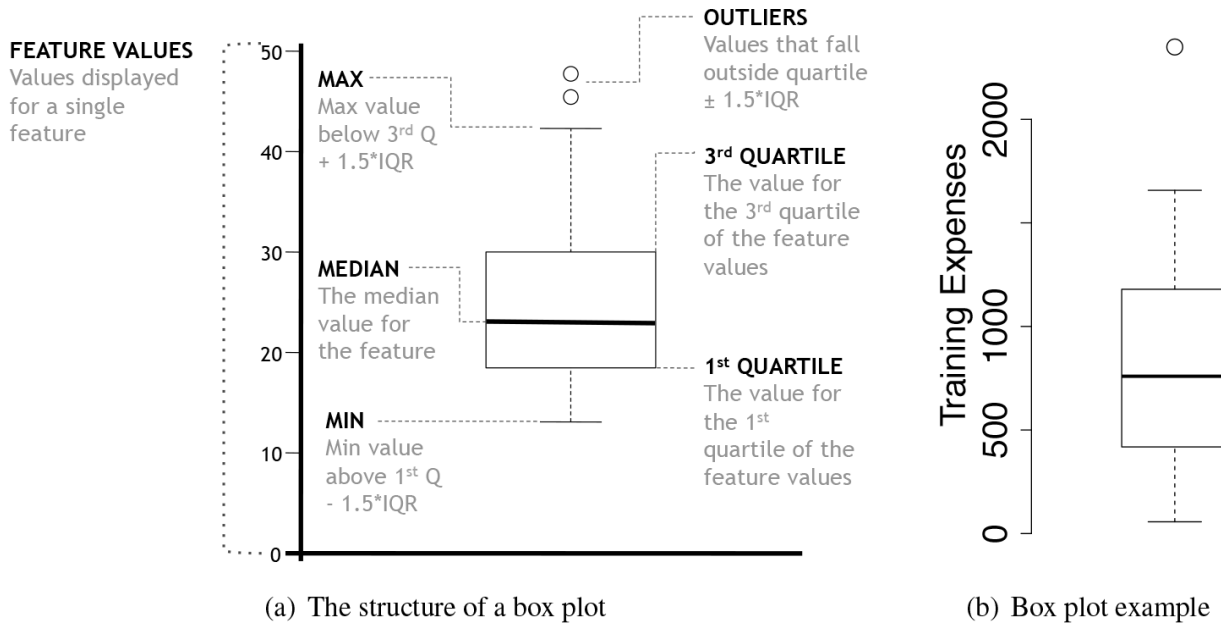


Figure A.8

(a) The structure of a box plot; and (b) a box plot for the TRAINING EXPENSES feature from the basketball team dataset in [Table A.1](#)^[750].

The whiskers that emerge from the top and bottom of the main rectangle in a box plot are designed to show the range of the data. The top whisker extends to whichever is lower of the maximum value of the feature or the upper quartile plus 1.5 times the IQR. Similarly, the bottom whisker extends to whichever is higher of the minimum value of the feature or the lower quartile minus 1.5 times the IQR. Values that fall outside the whiskers are referred to as **outliers** and are shown as small circles.

[Figure A.8\(b\)](#)^[756] shows a box plot for the TRAINING EXPENSES feature from the dataset in [Table A.1](#)^[750]. From this plot we can get a concise, but detailed, description of the feature and notice the inclusion of an outlier value. In comparison with a box plot, an individual histogram provides more information; for example, histograms show the distribution of the values of a feature. Box plots, however, can be placed side by side, and in [Section 3.5.1.2](#)^[74] we see that the ability to place multiple box plots side by side is the main advantage box plots have over histograms.

1. We divide by $n - 1$ (as opposed to n) because we are calculating the variance using only a sample, and on average, dividing by $n - 1$ gives a better estimate of the population variance than using n .
2. Remember, we refer to each value that a particular categorical feature can take as the levels of the categorical feature.

3. This data is taken from the collection at Real Clear Politics: www.realclearpolitics.com/epolls/2012/president/us/general_election_romney_vs_obama-1171.html.
4. Likely voters are the subset of registered voters who have been identified as most likely to actually vote in an election.
5. This size of margin of error is common for these types of election polls.
6. These charts are often referred to as **Pareto charts**, especially when they also include a line indicating the cumulative total frequency or density.
7. When defining intervals, a square bracket, [or], indicates that the boundary value is included in the interval, and a parenthesis, (or), indicates that it is excluded from the interval.
8. Box plots are one of the collection of visual data exploration techniques first presented in Tukey's influential 1977 book *Exploratory Data Analysis* (Tukey, 1977).

B

Introduction to Probability for Machine Learning

In this appendix we introduce the fundamental concepts of **probability theory** that are used in probability-based machine learning algorithms. Specifically, we present the basics of calculating probabilities based on **relative frequencies**, calculating **conditional probabilities**, the probability **product rule**, the probability **chain rule**, and the **Theorem of Total Probability**.

B.1 Probability Basics

Probability is the branch of mathematics that deals with measuring the likelihood (or uncertainty) around events. The roots of probability are in gambling, where, understandably, gamblers wanted to be able to predict future events based on their likelihood. There are two ways of computing the likelihood of a future event: (1) use the **relative frequency** of the event in the past, or (2) use a **subjective estimate** (ideally from an expert!). In the predictive analytics context, the standard approach is to use relative frequency, and we focus on this approach in this chapter.

Probability has a longer history, and broader applicability, than predictive analytics. Consequently, the standard language of probability has developed some esoteric terminology, including terms such as **sample space**, **experiment**, **outcome**, **event**, and **random variable**. So we will begin by first explaining this terminology and aligning it with the more familiar terminology of predictive analytics.

In probability a **domain** of interest is represented by a set of **random variables**. For example, if we want to model the behavior of a die using probability, we would begin by creating a random variable, let us call it X , that has a domain equal to the set of possible outcomes when we roll the die, namely, the set $\{\square, \square, \square, \square, \square, \square\}$. Extending this example, if we wanted

to study the behavior of two dice, we would create two random variables, we might call them $Dice_1$ and $Dice_2$, each having the domain $\{\square, \blacksquare, \blacksquare\blacksquare, \blacksquare\square, \square\square, \square\blacksquare\}$. In this extended context, an **experiment** involves rolling the two dice, and the **sample space** defines the set of all possible outcomes for this experiment (see [Figure B.1^{\[757\]}](#)). An **event** is then an experiment whose **outcome** fixes the values of the random variables. For example, an **event** in this domain would be represented as $Dice_1 = \square$, $Dice_2 = \blacksquare\square$.

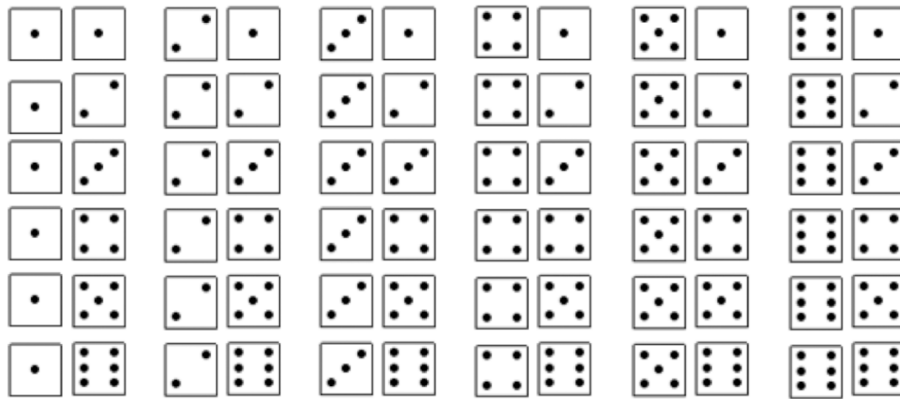


Figure B.1

The **sample space** for the domain of two dice.

Table B.1

A dataset of instances from the sample space in [Figure B.1^{\[757\]}](#).

ID	DICE1	DICE2
1	$\blacksquare\blacksquare$	$\blacksquare\blacksquare$
2	$\square\square$	$\blacksquare\blacksquare$
3	$\blacksquare\blacksquare\blacksquare$	$\blacksquare\blacksquare$
4	$\blacksquare\blacksquare$	$\blacksquare\blacksquare$
5	$\square\square$	$\square\square$

[Table B.1^{\[758\]}](#) lists a small dataset of instances from the sample space shown in [Figure B.1^{\[757\]}](#). We will use this example dataset to illustrate how to map the terminology of probability into the language of predictive analytics:

- The set of **random variables** in a domain maps to the set of features in a dataset (both descriptive and target). DICE1 and DICE2 are the equivalent of random variables.
- The **sample space** for a domain is the set of all possible combinations of assignments of values to features.
- An **experiment** whose outcome has been already been recorded is a row in the dataset. Each row in [Table B.1](#)^[757] records the outcome of a previous experiment.
- An **experiment** whose outcome we do not yet know but would like to predict is the prediction task for which we are building a model.
- An **event** is any subset of an experiment. An event may describe an assignment of values to all the features in the domain (e.g., a full row in the dataset) or an assignment to one or more features in the domain. $\text{DICE1} = \square$ is an example of an event. $\text{DICE1} = \square, \text{DICE2} = \square$ is also an event.

So that we are consistent with the terminology throughout this book, in the rest of this chapter, we use the predictive analytics terms (**feature**, **dataset**, **prediction**, and **event**) rather than the traditional terms from probability.

A feature can take one or more values from a domain, and we can find out the likelihood of a feature taking any particular value using a **probability function**, $P()$. A probability function is a function that takes an event (an assignment of values to features) as a parameter and returns the likelihood of that event. For example, $P(\text{DICE1} = \square)$ will return the likelihood of the event $\text{DICE1} = \square$, and $P(\text{DICE1} = \square, \text{DICE2} = \square)$ will return the likelihood of the event where $\text{DICE1} = \square$ and $\text{DICE2} = \square$. If we are defining the probability function for a categorical feature, then the function is known as a **probability mass function** because it can be understood as returning a discrete **probability mass** for each level in the domain of the feature. The probability mass is simply the probability of an event. Conversely, if the feature we are dealing with is a continuous feature, the probability function is known as a **probability density function**. For this introduction, we focus on categorical features and probability mass functions.

Probability mass functions have two properties: (1) they always return a value between 0.0 and 1.0; and (2) the sum of the probabilities over the set of events covering all the possible assignments of values to features must equal 1.0. Formally these properties are defined as follows:

$$0 \leq P(f = level) \leq 1$$

$$\sum_{l \in levels(f)} P(f = l) = 1.0$$

where $levels(f)$ returns the set of levels in the domain of the feature f .

Probability functions are the basic building blocks of probability theory, and they are very easy to create from a dataset. The value returned by a probability function for an event is simply the **relative frequency** of that event in the dataset. The relative frequency of an event is calculated as how often the event happened divided by how often it could have happened. For example, the relative frequency of the event $DICE1 = \square$ is simply the count of all the rows in the dataset where $DICE1$ has a value of \square divided by the number of rows in the dataset. Based on [Table B.1](#)^[758], the probability of the event $DICE1 = \square$ is¹

$$P(DICE1 = \square) = \frac{|\{\mathbf{d}_1, \mathbf{d}_4\}|}{|\{\mathbf{d}_1, \mathbf{d}_2, \mathbf{d}_3, \mathbf{d}_4, \mathbf{d}_5\}|} = \frac{2}{5} = 0.4$$

So far we have focused on calculating the probability of an individual event. In a predictive analytics task, we will often be interested in calculating the probability of more than one event. For example, we might want to know the probability of the target feature taking a particular value and one of the descriptive features taking a particular value at the same time. Technically, if an event involves more than one feature, it can be considered to be composed of several *simple* events. In these cases the probability calculated is known as a **joint probability**. The probability of a joint event is simply the relative frequency of the joint event within the dataset. In terms of rows in a dataset, this computation is simply the number of rows where the set of assignments listed in the joint event holds divided by the total number of rows in the dataset. For example, the probability of the joint event² $DICE1 = \square, DICE2 = \square$ would be calculated as

$$P(DICE1 = \square, DICE2 = \square) = \frac{|\{\mathbf{d}_3\}|}{|\{\mathbf{d}_1, \mathbf{d}_2, \mathbf{d}_3, \mathbf{d}_4, \mathbf{d}_5\}|} = \frac{1}{5} = 0.2$$

The type of probabilities we have calculated so far are known as **prior probabilities** or **unconditional probabilities**. Often, however, we want to know the probability of an event in the context where one or more other events are known to have happened. This type of probability, where we take one or more events to already hold, is known as a **posterior probability**, because it is calculated *after* other events have happened. It is also commonly known as a **conditional probability**, because the probability calculated is valid conditional on the given events (or evidence). When we want to express this type of probability, formally we use a vertical bar, |, to separate the events we want the probability for (listed on the left-hand side of the bar) from the events that we know have already happened. The vertical bar symbol can be read as *given that*. So the probability of DICE1 = \square *given that* DICE2 = \blacksquare would be written as

$$P(\text{DICE1} = \square \mid \text{DICE2} = \blacksquare)$$

The **conditional probability** for an event given that we know another event is true is calculated by dividing the number of rows in the dataset where both events are true by the number of rows in the dataset where just the given event is true. For example, the conditional probability for the event DICE1 = \square *given that* DICE2 = \blacksquare would be calculated as

$$P(\text{DICE1} = \square \mid \text{DICE2} = \blacksquare) = \frac{|\{\mathbf{d}_3\}|}{|\{\mathbf{d}_2, \mathbf{d}_3\}|} = \frac{1}{2} = 0.5$$

We now understand the theory of how to calculate a simple unconditional probability, a joint probability, and a conditional probability using a dataset. Now is a good point to ground this knowledge in a more interesting example focused on predictive data analytics. We will use the dataset in [Table B.2](#)^[760] for this.³ The target being predicted in this dataset is whether or not a patient is suffering from meningitis, and the descriptive features are common symptoms associated with meningitis.

Table B.2

A simple dataset for MENINGITIS with three common symptoms of the disease listed as descriptive features: HEADACHE, FEVER, and VOMITING.

ID	HEADACHE	FEVER	VOMITING	MENINGITIS
11	true	true	false	false
37	false	true	false	false
42	true	false	true	false
49	true	false	true	false
54	false	true	false	true
57	true	false	true	false
73	true	false	true	false
75	true	false	true	true
89	false	true	false	false
92	true	false	true	true

A quick comment on our notation. Throughout this chapter, named features will be denoted by the uppercase initial letters of their names—for example, a feature named MENINGITIS will be denoted by M . Also, where a named feature is binary, we will use the lowercase initial letter of the feature name to denote the event where the feature is true and the lowercase initial letter preceded by the \neg symbol to denote the event where it is false. So, m will denote the event $\text{MENINGITIS} = \text{true}$ and $\neg m$ will denote $\text{MENINGITIS} = \text{false}$. Given the dataset in [Table B.2](#)^[760], the probability of a patient having a headache is

$$P(h) = \frac{|\{\mathbf{d}_{11}, \mathbf{d}_{42}, \mathbf{d}_{49}, \mathbf{d}_{57}, \mathbf{d}_{73}, \mathbf{d}_{75}, \mathbf{d}_{92}\}|}{|\{\mathbf{d}_{11}, \mathbf{d}_{37}, \mathbf{d}_{42}, \mathbf{d}_{49}, \mathbf{d}_{54}, \mathbf{d}_{57}, \mathbf{d}_{73}, \mathbf{d}_{75}, \mathbf{d}_{89}, \mathbf{d}_{92}\}|} = \frac{7}{10} = 0.7 \quad (\text{B.1})$$

the probability of a patient having a headache and meningitis is

$$P(m, h) = \frac{|\{\mathbf{d}_{75}, \mathbf{d}_{92}\}|}{|\{\mathbf{d}_{11}, \mathbf{d}_{37}, \mathbf{d}_{42}, \mathbf{d}_{49}, \mathbf{d}_{54}, \mathbf{d}_{57}, \mathbf{d}_{73}, \mathbf{d}_{75}, \mathbf{d}_{89}, \mathbf{d}_{92}\}|} = \frac{2}{10} = 0.2 \quad (\text{B.2})$$

and the probability of a patient having meningitis given that we know that the patient has a headache is

$$P(m | h) = \frac{|\{\mathbf{d}_{75}, \mathbf{d}_{92}\}|}{|\{\mathbf{d}_{11}, \mathbf{d}_{42}, \mathbf{d}_{49}, \mathbf{d}_{57}, \mathbf{d}_{73}, \mathbf{d}_{75}, \mathbf{d}_{92}\}|} = \frac{2}{7} = 0.2857 \quad (\text{B.3})$$

B.2 Probability Distributions and Summing Out

Sometimes it is useful to talk about the probabilities for all the possible assignments to a feature. To do this we use the concept of a **probability distribution**. A probability distribution is a data structure that describes the probability of a feature taking a value for all the possible values the feature can take. The probability distribution for a categorical feature is a vector that lists the probabilities associated with each of the values in the domain of the feature. A vector is an ordered list, so the mechanism for matching a probability in the vector with a particular value in the domain is just to look up the position of the probability within the vector. We use bold notation $\mathbf{P}()$ to distinguish between a probability distribution and a probability function $P()$. For example, the probability distribution for the binary feature MENINGITIS from [Table B.2](#)^[760], with a probability of 0.3 of being *true* and using the convention of the first element in the vector being the probability for a *true* value, would be written as $\mathbf{P}(M) = \langle 0.3, 0.7 \rangle$.

The concept of a probability distribution also applies to joint probabilities, which gives us the concept of a **joint probability distribution**. A joint probability distribution is a multidimensional matrix where each cell in the matrix lists the probability for one of the events in the sample space defined by the combination of feature values. The dimensions of the matrix are dependent on the number of features and the number of values in the domains of the features. The joint probability distribution for the four binary features from [Table B.2](#)^[760] (HEADACHE, FEVER, VOMITING, and MENINGITIS) would be written as

$$\mathbf{P}(H, F, V, M) = \begin{bmatrix} P(h, f, v, m), & P(\neg h, f, v, m) \\ P(h, f, v, \neg m), & P(\neg h, f, v, \neg m) \\ P(h, f, \neg v, m), & P(\neg h, f, \neg v, m) \\ P(h, f, \neg v, \neg m), & P(\neg h, f, \neg v, \neg m) \\ P(h, \neg f, v, m), & P(\neg h, \neg f, v, m) \\ P(h, \neg f, v, \neg m), & P(\neg h, \neg f, v, \neg m) \\ P(h, \neg f, \neg v, m), & P(\neg h, \neg f, \neg v, m) \\ P(h, \neg f, \neg v, \neg m), & P(\neg h, \neg f, \neg v, \neg m) \end{bmatrix}$$

Remember that the sum of all the elements in a probability distribution must be 1.0. Consequently, the sum of all the cells in a joint probability distribution must be 1.0. A **full joint probability distribution** is simply a joint probability distribution over all the features in a domain. Given a full joint probability distribution, we can compute the probability of any event in a domain by summing over the cells in the distribution where that event is true. For example, imagine we want to compute the probability of $P(h)$ in the domain specified by the joint probability distribution $\mathbf{P}(H,F,V,M)$. To do this we simply sum the values in the cells containing h , in other words, the cells in the first column of the distribution. Calculating probabilities in this way is known as **summing out** or **marginalization**.⁴

We can also use summing out to compute conditional probabilities from a joint probability distribution. For example, imagine we wish to calculate the probability of h given f when we don't care what values V or M take. In this context, V and M are examples of **hidden features**. A hidden feature is a feature whose value is not specified as part of the evidence. We can calculate $P(h, V = ?, M = ? | f)$ from $\mathbf{P}(H,F,V,M)$ by summing the values in all the cells where h and f are the case (the top four cells in the first column).

The process of **summing out** is a key concept in probability-based prediction. In order to make a prediction, a model must compute the probability for a target event in the context where some other events are known (the evidence) and where there are potentially one or more hidden features. As we have seen, using a joint probability distribution, a model can carry out this calculation by simply conditioning on the evidence features and summing out the hidden features. Unfortunately, the size of a joint probability distribution grows exponentially as the number of features and the number of values in the domains of the features grow. Consequently, they are difficult to generate because of the curse of dimensionality: computing the probability for each cell in a joint probability table requires a set of instances and, because the number of cells grows exponentially as features and feature values are added, so does the size of the dataset required to generate the joint probability distribution. As a result, for any domain of reasonable complexity, it is not tractable to define the full joint probability distribution, and therefore probability-based

prediction models build more compact representations of full joint probability distributions instead.

B.3 Some Useful Probability Rules

Several important rules in probability theory allow us to compute new probabilities in terms of previously computed probabilities. Note that throughout the rest of the chapter, we use uppercase letters to denote generic events where an unspecified feature (or set of features) is assigned a value (or set of values). Typically we will use letters from the end of the alphabet (e.g., X , Y , Z) for this purpose. Also, we will use subscripts on uppercase letters to iterate over events. So, $\sum_i P(X_i)$ should be interpreted as summing over all the possible combinations of value assignments to the features in X .

The first rule we will introduce defines **conditional probability** in terms of joint probability:

$$P(X | Y) = \frac{P(X, Y)}{P(Y)} \quad (\text{B.4})$$

We have already calculated the conditional probability of the event m given h directly from the dataset in [Table B.2](#)^[760] as $P(m | h) = 0.2857$ (see [Equation \(B.3\)](#)^[761]). We will now recalculate this probability using our rule-based definition of conditional probability. From our previous calculations, we already know that $P(h) = 0.7$ (see [Equation \(B.1\)](#)^[760]) and $P(m, h) = 0.2$ (see [Equation \(B.2\)](#)^[760]). So our calculation for $P(m | h)$ is

$$P(m | h) = \frac{P(m, h)}{P(h)} = \frac{0.2}{0.7} = 0.2857$$

Using [Equation \(B.4\)](#)^[762], we can provide a second definition for the probability of a joint event, which is known as the **product rule**:

$$P(X, Y) = P(X | Y) \times P(Y) \quad (\text{B.5})$$

We can demonstrate the product rule by recalculating the probability $P(m, h)$ using previously computed probabilities:

$$P(m, h) = P(m | h) \times P(h) = 0.2857 \times 0.7 = 0.2$$

Again, the result of the calculation matches the probability computed directly from the dataset (see Equation (B.2)^[760]).

There are a few points worth noting about the product rule. First, it defines the probability of a joint event $P(X, Y)$ in terms of a conditional (or posterior) probability $P(X | Y)$ multiplied by an unconditional (or prior) probability $P(Y)$. Second, the order of the events in the product rule is not important, and we can condition the calculation on any of the events listed in the *and* (in logic, the *and* operation is symmetric):

$$P(X, Y) = P(X | Y)P(Y) = P(Y | X)P(X)$$

We can also extend the product rule to define the joint probability of more than two events. When we generalize the rule in this way, it is known as the probability **chain rule**:

$$P(A, B, C, \dots, Z) = P(Z) \times P(Y | Z) \times P(X | Y, Z) \times \dots \times P(A | B, \dots, X, Y, Z) \quad (\text{B.6})$$

As with the simple two-event version, the order of events in the chain rule is not important.

Finally, the **Theorem of Total Probability** defines the unconditional probability for any event X as

$$P(X) = \sum_i P(X | Y_i)P(Y_i) \quad (\text{B.7})$$

where each Y_i is one of a set of events Y_1 to Y_k that cover all the possible outcomes in a domain and have no overlap between them. Because an event defines a partition of a dataset (the rows from the dataset that match the event), then each Y_i defines a set of rows from a dataset, and the set of data partitions defined by Y_1 to Y_k must cover the full dataset and not overlap with each other. The Theorem of Total Probability is a formal specification of the **summing out** process we introduced earlier in Section B.2^[761].

To illustrate how the Theorem of Total Probability can be used to calculate probabilities, we will compute $P(h)$ by summing out M (note: earlier, in Equation (B.1)^[760], we computed $P(h) = 0.7$):

$$\begin{aligned} P(h) &= (P(h | m) \times P(m)) + (P(h | \neg m) \times P(\neg m)) \\ &= (0.6666 \times 0.3) + (0.7143 \times 0.7) = 0.7 \end{aligned}$$

We can, if we wish, sum out more than one feature. For example, we could compute $P(h)$ by summing out all the other features in the dataset:

$$P(h) = \sum_{i \in level(M)} \sum_{j \in level(F)} \sum_{k \in level(V)} P(h | M_i, F_j, V_k) \times P(M_i, F_j, V_k)$$

We will, however, leave this calculation to the interested reader (the result should still be 0.7).

B.4 Summary

Probability theory underpins a great deal of machine learning. This section has provided an overview of the aspects of probability that readers need to understand in order to follow the other sections in this book. One thing to note is that many of the rules and techniques we presented were different ways of achieving the same thing—for example, we can calculate $P(h)$ by simple counting, by summing out from a full joint probability distribution, or by using the Theorem of Total Probability. This is an aspect of probability theory with which beginners sometimes struggle. The important thing to remember, though, is that the different approaches exist because in different scenarios it will often be easier to apply one approach over the others. Just like the proverbial cat, there is more than one way to skin a probability problem!

1. In the notation used in this book, \mathbf{d}_1 refers to the instance in a dataset with an ID of 1, and so on.
2. When listing a joint event, we use a comma , to denote logical *and*.
3. This data has been artificially generated for this example.
4. Summing out is sometimes referred to as marginalization because statisticians used to carry out these calculations in the margins of the probability tables they were working with!

C

Differentiation Techniques for Machine Learning

In this appendix we present the basic differentiation techniques that are required to understand how linear regression can be used to build predictive analytics models. In particular we explain what a derivative is, how to calculate derivatives for continuous functions, the chain rule for differentiation, and what a partial derivative is.

To begin, imagine a car journey where we start out driving on a minor road at about 30mph and then move onto a highway, where we drive at about 80mph before noticing an accident and braking suddenly. [Figure C.1\(a\)](#)^[765] shows a profile of the *speed* during this journey measured at different points in time. [Figure C.1\(b\)](#)^[765] shows a profile of the *acceleration* during this journey. We can see that when the car is driving at a constant speed, on the minor road or the highway, acceleration is zero as the speed is not changing. In contrast, acceleration has modest positive values when we are taking off initially and slightly larger positive values when we increase speed on reaching the highway. The sudden braking at the end of the journey results in large negative values that slowly taper off to match the speed profile in [Figure C.1\(a\)](#)^[765].

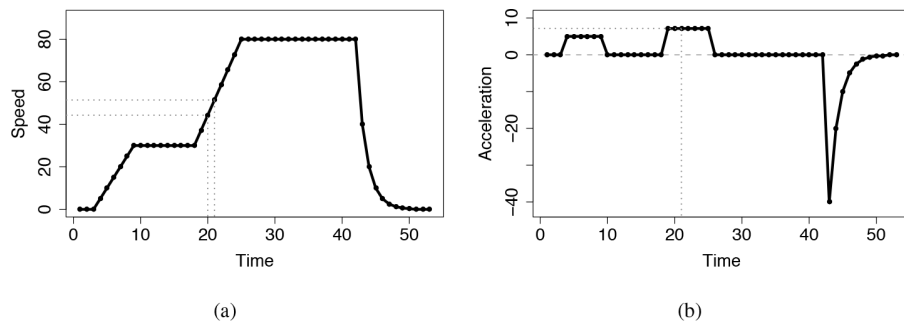


Figure C.1

(a) The speed of a car during a journey along a minor road before joining a highway and finally coming to a sudden halt; and (b) the acceleration, the derivative of speed with respect to time, for this journey.

Acceleration is a measure of the rate of change of speed over time. We can say more formally that acceleration is, in fact, the **derivative** of speed *with respect to* time. **Differentiation** is the set of techniques from **calculus** (the branch of mathematics that deals with how things change) that allows us to calculate **derivatives**. In an example like the car journey just described, where we have a set of discrete measurements, calculating the derivative is simply a matter of determining the difference between subsequent pairs of measurements. For example, the derivative of speed with respect to time at time index 21 is the speed at time index 21 minus the speed at time index 20, which is $44.28 - 51.42 = 7.14$. These values are marked in Figure C.1^[765]. All the values of acceleration have been calculated in this way.

C.1 Derivatives of Continuous Functions

While it is interesting to see how derivatives can be calculated for discrete examples, it is much more common that we need to calculate the derivative of a continuous function. A continuous function, $f(x)$, generates an output for every value of a variable x based on some expression involving x . For example:

$$\begin{aligned}f(x) &= 2x + 3 \\f(x) &= x^2 \\f(x) &= 3x^3 + 2x^2 - x - 2\end{aligned}$$

are continuous functions with a single variable x . Graphs of these functions are shown in Figure C.2^[767]. Each graph also shows the derivative of the

function. We will return to these shortly.

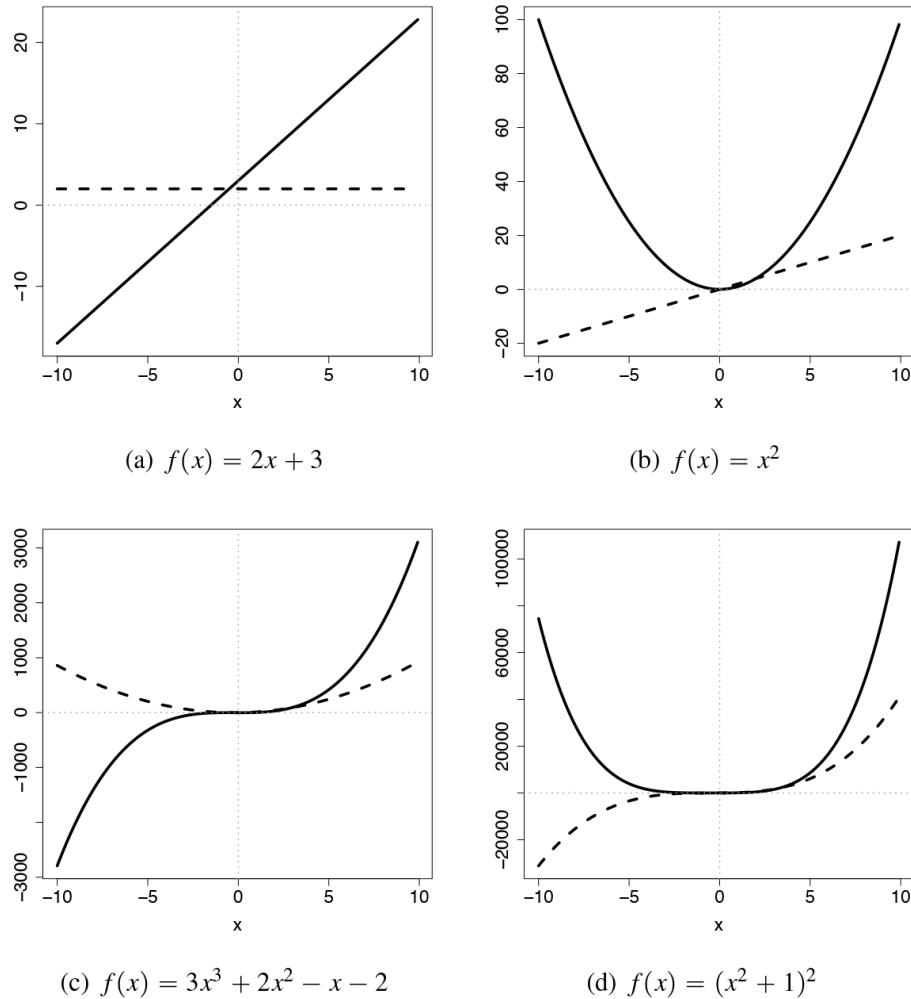


Figure C.2

Examples of continuous functions (shown as solid lines) and their derivatives (shown as dashed lines).

The function $f(x) = 2x + 3$ is known as a **linear function** because the output is a combination of only additions and multiplications¹ involving x . The other two functions are known as **polynomial functions** as they include addition, multiplication, and raising to exponents. Of those, $f(x) = x^2$ is an example of a **second order polynomial function**, also known as a **quadratic function**, as its highest exponent is 2, and $f(x) = 3x^3 + 2x^2 - x - 2$ is a **third order polynomial function**, also known as a **cubic function**, as its highest exponent is 3.

Looking first at [Figure C.2\(a\)](#)^[767], the function here is very simple, $f(x) = 2x + 3$, which results in a straight diagonal line. A straight diagonal line gives us a constant rate of change (in this case an increase of 2 in the value of the function for every change of 1 in x), so the derivative of this function with respect to x is just a constant. This is represented by the horizontal dashed line.

We can intuitively see from [Figure C.2\(b\)](#)^[767] for $f(x) = x^2$ that the rate of change of the value of this function is likely to be high at the steep edges of the curve and low at the bottom (imagine a ball rolling around inside this shape!). This intuition is mirrored in the derivative of the function with respect to x . We can see that on the left-hand side of the graph (for large negative values of x), the rate of change has a high negative value, while on the right-hand side of the graph (for large positive values of x), the rate of change has a large positive value. In the middle of the graph, at the bottom of the curve, the rate of change is zero. It should be no surprise to learn that the derivative of the function with respect to x also gives us the slope of the function at that value of x . The shape of the derivative in [Figure C.2\(c\)](#)^[767] can be understood similarly.

To actually calculate the derivative, referred to as $\frac{d}{dx}f(x)$, of a simple continuous function, $f(x)$, we use a small number of differentiation rules:

1. $\frac{d}{dx}\alpha = 0$ (where α is any constant)
2. $\frac{d}{dx}\alpha x^n = \alpha \times n \times x^{n-1}$
3. $\frac{d}{dx}a + b = \frac{d}{dx}a + \frac{d}{dx}b$ (where a and b are expressions that may or may not contain x)
4. $\frac{d}{dx}\alpha \times c = \alpha \times \frac{d}{dx}c$ (where α is any constant and c is an expression containing x)

Applying these rules to the first of our previous examples, $f(x) = 2x + 3$ ([Figure C.2\(a\)](#)^[767]), we first apply Rule 3 to split this function into two parts, $2x$ and 3 , and then apply differentiation rules to each. By Rule 2 we can differentiate $2x$ to 2 (remember that x is really x^1). The 3 is a constant, so by Rule 1 differentiates to zero. The derivative of the function, then, is $\frac{d}{dx}f(x) = 2$.

For the last function, $f(x) = 3x^3 + 2x^2 - x - 2$ ([Figure C.2\(c\)](#)^[767]), we first apply Rule 3 to divide this into four parts: $3x^3$, $2x^2$, x , and 2 . Applying Rule

2 to each of the first three parts gives $9x^2$, $4x$, and -1 . The final part, 2, is a constant and so differentiates to zero. The derivative of this function then is $\frac{d}{dx}f(x) = 9x^2 + 4x - 1$.

We can see from these examples that calculating derivatives of simple functions is a matter of, fairly mechanically, applying these four simple rules. Calculating the derivatives of the other two functions are left as exercises for the reader. Some of the functions that we will encounter later on in this chapter will be a little more complex, and we need two more differentiation rules to handle these.

C.2 The Chain Rule

The function $f(x) = (x^2 + 1)^2$ (shown in [Figure C.2\(d\)](#)^[767]) cannot be differentiated using the rules just described because it is a **composite function**—it is a *function of a function*. We can rewrite $f(x)$ as $f(x) = (g(x))^2$ where $g(x) = x^2 + 1$. The differentiation **chain rule** allows us to differentiate functions of this kind.² The chain rule is

$$\frac{d}{dx}f(g(x)) = \frac{d}{d g(x)}f(g(x)) \times \frac{d}{dx}g(x) \quad (\text{C.1})$$

The differentiation is performed in two steps. First, treating $g(x)$ as a unit, we differentiate $f(g(x))$ with respect to $g(x)$, and then we differentiate $g(x)$ with respect to x , in both cases using the differentiation rules from the previous section. The derivative of $f(g(x))$ with respect to x is the product of these two pieces.

Applying this to the example $f(x) = (x^2 + 1)^2$ we get

$$\begin{aligned} \frac{d}{dx}(x^2 + 1)^2 &= \frac{d}{d(x^2 + 1)}(x^2 + 1)^2 \times \frac{d}{dx}(x^2 + 1) \\ &= (2 \times (x^2 + 1)) \times (2x) \\ &= 4x^3 + 4x \end{aligned}$$

[Figure C.2\(d\)](#)^[767] shows this example function and its derivative calculated using the chain rule.

C.3 Partial Derivatives

Some functions are not defined in terms of just one variable. For example, $f(x,y) = x^2 - y^2 + 2x + 4y - xy + 2$ is a function defined in terms of two

variables, x and y . Rather than defining a curve (as was the case for all the previous examples), this function defines a surface, as shown in [Figure C.3\(a\)](#)^[769]. Using **partial derivatives** offers us an easy way to calculate the derivative of a function like this. A partial derivative (denoted by the symbol ∂) of a function of more than one variable is its derivative with respect to one of those variables with the other variables held constant.

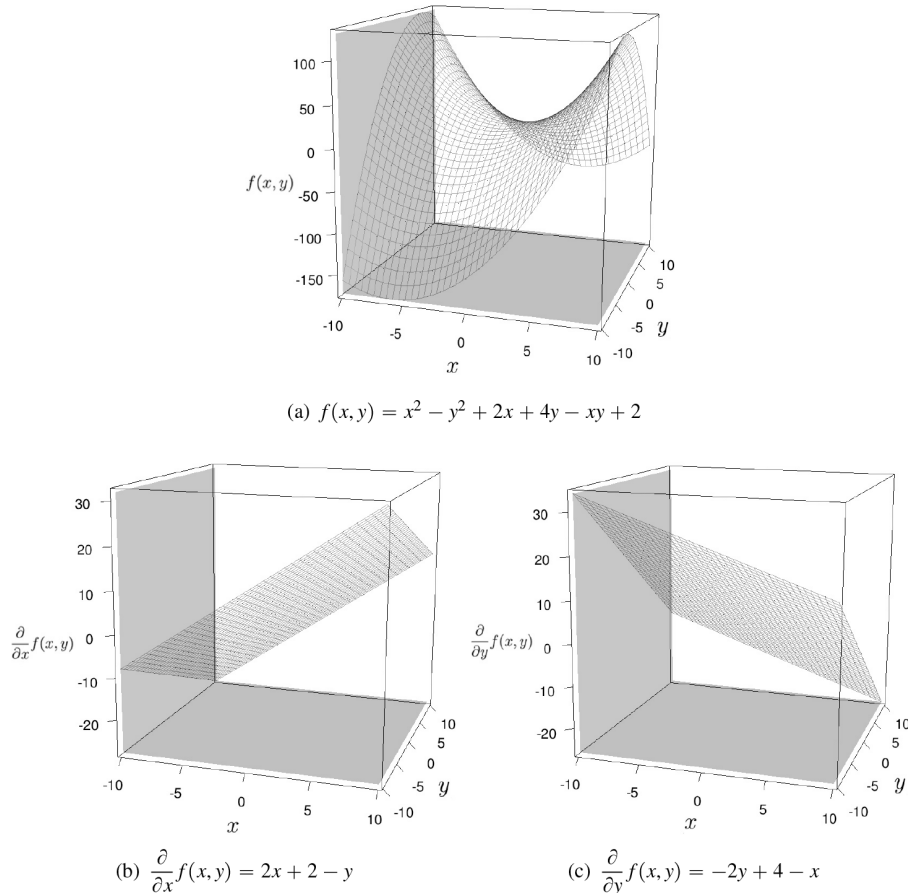


Figure C.3

(a) A continuous function in two variables, x and y ; (b) the partial derivative of this function with respect to x ; and (c) the partial derivative of this function with respect to y .

For the example function $f(x,y) = x^2 - y^2 + 2x + 4y - xy + 2$, we get two partial derivatives:

$$\frac{\partial}{\partial x}(x^2 - y^2 + 2x + 4y - xy + 2) = 2x + 2 - y$$

where the terms y^2 and $4y$ are treated as constants as they do not include x , and

$$\frac{\partial}{\partial y} (x^2 - y^2 + 2x + 4y - xy + 2) = -2y + 4 - x$$

where the terms x^2 and $2x$ are treated as constants as they do not include y . Figures C.3(b)^[769] and C.3(c)^[769] show these partial derivatives.

1. Note that subtraction is viewed as addition of negative numbers, and division is seen as multiplication by reciprocals, so both are also allowed.
2. This is not to be confused with the probability **chain rule** discussed in Section B.3^[762]. These are two completely different operations.

D

Introduction to Linear Algebra

In this appendix we introduce some of the fundamental operations in **linear algebra**. In particular, we introduce the vector and matrix operations that we use in the book.

D.1 Basic Types

There are a number of fundamental mathematical types that are the building blocks of linear algebra. These include

- A **scalar** is a single number.
- A **matrix** is a 2-dimensional ($n \times m$) array of numbers.

$$\mathbf{C} = \begin{bmatrix} c_{1,1} & c_{1,2} & \dots & c_{1,m} \\ c_{2,1} & c_{2,2} & \dots & c_{2,m} \\ \dots & \dots & \dots & \dots \\ c_{n,1} & c_{1,2} & \dots & c_{n,m} \end{bmatrix}$$

Each element in a matrix is identified by two indices, the row index and then the column index. For example,

$$\mathbf{C}[2, 2] = c_{2,2}$$

- A **vector** is an array of numbers, organized in a specific order. A vector can be either a column vector or a row vector. For example, **a** is a column vector, and **b** is a row vector.

$$\mathbf{a} = \begin{bmatrix} a_1 \\ a_2 \\ \dots \\ a_n \end{bmatrix}$$
$$\mathbf{b} = \begin{bmatrix} b_1 & b_2 & \dots & b_m \end{bmatrix}$$

Each element in a vector is identified by a single index. For example:

$$\begin{aligned}\mathbf{a}[2] &= a_2 \\ \mathbf{b}[2] &= b_2\end{aligned}$$

Vectors are often treated as special cases of matrices. For example, a column vector can be thought of as a matrix with just one column, and a row vector can be thought of as a matrix with a single row.

D.2 Transpose

A basic operation on vectors and matrices is the **transpose**. The transpose of a vector converts a column vector to a row vector, and vice versa. If \mathbf{a} is a vector, then we write \mathbf{a}^T for the transpose of \mathbf{a} . For example:

$$\begin{aligned}\mathbf{a} &= \begin{bmatrix} a_1 \\ a_2 \\ \dots \\ a_n \end{bmatrix} \\ \mathbf{a}^T &= \begin{bmatrix} a_1 & a_2 & \dots & a_n \end{bmatrix}\end{aligned}$$

The transpose of a matrix flips the matrix on its main diagonal (the main diagonal of a matrix contain all the elements whose indices are equal, e.g., $c_{1,1}, c_{2,2}$, and so on). To create the transpose of a matrix, take the first row of the matrix and write it as the first column; then write the second row of the matrix and write it as the second column; and so on. For example:

$$\begin{aligned}\mathbf{C} &= \begin{bmatrix} c_{1,1} & c_{1,2} & c_{1,3} & c_{1,4} \\ c_{2,1} & c_{2,2} & c_{2,3} & c_{2,4} \\ c_{3,1} & c_{3,2} & c_{3,3} & c_{3,4} \end{bmatrix} \\ \mathbf{C}^T &= \begin{bmatrix} c_{1,1} & c_{2,1} & c_{3,1} \\ c_{1,2} & c_{2,2} & c_{3,2} \\ c_{1,3} & c_{2,3} & c_{3,3} \\ c_{1,4} & c_{2,4} & c_{3,4} \end{bmatrix}\end{aligned}$$

D.3 Multiplication

In general, there is no special symbol used to denote a matrix product. Instead, we write the matrix product by writing the names of the two matrices side by side. For example, **DE** is the way we write the product for two matrices **D** and **E**, although sometimes a *dot* may be inserted between

the two matrices (\cdot is frequently used to highlight that one or both of the matrices is a vector):

$$\mathbf{DE} = \mathbf{D} \cdot \mathbf{E}$$

In order to multiply one matrix by another, the number of columns in the matrix on the left of the product must equal the number of rows in the matrix on the right. If this condition does not hold, then the product of the two matrices is not defined. For example, if \mathbf{D} is a 2×3 matrix (i.e., a matrix with 2 rows and 3 columns) and \mathbf{E} is a 3×3 matrix, then the product of these two matrices \mathbf{DE} is defined, because the number of columns in \mathbf{D} (3) equals the number of rows in \mathbf{E} (3). However, the matrix product \mathbf{ED} is not defined because the number of columns in \mathbf{E} (3) is not equal to the number of rows in \mathbf{D} (2). The product \mathbf{ED}^\top is however defined because \mathbf{D}^\top is a 3×2 matrix and the number of columns is \mathbf{E} (3) equals the number of rows in \mathbf{D}^\top (3).

The result of multiplying two matrices is another matrix whose dimensions are equal to the number of rows in the left matrix and the number of columns in the right matrix. For example, multiplying a 2×3 matrix by a 3×3 matrix results in a 2×3 . Each value in the resulting matrix is calculated as follows, where i iterates over the columns in the first matrix (\mathbf{D}) and the rows in the second matrix (\mathbf{E})

$$\mathbf{DE}_{r,c} = \sum_i \mathbf{D}[r, i] \times \mathbf{E}[i, c]$$

For example:

$$\mathbf{D} = \begin{bmatrix} d_{1,1} & d_{1,2} & d_{1,3} \\ d_{2,1} & d_{2,2} & d_{2,3} \end{bmatrix} \quad \mathbf{E} = \begin{bmatrix} e_{1,1} & e_{1,2} & e_{1,3} \\ e_{2,1} & e_{2,2} & e_{2,3} \\ e_{3,1} & e_{3,2} & e_{3,3} \end{bmatrix}$$

$$\mathbf{DE} =$$

$$\begin{bmatrix} (d_{1,1}e_{1,1}) + (d_{1,2}e_{2,1}) + (d_{1,3}e_{3,1}) & (d_{1,1}e_{1,2}) + (d_{1,2}e_{2,2}) + (d_{1,3}e_{3,2}) & (d_{1,1}e_{1,3}) + (d_{1,2}e_{2,3}) + (d_{1,3}e_{3,3}) \\ (d_{2,1}e_{1,1}) + (d_{2,2}e_{2,1}) + (d_{2,3}e_{3,1}) & (d_{2,1}e_{1,2}) + (d_{2,2}e_{2,2}) + (d_{2,3}e_{3,2}) & (d_{2,1}e_{1,3}) + (d_{2,2}e_{2,3}) + (d_{2,3}e_{3,3}) \end{bmatrix}$$

The product of two vectors of the same dimensions is known as the **dot product**. For example, given two row vectors \mathbf{F} and \mathbf{G} , both of which have

dimensions 1×3

$$\mathbf{F} = \begin{bmatrix} f_1 & f_2 & f_3 \end{bmatrix} \quad \mathbf{G} = \begin{bmatrix} g_1 & g_2 & g_3 \end{bmatrix}$$

The **dot product** of \mathbf{F} and \mathbf{G} , written $\mathbf{F} \cdot \mathbf{G}$ (and thus named) is equivalent to the matrix product \mathbf{FG}^\top

$$\mathbf{F} = \begin{bmatrix} f_1 & f_2 & f_3 \end{bmatrix} \quad \mathbf{G}^\top = \begin{bmatrix} g_1 \\ g_2 \\ g_3 \end{bmatrix}$$

$$\mathbf{F} \cdot \mathbf{G} = (f_1g_1) + (f_2g_2) + (f_3g_3)$$

Following the rules of standard matrix multiplication, the result of multiplying a 1×3 matrix by a 3×1 matrix is a 1×1 matrix (a matrix with a single value, i.e., a scalar).

Frequently, in discussing **deep learning** we use an elementwise product of two matrices, known as the **Hadamard product**. The symbol \odot denotes the Hadamard product, and the Hadamard product of two matrices \mathbf{D} and \mathbf{E} is written $\mathbf{D} \odot \mathbf{E}$. The Hadamard product assumes that both matrices have the same dimensions, and it produces a matrix with the same dimensions as the two inputs. Each value in the resulting matrix is the product of the corresponding cells in the two input matrices:

$$\mathbf{DE}_{r,c} = \mathbf{D}[r,c] \times \mathbf{E}[r,c]$$

For example

$$\mathbf{D} = \begin{bmatrix} d_{1,1} & d_{1,2} \\ d_{2,1} & d_{2,2} \end{bmatrix} \quad \mathbf{E} = \begin{bmatrix} e_{1,1} & e_{1,2} \\ e_{2,1} & e_{2,2} \end{bmatrix}$$

$$\mathbf{D} \odot \mathbf{E} = \begin{bmatrix} (d_{1,1}e_{1,1}) & (d_{1,2}e_{1,2}) \\ (d_{2,1}e_{2,1}) & (d_{2,2}e_{2,2}) \end{bmatrix}$$

D.4 Summary

Linear algebra is an important topic in machine learning. What we have presented here is a very short introduction to some of the most basic operations. This introduction is focused primarily on supporting your understanding of the content in this book, in particular the chapter on deep

learning, rather than on providing a comprehensive introduction to linear algebra. There are many excellent books on linear algebra; one of the standard textbooks on the topic is (Strang, 2016). Another relevant textbook by the same author is (Strang, 2019), which specifically focuses on introducing linear algebra from the perspective of understanding deep learning.

Bibliography

- Alimoglu, Fevzi, and Ethem Alpaydin. 1996. Methods of combining multiple classifiers based on different representations for pen-based handwritten digit recognition. In *Proceedings of the fifth Turkish artificial intelligence and artificial neural networks symposium (TAINN'96)*.
- Andoni, Alexandr, and Piotr Indyk. 2006. Near-optimal hashing algorithms for approximate nearest neighbor in high dimensions. In *Proceedings of the 47th annual IEEE symposium on foundations of computer science (FOCS'06)*, 459–468. IEEE.
- Anguita, Davide, Alessandro Ghio, Luca Oneto, Xavier Parra, and Jorge Luis Reyes-Ortiz. 2013. A public domain dataset for human activity recognition using smartphones. In *Proceedings of the 21st international European symposium on artificial neural networks, computational intelligence, and machine learning (ESANN'13)*, 437–442.
- Anscombe, Francis J. 1973. Graphs in statistical analysis. *American Statistician* 27 (1): 17–21.
- Anton, H., and C. Rorres. 2010. *Elementary linear algebra: Applications version*. Wiley. <http://books.google.ie/books?id=1PJ-WHepeBsC>.
- Ashenfelter, Orley. 2008. Predicting the quality and prices of bordeaux wine. *The Economic Journal* 118 (529): 174–184. doi:10.1111/j.1468-0297.2008.02148.x.
- Ashmore, Malcolm. 1993. The theatre of the blind: Starring a promethean prankster, a phoney phenomenon, a prism, a pocket, and a piece of wood. *Social Studies of Science* 23 (1): 67–106.
- Asimov, Isaac. 1950. *I, robot*. Gnome Press.
- Ayres, Ian. 2008. *Super crunchers: Why thinking-by-numbers is the new way to be smart*. Bantam.
- Bache, K., and M. Lichman. 2013. UCI Machine Learning Repository. <http://archive.ics.uci.edu/ml>.
- Ball, N. M., J. Loveday, M. Fukugita, O. Nakamura, S. Okamura, J. Brinkmann, and R. J. Brunner. 2004. Galaxy types in the Sloan Digital Sky Survey using supervised artificial neural networks. *Monthly Notices of the Royal Astronomical Society* 348 (3): 1038–1046. doi:10.1111/j.1365-2966.2004.07429.x. <http://mnras.oxfordjournals.org/content/348/3/1038.abstract>.
- Banerji, Manda, Ofer Lahav, Chris J. Lintott, Filipe B. Abdalla, Kevin Schawinski, Steven P. Bamford, Dan Andreescu, Phil Murray, M. Jordan Raddick, Anze Slosar, Alex Szalay, Daniel Thomas, and Jan Vandenberg. 2010. Galaxy Zoo: Reproducing galaxy morphologies via machine learning. *Monthly Notices of the Royal Astronomical Society* 406 (1): 342–353.

- Barber, David. 2012. *Bayesian reasoning and machine learning*. Cambridge University Press.
- Batista, Gustavo E. A. P. A., and Maria Carolina Monard. 2003. An analysis of four missing data treatment methods for supervised learning. *Applied Artificial Intelligence* 17 (5-6): 519–533.
- Bayes, Thomas, and Richard Price. 1763. An essay towards solving a problem in the doctrine of chances. By the late Rev. Mr. Bayes, FRS communicated by Mr. Price, in a letter to John Canton, AMFRS. *Philosophical Transactions (1683-1775)*.
- Bejar, J., U. Cortés, and M. Poch. 1991. LINNEO+: A classification methodology for ill-structured domains, Research report RT-93-10-R, Dept. Llenguatges i Sistemes Informatics, Universitat Politècnica de Catalunya.
- Bellman, R. E. 1957a. *Dynamic programming*. Princeton University Press.
- Bellman, R. E. 1957b. A markov decision process. *Journal of Mathematical Mechanics* 6: 679–684.
- Bentley, Jon Louis. 1975. Multidimensional binary search trees used for associative searching. *Communications of the ACM* 18 (9): 509–517. doi:10.1145/361002.361007.
- Berk, Richard A., and Justin Bleich. 2013. Statistical procedures for forecasting criminal behavior. *Criminology & Public Policy* 12 (3): 513–544.
- Bernstein, Peter L. 1996. *Against the gods: The remarkable story of risk*. Wiley.
- Berry, Michael J. A., and Gordon S. Linoff. 2004. *Data mining techniques: for marketing, sales, and customer relationship management*. Wiley.
- Bertin, Jacques. 2010. *Semiology of graphics: Diagrams, networks, maps*. ESRI Press.
- Bertsekas, Dimitri. 2017. *Dynamic programming and optimal control*. Athena Scientific.
- Bishop, Christopher M. 1996. *Neural networks for pattern recognition*. Oxford University Press.
- Bishop, C. M. 2006. *Pattern recognition and machine learning*. Springer.
- Blondlot, René. 1903. Sur une nouvelle action produite par les rayons n et sur plusieurs fait relatifs à ces radiations. *Comptes Rendus de l'Académie des Sciences de Paris* 137: 166–169.
- Bostrom, Nick. 2003. Ethical issues in advanced artificial intelligence. In *Science fiction and philosophy: From time travel to superintelligence*, 277–284. Wiley-Blackwell.
- Bray, Freddie, Jacques Ferlay, Isabelle Soerjomataram, Rebecca L. Siegel, Lindsey A. Torre, and Ahmedin Jemal. 2018. Global cancer statistics 2018: Globocan estimates of incidence and mortality worldwide for 36 cancers in 185 countries. *CA: A Cancer Journal for Clinicians* 68 (6): 394–424. doi:10.3322/caac.21492.
- Breiman, Leo. 1993. *Classification and regression trees*. CRC Press.
- Breiman, Leo. 1996. Bagging predictors. *Machine Learning* 24 (2): 123–140.
- Breiman, Leo. 2001. Random forests. *Machine Learning* 45 (1): 5–32.
- Brockman, Greg, Vicki Cheung, Ludwig Pettersson, Jonas Schneider, John Schulman, Jie Tang, and Wojciech Zaremba. 2016. OpenAI Gym. *arXiv:1606.01540*.
- Brown, Noam, and Tuomas Sandholm. 2017. Libratus: The superhuman AI for no-limit poker. In *Proceedings of the twenty-sixth international joint conference on artificial intelligence, IJCAI 2017, Melbourne, Australia, August 19–25, 2017*, 5226–5228. doi:10.24963/ijcai.2017/772.

- Burges, Christopher J. C. 1998. A tutorial on support vector machines for pattern recognition. *Data Mining and Knowledge Discovery* 2 (2): 121–167.
- Caruana, Rich, and Alexandru Niculescu-Mizil. 2006. An empirical comparison of supervised learning algorithms. In *Proceedings of the 23rd international conference on machine learning*, 161–168. ACM.
- Caruana, Rich, Nikos Karampatziakis, and Ainur Yessenalina. 2008. An empirical evaluation of supervised learning in high dimensions. In *Proceedings of the 25th international conference on machine learning*, 96–103. ACM.
- Casscells, Ward, Arno Schoenberger, and Thomas B. Graboys. 1978. Interpretation by physicians of clinical laboratory results. *New England Journal of Medicine* 299 (18): 999–1001.
- Chandola, Varun, Arindam Banerjee, and Vipin Kumar. 2009. Anomaly detection: A survey. *ACM computing surveys (CSUR)* 41 (3): 15.
- Chang, Winston. 2012. *R graphics cookbook: Practical recipes for visualizing data*. O'Reilly Media.
- Chapelle, Olivier, Bernhard Scholkopf, and Alexander Zien. 2009. Semi-supervised learning (Chapelle, O. et al., eds.; 2006) [book reviews]. *IEEE Transactions on Neural Networks* 20 (3): 542–542.
- Chapman, Pete, Julian Clinton, Randy Kerber, Thomas Khabaza, Thomas Reinartz, Colin Shearer, and Rudiger Wirth. 2000. CRISP-DM 1.0 Step-by-step data mining guide, Technical report, CRISP-DM consortium.
- Charniak, Eugene. 2019. *Introduction to deep learning*. MIT Press.
- Chen, Tianqi, and Carlos Guestrin. 2016. Xgboost: A scalable tree boosting system. In *Proceedings of the 22nd ACM SIGKDD international conference on knowledge discovery and data mining*, 785–794. ACM.
- Cleary, Duncan, and Revenue Irish Tax. 2011. Predictive analytics in the public sector: Using data mining to assist better target selection for audit. In *The proceedings of the 11th European conference on egovernment: Faculty of administration, University of Ljubljana, Ljubljana, Slovenia, 16–17 June 2011*, 168. Academic Conferences Limited.
- Cohen, Jacob. 1960. A coefficient of agreement for nominal scales. *Educational and Psychological Measurement* 20 (1): 34–46.
- Cooper, Gregory F., and Edward Herskovits. 1992. A Bayesian method for the induction of probabilistic networks from data. *Machine Learning* 9 (4): 309–347.
- Cover, T. M., and J. A. Thomas. 1991. *Elements of information theory*. Wiley.
- Crawford, Kate. 2017. The trouble with bias. Conference on Neural Information Processing Systems, invited speaker.
- Cristianini, Nello, and John Shawe-Taylor. 2000. *An introduction to support vector machines and other kernel-based learning methods*. Cambridge University Press.
- Cunningham, Padraig. 2009. A taxonomy of similarity mechanisms for case-based reasoning. *IEEE Transactions on Knowledge and Data Engineering* 21 (11): 1532–1543.
- Cybenko, George. 1988. Continuous valued neural networks with two hidden layers are sufficient, Technical report, Department of Computer Science, Tufts University.

- Cybenko, George. 1989. Approximation by superpositions of sigmoids. *Mathematics of Control, Signals and Systems* 2: 303–314.
- Daelemans, W., and A. van den Bosch. 2005. *Memory-based language processing. Studies in natural language processing*. Cambridge University Press.
- Dalgaard, Peter. 2008. *Introductory statistics with R*. Springer.
- Davenport, Thomas H. 2006. Competing on analytics. *Harvard Business Review* 84 (1): 98–107. <http://hbr.harvardbusiness.org/2006/01/competing-on-analytics/ar/1>.
- Davenport, Thomas H., and Jinho Kim. 2013. *Keeping up with the quants: Your guide to understanding and using analytics*. Harvard Business Press Books.
- Davies, E. R. 2005. *Machine vision: Theory, algorithms, practicalities*, 3rd ed. Elsevier.
- De Bruyne, Katrien, Bram Slabbinck, Willem Waegeman, Paul Vauterin, Bernard De Baets, and Peter Vandamme. 2011. Bacterial species identification from maldi-tof mass spectra through data analysis and machine learning. *Systematic and Applied Microbiology* 34 (1): 20–29.
- Demsar, Janez. 2006. Statistical comparisons of classifiers over multiple data sets. *Journal of Machine Learning Research* 7: 1–30.
- Dietterich, Thomas G. 2000. Ensemble methods in machine learning. In *International workshop on multiple classifier systems*, 1–15. Springer.
- Doctorow, Corey. 2010. *Little brother*. Macmillan.
- Drucker, Harris. 1997. Improving regressors using boosting techniques. In *International conference on machine learning ICML*, Vol. 97, 107–115.
- Dua, Dheeru, and Casey Graff. 2017. UCI Machine Learning Repository. <http://archive.ics.uci.edu/ml>.
- Dunn, Joseph C. 1974. Well-separated clusters and optimal fuzzy partitions. *Journal of Cybernetics* 4 (1): 95–104.
- Eco, Umberto. 1999. *Kant and the platypus*. Vintage U.K. Random House.
- Elman, Jeffrey L. 1990. Finding structure in time. *Cognitive Science* 14 (2): 179–211.
- Esposito, Floriana, Donato Malerba, and Giovanni Semeraro. 1997. A comparative analysis of methods for pruning decision trees. *IEEE Transactions on Pattern Analysis and Machine Intelligence* 19 (5): 476–491.
- Ester, Martin, Hans-Peter Kriegel, Jörg Sander, and Xiaowei Xu. 1996. A density-based algorithm for discovering clusters in large spatial databases with noise. In *Proceedings of the second international conference on knowledge discovery and data mining KDD*, Vol. 96, 226–231.
- Fanaee-T, Hadi, and Goao Gama. 2014. Event labeling combining ensemble detectors and background knowledge. *Progress in Artificial Intelligence* 2 (2-3): 113–127.
- Fawcett, Tom. 2006. An introduction to ROC analysis. *Pattern Recognition Letters* 27 (8): 861–874.
- Frank, Eibe. 2000. Pruning decision trees and lists. PhD dissertation, Department of Computer Science, University of Waikato.
- Franklin, Janet. 2009. *Mapping species distributions: Spatial inference and prediction (ecology, biodiversity and conservation)*. Cambridge University Press.

- Franklin, Janet, Paul McCullough, and Curtis Gray. 2000. Terrain variables used for predictive mapping of vegetation communities in Southern California. In *Terrain analysis: Principles and applications*, eds. John P. Wilson and John C. Gallant. Wiley.
- Freund, Yoav, and Robert E. Schapire. 1995. A desicion-theoretic generalization of on-line learning and an application to boosting. In *Computational Learning Theory*, 23–37. Springer.
- Friedman, J., J. Bently, and R. Finkel. 1977. An algorithm for finding the best matches in logarithmic expected time. *ACM Transactions on Mathematical Software* 3 (3): 209–226.
- Friedman, J., T. Hastie, and R. Tibshirani. 2001. *The elements of statistical learning*, Vol. 1. Springer.
- Friedman, Jerome, Trevor Hastie, and Robert Tibshirani. 2000. Additive logistic regression: A statistical view of boosting. *The Annals of Statistics* 28 (2): 337–407.
- Friedman, Jerome H. 2001. Greedy function approximation: A gradient boosting machine. *Annals of Statistics* 21 (5): 1189–1232.
- Fry, Ben. 2007. *Visualizing data: Exploring and explaining data with the processing environment*. O'Reilly Media.
- Gädenfors, Peter. 2004. *Conceptual spaces: The geometry of thought*. MIT Press.
- Gal, Yarin, and Zoubin Ghahramani. 2016. A theoretically grounded application of dropout in recurrent neural networks. In *Advances in neural information processing systems 29: Annual conference on neural information processing systems 2016, December 5–10, 2016, Barcelona, Spain*, 1019–1027.
- Gleick, James. 2011. *The information: A history, a theory, a flood*. HarperCollins UK.
- Glorot, Xavier, and Yoshua Bengio. 2010. Understanding the difficulty of training deep feedforward neural networks. In *Proceedings of the thirteenth international conference on artificial intelligence and statistics (AISTATS)*, 249–256. JMLR.
- Glorot, Xavier, Antoine Bordes, and Yoshua Bengio. 2011. Deep sparse rectifier neural networks. In *Proceedings of the fourteenth international conference on artificial intelligence and statistics (AISTATS)*, 315–323. JMLR.
- Goldberg, Yoav. 2017. *Neural network methods for natural language processing. Synthesis lectures on human language technology*. Morgan and Claypool.
- Goodfellow, Ian, Yoshua Bengio, and Aaron Courville. 2016. *Deep learning*. MIT Press.
- Goodfellow, Ian, Jean Pouget-Abadie, Mehdi Mirza, Bing Xu, David Warde-Farley, Sherjil Ozair, Aaron Courville, and Yoshua Bengio. 2014. Generative adversarial nets. In *Advances in neural information processing systems 27: Annual conference on neural information processing systems 2014, December 8–13, 2014, Montreal, Quebec, Canada*, 2672–2680.
- Gross, Philip, Albert Boulanger, Marta Arias, David L. Waltz, Philip M. Long, Charles Lawson, Roger Anderson, Matthew Koenig, Mark Mastrocinque, William Fairechio, et al.. 2006. Predicting electricity distribution feeder failures using machine learning susceptibility analysis. In *Proceedings of the twenty-first national conference on artificial intelligence (AAAI'06)*, 1705–1711. AAAI Press.
- Guisan, Antoine, and Niklaus E. Zimmermann. 2000. Predictive habitat distribution models in ecology. *Ecological Modelling* 135 (2): 147–186.

- Guo, Yanming, Yu Liu, Ard Oerlemans, Songyang Lao, Song Wu, and Michael S. Lew. 2016. Deep learning for visual understanding: A review. *Neurocomputing* 187: 27–48.
- Gwiazda, J., E. Ong, R. Held, and F. Thorn. 2000. Vision: Myopia and ambient night-time lighting. *Nature* 404 (6774): 144–144. <http://dx.doi.org/10.1038/35004663>.
- Han, Jiawei, Jian Pei, and Micheline Kamber. 2011. *Data mining: concepts and techniques*. Elsevier.
- Hand, David J., and Christoforos Anagnostopoulos. 2013. When is the area under the receiver operating characteristic curve an appropriate measure of classifier performance? *Pattern Recognition Letters* 34 (5): 492–495.
- Hart, P. 1968. The condensed nearest neighbor rule. *IEEE Transactions on Information Theory* 14 (3): 515–516.
- Hastie, T., R. Tibshirani, and J. Friedman. 2001. *The elements of statistical learning*. Springer.
- Hastie, T., R. Tibshirani, and J. Friedman. 2009. *The elements of statistical learning*. Springer.
- He, Kaiming, Xiangyu Zhang, Shaoqing Ren, and Jian Sun. 2015. Delving deep into rectifiers: Surpassing human-level performance on imagenet classification. In *Proceedings of the IEEE international conference on computer vision*, 1026–1034.
- Hebb, Donald O. 1949. *The organization of behavior; A neuropsychological theory*. Wiley.
- Hecht-Nielsen, Robert. 1987. Kolmogorov's mapping neural network existence theorem. In *Proceedings of the IEEE first international conference on neural networks*, Vol. 3, 11–13.
- Herculano-Houzel, Suzana. 2009. The human brain in numbers: A linearly scaled-up primate brain. *Frontiers in Human Neuroscience* 3: 31. doi:10.3389/neuro.09.031.2009.
- Hinton, G. E. 2005. What kind of graphical model is the brain? In *Proceedings of the 19th international joint conference on artificial intelligence (IJCAI-05)*. IJCAI.
- Hinton, G. E., S. Osindero, and Y. W. Teh. 2006. A fast learning algorithm for deep belief nets. *Neural Computing* 18: 1527–1554.
- Hirschowitz, Anton. 2001. Closing the CRM loop: The 21st century marketer's challenge: Transforming customer insight into customer value. *Journal of Targeting, Measurement and Analysis for Marketing* 10 (2): 168–178.
- Hochreiter, Sepp, and Jürgen Schmidhuber. 1997. Long short-term memory. *Neural Computation* 9 (8): 1735–1780.
- Hornik, Kur, Maxwell Stinchcombe, and Halber White. 1989. Multilayer feedforward networks are universal approximators. *Neural Networks* 2: 359–366.
- Howard, R. 1960. *Dynamic programming and Markov processes*. MIT Press.
- Hubble, E. 1936. *The realm of the nebulae*. Yale University Press.
- Hubel, D. H., and T. N. Wiesel. 1962. Receptive fields, binocular interation and functional architecture in the cat's visual cortex. *Journal of Physiology* 160: 106–154.
- Hunter, Elizabeth, Brian Mac Namee, and John Kelleher. 2018. An open-data-driven agent-based model to simulate infectious disease outbreaks. *PloS One* 13 (12): 0208775.
- Ioffe, Sergey, and Christian Szegedy. 2015. Batch normalization: Accelerating deep network training by reducing internal covariate shift. In *Proceedings of the thirty-second international conference on*

- machine learning*, 448–456. JMLR.
- Japkowicz, Nathalie, and Mohak Shah. 2011. *Evaluating learning algorithms: A classification perspective*. Cambridge University Press.
- Jaynes, Edwin T. 2003. *Probability theory: The logic of science*. Cambridge University Press.
- Jurafsky, Daniel, and James H. Martin. 2008. *Speech and language processing: An introduction to natural language processing, computational linguistics, and speech recognition*, 2nd ed. Prentice Hall.
- Kansagara, Devan, Honora Englander, Amanda Salanitro, David Kagen, Cecelia Theobald, Michele Freeman, and Sunil Kripalani. 2011. Risk prediction models for hospital readmission: A systematic review. *JAMA* 306 (15): 1688–1698.
- Kaufman, Leonard, and Peter J. Rousseeuw. 1990. *Finding groups in data: An introduction to cluster analysis*. Wiley.
- Kelleher, John D. 2016. Fundamentals of machine learning for neural machine translation. In *Translating europe forum 2016: Focus on translation technologies*. European Commission Directorate-General for Translation.
- Kelleher, John D. 2019. *Deep learning*. Essential Knowledge Series. MIT Press.
- Kelleher, John D., and Simon Dobnik. 2017. What is not where: The challenge of integrating spatial representations into deep learning architectures. In *Proceedings of the conference on logic and machine learning in natural language (LaML 17)*. Vol. 1 of *Clasp papers in computational linguistics*, 41–52.
- Keri, Jonah. 2007. *Baseball between the numbers: Why everything you know about the game is wrong*. Basic Books.
- Kingma, Diederik P., and Jimmy Ba. 2014. Adam: A method for stochastic optimization. *arXiv preprint arXiv:1412.6980*.
- Klotz, Irving M. 1980. The n-ray affair. *Scientific American* 242 (5): 122–131.
- Klubička, Filip, Giancarlo D. Salton, and John D. Kelleher. 2018. Is it worth it? Budget-related evaluation metrics for model selection. In *Proceedings of the eleventh international conference on language resources and evaluation (LREC 2018)*.
- Kohavi, Ron. 1996. Scaling up the accuracy of Naive-Bayes classifiers: A decision-tree hybrid. In *Proceedings of the twenty-fifth ACM SIGKDD international conference on knowledge discovery and data mining KDD*, 202–207.
- Kollar, Daphne, and Nir Friedman. 2009. *Probabilistic graphical models: Principles and techniques*. MIT Press.
- Kolmogorov, Andrei Nikolaevich. 1963. On the representation of continuous functions of several variables by superpositions of continuous functions of one variable and addition. *American Mathematical Society Translations*.
- Krizhevsky, A., I. Sutskever, and G. E. Hinton. 2012. Imagenet classification with deep convolutional neural networks. In *Advances in neural information processing systems*, 1097–1105.
- Kuncheva, Ludmila I. 2004. *Combining pattern classifiers: Methods and algorithms*. Wiley.

- Kutner, Michael, Christopher Nachtsheim, John Neter, and William Li. 2004. *Applied linear statistical models*. McGraw-Hill.
- Le Cun, Yann, Léon Bottou, Yoshua Bengio, and Haffner Patrick. 1998. Gradient-based learning applied to document recognition. *Proceedings of the IEEE* 86 (11): 2278–2324.
- Lehmann, Thomas Martin, Mark Oliver Güld, Daniel Keysers, Henning Schubert, Michael Kohnen, and Berthold B. Wein. 2003. Determining the view of chest radiographs. *Journal of Digital Imaging* 16 (3): 280–291.
- Leshno, Moshe, Vladimir Ya Lin, Allan Pinkus, and Shimon Schocken. 1993. Multilayer feedforward networks with a nonpolynomial activation function can approximate any function. *Neural Networks* 6: 861–867.
- Levitt, Steven D., and Stephen J. Dubner. 2005. *Freakonomics: A rogue economist explores the hidden side of everything*. Penguin.
- Lewis, Michael. 2004. *Moneyball: The art of winning an unfair game*. Norton.
- Li, Deren, Shuliang Wang, and Deyi Li. 2015. *Spatial data mining*. Springer.
- Lintott, C. J., K. Schawinski, A. Slosar, K. Land, S. Bamford, D. Thomas, M. J. Raddick, R. C. Nichol, A. Szalay, D. Andreescu, P. Murray, and J. Vandenberg. 2008. Galaxy Zoo: Morphologies derived from visual inspection of galaxies from the Sloan Digital Sky Survey. *Monthly Notices of the Royal Astronomical Society* 389: 1179–1189. doi:10.1111/j.1365-2966.2008.13689.x.
- Lintott, C., K. Schawinski, S. Bamford, A. Slosar, K. Land, D. Thomas, E. Edmondson, K. Masters, R. C. Nichol, M. J. Raddick, A. Szalay, D. Andreescu, P. Murray, and J. Vandenberg. 2011. Galaxy Zoo 1: Data release of morphological classifications for nearly 900 000 galaxies. *Monthly Notices of the Royal Astronomical Society* 410: 166–178. doi:10.1111/j.1365-2966.2010.17432.x.
- Loh, Wei-Yin. 2011. Classification and regression trees. *Wiley Interdisciplinary Reviews: Data Mining and Knowledge Discovery* 1 (1): 14–23.
- Maas, Andrew L., Awni Y. Hannun, and Andrew Y. Ng. 2013. Rectifier nonlinearities improve neural network acoustic models. In *Proceedings of thirtieth international conference on machine learning (ICML 13)*, Vol. 30. JMLR.
- Mac Namee, B., P. Cunningham, S. Byrne, and O. I. Corrigan. 2002. The problem of bias in training data in regression problems in medical decision support. *Artificial Intelligence in Medicine* 24 (1): 51–70.
- Mac Namee, Brian. 2009. Agent based modeling in computer graphics and games. In *Encyclopedia of complexity and systems science*, ed. R. A. Meyers. Dublin Institute of Technology.
- MacKay, David J. C. 2003. *Information theory, inference and learning algorithms*. Cambridge University Press.
- Mahalunkar, Abhijit, and John D Kelleher. 2018. Using regular languages to explore the representational capacity of recurrent neural architectures. In *International conference on artificial neural networks*, 189–198. Springer.
- Makhoul, John, Amro El-Jaroudi, and Richard Schwartz. 1989. Formation of disconnected decision regions with a single hidden layer. In *Proceedings of the international joint conference on neural networks*, Vol. 1, 455–460. IEEE.

- Mangasarian, Olvi L., and William H. Wolberg. 1990. Cancer diagnosis via linear programming. *SIAM News* 23 (5): 1–18.
- Marsland, Stephen. 2011. *Machine learning: An algorithmic perspective*. CRC Press.
- McCandlish, Sam, Jared Kaplan, Dario Amodei, and OpenAI Dota Team. 2018. An empirical model of large-batch training. *CoRR* abs/1812.06162. <http://arxiv.org/abs/1812.06162>.
- McCulloch, Warren S., and Walter Pitts. 1943. A logical calculus of the ideas immanent in the nervous system. *Bulletin of Mathematical Biophysics* 5: 115–133.
- McGrayne, Sharon Bertsch. 2011. *The theory that would not die: How Bayes' rule cracked the enigma code, hunted down Russian submarines, and emerged triumphant from two centuries of controversy*. Yale University Press.
- Michie, D. 1961. Trial and error. In *Science survey, part 2*, eds. S. A. Barnett and A. McLaren, 129–145. Penguin.
- Michie, D. 1963. Experiments on the mechanisation of game learning. *Computer Journal* 1: 232–263.
- Mingers, John. 1987. Expert systems - rule induction with statistical data. *Journal of the Operational Research Society* 38: 39–47.
- Mingers, John. 1989. An empirical comparison of selection measures for decision-tree induction. *Machine Learning* 3 (4): 319–342.
- Minsky, Marvin, and Seymour Papert. 1969. *Perceptrons*. MIT Press.
- Mishne, Gilad, and Natalie S. Glance. 2006. Predicting movie sales from blogger sentiment. In *AAAI spring symposium: Computational approaches to analyzing weblogs*, 155–158.
- Mitchell, T. 1997. *Machine learning*. McGraw Hill.
- Mitchell, Tom M., Svetlana V. Shinkareva, Andrew Carlson, Kai-Min Chang, Vicente L. Malave, Robert A. Mason, and Marcel A. Just. 2008. Predicting human brain activity associated with the meanings of nouns. *Science* 320 (5880): 1191–1195. doi:10.1126/science.1152876.
- Mnih, Volodymyr, Koray Kavukcuoglu, David Silver, Alex Graves, Ioannis Antonoglou, Daan Wierstra, and Martin Riedmiller. 2013. Playing atari with deep reinforcement learning. *arXiv preprint arXiv:1312.5602*.
- Montgomery, Douglas C. 2004. *Introduction to statistical quality control*. Wiley.
- Montgomery, Douglas C. 2012. *Design and analysis of experiments*. Wiley.
- Montgomery, Douglas C., and George C. Runger. 2010. *Applied statistics and probability for engineers*. Wiley.
- Montúfar, Guido. 2014. Universal approximation depth and errors of narrow belief networks with discrete units. *Neural Computation* 26 (7): 1386–1407.
- Moon, Todd K. 1996. The expectation-maximization algorithm. *IEEE Signal Processing Magazine* 13 (6): 47–60.
- Murphy, Kevin P. 2012. *Machine learning: A probabilistic perspective*. MIT Press.
- Neapolitan, Richard E. 2004. *Learning Bayesian networks*. Pearson Prentice Hall.

- Ng, Andrew Y., Michael I. Jordan, and Yair Weiss. 2002. On spectral clustering: Analysis and an algorithm. In *Advances in neural information processing systems*, 849–856.
- OECD. 2013. *The OECD privacy framework*. Organisation for Economic Co-operation and Development.
- Osowski, Stainslaw, Linh Tran Hoai, and T. Markiewicz. 2004. Support vector machine-based expert system for reliable heartbeat recognition. *IEEE Transactions on Biomedical Engineering* 51 (4): 582–589. doi:10.1109/TBME.2004.824138.
- Palaniappan, Sellappan, and Rafiah Awang. 2008. Intelligent heart disease prediction system using data mining techniques. *International Journal of Computer Science and Network Security* 8 (8): 343–350.
- Pearl, Judea. 1988. *Probabilistic reasoning in intelligent systems: Networks of plausible inference*. Morgan Kaufmann.
- Pearl, Judea. 2000. *Causality: Models, reasoning and inference*, Vol. 29. Cambridge University Press.
- Quinlan, J. Ross. 1986. Induction of decision trees. *Machine Learning* 1 (1): 81–106.
- Quinlan, J. Ross. 1987. Simplifying decision trees. *International Journal of Man-Machine Studies* 27 (3): 221–234.
- Quinlan, J. Ross. 1993. *C4.5: Programs for machine learning*. Morgan Kaufmann.
- Quinn, Graham E., Chai H. Shin, Maureen G. Maguire, and Richard A. Stone. 1999. Myopia and ambient lighting at night. *Nature* 399 (6732): 113–114. <http://dx.doi.org/10.1038/20094>.
- Reagen, Brandon, Robert Adolf, Paul Whatmough, Gu-Yeon Wei, and David Brooks. 2017. *Deep learning for computer architects*. Morgan and Claypool.
- Reed, Russell D., and Robert J. Marks. 1999. *Neural smithing: Supervised learning in feedforward artificial networks*. MIT Press.
- Rice, John A. 2006. *Mathematical statistics and data analysis*. Cengage Learning.
- Richter, Michael M., and Rosina O. Weber. 2013. *Case-based reasoning: A textbook*. Springer.
- Rosenblatt, Frank. 1958. The perceptron: A probabilistic model for information storage and organization in the brain. *Psychological Review* 65 (6): 386–408.
- Rousseeuw, Peter J. 1987. Silhouettes: A graphical aid to the interpretation and validation of cluster analysis. *Journal of computational and applied mathematics* 20: 53–65.
- Rubin, Daniel J. 2015. Hospital readmission of patients with diabetes. *Current Diabetes Reports* 15 (4): 17.
- Samet, Hanan. 1990. *The design and analysis of spatial data structures*, Vol. 199. Addison-Wesley.
- Sarle, Warren S. 1983. Cubic clustering criterion, Technical Report SAS Technical Report A-108, SAS Institute.
- Scarne, John. 1986. *Scarne's new complete guide to gambling*. Simon & Schuster.
- Schapire, Robert E. 1990. The strength of weak learnability. *Machine Learning* 5 (2): 197–227.

- Schapire, Robert E. 1999. A brief introduction to boosting. In *Proceedings of the sixteenth international joint conference on artificial intelligence (IJCAI-99)*, Vol. 2, 1401–1406.
- Schwartz, Paul M. 2010. Data protection law and the ethical use of analytics, Technical report, The Centre for Information Policy Leadership (at Hunton & Williams LLP).
- Scrucca, Luca, Michael Fop, T. Brendan Murphy, and Adrian E. Raftery. 2016. Mclust 5: Clustering, classification and density estimation using gaussian finite mixture models. *The R Journal* 8 (1): 289.
- Segata, N., E. Blanzieri, S. J. Delany, and Padraig Cunningham. 2009. Noise reduction for instance-based learning with a local maximal margin approach. *Journal of Intelligent Information Systems* 35: 301–331.
- Sejnowski, Terrence J. 2018. *The deep learning revolution*. MIT Press.
- Shannon, Claude E., and Warren Weaver. 1949. *The mathematical theory of communication*. University of Illinois Press.
- Siddiqi, Naeem. 2005. *Credit risk scorecards: Developing and implementing intelligent credit scoring*. Wiley.
- Siegel, Eric. 2013. *Predictive analytics: The power to predict who will click, buy, lie, or die*, 1st ed. Wiley.
- Silver, David, Aja Huang, Chris J. Maddison, Arthur Guez, Laurent Sifre, George van den Driessche, Julian Schrittwieser, Ioannis Antonoglou, Vedavyas Panneershelvam, Marc Lanctot, Sander Dieleman, Dominik Grewe, John Nham, Nal Kalchbrenner, Ilya Sutskever, Timothy P. Lillicrap, Madeleine Leach, Koray Kavukcuoglu, Thore Graepel, and Demis Hassabis. 2017. Mastering the game of go without human knowledge. *Nature* 550 (7676): 354.
- Silver, David, Thomas Hubert, Julian Schrittwieser, Ioannis Antonoglou, Matthew Lai, Arthur Guez, Marc Lanctot, Laurent Sifre, Dharshan Kumaran, Thore Graepel, Timothy Lillicrap, Karen Simonyan, and Demis Hassabis. 2018. A general reinforcement learning algorithm that masters chess, shogi, and go through self-play. *Science* 362 (6419): 1140–1144. doi:10.1126/science.aar6404.
- Silver, Nate. 2012. *The signal and the noise: Why so many predictions fail — but some don't*. Penguin Press.
- Sing, Tobias, Oliver Sander, Niko Beerenwinkel, and Thomas Lengauer. 2005. ROC: Visualizing classifier performance in R. *Bioinformatics* 21 (20): 3940–3941.
- Smyth, B., and M. Keane. 1995. Remembering to forget: A competence preserving case deletion policy for case-based reasoning systems. In *The fourteenth international joint conference on artificial intelligence (IJCAI-95)*, ed. C. Mellish, 337–382. ACM.
- Spercher, David A. 1965. On the structure of continuous functions of several variables. *Transactions of the American Mathematical Society* 115 (3): 340–355.
- Srivastava, Nitish, Geoffrey Hinton, Alex Krizhevsky, Ilya Sutskever, and Ruslan Salakhutdinov. 2014. Dropout: A simple way to prevent neural networks from overfitting. *Journal of Machine Learning Research* 15 (1): 1929–1958.
- Stewart, James. 2012. *Calculus*, 7th ed. Cengage Learning.
- Stoughton, Chris, Robert H. Lupton, Mariangela Bernardi, Michael R. Blanton, Scott Burles, Francisco J. Castander, A. J. Connolly, Daniel J. Eisenstein, Joshua A. Frieman, G. S. Hennessy, et

- al.. 2002. Sloan digital sky survey: Early data release. *The Astronomical Journal* 123 (1): 485. <http://stacks.iop.org/1538-3881/123/i=1/a=485>.
- Strang, Gilbert. 2016. *Introduction to linear algebra*, 5th ed. Wellesley-Cambridge Press.
- Strang, Gilbert. 2019. *Linear algebra and learning from data*. Wellesley-Cambridge Press.
- Sutton, Richard S., and Andrew G. Barto. 1998. *Reinforcement learning: An introduction*. MIT Press.
- Sutton, Richard S., and Andrew G. Barto. 2018. *Reinforcement learning: An introduction*. MIT Press.
- Svolba, Gerhard. 2007. *Data preparation for analytics using SAS*. SAS Institute.
- Svolba, Gerhard. 2012. *Data quality for analytics using SAS*. SAS Institute.
- Taleb, Nassim Nicholas. 2008. *The black swan: The impact of the highly improbable*. Penguin.
- Tempel, E., E. Saar, L. J. Liivamägi, A. Tamm, J. Einasto, M. Einasto, and V. Müller. 2011. Galaxy morphology, luminosity, and environment in the SDSS DR7. *A&A* 529: 53. doi:10.1051/0004-6361/201016196.
- Tene, Omer, and Jules Polonetsky. 2013. Big data for all: Privacy and user control in the age of analytics. *Northwestern Journal of Technology and Intellectual Property* 11 (5): 239–247.
- Tesauro, Gerald. 1994. TD-gammon, a self-teaching backgammon program, achieves master-level play. *Neural Computation* 6 (2): 215–219.
- Tijms, Henk. 2012. *Understanding probability*. Cambridge University Press.
- Trask, Andrew. 2019. *Grokking deep learning*. Manning.
- Tsanas, Athanasios, and Angeliki Xifara. 2012. Accurate quantitative estimation of energy performance of residential buildings using statistical machine learning tools. *Energy and Buildings* 49: 560–567.
- Tsoumacas, Grigorios, Min-Ling Zhang, and Zhi-Hua Zhou. 2012. Introduction to the special issue on learning from multi-label data. *Machine Learning* 88 (1-2): 1–4.
- Tüfekci, Pinar. 2014. Prediction of full load electrical power output of a base load operated combined cycle power plant using machine learning methods. *International Journal of Electrical Power & Energy Systems* 60: 126–140.
- Tufte, Edward R. 2001. *The visual display of quantitative information*. Graphics Press.
- Tukey, John W. 1977. *Exploratory data analysis*. Addison-Wesley.
- Vapnik, Vladimir. 2000. *The nature of statistical learning theory*. Springer.
- Vaswani, Ashish, Noam Shazeer, Niki Parmar, Jakob Uszkoreit, Llion Jones, Aidan N. Gomez, Łukasz Kaiser, and Illia Polosukhin. 2017. Attention is all you need. In *Advances in neural information processing systems*, 5998–6008.
- Widdows, Dominic. 2004. *Geometry and meaning*. CSLI Publications.
- Wirth, Rüdiger, and Jochen Hipp. 2000. CRISP-DM: Towards a standard process model for data mining. In *Proceedings of the 4th international conference on the practical applications of knowledge discovery and data mining*, 29–39. Citeseer.
- Wolpert David, H. 1996. The lack of a priori distinctions between learning algorithms. *Neural Computation* 8 (7): 1341–1390.

- Wood, Robert W. 1904. The n-rays. *Nature* 70: 530–531.
- Wooldridge, Michael. 2009. *An introduction to multiagent systems*. Wiley.
- Wooldridge, Michael, and Nicholas R. Jennings. 1995. Intelligent agents: Theory and practice. *The Knowledge Engineering Review* 10 (2): 115–152.
- Woolery, L., J. Grzymala-Busse, S. Summers, and A. Budihardjo. 1991. The use of machine learning program LERS-LB 2.5 in knowledge acquisition for expert system development in nursing. *Computers in Nursing* 9: 227–234.
- Zadnik, Karla, Lisa A. Jones, Brett C. Irvin, Robert N. Kleinstein, Ruth E. Manny, Julie A. Shin, and Donald O. Mutti. 2000. Vision: Myopia and ambient night-time lighting. *Nature* 404 (6774): 143–144. <http://dx.doi.org/10.1038/35004661>.
- Zhang, Nevin Lianwen, and David Poole. 1994. A simple approach to bayesian network computations. In *Proceedings of the tenth biennial Canadian artificial intelligence conference*, 171–178.
- Zhou, Zhi-Hua. 2012. *Ensemble methods: Foundations and algorithms*. CRC Press.

Index

68–95–99.7 rule, 62, 71
*, xx
 χ^2 pruning, 155
 χ^2 statistic, 583
 ϵ -greedy action selection policy, 656, 658, 674
 ϵ_0 bootstrap, 546

absence-presence, 214
absolute rarity, 720
ABT, 17
action, 643, 676
action-value behavior network, 672
action-value function, 642, 643, 651, 676
action-value table, 654
action-value target network, 672
activation function, 386
AdaBoost, 171
Adaboost.R2, 161
Adam, 523
additive models, 165
affine function, 385
agent, 639
agglomerative hierarchical clustering, 618, 618, 629, 635
aggregate features, 35
AHC, 618
AlphaGo, 677
AlphaZero, 677
analytics base table, 17, 23, 28, 28, 45, 49, 50, 52, 53, 94, 97, 600, 625, 688
analytics solution, 23, 24
ANOVA test, 86, 95
Anscombe's quartet, 84
anti-discrimination legislation, 40
approximate methods, 668, 676

area under the curve, 561, 590
arithmetic mean, 550, 551, 577, 591, 745, 745
artificial intelligence, 304, 677
artificial neural network, 369
artificial neuron, 383
astronomy, 703
AUC, 561
augment data, 599, 629
auto-encoder, 624, 624, 629, 733
average class accuracy, 550, 551, 554, 577, 586, 591, 698
average linkage, 619, 635

backpropagation of error, 387, 403, 404, 624, 731
backpropagation through time, 502, 518
backward sequential selection, 229
bag-of-words, 223, 236
bagging, 159, 159, 171, 179, 733, 735
balanced sample, 693
bar plot, 54, 745, 752
basis functions, 351, 365, 368
batch, 327, 417
batch gradient descent, 327, 416, 417
batch learning, 417
batch normalization, 523
batch size, 417
batches, 391, 417
Bayes' Theorem, 243, 245, 248, 731
Bayes, Thomas, 248
Bayesian information criterion, 292
Bayesian MAP prediction model, 254
Bayesian network, 243, 265, 285, 304, 732, 733, 735
Bayesian optimal classifier, 254
Bayesian score, 293
behavior policy, 657, 659, 664
Bellman Equations, 653
Bellman optimality equation, 653
bias, 91, 385, 751
bias term, 480, 493
BIC, 292
Bienaymé formula, 455
bimodal distribution, 60
binary data, 34
binary logarithm, 124
binary tree, 196
binning, 89, 102, 146, 280
binomial distribution, 178
bins, 89
bits, 126

black box model, 739
Blackjack, 645
blame assignment, 404, 405, 413
Blondlot, René, 533
Boltzmann action selection, 658
boosting, 159, 159, 171, 178, 179, 733, 735
bootstrap aggregating, 159
bootstrap samples, 159
bootstrapping, 546, 655, 662, 676
bottleneck layer, 624, 628
box plot, 54, 451, 745, 752, 755
branches, 121
breast cancer, 109
brute-force search, 318
burn-in time, 300
business problem, 23
Business Understanding, 16, 19, 24, 28, 46, 685, 704, 730

C4.5, 169
calculus, 765
capacity for model retraining, 739
Cardano, Gerolamo, 243
cardinality, 54, 54, 693
CART, 169
case-based reasoning, 234
categorical cross entropy, 378
categorical data, 34
causal graphs, 293
CBR, 234
cell, 508
central tendency, 54, 550, 745
centroid linkage, 619
chain rule (differentiation), 312, 325, 345, 381, 410, 413, 435, 731, 765, 768
chain rule (probability), 245, 251, 257, 291, 757, 763, 768
channel, 492
Chebyshev distance, 186
chessboard distance, 186
child node, 286
churn prediction, 584, 685
citizen science, 708
clamp transformation, 70, 715
classes, 551
classification accuracy, 539, 545, 550
cluster centroids, 600
clustering, 597, 599, 603, 629
clustering evaluation internal criterion, 608
clusters, 599
CNN, 477

co-absence, 212, 213
co-presence, 212, 213
Cohen's kappa, 726
collection limitation principle, 41
comparative experiments, 583
complete case analysis, 69, 712
complete linkage, 619
component, 274
composite function, 768
composition, 401
concept drift, 232, 578, 579, 657, 727
condensed nearest neighbor, 233
conditional independence, 256, 256, 261, 302
conditional maximum entropy model, 357
conditional probability, 245, 246, 251, 757, 759, 759, 762
conditional probability table, 286
conditionally independent, 285, 288
confidence factor, 161, 178
confounding feature, 85
confusion matrix, 537, 553, 572, 591
connectionism, 382
consistent model, 6, 7, 121, 141
constrained quadratic optimization problem, 363
constraints, 363
continuous data, 34
continuous function, 766
control group, 583
convergence, 323
convergence criterion, 418
convex surface, 318
convolutional auto-encoders, 630
convolutional neural network, 434, 477, 485, 673, 674
convolving a function, 485
coordinate system, 183
correlation, 81, 82, 94, 103, 223
correlation matrix, 83
Corruption Perception Index, 237, 294
cosine, 216
cosine similarity, 216, 223, 231, 237
cost function, 409
covariance, 81, 218
covariance matrix, 83, 219
CPI, 294
CPT, 286
credit scoring, 538, 553, 563
CRISP-DM, 16
critical value pruning, 155
CRM, 572

Cross Industry Standard Process for Data Mining, [16](#), [22](#), [28](#), [46](#), [53](#), [94](#), [534](#), [600](#), [730](#)
cross-correlation, [485](#)
cross-entropy, [434](#), [463](#), [465](#)
cross-sell model, [572](#)
crowdsourcing, [708](#)
cubic clustering criterion, [609](#)
cubic function, [766](#)
cumulative gain, [567](#), [567](#), [594](#), [700](#)
cumulative gain chart, [569](#), [570](#), [592](#)
cumulative lift, [567](#), [570](#), [700](#)
cumulative lift chart, [570](#)
cumulative lift curve, [570](#)
cumulative reward, [640](#), [643](#), [676](#)
curse of dimensionality, [225](#), [232](#), [255](#), [262](#), [740](#), [762](#)
customer churn, [48](#)
customer relationship management, [572](#)
customer segmentation, [599](#)
cut a hierarchical agglomeration, [622](#)

d-separation, [289](#)
data, [3](#)
data analytics, [3](#)
data availability, [33](#)
data exploration, [34](#), [53](#), [94](#)
data fragmentation, [255](#), [262](#)
data management tools, [42](#)
data manipulation, [42](#)
data manipulation tools, [42](#)
data mining, [16](#)
Data Preparation, [17](#), [19](#), [28](#), [46](#), [53](#), [87](#), [94](#), [95](#), [535](#), [691](#), [713](#), [730](#)
data preprocessing, [421](#)
data protection legislation, [40](#)
data quality issues, [53](#), [63](#), [94](#)
data quality plan, [64](#), [94](#)
data quality report, [53](#), [54](#), [94](#), [98](#), [105](#), [110](#), [614](#), [693](#), [710](#)
data subject, [40](#)
Data Understanding, [17](#), [19](#), [28](#), [46](#), [53](#), [94](#), [688](#), [707](#), [730](#)
data visualization, [99](#), [752](#)
data-driven decisions, [19](#)
database management systems, [42](#)
dataset, [5](#), [758](#)
DBScan, [630](#)
de Fermat, Pierre, [243](#)
de-noising auto-encoders, [630](#)
deciles, [567](#), [582](#)
decision boundary, [189](#), [338](#), [359](#), [396](#), [736](#)
decision stumps, [165](#)
decision surface, [341](#)

decision tree, 117, 121, 121, 169, 541, 554, 556, 732, 733, 735, 736
decisions, 3
decoder, 624
deep learning, xvi, 19, 381, 396, 599, 624, 629, 637, 676, 773
deep Q learning, 677
deep Q network, 637, 664, 671, 673, 676
degrees of freedom, 272
delta value, 323
dendrogram, 622
density, 752, 753
density curve, 61
density histogram, 753
Deployment, 17, 20, 702, 727, 730
depth of a filter, 492
depth of a neural network, 389
derivative, 765
derived features, 34, 41, 45
descriptive features, 5, 19, 23, 28, 598, 688
diabetes, 51
diagnosis, 4
differentiation, 370, 765
directed acyclic graph, 499
directed cyclic graph, 499
discontinuous function, 341
discount rate, 642
discounted return, 642
discriminative model, 733
disease diagnosis, 538
distance matrix, 620, 621
distance measure, 599, 601, 618
distance metric, 184, 231
distance weighted k nearest neighbor, 194
distributions, 102
document classification, 4, 223
domain, 34, 757
domain concept, 23, 30, 45, 688, 689, 707
domain representation, 732
domain subconcept, 32
dosage prediction, 3
dot product, 216, 320, 342, 385, 773
DQN, 664
DropMask, 530
dropout, 434, 472, 473, 507
Dunn index, 609
dying ReLU, 444
dynamic programming, 653, 677
eager learner, 232

early stopping, 418, 432, 434, 472, 472, 477
early stopping criteria, 152, 155
ecological modeling, 135
edges, 286
EEG, 353
electroencephalography pattern recognition, 353
eligibility traces, 655
email classification, 536
embedding, 624, 626
encoder, 624
enrich data, 599, 629
ensemble, 117
entropy, 43, 117, 120, 125, 149, 172, 173, 611, 731
environment, 643, 676
episode, 639
epoch, 416, 418
equal-frequency binning, 89, 91, 102, 280, 294, 307
equal-width binning, 89, 90, 102, 280
equation of a line, 313, 385
equivariant, 483
ergodic Markov chain, 299
error function, 312, 315, 315, 367, 409
error rate, 155
error surface, 311, 317
error-based learning, 19, 311, 599
ethics, 47
ETL, 42
Euclidean coordinate space, 185
Euclidean distance, 185, 200, 231, 237, 577, 601, 602, 620, 631, 632, 636, 731
Euclidean norm, 364
Euler's number, 342, 580
Evaluation, 17, 19, 534, 698, 725, 730
event, 246, 757, 758, 758
evolutionary reinforcement learning, 641
expectation, 652
expectation maximization algorithm, 600, 629
expected return, 642, 643, 676
expected reward, 651
experience replay, 671
experiment, 246, 757, 758
experimental design, 586
exploding gradients, 448, 452, 507
exploitation, 655, 656
exploration, 655, 656
exponential distribution, 60, 72, 270, 274
external criteria, 611
extract-transform-load, 42, 702

F measure, [549](#)
F score, [549](#)
 F_1 measure, [548](#), [549](#), [549–551](#), [611](#)
 F_1 score, [549](#)
factorization, [256](#), [302](#)
factors, [258](#)
false alarms, [538](#)
false negative, [537](#), [556](#)
false negative rate, [548](#)
false positive, [254](#), [537](#), [556](#)
false positive rate, [548](#)
fat tails, [272](#)
feature, [45](#), [758](#)
feature map, [485](#)
feature selection, [94](#), [181](#), [227](#), [227](#), [232](#), [614](#), [722](#), [740](#)
feature space, [181](#), [183](#), [184](#), [231](#), [599](#)
feature subset space, [228](#)
feedforward network, [389](#)
filter dimension, [486](#)
filters, [227](#), [482](#)
fit, [315](#), [367](#)
flag features, [35](#)
FN, [537](#)
FNR, [548](#)
folds, [543](#)
forget gate, [508](#)
forward reasoning, [248](#)
forward sequential selection, [229](#)
FP, [537](#)
FPR, [548](#)
fraud detection, [262](#), [538](#)
frequency counts, [749](#)
frequency histogram, [752](#)
frequency table, [749](#)
full joint probability distribution, [284](#), [302](#), [761](#)
fully connected network, [389](#)
fully observable environment, [640](#), [640](#), [673](#)

Gaeltacht, [655](#)
gain, [567](#), [569](#)
gain chart, [567](#), [570](#)
galaxy morphology, [704](#)
Galaxy Zoo, [708](#)
gamma function, [271](#)
Gapminder, [237](#)
gates, [508](#)
Gauss, Carl Friedrich, [317](#)

Gauss-Jordan elimination, 220
Gaussian distribution, 61
Gaussian mixture model, 629
Gaussian radial basis kernel, 366
generalization, 11, 14, 536
Generalized Bayes' Theorem, 251
Generative Adversarial Networks, 523
generative model, 733
Gibbs sampling, 298
Gini coefficient, 294, 563, 586, 590
Gini index, 145, 169, 174, 563
global minimum, 318, 319
Glorot initialization, 458
goal, 639, 643, 676
Goldilocks model, 14
GPUs, 394
gradient, 321, 368
gradient boosting, xvi, 159, 164
gradient descent, 168, 272, 274, 275, 319, 321, 368, 403, 541, 655
graphical models, 304, 742
greedy action selection policy, 641, 656, 680
greedy local search problem, 228
grid world, 659
ground truth, 607
group think, 158
guided search, 274, 319, 321

Hadamard product, xxvii, 475, 773
hamming distance, 240
Hand, David, 586
harmonic mean, 550, 551, 552, 554, 577, 586, 698
He initialization, 461
heating load prediction, 371
Hebb's Postulate, 404
heterogeneity, 126
hidden features, 762
hidden layers, 389
histogram, 54, 745, 752, 752
history, 639
hits, 538
hold-out sampling, 541, 547
hold-out test set, 533, 535, 540, 579, 719
Human Activity Recognition Using Smartphones Dataset, 636
hypercube, 224
hyperplane, 197, 197, 362
hypersphere, 201, 217

ID3, 133

identity criterion, 184, 211
identity function, 624
identity matrix, 219
ill-posed problem, 7, 10, 19, 21, 22, 145
imbalanced data, 193, 550, 693
imputation, 69, 296
incremental shrinkage, 168
independence, 256, 302
independent features, 83
index, 211, 212
inductive bias, 11, 11, 19, 22, 123, 141, 328, 357, 362, 729, 736
inductive learning, 11, 729
information, 120
information gain, 117, 120, 129, 130, 133, 135, 172, 174, 227, 614, 717
information gain ratio, 142, 174
information theory, 117, 126
information-based learning, 19, 117
input gate, 508, 511
insights, 3
instance, 5, 28
integration, 276
intelligent agent, 638, 639, 643, 676, 677
inter-annotator agreement, 726
inter-cluster distance, 608
inter-quartile range, 70, 749, 755
interacting features, 227
interaction effect, 169
interaction term, 355
interior nodes, 121
interpolate, 748
interpretability of models, 739
interval data, 34
interval size, 276
intra-cluster distance, 608
invalid data, 63, 94
invalid outliers, 65, 68, 715
invariant distribution, 299
inverse covariance matrix, 219, 242
inverse reasoning, 248
inverted dropout, 474, 475, 530
IQR, 749
irregular cardinality, 63, 65, 94
irrelevant features, 227
iteration, 416
Iterative Dichotomizer 3, 11, 117, 133, 133, 169, 173, 176, 541, 731

J48, 169
Jaccard index, 215, 231

Jaccard similarity measure, 635
jackknifing, 545
joint probability, 246, 251, 759
joint probability distribution, 247, 761

k nearest neighbor, 181, 192, 231, 536, 554, 575, 719, 731, 733, 735
k-d tree, 181, 196, 212, 232, 241
k-fold cross validation, 543, 611
k-means clustering, 597, 600, 601, 624, 629, 631, 636, 740
k-means++, 605, 607, 624
k-medoids clustering, 601
k-NN, 181
K-S chart, 563
K-S statistic, 563
K2 score, 293
Kaiming initialization, 461
kernel function, 366, 373
kernel trick, 366, 373
knowledge elicitation, 31
Kolmogorov-Smirnov chart, 563
Kolmogorov-Smirnov statistic, 563, 583
Kolmogorov-Smirnov test, 272
Kronecker delta, 192, 195

L₂ loss, 168
labeled dataset, 9
Lagrange multipliers, 363
Laplace smoothing, 267, 308
lazy learner, 232
leaf nodes, 121
leaky ReLU, 445
learning rate, 168, 323, 332, 379, 422, 654
learning rate decay, 334
least squares optimization, 318
leave-one-out cross validation, 545
left skew, 59
levels, 34
lift, 567, 569, 700
lift chart, 570
light tails, 272
linear, 386, 625
linear activations, 674
linear algebra, xvi, 771
linear annealing, 674
linear function, 766
linear kernel, 366
linear relationship, 312, 351, 368
linear separator, 339

linearly separable, 338, 354, 365, 396
linkage method, 618
local models, 189
local receptive field, 479
locality sensitive hashing, 233
location parameter, 271
location-scale family of distributions, 271
logarithm, 124
logistic function, 342, 386, 461
logistic regression, 311, 338, 342, 368, 556, 719, 732, 733, 735, 736
logistic unit, 386
logit, xxvii, 464
LogitBoost, 171
long short-term memory, 508
long tails, 59
longevity, 33
loss, 168, 625
loss function, 168, 315, 409, 670
loss given default, 554
lower quartile, 749, 755
LSTM, 508
LU decomposition, 220
lucky split, 543, 586
Lunar Lander, 668

machine learning, 4, 5
machine learning algorithm, 6, 19
MAE, 577
Mahalanobis distance, 217, 223, 231, 242
Manhattan distance, 185, 185, 231, 237, 577
MAP, 254
mapping features, 36, 65
margin, 361
margin extents, 361, 364
margin of error, 751
marginalization, 761
Markov assumption, 644
Markov blanket, 288
Markov chain, 298
Markov chain Monte Carlo, 298, 733
Markov decision process, 638, 643, 645
Markov process, 644, 679, 681
matrix, 771
matrix product, 385
max, 489
max pooling, 490
MaxEnt model, 357
maximum a posteriori, 254, 261, 556

maximum entropy model, 357
maximum likelihood, 301
MCMC, 298
MDP, 645
mean, 54, 69, 745, 746
mean absolute error, 577, 578
mean imputation, 374
mean squared error, 575
mean squared error loss, 625
measures of similarity, 181
median, 54, 69, 550, 745, 746, 749, 755
metric, 184, 211
mini-batch gradient descent, 417, 671
mini-batches, 417
minimum description length principle, 292
Minkowski distance, 185, 186
misclassification rate, 179, 533, 536, 539, 540, 549, 551
misses, 538
missing indicator feature, 69
missing values, 63, 64, 94, 231, 693
mixing time, 300
mixture of Gaussians distribution, 270, 274
MNIST, 477
mode, 54, 69, 746, 749
mode imputation, 374
model ensemble, xvi, 158, 170, 178, 476, 733
model parameters, 314
model residuals, 164
model-based clustering, 629
model-based reinforcement learning, 643
model-free reinforcement learning, 657, 676
Modeling, 17, 19, 20, 87, 697, 719, 730
Monte Carlo methods, 298, 677
MSE, 575
multi-armed bandit problem, 656
multi-feature, 319
multi-label classification, 742
multi-layer perceptron, 673
multimodal distribution, 60, 274
multinomial logistic regression, 357, 376
multinomial model, 311, 369, 572
multivariable, 319
multivariable linear regression, 319, 319, 575
multivariable linear regression with gradient descent, 11, 311, 731

N rays, 533
naive Bayes model, 243, 261, 284, 308, 309, 556, 731, 732, 735, 736
naive neural Q-learning, 671

natural language processing, 234
natural logarithm, 580
nearest neighbor, 303, 732, 736
nearest neighbor algorithm, 181, 187, 231
negative level, 537
negatively covariant, 74
network freezing, 671
neural network, 369, 381, 383, 599, 624, 629, 669, 735
next-best-offer model, 37
No Free Lunch Theorem, 13, 736
nodes, 286
noise, 7, 66, 69, 191
noise dampening mechanism, 157
non-linear model, 311
non-linear relationship, 368
non-negativity criterion, 184, 211
non-parametric model, 732
normal distribution, 59, 61, 71, 78, 269, 270, 557
normalization, 87, 181, 206, 231, 329, 332, 346, 421
normalization constant, 251
normalized mutual information, 611
null hypothesis, 333
numeric data, 34

observation period, 37, 689
Occam's razor, 123, 292
off-policy reinforcement learning, 659, 676
on-line gradient descent, 415
on-policy reinforcement learning, 664, 676
one-class classification, 235
one-hot encoding, 463
one-row-per-subject, 29
one-versus-all model, 357, 357, 358, 367, 369
ongoing model validation, 579, 702
OpenAI, 668
OpenAI Gym, 668
optimal control domain, 653
ordinal data, 34
other features, 36
out-of-time sampling, 546, 586
outcome, 757, 758
outcome period, 37, 689
outlier detection, 235
outliers, 63, 65, 87, 91, 94, 696, 745, 755
output gate, 508, 512
over-sampling, 93
overfitting, 14, 153, 157, 193, 256, 265, 432, 434, 472, 541
overlap metric, 240

p-value, 333
padding, 487
paperclip maximizer, 677
paradox of the false positive, 254
parameterized model, 311, 312, 314
parametric model, 732
Parametric ReLU, 445
parent node, 286
Pareto charts, 752
parsimony, 646
partial derivative, 312, 318, 381, 765, 768
partially observable environments, 640
Pascal, Blaise, 243
patience, 473
PDF, 269
Pearson correlation, 82, 223
Pearson, Karl, 82
peeking, 536
percentiles, 54, 91, 567, 748
perceptron, 396
perceptron learning rule, 342
performance measure, 535, 540
personal data, 40
placebo, 584
policy, 641, 643, 676
policy gradient, 641
policy-based reinforcement learning, 643
polynomial functions, 766
polynomial kernel, 366
polynomial relationship, 352
population, 750
population mean, 61
population parameters, 751
population standard deviation, 61
positive level, 537, 538
positively covariant, 74
post-pruning, 155, 698
posterior probability, 759
posterior probability distribution, 250
pre-pruning, 155, 169
precision, 548, 549, 572
prediction, 4, 758
prediction model, 3, 19
prediction score, 556, 574
prediction speed, 738
prediction subject, 23, 29, 689, 707
predictive data analytics, 3, 3, 21
predictive features, 227

preference bias, 11
presence-absence, 214
price prediction, 3
prior probability, 251, 759
probability density function, 61, 246, 269, 758
probability distribution, 59, 94, 247, 752, 761
probability function, 246, 758
probability mass, 266, 758
probability mass function, 246, 758
probability theory, 243, 757
probability-based learning, 19, 243
product rule, 245, 249, 757, 762
profit matrix, 553, 592
propensity modeling, 4, 36, 689
proportions, 749
proxy features, 33, 36
pruning, 117, 170
pruning dataset, 155
purpose specification principle, 41

Q-learning, 637, 657, 657, 676, 680, 741
quadratic function, 352, 766

R, 222, 276
 R^2 , 578, 586
r-trees, 233
random action selection policy, 656
random forest, 159, 159, 171, 175
random sampling, 92
random sampling with replacement, 93
random sampling without replacement, 94
random variable, 246, 652, 757, 758
range, 747
range normalization, 87, 87, 101, 206, 322, 340, 342, 374, 375, 421, 422
rank and prune, 227, 614
rate parameter, 274
ratio features, 35
raw features, 34, 41, 45
recall, 548, 549, 551, 572
receiver operating characteristic curve, 558, 589
receiver operating characteristic index, 558, 561, 586, 593
receiver operating characteristic space, 559
rectified linear activation function, 386, 625, 626, 674
rectified linear unit, 386
rectifier, 386
recurrent neural network, 434, 499
reduced error pruning, 155, 174, 698
redundant features, 227

regression task, 149
regression tree, 149, 165
regularization, 477
reinforcement learning, xvi, 5, 20, 637, 638, 674, 740
relative frequency, 245, 757, 759
relative rarity, 720
ReLU, 386
replay memory, 671
replicated training set, 160
representation learning, 401, 599, 624, 629
representational capacity, 396
residual, 315
restriction bias, 11, 357
return, 640
reward, 639, 643, 676
reward hypothesis, 640
right skew, 59
risk assessment, 3
RMSE, 577
RNN, 499
ROC curve, 558
ROC index, 558
ROC space, 559
root mean squared error, 577, 578
root node, 121
Russel-Rao index, 214, 231

S-I-R models, 644
sabremetrics, 183
sample, 541, 745, 750, 751
sample covariance, 81
sample mean, 745
sample space, 246, 757, 758
sampling, 87, 91
sampling bias, 12
sampling density, 224
sampling method, 541, 546
sampling variance, 153
sampling with replacement, 159
sampling without replacement, 159
SARSA, 664, 664, 666, 676
saturated, 437, 447
scalar, 771
scale parameter, 271
scatter plot, 73, 183
scatter plot matrix, 74, 84, 103
SDSS, 703
second mode, 749

second order polynomial function, 352, 766
seeds, 600
selection bias, 12
semi-supervised learning, 5, 742
sensitivity, 548, 559
separating hyperplane, 362
sequential gradient descent, 415
Shannon, Claude, 731
sigmoid, 625, 626
silhouette, 609, 610
silhouette method, 612
silhouette plot, 610
silhouette width, 609
similarity index, 212, 231
similarity measure, 181
similarity-based learning, 19, 181
simple linear regression, 314, 732, 735
simple multivariable linear regression, 367
simple random sample, 751
single linkage, 619, 620, 635
situational fluency, 24, 48, 686, 706
skew, 59
Sloan Digital Sky Survey, 703
slope of a line, 313, 766
small multiples, 75, 77
smoothing, 243, 265, 266, 282
social science, 293
soft margin, 366
softmax function, 463, 658
softmax output layer, 434, 463, 463, 495
Sokal-Michener index, 214, 231
spam filtering, 262
sparse, 443
sparse data, 215, 223, 225, 237, 262
specificity, 548, 559
spectral clustering, 629
SPLOM, 74
squared error, 378
stability index, 580, 590, 591, 727
stacked bar plot, 77
stale model, 578, 580, 583, 702
standard deviation, 54, 748
standard error, 333
standard normal distribution, 62
standard scores, 87, 717
standardization, 87, 101, 421, 450, 455
state, 640, 643, 676
state generation function, 640, 673

stationarity assumption, 234
stationary distribution, 299
statistical inference, 751
statistical significance, 585
statistical significance test, 333
statistics, 369
step-wise sequential search, 722, 723
stochastic, 415
stochastic gradient descent, 327, 415
stratification feature, 93
stratified sampling, 93, 710
stride, 486
student-*t* distribution, 271, 272
stunted trees, 701
sub-sampling layers, 489
subbagging, 159
subjective estimate, 757
subset generation, 228
subset selection, 228
subspace sampling, 159
sum of squared errors, 315, 367, 409, 411, 424, 426, 433, 441, 575, 578, 731
summary statistics, 96
summing out, 247, 761–763
supervised learning, 5, 21, 597, 598, 674
support vector machine, 311, 332, 361, 369, 373, 719, 732, 733, 735
support vectors, 362
SVM, 361
symmetry criterion, 184, 211

t-test, 333
tanh, 387, 461
Tanimoto similarity, 223
target feature, 5, 19, 28, 598
target hypersphere, 201
target level imbalance, 719
target network freezing, 672
target policy, 657, 664, 680
taxi-cab distance, 185
TD(0), 655
TD-Gammon, 677
temporal-difference learning, 637, 638, 654, 654, 676
termination condition, 229
test set, 535, 541
test statistic, 333
text analytics, 262
textual data, 34
Theorem of Total Probability, 245, 249–251, 757, 763, 764
thinning, 299

third order polynomial function, 766
Three Laws of Robotics, 677
timing, 33
TN, 537
TNR, 548
tolerance, 323
top sampling, 92
total sum of squares, 578
TP, 537
TPR, 548
training instance, 6
training set, 6, 541, 719
Transformer, 523
Transparency International, 237
transpose, 772
trapezoidal method, 562, 593
treatment group, 583
tree pruning, 154, 169
triangular inequality criterion, 184, 211
true negative, 537
true negative rate, 548, 558
true positive, 537
true positive rate, 548, 549, 558
TwentyTwos, 645, 647, 680
two-stage model, 722, 725
type I errors, 538
type II errors, 538

unbiased estimate, 752
unconditional probability, 759
under-sampled training set, 720
under-sampling, 93, 720
underfitting, 14, 193
uniform distribution, 59
unimodal distribution, 59, 272
unit hypercube, 224
units, 386
universal approximation theorem, 400
universal approximators, 400
unstable gradients, 449
unsupervised learning, xvi, 5, 20, 597, 598, 628, 674, 740
upper quartile, 749, 755
upsell model, 213, 572
use limitation principle, 41

valid data, 63, 94
valid outliers, 65, 68, 715
valid pixels, 487

validation dataset, 155, 473, 541, 541, 719
value function, 642
value-based reinforcement learning, 676
vanishing gradients, 387, 403, 435, 451, 507
variable elimination, 298
variable selection, 227
variance, 149, 206, 220, 747, 747, 748, 752
variation, 54, 745, 746
variational auto-encoders, 630
variational RNN, 507
vector, 216, 771
violin plot, 451
Voronoi region, 189
Voronoi tessellation, 189, 231

weak learners, 165
weight sharing, 483
weight space, 317, 321, 338, 369
weight update rule, 327, 403
weighted dataset, 160
weighted k nearest neighbor, 194, 209, 237, 238
weighted sum, 524
weighted variance, 149
weights, 314
Western Electric rules, 579
whiskers, 755
Wilcoxon-Mann-Whitney statistic, 563
Wisconsin breast cancer dataset, 109, 377
wrapper-based feature selection, 228, 541, 722

Xavier initialization, 458, 458, 459, 461
XGBoost, 171

z-score, 87
z-transform, 87